LHC OPERATION AT HIGHER ENERGY AND LUMINOSITY

G. Papotti, CERN, Geneva, Switzerland

Abstract

The Large Hadron Collider (LHC) at CERN (Geneva) was commissioned and operated in the years 2009-2013 up to a beam energy of 4 TeV. A peak luminosity of $0.77 \cdot 10^{34}\,\mathrm{cm}^{-2}\mathrm{s}^{-1}$ was reached and an integrated luminosity of around 29 fb^{-1} was delivered to both ATLAS and CMS. This performance allowed the discovery of a scalar boson. The LHC is presently in a shutdown phase dedicated to consolidation and maintenance that will allow the restart of beam operation in early 2015 at an increased beam energy of 6.5 to 7 TeV. Maximum acceptable pileup, effectiveness of electron-cloud scrubbing, and fast loss events are some of the issues that will shape the choice of operational parameters, cycle setup, and the commissioning strategy. The baseline choices and options for the restart after the shutdown are presented. In addition the roadmap for future performance upgrades is sketched.

INTRODUCTION

The Large Hadron Collider (LHC) at CERN is a 27 km long circular accelerator and collider based on superconducting two-in-one magnets and designed for a beam energy of 7 TeV [1]. It features 8 straight sections: 4 Interaction Points (IPs) are reserved for accelerator equipment and 4 house particle physics experiments. IP3 and 7 are dedicated to the collimation system, IP4 houses the RF system and most of the beam instrumentation, IP6 the beam dump system. IP1 and 5 contain ATLAS and CMS, the high luminosity experiments, while IP2 and 8 accommodate ALICE and LHCb, together with beam injection.

Initial commissioning with beam was re-started at the end of 2009, and first collisions at 3.5 TeV were achieved on 30 March 2010. The decision to limit the energy to 3.5 TeV was taken in order to reduce the risk of repeating events similar to the 2008 incident, when a highly resistive splice combined with a non-continuity in the copper stabilizer caused localized over-heating and an accidental release of the 600 MJ that were stored in the sector. After two years of successful running at 3.5 TeV with no accidental beam-induced quench at high energy, the decision was taken to run at 4 TeV per beam (in 2012 and 2013) until the start of the first Long Shutdown (LS1) during which the machine is being consolidated to run safely at 7 TeV.

The few weeks in 2009 and the year 2010 were dedicated to gaining the first operational experience. Initially, operation was with "pilot" bunch intensity (few 10^9 ppb), to commission the first squeeze. In June 2010 the bunch intensity was increased to "nominal" ($\approx 10^{11}$ ppb) and the summer was a period of steady running at $\approx$1 MJ to gain experience with intense beams and Machine Protection. In September the injection of bunch trains was commissioned (150 ns bunch spacing) and by mid-October the yearly target of an instantaneous luminosity of $10^{32}\,\mathrm{cm}^{-2}\mathrm{s}^{-1}$ was achieved.

Operation in 2011 started with 75 ns beams, and 50 ns beams were used only after a scrubbing run. With 50 ns beams, the number of bunches was slowly increased to 1380, then luminosity production was improved by reducing the transverse emittance, by squeezing further (from beta star 1.5 m to 1 m) and finally by gently increasing the bunch intensity. Squeezing to 0.6 m in 2012 allowed the production rates to increase even further and the year culminated with the discovery of the Higgs boson on 4 July 2012. The main machine and beam parameters are recalled in Table 1 for 2010-2012 and for the Design Report [1] for comparison. Operation with lead ions was also very successful [2, 3], but is not discussed here.

LONG SHUTDOWN 1

In the morning of 16 February 2013 the last LHC beam of run 1 was dumped and the LS1 started. The duration of the LS1 is planned to be approximately 20 months, and first beam is supposed to be back in the LHC in early 2015. This is to be compared to the winter shutdowns of 2010, 2011, 2012, that were as short as a couple of months and during which only fundamental maintenance was carried out.

The LS1 [4] firstly addresses the need to consolidate the interconnections between the LHC main magnets (soldered joints of two superconducting cables, splices, stabilized by a copper bus bar) to allow the LHC to operate at the nominal centre-of-mass energy of 14 TeV. It additionally targets consolidation activities to guarantee reliable operation of the LHC and its injectors until the next long shutdown (presently foreseen for 2018). Quality controls are performed on the splices and, in case of failure, the splices are remade. Consolidation activities include also the installation of shunts to improve electrical continuity and insulation boxes that provide mechanical restraints in addition to dielectric strength.

At the time of writing, the shutdown activities are progressing well. The consolidation activities spread across most of the machine, with hte interconnections being opened in sectors 12 and 23 being opened, the electrical

Copyright © 2013 CC-BY-3.0 and by the respective authors

ISBN 978-3-95450-138-0

THE CLIC PROJECT - STATUS AND PROSPECTS*

E. Adli†, University of Oslo, Norway
On behalf of the CLIC/CTF3 collaboration

Abstract

Following the feasibility demonstration of the novel CLIC technology and the publication in 2012 of a CLIC Conceptual Design Report for a Multi-TeV Linear Collider to be built in stages, a new phase towards a technical design is being launched by a global collaboration of volunteer institutes. This paper reviews the status and plans of the CLIC study outlining the developments planned for the next project phase.

INTRODUCTION

The CLIC project is a study for a Multi-TeV e+ e- collider based on normal-conducting X band technology, and a Two-Beam Acceleration scheme in order to provide compressed rf pulses for the main accelerating structures with high efficiency. The compressed rf pulses allow the main charge to be accelerated at a very high loaded gradient of 100 MV/m, in short pulses of 156 ns. CLIC completed the CDR in 2012 [1] and the project is currently in a project preparation phase where further optimization, system tests and detailed design of the machine will take place. In addition, the CLIC project has started collaborations for the use of CLIC X band technology in compact free electron lasers and medical applications.

The CLIC project is linked to the European Strategy Particle Physics priorities related to the Energy Frontier. The LHC may discover Beyond Standard Model physics when operation starts at full energy in 2015, and, depending on the findings, higher-energy hadrons as part of LHC energy upgrades or a high energy e+ e- collider might be the best option to access the new physics. The CLIC work in this period is also integrated under the Linear Collider collaboration, where the ILC technology provides an option for an early exploration of the Higgs sector in particular, while CLIC remains the only option for a Multi-TeV e+ e- collider. Wherever possible, shared activities for ILC and CLIC are being coordinated.

This paper will discuss the main conclusions of the Conceptual Design Report and highlight key activities foreseen in the project period from 2012 to 2018, which we will refer to as the "next period".

CONCEPTUAL DESIGN REPORT

The CLIC conceptual design report (CDR) was completed in 2012, and documents a proof of principle of all aspects related to the Two-Beam Acceleration scheme, both by comprehensive simulation studies of all parts of the machine and by a detailed experimental program in the CLIC Test Facility 3 at CERN [2]. Figure 1 shows a) the CLIC Test Facility Two-Beam Test Stand and b) data points for the achieved two-beam accelerating gradient as function of input power to the X band accelerating structure. Drive beam generation has been verified and the achieved gradient is up to and beyond the CLIC target of 100 MV/m. Furthermore, ongoing rf based tests of the main linac structure gradient are close to or on target for all parameters (gradient, pulse length and breakdown rate), and Figure 2 shows a summary of the latest results. Uncertainty from beam loading will be tested in the current next period. Studies of the deceleration versus power production shows good consistency [3]. Concerning emittance generation, the CLIC damping ring has similar specification to an ambitious light source, and no show stoppers were identified for generation of the ultra low emittances. Concerning emittance preservation, the alignment system principle has been demonstrated, the stabilization system have been developed and benchmarked and integrated simulations of emittance preservation in the main linac meet or exceed the luminosity targets.

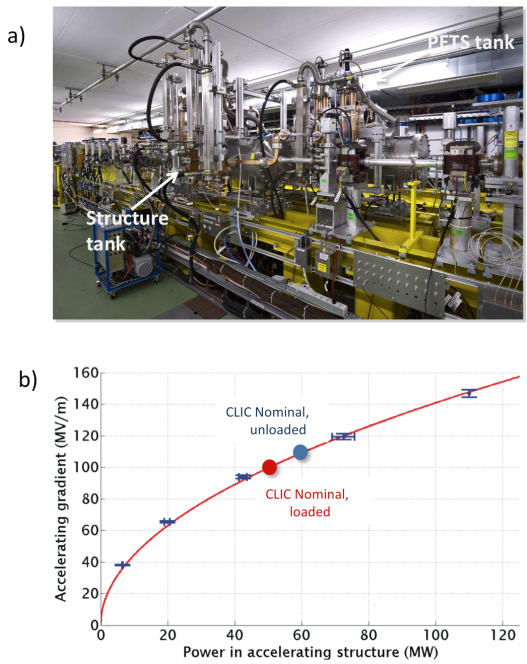


Figure 1: a) The Two-Beam Test Stand at the CLIC Test Facility. b) Experimental results of two-beam acceleration, up to and beyond the nominal CLIC gradient.

STAGING AND OPTIMIZATION

The Two-Beam Acceleration scheme is particularly suited for energy staging of the machine; once the drive

* This work is supported by the Research Council of Norway.
† Erik.Adli@fys.uio.no

Copyright © 2013 CC-BY-3.0 and by the respective authors

COLLIDERS – "QUO VADIS?" : PAST 20 YEARS, NEXT 20 YEARS, AND BEYOND*

V.Shiltsev#, Fermilab, Batavia, IL 60510, USA

Abstract

Particle colliders for high-energy physics have been in the forefront of scientific discoveries for more than half a century. The accelerator technology of the colliders has progressed immensely, while the beam energy, luminosity, facility size, and cost have grown by several orders of magnitude. The method of colliding beams has not fully exhausted its potential but has slowed down considerably in its progress. This paper briefly reviews the colliding beam method and the history of colliders, discusses the development of the method over the last two decades in detail, and examines near-term collider projects that are currently under development. The paper concludes with an attempt to look beyond the current horizon and to find what paradigm changes are necessary for breakthroughs in the field.

PAST AND PRESENT COLLIDERS

It is estimated that in the post-1938 era, accelerator science has influenced almost 1/3 of physicists and physics studies and on average contributed to physics Nobel Prize-winning research every 2.9 years [1]. Colliding beam facilities which produce high-energy collisions (interactions) between particles of approximately oppositely directed beams did pave the way for progress since the 1960's. Discussion in this section mainly follows recent publication [2].

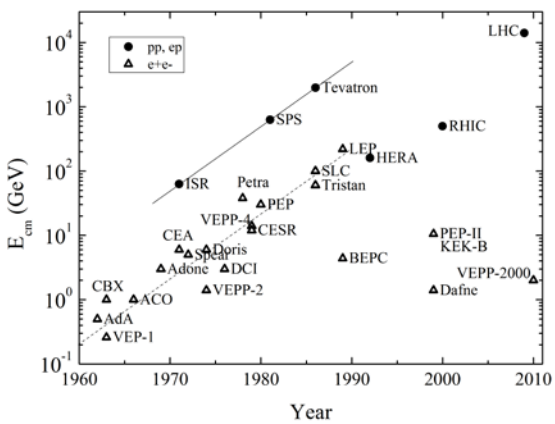


Figure 1: Colliders over the decades (after [2]).

Twenty nine colliders reached operational stage between the late 50's and now. The energy of colliders has been increasing over the years as demonstrated in Fig. 1. There, the triangles represent maximum CM energy and the start of operation for lepton (usually, *e+e-*) colliders and full circles are for hadron (protons, antiprotons, ions, proton-electron) colliders. One can see that until the early 1990's, the CM energy on average increased by a factor of 10 every decade and, notably, the hadron colliders were 10-20 times more powerful. Since then, following the demands of high energy physics, the paths of the colliders diverged to reach record high energies in the particle reaction. The Large Hadron Collider (LHC) was built at CERN, while new *e+e-* colliders called "particle factories" were focused on detail exploration of phenomena at much lower energies. Over the last 50 years, the luminosity of the colliders has improved by more than 6 orders of magnitude and reached record high values of over 10^{34}cm^{-2}s^{-1}. At such luminosity, one can expect to produce, e.g., 100 events over one year of operation (about 10^7 s) if the reaction cross section is 1 picobarn (pb)=10^{-39} cm^2.

Table 1: Past, Present and Possible Future Colliders; hadron colliders are in **bold**, lepton colliders in *Italic*, facilities under construction or in decisive design and planning stage are listed in parenthesis (…)

	early 1990's	early 2010's	2030's
Europe	**HERA, (LHC)** *LEP (Dafne)*	**LHC** (*Super-B,* **HL-LHC, LHeC,** *ENC*)	**HE-LHE** *CLIC?*
Russia	*VEPP2, VEPP4* (**UNK**, *VLEPP*)	*VEPP2000, VEPP-4M* (**NICA**, *Tau-C*)	**NICA** ? *Higgs Factory* ?
US	**Tevatron**, (**SSC**) *SLC, CESR,*(*PEPII*)	**RHIC** (*e***RHIC**, *ELIC*)	*Muon Collider* ? *PWLA/DLA* ?
Asia	*Tristan, BEPC* (*KEK-B*)	*BEPC* (*Super-KEKB*)	*ILC* ? *Higgs Factory* ?
Total	9 (7)	5 (9)	1 + ?

At the same time, the number of the facilities in operation has dropped from 9 to 5, as indicated in Table 1 which lists all operational colliders as of the early 1990's and now (early 2010's) and accounts for the projects under construction or under serious consideration at this time (in parenthesis).

NEXT TWO DECADES

There are several colliders currently under construction or at the design stage and which, therefore, have good prospects of becoming operational and deliver results in the next 20 years. Schematically they can be categorized by as follows:

Energy Frontier: the LHC luminosity upgrade project HL-LHC [3] to quintuple the performance of the energy frontier machine by mid-2020's to $5\cdot10^{34}$cm^{-2}s^{-1} with luminosity leveling at 14 TeV c.m. energy in proton-

*Fermi Research Alliance, LLC operates Fermilab under contract No. DE-AC02-07CH11359 with the U.S. Department of Energy
#shiltsev@fnal.gov

Copyright © 2013 CC-BY-3.0 and by the respective authors

STATUS OF THE ELECTRON-POSITRON COLLIDER VEPP-2000 *

A. Romanov, D. Berkaev, A. Kasaev, I. Koop, A. Kyrpotin, A. Lysenko, E. Perevedentsev, V. Prosvetov, Yu. Rogovsky, A. Senchenko, P. Shatunov, Yu. Shatunov, D. Shwartz, A. Skrinsky, I. Zemlyansky, Yu. Zharinov
BINP SB RAS and Novosibirsk State University, Russia

Abstract

VEPP-2000 began high energy physics experiments in the end of 2010 and finished its third experimental season in July of 2013. The last season was dedicated to the energy range of 160-510 MeV per beam. Compton back-scattering based energy measurements were used for the regular energy calibration of the VEPP-2000 together with resonance depolarization and NMR based methods. The concept of the round colliding beams lattice along with the precise orbit and lattice correction yielded the high peak luminosity of $1.2\times10^{31}cm^{-2}s^{-1}$ at 505 MeV with average luminosity of $0.9\times10^{31}cm^{-2}s^{-1}$ per run. The total beam-beam tune shift up to 0.174 was achieved in the runs at 392.5 MeV. This corresponds to beam-beam parameter $\xi = 0.125$ per one interaction point. The injection system is currently being upgraded to allow for the injection of particles at the top energy of VEPP-2000 collider and to eliminate the present lack of positrons.

COLLIDER OVERVIEW

VEPP-2000 collider was designed for the refinement of the cross section of the e^+e^- annihilation to hadrons in the energy range $0.4 \div 2$ GeV [1]. The lattice design was aimed to fulfill the conditions of round colliding beams [2], which promised higher luminosity performance because of an additional integral of motion.

The main proposed collider parameters are given in Table 1. VEPP-2000 was designed for one-by-one bunch operation with two functional interaction points. The ring consists of four 90 degree achromatic bends with four straight sections (Fig. 1). Two of the straight sections are occupied by the CMD-3 and SND detectors along with final focus superconducting solenoids, the third is used for injection, and the RF cavity is placed in the fourth.

The focusing system consists of six quadrupole families, three focusing and three defocussing, and four final focus configurable solenoids. Three sextupole families are available for the chromaticity correction. All sextupoles have additional coils that form skew-quadrupole fields to correct the coupling. Due to dense element placement, the orbit steering fields are generated by additional coils in main dipoles and quadrupoles resulting in 20 horizontal and 16 vertical correctors.

The beam diagnostics system consists of 4 electrostatic pickups that are capable of taking turn-by-turn data; 16

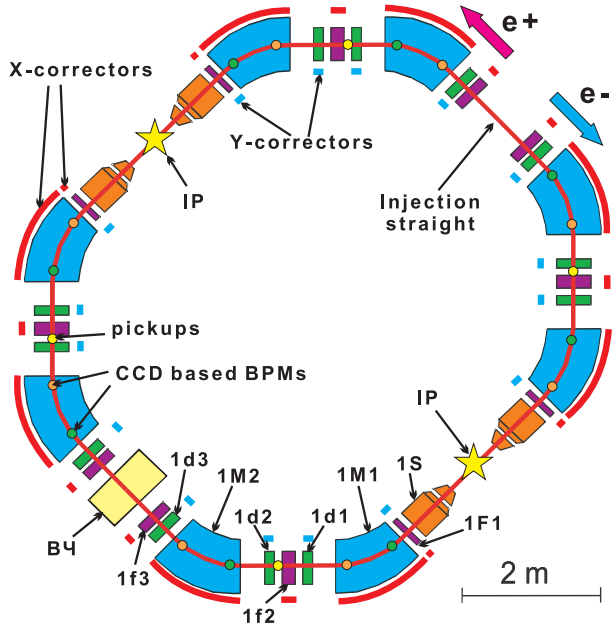


Figure 1: VEPP-2000 layout.

Table 1: VEPP-2000 Parameters at 900 MeV

Circumference, m	C	24.388
RF frequency, MHz	f_0	172
RF voltage, kV	V	100
RF harmonic number	q	14
Momentum compaction	α	0.036
Transverse emmitances, $cm \cdot rad$	ϵ_x, ϵ_y	$2.2 \cdot 10^{-5}$
Betatron tunes	ν_x, ν_y	4.1, 2.1
Twiss β at IP, cm	β_x, β_y	6.3
Particles/bunch	e^-, e^+	$1.0 \cdot 10^{11}$
Tune shifts	ξ_x, ξ_y	0.075
Luminosity/IP, $cm^{-2} \cdot s^{-1}$	L_{max}	$1.0 \cdot 10^{32}$

CCD cameras that take beam images using synchrotron light; two photomultipliers for bunch current measurements; one DCCT for measurements of full circulating current; two phi-dissectors [3] that give information about the longitudinal distributions of particles in both bunches.

The first beam was injected to the VEPP-2000 in the end of 2007 without final focus solenoids. This special "warm" configuration of lattice was used to test all vital systems of the collider. After installation of the final focus solenoids, the first luminosity runs were done in 2010. These runs were done only with SND detector, while the CMD-3 de-

* Work supported by the Ministry of Education and Science of the Russian Federation

Copyright © 2013 CC-BY-3.0 and by the respective authors

PERSPECTIVES AND CHALLENGES FOR DIFFRACTION-LIMITED STORAGE RING LIGHT SOURCES*

R. Hettel, SLAC NAL, Menlo Park, CA 94025, USA
M. Borland, ANL, Argonne, IL 60439, USA

Abstract

This paper provides an overview of the scientific motivation for developing diffraction limited storage ring (DLSR) light sources, reviews the main R&D challenges associated with DLSR implementation and summarizes the worldwide effort presently in progress to build a new generation of very low emittance rings.

INTRODUCTION

Synchrotron radiation from storage rings is the dominant source of high brightness photons from the infrared to hard X-rays, serving a multitude of scientific applications. Recently X-ray free electron lasers (FELs) have emerged, offering orders-of-magnitude higher peak brightness in ultra-short pulses. FELs offer nearly complete transverse coherence and energy bandwidth that will approach the transform-limit with seeding. Both ring- and FEL-based sources will play a vital role as they offer complementary beam properties, with rings providing low peak brightness with high average brightness and pulse repetition rate, which does not over-excite or damage samples as FELs do [1]. Another complementary capability for some storage ring sources is the production of high repetition rate (MHz), picosecond pulses for probing materials dynamics on the >10 ps timescale.

There are scientific applications and experimental methods that would greatly benefit from ring-based sources having much higher average brightness and transverse coherence. These include nanometer imaging applications; X-ray correlation spectroscopy and spectroscopic nanoprobes; and diffraction microscopy, holography and ptychography [2]. These applications will benefit from X-ray sources with average spectral brightness exceeding ~10^{22} photons/s/mm^2/mrad^2/0.1% BW and significantly higher coherent photon flux than presently available. This can best be provided only by reducing the electron beam emittance well below the present-day standard of nanometer-radians, towards the diffraction limit for X-ray beams.

WHAT IS A DLSR?

Diffraction-Limited Photon Emittance

While diffraction is typically associated with the divergence of a photon beam as it passes through a limiting aperture, it can be shown by solving the electric field wave equation that diffraction also occurs for a transverse spatially restricted photon beam, such as a Gaussian laser beam [3]. The transverse size and divergence of the electric field are related by a Fourier transform and the observed radiation intensity pattern, proportional to the square of electric field strength, satisfies the following:

$$\sigma_r(\lambda)\,\sigma'_r(\lambda) = \frac{\lambda}{4\pi} = \varepsilon_r(\lambda) \qquad (1)$$

where $\sigma_r(\lambda)$ and $\sigma'_r(\lambda)$ are the rms size and divergence, respectively, and $\varepsilon_r(\lambda)$ is the diffraction-limited emittance for a Gaussian photon beam having wavelength λ.

Extensive calculations of the radiation emitted by an undulator having N periods and length L have been carried out by several authors [3,4]. They reveal transverse beam size and divergence profiles that are only approximately Gaussian, so that the transform-limited value for the radiation emittance in (1) does not hold exactly. The rms size and divergence associated with the Gaussian fits to the calculated patterns are [4]

$$\sigma_r(\lambda) \approx 1.9\frac{\sqrt{2\lambda L}}{4\pi} \qquad \sigma'_r(\lambda) \approx \sqrt{\frac{\lambda}{2L}} \qquad (2)$$

and thus

$$\sigma_r(\lambda)\,\sigma'_r(\lambda) \approx \frac{\lambda}{2\pi} = \varepsilon_r(\lambda)\ . \qquad (3)$$

It should be noted that the factor of 1.9 for $\sigma_r(\lambda)$ in (2) is missing in [3]. This is not a serious issue – in fact, several other values can be derived depending on calculation and fitting assumptions. For the remainder of this paper, $\lambda/4\pi$ will be used since that value is commonly used by the synchrotron radiation community.

Diffraction-Limited Electron Emittance

A hypothetical filament of electrons having essentially no transverse size or divergence ("single electron" dimensions) passing through an undulator would emit radiation having the dimensions and emittance given in (2) and (3). A real electron beam has transverse size and divergence, which must be convolved with the single-electron photon parameters to determine the photon beam properties. Assuming Gaussian profiles, total horizontal or vertical emittance $\Sigma_{x,y}$ is given by

$$\Sigma_{x,y}(\lambda) = \varepsilon_r(\lambda) \oplus \varepsilon_{x,y}(e-) = \sqrt{\sigma_r{}^2(\lambda) + \sigma_{x,y}{}^2(e-)}\sqrt{\sigma'_r{}^2(\lambda) + \sigma'_{x,y}{}^2(e-)} \qquad (4)$$

where $\oplus$ denotes convolution, and $\sigma_{x,y}(e-)$ and $\sigma'_{x,y}(e-)$ are electron size and divergence, respectively, given by

$$\sigma_{x,y}(e-) = \sqrt{\beta_{x,y}\varepsilon_{x,y}(e-)} \quad \sigma'_{x,y}(e-) = \sqrt{\varepsilon_{x,y}(e-)/\beta_{x,y}} \qquad (5)$$

at the waist of the electron beam (and assuming zero dispersion). Total emittance is minimized when photon

†Work supported in part by Department of Energy Contract DE-AC02-76SF00515 and Office of Basic Energy Sciences, Division of Chemical Sciences

ISBN 978-3-95450-138-0

Copyright © 2013 CC-BY-3.0 and by the respective authors

ULTRA-LOW EMITTANCE UPGRADE OPTIONS FOR THE DIAMOND LIGHT SOURCE

R. Bartolini[1,2], N. Hammond[2], J. Kay[2], T. Pulampong[1] and R.P. Walker[2]
[1]John Adams Institute, University of Oxford, UK
[2]Diamond Light Source, Oxfordshire, UK

Abstract

Many synchrotron radiation facilities are studying lattice upgrades in order to lower the natural emittance and hence increase the radiation brilliance and transverse coherence. While large circumference rings are favoured for reaching ultra small emittance, recent advances in design and optimisation tools allow also medium size rings to reach emittances down to the some 100s of pm region, with workable lattices. Diamond is investigating a novel design whereby low emittance is conjugated with doubling of the capacity of the ring, based on a double-double bend achromat (DDBA) cell. Plans for the installation of one or more low emittance cells will be presented. This will serve as a prototype for a possible full phased upgrade of the storage ring in the longer term.

INTRODUCTION

The Diamond Light Source is actively pursuing a research programme for the development of an ultra-low emittance upgrade of the storage ring in order to achieve emittances in the range of 270 pm and below [1,2] which would improve the present emittance by a factor 10 or more. This emittance will allow the facility to remain competitive with the next generation high brightness light sources by substantially increasing the brilliance and the transverse coherence of the synchrotron radiation.

Accelerator physics studies have shown that lattices based on Multiple Bend Achromats (MBAs) can produce appealing emittance even with medium size rings such as the 561.6 m of the Diamond storage ring. The Diamond lattice upgrade is constrained by the requirement of maintaining the tunnel geometry and the position of the beamlines. The possibility of phasing the upgrade on a cell-by-cell basis to avoid long shutdowns was also considered in the studies. Reusing as much hardware as possible was considered, however it turned out that the magnets of the present lattice are not adequate for a reduced emittance lattice and so new magnet designs are now developed. Other technical subsystems are also under design, notably vacuum and diagnostics, while the RF system [3] and the power supplies will be reused. In this report we present the advances on the accelerator physics design.

MBAs have been proposed in the early '90s as a promising lattice design that allows reducing the emittance towards the diffraction limit [4] in the hard X-ray region. We therefore investigated the possibility of replacing our DBA lattice with an MBA. Various options were analysed starting with a very aggressive 7BA design with 45 pm emittance but with a very small dynamic aperture. More relaxed lattices 5BA and 4BA produced slightly larger emittance, 150 pm and 270 pm respectively. These values are in any case meeting the 10-fold emittance reduction target. In the analysis of the 4BA lattice it transpired that the 4BA cell can be split in two, inserting a new straight section in the middle of the cell. We later found that a similar concept was proposed in [5]. In this way the lattice strongly resembles again a DBA, despite the fact that the outer and inner dipoles in the cell have different lengths, and was therefore named "Double Double Bend Achromat" (DDBA). The additional straight section in the middle of the cell allows doubling the capacity of the present Diamond ring for Insertion Devices (IDs), while still maintaining a very small horizontal emittance.

The possibility of introducing an additional straight section has triggered the study of the installation of one or more such DDBA cells into the present Diamond lattice. The VMX [6] and the DIAD [7] beamlines have expressed strong interest in utilising a DDBA cell located in cell 2 and cell 11 respectively. A third modification of the lattice in cell 20 would allow the installation of a third harmonic cavity for bunch lengthening which will support the increase in the operational current to 500 mA and is in line with the potential phased upgrade of the full lattice.

The installation of the DDBA cells in the present lattice will provide the opportunity of testing many critical areas of a possible full upgrade of the machine. In particular it has kick-started the necessary R&D on several technical subsystems such as magnets, vacuum, diagnostics and the engineering integration of the subsystems.

MBA LATTICE STUDIES

The first options investigated to replace the existing DBA was a 7BA lattice, providing an emittance of 45 pm. The basic cell, shown in Fig. 1, is built on gradient dipoles with 0.45 T and 30 T/m quadrupole component and 90 cm length. The larger number of dipoles is accommodated by slightly reducing the lengths of straight sections. The natural chromaticity of this lattice is very high and requires strong sextupoles for correction. A dispersion bump is created between dipole 1 and 2 and symmetrically between dipole 6 and 7 to locate the chromatic sextupoles and reduce their required strength. The lack of a proper phase advance (π or 3π usually) between the chromatic sextupoles in the cell prevents the cancellation of the geometric driving terms. The phase advance was matched to complete 2π within one super period (4 cells). Most of the resonance driving terms (RDTs) can be cancelled in one super period in this way

Copyright © 2013 CC-BY-3.0 and by the respective authors

ISBN 978-3-95450-138-0

ANALYSIS OF TRANSVERSE INSTABILITIES OBSERVED AT J-PARC MR AND THEIR SUPPRESSION USING FEEDBACK SYSTEMS

Y. H. Chin, KEK/Sokendai, Tsukuba, Japan

Abstract

This paper presents an analysis of head-tail instabilities observed at the J-PARC MR (Main Ring) and their suppression using feedback systems. Instabilities were mainly observed at low energies. About 30% of particles are lost due to the instabilities if the feed-back system is turned off at the beam power of 120kW. Both horizontal and vertical instabilities were observed. Measurements of the horizontal oscillations initially suggested the excitation of higher-order head-tail modes during the injection. An analysis unveils that a dipole mode has a temporal appearance of higher-order head-tail modes if the chromaticity is sufficiently large. The development of instabilities in the presence of a large chromaticity should be considered for conditions beyond the Sacherer's text book case.

INTRODUCTION

J-PARC consists of three proton accelerators: a 400 MeV linear accelerator (currently operating at 180 MeV), a 3 GeV Rapid-Cycling Synchrotron (RCS) and a 50 GeV (currently 30 GeV) Main Ring (MR). The main parameters of the MR are summarized in Table 1.

Table 1: Main Parameters of the MR Ring

Circumference	1568 m
Injection Energy	3 GeV
Extraction Energy	30 GeV
Repetition Period	3 sec
RF Frequency	1.67-1.72 MHz
Number of bunches	8
Synchrotron tune	0.002-0.0001
Betatron tune	22.4, 20.77

In the normal operation mode, over 90% of the protons accelerated in the RCS are directed to the muon and neutron production targets in the Materials and Life Science Experimental Facility (MLF). The remaining protons are transported to the MR for further acceleration before being extracted via one of two (fast and slow) MR extraction ports.

The MR impedance is dominated by the transverse resistive-wall impedance of the stain-less steel chamber and the horizontal kicker impedance [1]. The kicker impedance has sharp peaks at about 1MHz and 10MHz. It is almost halved after four injection kickers were replaced by parasitic-impedance-free new models with HOM dampers (we still use five old-type kickers). The transverse resistive-wall impedance is exceptionally high, since the first betatron unstable line appears at around 40kHz on the vertical plane where the skin-depth is comparable to the wall thickness and the transverse impedance is proportional to the inverse of the frequency, not the square root of the frequency [2]. The beam instability evaluation before the commissioning of MR predicted that beam instabilities would start to hurt beam operation from the beam power of 100-200kW. Although the necessity of a damper system has been recognized, actual development has been delayed due to financial constraints. After the commissioning of MR started, the careful inventory of the existing hardware revealed that we already have some key components necessary to compose the damper system: several unused Stripline Position Monitors (SPM), and the exciters for tune measurements that can be exploited as damper kickers. It was found that only remaining component to be developed is a signal processing circuit to filter and process SPM data and then to produce kick signals. The whole project costs only less that 100k USD.

Figure 1 sketches the transverse (narrow-band) bunch-by-bunch feedback system. The beam position signals are sampled at an RF frequency times 64 rate (108.8MHz at 3GeV). The signal processing and digital filtering circuits consist of two LLRF4 boards with four 14-bit ADCs and two 14-bit DACs. They extract the betatron oscillation signals using 8-tap FIR filters. Its system integration and firmware development including EPICS interface was done by the Dimtel Inc. The kick signals are sent to the stripline damper kickers through the power amplifiers (two 500W/ 10kHz-250MHz ones for the horizontal plane and two 1kW/100kHz-8MHz ones for the vertical plane) to provide a single kick per bunch per passage for the both directions.

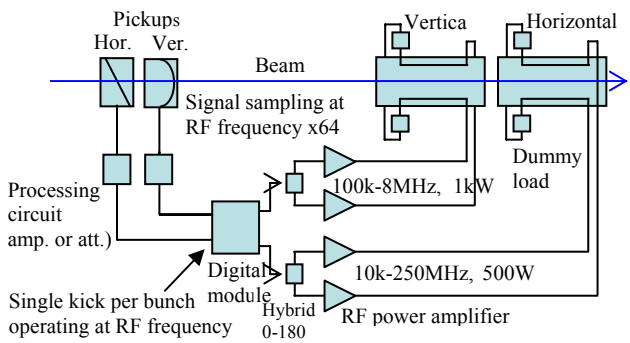


Figure 1: Schematic view of the transverse bunch-by-bunch feedback system (narrow-band).

Figures 2 (a) and (b) show the beam oscillation signals from the SPM recorded at a 500MHz sampling rate for the first 128ms period that covers the injection of the last batch of bunches from RCS (K4) and the onset of acceleration (P2) where all instabilities take place. The top figure (a) shows the signals with the feedback (FB) off, while the bottom figure (b) shows one with the FB on.

Copyright © 2013 CC-BY-3.0 and by the respective authors

ISBN 978-3-95450-138-0

TRANSVERSE IMPEDANCE AND TRANSVERSE INSTABILITIES IN THE FERMILAB BOOSTER*

A. Macridin, J. Amundson, P. Spentzouris, V. Lebedev, T. Zolkin Fermilab, Batavia, IL 60510, USA

Abstract

The Fermilab Booster is characterized by large space charge and large wake fields, leading to beam loss and instabilities at high intensity. Using the Synergia simulation package with a realistic lattice model and realistic wake functions we investigate the coherent tune shift and the instabilities at injection energy. We calculate the wake functions in the laminated magnets and find them to be four orders of magnitude larger than the wakes in the metallic straight sections. We find a large decrease of the vertical tune shift and a small increase of the horizontal tune shift with intensity, in good agreement with experiment. In agreement with measurements, we find that a large chromaticity is required to avoid a horizontal instability. The instability is caused by short-range bunch-bunch interaction and is due to the large coupling between the horizontal wake function and large lattice beta function at the locations of the focusing magnets.

INTRODUCTION

The Fermilab Booster [1] is a 40-year-old machine which provides protons for the Fermilab Main Injector. It runs at an intensity of 4.5×10^{12} protons per batch, which is about two times larger than the originally designed intensity. The machine shows beam loss and instabilities at high intensity. For machine improvements required by the demand of future Fermilab programs for high intensity beams, it is essential to have a good understanding of these instabilities.

The particular thing about the Booster is the presence of the dipole-quadrupole combined-function focusing (F) and defocusing (D) magnets, which cover about 60% of the machine length. The rest of the machine is made by straight metallic beam pipe sections. Since there is no beam pipe in the combined-functions magnets, the beam is exposed directly to the magnets' laminations. A consequence of the presence of bare laminations is the formation of very large wake fields. Since the machine runs at low energy (injection E/final $E = 0.4GeV/8GeV$), the space charge is also strong. The presence of both large wakes and space charge effects together with complex single-particle optics makes any attempt of analytical treatment very difficult.

We address these effects by using Synergia [2], a state of the art simulation package developed at Fermilab. We perform single- and multibunch simulations at the injection energy. Since the RF sets the number of buckets in the Booster to 84, a full machine simulations requires simulations with 84 bunches.

In order to properly take into account the wake fields, we calculate the wake functions in the laminated magnets. We find that the wake functions in the laminated magnets have a non-metallic behavior and are four orders of magnitude larger than the wakes in the metallic pipe section.

The measurements of the coherent tune shift show a large negative shift for the vertical tune and a small positive shift for the horizontal tune [3, 4]. Close to injection, the beam is horizontally unstable unless the machine runs with a large horizontal chromaticity [5]. The result of our simulations are in good agreement with experiment. We find that the instability is due to short range bunch-bunch interactions. The instability is caused by the large value of the coupling between the lattice horizontal beta function and the horizontal wake at the location of the F magnets.

SYNERGIA CODE

Synergia [2] is a simulation package for beam dynamics in accelerators developed at Fermilab. It can address single-particle optics by using direct symplectic integration through the lattice elements or/and by using arbitrary-order polynomial maps. Collective effects are incorporated by employing the split-operator method [6]. A variety of space-charge solvers (such as 3D Poisson solvers with different boundary conditions, 2.5D solversand semi-analytical 2D solvers) can be used with Synergia. Synergia can accommodate arbitrary wake functions by reading them from external files.

In our Booster simulations, in order to account for the large nonlinear lattice effects, we used direct symplectic integration for particle propagation. Space charge was addressed by using three different 3D Poisson solvers with appropriate boundary conditions for the F magnets, D magnets and straight sections, respectively. We used different wake functions for the F and the D magnets. The wake functions for the laminated magnets were calculated separately, as is described in the next section.

WAKE AND IMPEDANCE

The electromagnetic field created by a particle moving through the accelerator induces currents in the vacuum chamber walls. The field created by these currents will affect a trailing particle. This effect can be addressed by a

*This work was performed at Fermilab, operated by Fermi Research Alliance, LLC under Contract No. De-AC02-07CH11359 with the United States Department of Energy. It was also supported by the ComPASS project, funded through the Scientific Discovery through Advanced Computing program in the DOE Office of High Energy Physics. We also used resources of the Argonne Leadership Computing Facility at Argonne National Laboratory, which is supported by the Office of Science of the U.S. Department of Energy under contract DE-AC02-06CH11357.

Copyright © 2013 CC-BY-3.0 and by the respective authors

THE JLAB 12 GEV ENERGY UPGRADE OF CEBAF *

Leigh Harwood (for the JLab 12 GeV project team)
Thomas Jefferson National Accelerator Facility, Newport News, VA 23606 USA

Abstract

CEBAF at Jefferson Lab was a 5-pass, recirculating cw electron linac operating at ~6 GeV and devoted to basic research in nuclear physics. The 12 GeV Upgrade is a major project, sponsored by the DOE Office of Nuclear Physics, that is expanding its research capabilities substantially by doubling the maximum energy and adding major new experimental apparatus. The Upgrade is illustrated in Figure 1 includes: doubling the accelerating voltages of the linacs by adding 10 new high-performance cryomodules; the requisite expansion of the 2K cryogenics plant and rf power systems to support these cryomodules; upgrading the beam transport system from 6 to 12 GeV through extensive re-use and/or modification of existing hardware; and the addition of one recirculation arc, a new experimental area, and the beamline to it; and the construction of major new experimental equipment for the GPD, high-xBjorken, and hybrid meson programs. The accelerator upgrade is essentially complete and the construction of the new experimental apparatus is well underway. This paper provides some details about the accelerator upgrade.

OVERVIEW

Scientific Motivation

In the 20+ years since the original design parameters of CEBAF were defined the understanding of the behavior of strongly interacting matter has evolved significantly, and important new classes of experimental questions have been identified that can be addressed optimally by a CEBAF-type accelerator at higher energy. The original design of the facility, coupled with developments in superconducting RF technology, makes it feasible to triple the initial design value of CEBAF's beam energy to 12 GeV in a cost-effective manner, providing a new research tool capable of addressing the science.

The science motivating the 12 GeV Upgrade includes breakthrough programs that will be launched in four main areas (they are described in detail in [1]):

- Discovering the quark structure of nuclei
- Probe potential new physics through high precision tests of the Standard Model using precision, parity-violating electron scattering experiments.

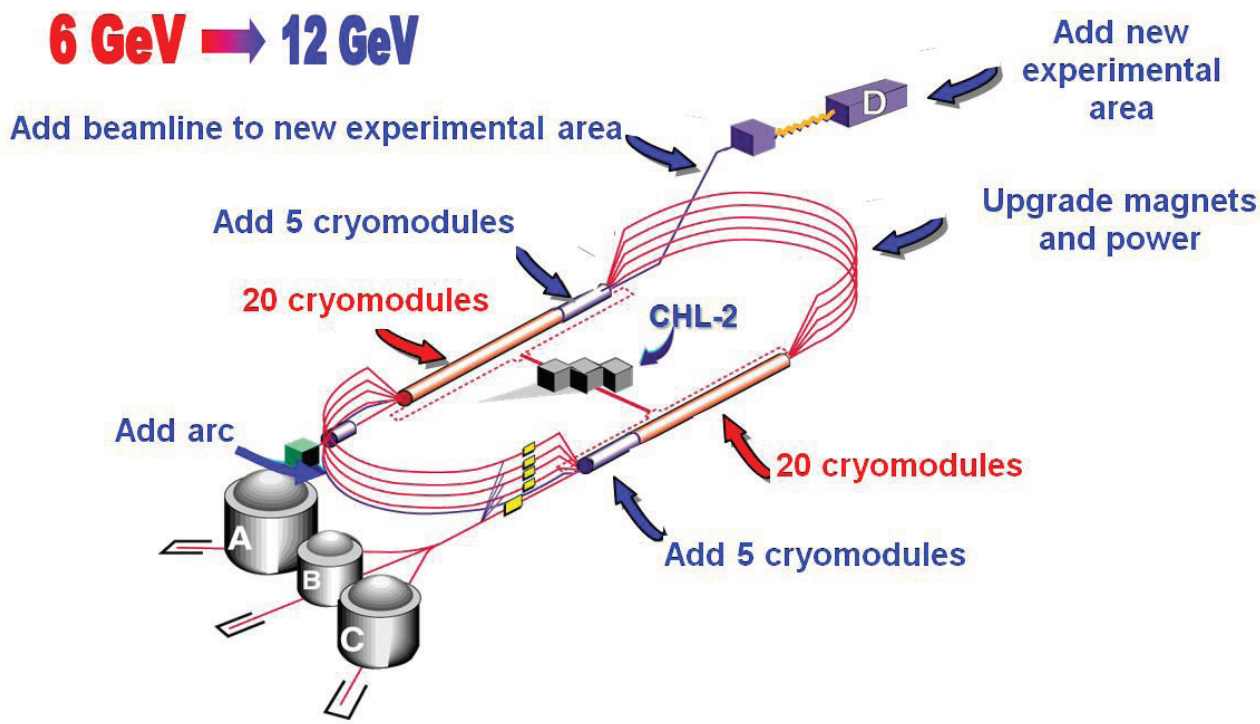


Figure 1: Changes to CEBAF.

* This work was supported by the U.S. Department of Energy Contract Number DE-AC05-06OR23177 under which Jefferson Science Associates, LLC operates Jefferson Lab

Copyright © 2013 CC-BY-3.0 and by the respective authors

FULL 3D STOCHASTIC COOLING AT RHIC*

K. Mernick#, M. Blaskiewicz, J.M. Brennan, BNL, Upton, NY 11973, USA

Abstract

Over the past several years, the installation of the full 3-dimensional stochastic cooling system in RHIC has been completed. The FY12 U-U and Cu-Au collider runs were the first to benefit from the full installation. In the U-U run, stochastic cooling improved the integrated luminosity by a factor of 5. This presentation provides an overview of the design of the stochastic cooling system and reviews the performance of the system during the FY12 heavy ion runs.

INTRODUCTION

Intra-beam scattering (IBS) is a primary cause of emittance growth of the heavy ion beams in the Relativistic Heavy Ion Collider (RHIC). A 3D bunched beam stochastic cooling system has been implemented to combat IBS and reduce the emittance of the beams. This system has been installed in stages over the past several years. The first operational use of stochastic cooling, in the longitudinal plane of the Yellow ring, began in 2007 [1,2]. The 2010 and 2011 collider runs had longitudinal and vertical cooling in both rings [3,4]. Commissioning of the horizontal cooling system in the 2012 run completed the full system.

SYSTEM DESIGN

The stochastic cooling system is essentially a wideband feedback damper. The momentum error of samples of particles within the bunch is measured and reduced via an applied kick. Longitudinal mixing randomizes the samples on subsequent turns and, over time, the emittance of the bunch is reduced. The time resolution of the samples and the resulting cooling rate are a function of the bandwidth of the system.

The layout of the fundamental components of the RHIC stochastic cooling systems is shown in Fig. 1. The longitudinal cooling pickups are located on either side of the 2 o'clock intersection region. The signals from these pickups are transmitted approximately 700m via microwave link to low-level electronics located near the kickers, which are in sector 4 for the Blue (clockwise) ring and sector 11 for the Yellow (counter-clockwise) ring. The longitudinal microwave links "cut the chord," transmitting the pickup signal across the center of the ring in the same direction the beam travels. This leaves only 200 ns for signal processing and cable delays. To minimize delay, the Blue ring electronics are located in the attic of the RF service building and cables are routed through a dedicated penetration to the tunnel. The Yellow ring electronics are located in a dedicated building on the berm above the tunnel.

*Work supported by Brookhaven Science Associates, LLC under Contract No. DE-AC02-98CH10886 with the U.S. Dept. of Energy.
#kmernick@bnl.gov

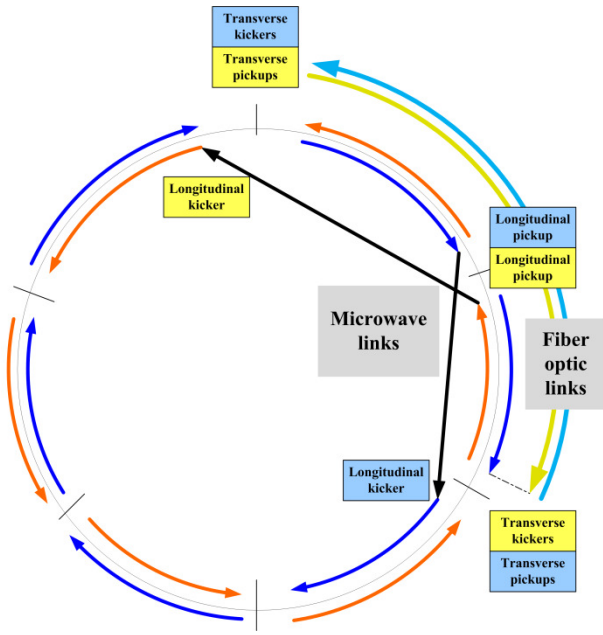


Figure 1: Locations of pickups and kickers (blue and yellow boxes), longitudinal system microwave links (black arrows), and transverse system fiber optic links (light blue and yellow arrows). The dark blue and orange arrows indicate the directions the beams travel.

In the Blue transverse system, signals from pickups in sector 3 are transmitted by fiber optic link to low-level electronics in the 12 o'clock service building, and from the electronics to the kickers in sector 12. The Yellow transverse system is the mirror-image of the Blue, with pickups in sector 12, electronics in a dedicated trailer outside the tunnel, and kickers in sector 3. The fiber optic link travels approximately 1/3 of the ring, while the beam travels 2/3 of the ring in the opposite direction.

Longitudinal Pickups

The longitudinal pickups measure fluctuations in the beam current as a function of the longitudinal position in the bunch. New longitudinal pickups have been designed and installed since the end of the 2012 run. These pickups consist of a keyhole-shaped vacuum chamber, shown in Fig. 2, with a 7 cm aperture round section and a 2 cm high rectangular section. During injection and ramping, the beam circulates in the large round section of the chamber. At top energy, the pickup chamber is moved, with pivoting double bellows on either side, to center the beam in the rectangular section. The small aperture cuts off the propagation of waveguide modes up to 9 GHz. The beam couples to top and bottom WRD-475 double-ridge waveguides parallel to the rectangular section through 8 mm by 6 mm slots. The top and bottom slots are offset in the beam direction, which improves the flatness of the pickup gain across the 6 to 9 GHz operating range.

Copyright © 2013 CC-BY-3.0 and by the respective authors

ISBN 978-3-95450-138-0

ARIEL ELECTRON LINAC

S. Koscielniak, F. Ames, R. Baartman, I. Bylinskii, Y.C. Chao, D. Dale, R. Dawson, I. Earle, K. Fong, E. Guetre, N. Kahn, A. Koveshnikov, R. Laxdal, F. Mammarella, L. Merminga, A.K. Mitra, T. Planche, Y.N. Rao, A. Trudel, V. Verzilov, D. Yosifov
TRIUMF*, 4004 Wesbrook Mall, Vancouver, B.C. Canada
D. Karlen, Victoria University, Victoria, B.C.

Abstract

The TRIUMF Advanced Rare Isotope Laboratory (ARIEL) phase I is funded since 2010 June by federal and BC provincial governments. ARIEL I comprises buildings and electron linac; the future phase II includes hot cells, target stations, mass separators and beam transport to ISAC experimental areas. The linac vault and He compressor building were completed 2012. The ARIEL targets building completion is 2013 August. With the exception of the 30 MeV accelerator cryomodule and second klystron and HV power supply, the linac major procurements are complete. This paper reports progress for the following systems: locally manufactured niobium 9-cell cavity, 300 keV electron gun, 4 K cryogenic plant and sub-atmospheric pumps, 290 kW cw klystron and 65 kV DC power supply. Status of the 10 MeV injector cryomodule assembly and beamlines construction will also be addressed.

CONVENTIONAL INFRASTRUCTURE

The ARIEL project, described in Refs. [1,2], is essentially a new front end for the existing ISAC I & II experimental complex. The project contains two new "drive beams" and two target stations to supplement those at ISAC. The conventional infrastructure consists of four main contracts: the ARIEL construction, demolition and excavation, the Stores building, and Badge building. The new Compressor Building forms part of the ARIEL package as does major renovation of the former Proton Hall that has segregated the Electron Hall (e-hall) area from the future BL4N protons vault.

The Stores and Badge building construction was completed in 2011. The e-hall and Compressor building occupancy were taken 2012 November 1st and December 1st respectively. The ARIEL building occupancy was taken 2013 September 1st; and the connecting tunnel was completed one month prior.

The ARIEL cooling water system which provides capacities of 3 MW each to the ARIEL building and e-linac, and 0.3 MW to the compressor building, was completed 2013 June 1st. The site electrical connections to the 5 MW utility feed are made through a 12.5 kV switchgear supplied by Siemens. This connection supplies up to 1.5 MW to klystrons, 0.5 MW emergency power, 1 MW to compressor building, and 2 MW to the ARIEL building. Switchgear was energized 2012 December. A rack farm for magnet power supplies, beam diagnostic and LLRF controls is now complete on the e-hall roof.

*TRIUMF is funded under a contribution agreement with the National Research Council of Canada.



Figure 1: ARIEL building, view south.

ELECTRON GUN

The thermionic gun provides 300 keV kinetic energy electron bunches with charge up to 16 pC at a repetition frequency of 650 MHz. Unique features of the gun are its inverted cathode/anode geometry to reduce dark current, and transmission of rf modulation via a ceramic waveguide through SF6 dielectric. An impedance network inside an HV shroud matches the waveguide to the gridded cathode. The waveguide was received 2012 September from Kyocera. The HV cage containing the Glassman 300 kV supply, isolation transformer and bias and heater supplies was completed 2013 March. The gun electrodes polishing and assembly to the ceramic was completed 2013 May. The SF6 vessel also was received and installed in May. The vessel internal corona domes and shroud were fabricated and installed in the SF6 vessel 2013 September. 200 kV High voltage was first applied in October and a breakdown encountered with the receptacle connecting to the conditioning resistor.

INJECTOR TEST FACILITY

The Injector test facility, under collaboration between TRIUMF and VECC of Kolkata, India, provides an ideal proving ground for e-linac design and operation strategies. It duplicates the e-linac up to the exit of the injector cryo-module with enhanced diagnostic capability. Commissioning this facility began Nov 2011 with a 100kV gun and low energy solenoid beam transport and continued to 2013 Feb. The primary objective is a complete 6D phase space characterisation of the 100 kV beam. The 99% longitudinal phase is ±18.8 deg at 650 MHz and $\Delta p/p \pm 3.7\times10^{-4}$. The measured transverse r.m.s. normalized emittance is 9.3 µm horizontal and

Copyright © 2013 CC-BY-3.0 and by the respective authors

ISBN 978-3-95450-138-0

THE RHIC POLARIZED SOURCE UPGRADE

A. Zelenski, G. Atoian, J. Fite, D. Raparia, J. Ritter, D. Steski, BNL, Upton, NY USA
V. Klenov, V. Zubets , INR Moscow, Russia
V. Davydenko, A. Ivanov, A. Kolmogorov, BINP, Novosibirsk, Russia

Abstract

A novel polarization technique has been successfully implemented for the upgrade of the RHIC polarized H^- ion source to higher intensity and polarization. In this technique, a proton beam inside the high magnetic field solenoid is produced by ionization of the atomic hydrogen beam (from an external source) in the He-gas ionizer cell. Proton polarization is produced by the process of polarized electron capture from the optically-pumped Rb vapor. Polarized beam intensity produced in the source exceeds 4.0 mA. Strong space-charge effects cause significant beam losses in the LEBT (Low Energy Beam Transport, 35.0 keV beam energy) line. The LEBT was modified to reduce losses. As a result, 1.4 mA of polarized beam was transported to the RFQ and 0.7 mA was accelerated in linac to 200 MeV. A maximum polarization of 84% (in the 200 MeV polarimeter) was measured at 0.3 mA beam intensity and 80% polarization was measured at 0.5 mA. The upgraded source reliably delivered beam for the 2013 polarized run in RHIC at √S=510 GeV. This was a major factor contributing to the increase in RHIC polarization to over 60 % for colliding beams.

OPPIS UPGRADE WITH THE ATOMIC HYDROGEN BEAM INJECTOR

The polarized beam for the RHIC spin physics experimental program is produced in the Optically-Pumped Polarized H^- Ion Source (OPPIS) [1].

An Electron Cyclotron Resonance (ECR) ion source was used as the primary proton source in the old operational polarized source. The ECR source was operated in a high magnetic field. The proton beam produced in the ECR source had a comparatively low emission current density and high beam divergence.

In pulsed operation, suitable for application at high-energy accelerators and colliders, the ECR source limitations can be overcome by using a high brightness proton source outside the magnetic field instead of the ECR source. In this technique (which was implemented for the first time at INR, Moscow [2]), the proton beam is focussed and neutralized in a hydrogen cell producing the high brightness 6.0-8.0 keV atomic H° beam. The atomic H^0 beam is injected into the superconducting solenoid, where both the He ionizer cell and the optically-pumped Rb cell are situated in the 25-30 kG solenoid field. The solenoid field is produced by a new superconducting solenoid with a re-condensing cooling system. The injected H atoms are ionized in the He cell with 60-80% efficiency to form a low emittance intense proton beam and then enter the polarized Rb vapour cell (see Figure 1). The protons pick up polarized electrons from the Rb atoms to become a beam of electron-spin polarized H atoms (similar to the ECR based OPPIS). A negative bias of about 3.0-5.0 kV applied to the He cell decelerate the proton beam produced in the cell to the 3.0 keV beam energy, optimal for the charge– exchange collisions in the rubidium and sodium cells. This allows energy separation of the polarized hydrogen atoms produced after lower energy proton neutralization in Rb-vapour and residual hydrogen atoms of the primary beam.

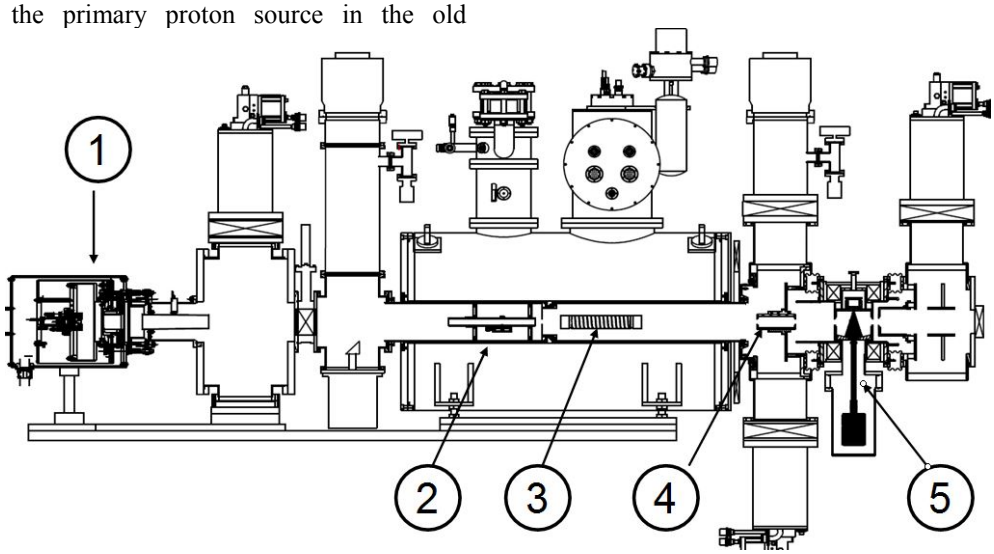


Figure 1: A new polarized source layout: 1–atomic hydrogen injector; 2–pulsed He –gaseous ionizer cell; 3–optically-pumped Rb-vapour cell; 4–Sona-transition; 5–Na-jet ionizer cell.

Copyright © 2013 CC-BY-3.0 and by the respective authors

ISBN 978-3-95450-138-0

FIRST COMMISSIONING EXPERIENCE WITH THE LINAC4 3 MEV FRONT-END AT CERN

J.B. Lallement, A. Akroh, G. Bellodi, J.F. Comblin, V.A. Dimov, E. Granemann Souza, J. Lettry, A.M. Lombardi, O. Midttun, E. Ovalle, U. Raich, F. Roncarolo, C. Rossi, J.L. Sanchez Alvarez, R. Scrivens, C.A. Valerio-Lizarraga, M. Vretenar, M. Yarmohammadi Satri
CERN, Geneva, Switzerland

Abstract

Linac4 is a normal-conducting 160 MeV H^- linear accelerator presently under construction at CERN. It will replace the present 50 MeV Linac2 as injector of the proton accelerator complex as part of a project to increase the LHC luminosity. The Linac front-end, composed of a 45 keV ion source, a Low Energy Beam Transport (LEBT), a 352.2 MHz Radio Frequency Quadrupole (RFQ) and a Medium Energy Beam Transport (MEBT) housing a beam chopper, have been commissioned at the 3 MeV test stand during the first half of 2013. The status of the installation and the results of the first commissioning stage are presented in this paper.

THE LINAC4 PROJECT

Linac4 is a new accelerator, first part of a project to improve the CERN proton accelerator chain [1]. The higher injection energy (160 MeV vs 50 MeV for Linac2) and the H^- charge exchange injection will make it possible to inject more intensity into the PS Booster. The 80 m long accelerator will be housed in a 101 m tunnel, 12 m underground. A view of the Linac in its tunnel is shown in Figure 1. It consists in a 45 keV RF ion source, a 2 magnetic solenoid LEBT; a 352.2 MHz RFQ accelerating the beam to 3 MeV; a MEBT housing a fast beam chopper; a 50 MeV Drift Tube Linac (DTL) composed of 3 tanks; a 100 MeV Coupled Cell Drift Tube Linac made of 7 modules of 3 coupled tanks and a Pi Mode Structure (PIMS) up to 160 MeV. The schematic layout is shown in Figure 2. The Linac will be connected by a 60 m transfer line to the present Linac2-PSB line. Figure 3 represents the integration of Linac4 in the PS complex. The linac positioning was also designed to be compatible with an extension to 5 GeV as part of the Superconducting Proton Linac (SPL) [2].

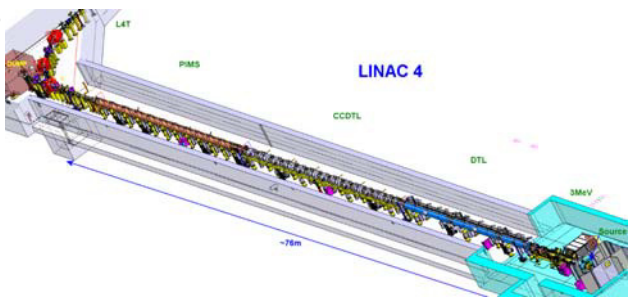


Figure 1: Linac4 in its tunnel.



Figure 2: Linac4 layout.

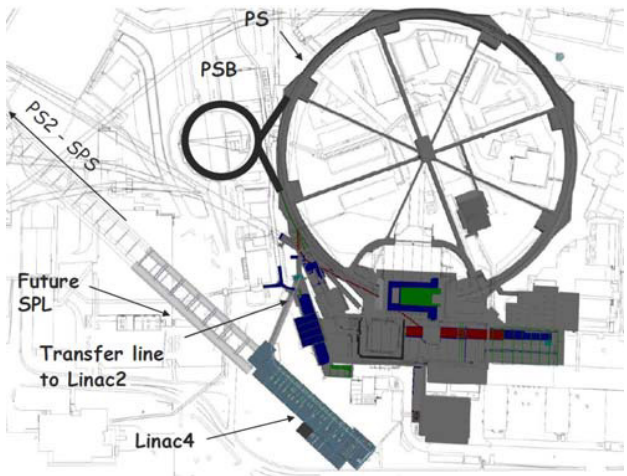


Figure 3: Linac4 integration in the CERN PS complex.

The Linac4 energy and repetition rate (160 MeV, 1.1 Hz) are defined by the PSB while the 352.2 MHz operation frequency is that of the LEP accelerator, from which a large inventory of RF equipment is recuperated. The design parameters are given in Table 1.

Table 1: Linac4 Design Parameters

Ion Species	H^-	
Length	77	m
Output Energy	160	MeV
Frequency	352.2	MHz
Repetition rate	1.1 (max. 2)	Hz
Pulse length	400 (max. 1200)	μs
Chopping factor	62	%
Source current	80	mA
Linac pulse current	40	mA

Copyright © 2013 CC-BY-3.0 and by the respective authors

PROTON ACCELERATOR DEVELOPMENT IN CHINA

S.N. Fu, IHEP, Beijing 100049, China

Abstract

The China Spallation Neutron Source (CSNS) and the Chinese Accelerator Driven Systems (C-ADS) projects are both underway in China. The CSNS includes a 100 kW RCS accelerator and first beam on target is planned for 2017. The C-ADS project includes a high power superconducting linac with a low energy (25-50 MeV) initial stage by 2015 and higher power deployment later. In addition to these intense-beam proton accelerators, some other proton accelerators for various applications are also under construction or planned. In this paper, the plans, R&D and construction activities of these projects will be discussed.

INTRODUCTION

Proton accelerator becomes a new direction in Chinese accelerator community for its many important applications. It will be used for neutron source for neutron scattering applications, Accelerator Driven Subcritical system (ADS) for nuclear waste transmutation, proton therapy for cancer treatment, as well as the space radiation effects research. China Spallation Neutron Source started construction in 2011[1]. Its accelerator provides a proton beam of 100 kW power onto the target in the first phase, and then will be upgraded to 500 kW beam power in the second phase. And meanwhile, a small neutron source is under construction in Tsinghua University[2]. In 2010 a Chinese roadmap for long-term development of ADS was proposed by Chinese Academy of Sciences[3] and the first budget of about $260M has be allocated for an ADS test setup construction. This year, Chinese central government has approved two proton accelerator-based big-science projects in its five-year plan: ADS program and space radiation effect research program. These proton accelerator-related projects, no matter big or small, give a great chance to Chinese accelerator community to develop the cutting-edge high-technology of proton accelerator in China. This paper will present an overview of these projects at different stage, including their design, key technology R&D, construction and future plan.

CHINA SPALLATION NEUTRON SOURCE

The CSNS is designed to accelerate proton beam pulses to 1.6 GeV kinetic energy at 25 Hz repetition rate, striking a solid metal target to produce spallation neutrons. The accelerator provides a beam power of 100 kW on the target in the first phase. It will be upgraded to 500kW beam power at the same repetition rate and same output energy in the second phase. For this reason, the present design has reserved a long beam line in LRBT for superconducting spoke cavity installation for the linac energy upgrade in order to compensate for space-charge effect in the RCS when the beam current becomes 5-times higher. Table 1 lists the major parameters of the accelerator in the two phases.

Table1: CSNS Design Parameters

Project Phase	I	II
Beam Power on target [kW]	100	500
Proton energy [GeV]	1.6	1.6
Average beam current [μ A]	62.5	312.5
Pulse repetition rate [Hz]	25	25
Linac energy [MeV]	80	250
Linac type	DTL	+Spoke
Linac RF frequency [MHz]	324	324
Macropulse. ave current [mA]	15	40
Macropulse duty factor	1.0	1.7
RCS circumference [m]	228	228
RCS harmonic number	2	2
RCS Acceptance [πmm-mrad]	540	540
Target Material	Tungsten	Tungsten

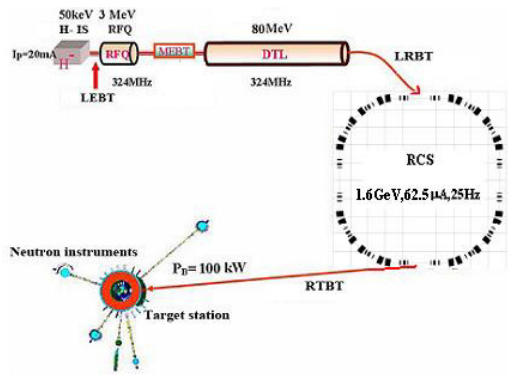


Figure 1: Schematics of the CSNS complex.

A schematic layout of CSNS phase-1 complex is shown in Figure 1. In the phase-1, an ion source produces a peak current of 25mA H^- beam. RFQ linac bunches and accelerates it to 3MeV. DTL linac raises the beam energy to 80MeV. After H^- beam is converted to proton beam via a stripping foil, RCS accumulates and accelerates the proton beam to 1.6GeV before extracting it to the target. 20 neutron channels are designed surrounding the target, but only 3 spectrometers will be built in the first phase due to limited budget.

The CSNS project started construction in September 2011 after the site land and the access road had been

Copyright © 2013 CC-BY-3.0 and by the respective authors

ISBN 978-3-95450-138-0

ACCELERATOR-DRIVEN SUBCRITICAL FISSION TO DESTROY TRANSURANICS AND CLOSE THE NUCLEAR FUEL CYCLE*

S. Assadi, C. Collins, J. Comeaux, K. Damborsky, J. Kellams, F. Lu, P. McIntyre#, K. Melconian, N. Pogue, M. Salanne, A. Sattarov, E. Sooby, and P. Tsvetkov, Texas A&M University, College Station, TX 77845 USA

Abstract

A design for accelerator-driven subcritical fission in a molten salt core (ADAM) has been made for the purpose of destroying the transuranic elements in used nuclear fuel as fast as they are made in a conventional nuclear power plant. The oxide fuel is extracted from the used fuel assemblies into molten chloride salt using pyroprocessing, and the transuranic, uranium, and fission product salts are separated into three batches using electroseparation. The transuranic salt is then transferred to a subcritical core, with neutron gain 0.97. The core is driven by 800 MeV proton beams from a 12 mA CW strong-focusing cyclotron. The transuranics are destroyed and the fission heat is used to produce electric power. Simulations of many potential failure modes have been performed; the core cannot reach criticality in any failure-mode scenario considered. It operates as an energy amplifier with an energy gain ~5.5.

INTRODUCTION

Today nuclear power plants generate 20% of the electric power in the United States [1]. Until recently nuclear power comprised 20% of the grid in Germany and 30% in Japan, but Germany has moved to end their nuclear power production and Japan has idled their reactor fleet. Those decisions reflect a growing public concern about the safety of nuclear power. The meltdowns at Three Mile Island [2], Chernobyl [3], and Fukushima [4] underscore that this abundant source of energy can also produce extreme hazards.

The most enduring hazard of nuclear power is the large quantity of hazardous radioisotopes in used nuclear fuel (UNF). The most dangerous among those are transuranics (TRU, elements beyond uranium in the periodic table). The transuranics contained in the ~70,000 tons of UNF in the US have a radiotoxicity $>10^{13}$ Sv and half-lives of 10^5-10^6 years. The present accumulation of UNF also still contains about 1/3 of the entire US reserves of uranium. Long-term storage would pose the risk unto the generations of future release of immense radiotoxicity, and would sequester a major portion of available uranium resources. ADAM has been designed to offer an alternative: to destroy the transuranics, to recover the uranium for future use, and to produce 10x more energy than was produced in the first use of the fuel.

* Work supported by State of Texas and the Mitchell Foundation.
# mcintyre@physics.tamu.edu

ADAM OVERVIEW

ADS Core Neutronics

The individual ADS core must be sized to optimize the normalized burn rate $\dot{T}/T$; i.e. to minimize the TRU inventory required to sustain core operation. Figure 3 shows the energy dependence for neutron capture on ^{238}Uwhich breeds TRU) and for n-induced fission of the dominant TRU isotopes. The fission cross sections for most TRU isotopes are significant only for ultra-fast neutrons (>1 MeV). Optimization of fast spectrum for the ADAM core places strong constraints upon the core size and geometry and upon the fuel salt composition. The optimized core is shown in Figure 1, and its neutronics properties are summarized in Table 1. In its spectrum 20% of the neutrons have >1 MeV energy. It operates with a neutron gain k_{eff} = 0.97, produces 280 MW_{th}, and requires a 10 MW proton driver. The optimized burn rate is $\dot{T}/T = 5.6\%/year$, corresponding to a destruction time of 18 years.

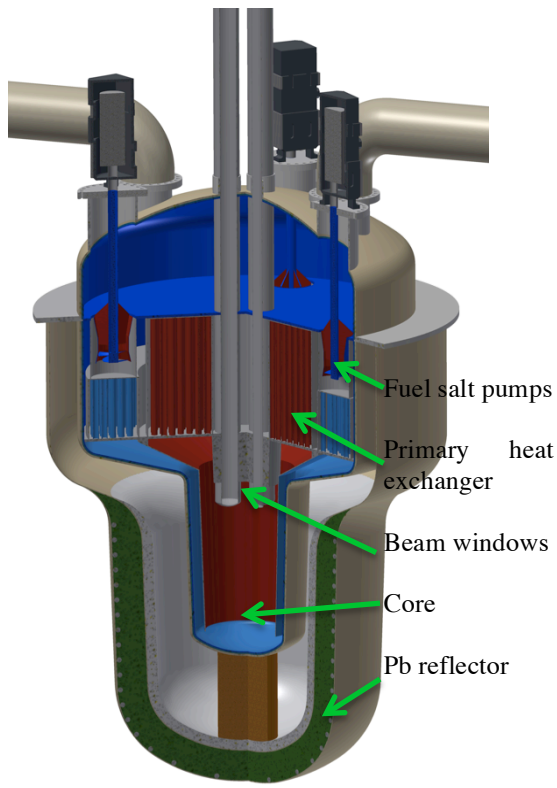


Figure 1: ADS molten salt core assembly.

Copyright © 2013 CC-BY-3.0 and by the respective authors

ISBN 978-3-95450-138-0

THE ADVANCED SUPERCONDUCTING TEST ACCELERATOR (ASTA) AT FERMILAB*

P. Piot[1,2], V. Shiltsev[1], M. Church[1], P. Garbincius[1], E. Harms[1],
S. Henderson[1], J. Leibfritz[1], S. Nagaitsev[1]
[1] Fermi National Accelerator Laboratory, Batavia, IL 60510, USA
[2] Department of Physics and Northern Illinois Center for Accelerator & Detector Development, Northern Illinois University DeKalb, IL 60115, USA

Abstract

The Advanced Superconducting Test Accelerator (ASTA) currently in construction at Fermilab will enable a broad range of beam-based experiments to study fundamental limitations to beam intensity and to develop transformative approaches to particle-beam generation, acceleration and manipulation. ASTA incorporates a superconducting radiofrequency (SRF) linac coupled to a photoinjector and small-circumference storage ring capable of storing electrons or protons.This report describes the facility, its capabilities, and provide an overview of enabled research thrusts.

INTRODUCTION

The Advanced Superconducting Test Accelerator (ASTA) currently in construction at Fermilab will establish a unique resource for R&D towards Energy Frontier facilities and a test-bed for superconducting radiofrequency (SRF) accelerators and high-brightness beam applications. The unique features of ASTA include: (1) a high repetition-rate, (2) one of the highest peak and average brightness within the U.S., (3) a GeV-scale beam energy, (4) an extremely stable beam, (5) the availability of SRF and high-quality beams together, and (6) a storage ring capable of supporting a broad range of ring-based advanced beam dynamics experiments. These unique features will foster a broad program in advanced accelerator R&D which cannot be carried out elsewhere.

ACCELERATOR OVERVIEW

The backbone of the ASTA facility is a radio-frequency (RF) photoinjector coupled with 1.3-GHz superconducting accelerating cryomodules (CMs); see Fig. 1 [1]. The electron source consists of a 1-1/2 cell 1.3-GHz cylindrical-symmetric RF gun comprising a Cs_2Te photocathode illuminated by an ultraviolet (UV, $\lambda = 263$ nm) laser pulse obtained from frequency quadrupling of an amplified infrared IR pulse The photocathode drive laser produces a train of bunches repeated at 3 MHz within a 1-ms-duration macropulse.

The $\sim$ 5-MeV electron bunches exiting the RF gun are then accelerated with two SRF TESLA-type cavities (CAV1 and CAV2) to approximately 50 MeV. Downstream of this accelerating section the beamline includes quadrupole and steering dipole magnets, along with a four-bend magnetic compression chicane (BC1) [2]. The beamline also incorporates a round-to-flat-beam transformer (RTFB) capable of manipulating the beam to generate a high transverse-emittance ratio. In the early stages of operation, the bunches will be compressed in BC1. In this scenario the longitudinal phase space is strongly distorted and the achievable peak current limited to less than 3 kA. Eventually, a third-harmonic cavity (CAV39) operating at 3.9 GHz will be added enabling the generation of bunches with $\sim$ 10 kA peak currents by linearizing the longitudinal phase space. In addition CAV39 could also be used

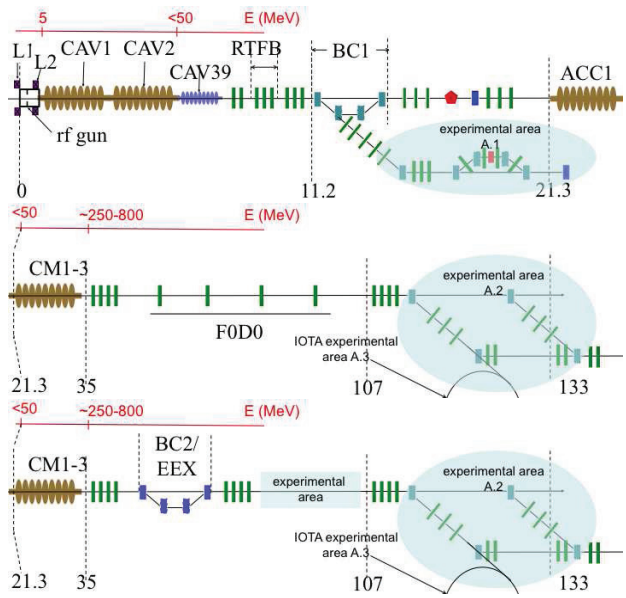


Figure 1: Overview of ASTA photoinjector (top); ASTA nominal high-energy transport beamline (middle) and modified high-energy transport beamline to accomodate a second-stage bunch compressor (bottom); "L1" "L2" stand for solenoids, "CAV1", "CAV2", and "CAV39" correspond to accelerating cavities, "CM1-3" to an ILC cryomodule string, "BC1" and "BC2/EEX" to bunch compressors, and "DL" to a dogleg beamline. "PEX" represents a possible reconfiguration of "BC2" to act as a transverse-to-longitudinal phase space exchanger.

* This work is supported by DOE contract DE-AC02-07CH11359 to the Fermi Research Alliance LLC

Copyright © 2013 CC-BY-3.0 and by the respective authors

ISBN 978-3-95450-138-0

THE AWAKE PROTON-DRIVEN PLASMA WAKEFIELD ACCELERATION EXPERIMENT AT CERN

P. Muggli*, Max Planck Institute for Physics, Munich, Germany
for the AWAKE Collaboration

Abstract

We briefly outline the proposed AWAKE plasma wakefield accelerator (PWFA) experiment to be performed with the CERN SPS proton bunches. We focus on the experimental setup, allude to some of the physics involved and describe some of the measurements that are planned.

INTRODUCTION

A new high-gradient acceleration technique for electrons (e^-) and positrons (e^+) is required. Among those currently proposed and explored, plasma-based acceleration has led to the largest energy gain (>40 GeV) over a meter-scale distance [1]. However, producing with plasmas beams with parameters equal to or better than those produced by conventional, RF-based accelerators remains challenging. One of the challenges arises from the energy of the drive bunch that limits the energy gain of the witness bunch. Current short laser pulses or e^- bunches carry less than ∼100 J. Therefore, staging of a large number of plasma accelerator sections, with all the ensuing issues (alignment, timing, gradient dilution, etc.), is required to reach the desired energy (TeV range).

Proton (p^+) bunches available today, e.g. at CERN, carry much more energy than that carried by a future e^-/e^+ collider bunches: ∼1.6 kJ for 2×10^{10} particles at 500 GeV. With 10^{11} p^+, CERN SPS (400 GeV) and LHC (7 TeV) bunches carry 6.4 and 112 kJ, respectively. However, these bunches are long (σ_z ∼10 cm). For single-bunch operation at a plasma e^- density n_{e0} such that the electron plasma wave period $\lambda_{pe} = 2\pi c\left(\epsilon_0 m_e/n_{e0}e^2\right)^{1/2}$ matches the bunch length ($\lambda_{pe}\sim\sigma_z$, as in [1]) would result in a very low maximum accelerating field: $\leq E_{WB} = \left(2\pi m_e c^2/e\right)/\lambda_{pe} \cong 3.2\times10^9/\sigma_z(mm) \cong$32 MV/m in a plasma with $n_{e0}\sim10^{11}$ cm^{-3}. Short p^+ bunches (σ_z ∼0.1-1 mm) are thus necessary to reach fields higher than in RF cavities (>200 MeV/m).

P^+-DRIVEN PWFA

The potential for a p^+-bunch driven, plasma-based accelerator to produce a high energy e^- bunch was demonstrated in proof-of-principle simulations [2, 3]. An energy gain of ∼500 GeV in a plasma ∼500 m-long with a density of 6×10^{14} cm^{-3} with a σ_z ∼100 μm-long drive bunch was achieved. A train of short bunches can be produced out of a long bunch ($\sigma_z \gg \lambda_{pe}$) by the plasma itself through a transverse self-modulation instability (SMI) [4]. Thanks to the periodic focusing/defocusing fields of the initial wakefields, the SMI produces a train of $\sim\lambda_{pe}/2$-long bunches separated by $\sim\lambda_{pe}$ that can then resonantly drive the wakefields to large amplitudes. Interestingly, the amplitude of the wakefields is comparable the one that would be driven if all the charge were in a single short bunch. However, using the long bunch and the SMI to drive wakefields brings new challenges.

When the SMI grows from noise it needs a long plasma length to saturate. Also, the final relative phase of the wakefields is unknown and varies from event to event, which prevents the deterministic injection of the witness bunch into the accelerating and focusing phase of the wakefields. Over this long propagation distance the long bunch is subject to a competing, but asymmetric transverse instability, the hose instability (HI) [5]. The HI can break-up the bunch before the SMI can grow or before the witness bunch can gain large amounts of energy. Calculations and simulations indicate that the growth length of the SMI can be shortened, the phase of the wakefields determined and the occurrence of the HI mitigated by seeding the SMI with a signal of large amplitude [6] and known phase. They also indicate that in certain regimes the full bunch self modulation can effectively prevent the HI from developing over the acceleration region [7].

Even when seeded, the phase velocity of the SMI is slower than that of the drive and witness bunch during the growth phase of the SMI [8]. This leads to dephasing of the witness bunch with respect to the wakefields and to its loss through strong defocusing. The witness bunch must therefore be injected after the SMI has saturated and the bunch is fully self-modulated.

The SMI also grows along the bunch (convective instability) and the witness bunch must be injected many plasma periods behind the start of the wakefields ($\sim1\sigma_z \gg \lambda_{pe}$). Therefore the proper position within the drive bunch for the witness bunch to be focused and accelerated ($\sim\lambda_{pe}/4$) over a long distance is rather sensitive to plasma density variations since $\delta\lambda_{pe}/\lambda_{pe} = -\frac{1}{2}(\delta n_{e0}/n_{e0})$. When injecting the witness bunch $N\sim\sigma_z/\lambda_{pe}$ periods after the start of the wakefields the density uniformity requirements becomes $|\delta n_{e0}/n_{e0}| \leq (1/2N)$ (for a $\leq\lambda_{pe}/4$ phase shift). This requirement must be met over the plasma length, but only over the time scale of the interaction ($\sim\sigma_z/c$).

THE AWAKE EXPERIMENT

The AWAKE collaboration proposed an experiment to be performed at CERN to study the physics of self-modulation of long p^+ bunches in plasmas, to determine the potential of plasma-based accelerators driven by self-

* muggli@mpp.mpg.de

Copyright © 2013 CC-BY-3.0 and by the respective authors

BEAM-BEAM LIMIT IN AN INTEGRABLE SYSTEM*

A. Valishev#, S. Nagaitsev, FNAL, Batavia, IL 60510, USA
D. Shatilov, BINP, Novosibirsk, 630090, Russia
V. Danilov, ORNL, Oak Ridge, TN 37831, USA

Abstract

Round colliding beams have been proposed as a way to push the attainable beam-beam tune shift limit, and recent successful experiments at the VEPP-2000 collider at BINP demonstrated the viability of the concept. In a round-beam system the dynamical stability is improved by introducing an additional integral of motion, which effectively reduces the system from a two and a half dimensional to one and a half dimensional. In this report we discuss the possible further improvement through adding the second integral of motion and thus making the system fully integrable. We explore the ultimate beam-beam limit in such a system using numerical simulations taking into account various imperfections.

INTRODUCTION

The strong nonlinearity of transverse focusing force is inherent to beam-beam interaction and affects the stability of particle motion in the present circular colliders. The beam-beam kick localized in a short interaction length along the accelerator circumference represents a nonlinear and time-dependent excitation of the otherwise linear betatron motion in the rest of the machine. In such systems, a multitude of resonances lead to particle diffusion and to chaotic-bounded motion, which limits the attainable beam brightness and collider performance. The typical maximum value of beam-beam parameter ξ in such 'conventional' machines is about 0.05÷0.06 for electron colliders, and up to 0.03 for hadron colliders due to the absence of synchrotron radiation damping.

In an attempt to mitigate the beam-beam effect, Krishnagopal and Siemann [1] analyzed the effect of the strong bunch length σ_z on the magnitude of resonances with the use of canonical perturbation theory. They concluded that '…the finite longitudinal extent of the beam-beam interaction results in averaging of the betatron phase over the collision, which mitigates the destructive effects of resonances'. Conversely, the synchrotron oscillations of the test particle lead to a greater depth of modulation and enhance the effect of resonances. Since the lengths of the two colliding bunches are usually equal, an optimal length should exist at which the two effects are compensating one another. The ratio of the bunch length to the beta-function of the order of one was determined as viable.

In further work along this direction Y. Alexahin [2] and T.Sen [3] studied the effect of phase averaging on the Tevatron performance, and also predicted the optimal $\sigma_z/b^* \approx 1$.

The growing interest to integrable systems in mathematical physics motivated Danilov and Perevedentsev to investigate the application of these systems to accelerators and colliding beams in particular [4, 5]. In a round colliding beams system, the beam-beam interactions as well as the transport through accelerator lattice possess axial symmetry. This results in the existence of an additional integral of motion, the longitudinal component of the angular momentum. An important consequence of the additional integral of motion is the elimination of transverse coupling resonances.

In Ref. [5], a round colliding beam system is proposed, which has two integrals of motion. The full integrability is achieved through proper shaping of the longitudinal bunch density, which makes the system Hamiltonian time-independent. The line charge density λ in this case must be inversely proportional to the beta-function β: $\lambda(2s)=C/\beta(s)$. In the case of no external focusing in the interaction region, the beta-function is a quadratic function of the azimuth s, $\beta(s)= \beta^*+s^2/\beta^*$, and the proper 'ideal' longitudinal distribution is

$$\lambda(s) = \frac{C}{1+(s/2\beta^*)^2}.$$

An important property of the fully integrable system is that the exact shape of transverse density distribution is irrelevant and does not affect the stability. However, the complete integrability is valid only for the center particles in the weak bunch, and synchrotron oscillations introduce modulation that disturbs the system. Also, the longitudinal distribution in a typical collider is Gaussian. Numerous numerical simulations have been performed to explore the stability of the round colliding beam systems to these imperfections (see e.g. [6, 7]). More importantly, the experimental implementation of the concept at the VEPP-2000 collider (BINP, Novosibirsk), where the record-high value of ξ=0.25 was achieved (at $\sigma_z/\beta^* \approx 1$), demonstrated its viability [8, 9].

This, and the recent progress in the development of nonlinear integrable systems [10] motivated us to re-visit the question of optimization of a round colliding beam system with the goal to achieve even higher beam-beam parameters. We use the Lifetrac weak-strong particle tracking code [11] to perform numerical simulations, and characterize the tracking data with the Frequency Map Analysis [12, 13].

*Fermi Research Alliance, LLC operates Fermilab under contract No. DE-AC02-07CH11359 with the U.S. Department of Energy.
#valishev@fnal.gov

Copyright © 2013 CC-BY-3.0 and by the respective authors

A MODEL RING WITH EXACTLY SOLVABLE NONLINEAR MOTION

T. Zolkin*, The University of Chicago, Department of Physics, Chicago, IL 60637–1434, USA
Y. Kharkov, I. Morozov†, BINP SB RAS, Novosibirsk 630090, Russia
S. Nagaitsev‡, FNAL, Batavia, IL 60510–5011, USA

Abstract

Recently, a concept of nonlinear accelerator lattices with two analytic invariants has been proposed [1]. Based on further studies [2], the Integrable Optics Test Accelerator (IOTA) was designed and is being constructed at FNAL. Despite the clarity and transparency of the proposed idea, the detailed analysis of the beam motion remains quite complicated and should be understood better even for the case when no perturbations are taken into account. In this paper we will review one of the three proposed realizations of integrable optics, where the variables separation is possible in polar coordinates. This system allows for an exact analytical solution expressed in terms of elliptic integrals and Jacobi elliptic functions [3]. It gives the possibility to check numerical algorithms used for tracking and to perform more rigorous analysis of the motion in comparison with the "crude" analysis of the topology of the phase space. In addition we will discuss some difficulties associated with numerical simulations of such a comparatively complex dynamical system and will take a look at the possible perturbations for a model machine.

INTRODUCTION

Below we will consider the design of the accelerator lattice which includes nonlinear lens, while the transverse motion remains integrable. Several such systems possessing a second invariant of motion, which is quadratic in momentum, have been proposed in [1]. One of the possible realization is based on the application of a point-like magnetic quadrupole inserted into the center of a vacuum pipe. In this case, the motion allows the variables separation in polar coordinates and its analytical solution was described in [3]. Here, we will focus on the implementation of this idea and will design a model accelerator ring. For more details on dynamics in such a magnetic field one should consult the list of references.

ACCELERATOR LATTICE DESIGN

The particle dynamics in the magnetic field of point-like magnetic quadrupole is unusual in that there is no equilibrium orbit of motion; trapped particles are only in dynamical equilibrium, i.e. in constant motion in at least one degree of freedom. This feature is related to the presence of singularity at the origin. On the other hand, it means that under the action of friction force, let say caused by the synchrotron radiation, particles will fall towards the singularity and eventually will be lost on the inner aperture of the vacuum pipe, ρ_{in}. Thus, below we will consider the design of an accelerator ring for protons, so far as the damping of oscillations due to radiation effects is negligible for them.

* zolkin@uchicago.edu
† imorozov@fnal.gov
‡ nsergei@fnal.gov

Axially Symmetric Focusing

As it was described in [1], the concept of nonlinear integrable optics under consideration requires an axially symmetric focusing in the accelerator ring. A super-period of such a lattice can be realized as $\frac{F}{2}O\frac{F}{2}$ lattice, with a drift space of length L, where the nonlinear lens is located, and an optics insert (also so-called T-insert), which is equivalent to a thin axially symmetric lens with the focal length equal to $1/k$ (see Fig. 1).

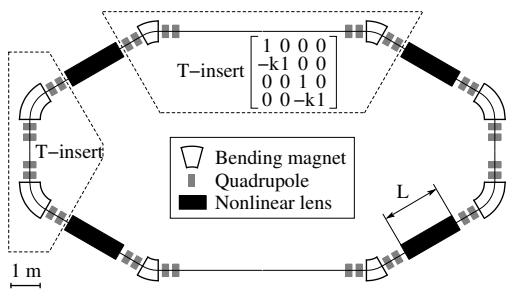


Figure 1: Schematic layout of the IOTA ring.

To study the transverse motion of the monochromatic beam the principal realization of the optics insert is not essential, and for all further simulations we will use a parameters designed for IOTA ring [2]. The dependence of the minimum and maximum of beta function in the drift space as well as betatron frequency as a function of the T-insert strength are show in Fig. 2. Main parameters of the ring are listed in Table 1.

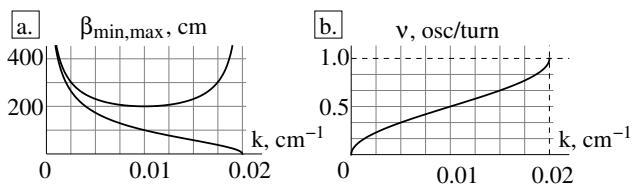


Figure 2: Minimum and maximum of beta-function (a.) and betatron frequency (b.) as a function of axially symmetric lens strength parameter, k.

Copyright © 2013 CC-BY-3.0 and by the respective authors

ISBN 978-3-95450-138-0

NONPARAXIAL TRANSVERSE EFFECTS ON THE PROPAGATION OF NONLINEAR ELECTROMAGNETIC PULSES *

A. Bonatto†, UFPR Curitiba, UFRGS Porto Alegre, Brasil
S.R.Lopes, UFPR, Curitiba, Brasil
R.P. Nunes, R. Pakter, F.B. Rizzato, UFRGS, Porto Alegre, Brasil
C. Bonatto, UFPel, Pelotas, Brasil

Abstract

In the present analysis we study the weakly nonlinear interaction between trains of electromagnetic pulses and space-charge fields in laser-plasma systems. We direct the analysis to regimes evolving with the co-moving coordinate of the beam frame, but do not make any assumptions on paraxial or underdense approximate conditions. The model thus constructed allows us to investigate regimes where transverse and longitudinal length scales of the pulses are comparable. Resonant and nonresonant regimes of space-charge wave excitation are analyzed. In both cases, with aid of analytical estimates and numerical simulations, we examine how far trains of electromagnetic pulses can travel before being affected by the destructive transverse effects.

INTRODUCTION

The propagation of localized radiation pulses in plasmas has been the subject of continuous interest in a variety of areas, including nonlinear wave excitation [1, 2] and particle acceleration [3, 4, 5]. Pulses are formed as large amplitude electromagnetic waves undergo the process of modulational instability in the plasma, breaking up into a series of narrow quasi-isolated structures. This is a typical behavior in soliton turbulence [6] and in self modulated laser accelerators, once an option in laser acceleration, whose interest has been reignited recently [7].

Pioneering works [8, 9] have studied the self-consistent problem of electromagnetic pulses propagating in plasmas and the space-charge waves generated by this propagation in one dimensional models. These models, however, usually refers to nonparaxial solutions (where dependence of the field on transverse coordinates is completely neglected) or the opposite, the paraxial limit (where transverse effects dominate the dynamics). In several occasions, a laser beam reaches operational conditions where longitudinal and transverse sizes become similar in magnitude [10, 11]. Under these conditions, an accurate account of the dynamics should treat transverse and longitudinal effects on the same footing.

The objective of the present work is to perform an analysis of the nonlinear interaction of electromagnetic and space-charge without invoking 1D, paraxial, or approximate nonparaxial approaches [12, 13]. Our main interest will be to determine how the the transverse structure affects a train of solitons, typically formed after an initially injected pulse breaks up through self-modulation [14].

* Work supported by CNPq, Brasil, and AFOSR Grant FA9550-12-1-0438, USA.
† abonatto@if.ufrgs.br

THE MODEL

We can model this system with the following coupled equations for the laser field a and for the space-charge potential $\varphi \equiv v_g^2 n - a^2/2$,

$$\kappa \frac{\partial^2 a}{\partial \xi^2} = \delta a + \frac{1}{v_g^2}\varphi\, a + \frac{\kappa}{2v_g^2} a^3 - \nabla_\perp^2 a, \qquad (1)$$

$$\frac{\partial^2 \varphi}{\partial \xi^2} + \frac{1}{v_g^2}\varphi = -\frac{1}{2v_g^2} a^2 + \frac{1}{2}\nabla_\perp^2 a^2, \qquad (2)$$

derived in details in our previous work [15]. If the transverse structure is neglected, this set becomes similar to models analyzed in the past [9] and one can think of it as describing the coupled nonlinear dynamics of fields a and φ as a function of the co-moving coordinate ξ, which plays the role of time. With the transverse structure included, it describes the weakly nonlinear, spatio-temporal interaction of laser and space-charge field. Coordinate ξ can still be seen as time, and space is associated with the transverse structure itself. These Eqs. are solved numerically with the following initial conditions

$$a(0, x_\perp) = a_0\, e^{-\lambda x_\perp^2} \;\;,\;\; \partial a/\partial\xi|_{\xi=0} = 0 \qquad (3)$$

$$\varphi(0, x_\perp) = -a(0, x_\perp)^2/2 \;\;,\;\; \partial\varphi/\partial\xi|_{\xi=0} = 0 \qquad (4)$$

EVOLUTION OF THE TRAIN OF PULSES.

Examining Eqs. (1) and (2) together with the initial conditions we find that $(\delta/\kappa)^{-1/2}$ is the time scale for pulse formation along the propagation axis, $(\lambda/\kappa)^{-1/2}$ is the time scale for transverse effects. When $\lambda \ll \delta$, pulses are formed before being affected by transversal effects, and when the inequality reverses, one recognizes the typical instability associated with the transverse term, shown in a recent work to be of the form $a \sim e^{\lambda\xi^2/\kappa}$ [15]. Depending on the relative magnitude of the parameters δ and λ one thus may or may not observe pulses in the system.

In order to see how the electromagnetic pulses evolve as they move into the plasma, we will split the analysis into nonresonant and resonant regimes. Nonresonant regimes are the ones where the adiabatic approximation would remain valid throughout the entire dynamics, if the transverse derivatives were turned off. Resonant regimes, on the other hand, are the ones where adiabaticity is broken and proper plasma waves are excited, even in the absence of the transverse structure.

Copyright © 2013 CC-BY-3.0 and by the respective authors

ISBN 978-3-95450-138-0

ELECTRON AND POSITRON BUNCH SELF-MODULATION EXPERIMENTS AT SLAC-FACET*

P. Muggli†, O. Reimann, Max Planck Institute for Physics, Munich, Germany
N. Lopes, L. Silva, J. Vieira, Instituto Superior Tecnico, Lisbon
E. Adli, S. Gessner, M. Hogan, S. Li, M. Litos, SLAC, Menlo Park, California
C. Joshi, K. Marsh, W. Mori, N. Vafaei-Najafabadi UCLA, Los Angeles, California
Y. Fang, USC, Los Angeles, California

Abstract

We describe some of the measurements that will be performed to study the physics of the self-modulation instability of electron and positron bunches. These measurements will be performed at SLAC-FACET in the E209 experiment. The effect of the SMI on the drive bunch itself (electron or positron) will be studied. Differences between electron and positron bunches are expected since the wakefields are driven into the nonlinear regime.

INTRODUCTION

It was recently proposed to use the self-modulation instability (SMI) of long charged particle bunches in dense plasmas to drive large amplitude (∼1 GV/m) accelerating wakefields [1]. Using the SMI is a method to produce a train of short bunches out of long bunches available today. Long bunches are interesting for driving wakefields and possibly accelerating particles because they can cary large amounts of energy, between 6 and 110 kJ for the p^+ bunches produced by the CERN SPS or LHC with σ_z ≅10-12 cm. Short bunches are desirable because the maximum amplitude of the accelerating field scales as $E_{WB} = \left(2\pi m_e c^2/e\right)/\lambda_{pe}$ and wakefields are most efficiently driven by bunches with $\sigma_z \cong \lambda_{pe}$, therefore $E_{max} \propto 1/\sigma_z$. Since $\lambda_{pe} = 2\pi c/\omega_{pe} = 2\pi c/\left(n_{e0}e^2/\epsilon_0 m_e\right)^{1/2}$, shorter bunches also require larger plasma densities n_{e0}.

We proposed to use the long e^- and e^+ bunches the SLAC linac produced for early plasma wakefield accelerator (PWFA) experiments (σ_z ≅500-700 μm) [2, 3, 4] and the high density plasma available for current experiments n_{e0} ≅10^{16}-10^{17} cm^{-3} [5] to test some of the SMI physics [6].

Theory and simulations predict that as long as the wakefields are in the linear regime, the SMI of positively and negatively charged particle bunches are identical (all other parameters being the same). The wakefields are in the linear regime as long as $E_z \approx (\delta n_e/n_{e0})\, E_{WB} \ll E_{WB}$, i.e., the electron density perturbation δn_e that sustains the wakefields satisfies $\delta n_e \ll n_{e0}$. But the nonlinear wakefield regime with $\delta n_e \sim n_{e0}$ is interesting because the accelerating field can reach the wave breaking field amplitude. In this regime the wakefields become anharmonic and in general more favorable for propagation and acceleration of negatively charged bunches. This is due to the pure ion column (focusing for electrons, defocusing for positrons, for example) occupying most of the phase of the wakefields. This regime is often referred to as the blowout or bubble regime. While the wakefields driven by the (long) unmodulated bunch are in the linear regime ($\delta n_{e0} \cong n_{b0} \ll n_{e0}$, see Table 1), the self-modulation and the ensuing resonant wakefield excitation drives the wakefields into the nonlinear regime. As a result, different quantitative outcomes are expected when changing only the sign of the drive bunch charge.

With the beam and plasma parameters available at SLAC-FACET many of the physics aspects of the SMI, including the asymmetry between negatively and positively charged drive bunches can be studied [6]. We outline here some of the measurements currently planned in experiment tentatively scheduled for this Fall and beyond.

PLANNED MEASUREMENTS

The experiment aims at observing as many of the characteristics of the SMI as possible with the FACET infrastructure. The nominal parameters for the beam and plasma are given in Table 1. However, these parameters will be varied over as large a range as possible depending on the setup that will be available at the time of the experiments.

Table 1: E209 Experiment Parameters

Parameter & Symbol	Value
Bunch population, N_b	<2× 10^{10}
Length, σ_z	500 μm
Radius, σ_r	>30 μm
Density, n_{b0}	<2.8 × 10^{15} cm^{-3}
Energy, W_b	20 GeV
Plasma density, n_{e0}	1-30 × 10^{16} cm^{-3}
Wavelength, λ_{pe}	334-61 μm
Frequency, f_{pe}	0.9-5 THz
Length, L_{plasma}	1 m
Relative bunch density, n_b/n_{e0}	0.1-0.003
Bunch length, $k_{pe}\sigma_z$	3.5-51
Bunch radius, $k_{pe}\sigma_r$	0.6-3
Plasma length, $k_{pe}L_{plasma}$	19,000-103,000

*This work performed [in part] under DOE Contract DE-AC02-7600515
† muggli@mpp.mpg.de

Copyright © 2013 CC-BY-3.0 and by the respective authors

PHOTONIC CRYSTAL AS A PASSIVELY DRIVEN STRUCTURE TO BOOST BEAM ENERGY*

B.R. Poole#, LLNL, Livermore, CA 94550, USA
J.R. Harris, S.V. Milton, Colorado State University, Fort Collins, CO 80523, USA

Abstract

The use of electromagnetic structures to couple energy to a charged particle beam is well known. These structures are usually driven by an external source of electromagnetic energy and the structure distributes that energy in such a way as being favorable to accelerate charged particles. Photonic crystals which typically consist of periodic arrays of metal and/or dielectric structures spaced on a scale comparable to the wavelength of interest, have been investigated for use both as sources of microwave radiation and as particle accelerators. In this case we consider driving a photonic crystal structure using a repetitive sequence of charge bunches driven from a photo-injector to resonantly excite the structure to produce an acceleration field to accelerate a suitably-delayed witness bunch to high energy. We examine the generation of the acceleration field as well as spurious modes. The characteristics of the witness bunch are examined to determine the longitudinal dynamics of the bunch and the energy spectra.

INTRODUCTION

Periodic structures are commonly used in the accelerator community for particle accelerators and as slow wave structures for microwave sources. The use of an L-band RF source to drive an X-band linac structure consisting of a disk loaded waveguide to accelerate properly phased electron bunches has been described [1]. Periodic structures with alternative geometries may be considered for the same task. For example, a structure consisting of a waveguide with a periodic array of metal rings at two radii was demonstrated as a microwave source operating as a backward wave oscillator [2] and such configurations in principle could be used to add energy to the beam rather than extracting energy from it In this paper we consider several structures for use with an L-band source for passive acceleration including the disk loaded waveguide and two ring array geometries The dispersion properties of various structures are determined using the COMSOL MultiPhysics RF package eigenmode solver [3]. The 2-D PIC code OOPIC [4] is then used to examine the excitation of the X-band structure at the 9th harmonic of the 1.3 GHz L-band source. The effect of higher order modes (HOMs) are investigated as well as the dynamics of a witness bunch.

MODELING AND SIMULATIONS

Three X-band structures were considered in this paper. All the structures have the same π-mode resonance at 11.7 GHz, the 9th harmonic of the 1.3 GHz electron source by adjusting various geometric structure parameters. The only fixed parameter was the spatial periodicity d, to maintain the π-mode axial wavenumber $k_z = \pi/d$. The drive beam consisted of 6 MeV, 1.3 GHz Gaussian-like bunches with 100 A peak current, 10 ps FWHM, and 1.23 nC of charge per bunch with a bunch radius of 2 mm. The Fourier spectrum of the drive beam current is a comb of frequencies with 1.3 GHz spacing as shown in Fig. 1. The witness bunch is injected into the structure typically after 50-100 ns (65-130 drive pulses) during the accelerating phase of the fields established by the drive bunch.

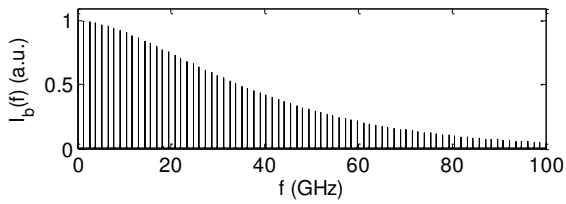


Figure 1: Beam current 1.3 GHz frequency comb.

Disk Loaded Waveguide

The first structure considered is the disk loaded waveguide shown in Fig. 2 with $R_0 = 1$ cm, $a = 0.3$ cm, $w = 0.2$ cm, and $d = 1.2$ cm.

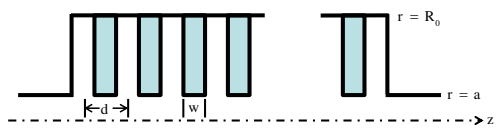


Figure 2: Disk loaded waveguide.

The TM_{0n} dispersion properties are shown in Fig. 3 and Fig.4 shows the axial electric field distribution for the 11.7 GHz π-mode.

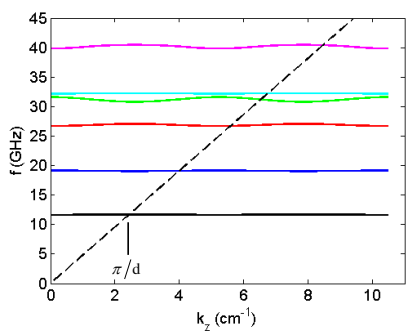


Figure 3: TM_{0n} modes of disk loaded waveguide.

The response of the structure to a single bunch was found using OOPIC to verify the various structure resonances. Figure 5 shows this response with resonances located at

* This work performed under the auspices of the U.S. Department of Energy by Lawrence Livermore National Laboratory under Contract DE-AC52-07NA27344
#poole1@llnl.gov

Copyright © 2013 CC-BY-3.0 and by the respective authors

ISBN 978-3-95450-138-0

LONG TERM EVOLUTION OF PLASMA WAKEFIELDS*

A.A. Sahai†, T.C. Katsouleas,
Electrical Engineering, Duke University, Durham, NC, 27708 USA
Frank S. Tsung, Warren B. Mori
Physics and Astronomy, UCLA, Los Angeles, CA, 90095 USA

Abstract

We study the long-term evolution (LTE) of plasma wakefields over multiple plasma-electron periods and few plasma-ion periods, much less than a recombination time. The evolution and relaxation of such a wakefield-perturbed plasma over these timescales has important implications for the upper limits of repetition-rates in plasma colliders. Intense fields in relativistic lasers (or intense beams) create plasma wakefields (modes around ω_{pe}) by transferring energy to the plasma electrons. Charged-particle beams in the right phase may be accelerated with acceleration/focusing gradients of tens of GeV/m. However, wakefields leave behind a plasma not in equilibrium, with a relaxation time of multiple plasma-electron periods. Ion motion over ion timescales, caused by energy transfer from the driven plasma-electrons to the plasma-ions can create interesting plasma states. Eventually during LTE, the dynamics of plasma de-coheres (multiple modes through instability driven mixing), thermalizing into random motion (second law of thermodynamics), dissipating energy away from the wakefields. Wakefield-drivers interacting with such a relativistically hot-plasma lead to plasma wakefields that differ from the wakefields in a cold-plasma.

INTRODUCTION

Intense laser and particle beams interacting with plasma can force plasma electrons to relativistic energies. Under the appropriate plasma conditions, energy gained by the plasma electrons can be used to create short-lived coherent structures in the plasma. These structures (such as linear electron waves and bubble) have been extensively studied and employed as accelerating and focussing systems for charged-particle beams. The structures created in the plasma have spatio-temporal scales that are defined by the characteristic of the plasma. The spatial scales by the plasma skin-depth, $\frac{c}{\omega_{pe}}$ ($\omega_{pe} = \sqrt{4\pi e^2/m_e}\sqrt{n_e/\gamma_e}$). And the temporal scales by the plasma frequency, $\frac{1}{\omega_{pe}}$. It should be noted that the wakefield theory assumes fixed background ions. In addition to this, the plasma structures are used only over a few plasma electron periods. However, when these plasma structures evolve over time, ion-dynamics which occurs over ion-acoustic wave times $\frac{1}{\omega_{ia}}$ ($\omega_{ia} = \omega_{pe}\sqrt{m_e/M_i}$) becomes significant. For instance, in electron-proton plasma, $\omega_{pe} = 43\ \omega_{ia}$. If plasma density, $n_e = 10^{18}$, $\frac{1}{\omega_{pe}} \simeq 20fs$ and $\frac{1}{\omega_{ia}} \simeq 1ps$. These timescales are important to understand the upper limits of the repetition-rate (and hence luminosity) in a future plasma collider [1]. Also, highly relativistic plasmas are created in astrophysical entities such as Active Galactic Nuclei (AGN such as Centaurus-A (NGC-5128), M-87) and lab-based hot plasmas can better explain phenomenon such as the relativistic jets emanating from AGNs. These particle jets interact with surrounding gravitationally heated hot plasma and can exhibit phenomenon such as self-focussing, hosing and radiation generation.

The plasma wave is *coherent* under the cold-plasma approximation as seen from its dispersion characteristic, $\omega^2 = \omega_{pe}^2 + 3k^2v_{th}^2$ which under, $v_{phase} \gg v_{th}$ is excited over a narrow-band mode centered around ω_{pe}. However, if the plasma is thermally inhomogeneous or the electrons have a large thermal spread the plasma wave mode begins to lose its narrowband characteristic. When a plasma wave evolves in time, plasma spatial inhomogeneities, driver spatial non-uniformity and ion motion introduce a new set of frequencies into the plasma. With non-linearity and instability driven phase mixing between these modes, the plasma wave further de-coheres and equilibriates into random thermal motion. This increase in the entropy of the system follows from the second law of thermodynamics which makes the energy distribution equipartitioned between all possible modes of a system, driving it towards equilibrium.

In a future plasma collider, the need for high luminosity would require each plasma stage to be re-used within a finite interval (depending upon the drive bunch-train design). The fraction of drive-bunch energy coupled into the plasma that is absorbed by the accelerated-bunch has been shown to be $\simeq 50\%$ under optimal non-linear beam-loading which implies significant energy leftover in the accelerating plasma structure. Hence the next drive bunch would be affected by the thermalization of the wake from the previous pulses. In this paper we discuss the long-term evolution of a wake-perturbed plasma in terms of its temperature and density profile. We look at the electron momenta to determine if unabsorbed energy from a previous drive-bunch could heat the plasma to relativistic temperatures ($k_BT_e \simeq 0.5MeV$). We use simulations to estimate the plasma diffusion timescales. Past experimental work have imaged about 10 plasma periods behind the driver [2].

ENERGY IN A PLASMA WAVE

The planar electron plasma wave in 1-D can be denoted as $\vec{E}_{pw}(x) = \hat{x}\ E^0_{pw}\ e^{\mathbf{i}(\omega_{pe}t - k_{pe}x)}$. The force equation of the plasma wave acting on a single plasma electron is $m_e\frac{d\vec{v_e}}{dt} =$

* Work supported by the National Science Foundation under NSF-PHY-0936278 and the US Department of Energy under DE-SC0010012
† aakash.sahai@duke.edu

Copyright © 2013 CC-BY-3.0 and by the respective authors

ANALYSIS OF HIGH REPETITION RATE EFFECTS IN DIELECTRIC WAKEFIELD ACCELERATORS*

Paul Schoessow#, Sergey P. Antipov, Chunguang Jing, Alexei Kanareykin, Stanley Zuo
Euclid Techlabs, 5900 Harper Rd 102, Solon, OH 44139, USA
John Gorham Power, Alexander Zholents, ANL, Argonne, IL 60439, USA

Abstract

Recently the question has arisen of whether dielectric charging might become a significant limiting effect on the performance of the DLAs (dielectric loaded accelerators), leading either to deflection of the beam by the static electric field generated, or to breakdown of the structure. In experiments to date this has not been problematic with appropriate choice of dielectric material. However, given the high repetition rate that would be required, the device would be subjected to essentially a dc bombardment from the beam halo and thus be vulnerable to these effects because there is no time between machine pulses for discharge of the dielectric. We have begun re-examining this problem, emphasizing the expected charging rate and charge distribution in a thin walled dielectric device and the physics of conductivity and discharge phenomena in a dielectric medium. Simulations of the charging process will be presented. We will review early work on beam-induced charging of dielectric structures and also results from deep charging of satellite components by cosmic rays. Ageing and induced conductivity under large radiation doses are also to be investigated.

IRRADIATION EFFECTS ON DLAS

The physical processes involved with the unwanted interception of beam electrons by a dielectric accelerating structure are complex and interacting:

- Asymmetric charging of the dielectric, leading to beam deflection;
- Breakdown (with structure damage). Although breakdown thresholds ~14 GV/m have been demonstrated for very short (<330 fs) pulses [1], maximum DC fields that can be supported are considerably lower;
- Changes in material properties with absorbed dose and repeated DC breakdowns;
- Dynamics of the charging/discharge process in the presence of high dose rates. Table 1 lists the characteristic discharge times for a number of dielectric materials used in DLAs, nearly all of which do not reflect the observed resistance to charging. This seems to suggest that other effects are compensating, for example ionization induced conductivity.

Charging effects were studied by the Argonne group as an incidental part of the first dielectric wakefield acceleration tests in 1988 [2]. In these experiments the charging originated from missteering of the drive beam through the dielectric structure. Transverse deflection of the beam through large angles by the induced DC field was sufficiently large as to deflect the beam outside the acceptance of the spectrometer focal plane detector. The initial tests used dielectric tubes made from plastics. Rexolite and Nylon dielectrics showed rather different behaviors under charging.

Table 1: Characteristic discharge times $\tau_c=\varepsilon/\sigma$ for commonly used dielectrics [6]. Here σ is the dc conductivity and ε is the (SI) permittivity.

Material	τ_c
Alumina	>0.78 s
Delrin ®	310 s
Kapton ®	3.5 d
Mylar ®	3.1 d
Polystyrene	37 min
Fused Quartz	>38 d
Borosilicate glass	0.41 s (variable) [7]
Teflon ®	2.1 d

Rexolite was found to charge until the beam was deflected and to hold its charge (and maintain the dc electrostatic field) for an extended time (~ 1 hr). No breakdowns were seen under the test conditions. Nylon would charge up and deflect the beam until breakdown occurred, snapping the beam back to its nominal undeflected position. The charge-discharge period was found to be ~ 30 s. It is worth noting that no permanent damage to the nylon structure was observed (based on repeated longitudinal wakefield measurements) despite being subjected to many charge-discharge cycles.

The rexolite structure was field-modified by depositing a thin layer of graphite powder on the interior surface of the tube. A thin conducting layer can short out the static field but be thin enough (<< 1 skin depth) to allow the rf fields of the structure to penetrate into the vacuum channel as before. It was determined that the graphite layer did in fact have the desired effect, although some trial and error was necessary to obtain a sufficiently thin layer. While use of graphite in this fashion is impractical for high energy acceleration, the principle of using an interior conductive coating was demonstrated. Ultimately the best approach was found to be tuning the beam through an electrically isolated aluminum tube in place of the dielectric, minimizing the intercepted beam current, and then swapping in the dielectric under test for the aluminum tube.

*Work supported by US Dept of Energy, SBIR Program
#paul.schoessow@euclidtechlabs.com

Copyright © 2013 CC-BY-3.0 and by the respective authors

ISBN 978-3-95450-138-0

ASTA AT FERMILAB: ACCELERATOR PHYSICS AND ACCELERATOR EDUCATION PROGRAMS AT THE MODERN ACCELERATOR R&D USERS FACILITY FOR HEP AND ACCELERATOR APPLICATIONS*

V. Shiltsev#, P. Piot, Fermilab, Batavia, IL 60510, USA

Abstract

We present the current and planned beam physics research program and accelerator education program at Advanced Superconducting Test Accelerator (ASTA) at Fermilab.

ASTA FACILITY

The Advanced Superconducting Test Accelerator (ASTA) at Fermilab will enable a broad range of beam-based experiments to study fundamental limitations to beam intensity and to develop transformative approaches to particle-beam generation, acceleration and manipulation. ASTA incorporates a superconducting radiofrequency (SRF) linac coupled to a photoinjector and small-circumference storage ring capable of storing electrons or protons. ASTA will establish a unique resource for R&D towards Energy Frontier facilities and a test-bed for SRF accelerators and high-brightness beam applications. The unique features of ASTA include: (1) a high repetition-rate, (2) one of the highest peak and average brightness within the U.S., (3) a GeV-scale beam energy, (4) an extremely stable beam, (5) the availability of SRF and high-quality beams together, and (6) a storage ring capable of supporting a broad range of ring-based advanced beam dynamics experiments. These unique features will foster a broad program in advanced accelerator R&D and accelerator education which cannot be carried out elsewhere. Several experiments and test can be carried out at ASTA simultaneously at three experimental areas – see Fig.1. Detail description of ASTA can be found elsewhere [1,2]

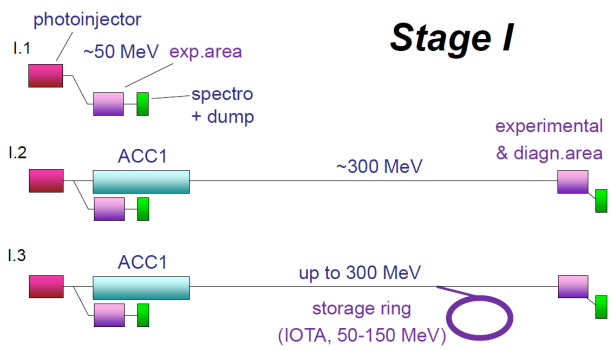


Figure 1: Schematics of ASTA (Stage I configuration).

*Fermi Research Alliance, LLC operates Fermilab under contract No. DE-AC02-07CH11359 with the U.S. Department of Energy
#shiltsev@fnal.gov

ASTA ACCELERATOR R&D THRUSTS

Accelerator R&D for Particle Physics at the Intensity and Energy Frontiers

The combination of a state-of-the-art superconducting linear accelerator and a flexible storage ring enables a broad research program directed at the particle physics accelerators of the future. The corresponding research program includes a number of proposals:

i) Test of non-linear, integrable, accelerator lattices (the Integrable Optics Test Accelerator) which have the potential to shift the paradigm of future circular accelerator design
ii) Test of space charge compensation in high intensity circular accelerators
iii) Advanced phase space manipulations
iv) Test of optical stochastic cooling
v) Flat-beam-driven dielectric-wakefield acceleration in slab structures
vi) Investigation of acceleration and cooling of carbon-based crystal structures for muon accelerators
vii) Measurement of the electron wave function size in a storage ring
viii) Studies of beam echo phenomena in a storage ring
ix) Development of a quadrupole pickup and study of the quadrupole mode dynamics in space-charge dominated beams
x) High power targetry studies for LBNE
xi) A tagged photon beam at ASTA for Detector R&D
xii) HEP applications of inverse Compton scattered photons.

It was specifically noted at the 2013 Community Summer Study ("Snowmass-2013" [2]) that there is obvious lack of accelerator test facilities where many burning accelerator science and technology issues of the Intensity Frontier (IF) accelerators [4] can be addressed. ASTA will provide this so-much needed platform for the IF accelerator R&D.

Accelerator R&D for Future SC RF Accelerators

High gradient, high power SC RF systems are critical for many accelerator facilities under planning for the needs of high-energy physics, basic energy sciences and other applications. ASTA offers a unique opportunity to explore the most critical issues related to SC RF technology and beam dynamics in SC RF cryomodules, such as:

Copyright © 2013 CC-BY-3.0 and by the respective authors

ISSUES AND R&D REQUIRED FOR THE INTENSITY FRONTIER ACCELERATORS*

V.Shiltsev#, S.Henderson, P.Hurh, I.Kourbanis, V.Lebedev, Fermilab, Batavia, IL 60510, USA

Abstract

Operation, upgrade and development of accelerators for Intensity Frontier face formidable challenges in order to satisfy both the near-term and long-term Particle Physics program. Here we discuss key issues and R&D required for the Intensity Frontier accelerators.

INTENSITY FRONTIER ACCELERATORS

The near-term program of HEP research at the Intensity Frontier continuing throughout this decade includes the long-baseline neutrino experiments and a muon program focused on precision/rare processes. It requires: a) double the beam power capability of the Booster; b) double the beam power capability of the Main Injector; and c) build-out the muon campus infrastructure and capability based on the 8 GeV proton source. The long-term needs of the Intensity Frontier community are expected to be based on the following experiments: a) long-baseline neutrino experiments to unravel neutrino sector, CP-violation, etc.; and b) rare and precision measurements of muons, kaons, neutrons to probe mass-scales beyond LHC.

Both types of experiments will require MW-class beams. The Project-X construction is expected to address these challenges [1]. The Project X represents a modern, flexible, Multi-MW proton accelerator (see Fig.1).

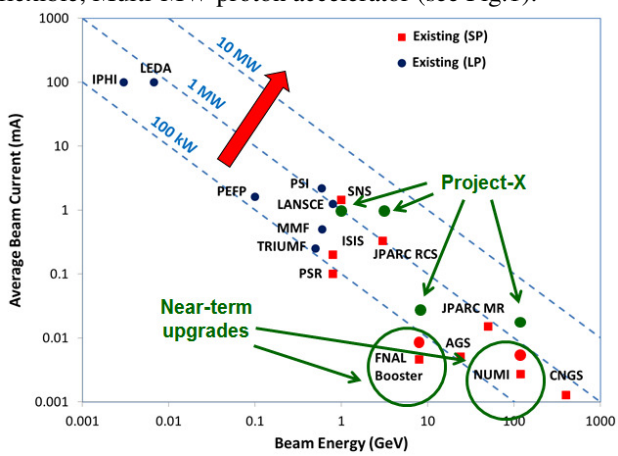


Figure 1: Accelerator beam power landscape.

High power hadron accelerators for the Intensity Frontier have two over-riding design constraints [2]:
Minimizing beam loss (typical beam loss requirements for a MW proton beam: < 1 Watt/m, or/and < 1×10^{-4} total beam loss), and
Proper beam structure (the required formats significantly vary from experiment to experiment – from a quasi-CW for rare particle decays to a single ~2-ns long bunch for MC/NF). The key challenges to satisfy these constrains include:

- Producing high current, high-quality and high brightness beams with required bunch structure;
- Accelerating high beam currents to high energy with (1) high-duty factors required for high resolution experiments and (2) very low duty factors for neutrino experiments;
- Running multiple experiments in parallel (quasi-simultaneously) required means for beam manipulations on the bunch-by-bunch base – see Fig.2;
- Transporting high power beams while maintaining beam loss at a level where routine maintenance is possible – see Fig.3;
- Acceleration of beams from keVs to GeVs preserving emittance and minimizing amplitude growth for large-amplitude particles ("beam halo");
- Low-loss extraction of the beams;
- Target systems capable of handling extreme power densities and extreme radiation environments – see Fig.4;
- A related challenge is producing intense, high-quality beams of secondary particles (muons, kaons, …).

ACCELERATOR R&D NEEDED

Below we outline the directions of the accelerator R&D needed to address the above challenges (we omit specific Project X R&D needs which are addressed elsewhere [3], and focus mostly on other important needs, especially, for the Fermilab's future intensity frontier program, which have not been articulated yet):

High Intensity beam sources: Radio-frequency quadrupoles (RFQs) are the injector technology of choice at present; the state of the art performance of 100 mA CW demonstrated at LANL/LEDA with 6.7 MeV output energy; is there an alternative technology which could compete with conventional technology?);

Beam dynamics issues with high intensity beams in existing accelerators (e-cloud, impedances/instabilities): RF systems (how to provide RF power for beam acceleration with many-fold higher beam current when the beam induced voltage greatly exceeds RF voltage?);

Space Charge issues (need to understand the Space Charge losses with the higher intensity slipped stacked bunches in MI and Recycler; the need collimators in

*Fermi Research Alliance, LLC operates Fermilab under contract No. DE-AC02-07CH11359 with the U.S. Department of Energy
#shiltsev@fnal.gov

Copyright © 2013 CC-BY-3.0 and by the respective authors

ISBN 978-3-95450-138-0

RF-COMPONENTS EMBEDDED WITH PHOTONIC-BAND-GAP (PBG) AND FISHNET-METAMATERIAL STRUCTURES FOR HIGH FREQUENCY ACCELERATOR APPLICATION

[1]Sara Robak, [1]Daniel Boyden, and [1, 2]Young-Min Shin
[1]Department of Physics, Northern Illinois University, Dekalb, IL, 60115, USA
[2]Fermi National Accelerator Laboratory (FNAL), Batavia, IL 60510, USA

Abstract

In the development of high efficiency and high gradient RF-accelerators, RF waveguides and cavities have been designed with Photonic Band Gap (PBG) and fishnet-metamaterial structures. The designed structures are comprised of a periodically corrugated channel sandwiched between two photonic crystal slabs with alternating high to low dielectric constants and a multi-cell cavity-resonator designed with fishnet-metamaterial apertures. The structural designs of our interest are intended to only allow an operating-mode or -band within a narrow frequency range to propagate. The simulation analysis shows that trapped non-PBG modes are effectively suppressed down to ~ -14.3 dB/cm, while PBG modes propagated with ~2 dB of insertion loss, corresponding to ~1.14 dB/cm attenuation. The pre-liminary modeling analysis on the fishnet-embedded cavity shows noticeable improvement of Q-factor and field gradient of the operating mode (TM_{010}) compared to those of typical pillbox- or PBG-cavities. Fabrication of the Ka-band PBG-waveguide and S-band fishnet cavity structures is currently underway and they will be tested with a microwave test bench/8510C Network Analyzer and 5.5 MW S-band klystron. These structures can be applied to stable short-bunch formation and mono chromatic radiation in high frequency accelerators.

INTRODUCTION

Periodic conducting structures have been utilized as active slow wave media interacting with high energy electron beams in a wide range of applications from high gradient linear accelerators to coherent power radiation sources. The distorted dispersion relation of metallic lattices constitutes effective plasmonic modes with negative permittivity (epsilon-negative materials, $\varepsilon < 0$) [1 – 4]. The non-radiative waves have been widely used in microwave regimes as they can be readily guided in passive components or strongly excited by energy-momentum-coupling with kinetic electrons as an active medium [5]. The confined evanescent waves induce electron bunches when the current density exceeds thermo-dynamic divergence ($\propto f^{-2}$) [6]. This gives rise to a strong coherent electron-photon interaction that is commonly used for high intensity photon generation or high gradient RF acceleration. The spectral regime of the electronic RF devices has rapidly increased from microwave to near terahertz (near-THz) wave regime (0.1–1 THz) as device size can be significantly reduced proportional to the wavelength.

Energy conversion efficiency on the photon- emission or -absorption process is thus noticeably reduced as the optical cycle is decreased [7, 8] Recent trends in the development of THz electron beam devices have gradually transitioned to elliptical sheet beams from round ones as enlarging the beam width either increases radiation intensity or reduces beam current loading. Among various planar slow wave structures (SWSs) recently micro-channels with an asymmetrically aligned double grating array [9] were intensively studied for frequency-tunable coherent radiation source application as they have large instantaneous bandwidth of plasmonic modes that are strongly confined in the beam channel with small ohmic losses. However, this broad band characteristic can lead to unstable oscillation of abnormal modes, which possibly destabilize beam-wave interactions, and perturb normal electronic energy conversion. In particular, the structure becomes heavily overmoded (TE → TEM) as its aspect ratio between x-y transverse dimensions is increased to expand the beam-wave interactive area. It is thus certain that there is a limitation in increasing the aspect ratio of the sheet beam structure due to low-energy mode excitation. A substantial solution to the issue could be obtained from bandgap structures. This paper will present the band-selective planar waveguide combined with the photonic crystal slabs and fishnet-type metamaterial slab. The composite structure permits only non-radiative photonic-band-gap (PBG) modes [2–4] to propagate through the sub-wavelength micro-channel. Comparative numerical analysis and test results on the spectral response and field distribution will be discussed in detail.

PHOTONIC BAND GAP WAVEGUIDE

In principle, the lowest frequency (cutoff) of a rectangular TE-mode waveguide is determined by waveguide width, so TE modes become closer to TEM modes as the cutoff decreases. Figure 1 shows the 0^{th} order dispersion curves (m = 0) of TE- and TEM-waveguides. Normalized structural dimensions of the designed models are specified with $a_0/d_0 = 0.75$, $L_0/d_0 = 0.6$, $b_0/d_0 = 0.33$, and $h_0/d_0 = 1.674$, where d_0 is the grating period of a unit cell. The surface wall conductivity is defined with oxygen-free high-conductivity (OFHC) copper ($\sigma = 5.8 \times 10^8$ [$\Omega^{-1}m^{-1}$]). With an increase in the guide width, the entire eigenfrequencies of the fundamental band (grey solid → grey dashed) are lowered as the other dimensions remain consistent with the ones of the TE mode waveguide. In the 2^{nd} TEM waveguide (grey

Copyright © 2013 CC-BY-3.0 and by the respective authors

ISBN 978-3-95450-138-0

FEASIBILITY STUDY OF CHANNELING ACCELERATION EXPERIMENT AT THE FERMILAB ASTA FACILITY

[1, 3]Young-Min Shin, [2]Tao Xu, [3]Dean A. Still, and [3]Vladimir Shiltsev
[1]Department of Physics, Northern Illinois University, Dekalb, IL, 60115, USA
[2]Department of Chemistry, Northern Illinois University, Dekalb, IL, 60115, USA
[3]Fermi National Accelerator Laboratory (FNAL), Batavia, IL 60510, USA

Abstract

Crystal channeling technology has offered various opportunities in accelerator community with a viability of ultrahigh gradient (TV/m) acceleration for future HEP collider in Energy Frontier. The major challenge of the channeling acceleration is that ultimate acceleration gradients might require high power driver at hard x-ray regime (~ 40 keV), exceeding those conceivable for x-rays as of today, though x-ray lasers can efficiently excite solid plasma and accelerate particles inside a crystal channel. Moreover, only disposable crystal accelerators are possible at such high externally excited fields which would exceed the ionization thresholds destroying the atomic structure, so acceleration will take place only in a short time before full dissociation of the lattice. Carbon-based nanostructures have great potential with a wide range of flexibility and superior physical strength, which can be applied to channeling acceleration. This paper present beam-driven channeling acceleration concept with CNTs and discuss feasible experiments with the Advanced Superconducting Test Area (ASTA) in Fermilab and beyond.

INTRODUCTION

The cost models of the modern colliders are quite complicated, but one may safely assume that a future facility should not exceed a few tens of km in length and simultaneously require less than 10 to a few tens of MW of beam. To get to the energies of interest within the given footprint, fast particle acceleration is inevitable. Plasma-wakefield acceleration (PWA) has become of great interest because of the promise to offer extremely large acceleration gradients, on the order of E0 ≈ n01/2 [GeV/m], where n0 is the ambient electron number density (n0 [1018cm-3]), on the order of 30-100 GV/m at plasma densities of n0 = 1017 – 1018 cm-3.[1] The density of charge carriers (conduction electrons) in solids n0 = ~ 1020 – 1023 cm-3 is significantly higher than what was considered above in plasma, and correspondingly, wakefields of up to 100 GeV/cm or 10 TV/m are possible. In the solid plasma, as escaping from a driving field due to fast pitch-angle diffusion resulting from increased scattering rates, particles must be accelerated along major crystallographic directions. This is called “channeling acceleration”. Normally, crystal channeling has been applied to high energy beam control such as collimation, bending, and refraction [2]. For high energy beam optics, carbon nanotubes (CNTs) have been considered for bending and collimation [3, 4] on account of the much wider range of flexibility, including superior physical strength, which also ideally fits with channeling acceleration. CNTs, composed of graphene sheets rolled into seamless hollow cylinders with diameters ranging from 1nm to about sub-micron, exhibit unique physical and chemical properties as a quasi-one dimensional material [5]. In principle, both straight and bent CNTs can effectively be used for high-energy particle channeling [6], provided the technological challenge of achieving an almost perfect alignment of CNTs with respect to the beam direction could be tackled effectively in the synthesis of samples.

Recently, Fermilab built the Advanced Superconducting Test Accelerator (ASTA) facility (50 MeV and several hundreds of MeV energy beams) that will enable a broad range of electron beam-based experiments to study fundamental limitations to beam intensity and to developing transformative approaches to particle-beam generation, acceleration and manipulation, which is ideally suited for the channeling acceleration experiment. We plan to detect a measurable energy gain from the electron bunches passing through CNTs. Successful demonstration of the experiment with this beam driven method will verify the viability of CNT channeling interaction for ultra-high gradient acceleration, which will also prove the feasibility of the laser-driven channeling acceleration. The experimental setup will be accommodated to a 50 MeV main stream beamline and high energy (50 – 300 MeV) beamline in our plan. In the research, beam energies and radiation spectra of CNT samples will be mainly characterized by beam tests at relativistic regimes.

CHANNELING ACCELERATION

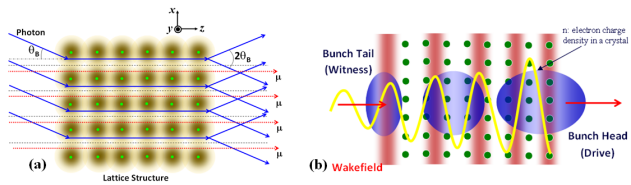


Figure 1: (a) Laser (x-ray) driven acceleration (muon, proton) (b) beam-driven acceleration (electron).

Wakefields in crystals can be excited by two sorts of driving sources: x-ray laser (Fig. 1(a)) or short electron bunch (Fig. 1(b)). With the x-ray pumping method [7], a crystal channel can hold > 1013 V/cm transverse and 109 V/cm longitudinal fields of diffracted traveling EM-waves at the Bragg diffraction condition ($\lambda/2b = \sin\theta B$), where b is the lattice constant and θB is the diffraction angle) However, to hold the ultimate gradients, the acceleration requires coherent hard x-rays ($\hbar\omega \approx 40$ keV) of ≥ 3 GW to compensate for radiation losses, which

Copyright © 2013 CC-BY-3.0 and by the respective authors

ISBN 978-3-95450-138-0

COMMISSIONING AND INITIAL EXPERIMENTS ON NDCX-II*

S. M. Lidia#, T. Schenkel##, W. G. Greenway, K. Murphy, T. Schenkel, C. D. Weis,
W. L. Waldron, Lawrence Berkeley National Laboratory, Berkeley, CA 94720, U.S.A.

Abstract

The Neutralized Drift Compression Experiment (NDCX-II) is a new induction accelerator facility designed to facilitate user experiments in high energy density laboratory physics, intense beam physics, and materials processing and testing with intense, pulsed ion beams. The facility has completed the initial commissioning phase of its injector, 27-cell solenoid transport lattice, induction accelerator modules and non-neutral pulse compression section. Space-charge-dominated Li^+ beams carrying 20-50 nC have been generated from the 133 kV pulsed, ~1.0 microsecond (FWHM), 65-mA injector, and compressed to 20-30 ns with 0.75-1.3 A peak currents and amplification factors of 10-20. We report results of non-neutral beam compression and transport studies to generate variable ion beam fluences on to solid targets. We also report on studies of dose rate effects in pulsed ion implantation and on the recombination dynamics of radiation-induced defects in semiconductors using the NDCX-II Li^+ beam.

INTRODUCTION

The NDCX-II facility [1, 2] was constructed between July 2009 and December 2012. Commissioning results of the source and injector systems has already been reported [3]. The induction accelerator modules with pulsed, 2-3 T solenoid magnet transport were added in several stages (5-cell, 11-cell, 27-cell) to facilitate the integration of diagnostic and controls systems [4].The 27-cell beamline configuration is shown in Fig. 1, with schematic representation indicating the position of the active induction cell modules, diagnostic cells, injector and end station. Each cell is instrumented with a pulse solenoid for transport.

The original complement of beam diagnostics for commissioning included a movable end station complemented with a Faraday cup, slit and slit-cup pairs, and scintillator viewable through downstream flange window. A pepper-pot mask and dedicated scintillator were added later, with the removal of the slit/slit-cup pairs. Other non-interceptive beam diagnostics included 6 capacitive plate beam position monitors at the diagnostic cell locations, solenoid current transformers, and accelerator cell voltage resistive monitors. This level of beam instrumentation was sufficient for initial beam transmission studies and beam quality measurements.

* This work is supported by the Director, Office of Science, Office of Fusion Energy Sciences, of the U.S. Department of Energy under Contract No. DE-AC02-05CH11231.

#smlidia@lbl.gov, ##T_Schenkel@LBL.gov

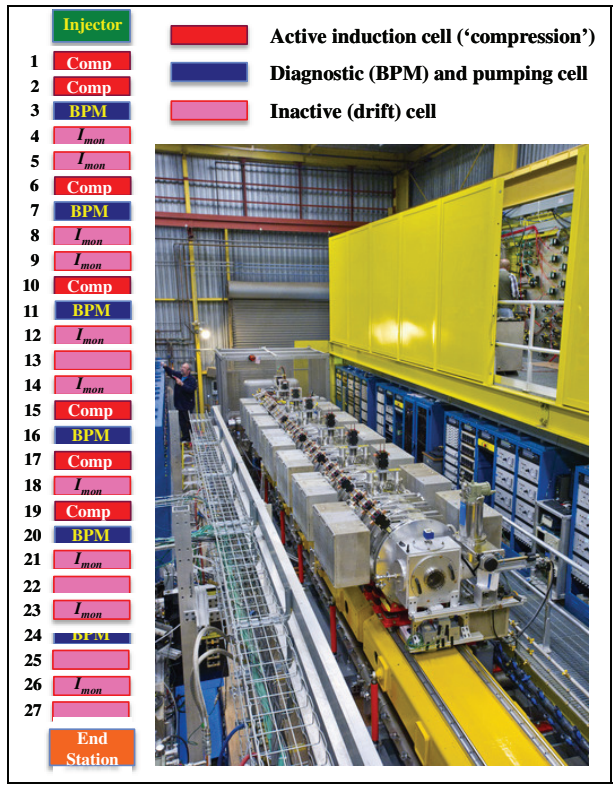


Figure 1: NDCX-II beamline and schematic.

ENHANCED DIAGNOSTICS AND COMMISSIONING STRATEGY

The modular beamline is built up from 21 identical induction cells and 6 diagnostic cells. For these commissioning exercises, only 7 of the induction cells are active, with the remaining inactive cells providing drift length for longitudinal compression. We utilized an additional 10 inactive cells as reciprocal inductive current monitors. The drive matching circuits for these cells were modified to provide a ~5Ω termination, and measured *L/R* response times were in the range of 1.6 – 2.2 µs.

These additional current diagnostics increased the spatial resolution of time-of-flight measurements along the beamline, and permitted determination of velocity and beam energy to within accepted error margins. Furthermore, interpolation of the beam arrival time and beam pulse duration to the active induction cell positions permits fine tuning of the accelerating voltage waveform amplitude and delay, enabling optimization of the bunch compression process and tailoring of the magnetic solenoid lattice.

Copyright © 2013 CC-BY-3.0 and by the respective authors

BETATRON X-RAYS FROM A LASER WAKEFIELD ACCELERATOR IN THE IONIZATION INDUCED TRAPPING REGIME *

F. Albert, B.B. Pollock, Y.-H. Chen, D. Alessi, J.E. Ralph, P.A. Michel, A. Pak,
LLNL, Livermore, CA 94550, USA
J. Shaw, K.A. Marsh, C.E. Clayton, C. Joshi, UCLA, CA 90095, USA
S.H. Glenzer, SLAC, Stanford, CA 94309, USA

Abstract

Betatron x-rays with multi-keV photon energies have been observed from a GeV-class laser-plasma accelerator. The experiment was performed using the 200 TW Callisto laser system at LLNL to produce and simultaneously observe GeV-class electron beams and keV Betatron x-rays. The laser was focused into various gas cells with sizes ranging from 3 to 10 mm, and containing mixed gases (He, N, CO2, Ar, Ne) to accelerate large amounts of charge in the ionization induced trapping regime. KeV betatron x-rays were observed for various concentrations of gases. Electron spectra were measured on large image plates with the two-screen method after being deflected by a large 0.42 Tesla magnet spectrometer.

INTRODUCTION

Laser Wakefield Acceleration (LWFA)[1] is one of the most notable applications of petawatt-class laser systems. Since the discovery that this mechanism can accelerate monoenergetic electron beams up to energies comparable to those obtained with conventional rf accelerators[2, 3, 4] but in a table-top setup, novel applications of these electron beams have been constantly increasing. Concurrently, x-ray sources such as synchrotrons, or more recently free-electrons lasers such as the Linac Coherent Light Source (LCLS)[5] continue to explore new properties of atoms, molecules, condensed matter, warm dense matter or plasmas. In this context, LWFA beams are very attractive to seed the next generation of light sources. Such beams can either be wiggled by an external periodic magnetic structure[6] or directly by the plasma in the wake of the laser pulse[7, 8] to produce keV x-rays. The latter example, the betatron x-ray source, first observed in a beam-driven plasma channel[9] is the subject of this work, and its mechanism can be described as follows: an ultrashort (femtosecond), ultraintense ($I > 10^{18}$ W/cm^2) laser pulse is focused under vacuum on the edge of a gas target. The gas is fully ionized to form a plasma. The laser ponderomotive force (proportional to the gradient of light intensity) plows the electrons of the plasma away from the strong light intensity regions. Because of the very short duration of the laser pulse, the heavier ions stay immobile and a bubble free of electrons is formed in the wake of the pulse. At the back of this bubble, some electrons are trapped, accelerated and wiggled by the electrical fields present in the plasma: these electrons emit the betatron x-rays. This source produces broadband, synchrotron-like radiation in the keV energy range[10, 11], within a source size of a few microns[12, 13], a divergence of less than 100 mrad[14], and a pulse duration of less than 100 fs[15]. Since betatron x-rays are directly related to the electrons emitting them, the source is also widely used as an electron beam diagnostic. The electron beam emittance and size can be deduced from the x-ray beam profile[14], spectrum[16] or source size[17], using various x-ray spectroscopy and imaging techniques. Traditionally, betatron x-rays are produced in the blowout regime of laser wakefield acceleration[18] using pure helium gas, where electrons are self-injected into the wake. This paper investigates the properties of betatron x-ray radiation produced in mixed gases.

BETATRON RADIATION MODELING

The motion of an electron accelerated along $\vec{u_z}$ with momentum $\vec{p}$ and position $\vec{r}$ in the wake of a laser pulse can be described by the Lorentz equation of motion:

$$\frac{d\vec{p}}{dt} = -m\omega_p^2 \frac{\vec{r}}{2} + \alpha \frac{mc\omega_p}{e}\vec{u_z}, \qquad (1)$$

where m is the electron rest mass, e the elementary charge, and $\omega_p = \sqrt{n_e e^2/m\epsilon_0}$ is the plasma frequency. Here, n_e is the electron density, and ϵ_0 the vacuum permittivity. In the blowout 3D nonlinear regime of laser wakefield acceleration [18], $\alpha = \frac{1}{2}\sqrt{a_0}$ is the normalized accelerating field, where a_0 is the laser normalized vector potential, typically around 2 for our experiments. Equation 1 can be solved by using a 4th order Runge-Kutta algorithm to obtain the single electron trajectories for given initial conditions and fields. The electron trajectory is used to calculate the intensity radiated by the particle per unit frequency ω and solid angle Ω [19]:

$$\frac{d^2I}{d\Omega d\omega} = \frac{e^2\omega^2}{4\pi c}\left|\int_{-\infty}^{\infty} \vec{n}\times(\vec{n}\times\beta)\, e^{i\omega(t-\frac{\vec{n}.\vec{r}}{c})}dt\right|^2, \qquad (2)$$

where $\vec{n}$ is the vector corresponding to the direction of observation, and $\beta = v/c$ the normalized electron velocity. The betatron x-ray beam profile is calculated by integrating Equation 2 over frequencies. Figure 1 shows an example of electron trajectory, with its corresponding betatron x-ray spectrum and beam profile. For this particular case, the parameters are $n_e = 10^{19}$ cm^{-3}, $\gamma = 200$, x_0=1 μm, $y_0 = 0$,

* This work was performed under the auspices of the U.S. Department of Energy under contract DE-AC52-07NA27344, and supported by the Laboratory Directed Research and Development (LDRD) Program under tracking code 13-LW-076.

ISBN 978-3-95450-138-0

Copyright © 2013 CC-BY-3.0 and by the respective authors

PARTICLE-IN-CELL MODELING OF DIELECTRIC WAKEFIELD ACCELERATOR*

C.-K. Huang#, T. J. T. Kwan, D. Yu. Shchegolkov, and E. I. Simakov, Los Alamos National Laboratory, Los Alamos, NM 87545, USA

Abstract

We explore the potential of Dielectric Wakefield Accelerator (DWA) to achieve compact high gradient acceleration of high brightness beams required by an X-ray Free Electron Laser (FEL). Particle-In-Cell (PIC) simulations of a LANL DWA experimental design utilizing a double triangle beam current profile indicate accelerating field >100 MV/m and large transformer ratio are accessible while the longitudinal wakefield phase is insensitive to beam parameters and radial offset for fixed longitudinal profile. End-to-end simulation is developed, which allows us to validate and optimize future DWA experimental design.

INTRODUCTION

The pre-conceptual design for Matter-Radiation Interactions in Extremes (MaRIE) future signature facility at LANL calls for a 12 GeV electron linear accelerator for hard X-ray FEL production. MaRIE demands a high quality electron beam with the electron bunch charges of 0.1 to 1 nC, normalized RMS emittances of 0.1 to 1 mm, and RMS energy spreads of less than 0.1%. A major deficiency of the conventional accelerator technology is the accelerating gradient that is limited to a few tens of MV/m, which put a severe restraint on the cost and future upgrade of such facility.

The wakefield which causes the dominant energy spread in beams in conventional linacs can be used in carefully designed electromagnetic structures, specifically, dielectric loaded waveguides in this study, to generate extraordinary gradients and potentially small energy spreads for electron beam acceleration. In this paper we present simulation study to assess the characteristics of DWA and its potential applications in advance of experimental validation.

THEORY ON WAKEFIELD IN DWA

Figure 1 shows the schematic of the dielectric-lined metallic waveguide. Here we confine our study to a waveguide with cylindrical symmetric geometry. The theory of wakefield generation in a cylindrical dielectric waveguide is generally formulated in frequency domain and dated back at least to 1951 in Ref. [1], where Bessel's equation for the fields is solved with boundary matching conditions at the dielectric-vacuum interface. In general, the dielectric-lined waveguide supports infinite number of discrete Hybrid EM modes. The supported EM modes have low frequency cut-off determined by the geometric

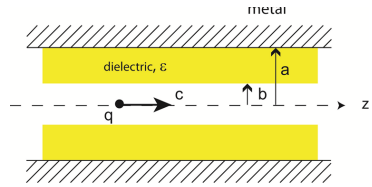


Figure 1: A schematic of the DWA consisting of a dielectric-lined metallic waveguide and an electron beam as the excitation source.

parameters of the waveguide and the dielectric constant ε of the liner materials.

However, for axial symmetric excitation (azimuthal mode number m=0), the TE and the TM modes are decoupled. For co-linear particle acceleration, the TM_{0n} modes are most useful for particle acceleration via the strong longitudinal electric field. While TE modes are detrimental to acceleration but can be used for beam deflection.

In Ref. [1], the dispersion of the TE, the TM and the HEM eigen modes are derived. Similar efforts are found in Ref. [2-4] for resonant modes driven by a moving particle. Here we adopt the notation used in Ref. [3] and summarize the key results relevant to our interests below:

(1) The conditional equation (dispersion relation) for modes with phase velocity $v_{ph} = \beta = v/c$,

$$C(s) = \frac{m^2 s k^2}{a^2}\beta^2\left(\frac{\varepsilon-1}{1-\beta^2}\right)^2 - s^3\left(\frac{kS_m'(sa)}{S_m(sa)} + \frac{sI_m'(ka)}{I_m(ka)}\right)\left(\frac{sI_m'(ka)}{I_m(ka)} + \frac{\varepsilon k R_m'(sa)}{R_m(sa)}\right) = 0 \quad (1)$$

where $k^2 = \omega^2(1-\beta^2)/v^2$, $s^2 = \omega^2(\varepsilon\beta^2-1)/v^2$, $k_0 = \omega/c$, and R_m, R'_m, S_m, S'_m are combinations of mth–order Bessel functions of the first and second kinds as defined in Eq. (35-38) in Ref. [3].

(2) The TM_{mn} longitudinal electric field for a single particle (Green's function),

$$E_{z,mn}(r,\theta,z-vt) = -8e\cos(m\theta)\cos\left(\frac{\omega}{v}(z-vt)\right) \times I_m(kr)I_m(kr_0)\times\frac{K_m(ka)}{I_m(ka)}\frac{T(s)}{sdC(s)/ds}\bigg|_{s=s_n} \quad (2)$$

where

$$T(s) = -\frac{m^2k^4\beta^2}{a^2}\left(\frac{\varepsilon-1}{1-\beta^2}\right)^2 - s^2k^2\left(\frac{kS_m'(sa)}{S_m(sa)} + \frac{sI_m'(ka)}{I_m(ka)}\right) \times\left(\frac{sK_m'(ka)}{K_m(ka)} + \frac{\varepsilon k R_m'(sa)}{R_m(sa)}\right)$$

and s_n is the solution of Eq. (1).

To obtain the wakefield generated by a beam, one can convolve (sum) the single particle field from Eq. (2) with the beam profile. For smooth beams, this can be done

*Work supported by the LDRD program at LANL.
#huangck@lanl.gov

Copyright © 2013 CC-BY-3.0 and by the respective authors

BEAM PULSE SHAPING EXPERIMENTS FOR UNIFORM HIGH GRADIENT DIELECTRIC WAKEFIELD ACCELERATION*

D. Shchegolkov#, E.I. Simakov, Los Alamos National Laboratory, Los Alamos, NM 87545, USA
S. Antipov, Euclid TechLabs, Solon, OH 44139, USA
M. Fedurin, C. Swinson, Brookhaven National Laboratory, Upton, NY 11973, USA

Abstract

Dielectric wakefield accelerators (DWA) can produce high accelerating gradients and could possibly be used as afterburners for the accelerators of future free electron lasers (FELs) such as X-ray FEL of the proposed Matter-Radiation Interactions in Extremes (MaRIE) experimental facility at LANL [1]. With a double triangular drive bunch DWAs can produce a high transformer ratio. Also, by slightly customizing the time profile of the accelerated bunch it is possible to achieve high gradient uniformity along the accelerated bunch resulting in a low induced energy spread [2]. We plan to test a DWA which would incorporate all those benefits. The only way to produce the desired current profile of the main and drive bunches is to use current shaping with a beam mask. A variation of this technique is currently used at Accelerator Test Facility (ATF) at Brookhaven National Laboratory (BNL) which is available for outside users' experiments.

We report our recent beam shaping experiments at BNL for a transformer ratio test. We used a 58 MeV energy chirped electron beam and a single dogleg with a beam mask inserted in a region where the beam transverse size was dominated by the correlated energy chirp. Both measurement results and Elegant simulation data are presented.

INTRODUCTION

A demand for compact accelerators has recently resulted in an increased interest in dielectric wakefield accelerators (DWAs). The DWA is formed by one or several co-axial dielectric layers surrounded by metal cladding (Fig. 1) [3]. Wakefields in dielectric structures may reach gradients on the order of 10 GV/m [4] with 100 MV/m being demonstrated in multiple experiments [5]. They also have the remarkable property that the wakefield's axial electric field and the transverse electric field are transversely uniform and linear, respectively. This is due to the fact that the relativistic drive beam and the subsequent wakefield travel very nearly at the speed of light. If one can make the wakefield to be longitudinally constant along the bunch it will result in no induced energy spread within the bunch, leading to an extraordinary condition of preserving the main beam brightness while providing high gradient acceleration. We have realized that by a proper longitudinal customization of the accelerated beam the induced energy spread in a DWA can be made small enough (<0.1%) to satisfy tight requirements for X-ray free electron laser linac afterburner of the proposed Matter-Radiation Interactions in Extremes (MaRIE) facility at LANL [1, 2, 6].

An important characteristic of the wakefield acceleration is a transformer ratio (TR). It is the ratio of the peak accelerating gradient to the peak decelerating gradient experienced by the drive bunch, and thus it determines how long the drive bunch will be stable before some part of it decelerates to low energies. For a finite length longitudinally symmetric bunch the TR can never exceed 2 [7]. An enhanced TR can be achieved with a ramped beam or a ramp-profiled bunch train [7]. Recently a Double Triangular (DT) beam shape was proposed making possible high TRs with almost uniform drive bunch deceleration [8]. In the DT bunch the TR is approximately proportional to the beam length in wavelengths of the induced wakefield radiation and thus can be made very large.

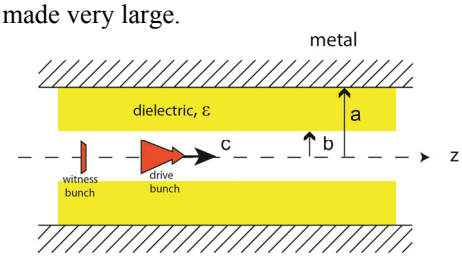


Figure 1: The schematic of a dielectric loaded waveguide with shaped electron bunches traveling on axis.

The main obstacle on the way to experimental demonstration of superior properties of the DWA with a DT drive beam is that the DT bunch shapes are difficult to produce in the submillimeter scale required for ~300 GHz DWAs using conventional methods based on direct beam current modulation. One of the actively popularized methods to shape the beam currents in such a small scale is based on an emittance exchanger technique [9]. It is easy to shape the transverse beam profile using a mask. The emittance exchanger allows to convert a transverse particle distribution into longitudinal. However this method is relatively new and not available at any user accelerator facility although it has already been verified at the Fermilab A0 Photoinjector [10]. A relatively simpler technique is used at Accelerator Test Facility (ATF) of BNL [11] which also allows current shaping on the required scale. It utilizes an energy chirped beam which is cut with a transverse beam mask placed inside of the beamline dispersive region where one transverse coordinate is linearly related to both the particle energy and arrival time.

We studied the possibility of using the ATF facility at BNL for demonstrating high gradient high transformer ratio operation of a DWA with a double triangular beam.

*Work supported by LDRD program at LANL
#d_shcheg@lanl.gov

Copyright © 2013 CC-BY-3.0 and by the respective authors

ISBN 978-3-95450-138-0

UPDATE ON FABRICATION AND TUNING OF THE PHOTONIC BAND GAP ACCELERATING STRUCTURE FOR THE WAKEFIELD EXPERIMENT*

Evgenya I. Simakov#, Sergey Arsenyev, Randall L. Edwards, Samuel Elson, Cynthia Heath, David Lizon, and William Romero, Los Alamos National Laboratory, Los Alamos, NM 87545, U.S.A.

Abstract

We designed an experiment to conduct a detailed investigation of higher order mode spectrum in a room-temperature traveling-wave photonic band gap (PBG) accelerating structure at 11.7 GHz. It has been long recognized that PBG structures have great potential in reducing long-range wakefields in accelerators. The first ever demonstration of acceleration in room-temperature PBG structures was conducted at MIT in 2005. Since then, the importance of that device has been recognized by many research institutions. However, the full experimental characterization of the wakefield spectrum in a beam test has not been performed to date. The Argonne Wakefield Accelerator (AWA) test facility at the Argonne National Laboratory represents a perfect site where this evaluation could be conducted with a single high charge electron bunch and with a train of bunches. We describe the design of the accelerating structure that will be tested at AWA in the near future. We also report the results of fabrication and tuning of PBG cells and the initial cold-testing of the traveling-wave accelerating structure. We discuss the plan for the wakefield experiment.

INTRODUCTION

The next generation of linear colliders with multi-hundred GeV to TeV beam energies pushes the frontiers of the current beam physics and technology with the goal of obtaining high luminosity of the beam and avoiding bunch to bunch beam breakup. Thus, the aaccelerating cavities for the future linear colliders must be selective with respect to the operating mode, and higher order mode (HOM) wakefields that affect the quality of the beam must be suppressed. Photonic Band Gap [1] (PBG) cavities have the unique potential to absorb all HOM power and greatly reduce wakefields. A PBG structure or simply, photonic crystal, represents a periodic lattice of macroscopic components (e.g., rods), metallic, dielectric or both. For accelerator applications, two-dimensional PBG resonators based on arrays of metal rods are commonly employed. The first ever demonstration of acceleration in a PBG resonator was conducted at Massachusetts Institute of Technology (MIT) in 2005 [2]. Since then, the importance of PBG structures for accelerators has been recognized by many research institutions worldwide.

*Work is supported by the U.S. Department of Energy (DOE) Office of Science Early Career Research Program.

#smirnova@lanl.gov

Two attempts to experimentally study wakefields in PBG accelerators were conducted to date, but were incomplete [3,4]. The MIT team [3] cold-tested the 6-cell PBG accelerator structure of [2] in a wide frequency range and recorded the wakefield spectrum. They also ran a beam test with a train of 200 picosecond electron bunches with the charge of 1-18 pC per bunch. Radiation was observed at the output port of the PBG structure and had a quadratic scaling with current at 17 GHz and at 34 GHz. However, with the MIT setup, observation of significant wakefield radiation into other important HOMs, such as a dipole mode was impossible. A more advanced test was conducted by a team at Argonne National Laboratory (ANL) [4]. They observed wakefields in a three-cell X-band standing wave PBG structure when driven by a single electron bunch with a charge up to 80 nC. Major monopole and dipole modes were identified in the collected signal. A variable delay low charge witness bunch following a high charge drive bunch was used to calibrate the gradient. However, this test was not the test of the actual traveling-wave PBG accelerator. At this point, the full experimental characterization of the wakefield spectrum in a traveling-wave PBG accelerator is overdue.

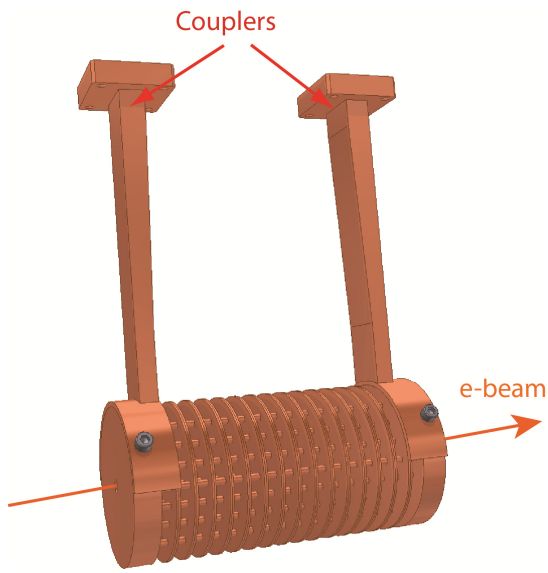


Figure 1: A 16-cell traveling-wave PBG accelerator structure with two waveguide couplers.

We have initiated a project at Los Alamos National Laboratory (LANL) to conduct the full experimental characterization of the wakefield spectrum of a traveling-wave PBG accelerator structure. We plan to put together an 11.7 GHz 2π/3-mode accelerating structure of 16 PBG

Copyright © 2013 CC-BY-3.0 and by the respective authors

BEAM BRIGHTNESS BOOSTER WITH IONIZATION COOLING

V. Dudnikov#, R. Johnson, L. Vorobiev and C. Ankenbrandt, Muons, Inc. Batavia, IL, 60510 USA

Abstract

The brightness and intensity of a circulating proton beam can be increased up to the space charge limit by means of charge exchange injection or by electron cooling but cannot be increased above that limit. Significantly higher brightness can be produced by means of charge exchange injection with space charge compensation [1]. The brightness of the space charge compensated beam is limited at low level by development of the electron-proton (e-p) instability. Fortunately, e-p instability can be self-stabilized at a high beam density. By development of surface plasma sources (SPS) with cesiation and RFQ, H^- beam injectors were prepared with intensity ~0.1 A. We discuss possibilities for production of a "superintense" circulating beam with intensity and brightness far above the space charge limit. A beam brightness booster (BBB) for significant increase of accumulated beam brightness is discussed. Ionization cooling can be used for suppression of the beam brightness dilution. The superintense beam production can be simplified by development of a nonlinear nearly integrable focusing system with broad spread of betatron tunes and the broadband feedback system for e-p instability suppression [2].

INTRODUCTION

Charge Exchange Injection (CEI) was developed for increasing the circulating beam intensity and brightness above injected beam parameters by multiturn injection of beam into the same transverse phase space areas [3-5]. At that time the intensity of H^- beam from plasma source was below 5 mA with normalized emittance ~1 π mm mrad. The intensity of H^- beam from charge exchange sources was up to 15 mA, but the brightness B of this H^- beam was ~100 times less than the brightness of a primary proton beam because only 2% of the proton beam was converted into the H^- ions. In this situation the increase of the circulating beam brightness up to 100 times was necessary for reaching of the brightness of primary proton beam which can be used for one or several turn injection. The intensity and brightness of H^- ion beams were increased by orders of magnitude by adding a trace of cesium into gas discharges (cesiation effect) [6]. After development of surface plasma source (SPS) with cesiation, the H^- beam intensity was increased up to 0.1 A with emittance ~0.2 π mm mrad [7,8], so the brightness of injected beam approached the space charge limit of real accelerators such as the Fermilab Booster [9]. With such beam the further increase of circulating beam brightness is impossible, but CEI is routinely used to increase the circulating beam intensity by many orders of magnitude by injection into different parts of the transverse phase space (painting in the transverse phase space) [5, 9, 10]. Further increase of circulating beam brightness is possible by using multiturn CEI with space charge compensation by particles with opposite charge (electrons or negative ions) [1, 11, 12]

Unfortunately, such possibility is complicated by strong transverse two-beam instability driven by beam interaction with accumulated compensating particles in the circulating beam.

The strong instability with fast loss of a bunched beam was discovered at 1965 in a small scale proton storage ring (PSR) during development of charge exchange injection and was stabilized by feedback [3, 4, 5, 12, 13]. This instability was explained in [4] as an inverse variant of the strong transverse instability of circulating electron beam caused by the interaction with compensating ions (beam- ion instability) predicted in 1965 by B. Chirikov [14]. An analogue of this instability, electron-proton (e-p) instability with very low threshold was observed experimentally at the same time during accumulation of a coasting beam [1, 5, 11-13]. The e-p instability of coasting beam was in good agreement with theory [14, 15].

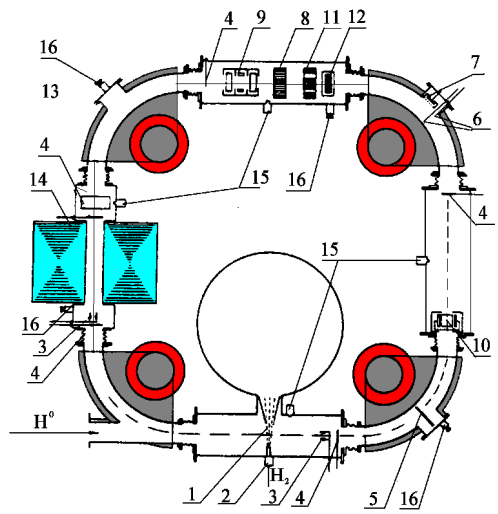


Figure 1: Schematic of storage ring with diagnostics and control. 1-stripping gas target; 2-gas pulser; 3-Faraday Cup; 4-Quartz screen; 5, 6-moving targets; 7-ion collectors; 8-current monitor; 9-Beam Position Monitor; 10-Quadrupole pick ups; 11-magnetic BPM; 12-beam loss monitor; 13-detector of secondary particle density; 14-inductor core; 15-gas pulses; 16-gas leaks.

Superintense circulating beam with intensity far above the space charge limit was produced in BINP in a simple race track ring [5,12,13,16] shown in Fig. 1.

#Vadim@muonsinc.com

ISBN 978-3-95450-138-0

Copyright © 2013 CC-BY-3.0 and by the respective authors

TRANSVERSE BEAM DYNAMICS IN PLASMA GUIDED LASER DRIVEN ACCELERATION

D. B. Cesar, P. Musumeci, UCLA *, PBPL, Los Angeles, CA 90095, USA

Abstract

An axially modulated plasma waveguide supports slow-wave laser modes suitable for direct laser acceleration. The channel studied here supports a gradient of 2 GeV/m driven by a 1 TW laser. The transverse beam dynamics are analyzed in the context of the envelope equation and simulated by particle tracing to demonstrate the feasibility of using a photogun as the electron source. External injection promises to take advantage of the precision offered by state-of-the-art RF photogun technology to increase shot-to-shot reproducibility.

INTRODUCTION

The acceleration of electrons directly by laser fields is an attractive design for a compact accelerator because of the large gradients lasers can provide. In particular, direct laser acceleration (DLA) requires less power than laser plasma wakefield acceleration (LWFA), which enables more compact designs. In order to take advantage of the high fields of the laser it is necessary to overcome the restrictions due to phase slippage implied by the Lawson-Woodward theorem [1]. The DLA scheme pursued here overcomes these limitations by guiding a high intensity pulse through a corrugated plasma channel [2]. Analogous to a conventional disk-loaded LINAC, the corrugations introduce slow wave components phase matched to the electron beam.

Corrugated plasma channels have been created in a laser-ionized plasma [3]. Gas clusters were ionized and then heated by a 100ps pulse focused to a line by an axicon. The corrugations considered for quasi-phase matching were created by using a ring diffraction grating to introduce radial modulations in the laser pulse. The axicon maps the radial intensity pattern to the axis, and uneven heating of the plasma leads to density modulations during the shock-wave expansion. The use of the heater pulse to shape the modulations offers control over the modulation parameters.

Here we propose fixing the modulation parameters to provide focusing for an emittance dominated beam. The transverse beam dynamics in an ideal channel are studied in the context of the envelope equation. A matched solution with asymptotically damped oscillations is calculated. The input beam to match the channel can be obtained from an RF photogun. This solution bypasses the problems LWFA experiments have faced with injecting bunches from the plasma into the accelerating field.

ANALYSIS

Following previous analysis [4], the density profile of the plasma channel used for Direct Laser Acceleration experiment can be approximately described as Eq.(1), with addition of a density ramp, $n_s(z)$ to be used for phase-matching throughout the accelerator [5].

Table 1: Channel Parameters

n_0	k_m	δ	w_{ch}	λ_0	a_0
$5 \cdot 10^{19}/\mathrm{cm}^3$	232200	.9	37 μm	800nm	.2

$$n(z) = n_0 \left[1 + \delta \sin\left(k_m z\right)\right] + n_0'' r^2/2 + n_s(z) \qquad (1)$$

The parabolic density channel supports TM guided modes of radially polarized waves. The lowest order solution is expanded into slow-wave components and the transverse forces due to the resonant and non-resonant components are studied and used as the basis for an envelope calculation. Channel parameters used throughout the paper are listed in table 1 and are chosen to be consistent with experiment [3]. The channel is taken to be 1.8cm long so that the length of the accelerating pulse does not limit acceleration [4]. A laser power of $a_0 = .20$ is chosen to correspond with the TW laser in construction at UCLA's Pegasus beamline.

Guided Modes

Since we want a longitudinal field component for acceleration, we seek the radially polarized component of the laser vector potential in the slowly varying envelope approximation: $A_\perp = \hat{A}_r e^{i(k_0 z - \omega_0 t)}$, with $\hat{A}_r$ satisfying:

$$\left[2ik_0\left(\frac{\partial}{\partial z} + \frac{1}{c}\frac{\partial}{\partial t}\right) + \nabla_\perp^2\right]\hat{A}_r = \frac{\omega_p^2}{c^2}\hat{A}_r$$

where $\omega_p^2 = \frac{ne^2}{m\epsilon_0}$. This can be solved using separation of variables and expanded into harmonics using the Jacobi-Anger expansion. Palastro [4] includes discussions of the assumptions behind this model. Ignoring time dependence in the laser envelope, the lowest order solution is written in the Columb gauge as:

$$\hat{A}_r = A_0 \frac{r}{w_{ch}} e^{\frac{-r^2}{w_{ch}^2}} \sum_{q=-\infty}^{+\infty} i^q J_q(\Psi) e^{i\left(-\Psi + (\delta k + q k_m)z - \frac{\int k_{ps}^2 dz}{2k_0}\right)} \qquad (2)$$

where:

- $w_{ch} = \left(\frac{8c^2}{\omega_{p0}''^2}\right)^{1/4}$
- $k_{ps}^2(z) = \frac{e^2 n_s(z)}{m\epsilon_0 c^2}$
- $\delta k = -\frac{1}{k_0}\left(\frac{\omega_{p0}}{2c^2} + \frac{4}{w_{ch}^2}\right)$
- $\Psi = \frac{\delta\omega_{p0}}{2c^2 k_0 k_m}$

The transverse potential peaks at $r = w_{ch}/\sqrt{2}$. For our parameters $\Psi \approx .5$ is small, so that the Bessel functions limit the relevant terms in Eq(2) to small q.

* dcesar@ucla.edu

Copyright © 2013 CC-BY-3.0 and by the respective authors

APPLICATIONS FOR OPTICAL-SCALE DIELECTRIC LASER ACCELERATORS

R.J. England, Z. Huang, R. J. Noble, J. E. Spencer, Z. Wu
SLAC National Accelerator Laboratory, Menlo Park, CA 94025, USA
B. Montazeri, E. Peralta, K. Soong, Stanford University, Stanford, CA, USA
C. Lee, M. Qi, Purdue University, West Lafayette, IN, USA
L. Schacter, The Technion, Haifa, Israel

Abstract

Particle acceleration in dielectric laser-driven microstructures, recently demonstrated at SLAC, holds the promise of providing low-cost compact accelerators for a wide variety of uses. Laser-driven undulators based upon this concept could attain very short (mm to sub-mm) periods with multi-Tesla field strengths. And since dielectric laser accelerators operate optimally with optical-scale electron bunch formats, radiation production with high repetition rate (10s of MHz) attosecond-scale pulses is a natural combination. We present preliminary analysis of the harmonic field structure for a periodic undulator based on this concept.

INTRODUCTION

The increasingly prohibitive cost and size of modern accelerator facilities has prompted interest in a variety of schemes for accelerating particles at higher gradients than traditional metallic cavity accelerators can provide, rapid fabrication techniques, and more readily available energy sources. One of the most promising of these schemes is the use of dielectric near-field structures powered by an infrared (IR) laser to produce a confined accelerating mode. Since the size of the confining beam channel scales with the wavelength of the source, the apertures of such structures are at most a few microns in transverse size. As a result, particle beam confinement requires a new operating regime with beams of low charge (10-100 fC) and ultra-low normalized emittance (1-10 nm). The bunches should ideally be short compared to the optical wavelength (10-100 fs), must be spaced at the optical period of the laser (or an integer multiple thereof), and should come in bunch trains commensurate with typical solid state laser pulse lengths (10 fs - 1 ps). The decrease in luminosity due to such small bunch charges are compensated by the fact that solid state lasers permit repetition rates 3 orders of magnitude higher than typical microwave sources. The requisite dielectric structures can be fabricated with nanometer-level precision on silicon wafers using modern solid state fabrication methods, and the first experimental demonstration of high-gradient acceleration in such structures has been recently reported [1].

The DLA concept leverages well-established industrial fabrication capabilities and the commercial availability of tabletop lasers to reduce cost, while offering significantly higher accelerating gradients, and therefore a smaller footprint. Power estimates for the DLA scenario are comparable with convention RF technology, assuming that similar power efficiency (near 100%) for guided wave systems can be achieved, 40% wall plug laser efficiencies (feasible with solid state Thulium fiber laser systems), and 40% laser to electron beam coupling (consistent with published calculations).

This research has significant near and long-term applications for energy frontier science [2, 3]. Additional applications including radiation production for compact medical x-ray sources, university-scale free electron lasers, NMR security scanners, and food sterilization are beginning to be explored. A dielectric laser-driven deflector, operating on the same basic principles as recently demonstrated accelerator devices, was proposed by Plettner and Byer [4]. The scheme uses a pair of dielectric gratings excited transversely by a laser beam and separated by a gap of order the laser wavelength where a beam of electrons would travel. By changing the sign of the excitation between successive structures (e.g. by alternating the direction of illumination) an optically powered undulator could be constructed to create laser driven micro-undulators for production of attosecond-scale radiation pulses synchronized with the electron bunch.

As a next step in exploring this concept in more detail, the commercial electromagnetic finite element code HFSS 12.0 was used to obtain realistic field profiles along the axis of an electron beam propagating in a single stage of deflection (representing half of one undulator period). These fields are analyzed with respect to the injection phase of a test electron and the deflecting forces calculated to produce a single-period model of the proposed undulator concept.

BACKGROUND

The deflector design proposed in Ref. [4] consists of a pair of coplanar gratings with a pillar height g separated by a gap of width w. If the gratings are constructed of an optically transmissive material (such as glass) an electromagnetic mode can be excited in the gap region by transverse illumination of the structure with a monochromatic plane wave. The resultant confined mode is found to produce a net deflecting force transverse on a trajectory lying in the midplane between the two gratings at an angle $\pi - \alpha$ relative to the direction of the grating lines. Consquently

Copyright © 2013 CC-BY-3.0 and by the respective authors

ISBN 978-3-95450-138-0

MULTIBUNCH BEAM PHYSICS AT FACET*

S. J. Gessner†, E. Adli, K. L. F. Bane, F. J. Decker, Z. D. Farkas, R. K. Jobe, M. D. Litos, M. Ross
SLAC, Menlo Park, CA, 94025, USA
T. Katsouleas, A. A. Sahai, Duke ECE, Durham, NC, 27708, USA

Abstract

Plasma wakefield studies are normally conducted as single-shot experiments. Here, single-shot means that the plasma returns to its original state before the next bunch passes through the plasma. The time scale for the plasma to return to equilibrium is 10-100 ns, which is comparable to the bunch separation in proposed linear colliders. The SLAC linac typically delivers beam at a rate of 10 Hz to FACET, but can also be operated in a manner that delivers two electron bunches per RF pulse to FACET. We explore operating modes with beam separations as small 5.6 ns so that high repetition rate plasma wakefield acceleration can be studied at FACET.

INTRODUCTION

The SLAC linac provides electron bunches with total beam charge of 3.2 nC to FACET experiments. The beam originates at Sector 0 from a thermionic cathode gun, passes through the sub-harmonic buncher for longitudinal compression, is captured and accelerated in the Sector 1 s-band linac and sent to the North Damping Ring (NDR) for beam cooling. After the emittance is damped in the ring, the beam is extracted into the Sector 2 linac, accelerated to 20.35 GeV, and delivered to Sector 20 for final compression and focusing. An overview of the linac and associated systems is given in Fig. 1. Each system imposes its own constraints on the possible bunch parameters and inter bunch spacings.

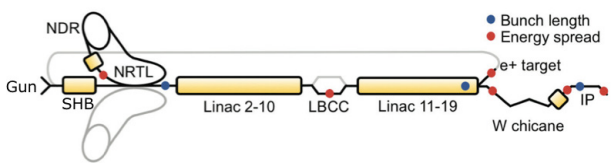


Figure 1: Overview of Linac with affected subsystems and diagnostics for multi-bunch operation.

BEAM GENERATION AND CAPTURE

Source

The electron source is a thermionic cathode driven by a multi-channel pulser. The pulser is a circuit with two planar triode amplifiers that couple into a common amplifier driving the cathode. The two triodes can be fired independently to produce electron pulses from the cathode with arbitrary separation in time. The gun can generate up to 27 nC of charge in a single pulse. We look to generate two pulses with 3.2 nC each. This can be achieved without changing the existing gun hardware [1].

Subharmonic Buncher

Immediately after the beam is generated it is captured in the sub-harmonic buncher (SHB). The SHB is operated at the $1/16^{th}$ sub-harmonic of the s-band linac. The bucket spacing for the SHB is 5.6 ns. The SHB bucket size sets the interbunch spacing in the rest of the machine. Without the SHB, most of the beam does not get captured in the linac and there is the potential for radiation damage in the injector. All of the interbunch spacings considered in this paper are multiples of 5.6 ns.

The longitudinally compressed bunches are captured in an s-band bucket at the start of Sector 1 and accelerated to 1.19 GeV before being sent to the NDR via the North Linac-to-Ring arc.

NORTH DAMPING RING

Kickers

A loaded ferrite kicker magnet with a flat-top of 30 ns kicks the bunches into the ring. This magnet was designed to have an extremely sharp rise and fall time, so as not to disturbed another bunch in the ring, which was typical during SLC operation. A second kicker magnet is located on the opposite side of the ring and is used to extract the bunches. This magnet is identical to the injection kicker except that it has a different pulse forming network that uses a Blumlein generator to produce an extremely flat pulse to the magnet [2]. The field in the magnet provides a uniform 7 mrad kick for more than 60 ns. The injection and extraction kickers set limits on the maximum separation between the two bunches. The maximum bunch spacing that is consistent with the NDR RF and SHB RF is 61.6 ns. The injection kicker would have to be equipped with a similar PFN as the extraction kicker to achieve this separation.

Instabilities

The NDR limits the bunch charge and separation in another manner due to single-bunch and coupled beam instabilities. The single bunch instability is a short range, microwave instability. With 3.2 nC per bunch, the ring is operated above the threshold for the instability. However, at this charge the instability is weak and does not degrade the bunch quality [3]. Note that having two 3.2 nC bunches

* Work supported by the U.S. Department of Energy under contract number DE-AC02-7600515.
† sgess@slac.stanford.edu

Copyright © 2013 CC-BY-3.0 and by the respective authors

SIMULATION OF POWER COUPLING AND WAKEFIELD IN PHOTONIC BANDGAP FIBERS FOR DIELECTRIC LASER ACCELERATION*

C.-K. Ng, R.J. England, A. Kwiatkowski, R.J. Noble, J.E. Spencer, SLAC, Menlo Park, U.S.A.

Abstract

A photonic bandgap (PBG) lattice in a dielectric fiber can provide high gradient acceleration in the optical regime, where the accelerating mode is obtained from the presence of a single defect in the lattice. In this paper, we will investigate two aspects of the PBG for acceleration. First, the excitation of the accelerating mode can be achieved by directing high-power lasers from free space. Simulation using ACE3P has demonstrated that, by appropriately shaping the end of the PBG fiber, power can be coupled into the fiber using a simple laser configuration. Second, the wakefield generated by the transit of a beam through a PBG fiber will be simulated. The radiation spectrum of the wakefield will be evaluated and corroborated with measurements from a commercial fiber.

INTRODUCTION

The photonic bandgap (PBG) structure proposed by Lin [1] has demonstrated the possibility of confining an accelerating mode in an energy bandgap existing in a periodic lattice of vacuum holes in a dielectric fiber with a central vacuum defect of larger diameter. High accelerating gradient can be achieved in such fibers in the optical regime using lasers for excitation of the accelerating mode. The mechanism of coupling power into the PBG fiber needs to be investigated to ensure efficient excitation of the accelerating mode. Previous studies have shown that a coupling scheme from free space by directly focusing laser pulses in a certain configuration into the fiber can excite the accelerating mode [2]. However, for best results the configuration requires an array of six laser beams arranged in a pattern that obeys the hexagonal symmetry of the Lin lattice. It is desirable to develop improved coupling schemes that can simplify the laser configuration by modification of the existing geometry. It will be shown in the next section that a simpler coupling scheme can be achieved by appropriately shaping the end of the PBG fiber.

While attempts to fabricate Lin-type PBG fibers that can support an accelerating mode are being explored, off-the-shelf telecom fibers are available in the commercial market place, providing samples that can be tested using high energy electron beams at the test facility at SLAC [3]. An example of these commercial fibers is the HC1060 fiber of NKT Photonics which supports the propagation of a telecom mode at the wavelength of 1060 nm. Although the HC1060 fiber does not support a strong TM-like accelerating mode, by measuring the radiated signal after the passage of an electron beam, it is possible to identify the modes that exist in the bandgap of the fiber. In order to corroborate with the measured radiation spectrum obtained from beam tests, simulations have been carried out using the 3D parallel electromagnetic code suite ACE3P [4] to model beam excitation in the HC1060 fiber to calculate wakefield effects and to compare with measurements.

* Work supported by the Department of Energy under Contract Number DE-AC02-76SF00515 and funds provided by Incom, Inc. through CRADA 383 from DOE STTR Grant DE-SC0007718.

POWER COUPLING IN LIN FIBER

The Lin PBG fiber consists of circular holes in a hexagonal lattice with spacing a between the centers of neighboring holes. The holes have a radius of $0.35a$. In order to introduce a defect in the lattice, one hole is replaced by another with a radius of $0.52a$. The material of the fiber has a dielectric constant of 2.13 for this glass at near IR wavelengths. A quarter of the model in the transverse plane is shown in Fig. 1, exhibiting a lattice with hexagonal symmetry and a central defect. The Lin PBG fiber supports a TM-like accelerating mode. For example, the wavelength of the defect mode is 2 μm for a = 2.61 μm. Using ACE3P's frequency domain eigensolver module Omega3P, the calculated longitudinal electric field pattern of the defect mode is shown in Fig. 1. It can be seen that a fairly uniform longitudinal electric field appears in the central circular hole and the field magnitude decays gradually at larger radial distances.

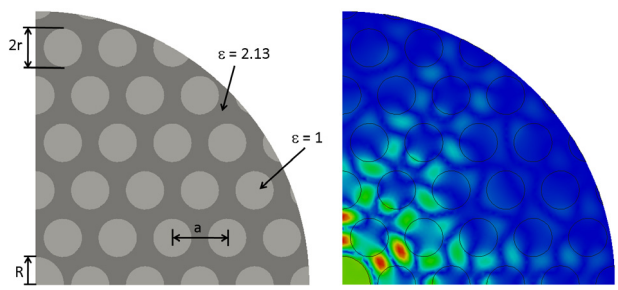


Figure 1: (Left) A quarter model of the Lin PBG fiber; (Right) The longitudinal component of the electric field of the defect mode in the Lin PBG fiber.

The study of power coupling from free space can be carried out through an inverse process by simulating the transmission and radiation of the accelerating mode through a slab of the fiber. The electric and magnetic field patterns calculated by Omega3P are loaded as an excitation at the incident port for ACE3P time domain simulation module T3P. The calculation has been reported in a previous work [2] and has shown that the radiation focuses in six hot spots, which observes the hexagonal symmetry of the Lin fiber. Figure 2 shows the model used in the simulation where a cylindrical slab of the fiber is placed in a hemisphere representing the free

Copyright © 2013 CC-BY-3.0 and by the respective authors

ISBN 978-3-95450-138-0

BEAM POSITION MONITOR FOR MICRO-ACCELERATORS*

K. Soong†, R.L. Byer, E.A. Peralta, Stanford University, Stanford, CA 94305, USA
R.J. England, Z. Wu, SLAC National Accelerator Laboratory, Menlo Park, CA 94025, USA

Abstract

Rapid progress in the development of laser technology and in the sophistication of semiconductor manufacturing has enabled the realization of the first dielectric laser-driven particle accelerator (DLA) on a chip [1]. Since the accelerating channel in DLA structures typically have dimensions in the sub-micron range, the ability to precisely control particle position within these structures will be critical for operation. A number of beam deflection and focusing schemes have been devised, but without the ability to measure the position of the particle beam to nanometer accuracy, these schemes will be extremely difficult to implement.

We present a new concept for a beam position monitor with the unique ability to map particle beam position to a measurable wavelength. Coupled with an optical spectrograph, this beam position monitor is capable of sub-nanometer resolution. We describe one possible design of this device, and present the current status of the structure fabrication and experimental demonstration.

INTRODUCTION

Recent success at SLAC and Stanford have demonstrated the proof-of-principle of the dielectric laser-driven accelerator (DLA) [1]. These dielectric accelerator structures are fabricated using commercially developed lithographic fabrication methods and can be mass produced on conventional dielectric wafers. The accelerator structures are powered using commercially available laser systems, rather than specialized klystrons, and can support peak electric fields well beyond those found in traditional accelerator components. Therefore, DLAs have the advantage of requiring a three-order of magnitude smaller footprint, while boasting significantly higher acceleration gradients than those achievable in traditional accelerator structures. With its inherent advantages, DLAs have the potential to revolutionize the concept of particle accelerators, moving the technology from expensive grand-scale machines to low cost printed microstructures. The applications of compact particle accelerators are numerous and extensive, spanning everything from radiation therapy to x-ray microscopy. While the recent proof-of-principle demonstration is a momentous occasion, the road to a complete particle accelerator-on-a-chip is still an arduous journey. A complete particle accelerator will require the staging of hundreds or thousands of individual dielectric accelerator microstructures, as well as beam focusing and beam deflecting elements – with submicron alignment tolerances. And although nanometer-class alignment of structures within a single wafer is inherent through well-established lithography methods, alignment from wafer-to-wafer does not have a corresponding process. For this reason, beam monitoring elements will necessarily be a critical component for DLA devices.

We present experimental demonstration towards a novel beam position monitor (BPM) which has the ability to map beam position to a measurable wavelength [2]. Coupled with a commercial optical spectrograph, this novel BPM device is capable of sub-nanometer resolution. Additionally, this BPM device can be easily fabricated alongside the DLA accelerator structures, using the same mass-producible lithographic processes; thereby ensuring nanometer-class alignment.

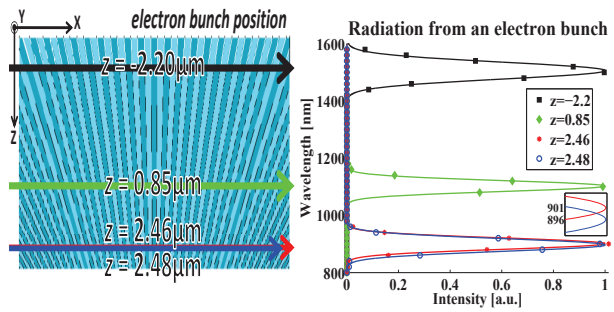


Figure 1: A top-down view of the grating BPM geometry (left), and the predicted normalized radiation spectrum from an electron bunch traversing the grating BPM at four unique positions (right). The markers on the plot represent simulation data, whereas the solid lines depict a Gaussian fit. The inset highlights the distinct radiation spectrum generated by two closely separated bunches.

The geometry of the proposed beam position monitor is shown in Fig. 1. The structure operates on the principles of an inverse-accelerator structure. If a grating accelerator structure can accelerate electrons with a laser pulse, then by reciprocity an electron beam traversing an unpowered grating structure will decelerate (slightly) and radiate. Based on the operating principles of the grating structure as an accelerator, we expect the generated wakefield radiation to be polarized in the direction of beam propagation. Additionally, from the phase-synchronicity condition ($\lambda_{laser} = \lambda_{grating}$), we expect a traversing electron beam to generate wakefield radiation with a center wavelength matching the observed structure periodicity. By varying the periodicity of the grating structure as a function of position, we create a structure which generates position-dependent

* Work supported by DOE (SLAC and LEAP), DARPA (AXiS), the Stanford Graduate Fellowship and the Robert Siemann Fellowship.
† kensoong@slac.stanford.edu

Copyright © 2013 CC-BY-3.0 and by the respective authors

SILICA ROD ARRAY FOR LASER DRIVEN PARTICLE ACCELERATION*

Z. Wu, J. England, R. Noble, SLAC, Menlo Park, CA 94025, USA
E. Peralta, K. Soong, Stanford University, Stanford, CA 94305, USA
M. Qi, Purdue University, West Lafayette, IN 47907, USA

Abstract

Here we describe a structure of double-row silica rods array for laser driven acceleration. Similar to the dual-layer rectangular grating structure, the periodic arrangement of the rods alongside the beam channel provides the necessary phase modulation of the electromagnetic fields, and therefore required phase synchronicity for laser acceleration of charged particles. Resonances among adjacent rods could enhance the near-fields in the gap region to achieve high gradient operation. Simulation has been carried out to optimize the structure dimensions for high accelerating gradient or high acceleration factor. Results show that acceleration factor up to 0.45 could be achieved from this rod array structure. One advantage of this structure is that all the rods are fabricated on one single substrate, therefore positioned and aligned with photolithographic level precision. Several prototype samples have been fabricated for potential laser acceleration experiments.

INTRODUCTION

To utilize the extraordinary electric field available from the state-of-the-art laser systems for charged particle acceleration has long been attractive in the advanced accelerator research. Laser driven dielectric accelerator structures possess advantages over conventional metallic RF structures in their miniaturized dimensions, greatly reduced manufacturing cost, larger breakdown threshold, and higher accelerating gradient [1]. Several resonant or waveguide based structures have been proposed theoretically [1-3]. Recently, near-Infrared laser induced electron energy modulation has been demonstrated for the first time on a fused silica near-field grating structure [4], with larger than 250 MV/m gradient observed.

The dual-layer rectangular grating structure [2] is advantageous for its structural simplicity and convenience of excitation (direct side illumination). However, on-chip power network of an integrated accelerator or accelerator-based light source usually employs a high-index-material waveguide sitting upon a planar low-index substrate, where laser light travels inside the waveguide parallel to the substrate. Side illumination then implies that grating teeth needs to stand up straight with respect to the chip substrate. Direct lithographic fabrication of these vertical teeth up to tens of micron tall is challenging. To vertically assemble a dual-layer, pre-bonded grating accelerator to the chip substrate also demands much fabrication and alignment effort.

*wzr@slac.stanford.edu Work supported by U.S. Department of Energy under Grants DE-AC02-76SF00515, DE-FG06-97ER41276 and by DARPA Grant N66001-11-1-4199.

Meanwhile, deep etching of silicon to form long cylinder array on a substrate has been demonstrated feasible. Oxidation process after etching is also demonstrated to transfer these rods to fused silica. This rod array may essentially serve as the phase-resetting dielectric mask just as well as the rectangular grating structure, but already integrated since it can share the same substrate with the on-chip waveguide network. This paper explores this possibility, by looking into achievable acceleration gradient from a silica rod array structure. Parametric study results of the structure dimensions will be shown, aiming for either optimal acceleration factor or large field enhancement. Following that will be an introduction to the manufacture of the structure.

DESIGN AND SIMULATION

Figure 1 below illustrates the proposed rod array accelerator structure. Two rows of dielectric rods with radius r and length l are laid on a substrate. The two lines are separated in the z direction by a gap width w, forming the electron accelerating channel. Rods across the gap have their centre positions aligned along the y direction. Within each row, the centre-to-centre periodicity between adjacent rods is p. Laser light is incident along the z direction to power this accelerator structure.

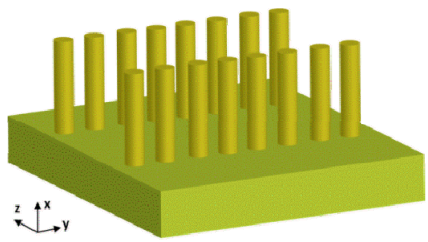


Figure 1: Layout of the rod array accelerator structure.

Silica Rod Array for Acceleration

The structure is modelled in Ansoft HFSS [5] to look for possible phase modulation for net acceleration gradient. Figure 2 shows the single-period structure simulated, with its geometrical parameters denoted on the schematic. Its y-direction periodicity is reflected by assigning master and slave boundary conditions to its left and right xz plane boundaries, with zero-degree phase delay. A plane wave excitation propagating towards the positive z direction is launched, with two perfect-matching-layer boundaries terminating the front and back xy planes to simulate infinite open spaces. The incident plane wave has its e-field polarized in the y direction, with magnitude of 1V/m. The top and bottom yz planes of the model are terminated by perfect magnetic boundary

Copyright © 2013 CC-BY-3.0 and by the respective authors

ISBN 978-3-95450-138-0

SPECTRAL BROADENING OF IONS ACCELERATED BY A RADIATION PRESSURE DRIVEN SHOCK *

N. Cook†, C.M. Maharjan, P. Shkolnikov, Stony Brook University, Stony Brook, NY 11790, USA
I. Pogorelsky, M.N. Polyanskiy, O. Tresca, BNL, Upton, NY 11973, USA
N.P. Dover, Z. Najmudin, Blackett Laboratory, Imperial College,
London SW7 2AZ, United Kingdom

Abstract

Laser driven ion acceleration has been the focus of considerable research efforts since multi-MeV energies were first demonstrated. Most experiments use solid state laser pulses focused onto thin foil targets. However, recent progress in CO_2 laser technology allows for the creation of intense pulses at lambda $\sim$10 μm. The longer wavelength permits the use of low density targets. In these conditions ion acceleration is primarily driven by a shock wave due to the radiation pressure of the laser. This acceleration mode has the advantage of producing narrow energy spectra while scaling well with laser intensity. New improvements to the CO_2 laser at the Accelerator Test Facility allow for the unique production of a single picoseconds-scale pulse with 1TW peak power. We report on the interaction of an intense CO_2 laser pulse with overdense hydrogen and helium gas jets. Using a two pulse optical probe, we are able to obtain real-time density profiles at different times during the interaction, allowing for the characterization of shock wave velocities and peak density conditions. Ion energy spectra are measured using a Thomson spectrometer and scintillating screen.

INTRODUCTION

Acceleration of protons by intense laser pulses has become an increasingly active area of study amongst nuclear, plasma, and accelerator physicists. Considerable progress has been made using thin foils as targets for high intensity lasers at optical wavelengths [1] [2] . These experiments utilize the highest intensity lasers to reach the highest proton energies, but at the expense of beam quality and energy spread.

An alternative is to use the radiation pressure of the laser to drive hole-boring or shock wave acceleration of ions from a low density target. The ponderomotive force of the laser can drive plasma electrons in an underdense plasma further into the target, forming a critical surface. For a cold electron population, hole-boring acceleration takes place. The plasma critical surface recedes at the hole-boring velocity, v_{HB}, reflecting ions at a velocity of $2v_{HB}$. Recent experiments with intense, circularly polarized, CO_2 laser pulses have demonstrated hole-boring acceleration by producing collimated bunches of protons with energies greater than 1 MeV and narrow energy spread [3] [4].

* Work supported by the United States Department of Energy, Grant DE-FG02-07ER41488.

† ncook@bnl.gov

In the case of a hot electron population, the strong charge separation at the critical surface launches a shockwave into the plasma, which reflects ions at nearly twice the shockwave velocity [5]. This mechanism requires a high electron temperature to reach high shock velocities. Collisionless shockwave acceleration has been shown to similarly produce quasi-monoenergetic proton beams [6].

Improvements to the CO_2 laser system at Brookhaven National Laboratory's Accelerator Test Facility have allowed for the production of ps-scale single pulses with TW peak power [7]. We report on the acceleration of protons using intense linearly polarized CO_2 pulses. With two pulse optical probing, we measure peak densities and shock wave velocities, while ion spectra are measured using a scintillator and Thomson spectrometer. Observed profiles correlate with 1D PIC simulations predicting declining shockwave velocity immediately following the laser plasma interaction (LPI).

EXPERIMENTAL METHOD

Utilizing a isotopic CO_2 mixture in a regenerative amplifier, we amplify a 10.2 μm CO_2 pulse centered on the R-branch of vibrational transitions. The pulse passes through a 10 bar amplifier resulting in a single 5 ps pulse providing a maximum of 1 TW power [7]. The pulse is then focused with an $f/3$ off-axis parabolic mirror to a focal spot of $w_0 = 50$ μm, providing a maximum on-target intensity of $I \sim 3 \times 10^{16} W cm^{-2}$ corresponding to $a_0 = 1.5$. The laser contrast is $> 10^5$ as measured by an infrared power meter.

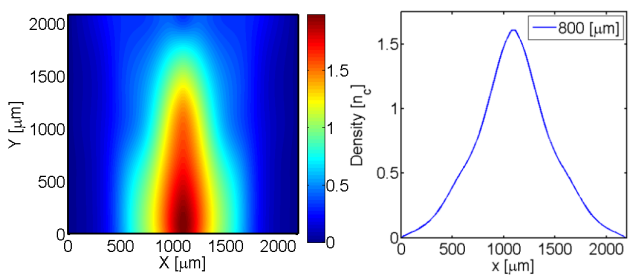


Figure 1: H_2 neutral density from a 1 mm nozzle at 15 bar backing pressure. Right, the density profile 800 μm above the nozzle.

We use 1 mm and 2 mm cylindrical nozzles to produce high density gas jets. Figure 1 shows the neutral density for H_2 gas with a backing pressure of 15 bar. A lineout is taken at 800 μm from the nozzle, showing a peak density

Copyright © 2013 CC-BY-3.0 and by the respective authors

A BETATRON-ANALYSIS TECHNIQUE FOR IDENTIFYING NARROWBAND TRAPPED CHARGE WITHIN A BROADBAND ENERGY TAIL IN PWFA EXPERIMENTS AT FACET*

Chris Clayton#, Weiming An, Chan Joshi, Kenneth Marsh, Warren Mori, Navid Vafaei- Najafabadi (UCLA, Los Angeles, California), Patric Muggli (MPI, Muenchen), Erik Adli, Christine Isabel Clarke, Sebastien Corde, Jean-Pierre Delahaye, Robert Joel England, Alan Stephen Fisher, Joel Frederico, Spencer Jake Gessner, Mark Hogan, Selina Zhao Li, Michael Dennis Litos, Dieter Walz, Ziran Wu (SLAC, Menlo Park, California), Wei Lu (TUB, Beijing)

Abstract

Plasma accelerators driven by ultra-relativistic electron beams have demonstrated greater than 50 GeV/m acceleration gradients over a distance of a meter [1] though the accelerated particles typically have had a 100% energy spread when a single drive bunch was used. However, it is known that by locally producing electrons via ionization within the beam-driven plasma wake, they can become trapped and accelerated so that high-energy, mono-energetic electron bunches can be produced [2]. Prior experiments and the associated simulations [3] suggested that, by augmenting the usual He buffer gas in the heat pipe oven plasma source [4] with a moderate ionization potential (IP) gas such as Ar or Ne, local injection can indeed occur. In a recent experiment associated with the E-200 plasma wakefield accelerator (PWFA) experiment at the Facility for Advanced Accelerator Experimental Tests (FACET) [5] at SLAC, the expected energy gain of these injected electrons (initially at rest) puts them within the energy range of the accelerated tail electrons of the FACET beam. We propose a technique to help identify bunchlets of electrons at the 10's of pC level arising from the ionization injection of Ar/Ne electrons that may otherwise be lost or overlooked as part of the discrete betatron-focusing maxima or the maxima inherent the chromaticity of the imaging electron spectrometer.

OBJECTIVES OF THE EXPERIMENT

For most applications of high-energy beams, narrow energy spreads are desired. By employing spatially localized ionization to produce and inject new electrons within the plasma wake, a PWFA can produce high-energy, mono-energetic electron "bunchlets".

When these bunchlets appear at the image plane of the imaging spectrometer, there are two other types of distinct features that may mask the bunchlets having only 10's of pC of charge. First is the fact that the highly chromatically aberrated electron imaging spectrometer has a very narrow energy range for which a stigmatic focus–a focus that is simultaneous focusing in x and in y (or energy) at the same spot–is located and thus there is always a "bright feature" in the spectrum due to this. Secondly, even with a broadband spectrometer, the electrons (both the FACET beam electrons and any injected electrons; i.e., the bunchlet) exit the plasma with an energy-dependent phase advance of their betatron envelope oscillations [6] that leads to an energy-dependent divergence of the electrons at the plasma exit. This fact also puts structure onto the final spectrum, as discussed below.

Let ζ_k represent the local (within the wake) longitudinal location of the k^{th} slice of the accelerated electrons. Suppose further that this k^{th} slice exits the plasma as a nearly parallel beam having undergone $N = N_k$ betatron oscillations. Due to the finite angular acceptance of the spectrometer coupled with the strong focusing force of the ion column within the wake in the blowout regime, and the finite bit-depth of the recording CCD cameras, this slice will appear relatively bright on the spectrometer. There will be another slice, the k+1$^{\text{th}}$ slice at a lower energy that has undergone $N = N_{k+1} = N_k + 1$ betatron oscillations and will likewise appear relatively bright at the spectrometer. In fact, for each final slice energy such that $N_{k,m} = N_k \pm m$ where $m = \pm 1, \pm 2$, etc., there will be a corresponding bright spot on the spectrometer. We call this series of spots the "betatron ladder". This ladder was clearly visible in the E-167 energy-doubling experiment of Ref. [1].

In the following Sections we will describe the experimental setup, derive the energy-locations of the betatron ladder, and finally suggest a strategy for identifying the bunchlets within the other structures appearing at the image plane of the spectrometer. Specifically, by placing the stigmatic focus on one "rung" of the ladder after another over a series of data aquistion runs, we can optimize our chances of observing accelerated bunchlets, especially if they lay between or straddle the rungs on the aforementioned betatron ladder.

* The work at UCLA was supported by DOE grant DE-FG02-92-ER40727 and NSF grant PHY-0936266. Work at SLAC was supported in part by Department of Energy contract DE-AC02-7600515.
#cclayton@ucla.edu

Copyright © 2013 CC-BY-3.0 and by the respective authors

ISBN 978-3-95450-138-0

SELF AND IONIZATION-INJECTION IN LFWA FOR NEAR-TERM LASERS*

A.W. Davidson, W. Lu, M. Zheng, C. Joshi, L.O. Silva, J. Martins, R.A. Fonseca, W.B. Mori
UCLA, Los Angeles, CA 90024, USA

Abstract

In plasma based acceleration (PBA), the methods of injecting high quality electron bunches into the accelerating wakefield is of utmost importance for various applications, including next generation light sources and high energy colliders. Numerous simulations are being conducted in order to study various methods of injection and to optimize the beam parameters. Particle-In-Cell simulations using codes such as OSIRIS are used to model PBA. 3D simulations are possible in some cases but are computationally expensive. 2D simulations are computationally less expensive, but 2D simulations in cartesian coordinates only provide qualitative agreement and 2D simulations in cylindrical coordinates cannot model laser wakefield acceleration (LWFA) at all and cannot include important physics such as hosing and low mode azimuthal mode asymmetries for particle beam drivers (PWFA). Here we discuss one method for reducing the computational load of a 3D simulation into those comparable to a 2D simulation that can model LWFA and include hosing. It utilizes a truncated azimuthal mode expansion. We describe how this expansion has been included into the OSIRIS simulation framework and show preliminary results.

INTRODUCTION

Simulations have played an essential role in the development of plasma based acceleration from the seminal work of Tajima and Dawson to the very present. Simulations are used to model both laser wakefield acceleration (LWFA) and plasma wakefield acceleration (PWFA). These simulations have evolved from 1D simulations to demonstrate the feasibility of new ideas to full 3D simulations that model current experiments one to one and that model parameters out of reach of current experiments. Although 3D simulations are now possible they are still computational expensive, therefore, when simulating LWFA and PWFA using we often begin with a series of 2D simulations over a range of parameters. The parameters are either for an ongoing experiment, for a future experiment, or for understanding a new theory or concept. We then have to perform a few large-scale 3D simulations to determine in what manner and to what degree the 2D simulations replicate a more realistic result.

*This work was supported by DOE awards DE-FC02-07ER41500, DE-SC0008491, DE-FG02-92ER40727, and DE-SC0008316, and by NSF grants NSF PHY-0904039 and NSF PHY- 0936266. Simulations were carried out on the UCLA Hoffman 2 Cluster, and Dawson 2 Cluster.

DIFFERENCES IN 2D AND 3D SIMULATIONS

One topic that is receiving much theoretical, computational, and experimental attention is how to best inject electrons into a plasma wave wakefield. One concept is to use field ionization to create electrons inside the wake. An important question is how do the 2D simulation results compare to those from otherwise identical 3D simulations. When using a laser, it is not possible to use 2D azimuthally symmetric simulations as such simulations only allow radially polarized modes. Therefore, 2D cartesian geometry are used and in such simulations both structure of the wakefield and the evolution of the laser can be very different. We provide examples of the differences by showing results from a a series of 2D and 3D simulations that were performed to model experiments conducted using the Callisto laser at LLNL. These simulations highlight some of the differences we see and the importance of the including full 3D physics. In these simulations a linearly polarized, 60 fs laser was focused into an "Injection Section" that is composed of 99.5% He and 0.5% N. After the laser propagates 1.5 mm in the injection section, it enters an "Acceleration Section" composed entirely of He. The total plasma density is $n_p = 1 \times 10^{18}$ cm^{-3} aside from the 0.5 mm up ramp at the beginning. Simulations were conducted with a 100 TW and a 500 TW laser beam. The spot size was 20.0 μm for the 100 TW case, and 26.2μm for the 500 TW simulation.

As can be seen from Table 1, the peak energy of the trapped electrons can be significantly different between the 2D and 3D simulations. Another notable difference is that in the two 2D simulations, a comparable number of particles are trapped whereas in the 3D simulations 3.9 times more particles are trapped for the 500TW laser than for the 100TW laser. And in the 2D cartesian simulations only the charge per unit length that is trapped can be obtained. These differences illustrate that if one uses 2D simulations to optimize the process one can be led very far astray.

There is another notable qualitative difference in the 2D and 3D 500 TW simulation. If you look at the particle energy spectrums about 3 mm into the plasma (Figures 1 and 2), you see that there is a large, lower-energy peak exclusively in the 3D simulation. Although this peak eventually falls out, it dynamically affects the shape and the evolution of the wake. The 2D simulation fails to capture this process. Although not shown the evolution of the laser is also very different.

Copyright © 2013 CC-BY-3.0 and by the respective authors

LASER-PLASMA INTERACTION STUDIES USING ABOVE CRITICAL DENSITY GAS JET PLASMAS AND A MULTI-TW CO_2 LASER*

C. Gong, S. Tochitsky, J. Pigeon, C. Joshi, Neptune Laboratory, Department of Electrical Engineering, University of California Los Angeles, CA, 90095, USA

Abstract

CO_2 laser-plasma interaction provides a unique parameter space for particle acceleration in a gas jet plasma taking place at a critical plasma density $n_{cr} \sim 10^{19}$ cm^{-3} and even at higher densities (3~10 n_{cr}) of 10μm radiation. Here we report the latest results of our study of electron acceleration in a wide range of plasma densities 1~10 n_{cr} using a multi-TW CO_2 laser system at the UCLA Neptune Laboratory. To gain insight into plasma density profile evolution during ~120 ps long CO_2 laser-plasma interaction, we used laser interferometry with two 1 ps, 532 nm probe pulses with variable delay of 5~120 ps. The knowledge of spatial distribution of accelerated electron beam transported through the overdense gas plasma is critically important for minimizing laser beam filamentation and for understanding influence of other laser-plasma instabilities. This should allow for optimization of CO_2 laser driven shock wave acceleration of low-divergence monoenergetic ion beams [1].

INTRODUCTION

The interaction of short high-intensity laser pulses with an overdense plasma can produce forward directed multi-MeV ions and electrons. Electrons heated/accelerated by the laser pulse can drag ions with them due to the space charge separation. Studying the spatial distribution of accelerated electrons can help to optimize the quality and yield of ion beams and is also important for understanding laser-plasma instabilities.

At the UCLA Neptune laboratory, a ~120 ps CO_2 laser train of 3ps pulses separated by 18ps with a peak intensity up to ~4×10^{16} W/cm^2 is used to study overdense laser plasma interaction in a helium gas jet. One of our goals is to optimize the ion acceleration by collisionless shock waves [1]. In order to gain an insight into the plasma density profile evolution during the CO_2 laser pulse train, a two-frame interferometry using 1ps, 532nm light has been developed. An adjustable temporal delay 5~120ps between pulses allows for optical probing of the laser/plasma interaction region. Through a careful analysis and comparison of the two-frame interferogram, the hole boring speed of the above critical density layer pushed by the radiation pressure along the laser propagation axis can be measured. Also, forward directed electron and ion beam is recorded on the LANEX phosphor screen to analyse its spatial distribution and divergence. A permanent magnetic dipole with ~600 Gauss magnetic field is placed before the LANEX phosphor screen to estimate the energy of particle beams.

*Work supported by DOE grant DE-FG02-92-ER40727, NSF grant PHY-0936266 at UCLA

EXPERIMENTAL SETUP

Target Chamber

The CO_2 Master Oscillator Power Amplifier system having a multi-terawatt peak power is used in the experiment. Due to a modulated gain spectrum of the CO_2 molecule, a ~3ps CO_2 laser seed pulse evolves into a ~120ps long pulse train after amplification. Each individual pulse within the pulse train preserves the original pulse width and is separated from the adjacent pulse by ~18ps.

The experimental arrangement in a target chamber is shown in Fig. 1.

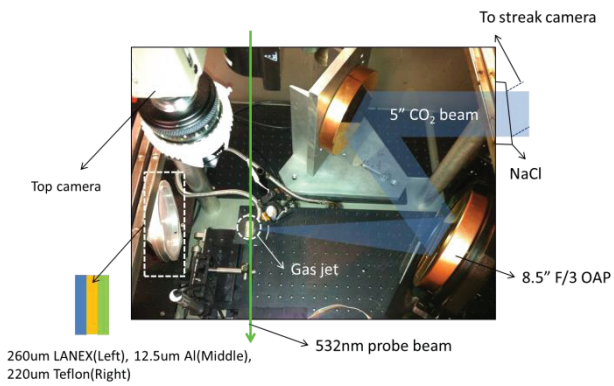


Figure 1: Experimental setup in the target chamber.

A 5" diameter CO_2 laser beam with an energy of ~60J is coupled into the target chamber through an 8" NaCl window mounted on a 4° wedged flange. The back reflection of the beam from the salt window is combined with a red diode laser beam in a CS_2 Kerr modulator. The red pulse modulated by the high intensity 10μm CO_2 laser is analysed by a Hamamatsu streak camera (Model: C5680-21) for the temporal structure measurement of the CO_2 pulse. The beam inside the chamber is focused in a 2mm diameter gas jet by an 8.5" F/3 off-axis parabolic mirror. Using an IR camera, we have characterized the spatial profile of the unamplified CO_2 laser beam by scanning along the laser axis (Z-scan) which is shown in Fig. 2. The measured spot size is w_o = 48μm. Using this spot size and an estimate of the energy contained in the most intense of the 3ps pulses (~20%) in the train of pulses, we estimate that a peak a_o of >1 can be achieved in these experiment. Here a_o is the normalized vector

Copyright © 2013 CC-BY-3.0 and by the respective authors

ISBN 978-3-95450-138-0

RESULTS OF THE SHORT PULSE DRIVEN LLNL/UCLA IFEL EXPERIMENT*

J.T. Moody, P. Musumeci
Department of Physics and Astronomy, UCLA, Los Angeles California, USA
G.G. Anderson, S.G. Anderson, S. Betts, S. Fisher, D. Gibson, A. Tremaine, and S. Wu
Lawrence Livermore National Laboratory, Livermore, California, USA

Abstract

The results of the LLNL/UCLA inverse free electron laser (IFEL) experiment are presented. A 500 mJ 120 fs Ti:Saph laser pulse interacts with a short electron beam in a planar undulator tapered both in magnetic field strength and period to accelerate the electron beam. The tapering of the undulator maintains resonant energy exchange between the laser and electron beam while the electron beam's energy increases. We observe an energy modulation from 77 MeV to 120 MeV. Through use of simulations that are consistent with the observed data, we report a peak acceleration gradient of at least 180 MeV/m.

INTRODUCTION

The growing expense of high energy electron accelerators has produced a demand for increasingly compact, high gradient accelerators than traditional rf accelerators. Because of breakdown which occurs at around 100 MeV/m for traditional rf structures, shorter wavelengths must be used to drive the acceleration. The inverse free electron laser (IFEL) [1] is a laser driven electron accelerating scheme that has the advantage of taking place in vacuum.

In this acceleration scheme, a high intensity laser copropagates with a relativistic electron beam through an undulator. As the electron beam oscillates in the periodic magnetic field, it's transverse velocity allows for coupling to the laser's transverse electric field. If the laser's frequency, electron beams energy, and the magnetic field's strength and period are set such that the electron beam slips one laser wavelength per undulator period, energy is maximally transferred between the laser and the electron beam. As the electron beam becomes accelerated by this period averaged effect, the undulator must be tapered in order to maintain the resonance condition and facilitate efficient energy exchange.

This concept was demonstrated at Neptune at UCLA [2], as well as STELLA at Brookhaven National Lab (BNL) [3]. Renewed interest in IFEL has allowed experiments to be performed at Lawrence Livermore National Lab and BNL. While BNL's Rubicon [4] focused on use of a helical undulator to give stronger coupling to a circularly polarized CO_2 laser at low rep rate (.05Hz), the LLNL IFEL Project focuses on exploiting the high repetition rate of TW class Titanium Sapphire laser systems (10 Hz) and achieving high gradient acceleration with a sub picosecond driving laser. This paper covers the preliminary results of the LLNL IFEL experiment.

THEORETICAL BACKGROUND

If we define a pondermotive phase as $\Psi = (k + k_w)z - \omega t - \Phi_G$, we can use this phase as the coordinate of an electron in the period averaged pondermotive field. Here k and k_w are the radiation wave number and undulator wave number, respectively, and ω is the radiation frequency, and Φ_G is the Guoy phase shift.The electron's conjugate momentum then can be described by γ, the electron's energy normalized by it's rest energy. The longitudinal equations of motion then can be described by:

$$\frac{d\gamma}{dz} = \frac{1}{2\gamma} k K_L K J J sin\Psi \tag{1}$$

$$\frac{d\Psi}{dz} = k_w - k\frac{1+\frac{K^2}{2}}{2\gamma^2} - \frac{1}{z_r(1+\frac{z}{z_r}^2)} \tag{2}$$

Where K_L is the radiation parameter equal to eE_0/kmc^2 and E_0 is the peak radiation electric field, m is the electron mass, and c is the speed of light. K is the undulator strength parameter and is equal to $eB_w/k_w mc^2$ and B_w is the peak undulator magnetic field. JJ is the coupling factor, which is a result of using a planar undulator. z_r is the Rayleigh range, and the final term in the pondermotive phase evolution is due to the Guoy phase shift.

If we allow the left hand side of Eq. 2 to go to zero, this gives the condition for which the pondermotive phase does not evolve. γ_r is then resonant electron's normalized energy. Plugging into Eq. 1 we have a description of evolution of a resonant particle as it is accelerated with a stationary phase. Expanding about the resonant phase,Ψ_r, we have a pondermotive potential that goes like $cos\Psi + \Psi sin(\Psi_r)$. This potential creates a stable accelerating bucket whose width in phase is dependent on the resonant phase. If the resonant phase is near zero, the bucket is wide and traps many particles at the cost of reduced accelerating gradient whereas if the resonant phase is near $\pi/2$ then the gradient is maximum but only a single point in phase space can be accelerated. If the laser intensity is not matched to the design, the injected electrons can fall out of the pondermotive bucket and resonant acceleration ceases. Non trapped particles interaction increases the energy spread of the non-captured distribution. Beyond the 1-D equations of motion, the particle tracking code cbeam [5] was used together with

* This work supported by US DOE Grant DE-FG02-92ER40693,Defense of Threat Reduction Agency award HDTRA1-10-1-0073 and University of California Office of the President award 09-LR-04-117055-MUSP.

Copyright © 2013 CC-BY-3.0 and by the respective authors

DEVELOPMENT OF A HIGH-REPETITION RATE TW CO_2 LASER DRIVER FOR A COMPACT, VARIABLE SPECIES ION SOURCE

J. Pigeon, S. Tochitsky, C. Joshi, UCLA, Los Angeles, CA 90095, USA

Abstract

CO_2 laser-driven ion acceleration has been used to generate monoenergetic, MeV proton beams from a gas jet plasma. Use of a gas jet is advantageous because it offers interactions at a density around the critical plasma density for 10 μm pulses (10^{19} cm^{-3}) and can be run at a repetition rate of 1-100 Hz. This opens the possibility to create a variable species ion source easily switchable from protons to light ions (*e.g.* He, N and Ne). A TW class high repetition rate CO_2 laser driver is required for implementing such a source. At the UCLA Neptune Laboratory we have built a 1 Hz CO_2 laser system and demonstrated the amplification of 20 GW, 3 ps laser pulses. However, peak powers on the order of 0.2-1 TW are required for producing ~ MeV proton beams. Here we report progress on an ongoing project in which the peak power of our laser system will be increased by nonlinear chirping and broadening followed by pulse compression. We also discuss a possible strategy for generating 300 mJ, 300 fs CO_2 laser pulses for driving a 1 – 10 Hz laboratory ion source.

INTRODUCTION

There are applications in material science, radiation biology and medical physics [1] that would benefit from a MeV class, multiple species ion accelerator. The cost of such a machine, if built using conventional accelerator technology, is prohibitively expensive for most universities and hospitals. Laser driven ion acceleration (LDIA) may be one avenue for reducing this cost, either as a stand-alone accelerator or as an injector for a conventional accelerator.

Recent experiments have demonstrated monoenergetic, MeV ion acceleration from over-dense ($\omega_{plasma} \geq \omega_{Laser}$) laser plasma interactions (LPI) [2]. High power CO_2 lasers are an attractive candidate for LDIA because, at a wavelength of 10 μm, the critical plasma density can be achieved using a gas jet or cell. In contrast, the majority of high power lasers operate at wavelengths from 0.8 – 1 μm and must use solid targets to study over-dense LPI. Due to the potential ease in targetry, 10 μm drivers are the most technological option for a multi-species, laser driven ion accelerator.

CO_2 LDIA studies have been limited to single shot experiments even though optimization of the laser-plasma interaction may only be possible at a high repetition rate. Although gas jet technology can be scaled up to 100 Hz, experiments have suffered due to limitations in the repetition rate of the driver. At the UCLA Neptune Laboratory we have recently developed a 20 GW, 3 ps CO_2 laser system which operates at 1 Hz [3]. Peak power on the order of 0.2 TW is required for acceleration of ~ 3 MeV protons from a H_2 plasma. In this paper we investigate a method to increase the peak power of our system by using nonlinear chirping and broadening followed by compression. Further we propose a path to a 300 mJ, 300 fs CO_2 laser to be used as a 1 – 10 Hz driver for a compact, multi-species ion source.

STATUS OF THE 1 HZ, PICOSECOND CO_2 LASER SYSTEM

CO_2 lasers have some technological advantages that cannot be matched by solid state laser systems. The gas medium can withstand intensities up to the ionization threshold, $\geq 10^{12} \frac{W}{cm^2}$, which allows for direct amplification of short pulses. Further, gas discharge technology can be scaled in repetition rate and provides high wall plug efficiency. Despite these advantages, high peak power amplification in CO_2 is difficult due to the relatively narrow bandwidth present in gaseous media. Gas lasers typically provide a bandwidth of 3.5 GHz/atm such that, at 1 atm of pressure, a CO_2 laser can only produce pulse lengths greater than 1 ns. Unfortunately, pulse lengths on the order of picoseconds or less are necessary to reach the relativistic intensities required for LDIA.

At the UCLA Neptune Laboratory we achieve broad band CO_2 laser amplification by relying on two broadening mechanisms: pressure and field broadening. Figure (1) shows simulated gain spectrums of the CO_2 medium at 1, 10 and 25 atm of pressure. At 1 atm of pressure the gain spectrum consists of a family of 3.5 GHz, rovibrational lines.

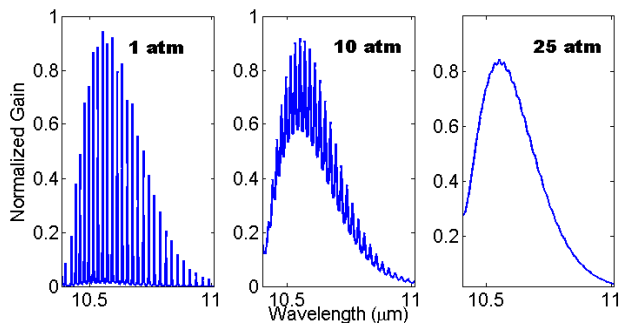


Figure 1: Simulations of the CO_2 gain medium at 1, 10 and 25 atm of pressure for the 10P branch.

At high pressures the collisional time becomes comparable to the radiative transition time which results in line broadening. At 25 atm of pressure the gain spectrum is a continuum across the entire 1.2 THz branch. In practice modules with 10 atm of pressure are used as it is difficult to obtain stable discharge at pressures greater than this. The presence of residual modulation in the gain

Copyright © 2013 CC-BY-3.0 and by the respective authors

ISBN 978-3-95450-138-0

TECHNIQUE FOR DETERMINING THE MAXIMUM ENERGY OF A DISPERSED ELECTRON BEAM FROM LASER WAKEFIELD ACCELERATORS*

J. Shaw#, N. Vafaei-Najafabadi, K.A. Marsh, C. Joshi, UCLA, Los Angeles CA 90024, USA

Abstract

We present a new curve-fitting method based on asymptotically fitting transverse size contributions to the measured electron spectrum that is capable of determining the maximum energy of a dispersed electron beam from a laser wakefield accelerator regardless of its transverse size. This method is applied to experimental spectra obtained in the characterization of a new injector stage to show that Direct Laser Acceleration may be an additional acceleration mechanism in laser wakefield accelerators where the laser pulse is long enough to overlap the trapped electrons.

INTRODUCTION

The energy of electron beams from an accelerator is typically measured by magnetically dispersing the electron beam onto a detector. Because the magnetic dispersion is highly nonlinear, the lower-energy charge generally experiences higher deflection and is well dispersed on the detector, whereas the higher-energy charge is deflected less and therefore is less dispersed. This small spatial separation leads to reduced resolution at higher energies and makes it challenging to accurately determine the maximum energy of an electron beam in the 10s to 100s of MeV energy range using a non-imaging but dispersive magnet. The issue of determining the maximum energy of an electron beam is further complicated when that beam has a large transverse size at the detection plane. In such a case, it is difficult to determine whether the signal at high energies on the detector is actually high-energy electrons or if it is an artifact of the transverse size of the beam. This proceedings describes a curve-fitting method to determine the maximum energy of an electron beam regardless of its transverse size.

EXPERIMENT

This curve-fitting method was developed to accurately characterize a newly-designed laser wakefield acceleration (LWFA) injector, which could produce ~100 MeV electron bunches in gas cells with lengths of 400 μm to 1100 μm [1, 2]. The Ti:Sapphire laser used to do this characterization had a pulse width of 45 fs FWHM and an a_0 of ~2. During the characterization, the injector was tested over a range of plasma densities from 8.1 x 10^{18} cm^{-3} to 2.5 x 10^{19} cm^{-3}. For these laser and plasma parameters, the LWFA is not operating in the ideal blowout regime [3]. Therefore, self-trapping of electrons in the wake will not occur without significant laser pulse evolution. To eliminate the need for laser pulse evolution and thus devote the length of the injector to acceleration, the ionization injection technique [4] was employed. As a result, the spectrum of the accelerated electrons was typically continuous with an exponentially decreasing tail as shown in Figure 1(a). To demonstrate that the injection stage was capable of producing ~100 MeV electrons as designed, it was critical to accurately measure the maximum energies of these electron beams even though they have exponentially decreasing tails. The method described here was found to converge on many real data sets and enabled us to determine the maximum energy of an electron beam regardless of its transverse size, its energy spread, or its exponentially decreasing tail.

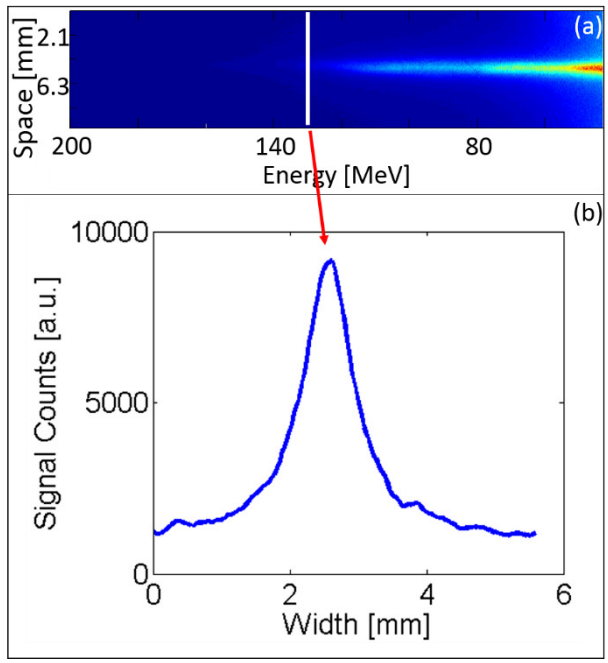


Figure 1: (a) Linearized electron spectrum showing the location of the transverse lineout taken at 130 MeV. (b) Typical raw transverse lineout of the electron spectrum taken at 130 MeV before being rotated and linearized.

DETAILS OF THE METHOD

The method separates out the transverse size contribution by comparing the signal in the dispersed plane to the signal in the transverse (undispersed) plane. In the dispersion plane, the lineout of the electron spectrum has the combined effects of energy dispersion and transverse size. The transverse lineout, however, only

*Work supported by: DE-AC52-07NA27344, DE-FG03-92ER40727, DE-FG02-92ER40727, NSF Grants No. PHY-0936266, DGE-0707424, PHY-0936266; DoD, Air Force Office of Scientific Research NDSEG Fellowship, 32 CFR 168a (Shaw).
#jshaw05@ucla.edu
Copyright © 2013 CC-BY-3.0 and by the respective authors

SUPPRESSION OF THE TRANSFORMER RATIO DUE TO DISTRIBUTED INJECTION OF ELECTRONS IN A PLASMA WAKEFIELD ACCELERATOR*

N. Vafaei-Najafabadi†, W. An, C.E. Clayton, C. Joshi, W. Lu‡, K.A. Marsh,
W.B. Mori, UCLA, Los Angeles, CA 90095, USA
E. Adli§, C.I. Clarke, S. Corde, J.-P. Delahaye, R.J. England, A.S. Fisher, J. Frederico, S.J. Gessner,
M.J. Hogan, S.Z. Li, M.D. Litos, D. Walz, Z. Wu, SLAC, Menlo Park, CA 94025, USA
P. Muggli, Max Planck Institute for Physics, Munich, Germany

Abstract

Evidence of beam loading due to distributed injection in Plasma Wakefield Accelerator experiments carried out at the FACET facility at SLAC during the year 2012 is presented. The source of the injected charge is tunnel ionization of Rb^+ inside the wake, which occurs along the length of the interaction at each minima of envelope betatron oscillation. Rb was used specifically to mitigate the problem of head erosion, which limited the energy gain in earlier experiments using Li that were carried out at FFTB in SLAC. In the present experiment however, electrons produced via secondary ionization of Rb were injected in the wake and led to a severe depletion of the accelerating wake, i.e. beam loading, which is observed as a reduction of mean, i.e. measured, transformer ratio. This "dark current" limitation on the maximum achievable accelerating gradient is also pertinent to other heavier ions that are potential candidates for high-gradient PWFA.

INTRODUCTION

A Plasma Wakefield Accelerator (PWFA) uses a short, dense, high current electron beam to drive a high amplitude wake [1], which can accelerate electrons with gradients that are orders of magnitude larger than the conventional accelerators [2]. When the beam density (n_b) is higher than the plasma density (n_p), the electron beam expels all of the plasma electrons locally and creates a blowout region, a structure of uniform ion density that accelerates and focuses electrons [3]. The FACET Facility at SLAC [4] is currently used for further research on PWFA.

Two particular physics problems that have to be addressed are the problems of head erosion [5] and ion motion [6]. Head erosion is a physical effect limiting the length of the acceleration. Briefly, if the plasma is generated by the beam via field ionization, as was the case in [2], the part of the beam that ionizes the medium into plasma is not in the blowout region and therefore continues to expand at a rate that is dependent on its emittance. The expansion then causes the ionization front to recede back in the frame of the beam. The rate of this "head erosion" effect is dependent on $1/\gamma$, ϵ_n, and $\mathrm{IP}^{1.73}$ [7], where ϵ_n is the normalized emittance and IP is the ionization potential of the element that is being ionized. Ion motion is a problem because it leads to distortion of the linear focusing force in the blowout regime, and it occurs for $n_b/n_p > m_i/m_e$.

Both of these problems can be addressed by switching Li (used previously [2]) to a higher Z element, such as Rb. With an ionization potential that is 23% smaller than Li, the application of the scaling equations for head erosion implies that the interaction length in Rb would be 40% longer, leading to a proportional increase in maximum achievable energy. Additionally, with an atomic mass of over 12 times larger than Li, Rb ions are an order of magnitude less mobile. On the other hand, the ionization potential of the second Li electron is so high (75.6 eV) that it is not exceeded during the experiment. This is not the case with Rb. The second ionization potential of Rb is 27.3 eV, which could be reached during the experiment. Here, we show that this secondary ionization of Rb is responsible for significantly reducing the energy gradient. The suppression of the accelerating gradient is diagnosed in this experiment by monitoring average transformer ratio $\langle T \rangle$, which can be measured in experiments as $\Delta W^+/\Delta W^- = \int E^+ dz / \int E^- dz$.

EXPERIMENTAL SETUP

The 3 nC, 20.35 GeV electron beam from the FACET facility at SLAC was focused on the rising edge of a column of Rb vapor at the neutral density of 2.7×10^{17} cm^{-3} in a heat pipe oven [8] (Fig. 1). Rb gas was contained in the oven using Ar as buffer. Therefore, the density of Ar rose as the density of Rb fell in such a way that the total pressure stayed the same. The bunch length of the beam was monitored for every shot using the integrated transition radiation signal, which was generated as the beam traversed a 1 μm thick Ti foil and was measured by a pyroelectric detector (pyro). This signal correlated with a THz Michelson interferometer (Fig. 1) and was the main diagnostic of the bunch length. Two absolutely calibrated toroids before and after

*The work at UCLA was supported by DOE grant DE-FG02-92-ER40727 and NSF grant PHY-0936266. The simulations were carried out on the Hoffman cluster at UCLA. Work at SLAC was supported by Department of Energy contract DE-AC02-7600515.

† navidvafa@ucla.edu
‡ Also at Tsinghua University, Beijing 100084, China
§ Also at Department of Physics, University of Oslo, 0316 Oslo, Norway

ISBN 978-3-95450-138-0

Copyright © 2013 CC-BY-3.0 and by the respective authors

SIMULATION OF LASER WAKEFIELD ACCELERATION IN THE LORENTZ BOOSTED FRAME WITH UPIC-EMMA

Peicheng Yu*, Viktor K. Decyk, Weiming An, Frank S. Tsung, Warren B. Mori, UCLA, CA 90024
Xinlu Xu, Wei Lu, Tsinghua University, Beijing 100084, China
Jorge Vieira, Ricardo A. Fonseca, Luis O. Silva, Instituto Superior Técnico, Lisbon, Portugal

Abstract

Simulating Laser wakefield acceleration (LWFA) in a Lorentz boosted frame in which the plasma drifts towards the laser with v_b can speedup the simulation by factors of γ_b^2, where γ_b is the Lorentz factor of the boosted frame. To eliminate the high frequency numerical instability induced by relativistic plasma drift in these simulations, we develop a fully parallelized, multi-dimensional, particle-in-cell code that uses a spectral solver to advance the Maxwell's equations. This new EM-PIC code is called UPIC-EMMA and it is based on the components of the UCLA PIC framework (UPIC). It is shown that using UPIC-EMMA, LWFA simulations in the boosted frames with large γ_b can be conducted without any notable numerical instability. We also benchmark the UPIC-EMMA results with OSIRIS in the lab frame, an EM-PIC code with a finite difference time domain (FDTD) Maxwell solver, and good agreements are found.

INTRODUCTION

Laser wakefield acceleration [1] offers the potential to construct compact accelerators that has a numerous potential applications, and the last ten years has seen an explosion of theoretical and experimental results. Due to the strong nonlinear effects in the laser plasma interaction involved, numerical simulations, in particular particle-in-cell (PIC) simulation, are critical in exploring the physics of LWFA. Recently, it was shown that by performing the simulation in an optimal Lorentz boosted frame with velocity v_b, the time and space scales to be resolved in a numerical simulation may be minimized [2, 3, 4]. The basic idea is that in the boosted frame the plasma length (the laser propagation distance) is Lorentz contracted while the plasma wake wavelength and laser pulse length are Lorentz expanded, which lead to savings of factors of $\gamma_b^2 = (1 - v_b^2/c^2)^{-1}$ as compared to a lab frame simulation using the so-called moving window [5].

However, in the boosted frame simulations noise from a numerical instability can be an issue. As discussed in [6, 7, 8, 9, 10], the noise results from a numerical Cerenkov instability induced by the plasma drifting with relativistic speeds on the grid. According to the dispersion relation this numerical instability is attributed to the coupling between the wave-particle resonances with EM modes (including aliased modes) in the numerical system. The pattern of the instability in Fourier space can be found at the intersections of the EM dispersion relation of the solver used in the simulation algorithm, and the wave-particle resonances [8, 9, 10].

In order to mitigate this instability, it is preferable to use an EM solver that eliminates the numerical instability at the main beam resonance [10]. When using a spectral solver that spatially advances the EM fields in Fourier space, its EM dispersion curve assures no instability pattern at the main beam resonance. In addition, the pattern at the first space aliasing beam mode is found to be located at high $|\vec{k}|$ values that are far away from the interested physics. For the spectral solver the numerical Cerenkov instability of the first aliased beam mode is located at a predicted pattern in $\vec{k}$ space so it can be conveniently eliminated by applying simple filters directly in $\vec{k}$ space.

We developed a fully parallelized three-dimensional electromagnetic spectral PIC code called UPIC-EMMA that was built using components of the UCLA PIC Framework called UPIC [11]. A spectral EM-PIC code has the same basic flow chart as a finite-difference-time-domain (FDTD) PIC code. In a spectral EM-PIC code both the charge and current are deposited on the mesh from the particles; the forces exerted on the particles are interpolated from the mesh points, and particles are advanced using the Lorentz forces. The main difference between the spectral PIC code and FDTD PIC code is the solver used to advance the electromagnetic field and that all field quantities, including the charge and current densities, are defined at the same locations on a cell (no Yee mesh [12] is needed). In a spectral PIC code the charge and current are directly deposited, and a strict charge conserving current deposit is not needed because Gauss's law is solved at each time step using the charge density.

There are no dispersion errors for light waves due to the grid (however there are errors from the finite time step). This is a significant advantage of the spectral solver, whereas a FDTD code describes the $[k]_i$ operator to $\mathcal{O}(k_i\Delta x_i)^3$, the spectral code has no errors in the finite $[\vec{k}]$ operator. In addition, when including time step errors, the numerical dispersion of a spectral PIC code is superluminal, while that of the FDTD code is sub-luminal. The more accurate and superluminal aspect of the EM dispersion relation provided by the spectral solver (together with the simple filters) is crucial for eliminating the numerical Cerenkov instability. This ensures no non-physical interaction between waves and particles in the first Brillouin zone for the spectral PIC code.

* tpc02@ucla.edu

Copyright © 2013 CC-BY-3.0 and by the respective authors

POSSIBILITY OF CONFIRMING SMI THROUGH ENERGY SPECTRUM WITH THE 1 nC ATF ELECTRON BUNCH

Y. Fang*, University of Southern California, Los Angeles, CA
P. Muggli, University of Southern California, Los Angeles, CA
and Max Planck Institute for Physics, Munich, Germany
W. Mori, University of California, Los Angeles, Los Angeles, CA

Abstract

In this paper, we demonstrate numerically the possibility of measuring the energy gain/loss experimentally to confirm the self-modulation instability (SMI) development with electron bunch parameter available at Accelerator Test Facility (ATF) of Brookhaven National Laboratory (BNL). The results also show that due to plasma wakefield dephasing during the SMI development, the actual energy gain/loss by drive bunch particles is lower than deduced from maximum accelerating fields. All the simulations are performed with the 2D-cylindrically symmetric partilcle-in-cell code OSIRIS [1].

INTRODUCTION

We have successfully demonstrated the excitation of multiple-periods plasma wakefields by a 50 pC bunch with square current profile available at the Accelerator Test Facility of Brookhaven National Laboratory (BNL-ATF) [2]. These wakefields act as the seed for self-modulation instability (SMI). The experimental data is in excellent agreement with the linear theory and OSIRIS-2D [1] simulation results. With this low 50 pC charge, the SMI does not grow within the 2 cm propagation distance in the plasma density range available in the experiment (10^{15}-10^{17} cm^{-3}), and therefore periodic energy modulation measurements were possible. However, simulations have shown that the SMI of the 1 nC bunch grows significantly and reaches saturation over the 2 cm propagation distance (see Fig. 1 b)). Note that for 1 nC bunch, the beam-plasma interaction is still in the linear regime of the PWFA for the plasma density range as indicated above, i.e., n_b/n_p <0.06. According to linear theory, the initial wakefield amplitude is 20 times higher for 1 nC bunch than that of 50 pC bunch, and this has been confirmed by previous simulations [3]. We here further analyze the simulation results of 1 nC bunch to examine the possibility of measuring the energy spectrum experimentally to confirm the development of SMI. As an example, we take the plasma density of $n_e = 4.85 \times 10^{15}$ cm^{-3} such that $L_{\rm beam}/\lambda_{pe} = 2$. It has been demonstrated that during the development of SMI, the plasma wave phase velocity becomes smaller than the beam velocity, resulting in dephasing between the bunch particles and the wakefields [4, 5]. The following results show that due to such dephasing, the actual energy gain/loss by drive bunch particles is $\approx 25\%$ lower than deduced from maximum accelerating field plots, i.e. assuming the wakefield on the particles do not dephase. However, the resulting energy gain is approximately 2.4 times larger than the case without SMI development. It is therefore still possible to confirm the SMI development through the measurement of resulting energy spectrum in the experiment.

ENERGY GAIN/LOSS

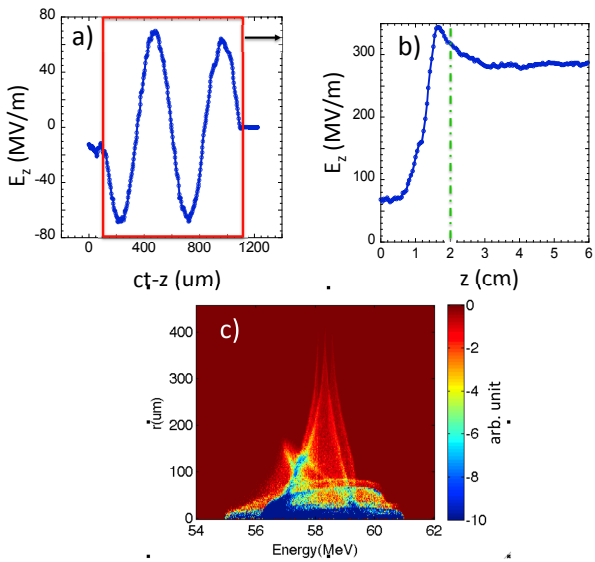


Figure 1: a) The longitudinal wakefield E_z on the axis ($r = 0$) at plasma entrance ($z = 0$) within the bunch. The red rectangle indicates position of the electron bunch. b) The evolution of maximum E_z on the axis ($r = 0$) along the propagation distance. The green line indicates the plasma length in the experiment. c) Electron bunch density in the r, E space, showing the energy spectrum of the beam at plasma exit ($z = 2$ cm). Results are obtained from OSIRIS 2D.

We first assume that there is no SMI growth during the 2 cm propagation for the 1 nC bunch, and therefore the energy gain/loss at the plasma exit can be estimated by multiplying the initial E_z amplitude (at $z = 0$) with 2 cm. Figure 1 a) shows the initial longitudinal wakefield E_z on the axis ($r = 0$) at the plasma entrance ($z = 0$) obtained from simulation, with an acceleration amplitude $E_{z0} \approx 67$ MV/m, which is within $\%5$ difference with the estimation of linear theory (≈ 64 MV/m). Therefore, assuming no SMI growth and hence no E_z amplitude evolution, the energy

* yunf@usc.edu

ISBN 978-3-95450-138-0

Copyright © 2013 CC-BY-3.0 and by the respective authors

CURRENT INDUCED IN VACUUM CHAMBER DURING NSLS-II BOOSTER RAMP*

S. Gurov#, V. Kiselev, S. Sinyatkin, BINP SB RAS, Novosibirsk, Russia

Abstract

Fields that arise in the booster magnets during a ramp induce currents in the vacuum chamber, including currents through the "ground". These induced currents produce magnetic fields, which influence the beam. Calculations and simulations for the NSLS-II booster are discussed.

INTRODUCTION

Budker Institute of Nuclear Physics has built the booster for NSLS-II. The booster has been designed [1, 2], produced [2], delivered, assembled and tested [3]. The booster is intended for continuous and reliable acceleration of electron beam from a minimum 170-MeV injection energy to a maximum energy of 3.15 GeV at an average beam current of 20 mA and a 2 Hz repetition rate.

The combined-function dipole magnets have magnetic fields with quadrupole and sextupole components. The basic parameters of the dipoles are given in Table 1.

Table 1: Specification of the Dipoles

Dipole parameters	BF	BD
Number	28	32
Effective magnetic length	1.24 m	1.30 m
Angle	3.2673°	8.3911°
Vertical gap	±14 mm	±13 mm
Field injection	0.03068 T	0.07516 T
Field extraction	0.46021 T	1.12734 T
Quadrupole K1, extraction	0.82 m^{-2}	-0.55509 m^{-2}
Sextupole K2, extraction	3.6 m^{-3}	-4.3 m^{-3}
Good field region	±12 x ±20 mm	
Field quality in the good field region, ΔB/B0	± 1·10^{-3}	

During a ramp, the fields arising in the booster magnets induce currents in the vacuum chamber, including currents through the "ground".

CURRENT THROUGH THE "GROUND"

The current through the "ground" is the total current I_{total} through the vacuum chamber:

$$I_{total} = \oint\!\!\iint \sigma E_z(r,\varphi,t)\,dS \qquad (1)$$

The integrating is done over the entire vacuum chamber cross-section with the conductivity σ.

The induced electric field can be found from the Maxwell-Faraday equation,

$$rot\vec{E} = -\frac{1}{c}\frac{\partial \vec{B}}{\partial t}, \qquad (2)$$

with $B_z = 0$ and $\frac{\partial \vec{E}}{\partial z} = 0$ taken into account.

We have the following equations:

$$\frac{1}{r}\frac{\partial E_z}{\partial \varphi} = -\frac{1}{c}\frac{\partial B_r}{\partial t} \quad \text{and} \quad \frac{\partial E_z}{\partial r} = \frac{1}{c}\frac{\partial B_\varphi}{\partial t} \qquad (3)$$

A magnet with symmetry in its median plane has the following magnetic field in the aperture:

$$B_r(r,\varphi,t) = \sum_{n=1}^{\infty} B_n(t)\cdot r^{n-1}\sin(n\varphi)$$
$$B_\varphi(r,\varphi,t) = \sum_{n=1}^{\infty} B_n(t)\cdot r^{n-1}\cos(n\varphi) \qquad (4)$$

As result,

$$E_z(r,\varphi,t) = E_{0z}(t) + \frac{1}{c}\sum_{n=1}^{\infty}\frac{\partial B_n(t)}{\partial t}\cdot\frac{r^n}{n}\cos(n\varphi) \qquad (5)$$

Here we get a component $E_{0z}(t)$, which is independent from the coordinates r and φ. This component depends on some external conditions.

If the vacuum chamber is isolated, I_{total}=0 and we get $E_{0z}(t)$ from Eq. (1) and Eq. (5).

If the vacuum chamber is grounded on the both sides of magnet, we can find $E_{0z}(t)$ in the following way. There is a field line that divides the magnetic field flow into two parts (see Fig. 1). This line crosses the magnet median plane at the point x_o. Let the circuit consist of the ground circuit and a line which is parallel to the beam axis and cross x_o. Then, the magnetic field flow through this circuit does not change during a ramp. Therefore, $E_z(r = x_o, \varphi = 0, t) = 0$, and from equation (4)

$$E_{0z}(t) = -\frac{1}{c}\sum_{n=1}^{\infty}\frac{\partial B_n(t)}{\partial t}\cdot\frac{x_0^n}{n}. \qquad (6)$$

#S.M.Gurov@inp.nsk.su

Copyright © 2013 CC-BY-3.0 and by the respective authors

SELF-CONSISTENT SIMULATIONS OF PASSIVE LANDAU CAVITY EFFECTS*

G. Bassi†, A. Blednykh, S. Krinsky, J. Rose, BNL, Upton, NY 11973-5000, USA.

Abstract

We discuss passive Landau cavity effects for arbitrary fill patterns. We present a new algorithm for the self-consistent calculation of the long-range multibunch interaction and implement it in the parallel OASIS code. As an application, we show numerical simulations with parameters of the passive Landau cavity system of the MAX-IV storage ring, which consists of normal conducting cavities. Together with with the uniform filling case, which is planned for nominal operations of the MAX-IV storage ring, we discuss the case with a gap in the fillings.

EQUATIONS OF MOTION

We assume M bunches, each with N electrons, circulating in a ring with circumference C and revolution period T_0. According to the steady state beam loading compensation scheme shown in Fig.1, for self-consistent simulations of passive Landau cavity effects, the dynamics of the particles in bunch m ($m = 0, .., M-1$), under the one-turn map approximation, is governed by (without radiation damping and quantum fluctuations)

$$\begin{aligned} \delta_{n+1} &= \delta_n \\ &+ \frac{e}{E_0}\Big[V_{gr}\cos\Psi\sin(\phi_s+\theta_L+\Psi-\omega_{rf}\tau_n) \\ &- V_m(\tau_n) - V_{rf}\sin\phi_{s0}\Big], \\ \tau_{n+1} &= \tau_n - \eta T_0\delta_{n+1}, \end{aligned} \tag{1}$$

where n is turn number, e the electron charge, δ is the relative energy deviation with respect to the nominal energy E_0, τ is arrival time and η the momentum compaction. Here V_{gr} (generator voltage) V_{rf} (rf voltage), ϕ_s (synchrotron phase), Ψ (detuning angle) and θ_L (load angle) are the parameters of the main cavity and $\sin\phi_{s0} = U_s/(eV_{rf})$, where U_s is the energy loss per turn. $V_m(\tau_n)$ is the collective voltage induced by the passages of the M bunches through the main and Landau cavities.

The self-consistent calculation of $V_m(\tau_n)$ for a narrow-band resonator wake can be done efficiently by computing averages, via a MonteCarlo integration, of trigonometric functions with respect to the "history" of the bunch densities [3]. For the case of an arbitrary long-range wakefield interaction, see [2], where the collective voltage is calculated via a Taylor series expansion. The algorithm is implemented in OASIS, a self-consistent parallel code for efficient simulations of instabilities driven by short and long-range wakefields [3], and allows the study of passive Landau cavity effects for normal conducting cavities. The case with superconducting cavities is at the moment computationally too expensive. However, we are planning to extend the capability of the algorithm to cover the superconducting case, since our ultimate goal is the study of the passive Landau cavity system of the NSLS-II storage ring, which is planned to operate with superconducting cavities. Notice that Eq.(1) provides Robinson damping of the 0 mode by properly detuning the main cavity. This is crucial vhenever the longitudinal radiation damping is not strong enough to suppress the Robinson instability induced by detuning the Landau cavity for bunch lengthening.

UNIFORM FILLINGS

As an application of our current algorithm, we study passive Landau cavity effects with parameters of the MAX-IV storage ring [1] (see Table 1), which will be operated with normal conducting cavities (see Table 2). In our simulations we include only the fundamental mode of the main and Landau cavity. The optimal bunch lengthening can be estimated by calculating the collective voltage induced by equally spaced stationary bunches [4]. According to the parameters of MAX-IV the optimal bunch lenghtening for uniform fillings is $\approx$ 200ps.

In Fig.2 we show self-consistent simulations of Eq.(1) with the OASIS code. OASIS is based on a Vlasov approach and implements a particle tracking method to solve the Vlasov equation, therefore uses $\mathcal{N}$ simulation or representive particles to sample the underlying phase space density, and its number is not necessarily related to the actual number of particles in the bunch N. The simulations of M bunches, each with $\mathcal{N}$ simulation particles, are done in parallel using M processors, by assigning $\mathcal{N}$ of each bunch to a single processor. Eq.(1) is integrated up to 300K turns. The parameters (per cavity) used to solve Eq.(1) are $V_{gr} = 0.495$MV, $\phi_s = 2.728$rad, $\Psi = -1.137$rad and $\theta_L = 0$. The detuning frequency of the Landau cavity is 47.53kHz and the number of simulation particles used is $\mathcal{N} = 100$K. In Fig.2 (left) we plot the bunch length of the bunch train after 300K turns. The red curve represents the numerical result with Landau cavities. The bunch length is roughly constant across the bunch train and approximately equal to 210ps. The curve in blue shows the nominal bunch length of 40ps without Landau cavities. In Fig.3 (top left) we plot the longitudinal density of the bunch train. We clearly see that for uniform fillings the Landau cavities induce roughly the same bunch lenghtening across the train without displacing the bunch centroid.

* Work supported by DOE contract DE-AC02-98CH10886
† gbassi@bnl.gov

ISBN 978-3-95450-138-0

Copyright © 2013 CC-BY-3.0 and by the respective authors

POLARIZATION PROFILE AND SPIN DYNAMICS SIMULATIONS IN THE AGS USING THE ZGOUBI CODE*

Y. Dutheil, L. Ahrens, H. Huang, F. Méot, V. Schoefer
BNL, Upton, Long Island, New York, USA

Abstract

Polarization transmission during the AGS acceleration cycle is critical for the RHIC polarized proton program.Thus drives a strong interest on the exploration of the polarization losses in the AGS. Intrinsic spin resonances are the main source of depolarization in the AGS. This results in the formation of a polarization profile since the strength of such depolarizing resonance depends on the Courant-Snyder invariant of each particle. The Zgoubi code and the AGS Zgoubi on-line model now allow exploration of the formation of the polarization profile during the acceleration cycle using multi-particle trackings with realistic beam and machine conditions. This paper introduces the specifics of these simulations and compares some of the latest simulated and experimental results.

INTRODUCTION

Acceleration of polarized protons in a synchrotron requires particular schemes to conserve the polarization. Two main types of depolarization resonances can reduce the overall polarization of the beam. The imperfection resonances are driven by vertical closed orbit distortions and occur when $Q_s = I$ with Q_s the spin tune and I an integer [1]. The intrinsic resonances are driven by the vertical betatron motion and occur when $Q_s = I \pm Q_y$ with Q_y the vertical tune.

The AGS uses two partial Siberian snakes to overcome the spin resonances [2], usually called *warm* and *cold* snakes. While in a regular synchrotron $Q_s = G\gamma$ (G is the anomalous gyromagnetic g-factor of the proton), the complex helical dipole fields of the Siberian snakes open forbidden bands in the spin tune around the integer values of $G\gamma$, the spin tune gap. The imperfection resonances are avoided since the integer values of Q_s are now forbidden. The vertical intrinsic resonances are overcome by keeping the vertical tune in the spin tune gap, typically around $Q_y = 8.98$.

Despite the use of Siberian snakes polarization losses are observed in the AGS and while the polarization profile at injection is negligible, measurements show significant profiles of polarization in both vertical and horizontal planes after the acceleration. We will present the main candidates that can explain the observed profiles then some simulation methods and results will be compared to measured polarization profiles.

* Work supported by Brookhaven Science Associates, LLC under Contract No. DE-AC02-98CH10886 with the U.S. Department of Energy.

Copyright © 2013 CC-BY-3.0 and by the respective authors

Sources of Polarization Profile

The strength of an intrinsic spin resonance depends on the *Courant-Snyder* invariant, hence the depolarization experienced by a particle across such a spin resonance also depends on the single particle emittance. The crossing of such resonance can result in the particles at larger amplitude being depolarized while the center of the beam remains polarized.

The injection in the AGS occurs at $G\gamma = 4.5$ and the vertical tune needs to be placed in the spin gap before the first vertical intrinsic resonance, around $G\gamma = 5$. Figure 1 shows the vertical tune crossing the spin tune around $G\gamma = 5$. Due to the strong optical distortions caused by the Siberian snakes it is not possible to push vertical tune high enough at low energy. We expect that the crossing of vertical intrinsic resonances in this region depolarizes part of the beam and induces a polarization profile in the vertical plane.

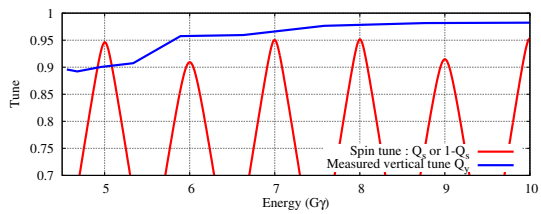


Figure 1: Fractional part of the vertical tune and spin tune at low energy.

While the partial Siberian snakes configuration avoid depolarizations caused by the imperfection and vertical intrinsic resonances, it can also induce depolarization through horizontal intrinsic resonances when $Q_s = I \pm Q_x$ with Q_x the horizontal tune. The stable spin direction is never perfectly vertical with partial snakes and therefore the non-zero horizontal component of the spin can resonate with the horizontal betatron tune. The strength of these resonances depends on the horizontal emittance and horizontal component of polarization. The crossing of these resonances builds up an horizontal polarization profile.

Other sources of depolarization can contribute to the polarization profile. For instance linear betatron coupling or high order partial snake resonances [3] can increase the polarization profile but will not be discussed here.

SIMULATIONS

Extensive development of the AGS Zgoubi on-line model provides a realistic model of the polarized proton

DESIGN OF THE INJECTION INTO THE 800 MeV/amu HIGH POWER CYCLOTRON*

M. Haj Tahar, Y. Dutheil, A. Morgan, F. Méot, N. Tsoupas
BNL, Upton, Long Island, New York, USA
L. Calabretta†, INFN/LNS, Catania, Italy; A. Calanna, MIT, Cambridge MA, USA

Abstract

We present the design of the injection into a separated sector cyclotron (SSC) aimed at the production of a high power beam of 800MeV/amu molecular H_2^+ for ADS-Reactor applications. To work out the beam line parameters and beam dynamics simulations, including the first accelerated turns, we used the ray-tracing code Zgoubi and the OPERA magnetic field map of the cyclotron sector. We simulated the injection path of the H_2^+ and evaluated radial injection scheme in order to evaluate the parameters so derived. The paper details and discusses various aspects of that design study and its outcomes.

INTRODUCTION

The present paper addresses an attempt to find an appropriate injection design for our SSC: the cyclotron complex consists of an injector cyclotron accelerating H_2^+ molecules from 50 KeV/amu up to 60 MeV/amu. The beam is then injected to our 6-sector cyclotron by means of electrostatic and magnetic elements, and accelerated up to 800 MeV/amu. In order to do so, 6 RF cavities, 4 single-gap and 2 double-gap are used, which are PSI-like. A plot of the OPERA magnetic field map in the median plane, for one sector is shown in Fig. 1. There are many considerations that explain the magnetic field shape [1]:

- The azimuthal variations show that the field is decreasing in the central region which ensures more focusing of the beam.
- The superconducting coils of each sector, which are wound around the hills, and the iron of the sector, produce the magnetic field that has to follow the γ(r) law in order to keep the isochronicity, where γ stands for the Lorentz factor.
- The isofield lines show that one edge of the sector has spiral shape while the other is quite straight: even though it is better to have spiral edges to increase the vertical focusing, the design of the magnet becomes problematic when it comes to using superconducting coils, because of the expansion radial force exerted from the inner region of the coil towards the outer radii. A superconducting magnet with a convex shape of the coil would be very difficult to build.

* Work supported by Brookhaven Science Associates, LLC under Contract No. DE-AC02-98CH10886 with the U.S. Department of Energy.
† calabretta@lns.infn.it

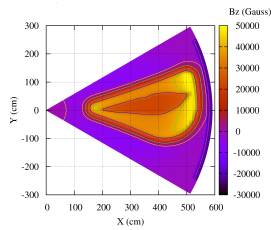


Figure 1: Plot of the z-component of the magnetic field in the median plane for one sector, with the isofield lines.

BEAM DYNAMICS AT INJECTION

Orbits at various energies from injection to nearby extraction are shown in Fig. 2. These orbits were obtained by Zgoubi [2] . It can be easily seen that the distance between consecutive turns (that have the same step size in energy) decreases quickly. In fact, the transverse separation of the turns is very important to consider in our design because it has to be maximized in order to allow clean injection. The step width per turn can be described by the formula [3]:

$$\frac{dR}{dn_t} = \frac{U_t}{m_0 c^2} \frac{R}{(\gamma^2 - 1)\gamma} \quad (1)$$

where U_t denotes the energy gain per turn. However, this assumes that the condition of isochronicity is perfectly satisified. It can be deduced from Eq. 1 that both the energy gain per turn and the injection radius should be made as big as possible in order to increase the step width per turn at injection as well. The transverse separation of the turns as a function of the kinetic energy is shown in Fig. 3.

The first orbit suitable for acceleration is the first closed orbit shown in Fig. 2. This orbit is very important to study in order to match the injected beam properly. Paraxial rays were generated around this orbit in order to compute the transfer matrix of the sector. From that, the betatron functions of the sector ensuring the 6-fold symmetry were computed. The beam envelope of the entire cyclotron was then obtained by multi-turn tracking of a set of particles generated around the eigen ellipse. Both axial and radial beam envelopes are shown in Fig. 4 and 5 respectively. All the results obtained here assume a H_2^+ beam energy of 60 MeV/amu and a normalized emittance of 13.5 π mm.mrad.

INJECTION LINE

The injection system needs to transport the beam from a point outside the cyclotron ring to the first orbit suitable for

Copyright © 2013 CC-BY-3.0 and by the respective authors

ISBN 978-3-95450-138-0

ALGORITHMS FOR SELF-CONSISTENT SIMULATIONS OF BEAM-INDUCED PLASMA IN MUON COOLING DEVICES

R. Samulyak*, Stony Brook University, Stony Brook, NY and BNL, Upton, NY, USA
K. Yu, Stony Brook University, Stony Brook, NY, M. Chung, A. Tollestrup,
K. Yonehara, FNAL, Batavia, IL, R. D. Ryne, LBNL, Berkeley, CA, USA

Abstract

A code called SPACE for the simulation of beam-induced plasma in gas-filled RF cavities has been developed. The core code uses the particle-in-cell (PIC) method for the Maxwell equations coupled to the dynamics of particles. In the SPACE code, the electromagnetic PIC methods are coupled with probabilistic treatment of atomic physics processes. The aim of the project is to demonstrate the feasibility of the RF cavity with muon collider beams. The most critical part is investigating how intense muon beams influence the plasma dynamics. Initial phase of simulations demonstrating the plasma generation and its short time dynamics in the high pressure hydrogen filled RF test cell has been performed.

INTRODUCTION

A dense hydrogen gas filled RF cavity has been proposed for muon beam phase space cooling and acceleration. The aim of the simulation program is the development of mathematical and numerical models and parallel software for the simulation of processes occurring in gas-filled RF cavities. An important issue in high-pressure gas filled cavity is a RF power loading due to beam-induced plasma [1]. Incident particle beam interacts with dense hydrogen gas and causes significant ionization level. Due to high frequency of collisions with neutrals, electrons reach equilibrium within picosecond time scale and move with a slow drift velocity. The recombination processes occur on the millisecond time scale. In order to induce the three-body electron capture, electronegtive gas has been tested in the test cell. This is the most critical process in the final cooling stage and should be modeled accurately in simulations. Other important processes include the interaction between positive and negative ions and the interaction of the beam with wakefields. A parallel electromagnetic PIC code with atomic physics, called SPACE, has been developed at Stony Brook University / BNL. It implements new mathematical models and numerical algorithms for the interaction of high-energy proton and muon beams with neutral gas and plasmas.

NUMERICAL METHODS

PIC method for Maxwell's equations

The system of Maxwells equations is discretized using the finite difference time domain (FDTD) method on a staggered mesh [2] that achieves second order accuracy in space and time. Electric charges are represented by discrete macroparticles coupled with electromagnetic fields by the action of Lorentz forces and electric currents. When one solves Maxwells equations analytically, solving two equations describing the Faraday and Ampere laws is sufficient as the equations expressing the Gauss law and the divergence-free constraint for the magnetic field are invariants of motion. The numerical method of Yee [2] for electromagnetic fields in vacuum also preserves the divergence-free properties of the electric and magnetic fields. To deal with the last two equations in the presence of charges and currents, the rigorous charge conservation method was developed within the PIC framework in [3]. The method calculates electric currents along computational grid edges by solving a geometrical problem of sweeping the computational mesh by finite volumes associated with each macroparticle. By using this method, we find first a set of initial conditions consistent with the Maxwell equations by either solving the Poisson problem for the electric potential or by a superposition of electric fields and changes created by each particle. Then only the first two Maxwell equations and the Newton-Lorentz equation are solved numerically thus avoiding solving the Poisson problem at each time step.

A schematic of processes computed at each time step is depicted in Figure 1. We would like to note that the conservative Leapfrog time discretization scheme for the Newton-Lorentz equations of particle motion becomes implicit. We use the Boris scheme for the time update [4], which is a modification of the Leapfrog scheme resulting in an explicit and conservative scheme. We also implement modifications of the Boris scheme proposed in [5] for dealing with rapidly accelerating particles for which the relativistic factor is not constant.

For accurate simulations of electromagnetic fields in geometrically complex structures, we have implemented the embedded boundary method [6] in a stand-alone Maxwell equation solver. The coupling of algorithms for complex boundaries with the main electromagnetic PIC code will be performed in the next phase.

Code Structure and Properties

The code is developed in C++ utilizing the advantages of Objected-Oriented Programming. The code is composed of three major parts. The first part, the FieldSolver class, contains FDTD solvers of the Maxwell equations. The second part, the ParticleMover class, contains solvers for the Newton-Lorentz equation. This class also includes various physics models describing particle interactions and trans-

* roman.samulyak@stonybrook.edu

Copyright © 2013 CC-BY-3.0 and by the respective authors

ISBN 978-3-95450-138-0

MULTIPLE SCATTERING EFFECTS IN A STRONG MAGNETIC FIELD*

P. Snopok, J. Ellison, Illinois Institute of Technology, Chicago, IL 60616, USA
T. Roberts, Fermilab, Batavia, IL 6051, USA

Abstract

New computational tools are essential for accurate modeling and simulation of the next generation of muon-based accelerator experiments at the energy and intensity frontiers. There is a long list of crucial physics processes specific to muon accelerators that have not yet been implemented adequately. One of the long-standing entries on that list is multiple scattering in the presence of strong magnetic field. Earlier studies showed significant discrepancies depending on the models used and step sizes when stepping through the field. A liquid Hydrogen (LH2) absorber in a strong longitudinal magnetic field is analyzed using G4beamline to study and mitigate the effects of step size, and compared to a past study. The updated results and an algorithm to limit step size depending on the field strength are presented.

INTRODUCTION

Though accelerator simulation codes have been steadily improving over the years, there is still much room for improvement. Many single-particle processes and collective effects in vacuum and matter, such as space charge, beam-beam effects, plasma effects from ionized electrons and ions, etc. have not been studied thoroughly or implemented. In order to ensure proper accuracy of simulations, these effects have to be either deemed negligible or taken into account.

One of the processes that is a source of concern is multiple scattering in a strong magnetic field. In a paper by P. Lebrun [1] scattering of muons through a 32 cm length of LH2 is compared between a Moliere (GEANT3) model and a Discrete Scattering model for both a zero field and a several Tesla magnetic field arrangement, showing significant discrepancies, especially in the tails of the distributions. This paper attempts to recreate the simulations of Lebrun as best as possible in G4beamline [2] based off the GEANT4 package. Several problems presented themselves during the recreation, and a complete recreation was not possible, however we believe it to be accurate enough for our purposes. Since [1], the PDG value for the radiation length of LH2 has been updated. Attaining a perfect match to the magnetic field profile in [1] was also not possible. Overall, GEANT4 shows a much better agreement with a Discrete Scattering model studied by Lebrun.

Another issue is that scattering in a strong magnetic field as simulated in G4beamline will yield different results for different step sizes as shown in the first plot in Fig. 4. Consistent results are achieved at very small step sizes, so an algorithm is required that will reduce step size in matter according to the field strength, so that the performance of tracking of particles in vacuum or in a relatively weak magnetic field is not affected.

OVERVIEW OF ALGORITHMS

The main difference in multiple scattering algorithms between GEANT3 and GEANT4 (and as a result G4beamline) was the change from the Moliere formalism to Lewis theory. In GEANT3, Moliere theory was used. This has a few limitations [1, 3]:

- the angular deflection is small;
- the theory applies only in semi-infinite homogeneous media;
- the absorber is not a very low Z material, as the Thomas-Fermi model could be inaccurate here;
- there is no energy loss built into the theory.

GEANT4 is based on the more complete Lewis theory. Like Moliere theory, this simulates the scattering of a particle after a step, but Lewis Theory also computes the path length correction and the lateral displacement, along with the moments of spatial distribution as well [4].

WITHOUT MAGNETIC FIELD

The simulation presented in Lebrun's paper was recreated as close as possible using G4beamline 2.14. A pencil beam of 180 MeV/c muons are scattered through a 32 cm length of LH2 in and out of an intense magnetic field. The magnetic field comes from the 2 m long Alternate Solenoid cooling channel [5] which reaches a peak field of 15 T. The 32 cm length of LH2 begins where the field is at peak. Ref. [1] makes a comparison between a Discrete Scattering model for LH2 and the Moliere model used in GEANT3 at the time, while we compare these to the current G4beamline 2.14 based on the GEANT4 package. The step sizes of the simulations were discussed in [1] and are set to 4 mm in the Moliere results and G4beamline results, and to a micron in the Discrete Scattering results.

Table 1 shows the compared results for the case with no magnetic field. Extensive track cuts were made by insisting on an aperture cut of 2.5 cm and angle cut of 250 mrad and maximum $r \cdot \theta$ of 500 mm·mrad.

WITH MAGNETIC FIELD

In recreating the coils, the data from [5] was used and is summarized in Table 2. The Z offsets were adjusted to

* Work supported by DOE.

ISBN 978-3-95450-138-0

Copyright © 2013 CC-BY-3.0 and by the respective authors

PROGRESS OF THE MATTER-DOMINATED MUON ACCELERATOR LATTICE SIMULATION TOOLS DEVELOPMENT FOR COSY INFINITY*

P. Snopok†, J. Kunz, Illinois Institute of Technology, Chicago, IL 60616, USA

Abstract

COSY Infinity is an arbitrary-order beam dynamics simulation and analysis code. It can determine high-order transfer maps of combinations of particle optical elements of arbitrary field configurations. For precision modeling, design, and optimization of next-generation muon beam facilities, its features make it the ideal code. The one component that needs to be included in COSY is the algorithm necessary to follow the distribution of charged particles through matter. Muon beams are tertiary production particles and high-intensity collection necessitates a large initial phase space volume. Therefore, accurate modeling of the dynamics and correction of aberrations is imperative. To study in detail some of the properties of particles passing through material, the transfer map approach alone is not sufficient. The interplay of beam optics and atomic processes must be studied by a hybrid transfer map–Monte-Carlo approach in which transfer map methods are used when there is no material in the accelerator channel, and Monte-Carlo methods when particles pass through material. Progress on the development of the hybrid algorithm is reported.

INTRODUCTION

Muon beams are tertiary production particles and high-intensity collection necessitates a large initial phase space volume. The resultant spray of muons must be collected, focused, and accelerated well within the muon lifetime (2.2 μs in the rest frame). The only technique fast enough to reduce the beam size within the muon lifetime is ionization cooling. Muons traverse a certain amount of material in order to lose energy in both longitudinal and transverse direction due to ionization. The energy is then restored in the longitudinal direction only, leading to an overall reduction in the transverse direction (cooling). In order to achieve cooling in the longitudinal direction, emittance exchange is used, usually involving wedge-shaped absorbers.

In order to carefully simulate the effect of the absorbers on the beam, one needs to take into account both deterministic and stochastic effects in the ionization energy loss. The deterministic effects in the form of the Bethe-Bloch formula with various theoretical and experimental corrections fit well into the transfer map methods approach, where the effect of the lattice on the particles is evaluated first by producing the so-called transfer map, and then applied to a given initial distribution of particles. The arbitrary-order simulation code COSY Infinity [1] is a key representative of the transfer map codes. COSY was chosen because of its built-in optomization tools, speed, its ability to produce high-order transfer maps, and its ability to control individual aberrations.

However, the stochastic effects are not easy to take into account in the framework of the transfer map paradigm. To compensate, we are interfacing COSY with select parts of another code, ICOOL [2], which was written specifically to study the ionization cooling of muon beams. The implementation of the stochastic effects due to various geometries and materials into COSY is reported with the most recent results.

CODE SELECTION PROCESS FOR STOCHASTIC PROCESSES

A variety of codes exists which would complement COSY. Initially, it was hoped that the implementation of a fragment separator into COSY that used a Monte-Carlo approach [3] could be repurposed; however, the libraries were heavily oriented towards electrons, protons, and heavy ions, with no muon data. Other codes that were considered included MUSIC [4], MARS [5], and GEANT4 [6], but were discarded either due to the code focusing on cosmic ray muons, difficulty in interfacing, or sheer bulk.

ICOOL was eventually chosen due to its modularity, compactness, and the fact that, like COSY, is written in FORTRAN. ICOOL's main purpose is to simulate particle-by-particle propogation through electromagnetic fields and matter, with roughly twenty built-in materials to call. The processes included are decays, delta rays, multiple scattering, energy loss, and straggling. Although built for muons, ICOOL can also keep track of other relevant particles such as electrons, pions, kaons, and protons. Additionally, ICOOL can either generate a beam with uniform or Gaussian distribution, or it can read particle information from an input file. This is advantageous since COSY also has a similar input/output file method, which makes direct comparison between the two codes simple.

INTERFACING DETAILS

While ICOOL has routines to calculate particles through, for example, an RF cavity, those were not used since there are corresponding routines in COSY that work faster since the transfer map is only calculated once and then applied to simultaneously to all particles. Therefore, only the routines that directly dealt with absorbers were interfaced. Currently, the following routines have been implemented into COSY: flat absorber (a cylindrical block of arbitrary thickness and radius), radially-symmetric wedge (where

* Work supported by the Department of Energy.
† psnopok@iit.edu

Copyright © 2013 CC-BY-3.0 and by the respective authors

SPACE CHARGE SIMULATION IN COSY USING FAST MULTIPOLE METHOD

B. Loseth*, M. Berz*, K. Makino*, H. Zhang*, P. Snopok**
* Michigan State University, East Lansing, MI 48824, USA
** Illinois Institute of Technology, Chicago, IL 60616, USA

Abstract

A method is presented that allows the computation of space charge effects of arbitrary and large distributions of particles in an efficient and accurate way based on a variant of the Fast Multipole Method (FMM). It relies on an automatic multigrid-based decomposition of charges in near and far regions and the use of high-order differential algebra methods to obtain decompositions of far fields that lead to an error that scales with a high power of the order. Given an ensemble of N particles, the method allows the computation of the self-fields of all particles on each other with a computational expense that scales as O(N). Using remainder-enhanced DA methods, it is also possible to obtain rigorous estimates of the errors of the methods. Furthermore, the method allows the computation of all high-order multipoles of the space charge fields that are necessary for the computation of high-order transfer maps and all resulting aberrations. This method has been implemented in COSY Infinity, and the progress of applying it to simulating the 6D cooling channel for the Muon Collider is reported.

FAST MULTIPOLE METHOD

The fast multipole method for the Coulomb interaction between many charged particles divides an arbitrary charge distribution into small boxes with a hierarchical structure. It then computes the multipole expansions and local expansions of charges far from the observer to achieve a computation efficiency that scales with the number of particles, N, and computational errors scaling with a high power of the differential algebra order. The FMM algorithm is especially suited for beam dynamic simulations because of the efficiency and low computational error compared to other spacecharge algorithms.

Other methods, such as the particle-particle interaction (PPI) and the particle in cell (PIC) method, while computationally efficient, incur excess error due to modeling and statistics. The PPI method uses macroparticles and assumes a particular distribution. The PIC method places the charge distribution onto a mesh, solves the Poisson equation on mesh points and interpolates between mesh points to find the field on each particle. Both of these methods suffer from an inability to precisely handle complicated charge distributions. This difficulty is overcome in the FMM by decomposing the charge distribution into boxes according to the charge density such that there are a pre-specified number of particles in each box to efficiently and accurately compute the multipole expansions.

FMM Algorithm

The principle of the FMM is to determine the potential of groups of source particles sufficiently far from the observer in terms of expansions in $1/r$, utilizing the fact that far away, high powers of $1/r$ become less significant. These multipole expansions can be translated and combined, and again locally expanded to determine the field on a group of nearby observer particles.

First, all of the charges are enclosed in a cube box called the zero-level box. A box is defined to be a parent box if the number of charges inside is larger than s, which we select. If a box is a parent box, it will be split into eight equal square boxes which are its child boxes and form a new level. If any of the child boxes have more than s charges, they will in turn be split into eight child boxes which form the next level. This process is iterated until no box has more than s charges. At each subdivision, we keep only the nonempty boxes, so the empty boxes are ignored by the subsequent field calculation.

Analytic Considerations

For a distribution of n particles of charge q_i located at $\mathbf{r_i}(x_i, y_i, z_i)$, the potential at a point $\mathbf{r}(x, y, z)$ can be expressed as

$$\phi = \sum_{i=1}^{n} \frac{d_r \cdot q_i}{\sqrt{1 + r_i^2 d_r^2 - 2x_i d_x - 2y_i d_y - 2z_i d_z}} \qquad (1)$$

with

$$d_x = \frac{x}{x^2+y^2+z^2} \quad d_y = \frac{y}{x^2+y^2+z^2}\ , \qquad (2)$$

$$d_z = \frac{z}{x^2+y^2+z^2} \quad d_r = \frac{1}{\sqrt{x^2+y^2+z^2}}\ . \qquad (3)$$

In COSY Infinity [1,2] we apply the DA techniques [3,4] to express ϕ as a DA vector by choosing d_x, d_y, and d_z as our DA variables. This DA vector is essentially the Taylor expansion of ϕ with respect to $1/d_x$, $1/d_y$, $1/d_z$, $1/d_r$, and can be translated into another multipole expansion at an arbitrary point and converted into a local expansion with a simple composition operation on the DA vector. Using the domain decomposition to determine near and far regions, the field in a box is computed using a combination of far multipole expansions and local expansions.

LINEAR COOLING CHANNEL IN COSY

The demonstration of muon ionization cooling is one of the key challenges for the Muon Accelerator Program

ISBN 978-3-95450-138-0

Copyright © 2013 CC-BY-3.0 and by the respective authors

MITIGATION OF NUMERICAL NOISE FOR SPACE CHARGE CALCULATIONS IN TRACKING CODES

L.G. Vorobiev, C. Ankenbrandt, T.J. Roberts, Muons, Inc., Batavia, IL 60510, USA
F. Schmidt, CERN, Geneva, Switzerland

Abstract

Modern tracking codes have very stringent requirements concerning space charge calculations. They should combine speed of calculations, in order to track particles for many turns (e.g. the LHC injection chain), with numerical accuracy while maintaining symplecticity. Grid solvers and modified Green's function algorithms have been compared, and upgrades were suggested.

INTRODUCTION

Multiple-particle tracking allows for accurate space charge (SC) beam simulations and design. However, in the particle-in-cell (PIC) formalism [1], spatial non-physical grid effects may jeopardize the validity of modeling in accelerator rings and colliders, especially during multi-turn particle tracking. To remedy artificial grid noise, PIC codes increasingly use more macro-particles, denser grids, and more SC kicks per bunch, requiring massive parallelization. Even so, numerical errors persist. The split operator method itself (unlike the general PIC paradigm) decouples three-dimensional (3D) SC forces and dynamics, possibly resulting in additional errors and faulty estimates of instabilities, dynamic aperture, emittance growth, etc. Recent numerical experiments demonstrated artificial noise due to mesh effects and interpolation, leading to micro-scale beam instability [2].

The situation can be improved in two ways. First, we perfect the components of the PIC formalism itself. We will develop a grid density module, suppressing numerical noise to upgrade the accuracy of Poisson solvers. Secondly, we avoid spatial grids entirely, because despite precautions the grid-related noise will always persist. The known grid-free SC solvers are based on the classic Green's function or direct Vlasov solvers (we are aware only of axi-symmetric ones) [3], but they are too slow for multiple particle tracking in rings and work only in free space without boundaries. Instead, we introduce hybrid SC solvers based on "space-charge templates", which represent macro Green's functions for macro-elements [4-5], from which a large family of beam distributions can be built. These SC templates calculate the 3D self-forces of a beam in the presence of conducting boundaries.

There is a gap in terms of generality and performance between fast but over-simplified "frozen" models and standard PIC codes. The proposed hybrid SC solvers fill that gap: they are more flexible than "frozen" models and approach the accuracy of PICs while being much faster. Template-based solvers can simulate rather arbitrary beam distributions within conducting boundaries and may be parallelized, boosting their performance even further.

ACCURACY OF MULTIPLE-PARTICLE TRACKING BY PICS

The computational flows of multiple-particle tracking codes are similar, and our analyses of the accuracy and performance of their components have much in common.

PIC Computational Modules

Each macro-particle in a 3D beam has six phase space coordinates, and a step-by-step evolution of the ensemble of N macro-particles $\mathbf{X}=(x_1, x'_1, y_1, y'_1, z_1, z'_1,\ldots, x_N, x'_N, y_N, y'_N, z_N, z'_N)$ looks like the following:

$$\mathbf{X}_{\text{old}} \rightarrow \underbrace{\rho_{3D}}_{\text{Space}}, \underbrace{u_{3D}}_{\text{Charge}}, \underbrace{\mathbf{E}_{3D}}_{\text{module}} \rightarrow \begin{bmatrix}\text{Trajectory}\\ \text{Integrator}\end{bmatrix} \rightarrow \mathbf{X}_{\text{new}} \quad (1).$$

Here the trajectories are integrated either by multi-step (2nd order leap-frog, or higher order) schemes, or symplectic maps, which are more customary for multi-turn modeling in the rings. These higher order maps take into account non-linearities of the lattice and SC forces, and they trace particles with any prescribed accuracy in the framework of the single particle approximation [6].

Contemporary Poisson solvers are able to derive nearly exact grid solutions by multi-grid techniques, assuming that the input, i.e. the grid density, is known exactly. The interpolation between grid nodes is also very accurate. Unfortunately, the grid density is evaluated only approximately, and moreover, it represents the main source of numerical noise in (1). We need to find remedies to manage this.

Space Charge Density on the Grid

The Cloud-In-Cell (CIC) technique was developed decades ago (see [1] and references therein). If a spatial grid has dimensions of $N_x \times N_y \times N_z$ and meshes $h_x \times h_y \times h_z$, then the macro-particle sizes are $\delta_{x,y,z}=\Delta \times h_{x,y,z}$ ($\Delta \geq 0.5$). A redistribution of elementary space charge among grid nodes must satisfy a conservation of space charge and should converge for higher order interpolations. A linear scheme is used in ORBIT, WARP, and Synergia codes. A quadratic interpolation is also possible.

Using finite clouds with bell-like shape functions is beyond linear/quadratic interpolation. One needs an infinite polynomial series to represent them. For example, Fig. 1 shows a family of one dimensional (1D) clouds:

$$S_2(\xi)=\frac{q}{2\Delta}, S_3(\xi)=\frac{3q}{4\Delta}\left[1-\frac{\xi^2}{\Delta^2}\right], S_4(\xi)=\frac{q}{2\Delta}\left[1+\cos\left(\frac{\pi\xi}{\Delta}\right)\right],$$

$$S_5(\xi)=\frac{q}{3\Delta}\left[1+\cos\left(\frac{\pi\xi}{\Delta}\right)\right]^2, S_6(\xi)=\frac{15q}{16\Delta}\left[1-\frac{\xi^2}{\Delta^2}\right]^2 \text{ for } |\xi| \leq \Delta.$$

Copyright © 2013 CC-BY-3.0 and by the respective authors

ISBN 978-3-95450-138-0

OPTIMIZATION OF THE MULTIPOLE TO LOCAL TRANSLATION OPERATOR IN THE ADAPTIVE FAST MULTIPOLE METHOD

S. Abeyratne[^], B. Erdelyi[*,^]
[^]Department of Physics, Northern Illinois University, DeKalb, IL 60115
*Physics Division, Argonne National Laboratory, Argonne, IL 60439

Abstract

The Fast Multipole Method (FMM) is an accurate and fast way to calculate potentials/fields created by a very large number of particles. The runtime of the FMM is significantly less than that of the pairwise calculation if the particle number, N, is sufficiently large. Two major parts in the FMM are the upward pass and the downward pass. The upward pass calculates multipole expansions and then performs multipole-to-multipole translations. The downward pass calculates multipole-to-local expansions and local-to-local expansions. The multipole-to-local translation in the downward pass is the most time consuming translation in the FMM. In order to make the FMM more efficient, we sought to minimize the time taken by the multipole-to-local translation. The promising and practical strategy to minimize the multipole-to-local translation time is to replace the 3D multipole-to-local translation with a 1D multipole-to-local translation in conjunction with rotations of the coordinate axes. In this paper we show how to perform the 1D multipole-to-local translation and the time comparisons between the two FMM variants.

INTRODUCTION

The traditional method to calculate the Coulomb interaction between charged particles is pairwise calculation. The computational power needed for this method is of the order O(N^2) and it is not practical if the number of particles is very large. The FMM can reduce the computational power to O(N).

The details of the two major components of the FMM, data structuring [1, 2] and calculation of the potential/field [3], are discussed in our previous papers. If the number of particle is large, the data structuring time scales linearly [2]. We have also shown that the total runtime, the addition of data structuring time and the time taken to calculate the potential, scales linearly with the number of particles, if the number is large enough [3].

The major components of runtime with optimized settings are the time taken by upward pass (~3%), the downward pass (~50%) and the direct calculation in the final summation (~47%). To decrease the runtime we need to decrease the downward pass time or the direct calculation time. As the direct calculation time solely depends on the optimum q (the parameter q has its usual meaning, the maximum number of sources allowed in the neighbourhood of a given target), it is no longer possible to reduce the direct calculation time. Hence, we focus on reducing the downward pass time. Further analysis showed that the multipole-to-local translation (M2L) used in the downward pass is the bottleneck. This paper places emphasis on the M2L operator and shows that the FMM runtime can be significantly reduced if the 3D M2L translation is replaced by the 1D M2L translation.

ALGORITHM

In the data structuring we create the C-forest (the collection of trees) and the D-tree (parent-child relations of all boxes which contain target particles) [1, 2] at the optimum q. Once the octree-type data structure is created we can implement the FMM proper to calculate the potentials/fields.

The FMM implementation consists of two key components, the upward pass and the downward pass [3]. The downward pass starts at level two and it has three steps. The first step is the M2L translation of the multipole expansions of the boxes in the interaction list of a particular box or leaf node, b. In the second step, we move to the next finer level and compute the local expansion of child nodes of b around their centers from the multipole expansions of the boxes in the interaction list of child nodes. In the third step, we re-expand the result in the first step to evaluate the contribution from the local expansion of the parent box and add that to the result obtained in the second step. In order to complete the downward pass the above three steps must be repeated until we reach the finest level.

After the upward pass and downward pass we move to the final summation [3]. In the second step of the final summation we calculate the potential at each target in b due to the sources in the neighbourhood of b. This is a pairwise calculation. We have noticed that the M2L translation in downward pass and direct calculation in final summation take a considerably longer amount of time compared to all the other operations in the FMM process. Since this pairwise calculation is unavoidable and we cannot reduce that time it becomes apparent that the FMM runtime can be further reduced by optimizing the M2L translation operator. At higher orders M2L translation takes more than 50% of the total FMM runtime.

In this translation, we perform a 3D M2L translation in all three directions, x, y and z. In 3D, the number of boxes in the interaction list varies from 27 to 189. Therefore, the M2L translation takes a longer time. If we rotate the coordinate system of the box with the multipole expansion to be translated in such a way that the z-axis of the box aligns with the line joining the centers of the box and the interaction list boxes, the 3D transformation of the M2L becomes a 1D transformation. Hence, the time taken

Copyright © 2013 CC-BY-3.0 and by the respective authors

ISBN 978-3-95450-138-0

NUMERICAL INTEGRATOR FOR COULOMB COLLISIONS

A. Al Marzouk*, B. Erdelyi*,^
*Department of Physics, Northern Illinois University, DeKalb, IL 60115
^Physics Division, Argonne National Laboratory, Argonne, IL 60439

Abstract

The trajectories of protons interacting through Coulomb forces were computed using a numerical integrator based on Picard's iteration method. This is a variable order, adaptive integrator with dense output. We show different cases by varying some parameters such as the impact parameter, the relative velocity of the protons and the order of the differential algebraic (DA) vector. The accuracy of the trajectories was tested by changing the order of the DA vector while fixing the other parameters. The impact parameter between the protons and the velocity of the incident proton has the most impact on the trajectories. The maximum time step is determined by the radius of convergence of the expansions, while a fixed accuracy is attained by varying the order.

INTRODUCTION

Many physical phenomena involve N bodies (particles) interacting with one another by long range forces which decrease inversely as the square of the distance. Examples include the gravitational interaction among the stars in a galaxy, and the Coulomb forces between charges. Many particle systems have wide range of applications in different areas such as biophysics, chemistry, astrophysics [1], etc.

This work includes the two-body problem, in which two charges interact through Coulomb forces. Coulomb's law describes the force between two point charges by the following equation:

$$\overrightarrow{F} = \frac{1}{4\pi\varepsilon_o}\frac{q_1 q_2 \vec{r}}{|\vec{r}|^3},$$

where $\overrightarrow{F}$ is the force, q is the charge, $\vec{r}$ is the radial distance between the two charges, and ε_o is the permittivity of free space.

It is complicated to solve the N-body problem numerically due to the singularity of very close encounters where $|\vec{r}| \to 0$ (very strong interaction $\overrightarrow{F} \to \infty$), and the requirements of high precision with violently varying time steps that are necessary to reduce errors to acceptable levels.

We consider the interaction between two protons in two dimensions. The first proton is initially at rest, and the second proton is moving horizontally towards the first one with a specific vertical distance between them. According to Coulomb's law, the electrostatic force between two similar charges is repulsive.

The integrator has applications in electron cooling of heavy ion beams, and any other beam dynamics problem where individual collisions need to be resolved.

ALGORITHM

To compute the trajectories of both of the protons, we used a code developed by us via COSY INFINITY [2]. The code is a numerical integrator based on Picard's iteration method (see [3] for details). Picard's method uses the initial conditions of the system and gives a sequence of functions that converge to the solution. This method can compute completely algebraically the Maclaurin polynomial (Taylor series expansion of a function about zero).

In this program, the Maclaurin polynomial of the solution is represented by DA vectors. The DA vector is an array of elements that describe a multi-variable function when given its value and derivatives at a specific point [4]. The integrator order is equivalent to the DA order, and we can vary this order to the one that we want to truncate the Taylor series at. At each time step, the program evaluates the change of the radius between the particles and compares it with the one at the next time step. Whenever the convergence radius is exceeded, the program will display an error message.

The maximum velocity (β_{max}) used for the incident proton is 0.283. Different fractions of this velocity were used as well. The initial horizontal distance between the protons was varied from 10^{-15}-10^{-9} m. The impact parameter (vertical distance between the particles) was varied from 10^{-15}-10^{-11} m. It is possible to use larger distances (horizontal or vertical), but the strong interactions are localized within these distances. Hence, larger distances would result into very small changes in the positions of the protons that would be hard to see.

EXAMPLES

The parameters of the system will be denoted as follows: d = horizontal distance (m), b = vertical distance (m), δt = time interval ($1/c$ s), N = number of time steps, and the DA order was set to be 4 unless specified otherwise.

Example 1

The impact parameter and the moving proton's velocity are fixed at 10^{-15} m and 10% β_{max}, respectively. The other parameters are varied in two instances:

- The parameters are: d = 10^{-15} m, N =10^4, δt = 3.6 × 10^{-17} $1/c$ s. The trajectories are shown in Fig. 1.
- Fig. 2 shows the protons' paths with the parameters: d = 10^{-10} m, N = 5.5 × 10^4, δt = 10^{-13} $1/c$ s.

The resulted trajectories in this example are as one would expect due to the Coulomb's interaction.

Copyright © 2013 CC-BY-3.0 and by the respective authors

STUDY AND COMPARISON OF THE METHOD OF MOMENTS AND THE SINGLE LEVEL FAST MULTIPOLE METHOD FOR 2D SPACE CHARGE TRACKING

Anthony Gee*[1] and Bela Erdelyi†[1,2]
[1]Physics Dept., NIU, DeKalb, IL, USA
[2]Physics Dept., ANL, Argonne, IL, USA

Abstract

Strong space charge is a significant impediment in charged particle beam physics, particularly at the high intensity frontier. For future applications, where particles must occupy the smallest region possible, quickly and accurately and efficient modeling space charge modeling is essential, for instance, to minimize the space charge contribution to beam dispersion. In this paper, we study and compare the performance for the method of moments (MoM) and the single-level fast multipole method (SLFMM) in 2D. The method of moments has been widely used to solve computational electromagnetic problems but assumes a series-expandable smooth distribution function, limiting its reliability in some cases. The fast multipole method was more recently developed and shows remarkable accuracy with difficult beam distributions. We demonstrate these methods using a simplified version of the University of Maryland electron ring (UMER). We present some multi-particle tracking results obtained using these methods. Future work will study the space charge inclusive transfer maps calculated from these methods.

INTRODUCTION

The general N body problem, although simple in principle, is computationally very challenging. The simplest method uses direct pair-wise interaction computations, where the complexity behaves like $O(N^2)$, and gives a machine precision solution for each pair. The mean field methods almost always involve some kind of numerical approximation. Two methods in particular were developed that approximate our solution to a significant degree of accuracy and reduce the scaling to $O(NlogN)$ or even $O(N)$ [1, 4, 5]. The method of moments (MoM) has been successfully used in several cases [1, 2]. As expected, it is most accurate for smooth unimodal distributions, where the relatively low order moments reliably approximate the distribution [4]. The fast multipole method (FMM), recently developed by Greengard and Rokhlin in 1987 [5], shows remarkable accuracy with arbitrary distributions, overcoming some weaknesses of the MoM. We are mainly interested in efficiently and accurately modeling the nonlinear effects present in a space charge dominant beam. The purpose of this paper is to evaluate and compare the MoM and FMM performance for a test case involving a simplified model of UMER.

* agee1@niu.edu
† erdelyi@anl.gov

IDEALIZED UMER

The University of Maryland electron storage ring has been designed and built specifically for the study of space charge dominated, high intensity beams in a localized, inexpensive setting. Some of the design specifications are shown in Table 1, with our specific settings in the lower section [3]. The design is such that the electron bunches fill the ring, allowing a quasi-2D approximation. We included only the main recirculation (RC) sections, each consisting of two equivalent FODO sections with a guiding dipole in the middle of each FODO section.

Table 1: The UMER Design Specifications are Listed in the Top Half and Our Relevant Simulation Conditions are in the Bottom Half

Circumference	11.52 m
Electron energy	10 keV
$\beta(=\frac{v}{c})$	0.2
Current	1–100 mA
Aperture	2.95 cm
Pulse Length	40 ns
Lap time	197 ns
Pulse repetition rate	60 Hz
Turns	30
Simulated current	6 mA
FODO period	0.32 m
# of FODO sections	36
Dipole bend	10°
Dipole effective length	3.82 cm
Quadrupole current	1.826 A
Quadrupole effective length	5.164 cm
Initial emittance (X,Y)	(5.28×10^{-8},4.94×10^{-8})
Integration region	5.25σ

RESULTS

MoM

Reference [1] explains the details of our implementation of the MoM and FMM. For the MoM, there are three separate orders to which we will refer. The space charge order (SO) is the order of computation for the space charge map. The map order is the order of computation for the regular transfer map or equivalently the order of the

Copyright © 2013 CC-BY-3.0 and by the respective authors

ISBN 978-3-95450-138-0

A PICARD ITERATION BASED INTEGRATOR *

H. Schaumburg, NIU, DeKalb, IL 60119, USA
B. Erdelyi, NIU, DeKalb, IL 60119, USA

Abstract

Picard iteration is mainly used as a theoretical tool to establish the existence and uniqueness of a solution to an initial value problem. We have developed a method based on Picard iteration that computes the exact Taylor polynomial of the solution to arbitrary order. The method has been implemented in COSY INFINITY to numerically solve Coulomb interactions.

INTRODUCTION AND BACKGROUND

Picard iteration generates a sequence of functions $\phi_n(t)$ related to the solution of the initial value problem

$$\begin{cases} \mathbf{y}' = \mathbf{f}(t, \mathbf{y}) \\ \mathbf{y}(t_0) = \mathbf{y}_0 \end{cases}.$$

When $\mathbf{f}$ satisfies a local Lipschitz condition with respect to $\mathbf{y}$ on U, a connected open subset of $\mathbb{R}^{m+1}$ and $(t_0, \mathbf{y}_0) \in U$, the Picard iterates given by

$$\phi_0(t) = \mathbf{y}_0$$
$$\phi_n(t) = \mathbf{y}_0 + \int_{t_0}^{t} \mathbf{f}\left(s, \phi_{n-1}(s)\right) ds.$$

converge to a unique solution of the IVP up to the boundary of U [1]. In general, ϕ_n may converge slowly to the exact solution.

The Picard iteration based integrator described in this paper has three main advantages. The the integrator has arbitrary order, is time adaptive, and has dense output. Dense output refers to the integrator being able to take time steps of variable length without having to recompute previous steps. These advantages are intertwined to balance local truncation error with computational efficiency. When smaller time steps are required, the order can be reduced to maintain efficiency. When a larger time step is appropriate, the order can be increased to maintain lower local truncation error.

The advantages of the integrator make it well suited for modelling the motion of charged particles. The forces in Coulomb interactions are proportional to the inverse of the square of the distances between particles. There are situations such as when two particles with same signed charges are on a near collision course. If too large of a time step is taken, the large repulsive force between the particles as they move closer to one another may not be considered and the integrator will give physically unrealistic results. An integrator with dense output can avoid these errors.

* This work was supported in part by the U.S. Department of Energy, Office of Nuclear Physics, under Contract No. DE-SC0008588, and Office of High Energy Physics, under Contract No. DE-FG02-08ER41532, with Northern Illinois University.

THEORY BEHIND THE INTEGRATOR

First, we will introduce notation to write Taylor polynomials. When f has a Taylor series centered at a with nonzero radius of convergence, define the operator $\mathcal{T}_{t,a}^{n}$ acting on function f to be the degree n Taylor polynomial centered at a for f. That is

$$\mathcal{T}_{t,a}^{n}[f] = \sum_{k=0}^{n} f^{(k)}(a) \frac{(t-a)^k}{k!}.$$

Main Theorem Statement

The main theorem below supplies two Picard iteration based integrators with different compositions. From the initial Taylor polynomial $\mathcal{T}_{t,0}^{0}[\mathbf{z}(t)] = \mathbf{z}_0$, we can find the next Taylor polynomials using either recursive relationship below. After each iteration, the local truncation error drops by an order of magnitude. Algorithm 1 in the implementation and results section shows how to implement the first composition.

Theorem 1. *Let* $\mathbf{z}\,'(t) = \mathbf{f}(t)$ *and* $\mathbf{z}_0 = \mathbf{z}(0)$. *Suppose* $\mathbf{z}$ *has a Taylor series centered at* 0 *with nonzero radius of convergence* R *and* $t < R$, *then*

$$\mathcal{T}_{t,0}^{n}[\mathbf{z}(t)] = \mathbf{z}_0 + \int_0^t \mathcal{T}_{s,0}^{n-1}\left[\mathbf{f}\left(\mathcal{T}_{s,0}^{n-1}[\mathbf{z}(s)]\right)\right] ds$$
$$= \mathbf{z}_0 + \int_0^t \mathcal{T}_{s,0}^{n-1}\left[\mathcal{T}_{s,\mathbf{z}_0}^{n-1}[\mathbf{f}] \circ \mathcal{T}_{s,0}^{n-1}[\mathbf{z}(s)]\right] ds.$$

In order to prove theorem 1, we need two lemmas. In order to show the first lemma, we will need the Faà Di Bruno formula [2], which is a generalization of the chain rule.

Theorem 2 (Faà Di Bruno)**.** *If* g *and* f *are functions with a sufficient number of derivatives, then*

$$\frac{\mathrm{d}^m}{\mathrm{d}t^m} f(g(t)) = \sum \frac{m!}{\prod_{i=1}^{m} b_i!} f^{(k)}(g(t)) \prod_{i=1}^{m} \left(\frac{g^{(i)}(t)}{i!}\right)^{b_i}$$

where the sum is over all different solutions in nonnegative integers $b_1, \ldots, b_m$ *of* $b_1 + 2b_2 + \cdots + mb_m = m$ *and* $k \equiv b_1 + b_2 + \cdots + b_m$.

Let $S_{m,k}$ denote the nonnegative integer solutions of $b_1 + 2b_2 + \cdots + mb_m = m$ and $k \equiv b_1 + b_2 + \cdots + b_m$, and $T_{n,m,k}$ denote the nonnegative integer solutions of $b_1 + 2b_2 + \cdots + nb_n = m$ and $k \equiv b_1 + b_2 + \cdots + b_m$.

Copyright © 2013 CC-BY-3.0 and by the respective authors

A USER FRIENDLY, MODULAR SIMULATION TOOL FOR LASER-ELECTRON INTERACTIONS*

S. Seung, G. Andonian, M. A. Harrison, S. Wu (RadiaBeam, Santa Monica), T. Shaftan (BNL, Upton, Long Island, New York), D. L. Bruhwiler (University of Colorado at Boulder, CIPS)

Abstract

The code RadTrack was developed to accurately model observable beam parameters in real laboratory environments RadTrack is a fast, reliable computational application that can calculate radiation observables in complex interactions between realistic laser and electron beam distributions. The interaction between laser and electron beams is important in processes such as inverse Compton scattering and inverse free electron laser schemes. Modeling these interactions, RadTrack incorporates functions from Synchrotron Radiation Workshop (SRW) with full parsing support to capitalize on well-established radiation generation and propagation code available for start-to-end simulations, while expanding simulated radiation to x-ray regimes [1]. RadTrack is based on the Python environment, which uses a hierarchal module system and possesses built-in data types that will allow further expansions of the code. The code provides an intuitive visualization work canvas that emphasizes the users overall objective.

INTRODUCTION

RadTrack is designed to addresses a number of issues in the accelerator community, with special attention to the radiation properties for direct comparison to available diagnostics. To achieve this, the code emphasizes modularity, breaking down these issues into digestible pieces. The graphical user interface is built on a visualization canvas that easily generates and displays important information. The interface is intuitive for seamless management of start-to-end simulations, which incorporate several codes. The interface allows for simple parallelization for complex, memory demanding calculations. RadTrack was developed as a code that can calculate beam dynamics as well as emitted radiation processes, in a transparent, intuitive manner,.

Complete modelling of a beam from its inception to detection, requires a complicated string of start-to-end studies, employing a concatenation of various function-specific simulations to achieve a high degree of confidence in the final outcome. RadTrack is specifically designed to address start-to-end simulations by seamlessly stitching I/O from various codes and file formats.

The code, RadTrack, was originally developed as an extension to the radiation code QUINDI [2] to calculate the radiative effects of bending beam trajectories. QUINDI was developed for a specific problem and its results benchmarked to experiments at Brookhaven National Laboratory Accelerator Test Facility [3]. RadTrack makes use of QUINDI's particle tracker and radiation field solver, which are based on the Lorentz for and Lienerd-Wiechert potentials, respectively [4]. RadTrack is able to generate laser and electron beam distributions and pass these distributions through an extensive library of optics, magnets and diagnostics, in particular, the use of undulators is important to many laser electron interaction schemes, such as laser heating, laser slicing and sub-femtosecond temporal diagnostics. Figure 1 displays the work flow and modular philosophy of the code; this is advantageous for implementation of the functions, where multiple outputs of codes are parsed as inputs into subsequent codes.

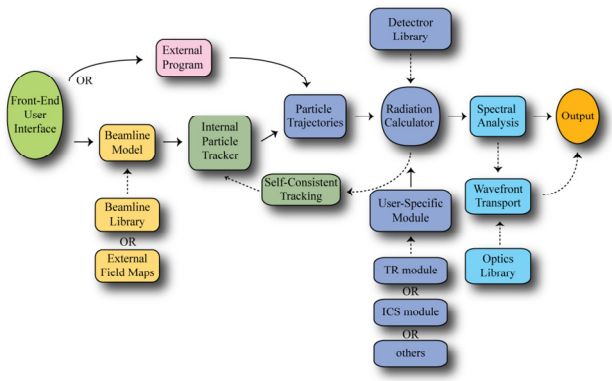


Figure 1: Work flow chart between physics modules, radiation modules, wave front propagator and various libraries.

LASER-ELECTRON INTERACTIONS

The motivation to develop a comprehensive software package that incorporates detailed beam dynamics calculations and radiation interactions has roots in many scientific cases prevalent throughout the advanced accelerator and light communities. Here are some laser electron interactions and their applications:

- The laser-heater is a laser-electron electron interaction in an undulator that increases the beam energy spread in a controllable way to reduce microbunching instability.
- The interaction between a relativistic electron beam and a high power laser induces an undulator-like radiation process that have the ability to produce short wavelength photons [5].
- The interaction between the laser and electron bunch is used to generate a beam energy modulation on the 100 femtosecond scale in storage rings.

* This work is supported by US DOE Grant No. DE-SC0006284.

ISBN 978-3-95450-138-0

Copyright © 2013 CC-BY-3.0 and by the respective authors

MULTIPACTING SIMULATION OF ACCELERATOR CAVITIES USING ACE3P*

Lixin Ge, Kwok Ko, Zenghai Li, Cho-Kuen Ng and Liling Xiao
SLAC, Menlo Park, CA 94025, U.S.A

Abstract

ACE3P [1] is a 3D parallel finite element code suite for cavity design and optimization including electromagnetic, thermal and mechanical effects. Taking advantages of the power of computing on multi processors, ACE3P's particle tracking module Track3P allows efficient multipacting (MP) simulation by extensive scanning in field gradient and on cavity surface to identify the occurrences of MP activities. The output from Track3P simulation includes the determination of resonant trajectories and their locations, the calculation of electron impact energy on cavity surface, and the evaluation of the electron enhancement counter as a function of field gradient. The sensitivity of MP on secondary emission yield can be readily obtained through post processing. The basic capabilities of Track3P for MP simulation will be presented.

INTRODUCTION

Multipacting (MP) is an undesireable, resonant built-up of electrons inside RF structures. It can cause wall heating and high power breakdown of RF components, prolong processing time and limit the achievable design field gradient. While most of the soft MP barriers could be processed through RF, the presence of a hard MP barrier prevents a RF component from reaching its design power or field gradient level.

Much work has been done on MP studies to identify potential MP events and to mitigate MP activities. In recent years, with more computing power, full 3D simulation tools have been developed to investigate potential MP activities. High resolution EM field, correct representation of particle emission from curved surface, realistic SEY curve for surface material and comprehensive post-processing of particle data to identify MP events are the basic requirements for accurately simulation of MP. Furthermore, the use of high performance computing allows efficient MP simulation by making use of hundreds to thousands of CPU cores running in parallel, by which the speedup in computation time facilitates extensive parameter scans. Track3P, a 3D parallel particle tracking code, provides a MP simulation tool with these advanced modeling and computational features. It has been extensively benchmarked against experiments and applied to model and predict MP activities for the design of many accelerator cavities and RF components.

* The work was supported by the U.S. DOE contract DE-AC02-76SF00515 and used the resources of NERSC at LBNL under US DOE Contract No. DE-AC03-76SF00098.
[1]lge@slac.stanford.edu

MULTIPACTING SIMULATION USING ACE3P

ACE3P

ACE3P (Advanced Computational Electromagnetics 3D Parallel) is a comprehensive set of conformal, higher-order, parallel finite-element electromagnetic codes with two unique features. First, it is based on higher-order curved finite element method for high-fidelity modeling and improved solution accuracy. Second, it is implemented on massively parallel computers for increased memory (problem size) and speed. The six modules of ACE3P cover a wide range of simulation capabilities for accelerators: Omega3P for calculating cavity modes and damping, and S3P for transmission in open structures in frequency domain; T3P for calculating wakefields and transients in time domain; Track3P for MP and dark current studies using particle tracking; Pic3P for RF gun design with particle-in-cell (PIC) method; and TEM3P for multi-physics analysis including EM, thermal and mechanical effects.

Track3P Characteristics

Track3P provides accurate and efficient simulation for MP by tracking particle trajectories under the influence of RF fields or external static fields. The RF field in an accelerator structure is first solved by Omega3P or S3P, which calculates the EM field to high accuracy using higher-order basis functions (up to 6^{th} order), and then loaded into Track3P for particle tracking. In a similar manner, external static electric and magnetic fields can be read into the code as input field data. The high-fidelity geometry representation built in the finite-element method allows realistic modeling of particle emission on cavity wall. Track3P constructs the MP map by identifying resonant particle trajectories. With a realistic secondary electron yield (SEY) curve provided by experiments, Track3P can calculate the particle enhancement counter and locate MP regions. This is achieved using the versatile postprocssing tools that have been developed to identify the onset of MP through various parameter scans.

MP Module in Track3P

The following describes the procedure for modeling MP in Track3P. Electrons with specified kinetic energy and emission direction are launched from specific surfaces at different phases over a full RF period. The initial launched electrons follow the electromagnetic fields in the structure and eventually hit the boundary,

Copyright © 2013 CC-BY-3.0 and by the respective authors

INTER-BUNCH COMMUNICATION THROUGH CSR IN WHISPERING GALLERY MODES*

R. Warnock †, SLAC National Accelerator Laboratory, Menlo Park, CA, USA
J. Bergstrom, Canadian Light Source, Saskatoon, SK, Canada
M. Klein, Synchrotron SOLEIL, Gif-sur-Yvette, France

Abstract

Theory predicts that coherent synchrotron radiation (CSR) in electron storage rings should appear in whispering gallery modes, which are resonant modes of the vacuum chamber, characterized by their high frequencies and concentration near the outer wall of the chamber. Such modes produce an extended wake field behind a particle bunch, which can influence the CSR from a succeeding bunch in a train. We review experimental evidence for the resonances and for the inter-bunch communication. We then present a calculation based on coupled Vlasov-Fokker-Planck equations which confirms an effect seen experimentally, namely that increasing the charge in a leading bunch increases the radiation from a following bunch.

RESONANCES: THEORY AND EVIDENCE

Synchrotron radiation in electron accelerators is strongly affected by the metallic vacuum chamber surrounding the beam, as was already shown theoretically by Schwinger in 1945 [1]. In the parallel plate model of the chamber [1] there is an exponential suppression of radiation at wavelengths greater than $\lambda_0 \approx 2h(h/R)^{1/2}$, where h is the separation of infinite conducting plates, and R is the radius of the particle's circular trajectory lying in the midplane. The model is made more realistic by adding conducting side walls perpendicular to the plates, so that the beam moves in a circular torus of rectangular cross section, with width w and height h. For w of order h, the cutoff λ_0 is roughly the same as before, but a markedly different physical picture emerges.

Radiation to infinity is now forbidden, and radiation synchronous with the beam appears in resonant modes, sharply concentrated in frequency [2]. We call these *whispering gallery modes*, because of a close analog in acoustics [3]; similar phenomena are widely studied in RF engineering and optics. .

A theoretical spectrum of resonant modes is shown in Fig. 1, which is a plot of the real part of the radiation impedance $Z(k)$ for a beam centered in a circular torus with rectangular cross-section and resistive walls of conductivity σ [2]. The parameters correspond to those of the ANKA light source in Karlsruhe: $R = 5.559$m, $w = 6.8$cm, $h = 3.2$cm, $\sigma = 1.33 \cdot 10^6$ (SI units). The power spectrum of CSR is proportional to $ReZ(k)|\hat{\lambda}(k)|^2$, where $\hat{\lambda}(k)$ is the Fourier transform of the bunch profile.

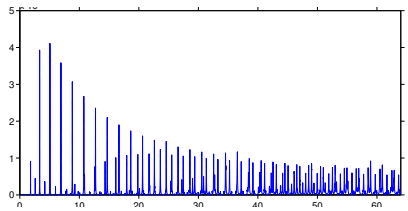


Figure 1: Re $Z(k)$ in ohms for ANKA parameters, vs. $k = 1/\lambda$ in cm^{-1}.

At ANKA and other light sources (CLS, BESSY, MLS, *et al.*) there are large flared vacuum chambers where the IR radiation is extracted, and these may alter the observed spectrum in comparison to that of the smooth toroidal model. The longitudinal electric field $E(s,t)$ may always be regarded as a function of the two independent variables $z = s - \beta ct$ and s. That leads to the concept of position dependent wake $\mathcal{W}(z,s)$. We define

$$\mathcal{W}(z,s) = E(s,t)\ ,\ \bar{\mathcal{W}}(z) = \frac{1}{C}\int_0^C \mathcal{W}(z,s)ds\ . \quad (1)$$

The average $\bar{\mathcal{W}}(z)$ over the circumference C is probably adequate to describe the bunch dynamics, since the synchrotron period is large compared to the revolution time. We suppose that $\bar{\mathcal{W}}$ can be approximated as the wake from the impedance of the smooth toroidal model, with central radius R equal to the bending radius of the dipoles.

Note that an interferometer at the position $s = s_{IR}$ of a flared IR chamber will see a field with time dependence given by $\mathcal{W}(z - \beta ct, s_{IR})$, in general different from the time dependence of $\bar{\mathcal{W}}(z - \beta ct)$. Specific theoretical modeling of fields in the flared chamber will be necessary to compare interferometer data with theory.

In an older ring, the NSLS-VUV at Brookhaven, the IR chamber is the same as in other dipoles, so the aforementioned difficulty is not so severe. Moreover, a power spectrum was measured at VUV in the bursting CSR mode, using a Michelson interferometer and also microwave techniques. In Ref.[4] a good fit of the model to experimental positions of spectral lines was shown. Zhou [5] did a similar fit including straight sections, but with less detailed discussion of low frequency lines. The straights induce a width of the lines, which could be part if not all of the explanation of experimental widths.

* Partial support at SLAC from U.S. Dept. of Energy contract DE-AC03-76SF00515; support at CLS from CFI, NSERC, NRC, The Canadian Institutes of Health Research, and the Government of Saskatchewan.
† warnock@slac.stanford.edu

ISBN 978-3-95450-138-0

Copyright © 2013 CC-BY-3.0 and by the respective authors

REVISED VIEW OF BASIC FEL EQUATIONS AND A NONLINEAR VLASOV DESCRIPTION*

R. Warnock †, SLAC National Accelerator Laboratory, Menlo Park, CA, USA

Abstract

The standard one-dimensional FEL equations are revised to incorporate a new approach to the wiggle average, in a context of continuous frequency. It has a firmer mathematical foundation, and leads to an interesting reformulation in the time domain. The equations are interpreted as a nonlinear Vlasov system for a continuous distribution function of ponderomotive angle and energy spread. Numerical solutions are illustrated.

VLASOV THEORY OF THE FEL

A linearized version of the Vlasov or Vlasov-Klimontovich equation is accepted as the natural mathematical framework for an analytic discussion of the basic mechanism of the FEL, at distances up to and including the exponential growth region. At greater distances along the undulator a nonlinear saturation comes into play, and to understand that regime one usually resorts to a simulation based on a limited number of representative particles. I explore an alternative approach, based on the full nonlinear Vlasov equation. The general advantage of nonlinear Vlasov over particle simulations is in reduction of modeling noise, but there may also be opportunities for analytic studies of the nonlinear equation. This approach requires a representation of the phase space distribution as a smooth function. To account for granularity from the finite particle number in the startup of the SASE process, I take the initial distribution to be noisy but smooth in the mathematical sense, namely a truncated formal Fourier series of a random discrete particle distribution.

REVISED TREATMENT OF BASIC FEL EQUATIONS

I first review a different treatment of basic FEL equations in one degree of freedom. I work with equations for general continuous frequency ν, and perform the wiggle average at general ν, not just at integers. Moreover, the averaging is now in a form that is justified by the mathematical theory of averaging of differential equations. The new equations suggest a more radical step, namely to reverse integration orders so as to pass from the frequency domain to the time domain (more exactly the domain of the ponderomotive angle). The kernel in the new scheme, analogous to a wake potential, has compact support and intriguing properties.

I consider planar electron motion in a planar undulator, with z and x being longitudinal and transverse position coordinates. A general representation of the transverse electric field is [1]

$$E_x(z,t) = \int_{-\infty}^{\infty} \hat{E}_x(\nu,z) e^{i\nu k_1(z-ct)} d\nu \ , \qquad (1)$$

assuming only that the field is smooth and decaying at infinity as a function of $\alpha = k_1(z-ct)$. Here $k_1 = 2\pi/\lambda_1$ is the wave number of the fundamental optical mode. A similar representation holds for the current density $J_x(z,t)$, in the sense of Fourier transforms of generalized functions if the source consists of point particles. A calculation invoking the wave equation and the slow variation approximation (dropping the second derivative), followed by the inverse FT with respect to α, yields the result

$$\frac{\partial \hat{E}_x(\nu,z)}{\partial z} = -\frac{Z_0}{2} \hat{J}_x(\nu,z) \ , \qquad (2)$$

with SI units, Z_0 being the impedance of free space.

To derive $\hat{J}_x$ assume a volume density of electrons

$$n_e(z,t) = -\frac{e}{\Sigma_\perp} \sum_{j=1}^{N} \delta(z - z_j(t)) \ , \qquad (3)$$

where $\Sigma_\perp$ is an average transverse area of the beam. Then by applying the formula for velocity v_x in the undulator one finds

$$J_x(z,t) \approx \frac{1}{\gamma_0} K \cos\zeta \ n_e(z,t) \ , \ \zeta = k_u z \ , \ \gamma = \gamma_0(1+\eta) \ , \qquad (4)$$

where $k_u = 2\pi/\lambda_u$ is the undulator wave number and the approximation is $|\eta| \ll 1$, used without comment henceforth. Now take the FT of J_x with respect to α, and for each j change the integration variable from α to u where $t = t_j(u) \ , z_j(t_j(u)) = u$. Next introduce the ponderomotive angle θ as a convenient phase space coordinate, namely

$$\theta = \alpha + \chi(\zeta) \ , \quad \chi(\zeta) = \zeta + \xi \sin 2\zeta \ , \quad \xi = \frac{1}{2 + 4/K^2} \ , \qquad (5)$$

and define

$$\theta_j(z) = \alpha_j(z) + \chi(\zeta) = k_1(z - ct_j(z)) + \chi(\zeta) \ . \qquad (6)$$

Then the FT of the current becomes

$$\hat{J}_x(\nu,z) = -\frac{ecNK}{\gamma_0 \Sigma_\perp \lambda_1} w(\zeta,\nu) < e^{-i\nu\theta(z)} > \ , \qquad (7)$$

$$w(\zeta,\nu) = \cos\zeta \ e^{i\nu\chi(\zeta)} \ , \qquad (8)$$

$$< e^{-i\nu\theta(z)} > = \frac{1}{N} \sum_{j=1}^{N} e^{-i\nu\theta_j(z)} \ . \qquad (9)$$

* Partially supported by U.S. Dept. of Energy contract DE-AC03-76SF00515

† warnock@slac.stanford.edu

Copyright © 2013 CC-BY-3.0 and by the respective authors

MODELING LOCALIZED STATES AND BAND BENDING EFFECTS ON ELECTRON EMISSION ION FROM GaAs*

D. A. Dimitrov, C. Nieter, Y. Choi, Tech-X Corp., Boulder, CO 80303, USA
I. Ben-Zvi, J. Smedley, T. Rao, BNL, Upton, NY 11973, USA
I. Bazarov, S. Karkare, W. Schaff, CLASSE, Cornell University, Ithaca, NY 14853, USA

Abstract

High acceptor doping of GaAs and (Cs, O) surface coating leads to downward band bending terminating with effective negative electron affinity surface. The periodicity breaking at the surface together with the formed potential leads to one or more localized states in the band bending region together with effective Fermi level pinning. We report results on how to calculate the band bending potential, the Fermi level pinning, and localized states as functions of GaAs p-doping density, surface density of states, and temperature. We also consider how these surface properties affect electron emission.

INTRODUCTION

High-average current and high-brightness electron beams are needed in advanced applications such as ultra-high Free-Electron Lasers, electron cooling of hadron accelerators, and Energy-Recovery Linac light sources. Semiconductor cathodes, such as negative electron affinity GaAs-based cathodes, are known [1] to have good quantum efficiency (QE) (10% achieved experimentally), low thermal emittance with prompt response time [2], and are candidates to achieve high average current up to 100 mA.

However, how to design, fabricate, and reliably operate semiconductor cathodes at high average current (reaching 100 mA) still represents a major problem. Some of the most important effects to understand are related to surface space charge region, controlling the electron affinity and band bending as a function of surface properties and charge propagation to the surface [3, 4].

In addition to experiments, simulations provide a complementary way to efficiently explore relevant parameter sets. Moreover, they allow us to obtain data on properties that are currently not accessible through experiments or very difficult to measure. For example, the energy distribution of electrons inside the cathode material in the region of the emission surface is directly accessible in the simulations but very difficult to measure in experiments. Producing high fidelity simulations data of semiconductor cathode properties depends on accurate modeling of the surface space-charge region. Specifically, the calculation of the band bending region (BBR) energy profile, determination of Fermi level pinning (e.g. for GaAs cathodes), development of localized electron levels with emission from them, and how the electron affinity depends on these properties significantly affect electron emission.

Emission from localized states has been shown to contribute to the observed energy distribution of electrons from GaAs and one approach was proposed to explain it [3] that depends on specific properties of the potential across the GaAs-vacuum interface. Similar effects were considered for emission from diamond but the model developed was based on a different surface potential [5].

We have already done simulations with a surface band bending profile that uses a quadratic approximation [6]. Here, we provide a general approach for calculation of the band bending profile and the Fermi level pinning for GaAs.

BAND BENDING AND LOCALIZED STATES

The surface band bending arises as a consequence of the space charge region that develops as a result of the symmetry breaking and appearance of surface states. The electrostatic potential in the band bending region (BBR) is determined from the solution of the Poisson equation:

$$\nabla \cdot (\varepsilon \nabla \phi) = q \left(n\left[\phi\right] - p\left[\phi\right] + N_A^-\left[\phi\right] - N_D^+\left[\phi\right] \right), \quad (1)$$

where $\varepsilon(\mathbf{r})$ is the dielectric constant, q is the fundamental charge, n and p are the electron and hole densities in the conduction and valence band, respectively, N_A^- and N_D^+ are the densities of ionized acceptor and donor impurities when present. Generally, all charge densities are non-linear functions of the potential. When periodicity is preserved in the emission surface, the resulting non-linear Poisson equation is effectively one-dimensional. For p-doped GaAs, when the donor density can be neglected and the acceptors are fully ionized, it has the form:

$$\frac{d^2U(x)}{dx^2} = \frac{q^2}{\varepsilon k_B T}\left(N_A - \frac{2N_V}{\sqrt{\pi}} F_{1/2}\left(\eta_V - U(x)\right)\right), \quad (2)$$

where $\eta_V = (E_V - E_F)/k_BT$ (with E_V the valence band maximum in bulk and E_F the Fermi level, k_B the Boltzmann constant and T the lattice temperature), $U(x) = q\phi(x)/k_BT$, $N_V = 2\left(\frac{m_{dh}k_BT}{2\pi\hbar^2}\right)^{3/2}$ with m_{dh} a hole-related effective mass, and $F_{1/2}(x) = \int_0^\infty \frac{\sqrt{u}}{1+e^{u-x}}du$. The boundary conditions imposed on the 1D non-linear Poisson equation are determined from the requirement of zero

* The authors wish to acknowledge the support of the U.S. Department of Energy (DOE) and the National Science Foundation (NSF) under grants DOE DE-SC0006246, NSF DMR-0807731, and DOE DE-SC0003965.

ISBN 978-3-95450-138-0

Copyright © 2013 CC-BY-3.0 and by the respective authors

INTEGRATED KINETIC AND PLASMA DIELECTRIC MODELS OF ELECTRON CLOUD BUILDUP AND TE WAVE TRANSMISSION *

S. A. Veitzer†, Tech-X Corporation, Boulder, CO, 80303 USA
P. H. Stoltz, Tech-X Corporation, Boulder, CO, 80303 USA
P. G. Lebrun, Fermilab, Batavia, IL, 60510 USA

Abstract

Buildup of electron plasmas in accelerator cavities poses a serious threat to performance for current and future accelerators. Traveling-wave rf diagnostics are an effective, non-destructive way to measure electron clouds, although determining the true cloud density from spectra is difficult due to the effects of reflections, non-uniform cloud density, and magnetic field effects. We model traveling-wave rf diagnostics of electron clouds by simulating spectra using both harmonically modulated plasma dielectric models, and dielectric models based on simulated electron cloud densities. We compare here the differences in computed side band spectra due to different magnetic field configurations for Main Injector parameters, and report on computational challenges inherent to numerical modeling of systems with large variances of spatial and temporal scales.

RF DIAGNOSTICS PROVIDE DIAGNOSTIC MEASUREMENT OF ELECTRON CLOUDS

Electron clouds have been identified as a potential performance-limiting element in both hadron and lepton accelerators [1]. Recently, methods for measuring electron cloud densities in a non-destructive manner have been developed. These methods rely on measurement of rf signals injected into the beam pipe, either at a frequency just below the cutoff frequency (resonant rf method) or above the cutoff frequency (traveling wave method). For traveling wave rf diagnostics, the presence of an electron cloud plasma in the beam pipe induces a phase shift due to changes in the dielectric properties of the medium in which the rf is traveling. The plasma dielectric strength is modulated at the revolution frequency as the plasma builds up during bunch passages, and dissipates during gaps in the bunch train. This is typically observed in experiments as side bands at the revolution frequency, with a height that is proportional (in the linear approximation) to the average plasma density. Magnetic field effects also come into play with these diagnostics in two ways. First, magnetic fields may excite a cyclotron resonance [2, 3] that increases the phase delay per unit length, and second, magnetic fields will affect the electron trajectories that will in turn change the spatial distribution of electrons in the beam pipe and hence the dielectric properties of the plasma. It has been observed in both experiments and in simulations that dipole fields tend to align electrons in vertical stripes [4, 5]. Recent studies indicate that quadrupole fields may be able to trap electron clouds thereby leading to negative effects on the lead bunch in a train [6].

* This work was performed under the auspices of the Department of Energy as part of the ComPASS SCiDAC-2 project (DE-FC02-07ER41499), and the SCiDAC-3 project (DE-SC0008920).

† veitzer@txcorp.com

SIMULATION RESULTS

We are developing numerical models that are appropriate for simulating electron clouds and rf diagnostics in the Main Injector at Fermilab, using the plasma simulation framework VSim [7]. In all of the simulations reported here, we use a circular cross section beam pipe with radius 7.46125 cm, and 50 cm long. We use a mesh with 48 computational cells in the longitudinal direction, and 16 cells in each of the transverse directions. We simplify the bunch train structure from that in the actual Main Injector by modeling one full revolution as a single continuous bunch train of 18.8 ns bunches of roughly 8 GeV protons. We artificially set one revolution time to $2.0\mu s$, including an abort gap of 0.4μ s during which time there are no beam bunches. This sets the modulation frequency to 500 kHz. The cutoff frequency for this beam pipe is 1.1774 GHz, and we drive rf above this frequency to model traveling wave diagnostics.

Kinetic PIC Simulations

We first perform detailed electrostatic Particle-In-Cell (PIC) simulations of electron cloud buildup using VSim. We start with a low-density, uniformly distributed, cold electron plasma in a circular beam pipe with radius 7.46 cm. We solve for the electric fields electrostatically given the overall charge distribution and subject to the appropriate boundary conditions; metallic boundaries on the beam pipe walls, and port boundaries on the open ends of the simulation domain. Port boundaries are a numerical filter model that effectively absorbs wave energy at a given phase velocity, preventing reflections from the boundary. We do not inject rf power in the kinetic simulations because we are focused on modeling cloud buildup here.

In buildup simulations we inject beam bunches with a spacing of 18.8 ns by specifying a time-dependent charge density that simulates the passage of proton beam bunches. Bunches cross the simulation domain for 1.2μs, followed by a 0.8μs abort gap, representing a single revolution. These times are chosen to demonstrate the physics of electron cloud buildup while maintaining numerical efficiency. In future simulations the actual Main Injector revolution period will be approached. Electrons that make up the plasma (cloud) are modeled as variable-weight kinetic par-

Copyright © 2013 CC-BY-3.0 and by the respective authors

ISBN 978-3-95450-138-0

CREATION OF GAMMA RADIATION USING ANNIHILATION OF CHANNELED POSITRONS IN CRYSTALS

Koryun B. Oganesyan*,
A.I.Alikhanyan National Science Lab, Yerevan, Armenia

Abstract

A possibility of channeling of low-energy ($5 \div 20\,Mev$) relativistic positrons with coaxial symmetry around separate crystal axes of negative ions in some types of crystals, is shown. The annihilation processes of positrons with medium electrons are investigated in details. The lifetime of a positron in the regime of channeling is estimated $10^{-6}\,sec$ which on a $10^9 \div 10^8$ is bigger than at usual cases.

INTRODUCTION

Studying of ways of generation of short-wave coherent radiation always was an essential problem of a science and was stimulated by its wide applied application. In work [1] one of the first the mechanism of radiation of relativistic electrons at their movement in periodic structures (see also [2]) was offered (later such types of structures have been named undulators). It at first sight imperceptible work later has essentially accelerated a process of creation of of modern devices the synchrophasotrons and the lasers on free electrons (see for example review [3]). In spite of the fact that the technology of generation of undulator radiation steadily is being developed and successes are obvious [4], however the problems also are obvious and they remain unresolved up to now. Let's note that the frequency of undulator radiation is being defined by length of its periodic element which in FELs and the undulators devices are macroscopic. Other defects of undulators their big sizes and used big energies of electrons. After opening of channeling of electrons (positrons) in crystals [5–7] and accompanying by its short-wave radiation [8] was appeared a hope to solve all the aforementioned problems. However these hopes up to now is justified only partially. In particular the problems of generation of short-wave radiation (x-ray) from less energetic electrons (of order a several Mev) on very small distances (of order a several micron) have been solved. Now a new problem arise. The point is that in the regime of channeling the particle (electrons and positrons) usually live very short time $\sim 10^{-14} \div 10^{-15}\,sec$. However this time is very short for conversion of a appreciable part of particle energy to energy of radiation. The short lifetime as well doesn't conduce to use of external factors for control by beam of channeling particles and to improving of spectral characteristics of radiation.

The quantum theory of channeling for electrons and positrons has been elaborated by many authors [8–10]. It is important to note that an electron in a crystal can commit both planar and axial channeling. At the same time only one type of real channeling for the positrons is known, the regime where a particle is localized between two adjacent planes. The possibility of axial channeling of positive particles has not been investigated, seriously up to now, because the crystallographic axes, irrespective of grade of crystal are been charged positively. However investigation of possibilities of axial channeling of positrons and, hence, the formation of metastable relativistic positron systems (PS) is a problem of utmost importance for a radiation physics.

In this work a role of different processes (scattering of positron on media electrons, the annihilation processes etc) in the expansion of energy levels of relativistic PS is analyzed and shown that PSs are metastable.

FORMATION OF RELATIVISTIC POSITRON SYSTEM (PS)

In previous work [11] we have shown, that if a low-energy relativistic positrons ($5 \div 20\,Mev$) are scattering under a small corners $\vartheta \le \vartheta_L$ (where ϑ_L is a Lindhard angle) on the axis $\langle 100 \rangle$ of chlorine ions Cl^- that they fall into regime of axial channeling. Moreover the motions of positrons concentrate between two cylinders that is very important from the point of view of movement stability. In particular, as was shown the effective $2D$ potential of channeling don't depend from temperature of media in a broad range of temperatures and has an order $-10\,eV$ depths of potential which is sufficient for formation a several quantum states of transverse motion. Recall that this type of effective potential can be in other crystals too. For example the effective potential of negatively charged ions O_2 axes often used in experiments of crystal SiO_2 is such.

In other words, the relativistic positrons in described regime of channeling don't interact with phonons subsystem. That means a main factor of de-channeling of particles in considered case is absent.

Taking into account the symmetry of effective potential for positrons around of the negative ions axis we can write the following analytical formula:

$$\begin{aligned} U_0(\rho) &= D_0(e^{-2\alpha\overline{\rho}} - 2e^{-\alpha\overline{\rho}}), \overline{\rho} = (\rho - \rho_0)/\rho_0, \\ \rho &= \sqrt{x^2 + y^2}, \end{aligned} \quad (1)$$

where the parameters for usual crystals are being found into intervals $D_0 = 5 \div 10eV$, $\alpha = 0.5 \div 0.8$ and $\rho_0 \sim 0.5d$, where d is a lattice constant.

* bsk@yerphi.am

ISBN 978-3-95450-138-0

Copyright © 2013 CC-BY-3.0 and by the respective authors

HOW ACTS PLANE WIGGLER MAGNETIC FIELD INHOMOGENEITY ON THE SPONTANEOUS RADIATION AND THE GAIN

Koryun B. Oganesyan*, A.I. Alikhanyan National Science Lab, Yerevan, Armenia

Abstract

A relativistic electron motion in a transversally inhomogeneous magnetic field of a wiggler is shown to consist of fast (undulator) and slow (strophotron) components. By separating fast and slow motions and by averaging equations of motion over fast undulator oscillations, we find spectral intensity of strophotron spontaneous emission in such a system. By solving similarly equations of motion in the presence of an external light wave, we find the gain in a Free-Electron Laser based on the interaction of light with the strophotron mode of the electron motion. Both the strophotron gain and the corresponding intensity of spontaneous emission are shown to be well separated spectrally from the usual undulator parts.

INTRODUCTION

Usually FEL [1, 2] use the kinetic energy of relativistic electrons moving through a spatially modulated magnetic field(wiggler) to produce coherent radiation. The frequency of radiation is determined by the energy of electrons, the spatial period of magnetic field and the magnetic field strength of the wiggler. This permits tuning a FEL in a wide range unlike atomic or molecular lasers. In usual FEL magnetic field of wiggler is supposed to be uniform. But really the magnetic field is inhomogeneous in transverse direction(see for example [3]). It is important to take into account this inhomogeneity. This account leads to complex motion of electrons: fast undulator oscillations along the wiggler axis and slow strophotron motion [4] – [9] in transverse direction . In the next section we describe the equation of motion of electrons moving along the axis of the wiggler with transversal inhomogeneous magnetic field. In the Sec. III and IV we calculate the spectral distribution of spontaneous emission and the gain correspondingly.

EQUATIONS OF MOTION

The vector potential of undulator's magnetic field has a form [10]

$$\overrightarrow{A_W} = -\frac{H_0}{q_0}\cosh q_0 x \sin q_0 z \;\; \hat{j} \tag{1}$$

where H_0 is the strength of magnetic field and $q_0 = 2\pi/\lambda_0$, λ_0 - period of wiggler, $\hat{j}$ unit vector in y direction.

The change of energy is

$$\frac{d\varepsilon}{dt} = 0, \qquad \varepsilon = const \tag{2}$$

* bsk@yerphi.am

Further we consider paraxial approximation when

$$q_0 x < 1 \tag{3}$$

Taking into account (3) the magnetic field (1) becomes

$$H_x = H_0\left(1+\frac{q_0^2x^2}{2}\right)\cos q_0 z; H_y = 0;$$
$$H_z = -H_0 q_0 x \sin q_0 z \tag{4}$$

Then we can write equations of motion taking into account (2) ($p_{x,y,z} = v_{x,y,z}\varepsilon$)

$$\begin{aligned}
\ddot{x} &= -\left(\frac{eH_0}{\varepsilon}\right)^2 x\sin^2 q_0 z \\
\dot{y} &= \frac{eH_0}{\varepsilon q_0}\left(1+\frac{q_0^2x^2}{2}\right)\sin q_0 z \\
\ddot{z} &= -\frac{1}{2q_0}\left(\frac{eH_0}{\varepsilon}\right)^2 \sin 2q_0 z(1+q_0^2x^2)
\end{aligned} \tag{5}$$

After averaging first equation of Eq. (5) on period $2\pi/q_0$ and taking into account that $\overline{\sin^2 q_0 z} = 1/2$ we have

$$\ddot{x} + \Omega^2\, x = 0 \tag{6}$$

which has a solution

$$x = a_0\cos(\Omega t + \theta_0) \tag{7}$$

where

$$\begin{aligned}
\Omega &= \frac{eH_0}{\sqrt{2}\varepsilon}; \qquad a_0 = \sqrt{x_0^2+\frac{\alpha^2}{\Omega^2}}; \\
\cos\theta_0 &= \frac{x_0}{a_0}; \quad \sin\theta_0 = -\frac{\alpha/\Omega}{a_0}; \\
\theta_0 &= -\arctan\frac{\alpha}{x_0\Omega}
\end{aligned} \tag{8}$$

Averaging of the second equation of Eq. (5) gives

$$\ddot{z}^{(0)} = 0; \quad \dot{z}^{(0)} = v; \quad z^{(0)} = vt. \tag{9}$$

The solution of the second equation of Eq. (5) using Eq. (7) and Eq. (9) has a form

$$\begin{aligned}
\delta z &= -\frac{\Omega^2}{2q_0^2}t + \frac{\Omega^2}{4q_0^3}\sin 2q_0 t \\
&+ \frac{a_0^2\Omega^2}{16q_0}\sin\{2(q_0+\Omega)t + 2\theta_0\} \\
&+ \frac{a_0^2\Omega^2}{16q_0}\sin\{2(q_0-\Omega)t - 2\theta_0\}
\end{aligned} \tag{10}$$

Copyright © 2013 CC-BY-3.0 and by the respective authors

GENERATION OF INTENSIVE TRANSITION RADIATION IN MODULATED MEDIUM

Koryun B. Oganesyan*, A.I.Alikhanyan National Science Lab, Yerevan, Armenia

Abstract

The 3D spin-glass system in the external standing electromagnetic field is considered. It is shown on an example of amorphous quartz, under the influence of a standing microwave field, at its certain parameters, superlattice is created in the medium where difference in values of dielectric constants of neighboring layers can be up to third order. This superlattice exists during the nanosecond, however it is sufficient for using it as a radiator for generation of transition radiation by relativistic electrons.

INTRODUCTION

The formation and governing of periodically modulated refractive index in media is a most important problem of solid state physics and material science. First of all it is related to the possibility of developing compact UV or X-ray Free-Electron Lasers (FEL) based on emission of transition radiation (TR) (see for example [1]). Currently the following two problems are discussed intensely:

1. A gas-plasma medium with periodically varied ionization density [2–9],

2. A special periodical solid-state superlattice-like (SSL) structures composed of layers with different refraction indexes [10–20].

TR is generated due to the difference in frequency-dependent dielectric constants (permittivity functions) of adjacent layers (remember that the radiation power is proportional to $[\epsilon_1^R(w) - \epsilon_2^R(w)]^2$, where $\epsilon_{1;2}^R(w) = Re[\epsilon_{1;2}(w)]$) [21]. Therefore, the possibility of controlling this difference by means of an external field is highly important. In other words, the problem here is to construct a superlattice with difference in dielectric constants of neighboring domains having the form $[\epsilon_1^R(w,\mathbf{g}) - \epsilon_2^R(w,\mathbf{g})]^2$, where $\mathbf{g}$ describes the controlling parameters, $\epsilon_1(w,\mathbf{g})$ and $\epsilon_2(w,\mathbf{g})$ are dielectric permittivity functions in neighboring regions. According to theoretical and experimental studies, the periodical structures may be formed in condensed matter by means of external electromagnetic or acoustic fields [22–25].

This idea was recently realized in TR generation experiments [26]. In particular, it was shown that at the passage of a beam of 20 Mev electrons through amorphous silicon dioxide $a - SiO_2$ with a standing electromagnetic wave (of 10 GHz frequency) inside, anomalous high short-wave radiation was produced. Preliminary studies explain this high intensity radiation as a result of multiple passage of the electron beam through interfaces between regions with different permittivity functions. Theoretically the appearance of $1D$ superlattice order in random media is explained by the polarization of media due to the orientational relaxation of elastic dipoles in the direction of external electromagnetic field propagation [27].

So, the main objective of this work is a systematic investigation of relaxation processes and critical effects in $a - SiO_2$ compound type disordered $3D$ systems under the action of external electromagnetic field that forms a standing wave in the medium, and in particular, to prove the possibility of formation of $1D$ periodic superlattice of permittivity function in the scales of space-time periods of standing wave.

FORMULATION OF THE PROBLEM

The starting point in our discussion will be the Clausius-Mossotti relation for dielectric constant. It is known that in isotropic media (as well as in crystals of cubic symmetry) the dielectric constant is well described by the Clausius-Mossotti equation [28–30]:

$$\frac{\epsilon_s - 1}{\epsilon_s + 2} = \frac{4\pi}{3}\sum_m N_m^0 \alpha_m^0, \qquad (1)$$

where N_m^0 is the concentration of particles (electrons, atoms, ions, molecules) with given m types of polarizability and α_m^0 correspondingly are polarizability coefficients. It follows from this formula that the static dielectric constant ϵ_s depends on the polarizability properties of particles as well as on their topological order. In the external field the homogeneity and isotropy of the medium is often lost. Then, it is expected that the formula (1) will be applicable after slight generalization.

The object of our investigation are solid state dielectrics of the amorphous silicon dioxide $a-SiO_2$ type. According to numerical $ab\ initio$ simulations [31], the structure of this type compound may be well described by the model of $3D$ disordered spin system.

In particular the $3D$ spin system we can represent as a $3D$ lattice with the lattice's constant $d_0(T) = \{m_0/\rho_0(T)\}^{1/3}$, where m_0 is the molecule mass, ρ_0 is the density and T is the temperature. We will assume also, that in each cell of this lattice there are only one randomly distributed spin (roughly polarized molecule).

We will suppose that the media under the influence of external standing electromagnetic field the electrical part

* bsk@yerphi.am

ISBN 978-3-95450-138-0

Copyright © 2013 CC-BY-3.0 and by the respective authors

ULTRA-LOW EMITTANCE LIGHT SOURCE WITH A TORUS-KNOT TYPE ACCUMULATOR RING

A. Miyamoto and S. Sasaki
HSRC; Hiroshima Synchrotron Radiation Center, Hiroshima University
2-313 Kagamiyama, Higashi-Hiroshima, Japan

Abstract

We proposed a torus knot type synchrotron radiation ring in that the beam orbit does not close in one turn but closes after multiple turns around the ring. This ring is capable to have many straight sections and it is advantageous to installation of many insertion devices. Currently, we are designing a new ring based on the shape of a (11, 3) torus knot for our future plan 'HiSOR-II.' This ring is mid-low energy light source ring with a beam energy of 700 MeV. It has eleven 3.6-m-long straight sections though the ring diameter is as compact as 15 m.

In late years, some compact light source rings achieved very low emittance of several tens of nmrad. However for the ring we propose, the emittance can be reached less than 10 nmrad when the multi-bend scheme is adopted to the arc section. With this ultra-low emittance, the size and divergence of electron beam is smaller than the diffraction limited light in lower energy part of VUV region, and it will be very useful for many synchrotron radiation users' experiments. Therefore we are designing this ultra-low emittance light source ring having innovatively odd shape.

INTRODUCTION

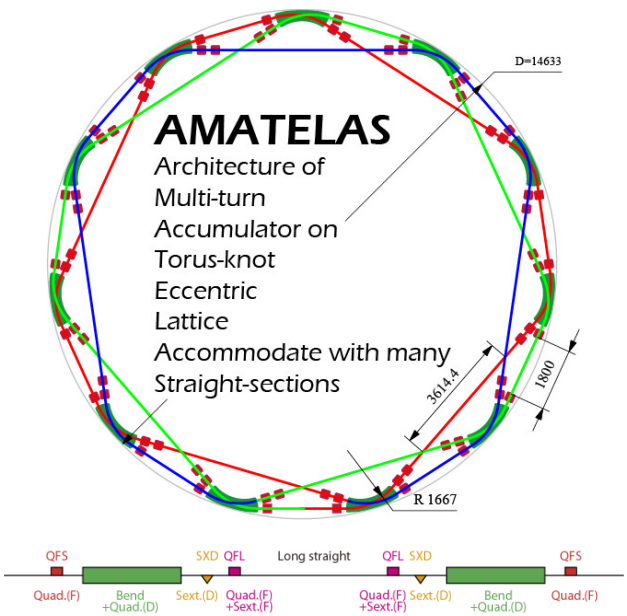


Figure 1: Schematic drawings of (11, 3) AMATELAS designed for HiSOR-II and the lattice of unit cell.

For small light source rings, it is very important to obtain a lot of straight sections in which we can install insertion devices, but it is difficult in reality because they are occupied by various magnets, RF systems or beam monitors. In this context we got a hint from the shape of the torus knot [1], and contrived the ring which had the orbit closed after multiple turns around the ring [2] and named it AMATELAS.

We are planning a new light source ring for our facility [3], therefore we are designing a new ring based on the shape of a (11, 3) torus knot for our future plan 'HiSOR-II' [4]. This ring has 11 long straight sections and we can place insertion devices efficiently by placing the elements such as quadrupole magnets near bending magnet, outside of the orbit crossing section. Furthermore, this ring has about 3 times longer closed orbit in comparison with the conventional ring, the diameter of this ring is as compact as 15 m, but its total orbit length is as long as 130 m. The AMATELAS ring designed for HiSOR-II and the lattice of unit cell are shown in Figure 1, and the main parameters of (11, 3) AMATELAS designed for HiSOR-II storage ring [5] is shown in Table 1, and beta or dispersion function of a unit cell is shown in Figure 2.

Table 1: The main parameters of (11, 3) AMATELAS for HiSOR-II storage ring

Perimeter	45.97 m
Orbit shape	(11,3) Torus knot
Perimeter	45.97 m
Orbit length	130.187 m
Beam energy	700 MeV
Straight sections	3.614 m ×11 1.728 m ×11
Betatron tune	(10.362, 7.807)
Natural emittance	17.9 nmrad
Chromaticity	(+1.0, +1.0)

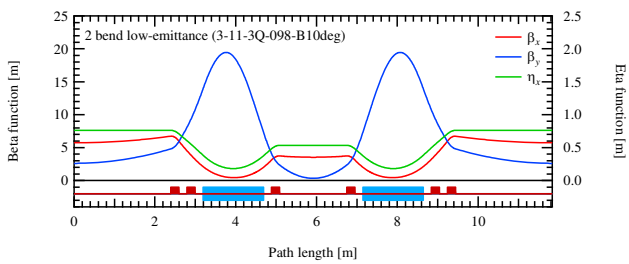


Figure 2: Optical function of (11, 3) AMATELAS for HiSOR-II storage ring.

Copyright © 2013 CC-BY-3.0 and by the respective authors

COUPLING AND BRIGHTNESS CONSIDERATIONS FOR THE MAX IV 3 GeV STORAGE RING

S.C. Leemann*, M. Eriksson, MAX IV Laboratory, Lund University, SE-22100 Lund, Sweden

Abstract

It is often suggested that the emittance coupling of a storage ring should be adjusted to the so-called diffraction limit corresponding to the shortest wavelength of interest. For 1 Å radiation this leads to a typical requirement of 8 pm rad vertical emittance. In ultralow-emittance storage rings like the MAX IV 3 GeV storage ring this corresponds to a comparably large setting of the emittance coupling (2.5%). This approach, however, does not produce the brightest radiation and needs to be revisited taking into account that overall photon brightness depends on the emittances of the electron beam and the intrinsic photon beam. This paper summarizes an analytic approach to maximizing brightness as a function of emittance coupling while retaining sufficient lifetime. Instead of "meeting the diffraction limit", we further reduce the coupling, thus increasing both the brightness and transverse coherence of the emitted radiation. We derive that reducing the MAX IV 3 GeV storage ring's vertical emittance to 2 pm rad (0.6% coupling) will increase brightness and transverse coherence by almost a factor two while 10 h overall lifetime can still be achieved.

INTRODUCTION

The MAX IV facility will use a 3 GeV linac and two storage rings to deliver synchrotron radiation to a broad and international user community across a wide spectral range and covering different temporal scales [1, 2]. The MAX IV 3 GeV storage ring has been optimized [3, 4] for insertion devices (ID's) producing high-brightness x-rays. A typical scenario is radiation at 1 Å produced in an in-vacuum undulator of roughly 4 m magnetic length. The intrinsic photon beam (i.e. the photon beam emitted by a single electron) emerging from such an ID [5] has a diffraction-limited RMS source size given by $\sigma_r = \sqrt{2L\lambda}/4\pi$ and its central cone has an RMS width $\sigma_{r'} = \sqrt{\lambda/2L}$ where L is the magnetic length of the ID and λ the (fundamental) emitted wavelength. This leads to the often quoted emittance criterion for diffraction limited radiation $\varepsilon_r = \sigma_r\sigma_{r'} = \lambda/4\pi$, which calls for 8 pm rad for 1 Å radiation.

In existing 3rd generation light sources, where the equilibrium emittance $\varepsilon_0 = \varepsilon_x + \varepsilon_y$ is several orders of magnitude larger than 8 pm rad, the conventional approach is to adjust the emittance coupling $\kappa = \varepsilon_y/\varepsilon_x$ by e.g. skew quadrupoles so that $\varepsilon_y \approx \varepsilon_r$. For small values of coupling $\varepsilon_x = \varepsilon_0/(1+\kappa) \approx$ const. The Touschek lifetime then scales like $\sqrt{\kappa}$ and the emittance coupling is therefore usually set "at the diffraction limit" and not much lower in order not to reduce overall beam lifetime.

This treatment, however, neglects the actual radiation process in the ID[1]. The brightness of the emitted radiation depends on the overlap of electron beam *and* intrinsic photon beam in phase space. This overlap, assuming a dispersion-free straight, is calculated as [5]

$$\Sigma_{x,y} = \sqrt{\sigma_r^2 + \sigma_{x,y}^2} = \sqrt{\frac{2L\lambda}{(4\pi)^2} + \varepsilon_{x,y}\beta_{x,y}}, \quad (1)$$

$$\Sigma_{x',y'} = \sqrt{\sigma_{r'}^2 + \sigma_{x',y'}^2} = \sqrt{\frac{\lambda}{2L} + \frac{\varepsilon_{x,y}}{\beta_{x,y}}}, \quad (2)$$

where $\beta_{x,y}$ is the beta function in the ID and we have assumed $\alpha_{x,y} = 0$ so that $\gamma_{x,y} = 1/\beta_{x,y}$. The spectral brightness of the emitted radiation is the flux at a specific wavelength[2] emitted from within a specific volume of transverse phase space volume, i.e.

$$\mathcal{B}(\lambda) = \frac{\mathcal{F}(\lambda)}{(2\pi)^2\mathcal{E}_x\mathcal{E}_y},$$

where $\mathcal{E}_{x,y} = \Sigma_{x,y}\Sigma_{x',y'}$ describes the effective emittance, i.e. the emittance of the overlap between electron beam and intrinsic photon beam[3]. In a nutshell, this motivates the push for low-emittance rings running with large amounts of stored current and long undulators with short period lengths.

Finally, since the transversely coherent flux emitted at a specific wavelength λ is given by

$$\mathcal{F}_c(\lambda) = \mathcal{B}(\lambda)\left(\frac{\lambda}{2}\right)^2,$$

the coherent fraction of the emitted radiation can be expressed as

$$\begin{aligned} f_c(\lambda) &= \frac{\mathcal{F}_c(\lambda)}{\mathcal{F}(\lambda)} = \frac{(\lambda/4\pi)^2}{\mathcal{E}_x\mathcal{E}_y} \\ &= \frac{1}{\sqrt{1+(\frac{\sigma_x}{\sigma_r})^2}\sqrt{1+(\frac{\sigma_{x'}}{\sigma_{r'}})^2}} \times \\ &\quad \frac{1}{\sqrt{1+(\frac{\sigma_y}{\sigma_r})^2}\sqrt{1+(\frac{\sigma_{y'}}{\sigma_{r'}})^2}}. \end{aligned} \quad (3)$$

* simon.leemann@maxlab.lu.se

[1] This approach also entirely neglects the horizontal plane and tacitly accepts that ID radiation will, at best, be diffraction-limited in the vertical plane only. Diffraction-limited light sources, i.e. storage rings where the equilibrium emittance is so low that both transverse planes can be operated at or below the diffraction limit, present a solution to this problem and have recently become a topic of great interest [6, 7].

[2] This spectral flux $\mathcal{F}(\lambda)$ is conventionally defined as the number of photons emitted per second and per 0.1% BW ($\Delta\lambda/\lambda$). It is proportional to the stored current and the number of undulator periods.

[3] A noteworthy consequence is that intrinsic photon and electron emittances are added linearly, not quadratically.

Copyright © 2013 CC-BY-3.0 and by the respective authors

ISBN 978-3-95450-138-0

SIMULATION OF USING ORBIT BUMPS TO TEST SEXTUPOLE COMPENSATION FOR THE SHORT PULSE X-RAY SYSTEM AT THE ADVANCED PHOTON SOURCE *

M. Borland†, V. Sajaev, ANL, Argonne, IL 60439, USA

Abstract

As part of an ongoing upgrade of the Advanced Photon Source (APS), a Short Pulse X-ray (SPX) system is being developed based on two sets of crab cavities separated by 180 degrees vertical phase advance. Emittance growth due to incomplete cancellation of the kicks from the sets of cavities is a concern. Simulations predict that it can be controlled by adjustment of the sextupoles between the cavities. To test these predictions, we can use orbit bumps that reproduce the trajectories of individual particles through the sectors in question. We present results of simulations of such tests, showing the degree to which the emittance growth and other properties of the machine will differ for optimized and unoptimized sextupoles. We also show results of recent experimental tests.

INTRODUCTION

One of the challenges of operating the Short Pulse X-ray (SPX) facility [1, 2] will be preserving the small vertical size of the APS beam. Vertical emittance increase was predicted in early simulations of SPX [3]. It results mainly from additional coupling occurring due to large vertical trajectories in sextupoles between the SPX cavities [4]. This emittance increase is undesirable because it decreases the x-ray brightness seen by all users. It also increases the minimum x-ray pulse duration that SPX can deliver.

We also found that lifetime and injection efficiency were negatively affected by this strong local coupling through stronger excitation of nearby nonlinear resonances. We resolved these problems in simulation by optimizing the sextupoles between the SPX cavities so as to minimize the vertical emittance growth, while at the same time preserving injection efficiency and lifetime [5].

Owing to the expense and complexity of SPX, it is desirable to test as many aspects of the beam dynamics ahead of time. With deflecting cavities, every longitudinal slice of the beam travels on its own vertical trajectory. The amplitudes of those trajectories depend on the longitudinal position of the slice. Without deflecting cavities, we cannot recreate this behavior completely, but we can generate a real orbit bump using orbit correctors where the entire beam would go on a trajectory corresponding to some beam slice. We could thus verify that the effect of the orbit bump on coupling and nonlinear dynamics is reduced when properly optimized sextupoles are used.

* Work supported by the U.S. Department of Energy, Office of Science, under Contract No. DE-AC02-06CH11357.

† borland@aps.anl.gov

Any two vertical correctors bracketing a straight section can be used to produce a trajectory that exactly corresponds to a trajectory originating from a single vertical kick somewhere in the straight section. Using existing correctors powered at modest levels, we can simulate deflections equivalent to a cavity deflecting voltage of about 4 MV without loss of stored beam. Note that this is a very stringent test, not only because it exceeds the intended maximum deflection by a factor of two, but because with actual deflecting cavities, very few electrons experience deflections that are close to the maximum possible deflection, owing to the small 33° rms phase spread of the bunch.

LATTICE OPTIMIZATION

The lattices used for the simulations and experiments are mock-ups of the planned operational lattices. The latter will differ from today's lattice by long straight sections (LSS) in straight sections 1, 5, and 7, as well as a special insertion with reduced horizontal beam size (RHB) in straight section 20. Two of the LSSs (in straights 5 and 7) are associated with SPX, being required in order to make room for the cryomodules. The vertical phase advance between these straights (i.e., through sectors 6 and 7) is ideally 2π. The LSSs are mocked up by setting to zero certain magnets that would be removed to make an actual long straight.

The tests require two lattices: one in which the sextupoles in sectors 6 and 7 are optimized to minimize SPX emittance growth, and a second with normal sextupoles in those sectors. The first lattice was optimized using a direct genetic algorithm [6] with fictitious zero-length crab cavities located located 1.2 m downstream of the center of straight sections 5 and 7. The cavities were powered at 2-MV deflection strength during the optimization of dynamic aperture, lifetime, and vertical emittance growth. The optimization was very effective, giving a nominal lifetime of over 11 hours for 24 bunches, 100 mA, 1% coupling, and $\xi_x = \xi_y = 5$; dynamic acceptance of -15 mm; and emittance growth of less than 1 pm on a base of 35 pm.

The second lattice started from the first, but the sextupoles in sectors 5 and 7 were identical to those in sector 1, while the sextupoles in sectors 6 and 8 were identical to those in sector 2. This condition results from the fact that straight sections 1, 5, and 7 are all long straights. This optimization also worked well, but not as well as the previous one, which is perhaps not surprising given that it had fewer knobs with which to work. The lifetime was just under 10 hours, with dynamic acceptance beyond -15 mm.

Copyright © 2013 CC-BY-3.0 and by the respective authors

A SEVEN-BEND-ACHROMAT LATTICE AS A POTENTIAL UPGRADE FOR THE ADVANCED PHOTON SOURCE*

M. Borland†, V. Sajaev, Y.-P. Sun, ANL, Argonne, IL 60439, USA

Abstract

The Advanced Photon Source (APS) is a 7-GeV storage ring light source that has been in operation since 1996. In that time, the emittance has dropped from 8 nm to 3 nm. The increasing feasibility of multi-bend-achromat lattices (e.g., the MAX-IV project) promises the possibility of a much greater reduction in emittance. In this paper, we show the design of a symmetric seven-bend-achromat lattice, including linear optics, nonlinear dynamics optimization, magnet requirements, and performance with errors.

INTRODUCTION

There is now wide-spread interest in multi-bend achromat lattices as a means of achieving significantly lower emittance in light source storage rings. Notable efforts include the MAX-IV [1] and SIRIUS projects [2], which are under construction, as well as proposed upgrades for ESRF and SPring-8. A recent report of the Basic Energy Sciences Advisory Committee recommended re-examination of existing upgrade plans for US storage rings to explore the potential of such a lattice. Such work was already on-going at the Advanced Photon Source (APS), but has now taken on renewed urgency.

We have explored a number of lattice concepts, including designs similar to the one being built at MAX-IV. In this paper, we present a design based on the hybrid-multi-bend achromat (HMBA) concept proposed by ESRF [3].

LATTICE OPTIMIZATION

The HMBA lattice is distinguished from the MAX-IV-style lattice by having a dispersion bump between the outer pairs of dipoles, which also feature a longitudinal gradient. Sextupoles are located only in the dispersion bump, by virtue of which their strengths are dramatically reduced. In addition, the phase advance between pairs of sextupole centers in the two dispersion bumps for any sector is 3π and π for the horizontal and vertical planes, respectively.

We started with a lattice file provided by N. Carmignani of ESRF. The first step was to modify the angles for a 40-sector ring (ESRF has only 32 sectors) and perform some basic matching to get a stable lattice. This gave acceptable dynamic acceptance (DA) and local momentum acceptance (LMA), albeit in the absence of errors, and an emittance of about 80 pm at 6 GeV.

For further development, our goal was to reduce the emittance as far as possible, consistent with workable lifetime and sufficient injection aperture for on-axis, swap-out injection [4]. Toward this end, we performed a wide-ranging scan of the integer and fractional tunes that covered over 4000 possible working points with $\nu_x : (99, 109)$ and $\nu_y : (32, 39)$. For each target working point, we used `elegant` [5] to perform linear optics optimization to minimize the emittance, obtain relatively small < 3 m beta functions at the insertion devices (IDs), restrain the maximum beta functions below 20 m, ensure the correct phase advance between sextupoles, ensure the correct overall geometry, etc. In this process, essentially every parameter of the lattice was allowed to vary, including strengths, lengths, and positions of all elements.

Once matching was completed, we corrected the chromaticity to $+2$ in both planes, using a reflection- and translationally-symmetric sextupole distribution. We then used `Pelegant` [6] to perform tracking without errors to determine the maximum stable amplitudes for momentum and amplitude deviations, which involved evaluation of particle survival, crossing of integer and half-integer resonances, and diffusion rates. Figures 1 and 2 show maps of natural emittance and minimum LMA. Note that the latter is often limited at the high-dispersion point and may be smaller than indicated by the tunes vs momentum offset. Figures 3 and 4 show maps of the beta functions at the IDs, which would ideally both be 1.5 m to maximize brightness.

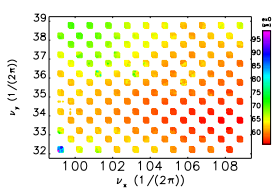


Figure 1: Map of natural emittance vs working point.

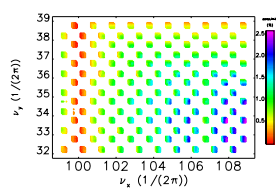


Figure 2: Map of minimum momentum acceptance vs working point.

Since not all parameters can be simultaneously optimized, we performed a non-dominated sort [7], which yielded a handful of superior solutions from which to choose. Dynamic acceptance (DA) and lifetime were optimized for several of these using a tracking-based multi-objective genetic algorithm (MOGA) [8]. This included fine adjustment of the working point and linear optics, as well as adjustment of individual sextupoles. Following ESRF, we organized the sextupoles into 12 families with

* Work supported by the U.S. Department of Energy, Office of Science, under Contract No. DE-AC02-06CH11357.

† borland@aps.anl.gov

Copyright © 2013 CC-BY-3.0 and by the respective authors

ISBN 978-3-95450-138-0

VARIOUS CANTING SCHEMES FOR UTILIZING MORE THAN ONE INSERTION DEVICE IN AN INSERTION DEVICE STRAIGHT SECTION *

V. Sajaev†, G. Decker, L. Emery, ANL, Argonne, IL 60439, USA

Abstract

Presently, the APS utilizes one simple canting scheme for separation of radiation generated by two insertion devices (IDs) located in the same ID straight section. This scheme is based on triangular horizontal orbit bump with one corrector located between the IDs and orbit distortion limited to the ID straight section only. However, this scheme does not allow for switching between the upstream and downstream devices, nor does it allow for one beamline to accept the combined radiation of both devices. These capabilities are being requested for future APS Upgrade. In this paper, we describe more advanced canting schemes that allow for these capabilities, and also present test results. The main complication here is that the orbit distortion is required to go through the storage ring magnets thus generating optics errors, which have to be corrected.

INTRODUCTION

The Advanced Photon Source (APS) is a 7-GeV third-generation synchrotron light source that has been serving a wide variety of users since operations began in 1996. 34 straight sections are used for installation of insertion devices, and each straight section allows space for up to two 2.4-meter-long devices. Because of ever-increasing demand for beam time from experimenters, over time several straight sections were modified to double the beamline capacity. This was done by introducing so called dual-canted undulators [1]. In this configuration, a chicane is created with a trio of dipole magnets with an undulator in each leg as shown in Figure 1 (1-mrad dipoles used to separate dipole radiation from the ID radiation [2] are omitted for simplicity). The result is an angular separation between the x-ray beams that can be exploited downstream to create two independent beamlines from a single straight section.

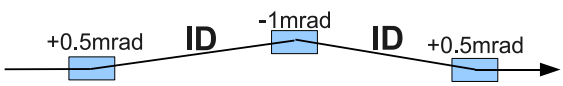


Figure 1: Canted ID straight section configuration presently used at the APS.

Since then, there have been a number of requests from user programs about the possibility of modifing this simple canting scheme to allow for better utilization of the insertion devices. The biggest problem with the present configuration is that the radiation from upstream and downstream devices cannot be switched between the two experimental stations. It is not a big issue presently because most of the insertion devices at the APS are similar to each other. But as more and more narrowly optimized devices are installed, the issue of switching the two photon beams can become more important. For example, the request to explore such a possibility already has come from the user group that plans to install one permanent magnet and one superconducting undulator in their straight section. In this paper, we will present several canting schemes and evaluate their performance from the accelerator physics point of view.

SWITCHABLE CONFIGURATIONS

The most straightforward way to switch radiation of upstream and downstream undulators is just to flip the signs of the correctors that create the triangular orbit bump. The advantage of this approach is its simplicity and the fact that the orbit does not change outside of the ID straight section. This approach, however, has a major deficiency — the position of the radiation source will be shifted transversely by several mm after the switching, as shown in Figure 2. The shift will present challenges in both designing the beamline front end and the beamline optics. Therefore, it is desirable to create such an orbit bump that the source position does not change during the switch.

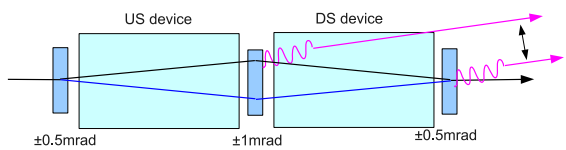


Figure 2: Diagram showing a position shift during ID switch in a triangular-bump configuration.

Symmetric Five-Corrector Bump (W-bump)

Using additional SR correctors outside of the ID straight section, we can make a bump such that source positions stay on the same line after the switch. Figure 3 illustrates the idea: when the beam travels along the trajectory shown in blue, the radiation of the upstream device goes into the inboard beamline; when the orbit is switched to the one shown in red, the downstream ID's radiation goes into the same inboard beamline. This configuration is strongly preferred by the users, but it presents difficulties for the storage ring operation – now the orbit will be changing outside of

* Work supported by the U.S. Department of Energy, Office of Science, under Contract No. DE-AC02-06CH11357.

† sajaev@aps.anl.gov

Copyright © 2013 CC-BY-3.0 and by the respective authors

NEW CONSIDERATION FOR INSERTION-DEVICE DIPOLE-ERROR PERTURBATION REQUIREMENTS WHEN INCLUDING THE EFFECTS OF ORBIT FEEDBACK*

L. Emery†, V. Sajaev‡ and A. Xiao§, ANL, Argonne, IL 60439, USA

Abstract

For various reasons insertion devices (IDs) in storage ring light sources generally produce small dipole perturbations on the stored beam, which is usually compensated by orbit correction. Tougher orbit stability requirements for the Advanced Photon Source Upgrade (APS-U) project have led us to revisit the requirements of these magnetic-field errors. When including the effect of orbit correction (slow orbit feedback plus fast orbit feedback), we realized that the field-error requirements change from a limit in absolute values of magnetic-field error integrals to that of *rates of change* in magnetic-field error integrals. Some modeling of the combined effect of ramping the strength of an ID with orbit correction will be presented. This new thinking has the potential of greatly alleviating the tuning requirements of insertion devices of all types.

INTRODUCTION

In the early stages of APS operation, perturbations from insertion device (ID) field errors was studied intensively, resulting in a set of ID field specifications [1]. Since then, many IDs have been built, measured, and placed into operation at APS. Their properties and the achievable manufacturing limits are by now well known.

The first- and second-field integrals of an ID are not zero, and also, very importantly, vary with gap. To maintain the source-point during user operations, these perturbations must be held within some limits relative to an appropriate short-term "average reference" condition, which is not necessarily the same as the open-gap condition or starting conditions.

The undulators are slow-moving devices; the induced perturbation on the stored beam has a time scale of 1 seconds to 2 to 3 minutes. When a device gap is scanned repeatedly near their closed position, the period could be a few seconds to a few minutes, depending on the experimenter's data collection requirements. At the smallest gap position a significant beam perturbation could take place within 1 second. Thus the frequency range of interest is, say, 0.01 to 1 Hz, the lower limit selected to be approximately the reciprocal of two minutes.

Given that the stored beam can be subjected to perturbations from general sources of all frequencies, a general beam stability requirement for APS-U was recently re-established (see Table 1). Just like the original APS beam stability requirement, this requirement is meant as a guide for setting limits on individual sources of perturbation. One of the specifications sets limits on all sources in the frequency range 0.01 to 200 Hz (middle column in Table 1).

As discussed previously, conventional undulators are expected to produce perturbations within a tiny fraction of that frequency range, while other sources produce perturbations over the whole frequency range. Thus some of the orbit motion spectrum integrals of Table 1 must be allocated to undulator perturbation limits. In other words, if 3 μm is the maximum allowable rms orbit motion in the x plane from all sources, then a smaller number, say, 1.0 μm, would have to be taken as the maximum allowable rms motion in the 0.01-1 Hz range for undulators.

NEW ALLEVIATING FACTORS

Restricting ID source perturbations to a small amount like 1 μm may seem impossible at first. However, there are many alleviating factors not considered until now and some complicating factors used for years that are no longer needed:

Previously it was assumed that ID gaps could be moving together. Actually, independently operated gaps rarely move together. This will remove a factor $\sqrt{N_{\mathrm{ID}}}$ due to the number of IDs.

If there are independent IDs whose gaps are scanned slowly for long periods, the perturbation frequency will be below the band (below 0.01 Hz), in which case orbit correction cancels the perturbation with very high (virtually "infinite") gain.

Two orbit correction systems are running full-time in different frequency bands and have particularly high gain (i.e., correction effectiveness) in the 0.01 - 1 Hz frequency range of interest. A high gain allows larger tolerances for ID perturbation. Figure 1 shows the gain of the orbit correction as presently configured.

ID gap feedforward on nearby storage ring dipole correctors can be used to reduce the effort from the feedback correctors by 90% in DC mode. However, we found that the EPICS network for communicating gap information is much slower than the dedicated reflective memory of the orbit feedback system. Thus a feedforward system for correcting the orbit perturbation would not be needed to improve stability.

The ID perturbation when the gap is moving is not really a sequence of steps but rather segments of ramp errors of

* Work supported by the U.S. Department of Energy, Office of Science, under Contract No. DE-AC02-06CH11357.

† lemery@aps.anl.gov
‡ sajaev@aps.anl.gov
§ xiaom@aps.anl.gov

ISBN 978-3-95450-138-0

Copyright © 2013 CC-BY-3.0 and by the respective authors

OPTICS DESIGN AND BEAM DYNAMICS OPTIMIZATION OF A FIVE-BEND ACHROMAT LATTICE FOR THE ADVANCED PHOTON SOURCE UPGRADE*

Yipeng Sun† and Michael Borland, ANL, Argonne, IL 60439, USA

Abstract

For the proposed future Advanced Photon Source (APS) upgrade, a multi-bend achromat design with very low emittance has been studied. Such a ring promises to enhance the photon brightness and transverse coherence by two orders of magnitude. In this paper, one possible lattice design is presented, which is composed of five-bend achromat arc cells. The linear optics design is done for an emittance of 150 pm at a beam energy of 6 GeV. The nonlinear optics are optimized using the Multi-objective Genetic Algorithm (MOGA) technique for good injection efficiency and beam lifetime. Beam dynamics performance is also preliminarily evaluated.

OVERVIEW

Storage rings based on alternate strong focusing have been widely used for many years in the design of colliders and synchrotron radiation light sources. Several focusing configurations have been invented and some of them applied in real ring construction and operation, including the separated-function FODO cell, combined function FD-cell, double-bend achromat (DBA), triple-bend achromat (TBA), and theoretical minimum emittance lattice (TME) [1].

In simplified form, the natural emittance in a storage ring scales as [2]

$$\epsilon_0 \sim \frac{F \cdot E^2}{(N_d N_s)^3 \cdot J_x}, \qquad (1)$$

where ϵ_0 is the equilibrium emittance in a storage ring, F is a dimensionless factor depending on the arc cell focusing, E is the electron energy, N_s is the number of sectors, N_d is the number of dipoles per sector, and J_x is the horizontal damping partition number.

To improve the photon brightness and coherence in a storage-ring-based light source, a low-emittance electron beam (matched to the photon beam) is needed. In general, the requirement to achieve very low emittance means employment of many weaker dipoles (smaller dispersion) and stronger quadrupoles (focusing). Stronger (or better) focusing approaches the ideal TME condition, while more dipole magnets direct us toward a multi-bend achromat (MBA) lattice where $M \geq 4$.

Such a lattice was first studied and proposed in the 1990s [3]. Similar ideas were also discussed for a future APS upgrade with MBA lattices [4] [5] [6], providing a lower natural emittance below 200 pm. The MAX-IV storage ring is the first MBA lattice being built and will be commissioned in 2015 [7]. It employs 20 seven-bend achromat (7BA) cells in a 528-m circumference, which provides an emittance of 330 pm at a beam energy of 3 GeV. ESRF is also proposing an upgrade using a hybrid multi-bend achromat lattice where larger dispersion is adopted to decrease sextupole strength [8].

Recently the APS has begun to explore replacing the current DBA lattice with a new MBA lattice as part of its ongoing upgrade project. A MAX-IV-like 7BA lattice [9], and an ESRF-like hybrid-7BA are being studied [5]. In this paper, another MBA design for the APS upgrade is presented, namely, a five-bend achromat lattice that provides an emittance of 150 pm at 6 GeV.

LINEAR OPTICS DESIGN

It is proposed to enhance the photon brightness and coherence by two orders of magnitude in the new APS MBA lattice. To achieve this goal, and to reuse as much existing hardware as possible, there are several optics design constraints:

- A natural emittance below 150 pm
- Match the existing ID beamline locations
- Maintain the bending-magnet beamlines
- 40 identical cells, each 27.6 m long
- Straight section length longer than 5 m
- Electron beam energy of 6 GeV
- Reuse the existing rf and injector system

Another important design constraint is from the available magnet technology. It is foreseen to use normal-conducting magnets with a bore radius around 12 mm. The drift length between magnets is limited to a minimum of 10 cm. The assumed maximum dipole, quadrupole, and sextupole strength are listed below.

- Combined dipole: dipole field $< 1\ T$; quadrupole gradient $< 50\ T/m$
- Quadrupole gradient $< 100\ T/m$
- Sextupole gradient $< 10000\ T/m^2$

Based on the above contraints, the linear optics matching is performed using ELEGANT [10]. The minimum magnet length is set to be 15 cm, with the magnet strength as low as possible. The linear optics in one sector is shown in Figure 1, where the starting and ending points are the insertion device (ID) center. One observes that the use of a triplet on either side of the ID straight has allowed tuning the beta

* Work supported by the U.S. Department of Energy, Office of Science, under Contract No. DE-AC02-06CH11357.

† yisun@aps.anl.gov

Copyright © 2013 CC-BY-3.0 and by the respective authors

LINEAR SCALING ON CHOOSING A BUNCH COMPRESSION RATIO FOR AN FEL DRIVER*

Yipeng Sun†, ANL, Argonne, IL 60439, USA

Abstract

In this paper, a proper initial bunch length as a function of the main rf frequency and rf phase is estimated analytically by several approaches, assuming that no harmonic rf section is needed to linearize the energy modulation introduced during main rf acceleration. Next the upper limit of the bunch compression ratio in a single stage is evaluated analytically. The analytical relations derived on choosing a proper initial bunch length as a function of main rf frequency are confirmed by numerical simulation. These simple limits provide rough analytical estimations and may be beneficial for choosing bunch compression ratios in different stages of an FEL driver, especially in a first-stage bunch compression system where an harmonic rf linearization is usually applied.

OVERVIEW

A magnetic bunch compression system is normally adopted during the acceleration process of the electron beam, usually in several (two) stages. The basic idea is to first introduce an energy modulation (chirp) along the electron bunch in its longitudinal direction by an rf acceleration off-crest, then let the electron beam pass by a dispersive region where electrons in the head and tail of the bunch all move relatively towards the bunch center. Chicane- and wiggler-based bunch compressor designs were proposed and studied thoroughly in the 1990s, mainly for linear collider projects [1] [2] [3].

Due to the nonlinear nature of the rf sinusoidal wave and an initially long bunch length, higher-order energy chirps can not be neglected. Harmonic rf linearization of the longitudinal phase space of the electron bunch is normally employed to generate a more uniformly compressed bunch in a first-stage bunch compression. This paper discusses what is the limit on the bunch compression ratio in order to achieve a quasi-linear bunch compression without harmonic rf.

PROPER INITIAL BUNCH LENGTH WITHOUT HARMONIC RF

In this section, only the main rf acceleration section is considered, and a proper initial bunch length is derived as a function of rf frequency and rf phase, given that a quasi-linear compression is achieved with a reasonable bunch compression ratio adopted for each stage. There are two possible ways to quantify a quasi-linear compression. First, the contribution to final bunch length from nonlinearities (from rf acceleration and bunch compressors) could be evaluated and limited to a certain percentage. A second way is to compare the final bunch length calculated as the root mean square of the distribution with the one derived from a numerical fit of the final distribution (Gaussian fit if the initial distribution is Gaussian), and limit the difference between these two to a certain amount.

Energy Chirp Approach

First let us recall the energy modulation formula. For any one particle in a bunch, its relative energy offset after passing by an rf acceleration off-crest can be expressed as shown below:

$$\begin{aligned}\delta(z) &= \delta_i \frac{E_{i0}}{E_{f0}} + \frac{eV_0\cos(\phi + kz_i)}{E_{f0}} \\ &= a\cdot\delta_i + \frac{eV_0\cos(\phi+kz_i)}{E_{f0}}. \end{aligned} \quad (1)$$

where δ_i denotes the initial uncorrelated energy offset, E_{i0} is the central energy before rf acceleration, E_{f0} is the central energy after rf acceleration, e is the electron charge, V_0 is the rf voltage, ϕ is the rf phase, $k = \frac{2\pi}{\lambda}$ is the rf wave number, λ is the rf wavelength, z_i is the particle's longitudinal coordinate relative to the bunch center, and $a = E_{i0}/E_{f0}$ is the energy damping ratio.

The first- and second-order energy chirp from the main rf acceleration could be described by the rf wave number, rf voltage, and rf phase, solved from the same Taylor expansions discussed above, as shown below:

$$h_1 = -\frac{keV_0\sin\phi}{E_{f0}} \quad (2)$$

$$h_2 = -\frac{k^2eV_0\cos\phi}{2E_{f0}}. \quad (3)$$

Neglecting the energy chirp above the third order, the overall energy modulation from this main rf section can then be rewritten as

$$\delta(z) = a\cdot\delta_i + (h_1 + h_2\cdot z)z, \quad (4)$$

where $h_1 + h_2\cdot z$ denotes the effective first-order energy chirp.

One then observes that if z is small enough to make $h_1 + h_2\cdot z \approx h_1$, the overall energy modulation is almost linear; in that case harmonic rf linearization is no longer necessary. This condition could be interpreted as $|h_1| \gg |h_2\cdot\sigma_z|$ and further derived to be

$$\frac{c\cdot\tan\phi}{\pi\cdot f_{rf}\cdot\sigma_z} \gg 1. \quad (5)$$

* Work supported by the U.S. Department of Energy, Office of Science, under Contract No. DE-AC02-06CH11357. Work also supported by the U.S. Department of Energy under Contract DE-AC02-76SF00515.

† yisun@aps.anl.gov

Copyright © 2013 CC-BY-3.0 and by the respective authors

ISBN 978-3-95450-138-0

SIMULATION OF AN X-BAND HARD X-RAY FEL WITH LCLS INJECTOR*

Yipeng Sun†, ANL, Argonne, IL 60439, USA
Tor Raubenheimer, SLAC, Menlo Park, California 94025, USA
Paul Emma, LBNL, Berkeley, California 94720, USA

Abstract

In this paper, the accelerator design and start-to-end 3D macro particle simulation (using ELEGANT and GENESIS) of an X-band rf-driven hard x-ray FEL with LCLS injector is briefly discussed. A preliminary design and LiTrack 1D simulation studies were presented earlier [1]. In numerical simulations this X-band rf-driven hard x-ray FEL achieves/exceeds LCLS-like performance in a much shorter overall length of 350 m, compared with 1200 m in the LCLS. One key feature of this design is that it may achieve a higher final beam current of 5 kA plus a uniform energy profile, mainly due to the employment of stronger longitudinal wakefields in the last X-band rf linac [2].

OVERVIEW AND ACCELERATOR DESIGN

LCLS is the world's first hard x-ray FEL in routine operation, providing soft and hard x-rays to its users with good spatial coherence at wavelengths from 2.2 nm to 0.12 nm by varying the bunch energy from 3.5 GeV to 15 GeV [3]. Design and beam dynamic studies are performed for several X-band rf-driven hard x-ray FEL drivers [4]. A low-charge hard x-ray FEL design [5] employs the entire X-band photoinjector and rf linac, which are optimized for a very low bunch charge of 10 pC and an average SASE FEL power of over 10 GW in a pulse length of 5 fs (start-to-end simulation in a short undulator length of 20 m). Thanks to the small 3D emittance associated with the low bunch charge (short initial bunch length from photoinjector, etc.), a linear bunch compression is achieved in two stages of bunch compressors without the assistance of harmonic rf linearization.

A second hard x-ray FEL design also features the entire X-band photoinjector and rf linac, but is dedicated for a normal bunch charge of 250 pC [6]. The longitudinal phase space linearization is done in its first-stage bunch compression with a specially designed bunch compressor composed of dipole, quadrupole, and sextupole magnets. From the start-to-end simulation using computer codes ASTRA [7], ELEGANT [8], and GENESIS [9], it is shown that this FEL achieves an average SASE FEL power of over 30 GW in a pulse length of 50 fs.

Both of these two hard X-ray FEL designs described above achieve a shorter SASE FEL saturation length due to a shorter undulator period and a weaker undulator field. It is also noted that the low-charge hard x-ray FEL design [5] achieves a better final beam quality than the LCLS case.

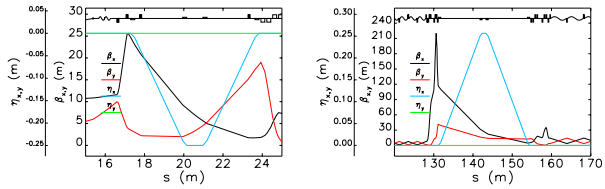


Figure 2: Beta functions and dispersion functions in the bunch compressors. Left: bunch compressor one, which is exactly the same as LCLS BC1; right: bunch compressor two, which is similar to LCLS BC2.

Analytical and numerical simulation studies show that the tolerance (charge and timing jitter, transverse misalignment) is acceptable for both of the above two hard X-ray FEL designs [5], [6].

A sketch of this compact (300 m) hard x-ray FEL driver using X-band accelerators plus an LCLS injector is shown in Figure 1. As previously mentioned, it employs an LCLS injector, which means that to the end of BC1 it is exactly the same as the LCLS. The only difference is that the S-band rf in Linac2 and Linac3 is replaced by an X-band rf. The BC2 design is similar to LCLS, at a beam energy of 4.3 GeV. For a bunch charge of 250 pC, the initial RMS bunch length is 690 μm from the S-band photoinjector. It is compressed to a final RMS length of either 6 μm (3-kA peak current) or 4 μm (5-kA peak current).

OPTICS DESIGN

The optics design of the linac, the bunch compressors, and the matching sections are done in MAD8 [10] and then converted to ELEGANT [8]. The TWISS parameters of bunch compressors one (BC1) and two (BC2), shown in Figure 2, are similar to the LCLS BC1 and BC2 (transverse phase-space matching to minimize CSR induced transverse emittance growth). The start-to-end TWISS parameters of the overall accelerator are shown in Figure 3. An average beta function of 10 meters and 20 meters are employed in Linac2X and Linac3X, respectively, to minimize both dispersive and wakefield-induced transverse emittance dilutions.

* Work at Argonne is supported by the U.S. Department of Energy, Office of Science, under Contract No. DE-AC02-06CH11357. Work also supported by the U.S. Department of Energy under Contract DE-AC02-76SF00515.

† yisun@aps.anl.gov

Copyright © 2013 CC-BY-3.0 and by the respective authors

ACHIEVING A QUASI-THIRD-ORDER ACHROMAT IN AN APS UPGRADE LATTICE*

Yipeng Sun† and Michael Borland, ANL, Argonne, IL 60439, USA

Abstract

The next-generation of storage rings will require stronger quadrupole focusing to achieve very low emittance. Stronger sextupoles (usually at smaller dispersion locations) are then necessary to correct the natural chromaticity and suppress the head-tail instability. The geometric and chromatic optics aberrations introduced by these sextupoles have a large impact on the beam dynamics performance. In this paper, it is discussed how to achieve a quasi-third-order achromat in a possible Advanced Photon Source (APS) multi-bend achromat (MBA) lattice. Repetitive identical MBA arc cells with specified phase advance and mirror symmetry are employed. The beam dynamics performance of such an achromat design is compared with a normal scheme.

OVERVIEW

The development of optical achromats started in the 1700s when achromatic doublets and triplets were invented to bring light of different frequencies to the same focal point. First-order achromats have been applied in particle accelerators for a long time. In the 1970s, K. Brown developed a systematic matrix-based approach to designing second-order achromats [1]. It adopts at least four identical cells with dipoles, quadrupoles, and sextupoles and can eliminate all geometric and chromatic aberrations up to second order. Two strong points being proposed are the integer phase advance in the entire beamline and the $-I$ phase separation between non-interleaved sextupoles to cancel even higher-order geometric aberrations. After that, similar third-order achromat design approaches were developed analytically and numerically [2] [3], where the concept of identical cells and integer phase advance is used again. Following these studies, W. Wan developed a general method with Lie algebra to design achromats to arbitrary order, taking advantage of mirror symmetry and using multipole magnets for each specified order (for example, octupoles for a third-order achromat) [4].

The latest PEPX design utilizes eight identical seven-bend achromat (7BA) cells in each arc section, where the total phase advance is an integer [5]. A third-order geometric achromat is achieved with the assistance of harmonic sextupoles [5]. In this paper, first a design similar to the APS storage ringe is presented. It employs more families of chromaticity sextupoles and may eliminate all geometric and chromatic aberrations up to third order. Then there is a discussion on how to achieve a quasi-third-order achromat in the APS upgrade lattices where 40 identical MBA cells have to be used and no dedicated straight sections are allowed.

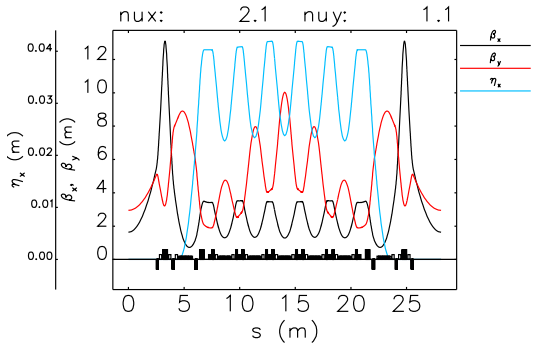


Figure 1: Twiss parameters in a 7BA arc cell with a length of 27.2 m. Natural emittance is 150 pm at a beam energy of 6 GeV. The black curve denotes horizontal beta function; red curve, vertical beta function; blue curve, horizontal dispersion function.

THIRD-ORDER ACHROMAT DESIGN

The current APS storage ring has a circumference of 1104 meters and is divided into 40 identical sectors. An APS-size ring is designed based on the third-order-achromat concept. Note that it may not fit in the current APS tunnel due to geometry, although the circumference is close to 1104 m. The ring consists of four arc sections plus short straight sections that are each 4 meters long. Each arc section has ten identical 7BA cells. The natural emittance is 150 pm at an electron beam energy of 6 GeV.

The linear and nonlinear optics optimization are performed with ELEGANT [6]. The Twiss parameters in a 7BA arc cell are shown in Figure 1. It is observed that in the central part there are five TME-like cells. Each cell consists of one combined function dipole (with defocusing quadrupole gradient), two focusing quadrupoles, and three sextupoles. The horizontal beta function and dispersion achieve a minimum in the center of the dipole magnet. The dispersion is matched to zero using two dedicated quadrupole magnets and an end dipole. A triplet is adopted outside of the end dipole to bring the beta functions down to β_x = 1.8 m and β_y = 3 m at the center of the insertion device (ID). The maximum dipole field is 0.45 Tesla and the maximum quadrupole gradient is 66 T/m.

The betatron phase advance of each 7BA cell is (2.1, 1.1) in units of 2π. The phase advance in each arc section is then (21, 11), i.e., multiples of 2π in both planes. In the 4-meter-

* Work supported by the U.S. Department of Energy, Office of Science, under Contract No. DE-AC02-06CH11357.

† yisun@aps.anl.gov

Copyright © 2013 CC-BY-3.0 and by the respective authors

ISBN 978-3-95450-138-0

ANALYTICAL EVALUATION OF CORRELATED TIMING JITTER CANCELLATION IN A STAGED BUNCH COMPRESSION SYSTEM*

Yipeng Sun†, ANL, Argonne, IL 60439, USA

Abstract

In this paper, the wakefield cancellation scheme on the timing jitter is revisited. The correlated timing jitter effects between the photoinjector laser and the linac rf phase are evaluated analytically. It is possible to minimize its impact on the final bunch length (peak current) variation by employing a longer linac with a lower acceleration gradient between bunch compressors one and two.

OVERVIEW

A staged magnetic bunch compression system is widely adopted in the acceleration process of the electron beam. It first introduces an energy modulation along the electron bunch in its longitudinal direction, then lets the electron beam pass by a dispersive region where electrons in the head and tail of the bunch all move relatively towards bunch center. Chicane- and wiggler-based bunch compressor designs were proposed and studied thoroughly in the 1990s, mainly for linear collider projects [1], [2], [3].

The stability of the final electron beam current depends on the timing and rf phase jitter, bunch compressor parameters, and electron beam charge variations. Gun laser to linac rf timing jitter (referred to as timing jitter)–the main timing error to be discussed in this paper–is considered to be correlated for all the linac sections as the sum of the uncorrelated (or random) rf phase jitter (different from rf source-to-source) tends to be small.

The bunch length variation due to jitter effects at the ends of the staged bunch compressors were studied in (and before) the LCLS initial design stage, and a longitudinal wakefield cancellation scheme was proposed with at least two stages of bunch compressions [4], [5], [6], [7], [8]. This scheme was also applied at the LCLS FEL [5], [7], [8]. A similar scheme is also proposed to reduce the energy chirp by employing the wake of coherent synchrotron radiation [9].

In this paper, this topic is revisited, while the associated formulae are rederived and extended analytically. The analytical result is verified by numerical simulations. It is possible to minimize the correlated timing jitter's impact on the final bunch length (peak current) variation by employing a longer linac with a lower acceleration gradient, between bunch compressors one and two.

* Work at Argonne is supported by the U.S. Department of Energy, Office of Science, under Contract No. DE-AC02-06CH11357. Work also supported by the U.S. Department of Energy under Contract DE-AC02-76SF00515.

† yisun@aps.anl.gov

ANALYTICAL DERIVATION

Neglecting the small initial un-correlated energy spread and considering only linear terms, the RMS bunch length after bunch compressor one can be expressed as

$$\sigma_{z1} = (1 + h_1 R_{56(1)}) \cdot \sigma_{z0}, \tag{1}$$

where σ_{z1} denotes the RMS bunch length after bunch compressor one, h_1 is the chirp of bunch compressor one, $R_{56(1)}$ is the first-order longitudinal dispersion in bunch compressor one, and σ_{z0} is the initial bunch length; and

$$h_1 = -\frac{k_1 e V_0 \sin\phi}{E_{f0}} \approx -k_1 \tan\phi \approx -k_1\phi_1, \tag{2}$$

where $k_1 = \frac{2\pi_1}{\lambda}$ denotes the rf wave number in the first rf section, E_{f0} is the central energy after rf acceleration, e is the electron charge, V_0 is the rf voltage, ϕ_1 is the rf phase, $k = \frac{2\pi}{\lambda}$ is the rf wave number, and λ is the rf wave length.

Given a timing jitter $\Delta\phi_1$, the change in the final bunch length is

$$\Delta\sigma_{z1} = -k_1 \Delta\phi_1 R_{56(1)} \cdot \sigma_{z0}. \tag{3}$$

Neglecting the residual damped energy chirp from the first rf linac $h_1 \cdot C_1 \cdot E_1/E_2$ ($C_1 = 1/(1 + h_1 R_{56(1)})$ denotes the compression ratio in BC1. Also the longitudinal wakefield effects in Linac2 only consider an energy chirp established in Linac2, which is h_2. The final RMS bunch length after the second bunch compressor can be calculated as

$$\sigma_{z2} = (1 + h_2 R_{56(2)}) \cdot \sigma_{z1}, \tag{4}$$

$$h_2 \approx -k_2\phi_2, \tag{5}$$

where σ_{z2} denotes the RMS bunch length after bunch compressor two, h_2 is the chirp of bunch compressor two, $R_{56(2)}$ is the first-order longitudinal dispersion in bunch compressor two, and $k_2 = \frac{2\pi_2}{\lambda}$ is the rf wave number in the second rf section.

After inserting the expression σ_{z1} into Eq. (4), one finds

$$\sigma_{z2} = (1 + h_2 R_{56(2)}) \cdot (1 + h_1 R_{56(1)}) \cdot \sigma_{z0}. \tag{6}$$

Given a linac rf timing jitter of $\Delta\phi_1$ and $\Delta\phi_2$ in the first and second rf linacs, the final bunch length is

$$\sigma_{z2} = \left[1 - k_2(\phi_2 + \Delta\phi_2) R_{56(2)}\right] \cdot \left[1 - k_1(\phi_1 + \Delta\phi_1) R_{56(1)}\right] \cdot \sigma_{z0}. \tag{7}$$

Copyright © 2013 CC-BY-3.0 and by the respective authors

X-BAND FEL DRIVER LINAC DESIGN WITH OPTICS LINEARIZATION*

Yipeng Sun†, ANL, Argonne, IL 60439, USA
Tor Raubenheimer, Juhao Wu, SLAC, Menlo Park, California 94025, USA
Paul Emma, LBNL, Berkeley, California 94720, USA

Abstract

In this paper, a compact hard x-ray FEL design is proposed with a single bunch charge of 250 pC, which is based on all X-band rf acceleration and two-stage bunch compression. It eliminates the need for a harmonic rf linearization section by employing optics linearization in its first-stage bunch compression. Emittance growth in the horizontal plane due to coherent synchrotron radiation (CSR) is investigated and minimized, to be on a similar level with the LCLS. An electron bunch distribution at the linac end is taken as the input for an FEL simulation in GENESIS, with a beam energy of 7 GeV. At an FEL radiation wavelength of 0.15 nm, a saturation length of roughly 40 meters can be achieved by employing an undulator with a period of 1.5 cm. Without tapering, an FEL radiation power above 10 GW is achieved with a photon pulse length of 50 fs, which is LCLS-like performance. The overall length of the accelerator plus undulator is around 250 meters, which is much shorter than the LCLS length of 1230 meters.

OVERVIEW AND ACCELERATOR DESIGN

In this paper, a very compact FEL driver is proposed with an accelerator length less than 200 m. An alternative way to do a linearized bunch compression in a first stage is proposed. The key point is to eliminate the harmonic rf section, and to apply an optics linearization instead, with a specially designed bunch compressor that includes quadrupole and sextupole magnets. Similar schemes have been proposed and studied preliminarily before, either in an analytical manner [1] [2] [3], by numerical simulations [1] [3] [4] [5], or in experimental measurements [3]. The second-order longitudinal dispersion T_{566} of this bunch compressor is precisely controlled and used to compensate the second-order curvature from the main rf acceleration. Third-order longitudinal dispersion U_{5666} can also be tuned to cancel the third-order rf curvature; however, in most cases this is not necessary as its impact is relatively small. Compared with a four-dipole chicane, this bunch compressor has the opposite sign of the linear longitudinal dispersion R_{56}. The main rf system in the first linac then has to work on the falling slope of the sinusoidal wave, which is the only way to shorten the bunch length; otherwise the bunch length is lengthened. In order to do a normal under-compression in the second stage, and still use longitudinal wakefields to remove the residual chirp in the last linac, one needs to do an over-compression in the first-stage bunch compressor. Over-compression may cause larger transverse emittance growth due to phase smear in the over-compression process, associated with energy change from coherent synchrotron radiation (CSR) in a dispersive region. The optics design of this bunch compressor needs to be investigated and optimized carefully to minimize these impacts.

The accelerator of this FEL driver is sketched in Figure 1. Compared with a similar hard x-ray FEL design based on S-band rf acceleration, this all X-band-based FEL has several potential advantages. One advantage is its compact size at the same final beam energy, due to the higher acceleration gradient provided by X-band rf cavities. In general the accelerator length is only one-fourth or one-third of the S-band-based accelerator. Besides, a shorter wavelength of X-band rf also makes the establishment of energy modulation easier, which then makes it possible to run on an rf phase closer to the crest and so save rf power. Another possible advantage is that it may be easier to manipulate the longitudinal phase space, especially in the second and last linac (for a two-stage bunch compression), mainly due to a much stronger longitudinal wake field of X-band rf. One may also benefit from a smaller CSR-induced emittance growth in bunch compressor two, as a larger energy correlation can be generated in Linac2 and then removed in Linac3, so the strength of the bunch compressor dipoles can be decreased.

NUMERICAL SIMULATION

In this section start-to-end ELEGANT [6] 6-D numerical simulation results are presented. The simulation starts at a beam energy of 50 MeV, where X-band photoinjector simulations show that an RMS bunch length of 160 μm could be achieved along with a normalized transverse emittance of 0.5 μm.rad at a bunch charge of 250 pC, by tuning the drive laser system, bunching system, and subsequent acceleration section [7]. Space-charge effect and velocity bunching are two dominant effects in this section from the production of the electron bunch and its acceleration to a beam energy of 50 MeV. The details on the simulation results of this part are not discussed here.

An electron bunch that consists of one million macro particles is then generated internally in ELEGANT, employing an RMS bunch length of 160 μm and a normalized transverse emittance of 0.5 μm.rad. The beam energy is 50 MeV and the single-bunch charge is 250 pC. The un-

* Work at Argonne is supported by the U.S. Department of Energy, Office of Science, under Contract No. DE-AC02-06CH11357. Work also supported by the U.S. Department of Energy under Contract DE-AC02-76SF00515.

† yisun@aps.anl.gov

Copyright © 2013 CC-BY-3.0 and by the respective authors

ISBN 978-3-95450-138-0

NSLS II COMMISSIONING TOOLS*

G.M. Wang#, T. Shaftan, B. Bacha, A. Blednykh, E. Blum, W.X. Cheng, J. Choi, M. Davidsaver, J. De Long, L. Dalesio, R. Fliller, M. Fulkerson, G. George, W. Guo, K. Ha, H. Hseuh, Y. Hu, W. Louie, M. Maggipinto, J. Mead, D. Padrazo, G. Shen, K. Shroff, O. Singh, K. Vetter; Y. Tian, H. Xu, L. Yang, X. Yang, F. Willeke. Photon Sciences, BNL, Upton, NY, 11973, U.S.A

V. Smalyuk, S. Karnaev, S. Sinyatkin, S. Gurov, A. Erokhin, E. Simonov, A. Derbenev, P. Cheblakov, R. Kadyrov BINP, SB, RUS

Abstract

NSLS-II is a state-of-the-art third-generation light source under construction at BNL. As many facilities worldwide, NSLS II uses the EPICS control system to monitor and control all accelerator hardware. CSS is used for simple tasks such as monitoring, display, setting of PVs and browsing the historical data. For more complex accelerator physics applications, a collection of scripts are mainly written in Python. The controls group developed the services, such as channel finder, machine snapshot, data archiving, twiss server, unit conversion etc. This paper will present the tools that we have been using for commissioning.

INTRODUCTION

The NSLS-II [1] is a state of the art 3 GeV synchrotron light source under construction at Brookhaven National Laboratory. It consists of a 200 MeV linac, a booster ring accelerating beam from 200 MeV to 3 GeV, a 3 GeV Storage ring and transport lines in between them.

As many other facilities [2,3], NSLS II chose the Experimental Physics and Industrial Control System (EPICS) as its control system to monitor and control the accelerator hardware. It interfaces to the accelerator instruments and devices (such as Power supply, digitizer, and motor) with IOC (Input Output Controllers). Channel Access is used as the interface to the machine process variables (PVs).

The typical control applications include two types, simple monitor/control device and complex accelerator physics application for studies and machine optimization (measurements, data analyses and applying correction). Mainly, we use cothread to access the process variables (PVs) in Python script for complex accelerator physics applications and the CSS (BOY) [4] panel for simple tasks such as monitoring, displaying and setting of the machine Process Variables (PVs). Besides, MATLAB is also available for programming and EDM panels are used for Linac control system from the linac vendor Research Instruments, GmbH. All source codes including panel configurations are controlled and managed by mercurial version in the control system.

To keep the beam commissioning time efficient, various tools were developed for data displaying, collecting and processing. Besides machine status and physics applications, we also developed the daily used operation tools, such as save/compare/restore tool, data archive, alarm and warning monitor, elog, eticket, channel finder service and applications.

Prior the beam commissioning, we have two stages test with above tools, subsystem integration testing (IT: the hardware system level function verification) and machine extended integration test (EIT: mimic the beam commissioning and tune the machine). These verifications require time and look boring and redundant, but it is necessary as it may take weeks of commissioning time to fix different technical problem.

MACHINE STATUS APPLICATION

All of the monitor and control panels are created with software tools in Control System Studio (CSS), which is an Eclipse-based collection of tools to monitor and operate large scale control systems. The interface allows the operators to edit the desired ramp/soak profiles and provides the option to use predefined recipes.

The NSLS-II operation panels [5] include the user panels and the expert panels. They display the device status and parameters (setpoint and readback) and show the device performance. A user panel shows only information that user is required, such as the magnet current setpoint and readback. The expert panel shows all the information that expert can fully control the device or diagnose the device, such as power supply operation mode and magnet temperature.

HIGH LEVEL APPLICATION

Besides the devices status and control, we also develop high level applications to realize the accelerator physics application tools. It is to translate the raw/processed data from PV to the "physics" parameters, such as from the beam size reading from flags for beam emittance or beam energy measurement. The code was programmed with Python. Although we programmed the high level applications with Python, some of their GUIs (depending on operation needs) are implemented in the CSS, as part of operator panels, so that the operators have consistent live information and interface environment. The user can set parameters and monitor the progress in GUI as regular device PV set and monitor. This feature is realized through soft IOCs.

* This manuscript has been authored by Brookhaven Science Associates, LLC under Contract No. DE-AC02-98CH10886 with the U.S. Department of Energy.

#gwang@bnl.gov

Copyright © 2013 CC-BY-3.0 and by the respective authors

A TUNABLE ENERGY CHIRP CORRECTION*

S. Antipov#, C. Jing, P. Schoessow, and A. Kanareykin,
Euclid Techlabs LLC, Solon, OH-44139
W. Gai, A. Zholents,
Argonne National Laboratory, Argonne, IL-60439
M. Fedurin, C. Swinson,
Brookhaven National Accelerator Laboratory, Upton, NY-11973
S. Baturin
St.Petersburg Electrotechnical University LETI, St.Petersburg Russia

Abstract

Short (subpicosecond) pulses are central to many of the next generation light source initiatives that are based on linear accelerators. Beam compression is performed by means of a chicane utilizing a correlated linear energy chirp. A small energy chirp is kept as the beam goes through the remaining accelerating stage to compensate for wakefield effects. It is necessary to compensate the residual energy spread before the beam enters the undulator stage. We present here a concept for a passive wakefield device - chirp corrector or dechirper, to perform this compensation. We have recently demonstrated a passive energy chirp correction by self-wakefield at the Brookhaven ATF facility. In this paper we present a progress report on development of these tunable chirp correction devices.

INTRODUCTION

Free Electron Laser (FEL) operation requires a high current beam. To reach high current, typically kA – level, the electron beam is compressed. Compression is performed by a chicane, a set of four dipole magnets arranged in a + - - + pattern. For the beam to be compressed by a chicane it has to have an energy chirp, a linear correlation between the energy and longitudinal coordinate. This correlation can be obtained by running beam off-crest in the accelerating section. A natural parameter to characterize the chirp is derived from the slope: the energy difference over the longitudinal coordinate difference in MeV/mm or equivalent. For compression in chicane a positive chirp required, i.e. the head of the beam has lower energy than the tail. In this case the lower energy particles (the head) have a longer path than the high energy particles in the tail. Hence the beam is compressed as the tail catches up with the head. After the compression the beam typically has a residual chirp on the order of 40 MeV/mm [1]. Prior to injection in the undulator this chirp has to be removed as it compromises the FEL lasing. In principle, this can be done by running the bunch off-crest in the accelerating section. Alternatively a passive wakefield device can be used by utilizing the self-acting wakefield induced by the electron bunch on itself [2]. In the original proposal such a device was called a "wakefield silencer". Similar proposals were also put forward in [3-5]. A new name "dechirper" or "chirp corrector" was used in [5] and adopted here as a generic name for the passive wake-inducing device whose sole purpose is to remove (or create) the energy chirp. Since the impact of the dechirper linearly scales with the length of the device and the charge of the electron bunch, it is convenient to characterize the dechirper strength in units of MeV/mm/m/nC. The experimental demonstration of the idea of the dechirper was first reported in [4] where a set of dielectric lined cylindrical waveguides with different apertures were used to produce wakefields with variable strengths. Although the use of different apertures in a cylindrical geometry gives a reasonable flexibility in adjusting the dechirper strength, a continuously tunable dechirper is nevertheless preferred. This device has been tested recently and in this paper we present some recent experimental results obtained using a tunable dechirper.

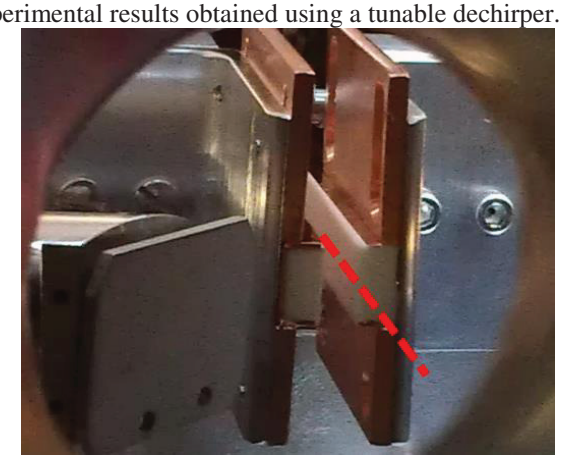


Figure 1: Tunable dechirper: two 10 cm long metallized alumina (ε=9.8) bars, 12 mm wide and 6.35 mm thick with 1 – 6 mm variable gap.

While propagating through the dechirper each electron emits Cherenkov radiation. For a particular structure this field can be simulated and in some cases calculated theoretically [6]. Integrating over the current distribution one can get the total wakefield inside the electron bunch. For dechirper operation we are interested in the self-wakefield, the fields inside the bunch. For a linear chirp correction the self-wakefield has to be quasi-linear. This can be obtained in a number of ways, using a single mode structure or a multimode structure. Naturally, a wake

*Work supported by the Department of Energy SBIR program under Contract #DE-SC0006299.
#s.antipov@euclidtechlabs.com

ISBN 978-3-95450-138-0

Copyright © 2013 CC-BY-3.0 and by the respective authors

DEMONSTRATION OF A COMPACT HIGH AVERAGE POWER THz LIGHT SOURCE AT THE IDAHO ACCELERATOR CENTER

Yujong Kim[†,‡,ǂ*], A. Andrews[†,‡], C. Eckman[†,‡], P. Buaphad[†,‡]
K. Folkman[†], C. O'Neill[†], B. Berls[†], J. Ralph[†], M. Smith[†], and A. V. Smirnov[ǁ]
[†]Idaho Acccelerator Center, Idaho State University, Pocatello, ID 83201, USA
[‡]Department of Physics, Idaho State University, Pocatello, ID 83209, USA
[ǂ]Thomas Jefferson National Accelerator Facility, Newport News, VA 23606, USA
[ǁ]RadiaBeam Technologies LLC, Santa Monica, CA 90404, USA

Abstract

The Idaho Accelerator Center (IAC) has been operating nine low energy accelerators for THz and X-ray light sources, nuclear physics, and medical isotope productions. In November 2012, the IAC and RadiaBeam collaborated to upgrade an IAC 44 MeV L-band RF linac with a chicane bunch compressor and a THz radiator with numerous periodic gratings for the resonant Cherenkov radiation. By using the THz radiator and the re-optimized L-band linac with a new operational energy of 5 MeV, we could demonstrate a THz resonant Cherenkov radiation with a high average power of about 17 W in an RF macropulse without using any sub-ps laser or undulator. In this paper, we describe our upgrades and accelerator optimization experiences to perform the proof-of-principle experiments at the IAC.

INTRODUCTION

As various user applications such as diagnosis of early stage cancers, 3D imaging of teeth, security and weapon scanning, and quality control of commercial products have been developing, recently, THz users strongly request coherent THz light source which can supply a high average power ($\geq$ 1 mW). Jefferson Lab and several other laboratories have demonstrated accelerator-based high average power THz light sources by using the Continuous Wave (CW) or Energy Recovery Linac (ERL) technology. However, we need a big budget to construct such an ERL based THz light source facility. To realize a compact and cheap high average THz light source facility, we have developed a resonant Cherenkov radiation based THz radiator [1–3], and performed its proof-of-principle experiments at the Idaho Accelerator Center (IAC) by upgrading an IAC 44 MeV L-band RF linac [4–6]. The parameters of the 44 MeV linac and the THz radiator are summarized in Table 1, and the layout of the upgraded IAC 44 MeV L-band linac is shown in Fig. 1. The upgraded linac has a 85 kV DC gun instead of an RF photoinjector and a THz radiator instead of a undulator as shown in Fig. 1. To perform the proof-of-principle experiments of narrow-bandwidth resonant Cherenkov radiation with a specially designed THz radiator, RF phases and gradients of the 44 MeV linac structures were re-optimized to have a new operational beam energy of 5 MeV and to have the shortest bunch length of about 500 fs (rms). It is well confirmed that the multi-bunch beam loading effects or the long-range longitudinal wakefields can be used to generate coherent narrow-bandwidth resonant Cherenkov radiation [1, 2, 7, 8]. In our experiments, we used a 85 kV DC gun to generate a long bunch train with 2600 short single bunches in a 2 μs long RF macropulse. By sending the 2600 short bunches with a single bunch charge of about 30 pC into the THz radiator, we could get strong multi-bunch beam loading effects to generate a high average power THz radiation at 0.316 THz. In this paper, we describe upgrades of the IAC L-band linac, the THz radiator, and linac optimization experiences to generate a high average power THz radiation at 0.316 THz with the compact THz radiator.

Table 1: Parameters of Linac and THz Radiator

Parameter	Value	Unit
Maximum beam energy	44	MeV
Minimum beam energy	5	MeV
RF frequency	1300	MHz
Repetition rate of RF macropulse	30	Hz
Length of RF macropulse	2	μs
Bunches in a macropulse	2600	·
Single bunch charge	30	pC
R_{56} of bunch compressor	13.7	mm
Minimum rms bunch length	500	fs
Resonance frequency of radiator	0.316	THz
Grating period	234	μm
Grating groove depth	80.86	μm
Grating structure length	30.4	mm
Grating structure width	6.3	mm
Grating structure gap	1.256	mm
Phase advance per period	88	deg
Quality factor	2150	·
Gap-averaged shunt impedance	4.3	MΩ/m
Nomalized group velocity	0.8	·
Average THz power per macropulse	17	W
Bandwidth of THz radiation	10	%

UPGRADES FOR EXPERIMENTS

For the THz experiments, as shown in Fig. 1, we installed a THz radiator, which had been fabricated with the conventional CNC milling, a chicane bunch com-

* Mail: yjkim@isu.edu

Copyright © 2013 CC-BY-3.0 and by the respective authors

PSEUDO SINGLE BUNCH WITH ADJUSTABLE FREQUENCY*

C. Sun†, M. Hertlein, J. Kirz, M. A. Marcus, G. Portmann, D.S. Robin and C. Steier
Lawrence Berkeley National Laboratory (LBNL), Berkeley, CA 94720, USA

Abstract

We present the concept and results of pseudo-single bunch (PSB) operation - a new operational mode at the Advanced Light Source (ALS) - that can greatly expand the capabilities of synchrotron light sources to carry out dynamics and time-of-flight experiments. In PSB operation, a single electron bunch is displaced transversely from the other electron bunches using a short pulse, high repetition rate kicker magnet. Experiments that require light emitted only from a single bunch can stop the light emitted from the other bunches using a collimator. Other beamlines will only see a small reduction in flux due to the displaced bunch. As a result, PSB eliminates the need to schedule multi-bunch and timing experiments during different running periods. Furthermore, the time spacing of PSB pulses can be adjusted from milliseconds to microseconds with a novel "kick-and-cancel" scheme, which can significantly alleviate complications of using high power choppers and substantially reduce the rate of sample damage.

INTRODUCTION

A major limitation of synchrotron light sources is the ability to easily serve two classes of experiments simultaneously, namely, brightness or flux limited experiments and timing experiments. High brightness experiments require filling most of the rf buckets with electrons, thus maximizing the total current while minimizing the current per bunch. In such a multibunch filling pattern, the bunch spacing is typically only a few nanoseconds between electron bunches. On the other hand, timing experiments require longer times between x-ray pulses. For example, in the case of laser-pump x-ray-probe timing experiments, it is desirable to have only one x-ray pulse per laser pulse. Since such lasers operate between kHz and MHz rates, this implies a distance between pulses of ms to μs.

At the Advanced Light Source (ALS) facility, we have been exploring a new mode of operation that we call pseudo-single-bunch (PSB) operation, the goals of which are to allow multibunch and timing experiments to run simultaneously [1, 2, 3]. The idea behind PSB operation is to use a high-repetition (MHz)-rate, short-pulse (<100 ns) kicker [4] to vertically displace a single camshaft bunch relative to the bunch train. Experiments that require light emitted only from a single bunch can block the light emitted from the other bunches using a collimator with only light from the camshaft bunch reaching the experiment. The PSB timing could be at the orbital period (656 ns) or longer, depending upon how frequently the bunch is displaced.

Here we discuss the results of our studies on the PSB operational mode, especially the novel kick-and-cancel (KAC) scheme that can deliver a single pulse with adjustable frequency [3]. A similar idea was previously suggested [5], but to our knowledge this is the first time that it has been realized.

KICK-AND-CANCEL SCHEME

The idea of the KAC scheme is that by adjusting the ring tune and the PSB kick pattern, the camshaft bunch can first be displaced to a different orbit and then kicked back to its original one within a few turns. This KAC process can be repeated at will to create a PSB pulse with an adjustable repetition rate. Mathematically, the KAC scheme can be shown as follows. Assuming that a camshaft bunch is kicked at the i^{th} turn with a kick angle of θ_y, the orbit offset and angle at the n^{th} turn due to this kick are given by

$$\begin{aligned} y_n^i &= \theta_y \beta_y \sin[2\pi(n-i)\nu_y], \\ y_n'^i &= \theta_y \{\cos[2\pi(n-i)\nu_y] - \alpha_y \sin[2\pi(n-i)\nu_y]\}. \end{aligned} \quad (1)$$

To restore the orbit after the n^{th} turn, the superpositions of orbit offsets and angles from each kick need to be zero, i.e.,

$$\sum_{i=0}^{n} y_n^i = 0, \qquad \sum_{i=0}^{n} y_n'^i = 0. \quad (2)$$

Using the two equations above, we can solve the required vertical tune for given number of kicks and orbit turns. There are many possible solutions to Eq. (2). Just one example is presented here. In this example we wish to restore the orbit after two turns within two kicks. The orbit offsets and angles are created by these two kicks at the 2^{th} turn are

$$\begin{aligned} y_2^0 = \theta_y^0 \beta_y \sin 4\pi\nu_y, y_2'^0 &= \theta_y(\cos 4\pi\nu_y - \alpha_y \sin 4\pi\nu_y) \\ y_2^2 = 0, y_2'^2 &= \theta_y^0. \end{aligned} \quad (3)$$

Applying Eq. (2), we can solve the vertical tune $\nu_y = 0.25$.

To test this scheme at the ALS, the vertical tune of the storage ring needs to be adjusted to 9.25 from the nominal tune of 9.20. Figure 1 shows simulated beam orbits for this KAC scheme with the kick angle of 73 μrad. We can see that the beam orbit is displaced for two turns and then kicked back to the nominal one. For example, at the undulator beam line 6.0.1 as indicated in Fig. 1(c), the two orbits are displaced on both sides of the unkicked one, and

* Work supported by the Director Office of Science of the U.S. Department of Energy under Contract No. DE-AC02-05CH11231.
† ccsun@lbl.gov

ISBN 978-3-95450-138-0

Copyright © 2013 CC-BY-3.0 and by the respective authors

INITIAL LATTICE DESIGN STUDIES FOR A DIFFRACTION LIMITED UPGRADE OF THE ADVANCED LIGHT SOURCE

H. Tarawneh#, C. Steier, D. Robin, H. Nishimura, C. Sun, W. Wan
Lawrence Berkeley National Laboratory, 1 Cyclotron Rd., Berkeley, CA 94720 USA

Abstract

The Advanced Light Source (ALS) at Berkeley Lab has seen many upgrades over the years, keeping it one of the brightest sources for soft x-rays worldwide. Recent developments in magnet technology and lattice design appear to open the door for very large further increases in brightness [1], particularly by reducing the horizontal emittance, even within the space constraints of the existing tunnel. We are investigating the possibility of a new storage ring lattice that could approach the soft x-ray diffraction limit around 2 keV in both planes within the ALS footprint.

This note presents an overview of a candidate lattice for diffraction limited ALS and describes the optimization of the dynamical performance of the lattice. In addition on-axis injection scheme is foreseen for this ring and a candidate lattice for an accumulator ring, which will be built and housed either in the ALS storage ring tunnel or the booster tunnel, is also presented.

INTRODUCTION

A new compact lattice based on Multiple Bend Achromat [2] that is going to replace the existing ALS Triple Bend Achromat is being investigated. This design study of diffraction limited ALS (ALS-II) lattice has a goal of achieving a natural emittance of about 100 pm.rad and beam energy around 2 GeV.

This candidate lattice takes advantage of the fact that the ring admittance is defined by the small gap insertion devices and hence the use of small aperture magnets. This leads to the introduction of high magnetic strength where very low emittance with short circumference can be achieved.

The small emittance achieved by the candidate ALS-II lattice requires the usage of double RF system to lengthen the bunch and to operate with round beam to mitigate the effect of Intra Beam Scattering (IBS) and for lifetime considerations [3]. Bunch lengthening will also have large impact on mitigating the effect of beam interaction with the resistive metallic chamber and the chamber geometric discontinuities due small momentum compaction factor.

The ALS-II lattice strong focusing limits the dynamic aperture to few millimetres which requires an on-axis injection scheme based on swap-out [4]. A relatively small emittance ring, Accumulator ring, is proposed to inject into the ALS-II ring as the current ALS booster has a large emittance and will not deliver full charge in a single bunch needed by the swap-out injection scheme.

In the following sections, the choice of the ALS-II lattice and characterization of its dynamical properties and performance are discussed. The bunch lengthening with double RF system and the implications on emittance, lifetime will be discussed.

Also a candidate lattice for the accumulator ring and achieved dynamic performance will be presented.

CANDIDATE ALS-II LATTICE

A study has been performed for a lattice that could approach the soft x-ray diffraction limit around 2 keV in both planes within the ALS footprint. This lattice, while not fully optimized, demonstrates the feasibility of the ALS-II concept. The new lattice is based on a Nine Bend Achromat replacing the existing ALS Triple Bend Achromat, see Figure 1. The lattice preserves the 12-fold symmetry and the circumference of the present ALS while ultimately achieving a natural emittance of about 100 pm.rad at 2 GeV beam energy. The proposed lattice follows the hybrid configuration of the ESRF upgrade design that takes advantage of a large number of combined function bending magnets to reduce the horizontal emittance [5]. The matched cell structure serves two goals, matching the dispersion to zero in the straight section since the lattice is optimized for high brightness production and to create a large horizontal dispersion bump and large beta function for efficient natural chromaticity correction. Figure 2 shows the layout of one arc of the candidate lattice.

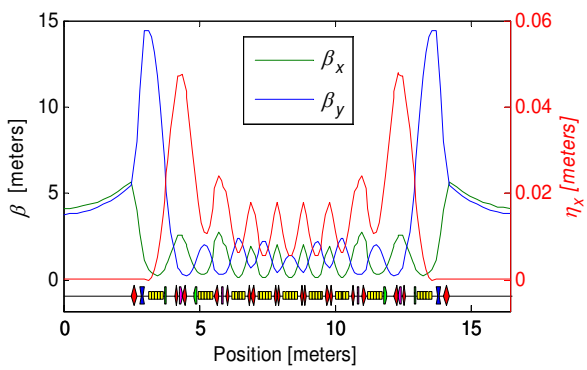


Figure 1: ALS-II candidate lattice Twiss functions.

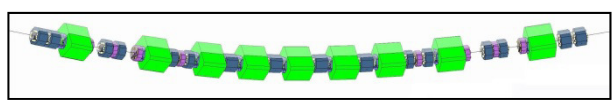


Figure 2: Layout of one arc of ALS-II lattice.

Multi-Objective Genetic Algorithm (MOGA) has been used to give an optimal solution based on the lattice elements [6]. The selected lattice provide identical optical functions in all straight sections with natural emittance of 100 pm.rad and horizontal and vertical beta functions of

(#) HITarawneh@lbl.gov

Copyright © 2013 CC-BY-3.0 and by the respective authors

REMOVAL OF RESIDUAL CHIRP IN COMPRESSED BEAMS USING A PASSIVE WAKEFIELD TECHNIQUE

M. Harrison*, G. Andonian, T. Campese, A. Murokh, F. H. O'Shea, M. Ruelas,
RadiaBeam Technologies, Santa Monica, CA 90404, USA
P. Frigola, RadiaBeam Systems, Santa Monica, CA 90404, USA
M. Fedurin, Brookhaven National Laboratory, NY 11961, USA

Abstract

The removal of residual chirp in XFELs is of paramount importance for efficient lasing. Although current S-band XFELs remove the unwanted residual chirp using off-crest acceleration after the final bunch compressor, this technique is not possible for XFELs with soft X-ray lines as there are no further accelerating structures. The off-crest dechirping technique is also expensive for future superconducting XFELs. In response, RadiaBeam Systems presents its work, building upon the theoretical work of Bane and Stupakov [1], in RF-free residual chirp mitigation using only passive techniques. Beam-induced longitudinal wakefields are produced with opposing corrugated plates which allow for an entirely RF-free chirp removal. Theory, engineering, and experimental results are presented.

INTRODUCTION

Beam dechirping is crucial for current and future XFELs. Accelerating and compressing sections of beamlines leave beam bunches with a residual chirp that must be removed for lasing. In the SLAC LCLS, dechirping requires hundreds of meters of off-crest accelerating structures. This is costly both in terms of accelerating cavity efficiency and beamline space [2].

RadiaBeam Systems has designed and manufactured a compact, low-cost corrugated plate system with an adjustable gap for tunable beam dechirping. Its dechirping characteristics were measured at the Brookhaven National Laboratory (BNL) Accelerator Test Facility (ATF).

THEORY

The driving theory for designing the passive dechirper system has been presented in papers by Bane, Stupakov, and Emma [2] [3]. The longitudinal wakefield generated by a single electron passing between the corrugated plates is given by

$$w(z) = \left(\frac{\pi^2}{16}\right)\frac{Z_0 c}{\pi a^2} H(z) cos\left(\frac{2\pi z}{\lambda}\right), \qquad (1)$$

where $Z_0 = \sqrt{\mu_0/\epsilon_0}$ is the impedance of free space, $H(z)$ is the unit step function, c is the speed of light, z is the coordinate along the beam path, and λ is the wavelength of the dominant mode of the wakefield given by

$$\lambda = 2\pi\sqrt{\frac{a\delta g}{2p}}. \qquad (2)$$

The remaining variables describe the dimensions of the corrugated plates. a is the distance of the plates from the beamline (half the plate separation); δ is the depth of the corrugations; g is the gap between corrugations; p is the period of the corrugations. These dimensions are listed in Table 1 and pictured in Figure 2. For compliance with the derivation assumptions, $p, d \ll a$ and $\delta \gtrsim p$ [2]. The transverse dimension of the plates is taken to be infinite.

The $\pi^2/16$ factor comes from the differing geometry between parallel plates and the circular pipe that was used in Stupakov and Bane's original derivation [4]. The wakefield produced by the bunch is found by convolving the single particle wakefield (Equation 1) with the longitudinal beam bunch charge density profile. For rectangular longitudinal profiles, the wakefield is linear in the region of the beam bunch as shown in Figure 1. For plates that satisfy the constraints above, the dechirping strength, h, is given by the slope of the linear region and can be calculated by

$$h = \left(\frac{\pi^2}{16}\right)\frac{Z_0 c Q L}{\pi a^2 l}, \qquad (3)$$

where Q is the bunch charge, L is the length of the dechirper, and l is the bunch length.

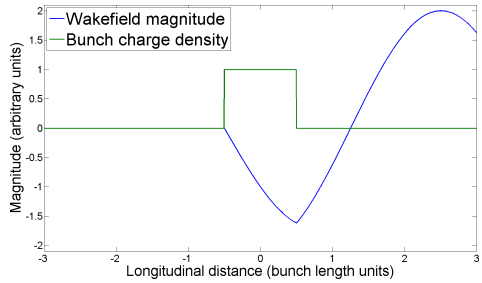


Figure 1: Bunch current profile and generated longitudinal wakefield.

CORRUGATED PLATE DIMENSIONS AND MANUFACTURE

The dimensions of the corrugated plates used in this experiment are listed in Table 1. The plates were fabricated

* harrison@radiabeam.com

ISBN 978-3-95450-138-0

Copyright © 2013 CC-BY-3.0 and by the respective authors

LASER-UNDULATOR FEL WITH NEARLY COPROPAGATING LASER PULSE*

R. A. Bosch#, J. E. Lawler, J. J. Bisognano, M. A. Green, K. D. Jacobs, R. Wehlitz, D. D. Yavuz,
University of Wisconsin-Madison, Madison, WI 53706, USA
R. C. York, Michigan State University, East Lansing, MI 48824, USA
T.-C. Chiang, T. J. Miller, University of Illinois, Urbana, IL 61801, USA

Abstract

A free-electron laser (FEL) may be obtained by interaction of an electron bunch and a nearly copropagating laser pulse, where the laser pulse is sheared to extend the interaction length. When the angle between the electron beam axis and the propagation direction of the laser pulse greatly exceeds the reciprocal of the relativistic factor, the output radiation is nearly on the axis, and the FEL may be approximated by an axially aligned magnetostatic undulator. For a feasible laser-undulator FEL, we calculate gain using a one-dimensional model, as well as a three-dimensional model that includes degradation from diffraction and electron velocity spread.

INTRODUCTION

An electromagnetic plane wave that collides head-on with an ultrarelativistic electron bunch may create an FEL [1] that amplifies xrays whose frequency is ~$4\gamma^2$ times that of the incident "pump" wave [2], where γ is the electron bunch's relativistic factor. To obtain softer xrays, one can propagate a pump wave in nearly the same direction as the electron beam. By using a sheared laser pulse [3, 4], the electromagnetic field affecting the bunch is similar to a plane wave over an extended interaction length [5–8].

For the case where the propagation directions of the electron beam and the pump wave differ by an angle >> $1/\gamma$, a one-dimensional (1D) FEL model predicts maximum gain for xrays whose propagation direction differs from that of the electron beam by an angle << $1/\gamma$, and nearly identical gain for xrays that propagate on the electron beam axis. For this practical case, a magnetostatic undulator that is aligned with the electron beam approximates the laser undulator.

For a circularly polarized laser-undulator FEL with output wavelength of 2.5 nm described in Ref. [8], we use this magnetostatic undulator to calculate gain using the 1D model as well as a three-dimensional (3D) model [9].

ONE-DIMENSIONAL MODEL

The 1D model describes a uniform density of cold electrons interacting with a plane electromagnetic pump wave. In this model, maximum gain occurs for the electromagnetic wave that is a 180º reflection of the pump wave, when viewed in the beam frame of reference where the average electron velocity is zero [10].

In the laboratory frame, consider a uniform density of cold electrons drifting with average velocity $\beta^* c$, where c is the speed of light, interacting with a pump wave. Let the z-axis describe the direction of the average electron motion while interacting with the pump laser, which propagates at an angle of θ_{pump} w.r.t the z-axis. A head-on collision is described by $\theta_{pump} = 180º$.

For small laser intensity, the forced electron oscillations in the beam frame are nonrelativistic, and the average axial velocity of the electrons in the lab frame is given by $\beta^* \approx \beta = (1-1/\gamma^2)^{1/2}$. In this case, the Lorentz-invariant undulator parameter K is << 1, where [2, 5, 8]

$$K^2 = 2 r_e I \lambda_{pump}^2 / (\pi m c^3) , \quad (1a)$$

$$K^2 = r_e I \lambda_{pump}^2 / (\pi m c^3) . \quad (1b)$$

Equation (1a) describes a planar undulator created by a linearly polarized pump wave, while eq. (1b) describes a helical undulator created by circular polarization. Here, r_e is the classical radius of the electron, I is the pump laser intensity, λ_{pump} is the pump wavelength and m is the electron mass. For larger values of K, the forced electron oscillations are relativistic in the beam frame. In the lab frame, $(K/\gamma)c$ is the maximum transverse electron velocity driven by the pump wave.

In the laboratory frame, the angular 4-frequency (c times the 4-vector) of the pump wave is

$$\overline{\omega}_{pump} = (\omega_{pump}, \omega_{pump} \sin\theta_{pump}, 0, \omega_{pump} \cos\theta_{pump}) . \quad (2)$$

A Lorentz transform gives the angular 4-frequency in the beam frame, which is moving at the velocity $\beta^* c$ [11]

$$\overline{\omega}'_{pump} = (\gamma^* \omega_{pump}(1-\beta^* \cos\theta_{pump}), \omega_{pump} \sin\theta_{pump}, 0, \gamma^* \omega_{pump}(\cos\theta_{pump} - \beta^*)) , \quad (3)$$

where the axial relativistic factor is defined by $\gamma^* = (1-\beta^{*2})^{-1/2}$. In the beam frame, the pump wave has angular frequency

$$\omega'_{pump} = \gamma^* \omega_{pump}(1-\beta^* \cos\theta_{pump}) , \quad (4)$$

and direction of propagation obeying

$$\cos\theta'_{pump} = \frac{\cos\theta_{pump} - \beta^*}{1-\beta^* \cos\theta_{pump}} . \quad (5)$$

For many cycles of interaction, the maximum FEL gain occurs for the wave given in the beam frame by a 180º reflection of the pump wave [10]. This wave is given in the beam frame by the same frequency as the pump

*Work supported by the University of Wisconsin-Madison
bosch@src.wisc.edu

Copyright © 2013 CC-BY-3.0 and by the respective authors

STUDIES ON SHORT-BUNCH EXTRACTION AT CSNS RCS

Ye Zou, Jingyu Tang, Jinfang Chen
Institute of High Energy Physics, Chinese Academy of Sciences, Beijing 100049

Abstract

White neutron application requires short proton pulse length to obtain high time resolution for nuclear data measurements. Back-streaming neutron beam at the CSNS spallation target is to be exploited as a white neutron source. The available high RF voltage in the high intensity rapid cycling synchrotron (RCS) of the CSNS makes it possible to extract very short bunches by using the bunch rotation method. Special attentions have been paid to the bunch rotation during the slow acceleration, space charge effect and beam loading effect in the high-intensity RCS. Different extraction scenarios together with the changes in the injection have been studied. Together with the calculations, multi-particle simulations have been carried out to show the effectiveness of the method. With a sacrifice of about two-third beam power, the rms bunch length of the extracted beam can be reduced to about one eighth of the one in the nominal operation mode. Other scenarios also show the improvement in the bunch length.

INTRODUCTION

Back-streaming neutrons from the spallation target of CSNS (China Spallation Neutron Source) are very strong and harmful to the proton beam transport line if they are not well treated [1]. The studies found that the neutron beam has excellent properties of wide energy spectrum and time structure, and has been proposed to build a white neutron source for nuclear data measurement [2, 3]. The neutron pulse length is critical in defining the neutrons' energy by the time-of-flight method, and should be reduced as short as possible. The time structure of the back-streaming neutrons is jointly determined by the pulse length of the impinging proton beam and the thickness of the spallation target. Simulations show that the target thickness dominates the time resolution for the lower energy part of the wide-range energy neutrons, while the proton pulse length dominates the higher energy part. As the target length cannot be changed for this parasitic application, it would be interesting to shorten the proton pulse length by designing a special dedicated working mode for the CSNS accelerators. This paper presents the study about using the bunch rotation method in the RCS (Rapid Cycling Synchrotron of CSNS) to obtain very short proton beam bunches.

CSNS is a multi-disciplinary research facility under construction [4], which is to be built in two or three phases. In the first phase, the RCS is to accelerate beam from 80 MeV to 1.6 GeV in a repetition rate of 25 Hz, and the extracted beam power is 100 kW. Figure 1 and Table 1 show the layout and some parameters of the RCS.

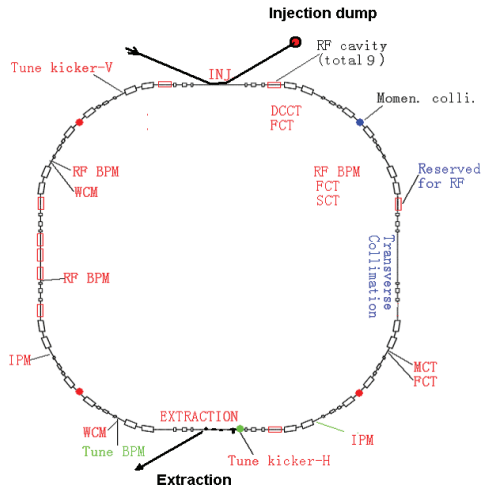


Figure 1: Layout of the CSNS RCS.

Table 1: Some Parameters of the CSNS RCS

Circumference (m)	227.92
Injection energy (GeV)	0.08
Extraction energy (GeV)	1.6
Maximum RF voltage (kV)	165
Betatron tunes (h/v)	4.82/4.80
RF harmonics	2
Transverse acceptance (πmm.mrad)	540
Collimation acceptance (πmm.mrad)	~350

SHORT-BUNCH EXTRACTION METHODS

There are two bunches per pulse in the extracted proton beam in the normal operation mode. The bunch length is determined by the RF voltage pattern and the longitudinal painting. The longitudinal painting is optimized to alleviate the space charge effects in such a high-intensity synchrotron. Compared with the simple method by designing a high RF voltage at the extraction, the bunch rotation method is more effective in shortening the bunch length for the extracted beam [5, 6]. The principle of the bunch rotation method is as follows: the RF voltage is adiabatically decreased from the normal extraction voltage to a low one, during which the bunch becomes gradually flat to follow the change of the RF bucket as long as the bucket still contain the beam with some margin. Then the RF voltage is quickly or non-

* zouye@ihep.ac.cn

Copyright © 2013 CC-BY-3.0 and by the respective authors

ISBN 978-3-95450-138-0

DESIGN CONSIDERATIONS FOR THE ESS ACCELERATOR-TO-TARGET REGION

Thomas J. Shea, Eric J. Pitcher, Ken Andersen, Phillip Bentley, Paul Henry,
Pascal Sabbagh, Alan Takibayev, ESS, Lund, Sweden
Heine Dølrath Thomsen, Søren Pape Møller, ISA, Aarhus, Denmark

Abstract

When the European Spallation Source (ESS) is completed in Lund, Sweden, a superconducting linac will deliver a 5 MW proton beam to a rotating tungsten target. Moderated neutrons from this target will be delivered to a suite of 22 neutron instruments. In the accelerator-to-target region, design choices must balance the demands of the accelerator, the target, and the neutron instruments. For example, the transport line upstream of the target station expands and shapes the small, low emittance linac beam into a large beam that is safe for the target components. It must do this with low loss in order to reduce activation of the beam line and minimize a potential source of background in the neutron instruments. To meet availability goals, beam-induced damage to critical components must be avoided by instrumenting beamline components, deploying a suite of beam instrumentation within the target monolith, and interfacing some of these devices to the machine protection system. This paper will describe recent design changes in this region, highlighting considerations that are applicable to most high power facilities and also those that are unique to a long-pulse source like the ESS.

GOALS

The accelerator-to-target region serves three primary stakeholders: Neutron Science, Target, and Accelerator. Because the long pulse concept couples these stakeholders, the design must balance the needs of all three.

Neutron Science

Neutron instrumentation at a long-pulse source requires a reproducible pulse, both in terms of the time structure and the brightness. Most long pulse instruments under development for ESS use a combination of choppers and the instrument's total flight path length to tailor the neutron pulse and the available wavelength band to the desired characteristics. For example, a truncated pulse will lead to a hole in the wavelength band at the sample position during the time-frame. Therefore, during neutron production, the facility should provide full length pulses with reproducible structure.

The long pulse places additional unique requirements on the neutron instrumentation in terms of dimensions and background. The optimal arrangement of the instrument geometry to exploit the long pulse requires measurement across a frame boundary. In other words, the instruments will perform measurements with slow-moving, meV-energy neutrons at the same time that the proton pulse hits the target for the next pulse. Any contamination from MeV particles emitted by the accelerator and target that can be picked up by the instrument appear as a time-dependent background superimposed on the weak meV signals of interest. This background manifests itself as a systematic error that is correlated with the measurement time (e.g. [5]), and is most efficiently mitigated at its source.

Target

To survive between reasonably long replacement intervals, target components that intercept the proton beam core impose restrictions on the beam's density. These components include the rotating tungsten target, and the proton beam window that separates this target's atmosphere from the accelerator's vacuum. In addition, surrounding components can only receive a limited volumetric power density, and this imposes a limit on beam outside of the core footprint.

Neutron moderator and reflector assemblies also reside within the target system. Because neutron intensity can depend on proton beam position and current, the time to moderate neutrons from the spallation spectrum down to desired energies will determine that timescale for allowable fluctuations in proton beam position and current.

Accelerator

To meet the target requirements above, the transport line leading to the target must expand the bright beam from the linac into an acceptable footprint. To meet the requirements for the neutron pulse, fluctuations in beam position and current must be repeatable and also limited in magnitude and/or characteristic timescale. The transport line should also allow hands-on maintenance by limiting beam loss to well under 1 W/m and by enabling isolation of the components from target back shine.

PROTON BEAM TRANSPORT

Table 1 summarizes the proton beam parameters at the output of the ESS linac. The accelerator-to-target line receives the beam with these parameters and transform it into a beam with the parameters at the proton beam window (PBW) and target (Tgt) listed in Table 2. It accomplishes this by scanning or rastering an expanded beamlet across the target surface.

Copyright © 2013 CC-BY-3.0 and by the respective authors

ISBN 978-3-95450-138-0

THERMAL DESIGN OF THE FETS CHOPPER BEAM DUMP

S. Mishra*, UROP student, Imperial College London
M. Aslaninejad, P. Savage§, P. A. Posocco, Imperial College London
J.K. Pozimski, Imperial College London and STFC/RAL
A.P. Letchford, STFC/RAL

Abstract

The Front End Test Stand Project (FETS) at RAL is being built to demonstrate fast beam chopping. This is required to create precisely defined gaps in the bunched H- beam which is essential in order to minimise beam losses in a synchrotron during injection. The gaps are created in the Medium Energy Beam Transport (MEBT) section of the FETS beam-line using a 'fast-slow' chopping scheme. This scheme uses two choppers, one fast and one slow, each kicks a portion of beam into its corresponding downstream beam dump. The challenge for the beam dump design is that it must occupy a limited longitudinal space to ensure that the beam transport is preserved and must absorb a beam power that is close to the sustainable stress limit of common engineering materials. This paper will describe the simulations made to study the cooling scheme required to absorb the power deposited in the dump plates for the fast and slow choppers.

INTRODUCTION

The FETS project requires two chopper beam dumps to withstand and safely dissipate power from the incident beam. The beam parameters, listed in Table 1, thus form the design criteria for these dumps [1].

Table 1: Parameters for the FETS Beam

Parameter	Value
Particle	H-
Beam Energy	3 MeV
Beam Current	60 mA
Pulse Length	20 ms
Duty Cycle	0.1
Maximum Power	180 kW
Average Power	18 kW

The beam is on for a 2 ms pulse in each 20 ms period. During this time, it is broken by choppers into a repeated cycle of ON/OFF states. The two choppers in the FETS project are denoted 'fast' and 'slow', based on their respective response times. During each ON stage of a chopper, it deflects beam particles to its corresponding downstream dump. The chopper timings have been designed in accordance with the ISIS synchrotron frequency of 1.5 MHz. The FETS beam has a frequency of 324 MHz, resulting in 216 periods of ON/OFF cycles, or beam bunches for each ISIS period [2]. Table 2 describes how these 216 beam bunches are broken by the fast and slow choppers.

*Supported by STFC
§ p.savage@imperial.ac.uk

Table 2: Sequenced Timing for the Fast / Slow Choppers

Number of bunches	Fast Chopper State	Slow Chopper State
4	ON	OFF
57	OFF	ON
4	ON	OFF
151	OFF	OFF

During an ON period of a chopper, its corresponding dump sees the full 180 kW of incident power. However, each chopper deflects only a certain proportion of the total 216 bunches, and the dump is required to dissipate power according to this proportion, as presented in Table 2. The sequence of states can be expressed in terms of the average power seen by the two dumps, shown in Table 3.

Table 3: Summary of Power Incident on Chopper Dumps

Number of bunches	Fast Chopper Dump	Slow Chopper Dump	Main FETS Dump
Percentage of total power dissipated	3.70%	26.39%	69.91%
Average power over 2 ms beam pulse	6.67 kW	47.50 kW	125.83 kW
Average power over 20 ms period	0.667 kW	4.750 kW	12.583 kW

PRELIMINARY DESIGN

This section describes the initial design decisions that have been taken for the chopper dumps. A rectangular plate-geometry was selected, with dimensions incorporating space constraints imposed by the FETS set-up. In this configuration, the deflected beam hits the plates at a shallow incident angle, with the power effectively distributed over a larger area, minimising the surface heat flux. Heat dissipates through the plate material, and is absorbed in water-cooled channels along the length of the plates.

The beam power must be safely dissipated by the plate and water cooling, and the material selection must be carried out accordingly. In order to select the material, existing beam dumps of similar specifications were first identified, and the materials used for these beam dumps were considered. Copper was then selected for the initial thermal analysis, with the possibility of using Nickel-coated copper in future simulations, should the radiation study deem this necessary. The subsequent analyses have all been carried out on a copper plate.

Copyright © 2013 CC-BY-3.0 and by the respective authors

ISBN 978-3-95450-138-0

PROPOSAL FOR SIMULTANEOUS ACCELERATION OF STABLE AND UNSTABLE IONS IN ATLAS†

A. Perry, ANL, Argonne, IL, 60439, USA; IIT, Chicago, IL, 60616, USA
B. Mustapha, P.N. Ostroumov, ANL, Argonne, IL, 60439, USA

Abstract

The Argonne Tandem Linac Accelerator System (ATLAS) is the only national user facility for low-energy stable heavy ion beams. With the recent commissioning of the Californium Rare Isotope Breeder Upgrade (CARIBU), ATLAS will also be used to accelerate radioactive beams. We here propose to convert ATLAS into a multi-user facility by simultaneously accelerating stable beams from the ECR ion source and radioactive beams from an Electron Beam Ion Source (EBIS) charge breeder under development for CARIBU. Radioactive beams produced from EBIS will contain several charge states of the same isotope, and could be injected into ATLAS in short (~10μs) pulses. We propose modifications of the existing ATLAS low energy beam transport line that will allow the simultaneous injection and acceleration of one or more charge states from EBIS and a stable ion beam from the ECR. Beam dynamics simulations using the code TRACK confirmed the feasibility of these modifications. The realization of this concept will increase the available beam time, the intensity of radioactive beams and improve the quality of the delivered beams as well.

INTRODUCTION

The Argonne Tandem Linac Accelerator System (ATLAS) is the only national user facility for low-energy stable heavy ion beams. On a yearly basis ATLAS provides beam time in excess of 5000 hours to domestic and international users.

Recently, the californium rare isotope breeder upgrade (CARIBU) had been successfully commissioned at ATLAS [1]. CARIBU will produce, at full capacity, beams of ~80-160 amu fission fragments from a 1 Curie ^{252}Cf source. After thermal stabilization and mass separation, the fragments will be charge bred in a charge breeder based on an electron beam ion source (EBIS) [2]. This type of charge breeders yield higher breeding efficiencies with fewer contaminations and shorter breeding times compared to electron cyclotron resonance (ECR) based charge breeders. After charge breeding in EBIS, the radioactive beams will be injected into ATLAS, used as a post accelerator.

When radioactive beams from CARIBU become available, the already high demand for ATLAS beam time is expected to further increase. It may therefore be necessary to upgrade ATLAS into a multi-user facility - capable of simultaneously accelerating multiple beams and delivering them to different experiments. The feasibility of the proposed upgrade project relies heavily on two features:

a. The accelerator structure of ATLAS, consisting of individually-phased superconducting cavities, is extremely versatile, as was best demonstrated in the simultaneous acceleration of 8 charge states of Uranium through the booster linac section [3]. This enables the acceleration of stable and radioactive beams with charge to mass ratios differing by as much as 5%. Amongst the beams available for injection into ATLAS are numerous examples that meet this criterion, as shown in Table 1 below.
b. The radioactive beam from CARIBU EBIS will be pulsed with a pulse repetition rate of ~30Hz and a pulse length of ~10μs for a duty cycle of 0.03%. During the remaining time it will be possible to feed the accelerator with the appropriate stable beam.

Table 1: Some Beams with Similar Charge-to-Mass Ratios which can be Accelerated Simultaneously in ATLAS

Nominal Charge/mass	Stable Beams from ECR2	Radioactive beams from EBIS
0.15	$^{20}Ne^{3+}$, $^{86}Kr^{13+}$ $^{238}U^{36+}$, $^{133}Cs^{20+}$	$^{86}As^{13+}$, $^{106}Nb^{16+}$ $^{93}Kr^{14+}$, $^{93}Rb^{14+}$
0.16	$^{208}Pb^{33+}$, $^{56}Fe^{9+}$	$^{100}Y^{16+}$, $^{87}Br^{14+}$
0.18	$^{128}Xe^{23+}$, $^{84}Kr^{15+}$	$^{111}Tc^{20+}$, $^{138}Te^{25+}$
0.20	$^{20}Ne^{4+}$, $^{90}Zr^{18+}$	$^{131}Sn^{26+}$, $^{124}Cd^{25+}$
0.23	$^{56}Fe^{13+}$	$^{105}Ru^{24+}$, $^{101}Mo^{23+}$ $^{91}Sr^{21+}$, $^{83}Se^{19+}$

In order to achieve multi-user capability, 3 main points were identified:

- Injection of beams from two sources into the ATLAS Low Energy Beam Transport (LEBT).
- Modification of the ATLAS LEBT, which contains a 180 degrees bend, to accommodate for the transport of two beams with slightly different charge-to-mass ratios while introducing minimal emittance growth.

† This work was supported by the U.S. Department of Energy, Office of Nuclear Physics, under Contract No. DE-AC02-06CH11357.

Copyright © 2013 CC-BY-3.0 and by the respective authors

THE D-LINE PROJECT AT MICHIGAN STATE UNIVERSITY *

J.A. Rodriguez#, S. Chouhan, A. Lapierre, D. Leitner, G. Perdikakis, M. Portillo, S. Schwarz, M. Steiner, C. Sumithrarachchi, S.J. Williams, W. Wittmer, X. Wu, NSCL, East Lansing, MI, USA

Abstract

The Coupled Cyclotron Facility (CCF) at Michigan State University (MSU) has been used to produce rare isotope beams for more than a decade. Ions produced by an ECR source are accelerated using two superconducting cyclotrons in tandem with a stripper foil in between to boost their charge state. After the second cyclotron, a target and a fragment separator produce and select the rare isotope beam that is sent to the different experimental vaults. A gas stopper can be used to thermalize the beam before sending it to a low energy experimental area or to a charge breeder before the ReA re-accelerator. The D-line project includes a mass separator after the gas stopper and several beam transfer lines that connect it to the low energy experimental stations and to the charge breeder. In this paper, we will describe the project and give an update of its status including the results of the commissioning.

INTRODUCTION

One of the most important developments at the National Superconducting Cyclotron Laboratory (NSCL) during this past year has been the successful delivery of the first radioactive reaccelerated beam to users [1]. Together with the commissioning of the gas cell in the ion beam thermalization area [2], the charge breeder [3] and the reaccelerator [4], the completion of the D-line was one of the steps necessary to make this possible.

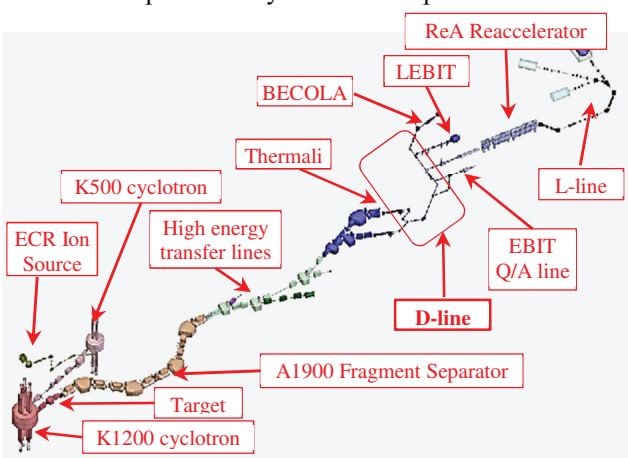


Figure 1: Layout of the CCF and ReA3 facilities (several high energy beam lines and experimental areas are not shown). The D-line connects the thermalization area with the low energy experimental hall and the charge breeder.

DESCRIPTION OF THE LINE

The main purpose of the D-line is to connect the beam thermalization area of the NSCL with the experimental devices in the low-energy experimental hall (LEBIT [5] and BECOLA [6]) or alternatively with the Q/A line before the charge breeder (EBIT) and the ReA3 reaccelerator. In addition, the line includes a mass separator that is used to select the Radioactive Isotope Beam (RIB) that is going to be studied and to clean the unwanted contaminants with a different momentum after extraction from the gas cell.

The line is designed to be able to transport efficiently beams with emittances of ~ 10 π·mm·mrad and energy lower than 60 keV. In its current configuration (Figure 3), the south line is used to transport stable beams from an off-line ion source. This beam has been used for commissioning of the D-line and downstream experimental devices. The north line is used to transport the RIBs previously thermalized in the gas cell.

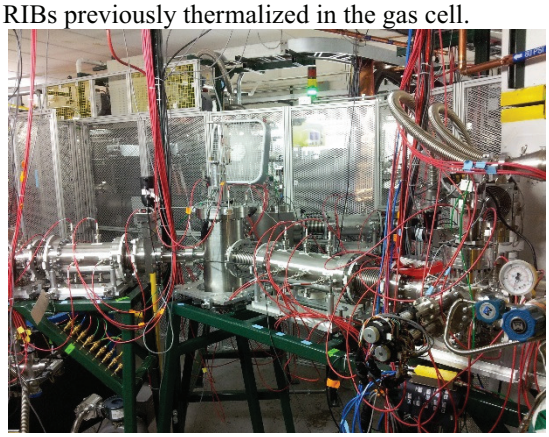


Figure 2: Merging point of the north and south lines. Starting from the left, the picture shows an electrostatic doublet, a bender and a triplet followed by the vacuum and diagnostic station before the mass separator.

With the exception of the dipole magnet used as a mass separator, all the other elements in the D-line are electrostatic. The beam is focused using electrostatic quads (10 cm long, 6 cm aperture, up to ±6 kV bias) normally grouped into doublets. In most cases, opposite electrodes are shorted inside the vacuum chamber and driven by a single power supply. However, some of them can be used as beam steerers since they can be biased independently. In addition, there are horizontal and vertical steering plates in all the diagnostic boxes. Spherical benders (up to ±10 kV bias) are used to deflect the beam 45 degrees at a time. Several of them have also been combined for deflection angles of 90 and 135 degrees. Some of them are mounted in movable drives in order to allow an inserted or retracted state to switch the desired beam and its destination.

A dipole magnet and two electrostatic doublets function

* This material is based upon work supported by the U.S. Department of Energy Office of Science under Cooperative Agreement DE-SC0000661, the State of Michigan and Michigan State University, and the National Science Foundation, under Cooperative Agreement PHY-1102511.
#rodriguez@frib.msu.edu

ISBN 978-3-95450-138-0

Copyright © 2013 CC-BY-3.0 and by the respective authors

SYSTEMS ENGINEERING AND INTEGRATION ON THE FRIB PROJECT*

D. Stout#, T. Borden, N. Bultman, R. Frazee, M. Leitner, P. Nguyen, T. Russo, E. Tanke, C. Thronson, Facility for Rare Isotope Beams, Michigan State University, East Lansing MI, 48824 USA

Abstract

The Facility for Rare Isotope Beams (FRIB) will be a world-leading, DOE Office of Science national user facility for the study of nuclear structure, reactions, and astrophysics on the campus of Michigan State University (MSU).

Systems Engineering and Integration has been implemented at the outset to ensure that a requirements-driven design process is followed, and to ensure intra and inter-system compatibility. Top-level requirements have been allocated and subsequently elaborated between the Accelerator Systems, Experimental Systems, and Conventional Facilities. FRIB has developed a number of methods and tools to track requirements, establish interfaces, monitor design progress, and ensure overall system integration. These will be described in the paper.

FRIB PROJECT INTEGRATION

A superconducting, heavy-ion, driver linac will be used to provide stable beams of >200 MeV/u at beam powers up to 400 kW (~650 electrical micro-amps for uranium). The stable beams will be used to produce rare isotopes by in flight fragment separation. After fragment selection, the rare isotopes will be used at velocity (~0.5c), stopped, or reaccelerated. The MSU-led design and construction effort is supported by collaborations with many National Laboratories and other scientific institutions [1].

FRIB is integrated both vertically and horizontally. The vertical integration is achieved by the Systems Engineering methods discussed in the next section. Horizontal integration is achieved by the project organizational structure and by adherence to a consistent design process.

Project Engineers are identified within the three main FRIB Divisions, Accelerator, Conventional Facilities, and Experimental, and are responsible for integration within their Division.

The overall project design process is shown in Figure 1. At each significant project design phase, the key design products and expectations are defined with respect to the major design aspects: requirements, interfaces, drawings and specifications, manufacturing, and project management. At the beginning of each major design phase (i.e. preliminary or final design) deliverables for each sub-system are identified. These include specific analyses, tests, and prototypes that must be completed to demonstrate readiness for the next design phase, or for construction.

Defining the deliverables for each sub-system ensures coherence between the sub-systems, either by keeping their efforts on a similar schedule, or by clearly defining the interface points between sub-systems on different development schedules. This latter point is important since most projects usually cannot complete all design work simultaneously due to cost and design resource limitations. The other main advantage of clearly defining the deliverables and design expectations is that each sub-system manager then has a clear work plan for design. On FRIB these deliverables are used as part of the Earned Value Management System to measure and quantify design progress.

SYSTEMS ENGINEERING AND INTEGRATION OVERVIEW

Systems Engineering, as defined by the International Council on Systems Engineering [2], is an inter-disciplinary approach and means to enable the realization of successful systems. It focuses on defining customer needs and required functionality early in the development cycle, documenting requirements, then proceeding with design synthesis and system validation while considering the complete problem: Performance; Operations; Cost & Schedule; Training & Support; Test; Manufacturing and Disposal. Systems Engineering integrates all the disciplines and specialty groups into a team effort forming a structured development process that proceeds from concept to production to operation. Systems Engineering considers both the business and the technical needs of all customers with the goal of providing a quality product that meets the user needs.

Implementation of Systems Engineering can be tailored for a specific industry or laboratory. Many industries can amortize software, staffing, training, and set-up expenses over multiple platforms or projects. For one-off projects like FRIB, the same methods can be used, but off the shelf software and a leaner System Engineering staff are more appropriate.

Irrespective of the scale of the implementation, the "V" model is at the core of the Systems Engineering approach, and has been fully implemented for FRIB. This model breaks a system into sub-systems, equipment, and components, with specific requirements and interfaces at each level of decomposition. The right hand side of the "V" model is the subsequent aggregation of components, equipment, and sub-systems into a fully functioning system. This aggregation is accomplished by increasingly sophisticated levels of testing and integration. A requirements-based design is fundamental to the use of this model. By starting from a limited number of top-level system requirements, one can define the overall architecture and decompose the project into essential sub-

*This is based upon work supported by the U.S. Department of Energy Office of Science under Cooperative Agreement DE-SC0000661, by Michigan State University and by the State of Michigan.

#stout@frib.msu.edu

Copyright © 2013 CC-BY-3.0 and by the respective authors

STATUS AND OPPORTUNITIES AT PROJECT X: A MULTI-MW FACILITY FOR INTENSITY FRONTIER RESEARCH*

S. D. Holmes, M. Kaducak, R. Kephart, I.Kourbanis, V. Lebedev, S. Mishra, S. Nagaitsev, N. Solyak, R. Tschirhart, Fermilab, Batavia, IL 60510, USA

Abstract

Project X is a multi-megawatt proton facility being developed to support a world-leading program in Intensity Frontier physics at Fermilab. The facility will support programs in elementary particle and nuclear physics, with the potential for broader applications in materials and energy research. Project X is in the development stage with an R&D program focused on front end and superconducting rf acceleration technologies, and with design concepts for a staged implementation. This paper will review the status of the Project X conceptual development and the associated R&D programs.

PROJECT X MISSION AND GOALS

Project X is a high intensity proton facility that will support a world-leading U.S. program in Intensity Frontier physics over the next several decades. Project X is currently under development by Fermilab in collaboration with national and international partners. Project X will be unique in its ability to deliver, simultaneously, up to 6 MW of site-wide beam power to multiple experiments, at energies ranging from 235 MeV to 120 GeV, and with flexible and independently controlled beam time patterns. Project X will support a wide range of experiments utilizing neutrino, muon, kaon, nucleon, and atomic probes [1,2]. In addition, Project X will lay the foundation for the long-term development of a Neutrino Factory and/or Muon Collider.

PROJECT X REFERENCE DESIGN

A complete design concept, designated the Project X Reference Design [3], has been established supporting the above-described mission in an innovative and flexible manner. The Reference Design is based on a 3-GeV superconducting (SC) continuous wave (CW) linac, followed by an 8-GeV superconducting pulsed linac, and improvements to the Main Injector complex at Fermilab. The primary elements of the Reference Design are:

- An H^- front end based on a 162.5 MHz RFQ delivering 5 mA of beam current at 2.1 MeV into a medium energy beam transport (MEBT) line containing a wideband, bunch-by-bunch, chopper capable of accepting or rejecting bunches in arbitrary patterns and leaving 1 mA average (averaged over ~1 μsec) current for further acceleration;
- A 3-GeV SC linac operating in CW mode and capable of accelerating an average beam current of 1mA;
- A 3 to 8-GeV pulsed SC linac capable of accelerating a peak current of 1 mA with a duty factor of 4.3%;
- Rf splitters that can deliver beams at 1 and 3 GeV to at least three experimental areas;
- Experimental facilities to support experiments at 1 and 3 GeV;
- Modifications to the Main Injector (MI) and Recycler complex required to support 2-MW operations in the energy range of 60-to-120 GeV;
- All interconnecting beam lines.

STAGING STRATEGY

Fiscal considerations have motivated development of a staging plan for Project X, consistent with the following principles:

- The plan should provide compelling physics opportunities at each stage;
- Each stage should cost substantially less than $1B;
- Each stage should utilize existing infrastructure to the extent possible;
- The construction of each stage should minimize interruptions to the on-going research program;
- The full Reference Design capabilities should be achieved at end of the final stage.

The Reference Design has been developed consistent with these principles – the associated layout on the Fermilab site is shown in Fig. 1.

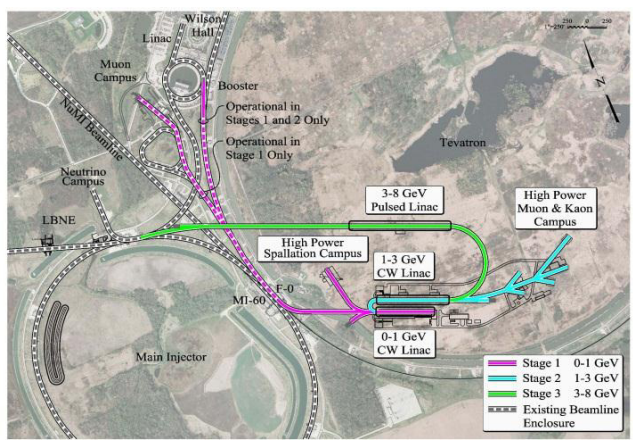


Figure 1: Project X Reference Design Stages.

Stage 1 is based on the 1-GeV CW linac. The 1-mA beam can be directed either to the existing 8-GeV Booster, the Muon Campus (currently under construction), or to a newly constructed High Power Spallation Campus. Stage 1 retires the existing 400-MeV linac and raises the Booster injection energy to 1 GeV,

* Work supported by the Fermi Research Alliance under U.S. Department of Energy contract number DE-AC02-07CH11359

Copyright © 2013 CC-BY-3.0 and by the respective authors

ISBN 978-3-95450-138-0

STUDIES OF FAULT SCENARIOS IN SC CW PROJECT-X LINAC*

A. Saini†, J.-F. Ostiguy, N. Solyak, V. P. Yakovlev
Fermilab, Batavia, IL 60510 USA.

Abstract

The success of the Project-X accelerator facility crucially depends on reliable operation of the 1 GeV superconducting (SC) continuous wave (CW) linac at stage-I. Operation at high intensity in CW mode puts stringent tolerances on beamline elements. Any fault affecting nominal operation of an accelerating or transverse focusing element will result in beam mismatch in the downstream sections. This in turn leads to emittance growth, and ultimately triggers beam losses. A robust lattice design allowing local retuning can make the machine operable even in the event of a fault, limiting the need for long unscheduled downtime. This paper presents studies performed to understand the consequences of failure of various elements. The outcomes of local retuning for different fault scenarios at critical locations in the linac are discussed.

INTRODUCTION

Project-X is a proposed multi-megawatt (MW) accelerator facility to be built at Fermilab[1]. It is envisioned as a multiuser facility that would support a diversified experimental program at the intensity frontier. In the current economic environment, funding profile limitations led to development of a staging strategy. The facility would be built in three stages. The first stage involves construction of 1 mA (average current), 1 GeV SC CW linac. The second stage would double the average current through stage I. Half of the beam would then be further accelerated in a 1-3 GeV SC CW linac. The final and third stage involves construction of 3-8 GeV SC pulsed linac. A detailed description of staging approach is presented elsewhere[2]. A schematic of the CW linac baseline configuration is shown in Fig. 1. It comprises a room temperature front end and a SC linac. The front-end includes an ion source, a low energy beam transport (LEBT) section, an RFQ and a medium energy beam transport (MEBT) section. The DC ion source delivers a nominal current of 5 mA at 30 keV. The beam is transported through the LEBT and matched to the RFQ. The RFQ operates at room temperature at a frequency of 162.5 MHz and accelerates the beam up to 2.1 MeV. The beam then enters the MEBT where it gets chopped to acquire the time structure required to drive different simultaneous experiments. Following the MEBT is a SC CW linac segmented into five sections. The first section is based on 162.5 MHz Half Wave Resonators (HWR) and accelerate the beam to $\sim$ 9 MeV. The next two sections use two types of 325 MHz Single Spoke Resonators (SSR) i.e. SSR1 and SSR2, to reach a kinetic energy of 156 MeV. The two final sections dubbed low beta (LB) and high beta are based on 5-cell, 650 MHz elliptical shaped cavities respectively designed for β_G = 0.61 and $\beta_G = 0.90$.

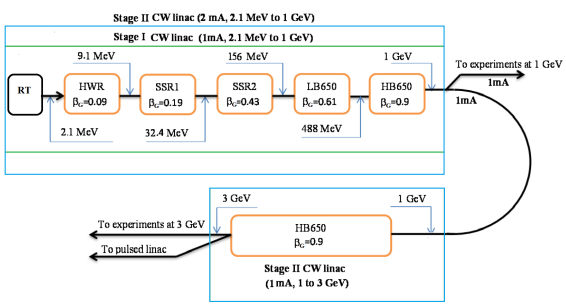


Figure 1: Acceleration scheme in Project-X CW linac.

GENERAL

Most of the complexity associated with a high intensity ion linac lays at low energy where dynamics is nonrelativistic and space charge effects are significant. The success of Project-X accelerator complex is therefore decisively dependent on reliable operation of the 1 GeV CW linac at stage-I. Failure of any element such as cavity, solenoid or quadrupole alters the focusing period of the beam, resulting in mismatch in the downstream sections. This, in turn, causes emittance growth and drives halo formation and beam losses. In some cases, the losses may be prevent safe operation. Unscheduled downtime is necessary to replace a faulty element and return to nominal operating conditions. Minimizing such unscheduled downtime is especially important in a multi-user facility where several experiments are running simultaneously. With that in mind, fault scenarios need to be accounted for in the optics design. The design should robust enough to allow localized compensation of the perturbation caused by an RF cavity or magnet failure. This paper presents studies performed to analyze various fault scenarios at critical locations in 1 GeV SC CW linac at stage-I of Project-X. Failure mitigation using localized compensation is demonstrated.

LOCAL COMPENSATION METHOD

The local compensation method involves re-tuning of elements in the vicinity of a failed element to restore a smooth beam envelope along the linac. Specifically, the RF phase and field amplitude of cavities are varied to recover the nominal beam energy and the longitudinal profile while

* Work supported by US DOE under contract DE- AC02-76CH03000.
† asaini@fnal.gov

Copyright © 2013 CC-BY-3.0 and by the respective authors

DESIGN ISSUES OF HIGH INTENSITY SC CW ION LINAC FOR PROJECT-X FACILITY*

A. Saini†, N. Solyak, V. P. Yakovlev, Fermilab, Batavia, IL 60510 U.S.A.

Abstract

Project-X is a high intensity proton facility which is primarily based on superconducting (SC) continuous wave (CW) linac. One of the most challenging tasks of Project-X facility is to have robust design of SC CW linac which can provide high quality beam to several experiments and subsequent pulsed linac simultaneously. Among the various technical problems associated with the SC CW linac, halo formation, beam mismatch, uncontrolled emittance growth and beam losses are the most crucial as they can limit overall performance and reliability. Scope of this paper is to address these issues for reference design of Project-X SC CW linac.

INTRODUCTION

The application horizon of particle accelerators has been widening significantly in recent decades. Where large accelerators have traditionally been the tools of the trade for high-energy nuclear and particle physics, applications in the last decade have grown to include large-scale accelerators like synchrotron light sources and spallation neutron sources. Applications like generation of rare isotopes, transmutation of nuclear reactor waste, sub-critical nuclear power, tritium production, radiation damage studies, studies of rare processes and generation of neutrino beams etc. are the next area of investigation for accelerator scientific community all over the world. Such applications require high beam power in the range of few mega-watts (MW). One such high intensity proton beam facility is proposed at Fermilab, named as Project-X [1]. The success of Project-X facility is primarily dependent on reliable operation of 1 GeV CW linac at first stage which is capable of delivering 2 MW beam power. A detailed description of baseline design of the CW linac is presented elsewhere [2].

Design of the high beam power accelerators are based on stringent beam losses limit. High beam losses can result in severe problem in terms of radio-activations. The cumulative experience of high intensity operation with existing facilities such as LANSCE [3] is utilized to set threshold limit of beam losses. In order to ensure hand-on-maintenance in safe environment, beam losses must be limited to 1 W/m for beam energy at 1 GeV. This paper addresses main characteristics and crucial beam dynamics design issues for the high intensity ion linac in framework of 1 GeV SC CW linac for the Project-X facility.

* Work supported by US DOE under contract DE- AC02-76CH03000.
† asaini@fnal.gov

EMITTANCE GROWTH

A low beam emittance ensures good output beam quality. Thus, minimal emittance growth along the linac is one of the primary objectives of optics design. The ion source determines initial transverse emittance of the beam which is transported to the RFQ through the low energy beam transport (LEBT) section. The magnets aberrations and non-linear space charge forces can result in a increase of transverse emittance in LEBT. It can be controlled, keeping beam size small and applying space charge neutralization. The longitudinal emittance is formed in the RFQ. A good beam matching at the upstream end of the RFQ minimizes transverse and longitudinal emittance growth along the RFQ. It is followed by the medium energy beam transport (MEBT) section which is comprised of bunching cavities and focusing magnets. Following is a SC CW linac. A robust design is capable to conserve emittance along the linac. It can be achieved using short regular focusing periods especially at low energy part of the linac. It results in smooth and linear changes in phase advance per meter (k). However, zero current phase advance in a focusing period should be kept below 90^0 to avoid envelope instability [4]. In order to avoid parametric resonance, focusing in linac is chosen such that $k_l \neq 2k_t$. Where k_l, k_t are wave numbers of the longitudinal and transverse oscillations respectively. Furthermore, non-linear space charge forces can result in excitation of coupling resonances which causes coupling between longitudinal and transverse motion. It results in abrupt emittance transfer between the planes. Figure 1 shows emittance coupling between longitudinal and transverse plane in first few sections of one of the variants of Project-X CW linac. It can be noticed that longitudinal emittance ϵ_l reduces at the expense of transverse emittance ϵ_t. In order to mitigate free energy transfer from one

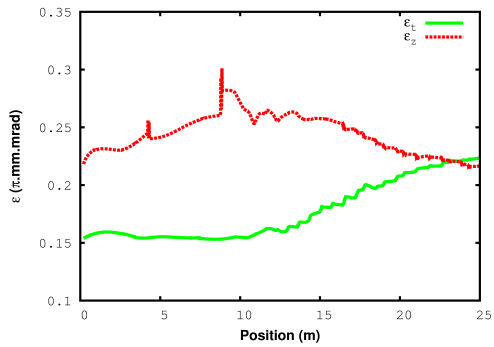


Figure 1: Emittance coupling between longitudinal and transverse plane.

Copyright © 2013 CC-BY-3.0 and by the respective authors

ISBN 978-3-95450-138-0

LAYOUT OF PROJECT-X FACILITY: A REFERENCE DESIGN*

A. Saini†, J.-P. Carneiro, D. Johnson, J.-F. Ostiguy, N. Solyak, V. P. Yakovlev
Fermilab, Batavia, IL 60510 USA.

Abstract

Project-X is a proposed high intensity proton facility to be built at Fermilab. It will be a multi-user facility which can support several experiments simultaneously. In the current scenario, the facility would be built in three stages. Each stage is associated with compelling scientific programs and is in synergy with existing Fermilab infrastructure. This paper presents the current reference design and discusses the main motivations and requirements driving the optics and physical layout.

INTRODUCTION

Project-X is a proposed high intensity proton facility to be built at Fermilab. Given the present economic environment, a staging strategy has been developed. The facility would be built in three stages. Each stage is associated with compelling scientific research programs and planned so that construction of each new stage has minimal influence on the operation of preceding ones. This approach has the benefit of limiting downtime during construction. A schematic of the Project-X facility is shown in Fig 1. A detailed description of the staging approach is presented elsewhere [1].

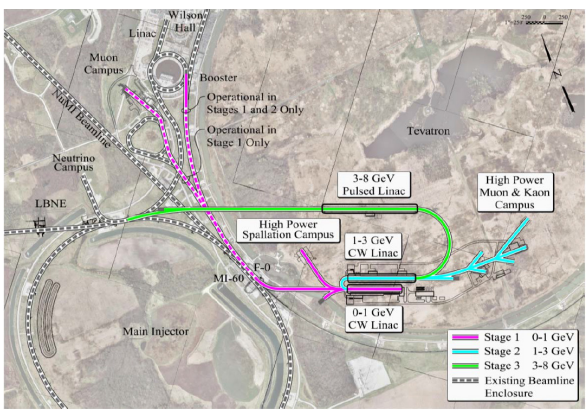


Figure 1: Layout of Project-X facility.

Success of the Project-X facility is critically dependent on the robustness of the superconducting (SC) continuous wave (CW) linear accelerator (Linac) design. While the reference design parameters [1] have been established, the optics is still evolving to incorporate technical constraints and to address issues that may potentially cause degradation of beam quality and particle losses. In this paper we describe recent changes in the beam optics.

* Work supported by US DOE under contract DE- AC02-76CH03000.
† asaini@fnal.gov

STAGE -I

The most challenging issues associated with Project-X facility would be addressed at Stage-1 which comprises a room temperature front-end followed by a 1 GeV SC CW linac delivering a 1 MW of beam power.

Ion Source, LEBT & RFQ

The front-end of Project-X consists of an ion source, a low energy beam transport (LEBT) section, an RFQ and a medium energy beam transport (MEBT) section. The ion source [2] operating in dc mode is capable of delivering a beam of H^- ion at 30 keV at maximum current of 10 mA. It is followed by the LEBT which includes three solenoids, a slow switching dipole magnet, a chopper assembly and diagnostic devices to characterize the beam. The chopper consists of a kicker and a beam absorber. It will primarily be used to produce variable low duty pulses during commissioning; it can also serve as pre-chopper to assist the MEBT high bandwidth chopping system. A detailed description of the LEBT layout and its component was presented elsewhere [1].

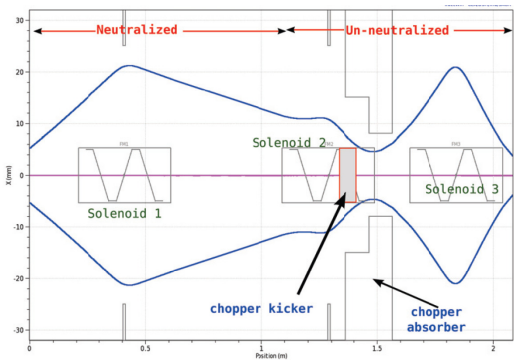


Figure 2: $3\sigma_{RMS}$ transverse beam envelope along LEBT (shown for fully neutralized operation).

A LEBT with solenoidal focusing usually requires neutralization to mitigate strong space charge defocusing. However, chopping of a neutralized beam can be problematic because the typical neutralization time is a few tens of micro-seconds, resulting in a time dependent optical perturbation. The Project-X LEBT design attempts to address this issue by incorporating two regions: (i) a fully neutralized region which extends from exit of the ion source to upstream edge of the second solenoid and (ii) an un-neutralized region from that point to the RFQ entrance port. Alternatively, the LEBT can also be operated in fully neutralized regime. Figure 2 shows a $3\sigma_{RMS}$ transverse beam envelope for fully neutralized operation. To

Copyright © 2013 CC-BY-3.0 and by the respective authors

STATUS OF THE LANSCE FRONT END UPGRADE*

R. W. Garnett#, Y. K. Batygin, I. N. Draganic, C. M. Fortgang, S. S. Kurennoy, R. C. McCrady, J. F. O'Hara, E. R. Olivas, R. J. Roybal, and L. J. Rybarcyk, LANL, Los Alamos, NM 87544, U.S.A., A. Schempp, IAP, Goethe University, Frankfurt am Main, Germany, J. Haeuser, Kress GmbH, Biebergemuend, Germany

Abstract

Initial acceleration of the beams in the LANSCE linear accelerator at Los Alamos National Laboratory is still presently accomplished through the use of two 750-keV Cockcroft-Walton (CW) based injectors. To reduce long-term operational risks and to realize future beam performance goals, plans are underway to replace the existing H^+ CW injector with a modern replacement, 4-rod Radio-Frequency Quadrupole (RFQ) based front end. Significant technical progress has been made since we last reported on this project. Status and progress of the design and fabrication of the RFQ, the RF system, beam transports, and integrated accelerator test stand will be discussed.

INTRODUCTION

The Los Alamos Neutron Science Center (LANSCE) currently supports a broad user base including the neutron scattering community, isotope production, basic science, and national security programs by providing multiple beams to several diverse experimental areas. The LANSCE linac accelerates negative hydrogen ions (H^-) and protons (H^+) simultaneously. An 800-MeV H^- beam is delivered at 20 Hz to the proton storage ring/moderated neutron production target for a suite of neutron-scattering instruments (Lujan Center), at 40 Hz to an un-moderated spallation target for nuclear physics cross-section measurements and microchip irradiations for industry (WNR), and on-demand at ~1 Hz for proton radiography (pRad), and at 20 Hz for ultra-cold neutron production (UCN). Protons are used for isotope production (IPF) at 100 MeV. High-power operation (10% total RF duty factor; 100 Hz x 625 μs; 16.5-mA peak proton beam current) has provided 800-kW average beam power at 800-MeV but was halted in 1998 after shut-down of the nuclear physics mission that supported high-power beam operations. Upgrades currently underway will restore full 120-Hz operations and allow high-power operation in support of planned new missions [1] that will require MW-level average beam powers.

Beams are delivered to the LANSCE experimental areas on a pulse-by-pulse basis, initially accelerated in two CW-based injectors, for H^+ and H^- beams, respectively. At present, LANSCE delivers up to three different H^- beams based on user requirements. The highest average-current H^- beam (100-125 μA) is first accumulated in the proton storage ring (PSR) and then extracted to the moderated neutron spallation target at the Lujan Center. This beam is chopped to provide an extraction gap in the PSR circulating bunch. By comparison, the WNR facility typically requires a single linac micropulse every few microseconds within the standard 625-μs macropulse. Producing the widely-spaced single micropulses requires the use of a chopper and low-frequency buncher in the H^- injector. These micropulses typically contain about 2.5 times more charge than the standard H^- linac microbunch. The other two H^- beam users, pRad and UCN, have beam requirements that require chopped and pre-bunched beams somewhat similar to the Lujan beam. The present dual-beam CW-based injector scheme for the LANSCE linac is shown in Fig. 1. The two beam species are merged into a common beam transport line and bunched before injection into the drift-tube linac (DTL) with a capture efficiency of approximately 80%.

Typical parameters for the 60-Hz (present maximum beam repetition rate) H^- beams are given in Table 1. Comparing chopping requirements against duty factor for these three beams, two categories emerge: low-duty factor beams with modest chopping requirements (Lujan, pRad) and a high-duty factor beam with demanding chopping requirements (WNR). H^+ beam parameters are also shown in Table 1. Future 120-Hz, H^+ beam requirements are shown in Table 2. An average H^+ beam power of 25 kW (250 μA) is required to be delivered to IPF at 100 MeV. An additional average beam power of 0.75 MW at 800 MeV is expected to be available for other applications beginning in 2017. Several options for enhanced future high-power beam operations can be found in Ref. 2.

Assessment of failure modes of our CW injectors revealed the potential for significant disruption of the beam operations at LANSCE [3] either due to catastrophic failure of major components and/or unavailability of spare parts.

Our strategy to reduce operational risks associated with the current CW-based injector systems involves the eventual replacement of these systems with modern radio-frequency quadrupole (RFQ) based injectors. Reliability is expected to improve due to reduced overall complexity of the systems and by modernization. RFQ accelerators are employed worldwide and have demonstrated stable and reliable operation.

To meet the above requirements while maintaining all existing beam delivery capabilities, including the high duty factor and demanding chopping requirements for the WNR beam, we are considering a 3-RFQ upgrade [3] to the present injector system that would be implemented in a staged approach with development of the H^+ RFQ having highest priority due to its impact on our near-term

* Work supported by the United States Department of Energy, National Nuclear Security Agency, under contract DE-AC52-06NA25396
# rgarnett@lanl.gov

Copyright © 2013 CC-BY-3.0 and by the respective authors

ISBN 978-3-95450-138-0

EXPERIMENTAL RESULTS FROM A "DIAGNOSTIC" PULSE FOR SINGLE-PARTICLE-LIKE BEAM POSITION MEASUREMENTS DURING ACCUMULATION/PRODUCTION MODE IN THE LOS ALAMOS PROTON STORAGE RING*

J. Kolski†, E. Bjorklund, M. Hall, M. Martinez, and F. Shelley, LANL, Los Alamos, NM, USA

Abstract

Beam position monitors (BPMs) are the diagnostic most used in setting up and documenting the Los Alamos Proton Storage Ring (PSR). One-turn injection can be approximated as single-particle injection with initial betatron position and angle (x_0 and x'_0). The turn-by-turn beam position data from single-turn injection allows measurement of the betatron tune, closed orbit (CO), and injection offset (x_0 and x'_0 at the injection point). In accumulation mode, many turns are injected into the ring, the transverse phase space is quickly filled, and there is no coherent betatron motion. The injection offset, which determines the accumulated beam size and is very sensitive to steering upstream of the ring, is not measurable during accumulation. We review our approach for measuring the injection offset during accumulation, focus discussion on recent experimental results, and compare measurements of the betatron tune, CO, and injection offset in single-turn injection mode and in a "diagnostic pulse" mode.

MOTIVATION

The PSR BPMs[1] are bi-directional, stripline-type with electrode length ∼37 cm (a quarter 201.25 MHz wavelength). The 201.25 MHz longitudinal beam structure, to which the PSR BPMs are sensitive, is imposed during acceleration and decoheres after ∼30 turns in the PSR due to momentum spread and synchrotron motion.

Single-turn injection mode is used to document the PSR. We measure 30 turns of beam position data before the longitudinal beam structure decoheres, which is sufficient to fit the betatron tunes, CO, and injection offset.

Normally, the PSR operates in production mode, where ∼1800 turns are accumulated. With the filled phase space, there is no coherent betatron motion in production mode, so the betatron tunes and injection offset can not be measured, but does yield the CO.

Aside from beam energy, the CO and betatron tunes are independent of machine operation upstream of the ring. The injection offset is very sensitive to steering upstream of the PSR, and we cannot measure this important operational parameter in production mode.

We develop an operation mode we call LBEG+ that enables us to document the PSR by measuring the betatron tunes, CO, and injection offset without affecting delivery of production beam[2]. The scheme is to inject a single turn (diagnostic pulse) on the same machine cycle as the production mode ∼50 μs after the accumulated beam is extracted, see Fig. 1. The 50 μs between production beam and the diagnostic pulse allows the linac RF to recover from the beam-off transient, the injection bump magnets to set to zero, and for residual field in the PSR buncher to dissipate. The diagnostic pulse coasts in the PSR and is lost.

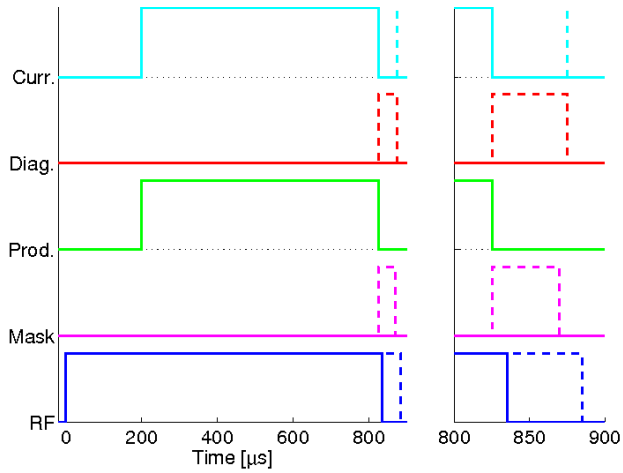


Figure 1: (Color) Timing scheme of one machine cycle for (from bottom to top) the linac RF gate (blue), RF system protect mask (magenta), production beam gate (green), diagnostic beam gate (red), and beam current in transport (cyan) for production (solid lines) and LBEG+ (dashed lines) modes. The right plot focuses on the end of the machine cycle.

LBEG+ AND SINGLE-SHOT MEASUREMENT COMPARISON

Operationally, the hope is for the LBEG+ scheme to replace the single-shot method for measurements of the CO, betatron tune, and injection offset during production. Thus, it is necessary for the CO, tune, and injection offset results measured via the LBEG+ scheme to be equal to the measurements taken in the single-shot scheme. We collected a set of BPM data in single-shot mode, and then collected another set of data in LBEG+ mode for comparison. In this section, we compare the LBEG+ and single-shot results for the CO, tune, and injection offset.

Thirty turns of betatron motion is digitized at each BPM.

* Work supported by in part by United States Department of Energy under contract DE-AC52-06NA25396. LA-UR 13-27450.

† Electronic address: jkolski@lanl.gov

Copyright © 2013 CC-BY-3.0 and by the respective authors

DESIGN ANALYSIS OF THE NEW LANL 4-ROD RFQ

S.S. Kurennoy, E.O. Olivas, and L.J. Rybarcyk, LANL, Los Alamos, NM 87545, USA

Abstract

An upgraded front end of the LANSCE linac will include a 4-rod RFQ replacing the aging Cockcroft-Walton injector, initially only for protons. We performed a detailed analysis of the proposed RFQ design using 3D modeling with the CST Studio Suite. The CAD-based RFQ model takes all design details into account. The electromagnetic analysis with MicroWave Studio (MWS) is followed by beam dynamics modeling with Particle Studio (PS) using the MWS-calculated fields. In addition, a thermal and stress analysis is performed with ANSYS, based on the power flux from MWS computations. Simulation results are used for design iterations aimed to satisfy special requirements imposed by an existing common transfer line for different beams injected into the 201.25-MHz drift-tube linac.

INTRODUCTION

LANL is moving forward with replacing the aging Cockcroft-Walton (C-W) injectors with an RFQ-based front end [1] for the LANSCE proton linac. A 4-rod type RFQ design was developed in collaboration between IAP (Frankfurt) and LANL. The LANL RFQ, operating at 201.25 MHz at the duty factor up to 15%, with 35-keV injection and 750-keV final energy, should satisfy special requirements due to its incorporation into the existing medium-energy beam transfer that works with multiple beams, see in [2]. The RFQ will be manufactured by Kress GmbH. We used the RFQ CAD files from Kress imported into CST Studio [3] to create a model of the LANL H^+ RFQ and evaluate its performance.

RFQ MODEL

The imported CAD model was simplified by removing details nonessential for EM analysis such as external supports, etc. The RFQ cavity walls were also removed, leaving only the resonator vacuum volume in the CST model. The resulting model is shown in Fig. 1. Here the RFQ vacuum vessel, in light-blue, is 175-cm long (wall-to-wall), 34-cm wide, and 30-cm high (along the stem direction, z). It also includes wide recesses on the thick end and front walls, of radius 8.5 cm and depth 1.5 cm, followed by 5-cm-long beam pipes of radius 2 cm. The RFQ vanes are supported by 24 stems that are spaced longitudinally with variable period, 75 mm in the center and 69.5 mm for three periods near each end. The tuners electrically short two adjacent stems and can be moved along them (in z direction) to adjust the mode frequency and voltage profile (flatness) along the structure length. The variable stem spacing simplifies tuning the voltage flatness along the structure. Our RFQ model uses the CAD model coordinates: x is along the RFQ axis, and the beam is moving in $-x$ direction (right to left in Fig. 1).

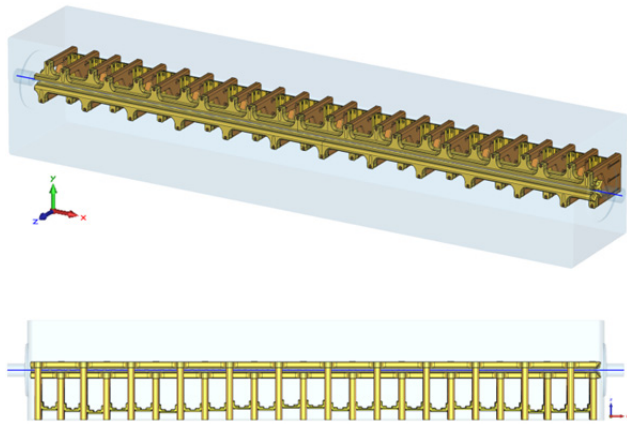


Figure 1: RFQ model (top) and its side view (bottom).

One can see in Fig. 1 (bottom) that the tuners are at different heights: they are adjusted to make the inter-vane voltage flat within ±1%. However, even with all tuners at the same height, the voltage is flat within ±5%, due to the variable stem spacing.

ELECTROMAGNETIC ANALYSIS

We studied the RFQ model using the CST MicroWave Studio (MWS). The mode frequencies and RF fields are calculated by the AKS eigensolver that provides more accurate surface approximations. The RF fields have some interesting features resembling those found in the FNAL 4-rod RFQ, see in [4, 5].

The first is the presence of a small transverse horizontal (parallel to the ground plane) electrical-field component, E_y, on the RFQ geometrical axis, sometimes referred to as a "dipole" component. This is due to the transverse electric fields being stronger between two upper vanes than between two lower ones, which results in the center of the transverse quadrupole field displaced down, to the ground plane, from the geometrical axis by 0.45 mm. The shift is small but not negligible when compared to the 4-mm vane aperture. This effect is known in 4-rod RFQs designed for higher frequencies [6]. The electric-field components on axis: longitudinal E_l, horizontal E_y, and vertical (along the stems) E_z are plotted in Fig. 2 versus the longitudinal coordinate $s = -x$. The fields are scaled to the nominal inter-vane voltage V_0=50 kV. In a similar plot along the axis shifted by -0.45 mm in z, the horizontal component E_y is close to zero, while the other two do not change much compared to Fig. 2.

Another important feature is the longitudinal electric field in the end gaps that separate the vane ends from the RFQ box walls (end-gap bumps). The red curve E_l in Fig. 2 shows the RFQ accelerating field – the oscillating part – produced by the vane modulation. The curve also has two peaks, near the entrance and exit.

Copyright © 2013 CC-BY-3.0 and by the respective authors

ISBN 978-3-95450-138-0

DESIGN REQUIREMENTS AND EXPECTED PERFORMANCE OF THE NEW LANSCE H^+ RFQ*

L.J. Rybarcyk#, Y.K. Batygin, I.H. Draganic, C. M. Fortgang, R.W. Garnett, S.S. Kurennoy, R.C. McCrady, and T.P. Wangler, Los Alamos National Laboratory, Los Alamos, NM 87545, U.S.A
A. Schempp, IAP, Goethe University, Frankfurt am Main, Germany
J. Haeuser, Kress GmbH, Biebergemuend, Germany

Abstract

LANSCE provides H^- and H^+ beams to several user facilities for fundamental and applied research, including a 100-MeV, 250-μA proton beam to the Isotope Production facility (IPF). Each beam species is initially accelerated to 750 keV in separate Cockcroft-Walton (C-W) accelerators. Due to the age and possible failure modes of the C-W's and the potential impact of a C-W failure to the IPF program, we have begun the process of replacing the aging H^+ C-W with a modern Radio Frequency Quadrupole (RFQ) accelerator-based system. In addition, the complexity of combined species operations imposes further restrictions on the beam performance and configuration that must be incorporated into the design process. This paper will cover the physics design requirements of this new RFQ and the expected performance based upon the results of PARMTEQM simulations.

INTRODUCTION

The Los Alamos Neutron Science Center (LANSCE) facility has a diverse user program that is possible in part because of the dual species operation, i.e. acceleration of both H^+ and H^- beams. IPF is one of those facilities and receives 100-MeV beam generated by our H^+ injector. IPF is one of only a few installations that produce a key radioisotope for medical procedures used across the nation and so high beam availability and reliability is critical to meeting their programmatic milestones. The H^+ injector utilizes an ~40 year old 750-keV C-W accelerator. The C-W has possible failure modes that include a failure of the accelerator column, which has already been replaced once and required 4 months to complete, and the collapse of a support leg that could lead to a catastrophic failure of the C-W. Concern over the potential likelihood of these types of failures and the severe impact to the IPF program has provided the impetus to pursue an RFQ-based replacement for the H^+ injector.

The RFQ is being designed and verified as a joint effort between the Institute of Applied Physics (IAP), Goethe University, Frankfurt, Germany and Los Alamos. The IAP team used a combination of PARMTEQM [1] and proprietary algorithms to develop the physics design for the 4-rod RFQ, which the Los Alamos team verified using PARMTEQM. Our project partner Kress GmbH, with input from IAP, is responsible for the engineering design and fabrication of the RFQ.

*Work supported by US DOE under contract DE-AC52-06NA25396.
#lrybarcyk@lanl.gov

REQUIREMENTS

The new H^+ RFQ will need to provide sufficient beam current to meet present and anticipated future programmatic needs and do so within the context of dual species operation. This includes the capability to operate the RFQ for a range of input beam currents depending upon the requirements of the user programs and the available beam duty factor. The LANSCE dual injector beam line layout that maintains the existing H^- and common LEBTs requires the new RFQ to be located several meters upstream from the entrance to the next accelerating structure, i.e. the 100-MeV drift tube linac (DTL). This places additional constraints on the transverse and longitudinal emittances so that the beam can be transported and properly matched without significant losses. A list of the RFQ requirements and expected performance based upon PARMTEQM simulation results for the IAP-developed physics design are given in Table 1. The frequency and output energy were chosen to be consistent with our present linac base

Table 1: Comparison of the Final, 201.25-MHz 4-rod RFQ Design Parameters with the Design Specifications

Parameter	Specification	Final Design
Injection Energy	35 keV	35 keV
Final Energy	750 keV	750 keV
Transmission	≥ 90%	96%
Peak Current	35 mA	35 mA
Current Limit	≥ 70 mA	60 mA
Output Energy Spread (FWHM)	< 3.0%	2%
Length	< 2.5 m	1.75 m
Peak Electric Field (E_K)	1.7	1.6
Input Trans. Emittance rms (cm-mr, norm.)	0.020	0.020
Exit Trans. Emittance rms (cm-mr, norm.)	0.023	0.022
Exit Long. Emittance rms (deg-MeV @201.25 MHz)	< 0.08	0.071

Copyright © 2013 CC-BY-3.0 and by the respective authors

GPU ACCELERATED ONLINE MULTI-PARTICLE BEAM DYNAMICS SIMULATOR FOR THE LANSCE LINAC*

X. Pang†, L. Rybarcyk, S. A. Baily, Los Alamos National Laboratory, Los Alamos, NM, 87544, USA

Abstract

A GPU-accelerated online multi-particle beam dynamics simulator is being developed for use in the LANSCE linac operation. The goal is to provide new insights on the beam distribution inside the linac and to help understand the impact of set point adjustments on it. Details regarding the code structure design, GPU programming and performance, code validation and status will be presented.

INTRODUCTION

The Los Alamos Neutron Science Center (LANSCE) linac can provide H^+ and H^- beam up to 800 MeV. Due to a lack of direct beam measurements during high power operation, small adjustments to linac operating set points are made primarily on the basis of beam loss along the linac. To provide more insight on the beam distributions along the linac and to better understand the effects of machine parameter changes on the beam, we are creating a virtual beam diagnostic tool for use in the LANSCE control room [1]. This tool is a Graphics Processing Unit (GPU)-accelerated multi-particle simulator whose beam dynamics algorithms are based upon the ion linac design and simulation code PARMILA [2]. PARMILA is a z-code which uses the R matrices to transfer particles through accelerator elements. The simulator is designed using modern software design techniques and coded in C++ and Python. Using NVIDIAs CUDA technology [3], the algorithms are recast to fully harvest the computing power of a GPU. Once connected to the EPICS control system, the simulator can track the real time machine parameter changes, convert control set points to model quantities and quickly update the simulation.

CODE STRUCTURE

Since the simulator is developed for use in the control room, fast execution and ease of use are both important design criteria. To meet these criteria, a combination of a high-level scripting language, i.e. Python, and a low level compiled language, i.e. C++, were adopted. Figure 1 shows the hierarchy of code layers that allows the user to take advantage of the fast number-crunching kernels written in C++ and CUDA C without having to deal with the complex syntax and the lengthy compilation process that is associated with them. The outermost shell of the code structure that a user directly interfaces with is written in Python. Python is chosen as the high-level scripting language because of its shallow learning curve, pseudo code like syntax, lack of compilation phase, easy integration with the compiled languages and the rich numerical and visualization libraries. Figure 2 shows the major components of the core part of the code that is written in C++ and CUDA C. Following the CUDA convention [3], we refer to the CPU as the host and the GPU as the device in the rest of this paper. The components colored in blue (left) are the ones that reside on the host while those colored in yellow (right) reside on the device. The *BeamLine* component (middle) resides in pinned, or page-locked memory on the host and the information stored is shared between the host and device and denoted by the green block. Each major component is described in detail as follows:

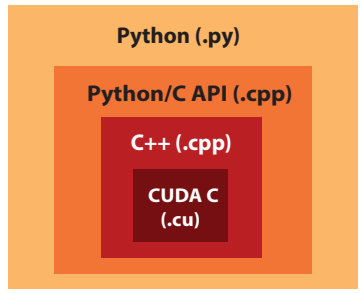


Figure 1: Code hierarchy. Lower level codes are wrapped by the higher level ones.

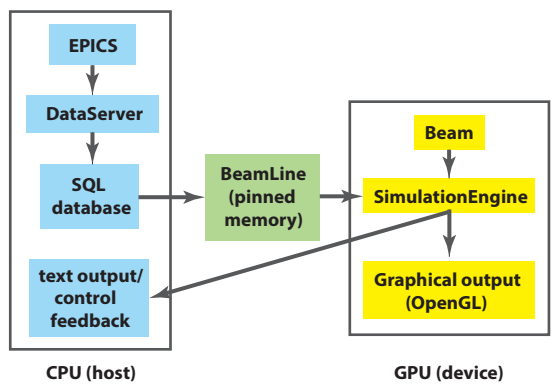


Figure 2: High level code structure and data flow indicated by the arrows.

The *DataServer* reads values from EPICS in multi-threaded fashion and stores the updated values to the SQL database.

The *SQL database* stores all the measured engineering values coming in from the *DataServer*, the conversion algorithms for every controllable accelerator element, and most importantly the converted physics quantities that are

* Work supported by U.S. DOE, NNSA under contract DE-AC52-06NA25396.

† xpang@lanl.gov

Copyright © 2013 CC-BY-3.0 and by the respective authors

ISBN 978-3-95450-138-0

PHASE STABILITY OF THE RF REFERENCE LINE FOR THE FRIB LINAC*

Q. Zhao#, J. Brandon, D. Morris, Y. Yamazaki, MSU, East Lansing, MI 48824, USA

Abstract

The phase stability of rf reference line is usually quite restricted in a high energy linac (very long linac, very high frequency). Due to the change of the ambience temperature in the linac tunnel, the electrical length of reference rf cables may change significantly, which results in unacceptable phase changes in cavities. So, sometimes the reference line is very expensive, for example, made of optical fiber housed in a lengthy thermostatic chamber. The frequencies of FRIB linac cavities are 80.5 and 322 MHz (not very high). We also take advantage of the double-folded linac geometry and feed the reference line in the center of the linac to effectively reduced the reference line by 6 times. Our studies show that the FRIB linac can tolerate up to 12ps phase stability of the rf reference line. Therefore, no is needed for the reference line.

INTRODUCTION

The Facility for Rare Isotope Beams (FRIB) [1], currently under establishment at the Michigan State University, will be a new national user facility for nuclear science. FRIB accelerator is a cw, high power, heavy-ion machine that will accelerate all stable isotopes to energies ≥ 200 MeV/u with a beam power of up to 400 kW. The driver linac consists of a front-end to generate ion beams and boost beam energy, a superconducting linac that is folded into three parallel segments and connected by a stripper station and two 180-degree bending sections, and a beam delivery system to transport output beam into the fragmentation target, as shown in Figure 1. The length of linac footprint is about 150m. Linac Segment 1 consists of 3 β=0.041 cryomodules and 11 β=0.085 cryomodules to increase the beam up to 20 MeV/u followed by a charge stripping system. All the cavities in Segment 1 are Quarter-wave Resonators (QWRs) with operating frequency of 80.5MHz. Half-wave Resonators (HWRs) with higher operating frequency of 322MHz are used for both Segment 2 and Segment 3. There are 12 β=0.29 cryomodules and 12 β=0.54 cryomodules in linac Segment 2 to accelerate beam energies ≥ 150 MeV/u. Additional 6 β=0.54 cryomodules in linac Segment 3 further push beam energies above 200 MeV/u, followed by a FODO quadruple lattice section that is reserved to place more cryomodules for future energy upgrade.

As a new generation national scientific user facility, the performance of FRIB has quite stringent requirements. Therefore, each system and its subassemblies become critical for the operation of such a complex machine. The rf field generated by cavities is one of the key factors that determine the beam performance of the linac. It is a challenging task to achieve good phase and amplitude regulation of the cavities in a large system. There are several types of errors or uncertainties related to the rf field of the cavities in linacs like the FRIB driver linac. For examples, (1) the random rf phase and amplitude fluctuation or jitter that changes very fast and dynamically and is regulated by low level rf controller, (2) misalignment of field axis with respect to the beam axis that is static and may be measureable thus be corrected or compensated, (3) deviation of amplitude settings with respect to the design that is static and determined mainly by calibration, (4) deviation of phase settings with respect to the design that is also static and usually more sensitive than that of field amplitude especially at low energy side, (5) phase change due to the variation of the electrical length of rf cable that is mainly due to thermal effect and thus a slow drift process. Therefore, each of them needs to be evaluated and controlled to meet requirements. In this paper, we discuss exclusively on the topic of the phase drift of the rf reference line for the FRIB linac.

CAVITY PHASE SETTINGS

There are total 330 cavities (including the rebuncher cryomodules between each segment) distributed in the three linac segments of the double-folded FRIB driver linac. All of the cavities (either QWRs or HWRs) have

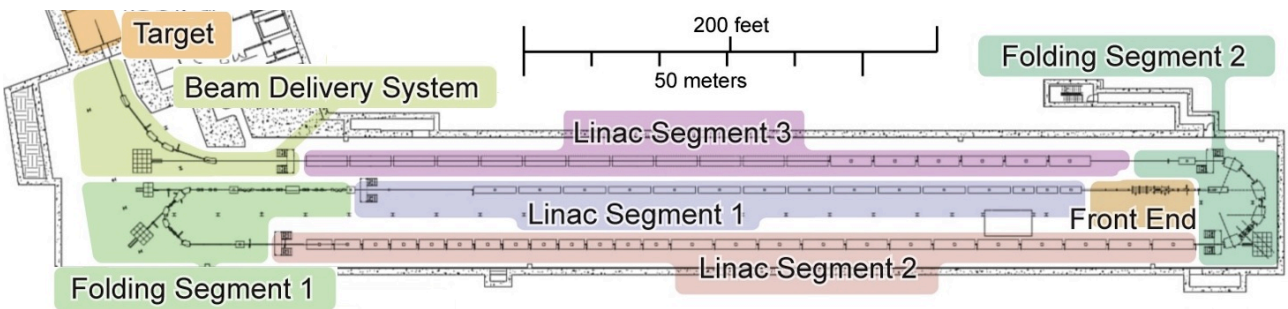


Figure 1: Layout of the FRIB driver linac.

* Work supported by the U.S. Department of Energy Office of Science under Cooperative Agreement DE-SC0000661
# zhao@frib.msu.edu

Copyright © 2013 CC-BY-3.0 and by the respective authors

AN OPTIMIZATION STUDY OF THE TARGET SUBSYSTEM FOR THE NEW G-2 EXPERIMENT*

C. Yoshikawa#, C. Ankenbrandt, Muons, Inc., Batavia, IL 60510, USA
A. Leveling, N.V. Mokhov, J. Morgan, D. Neuffer, S. Striganov, Fermilab, Batavia, IL 60510, USA

Abstract

A precision measurement of the muon anomalous magnetic moment, $a_\mu = (g-2)/2$, was previously performed at BNL with a result of 2.2 - 2.7 standard deviations above the Standard Model (SM) theoretical calculations. The same experimental apparatus is being planned to run in the new Muon Campus at Fermilab, where the muon beam is expected to have less pion contamination and the extended dataset may provide a possible 7.5σ deviation from the SM, creating a sensitive and complementary benchmark for proposed SM extensions. We report here on a study performed on the target subsystem utilizing a new optimization technique that overcomes complexities of asymmetric particle production and depth of focus of a Li lens. This new technique is applied to an apparatus that is optimized for pions that have favourable phase space to create polarized daughter muons around the magic momentum of 3.094 GeV/c, which is needed by the downstream g 2 muon ring.

INTRODUCTION

The New g-2 Experiment at Fermilab [1] aims to measure the muon anomalous magnetic moment to a precision of ±0.14 ppm — a fourfold improvement over the 0.54 ppm precision obtained in the g-2 BNL E821 experiment [2]. The present discrepancy, Δa_μ(Expt. — SM) = (255±80)×10^{-11}, is already suggestive of possible new physics contributions to the muon anomaly. Assuming that the current theory error of 49×10^{-11} is reduced to 30×10^{-11} on the time scale of the completion of our experiment, a future Δa_μ comparison would have a combined uncertainty of ≈ 34 × 10^{-11}, resulting in a 7.5σ deviation from the Standard Model, which will be a sensitive and complementary benchmark for proposed extensions to the Standard Model. Most of the improvement will be due to increased statistics and thus it is essential to maximize production of useful pions that create polarized muons which are in the acceptance of the g-2 muon storage ring. Furthermore, cost considerations favour a design that reuses the existing pbar production subsystem that worked well during the Tevatron operation. Hence, the pion production subsystem will begin with the pbar production subsystem scaled from 8 GeV (kinetic energy) protons to 3.1 GeV/c pions.

A preliminary study [3] revealed complexities in optimizing the target where there is interplay between the asymmetric pion production, the need to have the pions created near the target edges to minimize reabsorption, and the depth of focus of the Li lens. An optimization procedure was proposed in that early study to overcome those complications and its application and result is the focus of the study reported here.

THE LAYOUT

A graphical representation of the Fermilab pbar production target subsystem is shown in Figure 1 as implemented in Ref. [4] in the MARS15 code [5]. The proton beam with kinetic energy of 8 GeV impinges on the default target, which was previously used to create pbars. We considered two spot sizes for the proton. One is what we expect from a simple scaling from 120 GeV operation to 8 GeV. The other is the smallest we believe that can be achieved. Spot size information on both is provided in Table 1. The default pbar production target is a vertical cylinder (in-out of top view in Figure 1) composed primarily of inconel with a chord for the proton beam of ~7.5 cm. Pions produced in the target will be focused by the Li lens (yellow) that is 15 cm long, 1 cm in radius, and has a magnetic field gradient of 256.25 T/m, where the gradient has been scaled for 3.1 GeV/c pions to maintain proper focusing, while keeping the same focusing distance between centers of the target and Li lens of 25.16 cm. The focused pion beam is then collimated and bent through a pulsed magnet (PMAG) with a dipole field of 0.542219 T, also scaled for the 3.1 GeV/c pion beam, and bends the reference by 3 degrees to provide momentum selection.

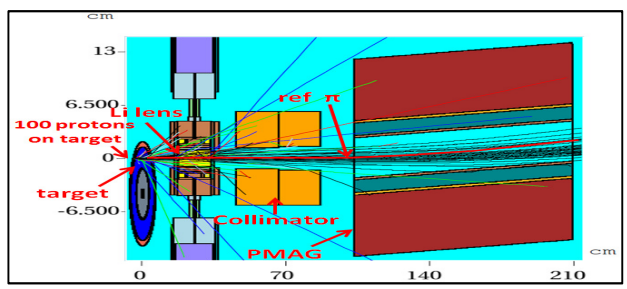


Figure 1: Zoomed in top view of pbar target subsystem.

Table 1: Proton Beam Spot Sizes

Proton spot size description	σ_x (mm)	σ_y (mm)	$\sigma_{x'}$ (mrad)	$\sigma_{y'}$ (mrad)
Default	0.55	1.1066	0.38	0.38
Small	0.15	0.15	0.6366	0.6366

A transition in our simulation between MARS that provides reliable particle generation and G4beamline [6] that is used for particle tracking, pion decay into muons, and effect of beam particles interacting with the beam line elements is shown in Figure 2. The MARS particle tracks that hit the virtual detector are converted and propagated in G4beamline through a set of four quads that refocuses

*Work supported by Fermi Research Alliance, LLC, under contract No. DE-AC02-07CH11359 with the U.S. Department of Energy
#cary.yoshikawa@muonsinc.com

ISBN 978-3-95450-138-0

Copyright © 2013 CC-BY-3.0 and by the respective authors

HIGH VOLTAGE STABILIZATION SYSTEM OF CARIBU/ECR FOR ATLAS

Yong Luo, Sergey Sharamentov, Richard Pardo, Rick Vondrasek, Guy Savard
ANL, Argonne, IL 60439, USA

Abstract

With the increased radioactive beam capabilities brought by new CARIBU (Californium Rare Isotope Breeder Upgrade) in ATLAS facility, highest charge breeder efficiency of ECR is desired. Experimental study shows that the best efficiency could be achieved when high voltages (up to 50 kV) of two platforms (CARIBU and ECR) are only different within less than 1V [1]. We have developed a system with some innovative ideas implemented to measure the required tiny voltage difference ratio (~0.002%) precisely and to protect the system too. High voltage (HV) filter is designed to protect it from severe HV sparks and multiple level of relays with high precision medium HV divider are used to protect it from possible power supply failure. Homemade HV divider is used for rough measurement and control. Measurement results are converted to optical signals and then used to control power supplies to achieve the desired platform voltages. The system has been partially tested and will be used in the future.

INTRODUCTION

When developing such a system with very high sensitivity and accuracy as mentioned above, at first we need to consider how to prevent damage from HV shock and power supply failure. We also need to think about how to measure the voltage difference precisely.

In ATLAS facility, both CARIBU and ECR1 are on a common HV platform of 350 kV. Then the 50 kV bias is applied to them on top of the 350 kV with separate power supplies. There are numerous instruments which are biased with different HV or high current power supplies on both platforms. Occasionally, HV sparks may occur. Those HV sparks are fatal to electronic measurement systems if they are not protected. Possible power supply failure is another threat we need to deal with. We cannot eliminate power supply failure, but we can protect the system with an appropriate design.

Using high voltage divider to measure the voltage difference is a simple and tempting idea. But careful study indicates that this approach has un-surmountable problem. Due to variation in resistor resistance caused by temperature and voltage bias variation, typical HV divider may only provide about 1% accuracy. Even for very expensive custom made high voltage divider with 0.1% tolerance, it still cannot provide the accuracy we need here. The high common mode noise also introduces more measurement error.

SOLUTION

Multiple levels of filter circuit are used to protect the system from HV, high current sparks in electrometer [2]. This kind of sixth-order low pass filter can achieve high-frequency attenuation exceeding 10^{+5}. So we adopted this approach for our HV spark protection.

Multiple levels of relay can be used to protect the system from power supply (PS) failure. Details will be explained in design and test section. Relays are turned off when PS fails. Homemade HV divider is used for coarse control and monitoring.

CARIBU side high voltage is used as floating GND for our measurement system. So when the tow platform HVs are very close, accurate measurement can be achieved without introducing big noise.

SIMULATION

Spice simulation is performed on a simplified low pass filter as shown in Fig. 1. In this simulation, a hypothetical high voltage spark source (I1, 20 kA, ~1ns rise time) shown in Fig. 1 is used.

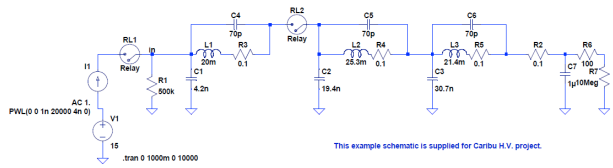


Figure 1: A simplified low pass filter with two relays.

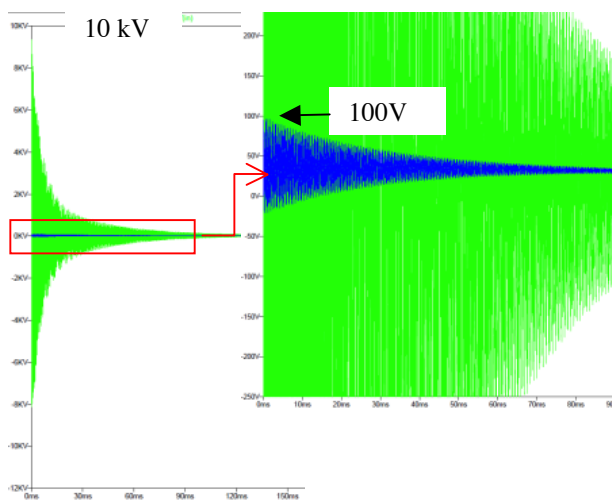


Figure 2: Simulation results of the filter shows the attenuation of HV shock

Copyright © 2013 CC-BY-3.0 and by the respective authors

DESIGN AND SIMULATION OF THE ARGONNE INFLIGHT RADIOACTIVE ION SEPARATOR (AIRIS)*

B. Mustapha#, M. Alcorta, B.B. Back and P.N. Ostroumov
Physics Division, ANL, Argonne, IL 60439, USA

Abstract

A new inflight radioactive ion separator (AIRIS) is being designed for the ATLAS facility at Argonne. AIRIS will be used to separate and produce secondary radioactive beams from the interaction of ATLAS primary beams in a production target. AIRIS will be at least 10 times more efficient than the existing radioactive beam capability. We have made significant progress in the design and simulations of AIRIS including full 3D models of all the elements to consider their real dimensions and produce realistic 3D fields. The resolving power of the device has been studied for several reaction cases using realistic cross sections and kinematics. In addition to the magnetic separation of the device, an RF sweeper is being designed to take advantage of the time separation of the different beams and reject the primary beam tail and other potential contaminants in order to produce higher purity secondary beams. The latest AIRIS design and simulation results will be presented and discussed.

AIRIS AT ATLAS

The Argonne Tandem Linac Accelerator System is undergoing an efficiency and intensity upgrade [1]. Most of the stable beams will have their intensities increased by one to two orders of magnitude. To take advantage of this intensity upgrade and enhance the radioactive beam capabilities at ATLAS, a new inflight radioactive beam production and separation system is being proposed. The new system will consist of a production target placed at the end of ATLAS followed by an ion separator called AIRIS. Figure 1 shows the location of AIRIS downstream of ATLAS and upstream of any experimental area. The main constraint on the AIRIS design is to preserve stable beam operations by moving the target out and using AIRIS as a transport line. For this purpose, AIRIS should have the same beam axis as ATLAS and the existing beamline. A broadband design has been proposed and developed for AIRIS [2]. It consists of four dipoles and four multipoles (quadrupoles) as shown in Figure 1. The original design was developed and simulated using COSY [3]. In this work, we have performed detailed simulations and parameter feasibility studies using the code TRACK [4], which has led to the new design parameters listed in Table 1. The dimensions and spacing of the elements have changed but not the overall layout.

Table 1: AIRIS Design Parameters

Parameter	Value
Number of dipoles	4
Dipole bend angle, deg	22.5
Dipole radius, m	1
Dipole full gap, cm	10
Max. dipole field, T	1.75
Number of quadrupoles	4
Quadrupole length, cm	30
Quadrupole full aperture, cm	15
Max. quadrupole field, T	1.0
Shortest drift, cm	20
Total chicane length, m	7.1
Angular acceptance, mrad	50
Dispersion at mid-plane, mm/%	1.2

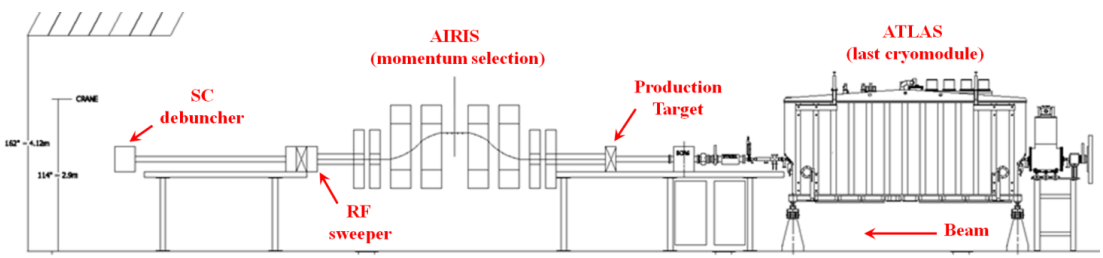


Figure 1: AIRIS, designed to be installed downstream of ATLAS and upstream of experimental areas for the production and separation of radioactive beams. An rf sweeper and a SC debuncher are included.

* This work was supported by the U.S. Department of Energy, Office of Nuclear Physics, under Contract DE-AC02-06CH11357.
# brahim@anl.gov

Copyright © 2013 CC-BY-3.0 and by the respective authors

ISBN 978-3-95450-138-0

DIAGNOSTICS FOR THE LANSCE RFQ FRONT-END TEST STAND*

R. C. McCrady#, Y. K. Batygin, I. N. Draganic, C. M. Fortgang, R. W. Garnett, S. S. Kurennoy, J. F. O'Hara, E. R. Olivas, R. J. Roybal, L. J. Rybarcyk, Los Alamos National Laboratory, Los Alamos, NM 87544, USA.

Abstract

Plans are underway at the Los Alamos Neutron Science Center (LANSCE) to replace the existing H^+ Cockcroft-Walton injector with a modern 4-rod Radio-Frequency Quadrupole (RFQ) based front end. This will provide protons for injection into the downstream linac, where H^- ions are also accelerated. This dual-species operation of the linac imposes constraints on the injectors, resulting in particular requirements on the transverse and longitudinal emittances and phase-space distributions of the beam from the RFQ proton injector. Good measurements of these quantities are therefore required during the testing phase of the RFQ injector. In this paper we describe the measurements to be made and plans for the systems for carrying out the measurements.

INTRODUCTION

The existing injectors at LANSCE for protons and H^- ions are based on Cockcroft-Walton (CW) generators and have been in use since the initial construction circa 1970. These CW-based injectors provide unbunched beams of protons and H^- ions at 750 keV with very little uncertainties in the beam energies. Precise matching of the beam energies is required for good dual-beam operation of the subsequent portions of the linac consisting of drift-tube linac (DTL) and coupled-cavity linac (CCL) sections. Additionally, the high average currents of the beams require good transverse matching from the injectors into the DTL to prevent large beam spill that results in high radiation fields.

An effort is underway to replace the proton injector with an RFQ-based system [1]. The initial phases of commissioning this system will involve operation in a test stand to characterize the system and to ensure that it operates as desired prior to installation in the production environment.

The present 750 keV beam-transport lines from the CW injectors to the DTL are rather long, at about 16m. The two beam species are merged in a 9° dipole magnet about 2.3 meters upstream of the DTL and pass through an RF buncher and a 4-quadrupole matching lens in the common section after the merging magnet. The 18° separation between the two beamlines upstream of the merging magnet limits the transverse space available for equipment in the two beamlines. For this reason, the RFQ must be placed rather far upstream of the DTL, about 4 meters. This distance, combined with the large energy spread of the beam produced by the RFQ, necessitates the use of 2 additional RF bunching cavities in the new proton transport line (shown in Fig. 1) in order to maintain a bunch length that will fit easily into the acceptance of the DTL. For this reason it is imperative that we measure the longitudinal bunch shape of the beam; ideally a full longitudinal phase-space distribution would be measured.

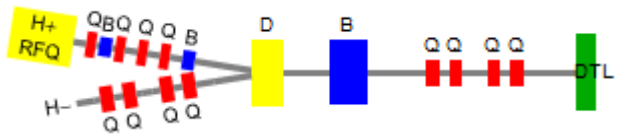


Figure 1: The proposed beam transport line from the proton (H^+) RFQ to the DTL. Also shown is a portion of the H^- transport line. Beamline elements are denoted by letters: Quadrupole magnets (Q), Dipole magnets (D) and Bunchers (B). Three of the bunchers are quarter-wave resonators, and one is a larger pillbox-style cavity.

The stringent requirements on the performance of the system drive the requirements for beam-measurement systems. In particular, we intend to measure beam current, transverse phase space, longitudinal bunch shape, and energy. The diagnostic systems for characterizing the beam produced by the new injector are described in the following sections.

TEST STAND

The RFQ-based proton injector will consist of a duoplasmatron proton source, a 35 kV accelerating column, a two-solenoid low-energy beam transport (LEBT), the RFQ, and a 750 keV medium-energy beam transport (MEBT) to the DTL.

We plan a phased approach to development of the RFQ test stand. The first phase will allow characterization of the LEBT that will transport the 35 keV beam from the source and extraction column to the entrance of the RFQ. The second phase will allow measurements of the beam delivered by the RFQ to assess its performance. The third phase will test the MEBT that will transport the beam from the RFQ to the DTL. Figure 2 shows the test stand phases and the associated beam measurements.

In the first phase, where the beam is not bunched, beam current and transverse emittance are of greatest importance. The beam energy is determined by the column voltage which can be measured precisely. The current and emittance provide input to models of the beam evolution in the LEBT. These models will be used in the process of transverse matching of the beam into the RFQ. We plan to have an emittance-measurement station near the middle of the LEBT; this apparatus will remain in place when the system transitions to the production

* Work supported by the United States Department of Energy, National Nuclear Security Agency, under contract DE-AC52-06NA25396
# mccrady@lanl.gov

Copyright © 2013 CC-BY-3.0 and by the respective authors

DESIGN AND COLD TEST OF A 17 GHz OVERMODED HYBRID PBG ACCELERATOR CAVITY*

JieXi Zhang†, Alan M. Cook, Brian J. Munroe, Michael A. Shapiro, Richard J. Temkin
MIT PSFC, Cambridge, MA 02139, USA

Abstract

An overmoded hybrid Photonic Band Gap (PBG) structure used as an accelerator cavity has been theoretically designed. The PBG structure consists of a triangular lattice of dielectric (sapphire) and metallic rods. The birefringence of the sapphire affects the PBG eigenmodes and must be taken into account. The PBG cavity formed by rods in between two copper plates will be operated in a TM_{02} mode at 17 GHz. Arrangement of the rods for higher-order-mode (HOM) damping demonstrates high frequency selectivity. Comparison with a disk-loaded waveguide (DLW) cavity gives a perspective of the dielectric PBG structure operated at an accelerating gradient of 100 MV/m. Cold test of a single hybrid PBG cell presents a high-Q resonance at 17 GHz. A standing-wave (SW) hybrid PBG structure will be tested in TM_{02} mode at 17 GHz.

INTRODUCTION

A periodic photonic structure, whose dispersion relation has photonic band gaps (PBG), can be applied to accelerators due to its good frequency selectivity [1]. A travelling-wave (TW) multi-cell metallic PBG structure has demonstrated successful acceleration of electrons with gradient of 35 MV/m [2]. More SW metallic PBG structures have been studied with high power breakdown tests at both SLAC and MIT [3, 4].

A theoretical study of a dielectric PBG structure was presented by Shapiro et al. [5]. A detailed design with isotropic sapphire rods using the commercially available code Ansys High Frequency Structure Simulator (HFSS) was reported in PAC11 [6]. The dielectric band gap allows a TM_{02}-mode operation without competing with the lower-frequency TM_{01} mode since the latter is not supported in the band gap. The TM_{02} mode helps in geometry design for a high frequency of 17 GHz and mitigates the central high field away from the innermost rods. Simulations showed an accelerating gradient of 100 MV/m with lower magnetic field than the metallic PBG structure, which may reduce the breakdown rate in high power testing. A sapphire rod structure was previously built and cold tested but not tested at high power [7].

In this paper, we analyze a sapphire PBG periodic unit cell with an anisotropic (birefringent) dielectric constant. 2D cross-section design in HFSS will give an optimal configuration of a hybrid PBG structure containing both dielectric rods and metallic rods. A single cell 3D structure has been theoretically designed and the cold test result will be presented.

ANISOTROPIC BAND GAP MAP

Sapphire is an optically anisotropic material with permittivity changing with the electromagnetic (EM) wave frequency [8]. At 17 GHz, with the orientation of the C-axis of the sapphire rods parallel to the particle beam axis in our design, the permittivity of the sapphire rod is $\epsilon_r = [9.398, 9.398, 11.587]$ by interpolation from [8].

Figure 1 shows the band gap map of a periodic sapphire lattice with the above anisotropic permittivity calculated in HFSS, as well as the comparison with an isotropic lattice of $\epsilon_r = 9.398$. The eigenmode frequency is normalized to $\omega b/2\pi c$ and the lattice is characterized by ratio $\frac{a}{b}$ with the rod radius a and the lattice spacing b. The lowest band gap can confine the TM_{02} mode while the TM_{01} mode is radiated out through the dielectric lattice.

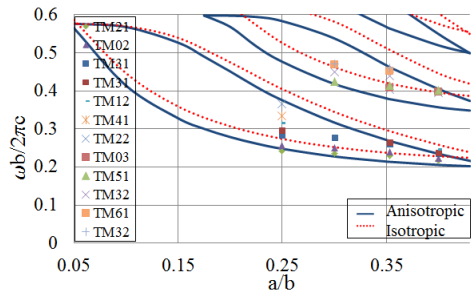


Figure 1: Band gap map of sapphire with isotropic and anisotropic permittivity.

In HFSS, to model a "2D structure", a very thin PBG layer is made with perfect E boundaries on top and bottom to limit the eigenmode solutions to TM modes. The calculated normalized frequencies of different modes in the 2D PBG structure are shown in Fig. 1; this helps to determine the design point $\frac{a}{b} \sim 0.35$, where the TM_{02} mode sits in the center of the band gap and few other modes are present in the same gap. The only HOM that is of concern is the TM_{31} mode. The final parameters of $a = 1.58$ mm and $b = 4.47$ mm have been chosen based on the 3D design shown later. Varying the arrangement of rods to achieve an improved Q of the TM_{02} mode and a reduced Q of the TM_{31} mode will be described in the following section.

CAVITY MODE IN 2D DESIGN

The birefringence of sapphire results in a discrepancy between the 2D and 3D simulations, but the study of the

* This work supported by Department of Energy High Energy Physics, Grant No. DE-SC0010075.
† zhangjx@mit.edu

Copyright © 2013 CC-BY-3.0 and by the respective authors

ISBN 978-3-95450-138-0

RESULTS FROM THE LINAC COMMISSIONING OF THE RARE ISOTOPE REACCELERATOR - ReA*

Walter Wittmer†, Daniel Alt, Thomas Baumann, Carla Benatti, Shannon Wayne Krause, Alain Lapierre, Daniela Leitner, Ling-Ying Lin, Fernando Montes, Samuel Nash, Randall Rencsok, Jose Alberto Rodriguez, Michael Syphers, Eugene Tanke, Xiaoyu Wu (NSCL, East Lansing, Michigan)

Abstract

ReA [1] is a radioactive ion beams post accelerator currently being completed at the National Superconducting Cyclotron Laboratory at Michigan State University. ReA is designed to reaccelerate rare isotopes to energies of a few MeV/u following production by projectile fragmentation and thermalization in a gas cell. The facility consists of five main components: an electron beam ion trap (EBIT) charge breeder, an achromatic charge over mass separator, a radiofrequency quadrupole (RFQ) accelerator, a superconducting radio frequency linear accelerator (SRF LINAC) and a transport line into the experimental hall. The first sections up to the SRF LINAC of ReA have been commissioned in the last two years using an offline stable ion beam source and heavy ion beams from the EBIT charge breeder. The final section, transporting beam from the LINAC into the experimental hall, was completed and commissioned this summer. This paper presents the results of the SRF cryo module characterization and the progress of the machine optics model.

INTRODUCTION

The Facility for Rare Isotope Beams (FRIB)[2], a 400kW superconducting heavy-ion driver LINAC, will produce beams of exotic nuclear species with increased intensity of up to three orders of magnitude more than the CCF after fast fragmentation. ReA will reaccelerate these beams with improved characteristics for experiments. Initially the energy of the Rare Isotope Beams (RIBs) will be 3 MeV/u with future upgrades reaching 12 MeV/u. Currently ReA is coupled to the Coupled Cyclotron Facility (CCF) at the National Superconducting Cyclotron Lab (NSCL) at Michigan State University and provides beam of up to 2.4 MeV/u.

Stable beams are accelerated to energies of approx. 100 MeV/u by the CCF and fragmented on a solid target. The secondary beam, comprised of a melange of fragments, is separated achromatically in the A1900 fragment separator. The selected isotope is then thermalized in a He gas cell and extracted at energies up to 60 keV. Following mass selection at a dipole magnet the beam is injected into the Electron Beam Ion Trap (EBIT) where it is charge bred. The beam is then extracted at 12keV/u (RFQ injection energy) and transported through a Q/A achromatic charge-over-mass separator for charge selection and accelerated in the LINAC. The initial acceleration occurs in a four rod RFQ to an energy of 600 keV/u. The beam is then rebunched in a rebunching module with a single quarter wave cavity ($\beta = 0.041$) followed by an accelerating module containing six cavities of the same type. Next, the beam is delivered into the experimental hall. The final accelerating cryo module, comprised of 8 quarter wave cavities ($\beta = 0.085$), is currently in construction and will complete the initial ReA3 installation next year.

The commissioning of the current installation of the reaccelerator has been successfully completed following a commissioning experiment where a ^{37}K ($T_{\frac{1}{2}} = 1.23$s) beam was delivered to the ANASEN [3] detector.

SRF LINAC

The first rebunching module comprises a single quarter wave cavity ($\beta = 0.041$) and two superconducting 9 Tesla solenoids with integrated steering magnets. The second accelerating module houses 6 cavities and 3 solenoids of the same type. Both modules are shown in Figure 1.

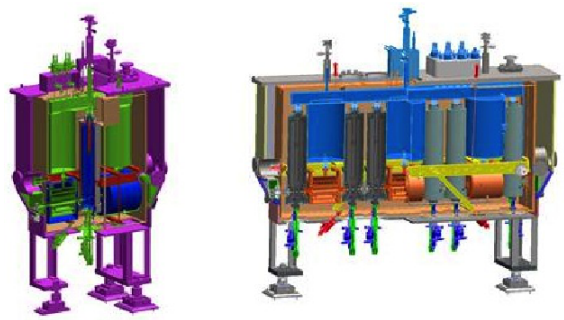


Figure 1: On the left the rebunching cryo module is shown with its cavity at the center between the solenoids. The right shows the first accelerating module with one cavity at each end and groups of two separated by the three solenoids.

Dipole Calibration and Energy Spread Measurement with CAESAR Detector

An experimental setup consisting of an Aluminum target inside the high-efficiency CsI(Na) scintillator array (CAESAR) [4] was used to obtain an energy calibration of a bend magnet, located after the second accelerating module, to measure the beam energy spread and to test the performance of the LINAC.

* Work supported by Michigan State University
† wittmer@nscl.msu.edu

Copyright © 2013 CC-BY-3.0 and by the respective authors

BUNCHED BEAM ELECTRON COOLER FOR LOW-ENERGY RHIC OPERATION*

A.V. Fedotov[1#], S. Belomestnykh[1,2], I. Ben-Zvi[1,2], M. Blaskiewicz[1], D. Gassner[1], D. Kayran[1], V.N. Litvinenko[1,2], B. Martin[1], W. Meng[1], I. Pinayev[1], B. Sheehy[1], S. Tepikian[1], J. Tuozzolo[1], G. Wang[1]
[1)] Brookhaven National Laboratory, Upton, NY 11973, U.S.A.
[2)] Stony Brook University, Stony Brook, NY 11794, U.S.A.

Abstract

Electron cooling was proposed to increase the luminosity of the Relativistic Heavy Ion Collider (RHIC) operation for heavy ion beam energies below 10 GeV/nucleon. The electron cooling system should be able to deliver an electron beam of adequate quality in a wide range of electron beam energies (0.9-5 MeV). An attractive option is to use electron bunches produced with the superconducting RF (SRF) injector. Such a scheme of cooling with bunched electron beam is also a natural approach for high-energy electron cooling which requires RF acceleration. In this paper, we describe the requirements and design aspects of such an approach.

INTRODUCTION

Mapping the Quantum-Chromo-Dynamics (QCD) phase diagram is one of the fundamental goals in the heavy-ion collision experiments. The QCD critical point is a distinct feature of the phase diagram, the existence of which is predicted by various QCD models. The beam energy scan phase-I (BES-I) runs for physics, motivated by the search of the QCD critical point, were successfully conducted at RHIC in 2010-11. During BES-I physics runs data sets were collected for Au+Au (center of mass) energies of 7.7, 11.5, 19.6 and 39 GeV. Driven by physics and the BES-I results, the future physics program called BES-II is proposed for Au+Au energies below 20 GeV (γ=10.7). However, required event statistics is much higher than previously achieved and relies on significant luminosity improvement in RHIC at energies below γ=10.7. Electron cooling was proposed to increase luminosity of the RHIC collider for heavy ion beams at these low energies [1-2].

In a collider, the maximum achievable luminosity is typically limited by the beam-beam effects. For heavy ion beams significant luminosity degradation via the bunch length and the transverse emittance growth comes from the intra-beam scattering (IBS). For low-energy RHIC such IBS growth can be counteracted with electron cooling. If IBS were the only limitation, one could achieve a small hadron beam emittance and bunch length with the help of cooling, resulting in a dramatic luminosity increase. However, as a result of low energies, the direct space-charge force from the beam itself is expected to become the dominant limitation [3-4]. The main role of electron cooling for the lowest energy points is thus to counteract IBS: this prevents transverse emittance growth and intensity loss from the RF bucket due to the longitudinal IBS. As the energy is increased, the space-charge effect on the hadron beam becomes smaller which permits additional cooling of the transverse or longitudinal emittances of the hadron beams. This, in turn, allows us to reduce the β^*, providing larger luminosity gain. Recently, operation with long ion bunches and a new low-frequency RHIC RF system was suggested which should help to mitigate some observed limitations of beam lifetime at low energies offering a better path towards luminosity improvement [5-6].

This electron cooling technique requires electron beam to co-propagate with the same velocity as the ion beam in a localized portion of circular collider called the cooling section. An electron beam up to 5 MeV kinetic energy is needed to cover the full energy range of interest.

Such Low Energy RHIC electron Cooler (LEReC) based on the SRF linac is presently under design at BNL.

COOLING CONSIDERATIONS

The energies of electron beam needed for low-energy RHIC are sufficiently high (0.9-5 MeV), which allows us to consider cooling using bunched electron beam. One of the challenges for bunched beam cooling is providing beam transport of electron bunches without significant degradation of beam emittance and energy spread. A low-frequency 84.5 MHz RF gun can provide relatively long electron bunches. As a result, even for high bunch charges, space-charge effects remain under control. One can then deliver an electron beam of the necessary quality to the cooling section. In addition, the use of long ion bunches [5-6] allows us place several electrons bunches on a single ion bunch, which in turn relaxes requirements on charge in individual electron bunch and should allow us to achieve good beam quality needed for cooling.

Since non-magnetized cooling significantly simplifies electron beam transport and reduces the cost of the cooler, it was chosen as our baseline approach. Due to a relatively low beam current required for our cooler (Table 1), an approach with zero magnetic field on the cathode and thus no magnetic field in the cooling section is feasible. Short solenoids will be placed every 2 m to correct the angular spread accumulated due to the electron beam space-charge self field in the cooling section.

*Work supported by the US Department of Energy under contract No. DE-AC02-98CH10886.
#fedotov@bnl.gov

Copyright © 2013 CC-BY-3.0 and by the respective authors

ISBN 978-3-95450-138-0

RHIC MACHINE STUDIES TOWARDS IMPROVING THE PERFORMANCE AT 2.5 GEV *

C. Montag, H. Huang, G. Marr, A. Marusic, G. Robert-Demolaize, T. Shrey, V. Schoefer, S. Tepikian, K. Zeno, BNL, Upton, NY 11973, USA

Abstract

To search for the critical point in the QCD phase diagram, Au-Au collisions at beam energies between 2.5 and 15 GeV/n are required. While RHIC has successfully operated at 3.85 and 5.75 GeV/n, the performance achieved at 2.5 GeV/n is not sufficient for a meaningful physics program. We report on dedicated beam experiments performed to understand and improve this situation.

INTRODUCTION

During the next 5 - 10 years, one of the major RHIC physics programs will be the search for the critical point in the QCD phase diagram, shown in Figure 1. This search requires a gold beam energy scan in the range between 2.5 and 15 GeV/nucleon, which extends well below the RHIC design energy range from 10 GeV/n at injection to 100 GeV/n at store.

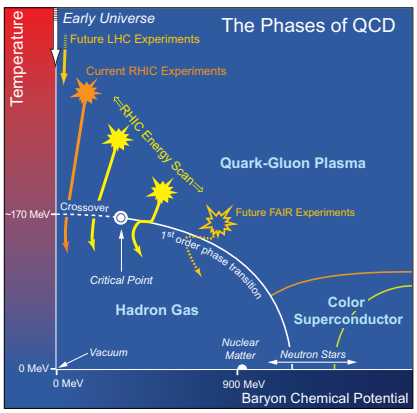


Figure 1: The QCD phase diagram, with the critical point expected in the center-of-mass energy range between $\sqrt{s_{\mathrm{NN}}} = 5$ and 30 GeV

Operating RHIC below its design energy range is very challenging for a number of reasons. First of all, beam emittances are large, resulting in a lower limit on the β-function at the interaction point, and therefore in low luminosity. Large space charge tune shifts are encountered even with moderate beam intensities. Last but not least, the multipole errors in the accelerator magnets are optimized at full energy, while they are an order of magnitude larger below the nominal injection energy.

* Work supported by Brookhaven Science Associates, LLC under Contract No. DE-AC02-98CH10886 with the U.S. Department of Energy.

Table 1: Beam Parameters Achieved at Three Different Energies During the Physics Runs of the First Phase of the Beam Energy Scan

	3.85 GeV	5.75 GeV	9.8 GeV
γ	4.1	6.1	10.7
σ_s [m]	1.5	1.5	1.5
ϵ_n [μm]	3	2.5	2.5
ϵ [μm]	0.73	0.41	0.23
I_{bunch} [10^9]	0.5	1.1	0.9
N_{bunches}	111	111	111
β^* [m]	6.0	6.0	2.5
ΔQ_{bb}	$1.2 \cdot 10^{-3}$	$1.7 \cdot 10^{-3}$	$1.4 \cdot 10^{-3}$
ΔQ_{sc}	0.035	0.047	0.012
τ_{beam} [sec]	1000	1500	3000

In the first phase of the beam energy scan in FY2010 and FY2011, RHIC operated at three different energies at and below its nominal injection energy [1, 2]. During these runs, beam lifetimes of roughly 15 minutes to one hour were achieved at gold bunch intensities of $0.5 \cdot 10^9$ to $1.1 \cdot 10^9$ ions per bunch; at the lower energies these intensities were limited by the space chage tune shift. Table 1 lists the beam parameters achieved during these runs.

In FY2012, RHIC operated for the first time successfully at a quarter of its nominal injection energy, namely at 2.5 GeV/nucleon [3]. During that test, beam lifetimes of approximately 4 minutes were achieved, see Figure 2. The bunch intensity was limited at $4 \cdot 10^7$ Au ions per bunch because of an injection efficiency of only 10 percent. Due to this short beam lifetime, only 27 bunches per ring were injected, since filling 110 bunches takes about two minutes per ring.

At these low bunch intensities, most of the RHIC beam instrumentation does not work properly, making it virtually impossible to understand and improve the machine performance. Most importantly, the transverse beam size and therefore the emittance were unknown because the ionization profile monitor (IPM) could not operate reliably.

EXPERIMENTS

In an effort to understand the single particle performance of the RHIC lattice at 2.5 GeV/nucleon Au beam energy, protons with the same rigidity of 19.3 Tm were injected and stored at an energy of 5.86 GeV, as listed in Table 2. Due to the different charge-to-mass ratio Z/A of protons compared to gold ions, the relativistic Lorentz factor γ is about

Copyright © 2013 CC-BY-3.0 and by the respective authors

BURN-OFF DOMINATED URANIUM AND ASYMMETRIC COPPER-GOLD OPERATION IN RHIC*

Y. Luo, W. Fischer, M. Blaskiewicz, J.M. Brennan, N. Kling, K. Mernick, T. Roser,
Brookhaven National Laboratory, Upton, NY, USA

Abstract

In the 2012 RHIC heavy ion run, we collided uranium-uranium (U-U) ions at 96.4 GeV/nucleon and copper-gold (Cu-Au) ions at 100 GeV/nucleon for the first time in RHIC. The new Electron-Beam Ion Source (EBIS) was used for the first time to provide ions for the RHIC physics program. After adding the horizontal cooling, 3-D stochastic cooling became operational in RHIC for the first time, which greatly enhanced the luminosity. In this article, we first review the improvements and performances in the 2012 RHIC ion runs. Then we discuss the approaches to achieve the burn-off dominated uranium beam lifetime at physics stores. And we also discuss the low copper beam lifetime in the asymmetric copper-gold collision with different intra-beam scattering (IBS) and stochastic cooling rates and the operational solutions to maximize the integrated luminosity.

PERFORMANCES

Improvements

The first high energy U-U collisions in RHIC were enabled by the versatile new Electron-Beam Ion Source (EBIS) [1]. EBIS can produce beams of essentially any ion species, and can switch rapidly between two different species. It was used for the first time to provide ions for the RHIC physics program.

To counter the intra-beam scattering (IBS) caused emittance growth in the RHIC heavy ion runs, stochastic cooling was implemented in RHIC in the past few years [2]. The longitudinal system was implemented in the Yellow ring in 2007, and longitudinal cooling in the Blue ring and the vertical stochastic cooling in both rings in 2010. In 2012, by adding cooling in the horizontal plane, full 3-D stochastic cooling became operational for the first time in RHIC for both rings.

In the previous 2010 and 2011 Au-Au runs, we observed large beam loss after RF re-bucketing and at store with the vertical cooling on. These losses were from particles with large off-momentum deviation. For the 2012 ion run, we chose a lattice with integer tunes (28, 29), which are 3 units lower than what was used in the previous ion runs. With this lattice, simulation shows that the off-momentum dynamic aperture increases from 2 σ to 5 σ with the maximum relative off-momentum deviation $\Delta p/p_0 = 0.0018$ [3].

The RHIC orbit feedback system became operational for the first time in the 2011 proton run. In the 2012 ion run, with numerous improvements in the control software and hardware, the orbit feedback became more robust. Together with tune/coupling feedback, the RHIC beam control feedback systems greatly reduces the beam time necessary for machine start-up and store tuning [4].

U-U Run

The 2012 RHIC U-U run began on April 19, 2012 and ended on May 15, 2012. The physics mode lasted for 22 days. Figure 1 shows the integrated luminosities for the two physics detectors PHENIX and STAR, together with their minimum and maximum projected luminosities. The minimum projected luminosity was based on the bunch intensity 0.6×10^9. However, the typical bunch intensity at the beginning of store was 0.3×10^9.

The luminosity in the U-U run was greatly enhanced with 3-D stochastic cooling. With 3-D cooling, the rms normalized transverse beam emittance was cooled down to 0.42 π mm mrad in 2 hours from 2.2 π mm mrad at the beginning of store. Figure 2 shows the luminosity with and without stochastic cooling. With 3-D cooling, the peak luminosity was 3 times the initial one, which was observed for the first time in a collider. The integrated luminosity per store is about 5 times that without any cooling. Despite the lower bunch intensity the integrated luminosity goals of both detectors were reached.

Figure 3 shows an example of the Zero Degree Calorimeter (ZDC) coincidence rates from the two detectors STAR and PHENIX, the actual beam loss rates, and the burn-off contributions to the beam loss in one store (fill number 16830). As mentioned above, this year we adopted a lattice which provides a large off-momentum dynamic aperture. The particle loss due to the momentum aperture limitation was essentially eliminated. Together with stochastic cooling, the beam loss was almost entirely due to burn-off [5], which is also the first time this was observed in a collider.

Cu-Au Run

The 2012 RHIC Cu-Au run began on May 15 and ended on June 25. Physics mode ran for 38 days. 3-D stochastic cooling was operational on May 23. Figure 4 shows the integrated luminosities for PHENIX and STAR. The achieved integrated luminosities for both detectors were above the maximum projection. We also reached

*This work was supported by Brookhaven Science Associates, LLC under Contract No. DE-AC02-98CH10886 with the U.S. Department of Energy.

Copyright © 2013 CC-BY-3.0 and by the respective authors

ISBN 978-3-95450-138-0

THE PROJECT-X INJECTOR EXPERIMENT: A NOVEL HIGH PERFORMANCE FRONT-END FOR A FUTURE HIGH POWER PROTON FACILITY AT FERMILAB*

S. Nagaitsev#, S. Holmes, D. Johnson, M. Kaducak, R. Kephart, V. Lebedev, S. Mishra, A. Shemyakin, N. Solyak, R. Stanek, V. Yakovlev, Fermilab, Batavia, IL 60510, USA
P. Ostroumov, ANL, Argonne, IL 60439, USA
D. Li, LBNL, Berkeley, CA 94720, USA
P. Singh, M. Pande, S. Malhotra, Bhabha Atomic Research Centre, Mumbai-400085, India

Abstract

A multi-MW proton facility, Project X, has been proposed and is currently under development at Fermilab. We are carrying out a program of research and development aimed at integrated systems testing of critical components comprising the front end of Project X. This program, known as the Project X Injector Experiment (PXIE), is being undertaken as a key component of the larger Project X R&D program. The successful completion of this program will validate the concept for the Project X front end, thereby minimizing a primary technical risk element within Project X. PXIE is currently under construction at Fermilab and will be completed over the period FY12-17. PXIE will include an H^- ion source, a CW 2.1-MeV RFQ and two superconductive RF (SRF) cryomodules providing up to 25 MeV energy gain at an average beam current of 1 mA (upgradable to 2 mA). Successful systems testing will also demonstrate the viability of novel front end technologies that are expected find applications beyond Project X.

PXIE GOALS AND PLAN

A unique feature of Project X [1] is the capability of delivering a MW-range proton beam to several experiments quasi-simultaneously with a beam structure that can be adjusted to each experiment's needs. In the suggested scheme, this is achieved as follows:

(a) Prepare a "nearly CW" beam, in which many RF buckets may be empty but the beam current, averaged over several μs, is constant. The undesired bunches are removed in the Medium Energy Beam Transport (MEBT) by a chopping system. This quasi-CW beam has a repetitive time structure (RS).

(b) Accelerate the prepared beam. The optimum solution requires acceleration by SRF cavities after MEB at 2.1 MeV;

(c) Distribute the beam to experimental stations by an RF separator at 1 GeV and 3 GeV.

The RF separation of bunches successfully supports multiple experiments operation at CEBAF [2]. The acceleration with SRF at low energies has been used for a long time at ANL [3] (at much lower average currents) and recently is being commissioned at SARAF [4], but has not been demonstrated at parameters required for the Project X. The wideband chopper, needed to prepare bunch patterns, is a unique device currently beyond state of the art.

The PXIE program [5] will address both (a) and (b) with the specific goals of demonstrating effective bunch-by-bunch chopping of the CW beam delivered from the RFQ and efficient acceleration of the 1 mA RS beam with minimal emittance dilution through at least 15 MeV.

PXIE consists of an H- ion source (IS); a Low Energy Beam Transport (LEBT); a CW 2.1-MeV RFQ; a MEBT; two SRF cryomodules (CM) operating at 2K - a Half Wave Resonator (HWR) and a Single Spoke Resonator (SSR1); a High Energy Beam Transport (HEBT); and a beam dump (Fig.1).

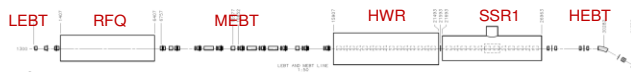


Figure 1: PXIE layout.

The concept of PXIE subsystems was described in [5]. The end-to-end simulations can be found in [6]. Main beam parameters are shown in Table 1.

Table 1: Nominal Beam Parameters at the Exit of Each Section

	IS/ LEBT	RFQ	MEBT	HWR	SSR1
Energy, MeV	0.03	2.1	2.1	11	25
Average current, mA	5	5	1	1	1
Time structure	DC	CW	RS	RS	RS
$\varepsilon_\perp$, μm					< 0.25
$\varepsilon_\parallel$, keV-ns					≤ 1

* $\varepsilon_\perp$ is the rms normalized transverse emittance, and $\varepsilon_\parallel$ is the rms longitudinal emittance.

The PXIE design and construction is being carried out by a collaboration between Fermilab, ANL, LBNL, SLAC, SNS, and Indian laboratories in a staged approach.

*Work supported by the U.S. Department of Energy under contract No. DE-AC02-07CH11359
#nsergei@fnal.gov

Copyright © 2013 CC-BY-3.0 and by the respective authors

HIGH POWER (MW-CLASS) TARGETS FOR PARTICLE BEAMS

E.J. Pitcher, European Spallation Source ESS AB, Lund, Sweden
C. Densham, Rutherford Appleton Laboratory, Abingdon, UK

Abstract

Many applications that use accelerators are demanding ever-higher beam powers, which place greater demands on accelerator design and operation. Equally demanding is the design of targets that can operate safely and optimally at these power levels. High-power target design considerations include performance optimization, heat load, radiation damage and lifetime, safety, operability, reliability, and for pulsed beams, dynamic stresses from thermal cycling. The design and operation of these targets draws upon the experience gained in operating lower power targets.

HEAT LOAD

Heat load in high-power targets can be a major driver in target design. For traditional targets made of solid metal, heat load is normally limited by heat flux at the target-coolant interface. Deposited power density goes linearly with beam power and inversely proportional to beam spot area on target. One way to address higher beam power is by increasing the size of the beam spot on target.

As beam power on target increases, so does the engineering complexity of the target. Solutions that are viable at low power, such as cooling at the periphery, are no longer viable. Figure 1 shows a spent tungsten target from the Manuel Lujan Neutron Scattering Center at Los Alamos National Laboratory [1]. This target is a solid cylinder of tungsten, 10 cm in diameter by 7.5 cm long, encased in an Alloy 718 shell that served to contain the water which passed over the tungsten surface to carry away the 60 kW of heat deposited by the 800-MeV proton beam. Two features are clearly evident. First, the target is broken into four quadrants, most likely caused by unacceptably high thermal stresses in the target. Second, substantial corrosion of the tungsten has occurred, which is due to the creation of short-lived highly oxidizing radicals in the cooling water. These radicals have been shown to be highly corrosive to tungsten [2]. Radioactive spallation products within the tungsten enter the coolant stream as the tungsten corrodes, leaving the cooling components, such as filters, ion exchange columns, highly radioactive.

At the megawatt level and higher, innovative solutions to the problem of target cooling have been proposed, such as flowing liquid metal [3,4,5,6] and rotating solid targets [SNQ, SNS TS2, Bilbao, ESS]. A liquid metal target, such as that shown in Fig. 2, has the potential to handle very high power densities due to its high heat capacity. Two liquid metals that have been successfully demonstrated as spallation targets are mercury [4,5] and lead-bismuth eutectic [6]. Lithium is proposed as the target material for the International Fusion Materials Irradiation Facility, (IFMIF) with a baseline 10 MW, 40-MeV deuteron beam. This project is now completing its engineering development and demonstration phase, including development of the lithium target [7].

At the megawatt level, full-scale thermal testing of the target prior to putting it into service is difficult and normally cost prohibitive. This is compounded by the complexity of trying to simulate the power deposition profile of the accelerator beam. As a consequence, normally small-scale tests are conducted instead. These tests are normally designed to validate uncertainties that may exist in the data or models in the simulations used in the thermo-mechanical design of the target.

SAFETY

Targets for high-power accelerators become radioactive as a consequence of beam-induced nuclear reactions within the target. For >100-MeV beams, a good rule of thumb is that the radioactive inventory within an accelerator target is on par with a nuclear fission reactor with one order of magnitude less power, e.g., a 1-MW proton beam on a spallation target will have a radionuclide inventory, as measured in becquerels, on par with that of a 100-kW fission reactor. This inventory will generate decay heat, or afterheat, following beam shutdown that must be removed in a robust and reliable manner.

Because of the risk to workers and the public presented by this radioactive material, designers of high-power targets do well to adopt a “safety by design” philosophy, whereby safety is an omnipresent consideration in the design optimization process. A number of recently designed high-power targets [APT, SNS, MTS] draw from the safety philosophy developed for the nuclear

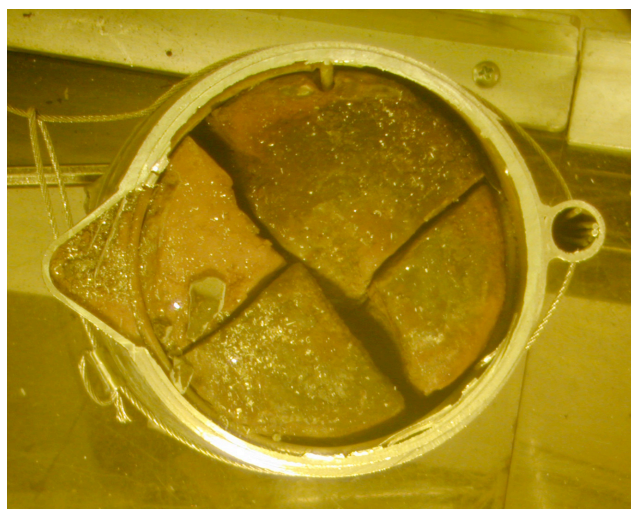


Figure 1: Broken and corroded Lujan Center tungsten target (from [1]).

Copyright © 2013 CC-BY-3.0 and by the respective authors

ISBN 978-3-95450-138-0

BEAM INSTRUMENTATION FOR HIGH POWER HADRON BEAMS

A. Aleksandrov
Oak Ridge National Laboratory, Oak Ridge, TN 37830, USA

Abstract

This presentation will describe developments in the beam diagnostics which support the understanding and operation of high power hadron accelerators. These include the measurement of large dynamic range transverse and longitudinal beam profiles, beam loss detection, and non-interceptive diagnostics.

INTRODUCTION

Beam instrumentation is an important part of any accelerator. Modern machines are equipped with large numbers of diagnostics for measuring various beam parameters as illustrated by the Spallation Neutron Source diagnostics map in Fig. 1. Many of the diagnostics systems are common for different types of accelerators and accelerated particles but some can work in specific conditions only. In this paper we will discuss beam instrumentation systems used for megawatt-class hadron machines with relatively low energy of no more than a few GeV (essentially non-relativistic beams). There is a significant number of operating and emerging accelerators in this class, such as SNS, PSI, J-PARC, ESS, FRIB, Project-X and others. The major factors specific for these machines are related to their high average beam power:

- Small fraction of lost beam is of importance. Large dynamic range diagnostics are required to follow the dynamics of these small fractions.
- The damage threshold is reached quickly with high average beam power. Diagnostics systems for machine protection must have a fast response.
- The power density in the beam core can be very large. This can prevent the use of interceptive diagnostics.
- The average peak beam current is large. The space-charge effects can be significant and affect operation of some types of diagnostics.

Another important factor is the use of a superconducting RF linac for all or part of the acceleration. Although this is not a necessary requirement and some high power accelerators, like the PSI cyclotron, do not use it, the majority of new projects include high power superconducting linac in the design. This adds two more important factors:

- New damage mechanisms related to the superconducting cavities. Additional diagnostics may be required to protect the SRF linac [1].
- The SRF technology requires maintaining a very clean environment for the cavities and the surrounding vacuum chambers. This can impose severe restrictions on the design of the diagnostics in these areas up to complete a ban on using interceptive diagnostics, like in the case of the SNS SRF linac.

In the following sections we will discuss how the above factors affect the diagnostics requirements and the design choices.

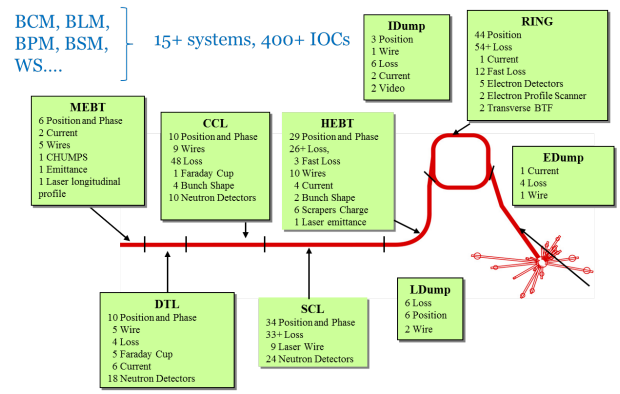


Figure 1: The Spallation Neutron Source diagnostics map.

MACHINE PROTECTION FROM LOST BEAM

Protecting the machine from damage by the lost beam is the most important application of the beam instrumentation. The main damaging factors are:

- Mechanical damage (melting, cracking, erosion). This mechanism is most important at lower energies (<10 MeV), where penetration depth for beam particles is relatively small. The damage threshold depends on many factors but typically it is of the order of magnitude of few hundred watts per meter, which represent a fraction of lost beam of few persent or higher. This level of fractional beam loss can be detected by a Differential Beam Current Monitor (DBCM) measuring beam current difference at two locations along the accelerator.
- Activation of the accelerator equipment. This mechanism is more important at higher energies and the commonly accepted threshold of 1 W/m is used for protons above 100 MeV, which corresponds to a very small fractional loss of $10^{-5} \div 10^{-7}$. As this threshold is significantly lower than the mechanical damage threshold, protection from the activation will automatically provide protection from the mechanical damage. Radiation Monitors (RM) are typically used for protection from small fractional beam loss at high energy [2].

The two above mechanisms are common for all types of the accelerators and a well-established protection strategy typically includes DBCMs at energy below 10 MeV, RMs

Copyright © 2013 CC-BY-3.0 and by the respective authors

A FAST ROTATING WIRE SCANNER FOR USE IN HIGH CURRENT ACCELERATORS*

T. Moore, N.I. Agladze, I.V. Bazarov†, A. Bartnik, J. Dobbins, B. Dunham,
S. Full, Y. Li, X. Liu, J. Savino, K. Smolenski
CLASSE, Cornell University, Ithaca, New York 14853, USA

Abstract

We have developed a cost-effective, fast rotating wire scanner for use in accelerators where high beam currents would otherwise melt even carbon wires. This new design uses a simple planetary gear setup to rotate a carbon wire, fixed at one end, through the beam at speeds in excess of 20 m/s. We present results from bench tests, as well as transverse beam profile measurements taken at Cornells high-brightness ERL photoinjector, for a beam energy of 4 MeV and beam currents up to 35 mA.

INTRODUCTION

Recently, a new regime of beam parameters has become accessible with the advent of very intense photoinjectors, such as the Cornell ERL photoinjector, which feature very high average beam currents (up to 100 mA) and low transverse beam emittances (<1 mm-mrad rms normalized) [1, 2]. The beam energy out of the photoinjectors is near or below 10 MeV, with very large beam powers (on the order of MW) contained inside a small beam cross-section (diameter of 1 mm or less).

This parameter range poses special challenges for diagnostics at full beam current operation, particularly due to the beam's high charge density. First, the beam power density is high enough that any material intercepting the beam will melt on the order of 10's of microseconds or less. Second, the beam energy is low enough that synchrotron or diffraction radiation, which are often the method of choice for beam profile measurements at higher energies, are generally not available without introducing strong magnetic fields or placing apertures undesirably close to the beam for diffraction radiation.

One obvious candidate for a beam profile diagnostic capable of measuring MW type electron beams is a wire scanner that can sample the beam profile at a suitable transverse resolution (on the order of microns or even better) [3]. However, particle beams with small transverse dimensions and high intensities require a wire scanner with a very fast scanning speed, as these beams can melt even carbon wires - one of the best materials for withstanding extremely high temperature rises[4]. For example, a beam current of 100 mA and both an electron beam diameter and a wire diameter of $34\mu m$, like those found in the Cornell photoinjector, require a minimal scanning speed of 20 m/s. In this paper, we describe the design and show tests of a simplified wire scanner capable of reaching this speed and optimized for a large quantity reproduction, resulting in significant cost reduction.

WIRE SCANNER CONSTRUCTION

The principle of operation of the new wire scanner is illustrated in Fig. 1. It consists of a stationary gear G_1 and a smaller gear G_2 rotating around the gear G_1. The blade attached to the gear G_2 holds the carbon fiber cemented on its end. If the center of the small gear moves with the linear velocity v_g then the fiber scanning speed is

$$v_s = v_g\left(\frac{R}{R_2}+1\right), \tag{1}$$

where R_2 is the radius of the gear G_2 and R is the distance from the center of the gear G_2 to the electron beam. Uncertainty of the beam position along the fiber results in the scanning speed variation

$$\frac{\delta v_s}{v_s} = \frac{\frac{\delta R}{R_2}+1}{\frac{R}{R_2}+1} \approx \frac{\delta R}{R}, \tag{2}$$

where it is assumed that $\delta R \ll R, R_2$. In the current prototype $R = 82.4$ mm, so for $\delta R = 5$ mm the relative scanning speed variation is $\delta v_s/v_s = 0.061$. This value sets the absolute precision of the transverse bunch profile measurement.

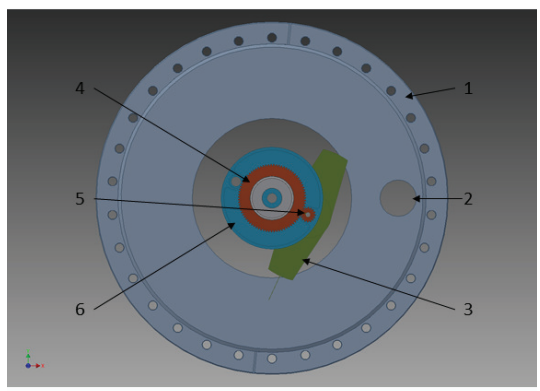


Figure 1: A 3D rendering of the gears setup. (1) - vacuum flange; (2) - beam pipe; (3) - blade with attached carbon wire; (4) - stationary gear G_1; (5) - rotating gear G_2; (6) - rotating gear box.

* This work was supported by the financial assistance from the National Science Foundation (Grant No. DMR-0807731).

† ib38@cornell.edu

ISBN 978-3-95450-138-0

Copyright © 2013 CC-BY-3.0 and by the respective authors

THE DOE-HEP ACCELERATOR R&D STEWARDSHIP PROGRAM*

Eric Colby, Michael S. Zisman#, U.S. Department of Energy, Washington, DC 20585, USA

Abstract

Since the Accelerators for America's Future (AfAF) Symposium in 2009, the U.S. Dept. of Energy's Office of High Energy Physics (DOE-HEP) has worked toward broadening its accelerator R&D activities beyond its support of only discovery science to include medicine, energy and environment, defense and security, and industry. Accelerators play a key role in many aspects of everyday life, and improving their capabilities will enhance U.S. economic competitiveness and the scientific research that drives it. In 2011, a community task force was initiated by DOE-HEP to develop more fully the information from the original AfAF Symposium. Subsequently, a DOE-HEP concept (coordinated with the other cognizant Office of Science program offices) was developed for accelerator R&D stewardship. Here, we describe the evolution of the stewardship task starting from its origins in the ongoing DOE-HEP accelerator R&D program, the mission of the new program, and initial steps being taken to implement it. Several initiatives are currently being considered to launch the program, and these will be indicated. Involvement of the accelerator community in developing ideas for future stewardship activities will be crucial to the ultimate success of the program.

ORIGIN AND MOTIVATION

Although DOE-HEP has historically taken a broad view of its accelerator R&D program, an effort to examine stewardship needs more formally began in 2009 with the sponsoring of the Accelerators for America's Future Symposium [1]. The report from this symposium, published in 2010 [2], identified the importance of accelerator technologies to broad sectors of the U.S. economy, including discovery science, medicine, defense and security, energy and environment, and industry. It also called out the needs for improved interagency, inter-program, and industry-agency coordination, and highlighted the value of expanded training and education of accelerator scientists and engineers.

In 2011, the Senate requested [3] DOE to prepare a 10-year strategic plan for "accelerator technology research and development to advance applications in energy and the environment, medicine, industry, national security, and discovery science." In preparation for developing such a strategic plan, Dr. Jim Siegrist, Associate Director of Science for High Energy Physics, in consultation with other Office of Science (SC) Associate Directors, asked Norbert Holtkamp from SLAC to convene a community task force to review and expand upon the findings of the earlier AfAF report. This group met during the period November 2011–February 2012 and provided information to:

- identify research opportunities with potential for broad national benefits
- summarize the status of key research and technology areas identified
- identify possible impediments to successful accelerator R&D stewardship activities for the broad user base envisioned

The task force report [4] was very helpful in preparing the DOE-HEP strategic plan, which was sent to Congress in October 2012.

DESCRIPTION OF STEWARDSHIP

Relationship with Current Program

The ongoing HEP accelerator R&D program develops the basic science and technologies needed to design, build, and operate state-of-the-art accelerators. Such accelerators are essential for making discoveries in HEP. Moreover, as is clear from the studies in Refs. [2] and [4], accelerators are likewise essential for serving the broader communities of medicine, defense and security, energy and environment, and industry as well as the discovery science community.

As indicated schematically in Fig. 1, there is already a strong connection between current R&D thrusts and stewardship program needs. The center portion of the figure lists the 8 program thrusts of the current HEP accelerator R&D program. The columns on the left indicate the science goals that motivate the program, namely, the desires for higher particle or photon beam quality, for higher beam intensity, and for higher beam energy (or, equivalently, more compact accelerators) and how they overlap with the program thrusts. The columns to the right indicate the overlap between the broader accelerator community needs and the ongoing R&D program thrust areas. The complete overlap with the needs of discovery science is by design, as this community has, to date, been the only consumer of the R&D work. It is interesting, however, that there is also substantial overlap with the needs of the other accelerator communities. We conclude from this that the existing skill set is already well matched to the needs of the broader accelerator community.

Accelerator Stewardship Mission

The mission of the accelerator R&D stewardship program is to support fundamental accelerator science and technology development of relevance to many fields, and to disseminate accelerator knowledge and training to the broad community of accelerator users and providers.

Carrying out this new mission—in addition to carrying out the current HEP programmatic accelerator R&D effort—will be accomplished through:

*Work supported by U.S. Dept. of Energy, Office of Science, Office of High Energy Physics
#michael.zisman@science.doe.gov
Copyright © 2013 CC-BY-3.0 and by the respective authors
ISBN 978-3-95450-138-0

ADVANCES IN PHOTOCATHODE TECHNOLOGY AT CORNELL UNIVERSITY*

S. Karkare†, I. V. Bazarov, L. E. Boulet, M. Brown, L. Cultrera, B. Dunham, N. Erickson, G. Denham, A. Kim, B. Lillard, T. P. Moore, C. Nguyen, W. Schaff, K. W. Smolenski, H. Wang, CLASSE, Cornell University, Ithaca, New York, USA

Abstract

Beam brightness from modern day photoinjectors is limited by the photocathode. A multifaceted photocathode development program has been undertaken at Cornell University with a goal to develop the ultimate photocathode which has high quantum efficiency, low mean transverse energy, quick response time and a long lifetime. Positive affinity cathodes like CsK_2Sb and Na_2KSb have been grown using different kinds of alkali metal sources (alkali-azide and pure metal), characterized and tested in the Cornell ERL photoinjector. Novel layered structures of various III-V semiconductors like GaAs and AlGaAs grown using Molecular Beam Epitaxy (MBE) and activated to negative electron affinity using Cs and NF_3 are also being investigated. Surface and photoemission diagnostics like Auger spectroscopy, LEED, RHEED and the 2D-electron energy analyzers have been connected in vacuum to the photocathode growth and preparation chambers to fully characterize the surface and emission properties of the materials grown. A Monte Carlo based simulation has also been developed to predict photoemission from layered semiconductor structures and help design novel structures to optimize the photoemission properties.

INTRODUCTION

Photocathodes used in photoinjectors that power modern and future 4^{th} generation light sources like the ERL's and FEL's have extremely stringent requirements. Moreover, the maximum achievable beam brightness from photoinjectors is limited by the photocathode [1]. For example, the photocathode in the Cornell ERL injector is required to have a high ($> 3\%$) QE (quantum efficiency) at 520nm laser wavelength, short ($<$ 2ps) response time, minimum possible MTE (mean transverse energy) with typical values being 150meV and a long lifetime during high current ($\sim$100mA) operation. Metallic cathodes are rugged and have a fast response time, but have very low ($< 0.1\%$) QE. Semiconductor cathodes provide a high QE in the visible and UV range. For this reason semiconductor cathodes are the choice for several photoinjectors around the world. However, they have very stringent vacuum conditions for longevity [2].

Several of the key emission properties required from semiconductor cathodes are conflicting. For example, at longer wavelengths, negative electron affinity (NEA) semiconductor cathodes give a small MTE ($\sim$25meV) but have a long ($>$100ps) response time [3]. Furthermore, the detailed physics of photoemission and the origin of the key photoemission properties like QE, response time and MTE are not well understood for semiconductor cathodes. This is largely due to lack of conclusive and self-consistent experimental data hampered by the demanding vacuum requirements and experimental difficulties associated with measuring key photoemission properties of MTE and response time from these cathode materials.

EXPERIMENTAL FACILITIES

A campus-wide photocathode investigation program has been initiated at Cornell University in order to address the need for experimental data. Both positive electron affinity (PEA) alkali-antimonide and NEA semiconductor photocathodes are under investigation. The alkali-antimonide photocathode growth chamber and GaAs activation chambers are connected in vacuum to surface analysis chamber with auger spectroscopy, RHEED and LEED capabilities. Abilities to measure spectral response, surface QE scan, activate NEA semiconductor cathodes using Cs and NF_3 while measuring QE at different wavelengths simultaneously have also been incorporated. Advanced photocathode diagnostics such as the electron energy analyzer [4] to measure simultaneously, transverse and longitudinal electron energy distributions have also been developed and added to the setup. Figure 1 shows the picture of the multipurpose vacuum system devoted to photocathode research. The entire assembly is under ultra high vacuum with a pressure of less than 10^{-10} Torr throughout and less than 10^{-11} Torr in the GaAs preparation chamber and the surface analysis chamber. Samples can be transferred from one part of the assembly to another in vacuum via use of magnetically coupled transfer arms.

Multialkali photocathodes developed and characterized here can be transferred to the Cornell ERL injector for studying their performance in a DC photoemission gun under high voltage (350kV) and high beam currents ($>$ 70mA) [5] via a vacuum suitcase capable of maintaining a pressure of a few 10^{-10} Torr during the transfer. Another facility is a semiconductor MBE reactor used to grow and activate III-V semiconductor photocathode structures. New layered structures of GaAs/AlGaAs can be grown with graded doping levels in order to optimize photoemission characteristics. These structures, once grown in the MBE reactor can be capped with a thick As layer and be transported in air to either the multipurpose photocathode

*This work has been funded by NSF under grant number DMR-0807731, DOE under grant number DE-SC0003965

† ssk226@cornell.edu

ISBN 978-3-95450-138-0

Copyright © 2013 CC-BY-3.0 and by the respective authors

CONTINUED DEVELOPMENT AND TESTING OF CARBON NANOTUBE CATHODES AT RADIABEAM*

J.J. Hartzell#, L. Faillace, R. Agustsson, S. Boucher, A. Murokh, A. S. Smirnov, RadiaBeam Technologies, Santa Monica, CA 90404, USA
B. C. Regan, W. Hubbard, UCLA, Los Angeles, CA 90095, USA

Abstract

RadiaBeam is continuing to develop carbon nanotube (CNT) cathodes for DC-pulsed and radio frequency (RF) driven electron sources. CNT cathodes, if fully realized, are capable of producing very high current density with low thermal emittance, due to ambient operating temperature. Experimental results of CNT cathodes are presented, including the high-voltage tests, and life time studies. CNT cathodes potential applications in accelerator science and microwave industry are discussed, and near term plans to test the CNT cathodes in the RF environment are presented.

INTRODUCTION

Carbon nanotubes are allotropes of carbon with a cylindrical nanostructure and exceptional electrical and mechanical properties [1]. They are typically fibers with a diameter of 1 to 50 nm, coming in either single-wall or multi-wall strands and an aspect ratio of up to 1000. Due to this very high aspect ratio, they have extremely large field enhancement factors, allowing efficient emission of electrons [2] at fields of only a few MV/m. Stable currents of more than 1μA have been measured from a single CNT fiber [3]. CNTs can also be fabricated in large, dense arrays, making them ideal as a cathode material. Peak current densities as high as 50 A/cm^2 have been reported from a macroscopic cathode operating in pulsed mode [4].

The use of a cathode fabricated with CNT technology has a high potential to replace thermionic cathodes in vacuum electronic devices, such as TWTs. Due to their high field enhancement factor, it is possible to operate in a "cold" field emission regime with relatively high current densities and affordable voltages in a much wider temperature range, including at room temperature [5]. Moreover, CNT cathodes are able to provide high current beams from a very small total gun size.

CNT CATHODE PRODUCTION

After early initial testing, we have focused on producing CNT cathodes via electrophoretic deposition (EPD) (see Figure 1). This method has proven to be rapid and economical. We are able to produce and characterize approximately one cathode per week. This allows us to produce a large number of samples with varying properties (deposition density, annealing temperatures, etc) to find the best combination of performance and durability.

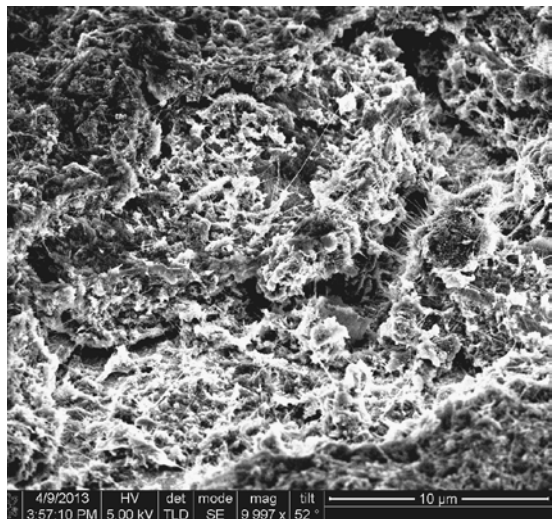


Figure 1: EPD deposition showing a very high density of CNTs.

As compared to earlier efforts, we have modified the substrate design to reduce the time required for machining and to accommodate the compact chemical vapor deposition (CVD) furnace that we helped our collaborators build. Our plan to eventually test the CNT cathodes inside the RF Gun at A0 (Fermilab) led to a design that has a reusable holder and removable cathode substrates. Figure 2 shows the new reusable holder with a variety of substrates ready for deposition.



Figure 2: Reusable cathode holder with molybdenum cathode substrate on the LEFT, based on Fermilab's A0 gun. Two undeposited cathodes (stainless steel and copper) on the RIGHT.

* This work is supported by DOE Grant DE-SC0004459
# Hartzell@radiabeam.com

Copyright © 2013 CC-BY-3.0 and by the respective authors

NOVEL METHODS FOR EXPERIMENTAL CHARACTERIZATION OF 3D SUPERCONDUCTING LINAC BEAM DYNAMICS

A. Shishlo#, ORNL, Oak Ridge, TN 37831, USA

Abstract

This paper describes an approach to measure initial Twiss parameters in transverse and longitudinal directions at the entrance of a linac with independent short accelerating cavities. For the transverse plane the usual technique of transverse profiles is used, and for the longitudinal direction a recently developed non-intercepting method is applied. The new method is based on a beam position monitor amplitudes analysis. The applicability of the methods are discussed and demonstrated on an example of the Spallation Neutron Source superconducting linac.

INTRODUCTION

Beam loss in accelerators should be low enough to allow "hands on" maintenance. This goal is achieved by a good design of the machine and a precise tuning before the operation phase. According to its design, the superconducting linac (SCL) of the Spallation Neutron Source (SNS) accelerator should be a almost loss-free part of the machine due to large apertures and low residual gas pressure. During the commissioning, it was found that SCL had significant beam loss and could be activated above the "hands on" maintenance level when the beam power reaches a design value of 1.4 MW. Fortunately, this beam loss was reduced to an acceptable level by reducing the strength of the quadrupoles in the SCL without a clear understanding the loss mechanism. After that, the power of SNS accelerator was not limited by SCL beam loss. Recently, the SCL beam loss mechanism was identified as intra-beam stripping (IBSt) [1,2]. IBSt is a process of stripping one loosely-bound electron from one of two H^- ions colliding inside the bunch. The neutral hydrogen atom created in this collision will not see any focusing fields, and it will be lost on the beam pipe. The reaction rate of IBSt is proportional to the square of the particle bunch density, so the reducing of the SCL quadrupole strengths made the beam bigger transversely and reduced the density and beam loss. The process of a quadrupole focusing fields tuning is and was a purely empirical beam loss reduction based on readings of Beam Loss Monitors (BLM). All previous attempt to use a model based approach to the SCL loss reduction failed, and this paper is an attempt to explain why we did not succeeded before.

RATIONALE

IBSt beam loss is defined by the core of the bunch where the most particles are located. It allows us to describe this loss with a simple envelope model instead of complicated and slow particle-in-cell tracking codes. After certain assumptions (the Gaussian particles distribution in the bunch), the only parameters needed for the loss calculation are Twiss parameters of the bunch for all three directions along the linac [1]. To calculate these Twiss parameters we need the following components:

- A validated envelope tracking accelerator model.
- The measured initial Twiss parameters for all three dimensions.

The present work describes how to get these components for the SNS superconducting linac tuning. The problem of loss reduction based on this model and the initial Twiss parameters is a subject of future studies.

THE SNS SUPERCONDUCTING LINAC

The SNS superconducting linac consists of Medium and High Beta sections named in accordance with the two types of superconducting cavities designed for geometrical relativistic β= 0.61 and 0.81 beams. The first section has 11 cryomodules with 3 cavities in each module, and the High Beta section has 12 modules, 4 cavities per module. Each 805 MHz cavity has independent control of the field gradient and phase. According to the design, the cavity field gradients in each section should be all the same, but in reality they are not. Instead, the gradient of each cavity is set to be as high as possible for stable operation. The input energy of the SCL is 185.6 MeV; the output energy is about 930 MeV, and it is defined by existing cavity gradients; the design peak current is 38 mA and the design energy 1 GeV. The bunch frequency of 402.5 MHz is defined by a normal conducting part of the linac. The SCL has 32 stripline beam position monitors (BPMs) installed along the linac between cryomodules and in the cavity-free part of SCL. The BPMs measure the transverse positions of the beam, the arrival phases of the bunches, and the amplitudes of the Fourier harmonics of the bunch longitudinal distributions at the bunch frequency. The SCL is also equipped with 9 Laser Wire (LW) Stations to measure transverse profiles of the beam. Four LWs are installed at the beginning of each of the two sections (one LW after each of the first four superconducting cavities) and one LW at the end of SCL.

XAL ONLINE MODEL

All simulations and analysis performed for this work used the XAL Online Model (OM) [3]. The OM is an envelope tracking accelerator code similar to TRACE3D [4]. The OM tracks the envelope parameters through the SCL lattice using transport matrices for each quadrupole, each RF gap in the accelerating cavities, and each drift space. The space charge kicks are accumulated in the total

shishlo@ornl.gov

Copyright © 2013 CC-BY-3.0 and by the respective authors

ISBN 978-3-95450-138-0

SPACE-CHARGE COMPENSATION FOR HIGH-INTENSITY LINEAR AND CIRCULAR ACCELERATORS AT FERMILAB*

M. Chung†, L. Prost, V. Shiltsev, Fermilab, Batavia, IL 60510, USA

Abstract

Space-charge effects have long been recognized as a fundamental intensity limitation in high-intensity linear and circular accelerators. As the mission of the US high energy physics program is pushing the Intensity Frontier, it is very timely to explore novel schemes of space-charge compensation that could significantly improve the performance of leading high-intensity proton accelerator facilities such as Project-X. In this work, we present two activities at Fermilab on space-charge compensation experiments based on residual gas ionization: 1) neutralized beam transport of continuous-wave (CW) H^- beam in Project-X Injector Experiment (PXIE); and 2) trapped electron plasmas for space-charge compensation in the newly proposed Integrable Optics Test Accelerator (IOTA) ring. Characteristics of the stability in the beam-plasma system, the dynamics of beam neutralization, and the transition between neutralized and un-neutralized beam transports are discussed for each experiment.

INTRODUCTION

The main idea of space-charge compensation considered in this work is based on the long-known fact that the negative effect of Coulomb repulsion can be mitigated if beams propagate through a plasma column of opposite charge. The plasma column can be formed by beam-induced residual gas ionization and/or by external plasma sources. This idea has been successfully applied to transport high-current low-energy proton and H^- beams into the RFQ in many linacs [1]. In circular machines, partial neutralization by ionization electrons was attempted with notable improvements in beam intensity, namely an order of magnitude higher than the space-charge limit [2].

BASIC DEFINITIONS

The time needed to generate enough electron-ion pairs for full space-charge compensation is called charge-neutralization time [1], $\tau_n = 1/n_g\sigma_i v_b$. The number density of the oppositely charged particles n_p (electrons for positive ion beams; positive ions for negative ion beams) grows linearly with time, and we have $n_p \approx n_b$ or $f_n \approx 1$ after the time duration of τ_n. Here, $f_n = n_p/n_b$ is the fractional charge neutralization. Note that the background gas density $n_g[\mathrm{m}^{-3}] = 3.54 \times 10^{22} \times p[\mathrm{Torr}] \gg n_b$ for nominal pressure range $p = 10^{-7} - 10^{-5}$ Torr. For the 30 keV H^- beam for the PXIE LEBT, $\sigma_i = 5 \times 10^{-20}\mathrm{m}^2$ and $\tau_n \approx 236$ μs for $p = 10^{-6}$ Torr. For a 2.5 MeV proton beam for the IOTA electron column, $\sigma_i = 1.5 \times 10^{-21}\mathrm{m}^2$ and $\tau_n \approx 862$ μs for $p = 10^{-6}$ Torr.

The electrostatic potential created by the uniform beam is $\phi(r=0) = V_s\left[1 + 2\ln\left(r_w/r_b\right)\right]$, where, $V_s = I_b(1 - f_n)/(4\pi\epsilon_0 v_b) > 0$ (< 0) for positive (negative) ion beams. Note that $\phi(r = r_b) = 2V_s \ln(r_w/r_b)$ and $\phi(r = r_w) = 0$. Here, r_b is the radius of the beam with constant density n_b and velocity v_b, and r_w is the radius of a perfectly conducting cylindrical wall.

PLASMA PROCESSES

We consider two cases: an H^- beam and a proton beam. Here, we listed only the dominant plasma processes for the space-charge compensation.

- H^- **beam:**

$$H^- + H_2 \rightarrow H(\mathrm{fast}) + H_2 + e \quad (1)$$

$$H^- + H_2 \rightarrow H^- + H_2^+(\mathrm{slow}) + e \quad (2)$$

$$e + H_2 \rightarrow H_2^+(\mathrm{slow}) + 2e \quad (3)$$

For the case with no solenoidal fields, ionization electrons are expelled by the beam space-charge immediately and the slow ions are oscillating inside the potential well of the beam. Initially, the ion density profile becomes highly peaked around beam center [3]. After a time duration of τ_n, a steady state is obtained. There is a critical value for the gas density, $n_{g,cr}$, in which $\tau_{i,exit} = \tau_n$, i.e., $n_{g,cr} \approx (1/\tau_{i,exit})/v_b\sigma_i$ [1]. Here, $\tau_{i,exit} = r_b/2v_i$ is the average time for an ion to exit the beam, and $v_i = \sqrt{T_i/m_i}$ is the ion thermal velocity. It is often assumed that T_i is on the order of 0.1 eV [1]. When $n_g = n_{g,cr}$, the potential difference between the beam center and edge, $V_s = 0$ and $f_n = 1$ at the steady state. For $n_g < n_{g,cr}$, $V_s < 0$ and $f_n < 1$. In this case, the beam is not fully neutralized and the system is essentially composed of two species ($n_e \ll n_i \sim n_b$). For $n_g > n_{g,cr}$, the beam becomes overcompensated, i.e., $V_s > 0$ and $f_n > 1$. In this case, $eV_s \sim T_e$ and $v_i \approx \sqrt{T_e/m_i}$.

For the nominal pressure range of PXIE, we always have $n_g < n_{g,cr}$, which is good for minimizing stripping loss, but not favorable for achieving full compensation. To achieve full compensation, use of Xe as a background gas is often considered, which decreases the critical density by a factor $\sim$ 45. Also, to reduce the loss of the H_2^+ ions through the longitudinal drift, positively biased electrodes may be used.

* Work supported by Fermilab Research Alliance, LLC under Contract No. DE-AC02-07CH11359 with the United States Department of Energy

† mchung@fnal.gov

Copyright © 2013 CC-BY-3.0 and by the respective authors

EXPERIMENTAL VERIFICATION OF SINGLE-BUNCH ACCUMULATION LIMIT DEPENDENCE ON IMPEDANCE AT THE APS *

V. Sajaev†, B. Borland, Y.-C. Chae, L. Emery, ANL, Argonne, IL 60439, USA

Abstract

One of the unique features of the Advanced Photon Source is operation with a small number of intense bunches — the standard operating mode has 24 16-nC bunches, while in a special operating mode one of the bunches has a charge of 60 nC. Such high single-bunch currents are achieved by a combination of high operational chromaticity and transverse bunch-by-bunch feedback. In the near future, more narrow-gap insertion device vacuum chambers will be installed, which will increase the impedance of the storage ring and make operation with high single-bunch current more problematic. Simulations exist that quantify the effects of increased impedance on the APS single-bunch accumulation limit; however, no direct experimental verification has yet been performed. In this paper, we will present a measurement of the single-bunch accumulation limit as a function of impedance. Different impedance values were achieved by changing the storage ring beta functions.

INTRODUCTION

The Advanced Photon Source (APS) is a 7-GeV third-generation synchrotron light source that has been in operation for almost 20 years. Presently, APS operates in three fill patterns: 24 equally spaced bunches — a pattern that is used for 60% of the time; 324 equally spaced bunches; and a special "hybrid" mode where one 60-nC bunch is separated from a train of weaker bunches by 1.5 μs. Total operating beam current is always 102 mA.

To achieve stable high-current single bunches, we operate at high chromaticities. Before introducing transverse bunch-by-bunch feedback, the operating chromaticity was +7 in both planes for the 24-bunch fill pattern and +11 for the "hybrid" pattern. The biggest downside of operating with high chromaticity is low lifetime. Even though APS operates in top-up mode, there is still a limit on how low the lifetime can be. The introduction of the feedback allowed us to lower chromaticity to +4 for the 24-bunches fill pattern and to +9 for the "hybrid" pattern.

The APS transverse impedance consists of three approximately equal parts [1]: the resistive-wall impedance of small-gap insertion device (ID) vacuum chambers, the geometrical impedance of the transitions from large- to small-gap chambers, and the geometrical impedance of the rest of the ring. Presently, there are 32 small-gap ID chambers installed. Of them, one has a 5-mm full gap, eight chambers have a 7.5-mm full gap, and the rest have an 8-mm gap. All ID chambers are 5 m long and are made of aluminum. At the time this work started, three ID locations were still unoccupied, meaning that three more small-gap vacuum chambers still needed to be installed. This would increase transverse impedance by about 6% and could affect our ability to provide users with 60 nC in a single bunch.

As we work on the APS Upgrade [2], a few things are clear: the lattice will be as strongly focusing as possible resulting in small dynamic aperture and short lifetime, the ID vacuum chambers will have as small gaps as possible resulting in higher impedance, and we still would need to provide high-charge bunches to the users performing timing experiments. In this situation, we need a good understanding of impedance effects in the APS and confidence in our simulation tools. We have developed an experimental program that would allow us to verify our simulation and predictive abilities.

SIMULATIONS

Simulation of the single-bunch accumulation limit is done by multi-particle tracking using `elegant` [3]. The impedance of the whole ring is represented as a single lumped element for each plane using the ZTRANSVERSE and ZLONGITUDINAL elements in `elegant`, which take calculated impedance as input. The ring itself is represented as a linear map of one sector (element ILMATRIX) with chromaticity. Special elements like cavities, radiation effects, etc. can be inserted between sectors. The simulated bunch consists of 200k particles, which is required for correct simulation of longitudinal effects. Wake potentials of all elements are computed using GdFidl [4] and a 1-mm-long bunch, in order to extend the resulting impedance bandwidth. Wake potentials are separated into dipole and quadrupolar components.

The simulated accumulation limit is strongly affected by the injection conditions, namely by the residual oscillations of the stored bunch. First, we used the most realistic approach and simulated both stored and injected bunches. But later we noticed that the losses that occur at the accumulation limit all come from the stored beam and are not affected by the injected bunch. After that, we simplified the simulation to a simple kick of the stored bunch. Ideally, there should be no vertical oscillations occurring after the injection, but due to small coupling inside the injection bump there is always some vertical motion of the

* Work supported by the U.S. Department of Energy, Office of Science, under Contract No. DE-AC02-06CH11357.

† sajaev@aps.anl.gov

Copyright © 2013 CC-BY-3.0 and by the respective authors

ISBN 978-3-95450-138-0

BEAM PHYSICS IN FUTURE ELECTRON HADRON COLLIDERS

A. Valloni*, O. Bruning, M. Klein, D. Schulte, F. Zimmermann, CERN, Geneva, Switzerland

Abstract

High-energy electron-hadron collisions could support a rich research programme in particle and nuclear physics. Several future projects are being proposed around the world, in particular eRHIC at BNL, MEIC at TJNAF in the US, and LHeC at CERN in Europe. This paper will highlight some of the accelerator physics issues, and describe related technical developments and challenges for these machines. In particular, optics design and beam dynamics studies are discussed, including longitudinal phase space manipulation, coherent synchrotron radiation, beam-beam kink instability, ion effects, as well as mitigation measures for beam break up and for space-charge induced emittance growth, all of which could limit the machine performance. Finally, first steps are presented towards an LHeC R&D facility, which should investigate relevant beam-physics processes.

INTRODUCTION

Particle colliders for high energy physics have been at the forefront of scientific discoveries for more than half a century. Leptons have been used to probe the partonic structure of the proton from the late 1960s, starting in fixed target deep inelastic scattering experiments, and continuing to the *e-p* collider HERA. With the first *e-p* collider HERA, remarkable results have been obtained on the parton structure of the proton, which are now crucial for the interpretation of the LHC data and include the discovery of a high density gluon and sea quark component in the proton. One can thus reflect on the valuable insight gained in revealing the structure of matter and evaluate priorities for future *e-p* or electron-ion (*e-A*) colliders [1]. Despite previous successes, many fundamental physics aspects have not yet been verified experimentally, and several future projects are under consideration in the USA and Europe and have good prospects of becoming operational and deliver results in the next 20 years. These projects intend to extend the knowledge achieved at HERA, and to provide new exploration tools by involving lepton collisions with heavy ions as well as with polarized protons and polarized light ions. These proposed colliders come in two varieties. One is an electron linear accelerator colliding with a proton or ion ring accelerator, the other, an *e*-ring accelerator colliding with a hadron ring. All of the future *e-A* colliders are based on the extension of already existing machines: LHeC at CERN [2], ENC at GSI [3], eRHIC at BNL [4] and MEIC at TJNAF [5]. Two colliders, ENC and MEIC are based on the ring-ring (RR) scenario, while the BNL and CERN teams selected the linac-ring (LR) option with energy recovery. The physics programs to a large degree are complimentary to each other and to the LHC physics [6]. In particular, with highest energies, the LHeC can be made a next Higgs factory. New ideas and technologies are applied in the accelerator designs and the intent of this paper is to present the key accelerator physics issues, referring to 3 possible future machines which are quite different in approach: eRHIC, MEIC and LHeC. This paper is organized as follows. The first part contains a brief overview on the parameter choices of the main future colliders worldwide. The focus here is on an understanding of the central characteristics of each machine and of the various common challenges. In the second part, among all the possible issues that these accelerators present, some selected subjects are described with related studies to analyze and compare the merits of different approaches. Special emphasis will be placed on the clear identification of the beam physics limits and accelerator technology limits highlighting aspects that need to be addressed by further research. The final section contains a summary of the future plans at CERN with special regard to the scientific and technical R&D activity for the development of an LHeC ERL test facility which will allow addressing relevant physics issues.

FUTURE ELECTRON-ION COLLIDERS

Since the very beginning, the focus of the *e-p* and *e-A* colliders studies has centered on achieving ultra-high luminosity and higher center-of-mass energy (CME). The eRHIC and ELIC machines consider their operation at the CME area of 20÷100 GeV, with luminosities ranging in 10^{32}÷10^{34} cm^{-2}s^{-1} values. Compared to the other machines, the LHeC provides the unique possibility of exploring *e-p* collisions in the TeV center of mass regime. The LHeC will collide the 7 TeV protons circulating in the LHC, therefore representing an interesting possibility for a further exploitation of the existing LHC infrastructure investment, with a high energy *e*-beam at a single collision point. As a result of the combination of SC accelerating structures and the energy recovery technique, a luminosity at least 2 orders of magnitude greater than the one achieved by HERA can be reached. The proposed machine layout consists of a 500 MeV polarized injector, two CW 10 GeV SC linacs and a recirculator system. Each beam recirculates up to 3 times through both linacs to boost the energy to 60 GeV. As the beam is focused and collided, it is bent by 180°, and then it is sent back through the first linac, at a decelerating phase. During deceleration the energy stored in the beam is converted to RF energy and the final beam, at its original injection energy, is directed to a beam dump. The baseline 60 GeV ERL option proposed can give an *e-p* luminosity of 10^{33} cm^{-2}s^{-1} (extensions to 10^{34} cm^{-2}s^{-1} and beyond are being considered), a beam current of 6.4 mA, with less than 100 MW total electrical power required.

* alessandra.valloni@cern.ch

Copyright © 2013 CC-BY-3.0 and by the respective authors

ISBN 978-3-95450-138-0

COLLIMATION WITH HOLLOW ELECTRON BEAMS: A PROPOSED DESIGN FOR THE LHC UPGRADE*

G. Stancari†, V. Previtali, A. Valishev, Fermilab, Batavia, IL 60510, USA
R. Bruce, S. Redaelli, A. Rossi, B. Salvachua Ferrando, CERN, Geneva, Switzerland
V. Moens, EPFL, Lausanne, Switzerland

Abstract

Collimation with hollow electron beams is a technique for halo removal in high-power hadron beams. The concept was tested experimentally at the Fermilab Tevatron collider using a hollow electron gun installed in one of the Tevatron electron lenses. Within the US LHC Accelerator Research Program and the European HiLumi LHC Design Study, we are investigating the applicability of this technique to the Large Hadron Collider and a conceptual design is being developed. We review some of the main topics related to this study: motivation; halo removal processes; development of hollow electron guns; effects on the proton beam core; and integration in the LHC machine.

INTRODUCTION

Hollow electron beam collimation is a new technique for beam collimation and halo scraping [1, 2, 3]. In a hollow electron beam collimator, a magnetically confined, pulsed, low-energy (a few keV) electron beam with a hollow current-density profile overlaps with the circulating beam over a short section of the ring. If the electron distribution is axially symmetric, the beam core is unperturbed, whereas the halo experiences smooth and tunable nonlinear transverse kicks. The electron beam is generated by a hollow cathode and transported by strong solenoidal fields. The size, position, intensity, and time structure of the electron beam can be controlled over a wide range of parameters.

The technique still relies on robust conventional collimators to absorb particles, but it has several features that can complement a classic multi-stage collimation system. In the case of high-power proton beams, for instance, scraping is smooth, controllable, and the issues of material damage and electromagnetic impedance of the collimator jaws are mitigated. In addition, a depletion zone is generated between the proton beam core and the collimator edges, making local energy deposition less sensitive to beam jitter, collimator movements, orbit and tune adjustments, or fast failures in the case of crab-cavity operation. In the case of ion collimation, it may be possible to reduce uncontrolled losses due to fragmentation. Hollow electron beam collimation is also being evaluated in comparison with other halo scraping techniques, such as tune modulation [4].

Hollow electron beam collimation is based on the technology of electron cooling and electron lenses. Electron lenses were developed for beam-beam compensation in colliders [5], enabling the first observation of long-range beam-beam compensation effects [6]. They were used for many years during regular Tevatron collider operations for cleaning uncaptured particles from the abort gap [7]. Thanks to the reliability of the hardware, one of the two Tevatron electron lenses could be used for experiments on head-on beam-beam compensation in 2009 [8], and for exploring hollow electron beam collimation in 2010–2011 [2, 3]. Electron lenses for beam-beam compensation were built for the Relativistic Heavy Ion Collider (RHIC) at Brookhaven National Laboratory and are currently being commissioned [9].

The Tevatron experiments on hollow electron beam collimation were conducted on antiprotons, mainly at the end of regular collider stores. In some cases, the electron beam was turned on for the whole duration of the fill. Because of the flexible pulsing pattern of the high-voltage modulator [10], the electron beam could be synchronized with a subset of bunches, providing a direct comparison with the unaffected beam.

The technique may provide a unique option to complement the LHC collimation system, but extending it from one machine to another is not trivial. To study these issues, a conceptual design of hollow electron beam collimation for the LHC upgrade is being developed within the US LHC Accelerator Research Program (LARP) and the European FP7 HiLumi LHC Design Study. If approved by the CERN management, this may then develop into a technical design in 2014, with the goal to build the devices in 2015–2017 and install them during the next long LHC shutdown, currently scheduled for 2018. In case of a resource-limited timeline, installation during the following long shutdown in 2022 is also an option.

HALO SCRAPING

For scraping the halo of a 7-TeV proton beam, we envision the inner radius of the electron beam to be placed between about 4σ and 6σ of the LHC proton rms beam size $\sigma = 0.32$ mm. This size is derived from the nominal normalized rms emittance $\varepsilon = 3.75\ \mu$m and the typical amplitude function at the candidate locations, $\beta = 200$ m. Scraping of elliptical proton beams is possible by displac-

* Fermilab is operated by Fermi Research Alliance, LLC under Contract No. DE-AC02-07CH11359 with the United States Department of Energy. This work was partially supported by the US DOE LHC Accelerator Research Program (LARP) and by the European FP7 HiLumi LHC Design Study, Grant Agreement 284404. Report number: FERMILAB-CONF-13-355-APC.

† Email: ⟨stancari@fnal.gov⟩.

ISBN 978-3-95450-138-0

Copyright © 2013 CC-BY-3.0 and by the respective authors

COMMISSIONING RHIC'S ELECTRON LENS *

X. Gu#, Z. Altinbas, M. Anerella, D. Bruno, M. Costanzo, W.C. Dawson, A.K. Drees, W. Fischer, B. M. Frak, D.M. Gassner, K. Hamdi, J. Hock, L.T. Hoff, A.K. Jain, J. Jamilkowski, R. Lambiase, Y. Luo, M. Mapes, A. Marone, C. Mi, R. Michnoff, T. Miller, M. Minty, C. Montag, S. Nemesure, W. Ng, D. Phillips, A.I. Pikin, S.R. Plate, P. J. Rosas, J. Sandberg, P. Sampson, L. Snydstrup, Y. Tan, R. Than, C.W. Theisen, P. Thieberger, J. Tuozzolo, P. Wanderer, and W. Zhang

Brookhaven National Laboratory, Upton, NY 11973

Abstract

In the 2013 RHIC polarized-proton run, it was found that the intensity of the RHIC bunch had reached a limit due to the head-on beam-beam interaction at intensity of $2x10^{11}$, as we expected from our simulations [1]. To overcome this limitation, we have planned to implement two electron lenses for beam-beam compensation. During and after the 2013 RHIC run, some e-lens systems were commissioned. The effect of the e-lens warm solenoids on the protons orbit was observed and corrected by orbit feedback. The blue electron-lens system was fully tested, except for the superconducting magnet; the electron beam was propagated from the gun to the collector, and most of the instrumentation for the blue e-lens was commissioned. The straightness of the superconducting solenoid #2 field was measured for the first time. The installation of the yellow e-lens system and two superconducting magnets are underway.

INTRODUCTION

Figure 1 schematically depicts the layout of the electron lens that was used during the 2013 run (A), and will be implemented for the upcoming 2014 run (B).

During the 2013 run, all e-lens warm magnets [2, 3] were ready and tested with proton beam; we placed the superconducting solenoid #1 on the yellow e-lens side and replaced the blue superconducting solenoid with a spare EBIS superconducting solenoid, which was operated at 3T. We tested the blue e-lens system with the electron beam.

For the 2014 run (Figure 1 B), the yellow e-lens system will also be available and the two e-lens systems will be ready for commissioning.

For commissioning the e-lens during the 2013 255 GeV polarized proton run, we first commissioned a new e-lens lattice [4]; then, we studied the effects of e-lens magnetic field on the proton beam with the e-lens warm solenoids. We found that when the currents from the warm solenoids were ramped up, there were some effects on the beam

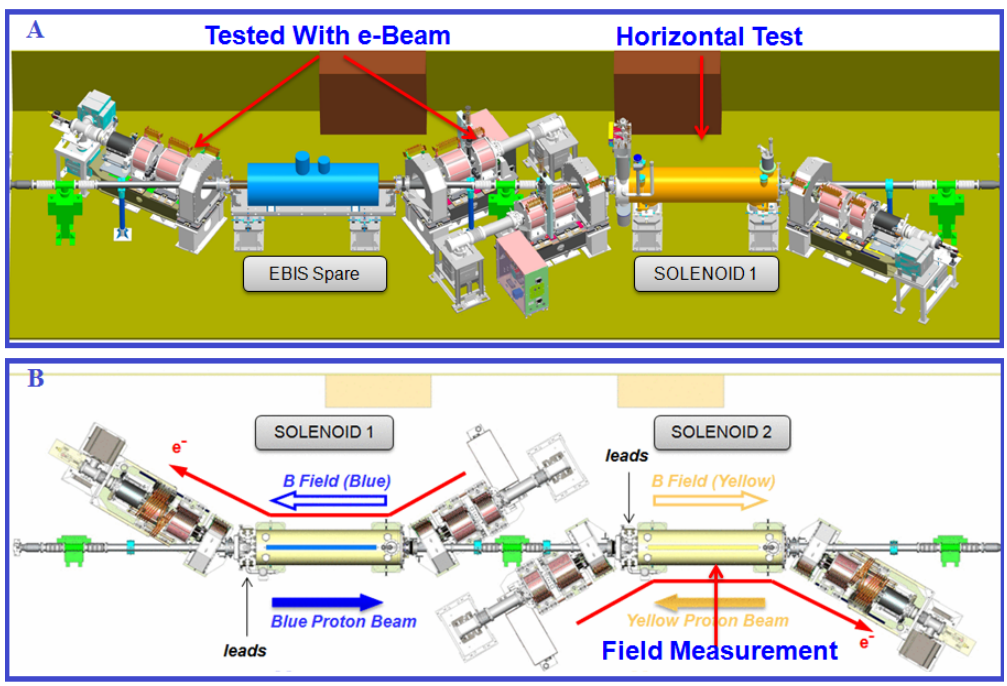


Figure 1: Schematic depictions of the layout of the electron lens during the 2013 run (upper) and the 2014 run (lower).

* Work supported by Brookhaven Science Associates, LLC under Contract No. DE-AC02-98CH10886 with the U.S. Department of Energy

#xgu@bnl.gov

Copyright © 2013 CC-BY-3.0 and by the respective authors

HIGH PRESSURE GAS-FILLED RF CAVITIES FOR USE IN A MUON COOLING CHANNEL

B. Freemire*, P.M. Hanlet, Y. Torun, IIT, Chicago, IL 60616, USA
M. Chung, M.R. Jana, M. Leonova, A. Moretti, T. Schwarz, A.V. Tollestrup, K. Yonehara, FNAL, Batavia, IL 60510, USA
R.P. Johnson, Muons, Inc., Batavia, IL 60510, USA
M.G. Collura, Politecnico di Torino, Torino, Italy

Abstract

A high pressure hydrogen gas-filled RF (HPRF) cavity can operate in the multi-Tesla magnetic fields required for a muon accelerator cooling channel. A beam test was performed at the Fermilab MuCool Test Area by sending a 400 MeV proton beam through an 805 MHz cavity and quantifying the effects of the resulting plasma within the cavity. The resulting energy loss per electron-ion pair produced has been measured at 10^{-18} to 10^{-16} J every RF cycle. Doping the hydrogen gas with oxygen greatly decreases the lifetime of an electron, thereby improving the performance of the HPRF cavity. Electron lifetimes as short as 1 ns have been measured, and electron-ion recombination rates are on the order of 10^{-6} cm^3/s. The recombination rate of positive and negative ions in the cavity has been measured on the order of 10^{-8} cm^3/s. Extrapolation in both gas pressure and beam intensity are required to obtain Muon Collider parameters, however the results indicate HPRF cavities can be used in a muon accelerator cooling channel.

INTRODUCTION

A recent White Paper submitted to the 2013 U.S. Community Summer Study of the Division of Particles and Fields by the U.S. Muon Accelerator Program (MAP) outlines a staged Muon Accelerator facility based at Fermilab [1]. The report outlines two main programs; a Neutrino Factory (NF), and a Muon Collider (MC). For the case of a MC, a Higgs Factory and multi-TeV collider are described. Because muons are created with a large initial phase space, the colliders requires significant (roughly six orders of magnitude) cooling.

The only cooling method that can work within the muon's lifetime is ionization cooling, and a so-called Helical Cooling Channel (HCC) has been proposed to do so [2]. The HCC is composed of normal conducting RF cavities arranged in a helix within a solenoidal magnetic field (see Fig. 1 & 2). The RF cavities are filled with a high pressure gas to allow operation in multi-Tesla magnetic fields. A series of six HCC cells, approximately 230 m long, reduces the 6D emittance by a factor of 175,000 [3].

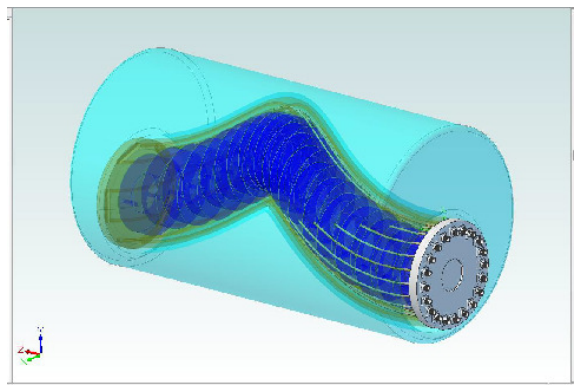


Figure 1: The 2D side view of one cell of the HCC, with components labeled. RF power is fed through the end. The solenoid coils are thermally isolated from the RF cavities [4].

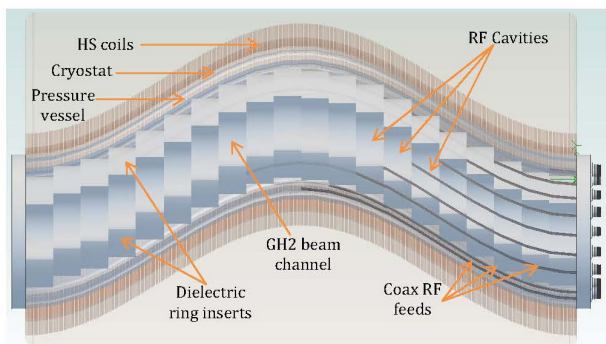


Figure 2: The 3D view of one cell of the HCC [4].

VALIDATION OF HIGH PRESSURE CAVITIES

A high pressure gas-filled RF (HPRF) cavity has been demonstrated to work in an external 3 T magnetic field without an ionizing beam [5, 6]. To validate its use in a HCC, a beam test using the 400 MeV Fermilab linac proton beam was performed at the MuCool Test Area (MTA). The cavity's performance using various beam intensities, gas pressures, dopant concentrations, and electric fields were studied with and without a 3 T magnetic field. Figure 3 shows a schematic of the experimental setup.

As the beam passes through the cavity, it ionizes the gas.

* freeben@iit.edu

ISBN 978-3-95450-138-0

Copyright © 2013 CC-BY-3.0 and by the respective authors

TEST OF OPTICAL STOCHASTIC COOLING IN THE IOTA RING*

V. A. Lebedev# and Yu. Tokpanov, FNAL, Batavia, IL 60510, USA
M. S. Zolotorev, LBNL, Berkeley, CA 94720, USA

Abstract

A new 150 MeV electron storage ring is being built at Fermilab. The construction of a new machine pursues two goals a test of highly non-linear integrable optics and a test of optical stochastic cooling. This paper discusses details of OSC arrangements, choice of major parameters of the cooling scheme and incoming experimental tests of the optical amplifier prototype which uses highly doped Ti-sapphire crystal as amplification medium.

INTRODUCTION

The stochastic cooling has been successfully used in a number of machines for particle cooling and accumulation. Cooling rates of few hours required for luminosity control in hadron colliders cannot be achieved in microwave frequency range (~10^9-10^{10} Hz) usually used in stochastic cooling. Large longitudinal particle density, N/σ_s, used in such colliders requires an increase of cooling bandwidth by a few orders of magnitude. To achieve such increase one needs to make a transition to much higher frequencies. A practical scheme operating in the optical frequency range was suggested in Ref. [1]. The method is named the optical stochastic cooling (OSC). It is based on the same principles as the stochastic cooling but uses much higher frequencies. Thus it is expected to have a bandwidth of ~10^{14} Hz and can create a way to attain required damping rates. Fermilab plans to make an experimental test of the OSC in IOTA ring [2].

In the OSC a particle emits e.-m. radiation in the first (pickup) wiggler. Then, the radiation amplified in an optical amplifier (OA) makes a longitudinal kick to the same particle in the second (kicker) wiggler as shown in Fig. 1. A magnetic chicane is used to make space for the OA and to delay a particle so that to compensate for a delay of its radiation in the OA resulting in simultaneous arrival of the particle and its amplified radiation to the kicker wiggler. A particle passage through the chicane has a coordinate-dependent correction of particle longitudinal position which, consequently, results in a correction of relative particle momentum, $\delta p/p$, with amplitude ξ_0 so that:

$$\delta p / p = -\xi_0 \sin\left(k\,\Delta s\right) . \qquad (1)$$

Here $k = 2\pi/\lambda$ is the radiation wave-number,

$$\Delta s = M_{51}x + M_{52}\theta_x + M_{56}\left(\Delta p / p\right) , \qquad (2)$$

is the particle displacement on the way from pickup to kicker relative to the reference particle which experiences zero displacement and obtains zero kick, M_{5n} are the elements of 6x6 transfer matrix from pickup to kicker, x, θ_x and $\Delta p/p$ are the particle coordinate, angle and relative momentum deviation in the pickup.

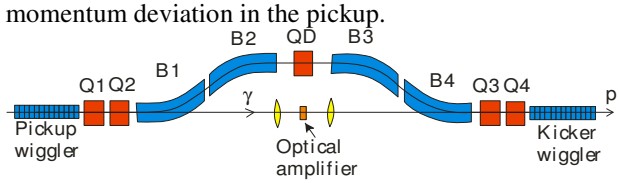


Figure 1: OSC schematic.

For small amplitude oscillations the horizontal and vertical cooling rates per turn are [3]:

$$\begin{bmatrix}\lambda_x\\ \lambda_s\end{bmatrix} = \frac{k\xi_0}{2}\begin{bmatrix}M_{56}-\tilde{M}_{56}\\ \tilde{M}_{56}\end{bmatrix} , \qquad (3)$$

where $\tilde{M}_{56} = M_{51}D_p + M_{52}D'_p + M_{56}$ is the partial slip-factor introduced so that for a particle without betatron oscillations and with momentum deviation $\Delta p/p$ the longitudinal displacement relative to the reference particle on the way from pickup to kicker is equal to $\tilde{M}_{56}\Delta p / p$, and D and D' are the dispersion and its derivative in the pickup. We assume that there is no x-y coupling in the chicane. Introduction of x-y coupling outside the cooling area allows a redistribution of the horizontal damping rate between two transverse planes. The sum of damping rates is: $\Sigma\lambda_n = k\xi_0 M_{56}/2$.

A non-linear dependence of kick on Δs in Eq. (1) results in a dependence of damping rates on amplitudes [3]:

$$\begin{aligned}\lambda_x(a_x,a_s) &= \left(2\,\mathrm{J}_0(a_s)\,\mathrm{J}_1(a_x)/a_x\right)\lambda_x \quad ,\\ \lambda_s(a_x,a_s) &= \left(2\,\mathrm{J}_0(a_x)\,\mathrm{J}_1(a_s)/a_s\right)\lambda_s \quad ,\end{aligned} \qquad (4)$$

where a_x and a_s are the amplitudes of longitudinal particle motion due to betatron and synchrotron oscillations expressed in the units of e.-m. wave phase:

$$\begin{aligned}a_x &= k\sqrt{\varepsilon_1\left(\beta_p M_{51}{}^2 - 2\alpha_p M_{51}M_{52} + \left(1+\alpha_p{}^2\right)M_{52}{}^2\right)},\\ a_p &= k\left|\tilde{M}_{51}\right|\left(\Delta p / p\right) \quad ,\end{aligned} \qquad (5)$$

ε_1 is the Courant-Snyder invariant of a particle, and $(\Delta p/p)$ is the amplitude of particle synchrotron motion. As one can see from Eq. (4) each damping rate changes its sign if any of amplitudes exceeds the first root, μ_0, of the Bessel function $\mathrm{J}_0(x)$. That determines that at the cooling area boundary $a_x=\mu_0$ or $a_y=\mu_0$ where $\mu_0\approx2.405$. That yields the cooling area boundaries:

$$\begin{aligned}\varepsilon_{\max} &= \frac{\mu_0{}^2}{k^2\left(\beta_p M_{51}{}^2 - 2\alpha_p M_{51}M_{52} + \left(1+\alpha_p{}^2\right)M_{52}{}^2\right)},\\ \left(\Delta p / p\right)_{\max} &= \mu_0 \Big/ \left(k\left|\tilde{M}_{51}\right|\right) \quad .\end{aligned} \qquad (6)$$

Although M_{56} and, consequently, the sum of damping rates depend only on focusing inside the chicane, $\tilde{M}_{56}$ and the ratio of damping rates depend on the dispersion at the chicane beginning, *i.e.* on the ring dispersion. Eq. (3) yields the ratio of damping rates,

*Work supported by Fermi Research Alliance, LLC, under Contract No. DE-AC02-07CH11359 with the United States Dep. of Energy
#val@fnal.gov

Copyright © 2013 CC-BY-3.0 and by the respective authors

FREE-ELECTRON LASERS IN THE SOFT X-RAY REGIME*

J. N. Corlett#, LBNL, Berkeley, CA, USA

Abstract

X-ray science in imaging, structure determination, and spectroscopy, as well as diffraction/scattering, requires intense ultrafast pulses in the soft X-ray range, uniquely provided by free electron lasers (FELs). In addition to operational soft X-ray FEL facilities, there are FEL construction projects under way that include soft X-ray laser capabilities, and planned facilities with novel capabilities. This paper provides a review of the exciting field of existing and planned soft X-ray FELs with emphasis on new schemes and new technologies to achieve better performance.

SCIENCE NEEDS FOR SOFT X-RAY FELS

The scientific innovation expected from the construction and operation of X-ray FEL facilities lies in their ability to provide tools that offer extreme spatial, temporal, and energy resolution. Properties of FEL sources are expected to include the ability to reach to the ultrafast timescales of atomic motion (about 100 fs), spin motion (down to about 1 fs), and electronic motion (down to attoseconds), the spatial scale of the atomic bond (down to Angstroms), and energy resolution on the scale of the bond that holds electrons in correlated motion with near neighbors (~10 meV and greater). X-ray FEL sources offer unique capabilities to combine information on atomic length scales with data on full-scale functional systems under realistic operational conditions. In addition, these sources have an intensity and brightness needed to observe the subtlest of nature's secrets at these frontier space, time, and energy scales, and with elemental specificity.

Critical X-ray science in imaging, structure determination, and spectroscopy needs new capabilities in the soft X-ray range, accessing K- and L-edges of the earth-abundant elements, as well as diffraction/scattering in the few to several keV photon energy range. These scientific requirements give rise to the following desirable FEL performance features:

- X-ray time structure
  - Control of longitudinal phase space, with Fourier-transform-limited pulse structure extending from ~100 fs pulses with ~10 meV bandwidths to sub-femtosecond pulses with ~10 eV bandwidths
  - Control of longitudinal pulse shape, amplitude and phase
  - Synchronization and full integration with conventional pulsed laser sources
  - High repetition rate with regularly spaced pulses
- Full transverse coherence
  - Requirements set by real-space imaging, diffractive imaging, and photon-correlation spectroscopy
  - Optical systems to preserve and exploit transverse coherence
- High peak flux and brightness
  - Requirements set by non-linear effects in materials
- High average flux and brightness
  - Short-pulse sources with high repetition rates (100 kHz or greater) providing average flux and/or brightness substantially beyond existing sources
- Tunability, polarization control, and extended photon energies
  - Tunability throughout the transition-metal L-edges and polarization control and modulation
  - Two-color capability for non-linear spectroscopies and X-ray pump/X-ray probe
- High degree of amplitude and wavelength stability
- Multiple simultaneous users

SOFT X-RAY FEL OVERVIEW

High-gain single pass FELs at wavelengths in the EUV and shorter have been operating as photon science user facilities for almost a decade – the TESLA Test Facility (TTF) became the Free Electron Laser in Hamburg (FLASH) in 2003, and user operations began in 2005 with lasing at 25 nm [1]. FLASH now operates at wavelengths in the water-window (~4 nm) and longer. The LCLS at SLAC is the world's first hard X-ray FEL [2], and also operates in the soft X-ray regime with wavelength ~4.5 nm and shorter [3]. Both of these facilities currently operate in SASE mode in the soft X-ray range (although the LCLS also offers a hard X-ray self-seeded mode [4]). FERMI@elettra is a seeded FEL facility, offering improved temporal coherence, with tunable user beam currently offered down to 20 nm [5]. The SACLA facility currently operates the shortest wavelength FEL, in SASE mode [6].

Upgrades of these facilities are planned or are in progress and include development of soft X-ray capabilities, in capacity (adding FEL beamlines), and also in capability by extending the tuning range, seeding (either self-seeding or external laser-seeding) and offering tunable undulators and new operating regimes of pulse duration and time structure. The FERMI team is now commissioning a 2-stage harmonic cascade to reach into the water window [7]. Upgrade plans at SACLA include the re-location of the SCSS test facility as a soft X-ray FEL driver [8]. FLASH-II will add variable-gap undulators in a separate beamline driven by the existing linac, and seeding. LCLS-II is planned to provide self-seeded capability from 0.25–5 nm, using a new CW superconducting linac.

The European XFEL [9], SwissFEL [10], and Korean PAL-XFEL [11] facilities are under construction, and

*Work supported by the Director, Office of Science, of the U.S. Department of Energy under Contract No. DE-AC02-05CH11231
#jncorlett@lbl.gov

Copyright © 2013 CC-BY-3.0 and by the respective authors

ISBN 978-3-95450-138-0

MACHINE BASED OPTIMIZATION USING GENETIC ALGORITHMS IN A STORAGE RING *

K. Tian#, J. Safranek, Y. Yan, SLAC, Menlo Park, CA 94025

Abstract

In this paper, instead of applying GA in the conventional numerical calculations, we present a successful experimental demonstration of implementing GA in real machine based optimization. We conduct the optimization of the average vertical beam size of the SPEAR3 storage ring using GA. Beam loss rate is chosen as the sole objective function because it is inversely proportional to the vertical beam size and can be measured quickly in SPEAR3. The decision variables are the strengths of SPEAR3 skew quadrupoles, by varying which we can change both the betatron coupling and the vertical dispersion to search for the minimum beam size. The results in this paper can shed light on new applications of GAs in particle accelerator community, for example, optimizing the luminosity of the high energy collider in real time.

INTRODUCTION

GAs have been successfully applied in areas such as designing injector systems [1], diagnosing and designing accelerating cavities [2], and optimizing beam optics design in storage rings [3]. One core process of the GA is to evaluate objective functions from a given set of decision variables, i.e. knobs to be adjusted for optimum search. In spite of various approaches used in previous efforts, all of them evaluate the objective functions based on numerical simulations using particle tracking codes. In principle, when the optimization targets or their correlating parameters are measurable experimentally, it is possible to use the real machine as the function evaluator to directly measure the objective functions, rather than using a computer model. Compared to the simulation based optimization, the machine based optimization has the most accurate representation of the machine condition that includes all lattice errors. Moreover, when the physics quantities of interest can be measured quickly in experiment but cost long time to be calculated in simulations, the machine based optimization will excel in speed too. One example of such quantity is the luminosity of the high energy colliders. In SPEAR3, we have identified a similar parameter of interest that can be measured nearly instantaneously. In this paper, we report an innovative application of GA to minimize the average vertical beam size of the SPEAR3 storage ring in real time. To construct the GA, we use 13 skew quadrupoles in the storage ring as decision variables and the measured beam loss rates as the objective function. The results can serve as a proof of principle for using GA in machine based optimization.

*Work supported by U.S. Department of Energy Contract No. DE-AC02-76SF00515

#ktian@slac.stanford.edu

MINIMIZE THE VERTICAL BEAM SIZE

In a storage ring, circulating electrons are lost due to collisions with gas molecules and electron-electron scattering inside the bunch, where the latter is known as the Touschek effect [4]. As in most modern electron storage rings, the loss of stored beam current in SPEAR3 is mainly due to the Touschek scattering. Thus, one can derive the simple scaling law between beam loss rates *dI/dt* and vertical beam size as shown below:

$$\frac{\left|\frac{dI}{dt}\right|}{I^2} \propto \frac{1}{\bar{\sigma}_y}, \qquad (1)$$

where I is the stored current and $\bar{\sigma}_y$ is the average vertical beam size.

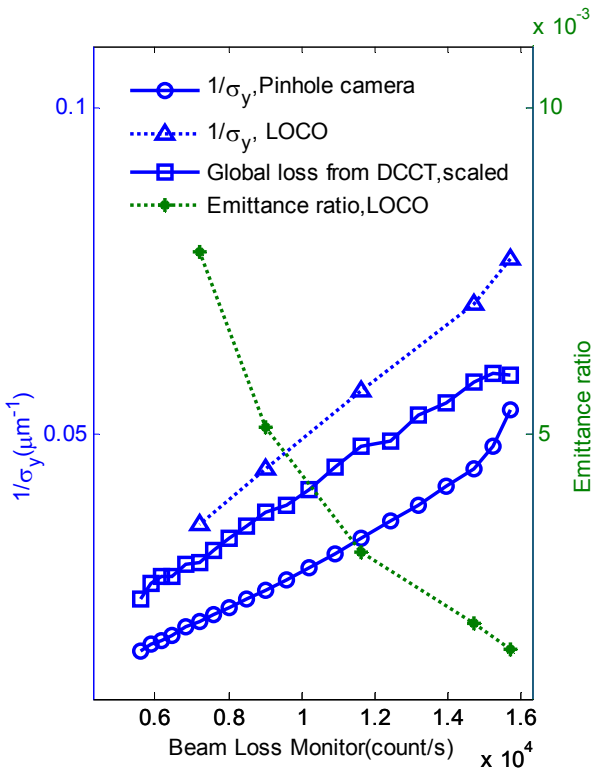


Figure 1: Experiment verification of Eq. (1).

In SPEAR3, Eq. (1) can be directly validated by experimentally measured data. During the experiment, 100 mA beam is filled in SPEAR3. We achieve 20 conditions in the ring by varying all skew quads in a fixed step size. For each condition, we measure the vertical beam size at 1Hz with an x-ray pinhole camera [5]. The beam loss rate is recorded instantaneously at 1Hz by a beam loss monitor (BLM) [6], installed next to the SPEAR3 beam horizontal scraper. The scraper is inserted close to the beam in order to capture nearly all of the beam loss at one point. The global beam loss is also

Copyright © 2013 CC-BY-3.0 and by the respective authors

SUCCESSFUL COMPLETION OF THE ALS BRIGHTNESS UPGRADE*

C. Steier†, A. Madur, B. Bailey, K. Berg, A. Biocca, A. Black, P. Casey, D. Colomb, B. Gunion, N. Li, S. Marks, H. Nishimura, C. Pappas, K. Petermann, G. Portmann, S. Prestemon, A. Rawlins, D. Robin, S. Rossi, T. Scarvie, R. Schlueter, C. Sun, H. Tarwaneh, W. Wan, E. Williams, LBNL, Berkeley, CA 94720, USA;
L. Yin, Q. Zhou, J. Jin, J. Zhang, C. Chen, Y. Wen, J. Wu, SINAP, Shanghai, China

Abstract

The Advanced Light Source (ALS) at Berkeley Lab is one of the brightest sources for soft x-rays worldwide. A multiyear upgrade of the ALS is underway, which includes new and replacement x-ray beamlines, a replacement of many of the original insertion devices and many upgrades to the accelerator. The accelerator upgrade that affects the ALS performance most directly is the brightness upgrade, which reduced the horizontal emittance from 6.3 nm to 2.0 nm (2.5 nm effective), resulting in one of the lowest horizontal emittances of operating light sources. Magnets for this upgrade were installed in late 2012 and early 2013 followed by successful commissioning and user operation with 2.0 nm horizontal emittance.

INTRODUCTION

Over the years, the brightness of the ALS has been steadily improved, keeping the ALS the brightest third generation light source in the energy range below 1 keV (see Fig. 1). The upgrades included improvements in beam parameters (current and emittance), addition of new radiation producing devices (Superbends and advanced insertion devices) as well as stability improvements going hand-in-hand with the brightness improvements.

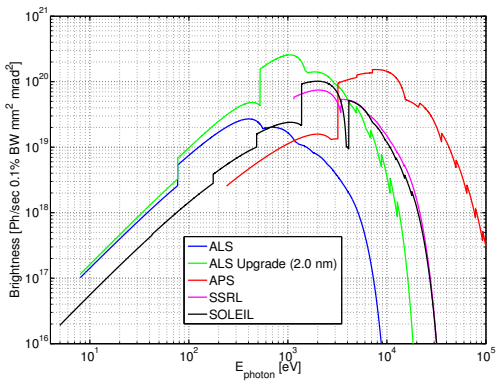


Figure 1: Comparison of the ALS brightness before and a after the low emittance upgrade with several other existing light sources.

The recent low emittance upgrade increased the brightness of the ALS by about a factor three in the bending magnet beamlines, and by about a factor two in the existing insertion device beamlines. The upgrade also opens the door to a potential further increase of the brightness by potentially implementing reduced horizontal beta functions in some straights.

BRIGHTNESS UPGRADE LATTICE

The ALS lattice has a triple bend achromat structure, with a fixed, large defocusing gradient in the bending magnets. Originally, there were only 2 families of sextupoles, with 4 sextupoles in each arc. An attractive set of possible upgrade lattices was found with higher straight section dispersion and an integer tune two units higher than the old lattice [1]. Those lattices have natural emittances of about 2 nm, compared to the more than 6 nm of the old lattice and horizontal beta functions of about 20 m in the straights.

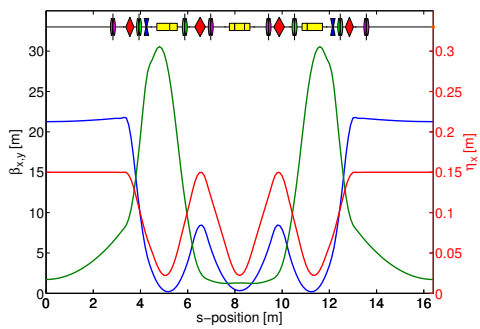


Figure 2: ALS upgrade lattice with 2.0 nm natural emittance at 1.9 GeV.

Later on, more systematic techniques [2, 3, 4] were used to find the global optimal lattices in terms of emittance or brightness. In those studies an additional family of low emittance lattices was found with very small horizontal beta function (order of 0.5 m) in the straights at much higher phase advance, which increase the brightness by better matching to the photon diffraction ellipse. Such low beta straights are still under investigation as an insertion for selected straights.

The high-beta lattices are within the range of the existing quadrupole magnets. However, the original sextupoles would not have been strong enough and the dynamic aperture would have been very poor. Both challenges were overcome with the addition of sextupoles in the straight sections.

* The Advanced Light Source is supported by the Director, Office of Science, Office of Basic Energy Sciences, of the U.S. Department of Energy under Contract No. DE-AC02-05CH11231.

† CSteier@lbl.gov

Copyright © 2013 CC-BY-3.0 and by the respective authors

ISBN 978-3-95450-138-0

STUDIES OF THE LOW ENERGY PROTON BEAM HALO EXPERIMENT

Hongping Jiang#,Shinian Fu, Jun Peng, Tao Huang, Fang Li, Peng Li, Huachang Liu, Cai Meng, Ming Meng, Zhencheng Mu, Huafu Ouyang, Peng Chen, Linyan Rong, Biao Sun, jianmin Tian, Biao Wang, Shengchang Wang, Wenqu Xin, Taoguang Xu, Lei Zeng, Fuxiang Zhao
Institute of High Energy Physic, Chinese Academy of Sciences, Beijing 100049, China

Abstract

We report measurements of transverse beam phase-space properties and transverse beam halo in mismatched proton beams in 28-quadrupole FODO transport channel following the 3.5-MeV IHEP RFQ. Beam profiles in both transverse planes are measured using beam-profile diagnostic. The gradients of the first four quadrupoles can be independently adjusted to match and mismatch the RFQ output beam into beam-transport channel. We also compare the measured beam profile with the 3-D nonlinear macro-particle code IMPACT simulations in the beam halo experiment. Quadrupole scans were used to determinate the transverse properties of the RFQ output beam. The Gaussian distribution was chosen as the initial particle distribution, which is well fit with the measured beam-core profile. We match the beam using the least-squares fitting procedure that adjusted the first four matching quadrupoles to produce equal rms beam size in the last six wire scanners. Simulations had been fairly successful in reproducing the core of the measured matched beam profiles, but there are some differences in the mismatched beam profiles.

INTRODUCTION

The interest in understanding the formation of a halo distribution around an intense proton beam has increased in recent years with the development of new applications requiring such beam, because the beam halo is a major source of beam loss and radioactivation in high-power and high-current proton linacs. Beam mismatch have been identified as the major source of the halo formation [1], space-charge forces in mismatched beam are the main source of beam halo in high current proton beams. Having well matched beam conditions is a fundamental requirement for the operation of proton linacs. And the macroparticle simulation method is widely used in modern accelerator design and beam dynamics studies [2].

In this paper, we present measurements of transverse beam phase-space properties and comparisons of simulation results using the code IMPACT [3] with experimental measurements of the beam profiles in a high-current matched and mismatched proton beam. The beam profiles were measured by the wire-scanners. The transport line was installed after the radio frequency quadrupole (RFQ) accelerator designated for ADS study at the Institute of High Energy Physics (IHEP).

Jianghp@ihep.ac.cn

THE BEAM-CORE MATCHING EXPERIMENT TRANSPORT LINE

The 28-quadrupole beam transport line is installed at the end of the IHEP RFQ, which accelerates the proton beam to 3.54MeV and operates at the frequency of 352MHz. The purpose of this transport line is the experimental study of the beam halo formation and the comparison of the experimental data with the simulations. The block diagram of this transport lattice is shown in Fig. 1. In this line, the first four quadrupoles are independently adjustable to match the beam or to produce mismatches; the last 24 quadrupoles form an FODO lattice.

The transverse beam profiles are measured using beam profile scanners, which consist of wire scanners for measurement of the dense beam core and halo scrapers for measurement of the outer halo regions [4]. In the beam halo experiment, we use the wire scanner to measure the beam profiles, and the wire scanner can provide intensity measurement over a dynamic range of about 10^3. The philosophy of the scanner placement is the following: the first group of two scanners is placed after quadrupole 5 and 6, they separately measure the beam vertical and horizontal profiles which are used to characterize the proton beam output from the RFQ. To observe beam profiles of matched or mismatched case, another two groups of scanners with 6 scanners for each group are placed after quadrupole 17 to 28, covering about two mismatch oscillations.

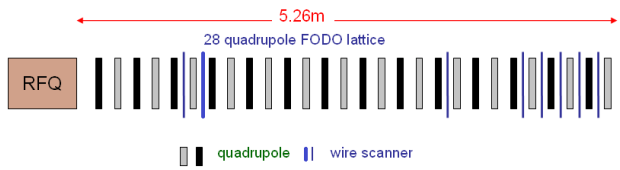


Figure 1: Block diagram of beam-core matching experiment transport line.

CHARACTERIZING THE PROTON BEAM OUTPUT FROM THE RFQ

In order to know the details of the beam, quadrupole scans and multi-wire scanner were used to characterize the transverse beam output from the IHEP RFQ [5]. In the scanning process, we kept the other three quadrupoles the same gradient 25.40T/m and obtained the Gaussian-like beam distributions with different rms radius compared with simulations shown in the Table 1 and Figure 2, the

Copyright © 2013 CC-BY-3.0 and by the respective authors

LONGITUDINAL BEAM DYNAMICS AND LLRF REQUIREMENTS FOR THE PROJECT X PULSED LINAC*

A. Vivoli†, G. I. Cancelo, B. Chase, N. Solyak, P. Varghese, FNAL, Batavia, IL 60510, USA

Abstract

Project X is a high intensity proton facility being developed to support the intensity frontier physics program over the next two decades at Fermilab. The Reference Design [1] is based on a continuous wave (CW) superconducting (SC) 3 GeV linac providing up to 1 and 3 MW of beam power at 1 and 3 GeV respectively, while a superconducting pulsed linac provides acceleration of roughly 4.3% of the beam delivered from the CW linac to the 8 GeV injection energy of the existing Recycler/Main Injector complex. In this paper we present the results of simulations of longitudinal beam dynamics and Low Level RF (LLRF) control system in the pulsed linac, operated for long pulses in presence of errors and cavity detuning for different RF configurations and settings, and set the requirements for the LLRF necessary to fulfill the specifications of the design.

INTRODUCTION

The pulsed linac is the main part of the third stage of Project X and will accelerate pulses of 4.3 ms duration and 1 mA average current of the H^- beam coming from the 3 GeV linac (and downstream transport beamlines) up to 8 GeV at a repetition rate of 10 Hz. The constraints on the output beam parameters come from the acceptance of the downstream 8 GeV transport line and efficient injection in the Recycler/Main Injector ring. The lattice of the pulsed linac is studied with computer codes for accelerator optics and particle tracking simulating a single bunch. Once a configuration and set of parameters that provide acceptable output are found, multi-bunch simulations are performed to study the behavior of the system (accelerator and beam) during the length of the pulse and in multi-pulse mode. The focus of this study is on the RF system and longitudinal beam dynamics, neglecting beam optics and effects from elements of the beamline except for the accelerating cavities.

SINGLE BUNCH SIMULATIONS

Single bunch simulations are performed with the computer code TraceWin [2]. The current lattice of the pulsed linac and simulation results for the bunch envelopes are showed in Fig. 1. The linac is composed of 3 cryo strings of, respectively, 10, 9 and 9 ILC Type-IV cyomodules [3]. Each cryomodule contains 8 ILC 9-cell cavities and a SC quadrupole at the center.

Each cryo string is preceded and followed by a 2.5 m service box and between service boxes of adjacent cryo strings

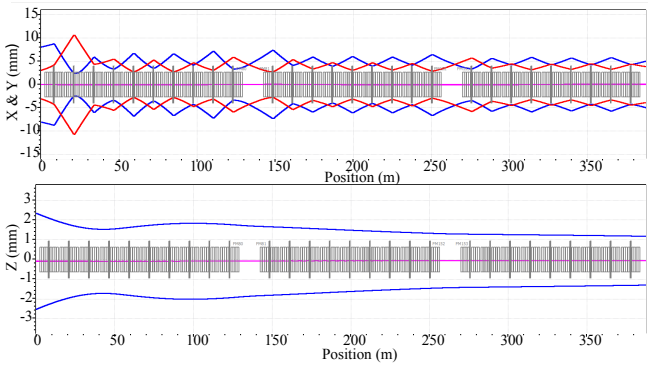


Figure 1: Beam envelopes (3 rms sigmas) in transverse (top) and longitudinal (bottom) coordinate spaces.

7.652 m room temperature areas are placed for beam collimation, diagnostics and maintenance operations. Table 1 shows relevant linac parameters and constraints to be fulfilled.

Table 1: Relevant Linac Parameters and Constraints

Beam Parameter	Initial value	Final value	Requirement
Kinetic Energy (MeV)	3000	8000	8000
Norm. hor. rms emit. (mm mrad)	0.516	0.516	≤ 0.6
Norm. vert. rms emit. (mm mrad)	0.281	0.311	≤ 0.6
Rms bunch length (ps)	2	1.3	≤ 100
Rms energy spread (MeV)	0.9	1.6	≤ 4

MULTI-BUNCH SIMULATIONS

Multi-bunch simulations are carried out employing a MATLAB based code written by the authors. The motivations for running multi-bunch simulations are various:

- To check that the configuration under study can fulfill consistently the specifications of the design during operation in presence of cavity detuning and errors in beam and RF components.
- To set the requirements for parameters of LLRF components to achieve an acceptable performance of the accelerator.

* Work supported by Fermi Research Alliance, LLC under Contract No. De-AC02-07CH11359 with the United States Department of Energy.
† vivoli@fnal.gov

Copyright © 2013 CC-BY-3.0 and by the respective authors

ISBN 978-3-95450-138-0

MULTI-TURN INJECTION OF 50 MEV PROTONS INTO THE CERN PROTON SYNCHROTRON BOOSTER

V. Raginel, E. Benedetto, C. Carli, B. Mikulec, CERN, Geneva, Switzerland

Abstract

Since 1978, Linac2 produces beams of 50 MeV protons with a current around 160 mA, which are injected into the CERN Proton Synchrotron Booster (PSB) with conventional multi-turn injection using a horizontal septum. It is planned to replace Linac2 during a future long stop with a new H^- linac, Linac4, injecting at higher energy (160 MeV) and making use of the modern charge-exchange injection principle. Due to the age of Linac2 and to a delicate vacuum situation the risk of a serious Linac2 breakdown has to be considered. Therefore it is necessary to study if the PSB could produce beams useful for the LHC and other experiments injecting a Linac4 proton beam at 50 MeV with much lower average current compared to Linac2 and without the need for a long installation of the 160 MeV H^- injection hardware. Benchmarking of the PSB injection model with the existing injection system with Linac2 using the ORBIT code has been done for a LHC-type beam and then the injection model was used to estimate the brightness for LHC-type beams that could potentially be reached in one PSB ring with the injection of a Linac4 proton beam at 50 MeV.

INTRODUCTION

The Proton Synchrotron Booster located at CERN, Geneva, Switzerland, is currently boosting protons injected by Linac2 from 50 MeV to 1.4 GeV. It is the second accelerator of the LHC injector chain and consists of four superposed rings. Linac4 is a 160 MeV linac under construction aiming at boosting the performance of the CERN PSB with higher injection energy and replacing the present conventional multi-turn injection of 50 MeV protons with a septum by H^- charge exchange injection. General planning of the CERN complex foresees the connection Linac4 – PSB not before the end of the second LHC long run. In case of a serious breakdown of the presently used Linac2, which is ageing and showing weaknesses in terms of vacuum tightness, it is envisaged to inject 50 MeV proton beams with lower beam current and emittance from Linac4 as emergency scenario.

This work indicates the brightness that can be expected for a LHC beam (LHC-25ns) in the PSB after a multi-turn injection of 50 MeV protons from Linac4. The results are derived from simulations done with ORBIT. The reference parameters of the PSB injection with Linac2 are first used to test the model and then parameters of Linac4 are used as input of the simulation. An optimization of the injection process can be done to obtain an estimate of the highest reachable brightness for the LHC beam.

PSB MULTI-TURN INJECTION

During injection into the PSB, the beam is stacked in horizontal betatron phase-space using a closed orbit bump generated by four slow kickers to bring the stacked beam very close to the injection septum to minimize the transverse emittance of the resulting beam in the PSB. The incoming beam is deflected by the injection septum, which results in an injection with small position and angle errors. Subsequently the bump decreases and the beam moves to the reference closed orbit (see Fig. 1). The injection septum blade has a thickness of 1 mm and is 40 mm away from the closed central orbit.

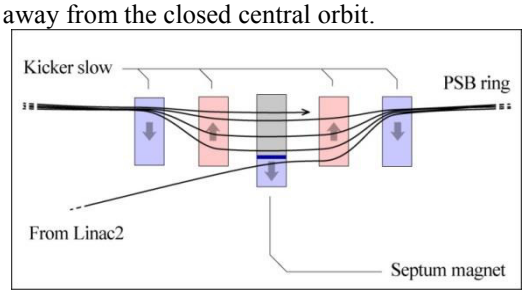


Figure 1: Multi-turn injection principle (after 4 turns).

During operation in order to produce all the required beam types, the following injection parameters can be optimized: the working point at injection, the injection timing and the horizontal and vertical positions and angles of the injected beam.

ORBIT CODE AND PSB MODEL

The ORBIT code (Objective Ring Beam Injection and Tracking) [1] was designed to track macro-particle coordinates through a set of accelerator elements and calculate space charge and other collective effects.

The model of the PSB lattice is composed of bending and quadrupole magnets imported with a special routine from MAD-8 [2] to ORBIT. The horizontal and vertical tune values are fixed in the MAD-8 model. The injection slow kickers are modelled in ORBIT with the ideal bump routine (linear decay of the bump). As ORBIT does not contain a septum module, a foil of thickness null as first element of the lattice and an aperture as last element of the lattice are used to simulate as realistically as possible the injection septum BI.SMH of the PSB [3]. The foil at the beginning of the lattice simulates the septum blade seen by the injected particles and the aperture at the end the septum blade seen by the circulating particles. The transverse space charge is modelled with the 2.5D FFT-PIC (Particle-In-Cell) modules without boundary condition(s). The FFT-PIC is a fast method to calculate transverse space charge, first by binning the

Copyright © 2013 CC-BY-3.0 and by the respective authors

ISBN 978-3-95450-138-0

nuSTORM: NEUTRINOS FROM STORED MUONS *

Alan D. Bross, Fermi National Accelerator Laboratory, Batavia, IL 60510, USA
for the nuSTORM Collaboration

Abstract

Neutrino beams produced from the decay of muons in a racetrack-like decay ring provide a powerful way to study short-baseline neutrino oscillation and neutrino interaction physics. In this paper, I describe the facility, nuSTORM, and show how the unique neutrino beam at the facility will enable experiments of unprecedented precision to be carried out. I will present sensitivity plots that indicated that this approach can provide 10 σ confirmation or rejection of the LSND/MinBooNE results and can be used to perform neutrino interaction measurements of unprecedented precision. The unique ν beam available at the nuSTORM facility has the potential to be transformational in our approach to ν interaction physics, offering a "ν light source" to physicists from a number of disciplines.

INTRODUCTION

The nuSTORM facility has been designed to deliver beams of $\overset{(-)}{\nu}_e$ and $\overset{(-)}{\nu}_\mu$ from the decay of a stored $\mu^{\pm}$ beam with a central momentum of 3.8 GeV/c and a momentum acceptance of 10% [1]. The facility is unique in that it will:

- Allow searches for sterile neutrinos of exquisite sensitivity to be carried out; and
- Serve future long- and short-baseline neutrino-oscillation programs by providing definitive measurements of $\overset{(-)}{\nu}_e N$ and $\overset{(-)}{\nu}_\mu N$ scattering cross sections with percent-level precision;
- Constitute the crucial first step in the development of muon accelerators as a powerful new technique for particle physics.

The nuSTORM facility represents the simplest implementation of the Neutrino Factory concept [2]. In our case, 120 GeV/c protons are used to produce pions off a conventional solid target. The pions are collected with a magnetic horn and quadrupole magnets and are then transported to, and injected into, a storage ring. The pions that decay in the first straight of the ring can yield muons that are captured in the ring. The circulating muons then subsequently decay into electrons and neutrinos. We are using a storage ring design that is optimized for 3.8 GeV/c muon central momentum. This momentum was selected to maximize the physics reach for both ν oscillation and the cross section physics. See Figure 1 for a schematic of the facility.

Muon decay yields a neutrino beam of precisely known flavor content and energy. In addition, if the circulating muon flux in the ring is measured accurately (with beam-current transformers, for example), then the neutrino beam flux is also accurately known. Near and far detectors are placed along the line of one of the straight sections of the racetrack decay ring. Purpose-specific near detectors can be located in the near hall and will measure neutrino-nucleon cross sections and can provide the first precision measurements of ν_e and $\bar{\nu}_e$ cross sections. A far detector at $\simeq$ 2000 m would study neutrino oscillation physics and would be capable of performing searches in both appearance and disappearance channels. The experiment will take advantage of the "golden channel" of oscillation appearance $\nu_e \rightarrow \nu_\mu$ (μ^+ stored in the ring), where the resulting final state has a muon of the wrong-sign from interactions of the $\bar{\nu}_\mu$ in the beam. This detector would need to be magnetized for the wrong-sign muon appearance channel, as is the case for the current baseline Neutrino Factory detector [3]. A number of possibilities for the far detector exist. However, a magnetized iron detector similar to that used in MINOS is seen to be the most straight forward and cost effective approach.

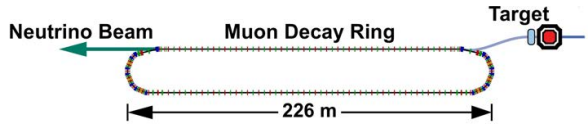


Figure 1: Schematic of the facility.

NUSTORM FACILITY OVERVIEW

The components of nuSTORM are anticipated to consist of six (6) functional areas consisting of the Primary Beamline, Target Station, Transport Line, Muon Decay Ring, Near and Far Detector Halls [4].

These areas will be located south of the existing Main Injector accelerator and west of Kautz Road on the Fermilab site. In general terms, a proton beam will be extracted from the Main Injector at the existing MI-40 absorber, directed east towards a new below grade target station, pion transport line and muon decay ring. The neutrino beam will be directed towards a Near Detector Hall located 20 m East of the muon decay ring and towards the Far Detector located approximately 1900 m away in the existing D0 Assembly Building (DAB). Figure 2 shows the nuSTORM facility components as they will be sited near the Fermilab Main Injector. The nuSTORM facility will follow, wherever possible (primary proton beam line, target, horn, etc.), NuMI [5] designs. Our plan is to extract one "booster batch" at

* Work supported by DOE under contract DE-AC02-07CH11359

ISBN 978-3-95450-138-0

Copyright © 2013 CC-BY-3.0 and by the respective authors

KINETIC THEORY OF HALO FORMATION IN CHARGED PARTICLE BEAMS*

Wilson Simeoni Jr.† and Felipe B. Rizzato
IF-UFRGS, 91501-970, Porto Alegre, RS Brasil

Abstract

The proceeding proposes a derivation of the Vlasov-Poisson equation where the distribution function is splitted in a main part standing for the core and a fluctuating part standing for the halo, with which the kinetic theory of halo formations and core-halo dynamics are analysed.

INTRODUCTION

High-power hadron beams are more and more requested in multiple research fields like fusion material studies, neutrino physics, nuclear transmutation, accelerator-driven systems. Among the most recent projects, the IFMIF accelerators [1] break the record of high intensity, leading to a multi-MW beam power at relatively low energy. The concern for such accelerated beams is the predominance of the self-field energy upon the beam energy. In these conditions, the space charge effect is at its maximum, which triggers different non-linear mechanisms implying emittance growth, halo formation and sudden particle lost. The challenge is then to be able to control the total beam size, to maintain it well inside the beam pipe, and to avoid particle losses on its wall at the level of 10^{-6} in order to preserve hands-on maintenance. Careful studies of the dynamics of high intensity charged particles are thus mandatory to better understand and characterise the beam non-linear behaviour.

In the space-charge dominated regime, the space-charge effects result in emittance growth and halo formation, which contribute to beam losses. A change of focusing lattice or inadequate knowledge of proper injection conditions can cause a mismatch between the beam and the transport system. This mismatch may result in an oscillation of the beam envelope and generally excite a superposition of the envelope eigenmodes. These envelope modes possess additional free energy compared with the stationary distribution. Particles with appropriate oscillation frequencies can resonate with these envelope modes through the so called parametric $2:1$ resonance and attain large amplitude to form a halo [2]. These halo particles extract the energy from the envelope modes and convert free energy from mismatch into thermal energy, which causes beam emittance growth. The goal of this proceeding is proposes a derivation of the Vlasov-Poisson equation where the distribution function is splitted in a main part standing for the core and a fluctuating part standing for the halo, with which core-halo interactions will be analysed.

* Work supported by CNPq
† wilson.simeoni@ufrgs.br

CORE-HALO EQUATIONS

The beam is assumed to propagate with a constant axial velocity $v_z\hat{\mathbf{e}}_z$, so that the axial coordinate $s = z = v_z t$ play the role of time. The external focusing field is given by $\mathbf{B} = B_0\hat{\mathbf{e}}_z$ and is used to compensate the repulsive Coulomb force between the beam particles. It is convenient to work in the Larmor frame [3] which rotates with respect to the laboratory frame with angular velocity $\Omega_L = qB_0/2\gamma_b mc$, where c is the speed of light in vacuo, and q, m, and $\gamma_b = 1/\sqrt{1-\beta_b^2}$ are the charge, mass and relativistic factor of the beam particles respectively.

A collisionless charged particle beam is usually described in a self-consistent mean-field approximation by the Vlasov-Poisson system :

$$\frac{df_b}{dt} = \frac{\partial f_b}{\partial t} + \mathbf{v}\cdot\frac{\partial f_b}{\partial \mathbf{r}} + \mathbf{F}\cdot\frac{\partial f_b}{\partial \mathbf{v}} = 0, \quad (1a)$$

$$\mathbf{F} = -\kappa_z\mathbf{r} - \nabla\phi, \quad (1b)$$

$$\nabla^2\phi = -4\pi q n_b(\mathbf{r}, s). \quad (1c)$$

where N_b is the number of particles per unit axial length, $\mathbf{r}$ is the position vector in the tranverse plane, $\mathbf{v} = \frac{d\mathbf{r}}{ds}$ is the transverse velocity, $n_b(\mathbf{r}, s) = q_b\int d\mathbf{v}^2 f_b(\mathbf{r}, \mathbf{v}, s)$ is the transverse beam density, $\kappa_{z_0} = qB_0/2\gamma_b\beta_b mc^2$ is the focusing field, and $K = 2q^2B_0^2/\gamma_b^3 v_z^2 m^2 c^2$ is the perveance, which is a measure of the beam space charge. In Eq. (1), ϕ is a scalar potential that incorporates both self-electric and self-magnetic fields, $\mathbf{E}^s$ and $\mathbf{B}^s$. We shall take zero of the scalar potential to be at r_w, the position of the conducting channel wall. The distribution function is normalized so that $\int d\mathbf{v}^2 d\mathbf{r}^2 f_b = 1$. In the Larmor frame, the system corresponds to a two dimensional non-neutral plasma of pseudo particles of mass $m = 1$ and charge $q = \sqrt{K/N_b}$ interacting by a repulsive logarithmic potential $\phi(\mathbf{r}) = -q^2\ln(r/r_w)$ confined in a parabolic potential well of $U(\mathbf{r}) = \kappa_z r^2/2$.

The Vlasov equation (1) express the conservation of the distribution function in phase space. We assume that the initial condition in phase space consists of a patch of uniform distribution function ($f_0 = \eta_0$) surrounded by vacuum ($f_0 = 0$). After some evolution, the patch mixes with vacuum and the coarse-grained (i.e. locally averaged) distribution function $\bar{f}$ takes values between 0 and η_0. The fact that the coarse-grained distribution function cannot exceed the maximum value η_0 of the initial condition is responsible for an effective "exclusion principle "leading to degeneracy effects. This degeneracy, resulting from the incompressibility of the Vlasov equation in phase space , was first recognized by Lynden-Bell [4] is his study of equilibrium.

Suppose that the *coarse-grained* [5] distribution function is the distribution f_c for *core* of the beam and the fluctua-

Copyright © 2013 CC-BY-3.0 and by the respective authors

BEAM DYNAMICS STUDIES OF A 30 MeV STANDING WAVE ELECTRON LINAC *

R. Dash#, HBNI, Mumbai 400094, India
J. Mondal, Archana Sharma, K.C. Mittal, BARC, Mumbai 400085, India

Abstract

For a high quality beam delivery to the users in application areas like material science and neutron spectroscopy, it is very important for the linac to keep the growth of transverse emittance and self field effects a minimum in order to limit the radioactivity and the cost of the linac itself and increase the transmission efficiency. This paper presents the results of electron beam tracking for a 30 MeV standing wave electron linac. This is a general purpose facility for neutron generation and will produce 10^{12}-10^{13} n/sec for measurement of neutron cross-section of (n, gamma), (n, xn) and (n, f) reactions. The effects of input beam size, divergence, field gradient and space charge effect on the beam quality have been studied with ASTRA beam dynamics code. This beam dynamics study explores the optimized beam parameters and beam quality for the linac operation.

INTRODUCTION

In this paper we have studied the beam dynamics of a 30 MeV, 6 kW bi-periodic coupled cavity standing wave electron linac under development at Electron Beam Centre (EBC) Kharghar, Navi Mumbai, India. In order to predict the quality of electron beam [1], [2], [3] the electron-tracking algorithm ASTRA [4] has been used. Although there are a few self-consistent space-charge codes that can be used to study the emittance evolution, we choose the ASTRA model in order to provide a fast parametric study.

The accelerating module (Fig. 1) contain a 85 keV thermionic electron gun, an injector section and two accelerating sections of 22 cell and 23 cell respectively operating in π/2 mode at a frequency of 2856 MHz. The injection section consists of three bunching cells and a power feed cell. The length of each accelerating cell is 52 mm, whereas the buncher cells are 45, 48 and 50 mm respectively. The bore radius is 5mm for all the buncher cells and accelerating cell. The effective shunt impedance for the buncher cells is ~ 80 MΩ/m, while for the accelerating cells, it is ~ 90 MΩ /m.

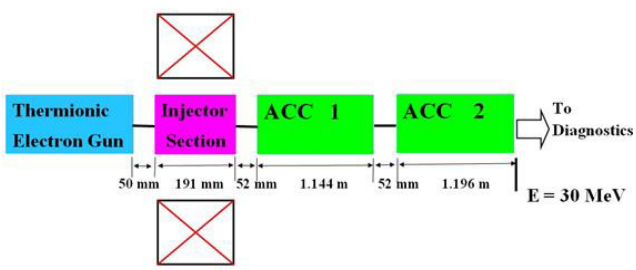


Figure 1: Schematic Layout of the 30 MeV Linac.

*Work supported by DAE, India
radhakanta.physics@gmail.com

MULTIPARTICLE SIMULATION WITH SPACE CHARGE

For the present work the longitudinal electric field components on the symmetry axis of the injector and accelerating sections have been computed using CST MWS [5]. The tracking code ASTRA does not need a geometrical description of the structures. For ASTRA code, the space-charge fields are calculated in the beam rest frame via Poisson's equation in free space and Lorentz's transformed back into the laboratory frame. ASTRA is based on Runge-Kutta integration of 4th order with fixed time step through the user defined external electric and magnetic fields, taking into account the space charge field of the particle cloud. A cylindrical grid, consisting of rings and slices, is set up over the bunch extension for the space charge calculations. The code automatically updates the mesh size as the simulation progresses. For all the simulations presented in the following, we have used 2.5 x 10^4 macro particles in uniform distribution. The initial energy of the particles injected in the guide is 85 keV. The particles are distributed quasi-randomly following the Hammersley sequence in such a way that statistical fluctuations are reduced and artificial correlations are avoided.

Effect of Space Charge on Beam Dynamics

Figure 2 gives the evolution of rms beam size for the nominal energy of 30 MeV. We have used a uniform distribution of particles having energy 85 ± 2 keV for the longitudinal direction with rms bunch length of 15.61 mm and bunch charge of 0.175 nC and Gaussian distribution in all transverse dimensions with rms beam sizes of 0.8 mm each. The results show that space charge gives rise to a transverse spread of the beam in the injection section and 1st cavity at low energies.

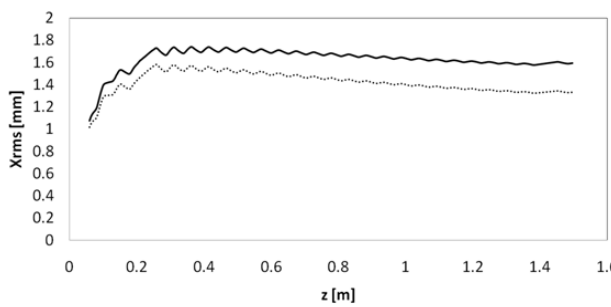


Figure 2: rms beam size without space charge (Dotted line) and with space charge (solid line).

Copyright © 2013 CC-BY-3.0 and by the respective authors

ISBN 978-3-95450-138-0

PRE-SEPARATOR DESIGN OF THE IN-FLIGHT FRAGMENT SEPARATOR USING HIGH-POWER BEAM*

J.Y. Kim, C.C. Yun, D.G. Kim, E.H. Kim, M.J. Kim, M. Kim, J.W. Kim#,
Institute for Basic Science, Daejeon, Korea

Abstract

In-flight fragment separator of the rare isotope science project (RISP) is a main device to produce isotope beams for nuclear science research and applications. The separator is divided into pre and main stages. The pre-separator contains a thin target to produce the isotope beam and beam dump to remove unreacted primary beam. The maximum primary beam power is 400 kW. As a result, radiation level is very high in the target area and some of the magnets will utilize high-Tc superconductor coils operating at 20-50 K to efficiently remove the radiation heat deposited on the coil. A major function of the pre-separator is to remove the primary beam, which is complicated by different charge states produced when the primary beam passes through the target and wedge-shaped energy degrader. Some detailed calculations in beam optics and on the layout of the major separator components have been performed using GICOSY and LISE++ considering contaminant isotope beams due to nuclear reactions.

INTRODUCTION

In-flight fragment separator using the high power primary beam with large acceptance will allow researches for rare isotopes near the boundary of the nuclear chart. The next-generation in-flight separator is characterised by two major features: large acceptances of wanted isotope beam and two-stage scheme [1]. In-flight fragmentation and in-flight fission by using U beam are two major reactions to produce RI beam with an in-flight fragmentation method. It is expected new understanding on the nuclear physics can be obtained with this new device.

Currently, rare isotope science project (RISP) to construct a next-generation radio-active isotope (RI) beam facility is underway in Korea. Both Isotope separation on-line (ISOL) and the in-flight fragment separation methods will be utilized [2]. A super-conducting linear accelerator is the main driver that can accelerate a uranium beam to 200 MeV/u at a maximum beam power of 400 kW. The optical design of the in-flight separator has been performed by using GICOSY [3].

Figure 1 shows a schematic layout of the two-stage separator, in which superconducting magnets with large aperture are used to achieve large acceptance. The first stage serves to produce an RI beam of interest and to remove the unreacted primary and unwanted RI beams. The second stage aims to purify and to identify the isotope beam of interest. Major technical challenges are associated to the design and construction of the pre-separator, where the target and beam dump are located. The area including the target and beam dump is under the influence of high radiation.

In this paper, in-flight fragment separator of RISP is briefly introduced. Then optical properties and performance of the pre-separator are mainly discussed.

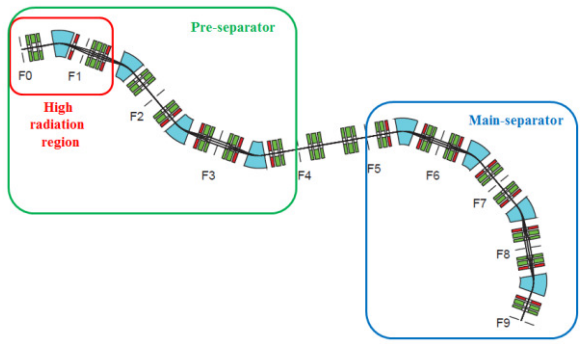


Figure 1: Schematic layout of the fragment separator.

DESIGN OF AN IN-FLIGHT SEPARATOR

The separator consists of pre and main separator, and a matching section in between is placed. The pre-separator from the production target to the F4 focus is composed of a four-bend achromatic spectrometer, consisting of four super-conducting dipole magnets with bending angle of 30 degree and seven superconducting quadrupole triplets.

As mentioned above, radiation level is very high in the target and beam dump area, so that radiation heating in superconducting coils is concerned. To remove the heat efficiently, one dipole and two quadrupole magnet triplets in the front end of the pre-separator will use high-Tc superconducting (HTS) coils. The rest of magnets in the pre-separator will use low-Tc superconducting (LTS) coils.

The main separator from the F5 focus to the F9 focus consists of eight superconducting quadrupole triplets and four dipole magnets. The F1, F3, F6 and F8 are momentum-dispersive focal planes, and the rest are achromatic planes. A wedge-shaped degrader can be used at each momentum dispersive focus to separate isotopes with the same q/A ratio by Z-dependent energy loss.

The goals of momentum acceptance and angular acceptance of the IF separator are ±5 % and ±50 mrad, respectively.

*Work supported by Rare Isotope Science Project
#jwkim@ibs.re.kr

Copyright © 2013 CC-BY-3.0 and by the respective authors

HORIZONTAL DISPERSION STUDIES FOR THE CERN PROTON SYNCHROTRON BOOSTER RINGS

V. Raginel, B. Mikulec, S. Gilardoni, CERN, Geneva, Switzerland

Abstract

In order to confirm the value of horizontal dispersion of the CERN Proton Synchrotron Booster (PSB) given by the MADX model, the horizontal dispersion has been measured using pick-ups and wire scanners on its four rings. The dispersion value of the PSB rings is of interest for example as input for the emittance measurements critical for high-brightness beam production for the LHC, for future optics studies related to the planned upgrades of the PSB or for optics studies of the ejection lines. In this study, the dispersion measurement protocol and the analysis of the measurements are presented. The measurement results point out differences with respect to the MADX model and also differences between the four rings. It was then investigated using horizontal orbit measurement and MADX matching routines whether misalignments of quadrupole magnets could explain these differences.

INTRODUCTION

The knowledge of the dispersion of the Proton Synchrotron Booster (PSB) rings is of interest for cross check the optics of the ring currently in use, but also as input for the emittance measurements [1] or for the optics matching studies of the injection/ejection lines. While the dispersion in the PSB is estimated by a MADX model [2], measurements of dispersion are necessary to validate the simulated optics. The horizontal dispersion $D_x(s)$ can be defined by:

$$\Delta x(s) = D_x(s) \cdot \delta$$

where $\Delta x(s)$ is the horizontal beam centroid displacement at the location s and $\delta=\Delta p/p_0$ is the relative momentum offset with respect to the nominal momemtum p_0. The dispersion can be measured by changing the beam momentum via the RF system, observing the beam displacement at the location of the beam position monitors and the variation of the revolution frequency. The momentum deviation is evaluated via the momentum compaction factor and the measured frequency change. The measurements were done for all four rings of the PSB. The dispersion was obtained off-line using a fitting routine on the beam position monitors data and then compared to the MADX model.

DISPERSION MEASUREMENTS

The dispersion was measured using a LHC 50 ns beam (the luminosity production beam for the LHC 2012 run) for each ring using the programmable RF radial position function which converts a given change in the average orbit into energy offset. The radial position function was modified 760 ms after the start of the cycle, just before the extraction flat top of the magnetic cycle when the beam momentum is 2126 MeV/c. The horizontal beam displacement and the revolution frequency were acquired for various values of the radial position function averaging over three measurements. The horizontal beam displacement was observed by the sixteen pick-ups of each ring (BRi.UES1L3, BRi.UES2L3 ..., and BRi.UES16L3, with i=1, 2, 3, 4 indicating the fours PSB rings), one pick-up per section, and by one wire scanner in the section 2 of each ring (BRi.BWS.2L1). The pick-ups of the PSB rings are installed in-between the first focusing quadrupole (QF) and the defocussing quadrupole (QD) with the basic optics cell of the PSB being bending1-QF1-QD-QF2-bending2. The readout chain per section of the pick-ups is the same for each ring (multiplexing) [3].

A too large horizontal beam displacement can cause beam losses when the aperture limit is reached. The maximum variations of the radial position function with no beam losses were determined for both positive and negative displacement. The measurements were done between these maximum variations.

DISPERSION ANALYSIS AND RESULTS

Determination of the Dispersion in Each Ring

The measurements yield the displacement of the center of the beam and the corresponding revolution frequency. The relative momentum deviation was derived from the relative variation of the revolution frequency thanks to the following relation:

$$\Delta f / f_0 = -\eta \cdot \delta$$

where $\eta = \eta_0 + \eta_1 \delta + O(\delta^2)$ is the phase slip factor [4]. The frequency f_0 corresponds to the naturally centered orbit by introducing no offset in the radial loop function. A first assumption is to simplify the phase slip factor to the first order. The analysis was done using the relation

$$\Delta f / f_0 = -\eta_0 \cdot \delta$$

where $\eta_0 = \alpha_0 - 1/\gamma^2$ with α_0 being the first order momentum compaction factor, which is equal to 0.0609 in the PSB, and γ being the relativistic gamma of the proton beam. Δx vs. δ is then plotted for each pick-up and the wire scanner, examples of a plot of Δx vs. δ is shown in Figure 1 (black dashed line). The data fits show that the data is not linear, but rather parabolic.

Copyright © 2013 CC-BY-3.0 and by the respective authors

ISBN 978-3-95450-138-0

BEAM DYNAMICS AND WAKEFIELD SUPPRESION IN INTERLEAVED DAMPED AND DETUNED STRUCTURES FOR CLIC*

A. D'Elia[1,2,3], T. Higo[4], V.F. Khan[3], R.M. Jones[1,2], A. Latina[3], I. Nesmiyan[1,2] and G. Riddone[3]
[1]School of Physics and Astronomy, The University of Manchester, Manchester, U.K,
[2]The Cockcroft Institute of Accelerator Science and Technology, Daresbury, U.K,
[3]CERN, Geneva, Switzerland, [4]KEK, Tsukuba, Japan

Abstract

Acceleration of multiple bunches of charged particles in the main linacs of the Compact Linear Collider (CLIC) with high accelerating fields provides two major challenges: firstly, to ensure the surface electromagnetic fields do not cause electrical breakdown and subsequent surface damage, and secondly, to ensure the beam-excited wakefields are sufficiently suppressed to avoid appreciable emittance dilution. In the baseline design for CLIC, heavy wakefield suppression is used (Q ~ 10) [1] and this ensures the beam quality is well-preserved [2]. Here we discuss an alternative means to suppress the wakefield which relies on strong detuning of the cell dipole frequencies, together with moderate damping, effected by manifolds which are slot-coupled to each accelerating cell. This damped and detuned wakefield suppression scheme is based on the methodology developed for the Japanese Linear Collider/Next Linear Collider (JLC/NLC) [3]. Here we track the multi-bunch beam down the complete collider, under the influence of transverse wakefields and record the final emittance dilution at the end of the linac. We utilize the code PLACET [4] for all tracking simulations and include systematic and random fabrication errors; the latter are particularly beneficial in reducing the impact of the wakefield on the beam quality. Results of some initial alignment studies are also provided.

INTRODUCTION

The CLIC scheme entails two beams, one of which is the high-current drive beam (~ 100 A), and the other is a low-current accelerated beam. The drive beam is decelerated and provides an electromagnetic field which is coupled to the main accelerating linac. These main linacs are required to accelerate electron-positron beams to a final collision centre of mass energy of 3 TeV. Recent studies anticipate a staging to a reduced centre of mass energy of 375 GeV, as a prelude to the full collision energy. Here we focus on the 3 TeV design, which requires more than 71,000 accelerating structures. In this baseline design, each structure accelerates 312 bunches, each of which consists of ~ 4 x10^9 particles per bunch. The corresponding beam current of ~ 1 A removes energy from the accelerating electric field, and loads it down. The beam-loaded accelerating field is designed, on average, to be 100 MV/m. The electric field is a little more than a factor of two larger on the walls and the magnetic field is constrained to provide a pulse temperature rise on the copper walls of no more than 56 K [5]. A relatively compact accelerating structure is obtained by adopting an X-band accelerating frequency of 11.994 GHz. The iris radius of each accelerating cell largely determines the shunt impedance, which ideally should be maximized, but since shrinking it down also enhances the transverse dipole fields, a compromise must be achieved. In our design we focus on an average iris radius to free space wavelength: $\langle a \rangle/\lambda \sim 0.13$. The average iris radius determines the short-range wakefield, or the field experienced along the bunch itself. The transverse wakefield experienced by succeeding bunches in the multi-bunch train is influenced by several factors. In principle it can be suppressed by heavy damping, and this is indeed the method adopted in the baseline design for CLIC in which field is coupled out from each cell and immediately dissipated in attached ceramics. This ensures the wakefield on the first trailing bunch is constrained to less than 6.7 V/pC/mm/mm [5] and all subsequent bunches experience an even lower wakefield. Recent high power tests have indicated this structure is able to sustain the requisite surface electromagnetic fields at the design gradient [6].

However, here we discuss a method which entails changing the dipole frequency of each of the cells within a given structure and hence ensuring the eigenmodes, corresponding to these fields, add up in a deconstructive manner [3]. In our alternative design the iris is tapered down in an erf function manner, and this ensures the wakefield decays with a Gaussian envelope. However, the finite number of cells within each structure corresponds to a sampling of the field. This will ultimately lead to a point at which the eigenmodes add together coherently and hence will force the wakefield to rise above the constrained value. We provide four waveguide-like manifolds, slot-coupled to each cell in the structure, to ensure this recoherence in the wakefield is sufficiently suppressed. We have constrained our design to utilize the same number of cells as the baseline design, namely 24. This short structure is of course insufficient to provide adequate sampling, and hence we interleave the frequencies of several neighbouring structures in order to obtained the requisite wakefield suppression -12 and 16 fold interleaving is focused on in this article (corresponding to an equivalent structure of 288 and 384 cells, respectively).

This paper is organized such that the next section provides a description of the wakefield suppression used, followed by a section entailing tracking the beam throughout the complete linac under the influence of expected fabrication errors, and finally by a penultimate

* This research has received funding from European Commission under the FP7 Research Infrastructure grant no. 227579

Copyright © 2013 CC-BY-3.0 and by the respective authors

BEAM-BASED ALIGNMENT OF SEXTUPOLES AT THE APS *

A. Xiao †, V. Sajaev, ANL, Argonne, IL 60439, USA

Abstract

Sextupole magnet offsets play a large role in modern storage ring coupling control. Due to the non-linear field of sextupoles, their beam-based alignment becomes more difficult and often requires a sophisticated post-data process. A simple method had been developed at the APS that measures the vertical orbit variation (orbit change at BPMs with sextupole strength) versus beam trajectory through a sextupole in one plane while keeping the trajectory in the other plane fixed. This method converts the non-linear problem into a linear one, and experiment results show very good reproducibility and accuracy.

INTRODUCTION

Given the strong sextupoles used in modern storage rings, such as light sources with emittance for producing x-rays near the diffraction limits and/or colliders (B-Factory or damping ring) with very low vertical emittance, misaligned sextupoles tend to be the main sources of large coupling and optics perturbation. It affects the ability to model the machine, and correct orbit, tune and coupling, often resulting in a reduced dynamic aperture and beam lifetime.

For a sextupole installed next to a quadruple, the alignment is as simple as aligning its magnet center to the next quadrupole, and then performing a commonly used beam-based alignment (BBA) technique on the quadrupole. At the APS, however, the majority of sextupoles (four of seven per cell) are on "dipole" girders that do not have quadrupoles, thus we cannot rely on BBA of quadrupoles. Other means of measuring the sextupole magnet offsets need to be developed.

In a previous paper [1], we presented a matrix fitting method to fit all sextupole offset errors together with other machine errors, so that the fitted model agrees with the response matrix measurement. The advantage of this method is that one can quickly get results. The disadvantage is that results are obtained in an "indirect" way and could be mixed up with other effects.

Similar to the beam-based quadrupole offset measurement method, a "direct" beam-based sextupole offset measurement method has been developed since then. This method measures the vertical orbit variation (orbit change at BPM with variation of sextupole strength) versus beam trajectory through a sextupole in one plane while keeping the trajectory in the other plane fixed. The small change of data acquisition and manipulation converts the non-linear problem into a linear one, and experiment results show very good reproducibility and accuracy. Details of the method, simulation, and experiment results are discussed in this paper.

PRINCIPLE

The closed orbit displacement (COD) at position s, rising from a kick error θ at position s_0, is given by

$$u(s) = \frac{\sqrt{\beta_{u,s_0}\beta_{u,s}}}{2\sin\pi\nu_u}\theta\cos[\pi\nu_u - (\phi_{u,s} - \phi_{u,s_0})] = A\cdot\theta, \tag{1}$$

where $u(s)$ represents x or y; β and ϕ are the β-function and the betatron phase; and ν is the betatron tune. For a sextupole with misalignment of x and y, the kick angle is given by

$$\begin{aligned}\theta_x &= \frac{1}{2}\cdot K2L\cdot(x^2 - y^2),\\ \theta_y &= K2L\cdot x\cdot y,\end{aligned} \tag{2}$$

where $K2L = \frac{e}{cp}\partial^2 By/\partial x^2\cdot L$ is the integrated sextupole strength. The corresponding kick angle from a misaligned quadrupole is given by

$$\theta_x = K1L\cdot x \qquad \theta_y = K1L\cdot y. \tag{3}$$

Equations (2) and (3) have different character, one is linear and the other is non-linear. However, if we keep either x or y unchanged during the measurement, i.e., $\theta_y = (K2L\cdot x)\cdot y$ or $\theta_y = (K2L\cdot y)\cdot x$, Eq. (2) becomes as linear as Eq. (3). In other words, by fixing x while varying y and the sextupole strength, we are doing the vertical offset measurement of a quadrupole with strength $K1L = K2L\cdot x$. Similarly, by fixing y while varying x and the sextupole strength, we are doing the horizontal offset measurement of a quadrupole with strength $K1L = K2L\cdot y$. The only difference in this case is that we measure the vertical orbit variation instead of the horizontal orbit variation for a real quadrupole offset measurement.

SIMULATION STUDY

The principle of the method is simple and straightforward. However, other effects, such as coupling from misaligned sextupole etc., need to be considered, too. We studied different misalignment scenarios through simulations before testing with beam. The calibrated lattice model obtained from LOCO fit [2] (includes normal- and skew-quad errors) is used for simulation. One sextupole (S17B:S3) is misaligned intentionally in three different sets: $DX = 2$ mm, $DY = 1$ mm; $DX = 1$ mm, $DY = 1$ mm; and $DX = 0$ mm, $DY = 0$ mm. Sextupoles within the measurement bump are kept on or turned off.

* Work supported by the U.S. Department of Energy, Office of Science, under Contract No. DE-AC02-06CH11357.

† xiaoam@aps.anl.gov

Copyright © 2013 CC-BY-3.0 and by the respective authors

ISBN 978-3-95450-138-0

ENERGY CALIBRATION IN THE AGS USING DEPOLARIZATION THROUGH VERTICAL INTRINSIC SPIN RESONANCES*

Y. Dutheil, L. Ahrens, H. Huang, F. Méot, V. Schoefer
BNL, Upton, Long Island, New York

Abstract

The AGS tune jump system consists of two fast pulsed quadrupoles used to accelerate the crossing of 82 horizontal intrinsic resonances. Timing of the tune jumps requires accurate tune and energy measurements. Although cross calibration using measurements of the beam revolution frequency shows good accuracy for most of the AGS energy range it is not adequately sensitive as the beam becomes highly relativistic. This drives a strong interest for a new independent energy measurement method.

Reduction in the vertical tune across vertical intrinsic spin resonances can induce significant depolarization of the beam. Therefore it was proposed to use the negative vertical tune shift created by this tune jump system to calibrate the energy measurement at few locations along the AGS acceleration cycle. The fast tune jump, of $\Delta Q \approx -0.02$ within $100\,\mu$s in the vertical plane, allows to accurately locate the spin resonant condition, independently from orbit or field conditions. Simulations using the AGS Zgoubi online model facilitate the interpretation of the experimental results. This paper introduces the experimental procedure and shows some of the latest results.

INTRODUCTION

The partial snakes configuration of the AGS creates horizontal intrinsic spin resonances by tilting the stable spin direction away from the vertical direction [1]. The resonant condition $Q_s \pm Q_x = n$ is satisfied twice per unit of $G\gamma$ during the ramp, inducing every time a small depolarization of the beam. The polarization losses are reduced by quickly changing the horizontal tune Q_x, increasing the crossing rate of the resonance [2].

The system is composed of two fast quadrupoles allowing a change in the horizontal tune of $\Delta Q_x = +0.04$ in $100\,\mu$s. One of the main challenge is the accurate timing required for each jump, such that the tune jump is centered around the resonance.

Tune Jump Timing

While the spin tune Q_s is a function of the energy, tune and energy measurements along the ramp allow precise timing of each jump. During the polarized protons operations these measurements are regularly used to generate new timings for the tune jumps. This is supposed to compensate for any drift in the location of the resonant condition, for instance due to a drift of the tune over time. During the AGS Polarized Proton Run 13, these measurements were regularly conducted to provide the highest polarization to the RHIC.

Table 1: Polarization Measurements During Run 13

Measurement date	Timings	Polarization
May 5th	from April 6th	$66.0 \pm 0.9\,\%$
May 5th	from April 29th	$59.7 \pm 1.1\,\%$
May 5th	from May 5th	$62.8 \pm 1.1\,\%$
June 6th	Uncalibrated	$64.4 \pm 3.9\,\%$
June 6th	Calibrated	$70.9 \pm 1.6\,\%$

In late April 2013, after a few weeks of running with the same tune jumps timings, new timings were generated but the polarization decreased. Table 1 shows that on May 5th the measured polarization was higher for the older timings. The two sets of timings more recently generated led to a consistently lower polarization.

To explain this deterioration the entire process from the computation of the jumps timing to the trigger of the pulsed power supply was verified, without finding any error. We decided to investigate on the measurements used to compute the jump timings : tune and energy measurements.

The tune measurement is based on the free oscillation of the beam, it is therefore an absolute measurement and is unlikely a source of significant error. The energy measurement is more complex and needs to be calibrated, making a possible suspect for our problems.

ENERGY MEASUREMENT IN THE AGS

The AGS uses a dedicated device called the *GgammaMeter* to measure the energy along the ramp. The energy is determined using the measured RF frequency f and average radius of the beam dR (Eq. 1) or the measured field $(B_{\text{inj}} + B_{\text{clock}}/C_{\text{scal}})$ and the average radius (Eq. 2) :

$$G\gamma = G\frac{1}{\sqrt{1-\frac{1}{c^2}\left(\frac{f}{h}\right)^2(2\pi)^2(R_0+dR)^2}} \quad (1)$$

$$G\gamma = G\sqrt{\left[\frac{(1+\gamma_{tr}^2 dR/R_0)\rho_0 c(B_{\text{inj}}+B_{\text{clock}}/C_{\text{scal}})}{M_0}\right]^2+1} \quad (2)$$

With γ_{tr} the transition energy, R_0 the radius and ρ_0 the radius of curvature of the AGS. The parameters in red (f, dR and B_{clock}) are measured quantities while the blue ones are machine parameters(R_0, γ_{tr}^2, ρ_0, B_{inj} and C_{scal}) that can be adjusted and the black are fixed physical constants.

The *GgammaMeter* is cross calibrated : at low energy the machine parameters in equations 2 and 1 are adjusted manually until the two methods report the same energy along

* Work supported by Brookhaven Science Associates, LLC under Contract No. DE-AC02-98CH10886 with the U.S. Department of Energy.

Copyright © 2013 CC-BY-3.0 and by the respective authors

HALO CONTROL AND GENERATION IN RHIC *

C. Montag, K. A. Drees, BNL, Upton, NY 11973, USA

Abstract

In the next 5-10 years, RHIC will be colliding gold ions in the center-of-mass energy range of 5 to 20 GeV, which is below the regular injection energy. Though the machine has already successfully provided collisions at CM-energies of 7.7 and 11.5 GeV, a significantly higher luminosity than so far achieved is required for a meaningful physics program. While an electron cooler is presently being designed to provide the desired luminosity gain, this is a long-term project that is expected to be completed in 2018. As a short-term alternative the STAR collaboration has proposed installation of an internal halo target in the STAR detector beam pipe. To study the generation and control of the beam halo, we have performed dedicated beam experiments aimed at the bunch-by-bunch uniformity, and long as well as short-term stability of collimator loss rates.

INTRODUCTION

The Relativistic Heavy Ion Collider (RHIC) consists of two superconducting storage rings with a circumference of 3.8 km. In heavy ion collider mode, beams are injected at a rigidity of $B\rho = 81\,\mathrm{Tm}$ and accelerated to $B\rho = 833\,\mathrm{Tm}$ before they are brought into collision in the two detectors STAR and PHENIX. In the case of fully stripped gold ions, these beam rigidities correspond to an injection energy of 9.8 GeV/nucleon and a storage energy of 100 GeV/nucleon.

In recent years, nuclear physicists have become increasingly interested in searching for the critical point in the phase diagram of nuclear matter, which is expected to occur in the center-of-mass energy range between $\sqrt{s_{\mathrm{NN}}} = 5$ and 30 GeV, see Figure 1. To provide collisions in the desired energy range in collider mode, gold beams therefore have to be stored and collided at energies as low as a quarter of the nominal RHIC injection energy, which is extremely challenging due to large multipole errors in the superconducting magnets at these energies, as well as space charge and intrabeam scattering effects.

In 2010, RHIC has been successfully operated at center-of-mass energies of 7.7 and 11.5 GeV per nucleon pair [1]. However, to reach the desired integrated luminosities for the beam energy scan, RHIC would have to operate for a total of 70 weeks at these energies. Furthermore, performance at $\sqrt{s_{\mathrm{NN}}} = 5\,\mathrm{GeV}$ has not yet reached any level sufficient for meaningful physics operations, though beams have already been stored successfully at this energy [2], albeit at tiny intensities, and studies are underway to improve the performance [3].

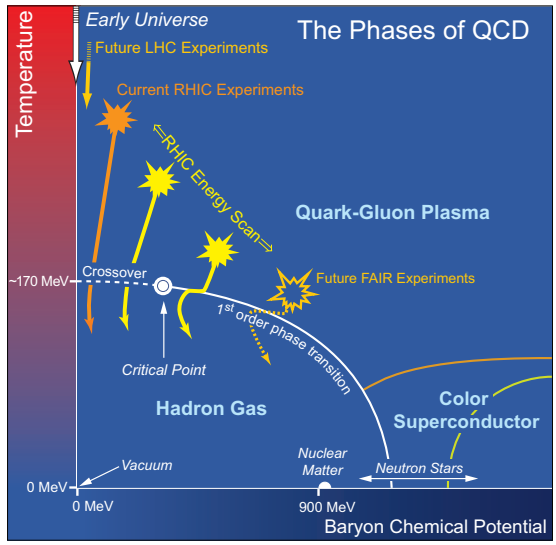


Figure 1: The QCD phase diagram, with the critical point expected in the center-of-mass energy range between $\sqrt{s_{\mathrm{NN}}} = 5$ and 30 GeV.

To improve the luminosity at low energies, an electron cooling system is currently being designed [4]. However, since this new device is scheduled to become operational in 2018, and because the lowest desired beam energy of 2.5 GeV per nucleon may turn out to be outside the useful reach of RHIC, the STAR collaboration has proposed the installation of a thin gold target in their detector area to study low energy gold-gold collisions in fix target mode rather than in collider mode [5].

The proposed internal target consists of a 30 mil (750 μm) thick gold foil that is installed in the RHIC beam pipe 2 m away from the STAR interaction point such that it intercepts the halo of the circulating Yellow beam upstream of the STAR detector, see Figure 2. To avoid potential damage to the target in case of an abort kicker pre-fire, which deflects the beam horizontally, the proposed target geometry is chosen such that it intercepts the beam halo only in the vertical plane. Furthermore, only the lower part of the beam pipe is equipped with the target foil, so in case the foil comes lose it does not drop into the beam path where it could block the aperture.

The aperture of the gold foil target needs to be chosen smaller than the 40 mm inner diameter detector beam pipe to make the target the local aperture limitation. On the

* Work supported by Brookhaven Science Associates, LLC under Contract No. DE-AC02-98CH10886 with the U.S. Department of Energy.

ISBN 978-3-95450-138-0

Copyright © 2013 CC-BY-3.0 and by the respective authors

A GRAPHIC INTERFACE FOR FULL CONTROL OF THE RHIC OPTICS*

G. Robert-Demolaize, M. Bai, Brookhaven National Laboratory, Upton, NY, USA
Xiaozhe Shen, Indiana University, Bloomington, IN, USA

Abstract

A high level application has been developed for the RHIC collider to provide a complete package for optics control. Optics can be measured using three different algorithms to process turn-by-turn (TBT) beam position monitor (BPM) data from either free (tune meter) or driven (AC dipole) betatron oscillations, and corrected via SVD on a response matrix built around specific sets of quadrupoles. The following reviews the details of those methods, and includes the first results of the operational commissioning of the application.

INTRODUCTION

One of the methods to measure the linear RHIC optics for any of its high energy heavy ions or polarized protons runs relies on AC dipoles (ACD's). In a particle accelerator, ACD's are designed to adiabatically drive coherent betatron beam oscillations with a frequency close to the beam tune. For RHIC, a GUI application called *loptics* was built to control the amplitude and frequency of the dipole field of a given ACD when measuring the optics of the corresponding beamline. Once the ACD is triggered, all BPM's around the considered ring record the beam oscillations over 1024 turns; linear optics are then derived using fitting algorithms on each BPM dataset [1]. With the recent successful developments of β_z-beating correction methods at RHIC in Run12 and Run13 [2], a major upgrade of *loptics* was to turn the application into a complete tool for measurement, correction as well as control of linear optic functions.

LINEAR OPTICS MEASUREMENTS

Fitting Driven and Free Oscillations

For coherent oscillations driven by an ACD at a tune $\nu_{\mathtt{AC}}$, the beam actually "sees" both $\nu_{\mathtt{AC}}$ and $1-\nu_{\mathtt{AC}}$ driving tunes according to the Nyquist sampling theorem. The transverse beam position $z_i^s(N)$ (for either plane) measured at the ith BPM and Nth turn at the longitudinal coordinate s in RHIC can then be derived as:

$$\begin{aligned} z_i^s(N) &= A_m \cos\left(2\pi\nu_{\mathtt{AC}}N + \psi_m(s)\right) \\ &-A_p \cos\left(2\pi\nu_{\mathtt{AC}}N - 2\pi\nu_{\mathtt{AC}} + 2\chi_{\mathtt{AC}} - \psi_m(s)\right), \end{aligned} \quad (1)$$

with $\psi_m(s) = -\pi\left(\nu_{\mathtt{AC}} - \nu_z\right) + \chi_{\mathtt{AC}} - \psi_z(s)$ and:

$$A_m = \frac{B_m L}{4\sin\left(\pi\left(\nu_{\mathtt{AC}} - \nu_z\right)\right) B\rho}\sqrt{\beta_z(s)\beta_z^0},$$

$$A_p = \frac{B_m L}{4\sin\left(\pi\left(\nu_{\mathtt{AC}} + \nu_z\right)\right) B\rho}\sqrt{\beta_z(s)\beta_z^0}.$$

where $B_m L$ is the integrated strength of the ACD field, $B\rho$ the magnetic rigidity, $\beta_z(s)$ and $\psi_z(s)$ the betatron function and phase advance at the ith BPM, β_z^0 the betatron function at the ACD, and $\chi_{\mathtt{AC}}$ the ACD initial phase. Eq. (1) can be written in both a compact form [3] (Eq. (2)) and a tune-phase dissociated form [4] (Eq. (3)):

$$z_i^s(N) = A_d\sqrt{\beta_d(s)}\cos\left(2\pi\nu_{\mathtt{AC}}N + [\psi_z(s) + \chi_{\mathtt{AC}}]\right), \quad (2)$$

$$z_i^s(N) = A_m\left[\cos(\psi_m(s))F_N - \sin(\psi_m(s))G_N\right]; \quad (3)$$

with $r = \sin\left(\pi\left(\nu_{\mathtt{AC}} + \nu_z\right)\right) / \sin\left(\pi\left(\nu_{\mathtt{AC}} - \nu_z\right)\right)$ one gets:

$$F_N = \cos\left(2\pi\nu_{\mathtt{AC}}N\right) - r\cos\left(2\pi\nu_{\mathtt{AC}}(N-1) + 2\chi_{\mathtt{AC}}\right),$$

$$G_N = \sin\left(2\pi\nu_{\mathtt{AC}}N\right) + r\sin\left(2\pi\nu_{\mathtt{AC}}(N-1) + 2\chi_{\mathtt{AC}}\right).$$

The compact form from Eq. (2) is then solved using the nonlinear Levenberg-Marquardt [5] fitting method on the three variables $A_{tot}(s) = A_d\sqrt{\beta_d(s)}$, $\nu_{\mathtt{AC}}$ and $\psi_{tot}(s) = \psi_z(s) + \chi_{\mathtt{AC}}$. The dissociated form in Eq. (3) can be solved with a linear fitting algorithm for the variables $A_m\cos(\psi_m(s))$ and $A_m\sin(\psi_m(s))$ once the driving tune $\nu_{\mathtt{AC}}$ is found using a fast Fourier transform (FFT) on the TBT data at the considered BPM. The ratio of amplitudes A_{tot} or A_m between two BPM's are then directly proportional to the ratio of the $\beta_z(s)$ functions at the BPM's locations. The phase advance $\psi_z(s)$ can only be calculated from $\psi_{tot}(s)$ or $\psi_m(s)$ with a precise knowledge of the initial ACD phase $\chi_{\mathtt{AC}}$; instead, *loptics* provides the phase difference $\Delta\psi_z(s)$ between two consecutive BPM's, which is independent of $\chi_{\mathtt{AC}}$.

The $\beta_z(s)$ and $\Delta\psi_z(s)$ derived from fitting Eq. (2) are actually the "driven" amplitude and phase of the beam oscillation. Results from the nonlinear fitting will therefore carry some artificial β_z-beating with an amplitude [6]:

$$\frac{\beta_d(s) - \beta_z(s)}{\beta_z(s)} \approx \frac{2\pi\left(\nu_{\mathtt{AC}} - \nu_z\right)}{\sin\left(2\pi\nu_z\right)}\cos\left(2\psi_z(s) - 2\pi\nu_z\right). \quad (4)$$

For typical ACD operations at RHIC, this amplitude is estimated at about 7% for $\nu_{\mathtt{AC}}$-ν_z=±0.01. For a linear machine, the artificial β_z-beat can be reduced experimentally to about 0.3% by driving the beam oscillations with $\nu_{\mathtt{AC}} > \nu_z$ in one measurement and $\nu_{\mathtt{AC}} < \nu_z$ in another, and averaging the fitted optics.

Free oscillations can be generated from beam injection oscillations or a coherent excitation by a single turn kicker magnet (e.g. for tune measurements), with $z_i^s(N)$ defined as:

* Work supported by Brookhaven Science Associates, LLC under Contract No. DE-AC02-98CH10886 with the U.S. Department of Energy.

Copyright © 2013 CC-BY-3.0 and by the respective authors

TRAJECTORIES OF LOW ENERGY ELECTRONS IN PARTICLE ACCELERATOR MAGNETIC STRUCTURES*

E.E. Cowan, Dept of Physics, Syracuse University, NY, USA
Kiran G. Sonnad†, CLASSE, Cornell University, NY, USA
Seth Veitzer, TechX Corp. Boulder, CO, USA

Abstract

It has been observed recently that low energy electrons, or electron clouds formed within quadrupoles can remain trapped for time periods beyond a beam revolution period at Cesr [1]. This paper provides some results obtained from analysis and numerical tracking of low energy electrons in quadrupoles under conditions similar to those when the above mentioned data was collected.

MOTION OF PARTICLES IN A NONUNIFORM MAGNETIC FIELD

Electron clouds generated in positively charged beams are known to negatively interfere with the beam. Most of the simulations done for various accelerators for estimating the cloud buildup have been for the duration of the passage of a single train of bunches. However if an electron remains trapped for long enough in a magnetic structure such as a quadrupole after the passage of a train, this trapped electron will encounter the next passage of a bunch train. The electron may then impinge upon the walls and potentially produce secondary electrons. Such a mechanism could lead to a progressive enhancement in cloud densities with repeated train passages and can have adverse consequences on the properties of the beam.

Trapping of electrons has been observed in the PSR [2]. In this experiment the proton beam was allowed to circulate and produce electrons and the beam was then deflected out of the storage ring, while the electron cloud was allowed to evolve. It was observed that electrons in quadrupoles persisted for a time period exceeding 50-100μs. More recently, experiments performed at Cesr observed electron trapping in quadrupoles in the presence of a beam [1]. The revolution period of the beam in Cesr is about 2.5 μs.

In this paper, we report results obtained from single particle tracking and compare them with theoretical expectations. The parameters of our computations were similar to those of the operating conditions when the data reported in Ref. [1] was taken. A similar study was performed earlier for the KEKB [3]. This study clearly showed that trapping of electron in quadrupoles can be important and requires a careful study.

Adiabatic Invariants

In dynamical systems exhibiting periodic motion, the quantity $\oint p \cdot dq$, which is the phase space area encompassed by the trajectory, also known as the Poincare invariant is a conserved quantity [4]. If a system undergoes a very gradual change, this quantity remains conserved so long as the relative value of this change over a full period of motion is very small, (see for example Ref. [4]). A classic example is a simple pendulum where the length of the string is gradually altered at a rate such that over the course of the oscillation period, $\delta l/l << 1$. Then the quantity E/ω remains constant and is the adiabatic invariant. The same principal of adiabatic invariance can be applied to a particle executing cyclotron motion in a magnetic field (see for example Ref. [5]). For a particle in this situation, the magnetic moment

$$\mu = IA = \frac{mv_\perp^2}{2B} \tag{1}$$

is conserved as long as $dB/B << 1$ over the cyclotron period T_c. This is equivalent to the following condition,

$$\frac{|\nabla B|}{B} r_c << 1, \tag{2}$$

where r_c is the cyclotron radius. On the other hand, energy which is given by

$$\mathcal{E} = \frac{1}{2} m(v_\perp^2 + v_\parallel^2) \tag{3}$$

being an absolute invariant always remains conserved. In the above equation, $v_\perp$ and $v_\parallel$ are velocities perpendicular and parallel with to the magnetic field, respectively.

Magnetic Mirroring

If energy and the magnetic moment are conserved, one can obtain a formula for magnetic mirroring. As B increases, $v_\perp$ increases and $v_\parallel$ decreases. If $v_\parallel$ decreases to zero, the trajectory turns around. This phenomenon is referred to magnetic mirroring. Since $v_\perp$ is rotating around the field line, one can associate this condition with a cone in velocity space. A particle would lie within the "loss" cone if

$$v_\parallel / v_\perp > 1 - (B_{bd}/B_{in})^{1/2}. \tag{4}$$

Here B_{in} is the magnetic field value at the initial point, and B_{bd} is the magnetic field on the same field line at the boundary of the vacuum chamber. A particle lying outside this cone in velocity space at the given point will remain trapped.

* Work supported by NSF (PHY-0734867, PHY-1002467, PHY-1068662), US DoE (DE-FC02-08ER41538)
† kgs52@cornell.edu

Copyright © 2013 CC-BY-3.0 and by the respective authors

A LINEAR ENVELOPE MODEL FOR MULTI-CHARGE STATE LINAC*

Z. He#, FRIB, Michigan State University, USA; Tsinghua University, China
J. Wei, Y. Zhang, Z. Liu, FRIB, Michigan State University, USA
R. M. Talman, Cornell University, USA

Abstract

The traditional linear envelope tracking model is widely used in linac design and on-line tuning. However, for multi-charge state acceleration, where the transfer matrix acts differently on different charge-states, the linear envelope tracking model cannot be utilized. A direct way to handle multi-charge state acceleration is using multi-particle tracking, which is usually high in precision, but lacking in efficiency, therefore is not suitable for linac on-line beam tuning. In this paper, a new approach of adapting linear envelope tracking model to multi-charge state acceleration is proposed. The lattice of FRIB is used to test this technique in both linac segment and folding segment. The result is then benchmarked with a multi-particle tracking program IMPACT to ensure its precision with enhancement in efficiency.

INTRODUCTION

The traditional linear envelope tracking model is widely used. Instead of tracking every particle, the method is capable of keeping track of beam envelopes by knowing an initial theta matrix and the transfer matrix between the initial point and the objective point, which is shown below.

$$x_i^{(1)} = R_{ij} x_j^{(0)}$$

$$\sigma_{ij}^{(0)} = \frac{\sum_n \left(x_{ni}^{(0)} x_{nj}^{(0)} \right)}{N}$$

$$\sigma_{ij}^{(1)} = \frac{\sum_n \left(R_{ik} x_{nk}^{(0)} R_{jm} x_{nj}^{(0)} \right)}{N} = R_{ik} \sigma_{km}^{(0)} R_{jm}$$

Numbers of linac code are based on or contains this scheme, such as Trace 3D. The advantage of envelope tracking model is obvious: fast in calculation speed, simple and clear in physics, therefore, remains to be a preferable way in computational intensive applications like case-by-case based linac lattice global optimization, and time restricted applications like linac on-line beam tuning.

For traditional accelerators like electron or proton machines, only one charge state is presented and the traditional linear envelope tracking model can be directly adopted. However, Facility for Rare Isotope Beams (FRIB) is accelerating multiple charge states in order to enhance the beam current. For this kind of accelerators, the traditional linear envelope tracking model can no longer be adopted directly, extensions onto multi-charge states acceleration problems are needed.

*This work was supported by the U.S. National Science Foundation under Grant No. PHY-11-02511, and the U.S. Department of Energy Office of Science under Cooperative Agreement DE-SC0000661.
hez@frib.msu.edu

HOW TO DEAL WITH MULTI-CHARGE STATE ACCELERATION

There are three different schemes to handle multi-charge state acceleration problem. The most simple and straight forward one is multi-particle tracking. The advantage is we can expect minimum change of existing tracking code, attain high precision and detailed information. Particle tracking code like IMPACT, is utilizing this scheme. However, the shortcoming is high computational intensity and slow speed. And computer takes over all the calculation would result physics to be unclear.

The second way is to treat charge state deviation as momentum deviation for magnetic field. This method can give exact result on transverse coordinates and can reuse most part of existing code. But the problem the method can only handle all-magnetic field lattice. The imaginary extra momentum deviation can cause imaginary change in time-of-flight for non-relativistic cases. This method is sometimes quite useful when calculating multi-charge beam behaviour in a bending magnet.

THREE-STEP SCHEME

The third way is to treat different charge states separately using envelope tracking scheme. This method can be divided into three steps:

Step 1: Use an ideal particle with centre charge state to initiate the machine parameters, such as RF phases, bending magnet strength. Keep record of the particle and make it the reference of the whole beam.

Step 2: Choose the particle located at beam centre of each charge state as a reference particle and do single particle tracking according to the initialized lattice parameter. Keep record of each particle and make it the reference for each charge state beam.

Step 3: Do envelope tracking for each charge state beam. The transfer matrix should be adjusted according to its own charge state and reference orbit.

This method of handling multi-charge state is a combination of precision of particle tracking method and efficiency of envelope tracking. The calculation efficiency is quite high. Details can vary while the three step scheme concept is universal. For next part, the FRIB lattice would be analysed as an example using this method.

APPLICATION TO FRIB LATTICE

The FRIB project, built at the Michigan State University in corporation with the US Department of

Copyright © 2013 CC-BY-3.0 and by the respective authors

CALCULATION OF THE KICK MAPS GENERATED BY A HOLLOW ELECTRON LENS FOR STUDIES OF HIGH-ENERGY HADRON BEAM COLLIMATION*

G. Stancari†, M. Chung, A. Valishev, Fermilab, Batavia, IL 60510, USA
V. Moens, EPFL, Lausanne, Switzerland, H. J. Lee, Pusan National University, Korea

Abstract

Collimation with hollow electron beams is a technique for halo removal in high-power hadron beams. It was experimentally studied at the Fermilab Tevatron collider using electron lenses and it is being considered as an option to complement the collimation system for the LHC upgrades. In the ideal case, the magnetically confined electron beam has a hollow, axially symmetric current-density distribution, whose fields affect the beam halo, leaving the core of the circulating beam unperturbed. We address the effects of imperfections in the current density based upon profiles measured in the Fermilab electron lens test stand. We also study the effect of the bends used to inject and to extract the electron beam from the overlap region. The calculated field distributions will serve as inputs for tracking simulations, which are needed to estimate the effects of the electron lens imperfections on beam core dynamics, such as nonlinearities and emittance growth.

INTRODUCTION

Hollow electron beam collimation is a new technique for collimation and halo scraping of intense hadron beams in storage rings and colliders [1]. In a hollow electron beam collimator, a magnetically confined, pulsed, low-energy electron beam with a hollow current-density profile overlaps with the circulating beam over a short section of the ring. Figure 1 shows the layout of one of the Tevatron electron lenses. The beam is formed in the electron gun inside a conventional solenoid and guided by strong axial magnetic fields. Inside the superconducting main solenoid, the circulating beam interacts with the electromagnetic fields generated by the charge distribution of electrons. The electron beam is then extracted and deposited in the collector. The halo of the circulating beam can be smoothly scraped. The core is unaffected if the distribution of the electron charge is axially symmetric. One cause of asymmetry is the space-charge evolution of the electron beam as it propagates through the electron lens. Another source of asymmetry are the bends that are usually used to inject and extract the electron beam from the interaction region. Although small, these asymmetries may have detectable effects on core lifetimes and emittances because of their nonlinear nature, especially when the current of the electron pulse is changed turn by turn to enhance the halo removal effect by resonant excitation of selected particles.

In this paper, we discuss the effects of these asymmetries from experimental data and from calculations. In particular, the asymmetries in the charge distribution are translated into transverse kick maps for the circulating beam. These kick maps are provided as inputs for numerical tracking simulations of the Fermilab Tevatron collider and of the Large Hadron Collider at CERN with the Lifetrac or SixTrack codes. This work is in support of a conceptual design for a proposed hollow electron beam collimator for the LHC upgrade [2]. The same techniques can be applied to different current-density profiles (Gaussian, flat, etc.) to study perturbations in nonlinear integrable optics with electron lenses for the IOTA ring at the Fermilab ASTA facility [3].

AZIMUTHAL ASYMMETRIES

Two-dimensional azimuthal asymmetries of the electron current density in the overlap region inside the main solenoid (neglecting the injection and extraction regions) may be caused by the space-charge evolution of the hollow electron beam as it propagates through the electron lens (diocotron instability), or by imperfections in the electron gun geometry, magnetic field lines, etc.

Electron guns are characterized at the Fermilab electron-lens test stand. Current-density profiles are measured as a function of beam current and axial magnetic field. Space-charge evolution of the electron beam profiles is mitigated by increasing the guiding magnetic fields. The measured profiles are used to calculate the corresponding transverse electric fields inside the beam pipe using the Poisson

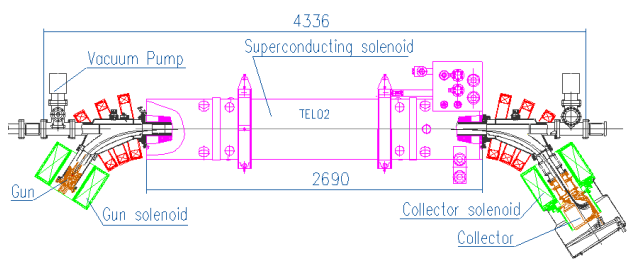


Figure 1: Layout of a Tevatron electron lens. (Dimensions in millimeters.)

* Fermilab is operated by Fermi Research Alliance, LLC under Contract No. DE-AC02-07CH11359 with the United States Department of Energy. This work was partially supported by the US LHC Accelerator Research Program (LARP) and by the European FP7 HiLumi LHC Design Study, Grant Agreement 284404. Report number: FERMILAB-CONF-13-356-APC.

† Email: ⟨stancari@fnal.gov⟩

Copyright © 2013 CC-BY-3.0 and by the respective authors

ISBN 978-3-95450-138-0

LIMITATIONS OF INCREASING THE INTENSITY OF A RELATIVISTIC ELECTRON BEAM*

J.E. Coleman#, D.C. Moir, C.A. Ekdahl, B.T. McCuistian, J.B. Johnson, G.A. Sullivan, and M.T. Crawford, LANL, Los Alamos, NM 87545, USA

Abstract

A 7 cm cathode has been deployed for use on a 3.8 MV, 80 ns (FWHM) Blumlein, to increase the extracted beam current from the nominal 1.7 kA to 2.9 kA. The intense relativistic electron bunch is accelerated and transported through a nested solenoid and ferrite induction core lattice consisting of 64 elements, exiting the accelerator with a nominal energy of 19.8 MeV. The principal objective of these experiments is to quantify the space charge limitations on the beam quality, in addition to its coupling with the corkscrew and the beam breakup (BBU) instabilities. Time resolved centroid measurements indicate a reduction in BBU >5x with simply a 20% increase in the average B-field used to transport the beam though the accelerator. A qualitative comparison of experimental and calculated results are presented, which include axial BBU amplitude with different accelerator lattice tunes.

INTRODUCTION

Relativistic electron beams used to study fundamental nuclear physics or provide intense sources of photons are challenged with instabilities to overcome when increasing the intensity of the beam. One of particular interest is the beam breakup (BBU) instability which manifests itself as a transverse magnet coupling to destroy the beam quality. BBU was first observed in the 1960s [1] and reported in detail by Stanford Linear Accelerator Center scientists in 1968 [2]. Shortly after its discovery, BBU was studied for the first time in detail on the Advanced Test Accelerator, a linear induction accelerator [3].

The first axis of the Dual-Axis Radiography for Hydrodynamic Testing (DARHT) facility is exploring the limitations of increasing the intensity of the electron beam for future radiographic capabilities. DARHT Axis-1 is unique for these studies because it is relatively simple to change the cathode emission size to increase or reduce the total current and therefore change the space charge of the beam while holding everything else constant. In order to effectively increase the intensity of the beam, the BBU instability must be quantitatively understood and effectively reduced. Beam Position Monitors (BPMs) provided time resolved centroid and BBU measurements.

EXPERIMENTAL SETUP

The experimental configuration used to study the BBU instability was the DARHT Axis-1 linear induction accelerator (Fig. 1). The accelerator is composed of a 4 MV Blumlein injector [4] and 32 Blumleins [5] used to drive at total of 64 induction cells (2 cells per Blumlein). The linear induction accelerator is broken up into 8 cell blocks consisting of 8 ferrite induction cores in each cell block for a total of 64 induction cells and 65 anode-cathode gaps. Each induction cell has the ability to impart 250 keV of energy into the beam for a total of 16 MeV in addition to the 3.8 MeV acquired in the diode.

Beam Position Monitors

The transported beam current and centroid is monitored by BPMs at the end of each cell block and internal to each cell block, so there is a BPM every 4 cells with axial spacing between 185-224 cm. The BPMs consist of 8 B-dots, or inductive monitors, oriented azimuthally every 45°. There are 4 position B-dots, 1 top and bottom for ±y measurements and 1 left and right for ±x measurements.

The ±x and ±y B-dots in each BPM were used to measure the BBU amplitude throughout the accelerator. This was done by measuring the unintegrated Δx and Δy which was sampled up to 8 GHz. A fast Fourier transform was applied to the signal over ± 50 ns in addition to the

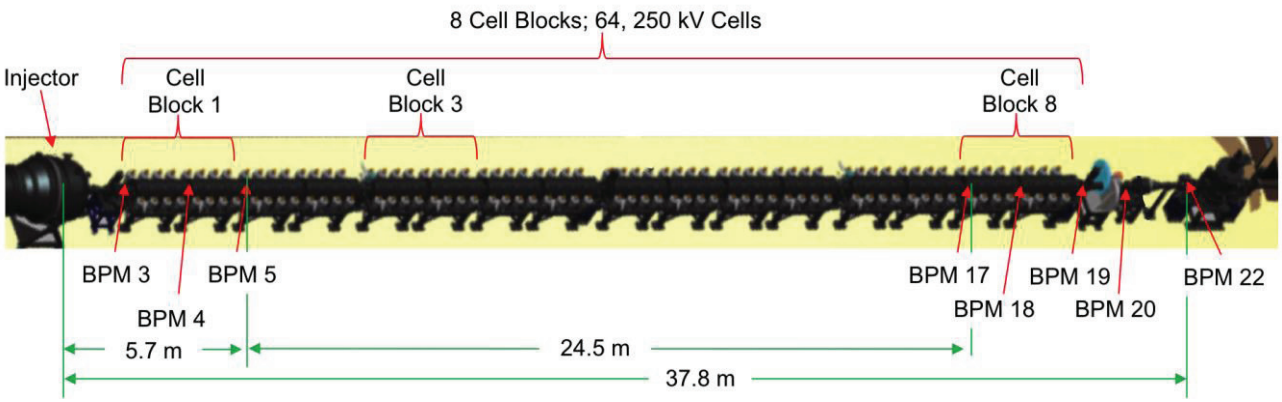


Figure 1: Model of the DARHT Axis-1 accelerator, consisting of the 4 MV injector, 64 induction cells and BPM located after every 4 cells.

* This work was supported by the National Nuclear Security Administration of the U.S. Department of Energy under contract DE-AC52-06NA25396.
#jecoleman@lanl.gov

Copyright © 2013 CC-BY-3.0 and by the respective authors

SYNCHROTRON RADIATION NEAR FIELD IN 3D*

C.-K. Huang#, B. E. Carlsten, and T. J. T. Kwan, Los Alamos National Laboratory,
Los Alamos, NM 87545, USA

Abstract

The Coherent Synchrotron Radiation (CSR) effect plays an important role in particle accelerators where high current electron beams are required, e.g., in X-ray Free Electron Laser. These electron beams are typically compressed to kA current in magnetic bends therefore they are subject to CSR effect. The widely used 1D CSR model relies on particle's radiation field along the circular trajectory near its present position, i.e., Green's function in 1D. We augment our previous 2D numerical CSR model by extending the synchrotron radiation near field calculation in the vertical direction. Our 3D calculation includes the dependence of the field on the relativistic beam energy through the scaled spatial variables and can be used to construct an efficient 3D CSR model due to the self-similarity of the field pattern in these variables.

INTRODUCTION

Coherent synchrotron radiation occurs in accelerators when high current beam bunches move along a circular beam path. It is a collective effect due to the coherence of the synchrotron radiation emitted by individual charge particle in the beam. As the radiation field on a particle is enhanced by the number of nearby particles if they emit coherently, the beam can undergo emittance growth or microbunching instabilities from interacting with its own coherent radiation. CSR is a major adverse effect on the performance of the FEL and has been investigated extensively in 1D and 2D [1-8]. As accurate understanding of the CSR effect requires modeling that accounts for the realistic beam shape and parameters, a 3D model will be essential and valuable. Although various CSR models have been developed so far, the most efficient and widely used models are based on a convolution approach using the time-independent longitudinal synchrotron radiation near-field, i.e., the "Green's function", of a single particle. We note that this near-field Green's function is relative to the present position of the radiating particle and in fact consists of both the near field and far field contributions from the particle at various retarded positions. Extending such CSR model into 3D requires an accurate description of the said Green's function in 3D, which is described in detail in the next two sections.

APPROXIMATE GREEN'S FUNCTION FOR RADIATION FIELD IN 2D

In this section we first review the 2D CSR model developed in Ref. [9]. This will serves as the premise of the 3D model discussed in the next section.

A diagram of the geometry is shown in Fig. 1. It is assumed that an electron is moving along a prescribed circular trajectory of radius R at constant angular velocity in the bending plane perpendicular to the magnetic field. The present and retarded positions of the particle are denoted as P and P', the corresponding velocities denoted as $\vec{\beta}$ and $\vec{\beta}'$, respectively. The field point A is represented by its coordinates (x, α) in this 2D geometry where x is the radial displacement of A relative to P and α is the angular difference between these two points.

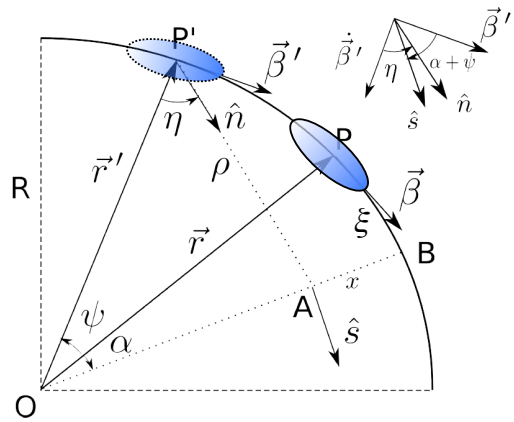


Figure 1: Geometry of the 2D model for calculating the longitudinal electric field from the synchrotron radiation of a particle in uniform circular motion. P and P' are the present and retarded positions of the particle, respectively.

The geometric relations that relate the present and retarded position of the particle are,

$$1+(1+x)^2-2(1+x)\cos(\alpha+\psi)=\psi^2/\beta^2 \qquad (1)$$

$$1+\psi^2/\beta^2-2(\psi/\beta)\cos\eta=(1+x)^2 \qquad (2)$$

where x has been normalized to R.

Using the Padé approximation

$$\cos(\zeta)\approx(1-5\zeta^2/12)/(1+\zeta^2/12)$$

and $|x|<<1$, $|\alpha|<<1$, $\psi^2<<12$, the transcendental equation Eq. (1) can be approximated as,

$$x^2+\alpha^2+2\alpha\psi+(x-\gamma^{-2}\beta^{-2})\psi^2-\psi^4/12\beta^2=0 \qquad (3)$$

After adopting the scaled variables $\tilde{x}=x\gamma^2$, $\tilde{\alpha}=\alpha\gamma^3$ and $\tilde{\psi}=\psi\gamma$, dropping the second term α^2 on the left hand side of Eq. (3) which is only important at the opposition

*Work supported by the LDRD program at LANL.
#huangck@lanl.gov

Copyright © 2013 CC-BY-3.0 and by the respective authors

EXPERIMENTAL VERIFICATION OF DIPOLE EDGE FOCUSING IN LINEAR MODEL BY OPERATING IN THE WEAK FOCUSING REGIME AT THE LOS ALAMOS PROTON STORAGE RING*

J. Kolski†, D. Barlow, R. Macek, and T. Spickermann, LANL, Los Alamos, NM, 87545, USA

Abstract

Linear optics models are important for the operation of circular accelerators because of their ability to predict the linear lattice functions, primarily betatron amplitude functions and betatron tunes. The accuracy of the liner model's prediction is dependent on how well the real machine's focusing lattice is known and represented. While quadrupoles may be mapped magnetically and their focusing properties well understood, the focusing effect due to dipole edge fields is less certain. For rings with rectangular dipoles like the Proton Storage Ring (PSR) at Los Alamos National Laboratory, the dipole edge focusing can be a significant contributor to the vertical focusing. Most accelerator modeling codes, like MAD and AT (Accelerator Toolbox), use the K. Brown formulation[1], but this approach can lead to errors ∼10% in the models betatron tune prediction[2]. Here we discuss particle tracking through simulated dipole fields, including edge effects, with TOSCA 3D to obtain the focal lengths of the edge focusing. We verify model and focal lengths by operating the PSR in the weak focusing regime (without vertically focusing quadrupoles) and show that the model predicts the betatron amplitude functions and tunes even in this unusual operating condition.

INTRODUCTION

The PSR is a 90 m circumference circular accelerator with broken ten-fold FODO cell symmetry, which occurs in the injection section (top of Fig. 1). While most cells have a 36° dipole magnet (SRBM), the injection section starts with a SRBM-type dipole that is shunted by 100 A (SRBM01) to allow room for RIBM09, which merges H- beam with the circulating H+ beam for charge-exchange injection. The dipole at the beginning of the next cell is replaced with two large gapped C-magnets (SRBM11 and SRBM12) accommodating a dump line. Relevant parameters for the five PSR dipoles types are listed in Tab. 1.

All PSR dipoles are rectangular, so including a good representation of the edge focusing is very important for the PSR linear model. There are three parameters in the edge focusing model: gap width, edge angle, and the fringe field integral (FINT) defined by

$$\kappa = \int_{-\infty}^{\infty} \frac{B_0 B_y(s) - B_y^2(s)}{g B_0^2} ds \qquad (1)$$

* Work supported by in part by United States Department of Energy under contract DE-AC52-06NA25396. LA-UR 13-27451.

† Electronic address: jkolski@lanl.gov

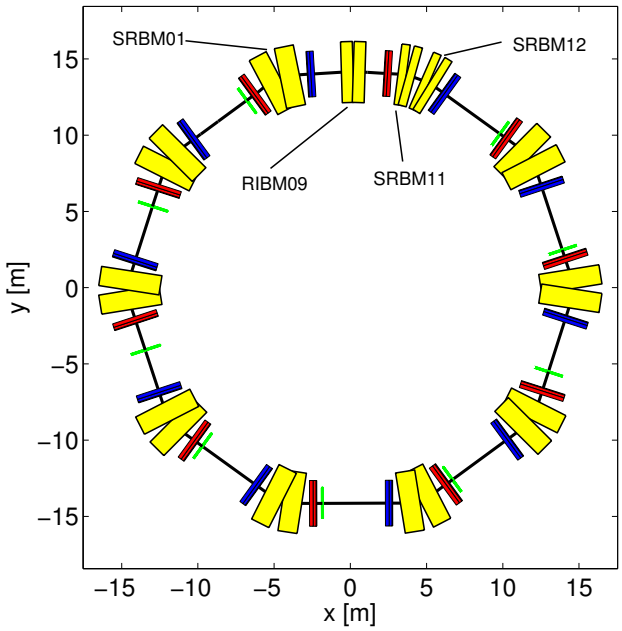


Figure 1: (Color) PSR model: dipoles (yellow) split into two model elements, focusing and defocusing quads (blue and red respectively), and vertical steering magnets (green).

Type	l [m]	θ°	$\theta/2$°	g [cm]
SRBM	2.550	36	18	10.478
RIBM09	1.553	6.8	3.4	12.852
SRBM01	2.542	32.8	11.9	10.478
SRBM11	1.095	16.2	8.1	18.059
SRBM12	1.080	16.2	8.1	12.852

Table 1: Five types of PSR rectangular dipoles.

and related to the edge focusing focal length by

$$\frac{1}{f} = \frac{1}{\rho} \tan\left(\frac{\theta}{2} - \psi\right), \qquad (2)$$

where

$$\psi = \frac{g\kappa}{\rho} \sec\left(\frac{\theta}{2}\right)\left(1 + \sin^2\frac{\theta}{2}\right). \qquad (3)$$

The initial (or baseline) PSR model uses gap width and edge angles from physical measurements and FINT based on applying Eq. (1) to results of a TOSCA 3D magnet field

Copyright © 2013 CC-BY-3.0 and by the respective authors

COHERENT SPACE CHARGE TUNE SHIFT MEASUREMENTS IN THE LOS ALAMOS PROTON STORAGE RING*

J. Kolski†, R. Macek, and T. Spickermann, LANL, Los Alamos, NM, 87545, USA

Abstract

The coherent space charge tune shift describes the average frequency shift experienced by particles due to the effects of the beam's image charge and current and is proportional to the instantaneous beam current. For long beam pulses like the 290 ns long accumulated beam bunch in the Los Alamos Proton Storage Ring (PSR), we can observe the change in the coherent space charge tune shift longitudinally along the pulse. We measure an asymmetric betatron tune profile about the bunch center even though the beam current profile is symmetric about the peak intensity. In addition, we observe the coherent space charge tune shift to vary as a function of turn during a store. Quality measurements of the coherent space charge tune shift may provide a unique handle on interesting physics including wake field effects and electron cloud (EC) buildup. We digitize the vertical sum and difference signals from a beam position monitor, stack the digitized vector turn-by-turn, and fit the tune for each slice (0.5 ns digitization bin) along the pulse after a single-turn vertical kick. We compare the difference between the measured/fitted tune and the measured bare tune with the theoretical tune shift and infer a charge neutralization, which we relate to the EC density along the pulse and buildup in turn number.

INTRODUCTION

The coherent space charge tune shift (measured tune − bare tune) is due to image charge and current effects[1, 2],

$$\Delta\nu_y = -\frac{r_p N}{\pi\beta^2\gamma}\left[\frac{\bar{\beta}_y(\text{ring})}{2\gamma^2 B_f h^2}(1-\eta)+\frac{\pi^2\beta^2 C_2\bar{\beta}_y(\text{bend})}{24g^2}\right], \quad (1)$$

where r_p and N are the classical proton radius, number of protons, β and γ are the relativistic Lorentz factors, $\bar{\beta}_y$ is the average beta function either around the ring or in the dipoles, and B_f, h, η, C_2, and g are the bunching factor (average / peak or instantaneous current), beam pipe radius, beam neutralization, fraction of circumference occupied by dipoles, and the dipole half gap respectively. The first term in Eq. (1) describes the dependence of the coherent tune shift on the instantaneous current, while the second term relates the contribution from the average current. For the PSR, the second contributes ∼15% to the tune shift[1].

We construct a simple simulation of the coherent space charge tune shift using the model in Eq. (1) and a measured beam profile, Fig. 1. To match our measurements (described later), we divide the beam longitudinally into 0.5 ns slices. Initially the simulated beam centroid is offset transversely to produce coherent betatron oscillation, then the transverse beam centroid position is tracked for 420 turns. The FFT along turn for each slice's position yields the tune. The simulation results in a symmetric tune distribution along the bunch as expected because the beam

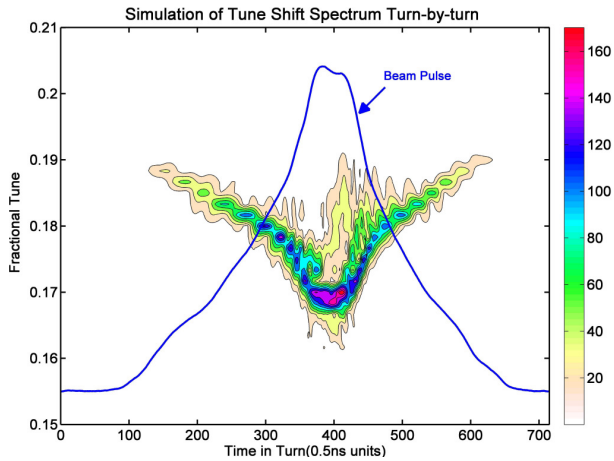


Figure 1: (Color) Simulation of tune distribution along the pulse using coherent space charge tune shift model Eq. (1) (contour) and measured longitudinal beam profile (blue line).

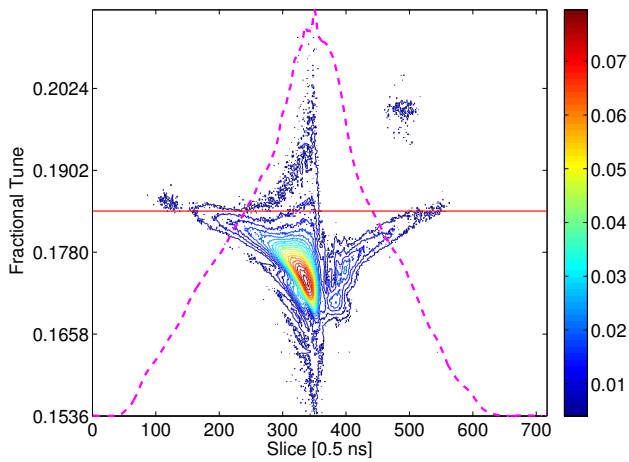


Figure 2: (Color) Measured tune distribution along the pulse (contour) and the last turn beam profile (dashed magenta line).

* Work supported by in part by United States Department of Energy under contract DE-AC52-06NA25396. LA-UR 13-27452.

† Electronic address: jkolski@lanl.gov

ISBN 978-3-95450-138-0

Copyright © 2013 CC-BY-3.0 and by the respective authors

PERFORMANCE COMPARISONS OF EMITTANCE-EXCHANGER BEAMLINES *

C.R. Prokop [1], P. Piot [1,2], B.E. Carlsten [3], M. Church[2]
[1] Department of Physics, Northern Illinois University DeKalb, IL 60115, USA
[2] Fermi National Accelerator Laboratory, Batavia, IL 60510, USA
[3] Los Alamos National Laboratory, Los Alamos, NM, 87544, USA

Abstract

Earlier experiments at Fermilab's A0 Photoinjector Laboratory demonstrated successful transverse-to-longitudinal emittance exchange (EEX) using a transverse-deflecting cavity (TDC) located between two identical doglegs. Such a design has the disadvantage of transversely displacing the beam. An alternative is an EEX beamline designed out of a variable R_{56} bunch compressor chicane. In this paper, we present designs and simulation comparisons for several emittance-exchanger beamlines, including the double-dogleg and chicane designs, as well as variations of the chicane design that allow for increasing its dispersion which proportionally decreases the field-strength requirements on the TDC. These comparisons are performed with PIC models of space charge and coherent synchrotron radiation.

INTRODUCTION

Transverse-to-longitudinal "emittance exchangers" (EEXs) allow for the exchange of a particle beam's transverse and longitudinal phase spaces. [1, 2] An early emittance exchanger design consisting of a transverse deflecting cavity (TDC) between two identical doglegs, each comprised of two opposite dipoles and a drift, was demonstrated at Fermilab's A0 Photoinjector Laboratory [3, 4]. A major disadvantage of such a configuration is its resulting offset of the beam's direction, which has significant impact on linac design as an elaborate dispersion correction scheme would be needed to operate the beamline in its non emittance-exchanging configuration.

A modification of the original design, based on a variable-R_{65} chicane, allows for the exiting beam to remain in-line with the incoming beam [5]. Furthermore, this design allows for almost-arbitrary adjustment of the dispersion at the TDC location, which reduces its power requirements. In this paper, we present three phase-space exchanger designs and performance comparisons between them.

We use two sets of beam parameters for these studies. The first is based on a study of partially compressed beams at ASTA [6], while the other is a smaller set of emittances used for comparisons with reduced second-order effects. Both are presented in Table 1.

Table 1: Initial Beam Parameters

Parameter	symbol	Value (case 1)	Value (case 2)	Units
hor. emittance	$\varepsilon_{x,0}$	10.0	1.0	μm
vert. emittance	$\varepsilon_{y,0}$	10.0	1.0	μm
long. emittance	$\varepsilon_{z,0}$	39.1	10.0	μm
bunch length	$\sigma_{z,0}$	0.8	0.4	mm
LPS chirp	$\mathcal{C}_{z,0}$	0.0	0.0	m^{-1}

OVERVIEW OF PHASE SPACE EXCHANGER DESIGNS

In this Section we summarize the properties of the three beamlines considered through out this paper. Each of the designs must generally satisfy three different requirements [7]. For the dispersive section upstream of the TDC, M_-, we must control of the upstream dispersive section's x dispersion, η_-, and its derivative, $\eta_-\prime$. For TDC section, M_{TDC}, we must control the strength of the TDC as $\kappa = -\frac{1}{\eta_-}$, operated at zero-crossing. For the downstream section, M_+, the dispersive section's transfer matrix must be finely controlled such that the properties satisfy

$$\mathbf{D}_+ = \begin{pmatrix} R_{11,+} & R_{12,+} \\ R_{21,+} & R_{22,+} \end{pmatrix} \mathbf{D}_-, \text{and} \quad (1)$$

$$\kappa = -1/\eta_-. \quad (2)$$

where the $+$ and $-$ signs refer to values associated to respectively the downstream and upstream dispersive sections and $\widetilde{\mathbf{D}} \equiv (\eta, \eta' \equiv d\eta/ds)$ is the dispersion vector.

The most basic design is the Double Dogleg EEX (DDEEX), of a design similar to that implemented at A0. The dispersion η of each dogleg is 0.5 m, and the TDC is centered between the upstream and downstream doglegs. An accelerating-mode cavity is placed immediately downstream of the TDC to correct for the R_{65} term [8]. The dipoles are rectangular, and the exact lengths and distances are described in Fig. 1.

A similar design is a the Nominal-Dispersion EEX (NDEEX), in which the bend angles and geometry of each dogleg are the same, except the bend angles of one of them are reversed such that it forms a chicane rather than a pair of symmetric doglegs. Quadrupoles are placed inside the

* Work supported by LDRD project #20110067DR and by the U.S. DoE Contract No. DE-FG02-08ER41532 with NIU and No. DE-AC02-07CH11359 with Fermilab.

Copyright © 2013 CC-BY-3.0 and by the respective authors

ION BEAM CHARGE NEUTRALIZATION BY FERROELECTRIC DISCHARGE PLASMA *

A.D. Stepanov, E.P Gilson, L.R. Grisham, R.C. Davidson
Princeton Plasma Physics Laboratory, Princeton, New Jersey, 08543, USA

Abstract

Space-charge forces limit the possible transverse compression of high perveance ion beams that are used in ion-beam-driven high energy density physics applications; the minimum radius to which a beam can be focused is an increasing function of perveance. The limit can be overcome if a plasma is introduced in the beam path between the focusing element and the target in order to neutralize the space charge of the beam. This concept has been implemented on the Neutralized Drift Compression eXperiment (NDCX) at LBNL using Ferroelectric Plasma Sources (FEPS). In experiments at PPPL, a perveance-dominated ion beam was propagated through a FEPS and the transverse beam phase space was measured with a slit-slit emittance scanner to characterize the effect of charge-neutralizing plasma on beam divergence.

INTRODUCTION

To reduce the divergence of high-perveance ion beams due to space charge, electrons can be introduced into the beam volume. In most experimental applications, electrons are produced by ion impact ionization of background gas and from secondary electron emission (SEE) from surfaces impacted by the beam. Electrons become confined the electrostatic potential well of the ions, reducing the magnitude of the potential well, which decreases until equilibrium is established between electron production and loss rates. For charge neutralization by ionization of background neutrals, this process typically takes 50 μs.

For charge neutralization of pulsed ion beams with duration < 100 μs, a volume plasma can be introduced into the beam path to provide electrons. Ferroelectric Plasma Sources (FEPS) can produce volume plasmas with low electron temperatures, and have been used successfully on NDCX-I to neutralize the space charge of a converging high-perveance ion beam pulse. Herein, experiments on charge neutralization of a 32-42 keV Ar+ beam with a plasma produced in a ferroelectric discharge are presented.

FERROELECTRIC PLASMA SOURCES

Ferroelectric materials (FE), such as PZT and ($BaTiO_3$) are characterized by a high relative dielectric constant ($\epsilon_r > 1000$) and the presence of a spontaneous electric polarization. It was found that under the application of a fast-changing electric field, high electron current densities are be emitted from the FE surface [1, 2], and plasma can be produced. Plasma sources based on $BaTiO_3$ have been built for use on NDCX-I/II [3] for ion beam charge neutralization. The basic configuration of a ferroelectric plasma source (FEPS) is a slab of ferroelectric material placed between two flat electrodes, one of which is perforated. When a fast-rising voltage pulse (~ 5 kV) is applied between the electrodes, a plasma is formed at the side of the perforated electrode at points of juncture between metal, ceramic, and vacuum. In addition, gas desorption occurs during FEPS discharge, which most likely plays a role in plasma formation. The precise mechanism of operation of FEPS is still under investigation [4].

EXPERIMENTAL SETUP

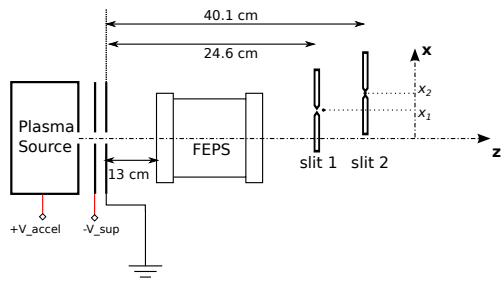


Figure 1: Diagram of the beamline used in the experiment. An Ar^+ beam, extracted from a plasma, propagates through a cylindrical FEPS. Downstream of the FEPS, the beam is intercepted by a two-slit emittance scanner which is used to measure the transverse current distribution of the beam.

The experiments were carried out on the Princeton Advanced Test Stand (PATS) at PPPL. Ar^+ ions are extracted from an RF-driven plasma and formed into a beam with a 3-electrode, accel-decel extraction system with gap length $d = 1.1$ cm and plasma aperture with radius $r_B = 1.5$ mm. The plasma is generated in a multicusp RF source with an internal antenna [5], driven by a pulsed RF power supply. Ion current density up to 28 mA/cm^2 can be extracted. Accelerating potential V_{accel} (30-60 kV) is supplied by an HV pulser [6].

The ion beam exits the accelerator through a grounded aperture at $z = 0$. At $z = 13$ cm, the beam enters a 10.1 cm long FEPS with an inner diameter of 7.62 cm. After the FEPS, the beam is intercepted by a slit-slit emittance scanner. The slits, located at $z_1 = 24.6$ cm and $z_2 = 40.1$ cm, are 2.5" long, 0.1 mm wide, and oriented horizontally. The second slit, referred to as the slit-cup, has a Faraday cup (FC) with SEE suppressor grid mounted directly behind it

* This work is supported by US DOE contract DE-AC02-09CH11466

ISBN 978-3-95450-138-0

Copyright © 2013 CC-BY-3.0 and by the respective authors

IDENTIFICATION OF INTRA-BUNCH DYNAMICS USING CERN SPS MACHINE MEASUREMENTS*

Ozhan Turgut†, John Cesaratto, John Dusatko, John D. Fox
Kristin Pollock, Claudio Rivetta, SLAC, Menlo Park 94025, USA

Abstract

Modern control techniques can be used to design feedback systems for stabilizing the intra-bunch dynamics in the presence of electron cloud (ECI) and transverse mode coupling (TMCI) instabilities. These techniques require reduced models of the bunch dynamics. We present a methodology to identify reduced order linear models representing single bunch dynamics using CERN SPS machine measurements. Vertical motion, in response to a wideband excitation signal, is sampled multiple times across the 5 ns bunch. The data and an observable canonical structure [1] are used to identify the dynamics, which is represented as a discrete time multi-input multi-output (MIMO) system. We focus on mode 0 (barycentric) and mode 1 (head-tail) data to identify a reduced order model. Results show that models clearly capture dominant dynamics and replicate machine measurements with corresponding central tune, damping value for each mode and correct separation between the modes.

INTRODUCTION

Electron cloud and machine impedance can cause intra-bunch instabilities [2]. Modern control techniques can be used to mitigate these problems but require reduced order models of intra-bunch dynamics to design optimal and robust controllers for wideband feedback systems [3]. We use system identification techniques to estimate parameters of linear models representing single bunch dynamics. We briefly explain the reduced order model and identification method. Experimental data was collected from a single bunch with 1×10^{11} protons at 26 GeV with low chromaticity configuration at CERN SPS. This paper includes results from mode 0 and mode 1 dynamics analysis but the methods are in principle applicable to N modes.

MODEL AND IDENTIFICATION

The physical system analyzed in this study is a nanosecond scale SPS bunch. The interaction with the bunch is done via control variables (momentum kick / driving signal) and measured variables (vertical displacement). The control variables and measured variables are discretized to represent the physical system in a MIMO form. The number of samples is arbitrary and depends on the sampling rate of the data acquisition system. These studies use 3.2 GS/s sampling rate allowing us to sample 16 different locations across 5 ns RF bucket [3]. The goal is to estimate the intra-bunch dynamics using these input and output signals.

Reduced Order Model

Any linear dynamical system can be represented in state space matrix form. A discrete time system sampled at every revolution period k with p inputs and q outputs is:

$$\begin{aligned} X_{k+1} &= AX_k + BU_k \\ Y_k &= CX_k \end{aligned} \tag{1}$$

where control variable (external excitation) $U \in R^p$, vertical displacement measurement $Y \in R^q$, system matrix $A \in R^{n\times n}$, input matrix $B \in R^{n\times p}$, and output matrix $C \in R^{q\times n}$. For a MIMO system, the model order determines the complexity.

Identification

Identification of a linear dynamical system is done by casting this problem into a linear least squares form. Assuming full observability, we can represent our state space in discrete time observable canonical form. This will enable us to estimate a minimum number of parameters [1]. However, even for linear systems there are two well known limitations for identification. These are the effect of noise and lack of persistent excitation.

Persistent Input

Input signal design and persistent excitation are critical aspects of system identification. Given a quasi-stationary input of u with a dimension nu and with a spectrum $\phi_u(\omega)$, $\phi_u(\omega) > 0$ should hold for at least n distinct frequencies for u to be a persistent excitation [4]. Random noise would be ideal to excite all the modes in the system but requires high excitation power and bandwidth. The hardware used in these measurements puts constraints on both power and bandwidth. The design of an input signal for identification under given constraints becomes an important question for the future studies.

Noise Sensitivity

Noise affects the performance of the identification, and in certain cases can make identification impossible. We can quantify the effect of the noise by adding noise on a known system until the identification can no longer clearly estimate the known dynamics. We drive a synthetic 2 × 2 coupled MIMO system using a frequency chirp signal with random noise added to the output signals. The effect of noise is tested by running the identification algorithm

* Work supported by U.S. Department of Energy under contract DE-AC02-76SF00515 and the US LHC Accelerator Research Program
† oturgut@stanford.edu

Copyright © 2013 CC-BY-3.0 and by the respective authors

NONLINEAR BEAM DYNAMICS STUDIES OF HIGH-INTENSITY, HIGH-BRIGHTNESS PROTON DRIVERS *

Saeed Assadi#, Karie Melconian, Peter McIntyre, Texas A&M University, College Station, TX

Abstract

Space charge effects, beam losses, wake fields, and orbital control are significant collective effects that affect beam dynamics. The strong-focusing cyclotron incorporates helical orbits with a strong-focusing lattice and high-gradient cavities. It makes it possible to fully separate orbits and suppress interaction between bunches on neighboring orbits. We simulate nonlinear synchro-betratron coupling and explore methods to use the tools of strong-focusing to suppress beam blowup mechanisms.

INTRODUCTION

The Accelerator Resarch Lab at Texas A&M University is developing designs for a strong-focusing cyclotron (SFC) as a high-current (12 mA CW) proton driver for ADS fission [1], production of medical isotopes, and neutron damage studies [2]. The purpose of this paper is to explore how the unique features of the SFC can be used to control nonlinear dynamical effects that limit beam current in accelerators.

Particle motion in the SFC is described in terms of six phase space coordinates (x,x',y,y',ΔE,Δϕ]. The lattice of the Strong Focusing Cyclotron (SFC) requires inclusion of longitudinal or synchrotron motion as one cannot decouple longitudinal and transverse planes past mid-plane analysis. In this case synchrotron motion causes modulations of the parameters or forces and sidebands appear as a result in the tune space. The effects of synchrobetatron couplings and resonance-crossing should become dominant as intensity increases or bunch length elongates.

The SFC lattice combines periodic quad-focusing elements [FD] with common sector magnets and RF cavities, and in this respect it is similar to a combined-function synchrotron. The orbits however are spirals, and dynamics is strongly dependent on initial conditions, and in this respect it is similar to linacs. This results in synchrotron sidebands [1] in the betatron motion with chromaticity as developed by Orlov [2] and synchrobetatron resonances caused by chromaticity as analyzed in a review by Suzuki [3]. The SFC lattice is highly regulated by the arrangement of superconducting beam transport channels (BTCs) [4], Mobius-geometry RF cavities [5], and low-field superconducting sector dipoles [6] to produce matched beta function [β_x, β_y], dispersion [D] and D' to manage emittances. We simulate the SFC as a spiral transmission line, and we include forces from error fields, wake fields, cavity-coupling of bunches, and space charge.

Designs have been developed for a 6-sector 100 MeV SFC (TAMU100, shown in Figure 1) and for a 12-sector 800 MeV SFC (TAMU800) for which TAMU100 would serve as injector. A key element of the SFC is its use of the beam transport channels (BTC), installed along the equilibrium trajectory or each orbit in each sector as shown in Figure 1b. Each BTC contains an FD doublet of Panovsky quadrupoles (up to 6 T/m, used to local tune) and a window-frame dipole (up to .02 T, used to control isochronicity).

Simulation of beam dynamics in both SFCs starts by tracking a 4D map of a bunch propagating through the lattice elements and interacting with EM fields, similarly to the kick codes COSY-INFINITY, Elegant, MADx, and CERN Mathematica. We have started with that framework and added complexity to the simulation as the design progresses. The framework utilizes a combination of mathematical scripts based on COSY-INFINITY fed by Madtomma. Tracking is made using CSRtrack. Figure 2 shows the elements of one cell of an SFC lattice.

We impose a shell on the kick code that operates a simultaneous quadratic optimization, in which we can optimize up to 48 variables that define the isochronous orbits. The framework has evolved to include space charge, chromatic effects, and evolution of bunch-length.

Beam position monitors are provided in a gap at the end of each sector for each orbit. In the planning for commissioning of TAMU100, we plan to inject low-power beam into the first two turns of the lattice with RF off and capture it on a retractable beam dump. That will enable us to verify injection matching and BTC alignment before

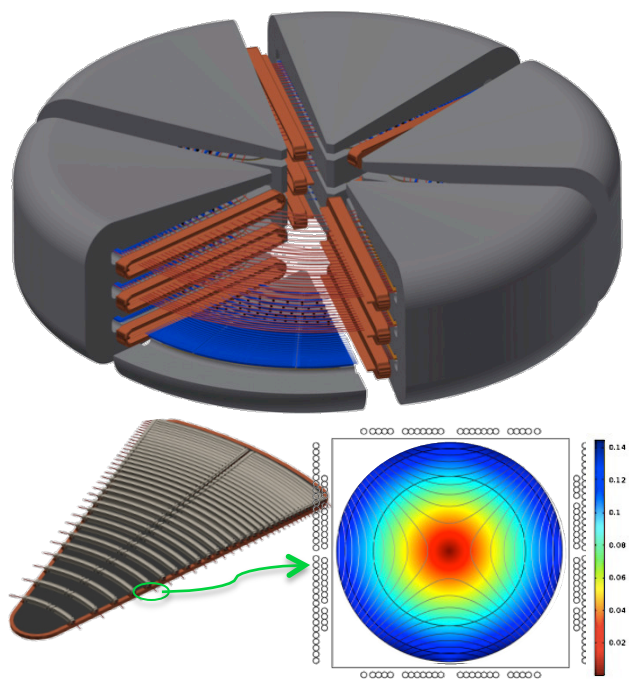


Figure 1. a) 3-stack of 100 MeV SFCs, with cutaway to show superconducting cavities, BTCs, and orbits; b) detail of a sector dipole flux plate and the arced BTCs.

*Work supported by grants from the State of Texas (ASE) and the George P. and Cynthia W. Mitchell Foundation.
assadi@tamu.edu

Copyright © 2013 CC-BY-3.0 and by the respective authors

ISBN 978-3-95450-138-0

INTERACTION REGION DESIGN AND DETECTOR INTEGRATION AT JLAB'S MEIC

F. Lin#, P. Brindza, Ya.S. Derbenev, V.S. Morozov, R. Ent, P. Nadel-Turonski, Y. Zhang,
Jefferson Lab, Newport News, VA, USA
C.E. Hyde, Old Dominion University, Norfolk, VA, USA
M. Sullivan, SLAC, Menlo Park, CA, USA

Abstract

The Electron Ion Collider (EIC) will be a next-generation facility for the study of the strong interaction (QCD). JLab's Medium-energy Electron Ion Collider (MEIC) is designed for high luminosities of up to 10^{34} $cm^{-2}s^{-1}$. This is achieved in part due to an aggressively small beta-star, which imposes stringent requirements on the collider rings' dynamical properties. Additionally, one of the unique features of MEIC is a full-acceptance detector with a dedicated, small-angle, high-resolution detection system, capable of covering a wide range of momenta (and charge-to-mass ratios) with respect to the original ion beam to enable access to new physics. The detector design relies on a number of features, such as a 50 mrad beam crossing angle, large-aperture ion and electron final focusing quads and spectrometer dipoles as well as a large machine-element-free detection space downstream of the final focusing quads. We present an interaction region (IR) design developed with close integration of the detection and beam dynamical aspects. The dynamical aspect of the design rests on a symmetry-based concept for compensation of non-linear effects. The optics and geometry have been optimized to accommodate the detection requirements and to ensure the interaction region's modularity for easiness of integration into the collider ring lattices. As a result, the design offers an excellent detector performance combined with the necessary non-linear dynamical properties.

INTRODUCTION

The MEIC accelerator complex at Jefferson Lab is designed to pursue a high luminosity to understand QCD in the nuclear physics programs [1]. As an interface between the beam acceleration/transport system and the detector, the interaction region (IR) is one of the most challenging parts of the MEIC design and largely determines the performance of the detectors and colliders. To achieve the required physics goals, the IR design should go through an optimization process between the physics requirements and accelerator performance. Besides, as part of the optics design of the complete accelerator complex, the IR design should also consider the modularity for its integration into the collider rings. This paper provides an overall consideration from the detection and accelerator performance points of view in the IR design and demonstrates a well-developed multi-function MEIC IR layout.

#fanglei@jlab.org

IR DESIGN REQUIREMENTS AND CONSTRAINTS

Detector Requirements

The primary full-acceptance detector has a sufficiently large magnet-free space near the interaction point (IP) for detection of particles down to about 0.5° in front of the final focus blocks. In addition, to allow detection of particles scattered between 0-0.5°, the hadrons and electrons need to pass through the large-aperture final focusing quadrupoles and are detected by the further downstream (up to 37 m) detector components. To maximize the detector's acceptance to the forwarding-scattered hadrons and electrons, both the ion and electron beams are focused downstream of the forward final focus so that small beam sizes at the focal points allow one to place the detectors closer to the beam centers. In combination with ~1 m dispersion at those points, this allows detection of particles with small momentum offset $\Delta p/p$. This optics was optimized to maximize its angular and momentum acceptance and detector resolution [2].

The considerations of detection performance in the IR design can be comprehensively described as follows,

1. large detector space (-4.4m / +7m) for a full-acceptance detector,
2. detection of forward scattered hadrons down to 0° achieved by
   - large aperture downstream ion final focusing quadrupoles,
   - strong spectrometer dipole,
   - large machine-element-free drift space after the spectrometer dipole,
   - secondary focus after the spectrometer dipole combined with large dispersion for better momentum resolution,
3. detection of low-Q^2 electrons and electron momentum analysis,
4. large 50 mrad crab crossing angle for faster beam separation to
   - reduce parasitic collisions due to high repetition rate,
   - increase space for magnets,
   - obtain better detector resolution,
5. IP locations
   - close to exit from ion arcs to reduce the residual gas scattering background,
   - far from exit from electron arcs to reduce synchrotron radiation background.

Copyright © 2013 CC-BY-3.0 and by the respective authors

MODELING SPACE CHARGE EFFECTS IN OPTICAL BUNCHERS*

L.V. Ho, P. Musumeci, J. P. Duris, R. K. Li, UCLA, Los Angeles, CA 90095, USA

Abstract

This paper introduces a 1-D, self-consistent simulation of Inverse Free Electron Laser (IFEL) based optical bunchers. Starting with a review of the conventional (monochromatic) IFEL bunching, we consider slow amplitude variation and multiple harmonics of the fundamental radiation wave. We model two new bunching schemes – the adiabatic and harmonic microbuncher and compare the bunching mechanisms between the optical bunchers as well as space charge effects to the modified IFEL interaction. Here, we present a model approximating the space charge fields and verification of the simulation with the well-known Free Electron Laser (FEL) simulator, Genesis 1.3.

INTRODUCTION

In recent years, the Inverse Free Electron Laser (IFEL) has gained popularity because of its accessibility as table-top accelerator with high energy gradient and most of all– because of its ability to microbunch beams on orders of the radiation scale [1]. Microbunched beams finds various applications throughout accelerator and beam physics including its use as a seed for high-gain harmonic generation (HGHG) FEL, preinjectors for advanced accelerators, and production of high quality, high current beams [2, 3].

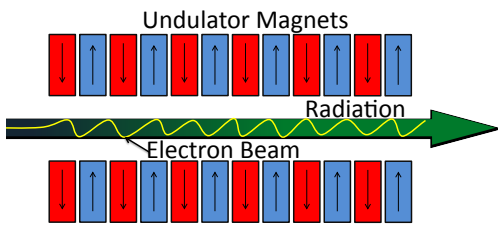


Figure 1: IFEL Interaction - Copropogating electron beam and laser within an undulator.

An IFEL consists of a laser and an electron beam copropogating within an undulator such that the electric field of the radiation is parallel to the wiggling of the electrons induced by the undulator (Figure 1). Efficient energy exchange between the beam and laser occurs when the resonant condition is satisfied – that is, when the electrons have energies such that the oscillation induced by the wiggler in its rest frame is in resonant with the electric field of the laser. This is satisfied when electrons has energy [1]:

$$\gamma_r^2 \simeq \frac{\lambda_\omega}{2\lambda}\left(1+\frac{K^2}{2}\right) \tag{1}$$

where γ_r is the resonant electron energy, λ_ω is the undulator wavelength, λ is the radiation wavelength, and $K = \frac{eB}{mck_\omega}$ is the normalized undulator parameter.

The IFEL was introduced by Palmer in 1972, who proposed the possibility of 10 GeV electron acceleration using the IFEL interaction [4]. In recent years, various experiments have shown the success of IFEL to achieve high-energy gradients with good beam quality [2], with experiments being done in national laboratories such as ATF and Livermore [5, 6]. In addition, the use of the IFEL microbunched beams have been demonstrated to increase radiation gain of over seven orders of magnitude in the HGHG FEL [3].

Here we present a 1-D IFEL simulation with the capability of including slow amplitude variation and multiple harmonics of the fundamental radiation wave. Thus, we can model the three different types of IFEL based optical bunchers: the conventional (monochromatic), harmonic, and the adiabatic microbuncher. With the newly proposed harmonic and adiabatic buncher, the ability to modulate the electron beam density is increased significantly, with bunching factors larger than 90 % [2, 7]. Space charge effects in ultra-relativistic electron beams may no longer be neglected, and considerations of its effects on the resulting beam becomes more important. We first present a review of the IFEL based optical bunchers. Then, we introduce a model approximating the space charge fields and verification of the bunching simulation with Genesis 1.3.

MICROBUNCHING THEORY

Monochromatic Microbuncher

The basic IFEL interaction of microbunching can be described in terms of phase space variables, γ and ψ, as alternative representations of the momentum and position of the electrons. The equations of motion are [1]:

$$\frac{d\gamma_i}{dz} = \frac{1}{2}kK_l\frac{KJJ}{\gamma_i}\sin\psi_i + \frac{e}{m_0c^2}E_i^{sc} \tag{2}$$

$$\frac{d\psi_i}{dz} \simeq k_\omega - k\frac{1+K^2/2}{2\gamma_i^2} \tag{3}$$

where the i denotes the i^{th} electron, $k_\omega = \frac{2\pi}{\lambda}$ is the undulator wavenumber, $k = \frac{2\pi}{\lambda}$ is the radiation wavenumber, $K_l = \frac{eE_0}{m_0c^2k}$ is the normalized radiation potential, and $JJ = J_0(G) - J_1(G)$ is the coupling factor due to the geometry of the undulator, where $G \approx \frac{K^2}{4+2K^2}$.

In the special case where there is no net energy exchange between the radiation and electrons, the resonant energy is constant, $d\gamma/dz = 0$, and modulation of the density of

* Work supported by DOE grant DE-FG02-92ER40693

ISBN 978-3-95450-138-0

Copyright © 2013 CC-BY-3.0 and by the respective authors

STABILITY OF EMITTANCE VS. SPACE-CHARGE DOMINATED BEAMS IN AN ELECTRON RECIRCULATOR *

S. Bernal†, B. Beaudoin, M. Cornacchia, and D. Sutter
IREAP, University of Maryland, College Park, MD, USA

Abstract

We report on experiments and simulations of beam lifetime at the University of Maryland Electron Ring (UMER) for an emittance as well as a strongly space-charge dominated beam. We note the presence of expected (and strong) integer resonances for both beam currents and the absence, for moderate envelope mismatch, of some half-integer resonances for the high current beam only. The observations are related to particle-tracking simulations with the matrix code ELEGANT. The simulations employ a simple incoherent space charge model for a continuous beam, as well as lattice and magnet errors.

INTRODUCTION

The operation of all circular accelerators rely on careful selection of the betatron tunes for optimal beam quality and lifetime. In addition, when collective effects are an important factor, systematic study of current-dependent phenomena, e.g. envelope resonance conditions, is required. The basis for our investigation is the University of Maryland Electron Ring (UMER), a low-energy, high-current compact machine dedicated to beam physics research [1, 2]. We discuss the use of a simple computer model and show that the results are consistent with the main features of experimental beam lifetime charts, i.e. charts that display the surviving fraction of injected beam current at a given turn as a function of betatron bare tunes. Of particular interest is to compare the beam lifetimes of emittance-dominated and space-charge dominated beams.

When space charge is a factor, realistic 6D computer simulations of beam evolution over even a few turns is very computer intensive. Customarily, particle-in-cell codes are employed for tracking hundreds of thousands or even million of macroparticles. Other calculations with space charge such as transverse rms envelope matching are performed with matrix codes such as TRACE3D [3] which employ a linear space charge model and do not allow particle tracking. By contrast, the matrix code ELEGANT [4] can be adapted to do particle tracking in the presence of strong transverse space charge including non-linearities. The ELEGANT model of transverse space charge is only approximate but has yielded satisfactory results in envelope as well as dispersion calculations in UMER [5].

EXPERIMENTS

We have conducted experiments with two electron beams, 0.6 mA and 6.0 mA, both at 10 keV. The initial normalized rms emittances are 0.4 μm (0.6 mA) and 1.3 μm (6.0 mA); the bunch duration is 100 ns for both beams. In one set of experiments, all 70 DC magnetic ring quadrupoles are powered with currents varying from 1.65 to 2.10 A in 10 mA steps, while the injection (pulsed) quadrupoles (YQ and QR1) are kept fixed at the nominal operating currents. For each operating set of quad currents, the transmitted peak beam current is measured with a wall-current monitor located roughly half-way around the ring. In the second set of experiments, the value of one of the injection quads (QR1) is also varied so its focal length equals the corresponding one for the ring focusing quadrupoles. The other injection quadrupole (YQ) could not be varied because it plays a critical role for the injection angle into the closed orbit.

Figure 1a displays the results of beam lifetime at the 10th turn as a function of *estimated* bare tunes for the 0.6 mA beam (emittance dominated) when varying the strength of QR1. Deep red in the figures indicates 90-100% transmission while deep blue or purple near complete loss. The overall beam transmission for the 0.6 mA beam at the 10th turn is slightly improved by varying QR1 (the results with fixed QR1 are not shown), particularly far from the nominal operating point (I_F, I_D) = (1.826,1.826)A, indicated in Fig. 1a by "0". "$I_{F,D}$" refer to the currents of focussing and defocussing ring quadrupoles. Also worth noting is that good transmission for 0.6 mA occurs for $\nu_{0x} \gtrsim 6.5$, but it is greatly reduced for $\nu_{0x} \lesssim 6.5$.

Figures 1 b-c illustrate the beam lifetime results for the 6.0 mA beam (space-charge dominated at injection). The results of varying QR1 are more dramatic for the 6.0 mA beam. In this case, the beam losses near the nominal horizontal bare tune ν_{0x} = 7.5 are markedly reduced. Further, significant beam transmission occurs for highly asymmetric focusing, around (ν_{0x}, ν_{0y}) = (5.5, 8.5), unlike the case for 0.6 mA (Fig. 1a.) Finally, beam transmission for 6.0 mA displays an asymmetry around the line defined by $\nu_{0x} + \nu_{0y}$ = 13, corresponding to a sum resonance. Notice that beam transmission, overall, is noticeably better for the 6.0 mA beam than for the 0.6 mA, with e.g. no visible beam loss at ν_{0x} = 6.5 for the former.

The *estimated* bare tunes in Fig. 1 are determined through a transformation of the quadrupole current space, which is square [(1.65, 2.09) A×(1.65, 2.09) A in 10 mA steps], into the trapezoidal tune space using an effective quadrupole peak gradient per amp of g_0 = 3.95 G/cmA and standard matrix formulas (specifically, the inversion of eqs. 18-ab in Ref. [6].) The choice of g_0 corresponds to a calibration to the observed integer-resonance bands for the *low-current* beam (Fig. 1a). Another model of UMER in ELEGANT based on fitting g_0 to match results from response matrix measurements leads to a slightly different tune calibration [7]. We stress the fact that the plots in Fig. 1 are meant mostly as a guide to study beam lifetime

* Work supported by the U.S. Department of Energy.
† sabern@umd.edu

Copyright © 2013 CC-BY-3.0 and by the respective authors

EXPERIMENTAL DETECTION OF ENVELOPE RESONANCE IN A SPACE-CHARGE-DOMINATED ELECTRON RING*

W.D. Stem, T.W. Koeth, I. Haber, B. Beaudoin, IREAP, University of Maryand, College Park, MD 20742, USA

Abstract

Linear perturbation analysis of the RMS envelope equations predicts a frequency splitting of the transverse envelope modes with the onset of space charge. The resulting resonances are a potential source of beam degradation for circular particle accelerators and storage rings encountering space charge. Following WARP simulations that predict measurable consequences of these resonances, an experiment has been designed for their direct detection. This paper provides a detailed description and preliminary results of an experiment to study envelope resonances in the beam at the University of Maryland Electron Ring (UMER), a scalable high intensity electron storage ring.

INTRODUCTION

In a particle beam, the set of particles that make up the transverse extremes of the beam at any given time is called the envelope. Because each particle oscillates sinusoidally in and out of the bulk, the envelope make-up changes in time. Independently of these particle oscillations, the envelope itself oscillates as described by the K-V equations [1,2,3]. These oscillations can be two different types as shown in Figure 1. The first type is called the breathing or even mode, in which the envelope oscillates in an azimuthally symmetric sense. The second is called the quadrupole or odd mode, in which the oscillations of the envelope are 90 degrees out of phase.

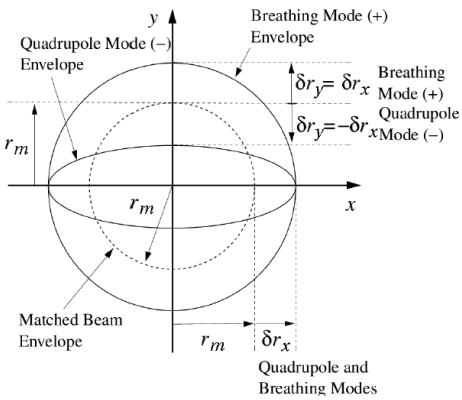


Figure 1: Transverse picture of the envelope modes [4].

At high energies, these envelope oscillations have the same frequency. This frequency occurs at a half-integer resonance, naturally determined from the geometry of the accelerator ring. At the onset of space charge a frequency splitting occurs and we can observe each of these oscillations independently. This frequency splitting is shown for UMER operating parameters in Figure 2.

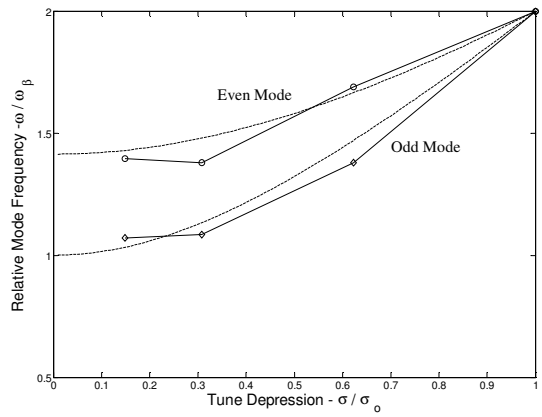


Figure 2: Relative envelope mode frequencies as a function of the tune depression for UMER operating parameters, plotted next to a calculation for the smooth approximation (dashed lines).

If we apply the appropriate perturbation to the envelope in phase with the mode we are trying to identify, the envelope will magnify in amplitude. This amplitude magnification results in the formation of a beam halo as shown in WARP simulation results [5]. After applying the perturbation, we can image the beam halo using a phosphor screen. Sweeping across frequencies, we can identify the resonant frequency of the oscillation as it will be proportional to the formation of beam halo. Applying the breathing mode perturbation may be possible with UMER's existing beam position monitors (BPMs), but the quadrupole mode requires the addition of an electrostatic quadrupole. This paper details the design, fabrication, and bench testing of the electrostatic quadrupole.

QUADRUPOLE DESIGN

In order to apply a quadrupole perturbation to the beam envelope, it is necessary to create a time-varying quadrupole field to match the oscillation frequency of the mode. To accomplish this, we create a resonant LC circuit using the quadrupole as a capacitor. The circuit design is shown in Figure 3.

*Work supported by US Dept. of Energy Offices of High Energy Physics and Fusion Energy Sciences, and by the Office of Naval Research and Joint Technology Office.

ISBN 978-3-95450-138-0

Copyright © 2013 CC-BY-3.0 and by the respective authors

MEASUREMENT OF PLASMA WAVE SPEED FROM ELECTRON BEAM END EROSION*

D. F. Sutter and B.L. Beaudoin, Institute for Research in Electronics and Applied Physics, University of Maryland, College Park, MD 20742, USA

Abstract

The University of Maryland Electron Ring (UMER) normally injects a beam that is square in longitudinal profile (constant line density), filling one half the ring. When operating without longitudinal focusing, the beam head and tail erode at a constant plasma wave speed. Because the beam is very long (580 cm) compared to the beam pipe diameter (5 cm), the two eroding edges remain sharply defined until they meet. This paper describes how the plasma wave speed in the beam can be obtained experimentally by measuring only the initial pulse length, the time it takes for the eroding ends to meet and the kinetic energy. The plasma wave velocity can then be used to get an estimate of the average beam radius during the erosion time. Experimental results are compared to theoretical predictions.

INTRODUCTION

The University of Maryland Electron Ring (UMER) was built to explore the physics of non relativistic, space charge dominated beams that would be relevant for an ion accumulator ring of the type originally envisaged for application in heavy ion fusion. While the operating kinetic energy of 10 keV is very low, it is sufficient at the range of available operating currents, 0.6 to 100 mA, to serve as a good analog model for such accumulator rings. Moreover, because the relativistic gamma factor is only 1.02, there also exist a whole range of non neutral plasma phenomena that cannot be so easily observed in a highly relativistic beam. One of these is the ready generation and observation of plasma density waves. In UMER the beam can be operated with or with out longitudinal confinement [1]. When there is no longitudinal confinement, the initially almost square ends of the injected pulse begin to immediately disperse, or "erode" in a characteristic debunching pattern as shown in Figure 1. The electrons at the leading edge are pushed forward, gaining kinetic energy from the potential energy stored in the electrical potential of the beam charge, and electrons at the trailing edge are decelerated, in effect losing kinetic energy. The edges where the beam is actively eroding into the constant line charge density in the longitudinal beam center retain a sharp definition up to the point where the two edges come together in what is called the "breakpoint" in Figure 1. The rate at which each edge moves toward the center is the plasma wave velocity, c_s, and that is what is measured in this experiment.

* Work funded by the US Dept. of Energy Office of High Energy Physics and the US Dept. of Defense Office of Naval Research and Joint Technology Office.

accelphys@aol.com

PHYSICS OF THE EXPERIMENT

Boundary Conditions

The general operating parameters of UMER have been described elsewhere [2] as has the generation of density waves and solitons [3][4][5][6]. The specific properties that support the non neutral plasma experiments and modelling with cold fluid equations for space charge dominated beams are, the very long bunch length compared to the beam pipe diameter, the low beam velocity, the presence of strong space charge (for beam currents > 1 mA), and a beam density that is approximately constant over the radius. As a consequence, the radial component of the electric field, E_r, points outward and $E_z = 0$ in the region between the eroding edges. In the region between an eroding edge and the head or tail end point, E_z is proportional to the gradient in z of the line charge density, which is no longer constant. Of particular importance to the present technique, the 10 keV beam injected into UMER has an almost rectangular, constant initial line charge density profile with rise and fall times of a few nanoseconds, and a flat top of adjustable pulse length (~20 to 145 ns).

Computing the Wave velocity

The wave velocity, usually referred to as the "sound velocity" of the density wave because it is analogous to the ion acoustic velocity in neutral plasma, can be computed from [4],

$$c_s = \sqrt{\frac{e}{4\pi\varepsilon_0}\frac{1}{m_0 v_{bm}}\frac{g}{\gamma^5} I_{bm}} \quad , \text{ where } \quad g = 2\ln\frac{b}{a} \qquad (1)$$

for space charge dominated beams [3]. Noting that the classical radius of the electron r_e and the "characteristic current" I_0 are defined, respectively, by

$$r_e = \frac{e^2}{4\pi\varepsilon_0 m_0 c^2} \text{ and } \quad I_0 = \frac{e\,c}{r_e},$$

Equation (1) can be rewritten in a more convenient form as

$$c_s = c\sqrt{\frac{1}{\beta\gamma^5}\frac{I_{bm}}{I_0}2\ln\frac{b}{a}}, \qquad (2)$$

where c is the velocity of light, β and γ are the usual relativistic parameters, b is the beam pipe inner diameter and a is the beam radius. Given a set of beam radii corresponding to the relevant operating parameters,

Copyright © 2013 CC-BY-3.0 and by the respective authors

PRELIMINARY ACCELERATOR DESIGN OF A CIRCULAR HIGGS FACTORY IN CHINA

Q. Qin, J.Y. Tang, Y.W. An, S. Bai, J. Gao, H.P. Geng, Y.Y. Guo, D. Wang, S. Wang, Y.W. Wang, M. Xiao, G. Xu, S.Y. Xu, T. Yue, J.Y. Zhai, C. Zhang, Institute of High Energy Physics, Chinese Academy of Sciences, P.O. Box 918-9, Beijing 100049, P. R. China

Abstract

Since the Higgs boson was announced to find at LHC in CERN last July, many labs around the world have showed their interests on building electron positron colliders as Higgs factories to investigate the features of the Higgs boson. IHEP also proposed a circular Higgs factory last Sept. with a circumference of 50 – 70 km, and can be converted to a super proton-proton collider, which can be a discovery machine for new particles and physics. A preliminary design of circular electron positron collider as a Higgs factory is given here.

INTRODUCTION

On July 4, 2012, CERN announced that the Higgs boson was found at the Atlas and CMS experiments of LHC. The mass of the Higgs boson is about 125 GeV, which is only 20 GeV higher than the maximum beam energy LEP reached. After that moment, concept of Higgs factory were proposed, including circular e^+-e^- collider, linear collider, muon collider and γ-γ collider. Among these machines, the international linear collider has been studied by global efforts for more than 10 years, with the TDR [1] just released, but the accelerator technologies of circular machine seem more mature after being developed during the past decades. Muon and γ-γ colliders are also considered as the candidates of Higgs factory, but some of their technologies are still under development. Reviews of these machines can be found in [2].

As the development of future high energy accelerator , a circular e^+-e^- collider (CEPC) as the Higgs factory was proposed in IHEP, China, last Sept. with a circumference of 50–70 km. It can also be converted to a super p-p collider (SppC), with the beam energy of 50 TeV or more, as a discovery machine in the far future. Figure 1 shows a schematic graph of the whole machine (CEPC+SppC).

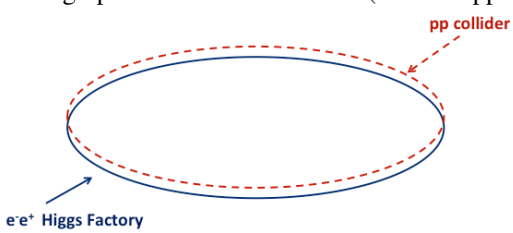


Figure 1: Schematic graph of the CEPC+SppC.

In this paper, we will first describe the determination of beam and machine parameters of the CEPC. Then, the linear lattice of the main ring will be given. The preliminary linear lattice design of the possible SppC converted from the CEPC by using the same tunnel is also presented. Some problems, covering both accelerator physics and technologies, are discussed at last.

PARAMETER DETERMINATION

In this section, main parameters for such a high energy collider will be given, after considering some important effects of beamstrahlung and the limit of synchrotron radiation power.

Beam Energy, Circumference, and Luminosity

As to a collider, beam energy and peak luminosity are the most important parameters.

Since the mass of Higgs particle is 125 GeV, the beam energy of CEPC can be set in the range of 120 – 125 GeV. In such a high energy region, beamstrahlung due to very strong synchrotron radiation (SR) when the two beams interact at IP, will be the main reason of the beam energy spread increase and thus the luminosity reduction. Under this concerning, we choose the lower limit of the Higgs particle, say 120 GeV, as the design energy of the storage ring of CEPC. Figure 2 shows the crossing-section of the Higgs at this energy region [3], from which we can see that though the lower beam energy was taken, the cross-section doesn't decrease too much.

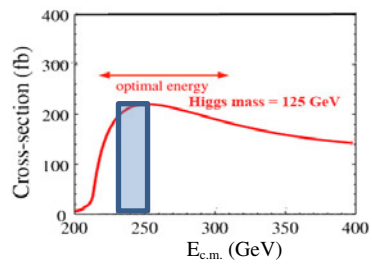


Figure 2: Cross-section at the Higgs energy region.

If we take cross-section of 200 fb and we need 20000 Higgs events per IP every year, we can easily get that the average luminosity will be $1\times10^{34}cm^{-2}s^{-1}$, which is then the design value for the CEPC.

The circumference of the CEPC storage ring can be determined by the future super p-p collider, converted from the CEPC. So the maximum proton beam energy, for example, E_{cm}=50–90 TeV, will be the energy of SppC, and thus we take 50–70 km as the circumference of the CEPC. Here we first use 50 km as the input parameter.

Considering the operation experience of LEP, we take the design value of vertical beam-beam parameter ξ_y as large as 0.1 for the CEPC, and 0.004 for the SppC. Besides these restrictions, another limit comes from the synchrotron radiation power of beam, which is taken as large as 50 MW. As to the 50 km circumference ring, if

Copyright © 2013 CC-BY-3.0 and by the respective authors

ISBN 978-3-95450-138-0

AC DIPOLE BASED OPTICS MEASUREMENT AND CORRECTION AT RHIC*

X. Shen†, S. Y. Lee, Indiana University of Bloomington, IN, 47405, USA
M. Bai, S. White, G. Robert-Domolaize, Y. Luo, A. Marusic, BNL, Upton, NY, 11973, USA
R. Tomás, CERN, CH1211 Geneva 23, Switzerland

Abstract

Independent component analysis (ICA) was applied to the AC dipole based optics measurement at RHIC to extract beta functions as well as phase advances at each BPM. Existence of excessive beta-beat was observed in both rings of RHIC at polarized proton store energy. A unique global optics correction scheme was then developed and tested successfully during the RHIC polarized proton run in 2013. The feasibility of using horizontal closed orbit bump at sextupole for arc beta-beat correction was also demonstrated.

INTRODUCTION

Accurate optics measurement and efficient optics correction schemes are highly demanded to provide more precise optics manipulation for further improvement of RHIC luminosity as well as its polarization performance.

ICA FOR AC DIPOLE BASED OPTICS MEASUREMENT

At RHIC, AC dipole has been routinely used to excite sustained coherent beam motion with large amplitude and preservation of beam emittance to facilitate acquisition of 1024 turn by turn beam position data at the beam position monitors (BPMs) [1]. Optical functions can then be extracted from the recorded BPM data by the technique of independent component analysis (ICA). ICA is more efficient than principle component analysis (PCA) because, in addition to correlations of data from all BPMs, it takes advantage of the time correlation between independent components to extract source signals with non-overlapping spectra [2]. From the spatial functions of source signals corresponding to AC dipole driven oscillation, one may extracted the modified betatron amplitude function β_d and phase advance ψ_d, which are related to the optical functions β_f and ψ_f of free betatron oscillation as [3]:

$$\beta_d = \frac{1+\lambda^2-2\lambda\cos[2(\psi_f-\pi\nu)]}{1-\lambda^2}\beta_f, \quad (1)$$

$$\tan(\psi_d-\pi\nu_d) = \frac{1+\lambda}{1-\lambda}\tan(\psi_f-\pi\nu_f), \quad (2)$$

where $\lambda = \sin[\pi(\nu_d-\nu_f)]/\sin[\pi(\nu_d+\nu_f)]$, ν_d is the driving tune of the AC dipole, and ν_f is the betatron tune of free oscillation. In Eq. (1) and (2), the reference point for phase advance is at the location of the AC dipole. In order to reconstruct the β_f and ψ_f, an accurate and efficient method was developed for routine operation. This method averages optical functions from two measurements in which ν_d is set on either side of ν_f with a distance of 0.01 to minimize the systematic errors from AC dipole driven oscillation. Details about the robustness of this averaging method against BPM errors can be found in Ref. [4].

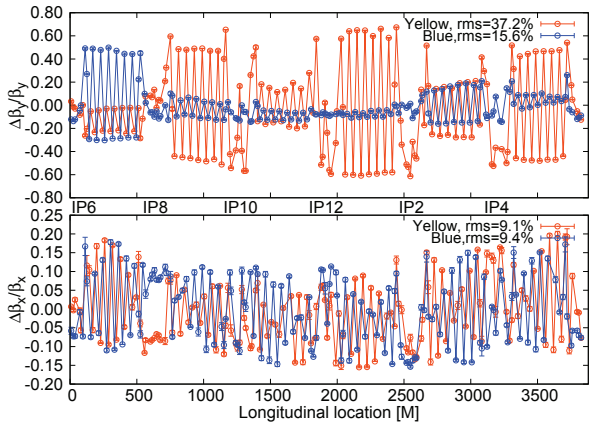


Figure 1: Measured beta-beat with error bars in the horizontal (bottom) and vertical (top) plane for both rings at RHIC. 15% peak beta-beat was observed in the horizontal plane for both rings. A 30% vertical peak beta-beat was found in the Blue ring and 60% in the Yellow ring

Figure 1 shows the beta-beat for the 255 GeV polarized proton beams in the Blue and Yellow rings during RHIC operation in 2013. In both rings, the horizontal peak beta-beat is approximately 15%. In the vertical plane, the peak beta-beat reaches 30% in the Blue ring and 60% in the Yellow ring. The excessively large beta-beat requires efficient correction to be explored.

BETA-BEAT RESPONSE MATRIX CORRECTION METHOD

The problem of beta-beat correction can be described by the following model:

$$\mathbf{WB} = \mathbf{WRK}, \quad (3)$$

where $\mathbf{B}^T = (\frac{\Delta\vec{\beta}_x}{\beta_x}, \frac{\Delta\vec{\beta}_y}{\beta_y}, \Delta\nu_x, \Delta\nu_y)$ is composed of the beta-beat vectors and tune variations, $\mathbf{K}^T = (\Delta K1L_1, \Delta K1L_2, \ldots, \Delta K1L_N)$ represents the change of integrated strength of N quadrupoles, and the superscript T means a transpose. $\mathbf{R}$ is the $M \times N$ beta-beat

* Work supported by grants from the US Department of Energy under contract DE-FG02-12ER41800 and the National Science Foundation NSF PHY-1205431.
† xiaoshen@indiana.edu

Copyright © 2013 CC-BY-3.0 and by the respective authors

IMPLEMENTATION OF OPTICS CORRECTION ON THE RAMP IN RHIC*

C. Liu†, A. Marusic, M. Minty, BNL, Upton, NY 11973, USA

Abstract

In this report we describe and present experimental results from correction of the accelerator optics during acceleration and preparation for collisions at the Relativistic Heavy Ion Collider (RHIC) at BNL. Past experiences with beam optics correction at RHIC have concentrated on measurements and corrections at store beam energies. While well-corrected store beam optics is desirable for maximizing beam and polarization lifetime, well-corrected beam optics during the ramp is also desirable for example to reduce the strength of depolarizing resonances. With optics measurements on the ramp at every 2 or 4 seconds, corrections were computed for several fixed points on the ramp using a well-tested weighted Singular Value Decomposition algorithm. Successful implementation of correction on the second part of the ramp (rotator ramp), together with some observations on the first part of the ramp (the energy ramp) will be presented.

INTRODUCTION

Analysis of depolarizing resonances on the ramp and dynamic aperture study are part of the ramp optics design nowadays in RHIC [1]. Acceptable intrinsic resonance strength and dynamic aperture are ensured by design. With optics errors, both of these quantities are hard to predict. Most likely the machine performance in both aspects will degrade to some extent with optics errors. Therefore, it is desirable to correct the optics on the ramp for better polarization and intensity transmission efficiencies.

Besides continuous efforts for improving TbT (turn-by-turn) BPM data quality over the years [2], there are two developments in 2013 that make ramp optics correction feasible. One of the developments is the precision optics measurement based on ARTUS kicker [3] which is critical for ramp optics analysis. Firing the AC dipole for optics measurement is operational and robust at injection and store energies [4], however, it has not been demonstrated on the ramp during acceleration. Exciting the beam periodically with the ARTUS tune meter kicker has been done previously for the purpose of ramp chromaticity control, however, no successful effort has been applied to extract accurate linear optics information along the ramp. The other development is the successful demonstration of global optics corrections based on both the ARTUS kicker and the AC dipole [5, 6].

* The work was performed under Contract No. DE-AC02-98CH10886 with the U.S. Department of Energy.

† cliu1@bnl.gov

RAMP OPTICS MEASUREMENT

By firing the ARTUS kicker every 2 or 4 seconds on the ramp, TbT BPM data of free betatron oscillations can be recorded in both planes [2]. The timing of the excitations in the two transverse planes is shifted by 510 turns to reduce coupling effects. Special care was taken to avoid interference between TbT and average orbit data taking. The option of 1k, 2k and 4k turns TbT orbit is available. The option of 1k is chosen for the ramp optics measurement since usually the oscillation lasts less than 500 turns due to decoherence. Examples of TbT BPM data are shown Fig. 1.

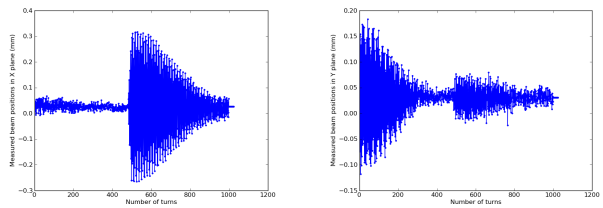


Figure 1: Turn by turn BPM positions in the horizontal (left) and the vertical (right) plane from ramp optics measurement, residual coupling (right) appears in the vertical plane where the horizontal oscillation starts.

As with usual optics analysis, beta functions and phase advances are determined for both planes from TbT BPM data. The analysis technique adopted by the author favors the data in the horizontal plane for better measurement resolution [3]. Therefore, the data in the vertical plane was shifted backwards by 500 turns (data after 500 turns being discarded) before windowed FFT being applied, which also reduces the impact of the residual coupling in the vertical plane after ∼500 turns.

The beta beats and phase errors at 289 s into the ramp are shown in Figs. 2 and 3. The whole ramp takes 320 s. Similar analyses were performed with data acquired every 4 seconds in the Blue ring and every 2 seconds for the Yellow ring. The overall trend of the optics errors is similar for both rings. As beam is being accelerated, the optics error decreases to its minmum in the middle of the ramp. Then the error goes up as beta stars are being squeezed.

RAMP OPTICS CORRECTION SCHEME

For the polarized proton program at RHIC in 2013, the ramp has two parts. The first one, during which the energy is ramped up and beta stars are squeezed, is called energy ramp. The second ramp, during which the rotator magnet ramps up, is called rotator ramp. There are 32 fixed points

Copyright © 2013 CC-BY-3.0 and by the respective authors

ISBN 978-3-95450-138-0

GLOBAL OPTICS CORRECTION IN RHIC BASED ON TURN-BY-TURN DATA FROM ARTUS TUNE METER*

C. Liu†, M. Blaskiewicz, K.A. Drees, A. Marusic, M. Minty, BNL, Upton, NY 11973, USA

Abstract

Deviation of the optical functions from the model may result in reduced dynamic aperture, luminosity and beam polarization all of which are of particular interest in the polarized proton program at RHIC. Peak to peak beta beats as large as +/- 80% have been observed. In Run-13, we demonstrated that the optical functions can be corrected globally by two different approaches, either beta beat or phase error correction. The optics measurement, correction algorithm and beta beat and phase error measurements before and after correction will be presented.

INTRODUCTION

RHIC (Relativistic Heavy Ion Collider) has been running with large beta beat over the years for both heavy ion and polarized proton programs. The impact on dynamic aperture and beam polarization from optics error are expected, however hard to quantify. The optics errors manifest themselves as beta beats (relative error of beta functions), or as phase advance errors, and as the integral, the tune errors. Usually, the luminosity decreases because of enlarged β^* from the presence of beta beat. Therefore, luminosity is expected to benefit from optics correction even though many other parameters contribute as well. Model optical functions are usually used in correction in accelerators, like orbit, tune and chromaticity corrections [1] since calibration of optical functions is non-trivial. The errors in optics obviously set a limitation on the best performance of the corrections. In addition, many critial diagnostics rely on model optics as well. For instance, IPM (Ionization Profile Monitor) uses model beta functions to calculate the beam emittance. The accuracy of all these diagnostics are expected to be improved with the measurement of optical functions and correction. The above facts justify the need of a robust fast turn-around optics measurement and correction scheme.

OPTICS MEASUREMENT

In RHIC, two types of TbT (turn-by-turn) BPM data can be acquired for optics measurement. One is the betatron oscillation driven by the AC dipole [2]; the other is the free betatron oscillation initiated by the ARTUS kicker [3] (tune meter). The oscillation caused by the AC dipole is adiabatical and renders high signal to noise ratio. The ARTUS kicker affects only one bunch, so it is more robust in practice. All measurments and corrections in this paper are based on TbT BPM data acquired using the ARTUS kicker.

TbT data analysis techniques, whether it is a time domain, frequency domain or any statistical method, should in principle deliver similar measurement resolutions provided they are employed to their best capacities. The author adopted a frequency domain method which produces ~0.2 deg phase measurement resolution [4] at RHIC.

In addition to measurements at BPM locations, beta functions at various critical devices can be interpolated based on the measured beta functions at nearby BPMs. First, one calculates the transfer matrices between the device and the upstream and downstream BPMs based on model optical functions. Then two equations can be established which relate the unknown beta and alpha at the device and the measured betas at the two BPMs.

$$\begin{cases} \beta_1 = R_{11}^2\beta_0 - 2R_{11}R_{12}\alpha_0 + R_{12}^2\frac{1+\alpha_0^2}{\beta_0} \\ \beta_2 = r_{11}^2\beta_0 - 2r_{11}r_{12}\alpha_0 + r_{12}^2\frac{1+\alpha_0^2}{\beta_0} \end{cases} \quad (1)$$

Here β_1, β_2 are the measured beta functions at BPM 1 and 2. R and r are the transfer matrices from the device to BPM 1 and 2 respectively. β_0 and α_0 are the unknown Twiss parameters at the device.

CORRECTION SCHEME

Global beta beat correction has been implemented on various accelerators successfully [5]. However, global phase error correction has been proposed but not demonstrated successfully [6]. The basics of the two corrections being applied in RHIC are similar. Suppose $(e_1, e_2, \ldots, e_m)'$ is the optics error (beta beat or phase error) being measured, M is the response of optics errors to quadrupole strength variationd in form of a matrix. The correction can be obtained by solving the following equations:

$$-\begin{pmatrix} e_1 \\ e_2 \\ \vdots \\ e_m \end{pmatrix} = \begin{pmatrix} M_{11} & M_{12} & \cdots & M_{1n} \\ M_{21} & M_{22} & \cdots & M_{2n} \\ \vdots & \vdots & \ddots & \vdots \\ M_{m1} & M_{m2} & \cdots & M_{mn} \end{pmatrix} * \begin{pmatrix} k_1 \\ k_2 \\ \vdots \\ k_n \end{pmatrix} \quad (2)$$

The optics error on the left side are from both planes, on which proper weights can be applied based on the scale of the errors. The correction knobs in RHIC are the 72 quadrupoles with trim power supplies which all reside in the interaction regions [7].

The response matrix for beta beat correction can be calculated either by an optics program (MAD-X) simulation or analytically based on the online model (OptiCalc) optical functions. The analytical formula are presented

* The work was performed under Contract No. DE-AC02-98CH10886 with the U.S. Department of Energy.

† cliu1@bnl.gov

Copyright © 2013 CC-BY-3.0 and by the respective authors

DYNAMIC APERTURE MAXIMIZATION WITH HEAD-ON BEAM-BEAM COMPENSATION IN RHIC*

Y. Luo, W. Fischer, S. White
Brookhaven National Laboratory, Upton, NY USA

Abstract

To reduce the large beam-beam tune spread and to compensate the beam-beam non-linear resonance driving terms, two electron lenses are being installed in the RHIC tunnel for head-on beam-beam compensation. In this article we discuss the approaches to maximize the proton dynamic aperture by adjusting the phase advances between beam-beam interaction points and the electron lenses. We present the beam-beam compensation lattice design, dynamic aperture calculation results, and comparisons between the lattices used in the previous RHIC proton operation.

INTRODUCTION

The working point in the polarized proton collision operation in the Relativistic Heavy Ion Collider (RHIC) is constrained between 2/3 and 7/10 to achieve a good beam lifetime with beam-beam interaction and to preserve the proton polarization on the energy acceleration and at the physics store. To further improve the luminosity, with an upgraded polarized proton source, the proton bunch intensity will be increased from currently 1.8×10^{11} up to 3.0×10^{11}. However, with such a high bunch intensity, there is not enough tune space between 2/3 and 7/10 to accommodate the large beam-beam tune spread.

To reduce the large beam-beam tune spread and compensate the large beam-beam resonance driving terms (RDTs), head-on beam-beam compensation with electron lenses (e-lenses) is adopted in RHIC [1]. Figure 1 shows the layout of RHIC head-on beam-beam compensation. The two proton beams collide at IP6 and IP8. Two e-lenses are being installed on either side of IP10, one for the Blue ring and one for the Yellow ring. To cancel the non-linear beam-beam RDTs from collision at IP8, we require the betatron phase advances between IP8 and the e-lens center to be $k\pi$, where k is an integer.

For the next 100 GeV polarized proton run, we will commission head-on beam-beam compensation for the first time in RHIC. To best utilize head-on beam-beam compensation and to maximize the proton dynamic aperture, we redesigned the proton lattices for both RHIC rings. On top of the above $k\pi$ phase advances between IP8 and the e-lenses, we also attempt to maximize the off-momentum dynamic aperture by adjusting the phase advances between the two collisional IP6 and IP8. In the following, we first discuss the phase requirements for head-on beam-beam compensation, then present the newly designed lattices and the calculated proton dynamic apertures compared with the previous RHIC proton operation lattices.

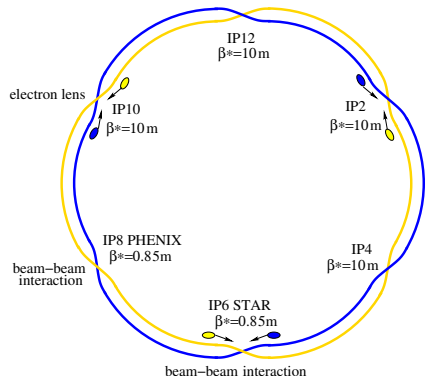


Figure 1: Layout of RHIC head-on beam-beam compensation. Proton beams collide at IP6 and IP8. E-lenses are located on both sides of IP10.

PHASE ADVANCE CONSIDERATIONS

For head-on beam-beam compensation in the proton operation in RHIC, simulation results show that full compensation gives a lower dynamic aperture than that with half beam-beam compensation. With half beam-beam comnpensation, if the phase advances between IP8 and the center of e-lenses is $k\pi$, k being an integer, the non-linear beam-beam RDTs from beam-beam interaction at IP8 will be exactly compensated by the e-lens at IP10 to the first order. For this purpose, we added two shunt power supplies to the main quadrupoles in the arc between IP8 and IP10.

In the previous proton runs, we observed that the particle loss at store took place in the transverse plane with beam-beam interaction. The proton loss rate was found to be proportional to the particle leakage rate from the proton bunch center to the tail. Since the particles in the bunch tail have bigger momentum errors, we concluded that the proton loss at store was caused by the low off-momentum dynamic aperture [2]. To improve it, we need to compensate the chromatic effects and compensate the higher order chromaticities.

In the early studies, we identified that the non-linear chromaticities for the RHIC proton lattices are mainly contributed by the triplet quadrupoles in the two interaction regions IR6 and IR8 where βs are much bigger than other non-collisional interaction regions [3]. From the

*This work was supported by Brookhaven Science Associates, LLC under Contract No. DE-AC02-98CH10886 with the U.S. Department of Energy.

Copyright © 2013 CC-BY-3.0 and by the respective authors

ISBN 978-3-95450-138-0

MEASUREMENT OF BEAM OPTICS DURING ACCELERATION IN THE RELATIVISTIC HEAVY ION COLLIDER

M. Minty#, K.A. Drees, R. Hulsart, C. Liu, A. Marusic, R. Michnoff, P. Thieberger
Brookhaven National Laboratory, Upton, NY 11973, U.S.A.

Abstract

Measurements of the beam optics during acceleration have been performed at the Relativistic Heavy Ion Collider (RHIC). The results were used to obtain a measure of the maximum amplitude of the beta-beat envelope during acceleration which are of interest in the context of emittance and polarization preservation. The measured beta functions were then interpolated to locations of beam profile monitors for more accurate determination of the transverse beam emittances during the energy ramp. In this report we summarize recent improvements in the experimental methods, describe the measurement procedure and present experimental results.

INTRODUCTION

Optics measurements during acceleration are here based on excitation of the beam using pulsed kicker magnets (from the RHIC tune measurement system, ARTUS [1]) as opposed to driven excitations using AC dipoles [2], which are not well suited for measurements during the energy ramp. The response of the beam's change in centroid position was measured using beam position monitors (BPMs). Compared to measurements made previously [3] using the ARTUS kicker magnet [1], the measurement precision has been substantially improved by numerous enhancements made in the BPM and data delivery systems and by the application of continuously operating orbit and tune/coupling feedback [4] used to ensure reproducible and stable conditions during acceleration. For beam optics measurement during the energy ramp, a coherent beam oscillation was excited and single-bunch turn-by-turn (TBT) BPM measurements were acquired. These were carefully interleaved with average orbit measurements used by the orbit feedback. The TBT data were acquired at a selectable maximum rate possible (depending on whether acquisitions were desirable in both RHIC accelerators simultaneously) as limited by the data delivery times. The results were analyzed using slightly modified adaptations of existing frequency-based analyses [5-7] as described in Ref. [8].

In this report we summarize the improvements leading to reliable and robust measurements, describe the measurement procedure and present experimental results.

* The work was performed under Contract No. DE-AC02-98CH10886 with the U.S. Department of Energy.
#minty@bnl.gov

TURN-BY-TURN BEAM POSITION MEASUREMENTS

Past beam optics measurements in RHIC were sometimes compromised by poor BPM performance [9]. During the early years of RHIC operation, modifications (e.g. electronics relocation, gain relay modifications) were made and automated timing scans were developed which contributed to substantially improved performance [10, 11]. Then several issues specific to the turn-by-turn BPM system were resolved: timestamp errors were eliminated (2008), FireWire (IEEE serial bus interface) error checking and staggering using software loop delays were implemented (2009), a RAM data corruption source was located in the integrated front end of the signal processing electronics and corrected (2009), changes were made to interrupt priorities (2009), and Sederta-card memory corruption was identified and eliminated (2010).

DETERMINISTIC DATA DELIVERY

During the shutdown before the RHIC FY11 run, a digital test mode was developed to ensure reliable and robust delivery of TBT BPM data and executed over many months. For each of the ~650 BPMs in RHIC, a test pattern was set at a 0.25 Hz rate in the TBT data array of the local signal processing unit. The received patterns, as logged by the RHIC control system, were subtracted from the expected patterns to detect data handling errors. While the symptoms of data delivery errors were varied (values missing, values repeated, etc.), it was found that they were primarily due to stale data being read back (if overloaded, the Sederta card lost a portion of data and delivered data previously saved in the circular buffer). The errors were solved by further staggering of data transmitted over FireWire using now the RHIC beam sync link turn counter to more precisely stagger the delays to prevent data transmission time overlaps between BPMs. After these modifications, error-free data delivery using the digital test mode was demonstrated: >100,000 acquisitions were performed, where 1 acquisition corresponds to readout of 1024 turns from all BPMs, or about 70 billion readings, with no errors.

ACQUISITION METHODOLOGY

Measurements of the beam optics were made reproducible by ensuring reproducible beam orbits and betatron tunes using the now standard beam feedback systems during acceleration. While orbit and tune

Copyright © 2013 CC-BY-3.0 and by the respective authors

SIMULATION OF HIGH-POWER MERCURY JET TARGETS FOR NEUTRINO FACTORY AND MUON COLLIDER*

R. Samulyak†, Stony Brook University, Stony Brook, NY 11794, BNL, Upton, NY 11973, USA
H.C. Chen, Stony Brook University, Stony Brook, NY 11794, USA
H. Kirk, BNL, Upton, NY 11973, USA
K. McDonald, Princeton University, Princeton, NJ 08544, USA

Abstract

Hydrodynamic behavior of high power targets for future particle accelerators, in particular for the proposed neutrino factory and muon collider, has been investigated via numerical simulations. The target will contain a series of mercury jet pulses of about 1 cm in diameter, interacting with intense proton pulses in 15 – 20 T magnetic fields. Simulations used a smoothed particle hydrodynamics code designed to accurately resolve free surface 3D hydrodynamic flows. Simulation results have been compared with existing experimental data and previous simulations performed with the front tracking code FronTier. New target parameters have also been investigated.

INTRODUCTION

The key element of the target system being designed for the future muon collider and / or neutrino factory is a liquid mercury jet interacting with powerful proton pulses inside a 15 – 20 T magnetic solenoid. The stability of the mercury jet after the proton pulse disruption is a major concern for the target design. The proof-of-principles experiment for high-power mercury target system was conducted at CERN in 2007 [1].

The problem of the slow distortion of the mercury jet entering the solenoid has been evaluated numerically using the FronTier code [2, 3]. FronTier is a hydro- and magnetohydrodynamic code that resolves material interfaces using the method of front tracking. FronTier simulations of the mercury jet cavitation and disruption caused by interaction with proton pulses were presented in [4] and previous works referenced therein. Previous studies have demonstrated that modeling of cavitation and surface dynamics is critical for the simulation of the mercury jet interaction with proton pulses. Cavitation is intrinsically a multiscale phenomenon involving scales from micron-size at the cavitation onset to global scales in later phases of the evolution of bubbles. In FronTier, cavitation was modeled by creating numerically grid-dependent initial cavitation bubbles with tracked surfaces in rarefaction waves of critical strength. Such a cavitation model depends on a number of artificial parameters and makes it difficult to resolve small scales typical for clouds of cavitating bubbles. It is also non-conservative in nature as it removes the liquid and replaces the corresponding volume with gas bubbles. Difficulties with cavitation models prevented us from simulating long time dynamics of mercury jets in 3D.

To improve the modeling of small scales and simulation of long time dynamics of free surfaces flows, we have developed a parallel code based on the smoothed particle hydrodynamics (SPH) [5]. The code has been applied for the simulation of mercury jet targets in the parameter range typical for the muon collider, neutrino factory, and other experimental designs. The present paper only deals with hydrodynamic effects. The study of influence of MHD on the mercury jet cavitation and disruption using particle methods is in progress and will be reported in forthcoming work.

NUMERICAL METHODS

SPH [5] is a Lagrangian particle method in computational fluid dynamics in which deforming Lagrangian cells are replaced with particles. SPH eliminates the main mesh tangling difficulty of the original Lagrangian method while retaining many of its advantages. Due to its Lagrangian nature, SPH is strictly mass-preserving and capable of robustly handling interfaces of arbitrary complexity in the simulation of free surface and multiphase flows. It has known accuracy issues in the numerical approximation of differential operators but these are compensated by the SPH properties of nonlinear stability and conservation, enabling successful usage of SPH for a wide class of problems. We have also developed necessary physics models pertinent to the mercury target problem.

To model properties of mercury, we use the stiffened polytropic equation of state (EOS) [6]

$$P = (\gamma_l - 1)\rho(E + E_\infty) - \gamma_l P_\infty$$

with the adiabatic exponent $\gamma_l = 6.0$ and the stiffening constant $P_\infty = 47$ kbar . The stiffened polytropic EOS extends the range of pressure to negative values in order to account for the transient effect of tension in liquids. When the pressure falls below the cavitation threshold, the interaction between the corresponding particles is eliminated. This causes internal liquid breakups or cavitation. Using this method, cavities can appear on particle-scale length. The particle interactions are resumed if the pressure equilibrates and particles move close to each other causing the merger of fluid fragments.

* Work supported by DOE MAP
† roman.samulyak@stonybrook.edu

ISBN 978-3-95450-138-0

Copyright © 2013 CC-BY-3.0 and by the respective authors

IMPACT OF THE INITIAL PROTON BUNCH LENGTH ON THE PERFORMANCE OF THE MUON FRONT END*

H.K. Sayed,† H.G. Kirk, J.S. Berg, Brookhaven National Laboratory, Upton, NY 11973, USA
K.T. McDonald, Joseph Henry Laboratories, Princeton University, NJ 08544, USA

Abstract

The dependence of the performance of the Front End of a Muon Collider/Neutrino Factory on the proton-beam bunch lengths of 0-20 ns is explored for beam kinetic energies of 3 and 8 GeV.

INTRODUCTION

Some of the requirements on the proton driver for a staged Neutrino Factory based on muons beams [1] are listed in Table 1. Efficient capture of muons in the Buncher of the Front End [2] of the Neutrino Factory favors very short proton bunch lengths. However, meeting the requirement of an intense proton bunch of length only 2 ns is challenging at 3-GeV beam energy because of space-charge effects [3]. We present here a study of the impact of a longer proton bunch on the performance of the Front End.

In the course of related studies [4], an advantage in capture efficiency was found in using a short "taper" to the profile of the capture-solenoid magnetic field, down from the 20 T peak at the target to 1.5-3.0 T at the beginning of the Decay Channel some 4-6 m downstream. Shorter tapers were found to deliver muon beams with smaller time spread at the Buncher for a given proton bunch length at the pion-production target, corresponding to increased capture efficiency of the Buncher. In this study we examined the performance of such short tapers, as well as long adiabatic ones, for proton bunches of 2-20 ns length.

The beam-dynamics simulations were performed using the ICOOL code [5], with input spectra of secondary particles produced at the proton-beam target as modeled by MARS15(2012) [6]. Figure 1 shows examples of pion beams at the end of the target, of length from 2-10 ns, before being tracked through the tapered capture-solenoid, Decay Channel, Buncher, Phase Rotator and Ionization Cooling sections.

CAPTURE EFFICIENCY VERSUS TARGET SOLENOID TAPER LENGTH

Pions (which later decay to muons) are generated at the target with a wide spread in transverse momentum, largely uncorrelated with their longitudinal momentum As they move through the high target solenoid field they develop a correlation between the longitudinal velocity and the initial transverse momentum. The higher the field integral $\int Bdl$ of the target solenoid leads to a larger time spread (*i.e.*, more muons sent out of the longitudinal acceptance of the buncher and rotator). Figure 2 shows the longitudinal phase space of muon beam at the end of the Decay Channel for a short taper of 4'm and a much longer adiabatic one of 40 m. The shorter solenoid taper delivers muon beam with smaller time spread at a fixed longitudinal momentum p_z to the Buncher. Consequently the short taper has an advantage over the more adiabatic long taper as it manages to pack more muons within the longitudinal acceptance of the buncher and phase rotation channels. Figure 3 shows the muon beam time spread at the end of decay channel (50 m from target) for various taper solenoid profiles.

Pions (later muons) produced off the target were tracked through the Front End starting from the end of the target, through the tapered solenoid, Decay Channel, Buncher,

Table 1: Proton-driver requirements for the final and initial stages of a Neutrino Factory.

Parameter	Final Stage	Initial Stage
Proton energy [GeV]	8	3
Beam power [MW]	4	1
Rep. frequency [Hz]	50	70
Bunch length [ns]	2 $\pm$1	2 $\pm$1

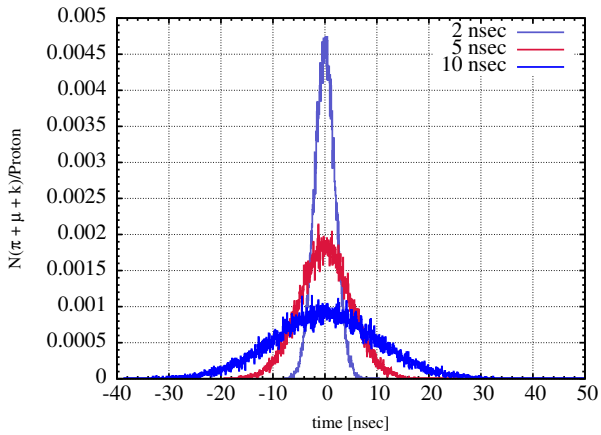


Figure 1: Pion beams with bunch lengths of 2-10 ns off the pion production target.

*Work supported by the US DOE Contract No. DE-AC02-98CHI10886.
† hsayed@bnl.gov

Copyright © 2013 CC-BY-3.0 and by the respective authors

TOWARDS A GLOBAL OPTIMIZATION OF THE MUON ACCELERATOR FRONT END *

H.K. Sayed,† J.S. Berg, H.G. Kirk, R.B. Palmer, D. Stratakis, BNL, Upton, NY 11973, USA
K.T. McDonald, Princeton University, Princeton, NJ 08544, USA
D. Neuffer, Fermilab, Batavia, IL 60510, USA
J. Qiang, R.D. Ryne, LBNL, Berkeley, CA 94720, USA

Abstract

The baseline design for the Front End of a Neutrino Factory and Muon Collider consists of a five major components, namely the Target System, Decay Channel, Buncher, Phase Rotator, and the Ionization Cooling Channel. Although each of the mentioned systems has a complex design which is optimized for the best performance with its own set of local objectives, the integration of all of them into one overall system requires a global optimization to insure the effectiveness of the local objectives and overall performance. This global optimization represents a highly constrained multi-objective optimization problem. The objectives are the number of muons captured into stable bunches of specified transverse and longitudinal emittances, as constrained by the momentum-and dynamic-acceptance of the subsequent acceleration systems in addition to the overall cost. A multi-objective global evolutionary algorithm is employed to address such a challenge. In this study a statement of optimization strategy is discussed along with preliminary results of the optimization.

INTRODUCTION

The capture efficiency of muon Front End [1] of a Neutrino Factory and Muon Collider [2] determines the luminosity of both machines. In the Neutrino Factory scenario only a 4D transverse Cooling Channel is considered, while in the Muon Collider a charge separation follows the Front End before the 6D Ionization Cooling.

The muon beam is produced by bombarding a pion-production target with a 4-MW proton beam that is pulsed at 50 Hz. Produced pions travel through a constant-field solenoid Decay Channel where they decay into muons. Following the Decay Channel, muons go through bunching, phase rotation, cooling, and acceleration sections. Previous studies [3] have shown that using the global Front End performance as the figure of merit in the optimization of local systems improves the performance in a significant way. In this study we identify the parameters in each of the major subsystems of the Front End major that have an impact on the integrated performance, then we optimize the design accordingly.

* Work supported by the US DOE Contract No. DE-AC02-98CHI10886 and DE-AC05-00OR22725.

† hsayed@bnl.gov

TARGET AND MUON FRONT END

The Target System is designed to deliver intense muon beam of 10^{14} muons/sec from an incident beam of 10^{15} protons/s. In the baseline design a liquid-mercury jet target intercepts the 8-GeV proton beam inside a solenoid field that peaks at $B_i = 20$ T at the target and tapers down to $B_f = 1.5$ T over a distance of $L_{\rm taper} = 15$ m. The portion of the mercury jet disrupted by the proton beam is replaced before the arrival of the following proton pulse. This baseline configuration produces 0.8 muons/proton at the end of the Target System.

After the particles leave the tapered target solenoid they are transported in the Decay Channel, Buncher, and Phase Rotator in a constant solenoid field, nominally 1.5 T. At the end of the Decay Channel, $\approx$ 70 m from the target, most pions have decayed into muons and the beam is about 15 m long. The beam is then bunched over $\approx$ 33 m in a sequence of RF cavities with frequencies from 320 to 230 MHz that capture muons with kinetic energy ranging from 50-400 MeV. The bunching cavities RF voltage increases linearly along the channel from 3.4 to 9 MV/m.

In the 42-m-long phase-rotation section, lower-energy muons are accelerated and higher-energy ones are decelerated, until at the end of the Rotator the central momentum is 232 MeV/c, and the original 15-m-long bunch of muons of both signs has been formed into a 48-m-long train with 33 bunches of μ^+ interleaved with 33 bunches of μ^-. The muon beam is then matched into the alternating, 2.8-T solenoid field in the Cooling Channel.

OPTIMIZATION STRATEGY

In this section we identify the parameters in each subsystem that we consider in the global optimization. In the next section we will show the improvement on the performance after optimizing each of those parameters.

Capture Solenoid

The target-solenoid field is parameterized in three variables, the peak initial field at the target location, the taper length, and the end solenoid field. For this study the peak field was either 20 or 15 T The effect of solenoid field profile on the phase space density and distribution of the captured muons was studied by simulating the particles produced at the target and transported through the rest of the Front End. The target-solenoid field profile was shown to

Copyright © 2013 CC-BY-3.0 and by the respective authors

ISBN 978-3-95450-138-0

DESIGN OF THE ILC RTML EXTRACTION LINES FOR THE RENOVATED TWO-STAGE BUNCH COMPRESSOR

S. Seletskiy#, NSLS, BNL, Upton, NY 11973, U.S.A.
N. Solyak, FNAL, Batavia, IL 60510, U.S.A.

Abstract

The renovated two-stage bunch compressor (BC) in the International Linear Collider (ILC) Damping Ring to the Main Linac (RTML) beamline requires new design for the extraction lines (ELs). The ELs located downstream of each stage of the BC will be used for both an emergency abort dumping of the beam and the tune-up continuous train-by-train extraction. They must accept both compressed and uncompressed beam with energy spread of 1.4% and 0.1% respectively. In this paper we report the design that allowed minimizing the length of such extraction lines while offsetting the beam dumps from the main line by 5 m distance required for acceptable radiation level in the service tunnel. Proposed extraction lines can accommodate beams with different energy spreads at the same time providing the beam size suitable for the aluminum ball dump window.

INTRODUCTION

It was decided [1-3] to incorporate a two stage bunch compressor [4] into the final design of the ILC [5]. The renovated two-stage BC compresses 6 mm long beam to 0.3 mm. The beam energy and energy spread after the first stage of the BC are 4.8 GeV and 1.4 % respectively. The beam energy after the second stage is 15 GeV and the beam energy spread, while it depends on the ILC operational mode, is 1.26 % at maximum.

The two extraction lines (ELBC1 and ELBC2) considered in this paper are located downstream of respective stages (BC1 and BC2) of the bunch compressor. The ELs can be used for either an emergency beam abort or for a train-by-train extraction. Since these ELs might receive both compressed and uncompressed beam, they must accept beams with both low and high energy spread.

Each extraction line is equipped with the 220 kW aluminum ball dump, which corresponds to the power of the continuously dumped beam with 5 GeV energy.

EXTRACTION LINES REQUIREMENTS

There are multiple requirements to the extraction lines:

- Due to the requirements of acceptable radiation levels in the service tunnel, horizontal offset of the dump from the main beamline must be at least 5 m center-to-center [6].
- The beam size on the dump window must be at least $\pi\sigma_x\sigma_y$=12 mm^2. Such beam size allows the use of an aluminum window on the dump.
- The beamline apertures have to be large enough to accommodate the beam. The RMS energy spread of the beam can be as large as 1.4% (for ELBC1). Additionally, a reasonable limit for the horizontal β-function is about 5 km. Since one might want to run beams with energy spread of 0.04% (for ELBC2 taking 15 GeV uncompressed beam) to the dump the beam size due to dispersion is no help in maintaining the required beam size on the dump window.
- The elements of the straight-ahead beamline and the extraction beamline must have enough transverse clearance.
- One has to arrange for both the train-by-train extraction and emergency abort of the beam, i.e., the emergency abort kicker has to ramp from zero to full strength in less than the minimum bunch spacing of 150 nsec.
- The magnets must be physically realizable. Here we limit ourselves to 1 T pole-tip fields for the quads, 1.5 T fields for the bends, and 0.05 T fields in septum magnets [6].
- The extraction line must be made as short as possible.

Requirements to the ELs in the final RTML are similar to the requirements specified in [6]. As a matter of fact the extraction system of new ELs is copied from 2008 solution.

EXTRACTION SYSTEM

The abort extraction of the beam is performed by four 2 m long fast kickers, which are powered to 35 G with a rise time of about 100 ns. Routine tune-up beam extraction is performed by a single 1 m long pulsed bend located between two central kickers. The bend is excited to 280 G to make its bending angle compatible with the cumulative angle provided by four fast kickers.

EXTRACTION LINES IN LINEAR APPROXIMATION

To satisfy aforementioned requirements, the linear lattices of ELBC1 and ELBC2 are designed in accordance with the concept considered in details in [6].

To decouple the dispersion and beam size issues we use Double Bend Achromats (DBA) as EL bending blocks. The extraction line is built of the cells, which have periodic solution for the Twiss parameters, and consist of DBA and focusing quads. Number of cells is determined by requirement to sufficient separation between the beam

#seletskiy@bnl.gov

Copyright © 2013 CC-BY-3.0 and by the respective authors

NS-FFAG FOR ELECTRON-ION COLLIDER IN RHIC (ERHIC)*

D. Trbojevic, J. S. Berg, S. Brooks, O. Chubar, Y. Hao, V. N. Litvinenko, C. Liu, W. Meng, F. Meot, B. Parker, V. Ptitsyn, T. Roser, N. Tsoupas, and W. T. Weng, BNL, Upton, New York, USA

Abstract

A future electron ion collider "QCD test facility" is designed in the present Relativistic Heavy Ion Collider (eRHIC) tunnel. Electron acceleration and de-acceleration is preformed with energy recovery linac with multiple passes. We report on a combination of a multi-pass linac with the Non-Scaling Fixed Field Alternating Gradient (NS-FFAG) arcs. A single NS-FFAG arc allows electrons to pass, in the first stage of eRHIC, through the same structure with an energy range between 1.28 and 10 GeV. The NS-FFAG is placed in the existing RHIC tunnel. The 100 MeV injector bring the polarized electrons to the 0.9 GeV superconducting linac. After three passes through the linac 2.8 GeV electrons enter NS-FFAG arc and after 8 passes reach the energy of 10 GeV. After collisions the beam is brought back by the NS-FFAG, decelerated to the initial energy and directed to the dump.

INTRODUCTION

The eRHIC, future "QCD factory", will provide collisions between polarized electrons and: polarized protons in an energy range of 100-250 (325) GeV; light ions (d, Si, Cu); heavy ions 50-200 (130) GeV/u; and, polarized He^3 215 GeV/u. Electrons will circulate in the present RHIC tunnel as shown in Figure 1.

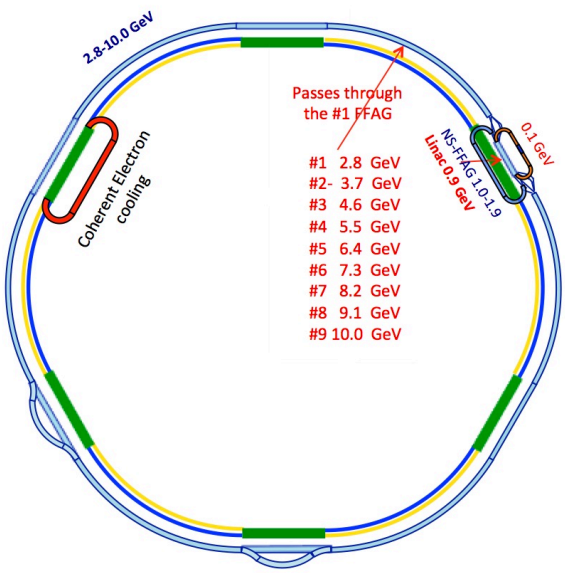


Figure1: Schematic layout of the electron NS-FFAG in the RHIC tunnel – blue and yellow superconducting ion rings are shown, as well as the position of the coherent electron cooling.

The Energy Recovery Linac (ERL) is proposed due to the beam-beam tune shift limitation in the ring-ring case for achieving higher luminosities and due to ability to recover the energy of ~1 GW with a dump energy equal to the injection energy. To reduce the cost and number of elements in the tunnel, a single NS-FFAG ring is proposed with an energy acceptance between 2.8-10 GeV for the first stage of eRHIC.

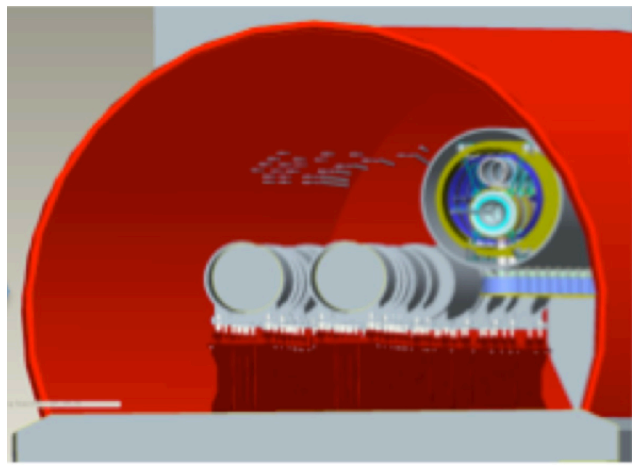


Figure 2: Two RHIC rings with electron linac on the right side above.

Non-Scaling FFAG

Revival of the Fixed Field Alternating Gradient (FFAG) accelerators previously developed in fifties [1,2,3] is very evident. They have very large momentum acceptance with beam accelerated under a constant magnetic field. The scaling FFAG have been mostly built in Japan: started with a the proof of principle (POP) proton accelerator at KEK, the 150 MeV proton accelerator (presently at the Kyushu University), 150 MeV accelerator at Osaka University, and many electron scaling FFAG's built for different applications. Although the scaling FFAG's have an advantage of the fixed magnetic field the synchrotrons are dominant accelerators in spite of magnetic field variation with energy. This is mostly due to significantly smaller aperture requirements. Large aperture magnets accommodate for the large orbit offsets. The aperture size is significantly reduced with the Non-Scaling FFAG's (NS-FFAG) [4]. The maximum of the orbit offsets are -18.6 mm<Δx<0 in the example presented. The NS-FFAG has fixed magnetic fields designed for the reference momentum. The maximum electron energy of 10 GeV, in the first stage of eRHIC, is selected for the reference energy with circular beam orbit. This is to reduce the synchrotron radiation, as the radius of the curvature is r=318 m.

NS-FFAG 2.8-10 GEV

The electron ring follows the shape of the RHIC tunnel and six arcs have 132 identical NS-FFAG cells. Each cell

* Work performed under Contract Number DE-AC02-98CH10886 with the auspices of the US Department of Energy

Copyright © 2013 CC-BY-3.0 and by the respective authors

ISBN 978-3-95450-138-0

DYNAMICAL BETA-SQUEEZE FROM 80 TO 40 CM AT RHIC*

Dejan Trbojevic, Jing Yichao, and Yun Luo, BNL, Upton, New York, USA

Abstract

Relativistic Heavy Ion Collider (RHIC) has been achieving record luminosities during the last decade. The latest stochastic cooling of the heavy ions, like uranium, achieved the largest luminosity at RHIC during the last heavy ion run. A betatron squeeze method, already used at LHC CERN, where a betatron wave is created through the arc up to the interaction region is applied at RHIC. When the heavy beam size is reduced due to stochastic cooling a dynamical beta squeeze is possible to apply in RHIC where the existing 75 cm value of beta-star could be reduced to 45 cm. This could be achieved by introducing the betatron wave in both planes throughout the arc before and after the interaction region. Higher values of dispersion and betatron functions in the arc, with a 90° degrees phase difference per FODO cell allow easier higher order chromatic corrections.

INTRODUCTION

The RHIC stunning discoveries in quark-gluon plasma in recent years went above any expectations that have captured worldwide attention. First and foremost was the unexpected "perfect"-liquid nature of the 4-trillion-degree quark-gluon plasma that permeated the early universe. RHIC is now closing in on the transition from this hot quark-gluon plasma into ordinary matter made of protons and neutrons—namely everything we see in today's world. This is a report on an attempt to improve on the RHIC existing large luminosity by dynamically squeezing the beam size as the stochastic cooling succeeds in reducing all three emittances. The stochastic cooling has already shown tremendous success during the previous RHIC runs. Under this assumption an additional step might be possible in an attempt to increase further the luminosity by additional beta squeeze at the interaction point (IP). This would be possible as the emittances are reduced and the triplet aperture would not present the aperture limitation anymore – as the beam is getting smaller at the IP the maximum of the betatron functions become larger at the focusing triplet quadrupoles. A complex of the RHIC accelerators used to make the latest achievements is shown in Figure 1.

RHIC 90° Lattice

Advantages of the 90° degrees per cell lattice have been well known [1]. The LHC chromatic and other non-linear compensations [2] were followed for the RHIC lattice chromatic corrections after encouraging results in the eRHIC lattice design.

* Work performed under Contract Number DE-AC02-98CH10886 with the auspices of the US Department of Energy



Figure 1: The RHIC accelerator complex shows the major components Linac, Booster, Alternating Gradient Synchrotron (AGS), and RHIC. The Electron Beam Ion Source EBIS is an additional important element.

Major advantage of the 90° lattice is not only reduction in the intra-beam scattering effect but easier linear and non-linear chromatic correction as there are 24 sextupole circuits available in RHIC. The sextupole correction has already shown very impressive results in dynamical aperture improvements during the eRHIC lattice study. The betatron functions of the 90° RHIC lattice with β^*=75 cm is shown in Figure 2.

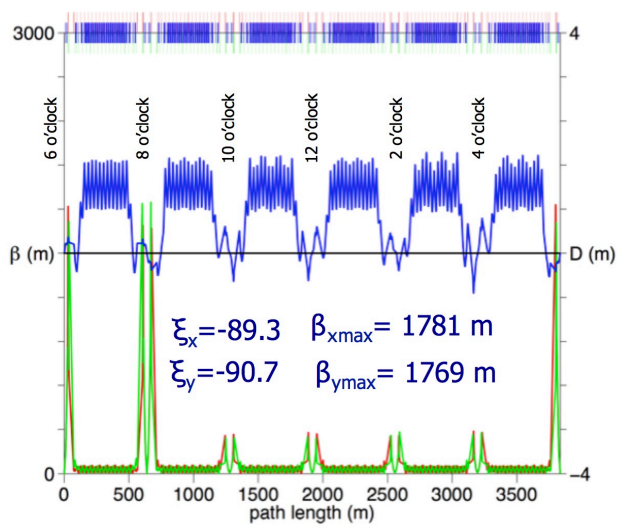


Figure 2: Betatron functions of the RHIC 90° degrees lattice with the β^*=80 cm. Two interaction regions at 6 and 8 o'clock have the same beam size.

Details of the lattice functions around one of interaction regions are shown in Figure 3. The maximum of the dispersion function is D_{max}=1.78 m. The lattice parameters

Copyright © 2013 CC-BY-3.0 and by the respective authors

ERHIC INTRACTION REGION AND LATTICE DESIGN*

D. Trbojevic, E. C. Aschenauer, V. N. Litvinenko, Y. Luo, Jing Yichao, B. Parker, and V. Ptitsyn
BNL, Upton, New York, USA

Abstract

A proposal for the new high luminosity L=10^{34} $s^{-1}cm^{-2}$ polarized electron proton/3He and other un-polarized heavy ions eRHIC based on Electron Recovery Linac (ERL), assumes a location in the existing tunnel of the operating Relativistic Heavy Ion Collider (RHIC). Requests of the experiments for the interaction region are very challenging: allow detection of neutrons, allow deep virtual scattering for protons-electron collisions, detection of partons with lower momentum, etc. We present an interaction region (IR) design with a vey high focusing where at the collision point IP of 5 cm, and a 10-mrad collision angle between electrons and ions using the crab cavities. We are introducing a combined function magnet for the first element in the high focusing triplet configuration to provide neutron and the lower energy parton detection, and allow at 4.5 cm distance passage of electrons through free magnetic field region. The 200 T/m gradient quadrupoles provide very small beam size at the IP and allows a passage with a very small magnetic field for electrons.

ERHIC PHYSICS

The RHIC stunning discoveries in quark-gluon plasma in recent years went above any expectations that have captured worldwide attention. First and foremost was the unexpected "perfect"-liquid nature of the 4-trillion-degree quark-gluon plasma that permeated the early universe. RHIC is now closing in on the transition from this hot quark-gluon plasma into ordinary matter made of protons and neutrons—namely everything we see in today's world. Continuation of the RHIC success will be a new polarized electron-polarized proton/He^3 and electron-ion collider the QCD lab (the quantum chromodynamics describes the strong forces). It would be determining quark and gluon contribution to the proton spin, what is the polarization of gluons, and what is the flavor decomposition of the polarized sea, what is the spatial distribution of quarks and gluons in nuclei, and to explore the strong forces – understand in detail the transition to the non-linear regime of strong gluon fields and the physics of saturation, and have a probe to study deep inelastic scattering.

IR LATTICE FOR HIGH LUMINOSITY

A choice for ERL in the eRHIC is due possibilities of obtaining higher luminosity as the beam-beam effect represents a limitation the ring-ring option. From an injector the beam is accelerated by the superconducting linac using several passes and reaching energies up to 20-30 GeV to be able to reach luminosities of L=10^{34} $s^{-1}cm^{-1}$. We describe an ion lattice and Interaction Region (IR) design to allow small beam sizes with β^*= 10 and 5 cm. It is assumed that coherent electron cooling will reduce the ion beam emittances, allowing very short bunches in the longitudinal space. The strong focusing is possible by placing the first magnet of the triplet at 4.5 m distance from the IP. The IR design is being developed together with the detector physicist designers. The IR in RHIC is made to be symmetric as shown in Figure 1 and in more detail in Figure 2.

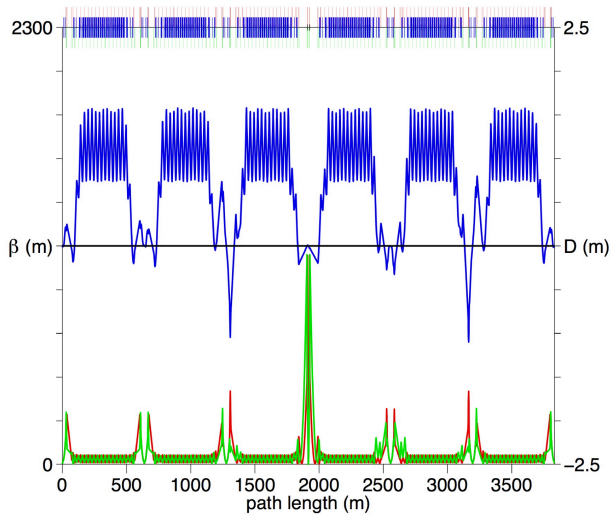


Figure 1: eRHIC lattice design with the β^*=10 cm at the single interaction region at 6 o'clock IP.

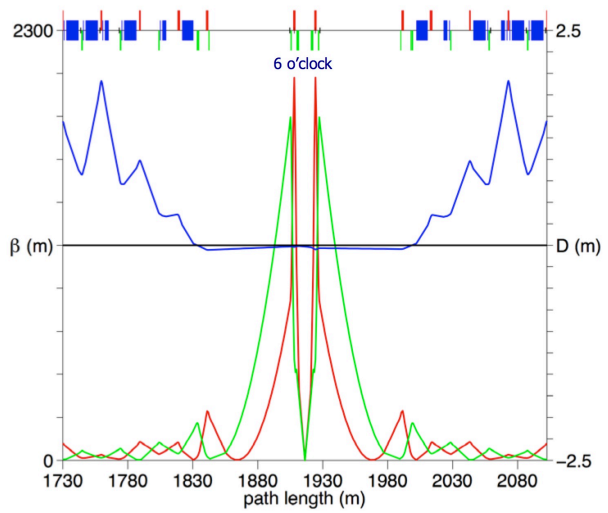


Figure 2: Details of betatron functions in the IR.

The maximum of the betatron function in the triplet magnets, the dispersion function, the chromaticities, and tunes for the β^*=10 cm are shown in Table 1. It is

* Work performed under Contract Number DE-AC02-98CH10886 with the auspices of the US Department of Energy

Copyright © 2013 CC-BY-3.0 and by the respective authors

ISBN 978-3-95450-138-0

nuSTORM PION BEAMLINE DESIGN UPDATE*

A. Liu†, A. Bross, D. Neuffer, Fermilab, Batavia, IL, 60510, USA
S.Y. Lee, Department of Physics, Indiana University, Bloomington, IN, 47405, USA

Abstract

A facility producing neutrinos from muons that decay in a racetrack ring can provide extremely well understood neutrino beams for oscillation physics and the search for sterile neutrinos. The "neutrinos from STORed Muons"(nuSTORM) facility based on this idea has been introduced by Bross, Neuffer et al. The design of the nuSTORM facility and the particle tracking have been presented in the paper of Liu, et al. This paper demonstrates the recent optimization results of the pion beamline, with G4beamline simulations. The optimum choice of pion beam center momentum, a new algorithm on fitting bivariate Gaussian distribution to the pion phase space data at the downstream side of the horn, and the comparison of the beamline performance with the optics designed based on Graphite and Inconel targets are also described.

INTRODUCTION

The overview of the nuSTORM project can be found in the nuSTORM Fermilab proposal [1]. A possible nuSTORM facility design was described in the paper of Liu, et al. [2]. An overview of the facility is displayed in Figure 1. In order to obtain as many useful muons from pion decay as possible, the pion beamline is designed to capture and transport pions within a $P_0 \pm 10\%$ GeV/c momentum range, where P_0 is the design momentum of the pion beamline [3]. P_0 is chosen to maximize the muon flux within a $3.8 \pm 10\%$ GeV/c range. This paper finds P_0=5 GeV/c, as determined by G4Beamline[4] simulations. We also inspect the possibility of using an Inconel target where the pion productivity is checked and compared with the graphite target scenario we proposed in our previous papers.

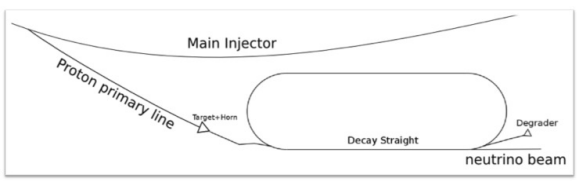


Figure 1: Overview of the nuSTORM facility. The Fermilab Main Injector places proton beam on a target, producing a large spectrum of secondary pions that are transported and injected into the decay ring. The pions then decay within the decay straight to muons , which are captured by the ring. Muons decay and produce neutrino beams with known flux and flavor in the decay straight.

Pions are produced by protons hitting the target, collected by a magnetic horn, transported and injected into the ring by a Beam Combination Section (BCS) and transmitted to the end of the decay straight until extracted. The beamline from the downstream end of the horn to the end of the racetrack ring decay straight is called the pion beamline of nuSTORM. A schematic drawing of the pion beamline in G4Beamline is shown in Figure 2.

PION PRODUCTION AND COLLECTION

nuSTORM is designed to use a 100 kW target station. A proton pulse with approximately 10^{13} protons at 120 GeV and pulse length of 1.6 μs will be extracted from the Fermilab Main Injector and bombarded onto a solid target. The target is partially inserted into a NuMI-like, 300 cm long magnetic horn to collect the pions produced from the target. The horn shape and length are designed to optimize the acceptance of pions within a momentum range of $P_0 \pm 10\%$. A schematic drawing of the horn with the target is shown in Figure 3

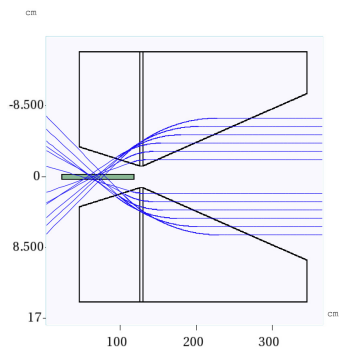


Figure 3: Schematic drawing of the nuSTORM horn and target (middle rod). Protons hit the target from the left.

Selecting The P_0 of The Pion Beam

The probability density of having a muon with momentum p_μ from the decay of a highly relativistic pion is $1/(2\gamma p'_\mu)$ for $0.573 P_0 \leq p_\mu \leq P_0$, where γ is the relativistic gamma of the pion, and $p'_\mu = 29.8$ MeV/c is the muon momentum in the rest frame of the pion. Assuming the pion beam has a uniform momentum distribution over the range $[0.9P_0, 1.1P_0]$, the probability of having a muon with momentum p_μ from this pion beam has a maximum constant value

$$f(p_\mu) = \int_{0.9P_0}^{1.1P_0} \frac{1}{0.2P_0} \frac{m'_\pi c}{2p_\pi p'_\mu} dp_\pi = \frac{2.35}{P_0} \left(\frac{\text{muons}}{\text{MeV/c}}\right)$$

* Work supported by DOE under contract DE-AC02-07CH11359
† aoliu@fnal.gov, also affiliated to Indiana University, supported in part by DE-FG02-12ER41800 and NSF Phys 1205431

Copyright © 2013 CC-BY-3.0 and by the respective authors

A STAGED MUON-BASED FACILITY TO ENABLE INTENSITY AND ENERGY FRONTIER SCIENCE IN THE US*

Jean-Pierre Delahaye (SLAC, Menlo Park, California),
Charles Ankenbrandt, Stephen Brice, Alan David Bross, Dmitri Denisov, Estia Eichten, Ronald Lipton, David Neuffer, Mark Alan Palmer (Fermilab, Batavia, Illinois),
S.Alex Bogacz (JLAB, Newport News, Virginia),
Patrick Huber (Virginia Polytechnic Institute and State University, Blacksburg)
Daniel M. Kaplan, Pavel Snopok (Illinois Institute of Technology, Chicago, Illinois),
Harold G. Kirk, Robert B. Palmer (BNL, Upton, Long Island, New York),
Robert D. Ryne (LBNL, Berkeley, California),

Abstract

Muon-based facilities offer a unique potential to provide capabilities at both the Intensity Frontier with Neutrino Factories and the Energy Frontier with Muon Colliders ranging from the Higgs energy to the multi-TeV energy range. They rely on novel technology with challenging parameters, for which the feasibility is currently being assessed by the U.S. Muon Accelerator Program (MAP) [1]. A realistic scenario for a complementary series of staged facilities with increasing complexity and significant physics potential at each stage has been developed. It takes advantage of and leverages the capabilities already planned at Fermilab, especially Project X and LBNE. Each stage is defined in such a way as to provide an R&D platform to validate the technologies required for subsequent stages. The rationale and sequence of a realistic staging process are presented.

INTRODUCTION

The major discoveries made in 2012, namely the large flavour mixing angle θ_{13} measured at Daya Bay in China and the Higgs boson by the LHC at CERN dramatically modified the Particle Physics landscape. Although the Higgs discovery corresponds to a splendid confirmation of the Standard Model (SM) and no sign of new physics Beyond the Standard Model (BSM) has (yet) been detected at LHC up to at least 1 TeV, BSM physics is necessary to address basic questions which the Standard Model cannot address especially the dark matter, the matter-antimatter asymmetry and the neutrino mass. Therefore the quest for BSM physics constitutes a high priority for the future of High Energy Physics. It requires facilities at both high energy and high intensity frontiers. Neutrino oscillations are irrefutable evidence for BSM physics with the potential to probe up to an extremely high energy range. Neutrino Factories with an intense and well defined flux of neutrinos from muon decay provide an ideal tool for high precision flavour physics at the high intensity frontier. At the high energy frontier, a multi-TeV lepton collider will be necessary as a precision facility to complement the LHC, if and when confirmed, for Physics exploration beyond the Standard Model.

* Work supported by the U.S. Dept. of Energy under contracts DE-AC02-07CH11359 and DE-AC02-76SF00515.

THE BEAUTY AND CHALLENGES OF MUON-BASED FACILITIES

Muon-based facilities [2] offer the unique potential to provide the next generation of capabilities and world-leading experimental support spanning physics at both the Intensity and Energy Frontiers. Building on the foundation of Project X at FNAL, muon accelerators can provide that next step with a high-intensity and precise source of neutrinos to support a world-leading research program in neutrino physics. Furthermore, the infrastructure developed to support such an Intensity Frontier research program can also enable the return of the U.S. high energy physics program to the Energy Frontier. This capability would be provided in a subsequent stage of the facility that would support one or more Muon Colliders, which could operate at center-of-mass energies from the Higgs resonance at 126 GeV up to the multi-TeV scale.

An ensemble of facilities built in stages is made possible by the strong synergies between Neutrino Factories and Muon Colliders, both of which require a high power proton source and target for muon generation followed by similar front-end and ionization cooling channels. These muon facilities rely on a number of systems with conventional technologies whose required operating parameters exceed the present state of the art as well as novel technologies unique to muon colliders. An R&D program to evaluate the feasibility of these technologies is being actively pursued within the framework of the U.S. Muon Accelerator Program (MAP) [1] with impressive R&D results already achieved and a definitive answer expected by 2018 as to whether or not muon-based facilities built in stages can be realistically contemplated.

RATIONALE FOR A STAGED APPROACH

The feasibility of the technologies required for Neutrino Factories and/or Muon Colliders must be validated before a facility based upon these could be proposed. Such validation is usually made in dedicated test facilities which are rather expensive to build and to operate over several years. They are therefore difficult to justify and fund, given especially that they are usually useful only for technology development rather than for physics.

Copyright © 2013 CC-BY-3.0 and by the respective authors

ISBN 978-3-95450-138-0

BEAM-BEAM STUDIES FOR HL-LHC*

A. Valishev#, FNAL, Batavia, IL 60510, USA, D. Shatilov, BINP, Novosibirsk 630090, Russia
T. Pieloni, CERN, Geneva, Switzerland, D. Banfi, J. Barranco, EPFL, Lausanne

Abstract

The analysis of beam-beam effects for the High Luminosity LHC upgrade is in progress as a part of HiLumi LHC Design Study. We report on the current status of beam-beam simulations with the particular emphasis on single and multi-particle weak-strong tracking studies. We evaluate the LH-LHC performance scenarios, and outline the plan of further research.

MOTIVATION AND APPROACH

A major upgrade of the Large Hadron Collider aiming at a significant increase of its luminosity beyond the design value is planned for around 2020. The machine configuration, called High Luminosity LHC (HL-LHC) will incorporate a number of technological advances bringing the beam intensity, brightness and overall accelerator precision to an unprecedented level. The global HiLumi LHC Design Study is in progress with the goal of delivering an integrated design to facilitate the upgrade [1]. Quite naturally, the examination of beam dynamics aspects constitutes an essential part of the effort. In the HiLumi structure, Work Package 2 covers accelerator physics subjects and combines the following Tasks: Coordination and Communication; Optics and Layout; Intensity Limitations; Beam-Beam Effects; Beam Parameter and Luminosity Optimization. The Tasks work in close collaboration with each other to enable the development of a coherent view on the beam dynamics. The goal of Beam-Beam Task is to evaluate the possible performance limitations arising from beam-beam interactions, to define key parameters such as minimum required beam separation and maximum acceptable beam brightness values and to identify optimum beam configurations for the different operating scenarios.

The studies of beam-beam interactions at HL-LHC are grouped into two categories: the weak-strong (incoherent) and the strong-strong (coherent) effects. The proposed values of beam brightness at HL-LHC suggest that the weak-strong effects are more likely to result in performance limitation through the creation of resonances causing particle losses and emittance growth. As such, the incoherent effects are the focus of the present report. For the strong-strong effects see e.g. Ref. [2, 3].

*Fermi Research Alliance, LLC operates Fermilab under contract No. DE-AC02-07CH11359 with the U.S. Department of Energy. This work was partially supported by the US LHC Accelerator Research Program (LARP). The HiLumi LHC Design Study is included in the High Luminosity LHC project and is partly funded by the European Commission within the Framework Programme 7 Capacities Specific Programme, Grant Agreement 284404.

#valishev@fnal.gov

PERFORMANCE SCENARIOS

A detailed description of the baseline HL-LHC scenario can be found in Refs. [4, 5]. Here we present the parameters relevant to the simulations reported further.

The so-called 'stretched' baseline HL-LHC scenario presumes that at the beginning of a high-energy run (fill), the beams collide at IP1 and IP5 (Atlas and CMS experiments) at the full crossing angle of 590 μrad. Due to the large geometrical reduction, the total beam-beam tune shift is quite moderate and does not exceed 0.015 for the case of 3 head-on collisions. The transverse separation at long-range collision points is 12.5 beam sigma. As the beam intensity decays due to the luminosity burn-off, the bunches are gradually tilted with respect to the reference trajectory (crabbed) using RF crab cavities, which results in a head-on collision at the end of the fill. This achieves a constant (leveled) luminosity of 5×10^{34} cm^{-2}s^{-1}, thus allowing to maximize the luminosity integral. The beta-function at IP1/5 during leveling remains constant at 15 cm.

Table 1: 'Stretched' Baseline HL-LHC Parameters for 25ns Bunch Spacing

Parameter	Value
Protons/bunch	2.2×10^{11}
Number of bunches	2808
Crossing angle	590 μrad
β*	15 cm
Normalized emittance	2.5 μm
Energy spread	1.2×10^{-4}
Bunch length	7.5 cm
Beam-beam tune shift per IP	0.0033

In the baseline HL-LHC scenario the luminosity is leveled such that the number of events per crossing (pile-up) does not exceed the limit set by experiments. However, it was recently recognized that the longitudinal pile-up density (the number of events per unit length or unit time) also needs to be limited. This can be achieved through maximizing the length of luminous area by keeping the bunches always colliding fully head-on (crabbed). The luminosity leveling in this scheme is performed by the transverse offset or change of beta-function, i.e. β*=70 cm at the beginning of a fill, and then is gradually reduced to 15 cm.

Copyright © 2013 CC-BY-3.0 and by the respective authors

COHERENT INSTABILITY DUE TO BEAM-BEAM INTERACTION IN HADRON COLLIDERS*

S. Paret, J. Qiang, LNBL, Berkeley, CA, 94720, USA

Abstract

Beam-beam effects can excite coherent modes in circular colliding beams and can thereby cause coherent instabilities. Nevertheless the beams in LHC have been well behaved and no fundamental limitation to the beam-beam parameter has been found in head-on collisions. In this paper we consider beams with much higher intensities than ever collided in any hadron collider. By virtue of 3D strong-strong computer simulations, we investigate the coherent stability and emittance growth of proton beams in head-on collision. The impact of a crossing angle between the beams and of a transverse damper is examined.

INTRODUCTION

In lepton colliders, a changed scaling of the luminosity and the beam-beam parameter with intensity has been observed when the intensity exceeded a threshold [1]. The dynamics of colliding hadron beams differs qualitatively from that of electron beams because radiation damping is negligible for hadrons. Therefore hadron beams are assumed to be more prone to instabilities. In the LHC however, the intensity or beam-beam parameter have not been limited by beam-beam effects due to head-on collisions [2]. Beam-beam effects at the highest beam-beam parameter achieved in LHC are discussed in Ref. [3, 4]. In this paper we consider the coherent stability at intensities well beyond the performance of present colliders to identify possible inherent beam-beam limitations for future colliders.

Analytic models of the coherent stability apply only to simplified cases, like assuming linear self-fields and no crossing angle [5, 6]. These models predict unstable regions in the parameter space. Head-tail modes, on the other hand, have been found to be generally stable as long as impedances are neglected [7]. The computer simulations discussed here are not subject to the limitations of the analytic models. In the next section the setup of our simulations is outlined. A discussion of results and conclusions follow in the subsequent sections.

SETUP

The beam parameters chosen for our simulations loosely follow the LHC setup, except for the intensity. The intensity of the beams in our simulations was increased until strong coherent effects were observed. Table 1 lists the simulation parameters. Initially, the particle distribution was Gaussian. One pair of bunches collided once per turn. The corresponding beam-beam parameter without crossing angle is 0.067. According to the linear model developed in Ref. [6], these bunches will experience a quadrupolar instability.

Table 1: Simulation Parameters

Parameter	Value	Unit
N	21×10^{11}	-
ϵ	0.512	nm
β^*	0.5	m
σ_L	0.077	m
δ_p	1.11×10^{-4}	-
Q_x, Q_y, Q_z	0.31, 0.32, 0.00212	-
E	7	TeV
N_m	1,000,000	-
Slices	10	-

Table 2: The Four Cases Discussed in This Paper

Case	Crossing angle	Damper
A	0	off
B	0	on
C	0.15 mrad	off
D	0.15 mrad	on

The beam-beam kicks were computed self-consistently using a Green's function method [8]. The numerical noise in self-consistent simulations can drive emittance growth [9, 10]. However, in the cases considered here, the physical emittance growth is so large that the numerical contribution is negligible. In fact, using 4 times more macro particles in a simulation of case D changed the emittance growth by about 3 % only. Impedances and electron clouds have been neglected because they would obscure the pure beam-beam effects.

Collisions with and without crossing angle as well as with and without transverse damper are discussed. In the following section these 4 cases will be referred to by the letters specified in Tab. 2. The damper model is described in Ref. [10].

RESULTS

First we consider the case A. The offset and emittance are shown as a function of time in Fig. 1. The centroid motion is unstable and the emittance grows by several 10 %/s. From 12,000 to 50,000 turns, the horizontal oscillation is damped while the emittance growth is accelerated. A list of emittance growths after different time intervals for all cases is provided in Fig. 3. For either plane, the average growth of both beams is given.

* This work was partially supported by the U. S. LARP and NERSC of the U. S. Department of Energy under contract No. DE-AC02-05CH11231.

ISBN 978-3-95450-138-0

Copyright © 2013 CC-BY-3.0 and by the respective authors

DESIGN AND HIGH ORDER OPTIMIZATION OF THE ATF2 LATTICES*

E. Marin†, G. White, M. Woodley, SLAC, Menlo Park, CA 94025, USA
K. Kubo, T. Okugi, T. Tauchi, J. Urakawa, KEK, Ibaraki, Japan
R. Tomás, CERN, Geneva, Switzerland

Abstract

The next generation of future linear colliders (LC) demands nano-meter beam sizes at the interaction point (IP) in order to reach the required luminosity. The final focus system (FFS) of a LC is meant to deliver such small beam sizes. The Accelerator Test Facility (ATF) aims to test the feasibility of the new local chromaticity correction scheme which the future LCs are based on. To this end the ATF2 nominal and ultra-low beta* lattices are design to vertically focus the beam at the IP to 37nm and 23nm, respectively if error-free lattices are considered. However simulations show that the measured field errors of the ATF2 magnets preclude to reach the mentioned spot sizes. This paper describes the optimization of high order aberrations of the ATF2 lattices in order to minimize the detrimental effect of the measured multipole components for both ATF2 lattices. Specifically three solutions are studied, the replacement of the last focusing quadrupole (QF1FF), insertion of octupole magnets and optics modification. By applying the mentioned cures the design vertical beam size at the IP is almost recovered for both ATF2 lattices.

INTRODUCTION

The International Linear Collider (ILC) [1] and the Compact Linear Collider (CLIC) [2] projects are designed to deliver a luminosity at the interaction point (IP) above $10^{34}\mathrm{cm}^{-2}\mathrm{s}^{-1}$ by colliding e^+e^- beams of vertical sizes in the nanometre scale. The final focus system (FFS) provides the required beam focusing by means of two strong quadrupole magnets, so called Final Doublet (FD), which are located at a distance L* upstream the collision point. The FD generates chromaticity due to the inherent energy spread of the particle beam which needs to be corrected in order to preserve the vertical IP beam size.

The ATF2 [3] beam line is the extension of the Accelerator Test Facility (ATF) meant to validate the feasibility of the final focus systems (FFS) based on the local chromaticity correction scheme, first proposed in [4]. To this end the ATF2 nominal and ultra-low lattices are designed to obtain a σ_y^* of 37 nm and 23 nm respectively. The nominal lattice is the scaled-down version of the FFS of ILC while the ATF2 ultra-low β^* lattice [5] features a β_y^* a factor 4 smaller than nominal, in order to increase the chromaticity to a value similar to that of the CLIC FFS. This challenging optics explores the feasibility of ultra-low β^* lattices.

Reducing the value of β_y^* imposes tight constraints on the magnetic field tolerances of the FFS magnets, particularly for those magnets located at high beta regions, e.g. FD. The lattice design that recovers the design vertical spot size σ_{y0}^* for both ATF2 lattices is described in the following.

LATTICE DESIGN

In order to overcome the destructive impact in terms $\sigma_{x,y}^*$ of the multipole components of the ATF2 magnets, described in [6], different solutions have been considered in [7]. These include replacing the FD, reducing the vertical emittance or increasing the β_x^*. Reducing the vertical emittance is not a cost effective solution. Increasing the value of the β_x^* by a factor 4 effectively reduces the impact of the multipole magnets for both ATF2 lattices, yet it is not the preferred solution since it deviates from the IP beam aspect ratio that the ATF2 nominal lattice was designed for to mirror that of the ILC FFS. In 2012 it was decided to insert 4 skew sextupole magnets [8] meant to compensate for the skew sextupole components of those quadrupole magnets that do not meet the required tolerances, see [9]. Further the focusing quadrupole magnet of the FD was replaced by a 4Q17 type recycled from the PEP-II ring, due to its better field quality. As a result of these beam line modifications the impact of the multipole components becomes negligible for the ATF2 nominal lattice. Although these modifications also minimise the impact of the multipole components for the ATF2 ultra-low β^* lattice, they are not sufficient. The σ_y^* obtained is still 30% larger than design value. The analysis of the high order aberrations of the IP beam size carried out in [10] by the MAPCLASS code [11] determines that a chromatic third order (octupole) component is the main contributor to the calculated $\Delta\sigma_y^*$. The insertion of a pair of octupole magnets is proposed in [10] as an effective solution for compensating this particular aberration.

Octupole Magnets

Two octupole magnets located at dispersion and dispersion-free regions of the ATF2 beam line, namely OCT1FF and OCT2FF respectively, counteract the effect of the chromatic octupole aberration on the vertical IP beam size. It is found that these octupole magnets can reduce the σ_y^* down to 24 nm. More details can be found in [10].

In terms of field quality, the tolerances have been evaluated for both decapole and dodecapole components, Table 1 summarises the tolerances for both octupole magnets. Tighter tolerances are found for the OCT1FF which is located at the dispersion region but all of them are easily achievable from the point of view of magnet design. CERN has taken the initiative to design and construct a pair

* Work supported by Department of Energy contract DE-AC02-76SF00515.
† emarinla@slac.stanford.edu

Copyright © 2013 CC-BY-3.0 and by the respective authors

COUPLING SPIN RESONANCES WITH SIBERIAN SNAKES*

Nermeen Khalil†, Stony Brook University, Stony Brook, NY 11794, U.S.A.
V. Ptitsyn, Brookhaven National Laboratory, Upton, NY 11973, U.S.A.

Abstract

The polarization of proton beam during the acceleration process in a particle accelerator is affected by the existence of spin resonances. Coupling spin resonances can be excited in the presence of the betatron coupling introduced by rolled quadrupoles and solenoids. A corresponding algorithm has been developed and added to the ASPIRRIN code to include the calculation of the first-order intrinsic resonance harmonics in the case of arbitrary strong betatron coupling and in the presence of Siberian Snakes and spin rotators.The analysis of the coupling resonance harmonics excited in RHIC collider is presented.

INTRODUCTION

Accelerating high energy polarized proton beams in a circular accelerator is complicated with the presence of depolarizing resonances. With the application of the various kind of spin rotating devices (like Snakes and spin rotators) the stable spin axis on the design closed orbit may deviate from the vertical, and an algorithm should be realized which would calculate the spin resonance harmonics with this complex configuration of the magnetic field on the design orbit. Main features of this algorithm for calculating the spin resonance strength were presented in [1]. In the work presented in this paper the algorithm has been extended to include the calculation of horizontal and vertical intrinsic spin resonance amplitudes for the case of strong betatron coupling, caused by rotated quadrupoles and solenoidal fields. We consider, as an example, the betatron coupling in RHIC accelerator which is originated mostly due to rolls of quadrupoles at the RHIC interaction regions and compensated using the local skew quadrupole correctors. In order to calculate the undesired coupling effects on the spin resonance strength an algorithm has been modified in ASPIRRIN [2] code to include the horizontal and vertical intrinsic spin resonance amplitude calculation for arbitrary rotated quadrupole in presence of the Siberian Snakes. In RHIC two Siberian Snakes are installed in each of the two RHIC rings [3].

ALGORITHM DESCRIPTION

In order to describe the spin motion which is initiated by the arbitrary rotated quadrupole , we would need to introduce the calculation of the spin perturbation in general. We consider the spin perturbation due to betatron oscillations as the linear form in the orbit variables $w_j = T_{iq}X_q$. The orbital coordinates and momenta of a particle will be defined as $X^T = (x, p_x, y, p_y)$, where x and y are the horizontal and vertical coordinates of a particle, and p_x and p_y are their conjugate momenta. The linear orbital motion can be defined as $X_q = F_{qr}A_r$ where F_{qr} is the matrix compiled from the complex eigenvectors of the orbital motion, and A_r is the vector of the betatron amplitudes.

Here we are considering the spin perturbation theory in the coordinate system $(\mathbf{l}, \mathbf{m}, \mathbf{n_0})$, where $\mathbf{n_0}$ is the stable spin solution on the design orbit. In this coordinate system a spin vector on the design orbit rotates with the constant spin precession tune ν around $\mathbf{n_0}$. The vector $\mathbf{k} = \mathbf{l}+\mathbf{im}$ is related with the spin eigenvector $\mathbf{k_0}$ by $\mathbf{k} = \mathbf{k_0}\cdot e^{i\nu\theta}$, where θ describes the accelerator azimuth. In Eq. 1 the first-order spin resonances are defined as the coefficients of Fourier decomposition of the spin perturbation term

$$\mathbf{w}\cdot\mathbf{k} = \sum_{r,p} \epsilon_{rp} e^{i(p+Q_r)\theta} = \sum_{r,p} A_r \tilde{v}_{rp} e^{i(p+Q_r)\theta} \qquad (1)$$

where p are integer numbers and Q_r present components of the orbital betatron tune vector $(Q_I, -Q_I, Q_{II}, -Q_{II})$. Q_I and Q_{II} are tunes of two betatron oscillation modes. In order to calculate $\tilde{v}_{rp}$ in the program the integral over one turn is taken doing element-by-element integration [1].

$$\tilde{v}_{rp} = \frac{1}{2\pi}\int_0^{2\pi} e^{i\delta_{rp}\theta} \sum_{j,q} T_{jq}\mathcal{F}_{qr}k_{0j}d\theta \qquad (2)$$

where $\delta_{rp} = \nu - (p + Q_r)$ describes detuning of the spin tune from a resonance tune.

In order to obtain $\tilde{v}_{rp}$ for rotated quadrupole we start with considering the following equations of motion of particle in arbitrary rotated quadrupole:

$$x'' = -g_c x - \kappa_c y \qquad y'' = g_c y - \kappa_c x \qquad (3)$$

where $g_c = g \cdot cos(2\phi)$ and $\kappa_c = g \cdot sin(2\phi)$ are defined by the quadrupole rotation angle ϕ and the quadrupole field gradient g.

From (3) we can get the expressions for the orbital motion eigenvectors which will be used later in the paper :

$$F_{3r} = -AF''_{3r} + BF''_{1r} \qquad F_{1r} = AF''_{1r} + BF''_{3r} \qquad (4)$$

Here:

$$A = -cos(2\phi)/g \qquad B = -sin(2\phi)/g \qquad (5)$$

The components of horizontal and vertical components of the spin perturbations in a quadrupole are given by:

$$w_x = (1+\nu_0)y'' \qquad w_y = -(1+\nu_0)x'' \qquad (6)$$

* Work supported by Brookhaven Science Associates, LLC under Contract No. DE-AC02-98CH10886 with the U.S. DOE
† nermeen.khalil@stonybrook.edu

ISBN 978-3-95450-138-0

Copyright © 2013 CC-BY-3.0 and by the respective authors

THE RHIC E-LENS TEST BENCH EXPERIMENTAL RESULTS *

X. Gu#, F.Z. Altinbas, J. Aronson, E. Beebe, W. Fischer, D.M. Gassner, K. Hamdi, J. Hock, L. Hoff, P. Kankiya, R. Lambiase, Y. Luo, M. Mapes, J. Mi, T. Miller, C. Montag, S. Nemesure, M. Okamura, R. H. Olsen, A.I. Pikin, D. Raparia, P. J. Rosas, J. Sandberg, Y. Tan, C. Theisen, P. Thieberger, J. Tuozzolo, and W. Zhang, BNL, Upton, NY 11973

Abstract

To commission some of the hardware and software for the RHIC electron lenses (e-lenses), we built a test bench based on BNL's EBIS test stand. Over several months, we tested the electron gun, the collector, the high-voltage gun-modulator, the instrumentation, the partial control system, and several software applications. A nominal DC-beam current of 0.85 A was demonstrated. And the electron beam transverse profiles were verified as being Gaussian with a small flat top. We also evaluated some e-lens power-supplies and the electronics for measuring current on our bench. The properties of the cathode and the profile of the beam were assessed. In this paper, we present some of our experimental findings.

INTRODUCTION

To improve the luminosity of the polarized protons in the Relativistic Heavy Ion Collider (RHIC), we are installing two electron lenses (e-lenses) in IR10 [1-4] to compensate for the head-on beam-beam effect. We designed an e-lens test bench to test some elements of the e-lens hardware, its controls, and some application software [5]. Figure 1 illustrates the layout of e-lens test bench; it encompasses an electron source, a beam-propagation system, an electron collector, and some instruments for beam diagnostics.

The electron source is an electron gun with a cathode designed to generate a beam with transverse Gaussian profile [3, 6]. After manufacturing it, we measured the actual shape of the cathode (its cross-sectional profile), then simulated the beam profile resulting from the cathode profile with the 2D program TRAK, and compared it to the obtained beam profile with the measured beam.

The system that propagates the beam encompasses a 4.6 T superconducting solenoid, a collector coil, gun dipoles, main dipoles, collector dipoles, and a drift tube.

When the electron beam arrives at the collector, we measured its current with the DCCT and the pulse CT [7]. The maximum temperature on the collector was determined by Resistance Temperature Detectors (RTDs) at the highest DC load. The eight RTDs on the cylindrical surface of the electron collector were arranged in two groups. Each group consisted of four RTDs in one longitudinal plane; the four thermocouples of one group were separated azimuthally by 90 degrees, while the two groups were separated longitudinally by 70 mm.

After several months of operation, we tested the electron gun, the collector, the high-voltage gun modulator and most of the instrumentation on the test bench. We also qualified parts of the control system and several software applications. The nominal pulse and the DC beam current of 0.85 A were demonstrated, and the electron beam transverse profiles were verified as being Gaussian. Some e-lens power supplies and the electronics for measuring the current were also assessed. The properties of the cathode and the profile of the beam were evaluated.

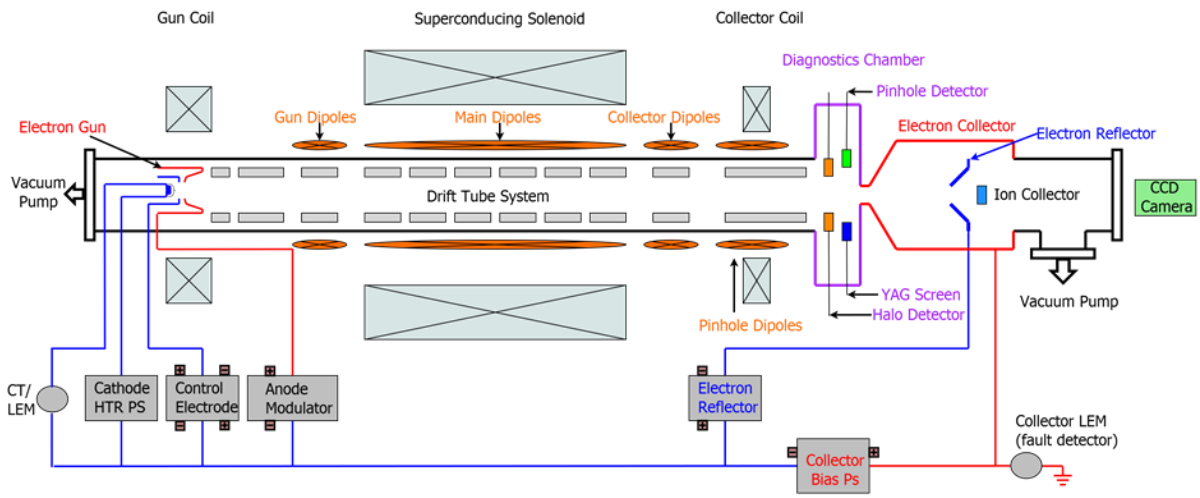


Figure 1: Layout of the electron lens test bench.

* Work supported by Brookhaven Science Associates, LLC under Contract No. DE-AC02-98CH10886 with the U.S. Department of Energy

#xgu@bnl.gov

Copyright © 2013 CC-BY-3.0 and by the respective authors

SINGLE PASS ELECTRON COOLING SIMULATIONS FOR MEIC*

G. I. Bell†, I. V. Pogorelov and B. T. Schwartz, Tech-X Corp, Boulder, CO, 80303, USA
Yuhong Zhang and He Zhang, Jefferson Lab, Newport News, VA, 23606, USA

Abstract

Cooling of medium energy protons is critical for the proposed Jefferson Lab Medium Energy Ion Collider (MEIC). We present simulations of electron cooling of protons up to 60 GeV. In the beam frame in which the proton and electrons are co-propagating, their motion is non-relativistic. We use a binary collision model which treats the cooling process as the sum of a large number of two-body collisions which are calculated exactly. This model can treat even very close collisions between an electron and ion with high accuracy. We also calculate dynamical friction using a δf PIC model. The parallel code VSim (formerly Vorpal) is used to perform the simulations. We compare the friction rates with that obtained by a 3D integral over electron velocities which is used by BETACOOL.

ELECTRON COOLING

In the simplest form of electron cooling [1], an electron beam is created with the same γ as a relativistic ion beam which we wish to cool. The two beams are then made to co-propagate over a section of a storage ring, the **cooling section**. In the **beam frame** traveling with the average velocity of the particles, their velocities are non-relativistic, and the particles interact by means of Coulomb collisions.

This paper explores the amount of dynamical friction which can be obtained in an (unmagnetized) cooling section of the Jefferson Lab Medium Energy Ion Collider. The particles to be cooled are protons with $\gamma = 65.4$. The cooling section is $s = 60$ m long. These simulations are done in 3D, where x and y are transverse coordinates and z is the direction of beam propagation.

The bunched electron beam is non-uniform, but suppose we consider a small region only a few Debye lengths wide in the center of the electron bunch. In this region, the electron density is nearly constant. We consider a distribution of electrons which is uniform in space and has a Maxwellian distribution in velocity

$$f_0(\vec{v}) = \frac{n_e}{(2\pi)^{3/2}\sigma_x\sigma_y\sigma_z}\exp\left[-\frac{v_x^2}{2\sigma_x^2}-\frac{v_y^2}{2\sigma_y^2}-\frac{v_z^2}{2\sigma_z^2}\right], \tag{1}$$

where n_e is the density in the center of the electron bunch. In the beam frame the RMS velocities $\vec{\sigma}$ are non-relativistic, specific values are given in Table 1. Note that

Table 1: Electron Beam Parameters Used in the Simulations, all Parameters are in the Beam Frame

parameter	symbol	value	unit
electrons per bunch		2.5	10^9 elec.
peak density	n_e	1.32	$10^{15}e/m^3$
plasma freq.	ω_p	3.26	10^8/sec
plasma per.		3.07	nanosec
interaction time	τ	3.06	nanosec
trans. RMS bunch size	r_x	303	μm
long. RMS bunch size	r_z	1.3	m
trans. RMS velocity	σ_x	2.35	10^5 m/sec
long. RMS velocity	σ_z	0.36	10^5 m/sec
trans. Debye length	λ_x	114	μm
long. Debye length	λ_z	17.5	μm

z is the direction of beam propagation, and because this is an accelerated beam it is not isotropic, and $\sigma_z < \sigma_x = \sigma_y$.

Consider now a single ion moving at velocity $\vec{v}_{ion}$, and let $\vec{v}_{\rm rel} = \vec{v}_{ion} - \vec{v}$ be the velocity of each electron relative to the ion. Assuming each collision is symmetric in time, the dynamical friction force on the ion can be calculated by the 3D integral over the electron velocity space [2]

$$\vec{F}_{\parallel} = -\frac{n_e Z^2 e^4}{4\pi\epsilon_0^2 m_e}\int_{-\infty}^{\infty}\Lambda\,\frac{\vec{v}_{\rm rel}}{|\vec{v}_{\rm rel}|^3}f_0(\vec{v})\,d^3\vec{v}. \tag{2}$$

Here Z is the ion charge number (for protons, $Z = 1$), $e < 0$ is the electron charge, and m_e is the electron mass. In the simplest case, the Coulomb logarithm

$$\Lambda = \log(\rho_{max}/\rho_{\perp}), \tag{3}$$

where ρ_{max} and $\rho_{\perp}$ are often called "the maximum and minimum impact parameters". This terminology is unfortunate, because equation (2) actually includes contributions from collisions with arbitrarily small impact parameters [2]. $\rho_{\perp}$ is the impact parameter for 90 degree scattering

$$\rho_{\perp}(\vec{v}_{\rm rel}) = \frac{Ze^2}{4\pi\epsilon_0 m_e|\vec{v}_{\rm rel}|^2}. \tag{4}$$

In the actual beam, collisions with arbitrarily small impact parameters can occur. In simulations, the problem is that very small impact collisions are rare, and there may not be enough of them to accumulate good statistics. Therefore, in simulations it is advantageous to introduce a cutoff

* This work is supported by the US DOE Office of Science, Office of Nuclear Physics, grant numbers DE-SC0009508 and DE-SC0000835; resources of NERSC were used under contract No. DE-AC02-05CH11231.
† gibell@txcorp.com

ISBN 978-3-95450-138-0

Copyright © 2013 CC-BY-3.0 and by the respective authors

MEIC ELECTRON COOLING SIMULATION USING BETACOOL*

He Zhang†, Yuhong Zhang, Jefferson Lab, Newport News, VA 23606, USA

Abstract

Electron cooling of ion beams is one critical R&D issue in Jefferson Lab's medium energy electron-ion collider (MEIC). In the present MEIC design concept, a multi-phase cooling scheme is adopted. In the ion pre-booster, a DC electron cooler is responsible for assisting ion beam accumulation and initial cooling. In the ion collider ring, the ion beams with energies up to 100 GeV/u are cooled by a high current bunched electron beam driven by an energy-recovery SRF linac assisted by a circulator ring. It is essential to understand how efficient that electron cooling is, particularly in the high energy range, and how the cooling electron bunches in the circulator cooler ring are affected by the cooling process and other collective beam effects, in order to confirm the feasibility of the design. Here we present first results of the simulation studies of electron cooling processes of MEIC using BETACOOL code.

INTRODUCTION

The MEIC is designed to deliver a peak luminosity above 10^{34} $\mathrm{cm}^{-2}\mathrm{s}^{-1}$ and covers a CM energy range up to 65 GeV. It offers an electron energy up to 12 GeV, a proton energy up to 100 GeV, and corresponding energies per nucleon for heavy ions with the same magnetic rigidity [1]. The MEIC ion complex consists of ion sources, a linac, two boosters and a medium energy collider ring, as shown in Fig. 1. The conventional electron cooling is chosen to assist cumulation of ions from the linac and to reduce and preserve the emittance of the MEIC ion beam. We propose to have electron coolers installed both in the pre-booster and in the collider ring, and our multi-phase electron cooling scheme includes the following steps: (1) low energy (up to 2 MeV) DC cooling at the pre-booster, (2) bunched electron cooling at the ion injection energy (up to 20 GeV/u) of the collider ring, and (3) bunched cooling at the top ion energy (100 GeV/u) of the collider ring. An important feature of this scheme is continuous electron cooling of the ion beams during their collision with the electron beam.

While the electron cooling mechanism is well developed and successfully tested with low energy DC beam applications world wide, we are challenged by the high density and high energy of the MEIC ion beam [2, 3]. The present design concept calls for an ERL for the high energy cooler in the collider ring for meeting the request of a very high RF power and additionally a circulator ring for mitigating the electron gun life time challenge [1]. There are a number of critical R&Ds for this design concept, for example, (1) what is the cooling efficiency at the high energy range with a bunched electron beam; (2) how the cooling electron bunches in the circulator cooler ring are affected by the cooling process and other collective beam effects; and further (3) how the cooling efficiency is affected by the continually (slow) degradation of the cooling bunches during circulation of the cooling. In the report, we present our initial results for the simulation studies of the first issue listed above. For simplicity, the coupling to the electron beam dynamics in the circulator cooler ring is ignored. The latter is currently also under studied [4]. In other words, the cooling electron bunches in the simulations are assumed ideal, fresh from the electron source, for each cooling, instead of being a real beam circulating in the cooler ring. At a later time, these two studies will be combined as we expect.

Table 1: Key Parameters for Different Cooling Schemes

		Pre-Booster	Collider Ring
p^+ Energy	GeV	3	20/100
p^+ Bunch Length	cm	Coasting	Coasting/1
Cooler Type		DC	ERL circulator
Magnetization	T	1	0
Cooler Length	m	10	2×30
e^- Beam Current	A	3	1.5
e^- Bunch Length	cm		1.2
Cooling Scheme 1		✓	
Cooling Scheme 2			✓
Cooling Scheme 3		✓	✓

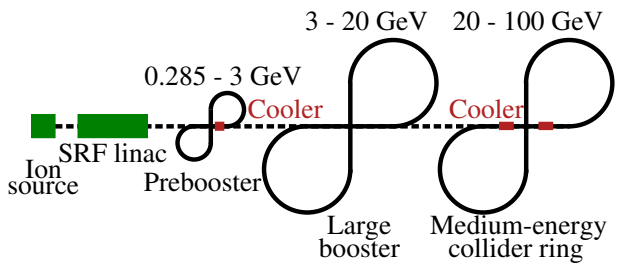


Figure 1: Components of MEIC ion complex

MODELS AND METHODS

Ideally a start-to-end simulation should be carried out for the entire process of MEIC ion beam formation and cooling, nevertheless, presently there is no such a code capa-

* Work supported by the U.S. Department of Energy, Office of Nuclear Physics, under Contract No. DE-AC05-06OR23177 and No. DE-AC02-06CH11357.

† hezhang@jlab.org

Copyright © 2013 CC-BY-3.0 and by the respective authors

STATUS AND FUTURE PLAN OF THE DEVELOPMENT OF A COMPACT X-RAY SOURCE BASED ON ICS AT LASER UNDULATOR COMPACT X-RAY (LUCX)*

M. Fukuda#, S. Araki, A. Aryshev, Y. Honda, N. Terunuma, J. Urakawa, KEK, Ibaraki, Japan
K. Sakaue, M. Washio, RISE, Tokyo, Japan

Abstract

We have developed a compact X-ray source via inverse Compton scattering (ICS) between multi-bunch electron beam and a laser pulse stacked in an optical cavity at Laser Undulator Compact X-ray (LUCX) accelerator in KEK. Since the autumn of 2011, we have begun X-ray imaging test. In the beginning, it had taken two hours to get an X-ray image because of low intensity of X-ray with 10^4 photons/pulse. To get a clear X-ray image in a shorter period of times, we have upgraded the accelerator, which consists of a 3.6 cell photo-cathode rf-gun, a 12cell standing wave accelerating structure and a 4-mirror planar optical cavity. The target intensity of an electron beam is 500nC/pulse with 1000 bunches at 30 MeV. The one of laser pulse is also 6mJ/pulse. The expected number of X-ray is $1.7\text{x}10^7$ photons/pulse with 10% bandwidth. We have already started the multi-bunch beam generation and X-ray imaging test after upgrade. The accelerator produces 26.8 MeV beam with the total charge of 380nC in 300 bunches per pulse. The aging process is also continued to increase energy and intensity. We will report the results of the beam test and future plan of the development of a compact X-ray source at LUCX.

INTRODUCTION

X-rays have various fields of application, such as medial application, biological science, material science etc. Synchrotron radiation produced by GeV order storage ring is commonly used for high brightness X-ray source. However the device is generally huge and expensive. On the other hand, the X-ray source based on ICS is compact and inexpensive because this method can decrease this energy of an electron beam by more than an order of magnitude when producing X-rays with the same energy.

We have constructed the LUCX accelerator at KEK in order to develop the compact X-ray source based on ICS. Since the autumn of 2011, we have begun X-ray imaging test and succeeded to take the X-ray image of fish bone[1]. However, it took two hours to get the image due to low intensity of X-ray with 10^4 photons/pulse.

We have upgraded this accelerator in order to increase the intensity of X-rays in last year. The 3.6cell rf-gun, 12cell booster and 4mirror cavity have been designed and constructed for this upgrade. The X-ray generation and the X-ray imaging are already started after upgrade[2]. We will report the current status and future plan of the X-ray experiment in the accelerator.

*Work supported by the Quantum Beam Technology Program and Photon and Quantum Basic Research Coordinated Development Program of MEXT.
#mfukuda@post.kek.jp

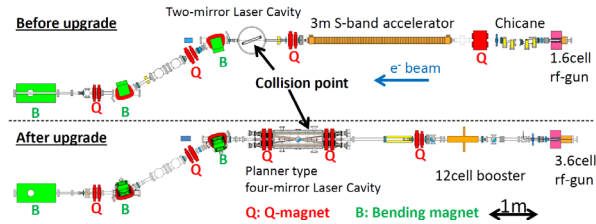


Figure 1: The beamline of the LUCX accelerator before/after upgrade.

LUCX ACCELERATOR

The upgraded beamline is shown in Fig. 1. A 3.6cell photo-cathode rf-gun generates an electron beam with the energy of 10MeV and then the beam is accelerated to 30MeV by a 12cell booster. After that, the beam is collided with a laser pulse in a 4-mirror planar optical cavity and then X-rays are generated by ICS. The X-rays are extracted into the atmosphere through a Be window with the thickness of 300μm. The electron beam is separated from the X-ray by a bending magnet and then is dumped to the beam dump.

3.6Cell Photo-Cathode Rf-Gun

An S-band 3.6cell rf-gun[3] has been installed instead of 1.6cell rf-gun to increase the beam energy. The cut view and the picture of the rf-gun is shown in Fig. 2. The cavity structure consists of smooth curves to increase the Q-value of the cavity and to reduce dark current from the surface. Cesium telluride (Cs_2Te) film is evaporated on the surface of the Mo cathode plug which is attached in the cavity by the load-lock system. An electron beam is emitted from the cathode by irradiating 266nm UV laser light. The beam is accelerated to 10MeV.

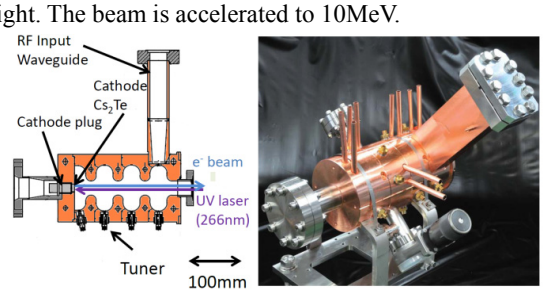


Figure 2: The cut view and the picture of 3.6cell rf-gun.

The cavity of the 3.6cell rf-gun has four resonance modes. Therefore the surface of the iris in the cavity has

Copyright © 2013 CC-BY-3.0 and by the respective authors

ISBN 978-3-95450-138-0

HIGH-CHROMATICITY OPTICS FOR THE MAX IV 3 GeV STORAGE RING

T. Olsson, S.C. Leemann, MAX IV Laboratory, Lund University, SE-22100 Lund, Sweden

Abstract

The ultralow emittance lattice of the MAX IV 3 GeV storage ring has a large negative natural chromaticity. This has to be corrected to positive values to prevent head-tail instabilities. On the other hand, high linear chromaticity can lead to a large tune footprint which limits Touschek lifetime. Therefore, the linear chromaticity is corrected to +1 in both planes with sextupoles while octupoles are used to further reduce the tune footprint. Studies indicate this design leads to threshold currents for resistive wall and transverse mode coupling instabilities beyond what is expected during regular user operation. However, since these are only preliminary studies based on approximations, the possibility of instability issues during commissioning needs to be considered. A short term solution is to operate the storage ring at a higher chromaticity. This paper describes the developed high-chromaticity optics for the MAX IV 3 GeV storage ring. It focuses on reduction of chromatic and amplitude-dependent tune shifts to maximize dynamic aperture and Touschek lifetime. A comparison between the performance of the new high-chromaticity optics and the design optics is also presented.

INTRODUCTION

The MAX IV facility is a 3rd generation state-of-the-art synchrotron light source currently under construction in Lund, Sweden [1]. The MAX IV 3 GeV storage ring has an ultralow emittance lattice with a large negative natural chromaticity in both planes [2]. To avoid head-tail instabilities, the linear chromaticity has to be corrected to positive values. On the other hand, a large linear chromaticity can lead to proximity to, or crossing of, potentially dangerous resonances, which can limit dynamic aperture and Touschek lifetime. To satisfy both constraints, the linear chromaticity in the design optics of the MAX IV 3 GeV storage ring has been corrected to +1 in both planes [2]. Initial instability studies indicate this design leads to threshold currents for resisitive wall instability and transverse mode coupling instability beyond what is expected during user operation [3]. However, since these are only preliminary studies based on initial estimates of the impedance budget the possibility of instability issues occurring during commissioning needs to be considered. The instability studies indicate that the threshold currents increase with chromaticity. A short term solution is therefore to operate the storage ring at a higher chromaticity. An alternate optics for the MAX IV 3 GeV storage ring with linear chromaticity +4 in both planes has therefore been developed [4]. This paper presents the performance of the newly developed high-chromaticity optics in comparison to the design optics. The challenges to achieve a high-chromaticity optics with sufficient performance are also described.

NONLINEAR OPTICS OPTIMIZATION

The MAX IV 3 GeV storage ring make use of strong sextupoles to correct the linear chromaticity, minimize chromatic tune shifts and tailor the chromatic tune footprint while minimizing first-order resonance driving terms. Octupoles are employed to minimize the amplitude-dependent tune shifts and further tailor the tune footprint. This approach is detailed in [5]. The same approach was used during the development of a high-chromaticity optics.

OPA [6] was used to correct the linear chromaticity to +4 in both planes using the two strongest chromatic sextupoles. All five sextupole families were then adjusted to optimize the chromatic tune footprint while constraining the linear chromaticities to +4.

The chromatic tune shifts for the high-chromaticity optics are displayed in Fig. 1. For both planes, the resulting chromatic tune shifts for the high-chromaticity optics are not unexpectedly larger than the corresponding tune shifts for the design optics across the entire range of interest.

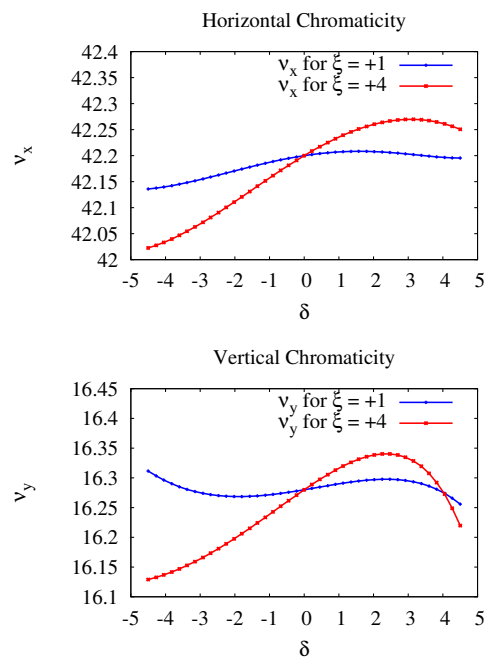


Figure 1: Chromatic tune shifts for the high-chromaticity optics calculated by TRACY-3 [7]. The chromatic tune shifts for the design optics are displayed for comparison.

Copyright © 2013 CC-BY-3.0 and by the respective authors

CREATION OF HIGH-CHARGE BUNCH TRAINS FROM THE APS INJECTOR FOR SWAP-OUT INJECTION*

C.-Y. Yao, M. Borland, L. Emery, L. Donley, F. Lenkszus, B.-X. Yang
Advanced Photon Source, Argonne National Laboratory, Argonne, IL 60439, USA

Abstract

A multi-bend-achromat (MBA) low-emittance lattice is being explored for a future APS Upgrade [1]. Due to its small dynamic aperture, the traditional injection scheme must be replaced with a "swap-out" scheme [2]. Several options were considered for the creation of a high-charge bunch train from the injector, and we selected an option that builds the bunch train in the existing particle accumulator ring (PAR). This option enables both single-bunch mode, which is necessary to support current APS operation, and bunch-train mode. This report provides a description of the injection process, simulation results, and specifications of injector timing, kicker, and rf subsystems.

INTRODUCTION

The APS injector consists of a 450-MeV electron linac, a particle accumulator ring (PAR), and a synchrotron booster. The PAR has a 9.77-MHz cw fundamental system (RF1) and a 117.3-MHz pulsed 12th-harmonic system (RF12). In the first 250 ms, beam is accumulated into the RF1 bucket and damped to a bunch length of ~0.86 ns. RF12 is turned on at 250 ms of the PAR cycle and compresses the bunch length to 0.3 ns. Bunch cleaning is performed at 350 ms, and beam is further damped and extracted at 483 ms. Currently the injector runs at a 2-Hz rate and provides a single bunch with a beam charge of up to 4 nC. For an APS MBA low-emittance lattice, the injection scheme would be replaced with a single-bunch or bunch train swap-out scheme. Several bunch fill patterns are being considered: a single-bunch high-charge mode with up to 4 mA per bunch, and a multiple bunch mode that consists of multiple bunch trains, each with up to 5 bunches per train.

HIGH-CHARGE SINGLE-BUNCH AND BUNCH TRAIN GENERATION

The APS MBA upgrade now under exploration envisions two types of fill patterns: a 48-singlet fill pattern with a single-bunch charge of up to 15 nC, and a multi-bunch-train fill pattern with up to 432 bunches.

For 48-singlet mode the injector would need to deliver up to a 20-nC single-bunch with an emittance of 30 nm-rad in the x and y planes. The rf gun, without major upgrade, can deliver about 1 nC per pulse with 30-Hz repetition rate. To reach 20 nC we would need to extend the PAR accumulation cycle from the current value of 0.5 second to 1 second or longer. Figure 1 shows a possible 1-second PAR accumulation cycle. During the first 633.33 ms, 20 linac pulses are accumulated, while the next 100 ms is used to damp the beam to about 0.8 ns in length. The 12th-harmonic rf is turned on around 733.33 ms, following which the beam is captured into the 12th-harmonic bucket and compressed to a bunch length of 0.3 ns. Bunch cleaning is then turned on for 20 ms. After a final damping of 100 ms, beam is extracted to the PAR-to-booster (PTB) beam transport line. The current rf system, with modest upgrades, can support this operating cycle.

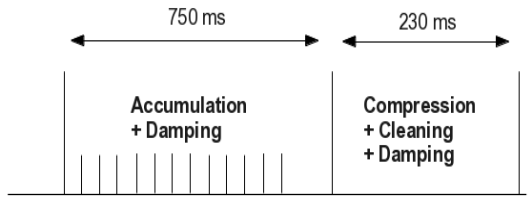


Figure 1: Accumulation of high-charge single-bunch beam in the PAR.

For the multiple bunch-train fill pattern, we consider 2 to 5 consecutive bunches per bunch train with a total of up to 432 bunches and flexible spacing between the trains. To build such bunch trains the PAR rf system must be replaced with a cw 352 MHz system. The bunches can be either accumulated one at a time with a linac micro-bunch length of less than 1.5 ns, or simultaneously with a long linac micro-bunch of up to 15 ns. In both cases a fast gun chopper with a rise time of ~1 ns is needed to accurately control the length of the linac micro-bunches. Bunch cleaning can be performed after accumulation to remove unwanted satellite bunches. Figure 2 shows one possible bunch-train fill pattern with 4 bunches per train.



Figure 2: A multiple bunch train fill pattern.

TIMING SYSTEM UPGRADE

The APS timing system would need to be upgraded to accommodate the new fill patterns and timing precision requirements. The "swap out" mode of operation and ns-level rise/fall time of the kickers requires much-reduced jitter time, estimated to be 50 ps or lower. The jitter time of the existing APS timing system, measured in the range of 200 to 500 ps, is apparently inadequate. A new timing infrastructure would need to be developed to achieve the required timing precision.

*Work supported by the U.S. Department of Energy, Office of Science, under Contract No. DE-ACO2-O6CH11357.
#cyao@aps.anl.gov

Copyright © 2013 CC-BY-3.0 and by the respective authors

ISBN 978-3-95450-138-0

OBSERVATION OF +1 BUCKET BUNCH IMPURITY GROWTH AT THE APS STORAGE RING*

C.-Y. Yao, B.-X. Yang, M. Borland, ANL, Argonne, IL 60439, USA

Abstract

The APS storage ring has three fill patterns: a 24-singlet, a 1+8x7 hybrid with a leading bunch of 16 mA, and a 324-singlet. Bunch purity of better than 1×10^{-6} is required for +3 and higher bucket numbers for the first two fill patterns during user operations. A PAR bunch cleaning system is used to clean the satellite bunches. During top-up user operation, beam charge in satellite bunches grows due to the long lifetime of the low charge satellites. Recent storage ring developments, including operating with the bunch-by-bunch feedback system, reduction of chromaticity, and lattice correction, have increased the dynamic and momentum aperture of the storage ring. We observed unusual beam charge growth in +1 buckets, which indicates leakage of electrons from the main bunches to the +1 satellite buckets. This report describes the observation and the dependence of leakage on chromaticity settings, and gives a brief analysis.

OBSERVATION OF ABNORMAL +1 BUNCH GROWTH

Figure 1 shows the normal growth of the +1 satellite bucket relative counts in the 24-singlet fill of the RHB (reduced horizontal β-function) lattice, recorded in the first run period of 2013. It has a typical growth rate of ~2×10^{-8} per hour. Figure 2 shows an abnormal growth of the +1 bucket counts with a growth rate of ~3×10^{-6}, about 150 times higher than normal value. Typical injector bunch impurity for the +1 satellite bucket is at the 8×10^{-7} level and can not explain this abnormal growth. A test was conducted with injected beam turned off and top-up injection systems continuously running. We observed significant growth of net counts in the +1 satellites while the -1 buckets showing no growth. A plot of the result is shown in Figure 3. This test confirmed that the +1 bucket counts come from leakage of main bunches.

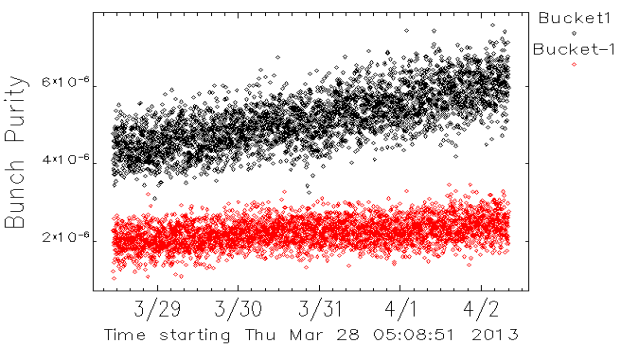


Figure 1: Normal accumulation of the +1 satellite bucket during user operations.

*Work supported by the U.S. Department of Energy, Office of Science, under Contract No. DE-ACO2-O6CH11357.
#cyao@aps.anl.gov

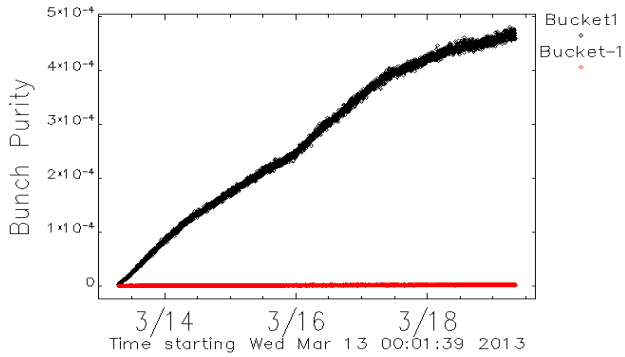


Figure 2: Abnormal growth of the +1 satellite bucket during top-up user operations with lower chromaticity.

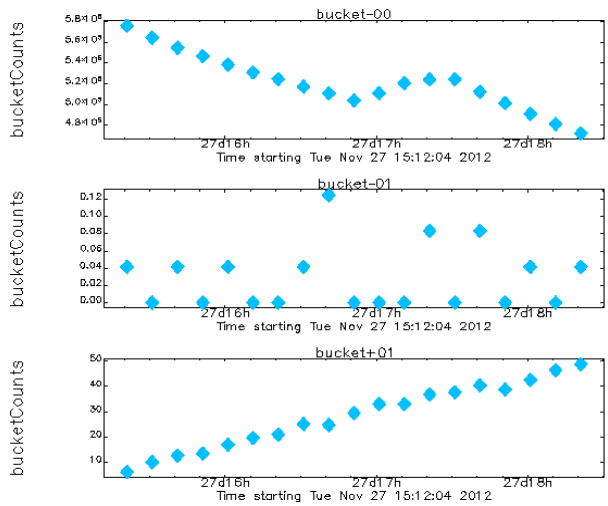


Figure 3: Average bucket count change during a test in which the injected beam is turned off while top-up injection systems were running. Top: main bucket. Middle: -1 bucket showing no growth. Bottom: +1 bucket showing steady growth.

LEAKAGE RATE FITTING

In order to find the relationship between the +1 bunch impurity and the change in storage ring chromaticity, we varied chromaticity in 0.5 steps and collected bunch purity data during Run-1 of 2013. We fit the resulting data with `sddsgenericfit` [1].

The +1 bucket relative counts can be expressed with the following differential equation:

$$dI = \frac{I_0}{T_0} C_{inj}\, dt - \frac{I}{T_b}\, dt + I_0\, R_{leak}\, dt \quad . \qquad (1)$$

The variables are defined as:
I_0 --- main bucket beam current

Copyright © 2013 CC-BY-3.0 and by the respective authors

FUTURE NSLS-II INJECTOR UPGRADES*

T. Shaftan#, G. Wang, J. Rose, R. Fliller, R. Heese, F. Willeke, BNL, Upton, New York

Abstract

Last year we began commissioning of the NSLS-II injection system. In 2013 the NSLS-II injector, which consists of 200 MeV linac, 3 GeV booster, transport lines and storage ring injection straight section, will be entering operations. During injection system development we invested substantial efforts in preserving options for future injector upgrades and enhancements. In this paper we discuss our vision and plans of incremental evolution of the NSLS-II injector by implementing planned upgrades, such as the second gun, flexible bunch patterns, beam stacking in the booster, emittance compensation techniques in the transport lines, etc. These upgrades will expand the facility capabilities, improve the beam quality and increase operational reliability.

INTRODUCTION

The NSLS-II [1] is a state-of-the-art 3 GeV synchrotron light source under construction at Brookhaven National Laboratory. It will provide ultra-bright synchrotron radiation of 10^{21}·photons·s^{-1}·mm^{2}mrad^2·0.1%BW^{-1} at 2 keV and high photon flux of 10^{15}·photons·s^{-1}·0.1%BW^{-1}. The facility will support a minimum of 60 beamlines. Construction started in 2009 and commissioning is expected to be completed in 2014.

The NSLS-II injector [2] is now being commissioned to deliver beam performance sufficient for initial storage ring operations at low current. At a later stage the NSLS-II storage ring capabilities will continuously expand to include high intensity operations and top-off mode. This expansion will require the NSLS-II injector to reliably deliver electron beam at a high charge rate, with low losses and high stability in all six phase space coordinates. To meet the requirements of high-intensity ring operation we designed in a large scope of the injector upgrades. The upgrades, described in this paper, aimed to increase the NSLS-II facility capabilities, improve beam quality and reliability of the facility operations.

LINAC UPGRADES

Production of Short Pulses

The 200-MeV NSLS-II linac is a high-performance accelerator delivering up to 15 nC per shot with the emittance of 70 nm rad within trains of 20 ps (RMS) bunches. These excellent beam properties can find applications in generating bright flashes of radiation in THz-visible and hard X-ray wavelength range. Top-off time format (1 injection cycle per minute) permits using the injector linac for other purposes during at least 50 seconds every minute.

*This manuscript has been authored by Brookhaven Science Associates, LLC under Contract No. DE-AC02-98CH10886 with the U.S. Department of Energy.

#shaftan@bnl.gov

Some of these parameters (bunch length and beam emittance) can be greatly improved by addition of an RF gun that delivers an LCLS-like beam performance.

With an RF gun the NSLS-II injector linac will gain potential in generating short bursts of radiation via:

- Short pulses of THz/IR via CTR or in an undulator
- Coherent sources in IR – DUV range of wavelengths
- Short pulse X-rays via Compton Scattering

We designed the linac tunnel in such a way that there exist an ample space ahead of the linac for developing a user end station and upgrading the linac energy for building a short radiation pulse facility (Fig. 1).

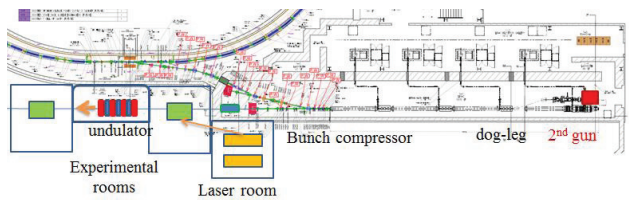


Figure 1: Potential layout of the short pulse facility.

Including the second gun [3] into the low-energy part of the linac will: a) increase reliability of the NSLS-II accelerator complex, b) enable more efficient operations in generating complex bunch patterns and, c) simplify switching between single-bunch and multi-bunch modes for the ring injection.

Generating Flexible Bunch Patterns

Specifications for the storage ring bunch pattern given by the NSLS-II users require sharp edges of the circulating bunch trains and uniform distribution of charge per bunch within a single train. This translates into challenging requirements on the gun pulser since its electronics defines the quality of the generated trains.

In order to enable generation of flat-top (relative bunch-to-bunch charge noise below 1%) trains with sharp edges (~2 ns) we proposed to include a short kicker (chopper) just upstream of the 100-keV gun (Fig. 2, [4]).

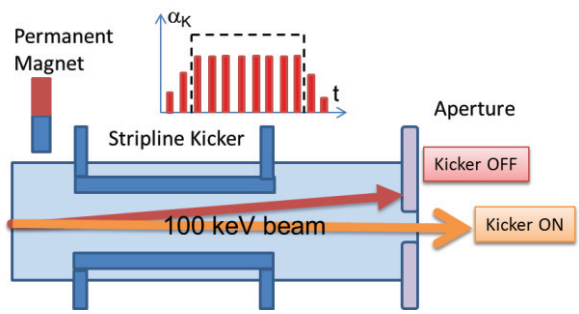


Figure 2: Schematics of the beam chopper.

This kicker will permit passing beam only inside the desired macropulse deflecting bunches outside to the

Copyright © 2013 CC-BY-3.0 and by the respective authors

ISBN 978-3-95450-138-0

SUBPICOSECOND BUNCH TRAIN PRODUCTION FOR HIGH POWER TUNABLE THZ SOURCE

S. Antipov#, C. Jing, P. Schoessow, and A. Kanareykin,
Euclid Techlabs LLC, Solon, OH-44139
W. Gai, A. Zholents, Argonne National Laboratory, Argonne, IL-60439
M. Fedurin, M. Babzien, K. Kusche
Brookhaven National Accelerator Laboratory, Upton, NY-11973
V. Yakimenko,
SLAC National Accelerator Laboratory, Menlo Park, CA-94025

Abstract

An effective method of introducing an energy modulation in an electron bunch by passing it through a dielectric-lined waveguide was recently demonstrated [1]. In the follow up experiment we successfully converted this energy modulation into a density modulation by means of a chicane beamline. The density modulated beam was sent through a foil target, producing THz transition radiation which was characterized using interferometric techniques. By changing the initial energy chirp of the beam we tuned the center frequency of the generated THz radiation in the range 0.68 – 0.9 THz. A table top high power narrowband tunable THz source based on this technique is proposed.

INTRODUCTION

In recent years there has been a large interest in the production of sub-picosecond bunch trains consisting of series of equally spaced electron micro bunches [2-6]. These bunch trains can be used for production of high power THz radiation [4–6, and references therein] and to drive resonant wakefields in plasma and dielectric wakefield accelerators [2, 3].

Sub-picosecond bunch trains can be generated directly from a photocathode of an electron gun using a series of uniformly spaced laser pulses [6-8]. Alternatively, a transverse-to-longitudinal phase space exchange in combination with a multi-slit mask [9-12] can be used. Another approach is to use difference frequency generation by double energy modulation of electrons in an undulator via interaction with optical lasers having slightly different carrier frequencies [13, 14]. In this paper we present an approach using energy modulation by means of the self-excited wake fields in a dielectric-lined [1] or corrugated waveguide [15] with subsequent conversion into a sub-picosecond period density modulation.

A strong energy modulation in an electron bunch passing through a dielectric-lined waveguide was recently demonstrated in reference [1]. Here, we report the successful conversion of this energy modulation into a density modulation and production of a picosecond bunch train. This result provides a foundation for a compact, tunable source of intense THz radiation [RSI].

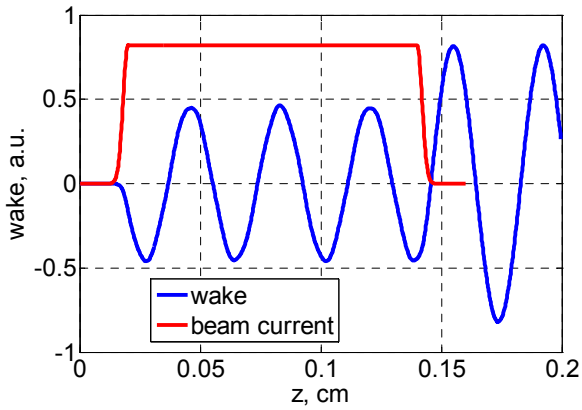


Figure 1: Periodic self-wakefield inside a long quasi-rectangular electron beam.

The principle of introducing an energy modulation in the beam is the following: when the bunch length is comparable or much longer than the wavelength of the fundamental mode of the wakefield, the wakefield inside the bunch will show an amplitude modulation, particularly for a triangular or rectangular shaped bunch (Fig. 1). If the beam has an energy chirp (linear correlation between energy and longitudinal coordinate) then the periodic self-wakefield (Fig. 1) produces an energy modulation (Fig. 2). This energy modulation can be converted into density modulation by means of chicane, a set of four dipoles arranged in a "+ - - +" fashion. Inside the chicane high energy particles travel a shorter distance than those at low energies, hence sections of the beam in which low energy particles are ahead of the high energy ones will be compressed (Fig. 2). If the beam has a positive chirp (head having a lower energy than the tail) initially, the whole beam is compresed as well. Hence the current is modulated at a higher frequency than the frequency of the wakefield mode that created the energy modulation in the first place!

Changing the energy chirp of the beam therefore allows us to tune the frequency of the current modulation. In the case of negative chirp the resulting modulation will be at a frequency lower than the energy-modulating frequency of the wakefield. This property allows us to tune the frequency over a wide range.

*Work supported by the Department of Energy SBIR program under Contract #DE-SC0006299.
#s.antipov@euclidtechlabs.com

Copyright © 2013 CC-BY-3.0 and by the respective authors

ANALYSIS AND OPTIMIZATION OF COUPLER KICK IN APEX*

H. Qian#, S.Kwiatkowski, C.F. Papadopoulos, Z. Paret, F. Sannibale, J. Staples, R. Wells, LBNL, Berkeley, CA 94720, USA

Abstract

A high repetition rate (~MHz) and high brightness photoinjector, based on VHF band CW normal conducting (NC) RF gun, is being developed under Advanced Photoinjector EXperiment (APEX) at Lawrence Berkeley Lab. A NC 30 MeV L-band linac system will be added after the gun to demonstrate beam brightness with lower repetition rate (~10 Hz). In this paper, coupler kicks from APEX buncher and acceleration cavities are evaluated by 3D RF simulation, analytical model and beam tracking, and coupler cells are optimized to minimize emittance dilution due to coupler kicks.

INTRODUCTION

The Advanced Photo-injector Experiment (APEX) is for demonstration of MHz repetition rate high brightness electron beam (~300 pC, ~0.6 mm mrad) injection for the next generation high repetition rate X-ray free electron lasers [1]. APEX is staged in 3 phases. In phase 0, the VHF-band normal conducting RF gun was successfully conditioned to achieve CW operation at nominal beam energy (750 keV) with low vacuum pressure performance (10^{-11} – 10^{-9} Torr). In phase I, a 6D beam phase space characterization will be conducted at 750 keV in CW mode. In phase II, a NC 30 MeV linac will compress and accelerate the beam to reduce space charge effects, so that beam brightness will be more reliably characterized. The APEX beamline is shown in Fig. 1.

The designs of buncher cavity and booster cavity are based on the ALS harmonic cavity and the ANL-AWA acceleration cavity respectively [2, 3], as shown in Fig. 2, both of which are not optimized for low energy and low emittance photoinjectors in terms of coupler kick. The RF input coupler breaks cylindrical symmetry of acceleration field and induces RF multipoles, which may perturb beam alignment and emittance compensation. Such effects can be even worse for beam near the gun due to relatively lower beam energy and thus bigger beam sizes, and has been taken care of in previous low emittance photoinjectors [4-9].

In the following, the RF coupler kicks will be evaluated for the APEX buncher and acceleration cavities through both simulations and simplified analytical models, and geometry modifications are suggested and evaluated.

ANALYTICAL EVALUATION OF COUPLER KICK EFFECT

RF coupler induced emittance growth has been well investigated during the development of low emittance photoinjectors [4-9]. Here a simplified analytical model is used to summarize the coupler kick effects when beam travels through a coupler cell (Fig. 2). Inside the model, only RF force is considered and beam size inside the cell is assumed to be relatively constant. The longitudinal paraxial electric field is expressed as follows:

$$E_z(x,y,z,t) = E_z(x,y,z)e^{i(\omega_0 t+\varphi_0+\Delta(x,y,z))}. \quad (1)$$

where amplitude asymmetry is included in $E_z(x,y,z)$,and phase asymmetry is included in $\Delta(x,y,z)$. $\varphi_0 = 0$ is defined as maximum acceleration phase.

Considering first order phase asymmetry and amplitude asymmetries induced by dipole and quadrupole, RF phase and amplitude can be expressed as,

$$\Delta(x,y,z) = k_y y\ . \quad (2)$$

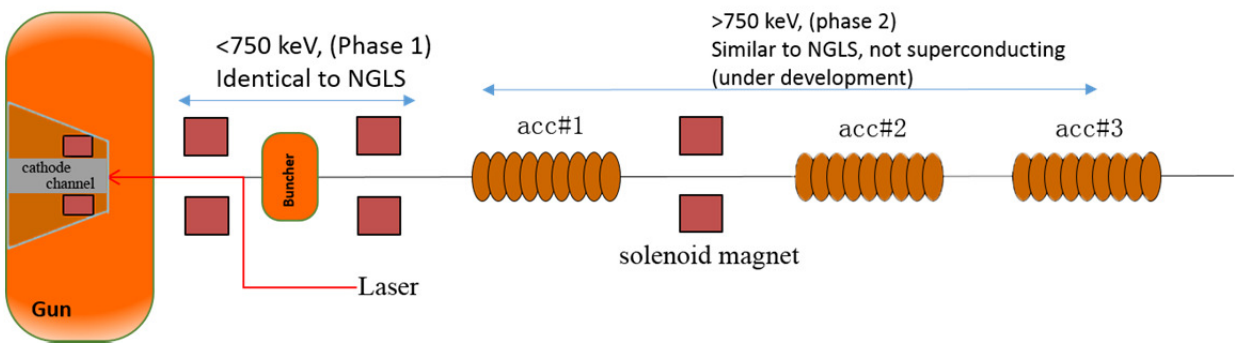


Figure 1: Schematic of the APEX injector beamline. Phase 1 is currently under operation. Phase 2 under development.

**This work was supported by the Director of the Office of Science of the US Department of Energy under Contract no. DEAC02-05CH11231

#hqian@lbl.gov

ISBN 978-3-95450-138-0

Copyright © 2013 CC-BY-3.0 and by the respective authors

LLNL X-BAND TEST STATION STATUS*

R.A. Marsh†, F. Albert, G. Anderson, S.G. Anderson, E.T. Dayton,
S.E. Fisher, D.J. Gibson, S.S. Wu, F.V. Hartemann, C.P.J. Barty
Lawrence Livermore National Laboratory, Livermore, CA 94550, USA

Abstract

An X-band test station is being built at LLNL to support inverse Compton-scattering x-ray and gamma-ray source development. The major components for the X-band test station have been designed, fabricated, installed, and aligned. The XL-4 klystron has been delivered, dressed and installed in the ScandiNova modulator, and tested to full peak power. Final assembly and bakeout of RF transport, test station supports, and accelerator components is complete, and the current status of commissioning and first beam will be presented and discussed. Future upgrade paths and configuration for a variety of x-ray and gamma-ray applications will be discussed along with schedule for planned experiments.

INTRODUCTION

Extremely bright narrow bandwidth gamma-ray sources are expanding the application of accelerator technology and light sources in new directions. LLNL has a successful history utilizing gamma-rays generated by a linac-driven, laser-based Compton scattering gamma-ray source [1, 2, 3, 4]. Next generation advancements in linac-based x-ray and gamma-ray production require increasing the average flux of gamma-rays at a specific energy (that is, $N/eV/sec$ at the energy of interest). One way to accomplish this is to increase the effective repetition rate by operating the RF photoinjector in a multi-bunch mode, accelerating multiple electron bunches per RF pulse. This multi-bunch mode will have stringent requirements for the electron bunch properties including low emittance and energy spread, but across multiple bunches. An X-band test station is under construction at LLNL to develop multi-bunch electron beams and generate x-rays. This paper summarizes progress and describes the current status of the project.

The RF gun is described in detail in [5]. Test station parameters are summarized in Table 1. Beam dynamics are summarized in Fig. 1 for a 250 pC bunch generated in the Mark 1 X-band RF gun and accelerated by a single T53 traveling wave accelerating section. Beam steering will use X-Y windowpane dipole magnets, and two quadrupole triplets will focus the beam for transport and quad-scan emittance measurement. A dump dipole magnet will double as a spectrometer once it has been calibrated.

Table 1: Test Station Parameters

Charge	25–250 pC
Normalized Emittance	<1 mm mrad
Gun Energy	7 MeV
Cathode Field	200 MV/m
Coupling β	1.7
Section Gradient	∼70 MV/m
Final Energy	30 MeV

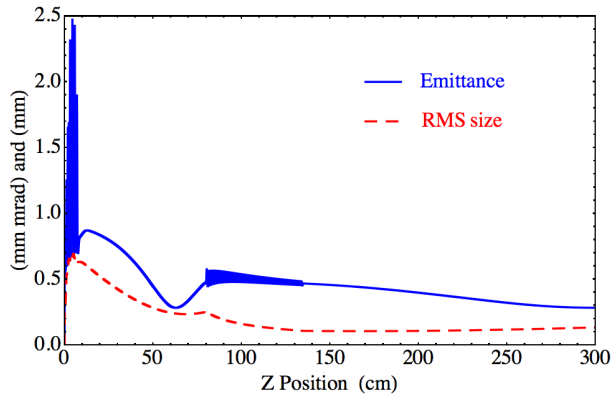


Figure 1: PARMELA beam dynamics simulation for a bunch charge of 250 pC.

TEST STATION

The test station layout is shown in Fig. 2. The high voltage modulator and X-band tube reside in a separate area with RF distribution fed through a hole in the wall to the linear accelerator. A manifold divides the power between the RF gun and the accelerating sections [6]. Testing of the klystron to full power is complete [7], and the RF load tree that was used for this testing is currently being disassembled to provide components for dressing the accelerating sections and provide components for the power division manifold. Support structures made from 80/20 mount to the laser tables and provide multi-dimensional adjustment for alignment of supported components to the beamline. The emittance compensation solenoid for the RF gun is mounted on precision ground rails so that it can be moved back to provide access to the gun. The gun support structure holds the RF gun, WR-90 pumpouts and pumps, as well as an RF gate valve on the beamline. The T53 accelerating structure is mounted on a SLAC designed strongback with end-to-end adjustment, which is then mounted on 80/20 supports that provide additional adjustment as well as support for RF distribution, loads, and vacuum pumps.

* This work performed under the auspices of the U.S. Department of Energy by Lawrence Livermore National Laboratory under Contract DE-AC52-07NA27344
† marsh19@llnl.gov

Copyright © 2013 CC-BY-3.0 and by the respective authors

SHAPING ELECTRON BUNCHES FOR ULTRA-BRIGHT ELECTRON BEAM ACCELERATION IN DIELECTRIC LOADED WAVEGUIDES*

Evgenya I. Simakov#, Dmitry Yu. Shchegolkov, C. Huang, and T.J. Kwan,
Los Alamos National Laboratory, Los Alamos, NM 87545, U.S.A.

Abstract

We describe a possible design of an Emittance Exchanger (EEX) which may be employed to generate a pair of a double-triangular drive bunch and a trapezoidal witness bunch for a Dielectric Wakefield Accelerator (DWA). We consider the concept of a high-brightness DWA with the gradient of above 100 MV/m and less than 0.1% induced energy spread in the accelerated beam as a possible afterburner for the proposed Los Alamos Matter-Radiation Interactions in Extremes (MaRIE) signature facility. We present the results of simulations with Elegant which take into account non-linear effects of the EEX beamline. Possibilities for producing ideal beam shapes to demonstrate low induced energy spread in a DWA are discussed.

INTRODUCTION

The modern discovery science has an emerging need for a very hard X-ray source, with high-peak fluxes of coherent 42-keV photons (~ 0.3 angstrom wavelength). High energy photons will allow resolving grain boundaries in materials in extreme states such as experiencing shock waves and being able to penetrate μm-to-mm sized samples. High photon energies are also required to prevent samples from disintegrating from a single X-ray pulse, allowing multiple images of transient effects. High-resolution imaging of these effects will optimally require up to 10^{12} photons per X-ray pulse, well above the ability of current technology. Los Alamos National Laboratory (LANL) has identified this discovery science frontier as an important part of its future mission and has proposed the Matter-Radiation Interactions in Extremes (MaRIE) facility [1], which includes an X-ray free electron laser (XFEL) as described in [2].

The number and the energy of photons produced by the XFEL is strongly dependent on the energy of the electron beam produced by the linear accelerator with the more energetic beam delivering more high energy photons to the user. Although generally the baseline design needs to be conservative and rely on existing technology, any future upgrade would immediately call for looking into the advanced accelerator concepts capable of boosting the electron beam energy up by a few GeV in a very short distance without degrading the beam quality. Typical electron beam quality parameters for XFEL applications are electron bunch charges of 0.1 to 1 nC, normalized rms emittances of 0.1 to 1 μm, and rms energy spreads of < 0.1%. By decreasing the bunch energy spread and emittance, it is possible to increase the total X-ray flux by orders of magnitude [2]. Dielectric Wakefield Accelerator (DWA) [3,4] has a potential to satisfy the required constraints of the afterburner and produce acceleration gradients above 100 MV/m and less than 0.1% spread in the gained beam energy [5].

We have initiated a project at LANL to demonstrate the proof-of-principle operation of a DWA with shaped drive and witness bunches at high gradient, and with enhanced transformer ratio and reduced energy spread.

REDUCING WITNESS BUNCH ENERGY SPREADS IN DWAs

DWAs are formed by one or several dielectric layers surrounded by metal cladding (Figure 1). The dielectric constant and the inner and outer radii of the dielectric tubes (or single tube in the simplest case) are chosen so that the phase velocity of the fundamental monopole mode (TM_{01}) is approximately equal to the speed of light and the mode is effectively excited by the beam passing in the central vacuum channel. In a collinear DWA the field generated by a leading, high-charge drive bunch is used to accelerate a trailing, low-charge main bunch which contains a relatively small amount of charge. The wakefields excited by a leading bunch have the remarkable property that the axial electric field and the transverse electric field are transversely uniform and linear, respectively. If one can make the wakefield to be axially constant along the bunch it will result in no induced energy spread within the bunch, leading to an extraordinary condition of preserving the main beam brightness while providing high gradient acceleration. We have realized that it is possible that an accelerated beam in a DWA can achieve the needed small energy spread if the longitudinal witness bunch profile is properly customized [5].

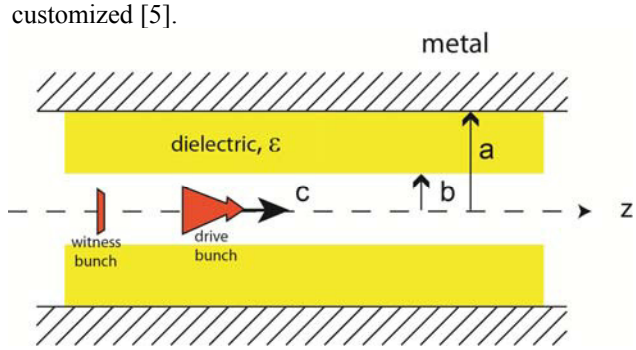


Figure 1: The schematic of a dielectric loaded waveguide with shaped electron beams traveling on axis.

Figure 2 shows the current profiles of the driving double triangular bunch and a trapezoidal witness bunch and their corresponding longitudinal wakefield generated

*Work is supported by the U.S. Department of Energy through the Laboratory Directed Research and Development (LDRD) program at Los Alamos National Laboratory.
#smirnova@lanl.gov

ISBN 978-3-95450-138-0

Copyright © 2013 CC-BY-3.0 and by the respective authors

MONTE CARLO SIMULATIONS OF CHARGE TRANSPORT AND ELECTRON EMISSION FROM GaAs PHOTOCATHODES*

Yongjun Choi†, Dimitre A. Dimitrov, Chet Nieter, Tech-X Corp., Boulder, CO, USA
Siddharth Karkare, and Ivan Bazarov, CLASSE, Cornell University, Ithaca, New York, USA

Abstract

The need for a bright electron beam is increasing in the fields of x-ray science, electron diffraction and electron microscopy which are required for colliders. GaAs-based photocathodes have the potential to produce high-brightness, unpolarized and polarized, electron beams with performance that meets modern collider requirements. Even after decades of investigation, however, the exact mechanism of electron emission from GaAs is not well understood. Therefore, we investigate photoemission from a GaAs photocathode using detailed Monte Carlo electron transport simulations. Instead of a simple stepwise potential, we consider a triangular barrier including the effect of the image charge to take into account the effect of the applied field on the emission probability. The simulation results are compared with the experimental results for quantum efficiency and energy distributions of emitted electrons without the assumption of any ad hoc parameters.

INTRODUCTION

The successful operation of X-ray light sources, free electron laser (FEL), and linear accelerator facilities depends on providing reliable photocathodes [1] for generation of low emittance, high-brightness electron beams using conventional lasers.

An ideal photocathode must have a high quantum efficiency (QE), low mean transverse energy (MTE), a quick response time and a good operational lifetime. GaAs-based photocathodes have been experimentally tested and shown [2] to have the potential to produce high-brightness unpolarized and polarized, electron beams with performance (e.g., high QE and low emittance) that meets FEL and modern collider requirements. A better understanding of the physics of photoemission in GaAs will open new possibilities for creating very low emittance high efficiency photoemitters.

However, there are still a number of issues [3] to solve in order to develop an optimized photocathode design. It is of interest to better understand the quantum efficiency and energy distribution of generated beams as a function of temperature, laser frequency, cathode material, doping concentration, electron affinity, and surface properties (e.g., roughness, band bending, charge trapping).

Accurate simulation capabilities help to optimize the design of a semiconductor photocathode. Three dimensional, particle-in-cell (PIC) codes can accurately simulate the evolution of electron beams for these purposes.

The VSim simulation and modeling framework [4] includes a variety of physical models that make it useful for a broad range of research in plasma physics and computational electrodynamics. It can model a plasma as particles, a fluid, or a particle-fluid hybrid; it can treat electromagnetic fields either self-consistently or in the electrostatic limit; and it provides both explicit and implicit time updates.

In a previous work [5], we investigated effects of charge transport and surface properties on electron emission from GaAs with a specific surface potential. However, it did not include the image charge effect, zero applied field was assumed, and the space-charge field was not included in the models. Here, we have started to consider electron emission properties when the space-charge field is included and the applied field is non-zero. We have done simulations with a surface potential that is often used to investigate electron emission and includes the image charge effect. Finally, we have used a reduced model for the calculation of the electron emission probability that is fast to evaluate but potentially less accurate than the model in Ref. [5].

MODEL

The simulation is based on the three-step model initially proposed by Spicer [6]. The three valley model is used to describe the band structure of GaAs. Here, we briefly describe these models. More detailed explanation can be found in Ref. [5].

Three Step Model

The three-step model takes into account the dependence on photon energy and (implicitly) on temperature. Fig. 1 shows a schematic representation of the three-step model for *p*-doped GaAs photocathode. The creation of electron-hole pairs due to absorption of photons is treated in the first step. A photon with sufficient energy is absorbed by a valence band electron leading to its transition to the conduction band and the formation of a hole in the valence band. The difference between the photon energy and the energy gap of the semiconductor material is transferred into kinetic energy of the created free charge carriers. In the second step, created conduction band electrons undergo different scattering processes and propagate diffusively. Some of these electrons will reach the photocathode surface and be

* The authors wish to acknowledge the support of the U.S. Department of Energy (DOE) under SBIR grant DE-SC0006246 and Early Career DE-SC0003965.

† yjchoi@txcorp.com

Copyright © 2013 CC-BY-3.0 and by the respective authors

HIGH CAPTURE LOW ENERGY SPREAD INVERSE FREE ELECTRON LASER ACCELERATOR

J. P. Duris, R. K. Li, P. Musumeci, E. Threlkeld
Department of Physics and Astronomy, UCLA, Los Angeles, CA 90095, USA

Abstract

We present the design and construction of a strongly period-, field-, and gap-tapered helical undulator for use in a high-gradient, high-efficiency helical IFEL experiment at Brookhaven ATF. The undulator design achieves efficient acceleration without prebunching by matching the ponderomotive and resonant energy gradients along the length of the interaction for the measured laser parameters. Simulations based on the measured undulator fields and experimental parameters suggest that as much as 43% of a 50 MeV beam will be accelerated to 94 MeV with 2.3% rms energy spread.

INTRODUCTION

Recent progress in inverse free electron laser acceleration (IFEL) has led to unprecedented acceleration gradients and energy gain for this class of accelerator. The STELLA experiment at ATF demonstrated efficient IFEL acceleration with gradients similar to conventional RF-accelerating cavities and captured up to 80% of the beam with the use of a prebunched beam [1]. The UCLA Neptune IFEL experiment first achieved accelerating gradients surpassing that of conventional rf-accelerators [2]. More recently, the UCLA-BNL helical IFEL collaboration at the Brookhaven Accelerator Test Facility (ATF) accelerated electrons from 52 MeV up to 106 MeV with a TW class CO_2 laser, averaging a 100 MeV/m accelerating gradient in the 54 cm long helical undulator [3]. The LLNL-UCLA IFEL effort currently underway at Lawrence Livermore National Lab aims to surpass these achievements by utilizing a multi-TW Ti:Sa laser [4] and has produced some significant initial results [5].

While IFEL accelerating gradients now outpace that of their rf counterparts, the higher gradients often come at the price of significant energy spread and low capture. One approach to improving capture is to match the longitudinal phase space of the beam to the longitudinal acceptance of the accelerator through microbunching as demonstrated by [1], and novel optical scale harmonic and adiabatic bunchers hold the promise of improved microbunching [6]. However, the efficiency of IFEL accelerators is often limited by spatiotemporal overlap of electron and laser beams as well as resonant energy and ponderomotive gradient mismatch. We aim to address these issues to allow monoenergetic acceleration with gradients larger than that of conventional accelerators without the use of prebunching.

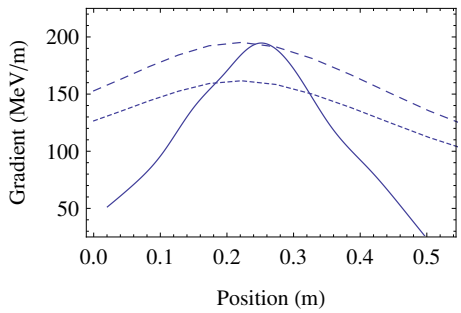


Figure 1: Resonant energy gradient set by the undulator tapering (solid) and ponderomotive gradients for the highest laser focal intensity of 23 TW/cm^2 (dashed) as well as for the median intensity of 18 TW/cm^2 (dotted).

GRADIENT MISMATCH

The UCLA-BNL helical IFEL collaboration at ATF was conceived to improve accelerating gradient through the use of the first strongly period- and field-tapered helical undulator. Whereas electrons propagating through a linear undulator undergo sinusoidal motion thereby reducing to zero twice per period their transverse velocity, the helical trajectories of the electrons propagating through the undulator provide continuous transverse velocity which in turn enables continuous energy transfer. This, coupled with a TW-class CO_2 laser, allowed for the acceleration of 52 MeV electrons up to 106 MeV [3].

The undulator was originally designed for use with a 9.6 cm Rayleigh range CO_2 laser. Unfortunately after construction, it was discovered that beam line space constraints and a restricting dipole aperture just upstream of the undulator necessitated a laser Rayleigh range of 30 cm. While the increased Rayleigh range had the positive benefit of easing transverse overlap tolerances by increasing the laser spot size, the on-axis intensity was reduced 3-fold, thereby significantly limiting the fraction captured and challenging the success of the experiment.

The problem can be better visualized by comparing the gradients set by the tapering of the undulator and that supplied by the ponderomotive interaction of the electrons in the combined undulator- and laser-fields. Figure 1 shows the resonant energy gradient set by the undulator and the ponderomotive gradient for various focal laser intensities (right plot). The resonant energy gradient usually exceeded the ponderomotive gradient, thereby significantly increasing the number of particles lost by reducing the ponderomotive bucket depth.

Copyright © 2013 CC-BY-3.0 and by the respective authors

ISBN 978-3-95450-138-0

WISCONSIN SRF ELECTRON GUN COMMISSIONING*

J. Bisognano,# M. Bissen, R. Bosch, M. Efremov, D. Eisert, M. Fisher,+ M. Green, K. Jacobs,
R. Keil, K. Kleman, G. Rogers, M. Severson, D. D. Yavuz
University of Wisconsin-Madison, Stoughton, WI 53589, USA
R. Legg, R. Bachimanchi, C. Hovater, T. Plawski, T. Powers
Jefferson Laboratory, Newport News, VA 23606, USA

Abstract

The University of Wisconsin-Madison has completed installation of a superconducting electron gun. Its concept was optimized to be the source for a CW free electron laser facility with multiple megahertz repetition rate end stations. This VHF superconducting configuration holds the promise of the highest performance for CW injectors. Initial commissioning efforts show that the cavity can achieve gradients of 35 MV/m at the cathode position. With the cathode inserted CW operation has been achieved at 20 MV/m with good control of microphonics, negligible dark current, and $Q_0 > 3\times10^9$ at 4 K. Bunch charges of ~100 pC have been delivered, and first simple beam measurements made. These preliminary results are very encouraging for production of 100s pC bunches with millimeter-milliradian or smaller normalized emittances.

MOTIVATION

An FEL complex operating at high repetition rates and delivering intense, ultra-short, fully-coherent, variably-polarized beams to multiple experiments enables transformational research in diverse science disciplines. The Wisconsin SRF electron gun program is a response to the demand for a very bright electron source that can be used for these next generation light sources. SRF guns hold the promise to produce very bright, CW beams because of the correlation between high electric field on the cathode and brightness [1].

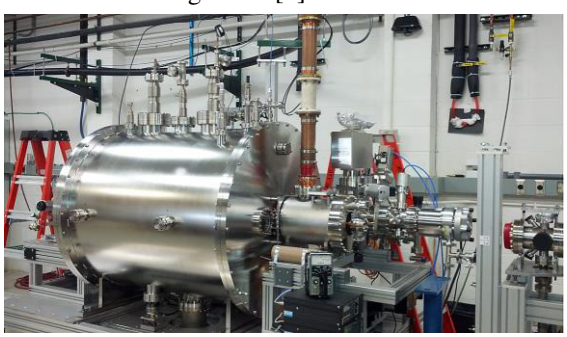


Figure 1: Electron gun installed in vault.

FACILITY OVERVIEW

The design uses a 199.6 MHz, quarter wave resonator geometry at a peak gradient up to 45 MV/m. Details of the superconducting cavity design, fabrication, and modeling have been presented in earlier publications [2]. The lower frequency design allows operation at 4 K and close to spatially constant electric field while the electron transits the accelerating gap. Thus, beam properties are expected to be superior to CW L-band guns, and relative to DC electron guns, should offer better performance with higher cathode fields. A copper photocathode was installed for initial testing with repetition rates limited to 1 kilohertz by the drive laser. Figure 1 shows the overall installation, and Table 1 contains key parameters for the gun.

Table 1: SRF Electron Gun Design Parameters

Max beam kinetic energy	4.0 MeV
Bunch charge	10–200 pC
Normalized trans. emittance	0.2–1 μm
Ultimate average beam current	1.0 mA
Peak current	50 A
Driving laser wavelength	266 nm

SUBSYSTEMS

RF System

The RF system utilizes a commercial, 30 kW, solid state transmitter driving coaxial waveguide through a circulator to the RF coupler. The low level RF controller (LLRF) [3] allows self-excited cavity operation and incorporates cavity fault and tuner control. It is based on the JLab upgrade design.

Magnets

The emittance compensation solenoid is of high temperature superconductor design. Nominal operating parameters are an integrated field of 3.1 T^2-mm at 38.45 A excitation at about 25-30 K (i.e., intermediate between LHe and LN_2 temperatures). An 18 bit AD7608 ADC is used to measure voltages at both ends and at the center of the solenoid for quench protection. The voltage difference between the two halves of the coil are compared and differences as small as 1 millivolt can be used to trigger a quench trip. There are two octupoles in the beamline. On each octupole the poles are independently powered with excitations mixed in software to produce normal and skew dipole and quadrupole correctors.

Cryostat

The cryostat consists of the helium vessel, internal tuner mechanism, cathode stalk, beam pipe, LN_2 cooled thermal radiation shield, magnetic shield, cryogenic plumbing and external vacuum vessel. The cavity is

*Work supported by DOE Award DE-SC0005264
#jbisognano@src.wisc.edu
+Current address: APS ANL

Copyright © 2013 CC-BY-3.0 and by the respective authors

EFFECT OF RF GRADIENT UPON THE PERFORMANCE OF THE WISCONSIN SRF ELECTRON GUN*

R. A. Bosch#, Synchrotron Radiation Center, University of Wisconsin-Madison,
3731 Schneider Dr., Stoughton, WI 53589, USA
R. A. Legg, Jefferson Lab, 12000 Jefferson Avenue, Newport News, VA 23606, USA

Abstract

The performance of the Wisconsin 200-MHz SRF electron gun is simulated for several values of the RF gradient. Bunches with charge of 200 pC are modeled for the case where emittance compensation is completed during post-acceleration to 85 MeV in a TESLA module. We first perform simulations in which the initial bunch radius is optimal for the design gradient of 41 MV/m. We then optimize the radius as a function of RF gradient to improve the performance for low gradients.

INTRODUCTION

A superconducting radiofrequency (SRF) electron gun has been designed and constructed to produce 200-pC bunches that are suitable for a high-repetition-rate (5 MHz) soft-xray free electron laser (FEL) [1–5]. Bunches are created by laser illumination of a photocathode and then accelerated to an energy of 4 MeV by a 200-MHz SRF cavity with peak electric field of 41 MV/m on the cathode. The electron gun utilizes a Cu photocathode, which can be replaced with a Cs_2Te photocathode whose higher quantum efficiency allows operation with lower laser power.

When a bunch is accelerated and compressed to achieve a peak current of ~1 kA for an FEL, current and energy modulations can cause microbunching that spoils the FEL process [1]. To minimize modulations in longitudinal phase space at the expense of slightly increased transverse emittance, "blowout" mode is employed, in which the initial bunch length is small compared to that of the accelerated bunch [6]. Simulations of blowout mode show that longitudinal and transverse modulations of the initial bunch distribution emitted from the photocathode are smoothed out by the self field space charge force [3].

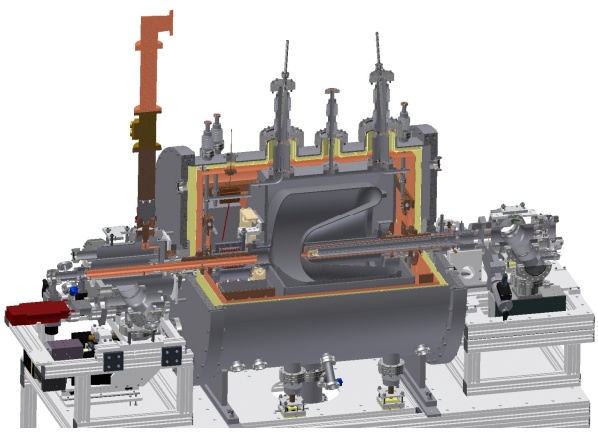


Figure 1: The photocathode, SRF cavity and high-temperature superconducting solenoid in the liquid-helium cryostat. Courtesy of G. C. Rogers.

We study the gun performance with simulations that include emittance compensation [7] from focusing the bunches in a high-temperature superconducting (HTS) solenoid [8] that is immediately downstream of the SRF cavity, and then accelerating them to 85 MeV in a cryomodule containing eight TESLA 1.3-GHz SRF cavities. The first TESLA cavity is used as a buncher, with the phase and gradient adjusted to control transverse focusing. The bunches become longitudinally frozen after travelling 3 m and reaching an energy of 6 MeV. For the design gradient of 41 MV/m, simulations indicate that bunches with normalized emittance of ~1 mm-mrad emerge from the cryomodule [5]. Figure 1 shows the photocathode, SRF cavity, and solenoid in the liquid-He-cooled cryostat.

In this article, we evaluate the production of 200-pC bunches when the peak electric field on the cathode of the 200-MHz cavity differs from the design gradient of 41 MV/m. The ASTRA [9] code is used to perform 100,000-particle simulations of a realistic bunch that initially has truncated Gaussian radial and longitudinal profiles, truncated at 0.8σ. (Note that for a Gaussian profile truncated at 0.8σ, σ is not the rms value.) For the Wisconsin electron gun, previous studies [5] have shown agreement between ASTRA simulations and simulations performed with the GPT code [10].

An initial longitudinal σ of 187.5 fs is studied; nearly identical results have been obtained with smaller values of the longitudinal σ, consistent with blowout mode. Since the electron velocity depends upon the RF gradient, we use the AUTOPHASE feature of the ASTRA code to set the RF phase when a bunch enters a TESLA cavity to equal the optimized phase for the design RF gradient of 41 MV/m.

A bunch is emitted from a Cu or Cs_2Te photocathode with initial transverse normalized slice emittances ε_x and ε_y that are related to the rms laser spot dimensions by $\varepsilon_{x,y}$ [mm-mrad] ≈ $\sigma_{x,y}$ [mm], and initial kinetic energy of ~0.5 eV [11, 12]. For a Gaussian radial profile truncated at $0.8\sigma_r$, the rms dimensions are given by $\sigma_{x,y} = 0.4\sigma_r$.

FIXED BUNCH RADIUS

We first considered the initial bunch radius that gives the lowest output emittance for the design gradient of 41 MV/m. For a truncated Gaussian radial profile truncated at $0.8\sigma_r$, this initial radius σ_r is 1.75 mm [5]. The rms

*Work supported by DOE Award DE-SC0005264
bosch@src.wisc.edu

ISBN 978-3-95450-138-0

Copyright © 2013 CC-BY-3.0 and by the respective authors

STUDY ON 2 CELL RF-DEFLECTOR CAVITY FOR ULTRA-SHORT ELECTRON BUNCH MEASUREMENT*

T. Takahashi†, Y. Nishimura, M. Nishiyama, K. Sakaue, M. Washio
Waseda University, Tokyo, Japan

T. Takatomi, J. Urakawa, KEK, Ibaraki, Japan

Abstract

We have been studying on an rf-deflector system to measure ultra-short electron beam bunch length at Waseda University. By using HFSS, we optimized the design of the 2 cell rf-deflector which is operating on π-mode, standing wave, dipole (TM_{110}-like) mode at 2856 MHz. We have finished manufacturing under the collaboration with High Energy Accelerator Research Organization (KEK) and installing the rf-deflector in the accelerator system of Waseda University. It is estimated that this rf-deflector has sufficient performance for measuring the ultra-short electron bunch. Now the experiment has just begun and confirmed electron beam is swept by this rf-deflector. Bunch length measurement will be soon carried out accurately. In this paper, the design of rf-deflector, the estimation for rf-deflector performance, the present progress and the future plan will be described.

INTRODUCTION

At Waseda University, a compact linear accelerator system based on photo-cathode rf electron gun is applied for the various researches and we have two kinds of rf electron guns as beam sources, 1.6 cell S-band Cs-Te photo-cathode rf gun (1.6 cell gun) for the pulse radiolysis [1] and the laser Compton scattering [2], Energy chirping cell attached rf gun (ECC gun) for the generation of coherent THz radiation [3]. It is necessary to measure time structure of electron beam on several picoseconds region on 1.6 cell gun and bunch length of several hundreds femtoseconds on ECC gun in the future. Therefore, we have been developing an rf-deflector system in order to achieve the bunch length measurement with high temporal resolution.

PRINCIPLE OF BUNCH LENGTH MEASUREMENT BY RF-DEFLECTOR

When rf electromagnetic wave is supplied into an rf-deflector, a proper resonant mode is excited. The resonant electromagnetic field in the beam line produces force on the beam. The magnitude of the force which influences on each part of the electron bunch is different in association with temporal change. When this force has vertical direction to the beam line, the beam after the passage of an rf-deflector is tilted as it drifts. This means the longitudinal distribution of the beam is converted to the transverse. The bunch length can be calculated by observing the transverse distribution. The outline of bunch length measurement by an rf-deflector is below (Fig.1).

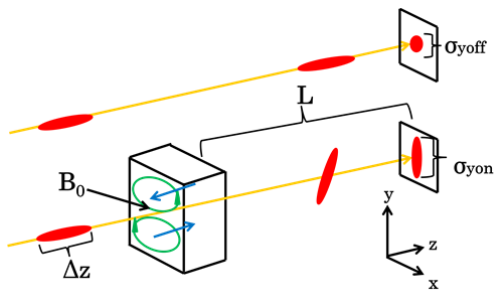


Figure 1: Outline of bunch length measurement.

In Waseda University, we have designed the rf-deflector which produces only Lorentz force to the beam by a magnetic field, using a TM110-like mode. By solving the equation of motion to electron, bunch length Δz is expressed by (assuming the Gaussian profile):

$$\Delta z = \frac{E\sqrt{{\sigma_{yon}}^2 - {\sigma_{yoff}}^2}}{2cB_0L\{\cos(\omega t_0 + \phi) - \cos\phi\}} \qquad (1)$$

where σ_{yon} and σ_{yoff} are the vertical beam size at the profile monitor when the rf-deflector is on and off, respectively, B_0 the peak magnetic field in the rf-deflector, L drift distance between the outlet of the rf-deflector and the profile monitor, φ the rf phase when the bunch enters the rf-deflector, ω the angular frequency of the rf-deflector, E the beam energy, t_0 the traveling time of the bunch in the rf-deflector, c the velocity of light. Then the number of 2 in the denominator represents the 2 cell structure of the rf-deflector. When σ_{yon} is measured, it is supposed that the time resolution becomes higher if the space covered by σ_{yoff} is smaller. So it is important to get large σ_{yon} and small σ_{yoff}. According to Eq. (1), the large magnitude of B_0 or L brings about the progress of time resolution, and ultra-short bunch length measurement could be possible. Because L has the limitation considering the size of the accelerator facility, we have designed the form of the rf-deflector with the larger

*Work supported by JSPS Grant-in-Aid for Scientific Research (A) 10001690 and the Quantum Beam Technology Program of MEXT.
†qwerty-ytrewq@toki.waseda.jp.

Copyright © 2013 CC-BY-3.0 and by the respective authors

10S FEMTOSECOND BUNCH LENGTH MEASUREMENT BASED ON COHERENT TRANSITION RADIATION*

Xianhai Lu†, Wenhui Huang, Chuanxiang Tang, Tsinghua University, Beijing 100084, P. R. China‡
K.G. Roberts, R.K. Li, P. Musumeci, H.S. To, UCLA, Los Angeles, CA 90095, USA

Abstract

In this paper, we discuss bunch length measurement based on coherent transition radiation for 10s femtosecond electron bunches with of several MeV energy and several pC charge. The ultrashort bunch length is obtained by velocity bunching using a compact dual slot resonantly coupled linac located after an RF photoinjector. Strong focusing with a solenoid is required to enhance the radiation generation. Filters are used to reconstruct coherent transition radiation spectrum. The transverse and longitudinal form factors are also studied with simulation.

INTRODUCTION

Bunch length measurement is a basic issue in beam diagnostic. Traditional methods for bunch length measurements includes using deflecting cavity[1], using radiation based spectrum methods[2] and electro-optic detection methods[3]. By using velocity bunching method, sub picosecond or 10s femtosecond bunch can be generated in several MeV energy and several pC charge regime, for applications such as ultrafast electron diffraction and Thomson scattering. To measure the bunch length at the maximum compression plain, coherent transition radiation (CTR) method is more appropriate than direct methods using deflecting cavity, since the latter measurements are extended in z and can only give an estimate for the average bunch length over the measurement distance. Another advantage of using CTR method for measuring ultrashort bunch is the energy of coherent transition radiation increases significantly as the bunch length decrease, which is favorable to detection.

In this paper, we discuss a bunch length measurement method based on coherent transition radiation, for 10s femtosecond electron bunch length obtained by velocity bunching using a linac. The method and setup are described in the following section. In the end, preliminary experimental results are also presented.

METHOD

For transition radiation generated by electron crossing metal boundary, the process can be viewed as collision process of electron with its image charge. The spectrum and angular distribution of energy generated in the collision can be obtained by calculating the Lienard-Wiechert potential as [4]:

$$\frac{\mathrm{d}E_s}{\mathrm{d}\omega\cdot\mathrm{d}\Omega}=\frac{e^2}{4\pi^2c^3}\left(\frac{\vec{v}\times\vec{n}}{1-\vec{n}\cdot\vec{v}/c}-\frac{\vec{v'}\times\vec{n}}{1-\vec{n}\cdot\vec{v'}/c}\right)^2, \quad (1)$$

where E_s is the radiation energy of single electron,ω is the angular frequency of radiation, Ω is the solid angle, e is the charge of electron, c is the speed of light in vacuum, $\vec{n}$ is the direction of radiation, $\vec{v}$ and $\vec{v'}$ are the velocities of electron and its image charge. It is noted that the angular distribution does not depend on frequency. For a 45 degree collision, the velocity $\vec{v}$ and $\vec{v'}$ are determined by the setup, then we can calculate the energy distribution by integrating over the solid angle collected by an off axis parabolic (OAP).

The total radiation energy of a bunch E_b is the sum of single electrons, taking consideration of phase effect into account. The expression can be written as:

$$\frac{\mathrm{d}E_b}{\mathrm{d}\omega\cdot\mathrm{d}\Omega}=|N\cdot f(\omega)|^2E_s(\omega) \quad (2)$$

$$=\frac{e^2|N\cdot f(\omega)|^2}{4\pi^2c^3}\left(\frac{\vec{v}\times\vec{n}}{1-\vec{n}\cdot\vec{v}/c}-\frac{\vec{v'}\times\vec{n}}{1-\vec{n}\cdot\vec{v'}/c}\right)^2, \quad (3)$$

where $f(\omega)$ is the coherent factor. When the longitudinal size of bunch is much longer than the transverse size and the radiation are concentrated in small angle around beam axis, transverse coherent effect can be neglect and the coherent factor can be written as:

$$f(\omega)=f_L(\omega)=\frac{1}{N}\sum_{j=1}^{N}e^{i\omega t_j}\cong\int_{-\infty}^{+\infty}\rho(t)e^{i\omega t}\mathrm{d}t, \quad (4)$$

where $\rho(t)$ is the normalized distribution function. For wavelength longer than bunch length, the field created by electrons are coherent and the total energy is proportional to the square of number of electrons. In the case of low energy bunch and comparable transverse bunch size and longitudinal size multiplied by γ ($\sigma_x \backsimeq \gamma\sigma_z$), the effect of transverse size of bunch should not be neglected. For a numerical example, the wavelength of CTR corresponding to 40 fs bunch ranges around 12 μm, assuming the transverse spot size is 100 μm, when viewed at the angle larger than 7 degree from the axis, the maximum phase difference of radiation emitting from different transverse position can be larger than one period. Then the coherent factor should be written as:

$$f(\omega)=f_L(\omega)f_T(\omega), \quad (5)$$

* U.S. DOE Grants No. DE-FG02-92ER40693, No. DEFG02-07ER46272
† sealuxh@gmail.com
‡ Key Laboratory of Particle & Radiation Imaging, Tsinghua University, Ministry of Education

ISBN 978-3-95450-138-0

Copyright © 2013 CC-BY-3.0 and by the respective authors

HIGH-CHARGE FEMTOSECOND ELECTRON GENERATIONS FOR ULTRAFAST, HIGH-BRIGHTNESS ELECTRON BEAM APPLICATIONS*

Jangho Park#, Hans Bluem, John Rathke, Tom Schultheiss, and Alan M. M. Todd
Advanced Energy Systems, Inc., Medford, New York 11763, USA

Abstract

Generation and preservation of ultrafast, high-brightness electron beams is one of the major challenges in accelerator research and development (R&D) for beam applications such as free electron lasers (FEL) and ultrafast electron diffraction (UED). Transverse and longitudinal space charge forces play a key role in emittance dilution and bunch lengthening respectively, for all high-brightness beams. We present a newly-designed, X-band, photocathode, radio frequency (RF), electron gun that utilizes radial bunch compression to deliver a compact ultrafast, high-brightness source. By compensating for the path length difference in an extremely-high-acceleration-gradient cavity with a curved cathode, we numerically demonstrate the potential for achieving more than an order of magnitude increase in beam brightness over existing electron guns. The thermo-mechanical analysis and conceptual design that demonstrate the viability and reliability of the concept are also presented.

INTRODUCTION

Ultrafast high-brightness electron beams are desired as injectors for light sources, including FELs, energy recovery linacs (ERL) and medical devices, amongst other applications. Brightness is the holy grail of most light sources and brighter, short-pulse electron injectors are to be prized where there are no downstream transport consequences of the short bunches. An example is micro bunching instabilities that can result from transport interactions with the energy modulations induced by the longitudinal space charge (LSC) forces in the bunches. These sources may also find direct application in advanced accelerators like the plasma wake-field accelerator (PWFA) and ultrafast electron diffraction (UED) [1]. Plasma accelerators promise orders-of magnitude increases in accelerating gradient to greater than 100 GeV/m and could lead to very compact and economical systems for those many accelerator applications that require high particle energies. Ultrafast diffraction techniques, which provide information about atomic-scale molecular structure, are critical to chemists and material scientist in their research and development activities.

In the generation of ultrafast, high-brightness electron beams, space-charge forces play a fundamental role in emittance dilution and bunch lengthening within the gun and subsequent emittance compensation drift. In order to generate and preserve the beam brightness, transverse and longitudinal space charge effects have to be precisely managed. Several different approaches have been reported and are being actively pursued within the worldwide accelerator community. These include various velocity bunching and magnetic compression techniques. However, each option suffers drawbacks that must be overcome in order to deliver a compact and economic ultrafast, high-brightness source.

In order to develop an improved ultrafast high-brightness electron source, we have proposed a scheme that compensates for path length differences by using a curved cathode [2]. This introduces radial compression that compensates for geometric bunch lengthening effects when coupled with extremely-high-acceleration-gradient to minimize the impact of space-charge forces. The AES-patented rear-fed coaxial cathode coupling eliminates contributions to transverse emittance from non-axisymmetric modes [3]. We show that combining these effects is feasible and does indeed deliver a more compact, economic, ultrafast high-brightness electron beam for the identified applications.

CAVITY AND COUPLING DESIGN

For a high-aspect-ratio (short bunch length) electron bunch, the asymptotic bunch length due to the space charge forces of a uniformly accelerated bunch is expressed by:

$$\Delta t_{sc}(\infty) = \frac{mc^2}{e}\frac{Q}{\pi R^2 \varepsilon_0 c E^2}. \qquad (1)$$

This ignores the drive laser duration and assumes prompt response from a copper cathode with a constant laser spot radius (R). Here, bunch lengthening due to space charge is inversely proportion to the square of the bunch radius (R) and the square of the accelerating field (E). The bunch lengthens due to the longer trajectories of the outer particles, compared to electrons emitted closer to the axis, and is proportional to the square of the beam radius.

Our previous upstream, coaxial, waveguide-fed gun cavity design had the drawback that the radial space for electron beam emission and drive laser insertion was relatively small [4]. We have now completed the RF analysis for a coaxial RF feed from the rear of the gun. Standard codes like the SLAC-developed S3P code [5] and SUPERFISH have been used to complete the RF design used in the reported beam dynamics analysis. Following Ref. [3], we focused on the geometry of the coaxial coupler and the iris between the cells, in order to maximize shunt impedance and thus minimize losses for a given cathode voltage. The coaxial coupler and the iris

* This work was supported by the U.S. Department of Energy, under Contract No. DE-SC0009556.
#jangho_park@mail.aesys.net

Copyright © 2013 CC-BY-3.0 and by the respective authors

STUDIES OF FIELD AND PHOTO-EMISSION IN A NEW SHORT-PULSE, HIGH-CHARGE Cs_2Te RF PHOTOCATHODE GUN

E. E. Wisniewski
Illinois Institute of Technology, Chicago, IL, USA and ANL/HEP, Argonne, IL, USA
M. Conde, W. Gai, C. Jing, W. Liu, and J. G. Power
ANL/HEP, Argonne, IL, USA
Z. Yusof and L. K. Spentzouris
Illinois Institute of Technology, Chicago, IL, USA

Abstract

A new high-charge RF gun is now operating at the Argonne Wakefield Accelerator (AWA) facility at Argonne National Laboratory (ANL). The 1.5 cell 1.3 GHz gun uses a Cesium telluride photocathode driven with a 248 nm laser to provide short-pulse, high charge electron beams for the new 75 MeV drive beamline. The high-gradient RF gun (peak field on the cathode $>$ 80MV/m) is a key piece of the facility upgrade. The large Cs_2Te photocathode (diameter $>$ 30 mm) is fabricated in-house. The photo-injector generates high-charge, short pulse, single bunches (Q $>$ 100 nC) or bunch-trains (Q$>$1000 nC) for wakefield experiments, typically involving dielectric-loaded accelerating structures. Field-emitted dark current from the Cs_2Te cathode was measured during RF conditioning. Fowler-Nordheim plots of the data are presented and compared to similar measurements made using a copper cathode in the initial phase of conditioning. Results of quantum efficiency (QE) studies are presented with the cathode operating in both single and bunch-train modes.

EMISSION STUDY PLAN AND GOALS

The 1.5 cell, 1.3 GHz, AWA drive-gun is now operating, using high Quantum Efficiency (QE) Cs_2Te photocathodes fabricated in-house [1]. The photocathode requirements are QE greater than 1% with a lifetime of weeks to months while experiencing a very high gradient (80 MV/m) peak RF field on the cathode. The primary function of the gun is to provide high-charge, short-pulse electron beams to drive wakefield structures [2]. As part of the turn-on process, we are conducting field emission and photoemission studies in the gun.

Photocathode Field Emission Study

We measured and characterized field emission from two different photocathodes used during the two phases of RF conditioning. Copper was used for the initial gun conditioning, followed by Cs_2Te thin film on Molybdenum for planned high-charge operation. We hope to use the data to better understand the relative impact of different factors influencing the level of field emission and its possible mitigation.

Photoemission Study

We characterized photoemission from the Cs_2Te photocathode under various conditions. Using 2-10 ps, 248 nm wavelength laser pulses, we are studying photoemission at high gradient to optimize the performance of the photocathode and the gun. At the time of the writing of this paper, QE measurements of the photocathode in the gun have been made over a period of about 6 weeks.

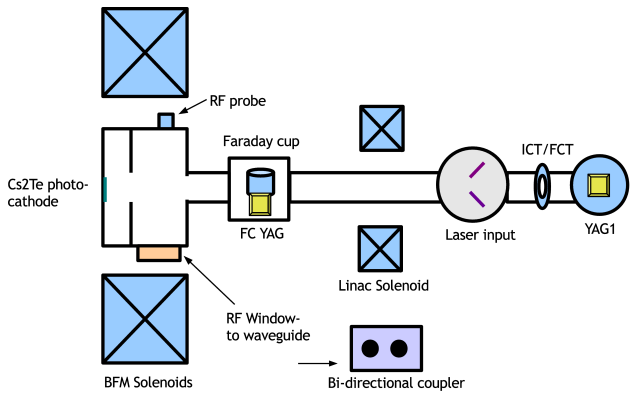


Figure 1: The L-band 1.5 cell photocathode gun with the relative positions of diagnostics to be used (cartoon - not to scale). The RF power input is measured near the RF window using a bi-directional coupler. The dark current is measured with a Faraday cup 58 cm from the cathode. The beam charge is measured using an Integrating Current Transformer (ICT). YAG(Ce) scintillating screens to image the beam and the dark current are available at two locations. In addition, an in-vacuum mirror at the Faraday cup location may be used to observe the photocathode and help to identify emission sites (not to scale).

EXPERIMENTAL SETUP

The beamline with the relative positions of diagnostics used for the experiments is depicted in a schematic shown in Fig. 1. RF power measurements were made using a dual-directional coupler connected in series in the waveguide just before the gun. The dark current was measured using a Faraday cup. The beam charge was measured using a Bergoz combination in-flange Integrating Current Transformer (ICT) and Fast Current Transformer (FCT).

Copyright © 2013 CC-BY-3.0 and by the respective authors

ISBN 978-3-95450-138-0

THE CATHODE PREPARATION CHAMBER FOR THE DC HIGH CURRENT HIGH POLARIZATION GUN*

O. Rahman†, I. Ben-Zvi, D. Gassner, A. Pikin, T. Rao, E. Riehn, B. Sheehy, J. Skartika, E. Wang, Q. Wu, BNL, Upton, NY 11973, USA.

Abstract

A compact cathode preparation chamber for the high current high polarization gun for the proposed eRHIC project has been designed and assembled at Brookhaven National Laboratory. This preparation chamber will be used to activate GaAs photocathodes to be used in the Gatling gun. The chamber is capable of achieving XHV on a consistent basis. Bulk GaAs samples were activated in this chamber with standard QE for the respective wavelength. In this paper, we discuss the design of this vacuum system, the heat cleaning and the activation procedure for the GaAs sample which will eventually be followed for the Gatling gun.

INTRODUCTION

The High Current High Polarization Electron Gun is one of the most important research projects for the proposed eRHIC project [1]. The average current is required to be 50 mA and the polarization requirement is more than 80%.For weekly exchange of cathodes, given that two guns are used, one cathode has to provide 50 mA of average current for 85 hours, which yields to 15300 C of charge. The maximum reported charge extracted is 1000 C, which is a order of magnitude lower than the requirement [2]. To solve this problem, 50 mA of current can be distributed over 20 photocathodes such that each cathode has to provide 2.5 mA of current for 85 hours, yielding 765 C of charge. This solution of combining 20 bunches to one common beam axis solves the problem of charge limitation without sacrificing the high average current requirement. The high polarization can be obtained using Superlattice GaAs which is able to provide polarization greater than 80% in a consistent basis [3]. For the R&D and "proof of principle" experiment, bulk GaAs will be used.

DESIGN OF THE CATHODE PREPARATION CHAMBER

The cathode preparation chamber is a compact design including 3 crosses, two of them are 6-way crosses and the other one is a standard 4 way cross. These three crosses are stacked on top of each other with the 4-way cross at the bottom. The cathode holder is moved up and down using a magnetic manipulator. One NEG pump and one turbo pump is attached to the bottom 4-way cross. The middle cross contains the tungsten filament, another NEG pump, one Ion pump and a view port. The top-most cross includes the Cs source, a pick up anode, a variable leak valve for Oxygen, an Extractor gauge to measure low pressure and a window through which laser shine the sample. A cross sectional view of the assembly is shown in Fig. 1 and the front view of the actual system is shown in Fig. 2. The vacuum and heat cleaning components are described in detail in the following sections.

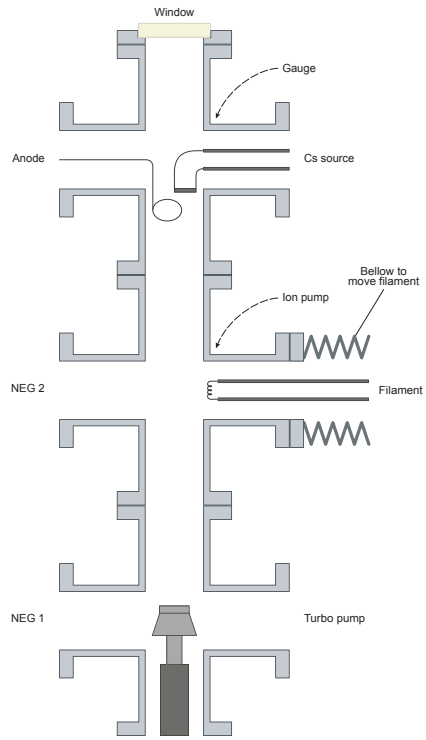


Figure 1: Cross sectional view of the cathode preparation chamber.

VACUUM COMPONENTS AND BAKE OUT PROCEDURE

The bake out procedure is extensive since activating GaAs requires XHV i.e low 10^{-11} Torr scale vacuum. The chamber at 200°C for approximately a week. Heater tapes are used to wrap the chamber and K-type thermocouples are used in 8 different locations of the chamber to make

* Work supported by Brookhaven Science Associates,LLC under contract no. DE-AC02-98CH10886 with the U.S. Department of Energy

† orahman@bnl.gov

Copyright © 2013 CC-BY-3.0 and by the respective authors

PARMELA SIMULATION FOR BNL 704MHZ SRF GUN IN LOW EMITTANCE OPERATION

E. Wang, J, Kewisch, I. Ben-zvi, BNL, Upton, NY 11973

Abstract

The BNL 704MHz 0.5 cell SRF gun is designed for an ERL prototype with high bunch charge and high average current, but may ultimately be used to generate a high brightness electron beam for a high power far infrared free electron laser (FEL) without energy recovery. In simulations with the space charge tracking code PARMELA we obtained a transverse normalized beam emittance of 0.22 mm-mrad for a bunch charge of 300 pC. The schematic layout of 704 MHz gun and its preliminary beam dynamics are presented in this paper. The emittance of electron beam was optimized for 300 pC bunch charge, 20 ps bunch length and 20 MeV operations.

INTRODUCTION

A high repetition rate FELs requires an electron beam with an extremely good emittance and operating in CW mode. The transverse normalized emittance of the electron bunch is matched to a FEL beam if

$$\gamma\varepsilon_{x,y} < \frac{1}{4\pi}\gamma\lambda_r$$

where γ is the electron energy and λr is the FEL wavelength. The reduction the transverse emittance from the RF gun and the optimization beam optics are the goals of this paper. To realize the high repetition rate and high average power FEL, the gun has to work in CW mode.

SRF gun combines the high gradients of normal conducting RF gun with the CW mode operation of superconducting RF technology. It is demonstrated to be capable of generating a low emittance beam in CW mode operation. The 704MHz superconducting gun for BNL ERL prototype is commissioned now[1]. As an ERL injector, this gun must accelerate electrons to 2-2.5MeV with bunch charge up to 5nC dependent on the operational parameters. In pervious simulations it was shown that this gun is capable of providing the beams with 1.4μm rms normalized emittance with a bunch charge of 1.4nC.

In our PARMELA simulation we reduced the bunch charge to 300 pC and obtained a normalized transverse emittance of 0.22 mm-mrad after acceleration to energy of 20MeV. The optimization code RTX was used in this work as a wrapper around the PARMELA program. The 2D electric field map of the gun and cavities was obtained with Superfish and passed into PARMELA. The average axial electric field in the gun is assuming 9.4MV/m.

BEAM OPTICS ARRANGEMENT

The layout of the accelerator is shown on Figure 1. The beam energy at half cell SRF gun exit is 2MeV. Then it will be boosted to 20MeV by a 5 cell cavity. Two solenoids are used to maintain the beam size and space charge compensation. A 3rd harmonic cavity is used to reduce the energy spread. A uniform spatial and temporal distributions laser shape was assumed to drive the beam from cathode. The 704MHz cavity shape is shown on Figure 2. The initial beam and accelerator parameters are listed as Table 1.

Multiple parameters including laser spot size, emission phase, beam length, solenoids' field, 3rd harmonic cavity parameters must be optimized.

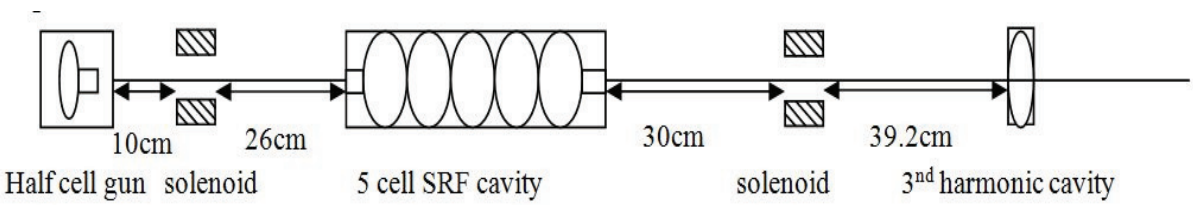


Figure 1: The layout of beam optics. The optimized distance is labelled.

*Work supported by Brookhaven Science associates, LLC under Contracts No.DE-AC02-98CH10886 with the U.S.DOE
#wange@bnl.gov

ISBN 978-3-95450-138-0

Copyright © 2013 CC-BY-3.0 and by the respective authors

BEAM DYNAMICS OF FUNNELING MULTIPLE BUNCHES ELECTRONS

E. Wang, I. Ben-zvi, D.M. Gassner, W. Meng, T. Rao, E. Riehn, J. Skaritka
Brookhaven National Laboratory, Upton, NY 11973, USA
O. Rahman, Stonybrook, NY 11974,USA

Abstract

The future electron ion collider (eRHIC) at Brookhaven National Laboratory requires a polarized electron source with high average current, short bunch length, and small emittance. The-state-of-the-art single polarized electron photocathode is far from delivering the required 50mA current due to ion back-bombardment limiting the cathode's lifetime and surface charge limit. In our design of the funnelling gun, currently under construction, the electron bunches generated from 20 photocathodes in a 220 kV DC gun are funnelled into a single common beam-axis. This article details design of the optics of our high-average-current polarized electron gun, and presents our simulation of the beam's dynamics and the design of the combiner. We also report herein our progress in constructing the funnelling gun.

INTRODUCTION

A key technological demand in constructing a future heavy-ion collider lies in assuring a high average-current, high-bunch-charge polarized electron source. To meet the requirements for luminosity and electron energy for an electron- and heavy-ion-collider, we are developing a polarized electron source with an average current of 50mA, and a 2.3A peak current. The quantum efficiency (QE) lifetime due to ion back-bombardment limits the level of the achievable average current, and bunch charge with a single GaAs photocathode in a DC gun. One approach to extending charge lifetime is to funnel the electron bunches generated from several photocathodes to a single common axis. In our design, each photocathode generates an average current of 2.5 mA. We placed twenty GaAs photocathodes along the rim of a 32 cm-diameter cathode electrode at a potential of -220 kV. A series of fixed magnetic field dipoles first bend the off-axis electron bunches that then are merged into the main axis by a rotating magnetic field. Figure 1 is the schematic layout of the funnelling gun for transporting current from the cathodes to the depressed collector that acts as a beam dump. Each cathode produces an electron bunch with a 700 kHz of repetition rate. The timing of the radiating laser to the cathode is such that each cathode emits with delay of 70ns after the previous one. After funnelling, the bunches' repetition frequency is 14 MHz; the total average current reaches 50 mA.

*Work supported by Brookhaven Science associates, LLC under Contracts No.DE-AC02-98CH10886 with the U.S.DOE
#wange@bnl.gov

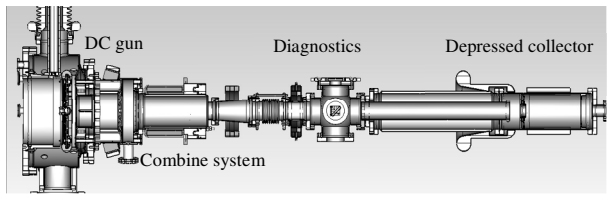


Figure 1: Schematic layout of funnelling gun.

GUN SETUP

The detailed design oft the gun was described earlier [1].We used a Pierce-like DC gun to accelerate the electrons. A focusing field near the cathode balances the effect of the strong space-charge from the bunch. The optimized angle between the cathode and the cathode's electrode is 157°; the gap voltage is 220V across 2.8mm. The maximum field on the cathode is 5.3MV/m. Solenoids placed after the anodes compensate for the defocusing of the space charge in the gun's DC gap. We designed compensated dogleg trajectories in the beam's funnelling system encompassing 20 fixed bending fields, one for each cathode, generated by 20 dipole-magnets, along with a single rotating bending-field generated by the magnetic combiner. Several components of the beam diagnostics are sited downstream, and finally, the beam will absorbed by a depressed collector. Two solenoids downstream of the combiner maintain the beam size.

SIMULATION OF THE COMBINER FIELD

We are using 20 dipole coils and 40 quadrupole ones with a sine AC current to generate rotational dipole- and quadrupole fields [2]. The OPERA AC steady-state solutions confirmed the degree of rotation of the fields, and also that the multicathode emitted beams are in phase. The effect on the beam of the rotating time-dependent field can be ignored. In simulating the gun , we used the static-field maps generated by Opera-3D/TOSCA for simulating the 3D beam in CST Particle Studio. We also generated a rotation dipole- and quadrupole-field from CST EM studio time-domain solver. The 20-sine excition signal is sent to the dipoles; each of them has an 18-degree phase shift. We obtained the animation of the rotating field in the time frame. We used the same setup for generating the rotational quadrupole field. Figure 2 shows the field distribution simulated by CST. The simulated rotated field was used in a PIC solver to assess the the funneling of the multiple bunches . However, the simulation consumed too much time and power due to the RAM limitation in the personal computer and its I/O speed.

Copyright © 2013 CC-BY-3.0 and by the respective authors

A TWO FREQUENCY GUN FOR HIGH CURRENT THERMIONIC CATHODE ELECTRON INJECTOR SYSTEMS

J. Edelen, S. Biedron, J. Harris, S.V. Milton, Colorado State University, Fort Collins, Colorado
J. Lewellen LANL, Los Alamos, NM

Abstract

This paper discusses work done at Colorado State University (CSU) on designing a radio frequency, thermionic cathode electron gun for high-current injection systems for free electron lasers. Some background and a brief overview of other facilities using this type of injector is provided followed by the basic theory of back-bombardment and why it is a problem for such high-current injectors. We then discuss the theory of how a second frequency in the gun could mitigate this back-bombardment effect. Scaling from a previous design to the relevant CSU frequencies and using beam simulations we show results comparable with previous work done in this field [1]. We found that for a 100-pC bunch charge operating at 10MV/m gradient the harmonic field produced a 63% reduction in the back-bombardment power.

INTRODUCTION

Production of 1) high-brightness, 2) low-emittance, and 3) high-average current beams is necessary for high average power free-electron lasers (FELs) and with regards to the first two the use of photocathode RF guns dominate. However, achieving high-average currents in the photocathode mode is complicated by the need of robust, high-quantum efficiency cathodes and complex laser systems. A simple thermionic cathode RF gun system can achieve quite high average currents and, properly designed, can achieve the high-brightness required for many FEL applications in the IR and longer wavelengths [2,3,4,5]; furthermore, the cathodes tend to be robust and long-lived (months to years).

While the use of thermionic cathodes can drastically increase the cathode lifetime, use of such cathodes presents two major complications. The first and foremost is how to prevent the potentially destructive electron back-bombardment, while of secondary concern is how to operate the accelerator in a pulsed mode, which is useful for characterizing the machine.

This paper does not address pulsed-power operation; however, previous work has analysed the possibility of both laser-gated thermionic emission or cathode grids to gate the emission [6]. Instead here we focus on a method to mitigate the electron back-bombardment heating effect.

BACK-BOMBARDMENT IN THERMIONIC RF GUNS

A thermionic cathode when held at a chosen elevated temperature will continuously emit electrons at a rate dependent on the cathode temperature. If the field on the cathode is positive there will be no emission because the field attracts the electrons back to the cathode. When the field is negative the emission from the cathode will be continuous. Some electrons, which are emitted late in the RF cycle, will not gain enough energy to exit the gun and will be accelerated back towards the cathode. These back-bombarded electrons transfer their energy to the cathode surface in the form of heat and subsequently can raise the cathode temperature. This effect is referred to as back-bombardment and is a negative feedback mechanism: higher temperatures produce more electrons, which in turn increase the back-bombardment. If left unchecked, cathode damage may occur.

Using a simple Newtonian model, we computed the trajectories of a single electron subjected to a time varying RF field. Figure 1 shows, as a function of injection phase, the resulting final position of these particles. A time domain overlay of the RF fields is also shown.

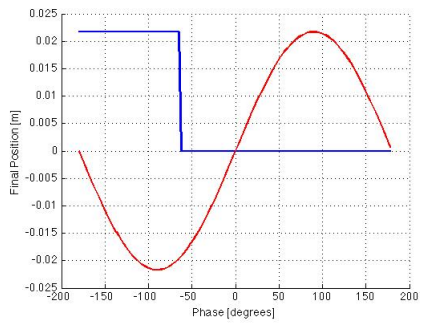


Figure 1: The resultant back-bombardment phase profile for a gap of 2cm and a RF frequency of 1.3GHz. Using a simple Newtonian model.

As stated previously, when the field is positive there is no emission so even though these particles have a final position of zero, they also never gain any energy. However for this model, there is a range of phases from roughly -63 to 0 degrees, where emission occurs but the particles ultimately are accelerated backwards by the rapidly changing field and strike the cathode. This corresponds to about 1/3rd of the region where emission is favourable and back-bombardment occurs.

THEORY OF BACK-BOMBARDMENT MITIGATION

In order to mitigate the back-bombardment effect we must consider what ideal waveform will completely eliminate this effect. A waveform that emits over some time, then holds zero long enough for the particles to

Copyright © 2013 CC-BY-3.0 and by the respective authors

ISBN 978-3-95450-138-0

THE CONCEPTUAL DESIGN OF PXIE VACUUM SYSTEM

A. Chen*, V. Lebedev, A. Shemyakin
Fermilab#, Batavia, IL 60510, USA

Abstract

The Project X Injector Experiment (PXIE) [1] will be a prototype of the Project X front end to validate the design concept and decrease technical risks. It consists of a 30 kV, 5mA DC H^- ion source (IS); Low Energy Beam Transport (LEBT); 2.1 MeV CW RFQ; Medium Energy Beam Transport (MEBT) that forms a desired bunch structure by removing ~80% of bunches; two SC cryomodules (CMs) accelerating the 1 mA beam to ~25 MeV; and High Energy Beam Transport with a dump (HEBT). Its vacuum system design will also establish the design guidance for the entire vacuum system of Project X, especially the requirement of low particulate vacuum that is sufficient in practise and at the same time is cost efficient to ensure the performance of CMs.

GAS LOADS AND LIMITATIONS

The PXIE vacuum system consists of four regions that can be separated by vacuum gate valves for commissioning or repairs: IS-LEBT-RFQ, MEBT, Cryomodules, and HEBT-DUMP. Different regions have different gas load sources and different limitations.

The main gas load in IS-LEBT-RFQ region is the gas flow from the IS, ~500 mTorr·l/s. Also, commissioning and machine tuning will be done in a pulse mode, when a chopper in the LEBT produces pulses of variable duration from 1 μs to 16 ms at 60 Hz repetition frequency. In this mode, almost all beam generated by the IS is absorbed in the chopper, and protons recombining inside the chopper's absorber into hydrogen, create an additional load ~1 mTorr·l/s. Vacuum limitations in this region are two-fold. First, the beam loss resulting from H^- stripping should be small, <5%. Second, the pressure in the RFQ and, consequently, gas flow from LEBT should be low to avoid discharges. From practical experience of other labs, pressure < 10^{-6} Torr should suffice.

The gas load in the MEBT region is a combination of outgassing of vacuum surfaces and gaskets; a hydrogen flux from the MEBT absorber irradiated by ~4 mA of the chopped-out beam; and a load from the MEBT scraping system. In the MEBT, vacuum restrictions are related to proximity to SRF. In addition to a gas and microparticles incoming to CMs, which is discussed in the next section, a flow of neutral hydrogen atoms created by stripping of H^- ions should be limited. Such atoms fly along the direction of the parent ions and can reach 2K surfaces of the cryomodules. To make irradiation of CMs by these atoms negligible (≤0.1 W of additional heat load), the vacuum integral over the MEBT length is limited to 1×10^{-6} Torr·m. Also, an aperture restriction after the MEBT absorber introduces differential pumping that dramatically improves pressure near the CM. Finally, scarpers installed at the end of MEBT additionally restrict the solid angle of penetration into the CMs.

Operating vacuum in the CMs is determined by the cryo-pumping and doesn't affect the beam directly. Vacuum limitations in the HEBT are determined mainly by the gas flow into SRF, and the main source of the gas is the beam dump.

Note that one of the vacuum-related effects considered in the course of PXIE design is a possibility of blistering. If hydrogen diffusion in a surface exposed to bombardment by the main beam or its tails is low, protons, implanted by an H^- ion impact, recombine in the bulk into hydrogen which is accumulated in dislocations until the built-up pressure breaks the overlaying material. Corresponding jump of local pressure can result in a beam loss. The issue is expected to be addressed by a system of collimation in LEBT and MEBT and preferential use of molybdenum for surfaces that are likely to be exposed to the beam irradiation.

THE SYSTEM DESIGN

A concept of beam line vacuum system derived from the limitations described above can be divided into three levels of vacuum environment (Figure 1):

1. Ultra High Vacuum and Low Particulate
2. High Vacuum areas (HV)
3. Transition areas

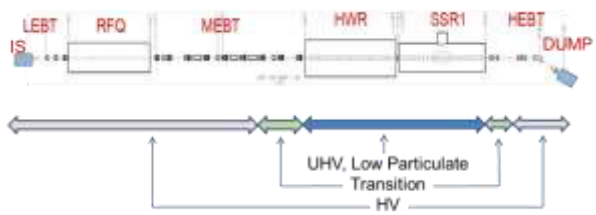


Figure 1: PXIE System Layout with classification of vacuum levels. HWR and SSR1 indicate location of two cryomodules.

UHV and Low Particulate Areas

These areas include two cryomodules, HWR and SSR1. With the cryomodules operating at 2K, cryo-pumping decreases the residual gas pressure below 10^{-10} Torr, mainly driven by the operation temperature. The challenge for this region is to achieve low enough pressure (10^{-7} Torr) at the room temperature before cooling down. Bypass vacuum pipe is designed to alleviate the conductance restriction due to the small aperture and large length of the cavity strings. To guarantee a low particulate environment for SRF operation, all necessary measures as proper handling,

Operated by Fermi Research Alliance, LLC, under Contract No. DE-AC02-07CH11359 with the United States Department of Energy
*alexchen@fnal.gov

Copyright © 2013 CC-BY-3.0 and by the respective authors

DEVELOPMENT OF A COMPACT PHOTO-INJECTOR WITH RF-FOCUSING LENS FOR SHORT PULSE ELECTRON SOURCE APPLICATION

[1]Alenxander Grabenhofer, [2]Douglas W. Eaton, and [1, 3]Young-Min Shin
[1]Department of Physics, Northern Illinois University, Dekalb, IL, 60115, USA
[2]ScandiNova Systems AB, Uppsala, Sweden
[3]Fermi National Accelerator Laboratory (FNAL), Batavia, IL 60510, USA

Abstract

For development of compact ultrafast electron source system, we are currently designing a short-pulse RF-gun with RF focusing structure by means of a series of comprehensive modeling analysis processes. EM design of a 2.5 cell resonant cavity with input coupler, acceleration dynamics of photo-emitted electron bunch, EM design of RF-lens with input coupler, and phase-space analysis of focused electron bunch are systematically examined with multi-physics simulators. All the features of the 2.856 GHz cavity geometry were precisely engineered for acceleration energies ranging from 100 keV to 500 keV (safety limited) to be powered by our 5 MW S-band klystron. The klystron (Thales TH2163) and modulator system (ScandiNova K1 turnkey system) were successfully installed and tested. Performance tests of the klystron system show peak output power > 5 MW, as per operation specifications. At the quasi-relativistic energies, the electron source is capable of generating 100fC – 1 pC electron bunch with pulse duration close to 30 fs – 1 ps and transverse size of a few hundred microns. PIC simulations have shown that the electron bunch undergoes fast RF acceleration, rapidly reaching the desired energies, which can be controlled by tuning RF injection phase and input driving power. It has been shown that it is possible to also focus/compress the bunch longitudinally using a RF-lens, which would allow us to control the temporal resolution of the system as well. While our primary analysis has been performed on a 2.5 cell design, we are also looking into half-cell (single cavity) design that is expected to provide the same range of beam energy with a simple configuration.

INTRODUCTION

The ultrafast electron diffraction (UED) source is one of the most powerful time-resolved spectroscopic/ microscopic tools capable of visualizing the sub-atomic world in a femto-second time frame. A successfully developed UED system will enable us to observe various ultrafast phenomena in chemical and biological substances of solid, gas and liquid phases. The instrument will be a useful tool for a wide range of scientific experiments in chemistry, biology, physics, radiolysis, and engineering on which accurate spatiotemporal analysis methodology is highly demanded. Ultrafast technology with sub-atomic resolution within the femto-second range, while still immature, far exceeds the current technical capacity of commercially available electron microscopes. This technology is not achievable from any single unit or commercial product, as integral parts and their systematic integration are still under development. For spectroscopic application, the main advantage of electron diffraction is that the electrons scatter off all atoms and atom-atom pairs in the molecular sample. Thus, unlike spectroscopy wherein the probe is turned to specific transitions, the electron probe is sensitive to all species in its path and can hence uncover structures that spectroscopy may be blind to. This type of spectroscopic imaging technique can offer spatiotemporal information of transitional dynamics and chemical reaction in liquid and solid states that are of main interest in NIU, as described in the next section, and the proposed UED system is expected to secure sufficient spatial and temporal resolution with good spatial coherence for those kinds of studies. The UED technique employs time-delayed ultrafast pulses – a laser pulse to initiate the reaction and an electron pulse to probe the ensuing structural change in the molecular sample. The resulting electron diffraction patterns are then recorded on a CCD camera. These processes can only produce femto-second electron diffraction when all the elements are properly orchestrated in harmony, which requires a sophisticated design process. In particular, as a key element of a UED system, a short pulse electron source must be capable of producing highly mono-energetic electron bunches of a few hundred keV to a few MeV to create dynamic scattering images with femto-second/sub-angstrom spatiotemporal resolution. Currently, we have a 5.5 MW S-band klystron driver for a photo-injector that has been designed with a 2.5 cell RF-gun to produce 100 ~ 500 keV electron bunches.

BACKGROUND AND OBJECTIVES

Most of UED systems have employed the photocathode-based DC gun with an energy in the range of 30 ~ 100keV（Max. DC field = 10 ~ 12 MV/m）and 400 ~ 600 fs at 10^3~10^4 e-/pulse. However, with the DC guns, bunch length and energy spread are increased during beam transport. The bunch length of a 30 keV e-beam is, for instance, increased from fs to a few ps and the energy spread ($\Delta E/E$) becomes ~ 3×10^{-3} to a distance of 40 cm. It is thus difficult to obtain a < 100 fs electron bunch with $\Delta E/E < 10^{-3}$ using DC guns. Also, to reduce the space charge effect in low energy DC gun system, the distance between sample and cathode should be minimized (4 ~ 5 cm) and/or the number of electrons in bunch should be decreased to 10^3 e-/bunch with 400 fs. It is difficult to observe the ultrafast dynamics with single-

ISBN 978-3-95450-138-0

Copyright © 2013 CC-BY-3.0 and by the respective authors

HIGH POWER TEST OF A 3.9 GHZ 5-CELL DEFLECTING-MODE CAVITY IN A CRYOGENIC OPERATION

Young-Min Shin[1, 2], and Michael Church[2]
[1]Department of Physics, Northern Illinois University, Dekalb, IL, 60115, USA
[2]Fermi National Accelerator Laboratory (FNAL), Batavia, IL 60510, USA

Abstract

A 3.9 GHz deflecting mode (π, TM_{110}) cavity has been long used for six-dimensional phase-space beam manipulation tests [1-5] at the A0 Photo-Injector Lab (16 MeV) in Fermilab and their extended applications with vacuum cryomodules are currently planned at the Advanced Superconducting Test Accelerator (ASTA) user facility (> 50 MeV). Despite the successful test results, the cavity, however, demonstrated limited RF performance during liquid nitrogen (LN_2) ambient operation that was inferior to theoretical prediction. We have been performing full analysis of the designed cavity by analytic calculation and comprehensive system simulation analysis to solve complex thermodynamics and mechanical stresses. The re-assembled cryomodule is currently under the test with a 50 kW klystron at the Fermilab A0 beamline, which will benchmark the modeling analysis. The test result will be used to design vacuum cryomodules for the 3.9 GHz deflecting mode cavity that will be employed at the ASTA facility for beam diagnostics and phase-space control.

INTRODUCTION

Over the past decade, a multi-cell deflecting (TM_{110}) mode cavity has been employed for phase-space manipulation tests of high brightness beams [1-6] at the Fermilab A0 photoinjector (A0PI), and extended applications are currently scheduled at the ASTA user facility (> 50 MeV). Despite the past successful experimental results, the cavity demonstrated a limited RF performance during liquid nitrogen (LN_2) operation, which did not reach the theoretically predicted gradient. The designed cavity has been fully examined with theoretical calculations, based on the Panofsky-Wenzel theorem, using an integrated modeling tool with a comprehensive system analysis capacity to solve complex thermodynamics and the mechanical stress of the multi-cell. This paper discusses the cryogenic RF performance of the 5-cell deflecting mode cavity with numerical modeling analysis. It also presents up-to-date test simulation results of an integrated thermo-stress analysis modeling tool on the deflecting cavity vacuum-cryomodule and low power RF-test results of warm (room-temp, 297 K) and cold (LN_2-temp, 80K) cavities.

SYSTEM DESCRIPTION

At the Fermilab A0PI, the deflecting mode cavity has been used for various beam optics experiments. The cavity was designed with 5 cells to maximize kick strength and powered with a 50 kW (peak), S-band (3.9 GHz) klystron. The RF power was coupled into the cavity through the high power TEM-mode coaxial coupler that was built in the liquid nitrogen (LN_2) vessel. The coupler design includes a temperature gradient from cryogenic temperature (80K) of a LN_2-ambient cavity to room temperature of an input waveguide. As the emittance exchange only requires modest fields and short pulse lengths, the TM_{110} mode cavity was constructed out of oxygen-free, high conductivity (OFHC) copper [7]. A higher Q_0 was required than what was achievable at room temperature with the OFHC copper. We see that Q_0 is proportional to the square root of the copper's bulk conductivity. A Q_0 2.4 times greater was achieved by simply incorporating a LN_2 cryogenic jacket into the design.

The system is designed with the LN_2 vessel because the conductivity of normal conducting copper is increased 6 times from $5.8 \times 10^7\ \Omega^{-1}m^{-1}$ at room temperature to $3.5 \times 10^8\ \Omega^{-1}m^{-1}$ at 80 K, which doubles the cavity Q. The cryo-vessel was designed with three frequency tuning screws, attached to the chamber-outside body at one end and the flange, brazed with the beam pipe at the other end, across the flexible bellows. The tuners push the flange against the body and the mechanical pressure is transferred to the cavity through the beam pipe so the structural distortion by the tuner induces frequency change. As this simple design did not include vacuum insulation, the LN_2-temperature (~ 80 K) was maintained by shielding the outer body with foam insulation. The coaxial input coupler was designed with the critical matching condition, $\beta = Q_0/Q_e \sim 1$, for maximum RF power coupling into the cavity. The original design includes many practical considerations in various technical aspects. However, a high-Q cavity sensitively responds to dimensional deviations and external perturbations, which could significantly limit the deflecting performance in a cryostat. In particular, structural variation of the input coupler can significantly influence RF coupling characteristics producing an unevenly distributed field profile. It is thus highly probable that the limited deflecting performance of the 5 cell can be attributed to an off-resonance RF coupling presumably owing to design error, fabrication error, and/or cryo-cooling contraction. In order to completely identify the operational constraints, we thus investigated the cavity design and estimated its performance with a theoretical assessment incorporated with numerical data of RF simulation modeling analysis.

We conclude that the off-resonance coupling leads to a reduction in the kick strength because it more likely perturbs the field distribution, decreasing cell-to-cell field uniformity, rather than directly weakening the field

Copyright © 2013 CC-BY-3.0 and by the respective authors

ISBN 978-3-95450-138-0

RF GUN WATER TEMPERATURE CONTROL SYSTEM AT ASTA *

P. Stabile#, M. Ball, J. Czajkowski, J. Firebaugh, P. Kasley, P.S. Prieto, T. Zuchnik,
Fermilab, Batavia, IL, 60510, USA

Abstract

A linear electron accelerator is in the late stage of construction at the Advanced Superconducting Test Accelerator (ASTA) facility at Fermilab. The purpose of this accelerator is to operate, study and develop the superconducting cavities and associated systems to be used in future superconducting accelerators. ASTA incorporates an L-band radiofrequency (RF) gun with a coaxial RF input operation at 1.3GHz, based on 1+1/2 cell DESY-type gun, followed by two superconducting cavities. A temperature control system regulates the RF power transmission between 5MW Klystron and the RF Gun. Its role is to maintain the resonant frequency by exploiting the 16.5ppm/ºC thermal expansion of the copper. Temperature is regulated by mixing chilled low conductivity water (LCW) with circulating water between the cavity and gun skid located outside the radiation cave. A fine pneumatic actuated valve controls the chilled water flow and in turn is controlled by a feedforward/feedback regulation algorithm. This paper will describe the water temperature control system used to stabilize the tuning frequency of the RF Gun.

INTRODUCTION

Fermilab is constructing ASTA at the existing New Muon Lab (NML) building. ASTA is part of Fermilab new state-of-the-art superconducting radio frequency (SRF) test facility complex. ASTA facility [1] consists of a shielding cave which houses the accelerator, as well as areas for support equipment and systems required for operation. The accelerator consists of three distinct sections: the injector, SRF accelerator, and the test beam lines including space for a small storage ring. The injector is a 1.3GHz photocathode electron RF gun which generates electron bunches repeated at 3MHz within a macro pulse of nominal duration of 1ms [2, 3].

The RF power to the gun is supplied by a 5MW, 1.3GHz klystron. The temperature control loop stabilizes the temperature of the RF Gun when RF power is applied and also during no RF power cycles.

The temperature control loop regulates the water temperature to ±0.18 ºC which, at a centre frequency of 1.3GHz, keeps the frequency shift of the Gun, within 5KHz (23KHz/ ºC). A 5KHz shift corresponds to a reflected power less than –22dB.

SYSTEM DESCRIPTION

The task of the cooling system is to mix the outgoing warm water with the supply LCW water regulating the desired temperature of the circulating water. Figure 1 shows the piping schematic of the RF gun cooling system. The cooling skid is located outside the radiation shielding and water is pumped through approximately 80 feet of piping. A PLC is integrated into the cooling skid to read back the temperature and flow measured by the different sensors and to control the flow rate of the LCW. The temperature of the LCW supply is stabilized to 90±1ºF (~32.22 ±0.5ºC) by an external control system running on an independent PLC. The amount of the incoming supply LCW is controlled by a fine pneumatic valve that allows a flow rate between 0 and 15GPM. The position of the valve is controlled by a dedicated PID loop build into the valve controller.

A heater is used to mix the LCW cold water and the warm water from the RF Gun and can supply between 0 and 12KW of power. The mixed water flows to the gun at a fixed rate of 15 GPM through nine cooling channels, seven with 10mm ID and two with 6mm ID tubing connections, cooling down the cavity. The return water from the gun is split between the heater and a return connection to the main chiller system.

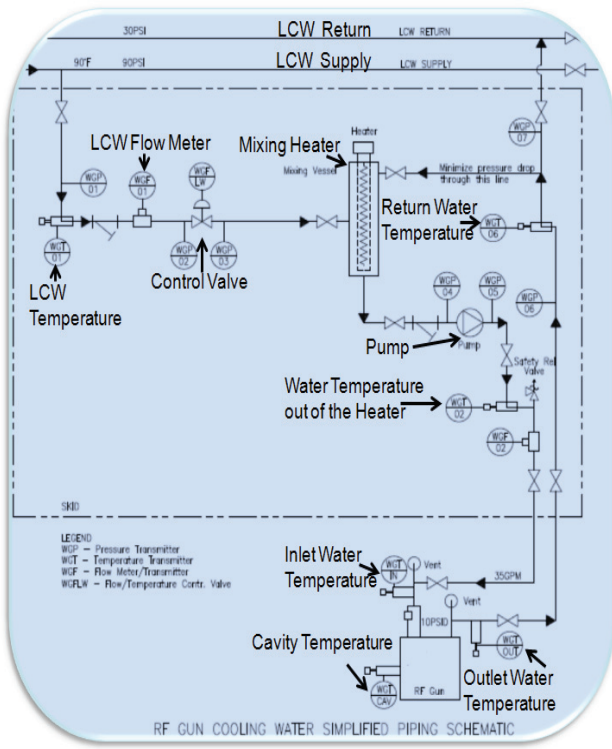


Figure 1: RF gun cooling system overview.

* This work was supported by the U.S. Department of Energy under contract No. DE-AC02-07CH11359

#stabile@fnal.gov

Copyright © 2013 CC-BY-3.0 and by the respective authors

ISBN 978-3-95450-138-0

EPICS ACCELERATOR CONTROL SYSTEMS FOR LAMBDA EMS AND TCR MAGNET POWER SUPPLIES

Anthony Andrews[1,2*], Y. Kim[1,2,3], C. Eckman[1,2]
P. Buaphad[1,2], C. O'Neill[2], B. Berls[2], K. Folkman[2], and J. Ralph[2]
[1]Department of Physics, Idaho State University, Pocatello, ID 83209, USA
[2]Idaho Accelerator Center, Idaho State University, Pocatello, ID 83201, USA
[3]Thomas Jefferson National Accelerator Facility, Newport News, VA 23606, USA

Abstract

The Idaho Accelerator Center (IAC) of Idaho State University has been operating a 44 MeV L-band linac for high average power THz generation, various nuclear physic related applications, medical isotope generation, and Laser Compton Scattering (LCS) based X-ray generation [1]. As of August 2012, the IAC has been upgrading the 44 MeV linac with a new computer based EPICS accelerator control system to replace the old analog control system. So far, this upgrade includes control of two GigE CCD cameras, and several magnet power supplies with embedded IEEE controllers [2]. However, the 44 MeV linac also has some magnet power supplies which are controlled with external RSTL controllers. This paper describes the development of the EPICS accelerator control system to control Lambda EMS and TCR magnet power supplies with these external RSTL controllers.

INTRODUCTION

To improve the reproducibility and stability of the 44 MeV linac, the previous analog control system was upgraded to a computer based control system. The control system chosen for this upgrade was the Experimental Physics and Industrial Control System (EPICS). As of August 2012, this upgrade included a control system for 2 Prosilica GigE CCD cameras, 32 TDK-Lambda ZUP power supplies, and 15 Lambda EMS power supplies with embedded controllers [2]. However, the 44 MeV linac also contains 3 Lambda EMS power supplies and one Lambda TCR power supply with external RSTL controllers. Figure 1 shows half of the control system for the magnet power supplies including Lambda EMS power supplies with embedded controllers, Lambda EMS with the external RSTL controllers, and a solitary Lambda TCR power supply with an external RSTL controller [3,4][1]. This paper describes how the control of these magnet power supplies with external RSTL controllers was accomplished. The full description of the EPICS accelerator control system for the 44 MeV linac will be published at another conference [5]. As shown in Fig. 1, the EMS power supplies and TCR power supplies were connected to their own dedicated MOXA terminal server with RS485-RS232 conversion interfaces [6]. Then, the terminal server was connected to the EPICS server via an isolated network using an Ethernet cable and a 3Com network switching hub. After that, a means to communicate with the power supplies was developed by using two EPICS modules (ASYN and StreamDevice) supplied with the synApps package [2]. Then, device support applications were manually programmed for the power supplies, and the current was controlled by manipulating process variables (PVs) using MEDM Operator Interface (OPI) panels.

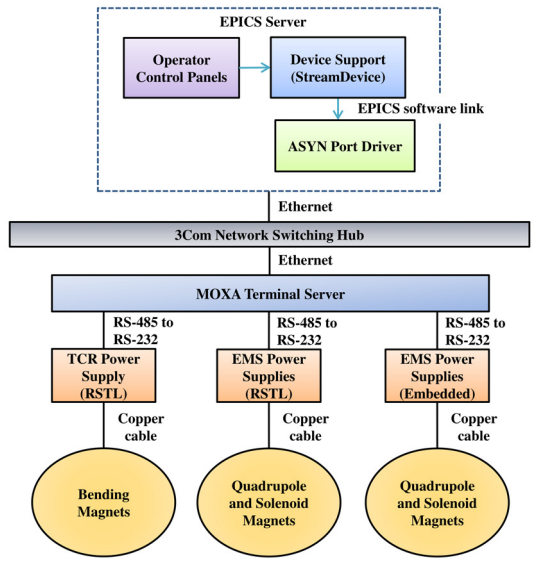


Figure 1: Experimental setup of EPICS server and hardware for the IAC 44 MeV linac.

HARDWARE CONFIGURATION

Before creating the PVs, the RSTL controllers had to be configured to work with the Lambda EMS and Lambda TCR power supplies. For the Lambda EMS power supplies, it was just a matter of following the connection diagram for the RSTL to TB1 connector in the manual [7]. However, the interface from the RSTL to the Lambda TCR power supply took some additional configuration for the RSTL. Since the RSTL was rated for a 40 V power supply and the Lambda TCR was a 160 V power supply, the first configuration detail was to add a couple resistors to the RSTL board. This was done to create a voltage divider and reduce the high voltage from the Lambda TCR to a level

* Mail: andranth@isu.edu
[1]For more information about the internally controlled EMS power supplies see reference [2,5]

Copyright © 2013 CC-BY-3.0 and by the respective authors

ISBN 978-3-95450-138-0

PROGRESS REPORT OF H⁻ ION BEAM PRODUCTION AT THE LANL ION SOURCE TEST STAND*

I.N. Draganić#, Y.K. Batygin, C.M. Fortgang, R. W. Garnett, J. Gioia, S. S. Kurennoy, R. C. McCrady, J. F. O'Hara, G. Rouleau, L. Rybarcyk, LANL, Los Alamos, NM 87545, USA

Abstract

As part of the Los Alamos Neutron Science Center (LANSCE) the Ion Source Test Stand (ISTS) is a flexible, stand-alone facility used for H⁻ ion beam source development and studies of low energy beam transport. It consists of a surface converter ion source with a multi-cusp permanent-magnet plasma confinement structure, an 80-kV high-voltage electrostatic extraction column, a low-energy ion beam transport line, and beam phase-space diagnostics. After resolving several technical issues, the ISTS was successfully restarted during the summer of 2012. Since then we have performed several long duration experiments. A development program is ongoing with the goals of improving source performance (e.g. reliability, availability, increased current, etc.) and beam transport efficiency (beam neutralization at low energy, beam dynamics with/without noble gas injection, etc.). Several enhancements to performance are being investigated in order to achieve a forthcoming upgrade requirement of LANSCE operations in 2014: beam current of 16-18 mA, 120-Hz operation at a duty factor of 10% and a source lifetime of greater than 28 days. We present a short description of the ISTS apparatus, obtained results and forthcoming experiments.

H⁻ ION SOURCE TEST STAND

The ion source test stand (ISTS) (Figure 1) was developed to perform H⁻ beam research in support of operation of H⁻ source of LANSCE user facility [1, 2]. It is a replica of the 80 keV injector in the H⁻ dome of LANSCE which is used to accelerate beam to 750 keV using a Cockcroft-Walton high-voltage generator. The ion beam optics consists of a four electrode electrostatic accelerating column (Pierce electrode -80 kV, extraction electrode -67 kV, column electrode -27 kV and grounded electrode), two focusing solenoid magnets separated by a distance of 1.9 m, two emittance measurement stations (IDEM02 and IDEM03), an electrostatic beam deflector, and a 4° bending magnet to separate H⁻ beam from electrons (see Fig 1). Beam current is measured by a calibrated current monitor and Faraday cup. The beam line is equipped with a residual gas analyzer (RGA) to characterize outgassing processes and a noble gas injection subsystem (Ar, Xe, etc.).

The first long ISTS run (over four weeks) was successfully performed during August and September 2012. The H⁻ ion beam was extracted in the range of 10 to 14 mA using a pulsed source gate of 835μs with repetition rate of 120 Hz (or ion source duty factor of 0.102).

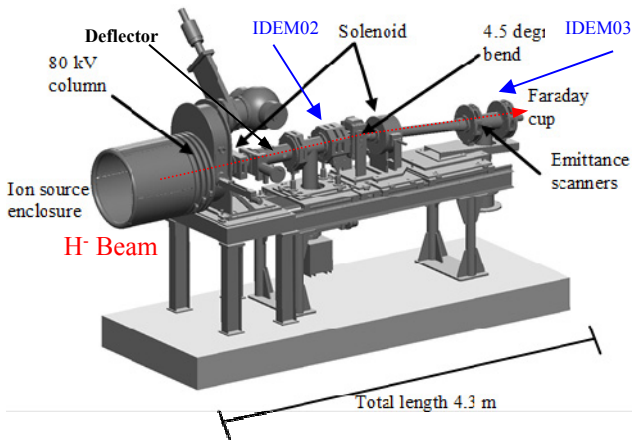


Figure 1: Schematic layout of the H⁻ ion source test stand.

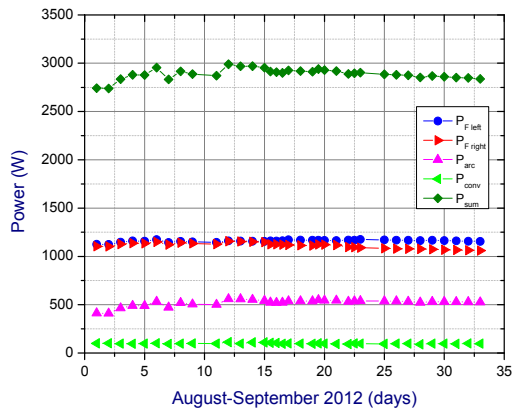


Figure 2: Source of power losses in the H⁻ ion source includes thermal dissipation of the two filaments, arc discharge and converter electrode loses at 120 Hz.

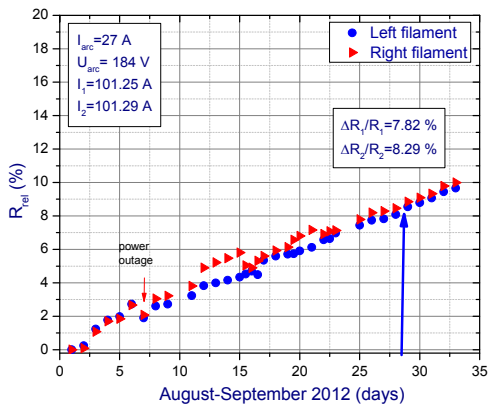


Figure 3: Recorded filament relative differential resistances (R1 - right filament and R2 - left filament).

*Work supported by the US Department of Energy under Contract Number DE-AC52-06NA25396.

#draganic@lanl.gov

Copyright © 2013 CC-BY-3.0 and by the respective authors

ISBN 978-3-95450-138-0

A SPECIALIZED MEBT DESIGN FOR THE LANSCE H+ RFQ UPGRADE PROJECT*

C. Fortgang#, Y. Batygin, R. Garnett, S. Kurennoy, L. Rybarcyk, LANL, Los Alamos, NM USA

Abstract

The LANSCE accelerator operates with both H^+ and H^- ions. Presently, each species has its own 750-keV Cockcroft-Walton (CW) and an initial transport line. The two transport lines merge into a common transport after which both species are injected into the 201.25-MHz DTL. The H^+ CW will be replaced with a 4-rod RFQ that is now in final design. Because of the complication of accommodating two beam species, the MEBT for the RFQ beam is much longer than usual. The length of the MEBT for the H+ beam, and a requirement to merge it with the existing common transport, present new and unique challenges for the MEBT design. In particular, multiple ¼-wave bunchers in addition to the existing final buncher upstream of the DTL are necessary to minimize phase spread of the RFQ output beam for DTL injection. Estimates of emittance growth, matching into the DTL over a range of H^+ beam currents, and simulations through the first two DTL tanks are presented.

INTRODUCTION

The LANSCE accelerator presently has 2 CWs for H^+ and H^- operation. The plan is to replace the H^+ CW with a 750-keV 4-rod RFQ being designed by IAP (Frankfurt) and Kress GmbH (with LANL input) and fabricated by Kress. The design of the RFQ transport line is complicated by the fact that it has to merge with the H^- transport line. The RFQ specifications that are relevant to the MEBT design are: RF frequency = 201.25 MHz, beam energy = 750 keV, RFQ maximum output emittance (rms, norm.) = 0.023 π cm-mrad, and maximum input current = 35 mA. The goals for the MEBT physics design are to minimize beam loss and emittance growth while maintaining the longitudinal bunching produced by the RFQ, under the constraint that the common transport for the 2 species not be modified. A discussion of the overall LANSCE RFQ project is given in [1].

PHYSICS DESIGN

Figure 1 shows the beam envelope and phase spread for the $5\varepsilon_{rms}$ beam from a TRACE-3D [2] simulation.

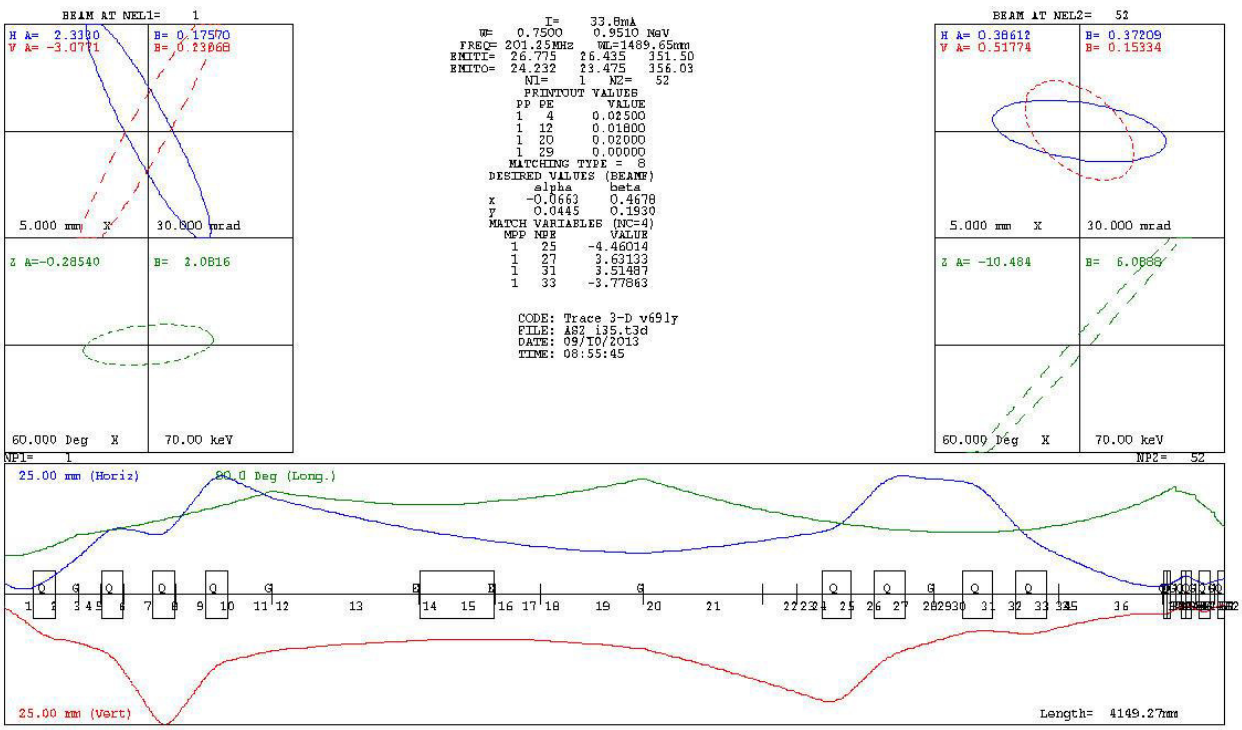


Figure 1: TRACE3D beam envelope for the $5\varepsilon_{rms}$ beam in the MEBT for ~34 mA.

*Work Supported by USDOE DE-AC52-06NA25396

cfortgang@lanl.gov

Copyright © 2013 CC-BY-3.0 and by the respective authors

DESIGN OF A DUOPLASMATRON EXTRACTION GEOMETRY AND LEBT FOR THE LANSCE H^+ RFQ PROJECT *

C. Fortgang#, Y. Batygin, I. Draganic, R. Garnett, R. McCrady, L. Rybarcyk, LANL, Los Alamos, NM USA

Abstract

The 750-keV H^+ Cockcroft-Walton at LANSCE will be replaced with a 4-rod RFQ with injection energy of 35 keV. The existing duoplasmatron source extraction optics need to be modified to produce up to 35 mA of H^+ current with an emittance <0.02 pi-cm-mrad (rms,norm) for injection into the RFQ. In addition to source modifications we need a new LEBT for transport and matching into the RFQ. The LEBT uses 2 magnetic solenoids with enough drift space between them to accommodate diagnostics and a beam deflector. The LEBT is designed to work over a range of space-charge neutralized currents and emittances. The LEBT is optimized in the sense that it minimizes the beam size in both solenoids for a point design of a given neutralized current and emittance. Special attention has been given to estimating emittance growth due to solenoid aberrations. Examples of source-to-RFQ matching and emittance growth (due to both non-linear space charge and solenoid aberrations) are presented over a range of currents and emittances about the design point. A preliminary mechanical layout drawing will also be presented.

INTRODUCTION

The LANSCE accelerator presently has 2 CWs for H^+ and H^- operation. The plan is to replace the H^+ CW with a 750-keV 4-rod RFQ being designed by IAP (Frankfurt) and Kress GmbH (with LANL input) and fabricated by Kress. The input energy of the RFQ is 35 keV at a maximum beam current of 35 mA. The design emittance for the RFQ input beam is 0.02 π-cm-mrad, rms-normalized. Presently the LANSCE users of H^+ require about 18 mA of extracted beam. The current H^+ duoplasmatron source is very reliable and has been used for decades at LANSCE. We will use the existing duoplasmatron source with a newly designed extraction system and LEBT for beam injection into the RFQ. For the LEBT a magnetic focusing system was chosen. Careful attention has been paid to the solenoid design so that emittance growth due to non-linear focusing terms is made negligible.

SOURCE EXTRACTION DESIGN

Figure 1 shows the extraction geometry for the 35 keV source. The source design was done using the finite element code TRAK [1]. The relevant parameters are: Pierce, extractor, electron suppressor and ground electrode apertures equal 5 mm, 6 mm, 8 mm and 16 mm, respectively. The gap between the Pierce aperture and the extractor is 12 mm. The Pierce and electron suppressor electrodes are held at 35 kV and -2 kV. The extractor voltage is varied to minimize the emittance for each extracted beam current, mainly determined by the source plasma density and T_e (proportional to source arc current). In Fig. 1 the extractor gap voltage (ΔV) is 22.6 kV and the extracted current is 18 mA. The maximum electric field is 3.44 kV/cm. For 35 mA of extracted current the extractor gap voltage is 35 kV and the maximum electric field is 5.3 kV/cm which is still below our goal of Epeak < 7 kV/cm. A cutaway view of the source design is shown in Fig. 2.

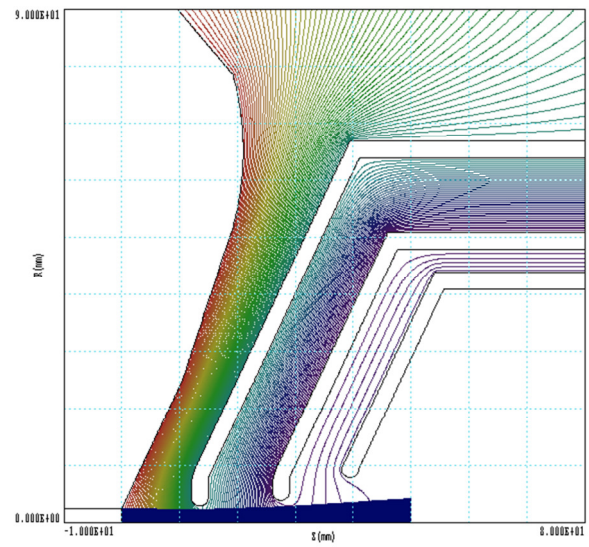


Figure 1: Electrode geometry and beam extraction for a 35 keV, 18 mA H^+ beam. Grid spacing is 10 mm/div.

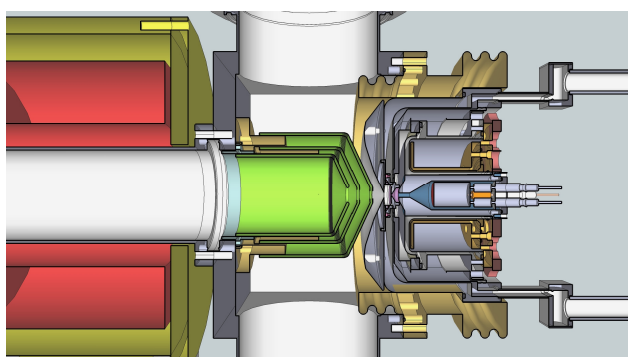


Figure 2: Duoplasmatron source is on the right. Extraction electrodes are in the center and the 1st LEBT solenoid is on the left. Pumps are above and below electrodes.

*Work Supported by USDOE DE-AC52-06NA25396
cfortgang@lanl.gov

Copyright © 2013 CC-BY-3.0 and by the respective authors

ISBN 978-3-95450-138-0

APPLICATION AND CALIBRATION ASPECTS OF A NEW HIGH-PERFORMANCE BEAM-DYNAMICS SIMULATOR FOR THE LANSCE LINAC *

L. J. Rybarcyk# and X. Pang, Los Alamos National Laboratory, Los Alamos, NM, 87545, USA

Abstract

The Los Alamos Neutron Science Center utilizes a linear accelerator (linac) consisting of two 750-keV injectors, a 100-MeV drift tube linac and an 800-MeV coupled cavity linac to provide both H^- and H^+ beams to several user facilities. We are presently developing a graphics processing unit (GPU)-based high-performance multiparticle beam-dynamics simulator to aid in tune-up and operation of the linac. Our primary goal is to create an on-line tool that will act as a virtual beam diagnostic and in pseudo real-time provide accelerator operators and physicists with insight into the evolution of the beam throughout the linac. This paper will discuss potential applications of this tool and aspects of the various calibrations that are a prerequisite to using the model.

INTRODUCTION

High power linacs, such as the Los Alamos Neutron Science Center (LANSCE) 800-MeV accelerator, use a combination of well defined physics-model based tune-up procedures and empirical optimization to establish low-loss operation under high-power beam conditions. Although the low beam power tune-up is typically performed with an array of beam diagnostics, the subsequent adjustments under high beam power conditions are performed with little or no direct beam information and focus mainly on reducing beam spill as measured with radiation monitors located along the linac and beam lines. A better situation would be one where tuning activities are guided by more detailed information about the beam properties along the linac. Although one possible option would be to install numerous beam diagnostic devices all along the accelerator, this is rather impractical due to cost considerations and the interceptive nature of many of the desired devices. Another possible option is to utilize a beam dynamics model along with a *realistic* beam distribution to predict the beam characteristics along the linac. The beam dynamics model would need to contain enough physics to predict with reasonable accuracy the properties of the beam along the linac, but also be fast enough to provide near real-time feedback, as an actual beam diagnostics device would. At LANSCE we are pursuing the latter approach as a means to provide additional information and insight into the evolution of the beam along the linac. Besides serving as a virtual beam diagnostic during tune-up and operation, this model can also serve other functions as will be discussed.

*Work supported by US DOE under contract DE-AC52-06NA25396.
#lrybarcyk@lanl.gov

THE SIMULATOR

The new high-performance, multi-particle, beam-dynamics simulator is based upon the widely used ion linac design and simulation code PARMILA [1], but rewritten in C++ and NVIDIA's CUDA C [2] to enable a modern code architecture that can utilize the power of the Graphics Processing Unit (GPU) technology for tremendous performance improvements [3]. PARMILA was chosen as it incorporates essential physics required to simulate a realistic beam distribution in various ion linac structures and beam line components, algorithms that have been tested and benchmarked and approximations that enable faster execution without sacrificing significant accuracy.

The physics model for the linac is based upon design and as-built information regarding the linac geometry and accelerating fields and is stored in an SQL database. When the simulator is used in an "on-line" mode, a *data server* reads in real-time the linac parameters from the EPICS control system and pipes the data into the SQL database, where they are converted into physics model quantities. Alternatively, in the "off-line" mode, the user may chose to modify the stored values of linac parameters, which are subsequently converted to physics model quantities. In either case, the simulator reads the database at the beginning of the simulation. This SQL database also contains the conversions and calibration constants that relate the data system set points to the corresponding physics model quantities. Specific procedures are performed to establish the correct value for each of the calibration constant required by the model.

APPLICATIONS

Although originally developed to serve as an online model for tune-up and operation of the linac, it has become clear that the high-performance, multi-particle, beam-dynamics simulator can also be used in other valuable ways. Many of the following activities could be performed with a standard off-line, "slow", beam dynamics code. However, the benefit for many of these applications is that the simulator response is rapid, i.e. pseudo real-time, and the connection to the accelerator control system conveys the sense of operating a real machine, not just a model, which facilitates these activities.

Virtual Beam Diagnostic

The main goal of the simulator development is to provide operations personnel with pseudo real-time information about the beam evolution along the linac to

Copyright © 2013 CC-BY-3.0 and by the respective authors

INTEGRATION BETWEEN THE FRIB LINAC MECHANICAL CAD MODEL GEOMETRY AND THE ACCELERATOR PHYSICS LATTICE DATABASE*

M. Johnson#, N. Bultman, I. Grender, M. Leitner, G. Morgan, O. Yair, Q. Zhao
Facility for Rare Isotope Beams (FRIB), Michigan State University, E. Lansing, MI 48824, USA

Abstract

This paper will summarize the systems engineering techniques utilized to translate the FRIB accelerator physics lattice file to actual three-dimensional CAD geometry for linac components. An automated approach of using the accelerator physics lattice database used for optics and particle simulation has been implemented to generate data points used to position the technical 3-dimensional CAD geometry. This coordinated method ensures consistency between the technical and scientific design domains throughout the project design phases. The FRIB configuration management used to control lattice and CAD model revisions is also discussed. In addition, the paper discusses fiducialization plans and tolerance stack up analysis to meet positional requirements for FRIB cryomodules, diagnostics, and the beam delivery magnet systems.

DATA MANAGEMENT

The layout of the FRIB accelerator physics lattice file is composed of the basic element layouts of the driver linac. This layout is accomplished using spreadsheet file to define the undeveloped geometry of ion sources, focusing and steering magnets, accelerating cryomodules, radio frequency quadrupole (RFQ), The alignment placement requirements of the accelerator components are summarized in [1,2]. An automated script imports the lattice points into our mechanical CAD software generating local coordinates for the centers of each component, called a skeleton file. The three-dimensional design geometry is then located to each coordinate in the skeleton file making up the complete linac geometry. The Survey and Alignment Group will develop and maintain a proprietal data handling system composed of a relational database and a workable simplified wireframe graphics model [3]. This system will be integrated with the FRIB project database currently under development within the Controls and Computing Group. All components requiring alignment will have associated fiducials. The fiducials are placed on the wireframe component model and these in turn are placed at the correct location in the design lattice based upon the data gathered during the fiducialization process. The wireframe graphical model is a single graphical representation of every point that the Survey and Alignment Group is given as a design location. The relational database provides functionality for archiving and retrieving data from various epochs of the project's evolution in order to keep abreast of revisions and network re-observation campaigns. In addition to coordinate data and associated uncertainties the database will hold information regarding nomenclature, instrumentation, tooling, fiducialization, and ideal component design lattice positions.

General Layout

As shown in Figure 1, the driver accelerator consists of Electron Cyclotron Resonance (ECR) ion sources, a low energy beam transport containing a pre-buncher and electrostatic deflectors for machine protection, a Radiofrequency Quadrupole (RFQ) linac, linac segment 1 (with Quarter-wave Resonators (QWR) of β=0.041 and 0.085) accelerating the beam up to 20 MeV/u where the beam is stripped to higher charge states, linac segments 2 and 3 (with Half-wave Resonators (HWR) of β=0.29 and 0.53) accelerating the beam above 200 MeV/u, folding segments to confine the footprint and facilitate beam collimation, and a beam delivery system to transport to the target a tightly focused beam.

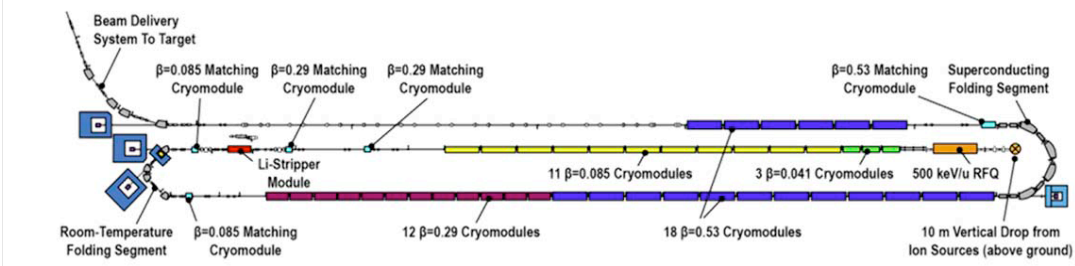


Figure 1: The FRIB accelerator layout at the tunnel level.

*This material is based upon work supported by the U.S. DOE Office of Science under Cooperative Agreement DE-SC0000661, the state of Michigan and Michigan State University
#mjohnson@frib.msu.edu

ISBN 978-3-95450-138-0

Copyright © 2013 CC-BY-3.0 and by the respective authors

IMPROVING EFFICIENCY OF IONS PRODUCTION IN ION SOURCE WITH SADDLE ANTENNA*

V. Dudnikov#, R. Johnson, Muons, Inc., Batavia, IL 60510, USA, S. Murrey, T. Pinnisi, C. Piller, M. Santana, M. Stockli, R. Welton, ORNL, Oak Ridge, TN 37831, USA

Abstract

Extraction of positive and negative ions from a saddle antenna radio-frequency surface plasma source (SA RF SPS) is considered. Several versions of new plasma generators with different antennas and magnetic field configurations were tested in the small Test Stand. The efficiency of positive ion generation in plasma has been improved up to 80 times from 2.5 mA/cm^2 kW to ~0.2 A/cm^2 per 1 kW. For cesiation was used a heating of the cesium chromate cartridges. A small oven for cesium compounds and alloys decomposition by heating was developed and tested. After cesiation a current of negative ions to the collector was increased from ~1 mA to 10 mA with RF power ~ 1.5 kW in the plasma and longitudinal magnetic field B_l~250 Gauss. A specific efficiency of H$^-$ production was increased up to ~ 20 mA/ cm^2 kW from previous ~2.5 mA/ cm^2 kW.

INTRODUCTION

Development of the saddle antenna RF surface plasma source (SA RF SPS) was proposed for improve efficiency of H$^-$ ion production and improve SPS reliability and availability [1-4]. Now RF SPS for accelerators with emission aperture 7 mm have the efficiency of H$^-$ ion generation ~1 mA/kW and RF power ~ 50 kW is needed for 50 mA beam current production [5]. With this efficiency delivered current is enough for 1 MW proton beam production but the high RF power required for the sources can create problems for very long term operation at higher beam power. This efficiency is too low for CW operation with current ~10 mA necessary for Project X and for cyclotrons injection.

In tested version of SA RF SPS the specific efficiency of positive ion generation was increased to ~0.2 A/ cm^2 kW and a specific efficiency of H- production was increased up to ~ 20 mA/cm^2 kW from previous ~2.5 mA/ cm^2 kW.

The total efficiency of the surface plasma produced fraction of the H$^-$ beam is a product of the probability of secondary emission of H$^-$ caused by plasma bombardment of the collar surface around the emission aperture, the probability of extraction of emitted H$^-$, and the rate of bombarding plasma flux [6,7].

The coefficient of secondary emission of H- is determined by surface properties (proper cesiation) and the spectrum of the plasma particles bombarding the collar/emitter surface around the emission aperture. The cesiation was improved recently [5] and appears to be nearly optimal. The probability of extraction of H$^-$ emitted from the collar surface is dependent on the surface collar shape [4-7], which was optimized recently to improve H$^-$ emission. The problem of efficient plasma generation is being addressed by the development of new RF plasma generators with higher plasma generation efficiency and better concentration of useful plasma flux onto the internal surfaces of the collar around the emission aperture for lower RF power [1-4]. In this project, we use the saddle antenna, which has its RF magnetic field transverse to the source axis, combined with an axial DC magnetic field, to concentrate the plasma on the collar where the negative ions are formed by secondary emission [1-4,6,7].

SA SPS DESIGN

The schematic of a large RF SA SPS with the AlN ceramic discharge chamber, saddle antenna, and DC solenoid is shown in Fig. 1. The chamber has an ID=68 mm. The saddle antenna in this SPS with inductance L=3.5 μH is made from water cooled copper tube. RF assisted triggering plasma gun (TPG) is attached to discharge chamber from left. An extraction system is attached from right side.

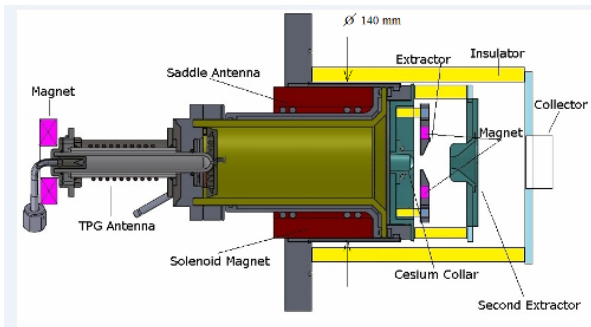


Figure 1: A schematic of the SA SPS with an extraction system and a collector.

Design of the extraction system is shown in Fig. 2. The strong transverse magnetic field (up to 1 kG) is created in the collar (4) by permanent magnets (7) inserted into water cooled extractor (6) attached to the plasma plate (1) through ceramic insulators (5). SA SPS was tested with emission and extractor's apertures of 6 mm diameters.
A Cesium vapor can be delivered to the emitter cone (2)

*Work supported by Contract DE-AC05-00OR22725 and by STTR grant DE-SC0002690.
#Vadim@muonsinc.com

Copyright © 2013 CC-BY-3.0 and by the respective authors

OPERATION OF A DIAMOND FIELD-EMISSION-ARRAY CATHODE IN A L-BAND RF GUN

P. Piot[1,2], B. Blomberg[1], C.A. Brau[3], B. K. Choi[4], W. Gabella[3], B. Ivanov[3],
J. D. Jarvis[5], M. Mendenhall[3], D. Mihalcea[1], H. Panuganti[1]
[1] Department of Physics and Northern Illinois Center for Accelerator &
Detector Development, Northern Illinois University DeKalb, IL 60115, USA
[2] Accelerator Physics Center, Fermi National Accelerator Laboratory, Batavia, IL 60510, USA
[3] Department of Physics and Astronomy, Vanderbilt University, Nashville, TN 37235, USA
[4] Department of Electrical Engineering and Computer Science, Vanderbilt University,
and Vanderbilt Institute of Nanoscale Science and Engineering, Vanderbilt University,
[5] Advanced Energy Systems Inc., Medford, NY 11763, USA.

Abstract

We report on the operation of a field-emission diamond cathode in a L-band RF-gun (1.3 GHz) at Fermilab's HBESL facility. The diamond cathode consists of an array of a million sub-micrometric pyramidal diamond tips.Beam currents in excess of 10 mA were observed and the cathode did not show appreciable signs of degradation after days of operation. Measured Fowler-Nordheim characteristics and transverse beam densities are also reported.

INTRODUCTION

Over the past years, field-emission (FE) electron sources have been the subject of intense researches due to several advantages they offer over photoemission and thermionic sources. The main advantages of FE sources stem from their ability to produce very low-emittance bunched beams, their capability to generate high-average current beams, and the absence of requirement for an auxiliary laser system. A single-tip FE emits electrons from a very small transverse area and can therefore produce beams with extremely small, quantum-degenerate, transverse emittances [1, 2]. When arranged as large arrays, field-emission-array (FEA) cathodes can provide substantial average currents [3] to the detriment of emittance which then scales linearly with the FEA macroscopic radius [4, 5].

Pulsed field-emission occurs when a FE cathode experiences a time-dependent field, e.g., when located in a resonant radiofrequency (RF) cavity and the root-mean-square (rms) duration of the bunch is $\sigma_t \simeq \omega^{-1}[\beta_e E_0/B(\phi)]^{-1/2}$ where $\omega \equiv 2\pi f$ where E_0 and f refer to the field amplitude and frequency. The latter pulse duration is obtained by taking the current density, $B(\phi)$ is a function of the workfunction ϕ associated to the cathode material and β_e is a field-enhancement factor [6, 7]. Nominally, the bunch rms duration is a significant fraction of the RF field period typically resulting in beams with large energy spread. This limitation can however be circumvented by exposing the FE cathode to superimposed electromagnetic fields [8].

In this paper we report on the first operation of a diamond FEA (DFEA) cathode in a conventional L-band RF gun nominally operated with a Cesium Telluride (Cs_2Te) photocathode. The DFEA is composed of ungated diamond pyramids which have proven to be rugged. Depending on the size and pitch of the pyramids, tests under DC voltages have showed field emission to begin at macroscopic fields $E_0 \simeq 5$ MV/m, and current density as high as 30 A.m^{-2} has been obtained [9].

EXPERIMENTAL SETUP

The geometry of the DFEA cathode used for the experiment reported below appears in Fig. 1(a,b). It consists of an array of $\sim 1000 \times 1000$ pyramidal diamond tips with their extremities separated by ~ 10 μm. The typical pyramid base is ~ 4 μm and the radius of curvature of the tip is on the order of 10 nm. Electrostatic simulations performed with the finite-difference element program POISSON [10], indicate that local fields in excess of ~ 0.9 GV/m are achieved at the tip when subjected to a macroscopic field $E_0 = 30$ MV/m (corresponding to $\beta_e \sim 30$).

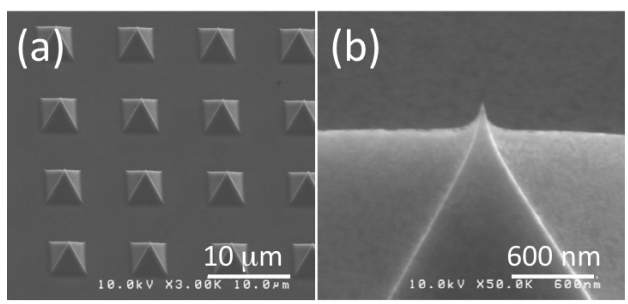


Figure 1: Electron-microscope photographs of the DFEA pattern (a) and close up of one pyramidal tip (b).

The cathode pattern was formed using a mold-transfer process whereby chemical vapor deposited (CVD) diamond is grown in sharpened silicon molds [11]. Using various techniques, DFEAs can be produced with single, double, or quadtip emitters. A variety of growth recipes

Copyright © 2013 CC-BY-3.0 and by the respective authors

ISBN 978-3-95450-138-0

MULTIPHOTON EMISSION FROM CESIUM TELLURIDE PHOTOCATHODES

H. Panuganti†, C. Prokop, Department of Physics, Northern Illinois University, DeKalb, IL, USA
P. Piot, Fermi National Accelerator Laboratory, Batavia, IL, USA

Abstract

The High-Brightness Electron Source Lab (HBESL) at Fermilab operates an L-band RF gun (1.3-GHz) that incorporates a Cesium Telluride (Cs_2Te) photocathode illuminated by an ultra-short (sub-100 fs) laser pulses. In this contribution we report recent studies on exploring the electron beam emission using 800 nm laser pulses (instead of the 266 nm nominal wavelength used for linear photoemission).

INTRODUCTION

Photocathodes are excellent sources for production of short electron bunches [1]. Production of short bunches is possible due to the advancements in the drive laser pulse times combined with availability of fast-response photocathodes. Photoemission allows generating higher charges compared to field- and thermionic emission, and also with small beam transverse emittance. One good parameter to characterize the performance of a photocathode is quantum efficiency (QE), which is defined as the number of electrons emitted for a unit photon. Cesium Telluride is considered to be an exceptionally high QE (up to 20 %) semiconductor photocathode [2]. The work function of Cs_2Te 4.6 eV corresponds to the laser wavelength of 266 nm falling in the ultraviolet (UV) region. Since most of the commercially available lasers include lasing media with high gain in the infrared (IR), frequency up-conversion to the UV is generally done for linear photoemission from metallic and some semiconductor cathodes. For titanium sapphire based laser systems (λ~800 nm), UV pulses for photoemission are obtained from frequency tripling of IR pulses using a two-stage process consisting of a second harmonic generation (SHG) stage followed by a sum frequency generation (SFG). In order to preserve the short pulse duration during the up-conversion process, both stages generally use thin BBO crystals which results in low IR-to-UV conversion efficiency typically < 10%. In this paper we present preliminary results toward attempting to generate electron bunches with commensurate charge directly using the amplifier IR pulse. We specifically report on the observation of two-photon emission from Cs_2Te.

PHOTOCATHODE THEORY

Spicer developed the first model in 1958 to explain photoemission in semiconductors, which is commonly referred to as the Three Step Model, which models the photoemission mechanism as a bulk effect [3]. In the first step, an electron absorbs a photon and gets excited from the valence band to the conduction band. In the second step, the excited electron transports to the surface. In the third step, the electron escapes to the vacuum level resulting in emission. The QE equation for a semi-infinite photocathode slab is given by [3]

$$QE = [1 - R]\frac{\frac{\alpha_{PE}}{\alpha}P_E}{1+\frac{1}{\alpha L}}$$

Where R is the reflectivity of the material; α is the intensity attenuation coefficient of the photocathode material; α_{PE} represents the coefficient of absorption for the vacuum level, or the number of electrons that are excited to the vacuum level that can possibly photoemit per unit laser intensity available; L is called the escape length which represents the strength of the electron scattering; P_E is the probability that an electron at the surface with sufficient energy to escape, escapes. Here all the parameters are functions of $h\upsilon$. Fowler-Dubridge model is derived for photoemission for metallic photocathodes based on similar approach. It is the first step (photo-absorption and excitation) that distinguishes between single-photon emission from multiphoton emission. Once the electrons get excited, the rest of the processes viz. electron transport to the surface and electron escape remain the same. In single photon emission the intensity dependence of QE goes away. But in multi-photon emission α_{PE} additionally depends on the intensity of the light (temporal) besides $h\upsilon$, as the non-linear "simultaneous" absorption of multiple photons (of lower energy) has to occur to excite an electron to the vacuum level. Hence shorter laser pulses are required for higher order photoemission.

EXPERIMENT

The experiment reported in this paper was carried at the high brightness electron source laboratory (HBESL). The HBESL facility consists of a 1.5 cell L-band 1.3 GHz RF gun powered by a 3 MW klystron. The photocathode drive laser consists of a broadband (200 nm) Octavius oscillator followed by a SpectraPhysics regenerative amplifier. The amplified IR pulse typically has 100 fs duration. The IR-to-UV SHG and SFG conversion processes incorporate respectively a 0.300 and 0.150 mm BBO crystals. The crystal thicknesses were optimized with SNLO and short UV pulse (130 fs), and were measured using a polarizing-gating UV FROG. The produced pulses were short enough to enable the production of uniformly charged ellipsoidal bunches using the blow-out regime [4]. A schematic of the experimental setup used for our experiment appears in Fig. 1. A 4 mJ amplified laser pulse is sent to the HBESL accelerator

† harsha.panuganti@gmail.com

Copyright © 2013 CC-BY-3.0 and by the respective authors

ANDROID APPLICATION FOR MONITORING THE STATUS OF THE ADVANCED PHOTON SOURCE

M. Borland*, Westmont, IL, USA

Abstract

Smartphones and tablets are nearly ubiquitous and have the ability to quickly access and display data from network sources. This suggests their suitability for remote monitoring of a facility such as the Advanced Photon Source (APS). While one possibility is to access data using a web browser running on the device, native applications offer attractive features, such as improved display and background execution. We report on development of an Android application for monitoring the status of the APS. In addition to displaying data, the application can issue alerts when beam is lost or restored. Home screen widgets of various sizes are also provided. We describe not only the features of the application, but also give details of the implementation. The application is free of advertising and is available free of charge on the Google Play store.

INTRODUCTION

Like many synchrotron radiation facilities, the Advanced Photon Source (APS) operates thousands of hours per year. During operating periods, it is expected to provide beam 24 hours a day, seven days a week. Getting information about status to accelerator staff, beamline staff, and beamline users is thus very important. The ubiquity of smartphones and tablets provides a way to do this.

These devices are internet-enabled, so it is of course possible to get information via a web browser. However, using a native Android application provides several advantages. One can provide high-level status on the notification bar, which is visible without unlocking the phone or opening the application. One can provide a home-screen widget that provides more information than will fit on the notification bar. The notification and widget can both be used to launch the full application. Another advantage of the native application over browser-based information delivery is that the native application can run in the background and provide audible alerts of significant events.

Inspired by these ideas, we developed an Android application that provides both high-level and detailed status data about the APS. The Android platform was chosen for its open-source nature and the low cost of entry for devices and development. Also, the Android home-screen widget feature provides a superior way to display very high level data without opening the application. Unlike other smartphone platforms, the Android Software Development Kit (SDK) is free and available for essentially all platforms, which allowed using Linux for development.

The application is called APSStatus and available free of charge on the Google Play store. The application is also free of advertising.

*michael.d.borland@gmail.com

FEATURES AND CAPABILITIES

The APSStatus package includes a main application and three home-screen widgets. The main application is organized into a series of pages or tabs, each of which displays information of a certain type. Presently there are tabs for overall status, status messages, 24-hour and 1-week history plots, superconducting undulator status, power supply summary status, power supply detailed status, vacuum system status, rf system status, personnel safety system status, and front-end equipment protection system status. Figure 1 shows the main status screen. This is typical of the status screens, in that it features a heading with a prominent date and time stamp, which allows the user to easily ascertain if the data is fresh. Data is updated at 1 minute intervals.

Since not all of the selections of data will be of interest to all users, the application menu's "Tab Settings" selection allows the user to determine which tabs will be displayed.

Most of the tabs supply snapshots of data without any history. One exception is the status messages display, which displays the history of recent status updates issued by control room staff. Two other exceptions are the 24-hour and 1-week history tabs, which provide plots of beam current, beam lifetime, rms beam motion, number of shutters open, horizontal emittance, and vertical emittance. Figure 3 shows an example of the 1-week history display. Touching a plot will bring up a zoomed-in version with pinch-to-zoom and scrolling features.

In addition to the main application, the user can add one or more of the three home-screen widgets to their home screen. These display small selections of data and require less than 300 bytes per update, i.e., less than 0.4 MB per day. Hence, these can be left running and provide the most essential information at a glance.

The largest of these widgets, which has some special features, is shown in Figure 4. It shows the beam current color-coded by status, the number of bunches, the beam lifetime, the number of operating beamlines, the horizontal and vertical emittance, and the injection efficiency on the last top-up shot. Unlike the other widgets, this widget also posts the beam current to the notification bar, where it can be seen from any home screen and even when the screen is locked. The beam current notification is color-coded to indicate whether it is within the expected range for the present machine mode or not.

Another special feature of this widget is that it can provide audible alerts when beam is lost or restored. The alerts are configured from the main application's menu. The user

Copyright © 2013 CC-BY-3.0 and by the respective authors

ISBN 978-3-95450-138-0

HIGH-POWER TESTS AND INITIAL ELECTRON BEAM MEASUREMENTS OF THE NEW HIGH-GRADIENT NORMAL CONDUCTING RF PHOTOINJECTOR SYSTEM FOR THE SINCROTRONE TRIESTE

L. Faillace#, R. Agustsson, P. Frigola, A. Verma, Radiabeam Technologies LLC, CA, USA
H. Badakov, A. Fukasawa, J. Rosenzweig, A. Yakub, Department of Physics and Astronomy, UCLA CA, USA
F. Cianciosi, P. Craievich, M. Trovo', Sincrotrone Trieste, Italy

Abstract

Radiabeam Technologies, in collaboration with UCLA, presents the development of a high gradient normal conducting radio frequency (NCRF) 1.6 cell photoinjector system, termed the Fermi Gun II, for the Sincrotrone Trieste (ST) facility. Designed to operate with a 120MV/m accelerating gradient, this single feed, fat lipped racetrack coupler design is modeled after the LCLS photoinjector with a novel demountable cathode which permits cost effective cathode exchange. Full overview of the project to date, installation, high-power RF conditioning and initial electron beam emittance measurements at Sincrotrone Trieste will be discussed along with basic design, engineering and manufacturing.

INTRODUCTION

Radiabeam is currently involved in the development of new technology aimed at high average power operation for a NCRF electron gun system, the FERMI II RF Gun, for the Sincrotrone Trieste facility operating at the frequency of 2.99801GHz with a repetition rate >50Hz.

The gun design was originally based on the UCLA-University of Roma-INFN-LNF [1] high repetition rate photoinjector for SPARX project, which borrowed the main features from the LCLS gun [2,3]. Nevertheless, the basic design was re-optimized by request of ST with two main changes: 1) an exchangeable cathode plate for easy exchange of different material samples; 2) single-feed for a cost-effective and more compact device.

RF GUN DESIGN

The RF design of the Gun has been performed by using the codes SuperFish [4] and HFSS [5]. Figure 1 shows half structure of the RF gun with surface electric field distribution calculated by HFSS. The RF power is fed through one waveguide only (top one); the symmetrical waveguide, acting as a dummy waveguide, forbids the propagation of the electromagnetic field that is below its cutoff value (i.e. the dummy waveguide has a width much smaller than the input one). The main purpose of the second waveguide is to cancel the field dipole component.

#faillace@radiabeam.com

Cell Design

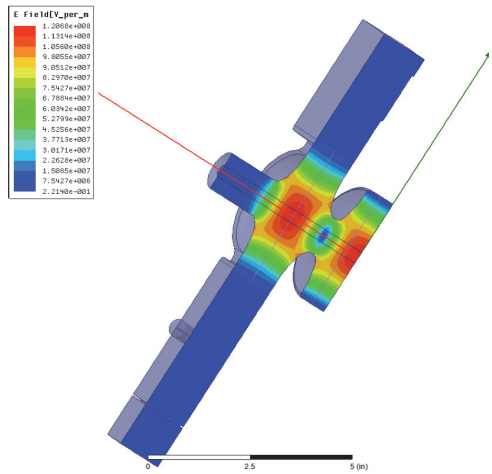


Figure 1: 3D model used for HFSS simulation. Surface electric field is shown.

The RF cavity shape, as proposed, has several innovative electromagnetic features, including Z-coupling and enhanced cell-to-cell coupling to produce higher mode separation, elliptical irises to reduce surface electric field, symmetric couplers for dipole mode minimization, racetrack geometry to minimize quadrupole field components. In contrast to the LCLS gun, which has these features, it is externally fed only by one side, avoiding the need of a power splitter and making the whole assembly much more compact, easier to handle and cost efficient.

In order to calculate the maximum surface electric field, we normalize the on-axis field to 120 MV/m at the cathode. The peak field on the iris is found to be 102 MV/m, below the breakdown safety threshold.

Per usual procedure, a first pass on the RF design was made with SUPERFISH and then HFSS was used to provide a complete picture of the RF performance, including mode frequencies, field balance, quality factor *Q,* shunt impedance and external coupling.

The design parameters achieved in simulation through this process are summarized below in Table 1.

Copyright © 2013 CC-BY-3.0 and by the respective authors

INNOVATIVE LOW-ENERGY ULTRA-FAST ELECTRON DIFFRACTION (UED) SYSTEM*

E. Threlkeld, L. Faillace#, S. Boucher, RadiaBeam Technologies, Santa Monica, CA 90404, USA
P. Musumeci, University of California, Los Angeles, CA 90095, USA

Abstract

RadiaBeam, in collaboration with UCLA, is developing an innovative, inexpensive, low-energy ultra-fast electron diffraction (UED) system which allows us to reconstruct a single ultrafast event with a single pulse of electrons. Time resolved measurement of atomic motion is one of the frontiers of modern science, and advancements in this area will greatly improve our understanding of the basic processes in materials science, chemistry and biology. The high-frequency (GHz), high voltage, phase-locked RF field in the deflector allows temporal resolution as fine as sub-100 fs. In this paper, we show the complete design of the UED system based on this concept, including initial beam measurements.

INTRODUCTION

Time resolved measurement of atomic motion is one of the frontiers of modern science, and advancements in this area will greatly improve our understanding of the basic processes in materials science, chemistry and biology. One technique under active development in this area is ultrafast electron diffraction (UED), which has several distinct advantages over X-ray diffraction for certain applications. UED utilizes a less expensive source; the electrons are less damaging to the specimen (at comparable energies); the scattering length of electrons better matches the penetration depth of the probe laser; UED is more suitable for gas phase samples; and it allows direct measurement of atomic positions, since the electron scatter mostly from nuclei. UED has already been used to study solid-state phase transitions [1, 2], gas phase reactions [3, 4], strongly coupled systems [5, 6] and surface dynamics [7]. In light of these results, researchers are demanding ever-shorter electron bunches in order to improve the resolution of their UED measurements. However producing intense sub-ps pulses of electrons in the desired energy range (30 - 100 kV) is challenging, due to space-charged induced longitudinal spreading. To date, efforts in this area have concentrated on either minimizing the bunch charge, which reduces the signal-to-noise ratio (SNR), or on using higher-energy electron beams, which reduces the diffraction angle and increases the size and the cost of the system. RadiaBeam, in collaboration with UCLA, is developing an innovative, inexpensive, low to moderate energy UED system which allows to reconstruct a single ultrafast event with a single pulse of moderate energy electrons (100 keV). By implementing a fast Radio-Frequency (RF) deflecting cavity immediately after the sample, the diffracted electron beam can be "streaked," transforming the temporal evolution of the diffraction pattern into a transverse image (see Figure 1). The high-frequency (GHz), high voltage, phase-locked RF field in the deflector allows temporal resolution as fine as 100-fs and below, while the probe electron beam can remain comparatively long (10's of ps), and contain a large number of electrons (~10^8).

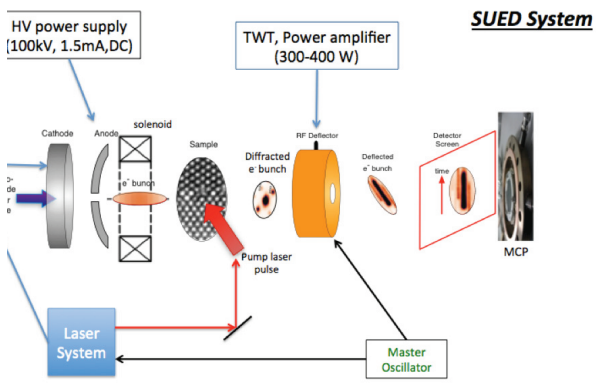


Figure 1: "streaked"- Ultra Electron Diffraction System.

ENGINEERING OF THE UED SYSTEM

The current setup of the UED system:

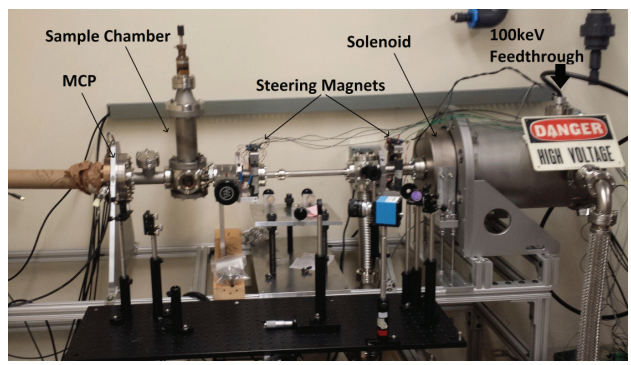


Figure 2: Current setup of the UED system.

The cathode location is set as z=0m. The solenoid is positioned at about z=6cm allowing a beam focusing point anywhere between the MCP (z=1m) and z=70cm. The sample is located at z=74cm and there is room for a second solenoid at z=40cm. Eventually the deflector can be put at z=50cm, just after the sample chamber to match previous resolution calculations.

PHOTOELECTRON GUN

The design of the 100 kV photocathode electron gun has been carried out by means of the 2D RF/Static simulation code SuperFish and the 2D gun design code

*Work supported by US DOE grant # DE-SC0006274
faillace@radiabeam.com

Copyright © 2013 CC-BY-3.0 and by the respective authors

ISBN 978-3-95450-138-0

MODELING THE DEVELOPMENT AND MITIGATION OF CHARGE ACCUMULATION FOR PHOTO EMISSION ELECTRON GUNS*

C. Nieter†, D.A. Dimitrov, Y. Choi, Tech-X Corporation, Boulder, CO 80234, USA

Abstract

One potential problem with the operation of photo emission electron guns is the potential for charge to accumulate on the emission surface depending on how the biasing voltage is applied to the gun. If the voltage is applied away from the emission surface there is the potential for charge to accumulate on the emission surface since not all electrons will necessarily be emitted. This charge accumulation may affect the gun operation by reducing the accelerating field in the gun. We report on simulations that demonstrate this potential issue as well as simulations that test a potential solution where a secondary voltage is applied periodically to clear the accumulated charge.

INTRODUCTION

New design for photoinjectors has been proposed that will address the need for high current, high brightness beams for future particle accelerators [1, 2]. The design takes a primary electron beam from a conventional photocathode which is accelerated to a diamond window. The diamond window consists of a layer of diamond followed by a high-vacuum gap with an applied voltage across the window. The primary electrons scatter in the diamond generating cascade of secondary electrons. The electrons drift across the diamond where most of them are emitted into the vacuum gap and then into the accelerating cavity of the gun.

Since not all of the electrons are emitted from the diamond surface charge can build up at the diamond/vacuum interface. If enough charge builds up the field in the diamond can be shorted out preventing further electrons from drifting across the diamond. Experimental studies have shown for a primary electron beam whose pulse length is long enough there is a drop in the emission gain for the cathode [3]. It is believed that this drop off is due to electrons accumulating at the surface of the diamond reducing the electric field in the diamond.

We ran a series of simulations with the Vorpal multiphysics code [4] to study the process of charge accumulation in the diamond window from first principles. These simulations can be challenging due to the relative long time scales of the primary electron pulse length relative to the electron scattering rates in diamond. However, we were able to demonstrate the build up of charge at the surface and look at possible ways to clear the charge with a second voltage applied after the primary electron pulse has passed.

* Work supported by by DOE SBIR grant DE-SC0007577
† nieter@txcorp.com

SIMULATIONS

We use the parameters given for the diamond window from Ref. [3] as a starting point for our simulations. To be able to complete the simulations in a reasonable amount of time the physical size was scaled down by a factor of 100 giving us a diamond thickness of 3 microns and the thickness of the full window (diamond plus vacuum gap) of 5.5 microns. Similarly the beam radius was reduced by a similar amount to 4 microns. We reduce the applied voltage by the same factor of 100 to keep the same electric field magnitude giving us a voltage of 30 volts across the diamond window.

We performed 3D simulations of the diamond window. The simulation domain was 5.5 microns in the direction of beam propagation and 10 microns in the transverse direction. We used Vorpal's electrostatic solver to solve for the electric field generated by the various applied voltages as well as the fields generated by the electrons themselves. The electrons are represented using the particle-in-cell (PIC) method with the addition of recently developed scattering models for electron propagation in diamond [5].

Since the time scales needed to cover the pulse width from from Ref. [3] are very long compared to the time scale needed to resolve the highest scattering rate for diamond we increased the beam current so the charge will accumulate faster in the simulations. We also apply a fully reflecting boundary condition for the particles at the diamond/vacuum interface effectively setting the emission probably at the surface to be zero. We run the simulation for the twice the pulse width so we can study the accumulation of the charge while the pulse is on and the dissipation of the charge after the pulse has passed.

Charge Accumulation Simulations

In the first simulation we maintain the voltage across the diamond window while the beam pulse is on. Once the beam pulse has passed we shut off the voltage across the diamond window. Figure 1 shows a scatter plot of the macroparticle positions projected into a plane with one direction along the direction of beam propagation in the simulation shortly before the voltage is shut off. This plot shows the charge accumulating at the diamond/vacuum interface.

In Figure 2 the electric field perpendicular to the diamond surface at the diamond/vacuum interface is plotted versus time. The magnitude of the electric field drops as more charge is introduced to the diamond and begins to accumulate at the diamond/vacuum interface. Eventually the field drops to zero as enough charge has accumulated to short out the field. Once the pulse has passed and the voltage across the diamond window is shut off the electric

Copyright © 2013 CC-BY-3.0 and by the respective authors

APS SUPERCONDUCTING UNDULATOR BEAM COMMISSIONING RESULTS*

Katherine C. Harkay#, Laura Boon, Michael Borland, Louis Emery, Glenn Decker, Roger Dejus, Jeffrey Dooling, Charles Doose, Joseph Gagliano, Quentin Hasse, Yury Ivanyushenkov, Matthew Kasa, Jonathan Lang, Douglas Robinson, Vadim Sajaev, Nicholas Sereno, Karen Schroeder, Yuko Shiroyanagi, Denise Skiadopoulos, Martin Smith, Emil Trakhtenberg, Aimin Xiao, Alexander Zholents, Efim Gluskin, ANL, Argonne, IL 60439, USA

Abstract

The first test superconducting undulator (SCU0) was successfully installed and commissioned at the Advanced Photon Source (APS) and is delivering 80- to 100-keV photons for user science. All the requirements before operating the SCU0 in the storage ring were satisfied during a short but detailed beam commissioning. The cryogenic system performed very well in the presence of the beam. The total beam-induced heat load on the SCU0 agreed well with the predictions, and the SCU0 is protected from excessive heat loads through a combination of orbit control and SCU0 alignment. When powered, the field integral measured with the beam agreed well with the magnet measurements. An induced quench caused very little beam motion and did not cause loss of the beam. The device was found to quench during unintentional beam dumps, but quench recovery is transparent to storage ring operation. There were no beam chamber vacuum pressure issues and no negative effect observed on the beam. Finally, the SCU0 was operated well beyond its design requirements, and no significant issues were identified. The beam commissioning results are described in this paper.

INTRODUCTION

Superconducting technology was used to build a fully functioning short-period test undulator (SCU0) at APS [1, 2]. Superconducting undulators allow a higher peak magnetic field compared to conventional devices, which can greatly benefit the light source community [3]. The SCU0 was designed and developed at APS in collaboration with Budker Institute of Nuclear Physics (BINP), Fermi National Accelerator Laboratory (FNAL), and U. Wisconsin, Madison. The SCU0 has a period length of 16 mm, magnetic gap of 9.5 mm, magnetic length of 0.34 m, and operates with photon energy in the first harmonic of 20-25 keV. The design operating current is 500 A, giving a design field of 0.64 T. The SCU0 incorporates several unique features, including an out-of-vacuum design, a beam chamber that is thermally isolated from the magnet cores, and a cryocooler cooling system. The SCU0, with a 2-m-long cryostat, was installed in the APS storage ring in Dec. 2012 (see Fig. 1).

SCU0 commissioning was completed over approx. 110 hr during an extended machine start-up period, and the device was released for user operation on Jan. 29, 2013.

* Work supported by U. S. Department of Energy, Office of Science, under Contract No. DE-AC02-06CH11357.

#harkay@aps.anl.gov



Figure 1: SCU0 installed in the APS storage ring.

COMMISSIONING PLAN

Prior to installing the SCU0, a test chamber with virtually the same length, aperture, and transitions as the SCU0 was installed in the storage ring. Beam-induced heat loads on the test chamber and transitions were tested, and key design improvements were implemented for the SCU0; in particular, a standard-aperture bellows, rf liner, and gate valve replaced a 7.2-mm-aperture assembly on the chamber transition upstream of the SCU0.

A detailed beam commissioning plan was carried out, and all the requirements were satisfied: (a) unpowered SCU0 is transparent to normal user operation; i.e., does not measurably increase storage ring impedance, nor decrease injection efficiency or lifetime; (b) powered SCU0 only perturbs the beam within the specifications; and (c) SCU0 is sufficiently protected from beam-induced heat loads. There were several commissioning goals, including assessment of thermal and vacuum monitoring, alignment procedures, cryogenic performance, beam orbit stability, quench response, field correction, x-ray performance, and operation procedures.

SCU0 EFFECT ON THE BEAM

An unpowered SCU0 is transparent to the beam if its contribution to the storage ring impedance and/or local vacuum pressure neither decreases the beam lifetime or injection efficiency nor lowers the beam instability threshold. As expected from the successful test chamber results, the SCU0 chamber was also transparent: the single bunch limit of 16 mA was preserved, and 100 mA could be stored in all three user bunch patterns. The measured betatron tune shift with current, which is a measure of the transverse impedance, did not change within the expected experimental error. The beam lifetime and injection efficiency were both in the normal range after the standard startup procedures were carried out.

Copyright © 2013 CC-BY-3.0 and by the respective authors

LOW EMITTANCE IN THE CORNELL ERL INJECTOR PROTOTYPE*

C. Gulliford, A. C. Bartnik, I. V. Bazarov, B. M. Dunham, for the Cornell ERL Team
CLASSE, Cornell University, Ithaca NY 14853 USA

Abstract

We present a detailed study of the six-dimensional phase space of the electron beam produced by the Cornell Energy Recovery Linac Photoinjector, a high-brightness, high repetition rate (1.3 GHz) DC photoemission source designed to drive a hard x-ray energy recovery linac (ERL). A complete simulation model of the injector has been constructed, verified by measurement, and optimized. Both the horizontal and vertical 2D transverse phase spaces, as well as the time-resolved (sliced) horizontal phase space, were simulated and directly measured at the end of the injector for 19 pC and 77 pC bunches at roughly 8 MeV. The resulting 90% normalized transverse emittances for 19 (77) pC/bunch were 0.23±0.02 (0.51±0.04) μm in the horizontal plane, and 0.14±0.01 (0.29±0.02) μm in the vertical plane, respectively. These emittances were measured with a corresponding bunch length of 2.1±0.1 (3.0±0.2) ps, respectively. In each case, the rms momentum spread was determined to be on the order of 10^{-3}. Excellent overall agreement between measurement and simulation has been demonstrated.

INTRODUCTION

Cornell University has recently designed, built, and commissioned a high repetition rate DC gun based photoinjector. One major goal for this project was the demonstration of low emittance at the end of the injector merger section. The results in this work demonstrate that it is possible to produce and transport beams from a DC source which have emittances at the point of injection approaching the diffraction limit for hard x-rays, and which have a bunch length and an energy spread within the parameter space required by the specifications of a full hard x-ray ERL. Table 1 shows these parameters for the Cornell Injector.

Table 1: List of Injector Design Specifications and Target Parameters

Parameter	Specification
Beam energy	5-15 MeV
Normalized emittance	$\epsilon_n \leq 0.3$ μm
RMS bunch length	$\sigma_t \leq 3$ ps
Bunch Charge	77 (19) pC
Average Current	100 (25) mA

One fundamental limit to achieving low emittance (high brightness) in a photoinjector occurs when the amount of charge extracted from the cathode nears the virtual cathode instability limit. A rough calculation shows that the lowest achievable emittance in this limit is proportional to the square root of the bunch charge q [1]:

$$\epsilon_n \propto \sqrt{q \cdot \frac{\mathrm{MTE}}{E_{\mathrm{cath}}}} \tag{1}$$

Here MTE and E_{cath} are the mean transverse energy of the cathode and the accelerating field at the cathode, respectively. Detailed simulations of well optimized DC gun photoinjectors support this square root dependence on the bunch charge and the cathode's MTE [2, 3]. In this paper, we show that the final measured emittance also scales in accordance with Eq. (1).

EXPERIMENTAL SET-UP

The injector features a high voltage DC gun operated at 350 kV, followed by emittance compensation solenoids and a buncher cavity. The beam is accelerated to 5-15 MeV using five superconducting srf cavities. The beamline section most relevant to this work is the B1 merger shown in detail in Fig. 1. The injector merger section is comprised of a conventional three-dipole achromat, a design chosen for its simplicity, and due to the limited space available for the injector experiment. The emittance measurement system (EMS) used for projected phase space measurements is the same two-slit system used in previous work [4]. For projected phase space measurements, the beamlet passed through the slits is collected using the Faraday cup at the end of the merger section. For time-resolved horizontal phase space measurements, the beamlet is passed through a horizontal deflecting cavity [5] in order to resolve the time axis of the beam on the viewscreen at the end of the merger [6]. The cathode used for this study was a GaAs wafer with a 4% quantum efficiency, and a MTE of 90 meV. The laser system used is a 50 MHz system, whose individual pulses have comparable pulse energy and duration to the our 1.3 GHz laser [7]. The final laser pulse train is chopped using a Pockells cell, and shaped using our temporal shaping system [8].

To arrive at the final optics used for these experiments, optimizations of a complete General Particle Tracer [9] model of the injector were carried out using a multi-objective genetic algorithm [2, 3]. For all optimizations, the gun voltage was fixed at 350 kV, and the beam energy was constrained to be $\leq$ 8 MeV to reduce neutron production from the tungsten slits in the EMS. The simulated temporal laser distribution was fixed to be roughly a flat-top

* Supported by NSF award DMR-0807731

Copyright © 2013 CC-BY-3.0 and by the respective authors

RECENT RESULTS FROM THE APEX PROJECT AT LBNL*

F. Sannibale, D. Filippetto, C. Cork, J. A. Doyle, G. Harris, T. Kramasz, S. Kwiatkoswski, R. E. Lellinger, V. Moroz, W. E. Norum, C. F. Papadopoulos, G. Portmann, H. Qian, J. Staples, R. Wells, K. Baptiste, J. Corlett, S. De Santis, L. Doolittle, G. Huang, R. Huang, M. Vinco, and M. Zolotorev, Lawrence Berkeley National Laboratory, Berkeley, CA 94720, USA

Abstract

The commissioning at the Lawrence Berkeley National Laboratory (LBNL) of a high-brightness high-repetition rate (MHz-class) photo-gun, based on a normal conducting 186 MHz (VHF-band) RF cavity operating in CW mode, is now completed. The gun has been designed to satisfy the requirements for operating high-repetition rate 4th generation light sources. Test of high quantum efficiency photocathodes with bunches of hundreds pC at MHz repetition rate are now underway. They include, Cs_2Te cathodes developed in collaboration with INFN-LASA and multialkali antimonides (CsK_2Sb), prepared by a collaborating group at LBNL. The present experimental results and the plan for future activities are presented.

INTRODUCTION

This paper describes the recent progress and experimental results obtained by the Advanced Photo-injector EXperiment (APEX) at the Lawrence Berkeley National Laboratory (LBNL).

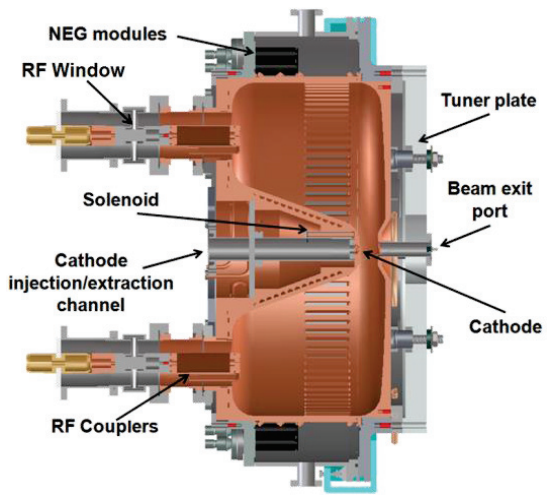


Figure 1: The VHF Gun cross sections.

The project main goal consists in the development and test of a new concept high-repetition rate high-brightness electron injector capable to operate in high-repetition rate free electron laser (FEL) and energy recovery linac (ERL) applications. The successful development of such an injector will critically impact the performance of future 4th generation light sources when high-repetition rates (> 10 kHz) are required, and of high repetition rate ultrafast electron diffraction (UED) and inverse Compton scattering (ICS) applications.

*Work supported by the Director of the Office of Science of the US Department of Energy under Contract no. DEAC02-05CH11231

The core of the system is represented by a normal-conducting (NC) continuous wave (CW) RF gun [1, 2] (see Fig. 1) where the electrons are generated by laser-induced photo-emission on high quantum efficiency (QE) photo-cathodes and accelerated by the cavity fields (~20 MV/m) to up to ~750 keV energy. The gun cavity has been designed to resonate at about 186 MHz (7^{th} subharmonic of 1.3 GHz) in the VHF frequency region. The low frequency choice makes the resonator size large enough to lower the power density on the structure walls at a level that conventional cooling techniques can be used when the cavity is run in CW mode.

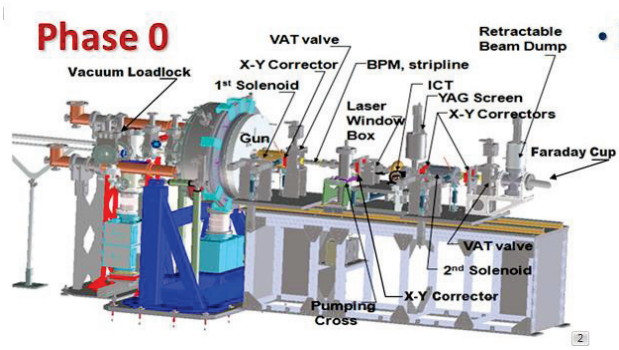


Figure 2: APEX Phase 0 CAD view.

A second advantage of the low frequency is the relatively long wavelength that allows for large apertures on the cavity walls with negligible distortion of the electromagnetic fields. Such apertures create the proper high-vacuum conductance path paving the way for the achievement of the very low pressures required by high-QE semiconductor cathodes (minimizing contamination and damage and hence ensuring longer QE lifetimes).

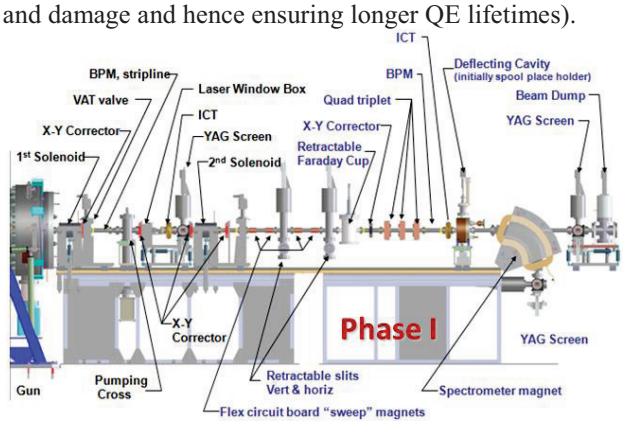


Figure 3: APEX Phase I CAD view.

Copyright © 2013 CC-BY-3.0 and by the respective authors

ISBN 978-3-95450-138-0

EXPERIENCE WITH THE SNS LOSS MONITORING AND MACHINE PROTECTION

A. Zhukov, ORNL, Oak Ridge, TN, USA

Abstract

The Spallation Neutron Source (SNS) is a megawatt-class hadron accelerator. Beam loss monitoring is essential for machine protection, residual activation control and machine tuning. We discuss all parts of our beam loss monitoring system including its detectors, electronics, machine protection system (MPS) interface and its role in the accelerator tuning process. The system was designed more than 10 years ago, so we are now addressing obsolescence problems by designing a new FPGA based replacement. The plans for this next generation Beam Loss Monitor (BLM) system are presented.

INTRODUCTION

At SNS a 1ms long H^- beam (macro-pulse) consisting of ~1000 mini-pulses (700 nS pulse and 300 nS gap) is accelerated from 2.5 MeV to 1 GeV in a linac and then converted into H+ by a stripping foil for injection into a storage ring. The mini pulses are accumulated and the resulting, ~700 nS, accumulated beam pulse is extracted and then hits a mercury target. This process runs at 60 Hz and delivers up to 1.4 MW of power to the target. Average beam current is ~24 mA over 1 ms [1].

The SNS BLM system consists of 378 radiation detectors measuring secondary radiation due to beam loss. BLMs are used as MPS devices to shut down the current beam pulse if the integral loss is above threshold and to limit average loss to be under 1 W/m. The MPS system has to be software and timing independent to increase reliability.

Since the beam parameters are different in different parts of the machine, the nature of the losses are also very different.

DETECTORS

The BLM system is used as an MPS device as well as a beam tuning diagnostics. The same detectors are playing two roles and so have to combine reliability for MPS and flexibility for beam diagnostics. SNS uses ionization chambers (IC) as its main BLM device. This is due to their simple design and immunity to radiation damage. In addition to ICs we use several type of photomultiplier tube (PMT) based detectors. The neutron detectors (ND) are neutron sensitive detectors that are useful in low energy part of the linac (where ICs lack sensitivity). The ICs are not fast enough to provide macro-pulse structure to physicists so the PMTs can be used for such diagnostics purposes. Also all PMT devices can adjust their sensitivity significantly (factor of ~100-1000) by changing their HV bias.

Detector Distribution

BLMs are evenly distributed along the accelerator with a typical distance to the beam line of 0-90 cm. In addition to fixed detectors we found moveable detectors to be very useful for investigating unexpected activation patterns.

Table 1: BLM Distribution

Detector	DTL	CCL	SCL	HEBT	Ring	RTBT
IC	11	50	79	59	71	40
ND	12	8	23			
PMT	6	6	3			
DBLM		2	5			3

Figure 1 shows moveable BLMs placed in the transition area between warm and superconducting linacs.

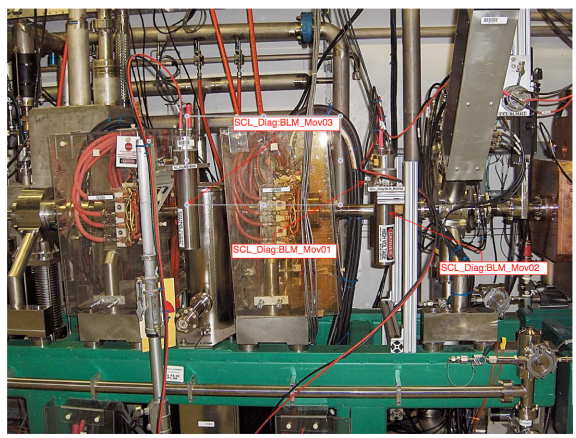


Figure 1: BLM placement for investigation of hot spot.

Detector Parameters

Most important detector parameters are shown in Table 2. Ionization chambers use daisy-chained HV lines since all of them have the same bias applied. All scintillator-based devices have dedicated HV power supply. In addition to signal and HV connections scintillator detectors have a test cable connected to an LED inside the detector. This connection allows testing and bias calibration for these detectors.

The slow response time of the neutron detector is caused by a polyethylene moderator that is needed to slow the neutrons down and increase cross section of neutron capture inside scintillator. Lead shielding around the scintillator helps to suppress sensitivity to x-rays (Fig. 2).

Copyright © 2013 CC-BY-3.0 and by the respective authors

ISBN 978-3-95450-138-0

ULTRA-SHORT ELECTRON BUNCH GENERATION BY A PHOTOCATHODE RF GUN*

M. Mizugaki#, Y. Koshiba, K. Sakaue, M. Washio, Waseda University, Tokyo, Japan
T. Takatomi, J. Urakawa, KEK, Ibaraki, Japan
R. Kuroda, AIST, Ibaraki, Japan

Abstract

We have been studying on the accelerator physics at Waseda University with BNL type 1.6cell RF gun. Such photocathode RF gun can generate low emittance and short bunch electron beam. Generating ultra-short electron bunch (shorter than 1ps) in a compact accelerator system would be meaningful because some applications need to be miniaturized, THz imaging, for example. However short the laser pulse is, the bunch length would be longer than 1ps due to the severe space charge effects. For the purpose of generating ultra-short electron bunch in compact system, we have newly designed Energy Chirping Cell attached RF gun (ECC RF gun). ECC is attached subsequently to the 1.6 cell. The role of ECC is to chirp the electron energy so that the electron bunch is compressed by velocity difference as it drifts. Simulation results show ECC RF gun can compress the electron bunch down to 200fs (rms) with 100pC electron charge. We have successfully measured the coherent THz light by synchrotron radiation and transition radiation. From these consequences, we infer that the bunch would be compressed into shorter than 500fs. In this paper, we report the results of the bunch length measuring experiments and future plans.

INTRODUCTION

At Waseda University, we have built a compact accelerator system (2m×3m), which consists of picosecond UV pulse laser and S-band Cs-Te photocathode RF electron gun . This RF gun is based on BNL type IV 1.6 cell cavity and capable accelerating high quality electron bunches up to the energy of 5MeV. In our system, the RF frequency is 2856MHz and Cs-Te is used for the cathode. Such photocathode RF guns can generate high-quality electron beam, that is to say low emittance, high brightness, and short pulse. At Waseda University, the beam has been used for applications such as pulse radiolysis experiment for radiation chemical reactions [1], soft X-ray generation via laser-Compton scattering [2] and a laser profiler [3]. Besides such beam applications, we have been developed an RF gun itself in cooperation with High Energy Accelerator Research Organization (KEK).

Ultra-short Electron Bunch

If ultra-short electron bunch (<1ps) is available from the RF gun, it leads some beam applications to be improved. At the least at Waseda, temporal resolution in pulse radiolysis system and luminosity in laser-Compton scattering will be improved. And in addition, ultra-short electron bunch is able to produce coherently enhanced THz radiation. At this time the intensity of THz radiation increases with the square of the bunch electron charge. Therefore in order to achieve high power THz radiation, it is necessary to keep a certain amount of the bunch charges besides bunch compression. The magnetic compression is widely used to compress energy chirped electron bunch. This method has made successful achievements [4], but leads the system to increase in size. The aim of our study is to generate ultra-short electron bunch by use of an RF gun alone.

BUNCH COMPRESSION

Generally in photocathode RF gun, the initial beam transverse/longitudinal profile can be controlled by the laser pulse. It seems that femtosecond laser would generate ultra-short bunch, but in simulation, we have confirmed that the bunch length gets longer than 1ps due to space charge effects. Therefore we have considered improving RF gun.

Energy Chirping Cell Attached RF Gun

Now we have newly designed an RF gun named Energy Chirping Cell attached RF gun (ECC RF gun) in order to achieve ultra-short bunch just with an RF gun itself [5][6].

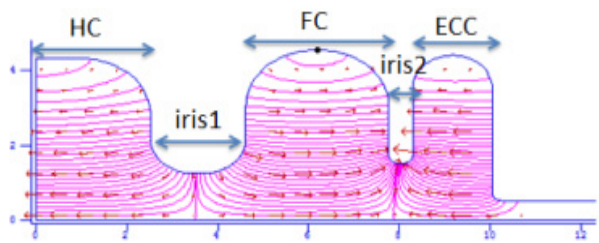


Figure 1: The cavity structure of the ECC RF gun.

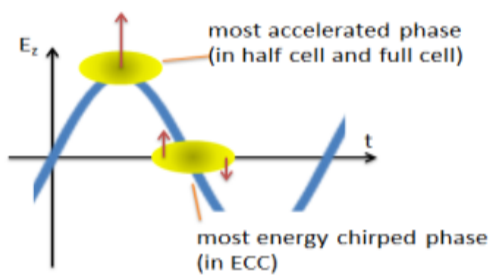


Figure 2: Off-crest acceleration in ECC.

*Work supported by JSPS Grant-in-Aid for Young Scientists (B) 23740203 and Scientific Research (A) 10001690
waterypersimmon7@fuji.waseda.jp

Copyright © 2013 CC-BY-3.0 and by the respective authors

ISBN 978-3-95450-138-0

REGULATOR / HARD SWITCH MODULATOR*

Ian Roth#, Neal Butler, Marcel Gaudreau, Michael Kempkes
Diversified Technologies, Inc., 35 Wiggins Avenue, Bedford, MA 01730

Abstract

Diversified Technologies Inc. (DTI) is developing a long-pulse modulator to meet the requirements of the Spallation Neutron Source (SNS) at Oak Ridge National Laboratory and the European Spallation Source (ESS), planned for Lund, Sweden. The modulator will deliver pulses at 100 kV at a pulse width of 3.5 ms, and a droop of less than 1%. The modulator will be delivered to Oak Ridge for conditioning klystron tubes before they are installed in the SNS accelerator.

INTRODUCTION

DTI is developing a long-pulse modulator as an alternative to the present Converter Modulator at SNS. The new Regulator / Hard Switch Modulator has two objectives: conditioning klystron tubes at SNS, and demonstrating the technology needed for future superconducting accelerators, such as ESS. The modulator specifications are given in Table 1. The key technical issue is meeting the 1% flatness specification without a large capacitor bank, using the minimum additional hardware. To meet these requirements, DTI's modulator has a small non-dissipative regulator that produces a tightly-controlled flattop and eliminates flicker on the input grid. The regulator is the major development for this new modulator design.

Table 1: Modulator Specifications (The frequency will be limited by the low-power supply used for klystron conditioning.)

Voltage (kV)	100
Current (A)	50
Pulse width (ms)	3.5
Frequency (Hz)	14
Voltage flatness (%)	<1
Ripple (% peak-peak)	<0.1

SYSTEM

Overview

The mechanical layout of the modulator is shown in Figure 1, and a highly-simplified schematic diagram is shown in Figure 2. The major elements of the system are the switch, regulator, capacitor, and transformer. This modulator is a 'hybrid' design, with a solid-state switch driving a pulse transformer. This design was chosen to accommodate the ESS preference to avoid DC high voltage and oil-immersed switching elements. The modulator could readily have been designed without a transformer; DTI has built many hard-switched solid-state modulators that reliably switch pulses over 100 kV, at much higher current and average power than required here.

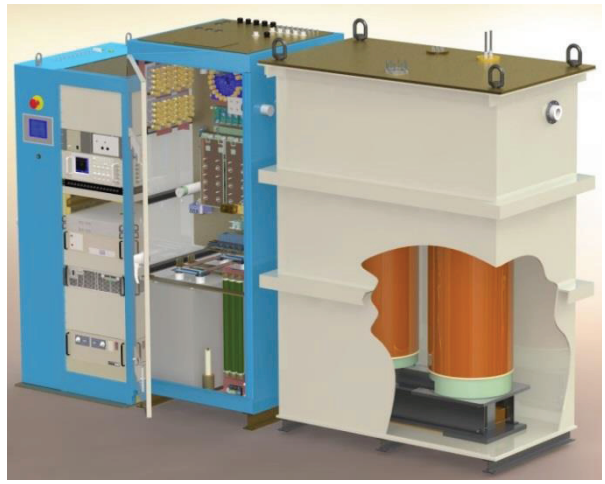


Figure 1: Mechanical layout of the system. The components are (from left to right) cabinet for PLC and AC power, rack-mount cabinet with power supplies and control boxes, power-conditioning cabinet (which contains the capacitor bank, switch, and regulator), and oil-filled transformer tank.

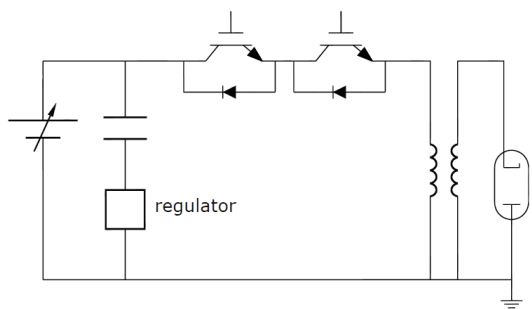


Figure 2: Highly-simplified schematic diagram. (The switch is made with seven IGBTs, not two.)

Switch

The switch is made with series-connected IGBTs, a well-established technology at DTI. The switch operates only once per pulse, in contrast to the 30 times needed by the SNS Converter Modulator. The lower switching frequency reduces the losses, and reduces the size of the switch.

The switch consists of seven modules in series; two of these are redundant. Since IGBTs fail short, if two modules short, the others will continue to support the voltage across the switch. The number of good IGBTs in the switch stack is monitored so that in the unlikely event

*Work supported by US DOE under an SBIR grant.
#roth@divtecs.com

Copyright © 2013 CC-BY-3.0 and by the respective authors

INDUCTIVELY COUPLED PULSED ENERGY EXTRACTION SYSTEM FOR 2G WIRE-BASED MAGNETS *

R. Agustsson#, J. Hartzell, S. Storms, RadiaBeam Technologies, Santa Monica, CA 90404

Abstract

This project seeks to develop a novel method for quench protection of high-temperature superconducting (HTS) magnets based on coupling the magnet with a high-power resonant coil. The quench protection is realized by applying an electromagnetic pulse through the resonant coil and disrupting the superconducting state in the conductor. This creates a large (10s of meters) normal zone in less than 10 ms thus ensuring even distribution of the energy dissipation. The proposed protection system does not involve generation of high voltage on the coil leads and does not contribute to cryogenic losses. The system is easily scaled to a magnet of arbitrary size. Preliminary design and POC bench top test preparations are presented below.

INTRODUCTION

Recent progress in high-field performance of the second-generation (2G) HTS conductors [1, 2] has enabled design and development of ultra-high field magnets. This is possible because YBCO, the core material of 2G wire, holds the record for the upper critical field, Hc2. A combination of high Hc2 and high mechanical strength (700 MPa yield strength [3] for SuperPower Hastelloy-based wire) position the 2G wire as the only viable conductor for ultra-high field, > 20 Tesla, superconducting magnets.

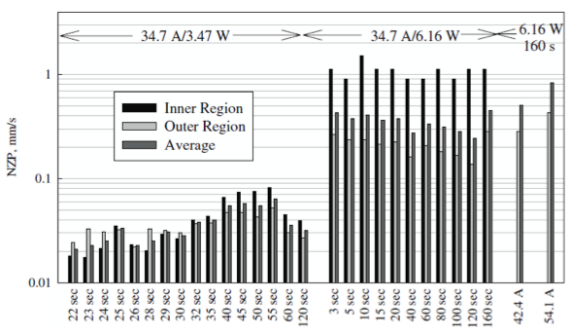


Figure 1: Typical NZP velocities measured in test 2G wire coils [4].

The key component of 2G wire is the epitaxial YBCO layer. This layer, which is only 1-1.5 micron thick, carries all the current of the superconductor. The major problem is its slow rate of Normal Zone Propagation (NZP). As shown in Figure 1, experimental measurement of NZP velocity in 2G wires yields values below 1 mm/s. Such a low propagation velocity results in concentrated energy dissipation and irreversible damage of the magnet during an unprotected quench. The problem is further exacerbated by the low thermal mass and poor thermal conductivity [5] of the YBCO layer. Thus carefully designed protection systems are required to protect 2G superconductors from catastrophic damage.

The established active and passive [6] quench protection systems for traditional low-temperature (LTS) magnets [7] are ill-suited for HTS magnets because their energy extraction is too slow. The measured NZP velocity means the stored energy has to be extracted or redistributed within a few seconds to prevent catastrophic damage. A traditional energy extraction system based on a dump resistor and a semiconducting switch would require several kilovolts on the coil to achieve fast extraction. Such a high voltage creates multiple problems for the interfacing electronics and the current source. Redistribution of the normal zone by resistive heaters is problematic since the thermal conductivity of insulating materials, used to separate the heater from the coil, drops at cryogenic temperatures due to the phonon freeze-out. This effect prevents efficient coupling of the heater elements to the superconductor.

TECHNICAL APPROACH

By inductively coupling a strong electromagnetic pulse via a resonant LC circuit, the normal zone propagation in the coil will be accelerated. The AC field induces currents in the superconducting layer with the current density exceeding that of the critical current density, J_c. This creates a large normal zone, uniformly distributing the dissipation through the magnet body. The method does not rely on thermal heating of the conductor, thus potentially enabling nearly instantaneous protection.

Quench Modeling

The 2G wire coil (in the following DC coil) was modeled as 120 mm OD, 80 mm ID double-pancacke stack. We used the following functional dependence to approximate the critical current field dependence: $I_c = I_0/(1+B/B_0)^a$, where I_0=300 A, critical current in self field, B_0=0.05 Tesla is the individual pinning field and a= 0.7 the pinning exponent. This is the typical I_c(H) behavior of SuperPower wire. The current density was calculated by dividing the current by the average area of the conductor, which was comprised of 50 micron Hastelloy substrate, 40 micron Copper stabilizer and 65

*Work supported by DOE Grant #DE-SC0009547

#agustsson@radiabeam.com

Copyright © 2013 CC-BY-3.0 and by the respective authors

ISBN 978-3-95450-138-0

PHYSICS OF POLARIZED PROTONS IN ACCELERATORS*

M. Bai
Brookhaven National Laboratory, Upton, NY 11973, USA

Abstract

Polarized proton beams have been one of the essential elements in fundamental research such as unveiling the deep secret of proton spin structure. Polarized proton beams can also be the tool for direct measurement of the proton's electric dipole moment (EDM). However, due to the interaction between spin motion and electric and magnetic fields, it is very challenging to overcome various depolarizing mechanisms through acceleration, and necessary spin manipulations at a store energy to meet the physics program requirements. Several decades of efforts have been devoted to develop techniques to preserve polarization and spin manipulation, as well as further our understanding of spin dynamics. These efforts directly led to the successful spin program at the Brookhaven Relativistic Heavy Ion Collider (RHIC), the world's first high energy polarized proton collider. This tutorial presentation introduces basic physics which governs the spin dynamics in accelerators. A brief history of polarized protons development, as well as what have been achieved at RHIC are also reported.

INTRODUCTION OF SPIN DYNAMICS BASICS

Just like charge and mass, spin is also an intrinsic property of elementary particles. Spin vector $\vec{S}$ for a particle is then defined as

$$\vec{S} = \langle\psi|\vec{\sigma}|\psi\rangle, \tag{1}$$

where $\vec{\sigma}$ is the Paul matrices, and ψ is the particle spin state. Proton, a spin of $\frac{1}{2}$ particle, has two eigenstates, i.e. $\psi_+ = |\frac{1}{2}, +\frac{1}{2}\rangle$ (up state) and $\psi_- = |\frac{1}{2}, -\frac{1}{2}\rangle$ (down state). The intrinsic magnetic moment of a particle is then given by

$$\vec{\mu} = g\frac{e}{2m}\vec{S} \tag{2}$$

where e and m are the electric charge and rest mass of the particle. g-factor for a perfect point-like particle is $\frac{1}{2}$. For proton, the anomalous g-factor $G = \frac{g-2}{2}$ is 1.7928474.

For a beam of spin-$\frac{1}{2}$ particles, polarization P, on the other hand, is a classical concept defined as

$$P = \frac{N_+ - N_-}{N_+ + N_-} \tag{3}$$

where $N_\pm$ are the number of particles in the two spin states, respectively [1].

In a circular accelerator, the spin motion is governed by the Thomas-BMT equation [2]. In the frame of particles orbital revolution, it is given by

$$\frac{d\vec{S}}{dt} = \frac{e}{\gamma m}\vec{S}\times[G\gamma\vec{B}_\perp + (1+G)\vec{B}_\parallel + (G\gamma + \frac{\gamma}{\gamma+1})\frac{\vec{E}\times\vec{\beta}}{c}], \tag{4}$$

where $\vec{S}$ is the spin vector in the particle's rest frame, $\vec{B}_\perp$ and $\vec{B}_\parallel$ are the transverse and longitudinal components of the magnetic fields in the laboratory frame with respect to the particle's velocity $\vec{\beta}c$, $\vec{E}$ is the electric field particle encounters and γ is the relativistic Lorentz factor. Here, Eq. 4 shows that in a perfect planar circular accelerator, the spin vector precesses $G\gamma$ times in one orbital revolution. $Q_s = G\gamma$ is then defined as spin tune.

In general, the effect on spin motion from electric field in an accelerator is negligible. Equation 4 can then also be expressed as

$$\frac{d\vec{S}}{ds} = \vec{n}\times\vec{S} = [G\gamma\hat{y} + G\gamma\frac{B_x}{B\rho}\hat{x} + (1+G)\frac{B_s}{B\rho}\hat{s}]\times\vec{S}, \tag{5}$$

where $\hat{x}$, $\hat{y}$, $\hat{s}$ are the unit vector along the direction of radial, vertical and longitudinal, respectively. $ds = \rho d\theta$, where θ is the bending angle. The equation of motion for the spin state in Eq. 1 also known as spinor for a $\frac{1}{2}$ particle is

$$\frac{d\psi}{d\theta} = -\frac{i}{2}(\vec{\sigma}\cdot\vec{n})\psi = -\frac{i}{2}H\psi. \tag{6}$$

For a constant H, Eq. 6 can be rigorously solved as

$$\psi(\theta_2) = e^{-\frac{i}{2}H(\theta_2-\theta_1)}\psi(\theta_1) = M(\theta_2-\theta_1)\psi(\theta_1) \tag{7}$$

where $M(\theta_2-\theta_1)$ is a 2×2 spinor transfer matrix. For a main bending sector dipole, the spinor transfer matrix is just $M(\theta_2-\theta_1) = e^{-\frac{i}{2}G\gamma(\theta_2-\theta_1)\sigma_3}$. For a thin quadruple, the spinor transfer matrix is $M = e^{-\frac{i}{2}(1+G\gamma)kly\sigma_1}$, where kl is the normalized integrated strength of the quadrupole and y is the vertical displacement of the particle from the center of the quadrupole [1]. For any spin rotator which rotates spin vector by ϕ around an axis $\hat{n}_{rot}$ is $M = e^{-\frac{i}{2}\phi\hat{n}_{rot}\cdot\vec{\sigma}}$. In general, in a circular accelerator, the one turn spin transfer matrix for a particle on the closed orbit is

$$M = e^{-\frac{i}{2}Q_s 2\pi\vec{\sigma}\cdot\hat{n}_{co}}, \tag{8}$$

where Q_s is the spin tune, and $\hat{n}_{co}$ is the stable spin direction. Equation 8 shows that for the particle's spin vector always returns to the same direction if it is initially aligned with the stable spin direction $\hat{n}_{co}$. Otherwise, the spin vector just simply precesses around the stable spin direction $\hat{n}_{co}$ Q_s times per orbital revolution. For a particle in a perfect circular accelerator where it only sees vertically aligned guiding magnetic fields, the stable spin direction is vertical and spin tune is $Q_s = G\gamma$, linearly proportional

*The work was performed under the US Department of Energy Contract No. DE-AC02-98CH1-886, and with support of RIKEN(Japan)

Copyright © 2013 CC-BY-3.0 and by the respective authors

STATUS OF THE FRIB FRONT END*

E. Pozdeyev#, N. Bultman, G. Machicoane, G. Morgan, X. Rao, and Q. Zhao
FRIB, East Lansing, MI 48824, USA

Abstract

The FRIB Front End will provide beams of stable ions with a mass up to uranium at a beam energy of 500 keV/u and intensity required to achieve a power of 400 kW on the fragmentation target. In this paper, we describe progress with the design and construction of the Front End and its systems.

DESIGN AND PERFORMANCE REQUIREMENTS

FRIB will be a premier multiuser nuclear physics facility providing stable ion beams accelerated to energies above 200 MeV/u and with a beam power on the target up to 400 kW [1]. These project requirements are translated into stringent requirements on the front end design and performance. The FRIB front end will provide stable ion beams up to uranium with an energy of 500 keV/u. The required intensity of uranium beam is 13.5 pμA and the charge state is 33+. This intensity is at the edge of performance demonstrated by modern ECR ion sources. To decrease technical risks and reduce operational stress on the sources, the front end is designed to transport two charge states simultaneously for all ions heavier than xenon with a charge state of 25 and higher. To control losses in the linac and meet experimental requirements the front end includes a collimation system to limit the transverse beam phase space. The longitudinal phase space is controlled by means of limiting the longitudinal acceptance of the RFQ. In addition, the front end will provide required variability of the bunch intensity by up to nine orders of magnitude to meet experimental needs. Beyond controlling the bunch intensity, it is also required to control the beam pulse length and the pulse repetition rate to simplify linac tuning and safely ramp up the beam power on the target.

High availability, maintainability, reliability, and tunability are required for the front end to operate FRIB as a national scientific user facility. These requirements, as well as project budget and schedule limitations require using proven, reliable technical solution as much as possible. However, those solutions frequently have to be taken to new levels with evolutionary changes and upgrades to demonstrate world-breaking performance required by the project.

Finally, to meet possible future programmatic demands the front end has to be upgradable and includes required provisions for future enhancements.

FRONT END LAYOUT

The FRIB front end includes two ECR sources, one of which is a room temperature 14 GHz source based on the ARTEMIS source developed at NSCL, and the other is a superconducting 28 GHz source based on VENUS design [2]. The beam extracted from the sources is transported through LEBT to the tunnel, where it is accelerated by an RFQ and injected into the SRF driver linac. The sources are placed on high voltage platforms that can be biased up to 100 kV to match the RFQ injection energy for all beams. Table 1 shows principle parameters of the Front End. The Front End layout is shown in Figure 1.

Table 1: Front End Principle Parameters

LEBT (before RFQ)	
Energy (keV/u)	12
Nominal beam current (eμA, typ.)	400
Emittance (πμm, 99.5%, norm.)	0.9
MEBT (after RFQ)	
Energy (keV/u)	500
Nominal current (eμA, typ.)	330
Emittance (πμm, 99.5%, norm.)	1.1
Long. Emittance (πkeV/u·ns, 99.5%)	1.5
Bunch repetition rate (MHz)	40.25, 80.5
Beam pulse length (μs)	0.6 – CW

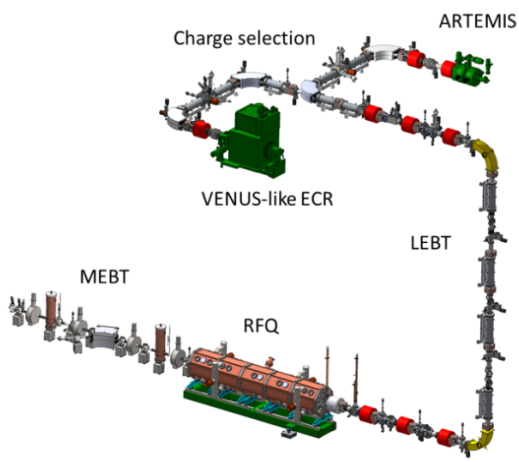


Figure 1: FRIB Front End layout.

FRONT END SYSTEMS

Ion Sources

The ARTEMIS ECR source, built at MSU and based on the AECR-U ECR developed at LBNL, operates at

*Work supported by the U.S. Department of Energy Office of Science under Cooperative Agreement DE-SC0000661 and grant #DE-FGO2-08ER41553
#pozdeyev@frib.msu.edu

Copyright © 2013 CC-BY-3.0 and by the respective authors

UPGRADE OF ARGONNE'S CW SC HEAVY ION ACCELERATOR*

P.N. Ostroumov#, A. Barcikowski, Z. Conway, S. Gerbick, M. Kedzie, M.P. Kelly, S. Kim, S. Kutsaev, R. Murphy, B. Mustapha, R. Pardo, D. Paskvan, T. Reid, S. Sharamentov, G. Zinkann
ANL, Argonne, IL 60439, U.S.A.

Abstract

The ATLAS National User Facility at Argonne National Laboratory is the world's first CW superconducting ion linac. The accelerator is being continuously upgraded to extend its scientific reach. To increase the efficiency and intensity of both stable and radioactive beams [1], we have developed, built and installed a new normal conducting CW RFQ capable of providing a 295 keV/u for any ion from proton to uranium. The RFQ has been fully integrated into ATLAS and in routine operation since January 2013.

A new cryomodule containing 7 high-performance 72.75 MHz SC QWRs and 4 SC solenoids was completed this year and has been commissioned off-line. New design and fabrication techniques for these QWRs resulted in record voltages up to 4-5 MV per cavity and low residual resistances of 2-3 nΩ at 2K were demonstrated in individual cold tests of several QWRs. The primary purpose of the new cryomodule is to replace 3 old cryomodules and to increase the intensities of accelerated stable ion beams up to several hundred electrical micro amps. Beam commissioning is expected by the end of the year after significant modification of the accelerator tunnel for increased shielding and installation of a redesigned beam transport system.

CW RFQ

Last summer we commissioned a CW RFQ designed and built for the ATLAS Facility [2, 3]. Several innovative ideas were implemented in this CW RFQ. By selecting a multi-segment split-coaxial structure we have achieved moderate transverse dimensions for a 60.625 MHz resonator. For the design of the RFQ resonator and vane tip modulations we have developed a full 3D approach which includes MW-Studio and TRACK simulations of the entire structure [4]. A novel trapezoidal vane tip modulation is used in the acceleration section of the RFQ which resulted in increased shunt impedance. To form an axially symmetric beam exiting the RFQ, a very short output radial matcher, only $0.75\beta\lambda$ long, was developed. Figure 1 shows an internal view of the RFQ's last two segments. The openings in the vane and trapezoidal modulation of vane tips are clearly seen.

An advanced fabrication technology was applied for the construction of the RFQ which included precise machining and two-step high temperature brazing. Thanks to the high accuracy of the overall fabrication, the assembly of the 5-segment RFQ was straightforward and no additional alignment was required. The resonance frequency control system based on water temperature regulation showed excellent performance. The RF measurements show very good RF properties for the resonator, with a measured intrinsic Q equal to 94% of the simulated value for OFE copper. The multi-segment split-coaxial structure creates strong coupling between the quadrants and individual RFQ segments which reduces the effect of local frequency deviations on electromagnetic field distortions. Therefore, no bead-pull measurements were required to tune the accelerating field.

An O^{5+} ion beam extracted from an Electron Cyclotron Resonance (ECR) ion source was used for the RFQ commissioning. In off-line beam testing, we found excellent agreement of the measured beam parameters with the results of beam dynamics simulations [3]. The great success of this advanced design and fabrication technology is reflected in the measured beam parameters after the RFQ which are nearly identical to the simulated data.

After the successful off-line commissioning of the ATLAS CW RFQ accelerator with oxygen and helium beams, the device was moved, installed and integrated into the ATLAS system during the October-November 2012 period. Fig. 2 displays the current view of the ATLAS front end. The RFQ is directly attached to the first SC cryomodule. For the RFQ beam matching we have incorporated a MEBT which includes 3 SC solenoids and a SC cavity as a buncher [1]. Since January 2013, the RFQ is in routine operation. The beam parameters have been measured after the Positive Ion Injector (PII) of ATLAS which includes three SC cryomodules. The beam energy and time spectra have been measured using silicon barrier detectors (Fig. 3). The results of these measurements are consistent with the TRACK simulations. The efficiency of ATLAS beams on

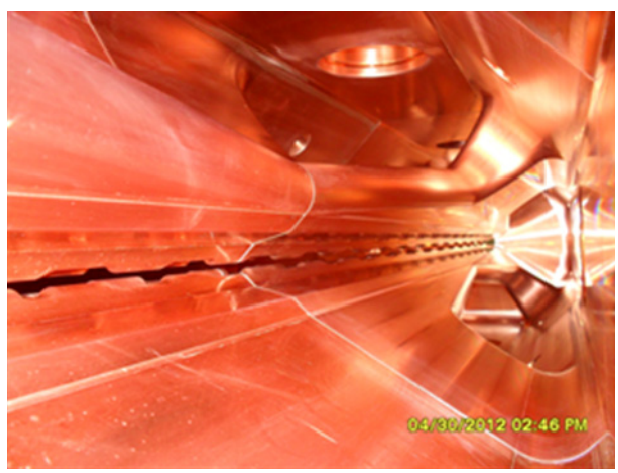


Figure 1: Internal view of the RFQ's high energy end.

* This work was supported by the U.S. Department of Energy, Office of High Energy Physics and Nuclear Physics, under Contract DE-AC02-06CH11357
#ostroumov@anl.gov

ISBN 978-3-95450-138-0

Copyright © 2013 CC-BY-3.0 and by the respective authors

ION IMPLANTATION FOR SEMICONDUCTOR DEVICES: THE LARGEST USE OF INDUSTRIAL ACCELERATORS

S.B. Felch, Susan Felch Consulting, Los Altos Hills, CA 94022, USA
M.I. Current, Current Scientific, San Jose, CA 95124, USA
M.C. Taylor, Taylor Consulting, Lake Oswego, OR 97034, USA

Abstract

Ion acceleration of dopants and other ions is a critical and nearly universally employed tool for the fabrication of transistors in semiconductor devices and the various forms of electronic, photovoltaic and photonic materials. This paper reviews the major types of accelerators, ion sources, and scanning methods used in contemporary practice for ion implantation for electronic applications.

INTRODUCTION

The use of accelerated ions to dope and modify semiconductor materials, generally called ion implantation, is a core technology for the fabrication of integrated circuits (IC), which form the backbone of the global communications and advanced computation capabilities that have transformed modern life over the last half-century. The use of ion implanters in the IC industry, starting in the 1970s for precision doping of channel structures at doping densities of ~10^{-4} monolayers to set the threshold conditions for transistor switching, enabled the practical fabrication of complementary metal-oxide-semiconductor (CMOS) transistors that are now the dominant form of IC devices. Development of accelerator technologies capable of delivering highly stable and collimated ion beam currents, ranging from a few μA to 100 mA, and incident ion energies, ranging from 100 eV to ~10 MeV, have provided a broad and capable technology for fabrication of ICs for logic, memory, and analog operations, as well as an increasingly varied array of optical sensors and imaging devices. Ion implantation is now used for the overwhelming majority of applications for doping of semiconductor materials and in an increasing array of applications for creation and modification of electronic and photonic materials.

The yearly revenues from the sale of industrial ion implantation and materials modification tools are a US$1.5B market (in "normal" economic environments). In addition, there are substantial markets for suppliers of dopant species materials (~US$140M/year) and a diverse array of suppliers of spare and upgrade parts and services. Additional parts of the ion implantation commercial infrastructure include the suppliers of system components, magnets, power supplies, and vacuum pumps, and a varied array of metrology tools focused on process characterization and control applications.

The average number of commercial ion implantation systems sold per year, predominantly for fabrication of Si-based IC devices, has increased from ~250 to ~400 per year since 1980, as seen in Fig. 1. The year-to-year sales show large fluctuations due to the highly cyclic nature of IC fab construction trends, especially when driven by additional factors, such as shifts in dominant wafer sizes, introduction of new implanter machine types and IC devices, expansion into new global regions, and variations driven by general economic cycles. The combination of these technology and market factors has resulted in a rather steady "5-year" cycle in units sold per year over the last 3 decades.

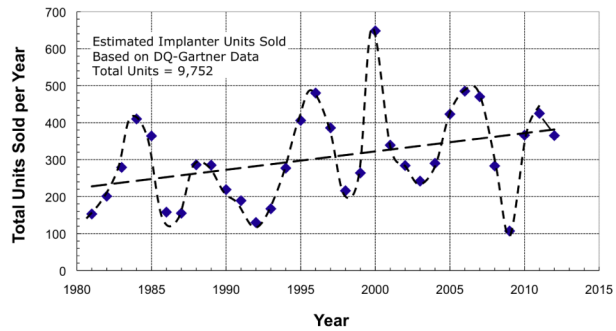


Figure 1: Estimates of the number of commercial ion implanters sold per year, mainly for IC fabrication. The data shown here are an underestimate, particularly for the earlier years.

SEMICONDUCTOR APPLICATIONS OF ION IMPLANTATION

The planar CMOS transistor, illustrated in Fig. 2, has been the workhorse device structure for IC devices for logic and memory applications since the mid-1980s.

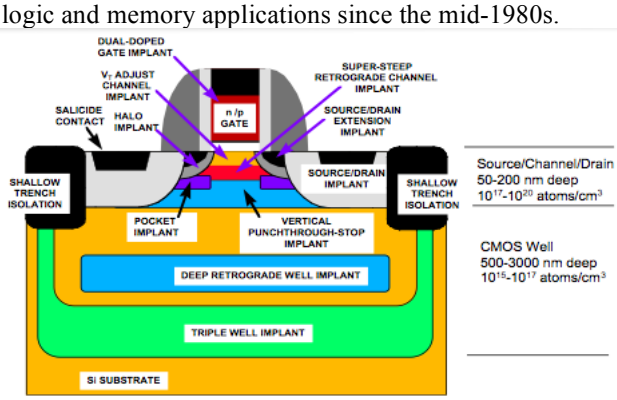


Figure 2: Sketch of major doped regions for a planar CMOS transistor.

For doping of near-surface (<100 nm) layers on Si with the common dopants B, As, and P, the beam energy

Copyright © 2013 CC-BY-3.0 and by the respective authors

ISBN 978-3-95450-138-0

ELECTRON BEAM IRRADIATION APPLICATIONS

Sunil Sabharwal#
Radioisotope Products and radiation Technology Section
International Atomic Energy Agency
Vienna, Austria

Abstract

The irradiation of materials with electron beams or X rays is used extensively to enhance or modify their physical, chemical or biological properties. These electron beam "irradiators" cover a very wide range of accelerators technology, beam current and energies to produce a wide variety of products, mostly with polymers. They also are used for curing ink, coatings, and adhesives as well as for the sterilization of medical products, disinfection and preservation of food. The emerging applications include treatment of waste waters and flue gases, and degradation of plastics for use in coatings and inks. The status of applications and the role of IAEA in enhancing these will be presented.

INTRODUCTION

High energy ionizing radiation has the unique ability to produce reactive species like free radicals in a variety of materials that can be used to modify physico-chemical properties of materials for a variety of industrial applications. Over the last 50 years, the subject of radiation chemistry and accelerator physics have developed simultaneously and from industrial applications point of view, the progress in one area has generally led to the advancement in the other area. While the basic radiation chemistry studies using the pulse radiolysis studies using nano-scale pulse electron beam accelerators led to understanding the basic fundamental aspects of radiation chemistry, the commercial applications based on radiation crosslinking of polymers or inactivation of pathogenic bacteria emerged as the driving force for developing high energy high current accelerators to ensure that the fruits of radiation chemical research are utilized for industrial applications. Radiation technologies based on electron beam accelerators today are used for applications such as crosslinking of wire& cables, producing heat-shrink materials, surface curing of materials, sterilization of medical products and for food irradiation [1]. Currently, world-wide, there are over 1400 industrial electron accelerators in operation that are being widely used for applications such as polymer processing, surface curing, sterilization of medical products and food irradiation [2]. A conservative market survey indicates that these high current EB units are providing an estimated over US $85 billion value added unique high-value products for mankind in an environmentally friendly manner [3]. Pollution of air, water and land resources due to industrial and human activities constitutes a major threat to sustainable development. While burning of fossil fuels lead to formation of sulphur oxides (SO_2 and SO_3), nitrogen oxides (NO_x), water resources are being polluted with industrial and human waste. The industrial effluents carry chemical contaminations like heavy metals, organic pollutants, petro-chemicals, pesticides and dyes while discharge of sewage and sludge giving rise to microbiological and chemical contamination of the water bodies. In the last few years, extensive work has been carried out for utilizing radiation technology for environmental remediation. Pilot or plant scale electron beam facilities have been set up to demonstrate the application of this technology for treatment of such pollutants in an effective and efficient manner [4,5]. This paper presents the present status of the established as well as emerging applications and the challenges that the accelerator technologists need to address for further implementation of this technology in these emerging areas.

TYPICAL CHARACRISTICS OF ELECTRON ACCELERATORS FOR INDUSTRIAL APPLICATIONS

For industrial radiation processing, the two main characteristics of an electron beam accelerator are energy and current. While energy of the accelerator determines the thickness of the product that can be uniformly processed, the current determines the productivity or the throughput of the process that can be achieved. A wide range of electron beams with energies varying from 0.15 to 10 MeV are used in radiation processing for varying applications (Table 1). The electron beam accelerators used in the industry typically have beam power (the product of electron energy and current) ranging from 5 to about 100 kW, although more powerful accelerators (400 kW and higher) have also been set up in recent years to demonstrate certain applications or for commercial irradiation. Low-energy accelerators having energies from 0.15 to 0.5 MeV, are generally constructed as self-shielded systems in the production. They are used mainly for the treatment of surfaces and the irradiation of coatings and thin materials, such as polymeric films. Medium-energy accelerators produce electrons with energies of 0.5 – 5 MeV at powers of up to 300 – 350 kW. High-energy accelerators, which for processing purposes generate electron beams with energies of 5 – 10 MeV, are linear accelerators giving pulsed beams of up to 50 kW. Such accelerators are used for radiation sterilization of medical products and, to a lesser extent, for the radiation treatment of foodstuffs. The applications of electron accelerators are summarized in Table 1.

#S.Sabharwal@iaea.org

Copyright © 2013 CC-BY-3.0 and by the respective authors

ISBN 978-3-95450-138-0

OVERVIEW AND LESSONS LEARNED OF THE JEFFERSON LAB CRYOMODULE PRODUCTION FOR THE CEBAF 12GEV UPGRADE*

J. Hogan, A. Burrill, M. Drury, L. Harwood, C. Hovater, C. Reece and M. Wiseman
Thomas Jefferson National Accelerator Facility, Newport News, VA 23606, USA

Abstract

The Continuous Electron Beam Accelerator Facility (CEBAF) at Jefferson Lab is nearing completion of an energy upgrade from 6 to 12 GeV. An integral part of the upgrade is the addition of ten new cryomodules, each consisting of eight seven-cell superconducting radio-frequency (SRF) cavities. An average performance of 100+MV of acceleration per cryomodule is needed to achieve the 12 GeV beam energy goal. The production methodology was for industry to provide and deliver the major components to Jefferson Lab, where they were tested and assembled into cryomodules. The production process begins with an inspection upon receiving of all major components followed by individual performance qualification testing. The SRF cavities received their final chemical processing and cleaning at Jefferson Lab. The qualified components along with all associated hardware and instrumentation are assembled, tested, installed into CEBAF and run through an integrated system checkout in preparation for beam operations. The production process is complete and one of the first completed cryomodules has successfully produced 108 MV of acceleration with a linac beam current of 465 μA.

INTRODUCTION

The ten C100 cryomodules accounted for approximately one-quarter of the accelerator budget and 10% of the total budget for the 12 GeV upgrade project. The scope of the cryomodule production run consisted of the design, procurement, assembly, acceptance testing and a final integrated performance checkout with all associated CEBAF operating systems. The first superconducting radio frequency (SRF) niobium cavities were delivered in 2010. These SRF cavities were individually qualified in vertical dewars [1] at Jefferson Lab. In 2011, (ahead of the baseline schedule) the first two production 12GeV-C100 cryomodules were installed and commissioned in the CEBAF machine. These first two cryomodules accelerated and delivered beam for six months of physics experiments. In May 2012, one of the 12GeV-C100 cryomodules was successfully operated at a total energy of 108MV (with a linac current of 465uA) while delivering three-pass beam to the experimental halls [2]. This beam loaded performance demonstrated the design and production process of the C100 cryomodules would meet the 12 GeV requirements.

*Work supported by Jefferson Science Associates, LLC under U.S. DOE Contract No. DE-AC05-06OR23177. The U.S. Government retains a non-exclusive, paid-up, irrevocable, world-wide license to publish or reproduce this manuscript for U.S. Government purposes.

DESIGN

The original CEBAF cryomodule design consists of 8-five-cell cavities and produces a nominal voltage of 20 MV per cryomodule. 40 cryomodules (20/linac) were installed in the original CEBAF and produced enough voltage to run the machine at 4GeV. Over time the performance of these cryomodules was improved and optimized to increase CEBAF operation to 6GeV. The C100 cryomodule design consists of 8-seven-cell cavities and produces 100 MV per cryomodule (500 MV/linac). By adding the ten new C100 cryomodules and an additional 1/2-pass (tenth arc) to the existing accelerator, the maximum operating energy of CEBAF will be doubled from 6GeV to 12GeV.

Parameters

The C100 cryomodule design was developed over several years and is based on a set of early developmental cryomodules designed, built and operated in the Jefferson Lab CEBAF and FEL accelerators. The C100 cryomodule design parameters (see Table 1) were developed in concert with the other associated 12GeV accelerator system upgrades [3]; including the 4.6kW (at 2K) Central Helium Liquefier (CHL) [4], High power (13kW) radio-frequency klystrons (HPRF) and a new digital low-level radio-frequency (LLRF) control system [2].

Table 1: C100 Design Specifications

Parameter	Design Specification	Units
Slot length (includes warm section)	9.8	Meters (m)
Voltage/Cryomodule	108	MeV
2K heat load	<300	Watts
50K heat load	<300	Watts
HOM Damping (transverse)	$<2.4\times10^{10}$	Ohms/meter
HOM Damping (longitudinal)	$<6.5\times10^{11}$	Ohms
Cavity Gradient	19.2	MeV/m
Qo (@19.2 MV/m)	7.2E9	N/A

To meet the 12 GeV performance criteria, each of the ten cryomodules will need to provide 98 MeV of energy. In order to provide performance margin, the cryomodule is designed to produce 108 MeV. This additional performance capability provides the option to run some cryomodules higher in voltage in the event that more energy is needed to make up for lesser performing cryomodules. Similarly, the SRF niobium cavities were

Copyright © 2013 CC-BY-3.0 and by the respective authors

ISBN 978-3-95450-138-0

SRF CAVITIES BEYOND NIOBIUM: CHALLENGES AND POTENTIAL*

S. Posen† and M. Liepe
Cornell Laboratory for Accelerator-Based Sciences and Education, Ithaca, NY, USA

Abstract

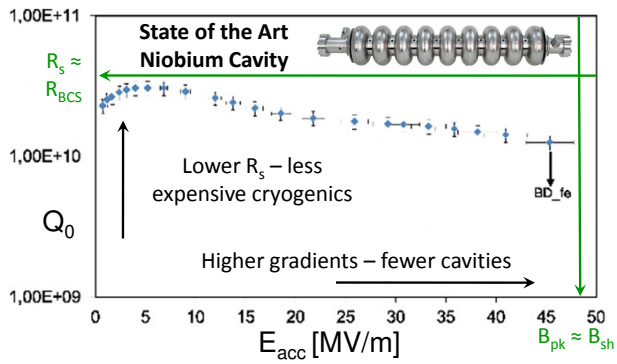
With niobium cavities now approaching the fundamental limits of the material, SRF researchers have begun a significant R&D effort to develop alternative materials to continue to keep up with the demands of new accelerator facilities. In this paper, the benefits of new materials are explored, as well as the critiria for selecting superconductors to use for SRF applications. The materials Nb_3Sn and MgB_2 are discussed in detail, including an exciting new result from a Nb_3Sn cavity that shows the great potential of alternative SRF materials. NbN and multilayers are also briefly discussed. The current status and the outlook for the future of alternative materials are reviewed.

WHY LOOK BEYOND NIOBIUM?

To accelerate beams of charged particles, superconducting radio-frequency (SRF) cavities are the technology of choice for many facilities. They can reach large accelerating gradients E_{acc} on the order of tens of MV/m, and though they require cryogenics for cooling below the superconducting transition temperature T_c of the material they are made from, they achieve high wall-power-to-beam-power efficiency due to their small surface resistances R_s. Modern SRF facilities use cavities made of niobium, either formed from bulk sheets, or sputtered in films onto copper. Early niobium cavities could operate at only small gradients of a few MV/m, but through years of research, preparation techniques were developed to avoid non-fundamental limitations, such as multipacting and field emission [1]. State-of-the-art production methods regularly produce cavities that operate very close to the fundamental limits of niobium: they have surface resistances R_s very close to the ideal BCS value at operating temperatures, and they sustain electromangetic fields very close to the material's superheating field B_{sh}, the field at which vortices penetrate the superconductor—creating unmanageable levels of heating in RF fields—for an ideal surface [2]. In Fig. 1, the qualification curve of a high-performing TESLA 9-cell niobium cavity (the proposed cavity design for ILC) is plotted. The curve tracks two figures of merit: E_{acc} and Q_0, which is inversely proportional to R_s. It shows that this cavity performs very close to the fundamental limits of the material.

To continue to keep up with continually increasing demands of future accelerator driven sciences, SRF researchers have begun a significant effort to develop alternative materials, chosen to have higher fundamental limits than niobium. The optimal material may depend on the type of facility. For low-duty-cycle high energy linacs, an alternative material would be chosen that can sustain very large surface magnetic fields, as this is what fundamentally limits E_{acc}, and therefore sets the minimum number of cavities requied to reach a given energy. On the other hand, for modern CW SRF linac designs, cryogenics is the cost driver, not the number of cavities. For niobium, low R_s operation requires the cavity to be cooled to ~2 K, where cryogenic efficiency often pushes the cost-optimum arrangement to using only modest gradients, because losses go quadratically with E_{acc}. At ~2 K, cavities made from an alternative material with lower R_s than niobium would have smaller losses at a given E_{acc}, so they would allow the cryogenic plant to be smaller and require less grid power, or they could operate at higher gradients, and therefore require fewer cavities. Furthermore, the temperature dependent part of R_s scales with $e^{-T_c/T}$, so if the alternative material had a large T_c, low R_s operation could be possible at 4.2 K, greatly simplifying the cryogenic plant by allowing it to operate at atmospheric pressure. Low R_s operation at even higher temperatures would open up the possibility of using helium gas for cooling.

Figure 1: Q_0 vs E_{acc} for a High Performing ILC 9-cell Niobium Cavity [3]. The maximum E_{acc} and the Q_0 over the entire range are very close to the fundamental limits of the material.



Long term R&D will be needed to reach the full potential of these alternative materials, but already new results (which will be shown later) on a Nb_3Sn cavity fabricated by Cornell show performances now superior to niobium for some applications requiring modest fields only.

* Work supported by DOE award number DE-SC0002329.
† sep93@cornell.edu

Copyright © 2013 CC-BY-3.0 and by the respective authors

DESIGN OF THE SUPERCONDUCTING MAGNET SYSTEM FOR THE SUPERKEKB INTERACTION REGION

N. Ohuchi#, Y. Arimoto, N. Higashi, H. Koiso, A. Morita, Y. Ohnishi, K. Oide, H. Sugimoto, M. Tawada, K. Tsuchiya, H. Yamaoka, Z. Zong, KEK, Tsukuba, Japan
M. Anerella, J. Escallier, A. Jain, A. Marone, B. Parker, P. Wanderer, BNL, Upton, NY, U.S.A.

Abstract

SuperKEKB is the upgraded accelerator of KEKB aiming at an extremely high luminosity. The machine is designed on the basis of nano-beam scheme. The beam final focusing system is the most important element for achieving the luminosity of this accelerator. The system consists of 8 quadrupoles, 4 solenoids and 43 correctors.

INTRODUCTION

The target luminosity of SuperKEKB [1] is 40 times higher luminosity of 8×10^{35} cm^{-2} s^{-1} than that of KEKB. The 7 GeV electrons in the high-energy ring (HER) and the 4 GeV positrons in the low-energy ring (LER) collide at a single interaction point, IP, with a finite crossing angle of 83 mrad.

The accelerator is designed on the basis of the nano-beam scheme [2], and the final beam focusing system has been designed with superconducting quadrupole doublets for each beam. Since the positions of quadrupole magnets must be aligned very precisely within several nano meters, the alignment of quadrupoles is performed by the correctors [3]. In addition, from the requirement of beam optics, 43 corrector coils are installed in the system. The system has four compensation solenoids to reduce the effect of the detector solenoid field on the beams. All magnets and correctors are assembled into two cryostats.

In the paper, the design of the system is described.

SUPERCONDUCTING MAGNET SYSTEM

Magnet Layout in the IR

Figure 1 shows the layout of the superconducting magnets near the interaction point, IP [4]. The system consists of 8 main quadrupole magnets, 4 compensation solenoids, 35 corrector coils and 8 coils to cancel the leakage magnetic fields of QC1LP/RP. The main quadrupole magnets (QC1s and QC2s) are designed to form a quadrupole doublet for each beam. Table 1 shows the main parameters of the quadrupole magnets at the colliding energy of 11 GeV. The QC1LP/RP magnets are located at the closest position, +/- 935mm, to IP. They are quadrupole magnets without magnetic yokes in order to make the solenoid field profile for minimizing vertical beam emittance. The other quadrupole magnets have magnetic yokes.

Since the QC1LP/RP magnets are non-yoked magnets, the leakage field from the magnets to the e- beam line contains all field components as shown in Fig. 2. In order to cancel these components, the B_3, B_4, B_5 and B_6 cancel coils [3] are wound using the helium inner vessel as the coil bobbin. A small twist of the windings which produce the normal cancel components also generates the needed skew cancel components. The B_1 and B_2 field components are included in the optics design.

The compensation solenoids, ESL, ESR1, ESR2 and ESR3, are designed to cancel the Belle-II solenoid field integrally along the beam lines [5]. In the ESL and ESR1 solenoids, two or three quadrupoles are assembled, respectively, as shown in Fig. 1. In the right cryostat, the additional solenoids, ERS2 and ESR3, are also installed.

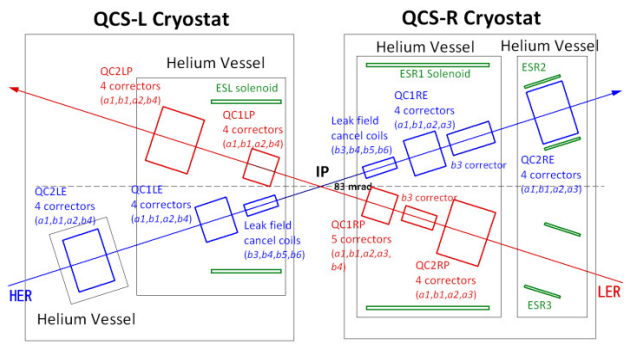


Figure 1: Layout of S.C. magnets near the IP of SuperKEKB.

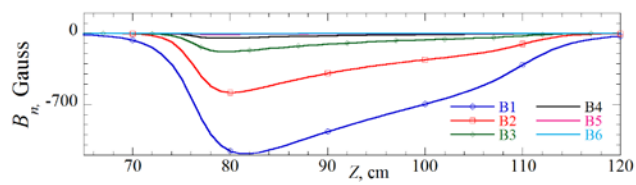


Figure 2: Leakage field profiles along the e- beam line.

Table 1: Main Quadrupole Parameters

Magnet	*GL*, T (T/m×m)	Type	*Z*, mm	*θ*, mrad
QC2RE	13.04 (31.12×0.419)	Yoke	2925	0
QC2RP	11.54 (28.15×0.410)	Yoke	1925	-2.114
QC1RE	25.39 (68.07×0.373)	Yoke	1410	0
QC1RP	22.96 (68.74×0.334)	no Yoke	935	7.204
QC1LP	22.96 (68.74×0.334)	no Yoke	-935	-13.65
QC1LE	26.94 (72.23×0.373)	Yoke	-1410	0
QC2LP	11.48 (28.00×0.410)	Yoke	-1925	-3.725
QC2LE	15.27 (28.44×0.537)	Yoke	-2700	0

GL is the integral field gradient (field gradient at center × effective magnetic length).

#norihito.ohuchi@kek.jp

ISBN 978-3-95450-138-0

Copyright © 2013 CC-BY-3.0 and by the respective authors

RAPID CYCLING DIPOLE MAGNET*

H. Witte†, J.S. Berg, P. Kovach, M.D. Anerella, Brookhaven National Laboratory, Upton, NY, USA
M. L. Lopes, Fermilab, Batavia, IL, USA

Abstract

Accelerating muons to 750 GeV and higher is most efficiently accomplished using a hybrid synchrotron. Such a machine interleaves superconducting dipoles with bipolar dipoles ramping at an effective frequency of 400–1000 Hz and with maximum fields of around 1.8 T. Previous designs for the rapid cycling dipoles for this lattice have been based on grain oriented steel, which possesses good magnetic properties in the direction of the grains. Grain oriented steel however is highly anisotropic, which can potentially lead to field quality problems. In this paper we present an alternative design, which we expect to have lower losses, a higher peak field, and better field quality.

INTRODUCTION

A hybrid synchrotron is the most efficient known option for accelerating muons to their highest energies in a TeV-scale muon collider. A hybrid synchrotron bends particles by interleaving fixed field superconducting dipoles with bipolar rapid cycling dipoles. This permits rapid acceleration, to reduce muon decay, while making a significant number of RF cavity passes to achieve good efficiency. To maximize the RF efficiency, minimize decay, and maximize the energy range of a single ring, it is essential to have the highest field possible for both the superconducting and the rapid cycling dipoles.

A design accelerating muons from 375 to 750 GeV has been proposed [1] (shown schamatically in Fig. 1), which was a variation and refinement on earlier designs [2]. It has a circumference of 6300 m, with arc cells containing 2.7 m 8 T dipoles and 7.9 m rapid cycling dipoles. The field in the rapid cycling dipoles swings from -1.8 T to $+1.8$ T in 0.5 ms; there are about 2200 m of these dipoles in the ring. The beam will be accelerated 15 times per second.

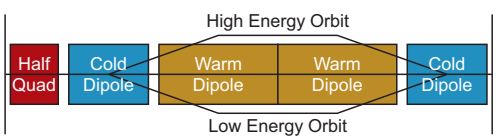


Figure 1: Structure of a quarter cell, showing the expected deviation of high and low energy closed orbits.

This report outlines a potential solution for the rapid cycling dipoles. We propose a solution operating at a frequency of 400 Hz (proposed in [2], gives more decays than [1]). The aperture required will be 60 mm horizontally (required for horizontal beam aperture) and 13 mm vertically (primarily to keep impedances reasonable). We also discuss a 25 mm vertical aperture, which might be required if a ceramic beam pipe is used.

MAGNET GEOMETRY

We consider the geometry shown in Fig. 2, which shows the 13 mm gap case. For a 25 mm gap the pole width increases to 132 mm because of field quality reasons. Each coil area is 87×30 mm^2 in cross-sectional area.

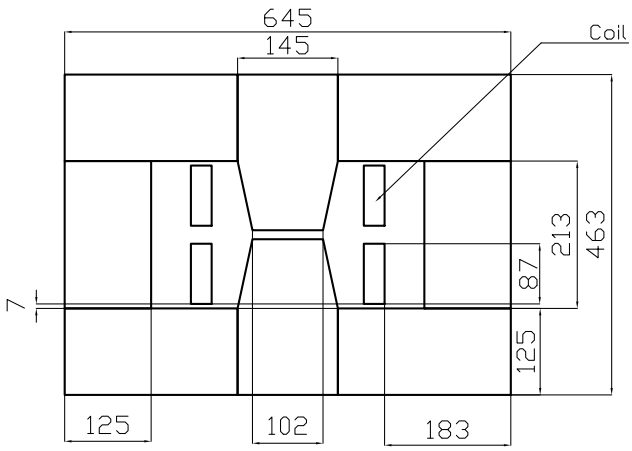


Figure 2: Geometry of the dipole magnet (in mm).

MATERIALS

Previous studies focused on grain-oriented 3% SiFe, which possesses good magnetic properties in the rolling direction [3]. A concern however is the high anisotropy of the material, which in studies has shown to affect the field quality.

For this study we focus on alternative isotropic materials, which promise lower losses while at the same time can achieve higher peak magnetic fields. The coil design employs two materials: 6.5 %SiFe and FeCo (49% Co, 1.9% V and 49% Fe). 6.5% SiFe, which has a relatively low magnetization saturation, is chosen for the very low losses. FeCo (with relatively large losses) has a very high magnetization saturation and is used for the poles of the magnet. For this design we consider Vacoflux 48 from Vac-

* Work supported by Brookhaven Science Associates, LLC under Contract No. DE-AC02-98CH10886 with the U.S. Department of Energy.
† hwitte@bnl.gov

Copyright © 2013 CC-BY-3.0 and by the respective authors

THE ILLINOIS ACCELERATOR RESEARCH CENTER

R. Kephart#, J. Anderson, C. Cooper, S. Henderson, C. Schmidt
Fermi National Accelerator Laboratory, Batavia, IL 60510, USA

Abstract

Particle accelerators are an enabling technology not only utilized in their traditional role for fundamental research, but also in such diverse fields as medicine, industrial processes, environmental mitigation, and national security. In recognition of this large impact on the US economy, the Fermi National Accelerator Laboratory (FNAL) has partnered with the Illinois Department of Commerce and Economic Opportunity (DCEO) and the Department of Energy's Office of High Energy Physics (DOE/OHEP) to build the Illinois Accelerator Research Center (IARC). Located on the Fermilab campus, this 83,000 square foot facility will house office, technical, and educational space in a state-of-the-art facility for accelerator research, development, and education. With a strong focus on industrial application of accelerator technologies, IARC will attract high-tech companies to Illinois and help train Illinois citizens in advanced technologies.

INTRODUCTION

IARC was conceived and proposed by Fermilab and DOE to the State of Illinois in 2007. The need for a US facility like IARC was recognized at the Accelerators for America's Future symposium held in Washington DC in Oct 2009. The 2010 report from this symposium contains a wealth of information on the basic justification for investment in accelerator applications as well as the opportunities for new accelerator applications for a facility like IARC [1]. Following the lead of this symposium, the 2012 Senate Water and Energy Bill encouraged DOE to pursue the development of accelerator applications more aggressively [2,3]. It requested DOE/OHEP to provide a plan to address the opportunities made evident in the Accelerators for America's Future symposium. In 2011, OHEP convened an Accelerator R&D Task Force to offer advice on the creation of such a plan. An interim report from this committee was presented at the High Energy Physics Advisory Panel (HEPAP) meeting in March 2012 [4]. The final report to the House and Senate Appropriations Subcommittees was completed in September 2012. Through this request by Congress, OHEP is now the designated steward of accelerator science and technology within the DOE Office of Science complex, with a new thrust toward applied technology.

Key to the success of IARC will be a shared understanding at the national, state, and local levels that translational technology, namely developing ideas from the laboratory into commercial practice, only happens when the proper environment is cultivated. The proper environment promotes friendly, flexible collaboration with industry and universities and provides sufficient seed resources such that non-traditional and multi-disciplinary efforts can flourish.

In 2014 Fermilab plans to increase its partnerships with industry via Work for Others (WFO) and Cooperative Research and Development Agreements (CRADA's). When the physical plant is completed for occupancy in 2015, the IARC facility will attract industrial partners to develop technology for accelerator applications, encourage development of intellectual property by laboratory and university accelerator staff, and provide a National Center for Accelerator Education. The goal is a successful IARC program that exploits and leverages resources from DOE OHEP, Small Business Innovation Research (SBIR) programs, DCEO, and other public funding with substantial private investment from industry and the venture capital community. These funds will be used to translate ideas in accelerator technology into new high tech products and industries and to create an educational program to train the skilled workforce to build and operate the accelerators of the future.

A key concept for the IARC program is that it serves as a portal to allow industrial access, not just to the IARC physical plant, but also to the facilities and technical expertise of the entire laboratory. A successful program at IARC will lower barriers for Laboratory – Industry cooperation on accelerator technology and applications and enable an entire new class of projects to be undertaken as Government-Industry partnerships.

MISSION STATEMENT

The mission of IARC is to partner with Industry, University, and Laboratory collaborators to promote the development of accelerator technology and applications, leading to new products, capabilities, and businesses. The IARC education program will support and enable the creation of the high technology workforce required for its mission.

THE VISION

The vision for IARC is the creation of a friendly, flexible environment to facilitate collaboration with industry, universities, and other national labs and to help provide sufficient seed resources such that non-traditional and multi-disciplinary efforts can flourish. The IARC environment will allow access and leverage of Fermilab's unique facilities and staff to create an innovation hub for new Accelerator based technologies and industries.

When the IARC physical plant is complete in 2015, the laboratory envisions attracting industrial partners to develop technology for industrial accelerator applications; encouraging the development of advanced innovative accelerator science and technology as well as intellectual

Copyright © 2013 CC-BY-3.0 and by the respective authors

ISBN 978-3-95450-138-0

DIAGNOSTIC PROTON COMPUTED TOMOGRAPHY USING LASER-DRIVEN ION ACCELERATION

K. Woods#, S. Boucher, RadiaBeam Technologies LLC, Santa Monica, CA 90404, U.S.A.
B.M. Hegelich, University of Texas at Austin, Austin, TX 78712, U.S.A.
V. Bashkirov, R. Schulte, Loma Linda University Medical Center, Loma Linda, CA 92354, U.S.A.

Abstract

Although the growing utilization of computed tomography (CT)-based imaging has led to major advances in diagnostic capabilities, it has also resulted in higher cumulative radiation doses to patients. In order to fully exploit the benefits of high-resolution diagnostic CT scans while minimizing the risks of radiation-induced cancer, the realization of low-dose CT is crucial. Recent research has shown that the use of protons, rather than X-rays, for CT has the potential to greatly reduce the radiation dose delivered to the patient without reducing image quality. RadiaBeam Technologies, in collaboration with the Loma Linda University Medical Center and the University of Texas at Austin, is proposing the development of a proton CT scanner utilizing laser-driven ion acceleration (LDIA) techniques. The initial design of this system is presented.

NEED FOR LOW-DOSE CT

With over 62 million scans performed each year in the United States alone, computed tomography (CT) is a crucial tool for diagnostic radiology. Over the last 15 years, there has been a large increase in the utilization of diagnostic CT imaging procedures and therefore a subsequent increase in radiation exposure. As CT scans are responsible for nearly 50% of the radiation exposure from medical imaging in the U.S., the risks associated with its relatively high radiation dose, which can be two orders of magnitude greater than corresponding X-ray radiographs, become more and more of a concern [1]. Dose reduction is especially important for pediatric diagnosis, since children are both more sensitive to radiation and have more time for developing radiation-induced secondary cancers.

PROTON CT

Recent research has shown that the use of protons, rather than X-rays, for CT has the potential to reduce the radiation dose by an order of magnitude without reducing image quality [2], [3]. Ongoing studies of proton CT (pCT) at Loma Linda University Medical Center (LLUMC) are being performed to develop this technology for improving the accuracy of treatment planning in hadron therapy.

Principles of pCT

The first requirement for pCT is the production of a proton beam with high enough energy to fully penetrate the body part to be imaged. Protons with energies 200 - 250 MeV would be necessary for performing a typical head scan, while 330 MeV protons would be able to span most human torsos (60 cm range). Position-sensitive detectors are placed on either side of the subject to track the entry and exit points of each proton. The energy loss of individual protons is then measured with an energy detector/range counter, as shown in Figure 1.

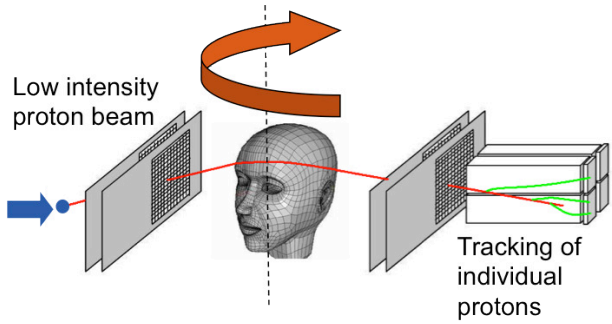


Figure 1: Conceptual design for a pCT scanner [Courtesy of R. Schulte, LLUMC].

Images can be created from the individual proton histories through the use of iterative reconstruction algorithms and path concepts such as the "most likely path" approach, as illustrated in Figure 2.

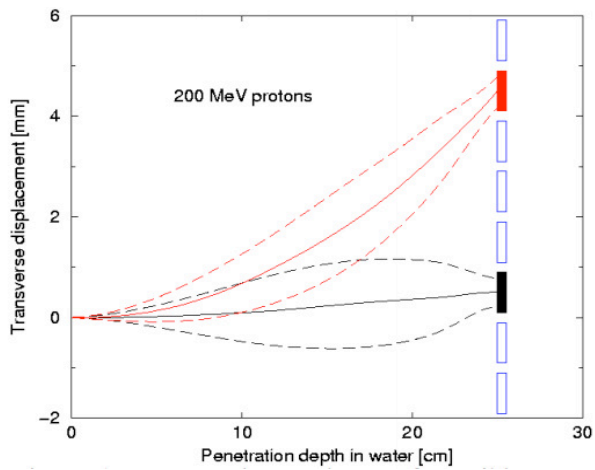


Figure 2: Monte Carlo simulation – solid lines: the most likely path of 200 MeV protons with exit displacements of 0 and 4 mm after traveling 25 cm in an object with water density; dashed lines: one sigma envelopes from Monte Carlo.

pCT Research at LLUMC

Over the last ten years, researchers at LLUMC have been developing pCT technology for improving the

Copyright © 2013 CC-BY-3.0 and by the respective authors

OPTIMAL 3D QUADRUPOLE SHAPES*

R. Baartman, TRIUMF, 4004 Wesbrook Mall, Vancouver, BC, V6T 2A3, Canada

Abstract

The usual practice of constructing quadrupoles from truncated cylindrical hyperbolae is put into question. A new shape is proposed. This shape has an analytic potential function. The exact shape of the analytic quadrupole may be impractical, but in the short case where aspect ratio ≈ 1, pole shapes can be spherical. The optimal spherical radius is found to be 1.54 times the aperture radius. An example is also given demonstrating that in the long quad limit, the aberrations of order 5 and higher are much lower for the optimized shape.

A somewhat extended version of this paper has been published previously [1].

INTRODUCTION

The multipole elements commonly used to control charged particle beams correspond to solution terms of the Laplace equation $\nabla^2 V = 0$, namely, in polar coordinates (r, θ), $r^n \cos n\theta$ in the system where the potential on axis is zero. Thus $n = 2$ for a quadrupole, 3 for a sextupole, etc. This implicitly assumes the elements are infinitely extended in the axial (z) direction, and of course in real beamlines, they are not. For $n = 2$, the intended linear dependence of the fields upon transverse coordinate is thus broken by the finiteness of the quadrupole. This results in nonlinear force terms and aberrations.

It is not obvious how to axially terminate the poles of a quadrupole. Often, they are simply truncated. Does the shape in the longitudinal direction matter? And if so, what shape is optimal? For very long quadrupoles, it can be argued that hyperbolic equipotential surfaces given by $r^2 \cos 2\theta$ = constant are optimal. However, this is only true sufficiently far from the ends; for quadrupoles whose length is comparable to or shorter than the aperture, the 2-D hyperbolic shape is clearly not optimal. What then is the optimal shape of quadrupoles in the short limit? What is the optimal shape in the long limit? Answering these questions is the subject of this paper.

Hardness of the Fringe Field

In the limit where the fringe field extent is short compared with the focal length of the quadrupole, the lowest order aberration (cubic force) effect is independent of fringe field shape. This was shown in 1997 [2].

Let the strength function of the quadrupole be $k(z)$. Rigourously, this means $\partial_{xx} V = -\partial_{yy} V = k(z)$ along the axis $x = y = 0$, so that

$$V(x, y, z) \to \frac{k(z)}{2}(x^2 - y^2) \text{ as } (x, y) \to (0, 0), \quad (1)$$

In the "hard-edge" limit, k is a step function. But using a discontinuous step function instead of an analytic function to calculate the optics leads to dramatically incorrect results. It is thus regrettable that almost all the major higher order optics codes allow calculation of third order optics in the "no fringe field" case. This case is unphysical because it brings a particle from the field-free region outside the quadrupole instantaneously into the region where $k \neq 0$ without traversing intermediate fields. For example, for electrostatic quadrupoles, this violates conservation of energy as the potential energy is thereby incremented without changing the kinetic energy (in magnetic quadrupoles, angular momentum conservation is violated).

The beamline designer may have learned that the third order aberrations calculated without fringe fields are incorrect, but he/she is still left with the impression that the fringe field is at fault and customizing it in some way will improve the third order optics. Further, of quadrupoles with the same effective length, those with short fringe fields are erroneously thought to be superior even though this often means they have smaller aperture. In fact, such quadrupoles are inferior, as their fifth order aberrations are worse: it can be shown that in the hard-edge limit, fifth order aberrations are singular [3].

ANALYTIC QUAD

A technique for finding the potential in all space given only the strength function $k(z)$ is given by Derevjankin [4, this reference is in Russian, but referred to by Vasil'ev [5]]:

$$V(x, y, z) = -\Re\left\{\int_{z+iy}^{z+ix} dt \int_0^t k(\zeta) d\zeta\right\} \quad (2)$$

A particularly simple case that is realistic for short quads is

$$k(z) = \frac{K}{2}\,\mathrm{sech}^2 z. \quad (3)$$

We find:

$$V = \frac{K}{2}\,\Re\{-\log[\cos(x - iz)] + \log[\cos(y - iz)]\}. \quad (4)$$

See Fig. 1 where equipotential contours are plotted using as scaling potential $V_0 \equiv V(\frac{\pi}{4}, 0, 0) = \frac{K}{4}\log 2$. The transverse fields are locally nonlinear; at $z = 0$, $F_x \propto \tan x$, $F_y \propto \tan y$. Nevertheless, the integral of the transverse field is exactly linear:

$$\int_{-\infty}^{\infty} F_x dz = Kx, \quad (5)$$

and similarly, $\int F_y dz = -Ky$. The reason for this behaviour is that farther from axis, the transverse field is

*TRIUMF receives federal funding via a contribution agreement through the National Research Council of Canada.

ISBN 978-3-95450-138-0

Copyright © 2013 CC-BY-3.0 and by the respective authors

NEW METHOD FOR POINT-CHARGE WAKEFIELD CALCULATION*

Boris Podobedov#, Brookhaven National Laboratory, Upton, NY 11973, USA
Gennady Stupakov, SLAC National Accelerator Laboratory, Menlo Park, CA 94025, USA

Abstract

Extending our approach recently described in [1] we present a new method to accurately calculate point-charge geometric wakefields from wake potentials due to a much longer bunch, typically obtained with a time-domain EM field solver. By allowing a relatively long bunch in the EM solver, this method can significantly reduce the need for computer resources as well as drastically shorten the computing time. On top of that, the method provides valuable physics insights. Since the method, applied to longitudinal wakes, was described in [1], the goal of this paper is to extend it to transverse wakes.

METHOD DESCRIPTION

Knowledge of geometric wakefields is critically important for studies of accelerator beam dynamics. While analytical solutions are known for a number of simple geometries, detailed wakefield calculations for realistic vacuum chamber components are typically done utilizing time domain EM solvers. They compute the fields due to finite length bunches, forcing one to use extremely fine mesh (small fraction of the bunch length) to compute wakes at small distances. This is where the longitudinal wakes are usually dominated by singularities, so that a wake potential due a bunch of rms length σ scales as $W_{\parallel}^{\sigma}(z) \propto \sigma^{-q}$, $q>0$ [2,3]. Utilizing fine meshes has severe implications for computer memory requirements as well as calculation speed. Furthermore, EM solvers cannot calculate point-charge wakes, $W_{\parallel}^{\delta}(z)$ and $W_{\perp}^{\delta}(z)$, - functions that often provide significant physics insights and simplify beam dynamics analysis.

Recently we developed a method to calculate arbitrarily short bunch wakes, including point-charge, from the wake potentials due to a relatively long bunch, thus avoiding the fine mesh requirements in the EM solver. For longitudinal wakes the method is applied as follows [1].

1. Determine analytical singular wake model for a given geometry. For collimator and cavity type structures these are usually given by the optical and diffraction models respectively, see i.e. [2].
2. Determine the length parameter λ_g, which is the first $z\neq 0$ location where $W_{\parallel}^{\delta}(z=\lambda_g)$ has a discontinuity or a singularity of its higher derivative with respect to z. The recipe is given in [1] and it is illustrated below.
3. Pick $\sigma_0 \ll \lambda_g$ (but not too short to keep the computation time reasonable) and calculate the wake potential $W_{\parallel}^{\sigma_0}(z)$ with an EM solver.
4. Subtract the singular wake model from the result:
$$D_{\parallel}^{\sigma_0}(z) = W_{\parallel}^{\sigma_0}(z) - W_{\parallel,s}^{\sigma_0}(z). \quad (1)$$
5. Fit the remainder as follows:
$$D_{\parallel}^{\sigma_0}(z \le 3\sigma_0) = \frac{\alpha+\beta z}{2}\left(1+\mathrm{erf}\left(\frac{z}{\sqrt{2}\sigma_0}\right)\right) + \frac{\beta\sigma_0}{\sqrt{2\pi}}\exp\left(-\frac{z^2}{2\sigma_0^2}\right), \quad (2)$$
where α and β are fit parameters. Fit range used here, $|z/\sigma_0|\le 3$, works very well. However, this choice is rather flexible and may be influenced by practical trade-offs, i.e. fit quality vs. computation time. Maximum z, however, must obey λ_g-z_{max}>few σ_0.
6. For arbitrary short $\sigma \le \sigma_0$, the wake is given by:
$$W_{\parallel}^{\sigma}(z \le 3\sigma_0) = \frac{\alpha+\beta z}{2}\left(1+\mathrm{erf}\left(\frac{z}{\sqrt{2}\sigma}\right)\right) + \frac{\beta\sigma}{\sqrt{2\pi}}\exp\left(-\frac{z^2}{2\sigma^2}\right) + W_{\parallel,s}^{\sigma}(z), \quad (3)$$
$$W_{\parallel}^{\sigma}(z > 3\sigma_0) = W_{\parallel}^{\sigma_0}(z). \quad (4)$$
7. Similarly, for the point-charge:
$$W_{\parallel}^{\delta}(z \le 3\sigma_0) = (\alpha+\beta z)H(z) + W_{\parallel,s}^{\delta}(z), \quad (5)$$
$$W_{\parallel}^{\delta}(z > 3\sigma_0) = W_{\parallel}^{\sigma_0}(z), \quad (6)$$
where $H(z>0)=1$ is the step-function required by causality ($z<0$ is ahead of the bunch).

Summarizing the steps above, the method basically states that for $0<z<\lambda_g$ the point-charge wakefield (with subtracted singular part) is a smooth, slowly varying function. For $0<z\ll\lambda_g$ it is well approximated by a linear polynomial with coefficients easily found by fitting.

PARAMETER λ_g

λ_g can be determined by a straightforward geometric analysis combined with the causality principle [1]. Figure 1 illustrates how to find λ_g for a simple axially symmetric cavity. In the left pipe, a bunch moving with the speed of light c, carries only static EM fields. As the bunch enters the cavity, the fields get disturbed, exciting the radiation of EM waves. Some wave-fronts (i.e. red or orange)

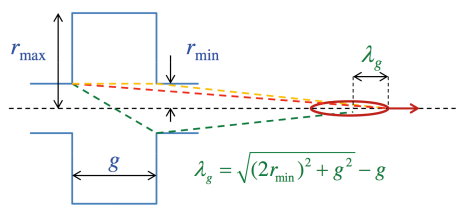


Figure 1: λ_g for a cavity with $r_{max}/r_{min}\ge 2$ and $g/r_{min}\ge 2^{-1/2}$.

*Work supported by DOE contracts DE-AC02-98CH10886 and DE-AC02-76SF00515.
#boris@bnl.gov

Copyright © 2013 CC-BY-3.0 and by the respective authors

SPACE CHARGE MODELS FOR PARTICLE TRACKING ON LONG TIME SCALES*

J.A. Holmes, S. Cousineau, A. Shishlo, ORNL, Oak Ridge, TN, 37830, USA
R. Potts, University of Tennessee, Knoxville, TN 37996, USA

Abstract

In order to efficiently track charged particles over long times, most tracking codes use either analytic charge distributions or particle-in-cell (PIC) methods based on fast Fourier transforms (FFTs). While useful for theoretical studies, analytic distribution models do not allow accurate simulation of real machines. PIC calculations can utilize realistic space charge distributions, but these methods suffer from the presence of discretization errors. We examine the situation for particle tracking with space charge over long times, and consider possible ideas to improve the accuracy of such calculations.

INTRODUCTION

Space charge physics has been successfully incorporated into numerous computational particle-tracking studies of linacs, accumulator rings, and rapid cycling synchrotrons. These space charge models have allowed the successful simulation of phenomena that would have been impossible otherwise. Particle-tracking simulations for these machines all involve following particle distributions over short to moderate time scales. With the emergence of ever-higher beam intensities, it is now necessary to incorporate space charge effects into simulations of storage rings [1]. Calculations for storage rings require tracking beams for far longer times than those in linacs, accumulator rings, or rapid cycling synchrotrons. These long time scales place severe requirements on the speed and accuracy of the physics models and call for innovative methods of solution. For example, Lie Algebraic methods have been used with great success in single particle tracking to provide fast symplectic high order maps for storage rings. Although it is difficult to conceive of full turn maps for collective effects, such as space charge, advances will be necessary to incorporate this physics reliably into storage ring applications.

The problems of simulating space charge over long times arise partly from simplifications in the physics required to obtain a computational model and, more seriously, from the numerical properties of the model so obtained. From the physics perspective, a beam consists of many identical indistinguishable particles interacting quantum mechanically with each other and with their surroundings. In order to perform tracking studies, we make a series of approximations to arrive at a picture in which we treat the beam as a collection of distinguishable particles moving and interacting with each other and their surroundings primarily according to classical physics. Within this picture, space charge is the inter-particle Coulomb force, and its evaluation requires the solution of Poisson's equation.

Thus, even at the outset, space charge models represent a very simplified picture of reality. Their success in predicting and describing the physics of accelerators on short to intermediate time scales is some testimony to the validity of these approximations. However, for extension to long time scales, we must keep in mind that many other effects, such as lattice imperfections and nonlinearities, wake forces, neutral gas ionization and scattering, electron cloud interaction, intrabeam scattering, beam loss, and others may be important. These effects may be relatively unimportant at short or intermediate time scales, but critical at longer times. To study them in the presence of space charge, it is necessary understand and to mitigate the numerically induced noise and errors in the space charge models. The challenge of simulating space charge over long times lies in the representation of the beam distribution and the discretization of the problem.

CHOICE OF PHYSICAL MODEL

The first issue in space charge modeling is to determine what type of model contains physics sufficient to your needs. One criterion is the dimensionality of the model. 1D longitudinal models are used in longitudinal beam dynamics codes and also in conjunction with 2D transverse space charge calculations in 3D tracking codes. 2D transverse models, including bunch factor effects, are the most widely used for calculation in rings. If transverse properties vary longitudinally or transverse impedances are of interest, 2.5D models are necessary. These consist of a series of 2D model slices along the longitudinal direction that are connected by a common boundary condition. 2.5D models provide both the longitudinal and transverse space charge force components. All the above models are valid only for long bunches in which the bunch length greatly exceeds the beam pipe radius. Finally, there are full 3D space charge models. These are essential for short bunches, where the longitudinal and transverse dimensions are comparable, and are widely used in linac studies. Computational requirements rise steeply with the dimensionality of the model, so it is important to adopt the simplest model that contains the necessary physics.

* ORNL/SNS is managed by UT-Battelle, LLC, for the U.S. Department of Energy under contract DE-AC05-00OR22725

ISBN 978-3-95450-138-0

Copyright © 2013 CC-BY-3.0 and by the respective authors

TIME-RESOLVED TEMPERATURE MAPPING SYSTEM FOR THE APS DEFLECTING CAVITIES*

Y. Yang †‖, P. Dhakal#, J. Fuerst, J. Holzbauer, J. Kaluzny, J. Mammosser#,
A. Nassiri, H. Wang#, G. Wu, Argonne National Laboratory, Argonne, IL 60439, USA
#Thomas Jefferson National Accelerator Facility, Newport News, VA 23606, USA
‖Tsinghua University, Beijing 100084, China

Abstract

Time-resolved temperature mapping of a superconducting cavity can give valuable information on the limiting process of the cavity performance. A fast temperature mapping system has been developed at Argonne National Laboratory (ANL) for a superconducting deflecting cavity test. The time resolution of the temperature mapping could be up to 50 μs. Not only the spatial distribution of surface heating but also the thermodynamics can be recorded, which helps to understand the limitation mechanism. This new temperature mapping system has helped us to understand the rf performance limitations during the cavity vertical tests. Based on the findings from the temperature mapping, proper cavity treatment has been applied and the cavity performances have been improved.

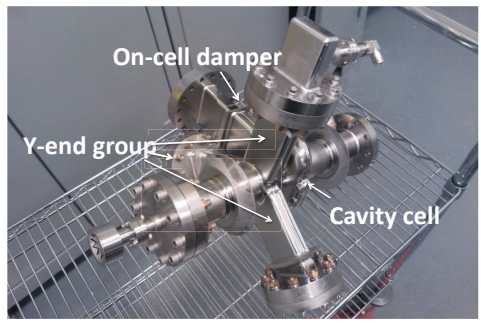


Figure 1: The APS superconducting deflecting cavity during assembling in a clean room. The cavity has a Y-end group on the beam pipe and a on-cell waveguide damper.

INTRODUCTION

The Advanced Photon Source (APS) at Argonne National Lab (ANL) has considered using the superconducting deflection technique to generate x-rays on the order of 2 ps or less [1]. A single-cell cavity design has been chosen as the baseline design and four superconducting deflecting cavities have been fabricated, as shown in Fig. 1. The cavity is a single squashed-cell cavity with an on-cell waveguide damper and a Y-end group on the beam pipe [2]. To provide sufficient deflecting modulation to the beam, a single-cavity deflecting voltage needs to reach 0.5 MV, which corresponds to a peak surface magnetic field of 106 mT. To accomplish this challenging goal, it is very important to understand the cavity performance limitations. Generally speaking, a number of processes, such as multipacting, field-emission, Q-slope, and thermal quench, might limit the superconducting cavity performance. All of these processes will eventually generate heat on the cavity wall. Temperature mapping is presently one of the most effective tools to gain insight into the cavity limitations.

Most conventional temperature mapping systems work for L-band accelerators [3][4]. Hundreds of sensors are required to cover the cavity surface. However, the sampling rate is limited to a few Hz, which is not fast enough to get a resolved signal. The APS deflecting cavity operates at 2815 MHz. The cavity size is much more compact compared to the L-band cavity, thus a fewer number of sensors are needed to cover the high magnetic field surface. A new time-resolved temperature mapping system has been developed for the APS deflecting cavity. It consists of 24 temperature sensors with a time resolution as high as 50 μs. A number of cavity tests made using this system have helped us understand cavity performance limitations. Compared to conventional temperature mapping, time-resolved temperature signals are much superior in classifying the limitations in terms of thermal dynamics. These findings from temperature mapping have led us to improve the cavity performance with the following treatment.

SENSOR MOUNTING AND DATA ACQUISITION

We used sensors made from Allen-Bradley carbon resistors. This resistor has a high thermal sensitivity of 10Ω/mK around 2 K. To thermally isolate the sensor from the helium bath, the resistor was enclosed in a G-10 container filled with epoxy. In order to make good thermal contact and provide electrical isolation to the cavity surface, the top surface of the resistor was ground away until the carbon was exposed and then a thin layer of a GE-varnish, toluene and alcohol mixture was applied.

The APS deflecting cavity operates at dipole mode, and the highest surface magnetic field region is the iris between the cavity cell and the Y-end group. The sensors were mounted around the cavity based on the surface magnetic field distribution, as shown in Fig. 2. Proper mounting techniques were developed. A cryogenic cable tie was applied as a band to mount the sensors around the iris. Two semi-circle bands made of cryogenic fiberglass weres used to attach the sensors on the cavity cell. Apiezon N grease

* Work supported by the U.S. Department of Energy, Office of Science, under Contract No. DE-AC02-06CH11357
† yaweiyang@aps.anl.gov

Copyright © 2013 CC-BY-3.0 and by the respective authors

MODE DAMPING MEASUREMENT FOR THE APS DEFLECTING CAVITY *

Y. Yang †‖, A. Nassiri, T. Smith, G. Waldschmidt, H. Wang#, G. Wu
Argonne National Laboratory, Argonne, IL 60439, USA,
‖Tsinghua University, Beijing 100084, China
#Thomas Jefferson National Accelerator Facility, Newport News, VA 23606, USA

Abstract

The Advanced Photon Source has considered using a deflecting-cavity-based scheme to produce short pulse x-rays. A deflecting cavity design has been completed. To verify the simulation result on this cavity, a copper prototype of the design has been fabricated for bench measurement. In this paper, we report our measurement results on this cavity. All the cavity modes below 5 GHz were identified by comparing the field distributions with calculations along different beam paths. After adding the damper, the measured Q_{ext}s of those modes were consistent with calculated values, which demonstrated that the cavity damping scheme was sufficient to reduce the wake impedances well below the safety thresholds.

INTRODUCTION

The Advanced Photon Source (APS) at Argonne National Lab (ANL) has considered using a superconducting deflecting-cavity-based scheme to generate x-rays on the order of 2 ps or less [1]. The unwanted cavity modes in cavities can drive coupled-bunch instabilities in high-current storage rings. Thus sufficient damping of those modes was very important. It is equally important to maximize the operating mode parameters and provide sufficient transverse kick to the beam. A cavity design has been proposed, as shown in Fig. 1. This cavity design is a single squashed-cell cavity with an on-cell waveguide damper and a Y-end group on the beam pipe [2]. The on-cell waveguide serves as lower-order mode (LOM) damper. One of the Y-end group waveguide damper works as a fundamental power coupler (FPC) and the other two dampers as higher-order mode (HOM) dampers. The cavity operates at 2815 MHz.

Extensive simulations have been performed, and we have demonstrated that the wake impedances are well below the stability thresholds [3]. In this paper, bench measurements were performed to verify numerical calculations. There were mainly two steps in the bench measurement. The first step was to identify the modes by measuring the field distributions using on-axis and off-axis bead-pulls. The second step was to characterize the damping performance by using actual high-power waveguide damper prototypes [4].

* Work supported by the U.S. Department of Energy, Office of Science, under Contract No. DE-AC02-06CH11357
† yaweiyang@aps.anl.gov

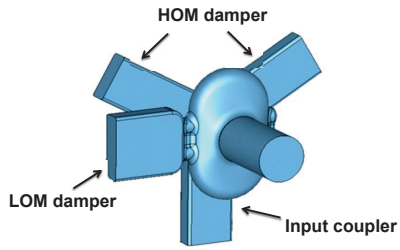


Figure 1: The APS deflecting cavity design.

COPPER PROTOTYPE CAVITY MEASUREMENT

Measurement Technique

The cavity modes were characterized by the Slater perturbation technique. With a small perturbing object, usually a dielectric bead or metal needle, passing through the cavity beam pipe, the longitudinal electrical field $E_z(r,\theta)$ along the beam path can be measured in terms of the frequency shift due to the perturbation. For a dielectric bead, the frequency perturbation can be related to the electric field strength as follows:

$$-\frac{\Delta\omega}{\omega} = g_1 e_{\parallel}^2 + g_2 e_{\perp}^2, \qquad (1)$$

where the coefficients g_1 and g_2 are geometric factors. They depend upon the bead size, material, and geometry. Eq. 1 shows that the electrical field in both longitudinal and transverse directions will contribute to the frequency change when the bead passes through the cavity. But for the R/Q measurement, only the longitudinal electrical field is of interest. In the APS deflecting cavity, there are many modes that have strong transverse electrical field compared to the longitudinal electrical field along the beam path. To get an accurate measurement of the R/Q, a slender bead with a length at least ten times larger than the diameter is required due to its insensitivity to the transverse electrical field with $g_1 \gg g_2$ [5]. However, our bead length needs to be relatively small to have adequate longitudinal resolution due to the compactness of the cavity. Given that, it is very difficult to have such a bead that can separate the transverse and longitudinal electrical fields. After exploring different beads and techniques, we selected a uniform dielectric bead with $g_1 \approx g_2$ to measure the electric field amplitude $E_{abs}(r,\theta)$ along different paths. Before the bead-pull mea-

Copyright © 2013 CC-BY-3.0 and by the respective authors

ISBN 978-3-95450-138-0

ELECTRO-MAGNETIC OPTIMIZATION AND ANALYSIS OF A QUARTER WAVE RESONATOR *

Z. Zheng[#, 1, 2], A. Facco[1, 3], Z. He[1, 2], Z. Liu[1], J. Wei[1], Y. Xu[1], Y. Zhang[1]
[1]Facility for Rare Isotope Beams, Michigan State University, East Lansing, MI 48824 USA
[2]Tsinghua University of Beijing, Beijing, 100084 China
[3]INFN - Laboratori Nazionali di Legnaro, Padova, Italy

Abstract

A β=0.085 quarter wave resonator (QWR) with resonant frequency=80.5 MHz is used in the Facility of Rare Isotope Beam (FRIB). Its baseline structure is designed to achieve the FRIB specifications with optimum cost to performance ratio. Electro-magnetic optimization is introduced in this paper to modify its internal geometry to reach instead maximum accelerating gradient, while preserving the original flange to flange length. Reduced peak magnetic field and increased shunt impedance are well achieved in the optimization while keeping the same stored energy. The maximum accelerating voltage is raised accordingly. Multipacting and steering are also analyzed for the optimized cavity. This resonator could be used in the ReA linac at MSU and in all applications where the maximum accelerating voltage should be achieved in a limited space, or where the accelerator cost is mainly driven by the resonator gradient.

INTRODUCTION

The baseline structure of FRIB QWR cavity is designed to achieve its goal with optimum cost to performance ratio. By further optimizing the baseline cavity, we aimed at a cavity design (that we nicknamed "race car") which provides significantly more accelerating gradient (E_a) still being affordable in cost, like an economy car in the auto world. The optimization is achieved mainly by reducing the peak magnetic field B_p and increasing the cavity shunt impedance R_{sh}. Lower B_p can speed up the "car" to higher cavity gradient, and increased R_{sh} allows keeping power consumption low, like saving "gasoline" for the "car". With high gradient, low-β resonators like this "race car" design, compact accelerators which can reach several MeV per nucleon in a limited space can be built for different applications. In this paper, section 1 introduces the method and procedure of the electromagnetic optimization. Section 2 discusses multipacting and beam steering issues before and after the optimization.

ELECTRO-MAGNETIC OPTIMIZATION

The main goal of the optimization is reducing the peak magnetic field (B_p) and increasing shunt impedance (R_{sh}/Q) while keeping good values for the stored energy, the peak electric field (E_p) and the geometric factor ($R_s \times Q$). To achieve the "economy" concept, we should limit rising of the cavity cost as little as possible. Thus, we maintained the radius of cavity outer conductor and optimized the cavity inner part.

Performance of FRIB QWR

Before cavity optimization, simulation was performed to get the parameters of FRIB QWR with MWS [1]. Table 1 shows the simulation results (effective length=βλ).

Table 1: Cavity Parameters of FRIB QWR

Parameter	Value	Units
Frequency	80.50	MHz
E_p/E_a	5.9	Abs.
B_p/E_a	12.6	mT/(MV/m)
R_{sh}/Q	452	Ω
$R_s \times Q$	22.3	Ω

In superconducting low-β resonators, the highest reported surface peak fields before quench are approximately 80 MV/m and 150 mT in cw mode. So there is a tradeoff between E_p and B_p that should be taken into account when designing a cavity, and B_p/E_p~1.8 should be nearly an optimum. For the FRIB β=0.085 QWR, B_p/E_p=2.14 which means the cavity can be expected to quench at high accelerating gradient due to B_p. To raise the maximum achievable gradient to this cavity, the most effective method is reducing its B_p.

Procedures of Optimization

First step:

The peak magnetic field of FRIB QWR is located at the inner conductor near the short plate (Fig. 1). To reduce the B_p/E_p, we optimized the structure of inner conductor by scanning two geometric parameters (R_1 and L_1 in Fig.2).

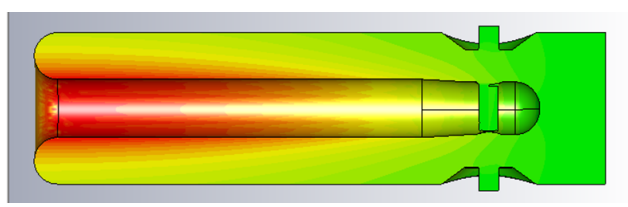


Figure 1: Magnetic field distribution of the FRIB QWR. Red means B_p. Cavity stored energy is normalized at 1J.

*Work supported by the U.S. Department of Energy Office of Science under Cooperative Agreement DE-SC0000661
#zhengw@frib.msu.edu

Copyright © 2013 CC-BY-3.0 and by the respective authors

HYDROGEN DEGASSING STUDY DURING THE HEAT TREATMENT OF 1.3-GHZ SRF CAVITIES

M.J. Joung[1#], H.J. Kim[1], A. Rowe[2], M. Wong[2]
[1]IBS, Daejeon, South Korea
[2]Fermi National Accelerator Laboratory, Batavia, USA

Abstract

Superconducting radio frequency (SRF) cavities undergo a number of processes as part of its manufacturing procedure in order to optimize their performance. Among these processes is a high temperature hydrogen degas heat treatment used to prevent 'Q' decrease. The heat treatment occurs in the processing sequence after either chemically or mechanically polishing the cavity. This paper summarizes the hydrogen measurements during the heat treatment of a sample of chemically and mechanically polished single-cell and nine-cell 1.3-GHz cavities. The hydrogen measurements are analyzed according the polishing method, the polishing history, the amount of time that the cavity was baked at 800°C, and the temperature ramp rate.

INTRODUCTION

The performance of superconducting radio frequency cavities is most important fact for a high gradient accelerator. However it is limited by field emission and thermal magnetic breakdown.[1] Most of the SRF cavities receive surface treatment to improve the performance of the cavity. A high temperature heat treatment degases the hydrogen gas that comes from the polishing process. High temperature heat treatment provides some stress-relief in the material in addition to degassing hydrogen gas [2] Hydrogen degassing studies were carried out at Jefferson Laboratory and Institut fuer Kernphysik using defference cavity. [3-4] The goal of the analysis in this paper was to evaluate whether a dependency exists between the cavity surface processing techniques, the kind of cavity and the hydrogen evolution during the heat treatment. The different polishing techniques and sequence are described. The methodology of determining the amount of degassed hydrogen is explained. Finally, the conclusion shows a comparison of the hydrogen amount.

DESCRIPTION OF CAVITIES & PROCESSING HISTORY

Nineteen single cell cavities and three nine-cell cavities, all 1.3-GHz cavities, were analyzed. All had a variety of processing steps. The cavities were polished using either EP (Electropolishing) or CBP (Centrifugal Barrel Polishing, or tumbling) to a mirror finish. [5]

The EP process polishes the surface using electrical current in acid solution at 30°C. It is a type of chemical polishing. The CBP (or tumbling) process polishes the surface using material (media) for many hours between 30°C and 50°C. It is a type of mechanical polishing.

The 800°C heat treatment takes place after the cavities were polished. During the heat treatment the temperature ramp rate was either 3°C per minute or 10°C per minute and the soak time at 800°C was either 2 hours or 3 hours. Table 1 shows the various sequences that different cavities experienced. It is noted that the amount of material removed during polishing did not correlate with the amount of degassed hydrogen.

Table 1: Polishing and Bake Sequences for the Cavities

Cavity No.	Process
1, 2, 3, 4, 9, 11, 13, 14, 15, 16, 17, 18, 20, 23, 25, 26	EP / bake
10, 12	CBP / bake
7, 19	EP / CBP / EP / bake
6	EP / CBP / bake
22, 24	CBP / EP / bake
5	CBP / bake / EP / bake

MEASURING AND CALCULATING THE H_2 AMOUNT

The vacuum furnace has a SRS 100 residual gas analyzer that measures the partial pressures of gasses during a bake. The RGA sits outside the furnace's hot zone and on the opposite end of the chamber's cryopumps. Figure 1 shows the hydrogen partial pressure curves for an electropolished cavity, a tumbled cavity and the baseline from an empty chamber for a temperature soak of 3 hours and a ramp rate of 3°C per minute. Of interest is the pressure data within the temperature range of 300°C to 300°C, as is shown in Figure 1.

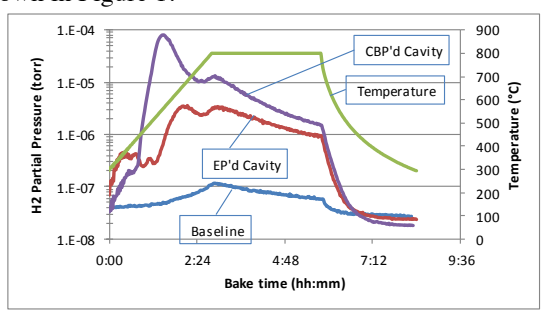


Figure 1: Typical H_2 partial pressures of an electropolished cavity, a tumbled cavity, and an empty chamber within 300°C to 300°C.

Copyright © 2013 CC-BY-3.0 and by the respective authors

ISBN 978-3-95450-138-0

MEASUREMENT OF A SUPERCONDUCTING SOLENOID WITH APPLICATIONS TO LOW-BETA SRF CRYOMODULES*

S.H. Kim#, M.P. Kelly, Z.A. Conway, P.N. Ostroumov, ANL, Argonne, IL 60439, USA
E.E. Burkhardt, Cryomagnetics, Inc., Oak Ridge, TN 37830, USA

Abstract

Proton and heavy-ion linacs with superconducting cavities require compact lattices to suppress emittance growth in the low-velocity region. For beam focusing superconducting solenoids are superior in this regard to normal conducting quadrupoles. A superconducting solenoid with integral x-y steering coils has been fabricated for the Project-X Injector Experiment (PXIE) half-wave resonator cryomodule. It is capable of generating 6 T solenoidal fields and dipole steering fields of 30 T·mm field integrals in both of transverse directions. We experimentally investigated issues for practical use of this solenoid in cryomodules including: 1) the superposition of dipole steering fields on solenoidal fields, 2) the magnetic axis of the solenoid with respect to the mechanical references in cryogenic temperatures, and 3) the residual magnetic field generated by the solenoid on the superconducting RF cavity surfaces even after degaussing; a 72 MHz quarter wave resonator was used for this experiment. In this paper, we present details of experimental setup and results.

INTRODUCTION

Proton and ion linacs require a compact focusing lattice in the low-velocity region to minimize the required real-estate and to minimize emittance growth and corresponding beam loss [1]. Superconducting solenoids are superior in this regard to normal conducting quadrupoles. To reduce the real-estate requirements further dipole steering coils are integrated with solenoids [2]. This superconducting solenoid with dipole steering coils is to be installed in a cryomodule with superconducting RF cavities so the following questions regarding beam and cavity performance need to be verified: 1) Are the dipole fields linearly superposed with the solenoid fields? 2) Is the solenoid aligned to the beam in the cryomodule? 3) Are the residual magnetic fields generated by the solenoids small enough not to degrade the cavity Q-factor?

We studied these issues with a superconducting solenoid prototype fabricated for the Project-X Injector Experiment (PXIE) Half-Wave Resonator (HWR) cryomodule [3]. This solenoid generates 6 T solenoidal fields and each pair of the dipole steering coils integrated with the solenoid produces up to 30 T·mm integrated deflecting fields. In this paper, we will briefly introduce the solenoid used in these experiments and present the dipole field measurements with and without the solenoidal field to discuss field superposition. Then, we will present magnetic axis measurements relative to the mechanical axis and discuss accuracy of this measurement method. Another alignment issue, the alignment of the solenoid to the beam axis in the cryomodule, is not discussed in this paper [4]. Next, measurements of the residual magnetic fields generated by the solenoid on the surface of a 72 MHz superconducting Quarter-Wave Resonator (QWR) will be presented with a discussion of the degaussing employed to reduce the residual magnetic fields on the cavity surface. Finally, a summary of these experimental results will conclude this paper.

FIELD PROFILES AND SUPERPOSITION

The solenoid contains two bucking coils at either end. The bucking coils are wired in series with the main solenoid to produce an opposing field polarity relative to the solenoidal field. There are no iron return yokes or magnetic shields surrounding the solenoid. The bucking coils minimize the axial fringe fields and stray fields on the cavity surfaces. The measured axial field profile is shown in Fig. 1. The measured solenoid field in the high field region is in good agreement with the design values; this ensures that the focal length will be the same as the designed value. The fringe fields are slightly higher than the design but are still small enough for the residual magnetic fields around the cavity wall to be successfully reduced by degaussing as will be discussed later in this paper.

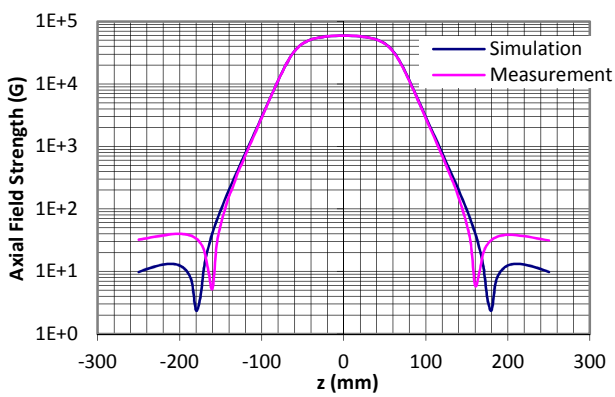


Figure 1: Axial field profiles on the axis. z is the longitudinal position which is 0 in the middle of the solenoid. Note that the magnetic field drops at z = ±160 mm in the measured data and at z = ±180 mm in the simulated response correspond to a polarity change in the axial field.

* Work supported by the U.S. Department of Energy, Office of High Energy Physics and Nuclear Physics, under Contract DE-AC02-76CH03000 and DE-AC02-06CH11357.
# shkim121@anl.gov

Copyright © 2013 CC-BY-3.0 and by the respective authors

MECHANICAL DESIGN OF THE 704 MHz 5-CELL SRF CAVITY COLD MASS FOR CeC PoP EXPERIMENT*

J. C. Brutus#,1, S. Belomestnykh1,2, I. Ben-Zvi1,2, T. Grimm3, Y. Huang1, R. Jecks3, V. Litvinenko1,2, I. Pinayev1, J. Skaritka1, L. Snydstrup1, R. Than1, J. Tuozzolo1, Wencan Xu1, J. Yancey3
1) Brookhaven National Laboratory, Upton, NY 11973-5000, U.S.A.
2) Stony Brook University, Stony Brook, NY 11794, U.S.A.
3) Niowave Inc., Lansing, MI 48906, U.S.A

Abstract

A 5-cell SRF cavity operating at 704 MHz will be used for Coherent Electron Cooling Proof of Principle (CeC PoP) system under development for the Relativistic Heavy Ion Collider (RHIC) at Brookhaven National Laboratory. The CeC PoP experiment will demonstrate the new technique of cooling proton and ion beams that may increase the beam luminosity in certain cases, by as much as tenfold. The 704 MHz cavity will accelerate 2 MeV electrons from a 112 MHz SRF gun up 22 MeV. Novel mechanical designs, including a super fluid heat exchanger, helium vessel, vacuum vessel, tuner mechanism, and fundamental power coupler (FPC) are presented. Structural and modal analysis, using ANSYS [1] were performed to confirm the cavity chamber and helium vessel structural stability and to calculate the tuning sensitivity of the cavity. This paper provides an overview of the design, the project status and schedule of the 704 MHz 5-cell SRF for CeC PoP experiment.

INTRODUCTION

The BNL3 5-cell 704 MHz SRF linac that is being designed and fabricated in collaboration between BNL and Niowave, will be used as the main 20 MeV accelerator for CeC PoP experiment under construction at IP2 of RHIC at BNL [2]. Phase II of this experiment is to be completed by the end of shutdown 2014 and will include the 704 MHz SRF linac. At the same time, with this project, BNL is pursuing R&D towards the electron-ion collider (eRHIC). This paper provides an overview of the design and structural analysis of the 704 MHz SRF linac. Two 5-cell Niobium cavities have been fabricated. The first one, BNL3-1 was manufactured by AES and the second one, BNL3-2 by Niowave.

704 MHZ DESIGN

Design Features

The 704 MHz 5-cell cavity cryostat consists of an internal phase separator, control valves, 5-cell cavity, two magnetic shields and a helium gas cooled thermal shield, a superfluid heat exchanger and an electrical heater. The helium supply and return lines are bayonet connections for quick assembly [3]. The layout of the 704 MHz SRF 5-cell SRF linac is shown in Figure 1.

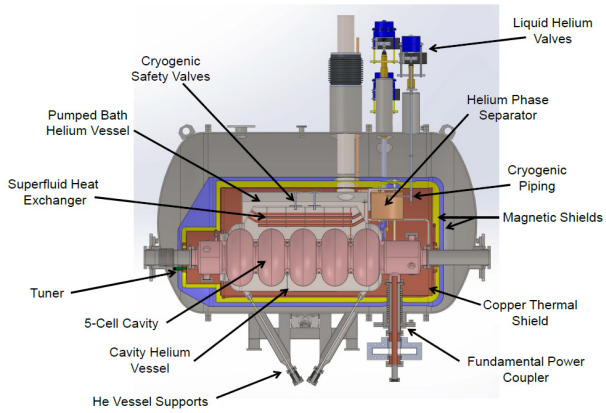


Figure 1: Layout of the 704 MHz SRF cryomodule.

The bottom of the helium vessel is a cylinder that incorporates the 5-cell cavity with the upper section modified to include the superfluid heat exchanger. Due to space constraint at IP2, the helium vessel was designed with the minimum real estate possible in order to keep the cryostat within the available space. The stiffeners shown in Figure 2 were added to the side of the helium vessel in order to reduce the deformation which translates to the cavity by deforming it through the supports attached to the helium vessel.

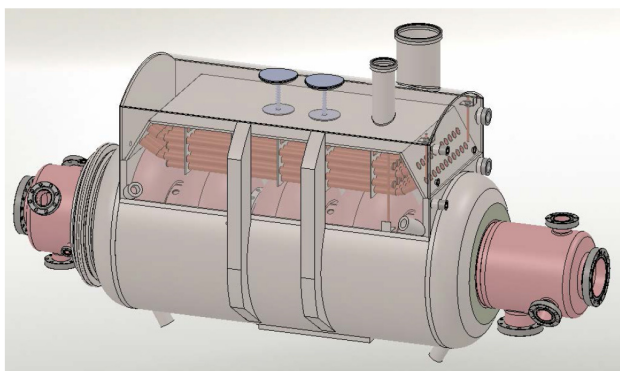


Figure 2: Layout of the 704 MHz cavity in a helium vessel.

Cavity Support

The support for the 5-cell cavity was designed in order to increase the natural frequency of the cavity in the helium vessel. The cavity is supported by three 1/8" Grade 5 titanium rods, symmetrically distributed around the beam axis. The support is located after the second

* Work is supported by Brookhaven Science Associates, LLC under contract No. DE-AC02-98CH10886 with the U.S. DOE.
#jcbrutus@bnl.gov

Copyright © 2013 CC-BY-3.0 and by the respective authors

ISBN 978-3-95450-138-0

MECHANICAL DESIGN OF 112 MHz SRF GUN FPC FOR CeC PoP EXPERIMENT*

J. C. Brutus#,1, S. Belomestnykh1,2, Y. Huang1,V. Litvinenko1,2, G. Mahler1, I. Pinayev1, J. Skaritka1, L. Snydstrup1, R. Than1, J. Tuozzolo1, Q. Wu1, T. Xin2
1) Brookhaven National Laboratory, Upton, NY 11973-5000, U.S.A.
2) Stony Brook University, Stony Brook, NY 11794, U.S.A.

Abstract

A Quarter-Wave Resonator (QWR) type SRF gun operating at 112 MHz will be used for Coherent Electron Cooling Proof of Principle (CeC PoP) system under development for the Relativistic Heavy Ion Collider (RHIC) at Brookhaven National Laboratory (BNL). The CeC PoP experiment will demonstrate the new technique of cooling proton and ion beams that may increase the beam luminosity in certain cases, by as much as tenfold. The 112 MHz cavity is designed to generate a 2 MeV, high charge (several nC), low repetition rate (78 kHz) electron beam using a new fundamental power coupler (FPC) design approach. Structural and thermal analysis, using ANSYS were performed to confirm the FPC structural stability and to calculate the deflection due to heat load from RF power generation. This paper provides an overview of the design, structural and thermal analysis, test results, and FPC tuning drive system for the 112 MHz gun.

INTRODUCTION

A 112 MHz superconducting quarter-wave resonator will be used as the injector for CeC PoP experiment under construction at IP2 of RHIC at BNL [1]. Phase I of this experiment is to be completed by the end of RHIC shutdown 2013 and will include the 112 MHz superconducting QWR and the fundamental power coupler that will be discussed in details in this paper. The paper provides an overview of the design, structural and thermal analysis, test results, and FPC tuning drive system for the 112 MHz gun.

112 MHZ FPC DESIGN AND FABRICATION

Design

The FPC is a coaxial structure, which provides tunable RF coupling and presents small interference to the electron beam output [2]. The FPC design couples the RF power into the cavity from the exit beam pipe of the cavity and allows the electron beam to travel through the hollow inner conductor of the FPC. An external linear motion system will be used to adjust the penetration of the coupling tube in order to fine tune the frequency of the cavity as well as to adjust the coupling strength [2]. The FPC was design to meet all the parameters listed in Table 1.

Table 1: Parameters of the Fundamental Power Coupler for 112 MHz QWR SRF gun

RF frequency	112 MHz
Frequency tuning range with FPC	3 kHz
FPC travel range	40 mm
Q_{ext} of FPC, min.	1.25×10^7
Max. RF power loss on the FPC inner conductor	898.6 W
Max. RF power loss on the FPC outer conductor	554.6 W
Available RF power	2 kW

The complete and detailed layout of the 112 MHz QWR and the FPC are shown in Figure 1 and Figure 2.

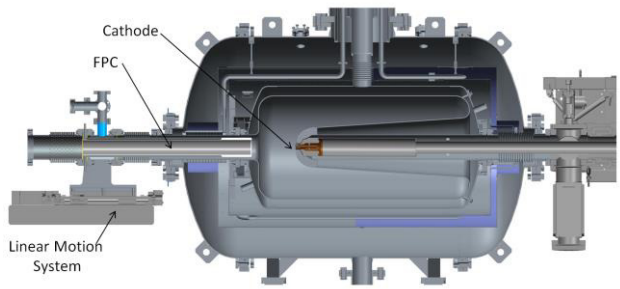


Figure 1: Layout of 112 MHz FPC in the QWR.

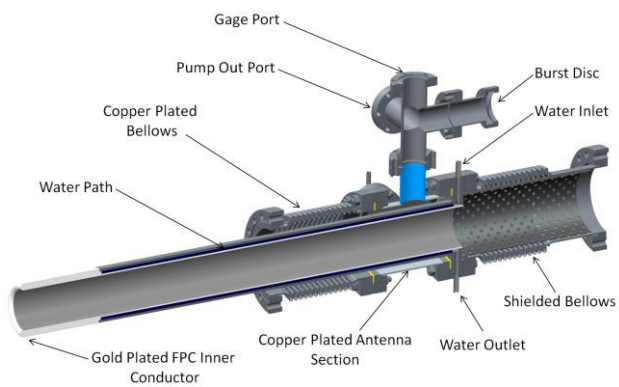


Figure 2: Detailed Layout of 112 MHz FPC.

In order to power the FPC, a BeCu connector was designed. The connector threads into the inner conductor of the FPC and slides inside an air cooled 7/16 UHF UHV cryogenic feedthrough designed by BNL. The FPC will be powered on both sides as shown in Figure 3.

* Work is supported by Brookhaven Science Associates, LLC under contract No. DE-AC02-98CH10886 with the U.S. DOE.
#jcbrutus@bnl.gov

Copyright © 2013 CC-BY-3.0 and by the respective authors

A TEMPERATURE-MAPPING SYSTEM FOR MULTI-CELL SRF ACCELERATING CAVITIES*

M. Ge, G. Hoffstaetter, F. Furuta, E. Smith, M. Liepe, S. Posen, H. Padamsee, D. Hartill, X. Mi,
Cornell University, Ithaca, NY 14850, USA.

Abstract

A Temperature mapping (T-map) system for Superconducting Radio Frequency (SRF) cavities consists of a thermometer array positioned precisely on an exterior cavity wall, capable of detecting small increases in temperature; therefore it is a powerful tool for research on the quality factor (Q_0) of SRF cavities. A new multi-cell T-mapping system has been developed at Cornell University. The system has nearly two thousand thermometers to cover 7-cell SRF cavities for Cornell's ERL project. A 1mK resolution of the temperature increase ΔT is achieved. A 9-cell cavity of TESLA geometry was tested with the T-map system.

INTRODUCTION

The quality factor (Q_0) of Superconducting Radio Frequency (SRF) cavities is a critical topic in the SRF field. High-Q cavities are able to save cryogenic capacities of accelerators. The definition of Q_0 is given by equation (1), where w is the angular frequency of the cavity, U is its stored energy, P_{loss} is the power loss on the cavity surface. The Q_0-value ranks the cavity's efficiency. If we define a geometry factor (G) as function (2), the Q_0 may be written as the ratio of the geometry factor and the surface resistance (R_s).

$$Q_0 = \frac{\omega U}{P_{loss}} = \frac{G}{R_s} \tag{1}$$

$$G = \frac{\omega\mu_0 \int_V \left|\vec{H}\right|^2 dV}{\int_A \left|\vec{H}\right|^2 dA} \tag{2}$$

The geometry factor is a constant determined by cavity geometry shapes, thus the Q_0 is dictated by cavity surface-resistance.

The T-map system, a thermometer array uniformly attached on a cavity exterior surface, is a powerful tool for surface resistance research. It is able to detect tiny heating on cavity wall during feeding RF power into cavity. Hence by the heating map of whole cavity, it is possible to calculate power loss and surface resistance, furthermore to calculate the Q_0-value of the cavity. The Q_0 of a multi-cell SRF cavity measured from RF is derived from the total value of all cells. The relationship between total Q_0 of a 9-cell cavity and Q_0-value of each cell at pi-mode is given by equation (3)

$$\frac{1}{Q_0^{tot}} = \frac{1}{n}\sum_{n=1}^{9} \frac{1}{Q_n^{cell}} \tag{3}$$

*This work has been supported by NSF award PHY-0969959 and DOE award DOE/SC00008431

Here Q_0^{tot} is total Q_0 of a 9-cell cavity, and Q_n^{tot} is Q_0 of cell n. The total Q_0 is unable to reflect which cell has low-Q and degrades the whole cavity. However, T-map can diagnose the Q_0-value of each cell by summing each cell's power loss. Hence T-map gives more information about cavity performance than RF measurement alone.

T-mapping history can be traced back to the 1980s. Cornell University was a pioneer in developing a 1-cell T-map system for 1.5GHz SRF cavity research [1, 2, and 3]. Now Jefferson Lab and Fermilab also have 1-cell or 2-cell T-map systems. These systems are used for fundamental SRF research via single-cell cavities. Therefore the development of a multi-cell T-mapping system is necessary and ultra-important. DESY and Los Alamos have multi-cell T-mapping systems for ILC 9-cell cavities [4, 5]. Those systems are mainly used to detect quench location.

TEMPERATURE-MAPPING SYSTEM DESCRIPTION

This multi-cell T-mapping system has been developed for the Cornell ERL project which requires the Q_0-value of 7-cell cavities to achieve 2×10^{10} at accelerating gradient 16MV/m [6]. For a 1.3GHz SRF cavity, the heating from RF causes on average about a 10mK temperature rise on the exterior wall at 25MV/m in a 2K helium bath [7]. Thus the resolution of this T-map is required to be approximately 1mK.

Thermometers and Boards

The Cornell multi-cell T-map has nearly two thousand thermometers. The temperature sensor is a 100Ω carbon Allen-Bradley resistor (5% 1/8 W). Carbon is a semiconductor, its resistance increases exponentially when temperature drops. Figure 1 (a) shows the schematic of sensor and its picture. APIEZON grease was applied on the varnished side of the thermometers prior to inserting the boards in cages. The sensor is able to detect the temperature rise of the cavity wall with 25% efficiency [3]. Two sets of 3-cell boards and one set of 1-cell boards were used for 7-cell SRF cavity. A 3-cell board has two channels addressed to the sensors for 3-cells. The sensor boards are spaced azimuthally every 15° around the cavity; totally it has 24 boards around the azimuth. Each cell is covered by an 11×24 thermometer array. Figure 1 (b) shows a 3-cell and a 1-cell board. The quantity of thermometers for the whole 7-cell cavity is 1848. Cornell constructed a new test insert for hanging the multi-cell cavity with full T-map. In Figure 1 (c) the left image shows the Cornell multi-cell T-map attached on middle 7-cells of a 1.3GHz 9-cell cavity; the right image is a picture showing several boards removed to expose the cavity. The

Copyright © 2013 CC-BY-3.0 and by the respective authors

ISBN 978-3-95450-138-0

INVESTIGATION OF THE SURFACE RESISTIVITY OF SRF CAVITIES VIA THE HEAT AND SRIMP PROGRAM AS WELL AS THE MULTI-CELL T-MAP SYSTEM*

M. Ge#, F. Furuta, D. Gonnella, G.H. Hoffstaetter, M, Liepe, H. Padamsee,
Cornell University, Ithaca, NY, 14853, USA

Abstract

The thermal feedback model with the linear BCS resistance which were believed not strong enough to explain medium-field Q-slope (MFQS) is still valid. The HEAT and SRIMP program (H&S program) which adopted the SRIMP code for BCS resistance calculation allows inputting full material parameters, hence is able to simulate different cavity cases e.g. baked, unbaked, BCP'd, EP'd, and so on. The results agree with the measurement data from the low-field up to the hot-spots onset field. With the T-map data, it's a clear view that the localized hot-spots occur above MFQS region and caused high-field Q-slope.

INTRODUCTION

The surface resistance of superconductor under RF field is a critical topic, because it determines the Q-value of SRF cavity in accelerating fields. The thermal feedback model with the linear BCS resistance was developed for Medium-Field Q-Slope (MFQS) study [1]. However, the thermal feedback model was believed not strong enough to account for the observed MFQS [1, 2, and 3]. In this work, we explain the thermal feedback model with linear BCS model is still valid for MFQS and the localized hot-spots cause the Q-slope in high fields.

HEAT AND SRIMP PROGRAM

The surface resistance of superconductor under RF field includes two parts, one is BCS resistance (R_{BCS}) and the other is residual resistance (R_0), shown in equation (1). And equation (2) is the simplified R_{BCS} forms.

$$R_s = R_{BCS} + R_0 \quad (1)$$

$$R_{BCS} = A\left(\frac{1}{T}\right) f^2 \exp\left(-\frac{\Delta}{kT}\right) \quad (2)$$

Here, the factor A is a constant which determined by material property such as mean free path (l) *etc.*, Δ is the energy gap, f is the frequency.

The traditional HEAT program [4] uses Pippard approximation [5]:

$$R_{BCS}(T) = (2.78\times10^{-5}\Omega)\frac{\nu^2}{t}\left(\frac{148t}{\nu}\right)\exp\left[-\frac{1.81g(t)}{t}\right] \quad (3)$$

$$t = \frac{T}{T_c}, \quad \nu = \frac{f}{2.86GHz}, \quad g(t) = \left[\cos\left(\frac{\pi t^2}{2}\right)\right]^{1/2} \quad (4)$$

where f is the frequency of the RF field, T is the temperature. However in equation (3) and (4), it doesn't consider the Nb property. Comparison between baked and un-baked cases, the mean free path l is reduced by baking. Hence the factor A in equation (2) is changed and decreases the BCS resistance after baking. But equation (3) and (4) are unable to reflect the changes.

The improved HEAT program, HEAT and SRIMP code (H&S code), uses SRIMP [6, 7] to replace the equation (3) and (4). The SRIMP was written by Jurgen Halbritter for the BCS surface resistance calculation. The method of calculation incorporates the full BCS theory. Five material parameters are required to describe the superconductor:

- The superconducting transition temperature T_c;
- The energy gap (entered as Δ/kT);
- The London penetration depth, λ at T=0;
- The coherence length, ξ at T=0;
- The electron mean free path, l, at 4.2K.

MULTI-CELL T-MAP SYSTEM

The T-map system is known as a powerful tool for surface resistance research. It's able to detect tiny heating on exterior wall on cavities. Cornell University developed a multi-cell T-map system [8].

SURFACE RESISTANCE ANALYSIS

The EP'd and BCP'd Cavity Cases

Figure 1 is the comparison Q vs. E curves between H&S program calculation and RF measurement from 1.7 to 2K. The plot shows the calculation agrees with the measurement results well. The cavity is TELSA single-cell cavity NR1-3. The cavity was EP'd and 120°C baked. During the test, the cavity was FE and quench free.

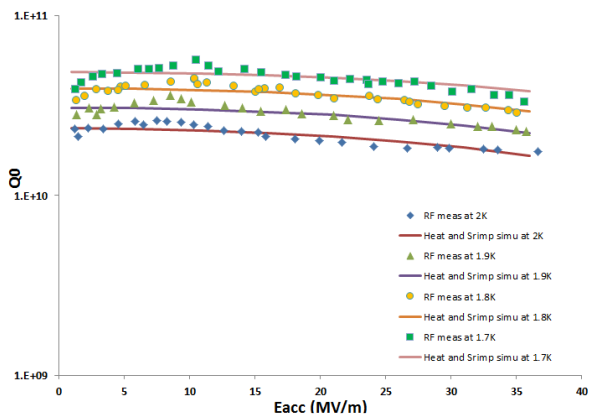


Figure 1: Comparison of H&S calculation and RF measurement at different temperatures for EP'd cavity.

*Work supported by NSF award PHY-0969959 and DOE award DOE/SC00008431
#mg574@cornell.edu

Copyright © 2013 CC-BY-3.0 and by the respective authors

CORNELL'S MAIN LINAC CRYO-MODULE PROTOTYPE

Ralf Eichhorn#, Yun He, Georg H. Hoffstaetter, Matthias Liepe, Tim O'Connel, Peter Quigley, Daniel Sabol, James Sears, Eric Smith, Vadim Veshcherevich
Cornell Laboratory for Accelerator-based Science and Education (CLASSE), Cornell University, Ithaca, NY 14853, USA

Abstract

In preparation for building an energy-recovery linac (ERL) based synchrotron-light facility at Cornell University which can provide greatly improved X-ray beams due to the high electron-beam quality that is available from a linac, a phase 1 R&D program was launched, addressing critical challenges in the design. One of them being a full linac cryo-module, housing 6 superconducting cavities operated at 1.8 K in continuous wave mode, 7 HOM absorbers and 1 magnet/ BPM section. The final design will be presented and a report on the fabrication status that started in late 2012 will be given.

INTRODUCTION

An NSF funded R&D program for the 5-GeV superconducting energy-recovery linac (ERL) [1] at Cornell University includes the design, build and thoroughly test all aspects of a complete cryomodule.

The almost 10 m long module (see Fig. 1) houses 6 superconducting cavities, operated in CW mode at 1.8 K. These 7-cells, 1.3 GHz cavities with an envisaged Q of $2*10^{10}$ will provide an energy gain of 16 MV/m. Each cavity is fed by a 5 kW power coupler. The Higher Order Modes (HOMs) absorbers are placed next to each cavity to obtain an efficient damping for the high beam current and short bunch operation. The series linac module will have a quadrupole/ steerer section which is omitted in the prototype as it technically does not present a challenge.

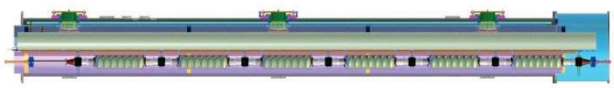


Figure 1: Cryomodule prototype.

COLD MASS SUPPORT SYSTEM

The beam-line string is suspended under the Helium Gas Return Pipe (HGRP) which acts as the beam-line backbone and is supported by three support posts to the vacuum vessel (see Fig. 2). The support system provides precision alignment and thermal insulation of the beamline string.

The HGRP is made of a Grade 2 Titanium pipe, with an outer diameter of 280 mm. With a 1 ton weight force of the beamline string, the maximum vertical displacement of the HGRP is estimated to be 0.1 mm and the natural frequency would be 88 Hz, indicating that a 3-posts support system is well suited to ensure an acceptable vertical displacement and vibration characteristics.

#r.eichhorn@cornell.edu

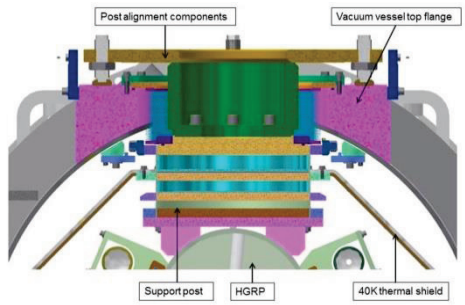


Figure 2: Cold mass support system.

The post has a same design as those used in the TTF cryomodule, which is an assembly of a low thermal conduction composite material pipe (G10 fiberglass pipe) and four stages of shrink-fit metal discs and rings. The two stainless steel disc/ring sets are connected respectively to the room temperature and to the 2 K cold mass environments. The two aluminum disc/ring sets provide thermal intercepts at 40 K and 5 K, with the 40 K set also providing structural support to the 40 K thermal shield. The heat load through conduction of each post (see Fig. 3) is estimated to be 8.58W to 40K, 0.54W to 5K and 0.05 W to 1.8K, respectively.

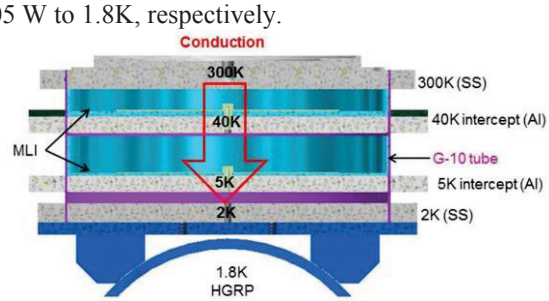


Figure 3: Support post.

The vacuum vessel is 965.2 mm in diameter, with a vessel cylinder made of carbon steel (A516 GR70) and stainless steel flanges that use O-ring seals. For the prototype the interior of the carbon steel portion will be painted with a low vapor pressure vacuum compatible epoxy, while the exterior will be painted with a marine paint product.

CYOGENIC PIPING SYSTEM

The cavities will be cooled by liquid helium sub-cooled to 1.8 K. Due to the fact that the half linac will be 350 m long, a big aperture (280 mm diameter) for the HGRP was chosen to provide the low flow impedance needed without excessive pressure drop. Connected to the HGRP at a single point in each module is a 100 mm diameter 2-phase helium manifold, show in Fig. 4. The purpose of this large 2-phase tube is to allow adequate surface area

Copyright © 2013 CC-BY-3.0 and by the respective authors

ISBN 978-3-95450-138-0

THEORETICAL DESCRIPTION OF SIS MULTILAYER FILMS FOR SRF CAVITIES*

Sam Posen[1†], Gianluigi Catelani[2], Matthias U. Liepe[1], James P. Sethna[3], and Mark K. Transtrum[4]
[1]Cornell Laboratory for Accelerator-Based Sciences and Education, Ithaca, NY, USA
[2]Forschungszentrum Jülich Peter Grünberg Institut (PGI-2), Jülich, Germany
[3]LASSP, Physics Department, Clark Hall, Cornell University, Ithaca, NY, USA
[4] Department of Bioinformatics and Computational Biology,
University of Texas M. D. Anderson Cancer Center, Houston, Texas, USA

Abstract

The SIS structure—a thin superconducting film on a bulk superconductor separated by a thin insulating film—was propsed as a method to protect alternative SRF materials from flux penetration by enhancing the first critical field B_{c1}. In this work, we calculate the gibbs free energy of a vortex in a superconductor, and we show that an isolated thin film can enhance B_{c1}, but when it is placed in a SIS structure, due to the gradient in field across the film, we show that in fact B_{c1} = 0. We argue that the SIS structure is not beneficial for SRF cavities, but it may be useful in DC and low frequency applications. However, due to recent experiments showing low-surface-resistance performance above B_{c1} in cavities made of superconductors with small coherence lengths, we argue that enhancement of B_{c1} is not necessary, and that bulk films of alternative materials show great promise.

INTRODUCTION

SRF researchers have begun a significant effort to develop alternative materials to niobium, superconductors that could offer higher accelerating gradients E_{acc} and/or lower surface resistances R_s at a given temperature. There are several promising candidates, but most of them suffer from two potential liabilities. First, they have relatively small first critical fields B_{c1}, the magnetic field at which it becomes energetically favorable for a vortex to be inside the superconductor. Second, they have relatively small coherence lengths ξ. Vortex penetration is prevented at fields significantly above B_{c1} by an energy barrier, but surface defects on the order of ξ can reduce this barrier. These materials have ξ on the order of a few nm, compared to tens of nm for niobium, making even very small defects a potential vulnerability. As a result, there has been significant concern in the SRF community over whether vortex dissipation will occur if these materials are exposed to fields that bring them into the metastable state between B_{c1} and B_{sh}, the superheating field at which the energy barrier is reduced to zero for an ideal surface.

A. Gurevich proposed [1] a method to avoid the potentially vulnerable metastable state altogether. Pointing to the enhancement of parallel B_{c1} in films with thickness d smaller than the penetration depth λ, he suggested coating a niobium cavity with alternating layers of insulator (I) and thin film superconductor (S). With such a SIS structure, he proposed it might be possible to take advantage of the high B_{sh} and low R_s of the alternative superconductors used in the thin films without the disadvantage of their small B_{c1}. SRF researchers have been putting significant effort into developing SIS multilayers, and they are producing excellent work [2, 3, 4, 5, 6, 7, 8].

CALCULATING BC1

Tinkham [9] defines B_{c1} as the field at which "the Gibbs free energy [has] the same value whether the first vortex is in or out of the sample." For a SIS, the sample under consideration should be the full structure [10]. Stejic et al. [11] calculate the Gibbs free energy of a vortex in a thin film superconductor immersed in a parallel external field. They show that B_{c1} of the film is enhanced relative to the bulk value, according to

$$B_{c1} = \frac{2\phi_0}{\pi d^2}\left(\ln\frac{d}{\xi} + \gamma\right) \quad (1)$$

where ϕ_0 is the flux quantum, $\gamma = -0.07$ and $d << \lambda$. However, if a SIS structure is used to screen Nb SRF cavities, the geometry is quite different than that of an isolated film. How does Stejic's expression for B_{c1} change when the film is screening a bulk superconductor? In this case, it will have a B-field gradient across it, which will affect the free energy. We can use the same formalism as Stejic to calculate the Gibbs free energy for this case, and use it to find B_{c1} and B_{sh}[12].

Consider a single layer SIS structure, as shown in Fig. 1. A strongly type II superconducting film of thickness d, penetration depth λ_f, and coherence length ξ_f is separated from a bulk superconductor with with penetration depth λ_b by an insulating film of thickness δ. The superconducting film is screening the bulk from a parallel magnetic field with amplitude B_0. The screened field inside the bulk region has amplitude B_i. In our geometry, the x-axis is perpendicular to the film, pointing into it, with origin at the interface with the exterior. The z-axis is aligned with the magnetic field.

* Work supported by DOE award number DE-SC0002329 and in part by the EU under REA grant agreement CIG-618258.
† sep93@cornell.edu

Copyright © 2013 CC-BY-3.0 and by the respective authors

ACHIEVING HIGH ACCURACY IN CORNELL'S ERL CAVITY PRODUCTION

R. Eichhorn#, B. Bullock, B. Clasby, J. Kaufman, J. Sears, V. Shemelin,
Cornell Laboratory for Accelerator-Based Sciences and Education, Cornell University,
Ithaca, NY 14853-5001, USA
B. Kilpatrick, Kutztown University of Pennsylvania
T. Kuerzeder, TU Darmstadt, Institut fuer Kernphysik, D-64291 Darmstadt, Germany

Abstract

The phase 1 R&D program launched in preparation to building a 5 GeV Energy Recovery Linac (ERL) at Cornell, a full main linac cryomodule is currently built, housing six 7-cell cavities. In order to control the beam break-up limit, the shape of the cavity was highly optimized and stringent tolerances on the cavity production were targeted. We will report on the details of the cavity production, the accuracy of the cups forming the individual cells, the trimming procedure for the dumbbells, the cavity tuning and final accuracy of the cavity concerning field flatness, resonant frequency and overall length within this small series production.

INTRODUCTION

Six Cornell ERL 7-cell cavities will be connected in each cryomodule in the full LINAC. Between each cavity there are bellows and HOM absorbers. Therefore a tight tolerance of +/- 0.5mm must be applied to the length of each cavity (see Table 1). Unfortunately, due to space restrictions in Cornell's electron-beam welder, the beam tubes must be welded to the cavity before the final equator weld, which does not allow the cavity to be trimmed to its final length. Therefore, the cavity length must be controlled through other means.

Table 1: Length and Frequency Tolerances

Length (mm)	1160	+/- 1
Frequency (MHz)	1298.985	+/- 0.100

The first series production of three unstiffened ERL cavities at Cornell was completed some time ago. Each of the cavities did not meet the length or frequency tolerance. The results of the production can be seen in (Table 2). Each cavity was long, as well as low in frequency. Adjusting the frequency through the use of tuning served only to lengthen the cavities even further. In an effort to avoid a situation such as this in the second production series of three stiffened cavities, the previous production steps were analysed and a new strategy was formed.

#r.eichhorn@cornell.edu

Table 2: Length and Frequency of Production Cavities

Pre-Tuning

	Length (mm)	Frequency (MHz)
ERL7-002	1161	1298.46
ERL7-003	1161.5	1298.459
ERL7-004	1160.7	1298.498

Post-Tuning

	Length (mm)	Frequency (MHz)
ERL7-002	1165.9	1297.462
ERL7-003	1163.9	1297.504
ERL7-004	1162.1	1297.541

RF AND MECHANICAL TOLERANCES AND GRADIENTS

The half-cell contour was designed using FEM to calculate the correct resonant frequency at 1.8 K under vacuum. The room temperature frequency at STP is then extrapolated from this calculation.

The half-cell contour, when combined with the end-groups, drives the overall cavity length. However, several manufacturing and processing steps can have an effect on either length, frequency, or both. For example, etching the cavity will drive the frequency of the cavity down, but has no consequence on the overall length. However, field flatness tuning can be used to adjust the frequency of the cavity while simultaneously changing the overall length of the cavity.

It is important to know how each process will affect both the frequency and length of a cavity. To do so, each process' "gradient" must be known. For example, the tuning gradient is 430 kHz/mm. This means tuning the cavity will change its frequency by 430 kHz for every on millimetre. Other gradients are shown in Table 3.

The trimming gradient is, perhaps, the most salient variable during production. This gradient was calculated

Table 3: Various Manufacturing Gradients

Dumbbell Trimming	5	kHz/µm
Etching	10	kHz/µm
Tuning	430	kHz/mm

Copyright © 2013 CC-BY-3.0 and by the respective authors

ISBN 978-3-95450-138-0

STUDIES OF THE SUPERCONDUCTING TRAVELLING WAVE CAVITY FOR HIGH GRADIENT LINAC*

Pavel Avrakhov#, Roman Kostin, Alexei Kanareykin (Euclid TechLabs, LLC, Solon, Ohio), Nikolay Solyak, Vyacheslav P. Yakovlev (Fermilab, Batavia)

Abstract

Use of a travelling wave (TW) accelerating structure with a small phase advance per cell instead of standing wave may provide a significant increase of accelerating gradient in a superconducting linear accelerator. The TW section achieves an accelerating gradient 1.2-1.4 larger than TESLA-shaped standing wave cavities for the same surface electric and magnetic fields [1]. Recent tests of an L-band single-cell cavity with a waveguide feedback [2] demonstrated an accelerating gradient comparable to the gradient in a single-cell ILC-type cavity from the same manufacturer. This article presents the next stage of the 3-cell TW resonance ring development which will be tested in the travelling wave regime. The main simulation results of the microphonics and Lorentz Force Detuning (LFD) are also considered.

INTRODUCTION

The primary advantage of a superconducting travelling wave accelerating (STWA) structure is an increased accelerating gradient up to a factor 1.24 for the same surface magnetic and electric field ratios E_{peak}/E_{acc} and B_{peak}/E_{acc} as for re-entrant [3] standing wave (SW) ILC [4] cavity. However, the TW regime for a high gradient linac requires too high level of RF power flux in the accelerating structure. Typical pulse power for L-band TW linac is a few hundred MW which is 10^3 times more than feeding power for superconducting SW cavities. Concept of the traveling wave resonator with a superconducting TW structure allows to keep pulse power on a reasonable low level

Figure 1 presents the first developed and tested 1.3 GHz prototype of a travelling wave SC resonator which consists of a single-cell cavity and a waveguide (WG) feedback [2]. The 1-cell model has the same shape as a regular full-sized cavity, which helped to understand the problems with mechanical manufacturing, assembly, and welding of this geometry as well as the surface processing issues.

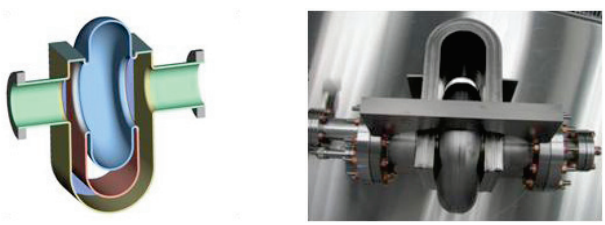


Figure 1: The single-cell model of a travelling wave cavity with waveguide loop.

Two single cell resonators were manufactured at Advanced Energy System, Inc. (AES) and processed in Argonne and Fermi National Labs. Despite the fact that the STWR processing was without electropolishing, high gradient tests showed that the surface electric and magnetic fields reached the same values as 31 MV/m of TESLA-shaped cavity with no field emission. There were problems with the waveguide processing such as high pressure rinsing. But these problems did not lead to quenching in the waveguide because the surface electric and magnetic field amplitudes in the feedback loop were 2-3 times less than in the accelerating cavity. It should be noted the 1-cell STWR model could be tested only in SW regime.

The next step in SC TW cavity studies will be developing and manufacturing a multicell cavity and testing it in the travelling wave regime.

A NEW 3-CELL SC TW RESONATOR DESIGN STUDIES

According to plan, a new 3-cell TW cavity design (schematically depicted in Figure 2) was developed [5] and now is prepared for fabrication. In spite of the fact that the 3-cell structure has only one regular cell (in the middle of the cavity), it retains the same field distribution as for the full-sized 1 meter, 15-cell pattern.

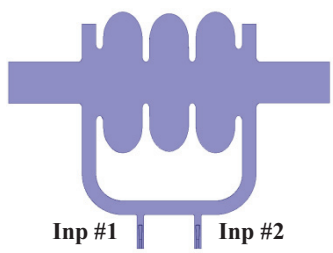


Figure 2: Traveling wave resonator with 3-cell TWaccelerating structure and two coaxial couplers.

As a standard for SC accelerating structure research it is testing on vertical test stand (VTS). Low level RF source of about 200-300 W at VTS requires the use of superconducting cavities with a high loaded quality factor Q_{load} of about 10^8. Well known problems for the SC high Q_{load} resonators are microphonics and Lorentz force detuning at the high gradient testing. But the TW structure detuning has specific feature when compared with the SW cavity - the degradation of the travelling wave regime. Unfortunately, TW operation cannot be restored only by frequency tuning as in the superconducting SW structure. Figure 3 illustrates

*Work supported by US Department of Energy
p.avrakhov@euclidtechlabs.com

Copyright © 2013 CC-BY-3.0 and by the respective authors

STUDY ON PARTICULATE RETENTION ON POLISHED NIOBIUM SURFACES AFTER BCP ETCHING*

I. Malloch#, C. Compton, L. Popielarski, Facility for Rare Isotope Beams (FRIB), Michigan State University, East Lansing, MI 48824, USA

Abstract

Niobium surface defects and inclusions can be introduced during the manufacturing processes used in the production of SRF cavities. Bulk removal methods (sanding, polishing, etc...) are frequently utilized to remove or smooth away these defects on the surface of the niobium metal. It is hypothesized that these mechanical removal methods are capable of trapping performance-degrading particulates, which are then exposed during subsequent chemical processing, potentially contaminating the cavity prior to RF testing. This paper summarizes results of a series of surface roughness and etching experiments performed to determine the relationship between the extent of polishing and trapped particulate, and to determine a method for mitigating this particulate contamination through BCP etching. The relationship between these experiments and RF cavity performance will be explored as well.

INTRODUCTION

The construction of the Facility for Rare Isotope Beams (FRIB) driver linac will require more than 350 niobium superconducting radio frequency (SRF) cavities. Four types of cavities will be used in the linac: 80.5 MHz β = 0.041 and β = 0.085 quarter-wave resonators, and 322 MHz β = 0.29 and β = 0.53 half wave resonators. Each of these cavities must be fabricated with utmost precision to ensure proper functionality of the cavities during RF testing and during the operation of the completed accelerator. Of the many critical aspects of these RF cavities, the surface finish of the niobium exposed to RF fields is paramount to the proper functionality of these cavities during testing. Unfortunately, despite the best of intentions and the most well-defined procedures and quality assurance protocols, issues can arise that compromise these niobium surfaces. Weld spatter deposited on the niobium during electron-beam welding of cavity components, foreign debris and inclusions imbedded in the niobium during sheet rolling or part stamping, and gouges or scratches occurring due to mishandling or machining errors can all impact the quality of the cavity surface [1]. Fortunately, these defects can frequently be fixed by means of mechanical abrasion. While these repairs are necessary, unfortunately, the use of abrasive media to repair the niobium surface can cause lasting degradation of the surface finish, and, as a result, potential degradation of cavity performance due to particulate contamination on the cavity surface. This study seeks to examine the lasting impact of these repairs, and to determine a method for mitigating the consequences by means of processing and analyzing a series of niobium samples.

EXPERIMENTAL

Two lots of niobium samples were used in this experiment. Each lot consisted of a series of small grain, high-RRR (>250), 3 mm thick sheet stock samples, shear-cut to approximately 2.5 cm square. Each sample was stamped with a serial number, photographed, degreased with acetone, ultrasonic cleaned, and precision measured for thickness (±0.0025 mm) with an NDT Systems Model TG900 ultrasonic thickness gauge.

As is typically performed with RF cavities, following cleaning, the samples were chemically etched with a standard solution of buffered chemical polish (BCP). The BCP mixture used at FRIB is a 1:1:2 mixture of concentrated hydrofluoric (49% w/w), nitric (70% w/w), and phosphoric (85% w/w) acids. The first lot of samples was divided into eight sub-lots. The sub-lots were each submerged in BCP and etched for between 60 and 480 minutes, removing up to 300 microns of niobium from the surface of the samples. Upon completion of the etching, the samples were thoroughly rinsed with ultrapure water (UPW) and set to dry in an ISO 5 cleanroom. Once dry, the surface roughness (both R_a and R_z) at six different locations on each sample was measured with a Fowler 54-410-500 X-Pro Portable Surface Roughness Tester.

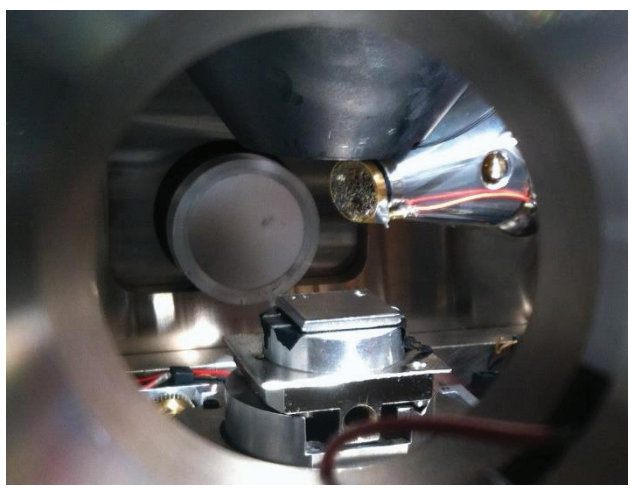


Figure 1: A niobium sample on the microscope stage as seen through the SEM's vacuum viewport.

To simulate a portion of an RF cavity repaired with an abrasive media, the second lot of samples was "polished"

* This material is based upon work supported by the U.S. Department of Energy Office of Science under Cooperative Agreement DE-SC0000661, The State of Michigan, and Michigan State University

malloch@frib.msu.edu

Copyright © 2013 CC-BY-3.0 and by the respective authors

ISBN 978-3-95450-138-0

SRF CAVITY ETCHING DEVELOPMENTS FOR FRIB CAVITY PROCESSING*

K. Elliott#, I. Malloch, L. Popielarski, N. Putman, Facility for Rare Isotope Beams (FRIB), Michigan State University, East Lansing, MI 48824, USA

Abstract

Updates to the FRIB beta=0.53 half wave resonator (HWR) design have provided an opportunity to test new buffered chemical polish (BCP) flow control techniques. New processing fixtures have been fabricated and used to process the FRIB beta=0.53 HWR. This paper will present details of the fixture mechanical design iterations, the resulting BCP flow simulations, a qualitative evaluation of the agreement between simulations and measured results, and developments in process validation techniques.

INTRODUCTION

Buffered chemical polish (BCP) processing techniques continue to progress with the FRIB β=0.53 half wave resonator (HWR) cavity. With the updated cavity design we were able to use new fixturing concepts and take a variety of measurements to better understand the processing parameters. The new β=0.53 HWR cavity has an internal volume of 76 L, and an internal surface area of 1.4 m^2.

The objectives for the design of the new chemistry fixtures were to reduce fixture complexity, reduce fixture installation time, and increase the etch uniformity.

FIXTURE DESIGN

Twelve different configurations were analyzed to determine the best concept for achieving uniform etch removal. Seven of the configurations were a derivative of the directional quill injection system used on the previous β=0.53 HWR cavity [1]. The other five configurations consisted of a single directional quill. Ultimately the single directional quill was chosen. The analysis of the single directional quill, and the four injection quill design, can be seen in Figure 1.

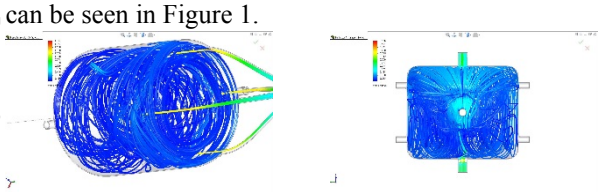


Figure 1: Left, analysis of four quill injection system. Right, analysis of single quill injection system.

* This material is based upon work supported by the U.S. Department of Energy Office of Science under Cooperative Agreement DE-SC0000661

#Elliott@FRIB.MSU.EDU

The single quill configuration shown in Figure 2 was chosen because it appeared to deliver equivalent mixing of the BCP compared to the four quill configuration, while reducing the complexity of the BCP delivery plumbing. The quality of the BCP mixing is determined qualitatively by choosing the fixture concept which produces the least velocity variation across the superconducting surface of the cavity.

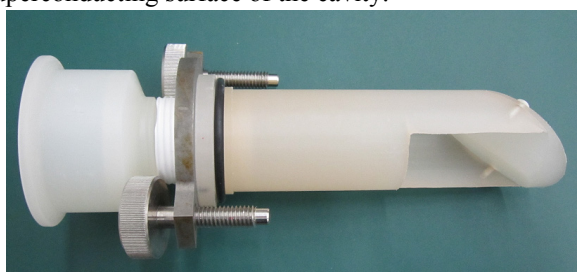


Figure 2: Single injection quill used for FRIB β=0.53 HWR cavity BCP processing.

One of the stated goals of this fixture iteration was to reduce installation time. This was done in two ways. First, the force needed to make the o-ring seal on each flange was carefully examined and revised. Second, we attempted to eliminate the need for tools during the fixture installation.

Past chemistry flanges were designed with a hole pattern to match the mating flange on the cavity. For example, one of the 2.75" ConFlat flanges of the prototype β=0.53 HWR cavity had six ¼" clearance holes (See Figure 3). Once the fasteners are were tightened there was nearly 12,000 lbs of force on the flange, though it is not known what portion of that force was transmitted to the o-ring.

O-ring Analysis

The Parker Hannifin o-ring handbook [2] indicates that only 20-30% compression is necessary to make a static o-ring seal. Given the o-ring hardness, thickness, and desired percent compression, the Parker Hannifin o-ring handbook indicates that 10-20 lbs of force per linear inch of o-ring is required to make a reliable seal. This means that only 300 lbs of force is needed for this seal.

A stainless steel backing plate was added to each flange to ensure that the tension from the fasteners was evenly distributed to the o-ring and, the number of fasteners was reduce from six to two. Because a well lubricated 1/4" fastener requires only 7.5 in*lbs of torque to produce 150 lbs of tension (half of the required 300 lbs), thumb screws

Copyright © 2013 CC-BY-3.0 and by the respective authors

MAGNETIC SHIELD OPTIMIZATION FOR THE FRIB SUPERCONDUCTING QUARTER-WAVE RESONATOR CRYOMODULE*

Y. Xu#, A. Fox, M. Johnson, M. Leitner, S. Miller, K. Saito, FRIB, East Lansing, MI 48824, USA

Abstract

The Facility for Rare Isotope Beams (FRIB) required 49 cryomodules containing 330 superconducting low-beta resonators, which have to be shielded from the earth magnetic field. Comprehensive magnetic shielding simulations have been conducted for 80.5 MHz β=0.085 cryomodules exposed to earth fields of 0.5 Gauss in different coordinate directions. The magnetic shield has to attenuate the earth magnetic field by a minimum factor of 33 (to less than 15 milli Gauss) in order to limit flux trapping in the resonators during cool-down. In the reported optimization studies, permeability of the magnetic shielding material, shield thickness, and number of magnetic shield layers have been varied. Different design concepts including global and local magnetic shielding have been evaluated. In addition, the design concepts are compared based on the cost of material, fabrication and assembly, the design complexity and compatibility with the overall cryomodule design to obtain an optimum solution.

INTRODUCTION

There are 49 cryomodules that will be built in FRIB: three 80.5 MHz β=0.041 cryomodules, eleven 80.5 MHz β=0.085 cryomodules, two 80.5 MHz β=0.085 matching cryomodules, twelve 322 MHz β=0.29 cryomodules, two 322 MHz β=0.29 matching cryomodules, eighteen 322 MHz β=0.53 cryomodules, and one 322 MHz β=0.53 matching cryomodule.

All cryomodules have to be shielded to attenuate the earth magnetic field in order to limit flux trapping in the cavities during cool-down to less than 15 milli Gauss. Two main different design concepts, room temperature global and low temperature local magnetic shielding as shown in Figure 1, have been compared on 80.5 MHz β=0.085 cryomodule from the attenuation ability, cost of material, fabrication and assembly, to the design and assembly complexity. The global magnetic shield locates between the vacuum vessel and the thermal shield and encompasses the entirety of cold mass, while the local magnetic shield is assembled around the resonators. Two local magnetic shielding designs are compared. One is to shield each resonator with individual shield, the other is to group the nearby resonators as much as possible.

ANSYS Magnetostatic is implemented to study the effects of permeability of material, size of magnetic shield, and the contribution from steel vacuum vessel. The magnetic flux on resonators is obtained to validate the effectiveness of the magnetic shield designs. Finally, Quality Function Deployment (QFD) is applied to compare different design concepts.

*Work supported by US DOE Cooperative Agreement DE-SC0000661
#xut@frib.msu.edu

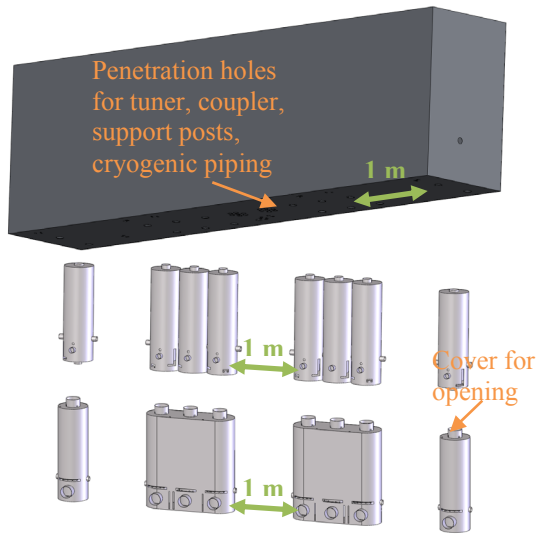


Figure 1: Global shield (top) and local single shield (middle) and local multi shield (bottom).

PERMEABILITY STUDY

The design of the magnetic shield starts with the proper material selection. Magnetic shielding materials should be chosen for their characteristic, usually in respect to permeability and saturation.

Manufacture Data

Amuneal Manufacturing Corporation compares the permeability of two products, Cryoperm 10 and Amumetal, as a function of ambient temperature shown in Figure 2 [1]. Amumetal has the maximum permeability at room temperature and is degraded at cryogenic temperature. Therefore, it is appropriate for the room temperature global magnetic shield. The permeability of Cryoperm 10 reaches its maximum at very low temperature (around 30 K) but is degraded at room temperature. Hence, it is proper for the low temperature local magnetic shield.

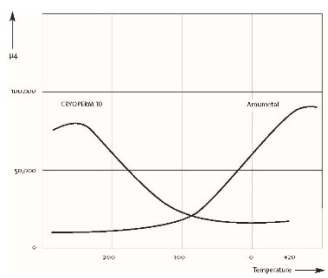


Figure 2: Permeability of Amumetal and Cryoperm 10 versus ambient temperature.

Recently, Amuneal developed a new shielding material Amuneal 4K (A4K) for cryogenic applications. A4K is

Copyright © 2013 CC-BY-3.0 and by the respective authors

ISBN 978-3-95450-138-0

TUNING PROCESS OF SSR1 CAVITY FOR PROJECT X AT FNAL*

P. Berrutti, M. Awida, T. Khabiboulline, D. Passarelli, L. Ristori, V. Yakovlev
Fermilab, Batavia, IL 60510, USA

Abstract

SSR1 is a family of single spoke resonators to be used in Project X at Fermi National Laboratory. These cavities operate in CW regime having nominal frequency of 325 MHz and optimal beta of 0.22. SSR1 cavities will accelerate H- ions after the Half Wave Resonator (HWR) section from 9 MeV to 32 MeV. In the near future this cavity will be used in Project X Injector Experiment (PXIE), which contains the ion source, the LEBT, the MEBT, the RFQ of Project X, and a cryogenic temperature section, having one HWR and one SSR1 cryomodule. SSR1 cavities have been built and tested at FNAL, the preparation of these resonators includes RF tuning which is the main focus of this paper. The frequency of the cavity is carefully chosen prior to the vertical test, and it is adjusted before welding the helium vessel to obtain 325 MHz nominal frequency for the dressed cavity in operating conditions. Several SSR1 cavities have been tuned at FNAL, the procedure, the hardware and the data are presented.

INTRODUCTION

SSR1 cavities have been built and tested at Fermilab [1] [2]. During cavity production it is necessary to set frequency goals throughout the entire process, to match the final target frequency of 325 MHz for a cold jacketed SSR1. After assembling and welding of the niobium, the cavity arrives at Fermilab and undergoes several quality control steps: visual inspection, CMM measurements, RF QC and leak check. The frequency is monitored throughout the entire cavity processing; when the cavity is received from the vendor several measurements are taken: fundamental frequency, high order modes frequencies, and field flatness. SSR1 cavity processing includes baking at high and low temperature and chemical polishing, bulk and light BCP. The leak check and the chemical processing are two main causes of frequency shifts. During the first vacuum check the cavity geometry is deformed by the atmospheric pressure, which shrinks the structure inducing permanent plastic deformations, even though very small. The average Δf for SSR1 due to the leak check is -80 kHz. The bulk BCP removes 150 µm in average from the cavity surface, while the light chemical processing results in 30 µm material removal. The Δf produced by the bulk BCP has been averaged over 10 cavities and it is 150 kHz, while the one due to light BCP is 30 kHz. Transition ring [3] and helium vessel welding makes the frequency change as well; the two processes have been recently started at FNAL. All these are causes of frequency deviations; in order to control and compensate for these shifts it is necessary to tune the cavities with a proper fixture.

*Work supported by D.O.E. Contract No. DE-AC02-07CH11359
#berrutti@fnal.gov

SSR1 BARE CAVITY TUNING

The first tuning step of SSR1 comes for the preparation to the vertical test, the frequency is adjusted to 324.6 MHz in order to reach approximately 325 MHz once the cavity is cooled down to 2 K in the test dewar. Usually the cavity received from the vendor has a resonant frequency of 325.6 (±0.2) MHz, after the leak check, first bake and bulk chemistry it is usually higher by 70 kHz. The total frequency shift to apply is approximately 1 MHz, taking into account the cavity sensitivity 540 kHz/mm (simulated) [4] and the spring constant 21 kN/mm, the tuning requires a robust fixture capable of delivering forces of several tens of kN. Figure 1 shows the tuning machine for SSR1 cavities, it consists in a box equipped with two rods which allow pushing or pulling on the cavity beam pipes. Two load cells measure the forces applied on each rod, four displacement gauges give reading of the deformations the cavity is subject to, and they are mounted between the beam pipes and the coupler ports. A set of antennae is mounted on the coupler ports to allow recording the frequency step by step with a network analyser.

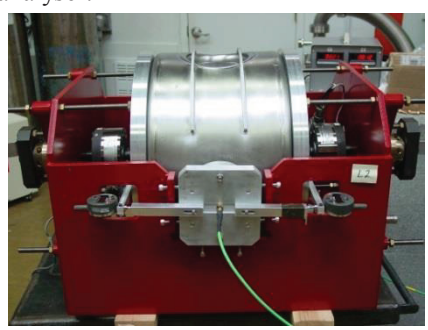


Figure 1: SSR1 tuning machine with a cavity in it.

To understand how the frequency changes when the tuning machine acts on the resonator, let us keep in mind Slater's rule:

$$\frac{\Delta f}{f_0} = \frac{1}{4W}\int_{V_i}^{V_f}(\varepsilon_0 E^2 - \mu_0 H^2)dV. \quad (1)$$

W is the stored energy in the cavity in initial conditions, V_i is the volume before tuning and V_f is the volume after deformations are applied. Since the rods are acting on the beam pipes the high electric field area is modified, consequently the change in frequency will have the same sign of the change in cavity volume: bigger volume means higher frequency.

Tuning Procedure

Before starting tuning the cavity, it has to be installed in the machine, which means have it fit centred in

Copyright © 2013 CC-BY-3.0 and by the respective authors

SINGLE SPOKE RESONATOR INNER ELECTRODE OPTIMIZATION DRIVEN BY REDUCTION OF MULTIPOLES*

P. Berrutti#, T. Khabiboulline, L. Ristori, N. Solyak, V. Yakovlev,
Fermilab, Batavia, IL 60510, USA

Abstract

Accelerating cavities based on coaxial resonators, half wave and spoke resonators for example, do not have azimuthal symmetry. This lack of symmetry introduces a transverse field perturbation which affects negatively the beam dynamic, since the particles traveling through the structure are crossing two accelerating gaps separated by the inner electrode. The field asymmetry induces an asymmetric transverse momentum gain which, once expanded in multipoles, appears to be due to a quadrupole perturbation. Depending on the cavity geometry and particle velocity, the influence of electric and magnetic fields may vary quite significantly. One solution to obtain symmetric transverse fields in spoke resonators consists in modifying the inner electrode shape from a pole to amore elaborated structure resembling an X or a Y letter shape. The application of these changes symmetrizes both electric and magnetic fields and reduces the multipoles amplitudes to negligible values. This paper presents the study aimed at reducing the multi-pole amplitudes for SSR2 cavity for Project X; the presented procedure, in general, is valid for any spoke cavity.

INTRODUCTION

Coaxial resonators are widely used for low-beta applications At Fermilab one family of half wave resonators (HWR) and two families of single spoke resonators (SSR) will be used in Project X. The geometry of both HWR and SSR is obtained from a coaxial line approximately half of a wave length long. The accelerating gaps of these cavities are formed by the inner and outer conductors of the coaxial resonator. Particles are travel along an axis perpendicular to the inner electrode. Let us assume that the particles are traveling through the gaps along the z axis, the lack of azimuthal symmetry leads to a different transverse momentum gain on x and y axes, acting as a quadrupole on the beam [1]. This issue has already been examined at Fermilab [1], [2] and a solution has been implemented to overcome HWR field asymmetry [3]: the central part of the inner electrode was modified using a radially symmetric circular shape. Such modification allows to obtain regular transverse electric field reducing asymmetric effects on the beam envelope. When the same approach was used on SSR2, the second family of spoke resonators for Project X, results were quite unexpected: the field asymmetry was even higher than before. This was caused by the magnetic transverse fields, which are not negligible in SSR2 cavities.

TRANSVERSE FIELD ASYMMETRY

Half wave and spoke resonators accelerating mode is quasi-TEM mode, that has non-zero transverse components on paths slightly off the ideal electric axis of the cavity. Considering the z axis as the longitudinal direction, electric and magnetic fields will be present in x and y. In figure 1 transverse field components of SSR2 cavity are plotted along z, for an offset of ten millimetres on the x-y plane: along x axis E_x and H_y are present, while for an offset on y direction E_y and H_x.

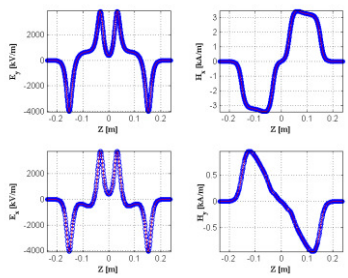


Figure 1: SSR2 electric and magnetic transverse fields.

A particle traveling with a radial offset r will experience a transverse kick due to the electric and magnetic fields:

$$\Delta p_x(r,\alpha)c = \int_{z_i}^{z_f}\left(\frac{E_{x(r,\alpha)}}{\beta} - i\boldsymbol{Z}_0 H_y(r,\alpha)\right)e^{i\frac{kz}{\beta}}dz \quad (1)$$

$$\Delta p_y(r,\alpha)c = \int_{z_i}^{z_f}\left(\frac{E_{y(r,\alpha)}}{\beta} + i\boldsymbol{Z}_0 H_x(r,\alpha)\right)e^{i\frac{kz}{\beta}}dz. \quad (2)$$

Where $\boldsymbol{Z}_0$is the impedance of free space, $\beta = v/c$ and α is an angle, taken with respect to the x axis: α=0 corresponds to x axis and α=π/2 refers to y axis. The momentum gain can be calculated in the whole beta range for the accelerated particles, and its components can be evaluated separately to highlight the difference between electric and magnetic contribution. The electric field line are directed from the spoke to the outer walls, while the magnetic field lines spin around the inner post, hence the magnetic field component orthogonal to the electrode will be higher than the one parallel to it. Figure 2 shows SSR2 single spoke geometry, the green arrows on the left (a) represent a sketch of the electric field lines while the orange circles on the right (b) show the magnetic field spinning around the electrode.

*Work supported by D.O.E. Contract No. DE-AC02-07CH11359
#berrutti@fnal.gov

Copyright © 2013 CC-BY-3.0 and by the respective authors

ISBN 978-3-95450-138-0

MULTIPACTING SIMULATIONS OF SSR2 CAVITY AT FNAL*

P. Berrutti#, T. Khabiboulline, L. Ristori, G. Romanov, A. Sukhanov, V. Yakovlev,
Fermilab, Batavia, IL 60510, USA

Abstract

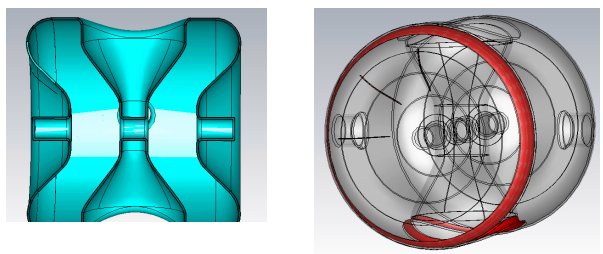
SSR2 is the second family of single spoke resonator under development at Fermi National Accelerator Laboratory (FNAL). These cavities will be placed in Project X front-end after SSR1 spoke resonators, which have already been built and tested and FNAL. Spoke cavities are affected by multipacting and the nature of their 3D geometry does not allow simulating the multipactor process using 2D tools. 3D tracking simulations, of electrons inside the cavity volume, have been carried out using CST Particle Studio. Different Secondary Emission Coefficients have been applied to the cavity walls in order to understand how strongly the multipacting depends on material properties. The power levels used in simulations cover the whole operating gradient range of SSR2 cavity. Results of these simulations are compared to the one given by SSR1 model, which demonstrated good agreement with experimental data. The purposes of this paper are to present the results gotten from the tracking solver, to give a prediction of what will be the multipacting scenario for SSR2 cavity and if there will be any dangerous zone for operation.

INTRODUCTION

Multipacting affects SRF cavities from high energy elliptical cavities to coaxial resonators for low-beta application. This work is focused on multipacting in low-beta structures; the main aim is to present the results of SSR2 cavity for Project X. SSR2 is a spoke resonator in development for Project X at Fermilab [1], it operates at 325 MHz and its optimal beta is 0.51. The design has been finalized recently it was necessary to understand at what level this resonator is affected by multipacting (MP), what the critical gradients are and where the MP develops in the cavity geometry. The software used for MP simulations is CST Particle Studio which provides a particle tracking solver that uses the field from the eigen-mode solver of Microwave Studio. The figure of merit chosen as a final result of tracking simulations is the growth rate, which gives information on how fast the number of particles increase with time. Simulation of MP in SSR2 cavity have been run for three different niobium secondary emission yields (SEY): in CST environment the highest emission for niobium is given by the wet treated material, a bake out model gives the intermediate one and the lowest yield is given by the discharge cleaned niobium. The growth rate has been calculated in a wide range of gradients and the MP locations have been identified for the major MP barriers. The experience of Fermilab with MP in low-beta structure started with SSR1, which is the lower optimal beta spoke resonator for Project X, operating at 325 MHz as well. Multipacting in SSR1 cavity has been simulated, using the same approach as for SSR2, and these results have been compared with experimental data from multipacting barriers found during the vertical test of SSR1 cavity [2], [3]. All this has been done in order to compare SSR1 and SSR2 multipacting simulations, and to understand how reliable and accurate the results of these simulations are.

SIMULATION SET UP

In order to simulate multipacting using CST particle studio it is necessary to create a shell all around the cavity volume to have an emitting material. The outer layer has been grown from the outside of the vacuum volume of the cavity, without interfering with the inner ideal surface. Figure 1(a) shows the geometry of SSR2 used for multipacting simulations in the x-y cut plane view. Once created the emitter shell the primary particle sources needed to be built. They were placed on the geometry taking advantage of the symmetry of the spoke resonator. Figure 1(b) shows the particle sources chosen for SSR2 MP simulations; red surfaces indicate sources of primary electrons. This set up has been used for SSR1 simulations as well; it has been previously described in [4] when the first multipacting simulations of SSR1 cavity were done.



(a) (b)

Figure 1: (a) outer shell built around SSR2 geometry x-y plane view, (b) particle sources are highlighted by red surfaces.

Primary particles were launched from the sources with an initial energy ranging from 2 to 6 eV, the angle was chosen randomly by the solver to get an isotropic electron emission. When simulating multipacting it is extremely important to have the mesh dense enough in the locations where the MP happens, the multipacting spatial scale is much smaller than the cavity dimensions. Multipacting occurs in regions where the electric field is not high, compared to the accelerating field, and the magnetic field bends the trajectories in a way that they satisfy the resonant condition. Electron trajectories could be very small compared to the cavity radius or length especially for complicated shapes like spoke resonators; thus a very fine mesh is required to get accurate EM field calculation

*Work supported by D.O.E. Contract No. DE-AC02-07CH11359
#berrutti@fnal.gov

Copyright © 2013 CC-BY-3.0 and by the respective authors

New Helium Vessel and Lever Tuner for the 650 Mhz Cavities for Project X*

I. Gonin#, M. Awida, E. Borissov, M. Foley, C. Grimm, T. Khabiboulline, M. Merio, Y. Pischalnikov, L.Ristori, V. Yakovlev, FNAL, Batavia, IL 60510, USA

Abstract

The proposed design of the 3 GeV Project X Superconducting Linac employs two families of 650 MHz 5-cell elliptical cavities with different β. The β_G =0.61 will cover the 177-467 MeV range. To cover the range between 467-3000 MeV two versions of 650 MHz 5-cell elliptical cavities with β_G =0.9 and β_G =0.92 has been proposed. The low beam current for CW operation of the Project X requires cavities to operate at a high loaded Q and thus, narrow bandwidth. Therefore it requires the optimal mechanical design of cavities to minimize the sensitivity to microphonics.

INTRODUCTION

Fermilab is currently developing a multi-MW proton source, Project-X (PX) [1], which will provide intense muon, kaon, neutrino and nuclei beams for broad and diverse program at the intensity frontier of particle physics. Possible future upgrades of Project-X may require operating linac in a regime of a high beam current, when an average beam current is 5 mA or even 10 mA. The design of 5-cell elliptical 650 MHz β_G =0.9 is under development at Fermilab. An alternative design of elliptical cavity with a larger aperture (59 mm) and β_G=0.92 is suggested for HE 650 MHz section in order to comply with various upgrade scenarios of the Project X linac [2]. The design of a dressed cavity (both β_G =0.9 and β_G =0.92) has been mechanically optimized by minimizing df/dP, the sensitivity to microphonics detuning due to fluctuations in helium pressure. The results for β_G =0.9 version has been presented at IPAC 2013 [3]. In this paper we will present the results of COMSOL simulations of df/dP, mechanical resonances and cavity tunability of an alternative β_G =0.92 cavity. We will also present the mechanical design of tuners and ANSYS analysis of their properties. The tuner system will be identical for both versions of cavities design.

HELIUM VESSEL DESIGN

The helium vessel assembly is constructed from a single 5 mm thick sheet of grade 2 titanium that is rolled and seam welded into a tube with an inside diameter of 441 mm and a length of 930 mm. Two helium fill ports are featured to allow for an even cool-down of the cavity. The helium vessel assembly is shown in Figure 1. The weld joint designs on the helium vessel satisfy the ASME Boiler & Pressure Vessel Code Section VIII Division 2. It is important to note that the 5 mm wall thickness for the helium vessel specification was not because of the ASME code, but rather to help in reducing *df/dP* by using the helium vessel to help stiffen the cavity.

* Operated by Fermi Research Alliance, LLC, under Contract DE-AC02-07CH11359 with the U.S. DOE

gonin@fnal.gov

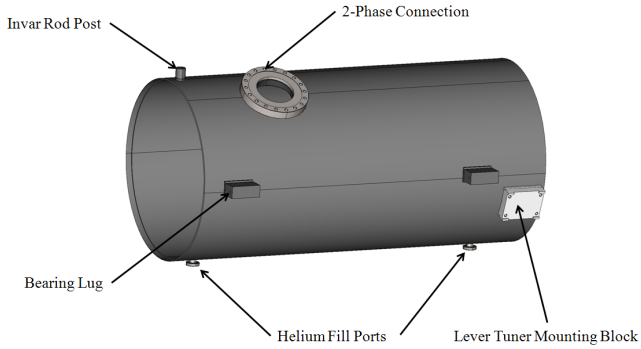


Figure 1: He vessel assembly.

The main coupler end and the field probe end of the helium vessel have slightly different joint designs due to the cavity installation sequence and variations in cavity lengths. The main coupler end of the vessel is considered a fixed position relative to the main coupler port of the cavity, and consistency between these key features for dressed cavities is maintained. Figure 2 shows the titanium-to-titanium TIG weld connection between the cavity and the helium vessel at the main coupler end. This joint design utilizes a backing ring and satisfies the ASME code.

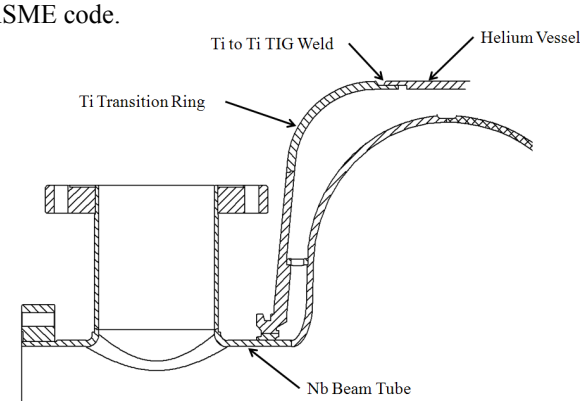


Figure 2: He vessel to cavity fixed joint design.

To allow for variations in the lengths of the manufactured cavities, the field probe end required a sliding joint design that would allow for cavity insertion from the field probe end to the main coupler end. As shown in Figure 3, cavities that vary by ±10 mm in length will not have any effect on the vessel design. This joint also satisfies the ASME code.

Copyright © 2013 CC-BY-3.0 and by the respective authors

ISBN 978-3-95450-138-0

CM2, SECOND 1.3 GHZ CRYOMODULE FABRICATION AT FERMILAB*

T. Arkan#, M. Awida, P. Berrutti, E. Borissov, C. Ginsburg, C. Grimm, E. Harms, A. Hocker, T. Khabiboulline, Y. Orlov, T. Peterson, R. Pilipenko, Y. Pischalnikov, K. Premo, L. Ristori, W. Schappert, V. Yakovlev, FNAL, Batavia, IL 60510, USA

Abstract

CM2 is the second 1.3GHz Cryomodule assembled at the Cryomodule Assembly Facility (CAF) in Fermi National Accelerator Laboratory. The string has a corrector coil magnet, a beam position monitor and eight cavities. All cavities are qualified at >= 33 MV/m gradient at the Horizontal Test Facility (HTS) before assembly. The dressed cavities were outfitted with magnetic shielding, blade tuner. The cold mass was assembled based on the Tesla TTF Type III+ cryomodule design. CM2 is currently being installed into the test stand in NML where it will be cooled down and high power tested. CM2 will also be the first cryomodule to be tested with an electron beam at the NML facility. This paper describes the assembly steps, the quality assurance methods and the challenges experienced during assembly and qualification at CAF.

INTRODUCTION

Fermilab's second 1.3 GHz cryomodule (aka CM2 or RFCA002) was assembled between July 2011 and March 2012. During the installation of this module at NML test facility, a vacuum leak was discovered in the 2-phase helium circuit. The module was brought back to CAF in June 2012 and was partially disassembled to find the location of the leak and to repair it. The module was then reassembled and transported to NML in April 2013. The module is currently being installed on the test stand. The cool-down and high power radio frequency (RF) test of the module is planned to start in September 2013.

CAVITIES AND COLD MASS COMPONENTS

All eight cavities manufactured by industrial vendors were specifically selected to be likely to achieve the ILC design goal based on their performance in individual RF tests [1]. The cavities were first tested "bare" in a vertical liquid helium dewar using low-power continuous-wave RF. Cavities which met the ILC vertical test specification ($E_{acc} \geq 35$ MV/m, $Q_0 \geq 0.8 \times 10^{10}$) were then welded into individual helium jackets at CAF and outfitted with a high-power input coupler. The high power couplers were purchased from CPI. The couplers were cleaned and high power conditioned at SLAC. These "dressed" cavities were then tested in the HTS using high-power pulsed RF. Qualified cavities along with a corrector coil magnet outfitted with XFEL style helium jacket and a button style beam position monitor (BPM) were all assembled into a cavity string in the CAF cleanroom. INFN design blade tuners [2] were purchased from Incodema. The tuner motors and gears were purchased from Phytron and Harmonic Drive Inc. The magnetic shielding parts were designed by Fermilab and were purchased from Amuneal. The vacuum vessel, gas return helium pipe (GRHP) assembly and cold mass support posts were procured from Zanon in Italy.

*Work supported by the U.S. Department of Energy
#arkan@fnal.gov

CRYOMODULE ASSEMBLY

Cavity String Assembly

The assembly of the cavity string was done in the CAF cleanroom situated in the CAF-MP9 building. Eight qualified cavities, a magnet, a BPM and two gate valves were interconnected using bellows in the Class 10 cleanroom. The assembly of the cavity string is the most important step throughout the cryomodule assembly to ensure that the measured gradient of the qualified cavities is preserved. Particulate-free-flange-assembly techniques were developed and optimized throughout the years at various institutions working on SRF R&D. CAF cleanroom technicians have over 7 year experience in particulate free ultra-high vacuum applications. CM2 cavity string (See Figure 1) was assembled while following the assembly travelers and working with strict adherence to the CAF cleanroom working protocols.

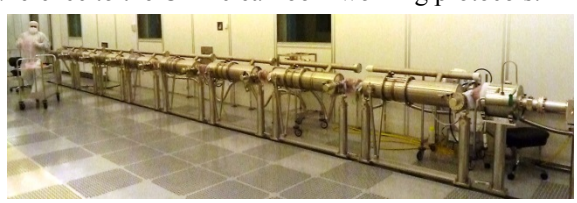


Figure 1: CM2 cavity string in the cleanroom.

Cold Mass and Final Assembly

After the string assembly was completed, the string was rolled out of the cleanroom into the cold mass assembly area at CAF-MP9 using the assembly rail. The 2-phase pipes of the cavities were interconnected using titanium (Ti) bellows welded using an automated orbital welding machine conforming to the ASME piping code. The cavities were then outfitted with magnetic shielding and blade tuner components. The cavity string was then lifted from the assembly fixtures and married to the GRHP assembly forming the cold mass assembly. The cold mass assembly was then transported to CAF-ICB building (See Figure 2). The X-Y axis alignment of the cavities to 250 microns was done using a laser tracker instrument. The cold mass was then transferred to the Big Bertha

Copyright © 2013 CC-BY-3.0 and by the respective authors

WAKEFIELD LOSS ANALYSIS OF THE ELLIPTICAL 3.9 GHZ THIRD HARMONIC CAVITY*

M. Awida#, P. Berrutti, A. Saini, T. Khabiboulline, and V. Yakovlev, Fermilab, Batavia, IL 60510, USA

Abstract

Third harmonic 3.9 GHz elliptical cavities are planned to be used in many particle accelerator projects such as XFEL, NGLS, and ASTA. In this paper, the wakefield losses due to bunches from 8 mm down to ultra short bunches of 10 μm are analysed. Both the loss and kick factors are numerically calculated for bunches of relatively long length (>1 mm) using CST wakefield solver. The data is then used to asymptotically extrapolate the values for ultra-short bunches by finding the wake functions. These calculations are essential to estimate the cryogenic losses in cryomodules and for beam dynamic analysis.

INTRODUCTION

Third harmonic cavities are commonly used in the particle accelerators of light sources to improve the bunch stability and compensate for the distortion that could happen between the sinusoidal accelerating field and the relatively long beam bunches [1-6].

Third harmonic 3.9 GHz cavities are currently under production for several projects. For instance, DESY's XFEL and FNAL's ASTA. Other future light sources (like NGLS) are also planning to use the third harmonic cavities.

In collaboration with DESY, Fermilab constructed a third harmonic cryomodule for the Free electron LASer in Hamburg (FLASH) facility [1-4]. Each cryomodule contains four superconducting radio frequency (SRF) cavities operating at 3.9 GHz. The third harmonic 9-cell cavities are designed to operate at 2 K in the TM_{010} π-mode at an accelerating gradient of 14 MV/m, summing up to a total energy gain of 20 MeV per cryomodule. These cavities operate in a decelerating phase of 179º relative to the beam phase, and are optimized for 9 mA of beam current.

In addition, another cryomodule will be fabricated for Fermilab Advanced Superconducting Test Accelerator (ASTA). ASTA plans to deliver 50 MeV beam for a broad range of beam-based experiments to push limits of particle-beam generation, acceleration and manipulation. ASTA plans to employ Superconducting 3.9 GHz cavities for bunch linearization.

Before accelerating beam with third harmonic cavities, it is imperative to estimate the cryogneic losses by analysing the wakefield losses. This paper reports on an extensive wakefield analysis, carried out on these third harmonic cavities, including the simulated loss and kick factors for sub cm beam bunches. Based on the simulated data and using an asymptotic approximation, we estimate the loss and kick factors for sub mm beam bunches.

WAKEFIELD SIMULATION FOR SUB CM BEAM BUNCHES

Figure 1 shows the geometry of the third harmonic 3.9 GHz 9-cells elliptical cavity. In different to the wakefield analysis in [5], we resorted to CST microwave studio to compute the wakefields inside a single cavity due to relatively long bunches, where the structure is excited by a longitudinal line current [7]. The line current is placed on the beam axis for the loss factor calculations, while the line is displaced off axis for the kick factor calculations. In both cases, the line current representing the beam is formed with a longitudinal, Gaussian shaped charge distribution.

Accuracy of the analysis was checked versus the mesh size. Typically, the ratio between the bunch sigma (standard deviation of the Gaussian distribution) to the mesh step size in the longitudinal direction *Sigma/h* is used to check the accuracy of the analysis with conventionally using *Sigma/h* of 20 as a satisfactory level of mesh refinement. In this analysis, we have used a *Sigma/h* of 30, as shown in Fig. 2. Mesh size of approximately 70 million elements (per quarter of cavity) was needed for the relatively short RMS bunch length of 2 mm, as shown in Fig. 2.

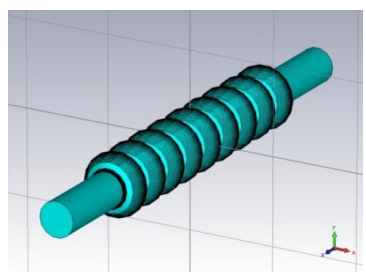


Figure 1: Geometry of the third harmonic 3.9 GHz cavity.

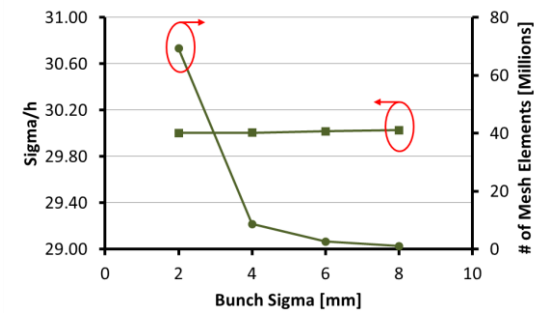


Figure 2: Sigma/h and number of mesh elements vs. bunch sigma.

*Operated by Fermi Research Alliance, LLC, under Contract DE-AC02-07CH11359 with the U.S. DOE

#mhassan@fnal.gov

ISBN 978-3-95450-138-0

Copyright © 2013 CC-BY-3.0 and by the respective authors

RESULTS OF THE NEW HIGH POWER TESTS OF SUPERCONDUCTING PHOTONIC BAND GAP STRUCTURE CELLS*

Evgenya I. Simakov#, Sergey A. Arsenyev, W. Brian Haynes, Sergey S. Kurennoy, David Lizon, James F. O'Hara, Eric F. Olivas, Dmitry Yu. Shchegolkov, Natalya A. Suvorova, and Tsuyoshi Tajima, Los Alamos National Laboratory, Los Alamos, NM 87545, U.S.A.
Chase H. Boulware, Terry L. Grimm, Niowave, Inc., Lansing, MI, 48906, U.S.A.

Abstract

We report the results of the recent 2.1 GHz superconducting rf (SRF) photonic band gap (PBG) resonator experiment in Los Alamos. The new SRF PBG cell was designed with the particular emphasis on changing the shape of PBG rods to reduce the peak magnetic fields and at the same time to preserve its effectiveness for suppression of the higher order modes (HOMs). The new PBG cells have great potential for outcoupling long-range wakefields in SRF accelerator structures without affecting the fundamental accelerating mode. Two 2.1 GHz PBG cells with elliptical rods were fabricated and tested with high power in a liquid helium bath at the temperature of 4 K and 2 K. The cells performed in accordance with simulation and the maximum achieved accelerating gradient was 18.3 MV/m.

INTRODUCTION

Superconducting radio frequency (SRF) cavities are the natural choice for the future generation of high-duty-factor accelerators for the high power free-electron lasers (FELs) where the heat produced in the accelerating structure must be effectively extracted [1]. Operating the accelerator at high frequency and low bunch charge reduces the risks of brightness degradation in electron beam transport. However, high frequencies become a disadvantage with respect to excitation of higher order mode (HOM) wakefields in the linac which get excited more easily and interact with the accelerated beam causing instabilities, energy spread and ultimately the beam breakup.

Photonic Band Gap [2] (PBG) cavities have the unique potential to filter out much of the HOM power and reduce the wakefields. A PBG resonator is capable of supporting the accelerating mode and not supporting any higher order modes which propagate towards the peripheries of the cavity and get filtered out with waveguides.

The first ever demonstration of acceleration in a PBG resonator was conducted at Massachusetts Institute of Technology (MIT) in 2005 [3]. Since then, the importance of PBG structures for accelerators has been recognized by many research institutions worldwide. In the experiment reported in [3], the 6-cell open copper PBG structure was employed to construct a room-temperature travelling-wave accelerator at 17.137 GHz with inherit ability to filter out wakefields.

* Work is supported by the Department of Defense High Energy Laser Joint Technology Office through the Office of Naval Research.
#smirnova@lanl.gov

A project funded by the U.S. Department of Energy (DOE) Office of Science Early Career Research Program at Los Alamos National Laboratory has recently demonstrated fabrication and high power operation of single-cell SRF PBG resonators at 2.1 GHz [4]. Two resonators were fabricated in 2012 and demonstrated solid high gradient performance with the maximum achieved gradient of 15 MV/m limited by the magnetic quench.

We have initiated a project at LANL to push the high gradient limitations of the SRF PBG resonators and demonstrate the possibility of a resonator with significantly reduced peak surface magnetic field and still excellent performance with respect to filtering out higher order modes.

2.1 GHz SRF PBG RESONATORS WITH REDUCED SURFACE FIELDS

We have followed the idea of [5] and changed the shapes of the 6 inner rods of the PBG resonator from cylindrical to elliptical. This produced the desirable effect reducing the surface fields up to 40 per cent depending on the major radius of the elliptical rods [6]. The question however was if the new resonators with elliptical rods were as effective with respect to filtering out wakefields as resonators with round rods. To answer this question we used the time-domain solver of the CST Microwave Studio [7] and analyzed the confinement of HOMs and the fundamental mode in a PBG resonator with elliptical rods. We discovered that if the periodicity of the PBG structure is broken and the elliptical rods are moved slightly toward the center of the resonator, then the fundamental mode in this structure becomes better confined than in the structure with round rods. At the same time HOMs in this structure are confined worse and can be extracted more efficiently than in the structure with round rods [6].

The final dimensions and the accelerator characteristics of the structure with the shifted elliptical rods are summarized in Table 1. The cells were designed with 18 hollow cylindrical rods: 6 elliptical and 12 round. The maximum surface electric field in the PBG cell is reached on the blended edge of the beam pipe, as was in the case of the cavity with round cylindrical rods [4]. The maximum surface magnetic field is again reached on the rods of the PBG structure; however it is 40% lower than the maximum surface magnetic field in the cavity with round cylindrical rods operating at the same gradient.

Copyright © 2013 CC-BY-3.0 and by the respective authors

UPDATE ON THE DESIGN OF A FIVE-CELL SUPERCONDUCTING RF MODULE WITH A PBG COUPLER CELL*

Sergey A. Arsenyev#, Massachusetts Institute of Technology, Cambridge, MA 02139, USA
Evgenya I. Simakov, Los Alamos National Laboratory, Los Alamos, NM 87545, USA

Abstract

We present a complete design of the 5-cell superconducting accelerating module incorporating a Photonic Band Gap (PBG) cell with couplers. The purpose of the PBG cell is to achieve better Higher Order Mode (HOM) damping which is vital for preserving the quality of high-current electron beams in novel linear accelerators used, for example, for free electron lasers. We first discuss the aspects of incorporating a PBG cell in a superconducting PBG module. The main goal is to ensure the equal probability of quench in each of the five cells, which can be achieved with significant geometry modifications. We then present the simulation data on HOM damping. Particularly, we calculate the external quality factors for the 10 most dangerous HOMs for this particular structure. HOM coupler configurations and modifications to the PBG geometry are discussed.

INTRODUCTION

Superconducting radio frequency (SRF) cavities are the natural choice for the future generation of high energy linacs, especially for high-duty-factor machines where the heat produced in the accelerating structure cannot be effectively extracted [1]. Going to higher frequencies in SRF cavities is desirable because of the lower cost and higher achievable luminosity of an electron beam. However, higher order mode (HOM) wakefields excited by a beam scale as frequency cubed and can easily destroy the beam in a high-frequency machine. If we want to go to the frequencies as high as 2.1 GHz, we have to find an effective way to suppress or outcouple HOMs.

PBG cavities are of interest to the particle accelerator community because they have reduced higher-order modes that can degrade beam quality [2, 3].

Waveguide couplers are commonly used as an HOM suppression mechanism (see, for example, [4]). Usually the couplers are attached to the beam pipe. In contrast with a room-temperature PBG cell, the superconducting cell is made closed in the transverse plane and utilizes waveguide couplers to extract the HOMs. Low field at the periphery of the PBG cell allows us to attach the waveguide couplers directly to the outside wall of the cell. This is beneficial to HOM damping because the HOMs are extracted at the point where their field is higher than at the beampipe. We also use less waveguides and increase real estate gradient.

*Work is supported by the U.S. Department of Energy (DOE) Office of Science Early Career Research Program
#arsenyev@mit.edu

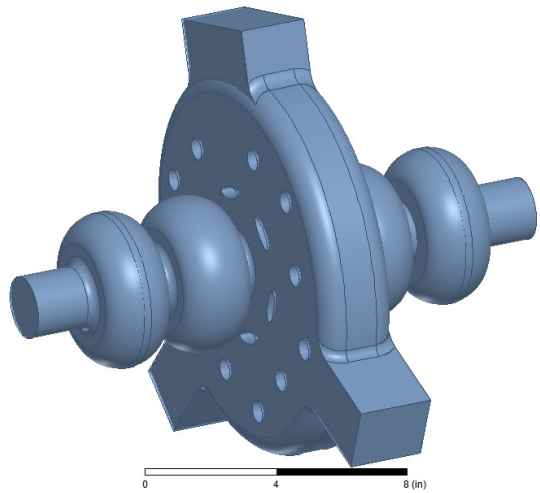


Figure 1: The 5-cell accelerating module with the central PBG cell.

Table 1: Dimensions and Accelerating Characteristics of the 5-cell Module

Frequency	2.1 GHz
Length of the module	14.05 in (35.69 cm)
Diameter of elliptical cells	4.95 in (12.57 cm)
Diameter of the PBG cell	12.32 in (31.3 cm)
Spacing of PBG rods	2.34 in (5.94 cm)
Radii of PBG rods	0.35 in (0.89 cm)
Beam pipe diameter	1.96 in (4.99 cm)
Angular position of the HOM couplers relative to the FM coupler	125°
r/Q	$1.44*10^3$ Ohm/m
E_{peak}/E_{acc}	2.65
B_{peak}/E_{acc}	4.48 mT/(MV/m)
Q_0 (4K)	$2.3*10^8$
Q_0 (2K)	$8.9*10^9$
Max theoretical gradient (for B_{peak}=200 mT)	45 MV/m

Copyright © 2013 CC-BY-3.0 and by the respective authors

ISBN 978-3-95450-138-0

INITIAL STUDIES OF MULTIPACTOR SUPPRESSION VIA TE AND TM MODES*

S. Rice[1] and J. Verboncoeur[2], Michigan State University, East Lansing, MI 48824, USA

Abstract

The formation of multipactor is strongly dependent upon the secondary electron yield (SEY) of a surface, and the emission velocities of the emitted electrons, in addition to the electric field. Since the secondary electron yield (SEY) of a material is dependent upon the kinetic energy and impact angle of the incident electron, we investigate use TE and TM coaxial cavity modes to modify the impacting electron velocities to reduce the average SEY and suppress multipactor, which builds upon our previous work examining TEM modes.

INTRODUCTION

Multipactor [1, 2] is a resonant phenomenon in which an electromagnetic field causes stray electrons to impact a surface, liberating secondary electrons, in such a way that the process can sustain itself. This phenomenon is of considerable practical interest in the design and operation of microwave windows, waveguides, and radio frequency resonant structures.

The formation of multipactor is strongly dependent upon the secondary electron yield (SEY) of a surface contributing to multipactor, since in order to initiate and sustain multipactor, the average number of emitted secondary electrons must be greater than or equal to unity. Multipactor is also dependent upon the system geometry and field excitation, which must be conducive to accelerating electrons into the boundaries at the proper RF phase to enable re-acceleration of the emitted secondary electrons.

When an electron impacts a boundary, the average secondary electron yield (SEY) is determined by the kinetic energy of the incident electron. Figure 1 shows a representative SEY curve. The specific SEY curve used in this present research was generated using Vaughan's model [3] with parameters chosen to match the impact energy location (E_{max}) and peak value (δ_{max}) of Furman's SEY model for copper [4], and is used for all the results presented in this study.

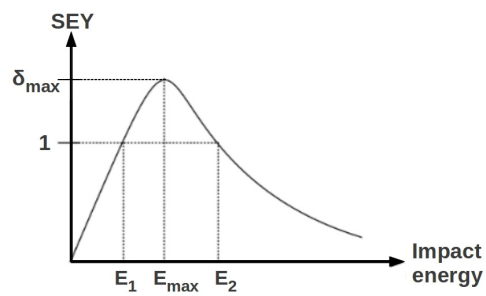


Figure 1: Typical SEY curve.

*Work supported by U.S. Air Force Office of Scientific Research (AFOSR) grant on the Basic Physics of Distributed Plasma Discharges.
[1]ricesco1@msu.com
[2]johnv@msu.edu

SIMULATION DESCRIPTION

Consider a coaxial cavity with conducting sidewalls, inner radius a, outer radius b, and longitudinal length L. The fundamental-mode TEM excitation at angular frequency ω can be parameterized by peak instantaneous voltage V_o and phase θ as $V_o \cdot \cos(\omega t+\theta) \cdot \sin(\pi z/L)$.

In our present research, we defined a=1 cm, b=5.65 cm, and L=1.86 m, and we used Vaughan's SEY model mentioned above. Unless otherwise noted, all secondary electron emission energies are set to zero to avoid the complication of the truly random (although typically low-energy) secondary emission energies. The selected geometrical values will allow a fundamental TEM mode to exist at 80.5 MHz, and the SEY model to yield maximum secondary electrons at $V_o \approx 1000$ V.

Electrons start from rest at the outer wall, and the net SEY is computed as the product of all the single-impact SEY values over 10 simulation steps, where each step is one fundamental mode period or boundary impact, whichever comes first. For each impact, a single simulated secondary electron is emitted and tracked. Only trajectories with at least two boundary impacts within ten fundamental-mode RF periods were considered to have net SEY > 0. The net SEY gives a proxy measure of the presence of the multipactor, since a net SEY < 1 would indicate that multipactor is not sustainable. Figure 2 shows the net SEY for the notional coaxial cavity for electrons starting at z values of 0.2L and 0.5L, where z=0 is defined to be the end of the cavity, and z=0.5L is halfway along the length of the cavity. The net SEY is displayed on a logarithmic scale, anything above 0 denotes a net increase in multipacting electrons. Note that to first order, the effect of changing z merely scales the multipactor voltage axis via the $\sin(\beta_z z)$ dependency.

MULTIPACTOR SUPPRESSION

Multipactor can only be sustained if the average SEY over the multipactor orbits is at least unity. This suggests a novel way to suppress multipactor, via the application of secondary excitation modes which result in the secondary electron impact energy being pushed away from the values where the SEY exceeds unity. Our previous work [5] explored multipactor suppression using an appropriately scaled and phase-referenced 3rd harmonic TEM mode, expressed mathematically as $-3V_o \cdot \cos(3\omega t+3\theta) \cdot \sin(3\pi z/L)$. The results are shown in Fig. 3, and it is apparent that the regions of sustainable multipactor have significantly decreased from the baseline case.

We now examine the use of TM and TE modes for the suppression of multipactor. This initial research examines the lowest order TM and TE modes, namely TM011 and TE011. The TM011 electric (E) and magnetic (H) field components are given by:

Copyright © 2013 CC-BY-3.0 and by the respective authors

TESTS OF AN RF DIPOLE CRABBING CAVITY FOR AN ELECTRON-ION COLLIDER *

A. Castilla[1,2,3†], J. R. Delayen[1,2],
[1]Center for Accelerator Science, Old Dominion University, Norfolk, VA 23529, USA.
[2]Thomas Jefferson National Accelerator Facility, Newport News, VA 23606, USA.
[3]Universidad de Guanajuato (DCI-UG), Departamento de Fisica, Leon, Gto. 37150, Mex.

Abstract

On the scheme of developing a medium energy electron-ion collider (MEIC) at Jefferson Lab, we have designed a compact superconducting rf dipole cavity at 750 MHz to crab both electron and ion bunches and increase luminosities at the interaction points (IP) of the machine. Following the design optimization and characterization of the electromagnetic properties such as peak surface fields and shunt impedance, along with field nonuniformities, multipole components content, higher order modes (HOM) and multipacting, a prototype cavity was built by Niowave Inc. The 750 MHz prototype crab cavity has been tested at 4 K and is ready for re-testing at 4 K and 2 K at Jefferson Lab. In this paper we present the detailed results of the rf tests performed on the 750 MHz crab cavity prototype.

INTRODUCTION

The rf dipole geometry has been studied as a compact and efficient design for an electron-ion crabbing scheme for electron-ion colliders [1]. Among some of the most attractive properties of this design are the lower balanced surface fields with higher net deflection, higher shunt impedance, the advantage of having the operating deflecting/crabbing mode as the lowest mode, and the simple dependency of the rf properties on just a few geometrical parameters [2]. It is for all these reasons that the designed 750 MHz crab cavity prototype shown in Fig. 1 built by Niowave Inc. [3] has been tested and characterized at its facilities and the Center for Accelerator Science at Old Dominion University (CASODU) to corroborate that the fields' symmetry, operation performance, conditioning to multipacting and external Q factor are in agreement with the designed values.

ROOM TEMPERATURE TESTS

Bead-Pull

In a TE_{11} deflector/crabber such as the rf dipole, the transverse kick has contributions from both the electric and the magnetic components of the fundamental mode, thus the symmetry of the field profiles is a key point in the fabrication of the cavity to avoid introducing higher-order nonlinear field effects on the beams.

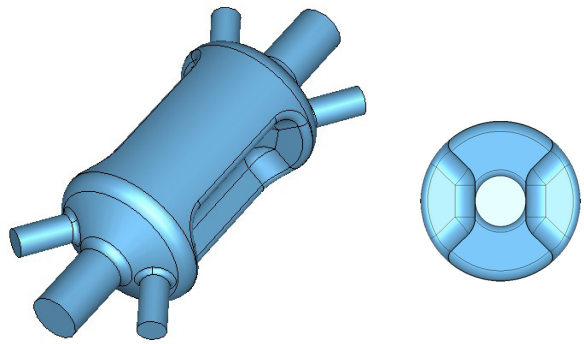


Figure 1: Rf dipole geometry and corresponding cross sections for the 750 MHz crab cavity design.

Table 1: Properties of the 750 MHz Crab Cavity

Parameter	750 MHz	Units
$\lambda/2$ of π mode	200.0	mm
Cavity length	341.2	mm
Cavity radius	93.7	mm
Aperture diameter d	60.0	mm
Deflecting voltage V_T^*	0.200	MV
Peak electric field E_P^*	4.45	MV/m
Peak magnetic field B_P^*	9.31	mT
B_P^*/E_P^*	2.09	mT/(MV/m)
Energy content U^*	0.068	J
Geometrical factor	131.4	Ω
$[R/Q]_T$	124.2	Ω
$R_T R_S$	1.65	$\times 10^4 \Omega^2$

At E_T^*= 1 MV/m

Once the electromagnetic design has been characterized using computer simulations, it is of utmost importance to characterize defects introduced during the fabrication and chemical treatment processes on the cavity, like assymmetries due to offsets on the load elements, perturbations induced by deformations on the volume, etc.

Different runs of bead-pull measurements were performed on the 750 MHz rf dipole crab cavity before and after e-welding using the automated bead-pull system set at CAS-ODU (see Fig. 2).

* Authored by Jefferson Science Associates, LLC under U.S. DOE Contract No. DE-AC05-06OR23177. The U.S. Government retains a nonexclusive, paid-up, irrevocable, world-wide license to publish or reproduce this manuscript for U.S. Government purposes. Part of this work was done in collaboration with and supported by Niowave Inc. under the DOE STTR Phase II program.

† acastill@jlab.org

ISBN 978-3-95450-138-0

Copyright © 2013 CC-BY-3.0 and by the respective authors

MECHANICAL ANALYSIS OF THE 400 MHz RF-DIPOLE CRABBING CAVITY PROTOTYPE FOR LHC HIGH LUMINOSITY UPGRADE*

S. U. De Silva[1,2#], H. Park[2,1], J. R. Delayen[1,2], Z. Li[3]
[1]Center for Accelerator Science, Old Dominion University, Norfolk, VA 23529, USA
[2]Thomas Jefferson National Accelerator Facility, Newport News, VA 23606, USA
[3]SLAC National Accelerator Facility, Menlo Park, CA 94025, USA

Abstract

The proposed LHC high luminosity upgrade requires two crabbing systems in increasing the peak luminosity, operating both vertically and horizontally at two interaction points of IP_1 and IP_5. The required system has tight dimensional constraints and needs to achieve higher operational gradients. A proof-of-principle 400 MHz crabbing cavity design has been successfully tested and has proven to be an ideal candidate for the crabbing system. The cylindrical proof-of-principle rf-dipole design has been adapted in to a square shaped design to further meet the dimensional requirements. The new rf-dipole design has been optimized in meeting the requirements in rf-properties, higher order mode damping, and multipole components. A crabbing system in a cryomodule is expected to be tested on the SPS beam line prior to the test at LHC. The new prototype is required to achieve the mechanical and thermal specifications of the SPS test followed by the test at LHC. This paper discusses the detailed mechanical and thermal analysis in minimizing Lorentz force detuning and sensitivity to liquid He pressure fluctuations.

INTRODUCTION

The rf-dipole design is a favorable design for compact deflecting and crabbing applications especially at low operating frequencies [1]. The LHC high luminosity upgrade is one such current application that requires a crabbing cavity system with stringent dimensional constraints that will be operating at 400 MHz [2].

The rf-dipole cavity is one of proposed crabbing cavity designs. The design is proven to have improved rf-properties with low and balanced peak surface fields with high transverse deflection and high shunt impedance. The non-existence of lower order modes and widely separated higher order mode spectrum is an added advantage for this high current application of LHC.

An rf-dipole cavity with a cylindrical outer conductor has been designed and fabricated as a proof-of-principle cavity. The rf tests have been carried successfully [3]. The expected goal of 3.4 MV was exceeded and a transverse voltage of 7.0 MV was achieved. The major unknown in the rf-dipole geometry was the expected multipacting levels during operation. The conditions were simulated using the SLAC ACE3P code [4] and compared with rf results, show similar behavior. These multipacting levels were easily processed during the first cryogenic rf test and did not reoccur during the tests followed.

*Authored by Jefferson Science Associates, LLC under U.S. DOE Contract No. DE-AC05-06OR23177. The U.S. Government retains a non-exclusive, paid-up, irrevocable, world-wide license to publish or reproduce this manuscript for U.S. Government purposes.
#sdesilva@jlab.org

400 MHz CRABBING CAVITY PROTOTYPE

The transverse dimensions of the proof-of-principle cavity design exceed the dimensional specifications required by the LHC crabbing system. The cylindrical outer conductor restricts in reducing the cavity size as the operating frequency is directly related to the cavity frequency. The rf geometry is modified into a square shape outer conductor with similar loading elements, where the operating frequency is adjusted by rounding the edges of the cavity (Fig. 1) [5]. The rf properties of the prototype in comparison with the cylindrical cavity are shown in Table 1.

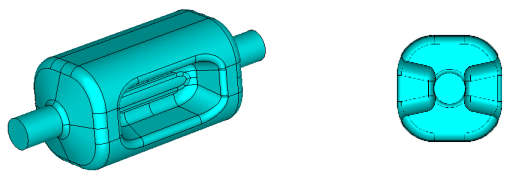


Figure 1: 400 MHz rf-dipole prototype with trapezoidal-shaped loading elements and the cross section.

Table 1: Properties of the Proof-of-principle and Prototype 400 MHz Rf-dipole Cavities

Parameter	Cylindrical shaped	Square shaped	Units
Cavity length	542.4	556.2	mm
Cavity diameter	339.9	281.0	mm
Aperture diameter (d)	84.0	84.0	mm
Bars length	350.3	293.0	mm
Bars inner height	80.0	117.5	mm
Angle	50.0	~12.0	deg
Deflecting voltage (V_T^*)	0.375	0.375	MV
Peak electric field (E_P^*)	4.02	3.65	MV/m
Peak magnetic field (B_P^*)	7.06	6.13	mT
B_P^* / E_P^*	1.76	1.68	
Energy content (U^*)	0.195	0.13	J
Geometrical factor	140.9	106.2	Ω
$[R/Q]_T$	287.0	429.2	Ω
$R_T R_S$	4.0×10^4	4.6×10^4	Ω^2

At $E_T^* = 1$ MV/m

The inner loading elements are curved to suppress the field non-uniformity across the beam aperture and to reduce the corresponding multipole components.

Copyright © 2013 CC-BY-3.0 and by the respective authors

COMPARISON OF ELECTROMAGNETIC, THERMAL AND MECHANICAL CALCULATIONS WITH RF TEST RESULTS IN RF-DIPOLE DEFLECTING/CRABBING CAVITIES*

H. Park[1,2#], S. U. De Silva[2,1], J. R. Delayen[2,1],
[1]Thomas Jefferson National Accelerator Facility, Newport News, VA 23606, USA.
[2]Center for Accelerator Science, Old Dominion University, Norfolk, VA 23529, USA.

Abstract

The current requirements of higher gradients and strict dimensional constraints in the emerging applications have required the designing of compact deflecting and crabbing rf structures. The superconducting rf-dipole cavity is one of the first novel compact designs with attractive properties such as higher gradients, higher shunt impedance and widely separated higher order modes. The recent tests performed on proof-of-principle designs of the rf-dipole geometry at 4.2 K and 2.0 K in the vertical test area at Jefferson Lab have proven the designs to achieve higher gradients with higher intrinsic quality factors and easily processed multipacting conditions. The cavity characteristics, such as pressure sensitivity and Lorentz force detuning, were studied using ANSYS before the fabrication. These characteristics were measured during the cavity test. The comparison between the simulation and the measurement provides insight how the simulation can be used for design and fabrication of future cavities.

INTRODUCTION

The Jefferson Lab 12 GeV [1] upgrade is in need of an rf separator system that separates the maximum energy beam in to the 3 experimental halls simultaneously. Figure 1 shows the 12 GeV beam line schematic with the rf separator systems required for the energy upgrade.

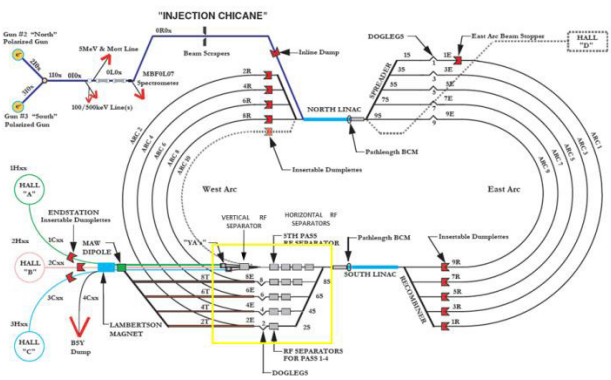


Figure 1: Jefferson Lab 12 GeV beam line.

The 6 GeV beam line has two separator systems for separating the beam horizontally and vertically. The horizontal separator system separates the beam that is recirculated into the linac from that sent to the experimental halls, where the vertical separator system separates the single beam into the 3 experimental halls. The existing rf separator system operates with a series of normal conducting rf separator cavities [2].

The 12 GeV energy upgrade requires a vertical rf separator system that operates at the increased beam energy. The superconducting rf-dipole cavity is one proposed options for the vertical separator system. Table 1 shows the optimized 499 MHz deflecting rf-dipole cavity [3]. The rf test results are shown in Figure 2.

Table 1: Properties of the 499 MHz Rf-dipole Deflecting Cavity

Parameter	Value	Units
Frequency	499.0	MHz
Cavity length	44	cm
Cavity diameter	25	cm
Aperture diameter (d)	40.0	mm
Deflecting voltage (V_T^*)	0.3	MV
Peak electric field (E_P^*)	2.86	MV/m
Peak magnetic field (B_P^*)	4.38	mT
Geometrical factor	105.9	Ω
$[R/Q]_T$	982.5	Ω
$R_T R_S$	1.0×10^5	Ω^2

At E_T^* = 1 MV/m

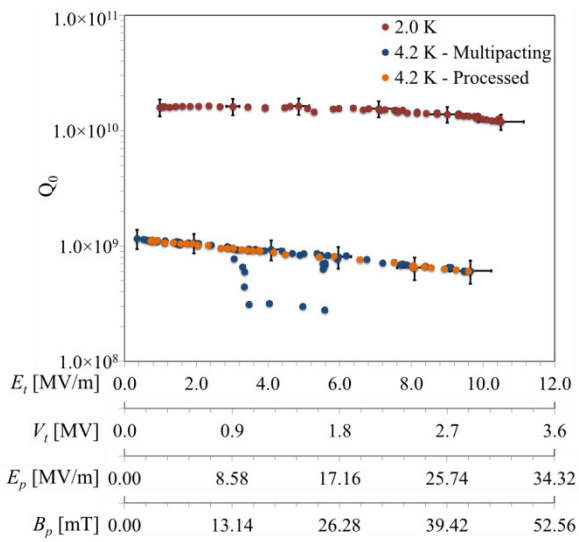


Figure 2: Q curve of the 499MHz rf dipole cavity.

*Authored by Jefferson Science Associates, LLC under U.S. DOE Contract No. DE-AC05-06OR23177. The U.S. Government retains a non-exclusive, paid-up, irrevocable, world-wide license to publish or reproduce this manuscript for U.S. Government purposes.
#hkpark@jlab.org

Copyright © 2013 CC-BY-3.0 and by the respective authors

ISBN 978-3-95450-138-0

GEOMETRY EFFECTS ON MULTIPOLE COMPONENTS AND BEAM OPTICS IN HIGH-VELOCITY MULTI-SPOKE CAVITIES*

C. S. Hopper†, K. Deitrick, and J. R. Delayen
Center for Accelerator Science, Department of Physics,
Old Dominion University, Norfolk, VA, 23529, USA and
Thomas Jefferson National Accelerator Facility, Newport News, VA 23606, USA

Abstract

Velocity-of-light, multi-spoke cavities are being proposed to accelerate electrons in a compact light-source [1]. There are strict requirements on the beam quality which require that the linac have only small non-uniformities in the accelerating field. Beam dynamics simulations have uncovered varying levels of focusing and defocusing in the proposed cavities, which are dependent on the geometry of the spoke in the vicinity of the beam path. Here we present the results for the influence different spoke geometries have on the multipole components of the accelerating field and how these components, in turn, impact the simulated beam properties.

INTRODUCTION

To address the varying levels of focusing and defocusing that beam dynamics simulations have shown exist, we first evaluate the higher order multipole components contained in the accelerating field to better understand what contributions could lead to the observed behavior. The design of the cavities, and the linac, are then evaluated using results generated by ASTRA particle tracking simulation code.

MULTIPOLE COMPONENTS

The higher order multipole components are analyzed using the method given in [2, 3]. Various cavities have been considered for fabrication, and the field non-uniformity for each of these cavities is shown in Fig. 2. The difference in the models essentially comes down to the shape of the spoke aperture region. A standard racetrack is preferred because of the rf properties, but a rounded square, ring [4], and elliptical aperture have also been studied, and are shown in Fig. 1.

These geometries have varying degrees of symmetry. The ring and racetrack apertures, for similar cavities, have been studied and presented elsewhere [3]. Additional optimization of apertures (c) and (d) is necessary. However, it is likely that some compromise would have to be made, in terms of increased peak surface fields, to decrease the multipole components. Figures 3 and 4 show the $E_z^{(2)}$ and $E_z^{(4)}$ components as a function of position. All the cavities have the same mesh, and similar $E_z^{(2)}$ components, however there is a clear difference in the $E_z^{(4)}$ components.

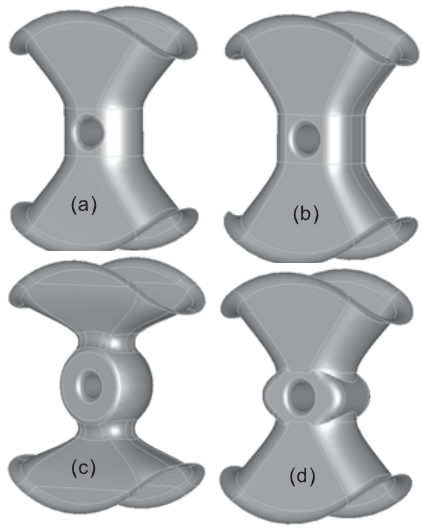


Figure 1: Various spoke aperture geometries studied. (a) racetrack, (b) rounded square, (c) ring, and (d) elliptical.

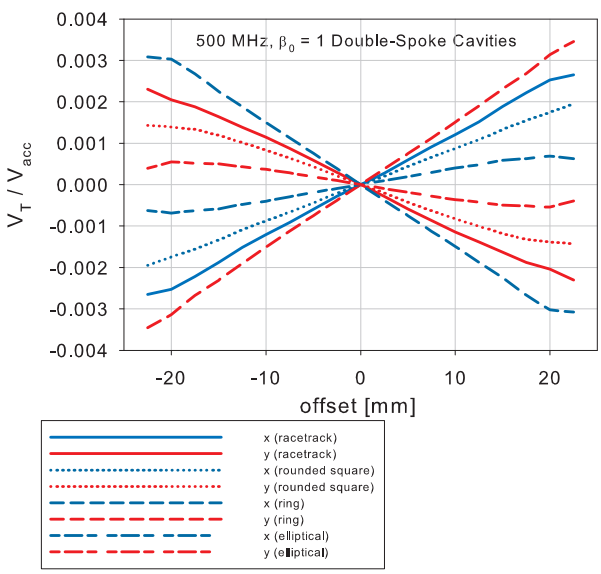


Figure 2: Dependence of transverse voltage (normalized to V_{acc}) on transverse offset for the aperture geometries presented in Fig. 1.

* Work supported by U.S. DOE Award No. DE-SC0004094
† chopp002@odu.edu

Copyright © 2013 CC-BY-3.0 and by the respective authors

STUDY OF CAVITY IMPERFECTION IMPACT ON RF-PARAMETERS AND MULTIPOLE COMPONENTS IN A SUPERCONDUCTING RF-DIPOLE CAVITY*

R. G. Olave, J. R. Delayen†, S. U. De Silva, Old Dominion University, Norfolk, VA, USA
Z. Li, SLAC National Accelerator Laboratory, Menlo Park, CA, USA

Abstract

The ODU/SLAC superconducting rf-dipole cavity is under consideration for the crab-crossing system in the upcoming LHC luminosity upgrade. While the proposed cavity complies well within the rf-parameters and multipolar component restrictions for the LHC system, cavity imperfections arising from cavity fabrication, welding and frequency tuning may have a significant effect in these parameters. We report on an initial study of the impact of deviation from the ideal shape on the cavity's performance in terms of rf-parameters and multipolar components.

INTRODUCTION

Due to transverse geometry constraints at the nominal operating rf frequency of 400 MHz, novel compact cavities are under consideration for the upcoming LHC High Luminosity upgrade. The ODU/SLAC superconducting rf-dipole cavity is a suitable candidate as it satisfies the requirements for high gradients, high shunt impedance, low surface fields, no lower order modes, and well-defined and widely-spaced higher order modes [1]-[3]. The cavity geometry, while compact, is not azimuthally symmetric and therefore it becomes important to identify any higher order multipolar components at the operating frequency, since these can lead to beam instabilities in the LHC system. The ODU/SLAC rf-dipole cavity satisfies all specifications for the LHC crab cavity system in terms of rf parameters and in terms of multipole contributions up to the octupole term [4]; Table 1 presents a list of the relevant rf parameters for the cavity. As we prepare for fabrication of a prototype cavity, we are analyzing the impact of individual imperfections or departures from the ideal cavity geometry, that may arise from fabrication or welding errors, while additional distortions would result from the tuning process. In this paper, we present an initial analysis on how such geometry imperfections, particularly those due to welding of the poles, would result in the introduction of undesired higher order multipole components.

IMPERFECTIONS IN THE POLES VS FIELD UNIFORMITY

The design optimization of the cavity showed quite clearly that the geometry of the aperture region of the poles near the beam axis is of vital importance in minimizing the contribution of the sextupole component, which results in a more uniform deflecting voltage across the beam aperture region. For this reason, we start by looking into imperfections in the shape or welding of the poles. Using CST Microwave Studio® 2012 (CST MWS) we have altered the optimized design near the beamline to introduce individual defects in the alignment or geometry of one of the poles, according to the following list:

Table 1: RF Parameters of the 400 MHz Rf-dipole Cavity (at E_T = 1 MV/m and Reference Length $\beta_0\lambda$)

Parameter		Units
Frequency	400.28	MHz
$(R/Q)_T$	412.7	Ω
$(R/Q)_T * (QR_s)$	4.43x10^4	Ω^2
E_p/E_T	3.66	
B_p/E_T	6.14	mT (MV/m)

- (A) Yaw (rotation about y-axis) of one pole.
- (B) Pitch (rotation about x-axis) of one pole.
- (C) Roll (rotation about z-axis) of one pole.
- (D) Horizontal displacement of one pole.
- (E) Vertical displacement of one pole.
- (F) Blending radius at the outer corner of one pole.
- (G) Blending radius of the feather-like structure near the beamline of one pole.
- (H) Aperture radius in one pole.

Figure 1 shows transverse and longitudinal views of the cavity, where the optimized pole geometry can clearly be seen, as well as the places where deformations have been added according to the previous list.

The robustness of the cavity design is such that none of the individual imperfections introduced so far produces drastic changes in the rf-parameters. For items (A), (F) and (G), the transverse voltages (normalized to the transverse voltage at the ideal cavity's beamline) barely change as function of transverse offset from the ideal beamline, from those of the ideal cavity geometry. This can be seen for example in Fig. 2, which includes a plots for different yaw (rotation about the y-axis) angles, as well as a plot (red) of the transverse voltage as a function of transverse offset of the ideal cavity for reference. As can be seen, there is field uniformity in a large region within the cavity's aperture, even for large yaw angles in one of the poles.

* Work supported by U.S. DOE through the US LHC Accelerator Research Program (LARP)
† jdelayen@odu.edu

Copyright © 2013 CC-BY-3.0 and by the respective authors

ISBN 978-3-95450-138-0

HIGHER ORDER MODES DAMPING AND MULTIPACTING ANALYSIS FOR THE SPX DEFLECTING CAVITY FOR THE APS UPGRADE*

Z. Li, L. Xiao, C. Ng, SLAC, Menlo Park, CA 94025, USA
A. Nassiri, G. Waldschmidt, G. Wu, ANL, Argonne, IL 60439, USA
H. Wang, R. Rimmer, Jefferson Lab, Newport News, VA 23606, USA

Abstract

A single-cell superconducting deflecting cavity operating at 2.815 GHz has been proposed and designed for the Short Pulse X-ray (SPX) project for the Advanced Photon Source (APS) upgrade. Each deflecting cavity is equipped with one fundamental power coupler (FPC), one lower order mode (LOM) coupler, and two higher order mode (HOM) couplers to achieve the stringent damping requirements for the unwanted modes. Using the electromagnetic simulation suite ACE3P, HOM damping was calculated for the cavity including the full engineering design waveguide configurations and rf windows. Trapped modes in the bellows located in the beampipes connecting the cavities in a two-cavity cryomodule were analyzed. Multipacting activities in the cavity and damping waveguides were simulated under the condition of field asymmetry due to a realistic cavity imperfection to assess possible problems during high power processing.

INTRODUCTION

The Advanced Photon Source (APS) can provide photon pulses of several tens to hundreds of picoseconds. There are growing requests from users to use shorter pulse X-rays (SPX) for the analysis of short time-scale physical processes. It has been proposed at APS [1,2] to utilize a pair of superconducting deflecting cavity modules to generate ~1ps X-ray pulses at one of the straight sections, without disrupting the regular X-ray pulse usage for other users. In the proposed scheme, the first set of cavities add a correlation between bunch longitudinal position and transverse momentum. X-Rays produced by this bunch will also have this correlation, and can be put through transverse slits to produce a much shorter X-Ray pulse. The second set of cavities are located a multiple of 180 degrees of phase advance to unchirp the beam, removing the effects of the first cavity set. A cryomodule of four such cavities on each side of the undulator will be needed to produce the required 2-MV deflecting voltage [3].

A two-cavity prototype cryomodule, Fig. 1, is currently under construction and to be tested before the full installation of the four-cavity cryomodules for the APS upgrade. Because of the added complicity of the multi-cavity system, understanding of potential trapped modes and multipacting issues in such a multi-cavity system is essential to validate the design concept. In addition to the planned test, detailed numerical analysis of the HOM damping and multipacting were carried out on the two-cavity prototype module. In this paper, we present the simulation results of HOM damping and multipacting analysis under realistic imperfection conditions.

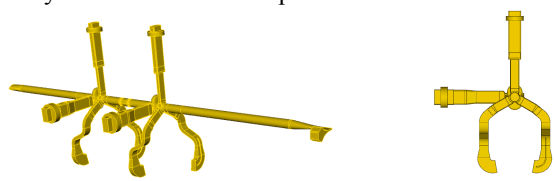


Figure 1: SPX two-cavity deflecting module, and the layout of the FPC and HOM/LOM damping couplers

TWO CAVITY PROTOTYPE MODULE

The layout of the two-cavity module, including the couplers, bellows, and extended beam pipes, is shown in Fig. 1. The cavity has a flattened oval shape and operates in the TM110 mode at 2.815 GHz, which has a strong magnetic field on the beam axis that produces transverse deflection. The RF power is fed from a fundamental power coupler (FPC) waveguide, the vertical waveguide in Fig. 1, which forms one of the legs of a ”Y”-end-group off-cell. The other two legs of the “Y”-end-group, the curved waveguide underneath the cavities, are for damping the higher-order modes. The cavity also supports a TM01 mode, which is at a lower frequency than the operating mode. An on-cell lower order mode (LOM) coupler, horizontal waveguide in Fig. 1, is directly attached to the cell at the cavity equator which offers a more compact geometry with enhanced LOM and HOM damping. Beampipe bellows are in between the two cavities for alignment flexibility.

We have used the parallel finite element EM code suite ACE3P [4] developed at SLAC to analyze the trapped mode damping and multipacting in the two-cavity cryomodule. Fig. 2 shows the finite element mesh around

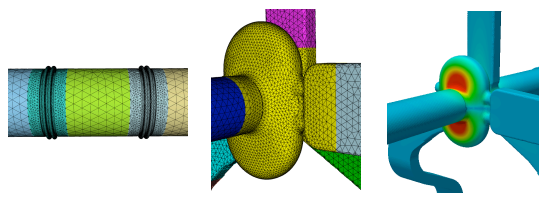


Figure 2: Finite-element mesh around the cavity and beam pipe bellows and the field profile of the operating mode.

*Work supported by the U.S. Department of Energy, Office of Science, Office of Basic Energy Sciences, under Contract No. DE-AC02-06CH11357

Copyright © 2013 CC-BY-3.0 and by the respective authors

WAKEFIELD COMPUTATIONS FOR A CORRUGATED PIPE AS A BEAM DECHIRPER FOR FEL APPLICATIONS*

C.-K. Ng, K.L.F. Bane, SLAC, Menlo Park, USA

Abstract

A beam "dechirper" based on a corrugated, metallic vacuum chamber has been proposed recently to cancel residual energy chirp in a beam before it enters the undulator in a linac-based X-ray FEL. Rather than the round geometry that was originally proposed, we consider a pipe composed of two parallel plates with corrugations. The advantage is that the strength of the wake effect can be tuned by adjusting the separation of the plates. The separation of the plates is on the order of millimeters, and the corrugations are fractions of a millimeter in size. The dechirper needs to be meters long in order to provide sufficient longitudinal wakefield to cancel the beam chirp. Considerable computation resources are required to determine accurately the wakefield for such a long structure with small corrugation gaps. Combining the moving window technique and parallel computing using multiple processors, the time domain module in the parallel finite-element electromagnetic suite ACE3P allows efficient determination of the wakefield through convergence studies. In this paper, we will calculate the longitudinal, dipole and quadrupole wakefields for the dechirper and compare the results with those of analytical and field matching approaches.

INTRODUCTION

In order to cancel the residual energy chirp in a beam before it enters the undulator in a linac-based FEL, a beam dechirper whose design consisting of periodic corrugations on the chamber walls has been proposed [1]. Such a dechirper is a passive device as it uses the longitudinal wakefield generated by the beam transit to compensate for the energy difference within the beam. The dechirper can be installed in machines such as LCLS-II where a superconducting linac will be used for beam acceleration and the wakefields generated in the superconducting cavities are not strong enough to dechirp the beam.

The original dechirper proposed for the light source NGLS was a round corrugated metallic pipe. The wakefields for the round geometry have been calculated using an analytical approach and formulas are available. Later, a flat rectangular geometry with corrugations on two parallel metallic plates was adopted and a dechirper was built and tested [2] at the injector test facility (ITF) for the PAL-XFEL in Korea [3]. The rectangular geometry has the advantage that the separation of the plates can be adjusted for different machine operation conditions. Formulas for the wakefields obtained by the analytical approach have been worked out recently for the rectangular case [4, 5]. Furthermore, numerical method using field matching in the frequency domain has been developed [4], which is believed to be more accurate than the analytical method.

The analytical approach is a good approximation when the depth and period of the corrugation are small compared with the separation of the plates. The corrugations in the dechirper being tested at PAL are small with respect to the chamber dimensions, but it is desirable to perform direct simulation by 3D electromagnetic code to verify the validity of the analytical approximation. This work focuses on numerical simulation using the finite-element electromagnetic code suite ACE3P [6] to calculate the wakefields of the dechirper and compare them with the analytical and field matching approaches. In addition to determining the longitudinal wakefield that is used to cancel the energy chirp of the beam, the dipole and quadrupole wakefields that kick and defocus the beam and hence increase its emittance will also be evaluated.

THE DECHIRPER MODEL

A sketch of the geometry of the dechirper is shown in Fig. 1. The corrugation is defined by the period p, the gap g, and the depth h. These corrugation parameters are fractions of a millimeter in size. The corrugations are located at the top and the bottom of the rectangular chamber with half height a and half width w. In order to provide sufficient longitudinal wakefield, the height of the dechirper needs to be small enough (on the order of millimeters), which is small compared with the chamber width, and the length of the dechirper needs to be long enough (on the order of meters). The dimension parameters of the dechirper tested at PAL are a = 3 mm, p = 0.5 mm, g = 0.3 mm, and h = 0.6 mm. In practice, a is adjustable from $2a$ = 5 mm to 28 mm. The validity of the analytical approximation is when p, $h \ll a$ and the corrugation depth h is much larger than its period p. It can be seen that the corrugation dimensions are about an order of magnitude smaller than the dechirper height. A direct 3D numerical simulation is required for cross check of the analytical calculation.

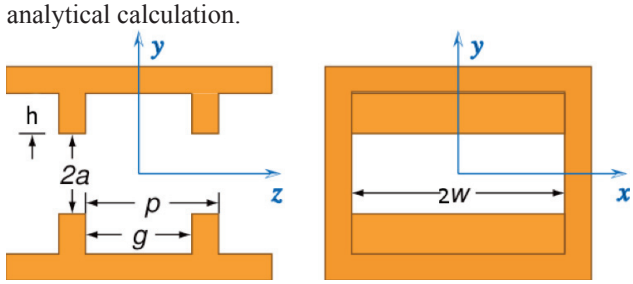


Figure 1: Sketch of the geometry of the dechirper.

* Work supported by the Department of Energy under Contract Number: DE-AC02-76SF00515.

Copyright © 2013 CC-BY-3.0 and by the respective authors

ISBN 978-3-95450-138-0

MECHANICAL DESIGN OF A NEW INJECTOR CRYOMODULE 2-CELL CAVITY AT CEBAF*

G. Cheng#, J. Henry, J. Mammosser, R. A. Rimmer, H. Wang, M. Wiseman, S. Yang, JLAB, Newport News, VA 23606, USA

Abstract

As a part of Jefferson Lab's 12 GeV upgrade, a new injector superconducting RF cryomodule is required. This unit consists of a 2-cell and 7-cell cavity, with the latter being refurbished from an existing cavity. The new 2-cell cavity requires electromagnetic design and optimization followed by mechanical design analyses. The electromagnetic design is reported elsewhere. This paper aims to present the procedures and conclusions of the analyses on cavity tuning sensitivity, pressure sensitivity, upset condition pressure induced stresses, and structural vibration frequencies. The purposes of such analyses include: 1) provide reference data for cavity tuner design; 2) examine the structural integrity of the cavity; and 3) evaluate the 2-cell cavity's resistance to microphonics. Design issues such as the location of stiffening rings, effect of tuner stiffness on cavity stress, choice of cavity wall thickness, etc. are investigated by conducting extensive finite element analyses. Progress in fabrication of the 2-cell cavity is also reported.

CEBAF NEW INJECTOR CRYOMODULE CAVITIES

Presently in the injector section of CEBAF there is a "Quarter Cryomodule", which has two 5-cell cavities. With the upgrade of operating energy from 6 GeV to 12 GeV, a few options for the booster cavity layout have been studied [1] and the 2-cell plus 7-cell cavities layout is deemed desirable. The demanded field amplitude for the 7-cell cavity is around 13 MV/m. An economic decision is made to refurbish a low loss JLAB Renascence cryomodule [2] 7-cell cavity, which is capable to provide 17-21 MV/m accelerating field amplitude, to be used in the new Injector Cryomodule. The 2-cell cavity is a new design based on the low loss cavity shape and is expected to provide approximately 4.6 MV/m accelerating field.

2-CELL CAVITY MECHANICAL DESIGN

The 2-cell cavity is made of high RRR fine grain niobium. Basic mechanical properties used in all design analyses are listed in Table 1. Note that the 2-cell cavity niobium material is the same as SNS cavity material and the cavity will be baked at 600 ^{o}C for 10 hours. Although niobium is not a "code material", the ASME Boiler & Pressure Vessel Code (BPVC) rules are referenced during the pressure induced stress analysis for the 2-cell cavity. The allowable stresses are determined per BPVC rules, i.e. the allowable stress is the lesser of 2/3 of yield strength or 1/3.5 of the tensile strength.

Among the major cavity mechanical design considerations, the choice of cavity wall thickness is mainly dictated by the upset condition pressure induced stress. The wall thickness also affects the cavity stiffness, tuning and pressure sensitivities, as well as vibration natural frequency. Similar theory applies to the option of using ring shape stiffeners. All mechanical design analyses are performed in ANSYS®. The tuning and pressure sensitivity calculations involve electromagnetic to structural coupled field analysis technique. Each design topics is addressed in a bit more details in the following sections.

Table 1: High RRR Niobium Mechanical Properties [3-5]

Properties	Room Temperature	Cryogenic Temperature
Young's Modulus, psi	1.49e7	1.79e7
Poisson's Ratio	0.38	0.38
Density, lb/in^3	0.31	0.31
Yield Strength, ksi	9.5	83.7
Tensile Strength, ksi	26.3	118.8
Allowable Stress, ksi	6.33	33.9

2-CELL CAVITY STRUCTURAL STRESS

Three loading conditions are examined for the stress state in the 2-cell cavity: 1) 2.2 atm pressure at room temperature (R.T.) simulating pressurization during the cryomodule cool down process, 2) 5 atm pressure at cryogenic temperature (C.T.) simulating pressurization caused by upset conditions [6], and 3) 5 atm pressure with 300 μm tuning displacement. The pressure chamber surrounding the niobium cavity is formed by the interior of a helium vessel and the cavity external surfaces. The helium vessel for this 2-cell cavity is made of stainless steel and has one bellows to mitigate the thermal stress developed during cool down and caused by the mismatch of expansion coefficients between niobium and stainless. The bellows also permits tuning of the cavity without holding up against an otherwise stiff helium vessel. Outside the helium vessel, a scissor-jack tuner is mounted. The helium vessel bellows and tuner are simulated as springs in the cavity stress analysis model. The bellows' longitudinal spring constant is relatively small. The tuner's warm and cold stiffnesses are analysed separately on a preliminary tuner design model.

*Authored by Jefferson Science Associates, LLC under U.S. DOE Contract No. DE-AC05-06OR23177. The U.S. Government retains a non-exclusive, paid-up, irrevocable, world-wide license to publish or reproduce this manuscript for U.S. Government purpose.
#cheng@jlab.org

Copyright © 2013 CC-BY-3.0 and by the respective authors

NOISE REDUCTION USING FILTERS ON TURN-BY-TURN LHC ORBITS TO OBTAIN MAGNETIC ERRORS WITH THE ACTION AND PHASE JUMP ANALYSIS METHOD

A.C. García B., J.F. Cardona, Universidad Nacional de Colombia*, Bogotá, Colombia

Abstract

The Action and Phase Jump analysis had been successfully used to obtain magnetic errors in RHIC. Analyses in LHC encountered significant noise. In this paper, a dual band-pass filter on LHC simulated orbits to reduce the noise is discussed. Gaussian and Uniform noise are studied independently. Results show that the best filter has a bandwidth of 0.0174 around the two transverse tunes. A low-pass band filter was also used to get the closed-orbit.

INTRODUCTION

The measurement of magnetic errors in an accelerator is an important task during the commissioning. One of the methods used to localize, to measure, and to correct magnetic errors is the Action and Phase Jump (APJ) Analysis. It is based on the theoretical principle of preservation of the Action and Phase variables in absence of a magnetic error. This method had been successfully tested in RHIC using closed-orbit data from experiments [1] and its theoretical development is fully presented in [2].

Preliminary analyses on turn-by-turn (TBT) orbits at the LHC show promising results [3, 4], but with a certain levels of noise than for the RHIC case, due to a bigger bandwidth of the LHC BPMs. Efforts to reduce the noise, like taking advantage of the thousands of turns provided by the LHC BPMs system (in contrast with the few orbits used in RHIC) have been done.

In this paper we discuss the use of pass-band digital filters to reduce noise in LHC TBT orbits; supplemented by an initial change of the PYTHON APJ code. A simulation of the beam trajectory, using MAD-X, is made for the thin LHC injection optics (V.6.5), where normal and skew linear quadrupole errors A_1 and B_1 were included, at the IR quadrupole MQXA.3L5 of beam 1.

Noise originated from the distribution of particles in the beam and noise originated from the misaligments of the BPMs are simulated using a Gaussian distribution and an Uniform distribution, respectively. The BPMs gain is also taking into account by using these distributions. This type of distributions had been used in noise studies for the closed-orbit measurement [5].

A BAND-PASS FILTER FOR THE LHC

The BPMs are the devices that provides measurements of the beam position in the transverse plane around the accelerator. For a fixed longitudinal position, the transverse position is sampled every turn leading to:

$$z(n) = \sqrt{2J_z\beta_{z,BPM}}\sin\left(\psi_{z,BPM} + 2\pi Q_z n - \delta_z\right) \quad (1)$$

where $z = \{x, y\}$ is the transverse plane coordinate, J_z is the Action, $\beta_{z,BPM}$ and $\psi_{z,BPM}$ are the beam β_z-function and phase advance at the BPM longitudinal position, δ_z is the Phase, and Q_z is the accelerator tune, at the transverse plane $z = \{x, y\}$. In this study, the data simulated with MAD-X on the acelerator LHC beam 1, is used to created new trajectories with simulated noise.In one case, the noise corresponds to a Gaussian distribution of $\sigma_{Gauss} = 0.1$ mm, which is added randomly to the each BPM data, and in the other case a Uniform distribution up to 0.3 mm is used. Then the resulting signal is filtered to evaluate wheter the filter help to reduce the uncertainty on the determination of magnetic errors using APJ method.

In this study, the filter was implemented using directly PYTHON functions, although trials were also made with own built transfer functions. From the available filters, the band-pass filter was chose, because it reduces the noise without damaging the magnetic error recovery. A second order filter is implemented, with Butterworth coefficients and the double run function [6].

Table 1: Frequencies Values for the Filter Bands. The overlapping is removed.

N.	$\omega_{pass}I$ [2π rad]	$\omega_{stop}I$ [2π rad]	$\Delta\omega$ [2π rad]	$\omega_{pass}II$ [2π rad]	$\omega_{stop}II$ [2π rad]
0	0.28025	0.28075	0.0005	0.30875	0.30925
1	0.28	0.281	0.001	0.3085	0.3095
...	...	...	...	...	...
25	0.01	0.49	0.48	0.01	0.49

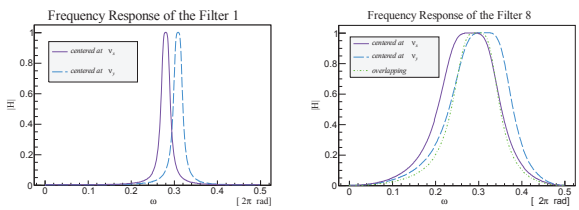


Figure 1: Dual Band-pass filter frequency response, if there is not overlapping (left) and with the corresponding overlapping band (right). Bands centered at 0.2805 and 0.309.

Also previous trials showed that the best results are obtained using a band-pass filter with two bands centered on the transverse tunes ν_x and ν_y (a 99% uncertainty is reached if only one tune band is used without noise). Table 1 presents the frequencies (ω) used to built the filter, where (N.) is the number of the case, the dots are the complementary values, such as an increment of 0.0005 in $\Delta\omega$ is

* Thanks to the DIB at Universidad Nacional de Colombia for the funding provided for computers and the support for this presentation.

ISBN 978-3-95450-138-0

Copyright © 2013 CC-BY-3.0 and by the respective authors

POSSIBLE OBSERVATION OF TRANSVERSE LASER COOLED ULTIMATE COLD ION BEAM IN S-LSR*

Kouichi Jimbo#, IAE, Kyoto University, Uji-city, Kyoto, Japan
Hikaru Souda, Gunma University Heavy Ion Medical Center, Maebashi-city, Gunma, Japan
Yosuke Yuri, TARRI, Japan Atomic Energy Agency, Takasaki-city, Gunma, Japan
Hiromu Tongu, ICR, Kyoto University, Uji-city, Kyoto, Japan
Masao Nakao, Toshiyuki Shirai, and Akira Noda, NIRS, Chiba-city, Chiba, Japan

Abstract

Transverse laser cooling is pursued at an ion storage/cooler ring, S-LSR, Kyoto University. An RF bunched Mg^+ beam was cooled transversely through synchro-betatron resonance coupling by a co-propagating laser. We investigated peaks of synchrotron oscillation spectroscopically so that we can observe them stably. Oscillation signals from a parallel-plate pickup were observed by a spectrum analyzer. We also observed the coherent synchrotron modes. As the beam temperature decreases, the ion beam would be in space charge limited region. According to the computer simulation, in the case the beam turns to be space charge limited, the disappearance of peaks of synchrotron oscillation is expected. We would like to propose a capability of detecting space charge limited region by observing such a frozen synchrotron oscillation.

INTRODUCTION

In Small Laser-equipped Storage Ring (S-LSR) at ICR, Kyoto University, a frequency tuneable laser of ~280 nm is co-propagating with a 40keV Mg^+ beam, as shown in Fig.1. It was cooled in the transverse direction through resonant coupling method [1]. The Horizontal and longitudinal oscillations are coupled by an RF voltage applied at the position with a finite dispersion when a synchro-betatron resonance coupling condition (SBRC) is satisfied: a cooling force in the longitudinal direction is transferred to the transverse direction [2].

The ion beam was bunched by the RF wave of frequency 2.5192MHz. Since the revolution frequency was 25.192kHz, it corresponded to the harmonic number 100. Frequency spectra, which were obtained from preamp signals of a parallel-plate pickup in the ring, were observed by a spectrum analyzer [3]. We hope to use these frequency spectra for diagnostic purpose of ultra cold ion beams.

The RF frequency of 2.5192MHz will be printed as 2.5MHz for abbreviation, which corresponds to 0Hz in Figure 2, 3, and 5. In Figure 4, 0Hz represents 2×2.5MHz. At this stage of transverse laser cooling where the beam temperature was not yet ultra-cold to be in space charged limited region, there was no clear difference in frequency spectra whether the ion beam was laser cooled or not.

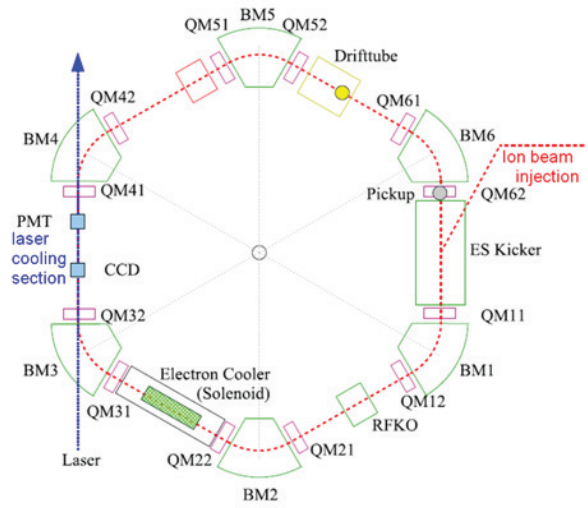


Figure 1: Layout of S-LSR.

Table 1 shows the main parameters of S-LSR.

Table 1: Main Parameter of S-LSR

Circumference	22.557 m
Average Radius	3.59 m
Length of straight section	1.86 m
Radius of curvature	1.05 m
Revolution frequency	25.192 kHz
Super periodicity	6
Ion species	$^{24}Mg^+$
Kinetic beam energy	40 keV
Transition wavelength	280 nm

EXPERIMENTAL RESULTS

The frequency spectra of around 2.5MHz, which is located at the centre, are shown in Fig. 2. To erase sidebands (2 peaks about ±1kHz, and about±2kHz from the centre), the RF frequency was varied ∓ 0.5kHz (Fig.2-a and 2-c) when SBRC was satisfied (Resonance tune ν_s=0.066、ν_h=2.066). However, we could not erase them. They were not noises. In fact the sidebands are small enough since the ordinate is the unit of dBm.

*Work supported by Advanced Compact Accelerator Development Project of MEXT, the Global COE program "The Next Generation of Physics, Spun from Universality and Emergence".
#jimbo@iae.kyoto-u.ac.jp

Copyright © 2013 CC-BY-3.0 and by the respective authors

LUMINOSITY ESTIMATION AND BEAM PHASE SPACE ANALYSIS AT VEPP-2000*

A. Romanov, I. Koop, E. Perevedentsev, D. Shwartz
BINP SB RAS and Novosibirsk State University

Abstract

Luminosity is the main output of colliders, so it is very important to measure it with speed and accuracy. VEPP-2000 has 16 beam profile monitors (BPM) which use CCD-cameras to register synchrotron light in the visible spectrum. Two luminosity estimation methods are presented, both based on beam size analysis. Although the luminosity measurements by particle detectors CMD-3 and SND are slow and have low statistical accuracy for low beam currents, their data can be used to test new faster methods. Additionally, an attempt of the phase space tomography is presented using the simulated BPM measurements of the particle distribution in a strongly non-gaussian beam.

INTRODUCTION

VEPP-2000 is used for hadron cross section measurements in the energy range of $0.4 \div 2$ GeV [1], hence it takes luminosity at several dozens of energies every season, thus emphasizing the tuning tools' importance. The collider has a two-fold symmetry lattice with 16 CCD cameras that take beam images using synchrotron light (Fig. 1). 8 CCDs are aimed at electrons and 8 at positrons.

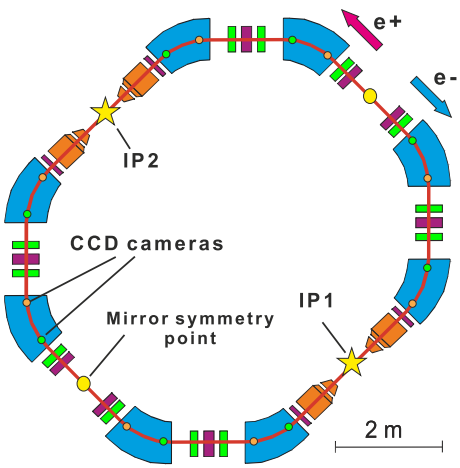


Figure 1: VEPP-2000 layout.

There are a number of theoretical and empirical considerations regarding lattice configuration depending on the energy [2], but the last step of the final tuning is almost always unique and done manually. To get the best luminosity output, the operator should tune parameters such as beta-functions at the IPs, closed orbit position, betatron tunes, chromaticity, betatron coupling and others. The crude effects such as "flip-flop" can be noticed by the naked eye, however fine tuning requires the fast and reliable luminosity estimation tools. Unfortunately, the speed and precision of the luminosity measurements from the detectors are not sufficient, especially at low energies.

Both presented methods of luminosity estimation assume that accurate optics model of the real accelerator ring is available. Assuming no focusing perturbations in the lattice other than those caused by the collision, and thus located at the IP, one can use known transport matrices to evaluate the beam sizes at the IP from the beam size measurements by CCDs.

FIRST LUMINOSITY ESTIMATION METHOD

Eight measurements are available for either transverse coordinates of the two beams, while there is only a pair of strongly indeterminate parameters - beam emittance ϵ and $\beta*$ - for each mode and each beam.

For the parameters fitting procedure, it is convenient to transport all the measured beam sizes to the point of mirror symmetry where Twiss $\alpha = 0$. The center of technical straight section is chosen since this point is not perturbed by the beam-beam focusing. The beta-function for $i-th$ profile monitor is transported as:

$$\beta_i = \beta_0 \cdot t_{11,i} + \beta_0^{-1} \cdot t_{12,i}, \quad (1)$$

where t_{kl} are the elements of known transport matrix. The fitting minimizes the difference between the model and measured beam sizes:

$$F = \sum_i \frac{\left(\sqrt{\epsilon\left(\beta_0 \cdot t_{11,i} + \beta_0^{-1} \cdot t_{12,i}\right)} - \sigma_i\right)^2}{\sigma_i^2 + o_i^2}. \quad (2)$$

Here, o_i is the size measurement error with a typical value of $3-5\mu m$, while the beam size σ_i is a pure betatron part of measured transverse size with excluded dispersion contribution

$$\sigma_\beta = \sigma - D \cdot \frac{\sigma_E}{E} \quad (3)$$

The fitted beta-function β_0 is transported to the IP together with the emittance that gives the size needed. The luminosity can be easily calculated as:

$$L = \frac{N_1 N_2 f_0}{2\pi\sqrt{\left(\sigma_{1x}^2 + \sigma_{2x}^2\right)\left(\sigma_{1y}^2 + \sigma_{2y}^2\right)}}. \quad (4)$$

The model is extremely simple, it uses several assumptions. 1) Well-known unperturbed optics between the IPs

* This work is supported by the Ministry of Education and Science of the Russian Federation.

ISBN 978-3-95450-138-0

Copyright © 2013 CC-BY-3.0 and by the respective authors

COMBINING MULTIPLE BPM MEASUREMENTS FOR PRECESSION AC DIPOLE BUMP CLOSURE*

P. Oddo, M. Bai, C. Dawson, J. Kewisch, Y. Makdisi, C. Pai, P. Pile, T. Roser
BNL, Upton, NY 11973, USA

Abstract

For the RHIC spin flipper to achieve a rotating field, it requires operating five AC dipoles as a pair of closed orbit bumps. One key requirement is to minimize the remnant AC dipole driven betatron oscillation outside of the spin flipper by 50 dB [1]. In the past, due to its inherent sensitivity, a single pickup with a direct-diode detector (3D) [2] and dynamic signal analyzer (DSA) were used to measure bump closure by measuring the remnant oscillations. This however proved to be inadequate, as the betatron phase advance between the AC dipoles is non-zero. A method of combining multiple BPMs into a sensitive measure of bump closure has been developed and was tested during RHIC polarized proton operation in 2013. This technique as well as the experimental results will be presented.

INTRODUCTION

A spin flipper for RHIC (Relativistic Heavy Ion Collider) has been developed for RHIC spin-physics experiments. It is needed to cancel systematic errors by reversing the spin direction of the two colliding beams multiple times during a store [3].

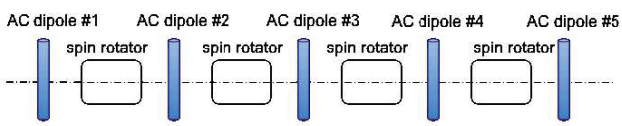


Figure 1: Spin flipper configuration.

The spin flipper system consists of four DC dipole magnets (spin rotators) and five AC dipole magnets (see fig. 1). The aim of this configuration is to produce a rotating field. Multiple AC dipoles are needed to localize the driven coherent betatron oscillation inside the spin flipper [1, 4]. While results from the 2012 run did suggest the presence of a rotating field, the polarization lifetime was degraded with the AC dipoles on. This suggested incomplete bump closure and/or incorrect phase between bumps [1] which lead to reinvestigating the method used to close the AC dipole bumps.

Operationally the AC dipoles form two bumps that minimize the effect of the AC dipoles outside of the spin flipper. The central AC dipole, #3 in figure 1, is common to both bumps. Both AC-dipole bumps operate at the same frequency, but are phase shifted from each other. The convention used when expressing closure in dB is to make the 0 dB reference the strongest AC dipole. In case of the dual bump, AC dipole #4 is used.

*Work supported by Brookhaven Science Associates, LLC under contract DE-AC02-98CH10886 with the U.S. Department of Energy and RIKEN, Japan.

BBQ 3D AFE & DSA

Up until the 2013 run the closure was only trimmed using the pickup and direct-diode detector (3D) analog front end (AFE) of the RHIC baseband tune meter (BBQ) processed via a DSA.

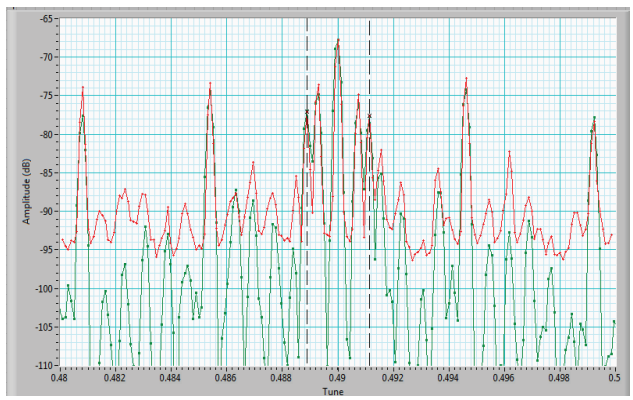


Figure 2: Closed bump DSA beam spectrum (green plot). The red plot is the fitted AC dipole magnet currents.

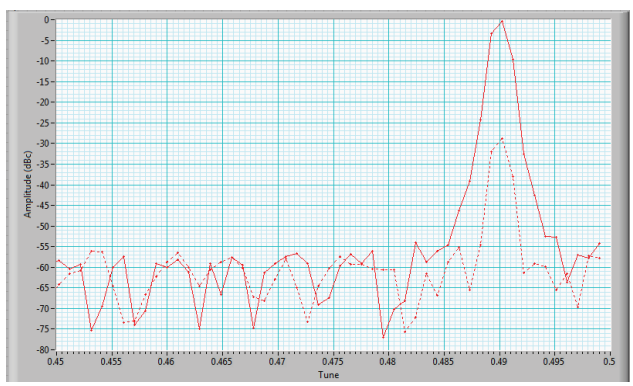


Figure 3: AC dipole #4 alone (solid) and closed bump (dotted) BPM beam spectrum of the most sensitive BPM.

The DSA spectrum in figure 2 (green plot) shows that the closure for the AC dipole bumps was 67 dB. However, the spectrum of the most sensitive BPM (fig. 3, dotted plot) shows a closure of only 28 dB. This nearly two order of magnitude difference clearly shows that it's not possible to determine closure using a single pickup (at a single frequency). The possibility of using a single pickup at multiple frequencies has not yet been fully explored.

COMBINING BPM MEASURMENTS

Even though discrete Fourier transform (DFT) spectrums, which typically are calculated using the fast Fourier transform (FFT) algorithm, are used here, these

Copyright © 2013 CC-BY-3.0 and by the respective authors

ISBN 978-3-95450-138-0

STRIPLINE BEAM IMPEDANCE*

A. Blednykh#, W. Cheng, S. Krinsky
BNL, Photon Science, NY 19973-5000, USA

Abstract

We discuss the Lambertson and Shafer formalisms for the longitudinal and transverse beam impedances of a stripline. The required characteristic impedances and the geometric factors are determined by the solution of Laplace's equation in 2-dimensions, which we find using the 2-D POISSON code. Lambertson's equations are compared with numerical results obtained using the 3-D electromagnetic simulation code GdfidL. Good agreement is found at low frequencies. The results differ at high frequencies, since the analytic results do not take into account higher order modes.

INTRODUCTION

Striplines [1-4] are often used in accelerator systems to serve as either pick-ups or kickers. These devices are comprised of the conducting surfaces of the vacuum envelope and inner conducting electrodes as illustrated in Fig. 1. An important issue in the design of a stripline is the impedance that it presents to the particle beam traveling along the axis through the device.

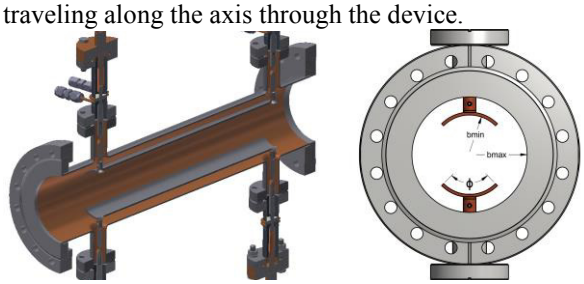


Figure 1: One half of the stripline kicker geometry. Two electrodes are located inside of the round pipe with $b_{min} = 24.1mm$ and $b_{max} = 38mm$ radii. The length of electrodes is 300mm. The electrode thickness is 2mm.

Lambertson [2,3] has presented a very interesting and comprehensive discussion of pick-ups and kickers. Following his formalism, one can express the longitudinal and transverse (vertical) beam impedances for a stripline in the form

$$Z_{||}(k) = g_{||}^2 Z_{ch,||}[sin^2(kL) + j\, sin(kL)cos(kL)] \quad (1)$$

$$Z_{\perp}(k) = \left(g_{\perp}^2 Z_{ch,\perp}/kb^2\right)[sin^2(kL) + jsin(kL)cos(kL)] \quad (2)$$

where k is the wave number, L is the longitudinal length of electrodes, b_{min} is the minimum distance between the beam axis and the electrodes, $g_{||}$ and $g_{\perp}$ are longitudinal and transverse geometric factors, and $Z_{ch,||}$ and $Z_{ch,\perp}$ are longitudinal and transverse characteristic impedances of the stripline. The geometric factors and the characteristic impedances are for the full structure containing all electrodes. We note that for a device comprised of two identical electrodes symmetrically placed as in Fig. 1, $Z_{ch,||} = Z_L/2$, where Z_L is the characteristic impedance of a single electrode.

At low frequency the longitudinal shunt impedance is related to the longitudinal beam impedance by [3]

$$R_{sh,||} = ReZ_{||}(k) \times 4, \quad (3)$$

and the transverse shunt impedance is related to the transverse beam impedance by

$$R_{sh,\perp} = ReZ_{\perp}(k) \times 4/k \quad (4)$$

To determine $Z_{ch,||}$ and $Z_{ch,\perp}$ for a given geometry, one needs to solve Laplace's equation in 2 dimensions. For this, we use the 2D POISSON electrostatic code [5]. The characteristic impedance is given by [6]

$$Z_{ch} = \frac{1}{cC}, \quad (5)$$

where c is the velocity of light and C is the capacitance of the stripline structure. For the longitudinal mode, both electrodes have voltage V_p, while for the transverse mode they have voltages of opposite polarity $\pm V_p$. In both cases, the capacitance is related to the stored energy W_e and voltage V_p via

$$C = \frac{2W_e}{V_p^2} \quad (6)$$

Given the magnitude of the voltage V_p, we calculate the stored energy using POISSON and in this manner determine the capacitance and thus the characteristic impedance for each mode.

First, as an illustration, we consider the ideal coaxial transmission line with geometric parameters $b_{min} = 24.1mm$ inner and $b_{max} = 38mm$ outer radius (Fig. 2a). The characteristic impedance determined from the stored energy computed by POISSON and using Eqs. (5 and 6) with specified positive voltage ($V_p = +1Volt$) on inner conductor is $Z_{ch}^{+} = 22.53\Omega$. This agrees with the well-known result, $Z_{ch}^{CXL} = \frac{Z_0}{2\pi} Log(b_{max}/b_{min})$ for the coaxial (CXL) transmission line.

Next, we consider the longitudinal and transverse characteristic impedances for the round stripline geometry shown in Fig. 2b,c. The electrode radius b_{min} and outer radius b_{max} are fixed. The angle subtended by an electrode is varied from $\phi = 10^{\circ}$ to $\phi = 170^{\circ}$. The longitudinal and transverse characteristic impedances of the structure with the two electrodes as a function of the electrode angle are shown in Fig. 3. The longitudinal characteristic impedance tends to 23Ω for $\phi \to 180^{\circ}$, approaching the result for the coaxial transmission line, as it must.

As can be seen from Fig. 3, for electrode angle $\phi \to 180^{\circ}$, the transverse characteristic impedance $Z_{ch,\perp}$ is about a factor of two less than the longitudinal $Z_{ch,||}$. For electrode angle $\phi \to 90^{\circ}$, their difference becomes

*Work supported by DOE contract DE-AC02-98CH10886.
#blednykh@bnl.gov

Copyright © 2013 CC-BY-3.0 and by the respective authors

ISBN 978-3-95450-138-0

LONGITUDINAL WAKEFIELD FOR AN AXISYMMETRIC COLLIMATOR*

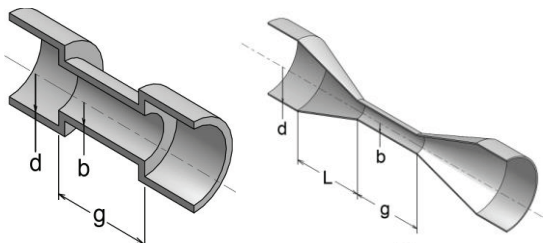
A. Blednykh# and S. Krinsky,
BNL, Photon Science, NY 11973-5000, USA

Abstract

We consider the longitudinal point-charge wakefield, *w(s),* for an axisymmetric collimator having inner radius *b*, outer radius *d*, inner length *g* and taper length *L*. The taper angle α is defined by $\tan\alpha = (d-b)/L$. Using the electromagnetic simulation code ECHO, we explore the dependence of the wakefield on a collimator's geometric parameters over a wide range of profiles: from small-angle tapers to step-function transitions.

INTRODUCTION

In this paper, using the 2-D electromagnetic simulation ECHO code [1,2], we carry out an investigation of the longitudinal short-range wakefield due to an axisymmetric collimator. More detail on this subject can be found in ref. [3].



a) b)

Figure 1: a) Step Collimator. b) Tapered Collimator.

We consider the highly relativistic limit in which a particle traveling at the speed of light *c*, passes through a step-function or tapered collimator illustrated in Figs. 1a,b. We denote: the smaller pipe radius by *b;* the larger radius by *d*; the length of the inner section of the collimator by *g;* and the length of the taper by *L*. The taper angle α is defined by $\tan\alpha = (d-b)/L$. The longitudinal wakefield produced by a point charge is denoted *w(s)*, where *s* is the distance of the test particle behind the driving particle.

Podobedov and Stupakov [4] have noted that the point-charge wakefield for a collimator can be written in the form,

$$w(s;b,d,g,L) = \frac{c\,Z_0}{\pi} log(d/b)\delta(s) + D(s;b,d,g,L), \quad (1)$$

where Z_0 is the impedance of free space. The delta function term corresponds to the result in the optical regime [5]. The causal function *D(s)*, vanishes for *s<0*, and is discontinuous at *s=0*. Since the impedance vanishes at zero frequency, it follows that

$$\int_0^\infty ds\, D(s) = -\frac{cZ_0}{\pi} log(d/b). \quad (2)$$

In this paper, in order to facilitate the illustration of the behavior of the wakefield over a wide range of parameters and for larger *s*, we prefer to introduce the normalized causal function $u(s)$, via

$$w(s;b,d,g,L) = \frac{c\,Z_0}{\pi} log(d/b)[\delta(s) - u(s;b,d,g,L)], \quad (3)$$

where

$$\int_0^\infty ds\, u(s) = 1. \quad (4)$$

Using this normalized function, the ratio of the loss factor k_{loss} to that in the optical regime [5,6] k_{loss}^{opt} is easily expressed. For a Gaussian bunch of rms width σ, this ratio is given by

$$k_{loss}(\sigma)/k_{loss}^{opt}(\sigma) = 1 - \int_0^\infty ds\, u(s) exp(-s^2/4\sigma^2), \quad (5)$$

where $k_{loss}^{opt}(\sigma) = \left(cZ_0/2\pi^{3/2}\sigma\right) log(d/b)$.

For a small-angle tapered collimator *(sat)*, it is shown in ref. [4] that,

$$D^{sat}(0) \cong -\frac{cZ_0}{\pi b\alpha}, \quad (6)$$

and for a step collimator *(st)*, it follows from the work of Okamoto, Jiang and Gluckstern [7] that

$$D^{st}(0) \cong -\frac{0.6\,cZ_0}{\pi b(\pi/2)}. \quad (7)$$

We now note that to within $\pm 10\%$ accuracy,

$$\frac{1}{\pi b} \cong \frac{log(d/b)}{d}, \quad (for\ 1.5 \leqslant d/b \leqslant 6). \quad (8)$$

In this paper, we shall restrict our attention to collimators with parameters within the range $1.5 \leqslant d/b \leqslant 6$. In this case, Eqs. (6,8) imply that for small-angle tapers,

$$u^{sat}(0) \cong \frac{\pi}{d\alpha}, \quad (9)$$

and Eqs. (7,8) show that for a step collimator,

$$u^{st}(0) \cong \frac{0.6\,\pi}{d(\pi/2)}. \quad (10)$$

The short-range wakefield depends predominantly on the two length scales $b\alpha$ and $d\alpha$. In illustrating its behavior, one can plot the wakefield versus the variable $s/b\alpha$ or $s/d\alpha$. In this paper, in order to illustrate more clearly the behavior of the wakefield at longer distances, we prefer to utilize the variable $s/d\alpha$.

For the short-range wakefield $(s/d\alpha \lesssim 0.3)$, our numerical calculations demonstrate that the dependence on g is very weak and they support the approximate validity of the scaling relation,

$$w(s;b,d,g,L) \cong \frac{c\,Z_0}{\pi} log\left(\frac{d}{b}\right)\left[\delta(s) - \frac{1}{d\alpha} f\left(\frac{s}{d\alpha}, \frac{b}{d}\right)\right]. \quad (11)$$

With the wakefield approximated by Eq. (11), it follows from Eq. (5) that the departure of the loss factor from the optical approximation for short bunches $(\sigma/d\alpha \lesssim 0.15)$ can be estimated by

$$k_{loss}(\sigma)/k_{loss}^{opt}(\sigma) \cong 1 - \sqrt{\pi} f\left(0, \frac{b}{d}\right)\frac{\sigma}{d\alpha}. \quad (12)$$

with $f\left(0, \frac{b}{d}\right)$ varying from ~3 for small-angle tapers to ~1.8 for step collimators. Eq. (12) is a more accurate expression for the loss factor than the similar relation given in Eq. (12.26) of ref. [8].

*Work supported by DOE contract DE-AC02-98CH10886.
#blednykh@bnl.gov

Copyright © 2013 CC-BY-3.0 and by the respective authors

WAKE FIELDS DUE TO WALL ROUGHNESS FOR REALISTIC SURFACES*

A.V. Fedotov#, I. Pinayev , BNL, Upton, NY 11973, USA
A. Novokhatski, SLAC National Accelerator Laboratory, Menlo Park, CA 94025, USA

Abstract

Wake fields due to the wall roughness of the vacuum chamber can catch up to the bunch causing energy spread and emittance growth. Several theoretical models were developed in the past which showed rather different importance of this effect. Some models suggest that the wall roughness effect can be minimized if the vacuum chamber surface is characterized by a large aspect ratio of the surface roughness (characteristic length to the height of the surface bumps). To explore these effects several surfaces were measured and direct numerical simulations were performed for such realistic surfaces. The studies were done both for the long bunches to provide estimates of this effect for parameters of the eRHIC project, as well as for very short bunches to explore parameter space of the wall roughness experiment proposed at BNL's ATF.

INTRODUCTION

This work was originally motivated by beam dynamics studies for the eRHIC project [1-3], which is a proposed upgrade of the Relativistic Heavy Ion Collider (RHIC). The present eRHIC design is based on the multi-pass electron beam transport in existing tunnel of RHIC. As a result of a high peak current and a very long beam transport, consideration of various collective beam dynamics effects becomes important [2, 3]. The contribution of the wall roughness to the coupling impedance (wake potential) can become significant, especially when the size of the vacuum chamber is small and length of the electron bunch is short.

Some models indicate that the wall roughness effects can be minimized if the vacuum chamber surface is characterized by a large aspect ratio of the surface roughness (characteristic length to the height of the surface bumps). We attempted to explore these effects for realistic surfaces by means of the direct numerical simulations. Several surfaces were measured, including extruded aluminium, for which such roughness aspect ratio is expected to be very large. The measured surface data was then used as an input parameter in electrodynamics code NOVO [4] to simulate the wake field.

Studies were done both for the long bunches (for the eRHIC parameters [2-3]) with the bunch length longer than a typical correlation length of the rough surface and for short bunches with bunch length much smaller than the correlation length of the surface roughness. In this paper, only results for the case of the short bunches are presented, as an illustrative example of our studies.

WALL ROUGHNESS

An effect of the wall roughness was first estimated based on the impedance of small protrusions of different configurations and orientations in Ref. [5]. Such an "inductive" model can lead to a very strict requirement on the surface polishing. The longitudinal wake potential in this model scales as h/b, where h is the height of the protrusion and b is the radius of the beam pipe.

Another model for the wall roughness was introduced in Refs. [6-7]. In this model the presence of roughness is equivalent to a pipe with a thin dielectric layer or periodic corrugation on the smooth wall surface. This model is typically referred to as the "dielectric" or "resonator" model. In the "resonator" model the coupling impedance also has a resistive part. A detailed comparison of the "resonator" and "inductive" models was given in [7]. The "resonator" model becomes invalid when the correlation length (or period of corrugation) is significantly larger than the height of the protrusion. This happens to be the case for realistic wall surfaces [8] and especially for the surfaces produced with extrusions.

The length of the protrusions along the surface (referred to as the "correlation length" l_c) was taken into account in the model developed in Refs. [8-9], which reduced the coupling impedance significantly for typical surfaces with the large correlation length, resulting in the scaling of the wake potential as $h \cdot h/(b \cdot l_c)$. A comparison of such model with the "inductive" model was given in Ref. [10].

In the eRHIC design, we relied on a significant reduction of the wall roughness effects due to the large aspect ratio of the wall roughness by choosing extruded aluminium vacuum chamber. Measurements of several surfaces were performed to allow systematic study of wake field dependences on the height and length of the roughness. In addition, rather than using measured surface data in approximate models for the estimates, we attempted to study wake fields directly, using numerical simulations with the code NOVO [4].

MEASURED SURFACES

In this paper, we limit our discussion to three measured surfaces: 1) "surface-1": sample of an extruded aluminium surface from the NSLS-II vacuum chamber; 2) "surface-2": rough aluminium surface without extrusions; 3) "surface-3": extruded aluminium surface from the superconducting undulator provided by ANL [11].

*Work supported by the US Department of Energy under contract No. DE-AC02-98CH10886 and DE-AC02-76SF00515.
#fedotov@bnl.gov

Copyright © 2013 CC-BY-3.0 and by the respective authors

ISBN 978-3-95450-138-0

CHANGES IN ELECTRON CLOUD DENSITY WITH BEAM CONDITIONING AT CESRTA*

J.P. Sikora†, J.A. Crittenden, D.O. Duggins, Y. Li, X. Liu, CLASSE, Ithaca, New York 14853 USA

Abstract

We compare measurements of electron cloud (EC) buildup in uncoated and TiN-coated aluminum vacuum chambers as a function of integrated beam dose up to 1140 amp-hours. The EC density in newly installed bare aluminum chambers increases with beam dose, while the EC density in the TiN-coated chambers decreases with dose under the same beam conditions. Several techniques are used to monitor EC buildup. These include shielded pickups that measure the flux of cloud electrons onto the beam-pipe wall, and a TE wave resonance technique that measures the EC density within the volume of the beam-pipe. These measurements were made at the Cornell Electron Storage Ring, which has been reconfigured as a test accelerator CESRTA, providing positron and electron beams with energies ranging from 2 GeV to 5 GeV and a variety of bunch train configurations.

INTRODUCTION

New chambers were installed at three locations in the Cornell Electron Storage Ring Test Accelerator (CESRTA) in August 2012 as shown in Fig. 1. We have previously reported on the effects of beam conditioning measured immediately after chamber installation and then again after a significant beam dose of up to 1140 amp-hours [1]. Data with beam dose that is between these two extremes is presented here in order to estimate the dose required to obtain this conditioning. Table 1 shows the number of amp-hours for each beam. The chambers in L3 were let up to atmosphere as part of a separate project in January 2013, but the chambers at 15W and 15E have been under vacuum throughout this period. The table shows two values for the beam dose in April 2013 to reflect this.

Using the TE wave technique, data was collected in the TiN and bare aluminum chambers in L3 as well as the bare aluminum chamber at 15E. The raw data is in the form of phase modulation sideband amplitudes from which the peak electron cloud (EC) density can be calculated [2, 3]. The 10-bunch TE wave data taken in this study use 14 ns spaced bunches.

Shielded pickups (SPU) collect data from the TiN chamber at 15W and the bare aluminum chamber at 15E. This data is in the form of an oscilloscope trace as the SPU samples the flux of cloud electrons onto the vacuum surface [4]. For the purpose of plotting, the averaged scope trace is integrated to obtain the charge into the 50 Ω scope input for each turn (including the preamplifier voltage gain of 100). The data presented here is from two bunches of equal charge spaced by 14 ns. A turn at CESRTA is 2.5 μs and data is recorded with a 100 ns span, which is enough time to capture the non-zero signal from two bunches.

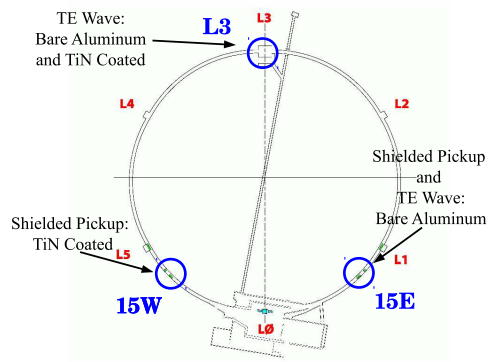


Figure 1: This sketch of the CESRTA storage ring shows the location of detectors used in this study: SPU in a chamber with TiN coating at 15W; SPU and TE wave measurements in the same aluminum chamber at 15E; TE wave measurements in the grooved TiN and bare aluminum chambers of L3.

Table 1: Beam Dose After Chamber Installation

Date (mm/dd/yy)	e- Amp-Hr	e+ Amp-Hr
08/22/12:	0.0068	0.028
08/23/12:	0.411	0.140
10/10/12:	167.9	166.2
11/19/12:	305.6	305.6
12/13/12:	306.0	308.0
(04/17/13):	(251.6)	(269.4)*
04/17/13:	558.8	579.7

*Since L3 at atmosphere during January 2013

CONDITIONING OF TITANIUM NITRIDE

There are two TiN-coated chambers in this study: the grooved chamber at L3 where there is TE wave data and the 15W chamber with SPU data. Figure 2 gives examples of the recorded 2-bunch SPU data at 8 mA/bunch. The signal from the first bunch peaks before 20 ns and is mostly composed of photo-electrons produced in the empty chamber. The larger second bunch signal at about 30 ns includes

*This work is supported by the US National Science Foundation PHY-0734867, PHY-1002467 and the US Department of Energy DE-FC02-08ER41538, DE-SC0006505.

† jps13@cornell.edu

Copyright © 2013 CC-BY-3.0 and by the respective authors

3D TOROIDAL FIELD MULTIPOLES FOR CURVED ACCELERATOR MAGNETS*

L. Brouwer †, S. Caspi, D. Robin, W. Wan, LBNL, Berkeley, CA 94720, USA

Abstract

Curved magnets producing continuously rotating field multipoles along the length of the bend can provide strong and continuous transverse focusing, making them of interest for accelerator systems such as compact ion beam gantries and synchrotron light sources. Evaluating the utility of such rotating multipole systems requires an accurate description of field behavior for beam physics calculations. This paper presents a helical scalar potential solution in 3D toroidal harmonics relevant to boundary conditions on the surface of a torus. The resulting fields are evaluated for a curved helical quadrupole channel to illustrate field rotation and the effect of magnet curvature.

INTRODUCTION

Previous analysis and use of accelerator magnets producing helical fields have focused on straight, cylindrical designs [1]-[5]. There is interest in studying the extension of this concept to curved magnets [6], requiring expressions for allowable fields rotating around the bend of torus. Previous work on field description and measurement of curved magnets is specific to cases of axial symmetry where the assumption of no field variation along the bend is made [7]-[9].

In these references Schinzer *et al.* present a method for finding scalar potential solutions in local polar coordinates using approximate R-separation of the scalar Laplace equation (expansion in the aspect ratio of the torus). In this paper a similar approach was taken to obtain expressions relevant to rotating fields on the bend of a torus, with the difference being the use of toroidal coordinates and full R-separation in 3D toroidal harmonics.

TOROIDAL COORDINATES

The right hand toroidal system of η, ξ, ϕ is formed by the rotation of bipolar coordinates η and ξ about the vertical axis (Fig. 1). Surfaces of constant η are tori, making toroidal coordinates a natural choice for problems with boundary conditions on the surface of a torus. Scale factors for this system are

$$h_\eta = h_\xi = \frac{a}{\cosh\eta - \cos\xi}$$
$$h_\phi = \frac{a\sinh\eta}{\cosh\eta - \cos\xi} \qquad (1)$$

where $(\pm a, 0)$ are foci of the bipolar system.

* Work supported by the U.S. Department of Energy under contract No. DE-AC02-05CH11231 and the National Science Foundation under grant No. DGE 1106400.

† lnbrouwer@lbl.gov

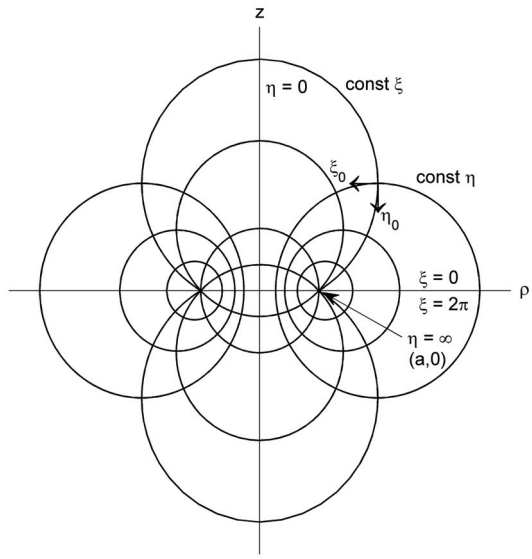


Figure 1: Bipolar coordinates $0 < \eta < \infty$ and $0 \le \xi \le 2\pi$ forming toroidal coordinates when rotated about the z-axis.

SCALAR LAPLACIAN

In a current free region the magnetic field can be expressed using only the gradient of a scalar potential $\vec{B} = -\nabla\psi$. The divergence of this field produces Laplace's equation for the scalar potential $\nabla\cdot\vec{B} = -\nabla^2\psi = 0$. In toroidal coordinates the scalar Laplace equation is

$$\nabla^2\psi = \frac{1}{h_\eta h_\xi h_\phi}\left[\frac{\partial}{\partial\eta}\left(\frac{h_\xi h_\phi}{h_\eta}\frac{\partial\psi}{\partial\eta}\right) + \frac{\partial}{\partial\xi}\left(\frac{h_\eta h_\phi}{h_\xi}\frac{\partial\psi}{\partial\xi}\right) + \frac{\partial}{\partial\phi}\left(\frac{h_\eta h_\xi}{h_\phi}\frac{\partial\psi}{\partial\phi}\right)\right] = 0. \qquad (2)$$

Substitution of the coordinate dependent scale factors (1) produces

$$\frac{k^2}{a^2}\left[\frac{\partial^2\psi}{\partial\eta^2} + \frac{\partial^2\psi}{\partial\xi^2} + \coth\eta\frac{\partial\psi}{\partial\eta} - k^{-1}\left(\sinh\eta\frac{\partial\psi}{\partial\eta} + \sin\xi\frac{\partial\psi}{\partial\xi}\right) + \frac{1}{\sinh^2\eta}\frac{\partial^2\psi}{\partial\phi^2}\right] = 0, \qquad (3)$$

where the simplification $k(\eta,\xi) = \cosh\eta - \cos\xi$ is made. The technique of R-separation is used, producing

$$\frac{k^{5/2}}{a^2}\left[\frac{\partial^2 u}{\partial\eta^2} + \frac{\partial^2 u}{\partial\xi^2} + \coth\eta\frac{\partial u}{\partial\eta} + \frac{1}{4}u + \frac{1}{\sinh^2\eta}\frac{\partial^2 u}{\partial\phi^2}\right] \qquad (4)$$

Copyright © 2013 CC-BY-3.0 and by the respective authors

ISBN 978-3-95450-138-0

RETRIEVAL OF EFFECTIVE PARAMETERS OF METAMATERIALS FOR ACCELERATOR AND VACUUM ELECTRON DEVICE APPLICATIONS *

Z. Y. Duan[1, 2, #], M. A. Shapiro[1], J. S. Hummelt[1], and R. J. Temkin[1]
[1]Plasma Science and Fusion Center, Massachusetts Institute of Technology, 167 Albany St., Cambridge, MA 02139, USA
[2]Institute of High Energy Electronics, School of Physical Electronics, University of Electronic Science and Technology of China, No.4, Section 2, North Jianshe Road, Chengdu 610054, China

Abstract

In this paper, we propose a new method to retrieve the effective material parameters, *i.e.*, the effective permittivity and permeability. We first obtain the effective permeability analytically and then retrieve the effective permittivity numerically from the structure's dispersion curve. This method is different from that one which is based on the scattering parameters for metamaterial slabs. The approach presented here offers an effective parameter retrieval for metamaterial-based accelerator and vacuum electron device applications.

INTRODUCTION

Metamaterials are artificial electromagnetic materials comprised of sub-wavelength elements. Metamaterials offer many new options for the design of components that use electromagnetic materials. A Double-Negative Metamaterial (DNM) has both negative permittivity and negative permeability and can be described by an effective medium theory [1, 2]. We investigate metamaterials at microwave, millimeter wave, and THz frequencies for application as accelerator structures, as interaction circuits of high-power microwave vacuum electron devices, and as beam diagnostics tools.

The present parameter retrieval method based on the scattering parameters (S_{11} and S_{21}) [3] is not suitable for the metamaterial-loaded waveguide case due to the waveguide dispersion and the anisotropy of the metamaterials as well as the complex mode. Up to now, the parameter retrieval method is only suitable for metamaterial slabs interacting with TEM mode in free space.

In this paper, we propose a metamaterial-loaded rectangular waveguide which is described by the effective medium theory and provide a method for the retrieval of the effective material parameters from the dispersion relation. The method presented here can offer a theoretical foundation for developing novel metamaterial-based accelerators and high-power vacuum electron devices [4]

*Work supported by DOE, High Energy Physics (Grant No. DE-SC0010075), AFOSR MURI Grant FA9550-12-1-0489 Administered by Univ. New Mexico and the Fundamental Research Funds for the Central Universities (Grant No. ZYGX2010X010).
#zhyduan@mit.edu

RETRIEVAL METHOD

A square waveguide operating below the cut-off frequency which is loaded by split-ring resonators (SRRs) was first proposed by Marques et al. [5] The empty waveguide can be considered as a negative permittivity medium only when the TE mode is excited, and the SRR array forms the effective negative permeability medium. As stated in [6], when metallic rods or stripes are loaded in the transverse direction of the waveguide operating below the cut-off frequency, the TM mode can be excited. Since TM modes are of interest in accelerator and vacuum electron device applications, we propose to use a rectangular waveguide loaded by complementary split-ring resonators (CSRRs) as shown in Fig. 1 (a). As opposed to SRRs on a dielectric in a waveguide where dielectrics can easily induce breakdown or damage [5], a CSRR-loaded waveguide is also completely composed of metallic elements and thus suitable for high-power applications.

The CSRR array can be characterized by an effective negative permittivity in the y direction. In addition, when the loss of the proposed waveguide is not considered, the corresponding empty rectangular waveguide operating below the cut-off frequency can be considered as a "magnetic" plasma and its relative permeability is given by [6]

$$\mathrm{Re}(\mu_{r,eff}) = 1 - \frac{\omega_c^2}{\omega^2}, \tag{1}$$

$$\omega_c = \frac{\pi}{\sqrt{\varepsilon_0 \mu_0}} \sqrt{\frac{1}{d^2} + \frac{1}{h^2}}. \tag{2}$$

Here ω_c is the cut-off frequency for the TM_{11} mode, ω is the angular frequency, and ε_0 and μ_0 are the vacuum permittivity and permeability, respectively, and d and h are the cross-section dimensions of the rectangular waveguide.

In Fig. 1 (b), two CSRR-loaded metallic plates are placed inside a rectangular waveguide and the beam is located between the two CSRR layers. In this waveguide, there is a TM-dominated hybrid mode. This mode is not pure TE or TM mode, but is a complex hybrid mode with field components both perpendicular and parallel to the electron beam direction. From the point of view of the effective medium theory, the "*macroscopic*" mode is

Copyright © 2013 CC-BY-3.0 and by the respective authors

SIMULATION OF WAKEFIELDS FROM AN ELECTRON BUNCH IN A METAMATERIAL WAVEGUIDE*

J. S. Hummelt[1], B. J. Munroe[1], S. M. Lewis[1], M. A. Shapiro[1#], and R. J. Temkin[1]
[1]Plasma Science and Fusion Center, Massachusetts Institute of Technology,
Cambridge, MA 02139, USA

Abstract

A metamaterial waveguide is proposed for use in a linear accelerator. The waveguide walls are made of a metamaterial structure composed of complementary split-ring resonators (CSRRs). In such a metamaterial waveguide, a TM-like mode exists that can be excited by an electron bunch. A complementary split-ring resonator is formed by slots machined in a metallic plate. The fact that the metamaterial waveguide is both planar and composed of elements that are direct machined makes it both easy to build and easily scalable to higher frequency linear accelerators. The metamaterial waveguide is coupled to single mode rectangular waveguides. These waveguides can then be connected to a microwave network to couple power into or out of the waveguide. The metamaterial waveguide that is presented was designed using electromagnetic simulations in HFSS, and wakefield as well as PIC simulations of the structure were carried out using the CST Particle Studio code.

INTRODUCTION

Metamaterial (MTM) structures [1] are periodic structures that are both sub-wavelength and operate in a frequency range in which the structures are resonant. In contrast to the disk-loaded waveguides used as accelerator structures, spatial harmonics do not play a role in the accelerating properties of MTM structures. Basic studies of MTMs for use in or as accelerator structures, beam diagnostics, and interaction structures of higher power microwave sources are of interest due to the potential benefits of using frequency selective materials in microwave generation and the advances in MTM fabrication that may allow for high frequency design.

A complementary split-ring resonator (CSRR) with negative permittivity has been introduced [1]. A medium formed of an infinite array of parallel plates with CSRRs machined into them was proposed as an accelerator structure [2,3]. This system can be considered as an infinite array of electric dipoles, and the effective permittivity and permeability of this MTM were determined and simulations showed that this MTM has a negative refractive index.

The CSRR MTM has been modified to be used as an accelerator structure. Instead of using an infinite medium, a MTM waveguide is formed by placing the CSRRs in a waveguide that is below cutoff. In this paper we study the dispersion properties of the MTM waveguide and the electron beam interaction with its field.

METAMATERIAL WAVEGUIDE

The MTM waveguide proposed (Fig. 1) is an assembly of four rectangular waveguides that have each had CSRRs machined into one of their faces as shown in Fig. 2. The waveguides are assembled such that the waveguide walls into which the CSRRs have been machined divide a 'cross' shaped pipe into four outer waveguide regions and one central waveguide region through which the electron beam passes. One period of the structure along the axial direction of the waveguide includes two split ring slots with openings facing each other, with total period p = 7 mm (Fig. 2). The MTM waveguide is designed in the S-band operating at 2.6 GHz. As the period is 7 mm, it is sub-wavelength at this frequency along the axial direction. The transverse dimension of the split rings is 41 mm. The slot width is g=2 mm and the CSRR thickness is 1.6 mm. In addition to the cross shaped structure shown in Fig. 1 we have investigated square, hexagonal, and triangular geometries as well.

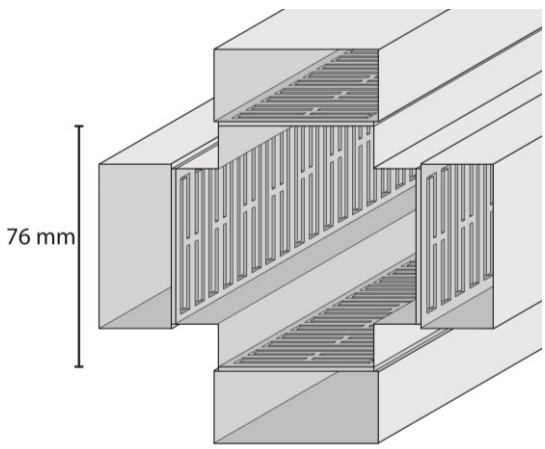


Figure 1: Metamaterial waveguide assembled from four WR187 waveguides (47.55 x 22.15 mm) with CSRRs machined into inner face of assembled structure.

*Work supported by AFOSR MURI Grant FA9550-12-1-0489 Administered by Univ. New Mexico and by DOE, High Energy Physics (Grant No. DE-SC0010075)
#shapiro@psfc.mit.edu

Copyright © 2013 CC-BY-3.0 and by the respective authors

ISBN 978-3-95450-138-0

RIBBON ELECTRON BEAM SOURCE FOR BUNCHED BEAM PROFILE MONITOR AND TOMOGRAPHY

V. Dudnikov, Muons, Inc., Batavia, IL 60510, USA
A. Aleksandrov, ORNL, Oak Ridge, TN 37831, USA

Abstract

Ribbon electron beam source with a strip cathode has been designed, fabricated and tested. Image of the ribbon electron beam with width up to 15 cm has been registered on the luminescent screen. This ribbon beam can be used for the large proton bunch profile monitoring in the Spallation Neutron Source (SNS) proton storage ring. Advanced beam diagnostics are essential for high performance accelerator beam production and for reliable accelerator operation. It is important to have non-invasive diagnostics which can be used continuously with intense beams of accelerated particles.

INTRODUCTION

Beam profile determination at high intensity ion accelerators requires the use of non-destructive methods. The basic physics and recent technical realizations of important non-intercepting profile diagnostics are summarized in Ref. [1]. Transverse electron beam scanners were realized recently for use in the SNS storage ring by Aleksandrov et al. [2, 3].

In the electron beam profile monitor (EBPM) developed at the SNS, a transverse beam profile is reconstructed from the deflection of electrons crossing the proton or ion beam after being influenced by the beam's space charge, as schematically shown in Fig. 1 [1]. A pencil electron probe is formed by an electron gun and scanned through the proton beam by the electric field of deflectors as in an oscilloscope tube. The position of the scanning electron probe after crossing the proton beam is visualized by a fluorescent screen and the image is captured by a camera for further processing. Assuming the electron beam has a much lower diameter than the proton or ion beam and the scan duration is much shorter than the ion bunch passage, the space charge field can be treated as constant. The beam profile can be reconstructed from the electron beam trace using the mathematical formalism given in Ref. [2].This method was considered for high energy synchrotrons and recently commissioned at the SNS [3]. A significant part of the scanner hardware is used for the extension of the scanning e-beam. Large quadrupole magnets also complicate the magnetic shielding of this version of scanner. For these reasons, electron beam profile monitors (EBPM) with electron beams formed by the deflection of pencil e-beams can be long, and fairly complex. Potentially more practical e-beam profile monitors that are more suitable for proton beam tomography can be developed using a strip cathode for formation of a ribbon beam as discussed below [4]. The analysis of the data for beam bunch transverse profiles for the system that we are proposing will be very similar to what has been developed for the EBPM as described below.

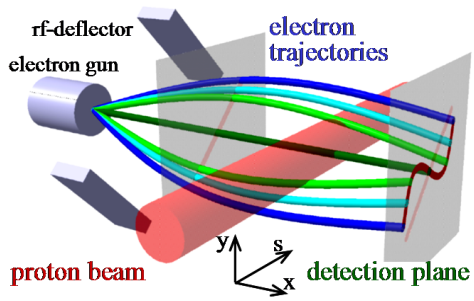


Figure 1: Schematic of an electron scanner for the vertical beam profile [1].

RIBBON ELECTRON BEAM PROFILE MONITOR (REBPM)

The ribbon electron probe beam profile monitor (REBPM) using a strip cathode is proposed as shown in Fig. 2. The electron ribbon (6) is generated by the strip cathode (1) with extractor (2). The transverse dimensions of the ribbon are defined by the collimator with two slits (3) and (5). The width or duration of the ribbon electron probe (6) is formed by the deflection of the ribbon electron beam across slit (5) by a pulsed voltage on the deflecting plates (4). Electrons of the ribbon electron probe after deflection by electric field of the proton bunch are visualized on the luminescent screen (7) and recorded by a fast CCD camera for further processing by the corresponding software discussed above.

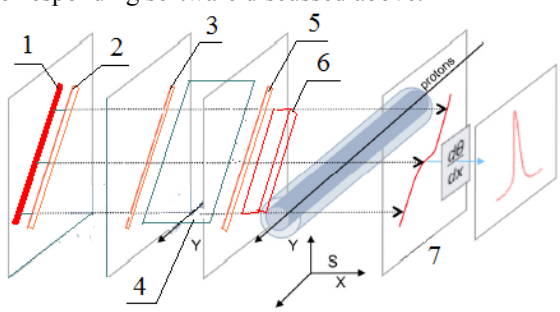


Figure 2: Electron probe beam profile monitor with a strip cathode.

The mechanical design of the system is shown in Fig. 3, the 3D models of the of the strip cathode electron gun with insulators and support insulators are shown in Figs. 4-6.

*Work supported by Contract DE-AC05-00OR22725 and by STTR grant DE-SC0007559.
#Vadim@muonsinc.com

Copyright © 2013 CC-BY-3.0 and by the respective authors

POSSIBLE EXPERIMENTS ON WAVE FUNCTION LOCALIZATION DUE TO COMPTON SCATTERING

V. Danilov, A. Aleksandrov, J. Galambos, T. Gorlov, Y. Liu, A. Shishlo, ORNL, Oak Ridge, TN 37831, U.S.A.
S. Nagaitsev, Fermilab, Batavia, IL 60510, U.S.A.

Abstract

The reduction of a particle's wave function in the process of radiation or light scattering is a longstanding problem. Its solution will give a clue on processes that form, for example, wave functions of electrons constantly emitting synchrotron radiation quanta in storage rings. On a more global scale, it may shed light on wave function collapse due to the process of measurement. In this paper we consider various experimental options using Fermilab electron beams and a possible electron beam from the SNS linac and lasers to detect electron wave function change due to Compton scattering.

INTRODUCTION

The first dedicated experiments to measure the wave function of an electron in accelerator were started in Novosibirsk about two decades ago and described in [1, 2]. The experiments showed that the wave function of an electron in a storage ring is very localized, and its motion is similar to the motion of a classical particle with random kicks without any sign of phase space dilution due to the potential well (RF) nonlinearities.

The experiments were performed in the VEPP-3 storage ring with a single circulating electron [2] and the light from an undulator that was detected by photomultipliers. The standard Brown-Twiss intensity interferometer scheme used a splitter to send the photons to two photomultipliers. The basic idea to measure the longitudinal wave function size was to detect two photons by different photomultipliers during one passage of an electron through the undulator and the rms difference in time, multiplied by velocity of light, was supposed to give the wave function size. Unfortunately, the photomultipliers were slow – their response time (called the dispersion in [2]) was around 160 ps. The signal time difference from two photomultipliers was well within this number, therefore it was concluded that the wave function size is much shorter than the available resolution.

Here we pursue another approach. Using scattered instead of radiated quanta, and knowing the precise energy of electrons and photons, we can measure the resulting energy distribution (and, consequently, the electron wave function) after the scattered photon is measured by a detector and after we employ coincidence scheme, i.e. take only pairs of related electrons and Compton photons with very small angle with the beam velocity vector. This results in a very small transverse recoil and the electrons have mostly longitudinal momentum (or energy) change. This is possible if the resolution of detectors is high and the repetition rate of events is low. If the repetition rate is high, the electron beam energy spread in its left shoulder (see Figure 1) gives the energy spread of scattered electrons even without precise knowledge of the measured gamma quanta if the quanta don't introduce a large angular spread for electrons (we discuss this in the next sections).

An experiment outline is shown schematically in Figure 1. An electron beam with very small energy spread from a linac with energy in the range of hundreds of MeV collides with a laser beam producing rare Compton quanta. The backward scattered quanta are measured in a small scattering angle range (to have precise knowledge of their energy) by an X-ray detector and the electron that scattered the quanta is measured in an energy analyser that separates this electron from the rest of the beam by, e.g., magnetic field.

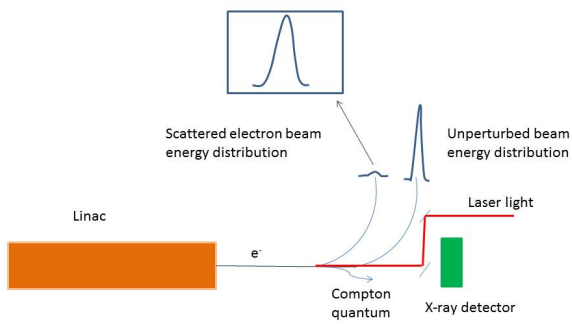


Figure 1: Experiment outline.

If the separation is larger than the width of the electron beam after the magnets, it is possible to measure the width of the energy distribution of the scattered electrons. This distribution, if different from the beam distribution, will give us the wave function width, or its localization, after the process of scattering and measurement of the photon. One has to notice that Figure 1 two-peak discontinuous distribution of electrons can be obtained if we cut out all electron-photon scatterings with large angles of Compton quanta with respect to beam axis pointing toward beam velocity. This procedure will eliminate the scattered-electron angular spread contribution to the left shoulder distribution and as a

Copyright © 2013 CC-BY-3.0 and by the respective authors

ISBN 978-3-95450-138-0

MEASUREMENT OF NON-LINEAR INSERT MAGNETS*

F. H. O'Shea†, R. Agustsson, A. Murokh, E. Spranza,
RadiaBeam Technologies, Santa Monica, CA 90404, USA
S. Nagaitsev, A Valishev, Fermilab, Batavia, IL 60510, USA

Abstract

Fermilab's Integrable Optics Test Accelerator (IOTA) is an electron storage ring designed for testing advanced accelerator physics concepts, including implementation of non-linear integrable beam optics and experiments on optical stochastic cooling. In this report we describe the contribution of RadiaBeam Technologies to the IOTA project which includes non-linear magnet engineering, prototype fabrication and measurement.

INTRODUCTION

IOTA is an electron ring designed as a proof-of-principle of non-linear integrable optics [1] at the ASTA facility [2]. Nonlinear optics are predicted to increase stability of the electron beam through Landau damping [3] and the natural tune spread of the electron beam will also increase dynamic aperture [1], leading to more intense beams in high-energy physics machines. The goal of the project is to study single particle dynamics in the non-linear regime using a 150 MeV electron beam in a ∼40 m circumference ring with 4 non-linear inserts that are each 2 m long [4]. While the beam dynamics of the non-linear optics system is being studied at Fermilab, the magnetic inserts are being designed and manufactured at RadiaBeam Technologies.

In this paper we discuss the magnetic design and tolerance requirements of the IOTA inserts and the measurement system being built to measure the first prototype of these unique magnets. The goals of the prototype magnet insert are to gain experience manufacturing a complex geometry, determine the cross-talk between adjacent magnet segments, and measure the field of a challenging insert that is tens of centimeters long with a sub-centimeter aperture.

DESIGN

The approach to this problem is the standard magnetostatic approach [5]: find the equipotential surfaces and choose one to fill with iron, correct the edge fields for the finite extent of the real magnets and then magnetize that iron via a current carrying coil on a "far off" yoke. The magnetostatic problem is defined in terms of the magnetic vector potential for a 2D object:

$$A_z(x,y,s) = \frac{B\rho\, c^2\, t}{\beta(s)} \sum_{n=1}^{\infty} \frac{2^{2n-1} n!(n-1)!}{(2n)!} \times \left(\frac{x^2+y^2}{\beta(s)\, c^2}\right)^n \cos\left[2n \arctan\left(\frac{y}{x}\right)\right]. \quad (1)$$

Where $B\rho$ is the magnetic rigidity of the particles, c is a scale factor with units $m^{1/2}$, t is a unitless strength parameter, x, y and s are the horizontal, vertical and longitudinal coordinates, respectively, and $\beta(s) = \beta^* + \frac{s^2}{\beta^*}$ is the beta-function in the non-linear insert with $\beta^* = 0.727$ m at the longitudinal center of the insert.

The vector potential (and as we will see, the scalar potential) is clearly continuous in the longitudinal coordinate but it would be very difficult to create a single 2 m long device that varies continuously to produce the desired scaling. Accordingly, the 2 m device is divided into 20 sections of constant parameters that are 6.5 cm long, between each section is a 3.5 cm long non-magnetic block (or air gap) used to separate the different segments. Because of the symmetry around the longitudinal center of the device, there are 10 different segments. The segments are labeled 1 through 10 with 1 being nearest the center of the 2 m device and 10

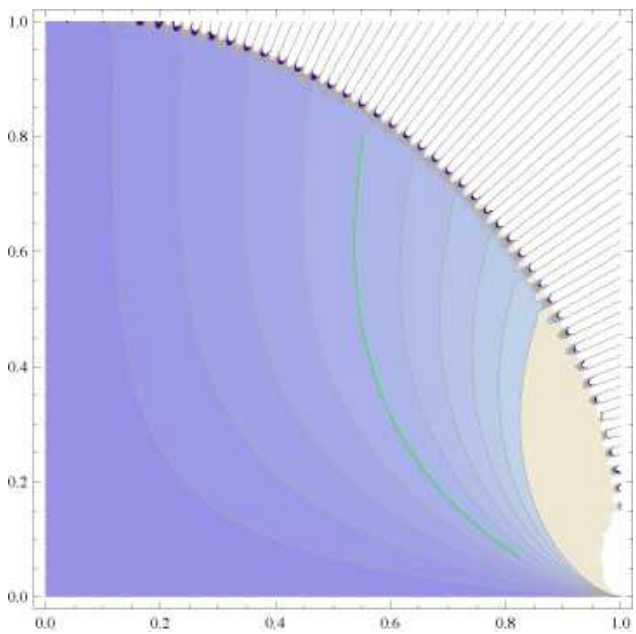


Figure 1: Contour plot of the equipotential lines of $\phi(x_N, y_N)$. The superimposed green line is the line taken for the face of the poles.

* Work supported by DOE under contract DE-SC0009531.
† oshea@radiabeam.com

Copyright © 2013 CC-BY-3.0 and by the respective authors

PERFORMANCE OF PLANAR RADIATOR IN THE RADIABEAM-IAC EXPERIMENT*

A. V. Smirnov#, R. Agustsson, S. Boucher, J. J. Hartzell, S. Storms, RadiaBeam Technologies Inc., Santa Monica, CA 90404, USA and Y. Kim Idaho Accelerator Center and Idaho State University, Pocatello, ID 83209, USA

Abstract

Planar gratings structure for generation of mm-sub-mm wavelength long-range wakefields is analysed. The rugged, side-open, slow wave structure can sustain substantial beam loading including long multi-bunch trains up to CW operation. Electromagnetic performance of the structure is characterized numerically vs. experiment with emphasis to application to flat beams. It is shown that such an electrically wide, wavelength-gap structure can operate at significantly reduced tolerances whereas substantial flatness of the wakefield can be obtained at essentially non-flat eigenmode profile.

INTRODUCTION

In the experiment [1] conducted at Idaho Accelerator Center (IAC) a side-open gratings planar structure (see Fig. 1) was used to generate and partially extract mm-sub-mm wave radiation induced by wakefields. Since the structure is relatively new the radiator performance needs more detailed characterization as well as to substantiate the measurements made and to support other potential applications such as compact THz sources [2], energy dechirping [3] and collinear wakefield acceleration.

We analyse here the structure performance with GdfidL code [4] in eigen- and time domains. The side opening has been modelled as a large space enclosed by low conductivity walls (see Fig. 1) with negligible influence on the frequencies of the modes of our interest.

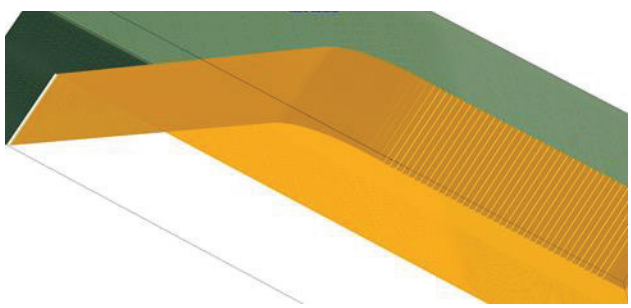


Figure 1: GdfidL model of one-quarter structure with horn antenna. Interaction gap: 1.26 mm, width: 6.3 mm, grating length L=30.4 mm (130 periods), period: 0.23 mm, and groove depth: 0.081 mm.

EIGENMODES

We analyse here eigenmodes that are in synchronism with the relativistic beam (v/c=0.996) using only one period of the regular part of the structure. Several modes with different horizontal variations can potentially interact with the beam in such an oversized structure. Field patterns for lowest modes are shown in Fig. 2. Side opening provides modal selection for the wakefield energy radiated forward [2,5] due to the side radiation losses via the factor $F = ((1-\exp(-\alpha L))/\alpha L)^2$, where $\alpha = \pi f / Q v_{gr}$ is the modal attenuation. Simulation results for the first few eigenmodes are shown in Table 1.

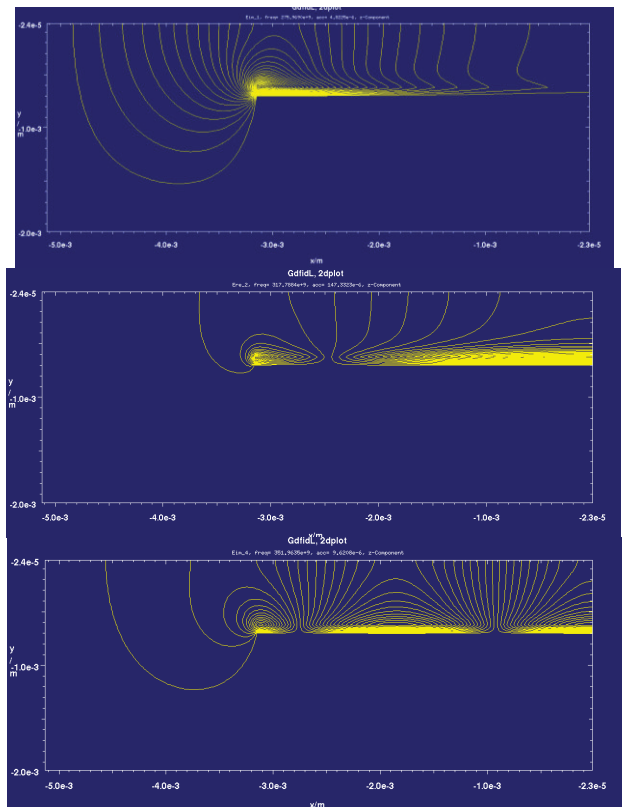


Figure 2: Contour plots in transverse XY plane for the Ez field for three lowest modes which are synchronous to 5MeV beam at 276, 312 and 352 GHz (one quarter model).

Table 1: F, group velocity, and r/Q [Ω/m] for different widths w [mm] of the beam filling the vertical gap.

f, GHz	F	r/Q, w=0	r/Q, w=2	r/Q, w=4.76	βgr
276	0.05	11	14.3	94	0.81
312	0.53	2450	2201	1343	0.844
352	0.27	1076	721	112	0.72
401	5e-4	459	180	23	0.79

*Work supported by US DoE Contract DE- SC-FOA-0000760
#asmirnov@radiabeam.com.

ISBN 978-3-95450-138-0

Copyright © 2013 CC-BY-3.0 and by the respective authors

WAKEFIELD CALCULATIONS FOR SEPTUM MAGNET IN LCLS–II*

K.L.F. Bane, T. Raubenheimer, SLAC, Menlo Park, CA 94025, USA

INTRODUCTION

The LCLS-II would have delivered low emittance beams with an energy in the range 7–13.5 GeV to one of two undulators, one for generating soft x-rays (SXR) and the other for hard x-rays (HXR) [1]. To allow for flexibility in the distribution of the beams to the two undulators, a fast kicker and Lambertson-type septum magnet would be installed just upstream of the undulator region. The septum itself is 2 m long and the beam is meant to traverse it while passing within millimeters of metallic walls, which will induce resistive wall wakefields. The longitudinal wakes will take energy from the beam and add a longitudinally correlated energy variation—an energy chirp. The transverse wakefields can increase the beam's projected emittance.

In this report we perform calculations of the longitudinal and transverse wakefields of the septum, find their effects on the beam, and put the results in the context of the wakes of other objects in the downstream part of LCLS-II.

Figure 1 gives the layout of the LCLS-II beamlines upstream of the undulators, showing the location of the fast kicker and septum magnets. The septum magnet geometry we consider is shown in Fig. 2. The design orbit for the unkicked (free) beam is 1.6 mm above a curved SS surface; the (horizontally) kicked beam moves in the middle of a flat, rectangular chamber with a vertical aperture of 5 mm.

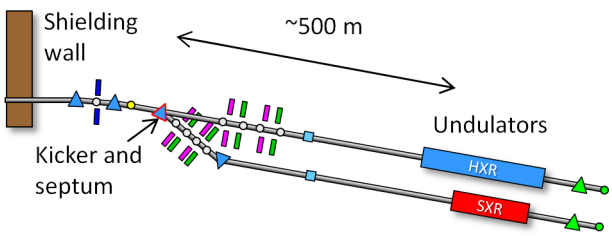


Figure 1: Layout of the LCLS-II beamlines in the vicinity and downstream of the fast kicker and septum magnet [2].

WAKES OF SHORT BUNCHES

Four bunch scenarios are considered for the operation of LCLS-II: short, relatively flat distributions with bunch charge eN = 250, 60, 12, 50 pC; peak current $\hat{I}$ = 3, 3, 3, 4 kA; full width t_{fw} = 70, 15, 3, 10 fs. With the peak current (relatively) fixed and the bunches quite short, the wake strength of a bunch tends to vary $\sim t_{fw}$—since the wake is normalized to total charge eN. Thus it is the first scenario, the so-called "high charge" case with eN = 250 pC that will induce the largest wake effects by far, and

* Work supported by the U.S. Department of Energy under contract DE-AC02-76SF00515.

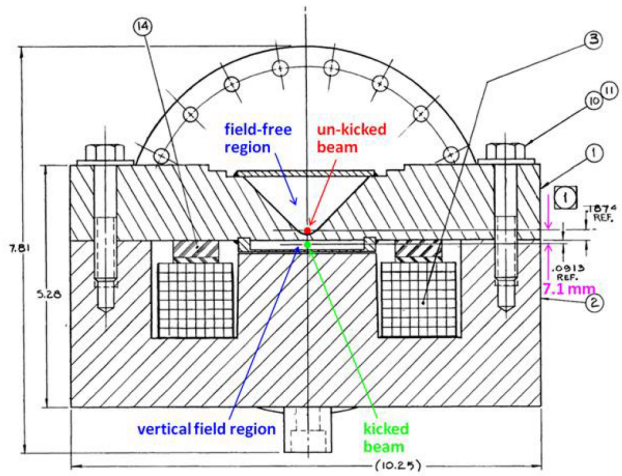


Figure 2: Cross-section the horizontally deflecting Lambertson septum magnet, "HLAM", considered in this report. The length of the chamber is 2.2 m. (Dimensions in the figure, unless otherwise specified, are in inches.)

in this report we limit our study to this case. The bunch distribution $I(s)$, to be used in calculations, is taken from the LCLS and is shown in Fig. 3 (the blue curve); note that the head is to the left, at positions $s < 0$. The distribution is double-horned, with an rms length $\sigma_z = 6.1$ μm; its core can be approximated by a uniform 3 kA (the red curve). Presumably, for the FEL we would like the entire beam core to reach saturation in the undulator together; thus the wake effects over the bunch core are most important.

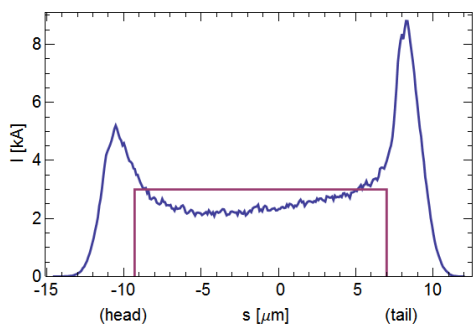


Figure 3: The bunch distribution used in the simulations, which represents the "high charge," 250 pC case (blue), and a uniform approximation of the core at 3 kA (red).

The energy variation induced in a bunch by the wake is

$$E_w(s) = -\frac{L}{c}\int_0^\infty W_z(s')I(s-s')\,ds'\,, \qquad (1)$$

Copyright © 2013 CC-BY-3.0 and by the respective authors

ISBN 978-3-95450-138-0

NEW TECHNIQUE TO MEASURE THE EMITTANCE OF BEAMS WITH SPACE CHARGE

K. Poorrezaei, R. B. Fiorito, and R. A. Kishek
Institute for Research in Electronics & Applied Physics,
University of Maryland, College Park, MD 20742, U.S.A.

Abstract

Characterization of the transverse phase space of electron beams with space charge is an important requirement for high brightness particle accelerators. We present a novel technique to measure the transverse rms emittance. The method uses the beam divergence, measured, e.g. with optical transition radiation interferometry, and the beam radius, obtained by imaging the beam, to determine the cross correlation term and thus all the terms in the equation for the rms emittance. The experimental data is obtained with a lens-drift-screen setup similar to what is used in a quadrupole scan. However, the analysis of the scan data is unique. It involves taking the cross-correlation term as a control variable in a procedure which matches the beam envelop radius and its derivative calculated from the envelope equation, with the measured radius and divergences at the screen. A linear space charge model is used in the envelope equations, hence the errors in the measurement relate to the nonuniformity of the beam transverse distribution. The technique is tested using simulated data.

INTRODUCTION

It is important to measure the transverse beam emittance in accelerators to quantify the beam quality and match the optics in an accelerator beam line. Most beams of interest are space-charge-dominated near the source and low energy transport section, where the beam dynamics are mostly determined by interparticle forces rather than the beam pressure represented by emittance. Space charge usually modifies and degrades the performance of emittance measurement methods such as quadrupole scan techniques [1]. Reference [2] presents a comprehensive analysis of space charge force effects on such measurements. Several amendments have been proposed in literature to enhance the accuracy of quadrupole scan method for high intensity beams [3].

From the symmetry of the expression for the rms emittance

$$\tilde{\epsilon}^2 = < x^2 >< x'^2 > - < x \cdot x' >^2$$

it is obviously possible to determine emittance with a quadrupole scan technique using measurements of either the beam radius or divergence . The usual implementation of the method is to perform a quadrupole scan of beam size only. However, it is possible to obtain simultaneous, high-quality measurements of beam size and divergence [4]. In this paper, we propose a method for measuring emittance, assuming a linear space charge model, from a small number of measurements of divergence and radius.

In order to use these observables to determine the rms emittance at arbitrary focus points we need a methodology which relates the measured observables, i.e. divergence and beam size to the cross-correlation ($< x \cdot x' >$) term. We will show how this can be done by taking the cross-correlation term as a control variable for matching beam envelopes to their actual envelopes with the constraint that the beam radii and divergences at the screen are same as the measured values.

MEASURING EMITTANCE FOR BEAM WITH SPACE CHARGE

Figure 1 shows a typical quadrupole scan setup. The focal length of the quadrupole (or solenoid) is scanned to achieve a minimum spot size on the screen located downstream at a distance L from the quadrupole.

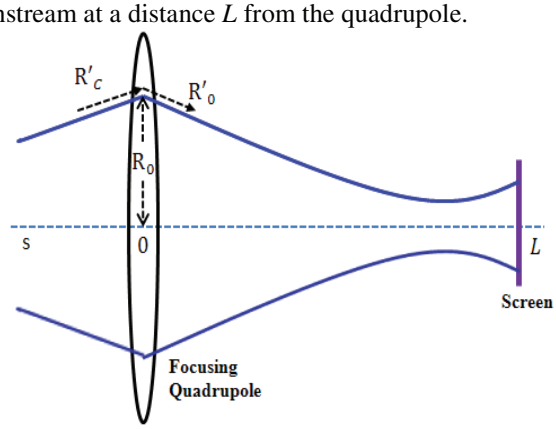


Figure 1: Diagram of a quadrupole scan setup to measure emittance. Beam enters the quadrupole with envelope R_0 and slope R'_C and leaves it with slope R'_0.

For a uniform round beam distribution where space charge is linear, the beam envelope evolution in a drift region is described by the following pair of coupled nonlinear ordinary differential equations (ODE):

$$R_j''(s) - \frac{K}{R_j(s)} - \frac{\epsilon_j^2}{R_j(s)^3} = 0 \quad (1)$$

where j ranges over transverse coordinates x and y, and dimensionless quantity

$$K = \frac{qI_b}{2\pi\epsilon_0 m(c\beta\gamma)^3} \quad (2)$$

is defined as the generalized perveance representing space charge defocusing forces. In Eq. (2), q is charge of the beam particles and I_b is the beam peak current.

Copyright © 2013 CC-BY-3.0 and by the respective authors

ISBN 978-3-95450-138-0

HIGH POWER RF SYSTEM FOR e-linac FOR TRIUMF

A.K. Mitra, Z. Ang, I. Bylinskii, S. Calic, D. Dale, S.R. Koscielniak, R.E. Laxdal, F. Mammarella
TRIUMF, 4004 Wesbrook Mall, Vancouver, BC, Canada, V6T 2A3

Abstract

The TRIUMF e-linac high power system will be built in stages. For the first phase of installation to be completed by September 2014, the injector cryomodule (EINJ) will be fed by a 290 kW cw klystron at a reduced power level and the accelerating cryomodule (EACA) will be powered by an identical klystron. The first 290 kW 1.3 GHz klystron has been purchased from CPI, USA and the high power supply system has been bought from AMPEGON, Switzerland. The second klystron and second high voltage power supply are being procured from the same manufacturers. The 290 kW cw 1.3 GHz klystron is a factory tuned multi-cavity, high efficiency, high gain, broadband, water cooled tube. The klystron has been tested at the factory. The maximum usable linear range of the rf output power of the klystron is 270 kW and is governed by the incremental gain of 0.5 dB/dB. Thus, rf power required for EACA of 200 kW cw is adequately met by the klystron after taking into account the loss in the waveguide components. and waveguides. The high voltage power supply system (KPS) for the klystron, based on a voltage controlled power module technology, consists of 65 kV beam power supply, focus supply, filament power supply and vacuum ion pump power supply. The klystron will be tested to full power on a dummy load by October 2013. At the same time, the KPS will be tested fully with all controls, interlocks, protections and integration of the klystron and a 300 kW high power circulator.

INTRODUCTION

The TRIUMF e-linac consists of an electron gun, buncher cavity, injector cryomodule, and two main-linac cryomodules [1]. The injector module has one 9 cell cavity whereas each of the accelerating (main-linac) cryomodules contains two 9-cell cavities. The cavities operate at 1.3 GHz at 2 Kelvin. The nominal energy of the e-linac is 50 MeV kinetic with an average current of 10 mA. Each 9 cell cavity has two 60 kW high power couplers. Two 290 kW CW klystrons will be employed to feed injector cryomodule (EINJ) and the accelerating cryomodule (EACA). However, the klystron for the injector will be operated at reduced output power. The linac will be built in stages. In the first stage, to be completed by September 2014, a minimum beam energy of 25 MeV, 4 mA will be obtained using the 290 kW klystrons. In the second stage, to be implemented in 2017, a second accelerating cryomodule (EACB) will be added and a 120 kW rf generator will be procured which will feed the injector. The two 290 kW Klystrons will be restored to full power operation to feed the first and the second accelerator cryomodules, to achieve the final beam power goal of 500 kW.

BASIC SCHEME OF THE HPRF SYSTEM

The basic scheme of the high power rf system for the first accelerating cryomodules is shown in Figure 1. The injector has 1 9-cell cavity and will be powered by one 290 kW klystron at a reduced power level whereas the accelerating cryomodule EACA will be run by the second klystron operating at full power. A variable power divider has been employed to facilitate rf conditioning of the two 9-cell cavities in EACA cryomodule. Also, variable phase shifters are employed to achieve phase balance between two couplers in the same cavity and for phase balance between adjacent cryomodules. The major components of the high power rf system is outlined in the following sections.

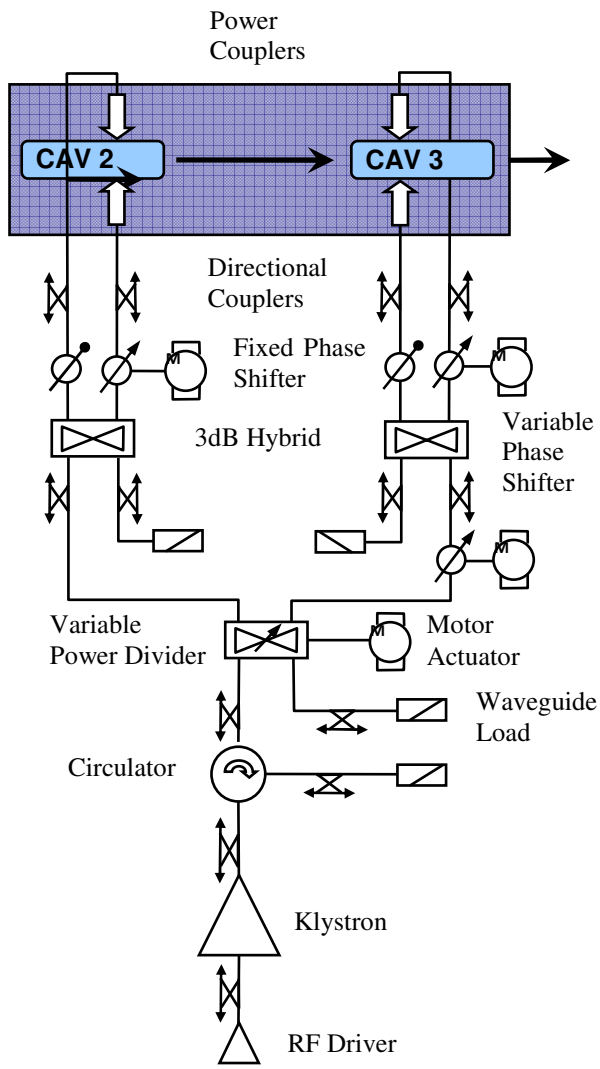


Figure 1: Basic schematic of HPRF system for the first accelerating cryomodule for e-linac

Copyright © 2013 CC-BY-3.0 and by the respective authors

ISBN 978-3-95450-138-0

THE LAYOUT OF 352 MHz 400 kW RF POWER AMPLIFIER

A. Smirnov, A. Krasnov, I. Rezanov, E. Ivanov, K. Nikolskiy, S. Polikhov, G. Sharkov
Siemens Research Center LLC, Moscow, Russia

Abstract

In this paper, we present the current status of the RF power amplifier under development for European Spallation Source (ESS, Sweden) normal conducting and superconducting accelerating sections based on solid-state architecture. A single 400 kW pulsed machine is represented with four standard 19" cabinets. Brief description and technical solutions regarding 8 kW (Class-AB, Si transistor based) RF modules, different power combiners and control system are shown.

INTRODUCTION

High power RF sources are important elements for most of linear accelerators that have found growing number of applications in science and medicine. Current power amplifier is being designed and developed to fulfil the requirements for superconducting cavities in ESS accelerator facility [1].

Main benefits of the generator under development are its smaller footprint, perspective of lower cost, better reliability and higher efficiency, achieved with class-AB operation, compared to conventional RF power sources like klystrons or other vacuum tubes generators. The solid-state microwave power amplifier modules based on Freescale LDMOS transistors arranged in parallel scheme with use of Wilkinson dividers/combiners are designed on PCB boards.

One machine is planned to be assembled inside set of four 19" cabinets. Each will contain 12 RF power amplifier modules with individual power combiner. All modules are connected to a power combiner with 50 Ohm coaxial cables. The set is terminated with a single common power combiner.

RF POWER MODULES

We have designed and manufactured compact RF power amplifier (RFPA) module prototype. The principal RFPA scheme is shown in Fig. 1. The driver stage is built using Freescale MRFE6VP100H transistor pair. The device is operated in Class-AB. Downstream the driver stage; there is a lumped element 1-to-8 Wilkinson-type splitter with final stage amplifiers at its outputs. All splitter ports have impedances of 50 Ohm.

Freescale MRFE6VP61K25H transistor pairs are being used for the final stage amplifying.

The second Wilkinson 8-to-1 power combiner is located downstream to the final stage amplifiers. The intermediate impedance of this combiner equals to 12.5 Ohms, which results in lower insertion loss. Additionally a lumped element mathing network is used to match the 12.5 Ohm intermediate impedance to output 50 Ohms. In Fig. 2, one of the fabricated RFPA modules is presented.

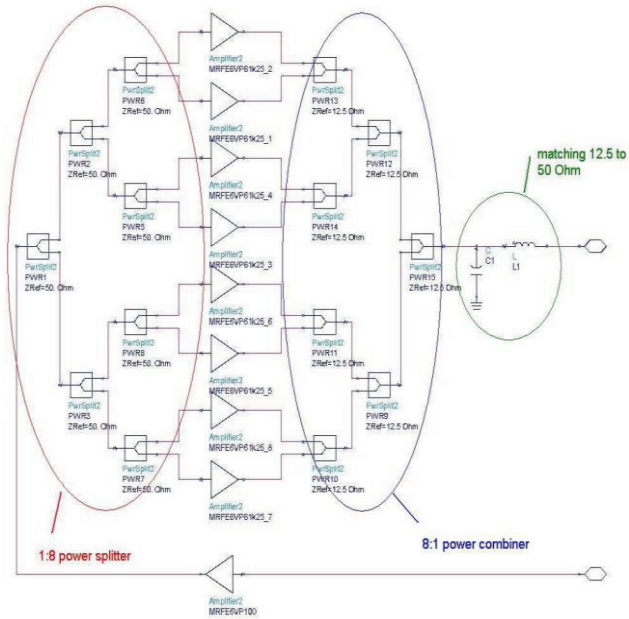


Figure 1: Single RFPA module principal scheme.

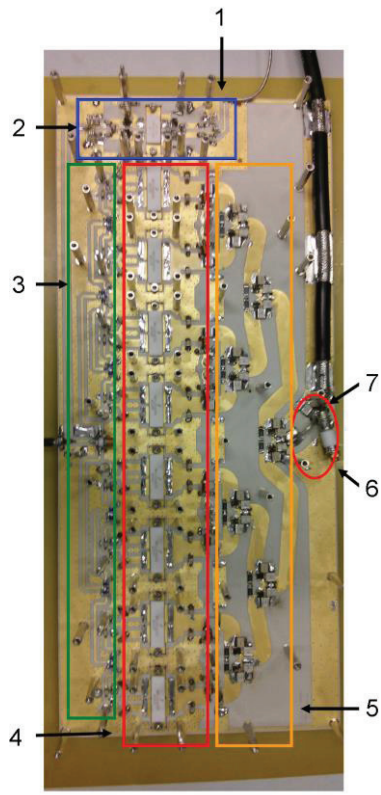


Figure 2: RFPA module: 1 – RF input; 2 – driver stage; 3 – input Wilkinson splitter; 4 – front-end amplifiers; 5 – output Wilkinson combiner; 6 – 12.5 to 50 Ohm matching circuit; 7 – RF output.

Copyright © 2013 CC-BY-3.0 and by the respective authors

ISBN 978-3-95450-138-0

THE LAYOUT OF 72 MHz 16 kW RF POWER GENERATOR

A. Smirnov, A. Krasnov, I. Rezanov, E. Ivanov, K. Nikolskiy, S. Polikhov, G. Sharkov,
Siemens Research Center LLC, Moscow, Russia

Abstract

In this paper, we present the current design of the RF power generator for medical cyclotron Eclipse (Siemens Healthcare) based on solid-state architecture. The 16 kW machine operating at 72 MHz in continuous wave regime is being assembled into standard 19" cabinet. Brief description and technical solutions regarding 2 k W (Class-AB, Si transistor based) RF modules, power combiner and control system are shown.

INTRODUCTION

High power RF sources are important elements for most of accelerators that have found growing number of applications in physics and medicine. Current power amplifier will feed Eclipse cyclotron that is being used for PET isotopes production (^{18}F, ^{11}C, ^{13}N and ^{15}O) with H- ions at 11 MeV [1].

The main benefits of the generator under development are its smaller footprint, perspective of lower cost, better reliability and higher efficiency, achieved with class-AB operation, compared to conventional RF power sources like klystrons or other vacuum tubes generators. The solid-state microwave power amplifier modules based on Freescale LDMOS transistors arranged in parallel push-pull circuits, are designed on PCB boards.

All modules are connected to a power combiner with 50 Ohm coaxial cables.

RF POWER MODULES

We have designed and manufactured compact RF power amplifier (RFPA) modules with two pairs of Freescale™ MRF6V2010NR1 (driver stage) and MRFE6VP1K2H (main stage) transistors arranged in push-pull topology as shown on Fig. 1.

The frequency is adjustable between 72 and 73 MHz because cyclotron resonant frequency changes in this range during operation.

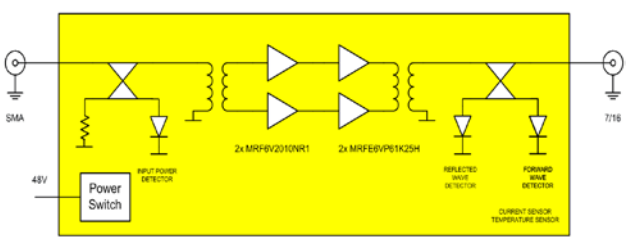


Figure 1: Parallel push-pull circuit.

The manufactured module prototype is presented on Fig. 2. Arlon AD255 with ε=2.55 is used a substrate material. The transistors are fed with 180^0 phaseshift, provided with an RF transformer. Achieved RF performance is shown in Table 1.

Table 1: RFPA Specifications

Parameter	Value
Bandwidth	72..73 MHz
Output RF power	max. 2100 W
RF efficiency	~75% (>80% planned)
Gain	52..55 dB
Input RF power	max. 30 mW
Supply voltage	48 V
Input/Output impedance	50 Ohm
Input/Output VSWR	max 1.3
Dimensions	16×25 cm^2

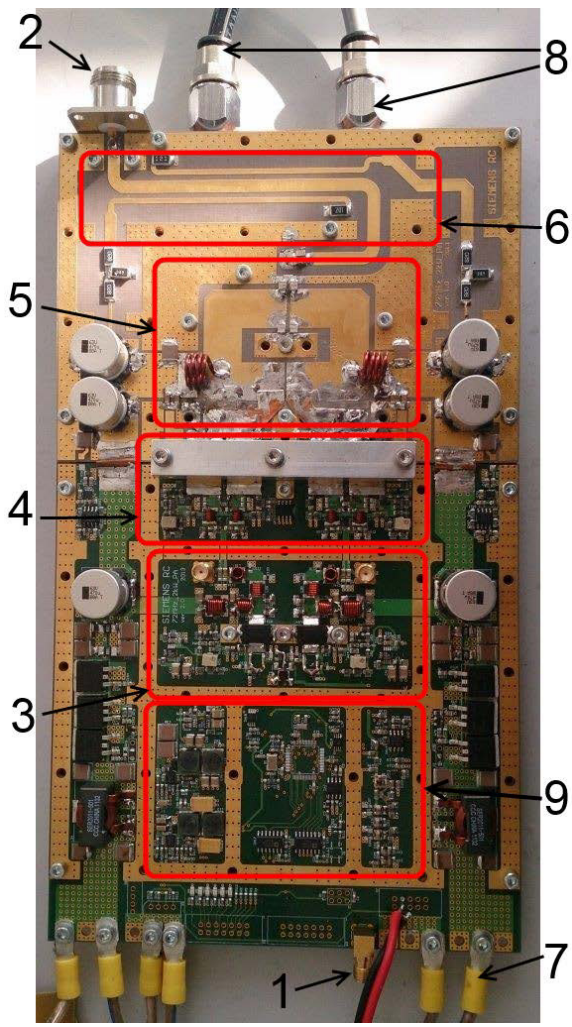


Figure 2: RFPA module: 1 – RF input; 2 – RF output; 3 – driver stage; 4 – main amp stage; 5 – output matching transformer; 6 – output directional coupler; 7 – DC supply; 8 – water cooling tubes; 9 – MCU unit.

Copyright © 2013 CC-BY-3.0 and by the respective authors

ISBN 978-3-95450-138-0

OVERVIEW OF THE RHIC E-LENS SUPERCONDUCTING MAGNET POWER SUPPLY SYSTEM *

D. Bruno#, A.Di Lieto, G. Ganetis, R.F. Lambiase, W. Louie, C. Mi, T. Samms, J. Sandberg,
Brookhaven National Laboratory, Brookhaven Science Associates, Upton, NY, 11973, USA.

Abstract

A new superconducting solenoid magnet was installed in the yellow ring of RHIC before Run 13 as part of the e-lens project. The second solenoid superconducting magnet will be installed in RHIC after Run 13 is over. There are 6 power supplies required for the solenoid, fringe and anti-fringe coils for both magnets. Commercial off the shelf unipolar power supplies are used to power the solenoid, fringe and anti-fringe coils. There are 24 corrector power supplies required for both magnets. Custom built 50A bipolar power supplies are used to power the correctors. Quench protection and quench detection have also been installed in this power supply system. In addition, 4 new phase shift power supplies have been installed in RHIC which are needed for the new e-lens system. These phase shift power supplies have been installed across the yellow focusing and defocusing arcs as well as the blue focusing and defocusing arcs from sector 8 to sector 10. Power Supply technology, control system, connections, the quench detection/protection system, and status will be presented.

E-LENS POWER SUPPLIES

Power Supplies Description

There are thirty power supplies (p.s.'s) used in the e-lens p.s. system. Fifteen p.s.'s for each magnet. These are all current regulated power supplies with a DC Current Transformer (DCCT) current sensing element.

The two Solenoid p.s.'s are rated at 20Volts and 750Amps dc. The ac input to both Solenoid p.s.'s is 480Vac. The two Fringe and two Anti-Fringe p.s.'s are rated at 15Volts and 534Amps dc. The ac input to the Fringe and Anti-Fringe p.s.'s is 480Vac. The Solenoid and Helical p.s.'s are commercially available voltage regulated switchmode p.s.'s which are used within the BNL designed current regulator. The required p.s. current reproducibility is 0.01% of maximum current.

The twenty four bipolar trim p.s.'s are 20Volts and 50Amps dc. The ac input to the bipolar trim p.s.'s is 208VAc. These are the same bipolar p.s.'s that are used for the RHIC corrector magnets. The required p.s. current reproducibility for the trim p.s.'s is 0.1% of maximum current.

During normal operation these p.s.'s ramp up slowly to a dc level and stay there.

The Solenoid, Fringe and Anti-Fringe p.s.'s are all connected to their own quench protection assemblies (QPA's). These QPA's contain an energy extraction resistor across an IGBT switch as well as a diode across the output of the p.s. The IGBT and energy extraction resistor are connected to the positive output terminal of the p.s. and the magnet. The diode is connected across the dc terminals of the p.s. When a fault occurs in the p.s. or the QPA, or if the magnet quenches, the diode conducts across the p.s. and the IGBT opens so the energy extraction resistor is now in series with the load. The current from the load goes through the diode and through the energy extraction resistor. The supply also trips to the STANDBY-FAULT state. A DCCT was installed in the QPA for the regulation of the e-lens p.s. The trim p.s.'s don't have a separate QPA; they have a crowbar with an energy extraction resistor built into them.

There is a quench detector (qd) for the e-lens p.s. system which monitors the voltage across the magnets and the current of the magnets. The qd trips the p.s. to STANDBY-FAULT if a quench is detected. Whenever the p.s. trips to the STANDBY-FAULT state, the energy extraction resistor becomes part of the circuit.

e-Lens P.S. Magnet Loads

There are 17 superconducting magnets in one cryostat. The main Solenoid is connected to one p.s. The two Fringe magnets are connected in series to one p.s. The two Anti-Fringe magnets are connected in series to one p.s. The 12 trim magnets are connected to 12 individual p.s.'s. The Solenoid magnet has an inductance of 14H. Each Fringe magnet has an inductance of 515mH. Each Anti-Fringe magnet has an inductance of 38.4mH. The two long (vertical and horizontal) trim magnets are 5.34mH each. The 5 short vertical and 5 short horizontal trim magnets are 19.2mH each. The dc resistance of the corrector cables to the magnets is between 74mohms and 120mohms depending on the cable size used.

Quench Detection for e-Lens

The yellow solenoid magnet is made up of 11 double layers (coils). In order to protect the magnet during a quench the coil difference is taken between 5 coils and 6 coils. If this coil difference ever exceeds 125mV the qd will tell the QPA to open the series IGBT, then the energy extraction resistor is connected in series with the load. The p.s. contactor opens after the IGBT in the QPA opens. The blue solenoid magnet is made up of 10 double layers. The coil difference is taken between 6 coils and 4 coils because of the available voltage taps.

There are 2 Fringe coils in each magnet and 2 Anti-Fringe coils in each magnet. Each Fringe coil has dc terminals that come out of the magnet. The Two Fringe coils are connected in series outside of the magnet to one

* Work supported by Brookhaven Science Associates, LLC under Contract No. DE-AC02-98CH10886 with the U.S. Department of Energy
# bruno@bnl.gov

Copyright © 2013 CC-BY-3.0 and by the respective authors

ISBN 978-3-95450-138-0

200 KW CW, 350 MHZ MULTIPLE BEAM INDUCTIVE OUTPUT TUBE

R. Lawrence Ives, Michael Read, David Marsden, George Collins, Rasul Karimov,
Calabazas Creek Research, Inc., San Mateo, CA 94404 USA
Takuji Kimura, Edward Eisen, Communications & Power Industries, LLC,
Palo Alto, CA 94304 USA

Abstract

Assembly is nearing completion of a 350 MHz, 200 kW CW, multiple beam, inductive output tube. The device incorporates seven electron beams interacting in a single, fundamental mode, output cavity. A single collector dissipates the spent beam power, and input and output power is transmitted in coaxial waveguide. Simulations predict 70 % efficiency with 23 dB gain. The tube is targeted for ion accelerators.

INTRODUCTION

Calabazas Creek Research, Inc. (CCR), in collaboration with Communications & Power Industries, LLC (CPI), is nearing completion of a 350 MHz, 200 kW CW, multiple beam, inductive output tube (MBIOT). This device is targeted for upgrade of the Advanced Photon Source (APS) at Argonne National Laboratory but will be applicable for a broad range of accelerator systems requiring RF power from 300 to 800 MHz. The MBIOT provides efficiencies higher than klystrons in a dramatically smaller device. The gain is limited to less than 24 dB; however, solid state drivers are commercially available providing several kilowatts of RF power. The principal challenge is designing an input cavity that will drive all electron guns at the same power and phase. This paper describes the design of the MBIOT and status of the assembly.

DESIGN

The MBIOT incorporates a single, coaxial input cavity to drive the seven electron guns. The tube uses electron guns produced by CPI for their single beam IOTs. The gun design is well established, and the performance has been verified through years of operation. Figure 1 shows the gun support plate and two of the guns.

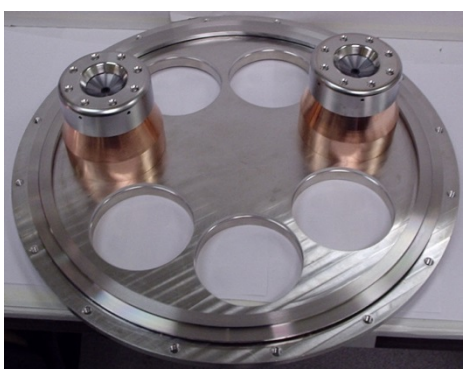


Figure 1: Gun support plate with two guns.

Figure 2 shows an HFSS simulation of the input cavity electric fields. The axis of the device is the Y-axis. Input power enters through a coax waveguide from the right. Heater power is provided by the leads emerging from the back of the gun and coupling to the top wall in the image.

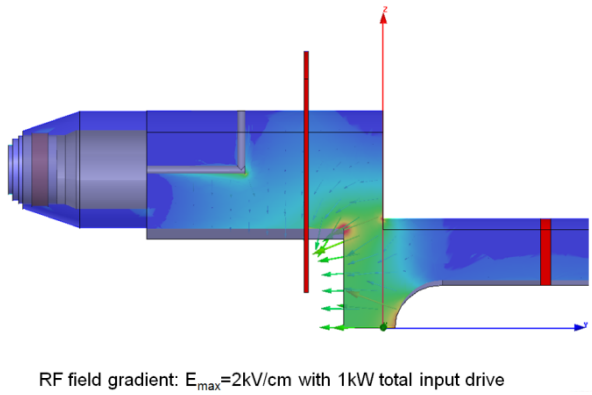


Figure 2: HFSS Simulation of MBIOT input cavity.

Figure 3 shows an HFSS simulation of the output cavity, with the beams entering from the left and the RF output power coupled to a coaxial waveguide on the axis. The external Q is determined by the penetration depth of the coax center conductor, which will be set during cold testing. The seven electron beams exit toward the right into a common collector that surrounds the output waveguide and window.

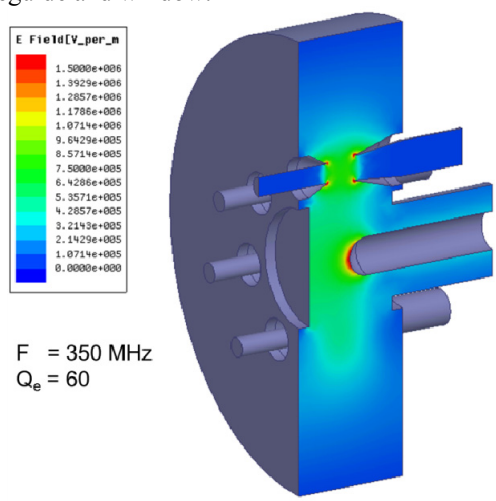


Figure 3: HFSS simulation of the output cavity.

Table 1 provides the performance specifications based on computer simulations. These satisfy the requirements for the APS upgrade and a number of anticipated accelerator systems.

Copyright © 2013 CC-BY-3.0 and by the respective authors

DESIGN AND FABRICATION OF A 10 MW, L-BAND, ANNULAR BEAM KLYSTRON*

Michael Read, Patrick Ferguson, R. Lawrence Ives, Robert Jackson, David Marsden, and George Collins
Calabazas Creek Research, Inc., 690 Port Drive, San Mateo, CA 94404

Abstract

Design improvements and fabrication of a 10 MW, 1.3 GHz Annular Beam Klystron are described. The principal improvement is the electron gun. Utilization of a Controlled Porosity Reservoir (CPR) cathode allows the use of a zero-compression gun, resulting in improved beam quality and reductions in the gun and solenoid diameters.

INTRODUCTION

Efforts to achieve a high efficiency 1.3 GHz, RF source for the International Linear Collider (ILC) and similar accelerators are centered on multiple beam klystrons (MBK) and, more recently, on a sheet beam klystron (SBK). CCR is developing an annular beam klystron (ABK) to fulfill the stringent requirements imposed by the ILC. That is, the minimum efficiency should be 65% at an RF output power of 10 MW, and the cathode current density should be less than 5 A/cm^2. The pulse width must be 1.5 milliseconds at a pulse frequency of 15 Hz.

Like the MBK, the ABK perveance can be much higher than in a traditional klystron. In contrast to the MBK, the ABK uses a single beam with simple transverse magnetic (TM) mode resonators. Thus, the tube is similar a traditional klystron and much simpler than an MBK. The ABK length, efficiency and gain are similar to those of an MBK with the same power, perveance and frequency.

The CCR ABK electron beam current is 140 A at 120 kV with inner and outer beam radii of 3.2 cm and 3.6 cm, respectively. The drift tube radius is 4 cm. The tube includes six cavities, and the solenoidal magnetic field is 1.5 kG. A schematic of the ABK electron gun and simulated beam is shown in Figure 1.

As previously reported [1], CCR created a design that met all requirements and was not significantly affected by the diocotron instability. However, the 2 kG magnetic field required more power than desired. With an ideal beam, calculations of the efficiency showed no degradation with fields down to at least 1.5 kG. However, lowering the field increased the beam ripple, which in turn decreased the efficiency. This ripple was due to gun optics.

Design of a gun using compression to create an annular beam is intrinsically difficult, due largely to the fact that there is no radial force on the inside surface of the beam. The original design with a 2 kG field used a complex interaction of the cyclotron motion with the radial fields of the anode to minimize the ripple. Unfortunately, it was not possible to maintain the balance of forces at lower magnetic fields.

Generating an annular beam without compression, i.e. with a uniform axial magnetic field, is much more straightforward. But, for this case, the beam density of 16 A/cm^2 is too high for conventional cathodes. This difficulty is avoided using a CCR Controlled Porosity Reservoir (CPR) cathode. Current densities to 50 A/cm^2 have been demonstrated with this type of cathode. At the required density of 16 A/cm^2, the predicted lifetime is 100,000 hours. This is more than adequate for most applications, including the ILC.

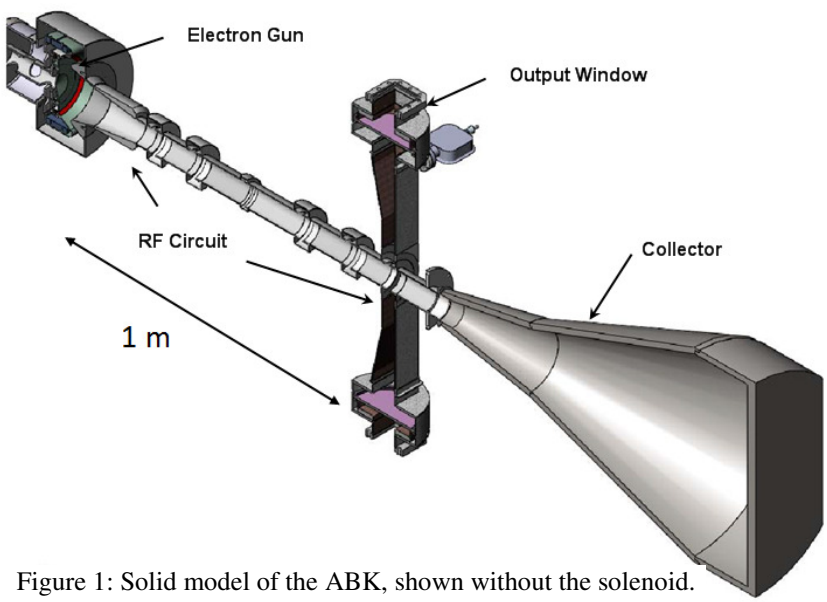


Figure 1: Solid model of the ABK, shown without the solenoid.

Copyright © 2013 CC-BY-3.0 and by the respective authors

ISBN 978-3-95450-138-0

X-BAND RF POWER GENERATION VIA AN L-BAND ACCELERATOR SYSTEM AND USES

N. Sipahi, T. Sipahi, S. G. Biedron, S. V. Milton, CSU, Fort Collins, Colorado, USA

Abstract

The development of compact, cost effective sources of high-energy electron beams is a major thrust of the Colorado State University Accelerator Laboratory team. In this paper we describe a way to generate usable X-Band RF power suitable for powering an X-Band accelerating structure to overall potentials significantly higher than what we are presently able to obtain from our L-Band photocathode RF gun system. The concept relies on the use of the L-band accelerator beam to generate the X-band power that is then delivered to a suitable X-band structure. Once powered this X-band structure can be used to accelerate an electron bunch to high beam energies.

GENERAL CONCEPT

The CSU Accelerator Facility will serve as a test bed for particle and laser beam research and development. Our major asset is an L-band rf gun system capable of delivering 6-MeV electron bunches [1], these parameters are given in Table 1. We would like to use this L-band linac as a drive source to generate X-band power for accelerating electron beam with an X-band rf structure without the need for an external X-band power source. This system could then be used to accelerate the beam to an even higher energy that possible with the L-band system alone.

Table 1: Parameters of CSU Accelerator Laboratory

Laser Frequency	81.25 MHz
L-Band RF Gun Frequency	1.3 GHz
L-Band RF Gun Energy	6 MeV
L-Band Macro pulse Length	10 μs
X-band Linac Frequency	11.7 GHz
Repetition Rate	10 Hz
RF gun Charge/Bunch	3.5 nC

From our earlier work, we found that although significant gradients could be achieved with an X-band structure powered via our L-band beam system the integrated potential in the X-band structure was fundamentally limited by the drive beam energy loss [2]. This led us to explore an alternative arrangement where power was generated in a TW structure and then transferred to a separate optimized structure used for acceleration of a secondary beam. This basic arrangement is shown in Figure 1.

Using such an arrangement, we would like to achieve the highest possible energies for our given beam parameters and proposed X-band drive system.

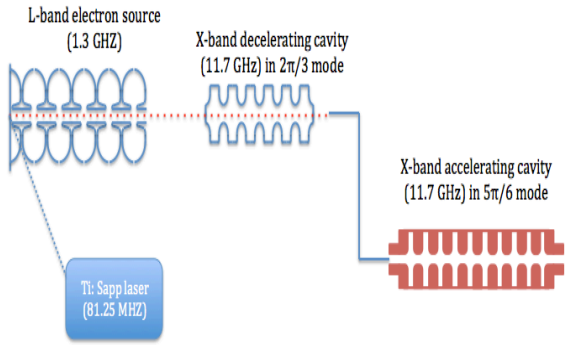


Figure 1: General layout of the two-beam X-band structure.

BEAM STUDIES FOR TWO DIFFERENT CAVITIES

Our study involves two different X-band accelerator structures, one to be used as a decelerating cavity that generates X-band power via the use of the beam from the L-band system, and the second one to be used as an accelerating cavity to achieve the highest practical potential for acceleration of the electron beam.

The one cell geometry for our X-band structures are defined in Figure 2 [3].

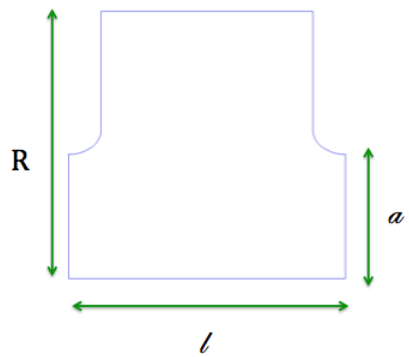


Figure 2: One cell structure of the X-band cavity.

The Beam – Cavity Interaction for the Decelerating Structure

In the decelerating cavity, the aim is to transfer energy from the L-Band RF system to the electron beam, consisting of bunches of charged particles, and then from the electron beam to the RF wave induced in the X-band decelerating structure, thus we design a structure that maximizes this interaction as in ref. 2.

The configuration is unconventional in that the X-band linac does not require a klystron system to achieve high accelerating fields. Rather it uses the power existing in the electron beam to resonantly power the fields in the structure.

Copyright © 2013 CC-BY-3.0 and by the respective authors

ISBN 978-3-95450-138-0

COMPONENTS OF HEATING AND FUELING OF FUSION PLASMAS*

K. Schrock, M. Gaudreau, J. Kinross-Wright, Diversified Technologies, Inc.,
35 Wiggins Ave., Bedford, MA 01730, USA

Abstract

Diversified Technologies, Inc. (DTI) has bench-tested a table-top scale 'Buck Matrix' modulator with an efficiency of ~96% which uses a single set of IGBT switches for voltage regulation, arc protection, and pulse modulation.

INTRODUCTION

Next generation fusion facilities will require many megawatts of RF power from dozens of gyrotrons. Each gyrotron requires a power system that must deliver high-voltage power, modulate cathode voltage, and protect these expensive gyrotrons from arcing damage. It must be highly efficient to minimize both the power and cooling costs associated with operation and to ensure high facility availability.

Conventional DC power systems, built from WWII era components, have provided the typical approach to powering this class of high-power RF vacuum devices for the last 50 years. These systems, with their variacs, inductrols, spark gaps, ignitrons, and tetrodes, traditionally suffer from reliability and availability problems and are often only 50 – 70% efficient. Scaling conventional RF power electronics technology for next generation high power fusion facilities is not practical in either cost or reliability.

The technology for off-the-shelf, reliable solid-state modulators does exist, but currently requires two layers of solid-state switches – a voltage regulation step followed by a modulator / opening switch for arc protection. These two-step approaches are unnecessarily large and expensive, and an approved approach will be presented.

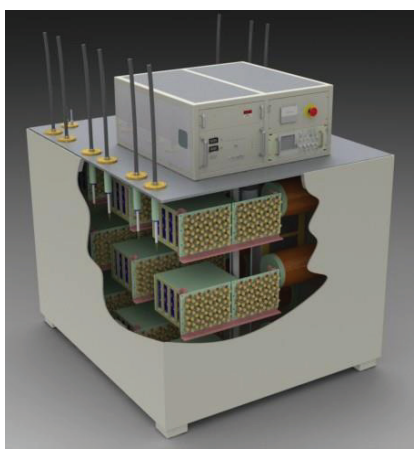


Figure 1: 75 kV, 45 A CW multi-phase buck-matrix regulator with low filter energy – serves dual purpose of regulating power and protecting a 1 - 1.5 MW gyrotron during arcs.

*Work supported by the Department of Energy

TECHNICAL APPROACH

Diversified Technologies, Inc. (DTI), under a DOE SBIR grant, has bench-tested a table-top scale 'Buck Matrix' modulator which uses a single set of IGBT switches for voltage regulation, arc protection, and pulse modulation.

DTI's Buck Matrix modulator (Figs. 1 and 2), with an efficiency of ~96%, cuts the size of the system in half, using a single layer of solid-state switches for both voltage regulation and arc protection/modulation. This cuts the total hardware costs by 30% or more, and eliminates the need for a separate opening switch or crowbar.

Although pulse step modulators also represent a one-step solution, their size and the complexity of their driving transformer make them more expensive than DTI's approach.

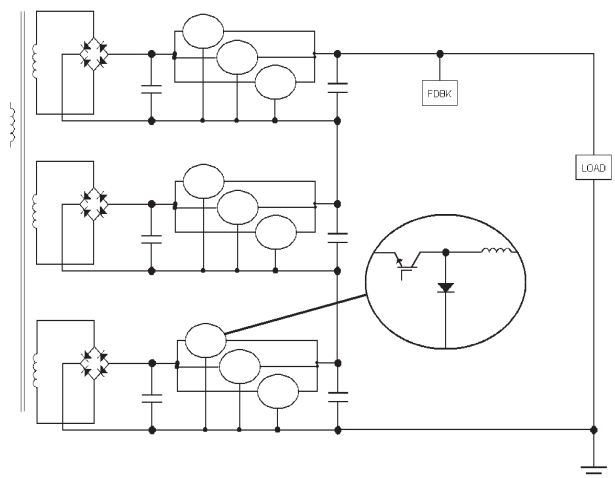


Figure 2: A series/parallel "Buck Matrix" topology combines superb ripple reduction and tube protection for minimum complexity and maximum efficiency. Transformer / Rectifier pairs are shown single-phase for simplicity.

OBJECTIVES

DTI focused on five primary objectives in developing the modulator. The first three focused on demonstrating the technical feasibility of the project: to assess any control system instabilities, to ensure the concept design would meet real gyrotron requirements, and to build and test a low voltage demonstration unit. The latter two tasks focused on the construction of a full-scale prototype. A high voltage electrical design for the full-scale system has been completed, as well as the ground work for the mechanical design, and the auxiliary systems have been

Copyright © 2013 CC-BY-3.0 and by the respective authors

ISBN 978-3-95450-138-0

AFFORDABLE, SHORT PULSE MARX MODULATOR*

R. Phillips, G. DelPriore, M. P.J. Gaudreau, R. Simpson
Diversified Technologies, Inc., 35 Wiggins Ave., Bedford, MA 01730, USA

J. Casey
Rockfield Research, Inc., 11010 Onslow Ct., Las Vegas, NV 89135, USA

Abstract

Under a U.S. Department of Energy grant, Diversified Technologies, Inc. (DTI) is developing a short pulse, solid-state Marx modulator (Fig. 1). The modulator is designed for high efficiency in the 100 kV to 500 kV range, for currents up to 250 A, pulse lengths of 0.2 to 5.0 μs, and risetimes <300 ns. Key objectives of the development effort are modularity and scalability, combined with low cost and ease of manufacture. For short-pulse modulators, this Marx topology provides a means to achieve fast risetimes and flattop control that are not available with hard switch or transformer-coupled topologies.

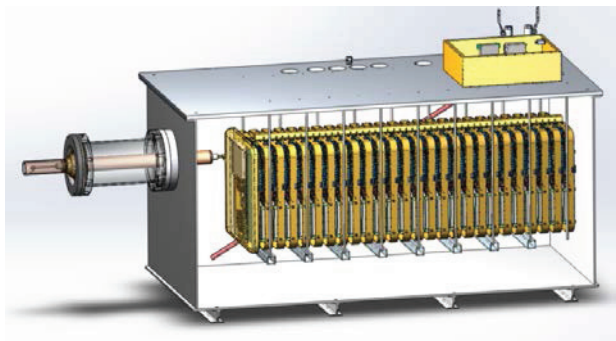


Figure 1 Planned 500 kV Marx modulator with an array of fifty of the plates shown in Figure 3.

INTRODUCTION

Under a DOE SBIR grant and based on research begun under the Next Generation Linear Collider (NLC) program, high energy, short-pulse modulators are being re-examined for the Compact Linear Collider (CLIC) and numerous X-Band accelerator designs. At the very high voltages required for these systems, however, all of the existing designs are based on pulse transformers, which significantly limit their performance and efficiency. There is not a fully optimized, transformerless modulator design capable of meeting the demanding requirements of very high voltage pulses at short pulsewidths.

BACKGROUND

A Marx generator is a system with energy storage capacitors which are charged in parallel at low voltage and discharged in series to provide high voltage output. This is a legacy idea, practiced for decades using resistor charging networks and spark-gaps for discharge. Constrained by the limits of closing switches, such systems required pulse forming networks and crowbars, with their attendant limitations

The Marx topology also enables features which are not common to hard switch modulators. Primary among these is the ability to control each module independently – and thus program the ultimate pulse voltage by choosing the number of modules triggered. The use of a bypass diode rated for full pulse current allows staggering of the modules' turn-on time, and ultimately enables full waveform synthesis in real-time.

TECHNICAL APPROACH

The Marx topology allows a new degree of freedom unavailable to other architectures – DTI can intentionally underdamp the series snubbing within the pulse circuit. This cannot be done conventionally – the reactive overshoot endangers the load. In a Marx, we can compensate for the overshoot by initially firing only a subset of the switches – thus "sling-shotting" the leading edge faster than otherwise possible. We can tune the number and timing of subsequent module firings to counter the reactive ringing, and hold a flattop pulse to the desired voltage and accuracy (Fig. 2).

Similarly, additional modules may be added to fire sequentially later in the pulse to compensate for capacitor droop. This is a critical enabling technology motivating Marx use for long-pulse accelerators (such as ILC), and yields valuable optimization even for very short-pulse systems. The reduction of capacitor size afforded by this flexibility further reduces parasitic capacitance, and thus reduces equipment size and cost while increasing power efficiency.

*Work supported by the Department of Energy

Copyright © 2013 CC-BY-3.0 and by the respective authors

ISBN 978-3-95450-138-0

TEST OF AN L-BAND ENERGY-EFFICIENT SOLID STATE RF POWER SOURCE*

X. Chang, N. Barov, D.J. Newsham, and R. Wu, FAR-TECH, Inc., San Diego, CA 92121, USA

Abstract

We present the test results of a 1.497 GHz Solid State RF Power Source for the CEBAF linac at Thomas Jefferson National Accelerator Facility. The power amplifier was designed to operate at output power of 6.4 kW, with an overall efficiency greater than 55% at peak power, and is sufficiently compact to fit the existing rack space and cooling requirements at the installation site. Our solid state amplifier is designed for high efficiency, band width of more than ±5MHz at 1.497GHz, and long lifetime. The test results of the whole unit test will be shown.

INTRODUCTION

Thomas Jefferson National Accelerator Facility (TJNAF, JLab) is upgrading their RF system [1] for upgrading their electron beam energy. One of the options is to replace the klystron RF sources with the solid state amplifiers. Compared to a conventional klystron RF source, the solid state amplifier is easier to obtain high efficiency, long lifetime, and is safer due to low operating voltage, with a lower maintenance cost.

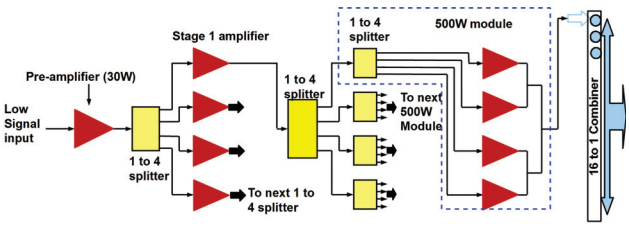


Figure 1: 8 kW Amplifier diagram. There are totally 16 of 500 W module.

Figure 1 is the diagram of an 8 kW solid state amplifier RF source. The low signal is amplified by a commercial 30 W amplifier (pre-amplifier) to drive the 4 transistors in the "stage 1" amplifier, which is contained in a single housing with 16 outputs. Each transistor in stage 1 has a peak output power of greater than 125 W. The output from each stage 1 transistor is split into 16 signals by two 1-to-4 splitters (one contained in the stage 1 amplifier housing and one contained in the 500 W module) and drive the 16 transistors in 4 of the 500 W modules. Isolators are placed between the two levels of splitting. Each transistor in the 500 W module has a circulator with load to prevent cross talking between transistor boards and to isolate the transistors from any reflected power. There are a total of 16 500 W modules and their outputs are combined in a 16-to-1 combiner.

EXPERIMENTS

Transistor Board Development

Our chose RF3934 [2] as our amplifier transistors. It's a wideband transistor which an operate at 120W power. Previous testing to combine the output of 4 transistor boards with a commercial combiner [3] helped improve the performance of the transistor board prior to incorporating the transistors and in-house 4-to-1 combiner into a single module. Figure 2 shows the test set up for testing the 500 W module.

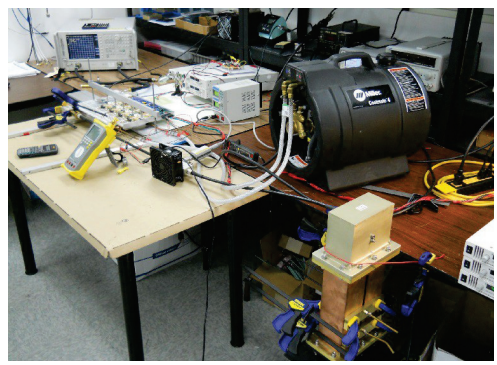


Figure 2: 500 W module test set-up. Output is connected through a 7/8" EIA connector.

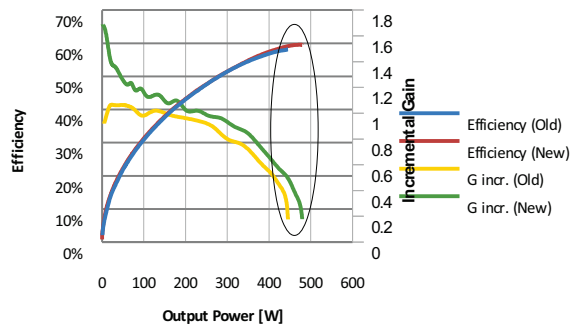


Figure 3: Peak power, efficiency, and incremental gain improvement by board modification.

The improvement of the 500 W module performance is shown in figure 3. With the improvement, the peak power increased from 445 W to 480 W, the peak drain efficiency increased from 58.2% to 59.5%, and incremental gain increased from 0.44 at 425 W to 0.57 at 425 W. The incremental gain here is defined as the change of output power in dB (P_{output}[dB]) divided by the change of input power in dB (P_{input}[dB]).

*Work supported by DOE Office of Nuclear Physics, DOE-SBIR #DE-SC0002529

Copyright © 2013 CC-BY-3.0 and by the respective authors

SYSTEM CONSIDERATIONS FOR 201.25 MHz RF SYSTEM FOR LANSCE*

John Lyles#, Walter Barkley, Jerry Davis, Angela Naranjo, Dan Rees, Gilbert Sandoval,
AOT Division, Los Alamos National Laboratory, Los Alamos, NM
D. Baca, R. Bratton, R. Summers, Compa Industries, Los Alamos, NM

Abstract

Acceleration of long pulses of proton current at high repetition rates (1 mS, 120 pps) at LANSCE have been impacted by reduced capability of the original 201.25 MHz RF system driving the 100 MeV DTL. The present operating point of the existing triode power amplifiers doesn't allow margin for tuning excursions with voltage standing wave effects or for tube manufacturing variations. This has led to the undesirable consequence of operating LANSCE at half of its original duty factor for the past seven years to maintain acceptable beam availability. A recent program has been initiated to restore the accelerator to its original high current operation. Investigated alternatives for high power RF included the development of physically large klystrons, solid-state and new power grid tube (tetrode) amplifiers. The power grid tube was favored as it reused much of the existing infrastructure including water-cooling systems, coaxial transmission lines, high voltage power supplies and capacitor banks. High duty factor tetrodes called Diacrodes®, are capable of supplying the DTL requirements with ample headroom. A LANL-designed power amplifier using the TH628L Diacrode® has produced 3 MW peak and 300 kW of mean power with > 14 dB of power gain and > 60% efficiency. It has been operating for over seven thousand hours generating RF power with a test load. Installation of the first new system begins in January of 2014.

RF SYSTEM SHORTCOMINGS

The LANSCE proton linac uses a DTL powered at 201.25 MHz, to accelerate both H^+ and H^- ions from 0.75 to 100 MeV in four Alvarez cavities, before injection into a coupled-cavity linac. The beam loading is 16.5 mA peak proton current at 120 pps. Nominal 8.7% beam duty factor (DF), with 1 pps of 1225 uS length. DTL cavity 2 has the highest energy gain of ~36 MeV, and requires the highest peak RF power of 3.6 MW, including excitation power. Significant average power (~430 KW) is required for each of three room temperature cavities to accelerate the long beam macro pulses. This is in contrast to the high-peak/low-average power regimes found at 200 MHz proton injector linacs at Fermilab, CERN, and BNL. Over the past 25 years, the manufacture of RF amplifier triodes with consistent lifetime has been challenging, when operating at the high average power needed at LANSCE. These tubes were originally commercialized in 1960, using unique processes such as pressed (non-brazed) seals. In the 1980s the company (RCA) quit the business, which was then bought by individuals. At this time there was concern about the longevity of the 7835 triode as a product.

Studies made in 1987-89 discussed alternatives to the triodes, including new tetrodes, klystrons, or IOTs. Through the last part of that century recurring problems were managed by having a larger supply of tested spare triodes. In 2006, the operating point of the power amplifiers had to be reduced in order to hold operating costs on budget (for all-too-frequent tube replacements) and prevent excess downtime. This led to the decision to operate LANSCE at half of its original duty factor to maintain acceptable beam availability.

A primary goal of the LANSCE Risk Mitigation (LRM) project has been to replace the original 201.25 MHz amplifiers with modern circuits having higher average power capability. Another goal has been to modernize the low level RF controls, to improve operational efficiency and reduce beam losses. In addition, end-of-life klystrons for the CCL are being replaced with forty-five new CPI VA862A1 klystrons.

ALTERNATIVES CONSIDERED

Solid State Amplifier

Broadcast transmitters have led development of solid state PAs. Units with up to 2 MW of modulated power have been installed at low frequencies up to a few MHz. In the VHF/UHF bands, however, power levels are predominantly in the tens of kW. In the past decade, development of CW PAs capable of 180kW was done at 352 MHz [1]. The Soleil group has pioneered using DMOS transistors in large combined circular arrays with 726 individual amplifier pallets for a booster synchrotron. Others have followed with similar designs. Transistors work best with continuous (CW) operation as wire bonds are weakened with pulsed currents, resulting in device derating [2]. The number of particular dies for a pulsed amplifier become similar to a CW rated amplifier, unlike with tubes where significantly higher peak power may be obtained from the same device. Technical problems are known to exist with LDMOS transistors, such as drift in quiescent current over time (aging and radiation-induced). MTBF for transistors are frequently quoted in tens to hundreds of years. In practical high power amplifiers such as at Soleil, the large number of passive and active devices required pushes down the MTBF to about 1 year, despite the inherent redundancies.

* Work supported by the United States Department of Energy, National Nuclear Security Agency, under contract DE-AC52-06NA25396
# jtml@lanl.gov

Copyright © 2013 CC-BY-3.0 and by the respective authors

ISBN 978-3-95450-138-0

MODELING OF MAGNETRON TRANSMITTER FOR THE PROJECT X CW 1 GeV LINAC*

Grigory Kazakevich#, Rolland Johnson,
Muons, Inc., Batavia, 60510 IL, USA

Vyacheslav P. Yakovlev, Brian E. Chase, Ralph J. Pasquinelli,
Fermilab, Batavia, 60510 IL, USA

Abstract

A 650 MHz 50 kW transmitter with a wide-band control in phase and power, based on injection-locked CW magnetrons has been proposed to drive individually Superconducting RF (SRF) cavities for the Project X CW 1 GeV H^- linac. Utilization of the magnetron RF sources for the intensity-frontier project will save a significant capital cost in comparison with traditional RF sources based on klystrons, Inductive Output Tubes (IOTs), solid-state amplifiers. The transmitter setup has been modelled experimentally using 2.45 GHz CW magnetrons with output power up to 1 kW operating in injection-locked mode in pulsed regime with long pulse duration. Measurements with the modelling setups indicated capability of the proposed transmitter to power the SRF cavities suppressing parasitic modulation of the accelerating field caused by mechanical oscillation (the microphonics), beam loading, dynamic tuning errors, and the low-frequency disturbances of the magnetron performance. Results of the experimental tests are analyzed and discussed in this paper.

INTRODUCTION

State of the art the intensity-frontier Project X H^- superconducting 1 GeV linac requires CW, 650 MHz RF sources to power SRF cavities. One of general requirements following from dynamic of non-relativistic or weakly relativistic beam is conservation of a small emittance during the process of acceleration. For this is necessary keeping the accelerating voltage phase and amplitude deviations to be less than 1 degree and 1% of nominal, respectively, [1].

To keep amplitude of accelerating voltage with the required accuracy in spite of microphonics, a dynamic control of the accelerating voltage is required, [2, 3].

The average RF power to feed each SRF cavity, providing an energy gain of ~17 MeV/m for average beam current of 2 mA at the microphonics magnitude, δf=20 Hz, one can determine by the following equation:

$$P_g = \frac{V^2}{4Q_E(r/Q)}\left[\left(1+\frac{I\cos\varphi(r/Q)Q_E}{V}\right)^2+\left(Q_E\frac{2\delta f}{f}\right)^2\right].$$

Here P_g is the RF source power, V is gradient of the accelerating field in the 1 m long SRF cavity for zero synchronous phase, (r/Q) is the cavity impedance, Q_E is the cavity external Q-factor, *f* is the cavity frequency, δ*f* is the microphonics magnitude, φ is the synchronous phase.

For ILC-type 650 MHz SRF cavity with (r/Q)≈ 638 and φ ≈-10 degrees the equation gives P_g≈ 38.5 kW at the necessary range of the power variation of ~ 5 kW. Considering reflections and insertion losses in the RF system one can evaluate the RF source nominal power of ≈ 50 kW necessary for each individual SRF cavity of the CW linac.

To compensate perturbations caused by beam loading, and dynamic tuning errors, a control of phase of the RF field is necessary in each individual SRF cavity.

Traditional RF sources based on klystrons, Inductive Output Tubes (IOTs), solid-state amplifiers are acceptable to provide the required power and the phase control, but the capital cost of the RF system is a significant part of the accelerator project. MW-scale CW klystrons powering groups of the cavities can reduce the costs, but this technique only allows a control of the vector sum of the accelerating voltage in the group. The vector sum control has not been tested in driving SRF cavities for non-relativistic or weakly relativistic particles; it may cause emittance growth because of non-optimized values of phase and amplitude of the field in individual SRF cavities.

The CW injection-locked magnetrons are efficient and less expensive than the aforementioned RF sources, [4].

Analysis of operation of magnetrons injection-locked by a phase-modulated signal, [5-7] demonstrates that the magnetron response on the locking signal is quite linear, has small phase error and quite fast, [8]. The features of the injection-locked magnetrons allow developing the RF source based on the CW magnetrons controlled in phase and power to suppress the perturbations of the magnetron phase performance inherent in magnetrons and moreover to satisfy requirements of the Project X H^- linac as well.

The experiments performed with CW 1 kW injection-locked magnetrons and evaluations presented in this paper indicate that the phase controlled transmitter based on the injection-locked magnetrons with a Low Level RF system including a closed wideband loop will allow eliminating all expected low-frequency perturbations of the accelerating field in SRF cavity including the perturbations caused by the phase performance of the injection-locked magnetron.

Results of the experimental tests are analyzed and discussed in this paper.

*Work is supported by the Fermilab and Muons, Inc. collaboration
#grigory@muonsinc.com; gkazakevitch@yahoo.com

Copyright © 2013 CC-BY-3.0 and by the respective authors

AN EFFICIENT RF SOURCE FOR JLAB*

M. Neubauer, A. Dudas, Muons, Inc. Batavia, IL 60510, USA
R. Rimmer, H. Wang, JLAB, Newport News, VA 23606, USA

Abstract

The original CEBAF accelerator at Thomas Jefferson National Accelerator Facility (JLAB) currently uses a system of 340 klystrons with relatively low efficiency, but an MTBF approaching 170,000 hours. Over the lifetime of the project 60% of the tubes have been replaced, giving an MTBF for a single tube of about five to six years. 45% of the klystrons were replaced over the thirteen years of full operation (1995-2007) with an average filament on time of 80% and high voltage on time of 75%, thus a utilization rate of 61% per year or ~4300 high voltage operating hours per year with an overall system efficiency of 35%. This represents 1.6M$ per year of electricity costs and over 20% of the total electricity usage of the high energy mission specific facilities (HEMSF).

We propose the development of a highly reliable high efficiency RF source for JLAB operating at ~80% efficiency yielding system operating costs of only about 0.7M$/year for the 6 GeV machine. A number of RF source designs are being evaluated including the concept of two injection locked magnetrons in a novel combining architecture for amplitude modulation. A cost analysis including efficiency and reliability will be performed to determine the optimum system architecture.

INTRODUCTION

The RF source for the CEBAF machine currently uses 5-8 kW klystrons operating at ~35% efficiency [1]. The annual electricity usage for the HEMSF for the 6 GeV machine is 130,000 MWhrs [2]. As shown in Table 1, the annual savings for the RF source alone would be about 1M$ per year, neglecting various cooling requirements for the power supply and microwave tube. The savings represent a reduction in the HEMSF usage from 130,000 MWhrs to about 113,000 MWhrs for the 6 GeV machine.

Table 1: Example calculations of the impact of a high efficiency RF source on the operating costs and electricity usage per year.

RF output power	5	5	kW
tube efficiency	35%	80%	
DC input power to each station	14.3	6.25	kW
number of stations	340	340	
DC Input power for HPRF sources	4857	2125	kW
Power supply conversion rate	95%	95%	
Total station input power for HPRF	5113	2237	kW
70% utilization rate	6132	6132	hrs/year
Yearly Electrical Useage	29784	13031	Mwh/year
Cost at 61$/Mwh	$1.82	$0.79	($M)
Savings		**$1.02**	**($M) per year**

The MTBF of individual tubes in the CEBAF system can be estimated to be 5-6 years or about 37,000 tube hours with a 75% utilization rate, while the MTBF of the system of 340 tubes is approximately 170,000 system hours (see Figure 1). Magnetrons have a similar MTBF. Varian (now CPII) reported lifetimes of 27,600 MTBF for a 65-80kW X-band coaxial magnetron [3]. In 2006, a study was made at the Naval Post Graduate School in Monterey, of the Total Ownership Cost (TOC) of the Aegis microwave power tubes. In the Aegis system, the MTBF of CFAs was improved from 6000 hours to 45,000 hours from 1983-2002 [4]. Cross-field amplifiers (CFA) are in the same class as magnetrons.

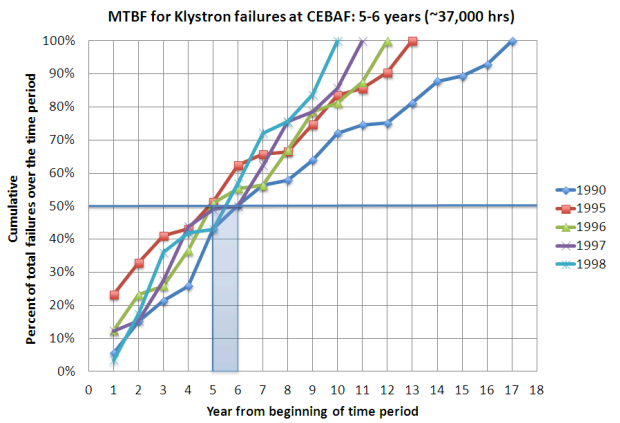


Figure 1: Data Collected from JLAB presentation, "Operating Experience and Reliability Update on the 5 kW CW klystrons at Jefferson Lab," [5].

Another primary use of magnetrons is in medical linear accelerators where they are operated at high peak powers with low utilization rates. The MTBF of the magnetrons in one linac system architecture was doubled from 20 months to 43 months over a four year period [6].

The point to be made is that, the system design and the interface between the tube(s) and power supplies dominates the MTBF of the RF source. It is reasonable to assume that the MTBF of a magnetron based system can be as good if not better, than the klystron MTBF when the system design is optimized at an early stage of development.

APPROACH

We have determined two basic designs which will be further analyzed. The first consists of a single RF source (klystron, magnetron, IOT, etc.), and the second would be a dual magnetron source in which the outputs of two injection locked magnetrons would be phased and combined to produce a required output power level and phase.

An initial power balance spreadsheet analysis has shown that a single magnetron would be more efficient that using either a klystron or IOT device. Thus our focus has narrowed to either a single or dual magnetron system.

*Work supported by DE-SC0009693

ISBN 978-3-95450-138-0

Copyright © 2013 CC-BY-3.0 and by the respective authors

HIGH POWER CO-AXIAL COUPLER*

M. Neubauer, A. Dudas, Muons, Inc., Batavia, IL 60510, USA
R. Rimmer, J. Guo, S. Williams, JLAB, Newport News, VA 23606, USA

Abstract

A superconducting RF (SRF) power coupler capable of handling 500 kW CW RF power at 750 MHz is required for present and future storage rings and linacs. There are over 35 coupler designs for SRF cavities ranging in frequency from 325 to 1500 MHz. Coupler windows vary from cylinders to cones to disks and RF power couplers will always be limited by the ability of ceramic windows and their matching systems to withstand the stresses due to non-uniform heating from dielectric and wall losses, multipactor, and mechanical flexure.

We have fabricated and tested a novel robust co-axial SRF coupler (400 MHz, 6 kW CW) design that uses two windows manufactured with compression ring technology and no matching elements in the coax line. This technology allows the use of high thermally conductive materials for cryogenic windows because the braze joint will be in compression. We have also incorporated "explosion bonded" technology into this design to reduce needed parts and simplify fabrication. In this phase, a scaled down version of the 500kW CW double window assembly has been built and tested.

A compressed co-axial window was designed and fabricated using standard ceramics [1]. Low power tests confirmed the broadband match characteristics of a double window design.

Double-window, coaxial input couplers or coaxial pressure barriers have high power CW applications ranging from RF guns for injectors to high power magnetron sputtering systems. Single half-wavelength coaxial windows built with our compression technology will handle significantly more power than standard windows.

INTRODUCTION

Dual-Window Concept

When two coax windows are placed in a length of line, the distance between them can be adjusted to create a perfect match. That distance is approximately a quarter-wavelength. The thickness of the window and its dielectric constant determine the exact distance for the cancellation of reflections. For EIA 3-1/8 50Ω coax line, the ceramic window has the same dimensions as the coax (76.9 mm and 33.4 mm). In our Phase I construction of a compressed window we used a window thickness of 7.6 mm. Using those dimensions the optimum spacing for various frequencies can be determined by various simulation tools. For EIA 3-1/8 coaxial line, Figure 1 shows the window spacing as a function of frequency, which provides a near perfect match.

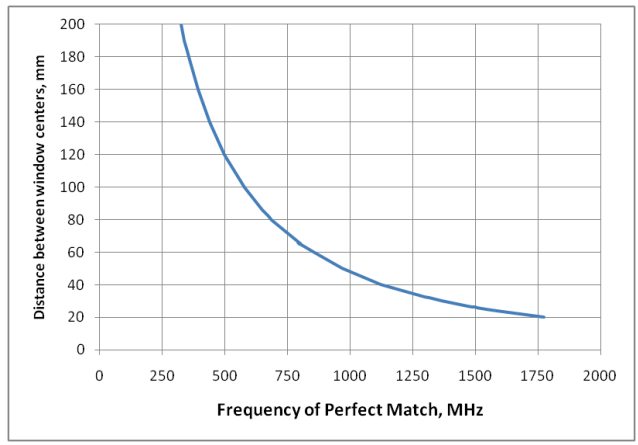


Figure 1: Two alumina windows 7.6 mm thick modeled in EIA 3-1/8 coax for the distance between them which creates a near perfect match.

As the thickness of the window becomes large compared to the wavelength of the match frequency, the actual distance to cancel reflections becomes smaller than the theoretical $\lambda_g/4$. The bandwidth of the match was calculated to be about 2-3% at a VSWR of 1.01:1.

Two windows of different materials can be matched in a similar manner by slightly changing the thickness of one window or the spacing between the two windows.

Explosion Bonding

Our coupler design was discussed previously [2], and illustrates the usefulness of fabricating the outer conductor, vacuum assembly, and window Compression Rings as one piece. A braze joint between the copper outer conductor and stainless vacuum tube, would be very difficult to make due to the large surface areas involved. Explosion Bonding (EB) a thin layer of copper onto the inner surface of a stainless steel tube then machining to size is a good and cost effective solution.

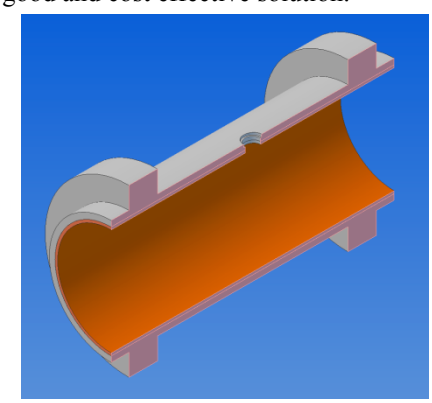


Figure 2: Explosion bonded copper outer conductor, compression rings, and vacuum tube assembly.

*Work supported by Dept. of Energy grant no. DE-SC0002769

Copyright © 2013 CC-BY-3.0 and by the respective authors

S-BAND LOAD DESIGN FOR SLAC*

M. Neubauer, A. Dudas, Muons, Inc., Batavia, IL 60510, USA
A. Krasnykh, SLAC, Menlo Park, CA 94025, USA

Abstract

S-Band vacuum loads at the SLAC linac are encountering operational problems, now that they have to operate under the stringent requirements of 50 MW peak power, 6 kW average power, and extremely-tight phase stability for the linac. Failure mechanisms have been studied which suggest an RF surface breakdown of the 200 µm Kanthal layer in original RF loads.

Currently there are two approaches for RF load design. The first is based on employing highly resistive materials inside of WR284 waveguide [see SLAC-PUB-15229 or MOPB087 in LINAC12]. An alternative approach is based on using lossy dielectric. This is the approach discussed in this paper.

We have proposed a novel solution which incorporates mode conversion from TE10 in rectangular waveguide to TE01 in round waveguide. Lossy material will be placed in the round waveguide, and the selection of the TE01 mode minimizes the electric field normal to the surface of the lossy material. This lossy material in the TE01 round waveguide will be mechanically confined in compression (without brazing), in order to eliminate tensile stresses in the lossy material. The mode converter will be based upon an X-band mode converter invented at SLAC, and the TE01waveguide load design is based upon HOM load designs developed by Muons, Inc.

We are presently performing additional materials testing, in preparation for fabrication of a full power prototype load. A TE10 to TE01 SLAC converter design will be fabricate for both cold and hot testing.

Operational improvements to the SLAC LCLS linac may require the replacement of all SLAC linac vacuum RF loads. The new design can be scaled for use at other frequencies in a multitude of commercial RF applications.

INTRODUCTION

Recently at SLAC, the increasingly-stringent requirements for phase and amplitude stability of the linac beam have increased the sensitivity to the performance of the present load design. Ten of the current Kanthal loads were inspected, and all ten showed evidence of multipactor. Fifteen spare loads were tested and exhibited multipactor between 1 and 20 MW. An attempt to shift the multipactoring resonance using permanent magnets was not successful.

Dry loads are generally designed using high strength lossy ceramics due to the manufacturing processes used in the construction of such loads. The interface between the lossy ceramic and the support structure is brazed or soldered to make a thermally conductive path between the lossy ceramic, mechanical support, and the cooling circuit. The fact that brazing or soldering is used requires the lossy ceramic to survive large tensile stresses due to the mismatch in thermal expansion between the ceramic and the mechanical support. Efforts to either reduce these thermal stresses, or survive these stresses during thermal cycling, has led to creating strengthened ceramics such as $SiC_{whiskers}$ + Al_2O_3, or using thermally matched materials for the mechanical support such as W_{powder} + Cu in a sintered alloy. Both of these techniques have led to expensive structures due to low manufacturing yields. These low yields are typically due to large manufacturing variables, and narrow process limits, for successful fabrication of dry loads.

In our design, the dry load operates in the TE01 mode to significantly reduce the chance of multipactor, and incorporates mode converters designed by SLAC. The lossy ceramic components are cast into cylinders, from slurries composed of mixtures of SiC and porcelain, and processed to full densification and vitrification. These lossy cylinders are held in mechanical compression rather than being brazed. The microwave characteristics of the lossy ceramic cylinders have been measured, and further measurements will be made to determine the optimum mixture for various loading elements.

TECHNICAL APPROACH

TE01 Mode

The most reliable high peak power load will have no normal electric field components on the lossy material. This should simply eliminate the occurrence of multipactoring and arcing. Since the TE01 mode is a low loss mode, the uniformity of loss within the lossy dielectric is not as critical as it would be if compared to operation using other modes. This fact serves to relax the manufacturing process limits, as compared to those which are required in loads utilizing other modes and designs, such as the TE10 mode in rectangular waveguide utilizing lossy walls.

A SLAC designed TE10 - TE01 mode converter from WR284 rectangular waveguide to 6 inch round waveguide was used for the initial measurements (Figure 1). With two mode converters the insertion loss of lossy cylinders can be measured in the TE01 circular mode. The wrap-around mode converter is primarily scaled from the X-band version that was invented by Sami Tantawi of SLAC [1]. The VSWR of these mode converters back-to-back was 1.13 at 2856 MHz, likely due to out-of-round circular waveguide and non-matching edges at the mating flanges. Some slight tuning on the endplates could improve that number to less than 1.11 at 2856 MHz.

*Work supported by Dept. of Energy contract DE-SC0007559

ISBN 978-3-95450-138-0

Copyright © 2013 CC-BY-3.0 and by the respective authors

HIGH-POWER LOW-VOLTAGE MULTI-BEAM KLYSTRONS FOR ILC AND PROJECT-X*

V. Teryaev[1], S.V. Shchelkunov[1,2], J.L. Hirshfield[1,2], N. Solyak[3], V. Yakovlev[3], S. Yu. Kazakov[3]
[1]Omega-P, Inc, New Haven, CT 06510, USA
[2]Yale University, New Haven, CT 06511, USA
[3]Fermilab, Batavia, IL 60510, USA

Abstract

Designs of two multi-beam klystrons with parameters suitable for ILC and for the 8-GeV pulsed stage of Project X (PX) have been developed. The chief distinction of these tubes from other MBKs is their low operating voltage, namely 60 kV for the ILC tube and 30 kV for the PX tube. Advantages of low voltage include no requirement for pulse transformers or oil-tanks for high-voltage components, and simpler modulators. A 6-beamlet quadrant of the ILC tube has been built and is soon to undergo tests; it is designed to produce 2.5 MW at 1.3 GHz in a 1.6 ms wide pulse at a 10 Hz pulse rate; a four-quadrant future version would produce 10 MW. The 6-beamlet PX tube is to produce 520kW, and would operate in one of two regimes, either at a repetition rate of 2 Hz delivering 30 ms pulses, or at 10 Hz delivering 8.5 ms-long pulses. The PX tube is currently undergoing engineering design, with construction scheduled for completion by the end of 2014.

INTRODUCTION

Multi-beam klystrons (MBKs) are the most advanced stage in the evolution of high-power klystron design. The distinct feature of MBKs is their relatively low-voltage beams (beam-lets) as compared to the single beam in traditional tubes. This provides numerous advantages: MBKs can use a simpler (and thus, a cheaper) modulator—or even a switched power supply; no pulse-transformer is required; and there is no need for a high-voltage oil tank to insulate the gun. An MBK can be made significantly shorter (e.g. by a factor at least 2) than a single-beam tube delivering the same power and pulse; in particular the collector length can be greatly reduced. The challenges associated with MBKs are typically to design the cavity chain where all parasitic modes are sufficiently detuned, which is accomplished by using a set of metal shunts inserted in some of the cavities to cause either inductive or capacitive detuning, particularly in the input and/or output cavities where the RF field interacts with all the beam-lets, or by using individual gain and penultimate cavities each serving a sub-group of beam-lets (beam-let cluster) and working at the fundamental mode. To easily match the beam between the gun, the cavities, and collector, the magnetic system is typically divided by iron pole-pieces into regions of independent control. An associated challenge is to have coil and pole-piece configurations where the transverse magnetic field on the axis of each beam-let is less than 0.5% of the longitudinal field, while keeping the magnetic system design relatively simple. In [1] and refs therein, detailed descriptions can be found of tools, methods, approaches and recipes to address the aforementioned challenges; in particular, contemporary state-of-the-art codes such as MAGIC [2], MERMAID [3], and DGUN [4] are invaluable in designing MBKs.

*Work supported by Office of High Energy Physics, U.S. Department of Energy;
sergey.shchelkunov@gmail.com

MBK FOR ILC

In [1], the tube's conceptual design was presented. Herein we mention briefly its parameters and main features. Figure 1 presents the layout; the design parameters are shown in Table 1.

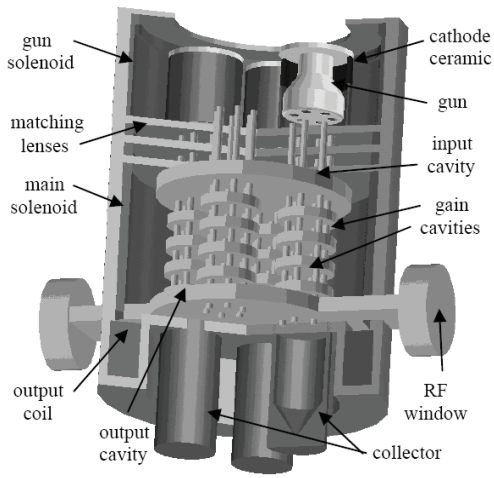


Figure 1: Layout of ILC MBK.

Table 1: Design Parameters of ILC–MBK

Operating frequency, MHz	1,300
Beam voltage, kV	60
Beam-let microperveance	0.85
Number of beam-lets	24
Beam-let current, Amps	12.5
Total current, Amps	300
Efficiency, %	65
Output RF power, MW	10
Average output power, kW	150
Pulse width, ms	1.6
Saturated gain, dB	50
Cathode loading, Amps/cm^2	2.7
Gun surface electric field, kV/cm	65
Total tube length, m	1

Copyright © 2013 CC-BY-3.0 and by the respective authors

ISBN 978-3-95450-138-0

OPTIMIZATION OF THE SLED PHASE MODULATION PARAMETERS OF THE FERMI LINAC*

C. Serpico, M. Dal Forno, A. Fabris, Elettra-Sincrotrone Trieste S.C.p.A., Trieste, ITALY

Abstract

FERMI is a single-pass, linac-based, FEL user-facility covering the wavelength range from 80 nm to 4 nm and is located next to the third generation synchrotron radiation facility Elettra in Trieste, Italy. The first FEL line in operation (FEL-1) has been opened to users at the end of 2012, while the second FEL line (FEL-2) covering the shorter wavelength down to 4 nm is in commissioning. The linac is composed of 16 S-band accelerating structures. Seven of them are Backward Traveling Wave (BTW) structures equipped with SLED system. Following the preliminary tests on one plant, in order to increase the operational accelerating gradient, phase modulation of the SLED drive power has been implemented on all BTW structures. The shape of the phase modulation is applied via the LLRF system firmware and can be modified if needed. This paper discusses the optimization of the phase modulation parameters.

INTRODUCTION

FERMI is a single-pass Free Electron Laser (FEL) driven by a normal conducting S-band linac composed of 16 accelerating structures. Seven of them are Backward Traveling Wave structures (BTW), coming from the old Elettra injector, with a filling time of 0.757μs. Each structure is fed by a $45MW$ peak power, 4.5μs pulse width Thales klystron. Taking advantage from the short accelerating structure filling time, the peak power to the structure is increased by shortening the pulse length: each power plant is equipped with PEN (Pulse Enhancement Network) system [1] that stores the energy at the beginning of the pulse and release it near the end of it.

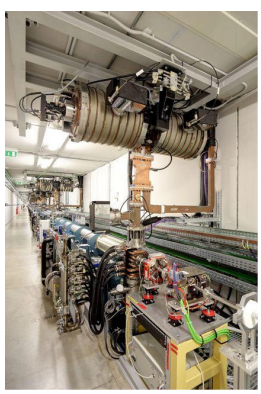


Figure 1: Pulse enhancement network system for a backward traveling wave structure.

* Work supported in part by the Italian Ministry of University and Research under grants FIRB-RBAP045JF2 and FIRB-RBAP06AWK3.

To achieve the Linac target energy of 1.5 GeV, each BTW structure needs to be operated at a gradient of 26 MV/m corresponding to an energy gain of about 155 MeV. Past operation of those structures, showed that breakdown problems inside the sections, associated with the very high peak-field built up during conventional SLED operation, prevented from reaching the desired gradient in a reliable way.

A phase modulation technique was implemented to lower the high peak field inhered with conventional SLED operation: while a preliminary linear phase modulation has allowed to demonstrate the utility of this technique in our application and has allowed to increase the energy gain in the structures, the possibility of an optimization of the phase modulation parameters has been studied to get the optimal trade-off between lowering the peak field, thus improving reliability, and still having an acceptable energy gain.

PRELIMINARY PHASE MODULATION

The phase modulation feature was integrated in the LLRF firmware of FERMI. The preliminary implementation of the phase modulation technique foresees just a linear modulation [2] where two parameters (i.e. the initial phase ϕ_0 and the phase modulation slope m) can be modified to change the shape of the modulation as depicted in Figure2.

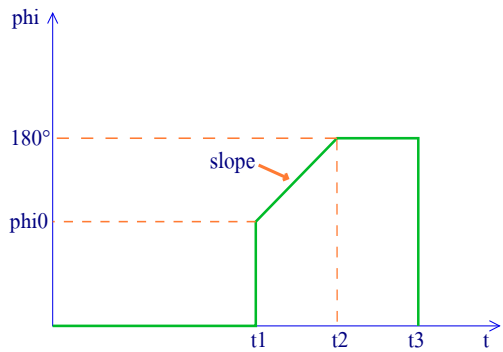


Figure 2: Linear phase modulation.

During a dedicated machine commissioning shift, different sets of parameters were tested: the optimal results (in terms of a trade-off between peak field and gradient loss) were achieved using an initial phase offset ϕ_0 of 95° and a slope m of 149 deg/μs.

A comparison between the pulse shape in case of conventional SLED operation and the one with the optimized linear phase modulation showed that for the same RF pulse

Copyright © 2013 CC-BY-3.0 and by the respective authors

ISBN 978-3-95450-138-0

ENERGY AND REPETITION RATE UPGRADE OF THE S-BAND RF SYSTEM OF THE FERMI LINAC*

A. Fabris#, P. Delgiusto, F. Gelmetti, M. Milloch, A. Milocco, F. Pribaz, C. Serpico, N. Sodomaco, R. Umer, L. Veljak, Elettra - Sincrotrone Trieste, S.S. 14 – km. 163,5, in Area Science Park, 34149 Basovizza, Trieste, Italy

Abstract

FERMI is a single-pass linac-based FEL user facility covering the wavelength range from 80 nm to 4 nm and is located next to the third generation synchrotron radiation facility Elettra in Trieste, Italy. The first FEL line in operation (FEL-1) has been opened to users at the end of 2012, while the second FEL line (FEL-2) covering the shorter wavelength range down to 4 nm is in commissioning. In 2013 the linac energy will be increased following the full RF conditioning of the backward traveling wave accelerating structures and of the SLED cavities. The repetition rate has been also increased to 50 Hz following the installation of the new RF gun and the completion of the upgrade program of the klystron modulators. This paper discusses the strategies adopted for the energy and repetition rate upgrade of the S-band linac and provides a description of the status and of the first results.

INTRODUCTION

FERMI is a FEL facility based on a warm linac followed by a single pass FEL [1]. Two FEL lines are installed: FEL-1 and FEL-2. The accelerator mainly consists of an RF photocathode gun, an S-band linac, an X-band structure, a laser heater, two bunch compressors and the beam transport line to the undulators of the two FEL lines.

The S-band linac is presently composed of sixteen accelerating structures. The first nine structures are forward traveling wave (TW) ones. Two of them are 3 m long and are from the old Elettra injector, while the remaining seven are 4.5 m long and are LIL type coming from CERN. The last seven structures of the machine are 6.2 m long backward traveling wave (BTW) type and are equipped with SLED systems. Also these structures were used in the old Elettra linac injector. The machine layout reserves the space for two more accelerating structures that will be added in the future [2].

Fifteen S-band 45 MW, 4.5 μs. pulsed klystrons are installed, powering the structures, the gun and the three RF diagnostic deflectors. Typical powering scheme is two structures per klystron for the TW case and one structure per klystron for the BTW one. The system is in operation on a 24h/day basis and the total operating hours/year is higher than 6000.

The commissioning of the facility is rapidly advancing [3]. The first FEL line (FEL-1) has been opened to the external users, while the commissioning of the second one (FEL-2) is advancing. FEL-1 is typically operating at 1.2 GeV beam energy and 10 Hz repetition rate. FEL-2 requires the increase of the beam energy to reach the final specifications in term of shorter wavelength. At the same time the installation of the new gun, capable of operating at 50 Hz, and the upgrade of the modulators, completed at the beginning of 2013, will allow to push the repetition rate of the machine from the present 10 Hz value to the design one, once the conditioning of the structures is completed.

REPETITION RATE UPGRADE

All the modulators installed in the machine are pulse forming network (pfn) type (see Fig.1). The first six modulators installed in the machine were assembled using the hardware of the plants of the old Elettra injector to allow the start of the commissioning studies. For this reason they were limited to 10 Hz by the hardware. The pulse forming network, the pulse transformer and the klystron tank were replaced to allow higher dissipation due to the augmented duty factor. The pfn is now water-cooled and has a better pulse flatness, while the pulse transformer has a reduced core dissipation and pulse droop. The klystron tank is water-cooled and additional lead shielding was added to the tube. The high voltage power supply was also replaced with a new one that has a higher range of current and voltage and better stability.



Figure 1: One of the RF power plants.

In addition to the replacement of some of the major components, a revision of the modulators was carried on in order to optimize the operation at 50 Hz and the stability of the klystron anodic voltage. The resonant charging scheme has been replaced by direct charging of the pfn. This allows to avoid the use of big storage capacitors and inductors, which means a reduction in stored energy, in space and in the dielectric oil. Other

*Work supported in part by the Italian Ministry of University and Research under grants FIRB-RBAP045JF2 and FIRB-RBAP06AWK3
#alessandro.fabris@elettra.eu

Copyright © 2013 CC-BY-3.0 and by the respective authors

TUNER SYSTEM ASSEMBLY AND TESTS FOR THE 201-MHZ MICE CAVITY

L.Somaschini, INFN-Pisa, Pisa, Italy
A. Moretti, R. J. Pasquinelli, D. W. Peterson, Y. Torun, FNAL, Batavia, USA
P. M. Hanlet, IIT, Chicago, USA
A. J. DeMello, D. Li, S. Virostek, LBNL, Berkeley, USA

Abstract

The MICE cavities include a mechanical tuning system consisting of stainless steel flexure forks attached to the cavity body and driven by pneumatic actuators. The first of these systems was assembled and tested at Fermilab for use at the MuCool Test Area. The actuators were calibrated on a test hoop. The cavity body was measured and the fork contact pads machined to fit. Actuators are going to be mounted on the vacuum vessel housing the cavity. The transfer function of the tuning system and the quality factor of the cavity will be measured with the recently implemented frequency control software.

MICE CAVITY AND TUNER

Each acceleration module (RFCC) of the MICE experiment [1] is composed of four normal-conducting cavities made of copper with a nominal resonant frequency of 201.25 MHz (fig. 1) [2]. The four cavities will be mounted into a vacuum vessel in order to have the same pressure on both sides and avoid deformation of the cavity when pulling vacuum. The cavities will have to work in a high magnetic field that can reach 3T on some points of the cavities surface [3]: a tuning system able to work in such an environment had to be designed. Each cavity will be equipped with a pneumatic system of 6 tuners composed of an actuator and a fork. Each fork, made of stainless steel, will be inside the vacuum vessel and it will stretch and squeeze the cavity when operated by the respective actuator. The actuators will be located outside of the vacuum vessel and will share vacuum with the vessel by means of bellows. All 6 actuators will be connected in parallel and will be controlled by two electronic valves, one responsible for pushing the actuator shaft and the other one for pulling the shaft. The main aim of the tuner will be to compensate for thermal drift of the cavity and for structural differences between the 4 of them, keeping all the cavities at the same resonant frequency.

A test module with only one cavity has been built and is about to be tested in the MuCool Test Area (MTA) at FNAL [4].

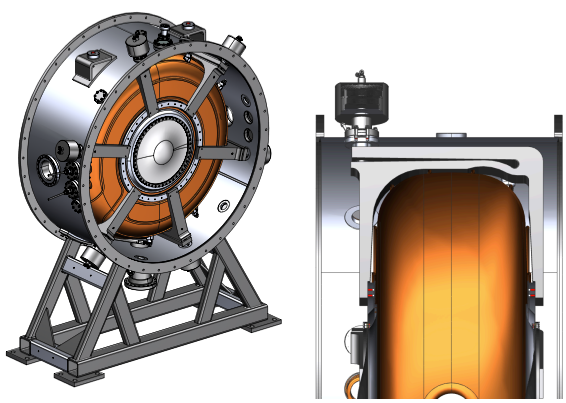


Figure 1: The MTA cavity module and the tuning system.

TEST STAND

Equipment

The six actuators, since working in parallel, had to be tested for possible gas leaks and for uniform response. To do that, a test stand was built at LBNL (fig. 2): a tuning fork was mounted on an aluminum hoop with a spring constant equal to 1/6 of the spring constant of the cavity. The test hoop was placed on an aluminum plate embedding a conflat flange necessary to screw the vacuum bellows of the actuators under test.

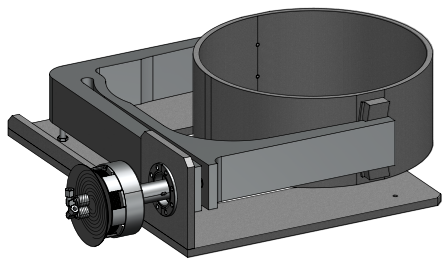


Figure 2: Tuning fork and actuator.

The actuators were controlled by two QPV proportional valves by ProportionAir. Those were connected to a computer running a LabView program. During the test, the pressure applied to each actuator was recorded from proportional valve readout and checked against an analog pressure gauge. The deflection on the test hoop diameter was measured with a dial gauge with a precision of 0.0005 inches, while a linear potentiometer was placed on the fork and aligned with the actuator shaft. The linear potentiometer used is by Novotechnik and it offers a 5 kΩ resistance over a mechanical range of 10 cm. It is powered with a stable 10V signal provided by a voltage regulator. The output voltage is directly proportional to the position of the shaft and consequently the voltage variation is proportional to the actuator shaft movement and to the variation in the fork gap (fig. 3). The voltage was read with a National Instrument ADC and recorded with a LabView code.

Copyright © 2013 CC-BY-3.0 and by the respective authors

ISBN 978-3-95450-138-0

RF DESIGN OPTIMIZATION OF A 176 MHZ CW RFQ*

B. Mustapha#, S.V. Kutsaev and P.N. Ostroumov
Physics Division, ANL, Argonne, IL 60439, USA

Abstract

We have recently designed a 176 MHz CW RFQ for the SARAF upgrade project. A full 3D model of the structure including vane modulation was developed. The design was heavily optimized using large scale electromagnetic simulations. Following the choice of the vane type and geometry, the shape and dimensions of the undercuts were optimized to produce a flat field along the structure. Simulations of the same structure with different lengths were performed to verify that the design length produced the best separation of the operating mode from neighboring modes. If built as designed, the RFQ should not need dipole rods for mode separation, but their effect were studied in the case of manufacturing errors. Finally, the tuners were designed and optimized to tune the main mode without affecting the field flatness. The design optimization was mainly performed using CST Micro-Wave Studio and the results were verified using both HFSS and ANSYS. The results of these studies will be presented and discussed.

INTRODUCTION

Soreq NRC, Israel's national laboratory, is exploring the possibilities of upgrading the existing SARAF linac [1]. One of the potential projects is an RFQ upgrade in collaboration with Argonne. In this paper, we present the rf design optimization for a 176 MHz cw RFQ. The proposed design is based on the successful ATLAS upgrade RFQ design [2].

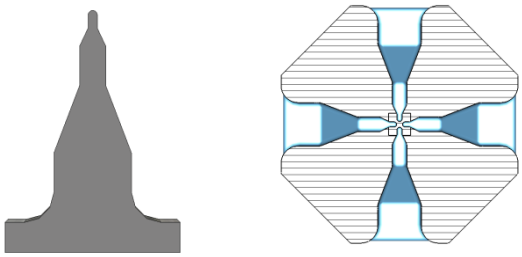


Figure 1: Vane profile (left) and RFQ cross section (right) with an inner diameter of ~ 36 cm.

RFQ STRUCTURE AND PARAMETERS

The selected structure for this RFQ is a 4-vane. The vane profile is based on the ATLAS upgrade RFQ except that this design is a full-vane, not a split-coaxial. At this frequency the transverse size of the RFQ is manageable. Both the vane profile and the RFQ cross section are shown in Figure 1. The structure is about 4 m long divided into 4 segments. The RFQ design parameters are summarized in Table 1. The output energy could be increased by applying trapezoidal modulation while keeping the same vane voltage and power.

Table 1: RFQ Design Parameters

Parameter	Value
q/A	½
Input energy, keV/u	20
Output energy, keV/u	1300
Frequency, MHz	176
Voltage, kV	75
Design current, mA	5
Power, kW	125
Average radius, mm	4.4
Max. modulation	2
Min. transverse phase advance, deg	33
Norm. trans. acceptance, π mm·mrad	2.2
Peak surface field, Kilpatrick units	1.6
Number of cells	250

RF MODELING AND OPTIMIZATION

The electromagnetic design and optimization were mainly performed using the CST Micro-Wave Studio (MWS) [3] and the final results were verified using HFSS and ANSYS. A full 3D model of the RFQ was developed in MWS. Detailed views of the geometry including the undercuts and the modulations are shown in figure 2. This model has pure sinusoidal modulations along the whole RFQ.

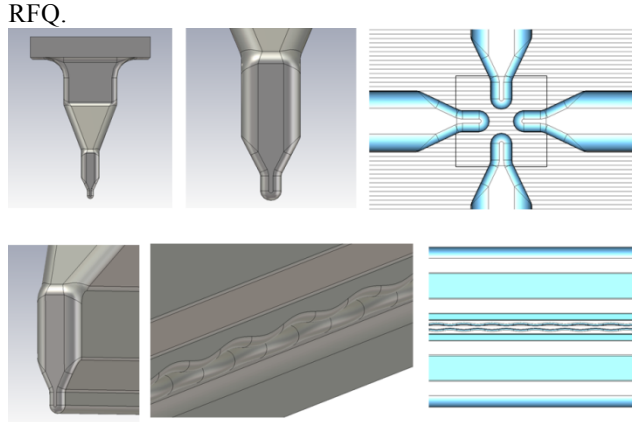


Figure 2: 3D modelling of the RFQ in MWS.

* This work was supported by the U.S. Department of Energy, Office of Nuclear Physics, under Contract DE-AC02-06CH11357 and ANL WFO No. 85Y4.
# brahim@anl.gov

Copyright © 2013 CC-BY-3.0 and by the respective authors

MODELING VACUUM ARCS IN LINAC STRUCTURES*

J. Norem#, ANL, Argonne, IL 60439, USA
A Moretti, Fermilab, Batavia, IL 60510 USA
Z. Insepov, S. Nurkenov, Nano Synergy Inc, Downers Grove, IL 60516 USA

Abstract

We describe our vacuum arc model, which divides breakdown into four stages: trigger, plasma formation, plasma evolution and surface damage. We have modeled all four stages numerically and find that the properties of surface cracks and unipolar arcs can explain essentially all the experimental data we have seen. In addition to linac breakdown, the model should apply to arcs in a wide variety of applications, such as laser ablation, tokamak edge plasmas and micrometeorite impacts. We also outline differences with other work.

THE MODEL

This effort began as an attempt to understand gradient limits in 805 MHz cavities used for muon cooling. We have described the overall picture of the model and some of the details in a number of papers in the context of accelerator breakdown [1-7].

Recent work has shown that the development of the arc can be explained by two mechanisms: 1) mechanical failure of the solid surface due to Coulomb explosions caused by high surface fields at crack junctions (see ref [5]) and, 2) the development of unipolar arcs that can act as virtual cathodes and produce currents that short the driving potential [3]. Once an arc starts, the surface electric field and field emission increase, increasing ionization of neutrals, increasing in the plasma density [4]. The density increase then reduces the Debye length that increases the surface electric field, thus both the electric field and the density increase approximately exponentially with time. PIC simulations of the unipolar arc model for vacuum arcs relevant to rf cavity breakdown show that the density of plasma formed above the field emitting asperities can be as high as 10^{26} m^{-3} [6]. The temperature of such plasma is low, in the range of 1-10 eV. These high densities can make the Debye screening length, λ_D, become smaller than the mean inter-particle distance or the number of particles in the Debye sphere, to become less that unity. This implies the failure of the ideal plasma approximation, as well as most of the assumptions used in simple calculations. Processes in such a dense plasma can be affected by three body particle collisions so that the Particle In Cell (PIC) method which relies on a simple collisional model, with two body collisions, becomes inappropriate and different methods, such as Molecular Dynamics (MD) must be used

Arrays of cracks are seen in many SEM images of arc damage. We believe these cracks are the result of the cooling of the melted surface that takes place in two stages; first cooling from high temperatures to the solidification point of the metal, followed by cooling from the freezing temperature to room temperature, where the solid contracts by an amount $\Delta x/x = \alpha\,\Delta T \sim 2$ %, where ΔT is the temperature change, x represents the dimension of the damage and α is the coefficient of linear expansion. The model is diagrammed in Fig. 1.

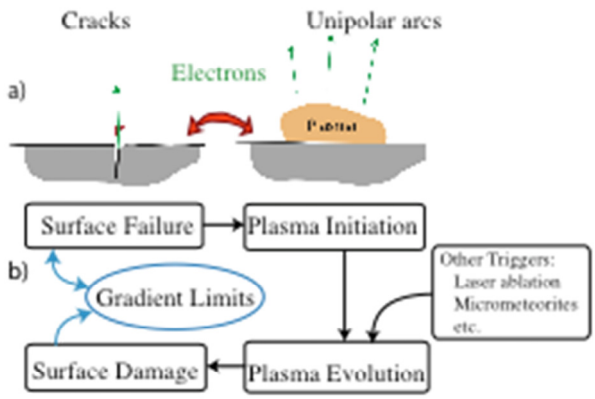


Figure 1: Breakdown proceeds through surface failure, plasma initiation, plasma evolution and surface damage. Part a) shows the physical picture, part b) shows active mechanisms.

The model provides a framework for prediction and experimental study of all aspects of the breakdown process in a variety of environments.

USING THE MODEL

In order to explore the reach of the model we consider the following issues:

Multipactor

We have reported surface damage in coupling cells where the scale of the structure was on the order of 10 nm, rather then the 1 μm commonly seen in 805 MHz Breakdown events. These are consistent with unipolar arcs caused by multipactor, and evidently are not associated with significant shorting currents. These occur at lower gradients and do not seem to be gradient limiting.

Magnetic Field Effects

The geometries of crack junctions can explain magnetic field effects. Data show similar breakdown thresholds with magnetic fields parallel and perpendicular to the surface, arguing for single surface breakdown. With B=0, melted areas are irregularly shaped, and cool so that

*Work supported by Office of High Energy Physics, USDOE
#norem@aps.gov

Copyright © 2013 CC-BY-3.0 and by the respective authors

ISBN 978-3-95450-138-0

TUNING, CONDITIONING, AND DARK CURRENT MEASUREMENTS: 1300 MHZ NCRF CAVITIES AT THE ARGONNE WAKEFIELD ACCELERATOR (AWA) FACILITY*

J.G. Power#, M. E. Conde, S.D. Doran, W. Gai, and E. Wisniewski ANL, Argonne, IL 60439
C. Jing, Euclid Techlabs, 5900 Harper Rd, Solon, OH 44139

Abstract

In this paper, we present data on: (i) tuning and balancing; (ii) high-power rf conditioning; and (iii) dark current measurements; of normal conducting, standing wave, 7 cell, 1300 MHz accelerating cavities. The six cavities were tuned to 1300 MHz and were balanced to >96% in all cells. They are designed to operate with 10 MW of rf input power but are being rf conditioned beyond this operating point to insure low dark current during operation. During rf conditioning, dark current measurements are being recorded to provide a history of the cavity's surface field enhancement factor, *"β"*, throughout the rf conditioning period. Finally, as the final step we plan to record the breakdown rate at 10 MW to add to the breakdown literature for L-band cavities.

INTRODUCTION

Six normal-conducting, L-band rf cavities are currently undergoing commissioning as part of the linac upgrade to the AWA facility [1] to increase the drive beam energy from 15 MeV to 75 MeV. The cavity design (Fig. 1) is a seven-cell, standing-wave, 1300 MHz cavity made with OFE copper and was reported on earlier [2]. As of September 2013, all six cavities have been tuned and balanced but only one of the six cavities has been conditioned. In the first section of this paper we describe the tuning and balancing of all six cavities and in the second half of the paper we describe the rf conditioning of the first of the six cavities including measurements of dark current and the field enhancement factor, β, during the rf conditioning process. The remaining 5 rf accelerating cavities will be rf conditioned during the Fall of 2013.

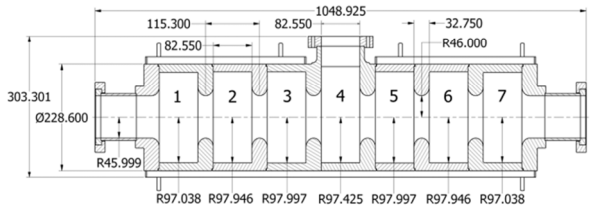


Figure 1: Cross section of the AWA rf cavity.

RF CAVITIES UPON ARRIVAL

Turnkey fabrication of the AWA cavities was enabled by a combination of high fidelity simulations using Omega3p [3], tight machining tolerances, push-pull tuning divots, and the adaptation of a well understood braze joint based on a SLAC design. Using this approach, the cavities were machined to final dimensions (i.e. without iterations), brazed together, and sent immediately to Argonne for tuning and balancing.

Table 1 lists the major figures of merit of the six cavities upon arrival from the vendor. The cavity Q0 was ~98% of ideal and the inter-cell coupling constant, k, was 99.5% of design. While neither of these is subject to adjustments during tuning they were within acceptable limits anyway. The cavities came back from the vendor with resonant frequency, f_0, that were between 290-568 kHz low and all cells had voltage field balance better than 87%. These values, for f_0 and balance, were very nearly acceptable without any tuning and balancing. Moreover, all cavities were within the estimated tuning range based on the combination of the push-pull divots and the temperature adjustment of the cooling water.

Table 1: Designed vs. Achieved Cavity Figures of Merit (upon arrival from vendor)

Parameter	Design	Cavity #1	Cavity #2	Cavity #3	Cavity #4	Cavity #5	Cavity #6
f0@38C	1300	-344 kHz	-290 kHz	-406 kHz	-568 kHz	-424 kHz	-360 kHz
T@1300	38^0C	38^0C	20.8^0C	23.6^0C	17.7^0C	9.6^0C	20.0^0C
Q0	25147	24911	24006	24798	24975	24768	24798
Beta	1.28	1.31	1.21	1.27	1.27	1.25	1.27
S11		-19.4dB	-20.2dB	-18.4	-18.5	-19.1	-18.5
Balance	100%	>93%	>90%	>95%	>93%	>87%	>99%
k	2.21%	2.2%	2.2%	2.2%	2.2%	2.2%	2.20%
S21-probe	-60dB				-61.95dB		-61.0dB

*The work is supported by the U.S. Department of Energy under Contract No. DE-AC02-06CH11357 with ANL.
#E-mail jp@anl.gov.

Copyright © 2013 CC-BY-3.0 and by the respective authors

PPM KLYSTRONS FOR ACCELERATOR SYSTEMS

Patrick Ferguson, Michael Read, R. Lawrence Ives and David Marsden
Calabazas Creek Research, Inc., 690 Port Drive, San Mateo, CA 94404

Abstract

Calabazas Creek Research, Inc. (CCR) is engaged in the development of high power periodic permanent magnetic (PPM) focused klystrons for Accelerator Systems. There are at present 3 ongoing development programs. A 10 kW CW S-band klystron for the Advanced Photon Source at Argonne National Laboratory is nearing completion. An SBIR Phase II grant to develop an S-band 5.5 MW pulsed klystron for the Varian Medical Systems, Inc. CLINAC was funded in April, 2013. An SBIR Phase I grant to develop an S-band 75 MW pulsed klystron for the X-FEL linac at Los Alamos National Laboratory was received in February, 2013. The present development status of these 3 klystrons will be presented.

INTRODUCTION

The impetus to develop high power CW and pulsed PPM focused klystrons is to reduce the cost of producing a large number of klystrons as required by pending high energy linacs. The electron beams for the majority of klystrons for these linacs are focused using electromagnets. These electromagnets require a DC power supply and external fluid cooling. In addition, the electromagnet adds size and weight to the klystron. Employing a PPM structure in lieu of the electromagnet with DC power supply reduces the cost, size and weight substantially with no degradation in operation and life time.

CCR is nearing completion of the fabrication of the 10 kW CW S-band klystron. A 3D pictorial of this klystron is shown in Figure 1 below. The PPM structure consists of as standard geometry with a fixed period where the conventional ring magnets have been replaced by 4 pill box magnets in each half period. This geometry allows ready access to cavity tuners and cooling lines. The four long magnets around the RF output cavity are required to focus the spent electron beam as it loses energy. Initial simulations predicted an efficiency of 70%. However, after determining that the spent electron beam was intercepted just after the output cavity, the PPM structure was redesigned to include the large magnets with the efficiency decreasing to 55%. The electrical parameters for this PPM klystron are listed in Table 1.

Table 1. Electrical Parameters for the APS Klystron

Frequency	2.815 GHz
Beam Voltage	20 kV
Beam Current	1.0 A
Efficiency	55%
RF Output Power	11 MW
Saturated Gain	49 dB
Frequency	>5 MHz

The second PPM program is the development of a 5.5 MW pulsed S-band klystron similar to the solenoid focused klystron presently used in the Varian Medical Systems, Inc. CLINAC. The CLINAC is an X-ray source for treating cancer. The initial SBIR Phase I addressed the L-band RF sources for Project X at Fermi National Laboratory. It was redirected to the 5.5 MW S-band klystron due to the reduction in funding for Project X. The revised program is

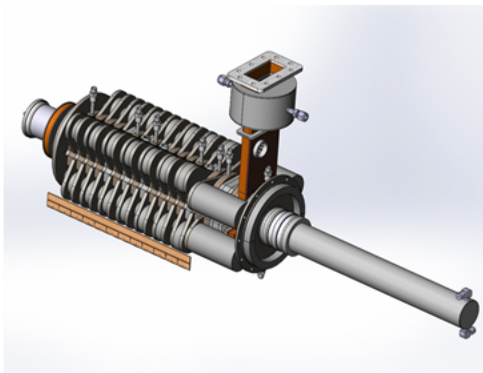


Figure 1: The 10 kW CW S-Band PPM Klystron.

Copyright © 2013 CC-BY-3.0 and by the respective authors

ISBN 978-3-95450-138-0

PASSIVELY DRIVEN X-BAND STRUCTURES

T. Sipahi, N. Sipahi, S. G. Biedron, S. V. Milton, CSU, Fort Collins, Colorado, USA

Abstract

Accelerating structures operated at X-band frequencies have been shown to regularly achieve gradients of around 100 MV/m or better. Obviously, use of such technology can lead to more compact particle accelerators. At the Colorado State University Accelerator Laboratory (CSUAL) we would like to adapt this technology to our L-band (1.3 GHz) accelerator system via a 2-beam configuration that capitalizes on the high gradients achievable in X-band accelerating structures in order to increase our overall beam energy in a manner that does not require investment in an expensive, custom, high-power X-band klystron system. Here we provide the design details of the X-band accelerator structures that will allow us to achieve our goal of reaching the maximum practical net potential across the X-band accelerating structure.

GENERAL CONCEPT

The CSUAL linac is an L-band system capable of generating 6-MeV electron bunches [1]. The parameters of L-band linac system are given in Table 1. For many reasons we would like to further increase the electron beam energy without additional significant investment. Our idea is to utilize the electron beam from our linac as a drive source for an otherwise unpowered (passive) X-band linac structure, thus allowing us to increase the beam energy by using the L-band power together with the inherent high shunt impedance of the X-band structure. In our previous study [2] we showed that by using a passive standing wave (SW) X-band cavity driven by our linac we had the potential to increase our 6-MeV electron bunch energy to 11 MeV in 15 cm, but there was a fundamental limit of that configuration. Here we utilize a two-beam configuration based on two traveling wave (TW) X-band structures, one used as an X-band power generator (the decelerator), and one as an accelerator. This configuration is shown in Figure 1. We exploit the TW structure's ability to provide continuous X-band power generated from the passing of the L-band system beam through it and then transfer this power to a second cavity that can be filled in a manner that does not limit as before the achievable integrated potential.

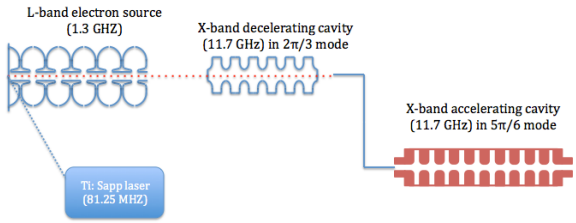


Figure 1: General layout of the two-beam X-band cavity structures [3].

Table 1: Parameters of CSU Accelerator Laboratory

Laser Frequency	81.25 MHz
L-Band RF Gun Frequency	1.3 GHz
L-Band RF Gun Energy	6 MeV
L-Band Macropulse Length	10 μs
X-band Linac Frequency	11.7 GHz
Repetition Rate	10 Hz
RF gun Charge/Bunch	3.5 nC

CAVITY CHOICE

General

We must design two separate cavities, one to be used as a decelerator and optimized to efficiently generate and allow extraction of X-band power without significant disruption to the passing beam, and the other optimized to efficiently accept X-band power and generate the highest practical integrated potential to be used for accelerating electron bunches.

We use a consistent description of cavity geometries as shown in Figure 2 where a is the iris radius, R is the cavity radius, h(=2r_1) is the disc thickness, l is the basic cell length, λ is the wavelength and r_1 is the radius of the iris poles.

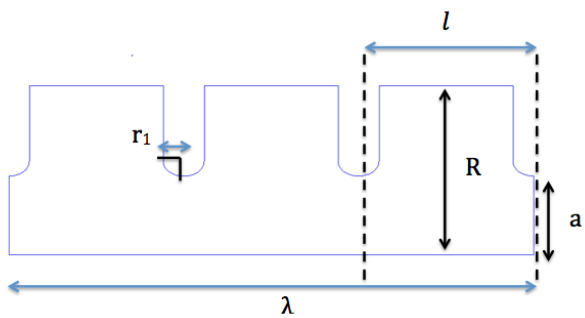


Figure 2: Schematic view of a generic X-band cavity.

In this example we show a configuration for a 2π/3 TW structure.

Copyright © 2013 CC-BY-3.0 and by the respective authors

ISBN 978-3-95450-138-0

PROGRESS TOWARD THE DEVELOPMENT OF A RAPIDLY TUNABLE RF CAVITY*

D.J. Newsham, X. Chang, and J.R. Thompson, FAR-TECH, Inc., San Diego, CA 92121, USA

Abstract

A major bottleneck in the development of compact, rapid-cycling particle accelerators is the ability to maintain phase coherence between the short orbit time of the particle bunch and the phase of the accelerating RF field. A ferroelectric loaded RF cavity can achieve the needed phase shift in a significantly shorter time than alternative technologies. The current status of the development of such a cavity including the cold test of a preliminary cartridge and the testing of the bias voltage subsystem will be presented.

INTRODUCTION

FAR-TECH, Inc. is developing a rapidly tunable RF cavity [1][2] that is specifically designed to provide the speed of frequency tuning required for use in modern rapid-cycling accelerator systems (rapid-cycling synchrotron or FFAG). Adjustment of the accelerating frequency between each cavity crossing of the particle bunch will maintain a synchronous phase between the bunch arrival time and the accelerating field on each pass.

The tuning is achieved by applying a bias voltage across a BST(M) [3] ferroelectric based load element placed within the cavity. The speed of frequency tuning is a combination of the fast response time of the BST(M) ($\lesssim 10$ ns) and the response time of the bias system (~ 55 ns). Several cooled tuning elements with bias voltages ramped to 40 kV placed near the periphery of pill-box structure can provide a few percent frequency shift on the microsecond time scale.

CARTRIDGE TESTING

The heart of the tunable cavity is the ferroelectric biasing cartridge. This cartridge contains the ferroelectric sample and biasing copper electrodes. This cartridge can be inserted and removed without breaking the vacuum of the main cavity. This separation from the vacuum will also allow a coolant flow of a dielectric fluid to cool the cartridge. Further, using a ferroelectric tube, rather than a solid cylinder will allow both the inner and outer surface to be cooled. To test the performance of the cavity a simplified cartridge and cavity structure was designed, simulated, constructed, and tested. Although an actual cavity would have multiple cartridges place off axis, the test cavity purposefully placed the cartridge on axis to increase the RF field and reduce the power requirement and increase the tuning range for the test. The structure was designed in SolidWorks and simulated with HFSS with several values of the dielectric constant and loss tangent.

Cavity parts and cartridges were constructed as shown in Fig. 1. The cartridge pieces were soldered in two stages using the appropriate alloy for each contact. Soldering was performed in a solder reflow oven with PID temperature control. Frequency and cavity Q-factor were measured at several bias voltages using an Agilent 8720ES network analyzer and a high voltage supply. Because the ferroelectric cylinders are 1 cm long, the conversion from bias voltage to bias electric field is trivial. Full air breakdown occurred at approximately 18 kV bias.

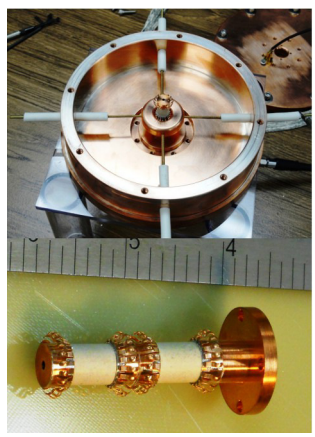


Figure 1: RF cavity used to characterize the biasing cartridge. Test cavity without top plate (*top)*. Biasing cartridge (*bottom*).

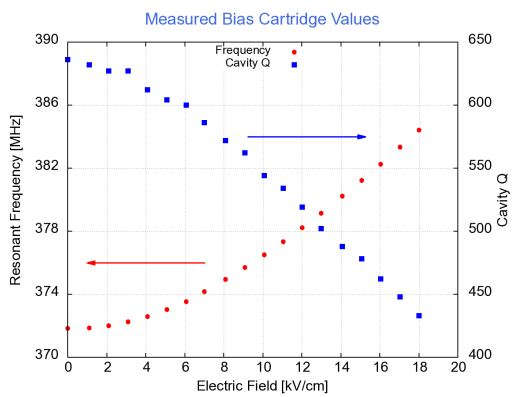


Figure 2: Measured resonant frequency and Q factor for the biasing cartridge in the test cell.

The measured frequency and Q-factor at different voltages are shown in Fig. 2. The HFSS simulation data relating dielectric constant and loss tangent to resonant frequency and Q-factor was inverted to convert the measure values to the values of interest. The result of this inversion are shown in Fig. 3 (dielectric constant) and Fig. 4 (loss tangent). Also included in these figures is

*Work supported by DOE Office of High Energy Physics, DOE-SBIR #DE-SC0006225

#newsham@far-tech.com

Copyright © 2013 CC-BY-3.0 and by the respective authors

INVESTIGATION OF BREAKDOWN INDUCED SURFACE DAMAGE ON 805 MHZ PILLBOX CAVITY INTERIOR SURFACES

M. R. Jana, M. Chung, M. Leonova, A. Moretti, A. Tollestrup and K. Yonehara,
Fermi National Accelerator Laboratory, Batavia, IL - 60510, USA
B. Freemire, and Y. Torun, IIT, Chicago, IL - 60616, USA
D. Bowring, LBNL, Berkeley, California - 94720, USA
G. Flanagan, Muons, Inc., Batavia, IL - 60134

Abstract

The MuCool Test Area (MTA) at Fermilab is a facility to develop the technology required for ionization cooling for a future Muon Collider and/or Neutrino Factory. As part of this research program, we have tested two 805 MHz vacuum RF cavities in a multi-Tesla magnetic field to study the effects of the static magnetic field on the cavity operation. This study gives useful information on field emitters in the cavity, dark current, surface conditioning, breakdown mechanisms and material properties of the cavity. All these factors determine the maximum accelerating gradient in the cavity. This paper discusses the image processing technique for quantitative estimation of spark damage spot distribution on cavity interior surfaces. The distribution is compared with the electric field distribution predicted by a computer code calculation. The local spark density is proportional to probability of surface breakdown and shows a power law dependence on the maximum electric field (E). This E dependence is consistent with the dark current calculated from the Fowler-Nordheim equation.

INTRODUCTION

High intensity, low emittance muon beams are essential requirements for a future Muon Collider and/or Neutrino Factory. Low emittance muon beams can be produced by ionization cooling. This consists of passing muon beams through low-Z absorber material (liquid H), to reduce all components of the momentum and replacing only longitudinal momentum with accelerating fields using RF cavities. At the same time, to keep the muon beam focused, both the absorbing material and RF cavities are placed inside a strong magnetic field provided by a superconducting solenoid. The ionization cooling process is most efficient if both the accelerating fields and magnetic fields are high. To study the interactions of a static magnetic field with operation at high accelerating fields, two 805 MHz RF cavities e.g. (i) LBNL-Pillbox (ii) All-Season have been tested in a multi-Tesla magnetic field at the Fermilab MuCool Test Area (MTA). During operation with high magnetic field B = 2 - 5 T, the cavity's accelerating field degrades significantly, dark current and X-rays are produced and interior surfaces suffer severe breakdown damage [1-3]. In this paper, we present the spatial distribution of the breakdown damage spots on the interior surface of the RF cavity using ImageJ [4] and Mathematica software [5]. The measured number of breakdown spots per unit area is compared with both the electric field distribution (calculated by computer code) and the dark current calculated from the Fowler-Nordheim equation. Finally a power law dependence on the maximum electric field is discussed.

805 MHZ CAVITIES

LBNL-Pill Box Cavity

A cross sectional view of the 805 MHz cylindrical pillbox cavity of inner diameter 312.4 mm is shown in Fig. 1. Two irises are covered by specially designed copper windows (separately shown). Each window has a radius of 97.9 mm. RF power at 805 MHz is fed in through a kidney shaped coupling slot on the cavity wall using WR975 rectangular waveguide [3] with 20 μs pulse duration and repetition rate of 15 Hz. The cavity is mounted inside a 44 cm bore diameter superconducting solenoid magnet which can generate magnetic fields up to 5 T. The peak electric field was 40 MV/m with RF power 4.2 MW at B=0 field and 16 MV/m with RF power 0.67 MW at B = 3 T.

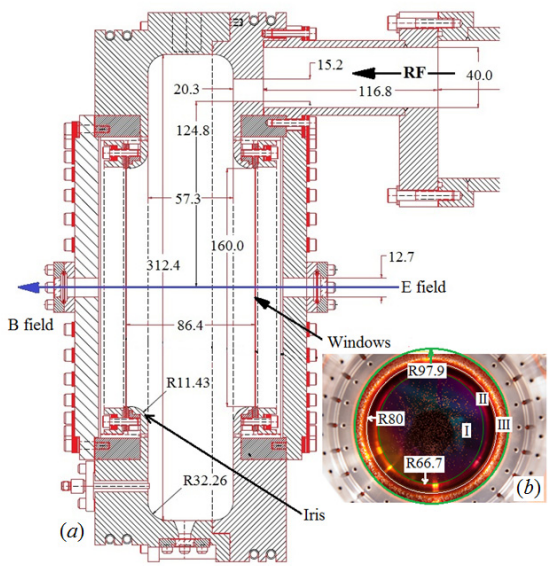


Figure 1: (*a*) Cross sectional view 805 MHz Pillbox RF cavity with copper window [3], (*b*) Copper window of radius 80 mm and iris of outer radius 97.95 mm.

Breakdown damaged spots on vacuum window is shown in Fig. 1(b) and the location of damaged spots are marked by crosshairs using ImageJ software shown in Fig. 2.

Copyright © 2013 CC-BY-3.0 and by the respective authors

ISBN 978-3-95450-138-0

DESIGN AND HIGH POWER TESTING OF 52.809 MHZ RF CAVITIES FOR SLIP STACKING IN THE FERMILAB RECYCLER*

R. Madrak#, D. Wildman, FNAL, Batavia, IL 60510, USA

Abstract

For NOvA and future experiments requiring high intensity proton beams, Fermilab is in the process of upgrading the existing accelerator complex for increased proton production. One such improvement is to reduce the Main Injector cycle time, by performing slip stacking, previously done in the Main Injector, in the now repurposed Recycler Ring. Recycler slip stacking requires two new RF cavities operating at slightly different frequencies (df = 1260Hz). These are copper, coaxial, quarter wave cavities with R/Q =13 ohms. They operate at a peak gap voltage of 150 kV with 150 kW peak drive power (60% duty factor), and are resonant at 52.809 MHz with a 10 kHz tuning range. Two have been completed and installed. The design, high power test results, and status of the cavities are presented.

INTRODUCTION

To increase beam power, the Recycler Ring has been converted from an antiproton storage ring to a proton preinjector for proton injection/slip stacking. The increase in power, which is projected to be 80%, is due to a shorter Main Injector cycle time (decreased from 2s to 1.33s), since injection/stacking and acceleration can now be performed in parallel. [1]

Slip stacking is a process in which 6 batches of 8 GeV protons from the Fermilab Booster are 'stacked' on top of an additional 6 batches of beam. It has been performed and studied previously in the Main Injector [2], using an RF system which was designed primarily for the acceleration of beam. The process is as follows: Six Booster batches are injected into the Recycler Ring and captured by one RF system at 52.809 MHz, and then decelerated slightly by changing the frequency of the RF system by 1260 Hz. Then, six more batches are injected and captured by a second RF system operating at 52.809 MHz. Since the two sets of batches have slightly different energies, one set 'slips' azimuthally with respect to the other. When the two sets of batches are aligned, they are injected into the Main Injector, captured, and then accelerated to 120 GeV.

CAVITY DESIGN PARAMETERS

Slip stacking requires two cavities with f_0 = 52.809 MHz, a maximum V_{peak}= 150 kV and approximately 10 kHz of tuning range. The cavities must be tuneable by 1260 Hz for slip stacking itself, and must also have compensation for frequency drift due to heating and variation of cooling water temperature (~ 0.5 kHz/°F). The maximum duty factor will be 60% with a pulse length of 0.8 s.

In the interest of minimizing beam loading, the cavity dimensions were chosen to minimize R/Q while taking into account other practical constraints, such as being able to fit in the allowed area in the tunnel.

The cavity geometry is shown in Figure 1. This is a quarter wave coaxial resonator. The R/Q of 13 Ω is substantially smaller than that in the Main Injector cavities (103 Ω). This is due mainly to the large ratio of diameters of the outer and center conductors. Other key parameters are shown in Table 1.

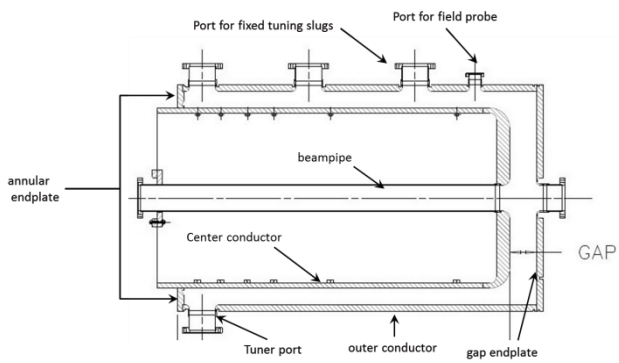


Figure 1: Cavity geometry and features.

Table 1: Cavity Design Parameters

f_0	52.809 MHz
Z_0	10.2 Ω
Vpeak (max)	150 kV
Maximum power	150 kW
Rshunt	75 kΩ
Q	5800
R/Q	13 Ω
Outer conductor ID	32 in
Inner conductor OD	27 in
nominal gap width*	2.9 in
Inner conductor length**	49.75 in
Step up ratio	6

*Based on pre-weld dimensions. Varied between cavities.
**Nominal length from cavity short to gap end

The initial design parameters and calculations were checked by constructing a model cavity from copper sheet metal [3]. Obviously this did not allow for vacuum or any high power tests, however, it was very useful for verifying and/or measuring key quantities at low power. These include factors such as resonant frequency

*Operated by Fermi Research Alliance, LLC under Contract No. DE-AC02-07CH11359 with the United States Department of Energy.
#madrak@fnal.gov

Copyright © 2013 CC-BY-3.0 and by the respective authors

PERPENDICULARLY BIASED YIG TUNERS FOR THE FERMILAB RECYCLER 52.809 MHZ RF CAVITIES*

R. Madrak#, V. Kashikhin, A. Makarov, D. Wildman, FNAL, Batavia, IL 60510, USA

Abstract

For NOvA and future experiments requiring high intensity proton beams, Fermilab is in the process of upgrading the existing accelerator complex for increased proton production. One such improvement is to reduce the Main Injector cycle time, by performing slip stacking, previously done in the Main Injector, in the now repurposed Recycler Ring. Recycler slip stacking requires new tuneable RF cavities, discussed separately in these proceedings. These are quarter wave cavities resonant at 52.809 MHz with a 10 kHz tuning range. The 10 kHz range is achieved by use of a tuner which has an electrical length of approximately one half wavelength at 52.809 MHz. The tuner is constructed from 3⅛″ diameter rigid coaxial line, with 5 inches of its length containing perpendicularly biased, Al doped Yttrium Iron Garnet (YIG). The tuner design, measurements, and high power test results are presented.

INTRODUCTION

Two new quarter wave copper cavities have been constructed and installed in the Fermilab Recycler Ring for the purpose of slip stacking protons to increase beam power. These have been described in detail in [1]. They are to operate at 52.809 MHz with a tuning range of 10 kHz. Tuning by 1260 Hz is required for slip stacking itself, and additional tuning is needed to compensate for temperature changes. The cavity maximum peak gap voltage is 150 kV with a shunt impedance of 75 kΩ and Q ~ 6000. The cavities will be pulsed for a maximum of 0.8 s every 1.33 s (the Main Injector cycle time).

The cavities are tuned using perpendicularly biased garnet in a coaxial line. This has been done previously and is described in [2] and [3]. The original concept, though not for cavity tuning in particular, is described in [4].

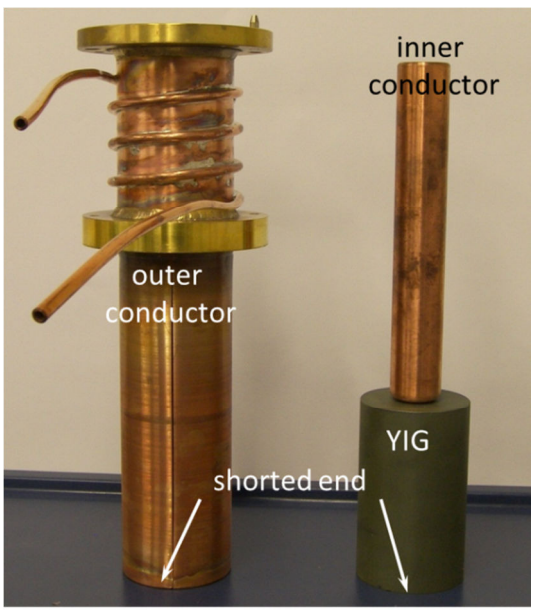


Figure 1: Tuner adjustable section with the inner conductor removed from the outer conductor.

DESIGN

In one of the ports located 3″ (on center) from the cavity shorted end, a fast tuner is loop-coupled to the cavity. The coupling is through a 2.5″ diameter coaxial ceramic window. The tuner loop area of 2.5 in^2 was adjusted to give a nominal coupling impedance of 50 Ω. The tuner is slightly less than a half-wavelength long and is made up of standard EIA 3⅛″ diameter, 50 Ω rigid copper transmission line, in addition to an "adjustable section" which is partially loaded with a 5″ long piece of Al doped Yttrium Iron Garnet (YIG). This section is immersed in a variable solenoidal magnetic field which provides a perpendicular bias for cavity tuning. A photo of the adjustable section, with the center conductor assembly removed from the outer conductor, is shown in Figure 1. The tuner line is shorted at the end opposite the cavity.

The garnet (TCI Ceramics type AL-400) has a saturation magnetization ($4\pi M_s$) of 400 gauss. Its OD and ID are 3.0″ and 0.65″ respectively. The center conductor used in the 15.75″ long adjustable section, which does not have the dimensions of standard 3⅛″ coax line, is shrink fit into the garnet. Over the 9″ length closest to the short, the outer conductor thickness has been reduced from the standard 3⅛″ coax line wall thickness to 0.020″. Both this 9″ section and the bottom copper shorting plate have a 0.0197″ wide slot machined through the copper to reduce eddy current effects.

For heat removal, the outer conductor is water cooled and the adjustable section is filled with a dielectric fluid (Diala AX).

The adjustable section had previously been designed for use as a fast phase shifter in vector modulators operating at 325 MHz [5].

The entire tuner, attached to the cavity and installed in the Recycler, is shown in Figure 2.

*Operated by Fermi Research Alliance, LLC under Contract No. DE-AC02-07CH11359 with the United States Department of Energy.
#madrak@fnal.gov

Copyright © 2013 CC-BY-3.0 and by the respective authors

ISBN 978-3-95450-138-0

ASSEMBLY AND TESTING OF THE FIRST 201-MHz MICE CAVITY AT FERMILAB*

Y. Torun †, P. Hanlet, Illinois Institute of Technology, Chicago, IL 60616, USA
M. Leonova, A. Moretti, R. J. Pasquinelli, D. W. Peterson,
R. P. Schultz, J. T. Volk, Fermilab, Batavia, IL 60510, USA
L. Somaschini, INFN, Pisa, Italy
J. Gaynier, Kettering University, Flint, MI, 48504, USA
D. Bowring, A. J. DeMello, D. Li, S. P. Virostek, LBNL, Berkeley, CA 94720, USA
T. Luo, University of Mississippi, University, MS 38677, USA

Abstract

The International Muon Ionization Cooling Experiment (MICE) [1] includes two linear accelerator sections with four RF cavities each within a shared vacuum vessel. Ten cavity bodies have been fabricated for MICE including two spares and one was electropolished at LBNL. A special vacuum vessel was built to house this cavity and form the 201-MHz Single-Cavity Module (SCM). The module and its instrumentation are being assembled and tested at Fermilab for installation and operation in the MuCool Test Area.

MICE RF SYSTEM

MICE is a demonstration of ionization cooling using a full cooling cell surrounded by tracking and particle identification detectors to measure each muon before and after it traverses the cooling cell [2]. It is under construction at Rutherford Appleton Laboratory (RAL). Figure 1 shows the RFCC (RF cavity and coupling coil) module [3, 4] which includes a large-diameter coil around a linac section. Each pair of cavities will be driven by a 2-MW amplifier system for a gradient of 8 MV/m per cavity. Parts of the power distribution network and LLRF system are being procured, developed, built and tested by teams from LBNL, University of Mississippi, Illinois Institute of Technology and Fermilab in the US and Strathclyde University, Daresbury Laboratory, Imperial College and RAL in the UK.

SINGLE CAVITY MODULE

In order to develop the assembly procedure for the RFCC modules and test cavity operation early on at the Fermilab MuCool Test Area (MTA), a special vacuum vessel was designed at LBNL to house a single MICE cavity. The single-cavity vacuum vessel has mostly the same mechanical interfaces as the RFCC module. Figure 2 shows the single-cavity module assembly. Ten RF cavity bodies have been manufactured in industry using techniques developed at LBNL. Cavity half shells were spun from 6mm-thick Cu sheet e-beam welded at the equator. Four ports were pulled around the equator on each cavity for couplers, vacuum pumping and instrumentation. Copper cooling tubes were brazed onto the cavity bodies. Each cavity has a pair of 0.35mm-thick curved beryllium windows for a pillbox-like geometry. Power is brought in through a pair of coaxial loop couplers. The first set of couplers is under fabrication at LBNL. The tuning system comprises stainless steel flexure arms driven by pneumatic actuators [5]. Figure 3 shows the basic design. The actuator body includes two concentric shafts screwed onto threaded holes in the tuner arm. As the shafts are pulled together or pushed apart by pneumatic action, the forces are transmitted to the cavity stiffener rings to elastically deform the cavity body. The actuator cover is attached to a vacuum vessel port with vacuum bellows while the body is thermally isolated from the

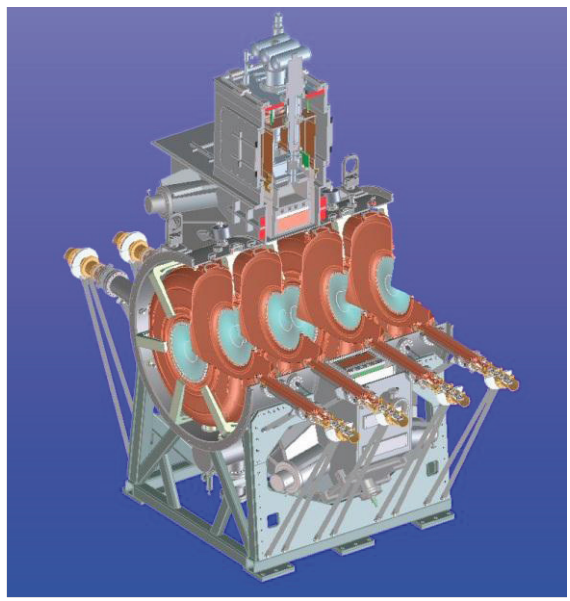


Figure 1: Partial cross section of a MICE RFCC module showing RF cavities, couplers and Be windows.

* This work was supported by the Office of Science, U.S. Department of Energy, through the Muon Accelerator Program.
† torun@iit.edu

Copyright © 2013 CC-BY-3.0 and by the respective authors

PROGRESS ON THE FABRICATION OF A CW RADIO-FREQUENCY QUADRUPOLE (RFQ) FOR THE PROJECT X INJECTOR EXPERIMENT (PXIE)*

M. D. Hoff, A. J. DeMello, A. R. Lambert, D. Li, J. W. Staples, and S. P. Virostek
Lawrence Berkeley National Laboratory, Berkeley CA 94720, USA

Abstract

The Project X Injector Experiment (PXIE), a prototype front end of the Project X accelerator [1] proposed by Fermilab, is currently under construction. The complete PXIE beamline [2] is made up of an H^- ion source, a low-energy beam transport (LEBT), a 2.1 MeV, 162.5 MHz radio-frequency quadrupole (RFQ) accelerator, a medium-energy beam transport (MEBT) and a 30 MeV section of superconducting cryomodules. The 4.45 m long CW RFQ consists of four separate modules that are joined by means of specially designed bolted joints. Each module consists of four solid copper vanes that are brazed together to form a 4-quadrant accelerating cavity. The ~100 kW of total wall power heat is removed by means of gun drilled water cooling passages. Mode stabilization is provided by a series of brazed, water cooled pi-mode rods. Tuning is achieved using a total of 80 fixed slug tuners. Fabrication of the PXIE RFQ is now under way at LBNL. Details of the RFQ mechanical design and an update of the fabrication progress are presented in this paper.

MODULES

The 4.45 m long RFQ is assembled from four approximately equal length modules. The modules are sized based on the available copper C101 billet size, available milling machine capacity, general handling considerations and the desire to minimize joints. Each module is fabricated from four tee shaped pieces of copper that weigh approximately 940 kg each before machining (see Fig. 1).

MACHINING

The outer wall features are machined first. The outer wall is machined flat, followed by the pi-mode rod holes, slug tuner ports, sensing loop ports and the vacuum pump port are cut. Then the vane is flipped over and mounted to a 3 inch stainless steel plate for cavity machining. The stainless plate allows easy handling and mounting of the part in the milling machines. The precise cavity contours, pi-mode rod clearance holes and then the four mating braze surfaces are cut with a standard shaped end mill (see Fig. 2 and Fig. 3). The last step is the machining of the vane tip modulations, as described later in this paper.



Figure 1: Raw tee shaped copper for vane fabrication.

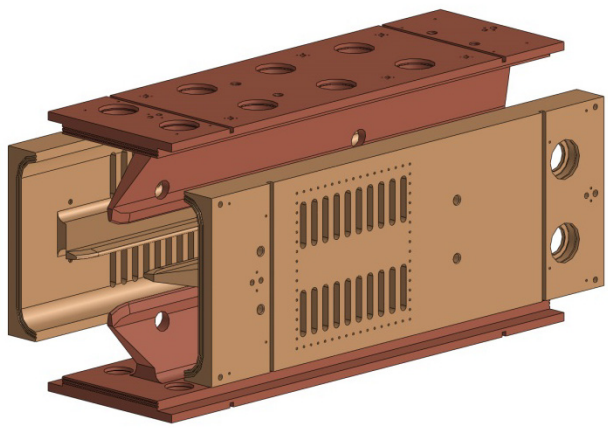


Figure 2: Exploded CAD model of four machined vane.

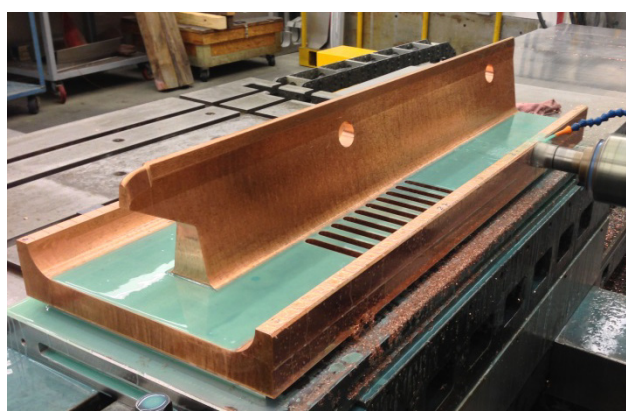


Figure 3: Module 1, horizontal vane being machined.

* This work is supported by the Office of Science, United States Department of Energy under DOE contract DE-AC02-05CH11231.

ISBN 978-3-95450-138-0

Copyright © 2013 CC-BY-3.0 and by the respective authors

RF, THERMAL, AND STRUCTURAL FINITE ELEMENT ANALYSIS OF THE PROJECT X INJECTOR EXPERIMENT (PXIE)* CW RADIO-FREQUENCY QUADRUPOLE (RFQ)

A.R. Lambert#, M.D. Hoff, D. Li, J.W. Staples, and S.P. Virostek
Lawrence Berkeley National Laboratory, Berkeley, CA 94804

ABSTRACT

PXIE (Project X Injector Experiment) is a prototype front end system for the proposed Project X accelerator complex at Fermilab [1]. An integral component of the front end is a 162.5 MHz normal conducting CW (continuous wave) radio-frequency quadrupole (RFQ) accelerator that has been designed and is being fabricated by LBNL. The RFQ will accelerate H^- ions from 30 keV to 2.1 MeV [2]. The four-vane RFQ consists of four modules with a total length of 4.45 meters. Through application of finite element analysis (FEA), the electromagnetic fields and their resultant effect on the RFQ body temperature and the subsequent deformations due to thermal expansion have been simulated. The analysis methodology developed at LBNL allows for quick evaluation of RFQ temperature, stress, deformation and the resulting effect on frequency without requiring the construction of a prototype. The technique has been applied to the following: RFQ body, RFQ cutbacks, fixed slug tuners, and pi-mode rods. The analysis indicates that the total heat load on the RFQ will be approximately 80 kW, which is removed via water-cooled passages.

INTRODUCTION

The PXIE RFQ is a front end injector for the proposed Project X experiment at FNAL. As this RFQ will operate in continuous-wave (CW) mode, the engineering design and analysis is critical for managing the thermal performance. The aim of this paper is to introduce that analysis method used to determine the heat loads experienced by the RFQ, how these loads affect operating temperature, and how temperature increase affects frequency and the methods by which the cooling water can be used to mitigate the RF heating effects on frequency.

RFQ BODY SIMULATION

The body of the RFQ is simulated using a thin 3D slice of the RFQ cross section. Only one-quarter of the geometry is simulated due to symmetry. The first step of this step in the simulation is to create a vacuum geometry that corresponds to the solid RFQ body. Once created, ANSYS Multiphysics [4] performs RF analysis on the vacuum geometry. Once complete, the RF heat load is calculated and applied to the inner cavity walls of the RFQ body model. Convective water cooling is applied to the gun-drilled cooling channels, as shown in Fig. 1.

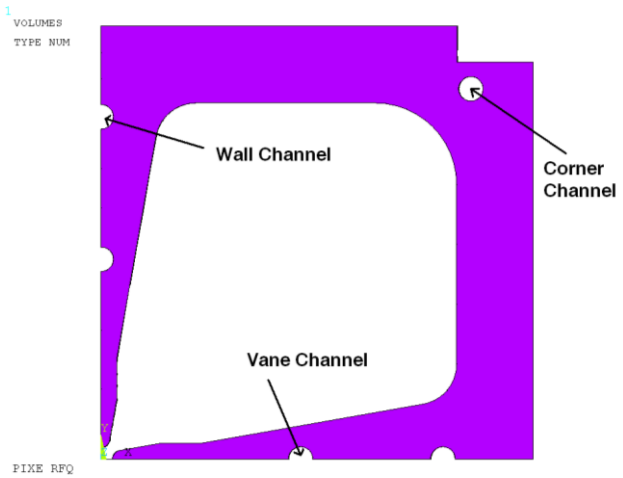


Figure 1: RFQ body cross section with gun-drilled cooling channels.

Assuming that the cooling water is at 30 °C, the resulting temperature profile at steady-state operation is shown in Fig. 2.

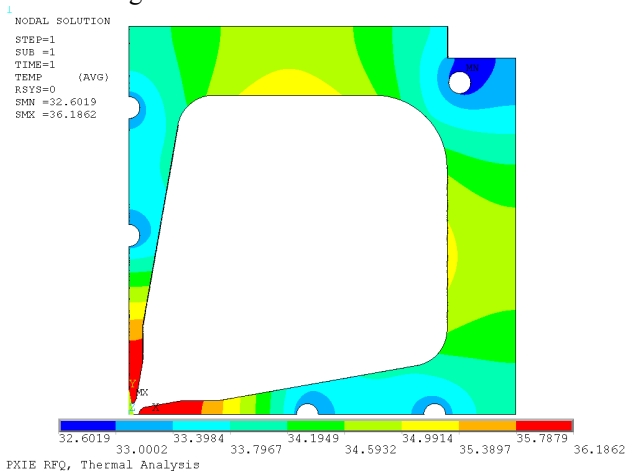


Figure 2: Temperature contours (°C) for steady-state RFQ operation.

The maximum temperature is 36.2 °C and is located at the vanetips. Minimum temperature is approximately 32.6 °C, and is found in the corner cooling passage. Overall, it is evident that with the current cooling scheme, the RFQ body temperature only rises 2.0 – 6.0 °C above nominal water temperature. This temperature rise causes expansion of the cavity walls away from the beam axis, and growth of the vanetips towards the beam axis. Both of these affect the resonant frequency of the cavity. The thermal results are piped into a structural analysis which determines the displacements due to thermal expansion, the results of which are shown in Fig. 3.

*Work supported by the Office of Science, U.S. Department of Energy under DOE contract number DE-AC02-05CH11231
#arlambert@lbl.gov

Copyright © 2013 CC-BY-3.0 and by the respective authors

FINAL DESIGN OF A CW RADIO-FREQUENCY QUADRUPOLE (RFQ) FOR THE PROJECT X INJECTOR EXPERIMENT (PXIE)*

S. P. Virostek#, A. J. DeMello, M. D. Hoff, A. R. Lambert, D. Li, and J. W. Staples
Lawrence Berkeley National Laboratory, Berkeley, CA, USA

Abstract

The Project X Injector Experiment (PXIE) now under construction at Fermilab is a prototype front end of the proposed Project X accelerator [1]. PXIE will consist of an H^- ion source, a low-energy beam transport (LEBT), a radio-frequency quadrupole (RFQ) accelerator, a medium-energy beam transport (MEBT) and a section of superconducting cryomodules [2]. The PXIE system will accelerate the beam from 30 keV to 30 MeV. The four-vane, brazed, solid copper design is a 4.45 m long CW RF accelerator with a resonant frequency of 162.5 MHz. The RFQ will provide bunching and acceleration of a nominal 5 mA H^- beam to an energy of 2.1 MeV. The average power density on the RFQ cavity walls is <0.7 W/cm^2 such that the total wall power losses are ~80 kW. LBNL has completed the final design of the PXIE RFQ, and fabrication is now under way. The completed PXIE RFQ will be assembled at LBNL and tested with low-level RF prior to shipping to Fermilab. Several aspects of the final RFQ mechanical design along with associated fabrication techniques are presented in this paper.

INTRODUCTION

The PXIE RFQ will operate at a 162.5 MHz resonant frequency and will accelerate a 5 mA H^- beam to 2.1 MeV using a 60 kV vane-to-vane voltage. The 4.45 m long, four-vane CW structure will be comprised of four approximately 1.1 m long longitudinal modules. Only about 12% of the total RF input power goes to beam loading with the rest dissipated on the cavity walls to generate the necessary RF field. The modules will consist of four solid OFHC copper sections that are fully machined with the vane tips modulated prior to being brazed together. Due to the high power CW operation of the PXIE RFQ, a brazed copper structure design has been developed. Final frequency adjustment and local field perturbation correction is accomplished by means of 80 evenly spaced fixed slug tuners. Quadrupole mode stabilization is achieved through a set of 32 water-cooled pi-mode rods. The overall approach for the PXIE RFQ was to combine specific proven fabrication and assembly techniques with other high reliability, low cost features in order to develop a design that poses low risk and is easily manufactured using readily available machinery.

Images from a 3-D CAD model of the completed RFQ design are used in this paper to present detailed descriptions of various design characteristics. A realistic CAD rendering of the full four-module RFQ is shown in Fig. 1 (rendering by Don Mitchell of Fermilab).

*This work was supported by the Office of Science, U. S. Department of Energy, under Contract No. DE-AC02-05CH11231.
spvirostek@lbl.gov



Figure 1: CAD model of the assembled RFQ.

RFQ DESIGN DETAILS

Cavity Body

Each module consists of four vanes that are to be machined from a single piece of OFHC copper and will incorporate simple cooling channels produced using a readily available gun drilling technique. Modulations will be machined on the RFQ vane tips with a custom designed fly cutter used in a computer controlled horizontal mill. In order to provide high precision during both machining and assembly, the mating surfaces where the vanes join together also serve as fiducial surfaces. Two different vane geometries will be used in each module (horizontal and vertical) with the opposing vanes being identical. Features located on the outer surface of the vanes such as tuner ports, RF coupling ports, cooling taps, vacuum pumping ports, pi-mode rod penetrations, sensing loop ports and tapped holes for the stainless steel module joining plates will be machined prior to finish machining of the inner cavity surfaces and vane tips. All of the vacuum and RF sealing surfaces for the cavity penetrations are recessed into the outer surface of the RFQ copper body to prevent damage during handling.

The modules will be formed by brazing together the finished vanes along the axially running joints. In order to maintain the tight vane tip-to-vane tip tolerances and ensure that the required field flatness and cavity resonant frequency can be achieved using the slug tuners, a zero-thickness brazing process will be used. Wire braze alloy will be loaded into grooves that are recessed into the joint surfaces. A series of specially designed clamps will hold the vane joints tightly together during the hydrogen oven braze. The alloy spreads throughout the close fitting joint during the braze cycle by means of capillary action. This

Copyright © 2013 CC-BY-3.0 and by the respective authors

ISBN 978-3-95450-138-0

INVESTIGATION ON DOUBLE DIPOLE FOUR-VANE RFQ STRUCTURE

Ki R. Shin[1], Yoon W. Kang, Aly E. Fathy[1], and Mark S. Champion
ORNL, Oak Ridge, TN 37831, [1]University of Tennessee, Knoxville, TN 37996, U. S. A.

Abstract

Four-vane RFQ is a general choice for the low energy injector of light ion accelerators. In this commonly used four-vane RFQ structure, each vane has undercuts at both ends to create open magnetic field paths that realize uniform electromagnetic fields along longitudinal direction. Meanwhile, there exists another undercut method called as double dipole (DD) that requires undercuts only on 2 vanes [1] that are interleaved with vanes with no undercut. The RFQ with DD cutback can provide a design option besides the traditional 4 vane cutback (4C) method. In this paper, we investigate and discuss some important DD RFQ features in detail: 1) Finite on-axis field at DD RFQ end section, 2) Dipole mode properties, and 3) Mode spectrum with respect to structure length. 3D simulation is utilized for this DD RFQ analysis.

INTRODUCTION

The radio frequency quadrupole (RFQ) has been widely used for focusing, bunching, and acceleration of ion particles [2]. The four-vane RFQ [3] with four vane cut-backs (4C) [2][4] is common design choice for light ion accelerator systems.

The four-vane RFQ is derived from the quadrupole ridge waveguide [3], and requires cut-backs on each vane ends. The cut-back is necessary to avoid perfect electric boundary condition on vane ends, which is essential to provide the required electric field uniformity in whole structure.

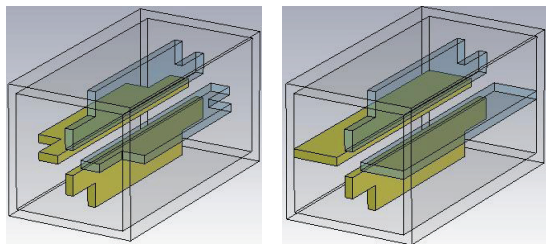
Researchers found that two other cut-back methods are possible to maintain the uniform quadrupole mode: double dipole (DD) and folded dipole (FD) [1][5]. These schemes were used in a $< 2.0\ \lambda$ length structure demonstration RFQ model at Chalk River. One drawback of the DD and FD structures is the generation of finite on-axis field at RFQ ends in quadrupole mode. However, these problems may be relieved by adjusting ion source energy level and RFQ radial matching section design [8].

The DD structure is of special interest in this paper because of its unique characteristics on dipole mode that leads to different mode spectrum results. This may provide an alternative design option in some cases where 4C RFQ mode separation is very small.

Therefore in this paper, we investigate some important features of DD RFQ. First, we discuss the on-axis voltage generation in DD RFQ. Next, some interesting dipole mode properties in DD RFQ are covered with qualitative description and discussion. Finally, a DD RFQ mode spectrum result with the Spallation Neutron Source (SNS) RFQ geometry is presented as an example case. The 3D simulation tool CST Microwave Studio [6] is utilized in this study.

ON-AXIS FIELD AT DD RFQ ENDS

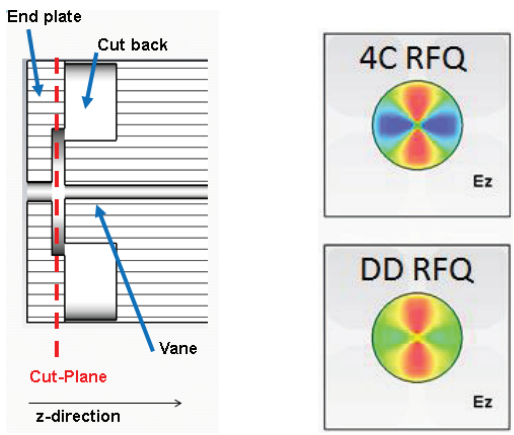
Fig. 1 shows a perspective view of 4C and DD RFQ cut-back geometries. In conventional 4C RFQ, all four vanes are not electrically touching the both end-plates. Meanwhile, only two opposing vanes make contacts to the end-plate in DD RFQ.



(a) (b)

Figure 1: RFQ cut-back - (a) 4C, (b) DD.

Because of this electrical contact of two vanes, DD RFQ generates a finite on-axis voltage. Fig. 2 describes how the on-axis voltage in z-direction is created. In 4C RFQ, the sum of Ez field on beam axis becomes zero. Each RFQ vane induces RF voltage of π phase difference from the adjacent vanes; hence cancellation of on-axis voltage occurs in 4C RFQ [7]. The short circuit condition of two vanes in DD RFQ, however, diminishes this cancellation and finite on-axis potential remains.



(a) (b)

Figure 2: RFQ end region - (a) geometry, (b) Ez field.

The existence of a finite on-axis voltage requires a different end-region design scheme as shown in Fig. 3. The conventional design for 4C RFQ in Fig. 3 (a) is not optimized to reduce the axial voltage. Previous work [1] suggested the design in Fig. 3 (b) which can decrease this axial voltage the most, however it may induce gas flow

Copyright © 2013 CC-BY-3.0 and by the respective authors

DESIGN AND MEASUREMENT OF DOUBLE GAP BUNCHER CAVITY PROPOSED FOR REDUCTION OF X-RAY RADIATION

Ki R. Shin[1], Yoon W. Kang, Aly E. Fathy[1], and Mark S. Champion
ORNL, Oak Ridge, TN 37831, [1]University of Tennessee, Knoxville, TN 37996, U. S. A.

Abstract

X-ray radiation from accelerating cavities can be serious problem not only in high energy section but also in certain low energy system including beam matching section with buncher cavity. In this paper we propose a double gap buncher cavity design for low energy part of H- ion accelerators which can reduce X-ray radiation. The cavity utilizes Transverse Magnetic (TM) mode at about 400MHz as the operating mode. A drift tube supported by a stem in the cavity can form two gaps that can divide the required gap voltage to a half per each gap. Lower peak field can be realized since this double gap cavity can avoid sharp geometry. 3D simulation is utilized to address the analysis of non-axisymmetric structure. An Aluminum scaled model is built and tested with low power measurement. The measured results are in good agreement with simulations.

INTRODUCTION

For safety, radiation shielding is an important part of a high energy accelerator design [1]. Concrete material surrounds accelerator system in a tunnel to shield any hazardous radiations. Often bunching cavities in low energy section of ion accelerator < 3MeV are placed outside the tunnel only with fundamental radiation shield. X-radiation with non-negligible level can occur, however, if cavities are not under good vacuum condition [2]. Therefore, more conservative design to prevent X-radiation can help to improve system operability.

Assuming a constant vacuum level, X-radiation intensity is related to the cavity gap voltage and discharge current [3][4]. Ref. [3][4] expects that the radiation intensity has quadratic to cubic relation with gap voltage. The radiation wavelength is inversely related to the gap voltage as well [4]. Consequently, lower gap voltage may decrease a radiation dose and hard X-ray generation.

The mechanism of discharge current is rather complex, but in general it is relevant to the field emission and explosive emission mechanism [5]. The electric field in cavity determines the discharge current, and lower electric field is expected. In other words, lower electric peak field with smooth gap geometry may help to minimize discharge current and radiation intensity.

With regarding these voltage and peak field requirements, a double gap buncher cavity design is proposed and its lab type measurement is presented in this paper. This design is aimed to fit the requirement of the cavity 4 with 30mm bore diameter in medium energy beam transport (MEBT) section in the Spallation Neutron Source (SNS) [6]. The cavity length and particle speed are about 13cm and 0.073 v/c, respectively.

X-RADIATION BY VACUUM DISCHARGE

At cavity gap, the X-ray radiation dose D_X is determined by the integration of the radiation intensity J_X over the particle commutation time t_c (1) [3][5].

$$D_X \cong \int_0^{t_c} J_X(t)dt \qquad (1)$$

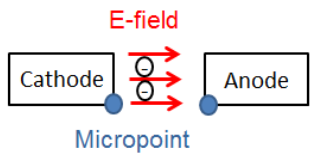
$$J_X \propto i(t)\cdot V^n(t) \qquad (2)$$

The radiation intensity J_X is related to the discharge current i(t) at cavity gap and the gap voltage V(t) likewise (2) [3][5]. The variable n commonly has values in range of 1.8~3.0 [3-5]. As a result, V(t) becomes an important parameter to determine J_X. The maximum X-radiation frequency also rises as the gap potential energy increases. This may induce a generation of hard X-ray. Therefore, low cavity gap voltage is desired to decrease X-radiation.

In accelerating cavities with high electric field intensity, the discharge current is generally formed by Fowler-Nordheim field emission mechanism [5]. Fig. 1 describes the field emission process at cavity gap (between cathode and anode), and the current density definition.

In field emission mechanism, some cathode electrons are stripped by strong electric field and collide to the anode. The emission current is a function of electric field; hence smaller electric field is desirable to decrease X-radiation by discharge current.

Most RF cavities are designed to have enough design margins until to reach the field breakdown limit, however, some micropoints on cathode and anode surface (Fig. 1) may lower the barrier of discharging. These micropoints can generate plasma around cathode, and as a result the discharging process starts earlier than as expected. This mechanism is called as explosive electron emission [5]. The anode part can also suffer from extra heating, evaporation, and ionization.



$$j = A\cdot E^2\cdot e^{-\frac{B}{E}}$$

A and B are constants

Figure 1: Field emission at cavity gap and Fowler-Nordheim current density.

The sharp gap shape in low energy ion accelerator section can be more vulnerable to explosive electron

Copyright © 2013 CC-BY-3.0 and by the respective authors

ISBN 978-3-95450-138-0

HARMONIC RATCHETING FOR FAST ACCELERATION*

N. Cook†, Stony Brook University, Stony Brook, NY 11790 USA
M. Brennan, S. Peggs, BNL, Upton, NY 11973, USA

Abstract

From medical synchrotrons to accelerator driven systems, there is a need for fast acceleration of protons and light ions. This can be a costly undertaking, requiring specially designed ferrite loaded cavities to be tuned across a wide range of frequencies. Ferromagnetic materials allow for the precise adjustment of cavity resonant frequency, but rapid tuning changes and operation outside material specific frequencies result in significant Q-loss. This leads to a considerable increase in power requirements. We introduce an acceleration scheme known as harmonic ratcheting which reduces the cavity frequency range when accelerating an ion beam in a synchrotron. This scheme addresses the needs of high repetition rate machines for applications in which low beam intensity is needed. We demonstrate with simulations the type of ramps achievable with ratcheting and consider its advantages.

INTRODUCTION

The potential for fast acceleration of low energy ion beams remains rich, with a host of applications proposed to take advantage of rapid cycling synchrotrons or FFAGs. Nonetheless, conventional acceleration of low β charged particles remains expensive and inefficient. The primary challenge of accelerating such particles lies in achieving robust and flexible tuning. Using speciality ferrites, tuning can be obtained at the cost of efficiency. Ferrite materials suffer dramatic loss effects when driven at high bias fields and high magnetic flux [1] [2]. These difficulties have stemmed the advancement of fast and efficient accelerators for low energy ion beams.

The integer harmonic number h relates the RF and revolution frequencies through the relationship $f_{RF} = h\, f_{ref}$. The relative RF frequency range can be significantly reduced below the revolution frequency range by decreasing h in steps as the ions accelerate and f_{rev} increases. This is the motivation and basic method of *harmonic ratcheting*.

HARMONIC RATCHETING

Suppose that two (or more) RF cavities take turns accelerating the beam – one turns on when the other turns off, at different RF frequencies – so that the RF frequency is always constrained to remain in the range

$$f_{min} \;\leq\; f_{RF} \;\leq\; f_{max} \tag{1}$$

where f_{min} and f_{max} are externally determined design parameters. It is possible to make the transition back or forth between harmonic numbers

$$\begin{aligned} h &= n \\ \text{and}\quad h &= n+\Delta \end{aligned} \tag{2}$$

where n and Δ are positive integers, if

$$\frac{f_{max}}{n+\Delta} \;>\; \frac{f_{min}}{n} \tag{3}$$

Equivalently, we have

$$\Delta \;<\; n\,r \tag{4}$$

where

$$r \;\equiv\; \frac{f_{max}}{f_{min}} - 1 \;>\; 0 \tag{5}$$

is the "ratcheting parameter". Equation 4 shows that Δ has a maximum permissible value, which must be greater than 1 if a harmonic transition is to be possible. A ratcheting transition is possible if the following conditions are met.

$$\begin{aligned} n &> 1 \quad &, r &> 1 \\ n &> \frac{1}{r} \quad &, r &< 1 \end{aligned} \tag{6}$$

Several harmonic ratchets can take place during one acceleration ramp. Figure 1 show an example with $r = 0.50$, where the revolution frequency increases from 0.61 MHz to 3.35 MHz, while the RF frequency is constrained to lie between 5.5 MHz and 8.25 MHz.

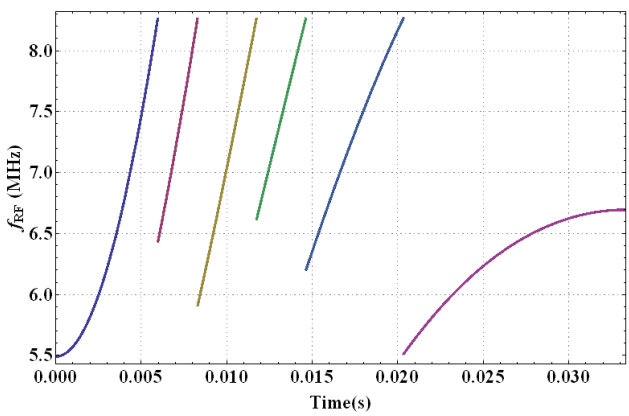


Figure 1: An example of harmonic ratcheting with $r = 0.50$. The plot shows one possible solution – with the harmonic number sequence $h = 9, 7, 5, 4, 3, 2$ – that maximizes RF frequency while minimizing ratcheting number.

* Work supported by Brookhaven Science Associates, LLC under Contract No. DE-AC02-98CH10886 with the U.S. Department of Energy.
† ncook@bnl.gov

Copyright © 2013 CC-BY-3.0 and by the respective authors

MULTIPACTING STUDY FOR THE RF TEST OF THE MICE 201 MHz RF CAVITY AT FERMILAB MTA*

T. Luo†, D. Summers, University of Mississippi, University, Mississippi, USA
A. DeMello, D. Li, H. Pan, S. Virostek, M. Zisman, LBNL, Berkeley, California, USA

Abstract

In this paper, we present a study of multipacting effects for the high power RF test, to be done at Fermilab's Mucool Test Area, of the 201 MHz RF cavity for the Muon Ionization Cooling Experiment. We show how the fringe field of the Lab_G magnet affects the cavity performance due to multipacting and predict the possible multipacting bands in the high power RF test with different magnetic field strengths.

INTRODUCTION

One cavity for the international Muon Ionization Cooling Experiment (MICE) [1], after being manufactured and electro-polished at LBNL, has been shipped to the Fermilab Mucool Test Area (MTA) for the single cavity test. To study the cavity performance in a strong magnetic field, this cavity will be tested in the fringe field of the 5-T Lab_G magnet before the MICE Coupling Coil is ready for operation.

In this paper, we study multipacting (MP) effects for the single cavity with and without the Lab_G magnet fringe field. We show possible MP bands with different magnetic field strengths expected in the high power RF test. The Lab_G magnetic field is calculated by ANSYS, the cavity RF field by S3p [2] and the MP effect by Track3p [3].

MAGNETIC FIELD OF THE LAB_G MAGNET

The magnetic field of the Lab_G magnet has been mapped both experimentally and numerically [4, 5]. However, none of the previous mappings cover the full region where the 201 MHz cavity will be placed. Thus we used ANSYS to recalculate the magnetic field. The field along the central axis is compared with previous mapping and shows good agreement, as shown in Fig. 1. Due to the uniqueness of the solution of Poisson equation, the ANSYS result should also give the correct field everywhere in space, including the fringe field region where the cavity will be placed, which is about 1.0 m away from the Lab_G magnet (center-to-center) if the Single Cavity Vessel is located as closely as possible to the Lab_G magnet.

* Work supported by NSF MRI Award 0959000, and by Office of Science, U.S. Department of Energy under DOE contract number DE-AC02-05CH11231, US Muon Accelerator Program.

† tluo@lbl.gov

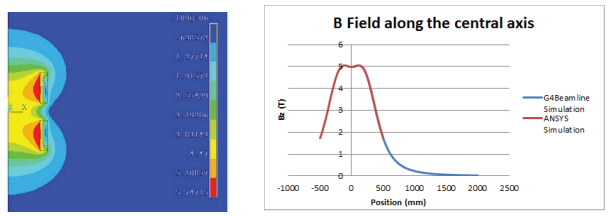


Figure 1: The ANSYS magnetic field calculation of the Lab_G magnet. The left figure is the contour plot of the field magnitude. The right figure is the comparison of magnetic fields from ANSYS with previous G4Beamline results [5] along the central axis.

RF FIELD IN THE 201 MHz CAVITY

The cavity model is built from its CAD drawing, including the curved beryllium windows, the coaxial waveguide and the loop coupler. To build an RF field with power propagating into the cavity and dissipating on the cavity walls, we use S3p with a "waveguide" boundary condition (BC) at the coaxial port and " impedance " BC on the cavity wall. The orientation of the coupler is adjusted to achieve critical coupling ($\beta \approx 1$), with coupling angle at about 17°. The E and B fields in the cavity are shown in Fig. 2.

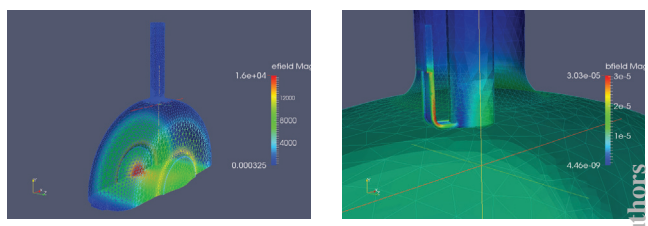


Figure 2: RF field of the cavity. The left figure shows the E field magnitude in the cavity. The right figure shows the maximum B field in the cavity on the coupler loop, where sufficient cooling should be supplied.

MULTIPACTING EFFECT ON 201 MHz CAVITY WITH LAB_G MAGNET

The MP effect is evaluated by the Enhancement Counter (EC) in the Track3P code. The electron is launched from its primary emission surface and tracked for 50 RF cycles, until its energy is too high or too low for MP, or until it hits the absorber surface. Every time it hits the second emission surface, the probability η to generate a secondary electron, which depends on impact energy and surface material, is

Copyright © 2013 CC-BY-3.0 and by the respective authors

ISBN 978-3-95450-138-0

MULTI-HARMONIC ACCELERATING CAVITIES FOR RF BREAKDOWN STUDIES*

Y. Jiang#, J. L. Hirshfield, Yale University, New Haven, CT 06511, USA

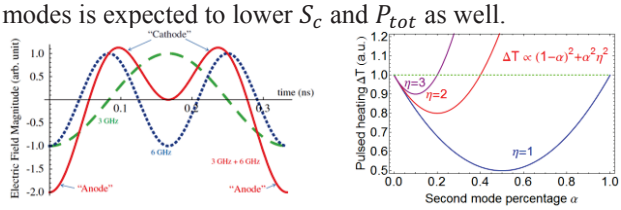
Abstract

Multi-harmonic accelerating cavities that are explicitly designed for RF breakdown experiments are described. The fundamental TM_{010} and its higher harmonic TM_{011} or TM_{012} modes of the cavities are to be excited coherently by an external RF source in the expectation of lowering surface pulsed heating and/or surface electric field, so as to reduce breakdown probability and possibly achieve an increase in acceleration gradient.

INTRODUCTION

In this paper, microwave cavities that support the superposition of the fundamental TM_{010} mode and at least one more mode whose eigen-frequency is a harmonic of the TM_{010} eigen-frequency are described. These bimodal cavities are explicitly intended to be vehicles that may deepen understanding of RF breakdown and pulsed heating, and as possible candidates for incorporation into multi-cavity high-gradient accelerator structures.

By selectively exciting synchronized multi-harmonic cavity modes driven externally in a precisely-controlled manner from a novel multi-frequency RF source available at Yale [1], unconventional spatiotemporal distributions of electromagnetic fields within a cavity can be realized, with the potential to lower field emission and/or pulsed heating at a given level of acceleration gradient; these effects are believed to be precursors to RF breakdown. In particular, two phenomena provide the main motivation for introduction of a 2nd mode at a harmonic frequency, namely: (a) the so-called anode-cathode effect [2]. In a longitudinally *asymmetric* cavity [2], phase-locked two-frequency operation, with the 2nd mode at a frequency double that of the fundamental, can allow the electric field pointing into one wall (cathode-like) to be significantly smaller than the field pointing out of that wall (anode-like), as shown in Fig. 1. A strong anode field will raise the work function barrier to suppress field and secondary emission; and (b) the suppression of pulsed heating, which is the focus of this paper. To model pulsed heating in a bimodal cavity, we characterize E-field superposition as $E_{total} = (1-\alpha)E_1 + \alpha E_2$, where $E_{1,2}$ is each electric field component with its associated acceleration gradient normalized to the same value, and α is the percentage of the 2nd mode such that E_{total} provides the same acceleration gradient. Similarly, the surface RF H-field is $H_{total} = (1-\alpha)H_1 + \alpha H_2$. Pulsed heating temperature rise ΔT can then be approximately scaled in terms of H_1 and H_2 as $\Delta T \propto (1-\alpha)^2 < H_1^2 > +\alpha^2\sqrt{f_2/f_1} < H_2^2 > =< H_1^2 > [(1-\alpha)^2 + \alpha^2\eta^2]$, where the frequency term $\sqrt{f_2/f_1}$ is related to the ratio of surface resistivities, $\eta = \sqrt{(f_2/f_1)^{1/2} < H_2^2 > / < H_1^2 >}$, and the cross term averages out over one period. Due to the quadratic dependence of ΔT upon α, it is possible to choose an optimal α such that $(1-\alpha)^2 + \alpha^2\eta^2 < 1$. In other words, to have lower temperature rise than for a single mode alone, while maintaining the same acceleration gradient; this is shown quantitatively in Fig. 1(b). The modified Poynting vector S_c [3], and total required RF power P_{tot}, also follow a quadratic dependence on the mode percentage α, so use of two modes is expected to lower S_c and P_{tot} as well.



(a) (b)

Figure 1: (a) Time dependence for a composite field (red line) excited at 3 GHz (green dashed) and 6 GHz (blue dotted), showing a factor-of-two anode-cathode field difference. (b) Dependence of the surface pulsed heating temperature rise ΔT on the 2nd mode percentage α. There is seen to be a range of α within which ΔT can be smaller than for a single mode (the green dashed horizontal line).

TM_{010} +TM_{011} CAVITY

For a simple pillbox designed as a bimodal cavity with a typical iris size of $0.1\lambda - 0.2\lambda$ to support the TM_{010} mode and a 2nd harmonic TM_{011} mode, our analysis shows that $\eta > 3$. This implies that ΔT could not decrease by more than 10% for a simple pillbox cavity. Consequently, a new software package is being developed by us to optimize cavity geometry to support multi-harmonic modes with desired RF properties, such as high shunt impedance and low surface fields, and maximize reduction in temperature rise ΔT. This code integrates *Finite Element Method* and *Generic Algorithm*, so that it can find global optimization of RF parameters. Currently the code package is to include beam-cavity interactions that allow multipactor, wake field, and beam dynamics studies to be carried out in our unconventional structures, so as to provide a single software suite to expedite cavity design and optimization of RF properties and beam dynamics.

Optimization of design for a bimodal cavity supporting the TM_{010} mode and its 2nd harmonic TM_{011} mode can be realized using this code, as shown in Fig. 2. It is a full π-mode accelerating cavity, longitudinally symmetric with iris and beam pipe. Its fundamental frequency is at X-

*Work supported by U.S. DOE
#yong.jiang@aya.yale.edu

Copyright © 2013 CC-BY-3.0 and by the respective authors

DESIGN STUDY OF KNOT-APPLE UNDULATOR FOR PES-BEAMLINE AT SSRF

Shigemi Sasaki#, Atsushi Miyamoto,
Hiroshima Synchrotron Radiation Center, Hiroshima University, Higashi-Hiroshima, Japan
Shan Qiao
Shanghai Institute of Microsystem and Information Technology, Chinese Academy of Sciences, People's Republic of China

Abstract

An intense on-axis radiation power from a linear undulator is a serious problem for a VUV/soft-X-ray beamline at medium or high energy light source facility. This problem may be solved by using a specially designed linear undulator such as the Figure-8, Pera, or Knot undulators. However, a permanent magnet undulator of such kind is not capable of changing polarization state. On the other hand, an APPLE undulator is able to generate variable polarization, but is not capable to reduce on-axis power density in linear modes. To solve these problems, we investigated various magnetic structures and found that the combination of Knot and APPLE undulator scheme works to generate low on-axis power density in every polarization mode.

INTRODUCTION

In order to generate the undulator radiation in VUV region at a medium energy storage ring facility, the undulator should have a very long period and a high K-value. In this case, especially for a linear undulator, unwanted high radiation power for higher harmonics concentrates on the radiation beam axis, and hence it give a heave heat load on optical components such as a mirror and a monochromator. To reduce the on-axis heat load, the Figure-8 undulator was proposed [1] and have been used in several synchrotron radiation facilities. Also, similar ides for the same purpose were proposed [2-4]. However, all those ideas except the Figure-8 were not realized may be due to the complicated structure and the advantages are not so significant compared with Figure-8. More importantly, all those exotic devices including the Figure-8 are not capable of varying polarization states. On the other hand, the APPLE-type undulators can generate various polarization states such as the right/left circular polarization, tilted linear polarization, and horizontal/vertical linear polarization. However, in the linear polarization modes, on-axis high power problem form higher harmonics is remaining as a serious problem.

In order to solve all problems described above, we propose a new scheme which is called a Knot-APPLE undulator to reduce on-axis radiation power in every polarization mode.

KNOT UNDULATOR

Figure 1 shows the magnetic structure of Knot undulator. This structure, similar to the Figure-8 undulator, the Halbach structure permanent magnet arrays locate above and below the beam axis, and magnet rows for generating horizontal magnetic field on the beam axis locate at both sides of central magnet rows. As shown in Figure 1, the dimension in the direction of beam axis of each magnet block in the horizontal row is the same with that in the vertical rows except the end structure.

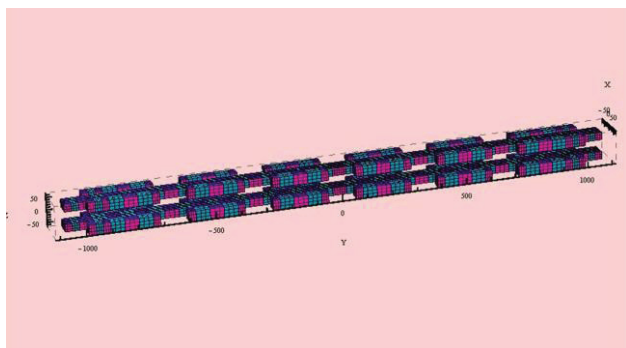


Figure 1: RADIA model of magnet structure for a Knot undulator.

As is seen in Figure 1, there is an empty space between segments in the horizontal structure in order to create the zero-field region. With this structure, the period length of horizontal field is one and a half of vertical field. Figure 2 shows the magnetic field distribution of Knot undulator having the structure of Figure 1.

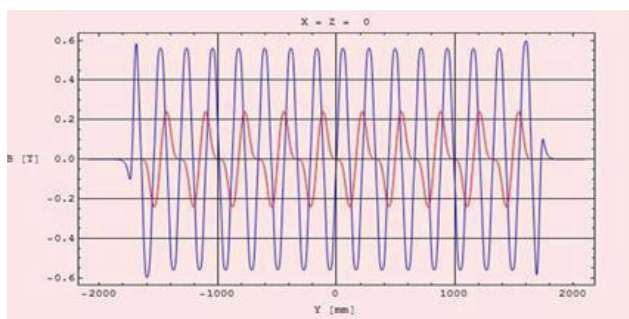


Figure 2: Field distribution of Knot undulator.

In Figure 2, blue line represents the vertical field and red line represents the horizontal field. The period lengths are 220 mm and 330 mm for vertical and horizontal, respectively. The magnet gap to generate the field in this figure is 40 mm.

Figure 3 shows the kick-angle map in an undulator having the field shown in Figure 2 for an electron beam with the energy of 3.5 GeV.

#sasakis@hiroshima-u.ac.jp

Copyright © 2013 CC-BY-3.0 and by the respective authors

ISBN 978-3-95450-138-0

CONCEPTS FOR SHORT PERIOD RF UNDULATORS

S.V. Kuzikov#, A.V. Savilov, A.A. Vikharev, IAP RAS, Nizhny Novgorod, Russia

Abstract

Two concepts for room-temperature RF undulators, fed by cm- or mm- wavelength radiation and aimed to produce ~1 nm wavelength radiation using relatively low energy electron beams, are considered. In accordance with the first considered concept each undulator segment introduces a high-Q cavity fed by its own multi-megawatt RF source. The 30 GHz pulsed gyroklystron or gyrotrons at 30 - 300 GHz, already elaborated and tested in IAP RAS, are appealing candidates. These sources can provide the effective undulator period of 0.5 - 0.05 cm, the undulator parameter up to 1, and the effective field length of 50 cm for each segment. The second concept implies using high-power short pulse propagating in a long helically corrugated waveguide where the -1st field harmonic is responsible for particle wiggling. High group velocity of this pulse allows providing long interaction of particles with RF fields.

RF UNDULATORS BASED ON HIGH-QUALITY CAVITIES

RF undulator in comparison with traditional undulator, consisting of DC magnets, introduces a strong appeal to use less energetic electron beam, in order to produce the same wavelength of Compton's scattered radiation [1-3]. For example, in order to achieve radiation of nanometer wavelength instead of 1-2 GeV beam in conventional undulator with several centimeters period, one can use several hundreds of MeV beam in RF undulator with period ~1 cm [4]. The inevitable payment for this evident advantage is a necessity to provide high power level of microwaves, in order to have acceptable undulator parameter to be competitive with conventional undulators. In Ka-band the necessary power of the wave (to be counter-propagating to electrons) in waveguide of ~1 cm size reaches GW level. That is why, the modern projects of RF undulators assume cavities of high Q-factors to be powered by existing RF sources (klystrons, gyroklystrons, magnikons) which itself are able to provide tens of megawatts. According to such a concept full RF undulator consists of many relatively short sections to be mutually phased ones. At centimeter wavelength range the bimodal TE_{01}-TE_{02} resonator looks promising [4], at millimeter or sub-millimeter range a multi-mirror Gaussian beam resonator is preferable.

High-Q cavities bring a threat of destroying phenomena like RF breakdown and pulsed heating [5-6]. In order to avoid these undesirable phenomena, a short-pulse RF radiation of GW power level is appealing. In particular, experiments carried out with particle accelerators show that nanosecond RF pulses of GW level can travel through electrodynamic structure without breakdown [7].

There are necessary RF sources of GW power level based on relativistic BWOs [8]. Such sources can deliver more than 1 GW power in X-band and about 1 GW in Ka-band in pulses of 0.1-20 ns duration with repetition rate as high as several kHz. It was proven in experiments that phases of separate sources might be mutually locked [9].

SHORT-PULSE, TRAVELING WAVE RF UNDULATOR BASED ON HELICAL CORRUGATED WAVEGUIDE

A short RF pulse of duration τ, propagating in a smooth waveguide with group velocity closed to light velocity c and directed toward an ultrarelativistic electron bunch, causes wiggling of particles at length $L_{eff}^{count} = c\tau/2$. If one takes 10 ns RF pulse, the interaction length does not exceed 2 m. Interaction distance can be much longer, if RF pulse is co-propagating with electrons. In this case the effective interaction length is:

$$L_{eff}^{co} = \frac{v_{gr}\tau}{1 - v_{gr}/c}, \qquad (1)$$

where v_{gr} – is a group velocity along electron beam.

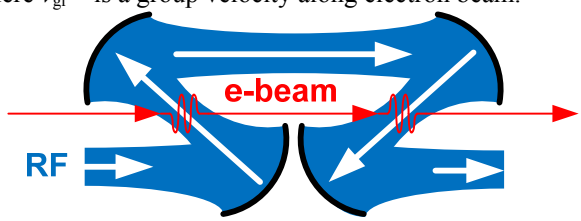


Figure 1: Mirror transfer line employing the "flying" RF undulator.

Of course, the co-propagating RF pulse in a smooth waveguide does not promise considerable Doppler's frequency up-shift. This problem is solved by using a so-called "flying" RF undulator, where a wavebeam spends a part of time moving toward electrons (Fig. 1).

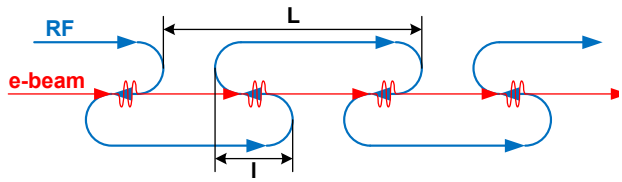


Figure 2: Equivalent scheme of "flying" RF undulator.

The simplified equivalent scheme of the "flying" undulator in Fig. 2 allows writing group velocity along beam in the mirror line:

$$v_{gr} = \frac{c}{1 + 2l/L}. \qquad (2)$$

#kuzikov@appl.sci-nnov.ru

Copyright © 2013 CC-BY-3.0 and by the respective authors

ISBN 978-3-95450-138-0

HELICAL SELF FOCUSING AND COOLING ACCELERATING STRUCTURE

S.V. Kuzikov#, S.V. Mishakin, A.A. Vikharev, IAP RAS, Nizhny Novgorod, Russia

Abstract

A new helical RF accelerating structure, which can provide emittance control of the electron beam, is proposed. This structure combines properties of a linear accelerator and a damping ring simultaneously. It makes acceleration of straight on-axis beam as well as beam cooling due to the synchrotron radiation of particles. These properties are provided by specific slow eigen mode which consists of two partial waves, TM_{01} and TM_{11} (near to cut off). The longitudinal field of the first wave is synchronous with electrons, the transverse fields of the second wave are far from synchronous condition and they cause electron wiggling like it occurs in RF undulator. As a result the emittance control might be employed at linear trajectory of the high-energy beam without decrease of the average gradient. Calculations show that surface electric field at level ~0,31 (relative to accelerating field) and shunt impedance ~20 MOhm/m at 30 GHz are achievable. Cooling rate at gradient 100 MV/m corresponds to the equivalent magnetic field ~0,75 T.

INTRODUCTION

High luminosity of colliding particles in meeting point is achievable for compact, well focused bunches. Such bunches are achievable using systems of particle's cooling. At energies up to several GeV dampling rings provides effective cooling [1]. In these rings particles move in spatially-periodic fields of DC magnets. There is cooling effect due to synchrotron radiation of particles [2]. In order to reach TeV level of energy, behind a cooling ring particles are directed in main linac. Unfortunately emittances of bunches propagating in high-gradient accelerator have tendency to increase, because long trains of particles inevitably excite wakefields which spoil beam quality.

At high energies (more than 10 GeV) rings cannot be used, because too high level of energy dissipation caused by radiation, and too big radius of a ring would be necessary. That is why, cooling undulator can be installed at the linear trajectory only. However, DC magnets around the accelerating structure would conflict with feeding, focusing, and diagnostic systems, and inevitably large period does not allow reaching small emittances, because the smallest achievable emittance is proportional to squared wiggler period [3]. Suggested in the paper [3] accelerator with alternating accelerating sections and wigglers would reduce effective gradient.

An accelerating RF structure, which also plays a role of RF undulator, does not reduce gradient. Such structure might be based on helical corrugated waveguide, where the operating normal mode consists of the 0^{th} spatial harmonic (with positive phase velocity), which is actually the accelerating mode, and the -1^{st} harmonic (with negative phase velocity) which is responsible for particle wiggling. The transverse non-synchronous field components can provide emittance control and beam focusing due to ponderomotive force which depends on transverse electric field gradient of the -1^{st} harmonic wave.

The enumerated properties allow to distinguish our new helical self focusing and cooling structure (HSFC) [4] among other helical structures investigated earlier [5, 6]. Nevertheless, there are important properties to be common for all helical structures. For example, like other helical structure a new structure has smooth shape of the constant circular cross-section (no expansions or narrowings) and big aperture (no small irises). A new technology of the mass production, based on a "corkscrew" in a copper mandrel, seems also possible which allows avoiding junctions inside sections.

TM01-TM11 HELICAL ACCELERATING STRUCTURE

Let us consider the accelerating structure based on helical waveguide described in cylindrical system of coordinates (r, z, φ) by equation:

$$r(z,\varphi) = R + a \cdot \sin\left(\frac{2\pi \cdot z}{L} + m\varphi\right). \qquad (1)$$

where R – is a waveguide radius, a and L – are amplitude and period of the corrugation. Period of the corrugation is close to $2\pi/h_{TM01}$, where h_{TM01} – is a propagation constant of the partial TM_{01} mode in smooth circular waveguide of the radius R. If index m equals 1, such helical structure couples partial waves TM_{01} and rotating on azimuth TM_{11}. The TM_{01} does not perturb transverse movement of on-axis electrons, the TM_{11} does not have longitudinal E_z component on axis.

Table 1: Parameters of TM_{01}-TM_{11} HSFC Structure

Radius, R	6.09 mm
Period, L	8 mm
Corrugation amplitude, a	1.25 mm
Azimuth index, m	1
Frequency, f	28.2 GHz
Phase advance, h_0L	4.727
Q-factor (copper)	10800
Norm. accelerating field, E_a / E_s^{max}	0.307
Shunt impedance, R_{sh}/L	18.9 MOhm/m

#kuzikov@apppl.sci-nnov.ru

ISBN 978-3-95450-138-0

Copyright © 2013 CC-BY-3.0 and by the respective authors

PROGRESS ON PULSED MULTIPOLE INJECTION FOR THE MAX IV STORAGE RINGS

S.C. Leemann*, MAX IV Laboratory, Lund University, SE-22100 Lund, Sweden
L.O. Dallin, Canadian Light Source, Saskatoon, Saskatchewan, S7N 2V3, Canada

Abstract

Injection into the MAX IV storage rings will not make use of a conventional local injection bump with four dipole kickers. Instead, pulsed multipole injection will be applied. Previously, it was foreseen to use a pulsed sextupole magnet similar to what KEK had originally designed for the PF ring. But after seeing encouraging results with a prototype nonlinear kicker magnet developed for BESSY II, pulsed multipole injection for the MAX IV storage rings was revisited. A nonlinear kicker magnet similar to the BESSY-type can be realized for both MAX IV storage rings. Such a nonlinear kicker offers a broad zero-field region around the center which does not perturb the stored beam, while offering a high-field region around the location of the injected beam making it ideal for top-up injection. This paper summarizes the proposed kicker magnet design and shows beam dynamics results from multi-particle tracking studies. A comparison with the previous PSM design is also included.

INTRODUCTION

Early in the design process of the MAX IV storage rings it was considered that injection into the rings could be performed using a single dipole kicker installed downstream of the DC Lambertson septum. In the meantime, detailed studies have demonstrated feasibility [1] and fabrication of these dipole kickers is well underway. However, a single dipole kicker is not suitable for top-up injection because injection and capture cannot be made transparent to users. Therefore, injection with a pulsed sextupole magnet (PSM) was studied as a means to perform fully transparent top-up injection. This avoids having to balance the four dipole kickers and pulsers required to cleanly open and close a local injection bump over prolonged periods of time. Detailed analysis [2] revealed the great potential of PSM injection and a reference design for the magnet was initiated following the experience gained at KEK in the design of the PSM for the PF ring [3].

The MAX IV storage rings require roughly the same kick from the PSM as the PSM in the KEK PF. However, the position of the injected beam in the MAX IV PSM's is only a third of that in the PF and therefore the required sextupole gradient in the MAX IV PSM is considerably higher. On the other hand, the aperture requirements in the MAX IV storage rings are significantly lower, thus allowing a reduction of magnet aperture and an increase in field strength. An initial reference design for a 300 mm long solid iron magnet (cf. Fig. 1) supplied roughly 1.2 mrad kick (at 3 GeV) at −4.7 mm from the center. The bore is 32 mm leading to a pole-tip field roughly 0.5 T. A single coil per yoke called for 2125 A current. With a stored energy of 20.6 J, the required pulser voltage was 19.3 kV for single-turn injection into the MAX IV 3 GeV storage ring. For the MAX IV 1.5 GeV storage ring a similar magnet was designed which relies on 1527 A current at 400 mm length. Here, however, single-turn injection calls for 640 ns pulse length which increases the required pulser voltage to 92.9 kV. Although two-turn injection is possible and reduces the voltage requirement by 50%, it remains desirable to further reduce this voltage, i.e. lower the inductance of the PSM. However, since the magnet bore already lies within only several mm of the beam-stay-clear area, a significant reduction of the inductance could not be expected for this type of magnet.

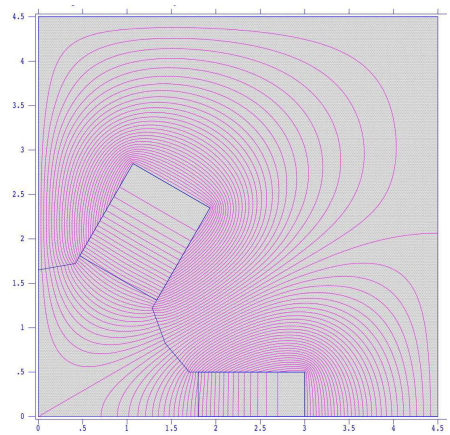


Figure 1: Pulsed sextupole magnet reference design for the MAX IV 3 GeV storage ring. One quarter of the magnet is shown. Scales are in cm. The magnet bore is 32 mm.

NONLINEAR INJECTION KICKER

Around the same time, first reports appeared of a novel nonlinear injection kicker (NLK) developed for BESSY II [4]. This kicker design expands on the original PSM idea to have a high field at the injected beam while keeping the field at the stored beam close to zero. It makes use of a stripline-like design with a geometry intended to create a high-field area strongly localized around the injected beam while suppressing the field at the stored beam through symmetry. Figure 2 shows an initial reference design for the MAX IV 3 GeV storage ring along with the

* simon.leemann@maxlab.lu.se

Copyright © 2013 CC-BY-3.0 and by the respective authors

BEAM-INDUCED HEAT LOAD PREDICTIONS AND MEASUREMENTS IN THE APS SUPERCONDUCTING UNDULATOR*

Katherine C. Harkay#, Laura Boon, Michael Borland, Yong-chul Chae, Roger Dejus, Jeffrey Dooling, Charles Doose, Louis Emery, Yury Ivanyushenkov, Mark Jaski, Matthew Kasa, Suk H. Kim, Robert L. Kustom, Vadim Sajaev, Yuko Shiroyanagi, Xiang Sun
ANL, Argonne, IL 60439, USA

Abstract

The first test superconducting undulator (SCU0) was successfully installed and commissioned at the Advanced Photon Source (APS) and is delivering 80- to 100-keV photons for user science. The cryosystem was designed to handle a beam-induced heat load of 40 W. Prior to operations, detailed predictions of this heat load were made, including that produced by resistive wall heating by the image current, geometric wakefields, synchrotron radiation, electron cloud, and beam losses. The dominant continuous wave (cw) source is the resistive wall heat load. The heat load predictions for standard 100-mA user operation were benchmarked using thermal sensors that measure temperatures along the SCU0 beam chamber. Analysis using the predicted heat loads from the electron beam agrees well with the observed measurements.

INTRODUCTION

A test superconducting undulator (SCU0) has been developed at APS [1] and was recently installed in the storage ring. A key design criterion was a vacuum and cooling system that keeps the NbTi coils cooled to 4 K in the presence of heating caused by the electron beam passing through the undulator beam chamber. The SCU0 beam chamber cooling system was designed for 40 W (at 20 K) of cooling capacity based on preliminary calculations of the beam-induced heat load [2]. In this paper, updated predicted heat loads are compared with measurements carried out during SCU0 commissioning [3].

Sources of beam-induced heat load on the SCU0 beam chamber include resistive-wall heating due to beam-induced image currents, synchrotron radiation generated in upstream dipole magnets, wakefield effects, direct beam interception and, potentially, electron cloud-induced multipacting effects. Under nominal operating conditions cw heat loads are present, while specific machine fault conditions may occur that give rise to individual transient heat loads.

Estimates of the various contributions to the heat load due to the beam are shown in Tables 1 and 2 for cw and transient sources, respectively, assuming 24-bunch operation. The central part of the chamber is nominally 20 K and is thermally isolated from the 4-K magnetic structure. The chamber transitions are in the 60- to 300-K cold-to-warm transition region. Where appropriate, the heat loads at 20 K and 60/300 K are given separately.

* Work supported by U. S. Department of Energy, Office of Science, under Contract No. DE-AC02-06CH11357.
#harkay@aps.anl.gov

Table 1: Estimated cw Beam-induced Heat Loads on the SCU0 Chamber, in 100-mA User Operations

Heat Source	Value at 20 K (60/300 K)
Resistive wall	4.7 W (11.3 W)
Wakefields	< 0.5 W (0.8 W)
Injection losses	2 W (non-top-up mode) 0.1 W (top-up mode)
Synchrotron radiation	0.2 W
Beam lifetime losses	<< 1 W
Electron cloud	< 2 W
Total heat load	10 W (12 W)

Table 2: Estimated Max. Transient Beam-induced Heat Loads on the SCU0 Chamber, in 100-mA User Operations

Heat Source	Value
Injected beam loss	13 W
Corrector failure	20 W
Synchrotron radiation with steering errors	25 W
Electron beam steering errors	20 W
Max. transient heat load	25 W

MEASUREMENTS

The beam-induced heating on the SCU0 beam chamber was measured using nine Cernox cryogenic thermal sensors mounted on the beam chamber, shown in Fig. 1 (Temp0-8). Sensors Temp2-6 are mounted on the outboard side of the aluminum section of the chamber, and Temp0,1,7,8 are mounted on the top side of the stainless steel (SS) cold-to-warm transition. The chamber heater is connected to a copper block mounted adjacent to sensor Temp5. A calibrated heat load was applied to the heater using a variable power supply. The chamber heater was used to calibrate the thermal sensors, allowing determination of the heat load from the temperature measurements. This calibration was used to both predict and benchmark the chamber temperatures for storage ring beam operation.

Chamber Heater Calibration

To simulate SCU0 operating conditions, the main coil current was set to 500 A, but there was no stored beam. An external supply current was used to vary the chamber heater power based on the known heater resistance. The chamber temperatures were recorded for P=0, 5, 10, 20, and 30 W, waiting 10-20 min per step. The equilibrium chamber temperatures were determined by fitting the measurements to an exponential function. The zero-power

Copyright © 2013 CC-BY-3.0 and by the respective authors

ISBN 978-3-95450-138-0

BEAM-BASED ALIGNMENT OF THE FIRST SUPERCONDUCTING UNDULATOR AT THE APS*

Katherine C. Harkay#, Laura Boon, Michael Borland, Louis Emery,
Robert L. Kustom, Vadim Sajaev, Yuko Shiroyanagi, Aimin Xiao
ANL, Argonne, IL 60439, USA

Abstract

The first test superconducting undulator (SCU0) was successfully installed and commissioned at the Advanced Photon Source (APS) and is delivering 80- to 100-keV photons for user science. The magnet cores are mounted on but thermally isolated from the beam vacuum chamber. Protecting the SCU0 from high beam-induced heat loads was an important requirement before operating the SCU0 in the storage ring. Precise alignment of the beam vacuum chamber with respect to both the electron beam orbit as well as the synchrotron radiation generated in the upstream dipole magnet was therefore extremely important. The beam vacuum chamber was instrumented with nine thermal sensors. Using the sensors, the chamber alignment was determined with 100-micron accuracy. This accuracy is 10 times higher than in a standard aperture scan. Other advantages of the thermal sensor-based alignment method include isolating the SCU0 alignment from other components in the orbit bump and providing good longitudinal spatial resolution. The chamber temperatures agreed well with the predicted heat load and dependence on steering. This novel beam-based alignment method and results will be presented.

INTRODUCTION

One of the many challenges of operating a small-gap superconducting undulator in a high-energy synchrotron light source is protection from excessive beam-induced heat loads [1]. For the test superconducting undulator (SCU0) recently installed in the APS [2], this is accomplished through several key features, including an out-of-vacuum design, thermal isolation of the beam chamber from the magnet coils, 40-W cooling capacity on the beam chamber, and a photon absorber to shield the SCU0 from synchrotron radiation from the upstream bending magnet (BM). Precise alignment of the magnet structure and beam vacuum chamber is also essential for proper heat-load protection, as is a well-controlled beam orbit while the device is in operation. Prior to installation in the APS, the SCU0 beam vacuum chamber and magnetic structure were transversely aligned to within ±150 μm relative to fiducials mounted on the vacuum vessel. Correction values were determined for a "cold fiducialization," based on measurements before and after cooldown on the test stand [3]. After installation and cooldown *in situ*, beam-based alignment was used to confirm that the SCU0 chamber position was reproduced and that it remained stable during operation. A standard aperture scan was performed first, followed by beam-based alignment using thermal sensors. The results are described below.

APERTURE SCAN

A standard aperture scan involves steering the electron beam vertically through the chamber until the edge of the beam scrapes the walls and the beam lifetime decays to a small value (typically < 10 min). The extreme values of the vertical beam position monitors (BPMs) are recorded to give a measure of the aperture. With a standard 5-m-long ID chamber, a combination of parallel- and angle-bumps can be used to determine the chamber alignment. However, the SCU0 was installed in sector 6 (ID6) downstream of a half-length ID chamber. Sector 6 thus has two small-aperture chambers and several transitions. Therefore, only parallel orbit bumps were implemented to confirm the overall chamber alignment.

The full vertical aperture of the SCU0 chamber is nominally 7.2 mm and the ID chamber is 7.5 mm. The aperture scan was performed using 2 mA in a single bunch, chosen low to protect the SCU0 but with sufficient BPM response. For comparison, the same measurement was repeated in ID21, a 5-m-long, 7.5-mm, full-height ID chamber known to be well aligned. A model four-corrector parallel bump was used to change the correctors, and a special global orbit configuration closes the bump, with the P1 BPM readings allowed to vary. P0 BPMs are located at the ends of the insertion device (ID) chamber, but they have inaccurate response at large orbit values (> 1 mm). P1 BPMs have a better response at large orbit values but there is a defocusing quadrupole between the P1s and the ID chamber ends. Because a model orbit bump produces a parallel orbit shift in the ID, it can be assumed that the orbit at P1 is nearly the same as P0. The aperture was determined from the P1 readings.

The results are given in Table 1. The ID6 results are very good in terms of symmetry, and the full range is comparable to ID21. The accuracy of this method in determining the chamber center is estimated to be about ±1 mm, given that the full range determined from the scan is ~3 mm smaller than the nominal chamber aperture.

Table 1: Aperture Scan Results for ID6/SCU0 and ID21

Sector	Steer up (mm)	Steer down (mm)	Full range (mm)
ID6	2.2	-2.2	4.4
ID21	2.2	-1.8	4.0

* Work supported by U. S. Department of Energy, Office of Science, under Contract No. DE-AC02-06CH11357.
#harkay@aps.anl.gov

Copyright © 2013 CC-BY-3.0 and by the respective authors

FAST-SWITCHING VARIABLY POLARIZING UNDULATOR*

M. Jaski, R. Dejus, B. Deriy, E. Moog, I. Vasserman, J. Wang, A. Xiao, E. Gluskin
Advanced Photon Source, Argonne National Laboratory, Argonne, Illinois 60439, USA

Abstract

Development of a new fast-switching electromagnetic variably polarizing undulator (EMVPU) is underway at the Advanced Photon Source (APS). The EMVPU can produce x-rays with left- and right-handed circular polarizations and horizontal and vertical linear polarizations in the energy range 400-2000 eV. The undulator will be able to switch between left- and right-handed circular polarizations at 10 Hz, fast enough to allow for magnetic circular dichroism studies that rely on lock-in amplifier techniques. The handedness switch will be accomplished by switching only the vertical component of the field while the horizontal component stays constant. Details of the EMVPU and its initial experimental test models are presented.

INTRODUCTION

The new EMVPU will join other all-electromagnetic undulators that are presently in use at APS—the CPU (circularly polarizing undulator) [1], with Eγ ≥ 500 eV and 1-Hz switching, that has been in operation since 2001; and the recently installed IEX undulator, a quasi-periodic variably polarizing undulator (Eγ ≥ 250 eV) that was designed and built at the APS [2] and commissioned successfully in 2012 [3]. The EMVPU, like those devices, will provide linear polarization (horizontal and vertical) and circular polarization (right- and left-handed) capabilities, but adds the capability of switching the circular polarization handedness at 10 Hz (with an 80% duty cycle), faster than previously available at APS. Fast-switching undulators are also in operation at ESRF [4] and SOLEIL [5] using a combination of electromagnets and permanent magnets.

The requirement for rapid handedness switching of the circular polarization is driven by the users' need to use lock-in detection for their magnetic scattering experiments. They require ample time between handedness switches—time when the photons produced are of the desired energy and polarization and when measurements can be made with a stable photon beam. Not only must the current in the coil stabilize to its new value rapidly, but any eddy currents and associated stray fields induced by the switching must be minimized.

In order to achieve fast switching in the EMVPU, the vertical (By) field coils are single-turn coils machined from a solid piece of copper. This minimizes the coil inductance to allow for the fastest possible switching speed. One-turn coils also provide right/left symmetry near the pole tips, reducing undesirable magnetic multipoles. Transient fields during the switching must also be minimized. Laminated cores minimize eddy currents in the By poles. Eddy currents in the vacuum chamber can significantly slow the switching speed so a vacuum chamber material with low electrical conductivity must be used. Any residual e-beam steering or multipole transients will be compensated during switching using corrector magnets on each end of the device.

*Work supported by U.S. Department of Energy, Office of Science, under Contract No. DE-AC02-06CH11357.

PARAMETERS

Table 1 lists selected parameters for the EMVPU.

Table 1: Selected Parameters

Parameter	Value	Unit
Period	12.5	cm
Gap	8.5	mm
Maximum effective field for linear polarization (horizontal or vertical)	3491	Gauss
Maximum effective field for circular polarization	2469	Gauss
Switching speed between right- and left-handed circular polarization	10	Hz

ONE-PERIOD TEST MODEL

General Concept

Figure 1 shows the general layout of the Bx and By coils, poles, and core for the lower jaw of the one-period test model. The upper jaw has similar geometry. The By coils are single-turn coils machined from oxygen-free copper. The By core is made from 0.64-mm-thick M-22 silicon steel laminations with a C5 coating. The laminations are laser-cut and epoxied together. The epoxy-impregnated Bx coils have 46 turns of square copper solid wire [6]. The Bx poles are made of heat-treated vanadium permendur, chosen because it gives 5% higher field than low-carbon steel. The Bx core is low-carbon steel with slots for stainless steel cooling-water tubes. These cooling-water tubes cool the Bx core, which cools the Bx poles; both in turn cool the Bx coils.

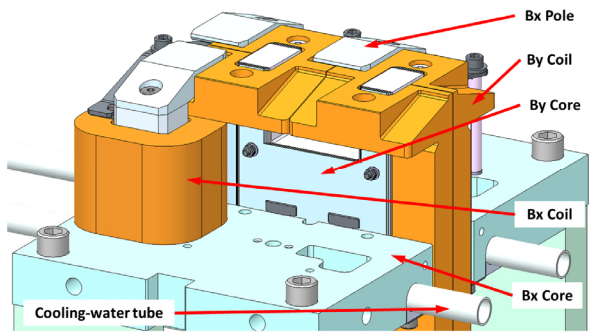


Figure 1: A 3-D CAD model of the one-period test model lower jaw (one Bx coil/pole assembly is hidden to show the By core).

Figure 2 shows a close-up of the one-period test model. The By coils are soldered to bus bars, after being tin plated to ease the soldering. The bus bars are water cooled

Copyright © 2013 CC-BY-3.0 and by the respective authors

ISBN 978-3-95450-138-0

AN ELECTROMAGNETIC VARIABLY POLARIZING QUASI-PERIODIC UNDULATOR*

M. Jaski, M. Abliz, R. Dejus, B. Deriy, E. Moog, I. Vasserman, A. Xiao, E. Gluskin
Advanced Photon Source, Argonne National Laboratory, Argonne, IL 60439, USA

Abstract

An electromagnetic variably polarizing quasi-periodic undulator was installed in the Advanced Photon Source (APS) storage ring in April 2012 and has been successfully commissioned with stored beam. This device is identified as the Intermediate Energy X-ray (IEX) undulator. The IEX undulator takes its name from the IEX beamline where it is installed. The IEX undulator is able to produce a variety of polarizations: linear vertical, linear horizontal, and right- or left-handed elliptical or circular. Ten pairs of poles, distributed quasi-periodically along the undulator length, are powered separately, allowing the field strength of the quasi-periodic poles to be adjusted. This adjustability allows the user to seek a balance between the suppression of the higher harmonics and the loss of flux in the fundamental that best suits the measurement being made. The IEX undulator has a 12.5-cm period and can achieve photon energies as low as 250 eV in horizontal polarization and 440 eV in vertical polarization. A description of the IEX undulator will be presented.

INTRODUCTION

The IEX beamline team, consisting of APS staff members along with researchers from the Universities of Illinois at Chicago and at Urbana-Champaign, is commissioning a new dual beamline with one leg dedicated to angle-resolved photoemission spectroscopy (ARPES) measurements and the other dedicated to resonant soft x-ray scattering (RSXS) [1]. The undulator needs to provide photons ranging from 250 to 2500 eV, with horizontal and vertical linear, and left- and right-circular and elliptical polarizations. (Vertical linear polarization only goes as low as 440 eV.) The presence of high harmonics in the spectrum degrades the signal-to-noise ratio in both techniques, so a quasiperiodic undulator is sought for its ability to shift the high harmonics in energy so they are eliminated by the beamline optics.

Several possible variably polarizing undulator designs were considered, including an Apple II (all permanent magnet), an electromagnetic/permanent magnet, and an all-electromagnetic design similar to the circularly polarizing undulator (CPU) [2] presently installed at the APS. The all-electromagnetic design was chosen, largely because of its ability to vary the magnetic strength reduction in the quasiperiodic poles so trade-offs could be made between additional high-harmonic reductions at the expense of a loss in photon beam intensity. Magnetic field simulation and optimization [3] were done, and prototypes were built and tested before building the full-length device. The full-length device was successfully commissioned at the APS in 2012 [4].

PARAMETERS

Table 1 lists selected parameters for the IEX undulator.

Table 1: IEX Undulator Selected Parameters

Title	Description	Value	Unit
General	Period	12.5	cm
	Gap	10.5	mm
	Periods per device (including end poles)	38	periods
Horizontal Linear Polarization	Minimum photon energy	240	eV
	Measured maximum vertical effective field	4614	Gauss
Vertical Linear Polarization	Minimum photon energy	440	eV
	Measured maximum horizontal effective field	3312	Gauss
Circular Polarization	Minimum photon energy	234	eV
	horizontal and vertical effective field	3312	Gauss

DESIGN AND ASSEMBLY

Figure 1 shows the IEX undulator at the magnetic measurement bench. The device is 958 mm wide × 2118 mm tall × 5044 mm long (37.7" × 83.4" × 198.6") and weighs 6350 kg (14,000 lbs). Casters attached to the base allow it to be manually rolled across a flat concrete floor by six people. The undulator is installed onto floor bases that are grouted to the floor. The undulator gap is fixed at 10.5 mm. The jaw assembly is mounted to high-precision linear roller bearings and can manually be moved



Figure 1: The IEX undulator at the magnet measurement bench.

*Work supported by U.S. Department of Energy, Office of Science, under Contract No. DE-AC02-06CH11357.

Copyright © 2013 CC-BY-3.0 and by the respective authors

DESIGN OF A 17.2-MM-PERIOD PLANAR UNDULATOR FOR THE APS *

E.R. Moog#, M. Abliz, R.J. Dejus, J.H. Grimmer, and M. Jaski, ANL, Argonne, IL 60439, USA

Abstract

The design process for a short-period planar undulator is described. This is a conventional planar design based on Nd-Fe-B magnets and vanadium permendur poles. The period length was driven by the users' request for a high flux of photons at 23.7 keV, with minimal tuning range. A shorter period gives higher flux; 17.2 mm was the shortest value consistent with the gap limitations of the vacuum chamber and with reaching the desired photon energy. Details of the design, especially the various chamfers of edges of the magnet and pole, were examined more closely than has been the standard past practice in order to minimize the period length.

INTRODUCTION

The majority of the insertion devices at the Advanced Photon Source (APS) are of the planar permanent magnet hybrid type, and a variety of period lengths have been installed. This 17.2-mm-period undulator will have the shortest period; it is being designed to meet the specific needs of a group of users who want to maximize their photon flux at 23.7 keV without any need for a significant tuning range. The ideal choice for such a short-period undulator would be to use superconducting technology, but that technology is only now being commissioned at the APS [1]. It will be several years before a customized device can be designed and built for these users. They have opted not to wait.

Keeping the beam impedance from the insertion device vacuum chamber walls low results in a minimum gap for the undulator of 10.4 mm (with a new ID vacuum chamber that is in the design stage; the present typical minimum gap is 11.0 mm). This, combined with the 23.7 keV desired energy, means that the operating point of the undulator is not at the peak in the tuning curve but rather on a slope where a small change in undulator period can have a noticeable effect on the on-axis flux, as shown in Fig. 1 where there is a 15% flux increase between the 17.5 and 17.2-mm period lengths. Shortening the undulator period gives more flux, until the field strength needed to reach the desired energy no longer lies within the achievable gap range. The steepness of the tuning curve for this design project places a high premium on achieving the shortest period possible, and the need for a single specific photon energy means that the magnetic field cannot be lower than expected. To add to the challenge, the required undulator field increases as the undulator period decreases, while a decrease in period generally comes with a decrease in field.

*Work supported by U.S. Dept. of Energy, Office of Science, under Contract No. DE-AC02-06CH11357.
#emoog@aps.anl.gov

CHOICE OF MAGNET GRADE

The considerations that drive the choice of a magnet grade are the remanent field B_r and the coercivity H_{cJ} of that grade. Recent magnet grades used for APS undulators are Shin-Etsu's N39UH and N42SH. With $B_r \geq 12.7$ kG and $H_{cJ} \geq 21$ kOe, N42SH has been used when the highest field strength was needed. Otherwise, N39UH with $B_r \geq 12.2$ kG and $H_{cJ} \geq 25$ kOe has been chosen for its higher coercivity.

The higher coercivity is desirable for two reasons: 1) for a particular demagnetizing field in the magnet, the higher-coercivity magnet can survive higher temperatures without ill effects, and 2) the higher coercivity correlates with higher resistance to radiation-induced demagnetization. Magnets of either grade, when installed in an undulator whose magnetic design considerations include maintaining a moderate demagnetizing field, will survive a hot day with broken air conditioning. Radiation susceptibility is harder to quantify because of many unknowns, including the spectral sensitivity of the magnets and the spectral distribution of the radiation at the magnets' locations. At the APS, except for two extremely high-dose sectors, the undulators have not been affected by radiation enough to affect users' programs, though small effects have been seen. A common difference between the maximum demagnetizing field and the magnet's H_{cJ} has been ~4 kOe, so a goal is to keep the demagnetizing field at least that far below H_{cJ}. For this short a period, a higher H_{cJ} than N42SH is not necessary.

The magnet grade characteristics given here are from the manufacturer's data sheets and are for 20°C. The temperature of the APS storage ring tunnel, however, is 25°C. Since the on-axis field in the simulations must be met in the real device, the reduction in the manufacturer's B_r due to the higher temperature must be taken into

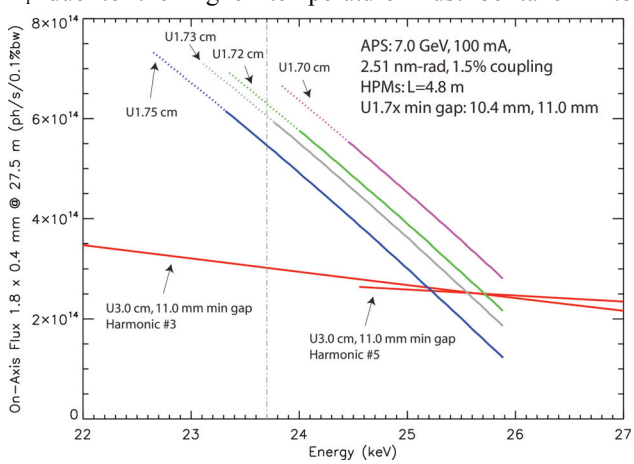


Figure 1: Tuning curves over a narrow photon energy range, for a few period lengths. The solid lines are for a minimum gap of 11 mm; the dotted extensions are for a reduction to 10.4-mm gap.

Copyright © 2013 CC-BY-3.0 and by the respective authors

ISBN 978-3-95450-138-0

THE INTERMEDIATE-ENERGY X-RAY (IEX) UNDULATOR COMMISSIONING RESULTS *

A. Xiao, M. Abliz, B. Deriy, M. Jaski, M. Smith, I. Vasserman, J. Xu
Argonne National Laboratory, Argonne, IL 60439, USA

Abstract

Strong beam perturbation from the intermediate-energy x-ray (IEX) undulator operation has been expected from the beginning. This paper describes our efforts including the initial magnet design, field measurements and compensation, special considerations of power supplies and the control system, and the final commissioning results with beam. Perturbations are well within the specified limits, and the IEX was made ready for user operation in less than six months.

INTRODUCTION

A 4.8-m electromagnetic undulator was designed, built, and installed at the APS to provide the Intermediate-Energy X-ray (IEX) beamline with variably polarized radiation. Details on the device itself are presented separately [1]. The main parameters of this device are listed in Table 1. Simulation results show that strong nonlinear fields are present in this device. To eliminate beam perturbations, 13 correction coils are included, which correct stray fields, orbit, tune, coupling, and some high-order perturbations. Together with four main coils (By, By-Quasi, Bx, Bx-Quasi), there are 17 power supplies for this single device. Besides the complexity of the device itself, special requirements from user operations are:

Table 1: IEX Main Parameters

Title	Description	Value	Unit
General	Length	4.8	m
	Period length	12.5	cm
Horizontal Linear	Energy	0.25-3	keV
	K Value	5.271-0.694	
Vertical Linear	Energy	0.44-3	keV
	K Value	3.863-0.694	
Circular Mode	Energy	0.44-3	keV
	K Value	3.863-0.694	

- Generates four polarization modes. Horizontal- and vertical-linear modes [H/V], clockwise and counter-clockwise circular modes [CW/CCW].
- In each mode, the quasi-periodic property can be switched on and off [1].
- Precise photon energy reproducibility.
- Polarization refinement at the sample location.

To satisfy requirements on energy reproducibility, the device is required to operate on a hysteresis loop. A special magnet degaussing and conditioning procedure also needs to be followed. The device provides radiation to two beamline branches in which, due to different properties of optical elements, different IEX settings are required for different branches to reach $> 99\%$ polarization purity at the sample location.

All facts added up together made IEX commissioning a difficult task. Commissioning started on May 2012 and by November 2012 all operational modes had been successfully commissioned with beam. This paper describes details of the commissioning efforts leading to eventual success.

MAGNET DESIGN AND MEASUREMENT

The magnet design and measurement were done in close coordination with simulation work. Simulation results [2] showed this device would be the strongest nonlinear perturbation source among all IDs that have been installed in the APS storage ring. Special measures were taken during the magnet design phase, including 2×6 correction coils added to each side of the device for making further corrections.

After magnet assembly, the field was measured over the entire excitation curve for each operational mode. Unlike other ID measurements, which measure B_y only in the xz plane (y=0) — i.e., 2D measurement—both B_x and B_y fields were measured in a 3D volume. One assembly fault (a magnet block was inadvertently made from a prototype part) was found through fitting the measured field map to the design model, and corrected. After fixing the fault, the IEX was re-measured and a full set of simulation work was done using the measured field map. For these simulations [3], field data were fitted to the wiggler field expansions while measured field error was represented by a kickmap element; other machine errors were also included. Simulation results showed that the magnet quality met our expections. The simulated dynamic aperture (see Figure 1) was only slightly reduced due to the strong nonlinear field errors. This reduction was expected based on design simulations and can be mitigated using the local correction coils based on later beam test.

POWER SUPPLY

As described in the previous section, the IEX has 17 individual power supplies (PSs) to provide field excitation and local beam perturbation corrections, making it one of the single most complicated powered elements in the ring. To reduce beam perturbations, all PSs are synchronized, and

* Work supported by the U.S. Department of Energy, Office of Science, under Contract No. DE-AC02-06CH11357.

Copyright © 2013 CC-BY-3.0 and by the respective authors

NON-LINEAR EFFECTS OF INSERTION DEVICES: SIMULATION AND EXPERIMENT RESULTS *

A. Xiao, M. Borland, L. Emery, V. Sajaev
Argonne National Laboratory, Argonne, IL 60439, USA

Abstract

The Advanced Photon Source (APS) Upgrade includes adding more insertion devices (IDs) to the storage ring. Perturbations from IDs have been reviewed, with the most significant sources coming from IDs that generate circular polarized light. To address this, we measured non-linear effects from the existing circular polarized undulator (CPU) and intermediate-energy x-ray (IEX) undulator. Measurement results were compared with simulation results. Proposed correction schemes were tested experimentally.

INTRODUCTION

The ongoing APS Upgrade (APS-U) project includes installing IDs in unused straights and replacing some IDs with devices better-optimized for user requirements. ID perturbations to the beam can be qualitatively expressed by [1]

$$\Delta x'(x) \propto \frac{L_w}{E^2} K^2 \frac{d}{dx} F^2(x), \qquad (1)$$

where L_w is the length of the wiggler, E is the beam energy, K is the wiggler strength, and $F(x) = B_y(x)/B_y(0)$. Non-linear effects come from the roll-off in $F(x)$.

For planar IDs, only one on-axis field (typically B_y) needs to be non-zero. Thus a generally wider ID pole and flatter $F(x)$ is possible, which reduces non-linearities. For IDs that generate elliptical radiation, both B_x and B_y are necessarily non-zero on axis. The required magnet structure is much more complicated, with narrower poles and, as a consequence, larger variation of $F(x)$. Figure 1 illustrates this difference for some of the typical and planned APS IDs. ID parameters are listed in Table 1.

To better understand the beam dynamics effects of ID field non-linearity, several simulation methods have been implemented in `elegant` [2]. Some of the methods require an analytical wiggler field expansion, which can be obtained through fitting a 3D magnetic field map to a model. In this paper, we first describe these simulation tools, fitting methods, and methods to reduce artificial errors from fitting. Then, using IEX as an example, we show simulation results from a measured field map. Finally, we present some experimental results from CPU and IEX operations.

SIMULATION TOOLS AND FITTING METHOD

There are four elements in `elegant` that simulate IDs: CWIGGLER, GFWIGGLER, UKICKMAP, and FTABLE.

* Work supported by the U. S. Department of Energy, Office of Science, under Contract No. DE-AC02-06CH11357.

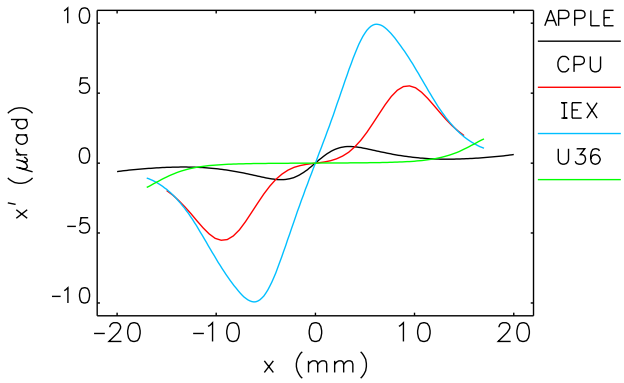


Figure 1: Comparison of simulated in-plane kick map ($y = 0$) for different types of IDs.

Table 1: Typical ID Parameters

ID Type	Length (m)	K_max+	By Pole Width (mm)
U33 *	2.4	2.75	51
U36 *	2.1	3.31	39.5
CPU*	1.8	2.77(H) 2.77(V) 2.5(C)	24
IEX*	4.75	5.27(H) 3.86(V) 3.86(C)	18.2
APPLE#	2.1	3.57(H) 2.7(V) 3.03(C)	35×35

+ H/V/C are different polarization mode for elliptical ID.
* Currently operated at APS.
# ID is under development, parameters are under consideration.

UKICKMAP uses kick maps [3] obtained from magnet design directly or from tracking results of the other three methods. All other methods use 3D field maps from ID design or field measurement. FTABLE uses the field map directly and is non-canonical, while CWIGGLER and GFWIGGLER require an analytical wiggler field expansion (from the 3D field map fitting) and are canonical. Our typical procedure for simulating nonlinear ID effects is: fit the 3D field map to a field expansion; using CWIGGLER or GFWIGGLER, track a bunch of particles through the element in a "grid" distribution on the $x - y$ plane with $x' = y' = 0$, and determine the kick map at the exit; use the kick map as input to UKICKMAP to perform various

Copyright © 2013 CC-BY-3.0 and by the respective authors

ISBN 978-3-95450-138-0

ON-AXIS INJECTION SCHEME FOR ULTRA-LOW-EMITTANCE LIGHT SOURCES *

A. Xiao†, M. Borland, C. Yao, ANL, Argonne, IL 60439, USA

Abstract

Injection design for an ultra-low-emittance light source is mainly limited by two effects. Due to intrabeam scattering and beam instabilities, multiple bunches with tight bunch spacing are injected into the ring to reach high average beam current, which limits the choices of injection technology. Strong non-linear effects due to the significant focusing force applied and the resultant strong sextupoles make the dynamic aperture very small, so that only on-axis "swap-out" beam injection is workable. Using a seven-bend-achromat (7BA) lattice designed for the Advanced Photon Source (APS) storage ring as an example, this paper presents an on-axis injection scheme based on the fast stripline technique together with discussions of the different configuration choices.

INTRODUCTION

When pushing a storage-ring-based light source emittance close to very low emittance, two primary consequences emerge: insufficient dynamic aperture for accumulation-based injection, so that only on-axis "swap-out" injection is workable [1]; and the maximum single-bunch intensity is significantly reduced due to the intrabeam scattering (IBS) and beam instabilities, so a significant fraction of the ring may need to be filled with beam to reach the required average beam current. Both factors put strict restrictions on the choice of injection technology and optics design.

In the scheme envisioned here, a single "swap-out" beam injection only replaces a portion of the stored beam, see Figure 1. The target bunches must be extracted and injected without affecting the emittance and stability of the remaining stored beam. For this to be the case, the kicker field must be negligible at the next upstream or downstream bunches, which requires kicker rise- and fall-times less than the spacing between bunches—usually one to a few rf buckets depending on the specific design, e.g., 10 rf buckets @500 MHz implies 20 ns. Commonly used ferrite kicker magnets cannot meet such requirements, but the stripline kicker technology proposed for the ILC damping ring [2] seems promising and is adopted in this paper.

A series of 40-sector, 6-GeV seven-bend achromat (7BA) lattices [3] have been studied for the future APS Upgrade. The lattice used is shown in Figure 2. In this paper, we will present an injection and extraction design for the 7BA lattice, with discussion of the different injection schemes.

* Work supported by the U.S. Department of Energy, Office of Science, under Contract No. DE-AC02-06CH11357.

† xiaoam@aps.anl.gov

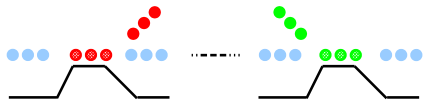


Figure 1: Sketch of on-axis "swap-out" injection (red: extraction bunches; green: injection bunches).

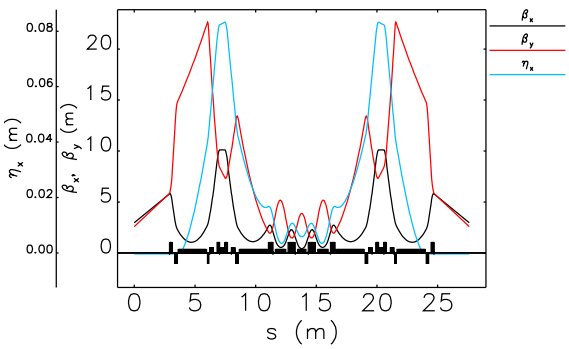


Figure 2: Single-cell optical functions of a 7BA lattice.

MAIN PARAMETERS

The kick angle from a stripline of length L with gap d between the electrodes is given by

$$\Delta\theta = 2g\frac{eV}{E}\frac{L}{d}, \tag{1}$$

where V is the voltage applied to the two electrodes, E is the beam energy, $g \leq 1$ is the geometry factor, and the factor 2 includes the force from both electric and magnetic fields. Using the stripline tested at ATF [4] (60 cm long, 10 mm gap, with $\pm$10 kV pulsers), the kick angle is 0.4 mrad.

The maximum achievable kick angle depends on two major factors: the available pulser strength V and the size of the stripline. Unlike the ILC damping ring, the required injection frequency is much lower, so a pulser with much higher output voltage [5] is available; V is then limited by the detailed design of the stripline (feed through). A smaller gap d increases $\Delta\theta$ for the same gap voltage V, while the maximum achievable V is also reduced due to reduction in the stripline size. As there is yet no detailed stripline design, we assume $V = 30$ kV at $d = 10$-mm gap compared with $V = 20$ kV at the same gap for the ILC damping ring. Larger L will make more efficient use of the limited space, but the maximum L is limited by the required rise/fall time. We choose $L = 0.6$ m, so that the rise/fall time is less than 5 ns. Altogether, the kick strength from a single stripline is 0.6 mrad. To accomplish the injection task, multiple striplines are needed.

Unlike other storage ring designs, an ultra-low-

Copyright © 2013 CC-BY-3.0 and by the respective authors

ADVANCED X-RAY BEAM POSITION MONITOR SYSTEM DESIGN AT THE APS*

B.X. Yang†, G. Decker, J. Downey, Y. Jaski, T. Kruy, S. H. Lee, M. Ramanathan and F. Westferro
Advanced Photon Source, Argonne National Laboratory, Argonne, IL 60439, USA

Abstract

As part of the Advanced Photon Source (APS) Upgrade, new x-ray beamline front ends are planned that include extensive integrated x-ray diagnostic capability. The high-heat-load front-end (HHLFE) design includes a grazing-incidence insertion device x-ray beam position monitor (GRID-XBPM) utilizing Cu K-edge x-ray fluorescence from x-rays striking a pair of copper absorbers. At a 1.0˚ grazing incidence angle, the XBPM assembly is designed to withstand 17 kW power from two inline Undulator A devices at 150-mA stored beam. A second XBPM located outside of the accelerator enclosure monitors fluorescence from the beamline exit mask, which is a critical beamline-defining aperture. In addition, an intensity monitor is used to detect x-ray flux passing through a front-end mask inside the enclosure, while a second intensity monitor is located immediately downstream of the exit mask. Details of these designs and expected performance will be presented.

INTRODUCTION

The ongoing Advanced Photon Source Upgrade (APS-U) requires major improvements in x-ray beam stability. The stability goals are to be achieved on multiple beamlines with two inline Undulators A's delivering beam power up to 17 kW at 150-mA stored current. Since the modern storage ring orbit feedback systems have demonstrated submicron stabilities, the actual x-ray beam stability delivered to the user is determined by the accuracy of the beam position monitors. In the past several years, the APS has made a major effort in developing a hard x-ray BPM. The new device uses the 8-keV Cu K-edge x-ray fluorescence (XRF) from the front-end limiting apertures to infer the undulator beam's core position [1,2]. An experimental test with two inline undulators showed that the XBPM has nearly 70-fold improvement in rejection of bend magnet radiation background and a gap-independent calibration in one of the two dimensions [3]. Based on this successful demonstration, the GRID-XBPM was included as a standard device for the new HHLFEs being developed for the APS-U. In this paper, we report the engineering design of the new XBPM system, including a GRID-XBPM, the second XBPM at the end of the front end, and the two intensity monitors to assist for beam-based alignment of front end apertures. We will also report on the latest design development of a new XBPM based on Compton scattering.

*Work supported by the U.S. Department of Energy, Office of Science, under Contract No. DE-AC02-06CH11357.
†bxyang@aps.anl.gov

THE FIRST XBPM

Figure 1 shows the first XBPM. It is a GRID-XBPM consisting of two GlidCop absorbers, positioned on the left and right sides of the undulator beam axis. At 1.0˚ grazing incidence angle, they intercept up to 11.5 kW of undulator power during user operations and are able to withstand the full beam in case of mis-steering. The XBPM reads out vertical positions using x-ray pinhole camera optics, with a calibration independent of undulator gaps. It derives horizontal beam position from the difference/sum of the x-ray detector signals from the left and right absorbers. Hence the horizontal position calibration depends on the beam sizes, or undulator gaps. To meet the stringent stability requirements, the pinhole camera and detectors are mechanically isolated from the absorbers, and its height above the floor is monitored in real time by a mechanical motion sensor mounted on an Invar rod. External perturbations to the XBPM include: (1) the annual air pressure variation of 0.6% [4], which distorts the XBPM support plate; and (2) the thermal load of the x-ray beam on the XBPM assembly. Table 1 summarizes the ANSYS analyses for the impacts of these external perturbations. We can see that most distortions are within specifications. The thermal-distortion-induced vertical detector position change will be monitored and corrected in real time with the mechanical motion sensor or treated as gap-dependent XBPM offset.

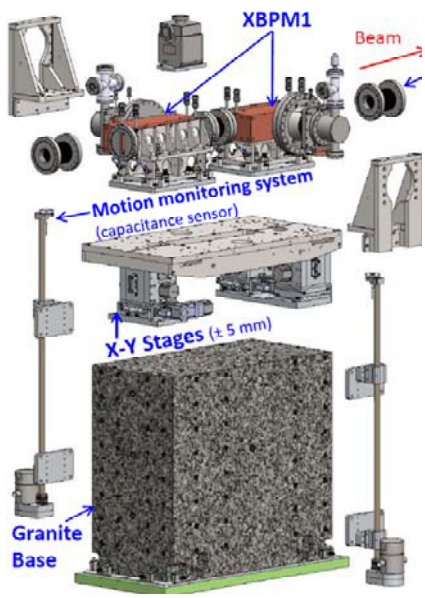


Figure 1: The GRID-XBPM for the APS-U high-heat-load front end.

Copyright © 2013 CC-BY-3.0 and by the respective authors

ISBN 978-3-95450-138-0

NON-INVASIVE BEAM DETECTION IN A HIGH-AVERAGE POWER ELECTRON ACCELERATOR

J. Williams, S. Biedron, J. Harris, J. Martinez, S. V. Milton, J. VanKeuren
Electrical and Computer Engineering, Colorado State University, Fort Collins, Colorado
S. V. Benson, P. Evtushenko, G. R. Neil, S. Zhang
Jefferson National Lab, Newport News, Virginia

Abstract

For a free-electron laser (FEL) to work effectively the electron beam quality must meet exceptional standards. In the case of an FEL operating at infrared wavelengths the critical phase space tends to be in the longitudinal direction. Achieving high enough longitudinal phase space density directly from the electron injector system in an FEL is difficult due to space charge effects, thus one needs to manipulate the longitudinal phase space once the beam energy reaches a sufficiently high value. However, this is fraught with problems. Longitudinal space charge and coherent synchrotron radiation can both disrupt the overall phase space, furthermore, the phase space disruption is exacerbated by the longitudinal phase space manipulation process required to achieve high peak current. To achieve and maintain good FEL performance one needs to investigate the longitudinal emittance and be able to measure it during operation preferably in a non-invasive manner. Using electro-optical (EO) methods, we plan to measure the bunch longitudinal profile of an energy (~120-MeV), high-power (~10kW or more average FEL output power) beam. Such a diagnostic could be critical in efforts to diagnose and help mitigate deleterious beam effects for high output power FELs.

INTRODUCTION

In order to operate an FEL of high quality, an electron beam with high-peak current, low transverse emittance and low energy spread is required. An operational understanding of electron bunch parameters through diagnostics is needed if one wishes to achieve the optimal desired beam qualities. There are a number of diagnostics of both invasive and non-invasive genres used to determine electron bunch parameters. Invasive diagnostics such as transition radiation (CTR) screens placed directly into the beam of electrons are great if one has a low power beam and does not care if operation is momentarily interrupted. Such diagnostics are not suitable for high power operation as they will be destroyed by the beam, or operational monitoring as they severly disrupt the beam properties upon impact with the diagnostic. As an FEL requires high longitudinal phase space density for optimal output, the required manipulations of the electron bunches can lend to undesirable additional effects which need to be monitored in-situ, and, if possible, avoided. One needs a non-invasive longitudinal phase space diagnostic to allow for the achievement and maintenance of the beam properties.

A method to sample the bunch's electric field without prohibitively disrupting the beam is to utilize a crystal with a birefringent property influenced by an electric field, known as the electro-optical (EO) method. This property is caused by the Pockel's effect and the crystal acts as a Pockel's Cell driven by the electric fields of the electron bunches. The different polarizations of light within a pulse traversing the crystal will have altered path lengths created by the birefringence. The altered pulse becomes elliptically polarized in a manner proportional to the influence of induced birefringence. Equation (1) (derived in Jamison, et al. [1]), gives the resultant Fourier transform of the electron beam's Coulomb field with a probing optical pulse, and the resultant inverse transform in Equation (2). The functions *R(t)* and *R(ω)* are the response of the crystal due its nonlinearity and phase matching.

$$E_{out}^{opt}(\omega) = E_{in}^{opt}(\omega) + i\omega E_{in}^{opt}(\omega) * [E^{Coul}(\omega)R(\omega)], \quad (1)$$

$$E_{out}^{opt}(t) = E_{in}^{opt}(t) + a[E^{Coul}(t) * R(t)]\frac{d}{dt}E_{in}^{opt}(t). \quad (2)$$

The Coulomb field becomes encoded in the optical pulse to later be processed in order to determine the longitudinal bunch profile.

For a relativistic electron, the radial Coulomb field is oriented perpendicular to propagation with an opening angle $\propto 1/\gamma^2$, where γ is the relativistic Lorentz factor. The strength of the field is a function of electron bunch distance, b, from the crystal as found in Eqn (3) below. This field is found to have an effect similar to radiation in the Terahertz region of the electromagnetic spectrum (~100-900μm wavelengths) [2]. Placing the desired (EO) crystal near the longitudinally propagating bunch charge encodes the electric field information in the crystal without directly altering the bunch. The induced birefringence is probed and encoded within an optical pulse incident normally on the crystal.

$$E_{y=b} = \frac{e}{4\pi\varepsilon_0}\frac{\gamma b}{(b^2+\gamma^2 z^2)^{3/2}} \quad (3)$$

The facilities where EO diagnostics have been implemented are in contrast to the CSU and JLab accelerators, typically feature beamline parameters with short bunches, low average power and high electron beam energies. As an example, one facility that has employed an EOS diagnostic is FERMI@Elettra [3], which features a bunch length of ~.54 ps FWHM, operational beam

Copyright © 2013 CC-BY-3.0 and by the respective authors

ISBN 978-3-95450-138-0

INVESTIGATION OF UPSTREAM TRANSIENT WAKEFIELDS DUE TO COHERENT SYNCHROTRON RADIATION IN BUNCH COMPRESSION CHICANES

Chad Mitchell* and Ji Qiang, LBNL, Berkeley, CA 94720, USA

Abstract

The longitudinal wakefield due to coherent synchrotron radiation (CSR) in the bending magnets of bunch compression chicanes can significantly impact the beam quality in high-brightness FEL light-sources. In addition to single-bend CSR effects, transient radiation that is generated within a bend can follow the electron bunch downstream through one or more lattice elements before interacting with the bunch. An analytical 1-D model is used to estimate the size of these upstream wakefields in the absence of vacuum chamber shielding, and an FFT-based, integrated Green function method for computing these wakefields has been implemented in the code IMPACT to investigate their dynamical effects in the second bunch compressor of a Next Generation Light Source.

INTRODUCTION

The bend-induced collective interaction due to CSR in bunch compression chicanes can pose a significant challenge in the design of FEL light sources, producing transverse emittance growth and increased energy spread in the beam delivery system that can result in decreased quality of the resulting FEL radiation. A variety of 1-D wakefield models of CSR have been developed to study these effects [1]-[3], and the primary difference between these models lies in the approximations made regarding the history of the particles over the transit time of the radiation.

The model described in [2] includes transient radiation due to bend entry and exit by assuming that all particles that lie upstream of the nearest dipole at their retarded times lie within an infinitely long drift space. By contrast, the model described in [3] makes use of more detailed information about the upstream lattice. As a result, it also includes radiation that has been emitted within upstream bending elements. This paper investigates the size of these upstream transient effects for chicanes of practical interest.

ANALYTICAL AND NUMERICAL MODELS

For a bunch with a longitudinal density profile λ, the longitudinal CSR wakefield in units of energy loss per unit length takes the form:

$$W(z,s) = \int_{-\infty}^{z} \lambda(z') K_{CSR}(z+s, z'+s) dz', \qquad (1)$$

where K_{CSR} is determined from the Liénard-Wiechert electric field of a point charge and the layout of the lattice [3], z is the longitudinal bunch coordinate, and s is a parameter that specifies the location of the bunch centroid within the lattice. The function K_{CSR} varies on a scale $\sim R/\gamma^3$ that can be many orders of magnitude shorter than the bunch length. One method for evaluating the integral (1) numerically given the density $\lambda(z_j)$ at a collection of longitudinal locations $z_j = z_0 + jh$, $(j = 0, \ldots, n)$ is to represent the density by an interpolating polynomial and to evaluate the integral analytically over each subinterval [4, 5]. For the case of piecewise constant interpolation, the result can be written in the form:

$$W(z_k, s) = \sum_{j=0}^{k} \lambda(z_j) w_{igf}^{k,j}(s), \qquad (2)$$

where for terms with $0 < j < k$,

$$w_{igf}^{k,j}(s) = \qquad (3)$$
$$I_{CSR}\left(z_k + s, z_j - \frac{h}{2} + s\right) - I_{CSR}\left(z_k, z_j + \frac{h}{2} + s\right),$$

and

$$I_{CSR}(s, s') = -\int_{-\infty}^{s'} K_{CSR}(s, s'') ds''. \qquad (4)$$

An explicit expression for I_{CSR} in the case of small bending angles and high energy for an arbitrary lattice consisting of circular arcs (bends) and drifts can be found in [3].

Implementation in IMPACT

The IMPACT code is a parallel particle-in-cell code suite for modeling high intensity, high brightness beams in rf proton linacs, electron linacs and photoinjectors [6]. The model for upstream radiation in equations (2-4) was implemented in IMPACT-Z using an FFT-based, integrated Green function algorithm [4, 5]. This feature provides a fast capability for computing the free-space 1D wakefield due to CSR in an arbitrary lattice consisting of bends and drifts.

To use this feature, an additional input parameter is required for the specification of each dipole and drift element in the IMPACT-Z input file. This parameter specifies the number of upstream elements whose CSR contribution is to be included in the wakefield calculation within that element. In order to provide consistency with the model of [2], it is assumed that the farthest upstream element used in the CSR calculation is an infinitely long drift space.

Upstream Radiation Effects

Consider a 4-bend magnetic chicane whose bends will be denoted as Bend $1, \ldots, 4$, moving downstream from the chicane entry. In this section, we will examine the CSR

* ChadMitchell@lbl.gov

ISBN 978-3-95450-138-0

Copyright © 2013 CC-BY-3.0 and by the respective authors

HIGH-GRADIENT METALLIC PHOTONIC BAND-GAP (PBG) STRUCTURE BREAKDOWN TESTING AT 17 GHz*

B.J. Munroe†, M.A. Shapiro, R.J. Temkin, MIT PSFC, Cambridge, MA 02139, USA

Abstract

Photonic Band-gap (PBG) structures continue to be a promising area of research for future accelerator structures. Previous experiments at X-Band have demonstrated that PBG structures can operate at high gradient and low breakdown probability, provided that pulsed heating is controlled. A metallic single-cell standing-wave structure has been constructed at MIT to investigate breakdown performance of PBG structures with very high surface temperature rise. The MIT standing-wave structure test stand has an available power of 4 MW for a maximum gradient of 130 MV/m; the actual realized gradient may be lower due to breakdown limitations. The MIT test stand will also utilize novel diagnostics, including fast camera imaging and optical spectroscopy of breakdowns.

INTRODUCTION

Photonic band-gap (PBG) structures, which use a lattice of metallic or dielectric rods to confine an accelerator mode while damping higher-order modes (HOMs), are a topic of ongoing experimental and theoretical work [1, 2, 3, 4]. Previous experimental work has demonstrated successful acceleration using a traveling-wave PBG structure [1] as well as suppression of wakefields [4, 5]. More recent work by MIT and SLAC National Accelerator Lab has shown that metallic PBG structures can operate at high gradient and low breakdown probability, achieving gradients of greater than 100 MV/m with a breakdown probability of less than 10^{-3} per pulse per meter of structure [6]. To expand on this X-band (11.4 GHz) testing a metallic PBG structure has been designed for testing at Ku-band (17.1 GHz). This metallic structure will be used to further investigate the role of pulsed heating on breakdown probability.

STRUCTURE DESIGN

The metallic PBG structure designed for high-gradient testing at MIT is designed as a scaled version of the round-rod PBG structure previously tested at SLAC and reported in [3]. The structure is axially powered via a scaled version of the SLAC $TM_{0,1}$ mode launcher. The PBG lattice has a filling factor, i.e. the ratio between the rod radius to the rod spacing, of $a/b = 0.18$, the same as the X-band structure. The high-field irises on either side of the PBG cell have an aperture of 0.216λ and a thickness of 0.176λ, again in agreement with the X-band structure. The main variation in structure design is that the Ku-band PBG cell has three rows of round rods, as opposed to the X-band structure's two, which is required by the Ku-band structure's open outer wall, as seen in Fig. 1. This open wall allows a direct line of sight to the high-field surface of the inner rods, allowing significantly greater diagnostic access to the structure during testing.

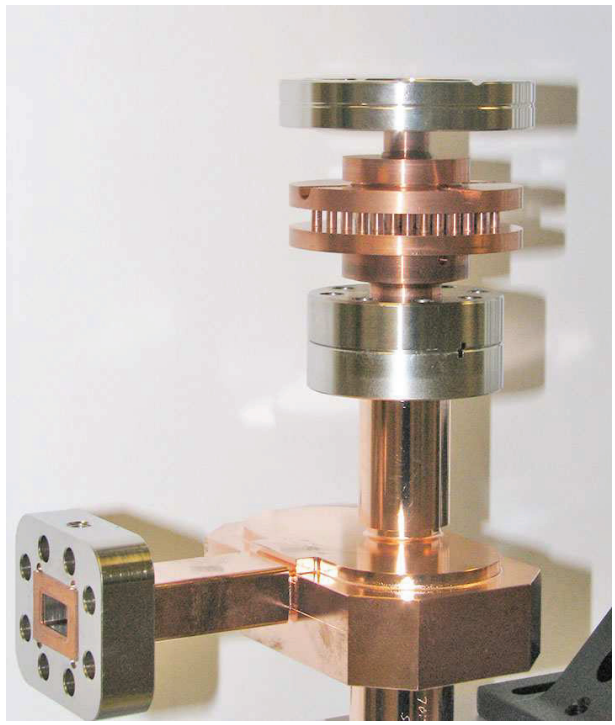


Figure 1: Metallic PBG structure and $TM_{0,1}$ mode launcher at MIT prior to structure brazing. Note the open outer wall of the PBG cell.

This structure will investigate the frequency scaling of breakdown behavior first observed in the testing of the PBG structure at X-band at SLAC, namely the effect of high surface magnetic fields on breakdown probability. To provide an accurate comparison the structure needs to be exposed, as limited by the breakdown probability, to gradients greater than 100 MV/m. The metallic PBG structure is expected to achieve 100 MV/m gradient at 2.4 MW of input rf power, as shown in Table 1. Note that the pulsed heating for this structure is higher than the X-band structure because of the increase in both the surface resistivity of copper and the power density with frequency. This power level is well below the approximately 4 MW of rf power available at the MIT test stand. The advanced optical diagnostics available at MIT combined with testing the structure at very high gradient should provide insight into how the structure fails and criteria for evaluating structure condition during testing.

* This work supported by Department of Energy High Energy Physics, Grant No. DE-SC0010075

† bmunroe@mit.edu

Copyright © 2013 CC-BY-3.0 and by the respective authors

FIRST CAVITY RESULTS FROM THE CORNELL SRF GROUP'S Nb_3Sn PROGRAM*

S. Posen† and M. Liepe
Cornell Laboratory for Accelerator-Based Sciences and Education, Ithaca, NY

Abstract

Breakthrough performance levels were achieved for a 1.3 GHz single cell cavity that was fabricated, coated with Nb_3Sn, and tested at Cornell. Unlike previous Nb_3Sn cavities, this cavity showed minimal R_s-increase up to medium fields. This disproves speculation that the R_s-increase in previous cavities was caused by vortex dissipation for $B > B_{c1}$, as surface fields far higher than the measured B_{c1} for this cavity were reached. At 2 K, quench occurred at ∼55 mT, apparently due to a defect, so additional treatment may increase the maximum gradient to even higher fields. At 4.2 K, at ∼12 MV/m, the cavity achieved Q_0∼1×10^{10}, approximately 20 times higher than niobium at this temperature. This makes it the first accelerator cavity made with an alternative superconductor to far outperform niobium at useable gradients.

INTRODUCTION

Superconducting Radio-Frequency (SRF) researchers have been highly effective at finding preparation methods that suppress performance-limiting effects in niobium particle accelerator cavities. Now cavities are regularly produced that operate very close to the fundamental limits of niobium: they have surface resistances R_s close to the ideal BCS value at operating temperatures, and they reach maximum surface magnetic fields close to the superheating field B_{sh}. To keep up with continually increasing demands of future SRF facilities, researchers have begun a significant effort to develop alternative materials to niobium, materials with smaller R_s and/or larger predicted B_{sh}.

Nb_3Sn is one of the most promising alternative SRF materials. Because it has a high critical temperature T_c of ∼18 K, compared to 9.2 K for niobium, its R_{BCS} at a given temperature is much smaller. This makes the material ideal for continuous wave (CW) linacs: benefits include a smaller and simpler cryogenic plant, the possibility of 4.2 K operation (no superfluid; atmospheric operation), and higher cost-optimum accelerating gradients in CW operation. Its predicted B_{sh} is nearly twice that of Nb, up to ∼400 mT depending on the material parameters used for the calculation. This makes the material ideal also for high energy linacs: it would allow Nb_3Sn cavities to operate at higher accelerating gradients than Nb cavities, and therefore fewer cavities would be required.

In the seventies, Siemens AG developed a method to fabricate Nb_3Sn coatings via vapor diffusion, which produced excellent RF results [1]. The University of Wuppertal applied this coating mechanism to particle accelerator cavities, achieving very small R_s at low fields, but their cavities showed a strong increase in surface resistance with increasing field (this effect is called Q-slope, for the shape of the graph of quality factor Q versus accelerating gradient E_{acc}). The Q_0 vs E_{acc} curve of one of the best cavities produced by University of Wuppertal and tested at JLab is shown in Fig. 1 [2].

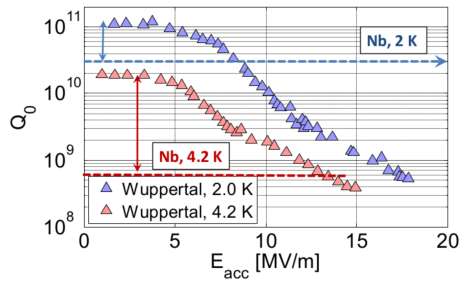


Figure 1: Q vs E curves at 2 K and 4.2 K for one of the best Nb_3Sn cavities produced by U. Wuppertal [2]. The approximate values for a Nb cavity are shown for comparison.

Various causes for the Q-slope were suggested, such as intergrain losses, imperfect stoichiometry [3], and dissipation due to vortex penetration beginning at the lower critical field B_{c1} [4]. As a result, it has been unclear whether or not this Q-slope behavior is fundamental to Nb_3Sn. In a recent historical review, Kneisel called finding the answer to this question and determining the origin of the Q-slope "the next important steps" for Nb_3Sn [5]. More importantly, if vortex penetration at B_{c1} were unavoidable, then bulk alternative SRF materials in general—which tend to have relatively small B_{c1} values—would be severely limited in the fields they could reach without strong dissipation. There is an energy barrier to vortex penetration, which for an ideal surface prevents strong vortex dissipation up to the superheating field B_{sh} [6], but small defects with size on the order of the coherence length ξ can decrease it. Other alternative materials also tend to have relatively small ξ, so the possiblity of vortex penetration above B_{c1} has been a serious concern.

Cornell University is now leading the program for new R&D efforts on Nb_3Sn SRF cavities. In 2009, Nb_3Sn development at Cornell began with the design, fabrication, and commissioning of a small coating chamber for samples. After establishing the capability to repeatably produce Nb_3Sn films of sufficiently high quality for cavity RF surfaces [7], Cornell researchers began work on a large coating chamber for single cell 1.3 GHz cavities, shown in

* Work supported by NSF Career award PHY-0841213, DOE award ER41628, and the Alfred P. Sloan Foundation.
† sep93@cornell.edu

Copyright © 2013 CC-BY-3.0 and by the respective authors

ISBN 978-3-95450-138-0

DEVELOPMENT OF Yb LASER FOR HIGH POWER ULTRA-SHORT PULSE*

Y. Matsumura†, K. Koyama, M. Uesaka,
The University of Tokyo, Bunkyo-ku, Tokyo, JAPAN
M. Yoshida, X. Zhou,
High Energy Accelerator Research Organization, Tsukuba, Ibaraki, Japan

Abstract

Ytterbium (Yb) lasers have good thermal and optical properties. The Yb lasers can be pumped by laser diodes. The oscillation wavelength is near the excitation wavelength. Yb can be highly doped in YAG crystal, so Yb-doped crystal has large gain even if the crystal is thin. These properties are advantages for high power operation. Additionally, because of broad emission spectrum of Yb, the passively mode-locked Yb lasers can easily generate femtosecond pulse at high repetition rate. The Yb lasers have been applied to many fields such as optical frequency comb and X-ray generation. Now, femtosecond pulse of much higher energy at high repetition rate is being required for dielectric laser accelerator (DLA) and lasertron. We have developed high power mode-locked Yb laser, and aim to generate 500 fs pulse of 500 W average power at 50 Hz. In this research, e acheived 20 W mode-locked Yb fiber laser amplification system at 1MHz. We report this achievement and the structure of our Yb laser system to achieve our final goal.

INTRODUCTION

Passively mode-locked lasers can easily generate femtosecond pulse at high repetition rate. The femtosecond pulses have been used in many scientific fields. In the accelerator field, femtosecond pulse of much higher energy at high repetition rate is required for new acceleration technologies such as DLA [1], lasertron [2] and laser wakefield plasma acceleration.

Yb lasers have many advantages for high power operation. Yb can be pumped directly by laser diodes (LD), which can convert electricity into light with as high efficiency as 60 percent. Since the difference between the oscillation wavelength and the excitation wavelength is as low as 90 nm, the quantum efficiency of Yb is very high. Furthermore, Yb can be doped in YAG crystal with high concentration, which enables thin disk lasers. The large surface to volume ratio of the thin disk enables efficient heat removal from the laser material and decreases the wavefront distortion due to the thermal lens effect.

Although the Ti:Sapphire lasers excel at less than 100 fs pulse generation, the Yb lasers have advantages over the Ti:Sapphire lasers when we need several hundreds fs pulse generation for high power operation.

* Work partly supported by KAKENHI, Grants-in-Aid for Scientific Research(C)24510120

† matsumura@nuclear.jp

In this research, we have developed a high power mode-locked Yb laser, and are aiming to generate 500 fs pulse with 500 W average power at 50 Hz for the new acceleration applications.

CPA SYSTEM OF YB LASER

To achieve the generation of 500 fs pulse of 500 W average power at 50 Hz, CPA was adopted. The schematic layout of the Yb laser is shown in Fig. 1. For amplification, Yb fiber and Yb:YAG lasers were used. The Yb fiber lasers have higher gain than the Yb solid lasers, and fibers can be cooled sufficiently by air. However, LDs for fiber lasers cost more than those for solid lasers, and power scaling cannot be applied for the fiber lasers. Additionally, the fiber lasers can't amplify high intensity pulse because of its damage threshold. For these reasons, the Yb fiber amplifiers were adopted at the first half part, while the Yb:YAG amplifiers were adopted at the second half part.

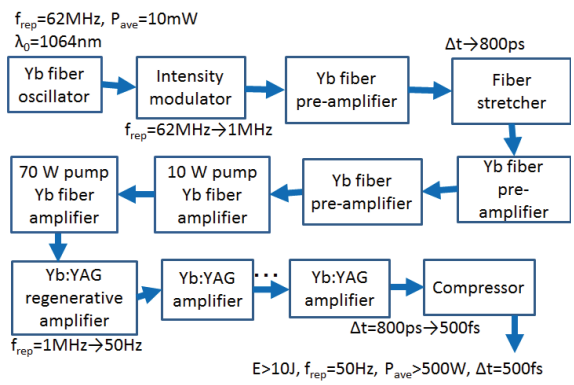


Figure 1: Schematic layout of Yb CPA system.

The ultra-short pulse at 62 MHz was emitted from a Yb fiber oscillator. After that, the pulse was picked up from the pulse train by an electro-optical (EO) module. The repetition rate was reduced from 62 MHz to 1 MHz. Then, the pulse was stretched to 800 ps by a fiber Bragg grating (FBG) stretcher. Through these fiber modules, the power of the pulse decreased. Therefore, three small Yb fiber pre-amplifiers were equipped. These pre-amplifications were needed to suppress amplified spontaneous emission (ASE) at the next amplifiers. After the three pre-amplifiers, the pulse was amplified up to several μJ by two Yb fiber amplifiers pumped by 10 W and 70 W LDs. Next amplifications are done by Yb:YAG lasers. A regenerative amplifier reduces repetition rate from 1 MHz to 50 Hz while amplifying the pulse. Finally, the pulse is amplified up to 10 J by

Copyright © 2013 CC-BY-3.0 and by the respective authors

ISBN 978-3-95450-138-0

BELLA LASER AND OPERATIONS*

W.P. Leemans, J. Daniels, A. Deshmukh, A.J. Gonsalves, A. Magana, H.S. Mao, D.E. Mittelberger, K. Nakamura, J.R. Riley, D. Syversrud, C. Toth, N. Ybarrolaza, LBNL, Berkeley, CA 94720, USA

Abstract

The BELLA laser system is the first high repetition rate petawatt class laser in the world. The laser was acquired from THALES to allow laser plasma acceleration (LPA) experiments that aim at exploring the physics of linear and non-linear interactions of intense lasers with plasmas towards the development of a 10 GeV module. Here we present details of the operation of the BELLA laser and beam line systems, including the control and data acquisition system.

INTRODUCTION

Laser plasma accelerators (LPA) [1] have the potential to drastically cut the cost of doing science with accelerators due to their much reduced size compared to conventional accelerators of the same energy. While it could be decades before a laser plasma accelerator can match or exceed the capabilities of something like the proposed International Linear Collider—a 25 miles (40 kilometers) long machine that would produce electrons and positrons at extremely high energies (0.5 TeV center of mass), straw man designs [2] and more detailed physics studies are underway to explore the possibility of LPA technology towards a linear collider [3,4]. In recent years, LPAs have made significant progress towards producing high quality beams with ever higher energy. In 2004, three independent groups showed the first demonstration of relatively narrow energy spread electron beams at the ~ 100 MeV level from mm-scale devices [5-7]. In 2006 the first production was shown of GeV electron beams from a 3 cm long plasma channel guided LPA at LBNL [8] and in 2011 a novel method for controlling injection via longitudinal tailored density profiles was demonstrated [9]. In the 2006 experiments, the laser peak power was of the order of 40 TW and the operating plasma density was a factor of ~10 lower but extended over a ~10 times longer distance than in the 2004 experiments. Motivated by the success of these experiments, designs were developed at LBNL to achieve 10 GeV electron beams from meter-scale accelerator structures using a PW-class laser system, which led to the formal BELLA (BErkeley Lab Laser Accelerator) project proposal to the Department of Energy, Office of High Energy Physics in 2007. BELLA represents an essential step towards investigating how more powerful accelerators of the future might be more compact. The initial experiments with the BELLA laser system and facility are aimed at demonstrating that high quality 10 GeV electron beams can be generated using a laser powered plasma structure that is about 1 meter long. The research supported by BELLA will also investigate fundamental laser-plasma interaction physics that aims at optimizing the coupling efficiency of laser to electron beam energy, controlling both the energy spread and emittance of the electron beams, and staging multiple LPA modules together. The 10 GeV beams could also be used to study beam driven plasma wakefield acceleration, as well as positron production and subsequent acceleration in plasma based accelerators. Although its main purpose is accelerator research, the development of a compact 10 GeV accelerator has several potential applications. BELLA could be used to build a free-electron laser (FEL) operating in the soft x-ray window that produces few femtosecond radiation pulses that are intrinsically synchronized to laser pulses, to THz radiation pulses or directly to the electron beam. Such a device could be an extraordinarily valuable tool for biologists, chemists, materials scientists, and biomedical researchers, allowing them to observe ultrashort, nanoscale phenomena.

We will next discuss the performance of the BELLA laser. As the key physics in the LPA studies are primarily dependent on laser intensity, the key parameters are laser pulse energy, pulse duration, laser beam profile and their stability. From an operational point-of-view, pointing stability is also essential. We also will introduce the BELLA control system, which is used for both control of all experimental subsystems and data acquisition. Details will be presented elsewhere.

BELLA PROJECT

The project phase of BELLA consisted of the construction and commissioning of a PW-class laser that supports the research aimed at the development of 10 GeV LPA modules. The project was formally launched in October 2007 and funded in 2009. The scope of the BELLA project included the design and construction of the conventional facilities required to house and safely operate the BELLA laser, the acquisition of the BELLA laser system itself, design and construction of ancillary systems to support the laser operations, site and system integration, and performance verification of the BELLA laser system.

The BELLA facility has been fully designed to achieve all key performance parameters of the laser system and future experimental systems. This includes clean-room (class 10,000 and 1,000) areas for the laser and experimental areas, with gowning area, assembly area and tightly controlled environmental conditions to minimize temperature and humidity effects as well as low vibration

*Work supported by DOE, Office of High Energy Physics and NSF

ISBN 978-3-95450-138-0

Copyright © 2013 CC-BY-3.0 and by the respective authors

LATEST PLASMA WAKEFIELD ACCELERATION RESULTS FROM THE FACET PROJECT *

M. D. Litos†, E. Adli‡, C. I. Clarke, S. Corde, J. P. Delahaye, R. J. England, A. S. Fisher, J. Frederico, S. Gessner, M. J. Hogan, S. Li, D. Walz, G. White, Z. Wu, V. Yakimenko
SLAC National Accelerator Laboratory, Menlo Park, California 94025, USA
‡ Department of Physics, University of Oslo, 0316 Oslo, Norway

W. An, C. E. Clayton, C. Joshi, W. Lu, K. A. Marsh, W. B. Mori, N. Vafaei-Najafabadi
University of California Los Angeles, Los Angeles, CA 90095, USA

P. Muggli
Max Planck Institute for Physics, Munich, Germany

Abstract

SLAC's new Facility for Advanced Accelerator Experimental Tests (FACET) had its second user run in April–June, 2013. Several new milestones were reached during this run, including the achievement of beam driven plasma wakefield acceleration of a discrete witness bunch for the first time, and energy doubling in a noble gas plasma source. The FACET beam is a 20 GeV electron bunch with a charge of 3.2 nC that can be compressed and focused to a size of 20 μm × 20 μm × 20 μm rms. To create the two-bunch, drive/witness beam structure, a chirped and over-compressed beam was dispersed horizontally in a chicane and a bite was taken from its middle with a tantalum finger collimator, corresponding to a longitudinal notching of the beam due to the head-tail energy correlation. A new 10 terawatt Ti:Sapphire laser was commissioned and used during this run to pre-ionize the plasma source in order to increase the efficiency of energy transfer from the beam to the wake. Ultimately, a witness beam of hundreds of pC in charge was accelerated by a drive beam of similar charge in a preformed lithium plasma with a density of $5 \times 10^{16}\,\mathrm{cm}^{-3}$, experiencing gradients reaching several GV/m in magnitude.

INTRODUCTION

The field of plasma wakefield acceleration (PWFA) has long been motivated by a need for new technologies that can provide higher accelerating gradients than conventional microwave powered metallic structures in order to make multi-TeV energies and beyond accessible to future generations of linear colliders. A conceptual design was recently developed for a plasma wakefield powered linear collider with a center of mass energy of 1 TeV that is extendible to the multi-TeV regime [1]. The main linac consists of modular plasma accelerator stages into each of which a fresh electron beam is injected to drive a wake over a meter-scale plasma source to provide an energy gain of 25 GeV per stage to the primary collider beam. Besides the high average gradient of such a collider design, the wall-plug efficiency is another very attractive feature, estimated to be well over ten percent. Current research efforts in beam driven plasma wakefield acceleration are largely devoted to creating a single plasma accelerator stage akin to what would be used in a collider, first as a proof-of-concept, and then as a test bed for studying the complex dynamics involved in the beam-plasma interaction.

In order to achieve accelerating gradients on the order of 10 GV/m with a GeV-scale drive beam, plasma densities on the order of $10^{17}\,\mathrm{cm}^{-3}$ are required. This sets the plasma wavelength, and thus the scale of the longitudinal spacing between the drive and witness bunch, to distances on the order of 150 μm (=500 fs temporal spacing). The drive beam must have a density that is > 1.8 times the background plasma density in order to produce a nonlinear blowout [2], which sets the scale for the peak current to the kA scale with a transverse size on the order of a few tens of microns, which is ultimately focused down to several microns by the strong fields generated in the plasma. FACET is the only facility in the world that can meet these demanding beam requirements, as well as produce a witness beam of several hundred pC or more to sample the large magnitude fields.

Previous electron-beam-driven plasma wakefield acceleration experiments that were performed at SLAC's Final Focus Test Beam (FFTB) facility have shown that the PWFA mechanism can produce accelerating gradients in excess of 50 GV/m by observing the energy gain in the low charge tail of the wake-driving electron beam. The tail trailing behind the head of the beam sampled the accelerating phase of the plasma wake, finally doubling the energy of the 42 GeV electrons [3]. What remained to be demonstrated, however, was the acceleration of a coherent beam of electrons, rather than individual particles. FFTB lacked the capability to produce a distinct drive and witness electron beam with the required temporal spacing, on the order of 500 fs from center to center. Several years after the FFTB was decommissioned, FACET was designed and constructed with this goal in mind, leveraging the knowledge gained from the FFTB experiments and the linac infrastructure available at SLAC [4]. Now, FACET has finally been able to fulfill the experimental requirements needed to study the acceleration of actual beams via

* Work supported by DOE contracts DE-AC02-76SF00515, DE-AC02-7600515, DE-FG02-92-ER40727, and NSF contract PHY-0936266.
† litos@slac.stanford.edu

ISBN 978-3-95450-138-0

Copyright © 2013 CC-BY-3.0 and by the respective authors

X-RAY RADIATION AND ELECTRON INJECTION FROM BEAM ENVELOPE OSCILLATIONS IN PLASMA WAKEFIELD ACCELERATOR EXPERIMENTS AT FACET

K. A. Marsh, W. An, C. E. Clayton, C. Joshi, W. B. Mori, N. Vafaei-Najafabadi (UCLA, Los Angeles, California, USA), P. Muggli (MPI, Munich, Germany), C. I. Clarke, S. Corde, J-P. Delahaye, R. J. England, A. S. Fisher, J. Frederico, S. J. Gessner, M. J. Hogan, S. Z. Li, M. D. Litos, D. Walz, Z. Wu (SLAC National Accelerator Laboratory, Menlo Park, California, USA), E. Adli (SLAC National Accelerator Laboratory, Menlo Park, California USA; University of Oslo, Oslo, Norway), Wei Lu (UCLA, Los Angeles, California, USA; Tsinghua University, Beijing, China)

Abstract

Plasma wakefield accelerator experiments at FACET at the SLAC National Accelerator Laboratory have shown a correlation between ionization-injected electrons and the betatron x-ray yield. Emittance spoiling foils were inserted into the beam and the x-ray yield, excess charge, and beam energy loss was measured. The excess charge and x-ray yield are attributed to the beam envelope oscillations where at the minima, the field of the beam is strong enough to create secondary ionization, and at the electron oscillation maxima, the beam electrons spontaneously radiate x-rays. Large amplitude beam oscillations are expected to yield more x-rays and create more excess charge, but the results show beam head erosion strongly limits the wakefield excitation.

INTRODUCTION

An important feature of any "blow out regime" plasma-based accelerator is the strong radial fields of the ion column, which creates electron betatron motion and x-ray radiation. This effect can be used to create MeV photons [1] and the x-ray characteristics can be used as a diagnostic of the electrons transverse motion. For example, matched beam propagation would be characterized by minimizing the x-ray radiation signal. Also, mismatched beams will collapse in size to where secondary ionization produces excess charge (i.e. dark current) [2]. Larger emittance beams have larger oscillation amplitudes and therefore they are expected to produce more x-rays and more excess charge. However, large emittance beams also have shorter head erosion lengths [3], which limits the distance over which x-rays and excess charge can be generated. In this paper we study experimentally which of these factors prevail.

SETUP

The experiments were performed at FACET at the SLAC National Accelerator Laboratory during the 2013 E200 PWFA experimental run. The 20.3 GeV electron bunch contained 2.0×10^{10} electrons with an rms bunch length of ~40 um. The x and y normalized emittances, ε_N, were designed to be 50 and 5 mm-mrad, respectively. Typically, the beam betas where 0.10 meter in x and 1.0 meter in y, giving a spot size at the plasma entrance of 11 μm in x and y. The beam was sent through a ~30 cm long rubidium heat pipe oven where the plasma was formed by the field of the beam via tunneling ionization. The Rb vapor was contained using argon as a buffer. The primary diagnostic measurements discussed here are: the x-ray radiation, beam charge, and beam energy. The x-ray yield was measured with a Lanex screen and CCD camera. A 1 mm thick Tungsten foil was placed in front of the screen, which gives a photon detection threshold of 200- 300 keV. SLAC toriods were used to measure the beam charge upstream and downstream of the plasma. The excess charge was measured using the difference between the toriod signals. The change in beam energy was measured with an imaging dipole spectrometer. To study emittance effects, emitttance spoiler foils were inserted into the beam 1 meter upstream of the plasma entrance. The foils and thickness used in the experiment were: Foil 1 Nicusil 3, 25.4 μm; Foil 2 25/75Au/Cu, 50.8 μm; and Foil 3 Nocoro, 80, 38 μm. The calculated rms scattering angles are 35, 58, and 64 μrad respectively. A figure showing the set up and the data analysis and methods can be can be found in [4, 5].

DENSITY RAMPS AND BEAM MATCHING

For a plasma with a sharp boundary, the beam matching condition is $\beta_{match} = 1/k_b$, where k_b is the plasma betatron wavenumber (Eqn. 2). For our experimental parameters, $\beta_{match} = 0.3$ cm. Beam matching on this scale is difficult to produce, but as shown in [1, 6] a density ramp can significantly reduce the oscillation amplitude of an unmatched beam, thereby reducing the expected x-ray yield. For the right beam parameters, the ramp can be used to produce matched beam propagation. A larger β can be used in proportion to the scale length of the ramp. For the plasma ramp at FACET, the matched β is 3.38 cm.

*The work at UCLA was supported by DOE grant DE-FG02-92-ER40727 and NSF grant PHY-0936266. Work at SLAC was supported in part by Department of Energy contract DE-AC02-7600515

ISBN 978-3-95450-138-0

Copyright © 2013 CC-BY-3.0 and by the respective authors

EXPERIMENTAL PROGRESS ON STAGED LASER-PLASMA ACCELERATION*

S. Shiraishi†, T. Sokollik‡, C. Benedetti, A. J. Gonsalves, N. H. Matlis, K. Nakamura, B. H. Shaw, S. Steinke, J. van Tilborg, C. G. R. Geddes, C. B. Schroeder, Cs. Tóth, E. Esarey, and W. P. Leemans
LOASIS Program, LBNL, Berkeley, CA 94720, USA

Abstract

Recent progress on a staged laser-plasma accelerator (LPA) experiment is reported. The experiment utilizes a 40 TW class laser which is split into two pulses. The first laser drives the first LPA stage to produce an electron beam. The second laser drives the second LPA stage in a dark-current free regime and accelerates the electron beam from the first LPA. Injection from the first stage, triggering of plasma mirror and reflection of the second laser, and laser guiding in the second stage have been demonstrated. Optical spectral redshift of driving laser has been analyzed to estimate the wakefield amplitude and electron energy gain in the second stage.

INTRODUCTION

Laser-plasma accelerators (LPAs) have demonstrated accelerating gradients thousands of times greater than those of conventional accelerators [1]. Employing a capillary discharge waveguide, a high-quality GeV electron beam (e-beam) has been produced within a few centimeters, demonstrating that LPAs have great potential for reducing accelerator size and cost.

For applications such as high energy colliders, LPA designs will rely on sequencing multiple acceleration stages, each driven by its own laser [2, 3]. Limitations to the energy gain in a single stage include diffraction, dephasing, and pump depletion. Using a capillary waveguide to create a preformed plasma channel, laser pulses have been guided over many Rayleigh lengths (z_R), minimizing diffraction and extending the accelerating length. If the laser is guided, and the e-beam dephasing controlled, energy gain is limited by depletion. To overcome pump depletion, staged acceleration is necessary to supply fresh laser pulses. Experiments performed so far utilize a single laser that drives the wakefield for both injection and acceleration. The on-going staging experiment at the LOASIS Program at Lawrence Berkeley National Laboratory will demonstrate driving of two modules with two independent laser pulses and coupling of the e-beam between them. Staged acceleration not only supplies fresh laser pulses to LPAs but it also allows independent control of electron injection and acceleration.

Experimental demonstration of staged LPAs requires understanding electron injection, performance of a plasma mirror (PM), and acceleration of externally injected e-beams. Controlled electron injection is an active area of research and various techniques such as self-trapping, density gradient, and ionization injections have been demonstrated [4, 5, 6, 7]. The PM is triggered when the leading edge of the pulse generates plasma on a solid target, reflecting the remainder of the pulse at the critical surface. The second laser pulse is coupled in to the acceleration beam line using the PM to keep the LPA compact [8]. Post-acceleration of e-beams requires understanding the amplitudes of wakefileds in the second stage. Laser spectra are analyzed as a diagnostic of plasma waves.

This paper reports the recent progress of the staged acceleration experiment at the LOASIS Program. Basic theory of laser propagation and redsfhit are presented to support the use of redshift as a wakefield diagnostic. Then, the experimental setup at the LOASIS Program is described. Initial results for electron injection, plasma mirror in-coupling and wake excitation performed independently of each other are presented in the results section followed by a concluding summary.

LASER PROPAGATION IN A PLASMA CHANNEL

Laser guiding is used to extend acceleration lengths in LPAs. However, accelerating fields, and hence redshifting of the laser, evolve differently depending on the guiding condition. In a capillary waveguide, the laser pulse transverse size can oscillate if the density profile is not matched to the laser spot size. The channel is characterized by a parabolic plasma density profile, $n(r) = n_0 + \Delta n r^2/r_\mathrm{m}^2$, where r is the radial position, n_0 is the on-axis density [9], and Δn is the channel depth at a matched spot size, r_m [10]. Such channels can provide guiding for a laser pulse with a Gaussian intensity profile, $|a|^2 = (a_0 r_0/r_\mathrm{s})^2 \exp(-2r^2/r_\mathrm{s}^2)$, where a_0 is the normalized laser vector potential given by $a_0^2 \simeq 7.3 \times 10^{-19}\ (\lambda[\mu\mathrm{m}])^2 I_0[\mathrm{Wcm}^{-2}]$, r_0 is the focal spot size, r_s is the spot size, and λ is the laser wavelength. Perfect guiding is achieved when $r_0 = r_\mathrm{m}$ and the laser is focused at the entrance of the channel ($r_\mathrm{i} = r_0$, $\mathrm{d}r_\mathrm{s}/\mathrm{d}z = 0$). Considering a low power pulse (without self-focusing), the laser pulse propagates in the channel according to

$$r_\mathrm{s}^2 = \frac{r_\mathrm{i}^2}{2}\left[1 + \frac{r_\mathrm{m}^4}{r_\mathrm{i}^4} + \left(1 - \frac{r_\mathrm{m}^4}{r_\mathrm{i}^4}\right)\cos\left(\frac{2\lambda z}{\pi r_\mathrm{m}^2}\right)\right], \quad (1)$$

where r_i is the spot size at the entrance of channel, and z is the propagation distance [10]. Examples of matched and mismatched guiding are shown in Fig. 1. The entrance of the capillary is set at $z = 0$, and the plasma channel is indicated with a cyan box. For matched guiding,

* Supported by DOE HEP, NSF and used the facilities at NERSC.
† Also at University of Chicago, Chicago, Illinois 60637, USA. Email: sshiraishi@lbl.gov
‡ Currently at Shanghai Jiao Tong University, Shanghai, China

Copyright © 2013 CC-BY-3.0 and by the respective authors

GENETIC ALGORITHMS AND THEIR APPLICATIONS IN ACCELERATOR PHYSICS*

A.S. Hofler†, Thomas Jefferson National Accelerator Facility, Newport News, VA 23608, USA

Abstract

Multi-objective optimization techniques are widely used in an extremely broad range of fields. Genetic optimization for multi-objective optimization was introduced in the accelerator community in relatively recent times and quickly spread becoming a fundamental tool in multi-dimensional optimization problems. This discussion introduces the basics of the technique and reviews applications in accelerator problems.

GENETIC ALGORITHM OVERVIEW

Genetic and evolutionary algorithms (GAs and EAs, respectively) are examples of adapting models for processes observed in nature to create novel approaches to solving seemingly unrelated problems. These methods mimic biological reproduction, the theory of evolution, and the behavior of biological populations to solve mathematical optimization problems. Sets of solutions to an optimization problem are considered successively. The solutions from set i that more closely meet the optimization goal(s) are considered fitter, more inclined to survive, and are used to create the next $i+1$ set of solutions. As the selection and reproduction cycle repeats, the solutions produced are refined, and the defining characteristics for the best solutions coalesce to the optimal value(s). While not an immediately obvious method for optimization, GAs and EAs have proven to be highly effective in solving engineering and accelerator physics problems. Two recommended references on GAs, EAs, and optimization in general are [1, 2].

Optimization Problem Statements

Commonly, optimization problems are cast as minimizing or maximizing a cost function, and optionally, the independent variables may be subject to boundary constraints. Real world optimization problems tend to be multi-objective meaning there are multiple cost functions that must be minimized or maximized simultaneously subject to bounds and inequality constraints. Written generally, a multi-dimensional, multi-objective optimization (MOO) problem is

$$\begin{aligned} &\text{Optimize } f_j\left(x_1, x_2, ..., x_N\right) && j = 1, 2, ..., J, \\ &g_k\left(x_1, x_2, ..., x_N\right) \geq 0 && k = 1, 2, ..., K, \\ &x_{\min}^{(n)} \leq x_n \leq x_{\max}^{(n)} && n = 1, 2, ..., N, \end{aligned} \quad (1)$$

where Optimize can be either Minimize or Maximize for each objective function f_j, J is the number of objective functions to be simultaneously optimized, g_k are K inequality constraints, and x_n are the N independent variables to vary subject to a set of bounds constraints, $x_{\min}^{(n)}$ and $x_{\max}^{(n)}$. For a single-objective optimization (SOO), $J = 1$ and $K = 0$. GAs and EAs can be applied to both single- and multi-objective problems.

Solution existence and uniqueness is not guaranteed for SOO and MOO making them difficult to perform, but MOO has the additional complication that the objectives may conflict, meaning a set of independent variables that satisfies one objective goal causes another to move away from its optimal value. An example is minimizing two objective functions that inversely depend on the same independent variable, e.g. $f_1 = x_1$ and $f_2 = x_1^{-1} + x_2$ for $0.5 \leq x_1 \leq 1$ and $0 \leq x_2 \leq 1$. No single combination of x_1 and x_2 clearly minimizes both f_1 and f_2 simultaneously. In contrast, changing the problem to minimize one function and maximize the other creates two different optimization problems where the objectives do not conflict, and fortunately, both problems have unique solutions ($x_1 = 0.5$ and $x_2 = 1$ minimize f_1 to 0.5 and maximize f_2 to 3, while $x_1 = 1$ and $x_2 = 0$ maximize f_1 to 1 and minimize f_2 to 1).

For the simultaneous minimization problem, each possible x_1 value gives an equally valid solution to the minimization problem for $x_2 = 0$. Absent additional information about a preferred solution or system behavior, there is nothing to differentiate any particular solution from the rest in the x_1 interval. For instance, at $x_1 = 0.5$ and $x_2 = 0$, while $f_2 = 2$ is not its minimum value on the x_1 interval, f_1 is minimized to 0.5. This is the best solution for $x_1 = 0.5$ since $f_2 > 2$ for $x_2 > 0$. Similarly, $f_1 = 1$ and $f_2 = 1$ comprise the best solution for $x_1 = 1$. For the remaining values of the x_1 interval with $x_2 = 0$, neither f_1 nor f_2 attains its individual minimum value, but their values are the optimal ones for each fixed value of x_1. These solutions for $0.5 \leq x_1 \leq 1$ and $x_2 = 0$ are equivalent in terms of the optimization goals, and they form the set of solutions to this optimization problem. When objective functions conflict, a series of individual optimizations must be considered and solved, and the set of solutions is called the Pareto optimal front. The Pareto optimal front is important because it elucidates trade-offs between objectives.

Comparison to Standard Techniques

Historically, standard techniques used for multidimensional optimization problems are either iterative derivative-based methods or systematic parameter scans. GAs and

*Authored by JSA, LLC under U.S. DOE Contract DE-AC05-06OR23177. The U.S. Govt. retains a non-exclusive, paid-up, irrevocable, world-wide license to publish or reproduce this for U.S. Govt. purposes.

† hofler@jlab.org

ISBN 978-3-95450-138-0

Copyright © 2013 CC-BY-3.0 and by the respective authors

A SPECIALIZED HIGH-POWER (50 kW) PROTON BEAMLINE FOR BNCT

Morgan P. Dehnel, Thomas M. Stewart, Tue Christensen, David E. Potkins, D-Pace, Inc., PO Box 201, Nelson, BC, Canada
Hirofumi Seki, Shinji Shibuya, Steve Domingo, Glenn James, Pat Creely, Steve Bucci, AccSys Technology, Inc., 1177 Quarry Lane, Pleasanton, CA 94566, USA

Abstract

D-Pace has developed a specialized high-power beamline for transporting a 20 mA, 2.5 MeV, CW proton beam for a Boron Neutron Capture Therapy (BNCT) application. The 2 m horizontal by 4 m vertical layout transports the space-charge dominated beam with less than 1% beam-spill using two sets of 10 T/m quadrupole doublets, DC XY steerer, 90 degree bending magnet, and AC XY magnets for raster-scanned, flat-topped, round or square intensity distributions deposited over targets with 40 – 100 mm maximum dimensions. Diagnostics include New Parametric Current Transformers (NPCT), graphite, water-cooled, electrically-isolated collimators with readbacks, and a low-power sapphire beam profile monitor for macro-pulsed beams (~100 micro-second wide pulses at low frequency). This paper describes the specialized: beam-optics, intensity distributions, and device designs.

INTRODUCTION

BNCT is a non-invasive therapeutic treatment of cancer (high-grade gliomas, cerebral metastases of melanoma; and head, neck, and liver cancer) [1] that involves two steps. First, tumour-localizing non-radioactive boron-10 delivery agents (such as boronophenylalanine i.e. BPA, or sodium borocaptate i.e. BSH) are injected into the patient [1]. Second, the patient is exposed to epithermal neutrons, which have a very high probability of reacting with the concentrated boron-10 residing in the cancer cells. This yields an energetic alpha particle, and a recoiling lithium nucleus which ionize a tremendous number of atoms and molecules within 5-9 microns (~size of cancer cell). This results in cancer cell death [1,2].

BNCT has a 50 year history at research nuclear reactors [3], and is established i.e. 16th International Congress on Neutron Capture Therapy, ICNCT (2014), is to be held in Helsinki. For widespread use of BNCT better delivery agents, improved dosimetry, and independence of nuclear reactors is required [3]. Barth [3], IAEA [4], Blue and Yanch [5] all emphasize the development of particle accelerators for BNCT. Strong growth in BNCT implementation in hospitals is anticipated since it can now be de-coupled from nuclear reactors through low energy (p,n) reactions provided by relatively inexpensive safe compact particle accelerator systems that can be turned off (as compared to a reactor) [6].

This paper describes the High Energy Beam Transport (HEBT) beamline developed for the BNCT treatment system utilizing an AccSys 2.5 MeV, 20 mA, CW proton Linac and the Li-7(p,n)Be-7 reaction.

HEBT BEAMLINE

The 10 rms RFQ beam was modeled thru HEBT (Figure 1) with 1st order Beamline Simulator [7] using acceptances greater than 3x the 10 rms emittances in both transverse phase-planes to define conservative apertures. TRACE-3D [7] simulations confirmed high beam transmission at 20 mA CW space-charge conditions. The finalized system in Figure 2 follows the principles [8-10].

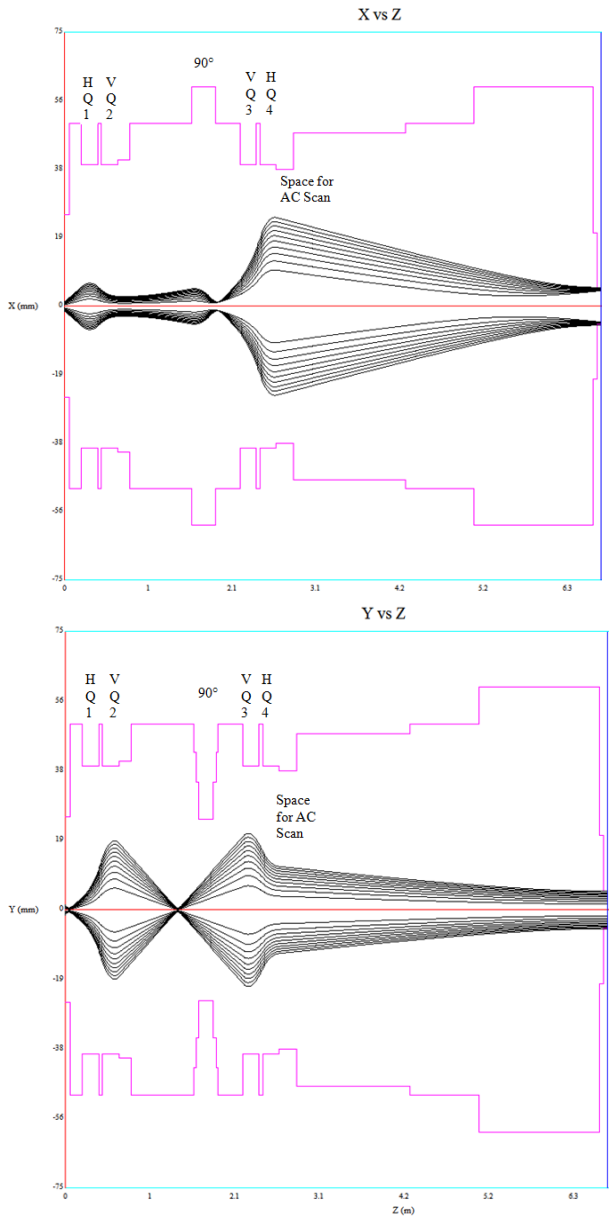


Figure 1: HEBT Horizontal & Vertical 1-10rms Beams.

Copyright © 2013 CC-BY-3.0 and by the respective authors

LARGE MOMENTUM ACCEPTANCE SUPERCONDUCTING NS-FFAG GANTRY FOR CARBON CANCER THERAPY*

Dejan Trbojevic, Brett Parker, BNL, Upton, New York, 11973, USA
Marco Pullia, CNAO, Pavia, Italy

Abstract

Carbon cancer radiation therapy has clear advantages with respect to the other radiation therapy treatments. Cost of the ion cancer facility is dominated by the delivery systems. New superconducting carbon ion gantry designs, based on the Non-Scaling FFAG (NS-FFAG) principle, are presented. The magnet size and weight is dramatically smaller with respect to existing gantries. The weight of the transport elements of the carbon isocentric gantry is estimated to be 1.5 tons to be compared to the 130 tons of the top-notch gantry in the Heidelberg ion therapy facility.

INTRODUCTION

A number of ion cancer therapy facilities are rapidly rising due to a clear advantage to any other radiation treatment of the cancerous tumors. This is due to a very localized energy deposition of ions at the "Bragg peak-as suggested by R. Wilson 1946 [1]. The ion cancer facility starts with an ion source, accelerator, and the delivery system (major cost). The Coulomb scattering and struggling define the final beam spot size–penumbra at the tumor. The best results in the cancer treatment are obtained by use of the spot size "pencil" beams with the transverse and longitudinal scanning technique. Usually the treatment time is of the order of couple of minutes. In proton cancer therapy the minimum beam volume size-voxel at the tumor (for the maximum distance of 27 cm in the patient) is ~715 mm^3, while for carbon ions it is ~14 mm^3. The transverse intrinsic spot for 206 MeV protons is ~11 mm, while for carbon ions is 2.9 mm. Carbon ions have advantage in the patient treatment, as they are more precise. Normal angle of ion arrival to the patient reduces the skin radiation. The Source to Axis Distance (SAD) parameter in the cancer treatment shows an optimum with SAD=∞ (beam arrives with normal angle of incidence to the patient skin).

A recommendation from the Workshop on Ion Therapy [1] in Bethesda MD (organized by Department of Energy (DOE), National Cancer Institute (NCI), National Institute of Health (NIH), and Department of Health & Human Services DHHS) was that the carbon or other ion therapy facility should include rotatable gantry, possibly made of superconducting magnets (to be able to reduce the size and cost) and with a large momentum acceptance.

This is a report on a large momentum acceptance superconducting NS-FFAG gantries. They have many advantages like: reduced size and weight, large momentum acceptance (200-400 MeV or 100-200 MeV/u etc.), fixed magnetic field, with the angle of incidence always normal to the patient (SAD=∞), and easy to operate, as the magnetic field is fixed during the treatment. We present two examples: the isocentric gantry and an eccentric gantry proposed, by Marco Pullia (CNAO-Italy). Both gantries have a large momentum acceptance – for one fixed magnetic field setting they can operate covering a large kinetic energy range (either between 200-400 MeV/u or 100-200 MeV/u). The normal angle of incidence is obtained by use of two scanning dual plane scanning magnets.

NS-FFAG PRINCIPLE

In recent years there has been a clear revival of the previous concept of the FFAG's, developed mostly in the 1950's. A concept of the NS-FFAG is based on strong focusing principle with a small dispersion function. The relationship: $\Delta x = D\ \delta p/p$ shows that the beam offset is small even for the large $\delta p/p$. Major differences between the NS-FFAG's with respect to the scaling FFAG's are variations of the tunes, time of flight, dispersion and amplitude functions with a momentum as shown in a gantry cell in Figure 1.

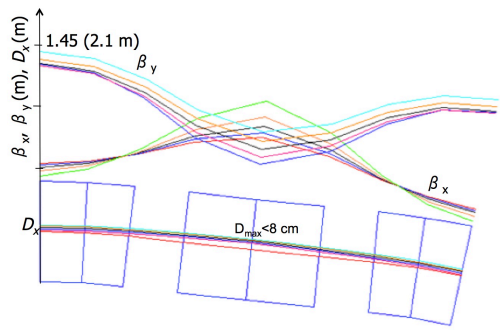


Figure 1: Betatron and dispersion functions in a gantry cell for the treatment energies.

BEAM DELIVERY - ION GANTRIES

The delivery system is the most expensive part of the ion cancer therapy facilities. Figure 2 shows the top-notch proton gantry at PSI in Switzerland. The scanning magnets are placed usually in front of the large 90°-bending magnet above the patient. This is to allow for the SAD=∞. To avoid the large magnet above the patient (for the proton gantries its weights is ~60 tons) a scanning system is placed above the patient. This solution (submitted to the Patent Office) not only removes the necessity of the large magnet but also always provides normal angle of incidence to the patient skin. A proton gantry design is shown in Figure 3.

* Work performed under Contract Number DE-AC02-98CH10886 with the auspices of the US Department of Energy

Copyright © 2013 CC-BY-3.0 and by the respective authors

ISBN 978-3-95450-138-0

CYCLOTRON PRODUCTION OF POSITRON EMITTING RADIOMETALS

S. E. Lapi and T. Voller, Washington University in St. Louis, MO, 63110, USA

Abstract

The increase in use of Positron Emission Tomography (PET) for medical imaging has led to the development of numerous radiopharmaceuticals for use in preclinical and clinical research for oncology, cardiology and neurology [1]. While many of these biological processes can be investigated with probes radiolabeled with the more commonly used positron emitters, ^{18}F ($t_{1/2}$ = 110 min) and ^{11}C ($t_{1/2}$ = 20 min), imaging at longer timepoints requires radionuclides with longer half-lives. Thus, the production and purification of longer-lived position emitting radiometals has been explored to allow for imaging of peptides, antibodies and nanoparticles. This brief review will focus on the production and purification of ^{64}Cu ($t_{1/2}$ = 12.7 h) and ^{89}Zr ($t_{1/2}$ = 3.27 d).

INTRODUCTION

Positron Emission Tomography (PET), with its high sensitivity and resolution, is growing rapidly as an imaging technology for the diagnosis of many disease states. The success of this modality is reliant on the development of effective imaging compounds. Initially, research in this area was focused on the relatively short-lived PET isotopes ^{11}C and ^{18}F, but the short half-lives of these isotopes limit radiopharmaceutical development to those that probe rapid biological processes. To overcome these limitations, there has been a rise in alternative radionuclide tracer development in recent years. Below, in Table 1, are some examples of radiometals for use in nuclear imaging (all data from [2]).

Table 1: Examples of Positron Emitting Radiometals

Isotope	Production Route	Half-Life
^{64}Cu	^{64}Ni(p,n)	12.7 h
^{68}Ga	^{68}Ge Generator	68 min
^{86}Y	^{86}Sr(p,n)	14.7 h
^{89}Zr	^{Nat}Y(p,n)	3.27 d

While ^{68}Ga use has also increased recently, this short review will focus on the cyclotron produced isotopes, namely ^{64}Cu and ^{89}Zr.

Washington University in St. Louis has been producing and distributing longer-lived PET radionuclides to the research community for over 15 years. The radionuclides that have been produced include ^{64}Cu, $^{76/77}$Br, ^{66}Ga, ^{86}Y, ^{124}I, and ^{89}Zr. Presently, ^{64}Cu and ^{89}Zr are produced on a regular basis (weekly and biweekly respectively), while ^{86}Y and ^{76}Br are produced intermittently in lower quantities. The recent increase in production and shipping of ^{64}Cu to external institutions is illustrated in Figure 1 and is mainly due to the increase in clinical trials with this isotope.

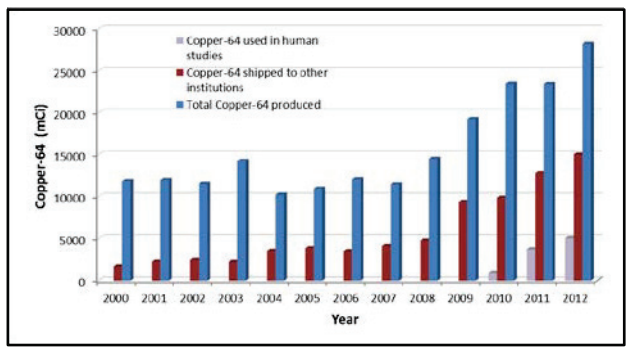


Figure 1: Production and Distribution of ^{64}Cu from Washington University in St. Louis.

TARGET PREPARATION AND BOMBARDMENT

Radiometal production starts with preparation of the target material on a suitable support for cyclotron bombardment. This may be an electroplated deposit, pressed powder pellet, or a foil placed in a suitable holder.

Preparation of ^{64}Ni Targets for Production of ^{64}Cu

Targets are prepared for ^{64}Cu production as per McCarthy *et al* [3]. Briefly ^{64}Ni metal is dissolved in 10 ml of 6.0 M nitric acid. The solution is then evaporated to dryness. The residue is dissolved in 1 ml of concentrated sulphuric acid and 5 mL deionized water and evaporated until slurry is formed. The resulting solution is diluted in 5 ml of deionized water. The pH was then adjusted to 9 with concentrated ammonium hydroxide (25%). Then 0.2 g of ammonium sulphate is added to the solution. This solution was transferred to an electrolytic cell with a graphite electrode as anode and a gold disc (target backing) as cathode. The cathode is cleaned with 6N HNO_3 to remove any metal residue on the surface. The cell is operated at 2.5 V with a starting current between 70-80 mA/cm^2. Final target weights are typically between 20 and 80 mg with a spot diameter of 5 mm.

The ^{64}Ni target is irradiated at a beam current of 20 µA for 60 to 80 µA-h with a Cyclotron Corporation CS-15 positive ion cyclotron, with a pneumatically-controlled cylinder sealing the back of the disc and providing cooling with recirculating chilled water. After irradiation,

*Work supported by the Department of Energy, Office of Science, Isotope Program under grant DESC0008657

Copyright © 2013 CC-BY-3.0 and by the respective authors

LOW ENERGY FUSION FOR A SAFE AND COMPACT NEUTRON SOURCE

S. Albright* and R. Seviour, IIAA, University of Huddersfield, UK, HD1 3DH

Abstract

Neutrons are primarily produced at large international facilities using either spallation reactions or nuclear fission. There is a demand for small scale neutron production for use at hospitals and borders for a variety of applications. Isolated fission sources and sealed tube deuterium-tritium fusors are able to provide a reliable neutron flux at small scale but are impractical due to the associated radioactivity. A beam of protons or deuterons accelerated onto a thin target will undergo a fusion reaction resulting in the emission of a quasi-monochromatic neutron beam. The total flux and energy spectrum of the neutrons produced through fusion is primarily dependent on target material, target thickness, beam energy and projectile. The use of neutrons for security screening at border crossings, ports and airports has the potential to drastically improve threat detection and contents verification. Monte Carlo code MCNPX is being used to investigate the most suitable target and beam characteristics for a neutron source for security applications.

INTRODUCTION

There are many areas of both science and industry which use neutron beams. There is growing interest in using neutrons for medical applications, such as Boron Neutron Capture Therapy (BNCT) [1], and for security applications, such as Pulsed Fast Neutron Analysis (PFNA) [2]. Medical and security applications in particular are not easily served by current neutron sources which tend to be either large and expensive or have radiotoxicology concerns.

For use in medical and security environments two important properties of a neutron source are that it be:

- Compact: Hospitals and airports in particular have limited space available.
- Clean: Radiotoxicity must be kept to a minimum to protect operators and reduce necessary safeguards.

Recently there has been an increased interest in using low energy accelerators (¡10MeV) to produce neutrons. There are sealed tube neutron sources on the market at present (such as the ING013 produced by the VNIIAA [3]) which use a Tritiated Titanium target bombarded by a deuteron beam to produce a high flux of quasi-monochromatic neutrons at $\approx$ 14MeV. Sealed tube sources are not practical for mass deployment due to both the radiotoxicology of Tritium and the legislative controls around their use and transport [4, 5].

In this paper we present simulated results showing that fusion reactions are capable of providing neutrons suitable for a range of industrial applications. Keeping the energy of the incident particles low enables the use of small accelerators and choosing the projectile/target combination correctly will prevent build up of any long lived radioisotopes.

Proton induced fusion reactions were simulated in the Monte Carlo code MCNPX [6] to show the effect of varying target and beam parameters on the neutron beam. The optimum parameters of the neutron beam depend upon the application. Fusion based neutron sources have been shown to satisfy the requirements of two very different applications. For PFNA the primary concern is that the neutron spectrum be both narrow and high energy. For BNCT the neutrons are moderated into the epithermal region therefore the spectrum from the source is unimportant and only the total flux and size of the source are of concern.

The nuclear inventory package EASY-II [7], which uses the fispact-II code [8], has been used to investigate the build up of isotopes in targets to ensure no long-lived radioisotopes are produced. EASY-II enables the build up, decay, and subsequent re-activation of isotopes to be simulated reducing the risk of potentially hazardous decay and transmutation chains being unidentified.

APPLICATIONS

A brief description of two valuable applications of a fusion based neutron source is given along with details of the optimum neutron beam properties for both applications. The two applications discussed are BNCT, a cancer treatment, and PFNA, a security technique.

BNCT uses a boronated drug, preferentially taken up by tumour tissue, and then bombarded by epithermal neutrons. The reaction ^{10}B + n $\rightarrow ^{7}$Li + α causes a massive dose of radiation to be delivered to the tumour whilst leaving surrounding tissue relatively untouched. As BNCT requires epithermal neutrons the beam must be moderated, the sourced neutron spectrum is therefore unimportant and instead maximising the flux whilst minimising the size of the source is the principle concern.

PFNA is a security technique which uses a high energy, monochromatic neutron beam to stimulate the emission of prompt gammas (γs) from material. The γs emitted in PFNA are unique to the element being interrogated allowing the precise content of cargo to be identified. By pulsing the source a volume can be broken into voxels giving a 3D breakdown of what is in a container and where it is located. For PFNA it is important that the neutron beam be; high energy, to maximise prompt gamma emission and minimise transmutation rates; and monochromatic, to minimise both voxel sizes and uncertainties in gamma emission rates.

* corresponding author: simon.albright@hud.ac.uk

ISBN 978-3-95450-138-0

Copyright © 2013 CC-BY-3.0 and by the respective authors

ACCELERATOR-BASED NEUTRON DAMAGE FACILITY USING LEDA*

N. Pogue, P. McIntyre, A. Sattarov, Texas A&M University, College Station, TX 77845, USA

Abstract

An accelerator based neutron damage facility (AND) is proposed to generate a high-dose fast neutron flux for testing of advanced reactor materials. The facility will be implemented in two stages. In AND-1, the 350 MHz LEDA RFQ will be re-commissioned to deliver 100 mA CW proton beam at 6.7 MeV. The beam will be targeted on a sheet-flow of Lithium to produce fast neutrons. Samples located at a target station behind the sheet flow will receive up to 10 dpa/year of neutron damage with a mean neutron energy of 2.37 MeV. In AND-2, the LEDA beam will be modulated to produce three 116 MHz bunch trains where they will be injected to three 100 MeV strong-focusing cyclotrons (SFC). The beams extracted from the three cyclotrons will be targeted 120 degrees apart onto sheet-flow Pb targets. Twenty one tensile samples located in the space between the three targets will receive up to 150 dpa/year of fast neutron damage with mean neutron energy ~8 MeV. AND-1 and AND-2 can provide the fast neutron flux needed for life-cycle damage studies for advance reactor technologies and for first-wall simulations for fusion systems.

INTRODUCTION

A design for an accelerator-based neutron damage (AND) facility has been devised to test advanced reactor materials. Since Three Mile Island there have been no new licenses issued for new construction in the US until just recently (2 reactors). Materials testing is one of the biggest hurdles and is of the utmost importance for two reasons: 1) The original lifetime for a nuclear power plant is 40 years and thus the current fleet has only remained operation due to lifetime extension every ten years, and 2) New reactor designs (Gen 4 and ADS systems) that are more efficient and clean require materials that remain unproven up to 200 dpa (displacement per atom). Currently, testing of materials to be used in advanced reactors is underway at facilities around the world such as HFIR and BOR60. However to reach 200 dpa within the sample takes over 15 years domestically and 10 years internationally. A decade long evaluation process enormously extends the selection process and material evolution.

As a consequence of this timeline, nuclear engineers have turned to the only method readily available, ions. Ions produce significantly more dpa per incident particle than neutrons. However, the mechanisms that ultimately dictate how the material swells and embrittles function differently for the two flavors of particles. Defect production, defect migration, defect annealing, production of interstitial clusters and loops, and H and He production, as well as how damage induced is effected by their presence, are all different for neutrons vs. ions. *Much has been learned about mechanisms that control damage from ion studies, but one cannot predict the damage a given neutron spectrum and dose will produce in a new material solely by experiments with ion damage.* Therefore, without a fast, high fluence neutron source, the ultimate lifetime and failure modes for materials to be used in advanced reactions cannot be ascertained.

Texas A&M Accelerator Research Lab (ARL) has devised an accelerator that can produce 200 dpa via neutron bombardment on several samples in less than 16 months, while also providing control of the temperature and chemical environment of the samples during exposure (problematic in reactors). The spectrum can be tuned to fully mimic conditions anticipated in future fission and fusion (currently not possible) reactors.

AND OVERVIEW

AND is comprised of two stages that utilizes several technologies developed by several groups. In the first stage the LEDA accelerator will be re-commissioned at ARL and send a 100 mA 6.7 MeV proton beam to a liquid Lithium sheet target similar to that developed by ANL. The second stage takes the proton beam from LEDA and accelerate 45 mA of the beam to 100 MeV using a set of 3 flux coupled Strong Focusing Cyclotrons (SFCs) developed at Texas A&M. The three beams are then directed to liquid Lead targets. The result of these two stages is a facility that can generate ~150 dpa/year using fast neutrons. An image of the facility is shown in Figure 1.

AND – PHASE 1

LEDA

The Low Energy Demonstration Accelerator, or LEDA, is one of the few RFQ accelerators that have achieved high current CW operation [1]. Initially built as the front end of the Accelerator Production of Tritium (APT), the accelerator was commissioned in 2003 and achieved in accelerating ~100 mA of beam to 6.7 MeV. In 2004, LEDA was decommissioned and remains in pristine condition within a high strength support structure, to maintain internal alignment among the cavity sections, while in storage (Figure 2). The current state of LEDA should assure that the time to re-commission at low power should be less than a year. Los Alamos National Lab (LANL) has agreed to make a 10-year loan of the LEDA system to Texas A&M University. ARL plans to move LEDA to Texas A&M along with pulsed RF power source, power supplies, transformers, and waveguides from LANL. The RF power loaned will be a pulsed system, but A&M has received commitment from CERN for two 1 MW 350 MHz CW power sources.

* Work supported by State of Texas and Mitchell Foundation
# npogue@physics.tamu.edu

Copyright © 2013 CC-BY-3.0 and by the respective authors

DEVELOPMENT OF LOW ENERGY ACCELERATOR-BASED PRODUCTION OF MEDICAL ISOTOPES

N. Ratcliffe*, R. Barlow, R. Cywinski, University of Huddersfield, Huddersfield, HD1 3BH, UK
P. Beasley, Siemens AG, Oxford, OX1 2EP, UK

Abstract

Here we present methods for production of new and existing isotopes for SPECT (Single Photon Emission Computed Tomography) and PET (Positron Emission Tomography) imaging using accelerator-based systems. Such isotopes are already widely used in medical diagnostics and research, and there is constant development of new drugs and isotopes. However the main production method for ^{99m}Tc, is currently in research reactors and is at risk due to scheduled and unscheduled shut downs. Therefore, a low cost an alternative accelerator-based system could provide many advantages. Various compact low energy proton machines are being proposed to enable cheap and accessible production: here we present a discussion of potential new SPECT isotopes and simulations of suitable targets for their manufacture.

INTRODUCTION

Currently the production of medical tracer isotopes for use in imaging techniques such as SPECT (Single Photon Emission Computed Tomography) and PET (Positron Emission Tomography) [1] relies principally upon an ageing fleet of nuclear reactors. For example the most common medical isotope ^{99m}Tc, used in over 80% of all radiopharmaceutical procedures, is currently produced, via its generator ^{99}Mo, by nuclear research reactors such as NRU-Canada and HFR-The Netherlands, which together produce over 60% of the worlds ^{99}Mo/^{99m}Tc supply. Both of these reactors are old (>50yrs) and close to decommissioning, and while several projects are looking at other production routes for this isotope, as yet there is no real replacement in place [2, 3]. As these reactors near their decommissioning, currently set at 2014-2016, there is considerable concern that we will soon be facing a similar situation to that of the 2010 isotope crisis, when both reactors were offline simultaneously resulting in a significant decrease in the supply of ^{99m}Tc and the postponing or cancelation of many vital radioisotope procedures [1–5]. Due to ^{99m}Tc monopolising the medical isotope market little work was done developing other isotopes and many potential isotopes fell by the wayside. The aim of this work is to resurrect some of these isotopes as alternatives to ^{99m}Tc as we head into another shortage in the hope of preventing another crisis. There are several short lived SPECT and PET isotopes that have the potential to take some of the workload from ^{99m}Tc.

* naomi.ratcliffe@hud.ac.uk

LOW ENERGY ISOTOPE PRODUCTION

We believe that the solution to this impending problem could lie in accelerator-based production methods, of both ^{99m}Tc and possible replacement isotopes. A collaboration with Siemens is focusing on the potential of a compact, low energy proton device for the generation of radioisotopes [6]. Such a machine could provide many more localised isotope production centres and allow for the use of isotopes with shorter halflives. A study of optimal target designs for such a system has been undertaken using GEANT4 simulations of low energy (<10MeV) proton induced reactions.

^{113M}INDIUM

^{113m}In is a metastable radioactive isotope that decays via a 392 keV γ into stable ^{113}In with a half life of 1.7hours [7]. In 1965 it was first proposed for use as an alternative medical tracer isotope to ^{99m}Tc for SPECT imaging in several applications such as brain and lung scanning. Trials of this isotope showed it to give results comparable to ^{99m}Tc images [7]. ^{113m}In showed several advantages over ^{99m}Tc such in terms of chemical properties. A successful generator production system for In was developed using ^{113}Sn [7, 8].

Generator Production

There are several advantages of a longer lived generator system, such as the Sn/In system. The longer gap between parent half life and daughter half life makes it easier to separate the two nuclei. It also increases the longevity of the system for example the Sn/In(parent half life approximately 118 days) system only needs replacing once every 6 months where as the Mo/Tc(parent half life approximately 3 days) system needs replacing weekly. However due the plentiful and cheap supply of Tc at the time very little serious work was carried forward with this isotope. The simplicity of the generator production system and the advantages available from such a system has prompted the exploration of a low energy method of production for this generator using the reaction:

^{113}In(p,n)^{113}Sn $\rightarrow$ ^{113m}In $\rightarrow$ ^{113}In

Preliminary simulation results from the TALYS data libraries show that such a reaction at 10 MeV gives a production cross section of 570mb. Further GEANT4 simulations have been used to study target designs and feasibility of this reaction using a <10MeV proton beam. In terms of daughter yield the most appropriate target thickness is that of just

Copyright © 2013 CC-BY-3.0 and by the respective authors

ISBN 978-3-95450-138-0

AN OVERVIEW OF LIE METHODS FOR ACCELERATOR PHYSICS*

Alex J. Dragt, Department of Physics, University of Maryland, College Park, MD, USA

Abstract

We sketch how Hamiltonian mechanics can be formulated in Lie algebraic terms (indeed Poisson and Jacobi almost invented Lie algebras without knowing it), and how this formulation can be applied to the description and computation of particle orbits in accelerators in a way that both unifies linear and nonlinear theory and leads to explicit results for realistic machines [1–5].

WHAT IS A LIE ALGEBRA?

In grade school we learned how to add numbers to get other numbers, and how to multiply numbers to get other numbers. Mathematicians call an *algebra* any collection of entities for which addition-like and multiplication-like operations are defined.

The concept of numbers and their addition can be extended to the concept of vectors and vector addition. With vectors in mind, is it possible to define multiplication for vectors in such a way that multiplication of any two vectors again yields a vector? There are various possibilities. We will select one. Suppose, for the moment, we denote such multiplication by the symbol $\circ$. Thus, we denote the product of two vectors u and v by the symbols $u \circ v$.

Consider a multiplication rule that has the two properties

$$v \circ u = -u \circ v, \tag{1}$$

$$u \circ (v \circ w) + v \circ (w \circ u) + w \circ (u \circ v) = 0. \tag{2}$$

A multiplication rule with the two properties (1) and (2) is called a *Lie product* rule, and a vector space equipped with a Lie product rule is called a *Lie algebra*. We remark, for reasons which will become evident, that the condition (2) is called the *Jacobi* condition or identity.

IS THERE A LIE ALGEBRAIC STRUCTURE IN HAMILTONIAN MECHANICS?

Notation

Consider a $2n$-dimensional phase space with position coordinates $q_1 \cdots q_n$ and momentum coordinates $p_1 \cdots p_n$. Also, for convenience, introduce the notation

$$z = (q_1 \cdots q_n; p_1 \cdots p_n). \tag{3}$$

That is, z denotes a collection of $2n$ variables with the first n of them being the q's and the remaining n being the p's.

* Work supported in part by the University of Maryland and the U.S. Department of Energy Grant DE-FG02-96ER4DOE.

The Set of Phase-Space Functions Forms a Vector Space

Next let $f(z,t)$ be any function of z and possibly the time t. Evidently, since phase-space functions can be added together and the result is again a phase-space function, the set of all phase-space functions forms a vector space.

The Poisson Bracket Provides a Lie Product

Is there a way of "multiplying" phase-space functions that will satisfy the Lie product requirements (1) and (2)? There is. The *Poisson bracket*, denoted by the symbols $[f,g]$, of any two phase-space functions f and g is defined by the rule

$$[f,g] = \sum_{k=1}^{n} (\partial f/\partial q_k)(\partial g/\partial p_k) - (\partial f/\partial p_k)(\partial g/\partial q_k). \tag{4}$$

Then, it is obvious from its definition that the Poisson bracket has the property

$$[g,f] = -[f,g]. \tag{5}$$

What is not so obvious, and was observed by *Jacobi*, is that the Poisson bracket also has the property

$$[f,[g,h]] + [g,[h,f]] + [h,[f,g]] = 0. \tag{6}$$

Evidently (5) and (6) are analogs of the properties (1) and (2). Only the symbols for a product have been changed, with $\circ$ replaced by $[,]$. We conclude that the set of all phase-space functions with the Lie multiplication rule (4) constitutes a Lie algebra.

The Fundamental Poisson Brackets

Simple calculation shows that for the phase-space coordinates themselves there are the Poisson bracket results

$$[z_a, z_b] = J_{ab}, \ a,b = 1 \cdots 2n \tag{7}$$

where J is the $2n \times 2n$ matrix, called the Poisson matrix,

$$J = \begin{pmatrix} 0 & I \\ -I & 0 \end{pmatrix}. \tag{8}$$

Here 0 and I denote the $n \times n$ zero and identity matrices.

A RELATED LIE ALGEBRA IN HAMILTONIAN MECHANICS

Lie Operators

Given any phase-space function $f(z,t)$ there is a related differential operator, called a *Lie operator* and denoted by the symbols $:f:$, defined by the rule

$$:f: = \sum_{k=1}^{n} (\partial f/\partial q_k)(\partial/\partial p_k) - (\partial f/\partial p_k)(\partial/\partial q_k). \tag{9}$$

Copyright © 2013 CC-BY-3.0 and by the respective authors

LONGITUDINAL EMITTANCE MEASUREMENT SYSTEM FOR THE ARIEL ELECTRON LINAC

A. Vrielink, Y.C. Chao, C. Gong, R. E. Laxdal, V. Zvyagintsev, TRIUMF, Vancouver, Canada

Abstract

As part of the ARIEL e-LINAC project at TRIUMF, a 1.3 GHz single-cell, room-temperature deflecting cavity has been developed to study the temporal distribution of an electron beam from a 300 kV thermionic gun. Beam bunches on the order of 100-200 ps long are produced from a biased grid with a 650 MHz RF voltage superimposed to periodically allow release of electrons. The RF deflector operates in a TM110-like mode, deflecting the electrons vertically with a magnitude dependent on their arrival phase. The cavity RF performance has been characterized through signal level and beam testing. The deflector is installed as part of a longitudinal emittance measurement system with beam collimation, a 90 degree analyzing magnet, the deflecting cavity and a final view screen. Initial beam bunch length measurements using this RF cavity, conducted in conjunction with the initial commissioning using a 100kV electron-gun and a 1.3GHz buncher, are presented. The beam bunch length was extracted by comparing data collected at a screen downstream of the deflector to an analytical model based on linear time-invariant system theory.

INTRODUCTION

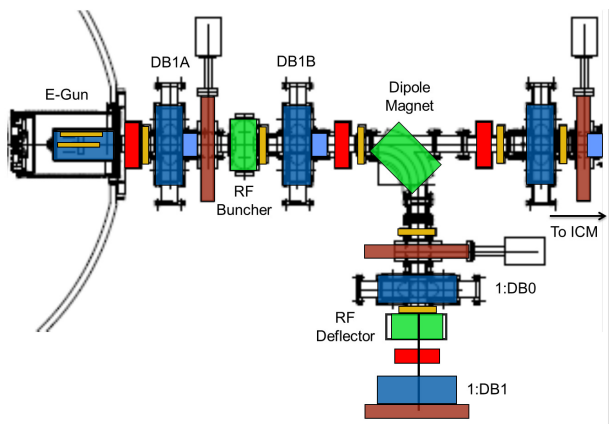


Figure 1: Low Energy Transport Line in the VECC Test Area.

The ARIEL project at TRIUMF is well under way, including a 50MeV linear accelerator using 1.3 GHz superconducting technology to accelerate a 10mA electron beam. TRIUMF is currently developing a 10MeV injection line for this electron linac in collaboration with the Variable Energy Cyclotron Center (VECC). A test area has been set up in the ISAC II building to commission various beamline components before installation in the ARIEL injection line and in Kolkata. The VECC Test Area consists of a 100kV (now 300kV) thermionic e-gun with an RF modulated gridded bias on the cathode at 650MHz, a low energy beam transport (LEBT), an injector cryomodule with a 1.3GHz superconducting 9 cell cavity, and a medium energy beam transport. Electron bunches ranging from 100-200ps long are emitted at a 1kHz repetition rate with a duty factor between 0.1% and 100%.

The LEBT section, pictured in Fig. 1, contains various beam diagnostics including linear profile monitors (LPMs), faraday cups, YAG screens and non intercepting beam profile monitors. The LPM consists of a vertical slit, horizontal slit and collimating hole which can be scanned across the beam to sweep the beam profile or inserted into the beam to select a beam profile.

THE LONGITUDINAL EMITTANCE MEASUREMENT SYSTEM

As part of the LEBT diagnostics, a longitudinal emittance measurement system was designed. It consists of an RF bunching cavity, dipole magnet, RF deflecting cavity in a 90° analyzing leg and downstream screen. The RF buncher manipulates the bunch length at a point downstream by accelerating late electrons in the bunch and decelerating early electrons. The dipole bends the beam into the analyzing leg, mapping the electron energy to the x axis through the dependence of the radius of curvature on electron energy, $\rho = \frac{\gamma\beta E_0}{qBc}$.

Circular apertures of 2mm diameter at the diagnostic boxes DB1A and DB1B (see figure 1) are used to limit the transverse emittance. The dipole magnet horizontal focusing is designed so an object at DB1B forms a dispersed focus at 1:DB0, such that a slit at 1:DB0 will select an energy slice of the beam.

In the analyzing leg, a 1.3GHz room temperature RF deflecting cavity maps the time spread of the beam to the vertical axis using E_y and B_x fields. A screen at 1:DB1 images the beam in the transverse plane. Using the deflector in conjunction with the dipole magnet, the beam energy and time spread can be extracted from the horizontal and vertical beam size, respectively. A solenoid upstream of 1:DB1 can be used to focus the beam at 1:DB1 with the RF devices off, producing a slight rotation of the $\Delta E/\Delta t$ (x/y) reference frame.

THE RF DEFLECTOR

The 1.3 GHz single cell deflecting cavity has been designed to analyze the temporal distribution of an electron

Copyright © 2013 CC-BY-3.0 and by the respective authors

ISBN 978-3-95450-138-0

BEAM DUMP DESIGN FOR THE IN-FLIGHT FRAGMENT SEPARATOR USING HIGH-POWER BEAM*

J.Y. Kim, M. Kim, J.W. Kim#, Institute for Basic Science, Daejeon, Korea

Abstract

The beam dump is a critical component for the in-flight fragment separator using high-power primary beams at the rare isotope science project (RISP) in Korea. The maximum beam power is planned to be 400 kW, and a third of the primary beam power deposits at the isotope production target and the rest are dissipated at the beam dump. The beam dump is designed to be a rotating water drum, which is movable in the perpendicular direction to the beam to select the isotope beam of interest. The main primary ion beam is U, and its range at the energy of 200 MeV/u is only a couple of mm after passing through the shell structure of the drum. This short range requires its internal structure to confine water flow on the wall and to keep high-pressure. Some detailed thermo-mechanical and thermo-fluid analysis has been done using ANSYS and other codes.

INTRODUCTION

Rare isotope science project (RISP), which is to produce rare isotope beams by using both the in-flight fragment (IF) separation and isotope separation on-line (ISOL) methods is undergoing in Korea [1]. The main accelerator, which can provide a wide range of heavy ion beams, accelerating ^{238}U beam to 200MeV/u and proton to 600 MeV, is a superconducting linear accelerator for the IF separator. The IF separator uses a thin target to produce rare isotope beams and a beam dump is located after the first dipole magnet so as to remove unwanted primary beam.

The design of beam dump for in-flight separator using high power primary beam has been performed considering high power density deposited in beam dump. Approximately 30% of the primary beam power, which is used to produce RI beam, will be dissipated in a production target with typical thickness of d/R = 0.3, whereas the rest of primary beam that does not react with production target, will pass through magnetic system and be absorbed in beam dump. The maximum beam power deposited in the beam dump is up to about 300 kW for 200 MeV/u ^{238}U beams and the beam size on beam dump is expected to be around 10 mm in diameter.

Removal of high power primary beam in an IF separator is complicated due to different charge states in primary beam, short range in material and high power density at beam dump. Furthermore, if assuming the primary beam directly impacted on beam dump in the case of target malfunction, the beam dump should be capable of absorbing up to 400 kW during a short time. The cooling system, which can handle high power, is required to avoid structural breakdown and thermal runaway.

If wanted fragment beam is close to the primary beam in rigidity, the task of separation becomes more difficult. Trajectories of off-rigidity fragments and non-reacted beam can overlap with that of the isotope beam of interest at the beam dump. Beam dump system is required to intercept unwanted fragments and non-reacted primary beam minimizing the loss of wanted beam. For the purpose of intercepting the primary beam and off-rigidity fragments with different trajectories, it is necessary that the beam dump has two units and is movable.

A conceptual design of beam dump, and thermal analysis using ANSYS [2] and PHITS [3] are described.

DESIGN OF BEAM DUMP

Figure 1 shows a schematic layout of the separator, which has been designed to consists of two-stages. The purpose of the first stage, pre-separator is to produce RI beams and then to separate the primary and unwanted RI beams, while the second stage, main separator serves to identify the RI beam of interest. The momentum and angular acceptance of the separator have been designed to be ±5 % and ±50 mrad, respectively.

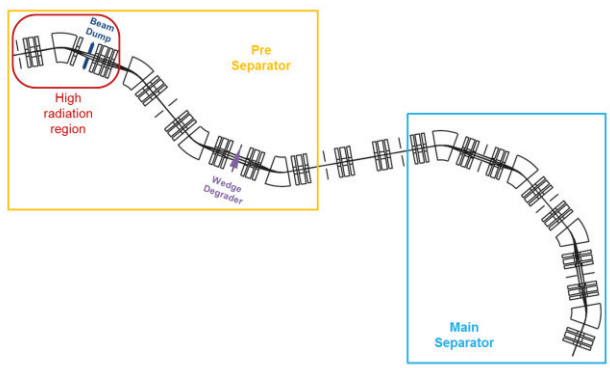


Figure 1: Schematic layout of the fragment separator.

As shown in Fig. 1, a dispersive focal plane is located after the first dipole magnet, and the beam dump is placed near the focal plane. The isotope beam of interest is separately by magnetic rigidity, but unwanted beam with the same Bρ is overlapped.

To remove the heat efficiently, we considered the beam dump consisting of two rotating water-filled cylinder as was adopted for FRIB [4]. A conceptual drawing of the beam dump system is shown in Fig. 2. The beam dump system will be located in a common vacuum space together with the dipole magnet and the production target. The beam dump rotates to prevent localized heating, and cooling water directly absorbs the beam power acting as a liquid beam dump. Titanium is chosen for the material of

* Work supported by Rare Isotope Science Project
#jwkim@ibs.re.kr

Copyright © 2013 CC-BY-3.0 and by the respective authors

BEAM POSITION ELECTRONICS BASED ON SYSTEM ON CHIP PLATFORM

M. Cargnelutti*, G. Jug, R. Hrovatin, Instrumentation Technologies#, Solkan, Slovenia

Abstract

With the advances in system-on-chip (SoC) technology, the CPU and FPGA are today enclosed in the same device. This enables high-speed processing, inherent fast communication and memory sharing between the two entities. However, dedicated tools for implementation are needed as the CPU and FPGA functionalities cannot easily be decoupled.

We used the advantages of the new architecture in the development of a booster BPM electronics. Its requirements are relaxed compared to up-to-now Libera beam position monitors. Proper design of the RF part of the instrument is still a challenge. Furthermore, with optimized FPGA design we target low overall power consumption so that the instrument can be cooled passively.

INTRODUCTION

Instrumentation used in particle accelerators is today one of the most demanding fields for electronic devices and of system integration. Required performances are usually at the cutting edge in terms of signal-to-noise ratio, computational power and data throughput. Even more impressive are the requirements in terms of reliability, long term stability and fault tolerance. As a consequence, instruments are usually a complex inter-connection of different boards that host RF circuits, field programmable gate arrays (FPGAs), communication buses and CPUs. Every logical component from hardware to software is optimized for the specific application.

On the other hand, not every accelerator, or at least not every part in it, needs a top-level device to work properly. A natural example here concerns beam position monitors (BPMs) used in synchrotrons boosters and injectors, compared to those used in the storage ring. Furthermore, a lot of applications have figures of merit such as low power consumption, no need for HW and SW maintenance, and user friendliness. This can be the case for a beam loss monitor (BLM), for example.

In this paper we introduce a compact platform that aims to host a wide range of applications, being able to cover all the points presented above. Details about the system design are presented in the third section. In order to give a real picture, we will consider the development of a BPM instrument for the European Synchrotron Radiation Facility (ESRF) booster [1] as an example.

* manuel.cargnelutti@i-tech.si
# www.i-tech.si

A NEW PLATFORM

Looking at the beam instrumentation used to monitor and stabilize an accelerator, every device suits a specific role, but it is possible to identify some key components that are always present:

- digital signal processing and elaboration units (e.g. FPGAs and CPUs)
- RF front-end and analogue signal processing chains
- internal communication buses
- power supply unit
- crate and cooling system (often is an active system with fans).

In this new development, we take advantage of the latest advances in SoC technology to introduce a compact platform that combines a high level of hardware integration with our knowledge regarding reconfigurable analogue signal processing.

HW and SW integration

Hardware and software are designed taking in account the balance between generality and optimization. It will be always possible to add specific features to customize it, opening at the same time the way for developing different applications, as shown in Fig. 1.

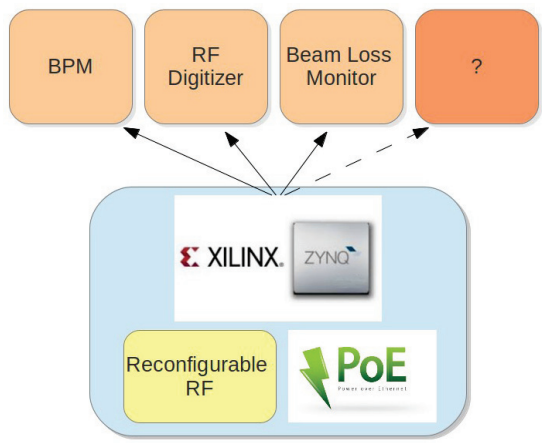


Figure 1: Platform concept based on SoC.

The core part is the SoC Xilinix Zynq 7020 [2] which combines the high-speed processing of the FPGA together with the flexibility of a CPU, all within the same chip. The inner communication between the two entities and the chance to share the same memory removes at the same time two of the biggest bottle-necks that still characterize separate-chip solutions:

- no communication protocols needed
- no data copy between FPGA and CPU.

Copyright © 2013 CC-BY-3.0 and by the respective authors

ISBN 978-3-95450-138-0

COMPARISON OF SIMULATIONS AND ANALYTICAL THEORY OF RADIATION HEATING ON THE ADVANCED PHOTON SOURCE SUPERCONDUCTING UNDULATOR*

Laura Boon†, Purdue University, West Lafayette, IN 47907, USA
Roger Dejus, Katherine C. Harkay and Mark Jaski, ANL, Argonne, IL 60439, USA

Abstract

Synchrotron radiation can potentially introduce large heat loads on the beam chamber of the superconducting undulator (SCU0) at the Advanced Photon Source (APS). With the photon absorber mask, a well-aligned centered beam in the upstream bending magnet allows only a small amount of radiation power, less than 1 W, to intercept the walls of the beam vacuum chamber in the cryostat, assuming no photon scattering. But beams with vertical orbit errors, especially, can deposit much higher heat loads on the beam chamber, above 100 W. An analysis was carried out to calculate the power on the vacuum chamber when the beam has an orbit error through the upstream bending magnet. This paper presents these analytical results compared to simulations that were performed using a 3D photon tracking code, Synrad3d.

INTRODUCTION

As part of the Advanced Photon Source Upgrade project [1], a test superconducting undulator (SCU0) was developed at Argonne National Laboratory [2]. The test SCU0 was installed in December 2012 [3]. To reduce heating on the superconducting coils, the beam chamber is thermally isolated from them. The cryo-coolers used to cool the beam chamber are able to handle up to 40 W of power (at 20 K) from transient and continuous wave sources. Radiation from the upstream dipole produces high amounts of power that can be incident on the beam chamber inside the SCU0 cryostat. SCU0 is in the downstream end of the straight section in sector 6, see Fig. 1. The upstream end of the straight section has a hybrid permanent magnet undulator (HPM). A photon absorber (PA) in the downstream end box of the HPM is used to shield the beam chamber outboard wall from direct, on-axis radiation.

CALCULATIONS

The power incident on the SCU0 beam chamber from primary photons can be calculated through ray tracings and analytically. Ray tracings are 2D projections of the dipole radiation fan on the 3D vacuum system layout. Ray tracings do not typically include the vertical distribution of the dipole radiation. So analytical calculations were performed to include the photon vertical distribution. Figure 2 shows the elliptical shape of the beam chamber in the SCU0 cryostat. The shape was taken into account for all the calculations and simulations shown in this paper. All calculations assume a beam current of 100 mA. Beam orbits are referenced to the dipole exit.

Ray Tracings

The layout of the radiation fan is seen in Fig. 1. By applying an off-axis electron beam orbit through the radiation source, the horizontal steering offset (x) and angle (x') limits can be determined. The steering limit is defined by when the radiation fan begins to intercept the outside edge of the beam chamber. The steering limit defined by ray tracings is shown in Fig. 3 (red dotted line). Due to the wide horizontal aperture of the beam chamber, only for very large steerings is there a concern about radiation heating. For positive offsets the photon absorber shields the beam chamber. The power incident on the beam chamber is calculated as follows. The APS main dipole magnet generates 6.65 kW of synchrotron radiation power per 100 mA. The horizontal fraction of energy that is incident on the SCU0 chamber is calculated using α/θ_{dipole} where $\theta_{dipole} = 77.54$ mrad is the full bending angle and α is the angle subtended by the SCU0 chamber. The power incident on the beam chamber is greatest for an electron beam that has a negative orbit offset. The power on the outside edge ranges from 0.3 W to 22.8 W. The power increases for larger negative offsets.

Analytical Calculations

The radiation heating load is calculated analytically using the method described in [4]. The following equation is integrated over the vertical opening angle in which the photon beam is incident on the beam chamber:

$$F = P_0 \frac{1}{(1+X^2)^{5/2}} \left[1 + \frac{5}{7}\frac{X^2}{1+X^2}\right]. \qquad (1)$$

In Eq. 1, P_0 is the fraction of total power produced by the dipole magnet that passes the photon absorber, and $X = \gamma\psi$, where γ is the relativistic factor, and ψ is the vertical opening angle between the radiation source and the SCU0 beam chamber.

Figure 3 is a contour plot of the power incident on the SCU0 chamber when the beam has a horizontal offset. The vertical photon distribution is included in the calculation. Radiation intercepts the top and bottom of the beam vacuum chamber and not just the outside edge. Again the contour plot shows that large negative offsets through the

* Work supported by U.S. Department of Energy, Office of Science, under Contract No. DE-AC02-06CH11357
† lboon@purdue.edu

Copyright © 2013 CC-BY-3.0 and by the respective authors

THERMAL MODELING OF THE PROTOTYPE SUPERCONDUCTING UNDULATOR (SCU0)*

Y. Shiroyanagi, C. Doose, J. Fuerst, K. Harkay, Q. Hasse, Y. Ivanyushenkov, M. Kasa
Argonne National Laboratory, Argonne, IL 60439, USA

Abstract

A cryocooler-cooled superconducting undulator (SCU0) has been built, and cryogenic and magnetic tests have been completed. The device is currently installed in the Advanced Photon Source (APS) beamline. The device consists of a dual-core 42-pole magnet structure that is cooled to 4.2K with a system of four cryocoolers operating in a zero-boil-off configuration. In this paper, a thermal model of the beam chamber and its cooling circuit are presented. A temperature profile of the cooling circuit and heat load to cryocoolers are calculated based on steady-state temperatures. Comparison with cryogenic test results and future improvements will be discussed.

BACKGROUND

The superconducting undulator (SCU0) consists of a dual-core 42-pole magnetic structure that is cooled to 4.2K with a system of four cryocoolers operating in a zero-boil-off configuration. The design of the cryostat is based on a concept developed at the Budker Institute, Novosibirsk [1]. Figure 1 shows the overall cooling scheme of the cryostat. The beam chamber is cooled by the two bottom cryocoolers (Sumitomo RDK-408S) together with the inner thermal radiation shield, which is called the 20K circuit. The main and correction magnet leads and the thermal transitions of the beam chamber are connected to the first stages of all four cryocoolers through the outer thermal radiation shield, which is called the 60K circuit. The 4K circuit consists of the helium vessel, the magnetic structure, and the superconducting part of magnet leads. These are cooled by the 2nd stage of the top cryocoolers (Sumitomo RDK-415D). The magnet is cooled by circulating LHe, and it is thermally isolated from the beam chamber [2-4].

FEA MODEL

Finite element analysis (FEA) was conducted using ANSYS 14.5. Initially, heat loads at individual parts of the cryostat were calculated with fixed end temperatures. Thermal radiation heat was calculated in a separate model. Joule heating of the resistive parts of the current leads was also calculated separately. Then using these results, the 20K and 60K circuits were modeled including a simulated heat load imposed by the circulating electron beam. Temperatures and heat load at each cryocooler were calculated and compared with measured data. Table 1 is the calculated heat load of the individual parts of the cryostat based on the original design before the installation [1]. The 60K circuit heat loads are dominated by the magnet current leads. Static heat load through the main current leads are 47 W and through the correction current leads are 8.0 W. Main current lead heat increases to 63.85 W when they are energized to 650 A. The correction current lead heat increases to 12.2 W when they are energized to 70 A. Other sources include beam tube conduction and radiation from 295K to the outer shield. The 20K circuit heat loads are primarily the beam-induced heat load in the beam chamber that goes to the second stages of the bottom cryocoolers (408S) through the copper busbar and thermal links. The beam heat load is predicted to be 10 W at the 20K circuit and 6 W at the 60K circuit. The 4K circuit heat loads consist of the high-temperature superconducting (HTS) section of the magnet current leads, a very small portion of the beam heat through the beam chamber supports, heat through the cold mass supports made of Kevlar strings, and radiation from the inner shield to the cold mass.

In order to calculate the 20K and 60K circuit temperatures and heat, the magnet leads, the beam chamber, and the outer shield are modeled at steady state conditions. Figure 2 shows the overall temperatures of the 20K and 60K circuits as well as boundary conditions of this model. The outer shield is included in the calculation but not shown. Temperatures of the end flanges of the beam chamber and the top of the magnet leads are fixed at 295K. The coldest ends of the magnet leads are fixed at 3.42K, which is the measured temperature of the 2nd stage of the top cryocooler (415D). The load maps of the 1st stage top and 1st and 2nd stages of the bottom cryocoolers are implemented as temperature-dependent heat flow at each cold head.

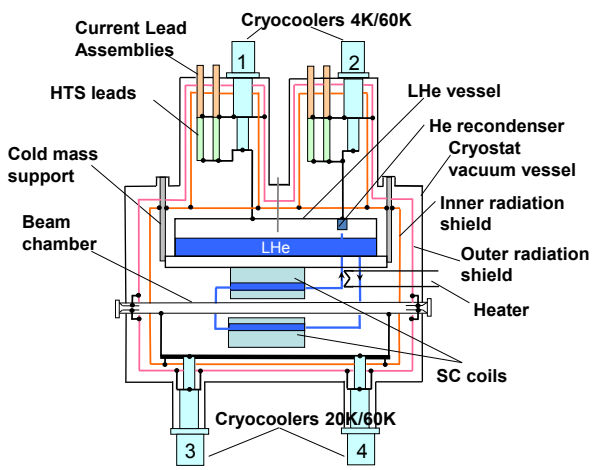


Figure 1: Cooling schematic.

*Work supported by the U.S. Department of Energy, Office of Science, under Contract No. DE-AC02-06CH11357
#yshiroyanagi@aps.anl.gov

ISBN 978-3-95450-138-0

Copyright © 2013 CC-BY-3.0 and by the respective authors

MODERNIZATION OF THE BERGOZ MULTIPLEXED BPM SYSTEM FOR THE APS UPGRADE*

X. Sun#, R. Lill, H. Bui, R. Keane, G. Decker, B. Yang, ANL, Argonne, IL 60439, USA

Abstract

The APS upgrade includes improvements to the Bergoz Multiplexed BPM system, which presently suffers from an aging data acquisition system. The upgrade leverages off the development of an eight-channel data acquisition system featuring modern FPGA flexibility that was designed for the monopulse BPM system. This upgrade also provides an external clock signal synchronized to the APS revolution clock that will eliminate the aliasing caused by the Bergoz asynchronous multiplexing interacting with different accelerator fill patterns. The upgrade will revitalize this system and demonstrate a cost-effective approach to improved beam stability, reliability, and enhanced postmortem capabilities. In this paper we will discuss the upgrade system specifications, design, and prototype test results.

INTRODUCTION

The Advanced Photon Source Upgrade (APS-U) project includes improvements to the commercial narrowband (Nb) Bergoz multiplexed Beam Position Monitor (BPM) systems [1], which were installed in 2000. The APS storage ring now makes use of 80 Bergoz modules that are connected to 10-mm buttons on a large-aperture, standard elliptical (42 mm by 85 mm) vacuum chamber. This NbBPM system presently suffers from an aging data acquisition system. The upgrade leverages off the development of an eight-channel data acquisition system featuring modern field-programmable gate array (FPGA) flexibility that was designed for the monopulse BPM system [2]. The new FPGA-based Beam Signal Processor (BSP100) will replace the old data acquisition system and controls for the existing Bergoz receivers located at P1s on the standard elliptical vacuum chambers.

The upgrade will revitalize this system and demonstrate a cost-effective approach to improved beam stability, reliability, and enhanced postmortem capabilities.

The noise floor, fill-pattern dependence, and intensity dependence of the prototype upgrade NbBPM system will be investigated.

UPGRADE SYSTEM SPECIFICATIONS

Beam stability improvement is an important part of the APS-U project, which will be supported by new and upgraded BPM electronic systems. Listed in Table 1 [3] are APS-U beam stability performance and goals for ID sources. To achieve these goals, the obsolete BPM electronics for the NbBPM, located at the standard elliptical vacuum chambers, will be replaced with a modern system providing improved resolution and drift characteristics.

Table 1: APS-U Beam Stability Performance and Goals

		AC rms motion 0.01-200 Hz		AC rms motion 0.01-1 k Hz		Long-term drift (One Week)	
		µm rms	µrad rms	µm rms	µrad rms	µm rms	µrad rms
Horizontal	Present	5.0	0.85	5.0-7.0*	NA	7.0	1.4
	Upgrade	3.0	0.53	6.0	1.14	5.0	1.0
Vertical	Present	1.6	0.80	3.7*	NA	5.0	2.5
	Upgrade	0.42	0.22	0.84	0.44	1.0	0.5

* Measurement up to 767 Hz

DESIGN

The BSP100 is a standalone Experimental Physics and Industrial Control System (EPICS) input/output controller (IOC), an FPGA-based (Altera Stratix® II), a C-sized VXI form factor, with eight high-speed 14-bit digitizers (Analog Device AD6645) running at 88 MSPS (one-fourth of the APS rf frequency) [2, 4]. The baseline design replaces the aging Bergoz data acquisition with the BSP100. The position signals from four Bergoz BPMs will be digitized with a single module. The BSP100's FPGA has five major blocks, the APS timing system receiver, the acquisition control block, the preliminary processing block, the continuous signal processing block, and the triggered processing block.

The turn-by-turn average from the preliminary processing block, which is same as that in the monopulse BPM system, is passed through a first-order low-pass filter with a cutoff frequency of about 1.4 kHz. Then it is converted to the engineering units and sent to several other blocks for processing, as shown in Figure 1.

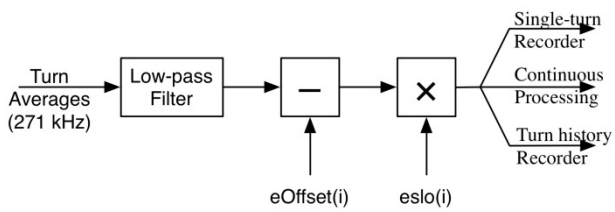


Figure 1: BSP100 Bergoz signal processing block diagram.

In the continuous processing block (shown in Figure 2), acquired data from the Bergoz BPMs will be available at EPICS rate and at a fast data stream. The BSP100

*Work supported by U.S. Department of Energy, Office of Science, under Contract No. DE-AC02-06CH11357.

#xiang@aps.anl.gov

Copyright © 2013 CC-BY-3.0 and by the respective authors

ULTRA-HIGH VACUUM SEAL FOR LONG CHAMBERS USING WIRE SEALS*

H. Fernandes#, P. Cappadoro, T. Corwin, D. Harder, P. He, C. A. Kitegi, W. Licciardi, M. Musardo, G. Rakowsky, J. Rank, C. Rhein, and T. Tanabe,
National Synchrotron Light Source II, Brookhaven National Laboratory, Upton, NY 11793, USA

Abstract

As the length of insertion devices (ID's) increase for synchrotron light sources, so does the need to have larger ultra high vacuum (UHV) sealed chambers, which in turn necessitates the use of creative ways of sealing these large chambers in the UHV range (10^{-11} torrs).The method specified below was used to seal a 4-meter test vacuum chamber successfully in the ultra high vacuum range. This method could be used for sealing ID chambers of lengths larger than 4 meters in the UHV range due to its simplicity and reduced cost advantage. This test chamber was also baked for 3 cycles to check for the integrity of the seals and final vacuum levels.

INTRODUCTION

The ultra high brightness NSLS-II storage ring is under construction at Brookhaven National Laboratory. It will have 3GeV, 500mA electron beam circulating in the 792m ring, with very low emittance (0.9nm.rad horizontal and 8pm.rad vertical). Significant increases in brightness requirements for the third generation ID has led to increased length of ID and hence increased length of vacuum chambers. The wire seal method outlined below depicts a way of sealing these long vacuum chambers in a cost efficient way. Other sealing methods for chambers such as Helicoflex ™ seals, metal gaskets, metal O-ring seals and differential pumping methods were studied as potential sources for sealing large vacuum chambers (>2.5 meters) [4]. Of these methods, only the wire seal made it to manufacturing, testing and optimization; the other methods were ruled out due to their high cost, difficulty in manufacturability by vendors due to low production quantities, or failure to meet UHV requirements in terms of operational efficiency and difficulty in installation. The wire seal was able to seal a 4-meter-long vacuum chamber in the UHV range and was also able to maintain the same vacuum specifications during and after baking. Here, we outline the procedure used to seal a 4 meter test vacuum chamber, specify the test results for this chamber, and mention possible methods to improve the wire seal.

TEST CHAMBER CONSTRUCTION SPECIFICATIONS

The seal was tested on a 4-meter test chamber that had a modular design. This design reduces the cost of the R&D chamber to a minimum, as it consists of mainly steel plates. The modular design of the vacuum chamber consists of a base plate as shown in Figure 1. A spacer plate has grooves cut for o-ring seals, which are placed between the front plate and the back plate. The distance between the front plate and the base plate is 0.75". This is maintained to a minimum in order to keep just enough room for bowing of the chamber inwards.

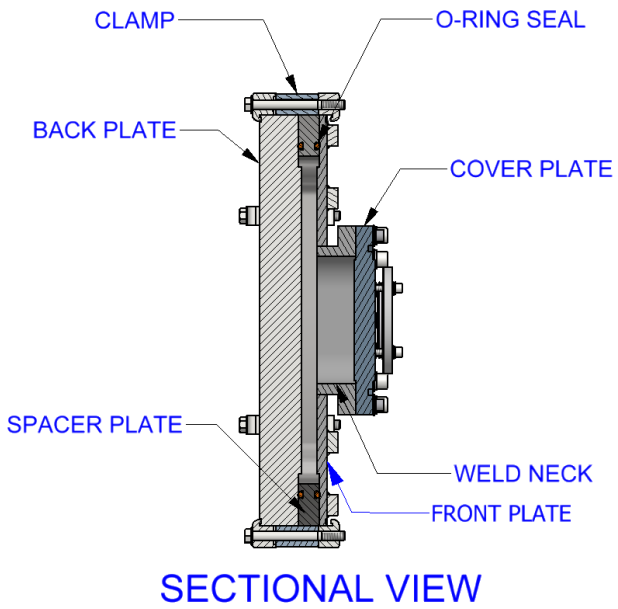


Figure 1: Construction details of test chamber.

O-ring seals were used on either side of the spacer plate to seal the spacer plate with the front plate and back plate. A weld neck was welded onto the front plate. During the first phase of the testing procedure, the top surface of the cover plate and the mating face of the weld neck were polished to 32 micro-inches surface finish because a wire seal would be placed and tested on this surface. During the second phase of the testing procedure, the two mating surfaces were polished to a 16 micro-inch surface finish. The length of the testing surface for the wire seal is approximately 3.6 meters. The entire vacuum chamber from end to end is 4 meters, as shown in Figure 2 below. Stiffening ribs were welded onto the surface of the front plate toward the cover plate. The main reason for the stiffening ribs was to have a chamber with adjustable stiffness which could be either increased or decreased by inserting stiffeners along the length of the stiffening ribs.

Copyright © 2013 CC-BY-3.0 and by the respective authors

ISBN 978-3-95450-138-0

DESIGN AND TESTING OF FARADAY'S CUP FOR NSLS-II LINAC AND BOOSTER*

H. Fernandes#, B. Belkacem, W. Cheng, W. Guo, B. Kosciuk, J. Rank, S. Sharma, O. Singh, T. Tanabe and G. Wang
National Synchrotron Light Source II, Brookhaven National Laboratory, Upton, NY 11793, USA

Abstract

NSLS-II will provide 500 mA, 3 GeV beam of 1 nm emittance. It's planned to have top-off operation. To ensure bunch uniformity and constant current, the precise measurement of the charge becomes necessary. There are three Faraday Cup's at the end of the transport line in the Linac and Booster transport lines which serve this purpose. The details of the design consideration are presented in this paper. The Diagnostic group at NSLS-II, designed, prototyped and tested the Faraday Cup (FC). Power density calculations and FEA simulations were carried out for the three cases.

INTRODUCTION

At NSLS-II, the FC's serve as a beam dump and a charge measuring device, therefore we have three such devices at the end of each of the test beamlines. The beam energy in the Linac area is 200 MeV [1]. The beam size at FC1 and FC2 in the Linac transport line was found to be 0.2 mm horizontally and 0.5 mm vertically. Figure1 below indicates the location of FC1 and FC2 in the Linac area. Figure 2 indicates FC3 in the Booster area. The beam energy in the Booster area is 3 GeV with a beam size of 2.3 mm in the horizontal direction and 0.27 mm in the vertical direction.

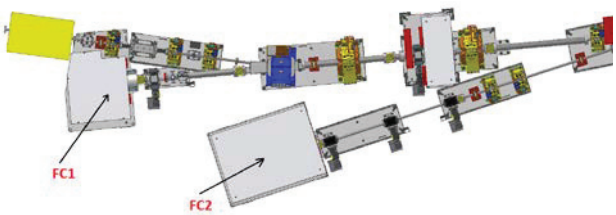


Figure 1: Location of Faraday's Cup in the linac area.

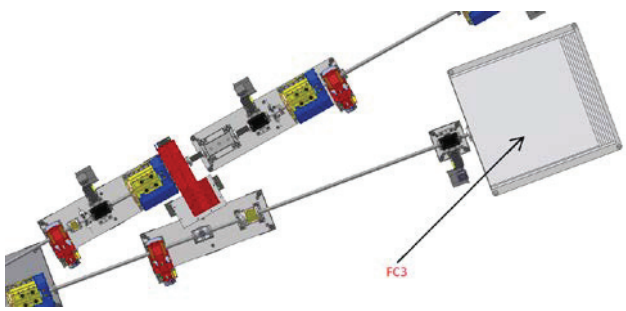


Figure 2: Location of the Faraday's Cup in booster area.

- Different devices are used to measure beam current. One way to measure the total charge of the beam in normal operation is by non intercepting devices such as current transformers (ICT, and DCCT). This non destructive method is independent of beam energy. These devices have to be calibrated to a device that will collect the totality of the electrons. For this reason an FC have to be installed close to the device to be calibrated (unknown losses between the two instruments introduce systematic errors).
- Another method to measure the charge is by using FCs. In this case, we need to stop and dump the electron beam for a certain period, preferably at full energy and bunch repetition rate. FCs are installed at the end of the transport lines. The beam will be sent to the FC during beam tune ups. Beam stops are used to absorb the entire beam.

MECHANICAL DESIGN

The designed Faraday Cup consists of a beam stop (graphite and copper pieces), which is essentially used to stop the beam. This is followed by a beam dump (stainless steel pieces). Details of this design are indicated in Figure 3.The radiation shower produced after stopping the beam must be absorbed. This is achieved by using layers of lead and borated polyethylene sheets. The third most critical component of the Faradays cup is its electrical circuit, which consists of an integrator followed by a digitizer. The ceramic brake isolates the beam dump from the rest of the assembly. The charge is measured by integrating the output voltage across the ceramic break. The beam dump consists of six plates which are one inch thick made of SS-304 and are bolted together. A knife-edge seal would ensure that the integrity of vacuum is maintained. This is machined on the first plate face of the SS-304 plate.

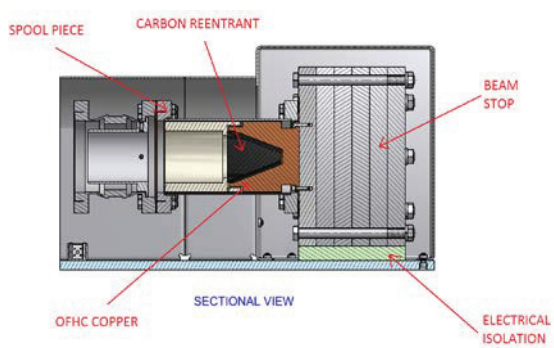


Figure 3: Construction details of FC.

Copyright © 2013 CC-BY-3.0 and by the respective authors

PREPARATION AND INVESTIGATION OF ANTIMONY THIN FILMS FOR MULTI-ALKALI PHOTOCATHODES

X. Liang, M. Ruiz-Osés, I. Ben-Zvi, Stony Brook University, Stony Brook, NY, 11794, USA
S. Schubert, E. Wang, Q. Wu, T. Rao, K. Attenkofer, J. Smedley, BNL, Upton, NY, 11793, USA
J. Wong, H. Padmore, LBNL, Berkeley, CA, 94720, USA
J. Jordan-Sweet. IBM T. J. Watson Research Center, Yorktown Heights, NY, 10598, USA

Abstract

Multialikali antimonide photocathodes exhibit high quantum efficiency in the visible light range, with low thermal emittance and are excellent candidate materials for high average current next generation ERLs or high repetition rate FELs. Although these materials have some excellent characteristics, control of the growth mode of the thin film and ultimately the surface roughness is difficult and will affect the emittance that can be obtained in high gradient fields. Being the first step in multi-alkali photocathode growth, the morphology of Sb films was investigated. X-ray diffraction pole figure (PF) measurement was used to determine the crystallinity of the Sb films. The measurements were complemented by atomic force microscopy (AFM) to determine the roughness and particle size. This study demonstrates how minor changes in deposition rate, thickness and substrate temperature can influence the Sb film properties.

INTRODUCTION

A.H. Sommer discovered that alkali metals such as Sodium (Na), Potassium (K), combined with antimony (Sb) result in photocathodes with high sensitivity and wide spectral response. Although methods for producing high QE films were established long ago, the remaining problems are mainly how to achieve good stoichiometric control so that long wavelength behaviour is reproducible and how to make very smooth films as required for high gradient photoinjectors. A collaboration of Stony Brook University, Brookhaven National Lab and Lawrence Berkeley National Laboratory aims to improve the performance of alkali antimonide photocathodes by using the tools of modern materials techniques such as X-ray diffraction (XRD), grazing incidence small angle X-ray scattering (GI-SAXS), X-ray reflectivity (XRR), AFM and X-ray photoelectron spectroscopy (XPS). [1-5]

This report will focus on recent progress in the analysis of the relationship between evaporation rates, film thickness and roughness.

EXPERIMENTALS

Ex-situ X-ray diffraction pole figure measurement was performed at the National Synchrotron Light Source (NSLS) X20A beam line at Brookhaven National Laboratory (BNL). For the PF measurement, the incident X-ray flux is approximately $8*10^{10}$ photons/second and the energy of the X-rays is 8.05KeV (λ = 1.5406Å). The size of the incident X-ray beam is 0.7 mm high and 0.7mm wide. The incident angle at the center of the linear detector was 20 degrees.

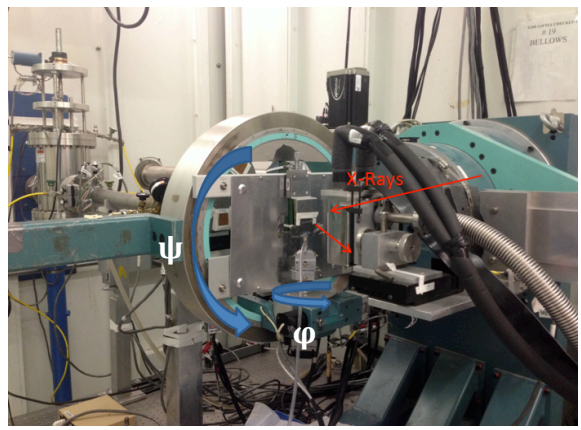


Figure 1: The experimental set up at the X20A beam line at NSLS. The beam line has a 4 circle Huber diffractometer, here just ψ and φ are moveable.

Si (100) wafers were used as the substrate, and all wafers were cleaned using hydrofluoric acid (HF), rinsed in deionized water and dried. The deposition was performed in a UHV chamber with a base pressure of 4×10^{-9} mbar; a Pfeiffer® Prisma QMG 200 residual gas analyzer (RGA) was used to monitored contaminants during growth. Values of H2O never exceeded 5.8×10^{-10} mbar, and CO/CO2 partial pressures were $< 1\times10^{-10}$ mbar during deposition. Deposition rates were monitored using an INFICON® quartz crystal film thickness monitor (FTM).

Surface topography was measured in air over a 1.5 × 1.5 micron area using a Nanosurf® Easyscan 2 AFM with a pyramidal Si (A-CLA mode) probe in BNL building 911 room 210A.

GROWTH PROCESS AND ANALYSIS

Ex-situ XRD PF measurement has been used to characterize the phases and texture changes of Sb thin films. The substrate size of 2cm ×1cm was used. Sb thin films were deposited on these in the UHV chamber by thermal evaporation, with the Sb being evaporated from

*Work supported by the United States Department of Energy through Contract numbers DE-AC02-98CH10886 and at Stony Brook University under Grant No. DE-SC0005713 with the U.S.DOE.
#liangx@bnl.gov

Copyright © 2013 CC-BY-3.0 and by the respective authors

ISBN 978-3-95450-138-0

SIMULATION AND OPTIMIZATION OF MULTI-SLIT BASED EMITTANCE MEASUREMENT FOR BNL ERL*

C. Liu†, D. Gassner, D. Kayran, M. Minty, P. Thieberger, BNL, Upton, NY 11973, USA

Abstract

A code for determining the beam emittance from a multi-slit image has been developed. To verify its validity, we simulated a beam distribution in 4D phase space at the multi-slit position and the resulting image at a downstream profile measurement device. We applied the algorithm to this image pattern to recover the beam emittance at the slit position. The dependence of the relative difference of the inferred emittance and the input emittance on the slit width and drift length are studied in detail and presented in this report.

INTRODUCTION

At the BNL ERL, a multi-slit device will be used for direct measurement of two dimensional beam phase space, which samples particles at discrete horizontal (or vertical) positions and projects the sampled beam on a downstream screen. The beam size and divergence of the sampled beam can be determined using the image acquired by the downstream profile device and the mask pattern dimensions. The emittance of the beamlets sampled by the multi-slit mask will be shown to be representative of the emittance of the beam incident on the mask. Here we will present the algorithm and its application using simulated data, and a study of geometry-dependent systematic errors in the inferred emittance.

ALGORITHM

The schematic for a multi-slit emittance measurement device is shown in Fig. 1. The incoming beam is sampled by a multi-slit mask. Beamlets formed by the mask project onto a profile measurement device and the resulting image is recorded. The beam size at the slits can be determined by the dimension of the slit pattern and the intensity of the beamlets. The beam divergence can be determined by the intensity distribution on the profiler.

The well accepted rules for multi-slit mask design [1, 2] are: the slit spacing is chosen such that beam is divided to 4-8 beamlets; the slit width is as narrow as possible as limited by current fabrication techniques; the drift length between mask and profiler is such that beamlets will spread out on the profiler until they overlap; the mask thickness is thick enough to stop most incoming particles; and the opening angle of the slit is comparable to the anticipated beam divergence.

Detailed formulas for slits emittance measurement can be found in Ref. [3]. The projection of the recorded image is usually treated as a multi-Gaussian distribution. The average divergence of each beamlet is calculated based on slit positions and peak positions. The rms divergence of the beamlets is calculated from the rms of the fitted Gaussian peaks. Suppose we get three arrays of parameters from multi-Gaussian fits of the projection, a, b and c, which are the intensity, peak position and sigma of the peaks. The slit positions are represented by an array x. The centroid of the beam at the mask is $< x >= \frac{1}{\sum_{i=1}^{n} a_i} \sum_{i=1}^{n} (a_i * x_i)$, here n is the number of beamlets. The rms size at the mask is

$$< x^2 >= \frac{1}{\sum_{i=1}^{n} a_i} \sum_{i=1}^{n} (a_i * (x_i - < x >)^2)$$

The average divergence of the beamlets is given by $x'_i = (b_i - x_i)/L$. The average divergence of the sampled beam is $< x' >= \frac{1}{\sum_{i=1}^{n} a_i} \sum_{i=1}^{n} (a_i * x'_i)$. The rms divergence of the beamlets is $\sigma'_i = c_i/L$. The rms divergence of the sampled beam at the mask is

$$< x'^2 >= \frac{1}{\sum_{i=1}^{n} a_i} \sum_{i=1}^{n} (a_i * \sigma_i'^2 + a_i * (\sigma'_i - < x' >)^2)$$

The position angle correlation term is

$$< xx' >= \frac{1}{\sum_{i=1}^{n} a_i} (\sum_{i=1}^{n} a_i * x_i * x'_i - \sum_{i=1}^{n} a_i < x >< x' >)$$

Then the emittance is calculated by

$$\epsilon = \sqrt{< x^2 >< x'^2 > - < xx' >^2}$$

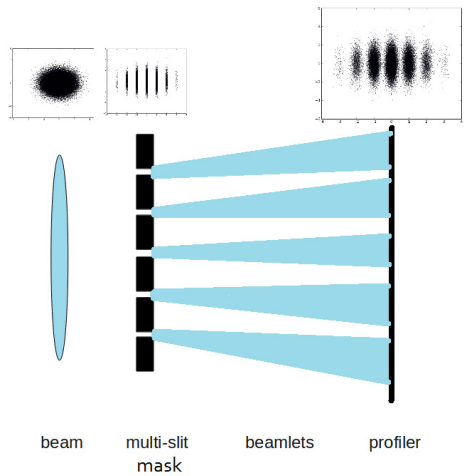


Figure 1: Schematic of a multi-slit emittance measurement device (not to scale).

* The work was performed under Contract No. DE-AC02-98CH10886 with the U.S. Department of Energy.

† cliu1@bnl.gov

Copyright © 2013 CC-BY-3.0 and by the respective authors

3D HALL PROBE CALIBRATION SYSTEM AT INSERTION DEVICE MAGNETIC MEASUREMENT FACILITY AT BNL *

M. Musardo#, T. Corwin, D. Harder, P. He, C. A. Kitegi, W. Licciardi, G. Rakowsky and T. Tanabe,
National Synchrotron Light Source II, Brookhaven National Laboratory, Upton, NY 11793, USA

Abstract

Hall probes are commonly used to measure local magnetic field, however they need to be calibrated. This paper describes the accurate 3D Hall probe calibration system developed by the NSLS-II Insertion devices group. The calibration system and the calibration curves are presented. An Arepoc 3D Hall probe used to characterize the Insertion Devices (IDs) has been calibrated. The probe contains three sensors oriented perpendicular to each other in order to measure three components of the magnetic field. The three Hall sensors are mounted on a circuit board and their active area dimensions are 0.05 mm x 0.05 mm with a linearity error up to 1 T less of 0.2%.

INTRODUCTION

The 3D Hall probe calibration system consists of a GMW dipole electromagnet, a precision magnet power supply system, a nuclear magnetic resonant teslameter (NMR) and a motorized probes supporting stage.

In order to perform an absolute and precise calibration, the Arepoc 3D Hall probe must be positioned in a known magnetic field. The coordinate frame of the probe is indicated in Fig. 2. Sensor 1 is perpendicular to z direction (longitudinal direction), sensor 2 is perpendicular to x direction (horizontal direction) and sensor 3 is perpendicular to y direction (vertical direction).

HALL PROBE CALIBRATION SYSTEM

GMW dipole electromagnet (see Fig. 1) and a low noise and high stability Danfysik System 8500 Power Supply are used to create a constant and uniform magnetic field in the region around the point midway between the coils. The maximum magnetic field obtained with a current of 140 A at pole gap of 30 mm is of about 2.148 T and the uniformity achieved is of 110 ppm in 10 mm^3. The magnet and the power supply are water cooled.

A Metrolab PT-2025 NMR Teslameter System (Fig. 1) precisely measures the absolute magnetic field produced by the GMW dipole magnet. It is based on the nuclear magnetic resonance effect and achieves 5-ppm absolute accuracy and 1mG resolution for measurements in the range from 430 G to 137 kG. A multiplexer with different NMR probes is used, because the magnetic field value could be in one of several probe's ranges. So the proper NMR probe needs to be chosen and positioned within the magnetic field in the right position. A motorized *NMR Probe Supporting Stage* (see Fig. 3) is used to manage the NMR probe and to position it in the center of the electromagnet.

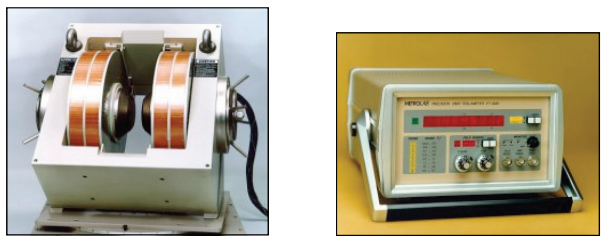


Figure 1: GMW dipole electromagnet and metrolab NMR teslameter.

An integrated digital multimeter is used to measure the Hall voltages of the sensor under calibration and a *Hall Probe Supporting Stage* (see Fig. 4), needed to move and rotate the probe during the calibration, provides precise controlled linear and angular motions in all required directions.

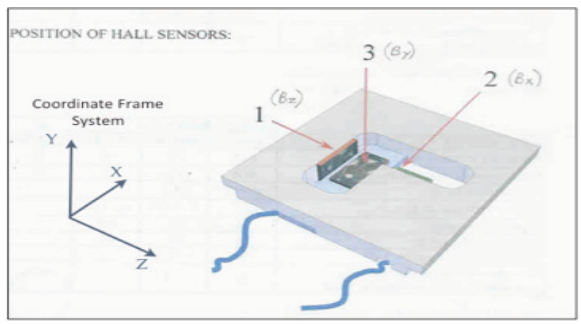


Figure 2: Coordinate frame system.

The control system written in LabView coordinates and automates the calibration measurements.

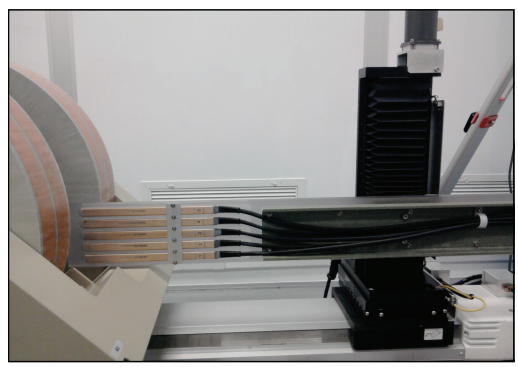


Figure 3: NMR probe supporting stage.

*Work supported by DOE contract DE-AC02-98CH10886
#musardo@bnl.gov

ISBN 978-3-95450-138-0

Copyright © 2013 CC-BY-3.0 and by the respective authors

NSLS-II MAGNETIC MEASUREMENT SYSTEM FACILITY*

M. Musardo#, T. Corwin, D. Harder, P. He, C. A. Kitegi,
W. Licciardi, G. Rakowsky, J. Rank, C. Rhein and T. Tanabe,
National Synchrotron Light Source II, Brookhaven National Laboratory, Upton, NY 11793, USA

Abstract

The National Synchrotron Light Source II at Brookhaven National Laboratory (BNL) is a storage ring of 3 GeV electron beam energy that will provide ultra high brightness and flux and exceptional beam stability using advanced insertion devices (IDs). The magnetic characterization of these devices is important to achieve these performances. In order to perform precise and accurate measurements of the NSLS-II IDs, several recent improvements on actual magnetic measurement system have been developed. The system includes a flipping coil bench to measure the first and second magnetic field integrals and a Hall probe bench to perform magnetic field measurements of different types of IDs.

The main features of the hardware system, control program and the recent improvements in the magnetic measurements system are presented.

INTRODUCTION

All insertion devices for NSLS-II have been bought from different vendors. It is planned to measure these devices at NSLS-II in order to confirm vendors. Our magnetic measurements are the final verification of the complex design and fabrication process, so that proper certification of device can be made. The magnetic measurement system facility at BNL consists in a Hall probe bench MMB-6500, built by Kugler, GmbH and an Integrated Field Measurement System (IFMS), provided by ADC [1].

HALL PROBE BENCH

The Hall probe mapping bench has an ultra-precision granite guide beam. There are nine conrolled axes. The air-ride Z axis has a travel distance of 6.5 meters. The trajectory deviation for the Z axis carriage is ± 7 µm and the positioning accuracy is ± 1 µm. The X and Y axes are high precision stages. Mounted to the Y stage carriage is a rotary stage. Mounted to the rotary stage is a small X-Y stage. Mounted to that is a pair of goniometers. Thus the extended Hall probe can be positioned in any orientation and then translated (see Fig. 1). The Z' axis is used as a follower stage for transporting the cables, so that cable loading does not affect the Z axis trajectory. Instrumentation is also carried on the follower stage (see Fig. 2).

The Z axis has two encoders. A linear scale encoder is used for the motion control and a laser interferometric encoder is used for generating triggers. A Delta Tau controller is used for motion control. A Senis 3D probe is used as the Hall sensor.

Each Hall sensor, arranged along X-axis, has been accurately calibrated to provide a calibration curve of its response to the strength of the magnetic field up 1.9 Tesla. The magnetic field sensitive volume for each sensor is 150x150x1 µm and the angular accuracy of axes with respect to the reference surface is about of ± 2°.

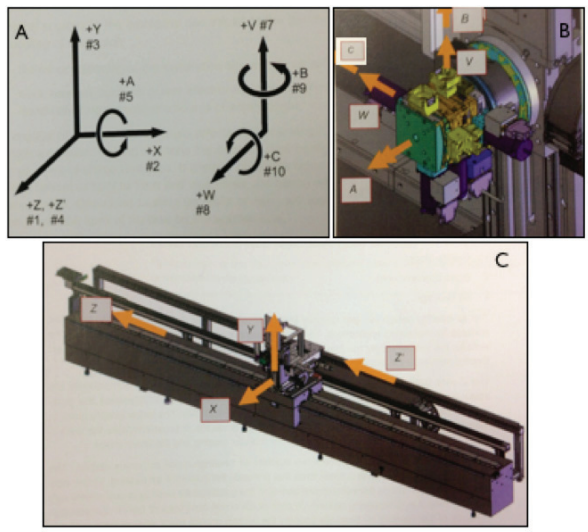


Figure 1: A: Machine coordinate system. Axis movements viewed from undulator towards granite. B: Arrangement of the goniometer head axes V, W, A, B and C. C: Arrangement of the three main linear axes X, Y, Z and auxiliary axis Z'.

In order to improve the accuracy and the repeatability of the Hall probe measurements, the electronics of the data acquisition have been upgraded. In particular a new time synchronization system has been developed in order to optimize the first integral repeatability and the precision of magnetic field measurements. Figure 3 shows the vertical field of a Damping Wiggler with period length of 100 mm at the minimum gap of 15 mm (blue line) and the field difference between two consecutive Hall scans (red line), which represents an absolute error of the magnetic field, measured with the initial triggering method. This error is a periodic and systematic curve with precise harmonic frequencies (see Fig. 4). The peak-to-peak amplitude is about of 30 G and occurs around the magnetic field gradient. It is a strong indication of a small jitter in the start trigger of the Hall probe measurements. This trigger jitter was reduced by changing from a motion controller generated trigger to a trigger generated by external Hardware, the parallel digital signal from the laser encoder is processed in external logic which feeds a trigger signal into an FPGA aboard a National Instruments CompactRIO real-time PAC. The

Copyright © 2013 CC-BY-3.0 and by the respective authors

ISBN 978-3-95450-138-0

UPGRADE OF BEAM INJECTION DIAGNOSTICS AT BNL NSLS

S. Seletskiy#, Y. Hidaka, B. Podobedov, X. Yang, BNL, Upton, NY 11973, USA

Abstract

In this paper we report the upgrade of the diagnostics of the beam injection system at BNL NSLS. Installation of commercially available turn-by-turn beam position monitors (BPMs) in the VUV and X-Ray rings allowed us to build the detailed injection models for each of the rings. In addition we built the tools for real time monitoring of and troubleshooting the beam injection into the rings.

INTRODUCTION

The NSLS accelerator complex consists of the 120 MeV linac, the booster accelerating the beam to 740 MeV and the two storage rings: 800 MeV VUV ring and 2.8 GeV X-Ray ring. Injection into each of the rings is performed at 740 MeV energy. The injection hardware in each of the rings consists of an injection septum (DC-magnet in case of the VUV ring and pulsed one for the X-Ray ring) and three fast multi-turn kickers. A single turn-by-turn (TBT) BPM was added to each ring for the purpose of injection monitoring. As a result a set of tools was created which are successfully used for troubleshooting injection problems. In this paper we discuss the operation of this diagnostics using the VUV ring as an example.

VUV RING INJECTION SETUP

The beam is injected into the VUV ring through the septum (BUISH) when the amplitudes of the three injection kickers (bumps BUIFB1, BUIFB2 and BUIFB3) are close to their peak values. Fig. 1 schematically shows the locations of the injection hardware and the fast kicker waveforms.

Since the duration of the kicker pulse is 1.3 us and the electron orbital period in the VUV ring is 170 ns the injected beam is affected by the kickers on multiple turns after the injection. This substantially complicates the injection process. At pick-up 5 (see Fig. 1) we installed a dedicated turn-by-turn BPM (Libera Electron [1]) to study and monitor the injection. The Libera unit is synchronized with the VUV ring orbital period and is triggered by the Booster extraction kicker trigger.

Since we can communicate to the machine from MATLAB through the "middle layer" software [2] and since the Libera settings and readings are easily accessible from MATLAB, Accelerator Toolbox (AT [3]) is a natural environment to model the ring injection. Thus we built the injection model by integrating the fast kickers into the AT model of the VUV ring.

The AT provides tools for beam tracking and calculation of lattice functions. Our AT model includes the linear ring lattice as well as kicks from sextupoles. It was calibrated with MATLAB-based LOCO [4].

#seletskiy@bnl.gov

BUILDING INJECTION MODEL

Since the kicker waveforms are nearly identical up to a scaling factor, we used the measured BUIFB2 waveform for each modelled bump. In simulations we only use half-wave of the sinusoid and ignore the residual kicker field. Each kicker's amplitude in the model is scalable, but the width of the waveform is kept constant.

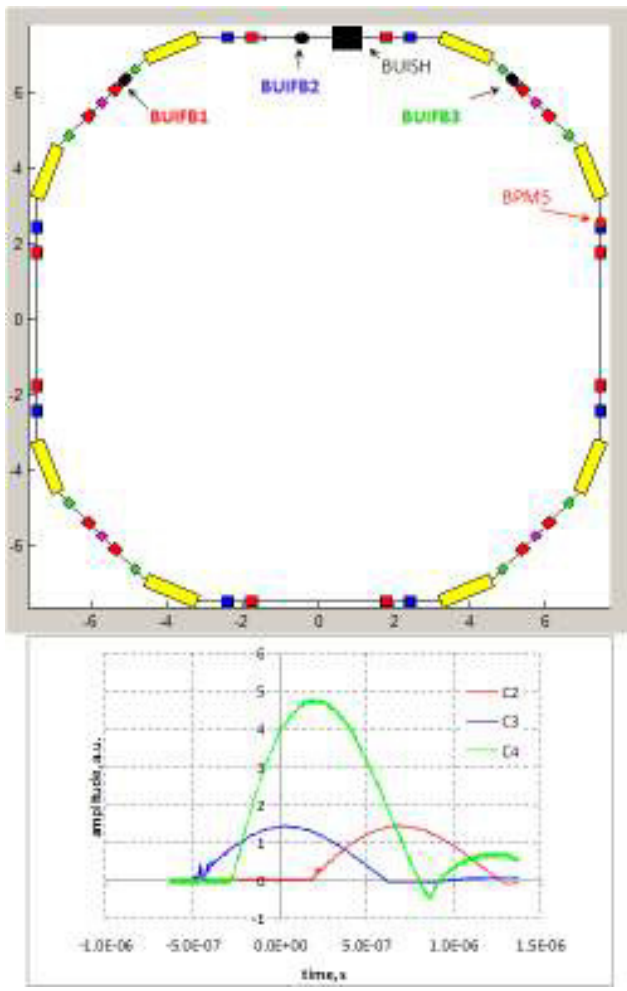


Figure 1: Locations of injection septum and fast injection kickers in the VUV ring (upper plot). The turn-by-turn diagnostics is connected to BPM5. Lower plot shows measured fast kicker waveforms in arbitrary units. Red line is BUIFB1, blue is BUIFB2 and green is BUIFB3.

Initial benchmarking of the model was performed with the stored single-bunch beam. Fig. 2 shows the readings of the TBT BPM over 20 turns versus the model predictions for the stored beam kicked with BUIFB1.

As one can see, there is a good agreement between the model predictions and the measured data. The same level of agreement was obtained for BUIFB2 and BUIFB3, as well as all three kickers turned on simultaneously. The benchmarking was performed both at the stored beam

Copyright © 2013 CC-BY-3.0 and by the respective authors

ISBN 978-3-95450-138-0

ALKALI ANTIMONIDE PHOTOCATHODES FOR EVERYONE

J. Smedley, K. Attenkofer, S. G. Schubert, BNL, Upton, NY 11973, USA
H. A. Padmore, J. Wong, LBNL, Berkeley, CA 94720, USA
J. Xie, ANL, Argonne, IL 60439, USA
M. Ruiz-Oses, I. Ben-Zvi, X. Liang, E. M. Muller, Stony Brook University, Stony Brook, NY 11794, USA
J. DeFazio, Photonis USA PA, Inc., Lancaster, PA, 17601, USA

Abstract

The next generation of x-ray light sources will need reliable, high quantum efficiency photocathodes. These cathodes will likely be from the alkali antimonide family, which currently holds the record for highest average current achieved from a photoinjector. In this work, we explore a new option for delivering these cathodes to a machine which requires them: use of sealed commercial vacuum tubes. Two sealed tubes have been introduced into a vacuum system and separated from their housing, exposing the active photocathode on a transport arm suitable for insertion into an injector. The separation was achieved without loss of QE in one case. These cathodes are compared to those grown via traditional methods, both in terms of QE and in terms of crystalline structure, and found to be similar.

INTRODUCTION

Alkali antimonide photocathodes have a long history in low-light photodetection, including image intensifiers. These needs have been met by commercial production; principally by RCA and its successors. The accelerator community also has great interest in alkali antimonide photocathodes – they are a prime candidate for use in high-brightness photoinjectors of free electron lasers and 4th generation light sources [1-3]. However, within the accelerator community, cathodes have traditionally been grown in dedicated vacuum systems tied to specific injectors. In some cases cathodes have been transferred from one system to multiple injectors, typically on a limited basis [2,4].

We have developed tools to understand the formation of these materials, both structurally and chemically, with the goal of altering the growth to produce cathodes with less roughness, better stoichometry, and larger crystal grains. The *in situ* techniques being used are x-ray diffraction (XRD), grazing incidence small angle x-ray scattering (GISAXS) and x-ray reflection (XRR). These tools enable determination of the crystal form of the cathode at each phase of growth, the film thickness and roughness, the texture and grain size of the film, and the presence of "imperfectly reacted" material. This work has been carried out at the National Synchrotron Light Source (NSLS) using beamline X21 and at the Cornell High Energy Synchrotron Source (CHESS) using beamline G3.

The goal of this work is to enable the large scale production of identical photocathodes, using recipes developed in the *in situ* analysis chamber, which will provide high QE while minimizing the surface roughness which can dominate the intrinsic emittance [5,6]. One aspect of this effort is collaboration with an industrial partner to produce photocathodes in sealed tubes which can be separated in vacuum.

Figure 1 shows a prototype photocathode in a sealed vacuum capsule. The substrate for growth is polycrystalline Molybdenum, which is brazed to the copper plug shown in the picture to the left. The capsule is sealed with a low temperature solder visible around the copper. A window on the isolated top electrode enables the QE of the device to be measured while the capsule is still sealed. The photocathode is visible as the blue area in the picture on the right, through this window.



Figure 1: Sealed photocathode.

EXPERIMENT

In the interest of space, the growth chamber with *in situ* x-ray analysis is described elsewhere [7]. This chamber has been used to measure both the capsule photocathodes, and to grow cathodes for comparison. The comparison cathodes are grown in a UHV chamber, with a typical operating pressure of 0.2 nTorr. Residual gas analysis confirms that the partial pressures of reactive gases (H_2O, CO) are better than 0.05 nTorr. Silicon [100] wafers 1x2 cm^2 are used as substrates; these are exposed to HF prior to installation, and baked to 500 C for an hour prior to growth. Once the substrate has cooled to 160 C, a further cleaning of the substrate is achieved by an initial potassium evaporation – XRR measurements confirm that this K does not remain resident on the surface, however the QE of cathodes grown is significantly improved by this initial step. Antimony is evaporated from PtSb beads; alkali-Bi sources from Alvatech are used to supply Potassium and Cesium. Deposition is sequential, with Sb evaporated, then K, then Cs, all at ~0.2 Å/s. The QE is observed during K and Cs evaporation, and the deposition is halted when the QE reaches a plateau. The "traditional" cathode is a multi-layer growth on a single substrate, with the first cathode "baked off" (substrate raised to 500 C for 10 min) prior to the growth of a second (recipe in Table 1).

Copyright © 2013 CC-BY-3.0 and by the respective authors

ISBN 978-3-95450-138-0

PROGRESS ON GROWING A MULTI-ALKALI PHOTOCATHODE FOR ERL AT BNL

E. Wang I. Ben-Zvi, S. Belomestnykh, T. Rao, J. Smedley, BNL, Upton, NY 11973, USA
X. Liang, M. Ruiz-Oses, Stony Brook University, Stony Brook, New York 11794, USA

Abstract

K_2CsSb is a robust photocathode capable of generating electron beams with high peak, high average current and low thermal emittance. During the last two years, a great improvement in the design and fabrication of a reliable deposition system suitable for K_2CsSb cathode growth and its insertion into BNL high current ERL SRF gun has been achieved. A standard procedure for the growth of multi-alkali cathodes combined with another procedure to transport these cathodes into the SRF gun was developed. The first cathode is planned to be grown on a copper insert and mounted into the 704 MHz gun. In this article, we will describe the progress of cathode growth and transport for ERL project. In particular, effect of excimer laser exposure and the cathode growth on Ta will be included.

INTRODUCTION

The multi-alkali photocathode is considered to be suitable for high current applications due to its high quantum efficiency at visible wavelengths. The photocathode of choice for BNL-ERL photo-injector is K_2CsSb due to its capability to generate high average current and low emittance electron beams. The 704 MHz SRF photoinjector is built for testing ERL concept up to 500 mA high average current. A multi-alkali photocathode deposition system for this gun was built by Advanced Energy Systems (AES) [1]. In last two years, we assembled entire system and grew several cathodes to find the optimal cathode preparation parameters. We also tested the transport cart and insertion of the cathode plug through the load-lock system. 0.2% QE was obtained from a K_2CsSb cathode grown on the copper substrate. Currently, the gun is being conditioned for CW SRF operation with a copper cathode plug and the vacuum in both the deposition chamber and the transport cart is maintained in low 10^{-10} torr range. The cathode will be deposited on this plug soon after the conditioning. The first cathode test in the gun is scheduled for November.

DESCRIPTION OF THE DEPOSITION SYSTEM

The K_2CsSb deposition system consists of a main deposition chamber and three source chambers attached to the main chamber but isolated from each other and the main chamber through gate valves. The main chamber is equipped with two view ports, an RGA, a quartz crystal monitor, anode, resistive heater and load-lock port. Ion pumps integrated with NEG pumps maintain the vacuum in low-10^{-10} torr scale. Each of the source chambers has one ion pump keeping the vacuum in mid-10^{-10} torr range. Bellows coupled manipulator can move the sources into the deposition chamber and locate them in front of the substrate. We use Alvatec Alkali metal source of type S and 99.999% purity pellets antimony source. The alkali sources are evaporated by resistive heating of the source container and the Sb is evaporated by heating a boat which holds the crucible containing Sb pellets. Each alkali arm contains two Cs or K sources to increase the evaporation area and cathode uniformity. To protect the sides of the cathode plug from being coated with the cathode material, an aperture is placed between the substrate and the source to limit the deposition area to a 0.75 inches diameter. The substrate can be heated or cooled by flowing dry N_2 gas through a pipe in contact with the stalk. With the same pipe, the stalk is maintained at LN_2 temperature when in the SRF gun. The stalk can be heated up to 200° C and maintained at optimal temperature for evaporation. To determine the initial quantum efficiency, the cathode is irradiated with a low power CW laser. Emitted electrons are collected at the anode in front of the cathode. The whole deposition system is placed in a class 10,000 clean room shown in Figure 1. The load lock connection port is inside a class 100 clean room to avoid accumulation of the particulates in section that comes in contact with the SRF gun.

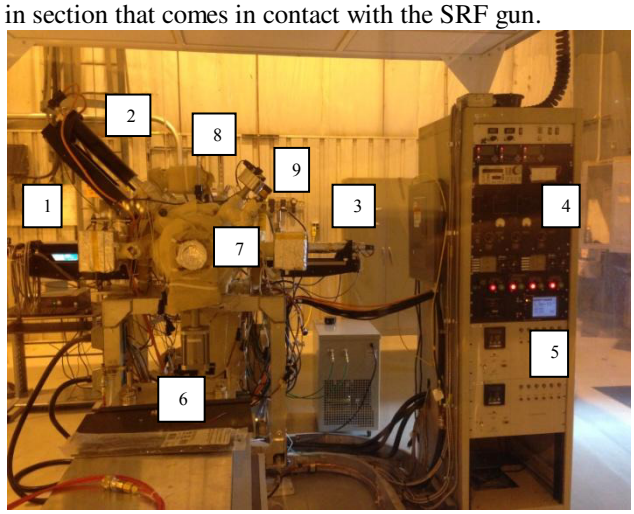


Figure 1: The picture of ERL-deposition system: 1 – K source; 2 – Sb source; 3 – Cs source; 4 – control system for valves and source; 5 – power supply for baking; 6 – table for supporting cathode transport cart; 7 – load lock port; 8 – heater; 9 – crystal monitor.

*Work supported by the United States Department of Energy through Contract numbers DE-AC02-98CH10886 and at Stony Brook University under Grant No. DE-SC0005713 with the U.S.DOE.
#wange@bnl.gov

Copyright © 2013 CC-BY-3.0 and by the respective authors

ISBN 978-3-95450-138-0

TEMPERATURE DEPENDENCE OF PHOTOEMISSION FROM COPPER AND NIOBIUM*

J.R. Harris[1,#], A. Kara[2,3], C.W. Bennett[2], M. Galt[2],
A.D. Holmes[2], R.L. Swent[2], J.W. Lewellen[4], and J. Sears[5]

[1]Dept. of Electr. & Computer Engineering, Colorado State University, Fort Collins, CO 80523
[2]Department of Physics, Naval Postgraduate School, Monterey, CA 93943
[3]Lieutenant (Junior Grade), Turkish Navy
[4]Los Alamos National Laboratory, Los Alamos, NM 87545
[5]Laboratory for Elementary-Particle Physics, Cornell University, Ithaca, NY 14853

Abstract

Photocathodes remain the principal electron sources for many particle accelerators. With the increasing interest in the use of superconducting radiofrequency electron guns, it is important to understand how operation at cryogenic temperatures affects the performance of photocathodes. Here we report measurements of the quantum efficiency of copper and niobium under illumination with 266 nm light at temperatures between 85 K and 400 K. The quantum efficiency of copper was found to vary strongly over this range, while there was only a minimal change in the quantum efficiency of niobium.

INTRODUCTION

Superconducting radio-frequency (SRF) electron guns combine efficient CW operation with the excellent vacuum needed for high-quantum efficiency (QE) photocathodes and the high surface gradients needed to maintain the quality of high-charge bunches. However, they remain an immature technology, with a number of very different configurations currently being investigated [1]. One major concern has been how to best balance the tradeoffs associated with integrating photocathodes into these devices. As part of its research program on SRF guns [2,3,4,5], the Naval Postgraduate School has studied some of these issues, including the potential contamination from dispenser photocathodes [6,7] and cathode stalk cooling to mitigate thermal and RF losses [8]. Many SRF guns use a normal-conducting cathode which is mechanically isolated from the cavity to minimize heat leaks. But even without mechanical contact between the cavity and the cathode, the cathode will be radiatively cooled due to the surrounding 2 - 4 K environment. This raises the interesting question of how the cryogenic environment affects the performance of photocathodes. There have been many measurements of the QE of metal cathodes, including at cryogenic temperatures. However, comparing QE measurements from one experiment to the next is difficult because of differences in sample and testing conditions. Having a single experimental apparatus where the temperature of a cathode can be varied, while keeping other influences largely constant, aids in effectively isolating the dependence of QE on temperature. Accordingly, we modified the cathode stalk cooling experiment to serve as a temperature-controlled photoemission test stand, and used it to measure the QE of copper and niobium at temperatures from 85 K to 400 K with 266 nm light [9]. Our experimental apparatus and results are reported here.

EXPERIMENTAL APPARATUS

Figure 1 shows a schematic of the test stand. The cathode stalk (Fig. 2) was formed from a copper cylinder with a recess in the front surface to accept metal cathode samples, with the samples held in place by a copper retaining ring to provide good thermal and electrical contact between the samples and the stalk. Temperature control was provided by a liquid nitrogen line and a pair of resistive heaters in the back of the cylinder. The heaters were supplied from a variable autotransformer, while liquid nitrogen was supplied from a pressurized fill pot used for the experiments described in Ref. [8]. Temperature measurements were made with LakeShore DT-670-SD and DT-670-CU-HT diodes placed on the front and back faces of the cathode, respectively; these limited operation to temperatures at or below 400 K. The diodes were connected to a computer by a LakeShore 218 temperature monitor, and the data was recorded every 5 seconds by a LabView program.

The vacuum envelope was made from conventional UHV components, with an ion pump providing typical pressures of 3×10^{-8} - 4×10^{-7} Torr at room temperature during testing. In operation, the rate of cathode heating had to be limited to prevent vacuum pressure spikes. A ceramic break was placed around the cathode stalk, with the downstream end electrically isolated from the rest of the experiment to serve as the anode, and connected to a 10 kV Glassman high voltage supply. The floating end also contained a UV window and a small magnet to disperse the photoelectrons to prevent charging of the window. A Bergoz fast current transformer mounted outside the ceramic break provided a time-resolved measurement of the current flow on the stalk, and therefore served as a measure of emitted current.

*Work supported by the Office of Naval Research and the High Energy Laser Joint Technology Office.
#john.harris@colostate.edu

Copyright © 2013 CC-BY-3.0 and by the respective authors

BEAM POSITION AND PHASE MEASUREMENTS OF MICROAMPERE BEAMS AT THE MICHIGAN STATE UNIVERSITY REA3 FACILITY*

J. Crisp, D. Constan-Wahl, B. Durickovic, G. Kiupel, S. Krause, D. Leitner, S. Nash, J. A. Rodriguez#, T. Russo, R. Webber, W. Wittmer, NSCL/FRIB, MSU, East Lansing, MI 48824, USA
N. Eddy, C. Briegel, B. Fellenz, D. Slimmer, FNAL, Batavia, IL 60510, USA
M. Wendt, CERN, Geneva, Switzerland

Abstract

A high power CW, heavy ion linac will be the driver accelerator for the Facility for Rare Isotope Beams (FRIB) being designed at Michigan State University (MSU). The linac requires a Beam Position Monitoring (BPM) system with better than 100 micron resolution at 100 microamperes beam current. A low beam current test of the candidate technology, button pick-ups and direct digital down-conversion signal processing, was conducted in the ReA3 re-accelerated beam facility at Michigan State University. The test is described. Beam position and phase measurement results, demonstrating ~250 micron and ~1.5 degree resolution in a 45 kHz bandwidth for a 1.0 microampere beam current, are reported.

INTRODUCTION

The Facility for Rare Isotope Beams (FRIB) [1] will be a new accelerator-based user facility for research in nuclear physics. It will be located in the MSU campus and it is scheduled for completion in 2022. Its driver linac will accelerate ions as heavy as Uranium to energies higher than 200 MeV/u delivering up to 400 kW of beam power into a target. The desired Rare Isotope Beam (RIB) product of the reactions in the target will be transported to the different experimental areas after being selected in a fragment separator. Alternatively, the RIB can be thermalized, charge-bred and postaccelerated in the ReA re-accelerator [2] before being sent to an alternative experimental hall.

While the FRIB facility completion is scheduled for 2022, the first stage of the ReA re-accelerator was recently completed and connected to the Coupled Cyclotron facility (CCF) [2, 3]. During the measurements described in this paper, it has been used as a stand-alone accelerator to test the FRIB's prototype BPM system using a molecular Hydrogen beam produced by the off-line stable ion source.

DESCRIPTION OF REA3 AND THE BPMS

A Colutron-type ion source is used to produce several microamps of H_2^+ beam with an initial energy of 24 keV (defined by the 12 keV/u injection energy of the RFQ). The beam is then transported through an electrostatic transfer line and injected into a 4-rod 80.5 MHz RFQ after being bunched using a multiharmonic buncher. After the RFQ, the 600 keV/u beam is rebunched as it passes through a $\beta = 0.041$ SRF cavity operated at its zero-crossing phase (located in the first cryomodule (CM1) of the linac) and then accelerated to a few MeV/u when it passes through six more $\beta = 0.041$ SRF cavities located in the second cryomodule (CM2). Superconducting solenoids equipped with corrector coils inside the cryomodules are used to focus and steer the beam. During the tests, the two BPM sensors were installed in a drift space approximately 0.6 m down-stream of CM2 and separated by 2.08 m (Figure 1). Movable slits and Faraday cups in diagnostics stations before and after the BPMs were used to center and characterize the beam during the tests and beam attenuators and collimator slits were used to change the beam current.

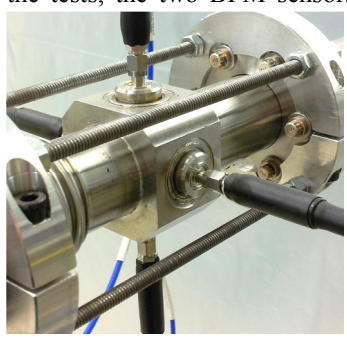


Figure 2: Prototype BPM as tested in ReA3.

The BPM system comprises two button-type BPM sensors (Figure 2, Table 1), signal amplifiers and digitizers that provide raw and processed data via EPICS channels to the control room. The button pickup has a design capacitance of 2 pF and impedance of 50 Ω. The

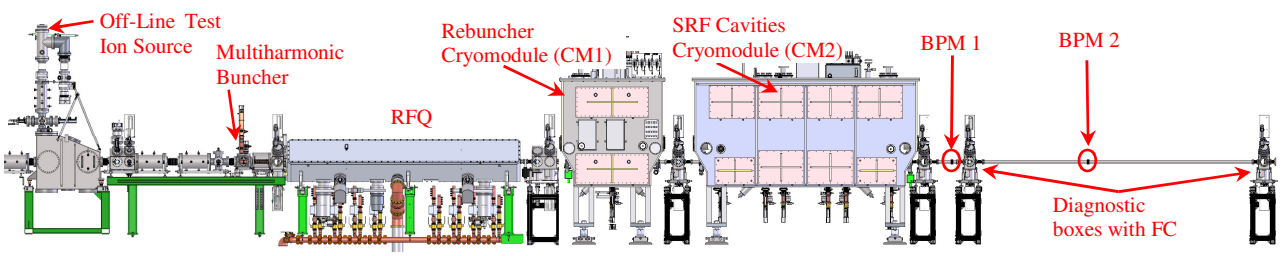


Figure 1: Layout of the ReA3 re-accelerator during the BPM tests.

* This material is based upon work supported by the U.S. Department of Energy Office of Science under Cooperative Agreement DE-SC0000661, the State of Michigan and Michigan State University, and the National Science Foundation, under Cooperative Agreement PHY-1102511.
#rodriguez@frib.msu.edu

ISBN 978-3-95450-138-0

Copyright © 2013 CC-BY-3.0 and by the respective authors

LIFETIME STUDY OF TUNGSTEN FILAMENTS IN AN H- SURFACE CONVERTER ION SOURCE*

I.N. Draganic#, J. F. O'Hara, and L. Rybarcyk, LANL, Los Alamos, NM 87545, USA

Abstract

The tungsten filaments are critical components that limit the lifetime of the H- surface converter ion source. Their finite lifetime has a huge impact on the maintenance schedules and overall availability of an accelerator facility. We present in this work a simple analytical filament lifetime model and 3D thermal simulation explaining basic phenomena of filament erosion and electrical resistance changes during a normal run of an H- production ion source at the Los Alamos Neutron Science Center (LANSCE). The calculation of filament longitudinal temperature profile takes into consideration the effects of ohmic heating, thermal conductivity and total emissivity for tungsten wires in high vacuum. The simulation includes the DC voltage operation of the filament with and without pulsed arc discharge current and gives the differential filament resistance changes, metal evaporation rates and theoretical electron emission currents. The results of the computation are compared with observed experimental data recorded using the EPICS control system during a normal LANSCE production cycle of 28 days with pulse repetition of 60 Hz and duty factor of 5%.

H- ION SOURCE LIFETIME

H- surface converter ion sources are well described elsewhere [1-4]. Three nearly-identical H- radial extraction converter ion sources (see Fig. 1A) have been utilized for proton beam production at LANSCE for more than 25 years. These H- sources deliver typical beam current up to 18 mA into an 80-kV electrostatic column and have operational lifetimes more than four weeks between accelerators maintains periods at a repetition rate of 60 Hz and duty factor of 5 %. Typical EPICS-recorded data of the extracted H- ion beams and an evolution of each filament's relative differential resistance during an entire cycle are presented in Figure 2. The negative-ion source consists of a filament driven arc discharge in a permanent-magnet, multi-cusp vacuum chamber for plasma confinement and a negatively biased converter electrode for H- beam production. The source uses two filaments made of high purity tungsten wires (99.99%), bent in a characteristic shape (see Figure 1B) with length of 297 mm, 1.6 mm thick diameter, weight of ~12 g and resistance of 7.8 mΩ at 295 K. Nominal filament currents of 100 to 106 A are driven by DC constant voltage power supplies (11 - 12V) bringing the wires to working temperature range of 2600 to 2700 K. The increase of filament temperature for higher electron output (plasma discharge) or more intense H- current is limited by the increasing of evaporation of filament material, which

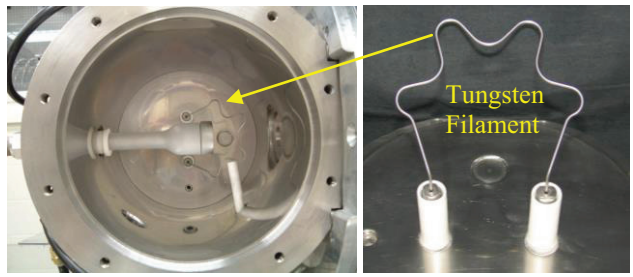


Figure 1: An internal side view of the LANSCE H- ion source is shown (A). New tungsten wire mounted on the water cooled ports (B).

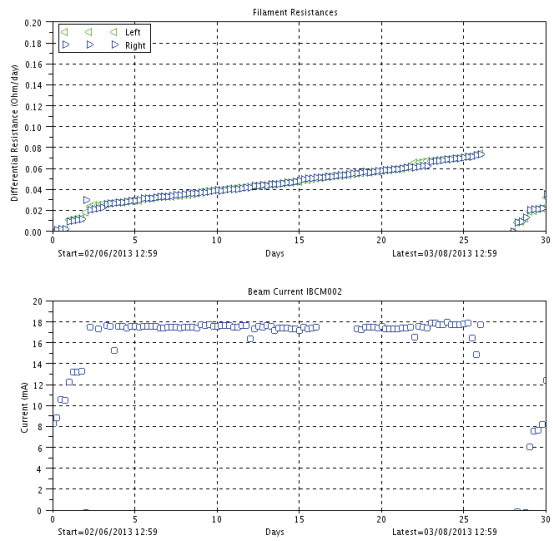


Figure 2: An EPICS application plots for operation monitoring purposes the filament relative differential resistances and the 80 keV extracted beam currents during a LANSCE beam production cycle (points every 6 hours).

decreases the lifetimes of the filaments, and ultimately limits the ion source operating period before replacement. The characteristics of tungsten filaments in vacuum at various high temperatures were studied in detail for incandescent lamps, radio tubes and in other scientific and engineering investigations [5-12]. There are two empirical criteria for critical differential resistance that predict the onset of filament failure: a) 12% of total increase in filament resistance or decrease in mass weight [5, 6] and b) 19 % of total increase in filament resistance or 10% of reduction in wire diameter [4, 8-12].

FILAMENT RELATIVE DIFFERENTIAL RESISTANCE

The LANSCE EPICS control system continuously records (a sample per minute) the filament currents and voltages, as well as the arc discharge peak currents and voltages. The filament resistances, based on U/I

*Work supported by the US Department of Energy under Contract Number DE-AC52-06NA25396

#draganic@lanl.gov

Copyright © 2013 CC-BY-3.0 and by the respective authors

PIN DIODE DETECTORS AT DARHT II*

Jeffrey B. Johnson, LANL, Los Alamos, NM 87544, USA

Abstract

PIN diode detectors are a useful diagnostic tool for accelerator operations. The DARHT Axis II electron beam accelerator utilizes an array of twelve PIN diodes to detect the location of high voltage column electron emissions during abnormal injector events. The PIN diodes are located outside the injector vacuum vessel and detect the x-rays that are produced when the -2 MeV column electrons strike the vacuum vessel wall. This paper describes the PIN diode selection, calibration and use on the accelerator.

INTRODUCTION

An array of twelve PIN diode detectors is used on the DARHT Axis II accelerator injector to monitor for abnormal high voltage events. The injector consists of a Marx bank pulse generator, high voltage column, thermionic cathode and a vacuum vessel as shown in Figure 1.

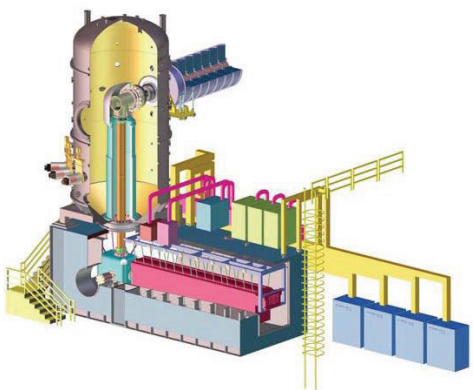


Figure 1: DARHT Axis II Injector.

During operation of the injector, abnormal events may occur. These include explosive electron emissions from the cathode and injector voltage droops from high voltage breakdowns of the cathode region or column. To help identify the precise location of such events, a PIN diode detector system was developed and installed on the injector. The PIN diodes detect the Bremsstrahlung radiation created when high energy electrons emitted during an abnormal event intercept the vacuum vessel wall. The array of twelve detectors is evenly spaced around the outside of the vacuum vessel.

PIN DIODE SELECTION

The sensitivity required for the PIN diodes was determined experimentally. A PIN diode detector assembly made by Emerge Semiconductors (100-PIN-250-HN-BG) was initially used as a single channel monitor for abnormal events. Data collected during a few abnormal events showed that this diode had the appropriate sensitivity to make the measurements. Unfortunately, the Emerge PIN diode assemblies are no longer available. An equivalent PIN diode assembly needed to be identified or built in order to construct the detector array. A market survey was conducted for a silicon PIN diode assembly similar to the Emerge detector and none could be found. This lead to the development a LANL designed detector assembly which uses a low cost commercial PIN diode chip and a custom made housing shown in Figure 2. The PIN diode chip selected was the OSI Optoelectronics PIN-RD-100. This chip has similar geometry (area and Si depth) compared to the Emerge diode. A steel housing was designed to hold the chip and provide some degree of collimation and shielding.

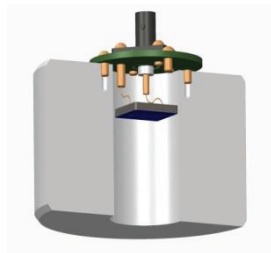


Figure 2: LANL PIN diode assembly.

CALIBRATION

The LANL PIN Diode detector assembly was calibrated against the Emerge detector using the DARHT Axis II accelerator Beam Clean up Zone (BCUZ) [1] as a radiation source. The BCUZ, shown in Figure 3, is an energy filter which absorbs beam energies below 3 MeV which occur during the rising and falling edges of the accelerator beam pulse.

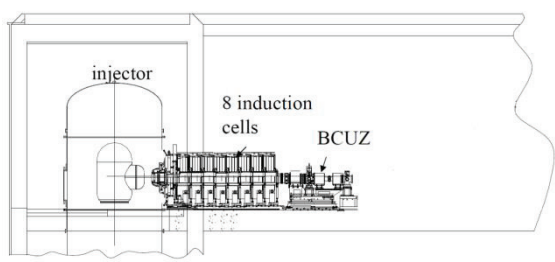


Figure 3: BCUZ region used for calibration.

The absorbed energy creates a pulse of broad band X-rays for the calibration. The central portion of the signal from the rising edge was used for the calibration. During calibration, the detectors were placed downstream from and just above the BCUZ. Detector reverse bias voltages

*Work supported by the U.S. Department of Energy under contract DE-AC52-06NA25396
johnsojb@lanl.gov

Copyright © 2013 CC-BY-3.0 and by the respective authors

ISBN 978-3-95450-138-0

LANSCE-RM WIRE SCANNERS: SLIP-ENCODED SERIAL COMMUNICATION FOR MAINTENANCE DISPLAY AT THE INSTRUMENT*

J. Sedillo, J.D. Gilpatrick, LANL, Los Alamos 87545, USA

Abstract

The newest LANSCE-RM wire scanner control systems at Los Alamos National Laboratory's LANSCE particle accelerator facility utilize touch-panel displays for limited status and control at the instrument. Since the wire scanner control hardware utilizes a National Instruments CompactRIO embedded controller, no display may be interfaced to the CompactRIO via conventional means. Thus, in order to display information from the CompactRIO, a touch-panel display and computer combo unit has been added to each wire scanner control chassis with information being exchanged via a common, RS-232 interface. This paper describes the maintenance features available at the touch screen and the underlying SLIP communication scheme used for simple packetized transfer of data between the touch-panel display and the CompactRIO.

INTRODUCTION

The control system outlined in figure 1 represents the solution developed by LANSCE staff for wire scanner actuator control and data acquisition [1]. Among its assortment of features is the control system's chassis-mounted, touch-panel PC (TPC) for localized control and diagnostics of the wire scanner system.

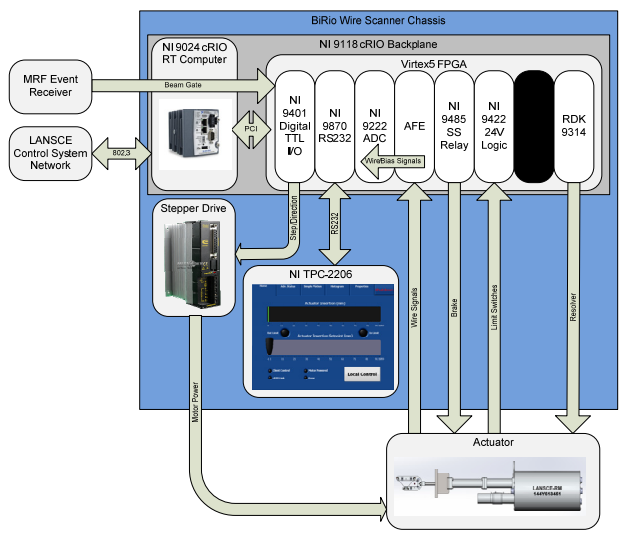


Figure 1: LANSCE-RM Wire Scanner Controller.

Although the touch panel PC offers a variety of high-bitrate interfaces (e.g. Ethernet and USB), the touch panel's RS-232, null-modem interface was chosen due to its ease of use and its common and direct interface to the compactRIO (cRIO) controller's FPGA (via the FPGA's NI 9870 RS-232 c-series module).

*Work supported by the U.S. Department of Energy.

MOTIVATION

RS-232 null-modem links offer a great deal of flexibility with how data is communicated since the hardware does not inherently provide the means to organize data meaningfully other than its FIFO approach. If context of the data may be derived from each individual byte communicated, then no expanded form of data encapsulation may be necessary. However, for more common situations where the data varies in content (e.g. varying data structures) and size (the size of the data structure in bytes), the implementation of a data encapsulation scheme will assist the receiver with making a clear determination of data boundaries by placing the data in "packets".

Data encapsulation schemes are fundamental to many familiar hardware communication systems, the most prevalent of which is 802.3 ethernet. Common encapsulation schemes leveraged on 802.3 networks include the familiar IP, TCP, UDP, etc. Given the successful standardization and implementation of these protocols, almost any one of them may be utilized for serial links implemented on hardware other than 802.3, depending on the application. Since the wire scanner's cRIO transmits a variety of data structures to the TPC and since the data can arrive in an unpredictable order, a data encapsulation method was required to assist both the TPC and cRIO to 1: understand the where a packetized data structure begins and ends, and 2: to determine how to direct the data to the proper methods for processing.

SLIP

IETF de-facto standard RFC1055, otherwise known as SLIP, was deemed the most suitable protocol for data encapsulation [3]. SLIP is an acronym for Serial-Line Internet Protocol and is a data-link layer protocol in the OSI conceptual model. SLIP was developed as a simple means of transmitting TCP/IP datagrams over serial lines when no standard yet existed and has since been replaced by PPP (Point-to-Point Protocol, RFC1661) in most applications. SLIP focuses only on packet framing, and therefore does not inherently provide a means for addressing, packet type identification, error detection/correction, or compression [2].

SLIP's simplicity made it an attractive choice for this application since encoding and decoding methods of more complex protocols would have been needlessly difficult to develop for the cRIO FPGA. Furthermore, the limitations of the SLIP protocol were of little concern since the wire scanner controller can operate without proper operation the TPC; and because the414-6541 link was short (<1 ft),

Copyright © 2013 CC-BY-3.0 and by the respective authors

ANALOG FRONT END DESIGN FOR HIGH SPEED DIGITIZING OF BEAM POSITION AND PHASE MEASUREMENTS AT LANSCE*

H. Watkins#, J.D. Gilpatrick, R. McCrady, LANL, Los Alamos, NM 87544, USA

Abstract

The Los Alamos Neutron Science Center (LANSCE) is currently developing beam position and phase measurements for its 805-MHz linac as part of the LANSCE risk mitigation project. Beam position and phase monitors (BPPMs) with four shorted strip lines have been installed throughout the linac. The BPPM electronics will sample each strip line at 240 MSPS and use a field programmable gate array (FPGA) to calculate position and phase of the beam relative to the linac reference. The beam micro-pulses from each electrode must be filtered and amplified to provide the correct frequency and amplitude level to the digitizer. This paper describes the signal conditioning required to interface LANSCE BPPMs to high speed digitizers, the diagnostic capabilities of the analog front end (AFE) module, digital control of the AFE module and design considerations to meet these objectives.

INTRODUCTION

Today's analog to digital converters (ADCs) are supporting higher sample rates and signal bandwidths allowing for direct sampling of RF signals that once required analog down conversion. The TI ADS62P49 14-bit ADC is being used at LANSCE to sample beam position and phase monitor (BPPM) signals. These signals are down converted digitally in a field programmable gate array (FPGA) to in-phase and quadrature-phase (I & Q) signals that are used to calculate position and phase of the beam centroid.

To take advantage of high speed digitizing and digital down conversion the micro-pulses from the BPPM's must be conditioned in frequency and amplitude to match the input range of the ADC. The analog front end (AFE) module was designed to interface between the BPPM and the digitizer to provide optimal signals for position and phase measurements.

This BPPM system is being developed as a replacement for LANSCE's legacy Δt system used for phase and amplitude adjustment of RF accelerating fields in the 805-MHz linac with the addition of measuring transverse beam position [1].

ARCHITECTURE

The hardware architecture for the system includes a 4-port BPPM, an AFE module, a 5-channel digitizer module and a Stratix 4 FPGA carrier board shown in Figure 1. The electronics system is housed in a VPX chassis that conforms to the ANSI/VITA 46.0-2007 standard [2].

The AFE module's printed circuit board design will conform to the VPX standard for size and backplane connections. Its power and control signals will come through the VPX backplane from the FPGA.

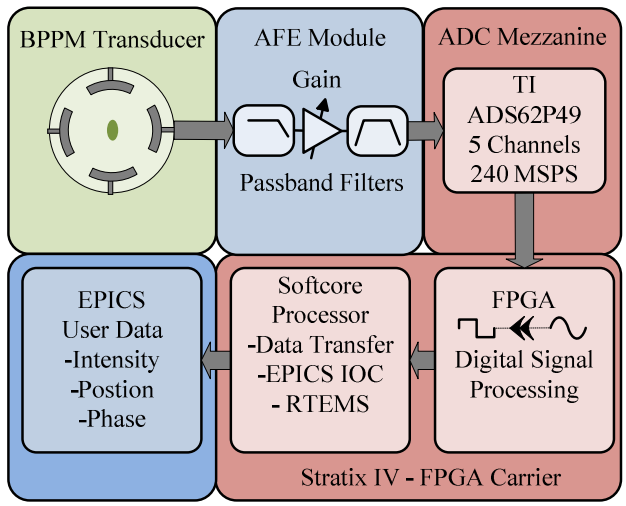


Figure 1: System Diagram

AFE DESIGN REQUIREMENTS

The following lists the design requirements for the AFE module to interface to the ADC. [1]

- Filter the micro-pulse signal to a fundamental frequency of 201.25MHz for sampling by the ADC while preserving pulse information.
- Increase the signal amplitude to match the dynamic range of the ADC without exceeding the 2Vp-p full scale range of the ADC.
- Provide a method of self calibration and signal integrity checks without beam present.
- Protect the digitizer from overdrive events.
- Provide conditioning for single micro-pulse position measurements.
- Provide remote control of the AFE gain and switching.

SIGNAL CONDITIONING

The AFE is designed to provide the filtering and gain to convert a micro-pulse from the BPPM to a sine wave that can be sampled by the ADC and analyzed by the FPGA.

Selectivity and Filtering

The beam doublets produced by the BPPM transducers are narrow micro-pulses occurring at the fundamental accelerating frequency (201.25MHz) with a pulse width of approximately one nanosecond. The ADC can only sample every four nanoseconds so the bandwidth of the pulse must be limited to provide a signal slow enough for the ADC to capture frequency and phase information.

*Work supported by the U.S. Department of Energy
#hwatkins@lanl.gov

ISBN 978-3-95450-138-0

Copyright © 2013 CC-BY-3.0 and by the respective authors

FABRICATION AND VALIDATION OF A NORMAL CONDUCTING RADIO FREQUENCY S-BAND DEFLECTING CAVITY FOR THE POHANG ACCELERATOR LABORATORY (PAL)

L. Faillace#, R. Agustsson, J. Hartzell, A. Murokh, S. Storms
RadiaBeam Technologies, 1717 Stewart St, Santa Monica CA, USA

Abstract

Radiabeam Technologies recently developed an S-Band normal-conducting Radio-Frequency (NCRF) deflecting cavity for the Pohang Accelerator Laboratory (PAL) in order to perform longitudinal characterization of the sub-picosecond ultra-relativistic electron beams. The device is optimized for the 135 MeV electron beam parameters. The 1m-long PAL deflector is designed to operate at 2.856 GHz and features short filling time and femtosecond resolution. RF design, fabrication, RF validation and tuning will be presented, as well as initial beam measurements.

INTRODUCTION

Some of the most compelling and demanding applications in high-energy electron beam-based physics, such as linear colliders [1], X-ray free-electron lasers [2], inverse Compton scattering (ICS) sources [3,4], and excitation of wakefields in plasma for future high energy physics accelerators [5,6] now require sub-picosecond pulses. Thus, improvement in resolution and capabilities of fast longitudinal diagnostics is needed.

RadiaBeam has recently developed and delivered an S-Band Traveling wave Deflecting mode cavity to be utilized for direct longitudinal phase space measurements of compressed electron beams at the Pohang Accelerator Laboratory X-ray SASE-FEL [7]. The PAL deflector takes advantage of the well-established cell machining in S-Band as well as our version of the SLAC-modified procedure for surface preparation for high RF power operation.

RF/THERMAL DESIGN

The initial 3D surface model used for RF simulations with HFSS [8] is shown in Figure 1. It is a disc-loaded traveling-wave (TW) structure operating in the TM_{110} mode at 2.856 GHz. Two coupler cells allow the input and output of the RF power provided by a standard WR284 metallic waveguide. The main deflecting cells, stacked in between the couplers, have a pillbox-like shape, each with holes located perpendicular to the deflection plane for the separation of the two dipole-mode field polarizations.

#faillace@radiabeam.com

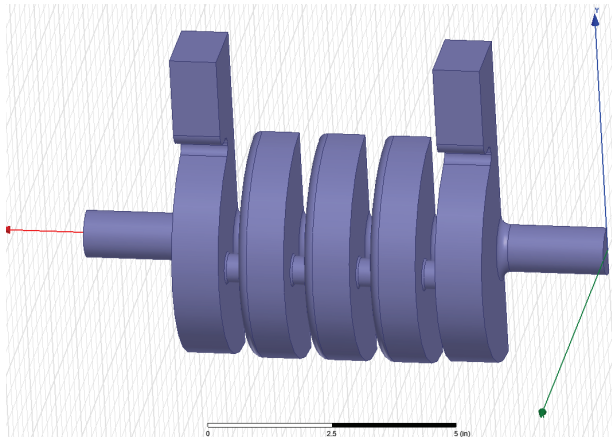


Figure 1: 3D surface model used for RF simulations in HFSS.

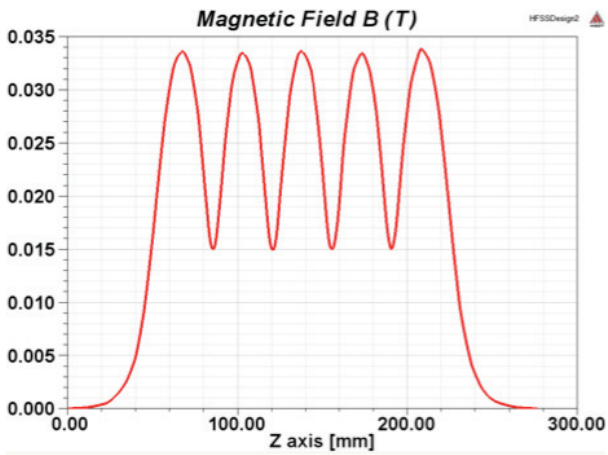


Figure 3: On-axis deflecting magnetic field profile.

The plot on the resulting on-axis deflecting magnetic field is given in Figure 2. The cell-to-cell phase shift is 120 degrees. The final full PAL deflector consists of an overall number (couplers plus main cells) of 28 cells. The main RF parameters for the L=1m long PAL deflector is listed in Table 1. The total deflecting voltage is equal to 8.5 MV, assuming an input RF power value of 10MW. Very good agreement was found between the simulated and the measured values.

Copyright © 2013 CC-BY-3.0 and by the respective authors

ISBN 978-3-95450-138-0

TRANSVERSE BEAM PROFILE DIAGNOSTIC USING FIBER OPTIC ARRAY*

S. Wu#, G. Andonian, T. Campese, A. Murokh, R. Agustsson,
RadiaBeam Technologies, Santa Monica, CA 90404, USA
R.K. Li, UCLA, Los Angeles, CA 90095, USA
M. Fedurin, R. Malone, K. Kusche, C. Swinson,
Brookhaven National Laboratory, NY 11961, USA

Abstract

The fiber-mesh diagnostic (FMD) is a transverse beam profile diagnostic based on the emission and detection of Cherenkov radiation produced as a relativistic electron beam traverses through an ordered bundle of fiber optics (SiO_2), arranged in a hexagonal close-pack configuration. Sub-10μm transverse beam profile resolution is attainable due to fiber optic core concentricity. Adequate SNR is achieved using a standard CCD sensor. A fiber optic taper input maximizes light collection efficiency by coupling each output channel to approximately single-pixel pitch. A v-groove holder and assembly process was developed to hold many fiber layers in the desired configuration. In this paper, we present results from a fully functional FMD prototype evaluated at the BNL ATF facility that demonstrates the efficacy of this diagnostic.

INTRODUCTION

The FMD was developed to address the need for higher resolution transverse profiling in low emittance electron beams. Standard techniques to measure the transverse extent of beams include fluorescent screens (such as YAG), observation of optical transition radiation, wire scanners and others. The resolution limit of these diagnostics hovers around >20μm. In the FMD, Cherenkov radiation is generated when a charged particle strikes a dielectric fiber that is placed at the Cherenkov angle. The device collects incoherent Cherenkov radiation, so the spatial profile is an accurate representation of the beam transverse charge distribution.

For a relativistic beam striking a dielectric, the Cherenkov angle, θ_C, is:

$$\theta_C = \cos^{-1}\frac{1}{n} \cong 46.5° \quad (1)$$

where n is refractive index of the fiber.

The approximate photons generated in each fiber are:

$$N_{photons} \approx \frac{2\alpha}{\sqrt{\pi}} N_e \left[\frac{d^2}{\lambda\sigma_x}\right]\left(\frac{\Delta\omega}{\omega}\right) NA \quad (2)$$

where α is the fine structure constant, d is the fiber core diameter, λ is the wavelength of light, N_e is the number of electrons, σ_x is electron beam RMS width, and Δω/ω is the fiber bandwidth.

A proof-of-concept experiment was executed at the UCLA Pegasus lab to demonstrate adequate photon yield for a single fiber [1]. The experiment results and theory were scaled for Brookhaven ATF parameters (Table 1). These results proved the feasibility to build a functioning prototype.

Table 1: Electron Beam Test Parameters

Facility	Energy (MeV)	Charge (pC)	Expected Photon Yield
UCLA Pegasus	2.5	25	10^4
Brookhaven ATF	57.6	100-1000	10^5-10^6

SYSTEM DESCRIPTION

The interaction point consists of an ordered array of single mode fiber optics (Fluorine-doped SiO_2, 6.8μm MFD, 245μm OD), which are also used at CERN for their radiation resistant qualities [2], to obtain multiple measurements in one instance. Cherenkov radiation is generated within the fibers, which also guide the radiation to an external CCD detector. Custom algorithms convert the multiple-fiber signals to a transverse profile charge distribution on a shot-to-shot basis.

The system consists of three key components:

(1) The fiber array at the interaction point
(2) The CCD acquires the Cherenkov signal
(3) DAQ logic converts signals to beam profile

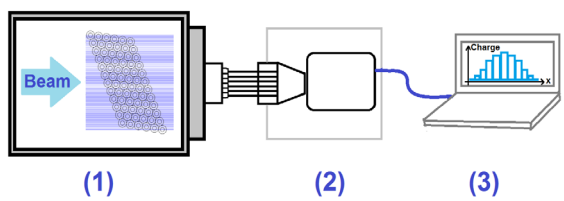


Figure 1: Diagram of System Design.

*Work is supported by U.S. D.O.E. Contract Number DE-SC0000870
#swu@radiabeam.com

Copyright © 2013 CC-BY-3.0 and by the respective authors

ISBN 978-3-95450-138-0

SCINTILLATOR DIAGNOSTICS FOR THE DETECTION OF LASER ACCELERATED ION BEAMS *

N. Cook†, R. Lefferts, Stony Brook University, Stony Brook, NY 11790 USA
O. Tresca, BNL, Upton, NY 11973, USA
V. Yakimenko, SLAC, Menlo Park, CA 94025, USA

Abstract

Radiation pressure acceleration with ultraintense laser pulses presents an exciting new scheme for accelerating ions. One of the advantages conferred by using a gaseous laser and target is the potential for a fast (several Hz) repetition rate. This requires diagnostics which are not only comprehensive for a single shot, but also capable of repeated use. We consider several scintillators as candidates for an imaging diagnostic for protons accelerated to MeV energies by a CO_2 laser focused on a gas jet target. We have measured the response of chromium-doped alumina (Chromox), CsI:Tl, and polyvinyl toluene (PVT) screens to protons in the $2-8$ MeV range using a CCD camera. We have calibrated the luminescent yield in terms of photons emitted per incident proton for each scintillator. We also discuss how light scattering and material properties affect detector resolution. Furthermore, we consider material damage and the presence of an afterglow under intense exposures. Our analysis reveals a near order of magnitude greater yield from Chromox in response to proton beams at >5 MeV energies, while scattering effects favor PVT at lower energies.

INTRODUCTION

Acceleration of protons by intense laser pulses has become an increasingly active area of study amongst nuclear, plasma, and accelerator physicists. Recent experiments with intense CO_2 laser pulses have produced collimated bunches of protons with energies greater than 1 MeV and narrow energy spread with the potential to do so at repetition rates on the order of $1-10$ Hz [1] [2]. The evolving nature of this field necessitates flexible diagnostic techniques suited to measure a myriad of experimental outputs.

Film and resin diagnostics offer single particle sensitivity but require weeks of analysis. MCPs offer a controlled gain curve and excellent resolution but are extremely delicate and ill-suited to high energy radiation. The use of scintillators has emerged as a flexible diagnostic as they may exhibit strong luminescence in response to an array of radiation types and energies; nonetheless their use necessitates precise calibration and their specific responses may vary by orders of magnitude [3]. The goal of these tests was to find a material which produces an adequate and consistent light yield under expected conditions (10^4-10^6 protons with energies $\sim 1-20$ MeV). The material should have sufficient resolution to determine bunch size, and should be relatively inexpensive and robust when exposed to high radiation flux at a repetition rate near 1 Hz.

EXPERIMENTAL METHOD

We narrowed our potential candidates to three scintillators: Chromox, CsI:Tl, and PVT. Chromox (Al_2O_3 : Cr_2O_3) is a ceramic phosphor designed to be durable under high radiation exposure and is responsive to ions in the MeV range [4] [5]. Chromox emits at ~693 nm. CsI:Tl is an inorganic crystal scintillator which emits at 550 nm. Though designed for photon detection, it's high-Z composition improves proton stopping power and makes it a high yield candidate. PVT is a low Z organic compound comprised of covalently bonded vinyl toluene chains, and as such it is easily damaged by high linear energy transfer (LET) radiation [6] [7]. BC-416 is the specific PVT variant tested, featuring added fluorophores as solvents to adjust the emission spectrum. It emits light through several channels, due to the presence of several solvents; the maximum of its emission spectrum occurs at 434nm, and its stated decay time is 4 ns.

We obtained a 1 inch diameter, 0.82 mm thick Chromox disc from Morgan Advanced Ceramics. We evaporated a 225 nm thick aluminium coating on the disc to diminish noise from electrons and X-rays. An uncoated 25 mm diameter by 1 mm thick CsI:Tl disc was purchased from Marketech International Ltd. The plastic scintillator is a 2" $\times$ 2" square, 1 mm thick, with a 50 μm Al coat, and has been used for previous proton experiments at the Accelerator Test Facility at BNL.

Experiments were performed at Stony Brook University using the Stony Brook Tandem Van de Graaff. Protons may be accelerated to total energies of $2-12$ MeV with 0.01% accuracy. Beam currents are flexible from 200 pA to 8.0 nA. Current regulation limits instantaneous uncertainties to no less than 10% regardless of beam parameters.

We used a Basler scA1400-17gm monochrome CCD camera to image the scintillator output. It features a 58% quantum efficiency at 545 nm, 12-bit image depth, and a 1392×1040 pixels sensor with 6.45μm $\times$ 6.45μm pixel size. The camera is paired with 75 mm $f\#/1.4$ tv-lens which corresponds to a maximum aperture of 0.414 sr.

RESULTS AND ANALYSIS

Captured images are analyzed following the European Machine Vision Association (EMVA) Model 1288 [8]. 300

* Work supported by Brookhaven Science Associates, LLC under Contract No. DE-AC02-98CH10886 with the U.S. Department of Energy.
† ncook@bnl.gov

Copyright © 2013 CC-BY-3.0 and by the respective authors

DIAMOND AMPLIFIER DESIGN AND PRELIMINARY TEST RESULTS

T. Xin#, [1, 2], S. Belomestnykh[1, 2], I. Ben-Zvi[1, 2], M. Gaowei[1, 2], E. Muller[1, 2], T. Rao[1], J. Skaritka[1]
J. Smedley[1], E. Wang[1], Q. Wu[1],

[1]Brookhaven National Laboratory, Upton NY 11973
[2]Stony Brook University, Stony Brook NY 11794

Abstract

Diamond as a large band gap material can be easily made to have negative electron affinity (NEA) surface. Using a few keV primary electrons as input and a few kV bias, the NEA diamond will emit cold electrons into vacuum with a large gain. We had tested and reported the performance of the diamond amplifier in our DC system. The best amplification achieved so far was above 170. Next step of the experiment is to test the diamond amplifier in a 112 MHz superconducting RF electron gun. In this report we describe the design of the amplifier containing a DC primary gun and light optics, to be tested in our SRF gun and relevant simulations. We also provide preliminary test results of the laser and electron beam transport.

INTRODUCTION

In previous papers, works on hydrogenation of CVD diamond and on measurements of secondary electron gain in a DC system at Brookhaven National Lab were reported [1-3]. The next step will be testing the diamond amplifier in a Superconducting RF (SRF) gun. For this purpose a specially designed cathode stalk is needed to work as a transporter/holder of a diamond in the gun. Besides that, we also designed a subsystem, which will be inserted into the cathode stalk and act as the DC stage of the amplifier.

DIAMOND AMPLIFIER

A basic diagram of a diamond amplifier is shown in Figure 1. A primary beam, with a few keV energy, hits the Pt coated back of the diamond and generates a cloud of electron/hole pairs inside the diamond. This entrance surface of the diamond is negatively biased hence the electrons separate from the cloud and drift across the bulk of diamond to the opposite, hydrogenated NEA emission surface. An anode is placed 200 μm away from the emission surface so that the electric field will extract the secondary electrons from the NEA surface of diamond into vacuum.

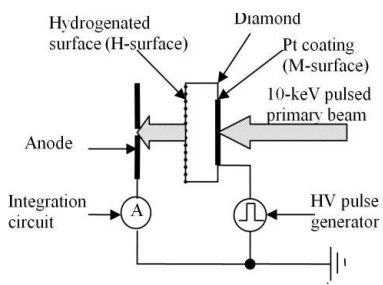


Figure 1: DC test of Diamond Amplifier (conceptual diagram) [1].

* This work was carried out at Brookhaven Science Associates, LLC under Contracts No. DE-AC02-98CH10886 and at Stony Brook University under grant DE-SC0005713 with the U.S. DOE.
#txin@bnl.gov

Design of Amplifier for SRF Gun Test

For the test of the Diamond Amplifier in an SRF gun, we need a special stalk to position the diamond in right location in the cavity and hold it there. The detailed description of the stalk can be found in previous papers [4, 5]. As for the source of primary electrons, we decided to use a newly designed DC assembly with a UV driven copper cathode. A CAD model and a photo of this system, which will hereby be called Amplifier, is shown in Figure 2.

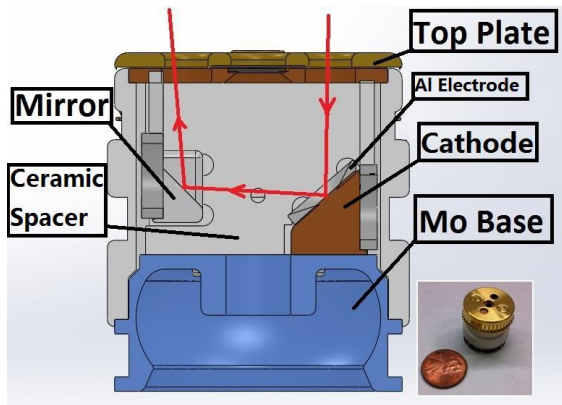


Figure 2: Section view of the Amplifier: red lines show the path of UV light. Smal insert is a photo of the first prototype Amplifier with a penny on the side as size reference.

This is the first prototype amplifier we made for SRF test. There are four major pieces. A gold plated copper top plate is used to hold the diamond and ground it to the cavity. A ceramic spacer serves as an insulator between the grounded top plate and biased molybdenum base. It also acts as a holder for the cathode and mirror and defines the crucial distance between the cathode and diamond. The third part is the cathode/mirror pair that will provide electron beam and guide the laser beam out of the cavity. The fourth part is the molybdenum base that works as the connection between the Amplifier and the transport arm.

Laser will come in through a hole in the top plate and illuminate the cathode. There is an aluminium electrode surrounding the cathode optimized for beam focusing. After the laser bounces off the mirror-finished cathode, it will hit a metal-coated mirror on the other side, which will redirect the laser out of the amplifier through an exit hole in the top plate. Figure 3 shows how the amplifier will be positioned in the stalk and cavity as well as depicts the paths of laser and electron beams. The angles of the cathode and mirror are chosen to meet two conditions. The first one allows the laser beam to escape the cavity with no obstacles. And the second condition is that the electron beam must hit the center of the diamond so that we do not

Copyright © 2013 CC-BY-3.0 and by the respective authors

ISBN 978-3-95450-138-0

MULTIPACTING STUDY OF 112 MHZ SRF ELECTRON GUN*

T. Xin#,1, S. Belomestnykh1,2, I. Ben-Zvi1,2, C. H. Boulware3, T. L. Grimm3, X. Liang1, T. Rao2, J. Skaritka2, E. Wang2, Q. Wu2
1) Stony Brook University, Stony Brook, NY 11794, U.S.A.
2) Brookhaven National Laboratory, Upton, NY 11973-5000, U.S.A.
3) Niowave, Inc., Lansing, MI 48906, U.S.A

Abstract

The 112 MHz quarter wave superconducting electron gun was designed and built as an injector for the coherent electron cooling experiment. Besides that, the gun is suitable for testing various types of photocathodes thanks to its specially designed cathode holder. In recent RF tests of the gun at 4 K, the accelerating voltage reached 0.9 MV CW and more than 1 MV in pulsed mode. During this testing, we observed several multipacting barriers at low electromagnetic field levels. Since the final setup of the gun will be different from the cool down test configuration, we want to understand the exact location of the multipacting sites. We used Track3P to simulate multipacting. The results show several resonant trajectories that might be responsible for the observed barriers, but fortunately no strong multipacting barriers have been found in the cavity.

INTRODUCTION

The fabrication of the 112 MHz SRF quarter wave cavity as well as the cryomodule has been finished and the cold test was successfully conducted early this year. The gap voltage had reached 0.9 MV in CW mode test and 1 MV in pulsed mode. Further increase in gap voltage was limited by radiation. During the conditioning process we encountered several multipacting barriers. The purpose of study shown in this paper is to investigate the relative strength of the known barriers to the ones that are predicted by the simulation under higher field level with different FPC and cathode stalk for future test so that the difficulty of future conditioning can be estimated.

EXPERIMENTAL ASPECTS

General Layout

The cavity and a new cryomodule were built and assembled at Niowave. The layout of the cavity, fundamental power coupler (FPC) and pickup antenna is shown in Figure 1. The FPC antenna was designed with an adjustment range allowing critical coupling at different levels of RF losses in the cavity. Special precaution was taken during the cool down to avoid the accumulation of residual gas on the outer conductor of the FPC. We suspected that changing of surface condition might explain multipacting in a previous cold test. Also a standing wave structure was introduced between the RF amplifier and the feed through of the FPC to further enhance the coupling in case stronger coupling is needed to condition a multipacting barrier. The design parameters of the 112 MHz electron gun are shown in Table 1.

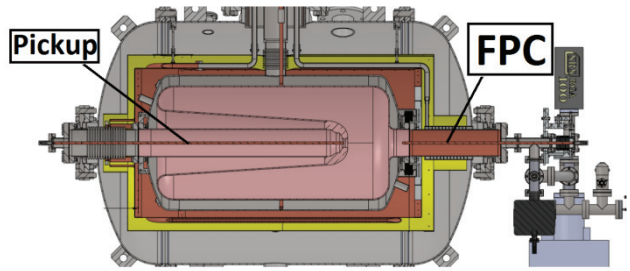


Figure 1: Layout of the 112 MHz SRF cavity horizontal test. The coaxial FPC approaches from the exit of the cavity and the pickup antenna goes through the nose cone part of the cavity and positioned 2 cm behind the entrance of the cavity.

Table 1: Design Parameters of the 112 MHz Electron Gun

Parameters	Value
Frequency	112 MHz
Charge per Bunch	1~3 nC
Repetition Rate	78 kHz
Acceleration Voltage	1~2 MV
Cavity Q_0	1.8e8
R/Q	122 Ω

Experimental Results

The cool down took about 4 hours to bring the cavity to superconducting status. To avoid condensation of residual gas on the FPC, the thermal shield was not cooled until later in the process.

Soon after the superconducting status was reached, the multipacting barriers were observed at relatively low field level. The corresponding gap voltage was estimated to be below 50 kV and the more accurate value was later confirmed to be in the range of 30 kV to 40 kV by Track3P simulation.

After overcoming the multipacting barriers, the cavity Q *vs.* accelerating voltage Vc was measured. Figure 2 shows the result of the measurement.

*This work was carried out at Brookhaven Science Associates, LLC under Contracts No. DE-AC02-98CH10886 and at Stony Brook University under grant DE-SC0005713 with the U.S. DOE.
#txin@bnl.gov

Copyright © 2013 CC-BY-3.0 and by the respective authors

PROGRESS IN THE DEVELOPMENT OF TEXTURED DYSPROSIUM FOR UNDULATOR APPLICATIONS*

F. H. O'Shea†, R. Agustsson, Y.-C. Chen, T. Grandsaert II, A. Murokh and K. Woods
RadiaBeam Technologies, Santa Monica, CA 90404, USA
J.-H. Park, R. Stillwell, NHMFL, Tallahassee, FL 32310, USA

Abstract

RadiaBeam Technologies is in the process of developing bulk textured dysprosium as a potential replacement for CoFe steel as undulator poles. For cryogenic undulators that can be cooled below the ferromagnetic transition of dysprosium, textured dysprosium offers potential increase in the peak field of the undulator. Here we report on the progress of the project, including magnetization curves for the material.

INTRODUCTION

The operation of cryogenic permanent magnet undulators (CPMUs) at temperatures below the Curie transition of rare-earth metals offers the opportunity to develop new pole materials that take advantage of the existing cryogenic conditions to potentially produce higher peak field undulators. To this end, RadiaBeam Technologies has been investigating the use of dysprosium and gadolinium to replace the cobalt-iron (CoFe) typically used in high field hybrid undulators. CoFe is the pole material of choice for high field undulators because of its large saturation magnetization (2.35 T), very large initial permeability ($\mu_i \sim 10^4$) and small non-linear knee region which is the transition between the two regions. In single crystal form, dysprosium demonstrates much higher magnetic moment (>3 T [1]) at low applied field and cryogenic temperatures than CoFe [2]. However, single crystals of these materials are difficult and expensive to produce at the dimensions and scale required for undulator fabrication and polycrystalline versions of the materials are not useful for undulator applications because of low initial permeability.

A compromise between the single crystal and polycrystalline forms can be reached through a processing technique that generates so-called texture in the material. This technique takes advantage of a favorable energy difference between crystallographic orientations during a rolling and annealing cycle [3]. Briefly, the polycrystalline material is rolled out and then annealed near the melting point. For dysprosium, which has an *hcp* structure, grains within the foil that are oriented with the hardest axis within the plane of the foil are taken over by grains that have the hardest axis pointed normal to the plane of the foil in a process known as secondary re-crystallization. This process dramatically increases the permeability within the plane of the foil [1]. The foils can then be annealed together in stacks to produce a macroscopic piece for further machining.

MATERIAL DEVELOPMENT

We have previously reported the results of magnetic measurement of the textured dysprosium [2]. Those results showed that the textured dysprosium, made up of 100 μm thick foils, used in the initial 2-period prototype would not produce an improvement in peak field over CoFe poles. In that publication we suggested several changes that might increase the performance of the the textured dysprosium poles: operate the undulator at lower temperature, use thinner foils in the poles, and increase the complexity of the design of the undulator by installing backing magnets on the side of the poles opposite the magnetic gap. Because of those observations, all foils created subsequently have been 25 μm thick. Since that previous publication we have found evidence of another feature of the textured dysprosium that will influence future magnetic designs, namely that the direction of rolling affects the orientation of the easy axes of magnetization. Unfortunately, because cryogenic magnetic measurement techniques below 77 K require the use of liquid helium, we have had difficultly finding facilities willing to perform these measurements until recently.

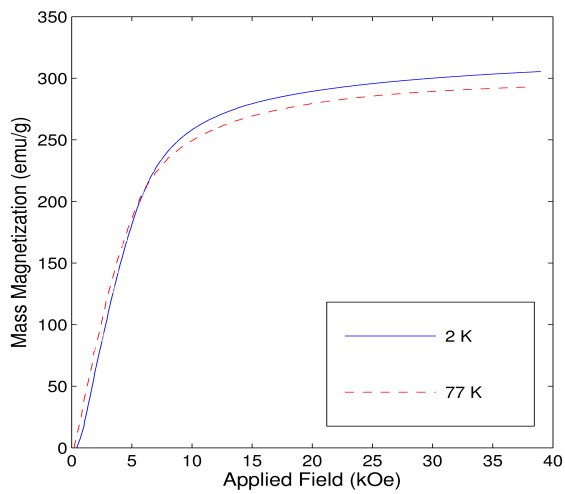


Figure 1: Comparison of the magnetic performance of textured dysprosium at 2 K and 77 K. The sample was cut such that the direction of measurement was within the rolling plane.

* Work supported by DOE under contracts DE-SC0006288 and NNSA SSAA DE-NA0001979
† oshea@radiabeam.com

ISBN 978-3-95450-138-0

Copyright © 2013 CC-BY-3.0 and by the respective authors

SURFACE PLASMON RESONANCE ENHANCED MULTIPHOTON EMISSION FROM METALLIC CATHODE*

H. To, R. Li, P. Musumeci, UCLA, Los Angeles, CA 90095, USA
G. Andonian, Radiabeam Technologies, Santa Monica, CA 90404, USA

Abstract

We investigate the use of surface plasmonic nanostructures in increasing the efficiency of copper photocathodes for high-brightness electron sources. A nanohole structure was fabricated, using focused ion beam milling, such that it exhibited a strong plasmonic response near 800 nm. The reflectivity of the nanostructured surface was significantly lower compared to that of a flat surface, due to plasmonic resonance effects. A previous experiment [1] demonstrated an increase in charge yield by over a factor of 100, using a slightly off-resonance structure. With this new near-resonant structure, the reflectivity is expected to be even lower and the charge yield enhancement factor even larger.

INTRODUCTION

Recently, progress has been made in using metal photocathodes to generate high brightness electron beams, as an alternative to using semiconductor cathodes [2]. Because of their prompt response, low vacuum requirements, robustness, and fabrication simplicity, metals are typically the preferred choice in high peak brightness photoguns [1]. However, metal cathodes are not without disadvantages, a significant one being that they are often highly reflective at optical and infrared wavelengths and in general offer lower QE than semiconductors [3].

We, at the UCLA Pegasus laboratory, have demonstrated the generation of electron beams through multiphoton emission using a copper photocathode with an 800 nm Ti:Sa incident laser [2]. At 800 nm, copper is ~95% reflective, and thus, most of the photons from the incident laser are wasted and do not participate in the multiphoton emission process [3]. To increase the efficiency of the cathode, an obvious solution would be to increase the absorptivity of copper at 800 nm. One way we propose to do this is to pattern a cathode surface with nanoscale features that take advantage of plasmonic effects.

THEORY

Recent advances in nano-plasmonics have enabled fine control of optical properties of metal surfaces by patterning them with sub-wavelength or nanoscale features [4]. Nanoscale features of the correct geometry can lead to surface plasmon resonance, or a resonant interaction between surface plasmons and incident photons [5]. This produces two major effects [4]: 1) significant reductions in metal reflectivity due to photons being absorbed by surface plasmons, and 2) large enhancements of local optical field intensity due to photon energy being stored in the surface plasmons. These nano-plasmonic phenomena could be applied to optimize the optical response of a cathode and obtain high efficiencies in photoemission charge yield.

Previously, we reported the first experimental results of the generation of relativistic electron beams from a nanostructured photocathode in a high gradient RF gun [2]. The aforementioned nanohole array structure exhibited a resonant response at ~810 nm. At 800 nm, the reflectivity of the nanopattern was ~60%, still producing a >100-fold enhancement in the multiphoton charge yield. With a nanopattern that is resonant closer to 800 nm, the charge yield can be expected to be greater.

SETUP

The geometry of the nanopatterns consist of rectangular arrays of nanoholes fabricated with focused ion beam (FIB) milling, as shown in Fig. 1. The patterns were milled onto a single crystal Cu(100) substrate to avoid pattern variation due to the random grain sizes and orientations associated with polycrystalline substrates.

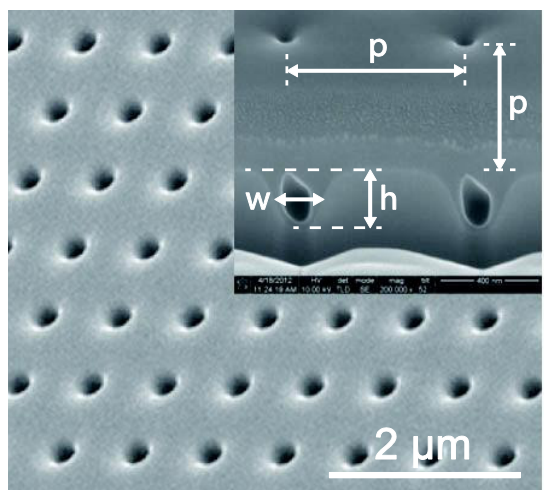


Figure 1 [1]: Scanning electron microscopy images of a nanohole array. Inset: Zoomed in profile view of nanoholes.

When using the nanohole array geometry, the resonant wavelength is much more sensitive to the spacing of the holes than to their depth, width, and even their shape [1]. Each nanohole has an approximately Gaussian profile, mainly due to the current density distribution of the milling ion beam. Finite Difference Time Domain (FDTD) simulations were performed to compare the

*Work supported by U.S. DOE Grants No. DE-FG02-92ER40693 and U.S. DOE SBIR Grant No. DE-SC0009656

Copyright © 2013 CC-BY-3.0 and by the respective authors

BEAM DYNAMICS DRIVEN REQUIREMENTS ON THE ARIEL E-LINAC SRF SEPARATOR CAVITY*

Douglas W Storey[1,2†], Yu-Chiu Chao[2], Lia Merminga[2],
[1]University of Victoria, Victoria, B.C, Canada, [2]TRIUMF, Vancouver, B.C, Canada

Abstract

A possible future extension to TRIUMF's ARIEL e-linac is the addition of a recirculation path for an Energy Recovery Linac (ERL), which will drive an Infrared or THz Free Electron Laser (FEL). The ERL electron beam will be interleaved with the single-pass beam bound for Rare Isotope Beam (RIB) production in the ARIEL facilities, allowing for simultaneous beam delivery to both FEL and RIB users. A superconducting RF separator will separate the beams at the exit of the linac at a frequency of 650 MHz in CW mode. After a second pass through the linac, the energy recovered ERL beam will pass through the separator cavity out of phase with the deflecting fields, and at a much lower energy, before continuing to a beam dump. Using the General Particle Tracer software, three-dimensional simulations of the beam dynamics of the passing beams have been performed to determine the requirements on the SRF separator's deflecting field uniformity. Operation of the FEL requires minimal emittance dilution of the ERL beam from the separator. This contribution describes the results of these studies and the requirements imposed on the SRF beam separator.

INTRODUCTION

The ARIEL e-linac will produce a 50 MeV, 10mA CW electron beam as the photo-fission driver for the production of neutron rich Rare Isotope Beams (RIB). This complementary RIB source will expand TRIUMF's existing ISAC experimental program. The electron beam is accelerated through an injector cryomodule to an energy up to 10 MeV, and two accelerating cryomodules (ACM) up to an energy of 50 MeV in cavities operating at 1.3 GHz [1].

A future phase will be the addition of a recirculation loop to return the electrons for a second pass through the main linac. This may be configured as a recirculated linac (RLA), accelerating the beam up to 75 MeV before continuing on for RIB production, or as an Energy Recovery Linac (ERL) with a Free Electron Laser operating in the back leg of the recirculation loop and interleaved with the RIB beam in the main linac.

Successful operation of the FEL depends on a low emittance beam, requiring minimal emittance dilution imparted during the separation of the beams at the exit to the main linac.

* Work supported by the Natural Sciences and Engineering Research Council of Canada.

† dstorey@uvic.ca

RF Separator Layout

Bunches bound for either RIB production or the ERL will have the same energy when reaching the separator section and will occupy alternating buckets of the 1.3 GHz accelerating RF. Separation of the bunches will then require RF separation at a frequency of 650 MHz at the exit of the main linac. Furthermore, the separator layout must also be compatible with the RLA operating mode, which will rely on the static magnetic separation of the two beams.

The basis of this separation scheme has been developed in [2] and comprises of an RF separator cavity imparting an initial differential transverse kick to the two beam types, followed by a steering dipole, a defocusing quadrupole to further enhance the separation, and finally a septum magnet to perform the final separation of the beams. This scheme is driven by rigid space constraints that require the full separation of the beams within a distance of about 3 m. The layout of the separation section of the e-linac is depicted in Fig. 1.

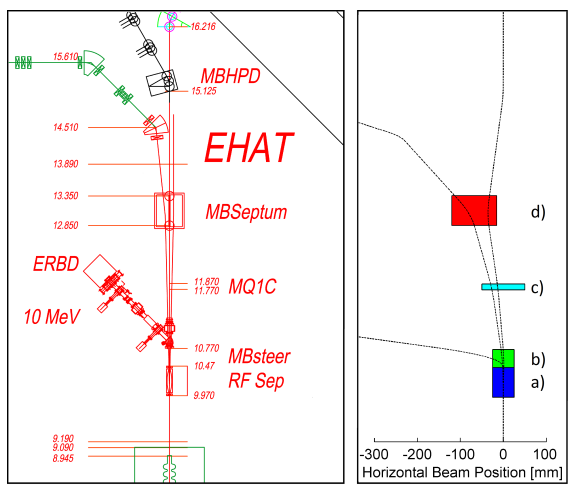


Figure 1: The layout of the ARIEL RF separator on the left with the beam deflections shown on the right. The elements shown are the a) RF separator cavity, b) dipole magnet, c) quadrupole, and d) septum.

In addition to the RIB and ERL beams, the decelerated beam after making its second pass through the ACM, will reach the RF separator with energy of 5 to 10 MeV and 90°out of phase with the cavities deflecting phase. It will therefore pass mostly unaffected through the separator cavity and receive a sharp deflection by the dipole magnet due to its low energy to be directed down a short transport line to a beam dump.

Copyright © 2013 CC-BY-3.0 and by the respective authors

ISBN 978-3-95450-138-0

FEASIBILITY OF AN RF DIPOLE CAVITY FOR THE ARIEL E-LINAC SRF SEPARATOR*

Douglas W. Storey[1,2†], Robert Edward Laxdal[2], Lia Merminga[2], Vladimir Zvyagintsev[2]
[1]University of Victoria, Victoria, B.C, Canada, [2]TRIUMF, Vancouver, BC, Canada

Abstract

A megawatt class CW e-linac is being designed and constructed at TRIUMF with the main goal of producing neutron rich isotopes for TRIUMF's Rare Isotope Beam (RIB) program. A possible extension of the beam-line will allow recirculation of the beam for an Energy Recovery Linac (ERL) to operate in tandem with the RIB user program. A superconducting cavity with RF dipole geometry is being considered for separation of the ERL and RIB beams at the end of the linac to provide simultaneous beams to both the ERL and RIB programs. This contribution describes optimization studies performed on the RF dipole design to determine if this geometry will meet the requirements of the ARIEL e-linac. The resulting 650 MHz structure has compact cavity dimensions, low peak fields, and high transverse shunt impedance. Due to the large aperture beam-line and stringent requirement on preserving beam quality, extensive focus has been placed on transverse uniformity of the deflecting fields.

INTRODUCTION

A future extension to the ARIEL e-linac [1] will be the addition of a recirculation path to the beam-line for an Energy Recovery Linac (ERL), the driver for an Infrared or THz Free Electron Laser (FEL). The ERL electron beam will be interleaved with the single-pass beam bound for Rare Isotope Beam (RIB) production in the ARIEL facilities, allowing for simultaneous beam delivery to both FEL and RIB users.

Bunches of electrons bound for either the ERL or RIB will occupy alternating buckets of the 1.3 GHz accelerating RF. The separation of the beams will take place at the exit of the main linac. The basis of this separation scheme is introduced in [2], which describes the layout and deflections required by each element in the separation complex: an RF separator, steering dipole, defocusing quadrupole, and septum magnet. This scheme is driven by the rigid space constraints that require the separation of the beams within a distance of about 3 m.

After energy recovery in its second pass through the accelerating modules, the recirculated ERL beam will reach the RF separator with beam energy of approximately 5 to 10 MeV, and 90°out of phase with the deflecting phase of the cavity. It will therefore pass mostly unaffected through the separator cavity and receive a sharp deflection in the dipole magnet and be directed down a short beam-line to a beam dump.

The initial separation will take place in an RF separator cavity operating at a frequency of 650 MHz, imparting opposing transverse momentum kicks to the ERL and RIB bound beams and deflecting them by ±4.5 mrad in the horizontal direction. This deflection will be amplified by the quadrupole magnet with the final separation of the beams reaching $\sim$ 35 mm by the time they reach the septum. At this point, the ERL beam will be directed around the recirculation loop and the RIB beam back towards the main linac axis.

Additionally, the layout of the separator section of the linac is compatible with a two pass Recirculating Linac in which the beam is directed around the recirculation loop after its first pass to be accelerated a second time in the main linac before continuing on for RIB production. This mode would not employ the RF separator cavity, but would rely on the static magnetic separation of the beams with different energies in the dipole.

The maximum beam energy at the exit of the main linac will be 66 MeV. This translates to a 0.3 MV transverse momentum kick imparted by the RF separator cavity and transverse deflecting field of $E_\perp = 1.3$ MV/m for a single deflecting cavity.

SRF SEPARATOR CAVITY

The RF dipole deflecting cavity is being considered for use in the ARIEL separator complex. This cavity is compact in size and the transverse deflections are high with low peak electric and magnetic fields. Extensive scaling studies have been performed on this geometry [3], however detailed optimization is required to fully access the suitability of this cavity design for the ARIEL e-linac separator.

The geometry of the RF dipole separator cavity is shown in Fig. 1. The inner ridge length of the cavity will be of order $\beta\lambda/2 = 230$ mm at 650 MHz, and the aperture 50 mm, the same as along the rest of the length of the e-linac.

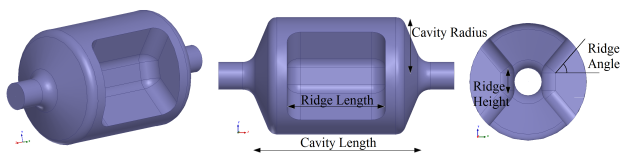


Figure 1: The RF dipole geometry showing the key parameters affecting the cavity performance.

* Work supported by the Natural Sciences and Engineering Research Council of Canada
† dstorey@uvic.ca

Copyright © 2013 CC-BY-3.0 and by the respective authors

DESIGN, FABRICATION, MEASUREMENT, INSTALLATION AND ALIGNMENT OF 2 TYPES OF QUADRUPOLE-SEXTUPOLE COMBINED MAGNETS FOR THE UPGRADE OF THE 1.2 GEV BOOSTER SYNCHROTRON AT TOHOKU UNIVERSITY

W.Beeckman, S.Antoine, P.Bocher, F.Forest, P.Jehanno, P.Jivkov, M.J.Leray, L.Swinnen, S.Taillardat, , SIGMAPHI, Vannes, France
H.Hama, F.Hinode, Electron Light Science Centre, Tohoku University, Sendai, Japan

Abstract

The upgrade of the 1.2 GeV booster synchrotron is part of the recovery program from the March 11 2011, Great East Japan Earthquake. The replacement of standard quadrupoles by combined quadrupole-sextupole magnets will tame the head-tail instability by changing the chromaticity from the natural, negative, values to positive values, and prevent the unstable m=0 mode to develop.

In January 2012, Sigmaphi was awarded a contract for the design of 2 kinds of combined magnets and the fabrication of 8 magnets of each type, including rotating coil and Hall probe measurements of every unit. The contract also required disassembly of the old quadrupoles and installation of the new combined magnets, including disassembly/reassembly of the vacuum chambers and fitting with new UHV gaskets. Finally, all the booster magnets, namely 8 dipoles, 4 achromat quadrupoles and the 16 new combined function magnets were to be realigned within ±0.2 mm accuracy by mid-January 2013. The presentation outlines the main steps of the different operations and presents the achievements and results.

DESIGN

A general overview of the status of the project is given in [1] and we concentrate here on the magnets.

Table 1 presents the requirements for the new magnets.

Table 1: Magnet Requirements

Requirement	QSF	QSD
Quadrupole	k=2.01044 m^{-2}	k=2.21750 m^{-2}
Sextupole	2.4 times 4-pole m=4.825061 m^{-3}	3.8 times 4-pole m=8.426508 m^{-3}

Additional requirements are listed below

- Same geometry as old magnets including coil shape and electrical/water connections. Only the pole face may be changed.
- Magnetic centre at ±0.5 mm from mechanical centre in both transverse dimensions
- Alignment error may not be larger than ±0.2 mm
- 1 year from contract to end

All these requirements put together make a very demanding job with little freedom.

Many different designs of such combined magnets can be found in the literature. The extra function is added on top of the main multipole either through pole shaping [2][3], or by using extra coils that superimpose a second multipole [4][5]. By requirement, we must not only adopt the first scheme but we must also abide to the very strong constraint of keeping the magnetic circuit within the yoke shape of the existing magnets.

The pole profile [6] of such a combined function magnet is a superposition of the potentials, hence an equation $kxy+\frac{1}{6}m\left(3x^2y-y^3\right)=\frac{1}{2}kR^2+\frac{1}{6}mR^3$

The field components are summarized in table 2.

Table 2: Field Components

Field component	Bx	By
Quadrupole	ky	kx
Sextupole	mxy	$\frac{1}{2}m\left(x^2-y^2\right)$

Thus, the vertical component in the horizontal plane (y=0) is equal to $B_y = kx+\frac{1}{2}mx^2$

Starting from the above theoretical pole profile with a pole radius of 50 mm and maximum coil current of 700 A we can aim at designing a pole profile that satisfies the requirements. However, as shown below, incompatible symmetries generate differential saturations which prevent required fields to be achieved with the prescribed yoke thickness. The possible m/k ratio was redefined as m/k(QSF) ~ 1.0 (2.4) and m/k(QSD) ~ 1.8 (3.8)

The pink and green rectangles locate the 4 and 6-poles and the matching arrows the resulting field, adding on the right and subtracting on the left.

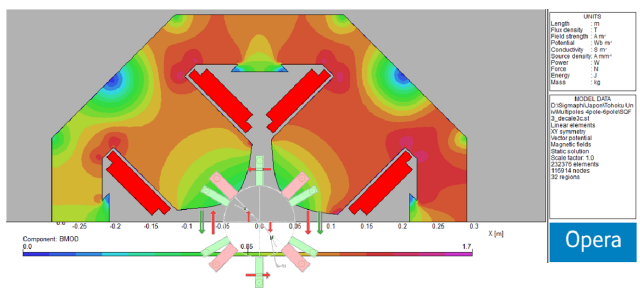


Figure 1: 2d cross-section of a combined magnet showing the strong differential yoke saturation.

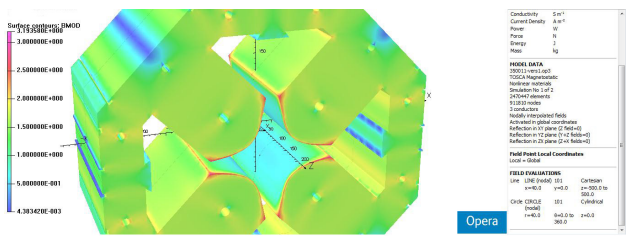


Figure 2: Opera3d model

Copyright © 2013 CC-BY-3.0 and by the respective authors

ISBN 978-3-95450-138-0

DESIGN AND CONSTRUCTION OF THE PROTO-TYPE QUADRUPOLE MAGNTS FOR THE SUPERKEKB INTERACTION REGION

N. Ohuchi#, Y. Arimoto, H. Yamaoka, Z. Zong, M. Tawada, K. Tsuchiya, H. Koiso, Y. Ohnishi, A. Morita, H. Sugimoto, K. Oide, KEK, Tsukuba, Japan

Abstract

Construction of the SuperKEKB accelerator started from 2010. The final focusing system in SuperKEKB was designed, and it consisted of 8 superconducting quadrupole magnets. As part of the R&D of the final focusing system, two prototype magnets were designed and constructed. The magnets were cooled to 4 K, and they were excited over the design current and the field measurements were performed.

INTRODUCTION

SuperKEKB [1] is the upgraded machine of KEKB, and the design luminosity is $8\times10^{35}\mathrm{cm}^{-2}\mathrm{s}^{-1}$, which is 40 times higher than that achieved at KEKB. SuperKEKB has a single interaction point, IP, to collide the 7 GeV e- beam and the 4 GeV e+ beam with a finite crossing angle of 83 mrad. The colliding energy is planned to be increased to 12 GeV. The design concept of SuperKEKB is based on the Nano-Beam Scheme, originally proposed by P. Raimondi for SuperB [2]. In order to focus the beam at IP with the vertical beam size of about 50 nm, a pair of the quadrupole doublet system for LER and HER [3, 4], respectively, was designed with 8 superconducting magnets. As the R&D of the final focusing system, the QC1P and QC1E prototype magnets were constructed and cold tested at 4K. In this paper, the magnet designs, constructions and test results are reported.

DESIGNS OF QC1P/QC1E MAGNETS

The QC1P and QC1E magnets were designed for the e+ and e- beams, respectively, and they are located at the closest position to IP on each beam line [3].

QC1P Magnet Design

The QC1P is the collared quadrupole magnet without iron yokes in order to make the solenoid field profile required from beam optics. The magnet cross section is shown in Fig. 1, and the parameters are summarized in Table 1. The magnet consists of two layers of the superconducting coil, and the thickness of the two-layers is 5.425 mm. Because the separation between two beams at the front end of the QC1P magnet is only 61 mm, the outer radius of the magnet was designed to be 30.425 mm while the coil inner radius was 25 mm. The field gradient of the magnet was 76.17 T/m at the design current, I_d=1800 A, and the magnetic length was 0.3372 m. I_d was for the colliding energy of 12 GeV, and the magnet current for 11 GeV was 1624 A. For this magnet, the small Rutherford cable, which consisted of 10 strands, was developed. The cable size was 0.93 mm in mid-thickness × 2.5 mm in height, and the key stone angle of the cable was 2.09 degree because the coil inner radius was 25 mm. I_d is 60 % of the critical current of the cable, I_c, at 4.7 K. The cable parameters are listed in Table 2.

The magnetic field of the QC1P magnet was calculated with the magnet cross section model and with the whole magnet model including the lead end and the non-lead end. They are summarized in Table 3. The each coil was designed with three coil blocks, and b_6 and b_{10} of two layer coils were optimized to be 0.16 units and -0.02 units in the cross section, and -0.11 units and -0.05 units in the whole magnet, respectively, at the reference radius of R_{ref}=10mm.

QC1E Magnet Design

The QC1E magnet was located behind the QC1P magnet from the IP. The prototype magnet was designed with iron yokes, and the yoke outer radius was 70 mm. The magnet consisted of two layer coils, and the inner radius was 33 mm. The superconducting cable had same parameters as those for the QC1P magnet except for the cable keystone angle of 1.59 degree. The QC1E was designed to generate the field gradient of 91.73 T/m at I_d=2000 A, and the magnetic length was 0.3774m. The magnet current for 11 GeV was 1577 A. The magnet cross section was optimized with three coil blocks of each layer as same as the QC1P magnet, for b_6 and b_{10} to be -0.04 units and -0.08 units at R_{ref}=15mm, respectively. In the whole magnet, b_6 and b_{10} were optimized to be -0.17 units and -0.20 units, respectively.

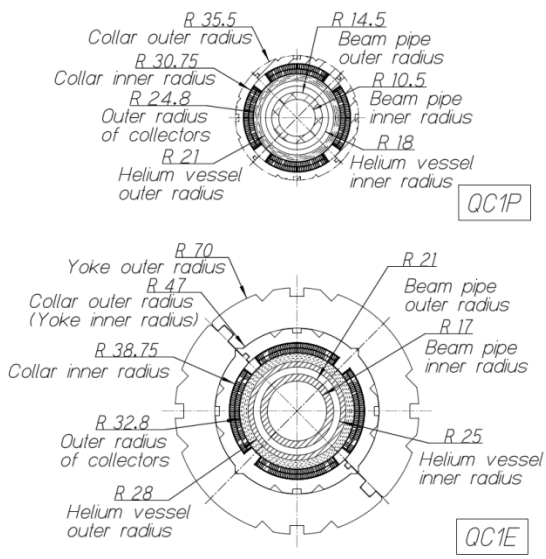


Figure 1: Cross sections of QC1P/1E prototypes.

#norihito.ohuchi@kek.jp

Copyright © 2013 CC-BY-3.0 and by the respective authors

MULTIPOLE MAGNETIC MEASUREMENTS USING A LOCK-IN AMPLIFIER TECHNIQUE*

C. Doose, M. Kasa, ANL, Argonne, IL 60439, USA

Abstract

Magnetic measurement systems for accelerator magnets typically use relatively complicated rigid rotating coils and digital integrators to capture the integrated coil signal as a function of angular position of the coil. This technique has proven to be reliable and accurate for measuring the field quality of conventional multipole magnets; however, the design and construction of the rotating coils ultimately determine the accuracy of the measurement system. A different concept and implementation of a simple stretched-wire rotating coil will be described. This system utilizes a single-turn radial coil continuously rotating at a fixed angular velocity. The coil signal and a reference pulse are sampled with a 24-bit ADC. A lock-in technique or an FFT can be used to determine the harmonic content of the signal and thus calculate the main field strength and angle, multipole coefficients, and magnetic center offsets. The main advantages of such a system are ease of coil manufacturing and simple mechanical system design.

INTRODUCTION

Motivation for this project was prompted by the need to quickly measure modified multipole magnets for the APS storage ring. Existing six-pole horizontal/vertical dipole corrector magnets were modified to become horizontal correctors and skew quadrupoles. A need to measure the multipole components and magnetic center of these new combination magnets prompted the design of a new, relatively simple multipole magnet measurement system.

The previous APS multipole magnetic measurement system used G-10 and ceramic Morgan coils that were supported in air bearings and driven by a DC motor. A 16-bit absolute encoder was used to trigger an integrator based on rotary position. This system had not been used in many years and the quality of the coil assemblies was questionable. We had recently completed magnetic measurements of a superconducting undulator (SCU) and had used a single-turn stretched coil to measure the integrated dipole components. Since we already had much of the hardware required, we decided to use a single-turn radial coil for harmonic field measurements of multipole magnets.

SYSTEM OVERVIEW

The following is a list of some of the features of the new multipole measurement system:

- Continuous coil rotation without slip rings
- Quasi-real-time measurements of individual multipole components using a lock-in amplifier (LIA)
- Measurement of the integrated magnetic field strength, multipole coefficients, magnetic-center offsets, and magnetic angle
- Automatic alignment of quadrupole and sextupole magnet positions relative to the center of rotation of the coil

The key components for the multipole measurement system were two Newport RGV100BL precision rotary stages. The precise control of position, velocity, and simultaneous timing allowed synchronous operation of both stages as if the coil wires were rigidly linked.

The system utilized a single-turn stretched coil in a radial configuration, as shown in Fig. 1. The coil-wire was 100-µm-diameter CuBe. The coil-wire ends were held in place with plastic fixtures connected to the rotary stages, as shown in Fig. 2. Coil fixtures can easily be made overnight on a 3D printer, so changing the radius of the coil would be a simple matter of changing the fixture radius. The coil was tensioned by moving the signal-end rotary stage in the longitudinal direction until the sag was minimized. The coil-wire sag was typically less than 200 µm when using a 1.5-m-long coil. Optical alignment telescopes were used to confirm the coil dimensions and alignment to approximately 50-µm accuracy.

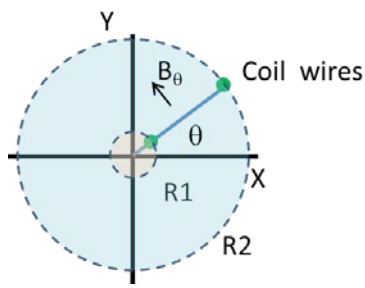


Figure 1: Radial coil configuration is sensitive to the radial component of the B field.

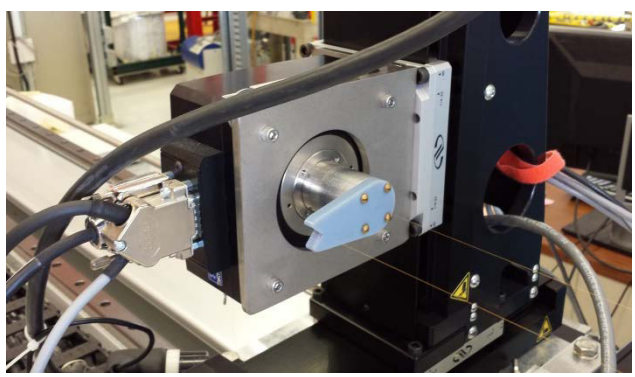


Figure 2: Signal-end rotary stage looking at the plastic coil positioning fixture.

*Work supported by the U.S. Department of Energy, Office of Science, under Contract No. DE-AC02-06CH11357

ISBN 978-3-95450-138-0

Copyright © 2013 CC-BY-3.0 and by the respective authors

MAGNETIC MEASUREMENTS OF THE FIRST SUPERCONDUCTING UNDULATOR AT THE ADVANCED PHOTON SOURCE*

C. Doose, M. Kasa, ANL, Argonne, IL 60439, USA

Abstract

A superconducting (SC) undulator prototype designated SCU0 was installed in the APS storage ring in December, 2012, and is providing users with photons in the energy range of 80-100 keV. This device was assembled and tested during the majority of 2012. Detailed tests were performed related to cryogenics, vacuum, mechanical motion due to thermal contraction, and magnetic performance. Magnetic measurements have been performed using a horizontal measurement system, which utilizes Hall probes and an integral coil. The measurement system was configured without interfering with the cryogenic or vacuum systems of the SCU0 cryomodule. Some of the magnetic measurement results will be presented for local and integrated field measurements, integrated field uniformity, and integrated fields during a quench. The measured rms phase errors were typically less than two degrees. The measured change in the integrated field during an intentional quench was less than 35 G-cm. The magnetic performance of SCU0 has proven to be within design tolerance for field quality and quench characteristics. Beam-based integral measurements agree well with the magnetic measurements.

SCU0 BACKGROUND

SCU0 is a prototype superconducting undulator (SCU) that was installed in the APS storage ring during December 2012, and is presently operating successfully at the APS sector 6 beamline [1,2].

Table 1: SCU0 Magnetic Specifications

Period	16 mm
Magnetic gap	9.5 mm
Magnet length	331 mm
Design peak field	0.4 - 0.65 T
Design Current	200 - 500 A
Maximum achieved peak field	0.82 T
Maximum achieved current	740 A

Table 2: APS Undulator Error Tolerance

1st Vertical Field Integral	100 G*cm
1st Horizontal Field Integral	50 G*cm
1st Vert. Field Integral during quench	2100 G*cm
2nd Horz. And Vert. Integrals	1×10^{-5} G*cm^2
Normal and Skew Integrated Quadrupole	50 G

*Work supported by the U.S. Department of Energy, Office of Science, under Contract No. DE-AC02-06CH11357

The assembly of the SCU0 cryomodule began in January, 2012; the first magnetic measurements of the assembled device began in June 2012 and were completed in August. A second set of magnetic measurements was done in November and December of 2012. The first set of measurements was performed with the original pair of SC magnetic structures. From September to October, the SCU0 was disassembled to replace the Al beam chamber with a new design. In the process of disassembly one of the SC wires was possibly damaged. A spare magnet structure was available so it was installed rather than risk a failure of the suspect SC wire.

HALL PROBE MEASUREMENT RESULTS

The following section describes some of the typical measurement results while using a room temperature Hall probe to measure the local fields along the longitudinal axis (z). The measurement system utilizes a room-temperature Ti tubing, "warm-bore," as a guide tube for the carbon fiber Hall probe assembly. The Ti tubing is tensioned inside but isolated from the cold (~10 K) Al beam chamber. A similar concept is used by the Budker Institiute for SC wiggler magnetic measurements.

An overview of the measurement system is shown in Fig. 1. The 3.5-m-long stage is used to drive a carbon fiber Hall probe assembly through the Ti guide tube. Stages mounted to the ends of the SCU0 cryomodule provide support and tension for the Ti guide tube and horizontal transverse motion (x) for measuring up to ±10 mm from the central axis.



Figure 1: SCU horizontal magnetic measurement system with 3.5-m linear stage for Hall probe scans. SCU0 cryomodule is on the left.

1st and 2nd Field Integrals and Phase Errors

The measured 1st and 2nd vertical field (B_y) integrals from the measurements performed in August and December of 2012 are shown in Fig. 2 and Fig. 3. The final 1st integral values were +31 and -87 G*cm in August and December, respectively. The August measurements of

Copyright © 2013 CC-BY-3.0 and by the respective authors

SUPERCONDUCTING CORRECTOR IR MAGNET PRODUCTION FOR SUPERKEKB*

B. Parker#, M. Anerella, J. Escallier, A. Ghosh, H. Hocker, A. Jain, A. Marone, P. Wanderer
BNL, Upton, NY 11973, USA
Y. Arimoto, M. Iwasaki, N. Ohuchi, M. Tawada, K. Tsuchiya, H. Yamaoka, Z. Zong
KEK, Tsukuba, Ibaraki 305-0801 Japan

Abstract

SuperKEKB is an upgrade project underway at KEK, to increase the KEKB b-factory luminosity 40-fold by using nanobeam Interaction Region (IR) focusing optics [1] for which the production of new superconducting IR magnets and correctors is critical [2]. SuperKEKB corrector design and production is challenging since many different coils are needed for precise control of IR magnetic fields, in order to ensure good beam lifetime and there is very little space for them. SuperKEKB corrector production is about half completed and we report here on new techniques recently developed to address production challenges.

INTRODUCTION

The SuperKEKB IR magnet layout in the left-side and right-side cryostats is shown in Fig. 1. The SuperKEKB design has 83 mrad total crossing angle to separate the e^- (E) High Energy Ring (HER) and e^+ (P) Low Energy Ring (LER) beam lines in independent non-cryogenic vacuum apertures. A few millimetres of radial space is available for corrector coils atop support bobbins that serve as the inner cold mass containment wall and the main quadrupole coils' inner surface. The corrector requirements, presented in Table 1, evolved in response to results from optics optimization and tracking studies and differ from those available before production started [3].

Left-side corrector production commenced first using preliminary specifications provided before the right-side requirements were set. Later optics studies found that sextupole coils, b_3 and a_3, not in the original design, are needed; so these coils are added to the right-side layout. The majority of the corrector coils are located inside a main quadrupole coil; however, with insufficient space inside the first IR quadrupoles, QC1LP/RP, their b_4 correctors are wound on bobbins placed just outside the main coil (along with an a_3 corrector only for QC1RP). Because these first LER quadrupoles have insufficient space for magnetic flux return yokes between their coils and the nearby HER beam, there is significant external field leakage that must be dealt with so as not to adversely impact the HER optics. Requirements for these additional external field cancel coils for the HER are discussed later.

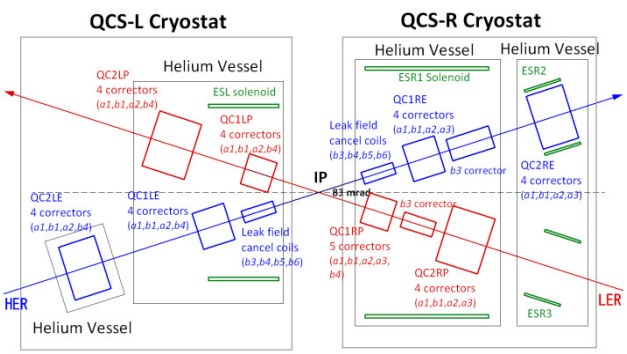


Figure 1: SuperKEKB IR magnet layout schematic.

Table 1: Corrector Integral Field Strength Requirements. Here R/L denote left- and right-side magnets and P/E denote the LER and HER beam lines. The right-side b_3 coils are placed between main magnets. The external field cancel coils for the HER are not included in this table.

Magnet	R_r	A_1	B_1	A_2	A_3	B_3	B_4
	mm	T•m	T•m	T	T/m	T/m	T/m^2
QC1RP	10	0.016	0.016	0.64	7.6	17.2	60
QC2RP	30	0.03	0.03	0.31	1.36		-
QC1RE	15	0.027	0.046	0.75	7	27	-
QC2RE	35	0.015	0.015	0.37	1.5		-
QC1LP	10	0.016	0.016	0.64	-	-	60
QC2LP	30	0.03	0.03	0.31	-	-	60
QC1LE	15	0.027	0.046	0.75	-	-	60
QC2LE	35	0.015	0.015	0.37	-	-	60

Both the corrector and cancel coils are attached to support bobbins via the BNL Direct Wind technique [4] using 0.35 mm diameter, single-strand superconducting round wire from Furukawa with a 1:1 Cu:NbTi ratio and critical current at 4.2K greater than 130 amps in a 5 T background field [5]. The wire is Kapton® overwrap insulated and adhesive coated to be compatible for use with BNL Direct Wind ultrasonic bonding technology.

CORRECTION COIL PRODUCTION

The SuperKEKB corrector requirements span a broad range of field harmonics and focusing strengths and are manufactured in many radius and length combinations. In order to make the best use of the available space attention to detail is needed regarding the careful nesting of coil layers. The QC2LE multi-layer arrangement shown in Fig. 2 offers an example of how lead management is an important consideration. At the bottom of the QC2LE coil stack is a single layer planar pattern [6] dipole winding over which skew dipole and then skew quadrupole planar coils are wound. The skew quadrupole is topmost because its ends, with fewer turns, are naturally shorter than those of the layers below and its four pole regions line up with

#parker@bnl.gov

Copyright © 2013 CC-BY-3.0 and by the respective authors

ISBN 978-3-95450-138-0

PARTIAL RETURN YOKE FOR MICE – ENGINEERING DESIGN*

H. Witte†, S. Plate, Brookhaven National Laboratory, Upton, NY, USA
J. Tarrant, STFC Rutherford Appleton Laboratory, Didcot, UK
A. Bross, Fermilab, Batavia, IL, USA

Abstract

MICE, which is an acronym for Muon Ionization Cooling Experiment, is a technology demonstration which is presently assembled at the Rutherford Appleton Laboratory in Didcot, UK. MICE aims to demonstrate ionization cooling experimentally, which is an essential technology for potential future accelerators such as a muon collider.

The MICE channel consists of up to 18 large bore superconducting solenoids, which produce a substantial stray field. This stray field can jeopardize the operation of electrical and electronic equipment in the MICE hall.

The concept of a partial flux return yoke has been developed, which reduces the stray field in the MICE hall to a safe level. This paper discusses the engineering design of the partial return yoke.

INTRODUCTION

MICE will be assembled in several steps [1]. At the time of writing it is aimed to finish construction of Step IV by summer/autumn 2014. MICE Step IV consists of 12 large bore superconducting solenoids (18 for Step VI). The MICE solenoids produce a substantial amount of stray field, which is a concern as some of the technical equipment in the MICE hall may not work.

This paper discusses the engineering aspects of a partial return yoke (PRY) for the MICE solenoids for Step IV; the partial enclosure is sufficient to reduce the stray fields to an acceptable level.

Details on the general design approach, the coil configuration of Step IV, expected shielding performance and effect on the performance of MICE are given in [2, 3].

ENGINEERING CONCEPT

The evolution of the PRY geometries is shown in Fig. 1. It is important to note that in general all shown geometries have a similar shielding performance. The vertical extensions (middle plot) have been found to further reduce the stray field behind the PRY by preventing flux leakage from the unshielded part. The final geometry, shown on the right, was chosen because of engineering considerations.

The MICE PRY will consist of in total eight shielding plates, each of which is about 4 m long and 1.5 m wide. The thickness of each shielding plate is 10 cm or 12 cm depending on the desired shielding performance. The weight

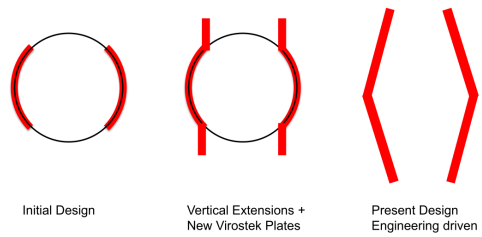


Figure 1: Evolution of the PRY geometry.

of a 10 cm thick shielding plate is about 4.8 tons, which is less than the limit of the lifting crane in the MICE hall.

To avoid field leakage (see section 'Vertical Gaps') two backing plates are installed on the inside and outside of the PRY covering the vertical joint. The thickness of each backing plate is half that of the PRY.

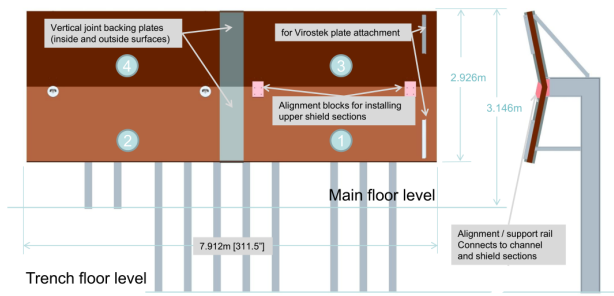


Figure 2: MICE partial return yoke.

SUPPORT STRUCTURE

The support structure has been designed to cope with the dead weight of the PRY as well as magnetic forces. The magnetic forces on the structure were evaluated using the Maxwell stress tensor. The forces were evaluated for each of the shielding plates separately. The main force component is in horizontal direction, directed such that the shielding plates want to move towards the MICE experiment. The maximum force is equivalent to 34 tons for half of the PRY (four shielding plates) and occurs for the 240 MeV flip mode. There is no net longitudinal or vertical magnetic force on the PRY due to symmetry reasons.

The support structure, as shown in Fig. 2, consists of several S-beams which are anchored in the floor of the MICE hall. An ANSYS study was carried out to evaluate peak stresses and deflections. While the stresses are not a concern (123 MPa) a maximum deflection of 5 mm was ob-

* Work supported by Brookhaven Science Associates, LLC under Contract No. DE-AC02-98CH10886 with the U.S. Department of Energy.
† hwitte@bnl.gov

Copyright © 2013 CC-BY-3.0 and by the respective authors

PARTIAL RETURN YOKE FOR MICE – GENERAL CONCEPT AND PERFORMANCE*

H. Witte†, S. Plate, Brookhaven National Laboratory, Upton, NY, USA
J. Tarrant, STFC Rutherford Appleton Laboratory, Didcot, UK
A. Bross, Fermilab, Batavia, IL, USA

Abstract

MICE, which is an acronym for Muon Ionization Cooling Experiment, is a technology demonstration which is presently assembled at the Rutherford Appleton Laboratory in Didcot, UK. MICE aims to demonstrate ionization cooling experimentally, which is an essential technology for potential future accelerators such as a muon collider.

The MICE channel consists of up to 18 large bore superconducting solenoids, which produce a substantial stray field. This stray field can jeopardize the operation of electrical and electronic equipment in the MICE hall.

The concept of a partial flux return yoke has been developed, which reduces the stray field in the MICE hall to a safe level. This paper discusses the general concept and expected performance.

INTRODUCTION

Ionization cooling can be regarded as an essential technology for future HEP particle accelerators such as the muon collider, as it is the only known technology fast enough to reduce the emittance of a muon beam.

MICE, which aiming to demonstrate the concept [1], will be assembled in several steps. At the time of writing it is aimed to finish construction of Step IV by summer/autumn 2014. MICE Step IV consists of 12 large bore superconducting solenoids. The MICE solenoids produce a substantial amount of stray field (in excess of 50 mT), which is a concern as some of the technical equipment in the MICE hall may not work.

This paper discusses the design concept of a partial return yoke (PRY) for the MICE solenoids for Step IV. The engineering design is described in [2, 3].

METHODOLOGY

For the analysis of the problem and performance estimate two commercial finite element packages are employed: COMSOL Multiphysics (COMSOL AB, Tegnergatan 23, SE-111 40 Stockholm, Sweden) and Opera 3D from Cobham/Vectorfields (Cobham CTS Limited trading, 24 Bankside, Kidlington, Oxfordshire, OX5 1JE, UK).

The two software packages use different physics implementations, which allows to verify the obtained results. COMSOL solves for the magnetic vector potential:

$$\nabla \times \left(\mu^{-1}\nabla \times A\right) = J \ . \tag{1}$$

In this equation μ is the magnetic permeability, A the magnetic vector potential and J a current density. In contrast to this Opera 3D solves for the magnetic scalar potential ϕ:

$$\nabla\mu\nabla\phi - \nabla\mu\left(\int_{\Omega_J}\frac{J\times R}{|R^3|}\mathrm{d}\Omega_J\right) = 0 \ . \tag{2}$$

Contributions to the magnetic field from current carrying structures at a distance R are usually evaluated using Biot-Savart law and integrated over the domain Ω.

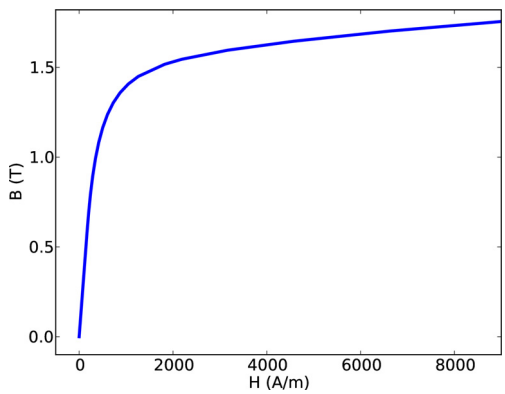


Figure 1: Magnetization curve of AISI 1010 steel.

For the simulations we assume that shielding iron will have the magnetic properties shown in Fig. 1. The magnetization curve was taken from Opera and is valid for AISI 1010 steel.

The coil geometries used in the simulation are summarized in Table 1.The MICE solenoids will be run in five different configurations. In two configurations the magnetic field flips in the centre of the MICE channel ('flip modes') whereas in three it does not ('solenoid modes'). The current densities for all cases are summarized in Table 2.

GENERAL CONCEPT

All MICE magnets are large diameter solenoids, which are relatively thin and short. From a shielding point of view an ideal solution is to encase the MICE magnets in a soft-iron cylinder. This is of course not practical; however, it is possible to achieve good shielding by only encasing MICE partially in this way. Fig. 2 shows the concept.

* Work supported by Brookhaven Science Associates, LLC under Contract No. DE-AC02-98CH10886 with the U.S. Department of Energy.
† hwitte@bnl.gov

ISBN 978-3-95450-138-0

Copyright © 2013 CC-BY-3.0 and by the respective authors

A STRIPLINE KICKER DRIVER FOR THE NEXT GENERATION LIGHT SOURCE*

N. Butler, F. Niell, J. Kinross-Wright, M. Gaudreau, M. Kempkes,
Diversified Technologies, Inc., Bedford, MA 01730, USA

Abstract

Diversified Technologies, Inc. (DTI) has designed and prototyped a novel high voltage pulse generator applicable to beam deflector applications. This work is funded by an SBIR grant from the U.S. Department of Energy in support of advanced accelerator development. The technical goals include 10 kV output into 50 Ω with 2 ns rise time and a repetition rate of 100 kHz. These challenging specifications were based on the original Next Generation Light Source (NGLS) fast deflectors (stripline kicker) required in the proposed beam switchyard. DTI believes the advanced pulse generator will have numerous applications requiring fast risetime and high repetition rate. This paper describes the current status of the project.

BACKGROUND

In Phase I of the project, DTI investigated several high-speed switching circuits, using a variety of emerging solid-state switch technologies, including GaN and SiC. After much experimentation, DTI has settled on an inductive adder circuit topology, using a two-step, silicon MOSFET Marx approach in each stage. The use of parallel FETs at each stage of the inductive adder allows a flexible design which can be adapted to new requirements. The Phase II prototyping efforts have validated the design approach. Figure 1 shows an operational prototype pulse generator.

Motivation

The NGLS facility concept uses a high bunch rate accelerator (1 MHz) to efficiently supply beam to 10 independent X-ray FEL beam lines. Each beam line receives pulses at 100 kHz, though the fields in the deflector must settle in less than 1 μs to avoid perturbation of un-deflected pulses in the bunch train from the accelerator.

It is envisioned that the deflection will be imparted by a symmetric pair of shaped parallel deflection electrodes, pulsed in opposition at 10 kV. Matching 50 Ω resistors terminate the deflector to avoid the creation of backward-traveling waves.

SYSTEM ARCHITECTURES

Various system designs were explored for producing the required pulse wave forms. The options included a direct series high voltage switch, solid-state Marx bank, inductive adder, or more conventional pulse transformers and transmission-line adders, several of which were considered in detail. The inductive adder was ultimately selected as the preferred development path for the remainder of the program. The favored embodiment of the overall pulse generator was based on measurements, multiple circuit test boards, extensive modeling, and practical considerations regarding component performance in the sub-nanosecond regime.

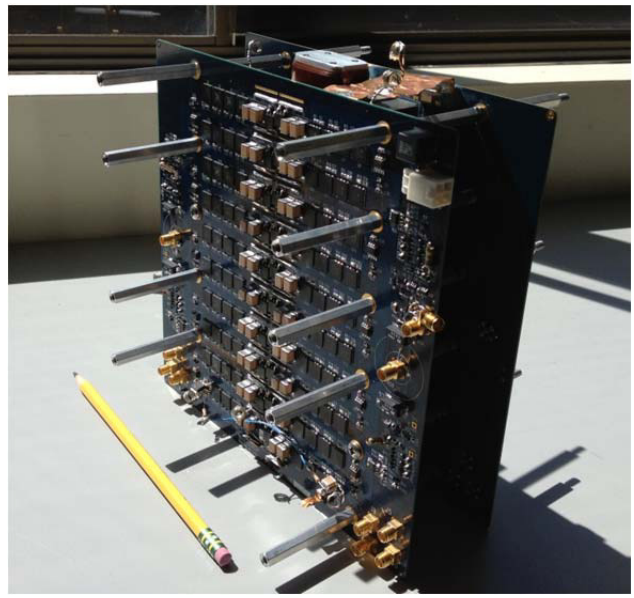


Figure 1: Prototype pulser hardware. In the center of the rectangle at the top is the output connection, and the two circuit boards on either side carry the pulse amplifiers and MOSFETs.

Pulse Generation

The overall pulse generation network is presented in Figure 2. This represents the principal schema, but variants on this approach have been developed as well. The key components exhibited in this figure include:

- Each stage is comprised of a pair of STMicroelectronics STL21N650 compensated silicon MOSFETs, capable of 2 nanosecond-class switching speed, along with extremely fast charge-pump driver circuitry to enable such fast switching. Note that the gate drivers must be referenced to the source pins in the diagram, meaning that one set of gate drivers must be floating – a key technological issue in this speed domain.
- A set of transformer cores, Tn, to couple the 1 kV pulses into a common tapered secondary structure. Matching the impedance of the output structure to

*Work supported by the Department of Energy

Copyright © 2013 CC-BY-3.0 and by the respective authors

PROGRESS ON THE MSU SUPERFERRIC CYCLOTRON GAS STOPPER MAGNET QUENCH PROTECTION AND COOLING SYSTEM

S. Chouhan, M. A. Green, G. Bollen, and A. F. Zeller, FRIB, Michigan State University, East Lansing MI 48824, USA; J. DeKamp, C. Magsig, D. Morrissey, J. Ottarson, and S. Schwarz, NSCL Michigan State University, East Lansing MI 48824, USA

Abstract

The MSU gas cyclotron stopper system is designed to decelerate rare isotope ions from energies from >50 MeV to energies in the 10 keV range. The ions are decelerated in low-pressure helium gas in vertical cyclotron magnet. The magnet and the system for decelerating the ions are mounted on a high voltage platform. The cyclotron gas stopper magnet is a warm iron superconducting cyclotron sector dipole. The maximum field in the gap (0.18 m) is 2.7 T. The outer diameter of magnet yoke is 3.8 m, with a pole radius of 1.1 m and Br = 1.8 T m. The desired field shape is obtained by the pole profile. Each coil of the two halves is in a separate cryostat and connected in series through a warm electrical connection. The entire magnet system will be mounted on a high voltage platform. The magnet coils have been fabricated and installed in their cryostats. The iron poles have been machined and assembled. This paper presents the progress on the magnet system fabrication and assembly.

INTRODUCTION

The fragmentation of fast heavy-ion particles enables fast, chemistry-independent production, separation and delivery of exotic isotope beams. The resulting beams of exotic nuclei have high energies (>50 MeV/u) and large emittances. The range of possible experiments with the fast beams can be extended by slowing down the fast ions. The ReA3 [1] re-accelerator under construction at MSU will re-accelerate the thermalized ions to provide low emittance exotic beams over a range of energies. The thermalization of the fast ions and their extraction using existing techniques are limited by space charge and other limitations.

A proposed solution to thermalize and extract light to medium mass ions and high intensity beams is to apply strong gradient-dipole magnetic field in a large magnetic gap (0.18 m) that forces the fast ion beams to follow spiral trajectory while slowing down in the gas. Concentrated thermalized ions near the central extraction port are then transported in to central extraction orifice via an RF-carpet. These extracted ions will be transformed into low energy beams using a differentially pumped ion-guide. The low energy ion beams can be transported directly to low-energy experiments or to other accelerators for reacceleration. The high performance and high field (2.7 T) super-ferric cyclotron gas stopper sector-magnet at National Superconducting Cyclotron Laboratory (NSCL), Michigan State University (MSU) will enable the capture of short-lived rare isotopes produced in nuclear reactions.

The cyclotron gas-stopper magnet design has evolved since its original design in 2007 [2]. A gradient dipole field is produced in a gap of 180 mm between sector cyclotron iron poles. The peak field in the gap is ~2.7 T. A pair of superconducting solenoid coils produce the field. The warm iron poles can be separated so that the deceleration system can be maintained. Each pole coil has its own helium cryostat and superconducting coil that operate at 4.3 K. The 300 K iron poles are physically connected through the magnet iron flux return path, but the superconducting coils are not physically connected. The forces on the magnet coils are transported to the iron return yoke through the cold mass supports. The magnet is oriented so that the common axis of the solenoid coils is horizontal. Thus the beam plane for the super-ferric cyclotron magnet is vertical. Each of the two magnet superconducting coils will be cooled using three PT-415 pulse-tube 4 K coolers with remote valves.

IRON POLES AND RETURN YOKE

The split iron poles and return yoke are shown in Fig. 1. One of the sector cyclotron pole pieces is shown in Fig. 2. Table 1 presents the parameters for the magnet [3].



Figure 1: The split magnet iron return path and poles.

*The material in this paper was supported in part by a grant for the National Science foundation under MSU grant number PHY-0958726.

ISBN 978-3-95450-138-0

Copyright © 2013 CC-BY-3.0 and by the respective authors

MECHANICAL DESIGN OF THE CRYOGENIC SUB-SYSTEMS FOR ReA6 QUARTER WAVE RESONATOR CRYOMODULE*

M. Shuptar#, F. Casagrande, A. Fox, M. Johnson, M. Leitner, S. Miller, T. Nellis, M. Patil, T. Xu, Y. Xu, Facility for Rare Isotope Beams (FRIB), East Lansing, MI 48824, USA

Abstract

The driver linac for the Facility for Rare Isotope Beams (FRIB) consists of 49 cryomodules operated at 2 K utilizing 4 different types of superconducting resonators and 2 solenoid lengths which in turn requires 7 individual cryomodule configurations. The mechanical design requirements of the internal cryogenics of an FRIB cryomodule are determined by the piping and instrumentation diagram, which is discussed in the paper based on the FRIB quarter wave cryomodule type. In addition, heat load requirements and spatial constraints of other cryomodule sub-systems influence the cryomodule cryogenics design. The paper describes detailed design choices for the cryogenic headers and piping, a 2 K heat exchanger inside the cryomodule, solenoid current leads, and the bayonet connections to the cryogenic distribution system inside the accelerator tunnel. Different operating modes, which influence the cryogenic design, are summarized.

INTRODUCTION

FRIB is a US $700 million nuclear physics project to be built at the Michigan State University under a corporate agreement with the US Department of Energy (DOE) with a 7-year timetable [1]. According to the current FRIB baseline schedule fabrication and procurement of linac components will start mid-2014. Actual linac installation will begin end of 2016 after completion of conventional facilities and cryoplant construction [2].

Due to the heavy mass and correspondingly low velocity of the accelerated ions the FRIB driver linac [1] utilizes four different low-beta SRF resonator designs in cryomodules. Each cryomodule is equipped with niobium cavities which will operate at 2 K providing acceleration to the heavy ions. Due to the large number of cryomodules the FRIB project lends itself to a manufacturing mind-set that incorporates large scale production into the design of individual modules types. As a part of the manufacturing mind-set FRIB is currently developing a prototype cryomodule that will utilize 8 superconducting quarter-wave cavities, and is referred to as the ReA6 cryomodule. Upon completion the ReA6 cryomodule will test not only the general cryomodule design, but also the manufacturing methodology [3]. Even though ReA6 is a prototype module it will implement some design choices that differ from a typical FRIB cryomodule. The usefulness of the ReA6 module will not end with proof of concept of mechanical and manufacturing principals; after testing the module becomes a permanent part of FRIB's Re-Accelerator located in the experimental area of the facility.

* This material is based upon work supported by the U.S. Department of Energy Office of Science under Cooperative Agreement DE-SC0000661. Michigan State University designs and establishes FRIB as a DOE Office of Science National User Facility in support of the mission of the Office of Nuclear Physics.

shuptar@frib.msu.edu

BASIS OF REQUIREMENTS

Each cryomodule design starts by obtaining the system's requirements and then designing the specifications. For the cryogenics inside the ReA6 Quarter Wave Resonator (QWR) cryomodule the requirements are defined by; piping and instrumentation diagram (P&ID), heat load budget, cost and spatial constraints.

The ReA6 P&ID differs from an FRIB module because the operating constraints of the ReA6 are slightly different from an FRIB module. Since the ReA6 module will be built ahead of the FRIB cryoplant and will not be located in the tunnel its cryogenic layout specified on the P&ID includes a liquid nitrogen circuit not present in FRIB Cryomodules. ReA6 Resonators will also operate a 4.5 K compared to an FRIB module's resonators operating a 2 K [4].

Heat Load Budget

The heat load calculations outline the allowed heat load for each module. Constraining the heat load to each module budget ensures that the cryoplant is sized correctly. The heat load budget requirement for ReA6 cryomodule is shown in Table 1 [5].

Table 1: ReA6 β=0.085 Cryomodule Heat Loads

	Resonators (4.5 K)	**Focusing Magnets (4.5 K)**	**Thermal Shield (80 K)**
Static (W)	6.0	50.7	180.6
Dynamic (W)	80.0	1.3	23.2
Total (W)	**86**	**52**	**204**

The heat load budgets are also necessary to estimate the mass flow for three separate cryogenic loops. Calculation of the helium and nitrogen interfaces to the cryogenic distribution are given in (Table 2) [5]. To minimize vapour velocity and maximize helium capacity the headers needs to be sized effectively.

Copyright © 2013 CC-BY-3.0 and by the respective authors

IMPACT OF RADIATION ON THE MU2E PRODUCTION SOLENOID PERFORMANCE*

V.V. Kashikhin#, N. Dhanaraj, M.J. Lamm, N.V. Mokhov, V.S. Pronskikh,
FNAL, Batavia, IL 60510, USA

Abstract

The Muon-to-Electron conversion experiment (Mu2e) is under development at Fermilab to detect direct muon to electron conversion and provide evidence for processes violating muon and electron lepton number conservation not explained by the Standard Model of particle physics.

The Mu2e magnet system consists of three large superconducting solenoids. One of the magnets is Production Solenoid (PS) named after the pion production target installed in the magnet bore. The superconducting coils are protected from the secondary particle radiation by a massive Heat and Radiation Shield (HRS) made of bronze, which was optimized for the energy absorption and cost. This paper describes the impact of radiation on the magnet cooling, stability and quench.

INTRODUCTION

The Mu2e magnet system consists of three large superconducting solenoids [1]. PS is the first magnet in the chain [2], which collects and focuses pions and muons generated in interactions of an 8-GeV proton beam with a tilted high-Z target and directs them towards Transport Solenoid (TS), by supplying a peak axial field of 4.6-5.0 T and ~1 T/m gradient within a 1.5 m warm bore.

It is a challenging magnet because of the relatively high magnetic field and a harsh radiation environment. The PS coils are protected from radiation by 50-cm thick water-cooled HRS made of high-resistivity bronze, placed within the warm magnet bore. An extensive simulation effort has been carried out to optimize the shield parameters and get the radiation load below the tolerable levels with a sufficient safety margin [3].

The radiation heat reaching the coils must be extracted to the cryogenic system to maintain the necessary operating margin. It is achieved using a system of thermal bridges made of pure Al connected to the cooling tubes [4]. Electrical and thermal properties of the thermal bridges and the cable stabilizer are significantly degraded under the irradiation that impacts the cooling efficiency, magnet stability and quench performance.

RADIATION ANALYSIS

Simulations were performed with the MARS15 code [5] on the model shown in Fig. 1. The neutrons were propagated down to 0.001 eV. The full set of critical radiation quantities was calculated. The superconducting coil material was described using homogeneous approach (the material was represented as a mix of all elements with appropriate weight factors).

* This work was supported in part by Fermi Research Alliance under the U.S. Department of Energy Contract DE-AC02-07CH11359.
#vadim@fnal.gov

The peak calculated Displacement Per Atom (DPA), which characterizes the radiation damage in metals, was ~$2.5 \cdot 10^{-5}$ yr^{-1} and the peak power density was 12.6 μW/g [3]. Corresponding peak absorbed dose for the coil insulation is 240 kGy/yr; total dynamic heat load in the cold mass is 28 W. While the total dynamic heat load is relatively small, the power density distribution in the cold mass is strongly non-uniform, as shown in Fig. 2 that creates a localized hot spot in the middle of the first coil.

Taking conservative safety factors into account, the calculated DPA translates into the degradation of RRR in Al and Cu from the initial values of 600 and 80 to 100 and 50 respectively in about one year of experiment's operation [6]. These numbers are regarded as the minimum allowable values. The magnet will be equipped with RRR gauges that monitor the material property changes during the operation. Once the critical resistivity degradation is detected, the magnet will be thermo-cycled to the room temperature that restores the original resistivity in Al and ~87% of that in Cu [7]-[8].

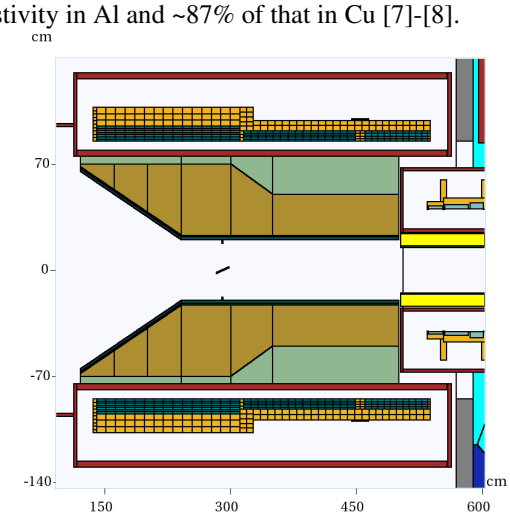


Figure 1: MARS model.

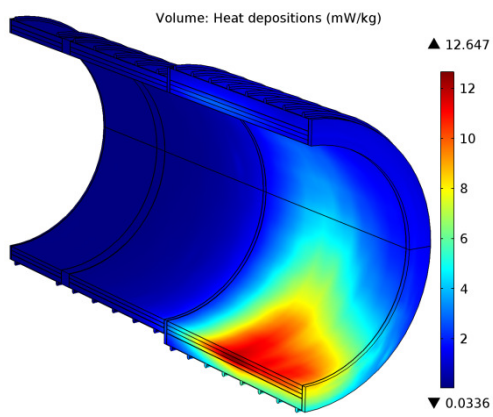


Figure 2: Radiation power distribution in the cold mass.

Copyright © 2013 CC-BY-3.0 and by the respective authors

ISBN 978-3-95450-138-0

A HIGHLY CONFIGURABLE AND SCRIPTABLE SOFTWARE SYSTEM FOR FULLY AUTOMATED TUNING OF ACCELERATOR CAVITIES *

J. M. Nogiec#, R. Carcagno, S. Kotelnikov, A. Makulski, R. Nehring, D. Orris, W. Schappert,
FNAL, Batavia, IL 60510, USA

Abstract

A software system has been developed to automate cavity tuning machines as part of a multi-laboratory collaboration. The system is based on a plugin framework containing a configurable set of components. Each component runs asynchronously and uses a framework for message based communication. Components run in either manual or automatic mode. In automatic mode, the system interprets a user-selected control script which executes a sequence of measurements, model calculations and tuning operations. A tuning script iterates until the prescribed tuning criteria are satisfied, or until aborted or paused by the user. In manual mode, the user controls the tuning process, deciding when and which component to run, and when tuning is complete. The software framework incorporates the blackboard architecture for sharing data and results between the various plugins. The results of the measurements and tuning are persisted in an XML-based data store, and components exist that retrieve and visualize the data. The software system is portable (Linux, Windows) and has been successfully deployed and used by Fermilab, DESY, and KEK.

INTRODUCTION

The Cavity Tuning Machine (CTM) is a result of collaborative efforts among DESY, KEK and Fermilab [1] [2], with the Fermilab team responsible for developing system electronics and software [3]. The goal for the project was to automate tuning of accelerator cavities with the intention to support high-throughput cavity fabrication for construction of large SRF-based projects.

The tuning process includes a sequence of measurements and model-based calculations to determine the required tuning parameters, followed by the actual tuning. This process is iterative and is continued until the π-mode frequency and field flatness as well as the cavity mechanical alignment are all within the required tolerances. Automating the tuning process shortens the time required to tune the cavity and ensures the repeatability and predictability of this process. In addition, trained operators can replace RF experts at performing cavity tuning.

The main building blocks of the CTM apparatus include the base frame with a positioning system that moves the cavity between various positions, the eccentricity measurement device to measure the shape of the cavity, the gate with actuators for tuning (mechanically deforming) the cavity cells, the bead-pull measurement system, the laser-based alignment setup, and various electronic components, such as motion controls, interlocks, a network analyser, DAQ boards, and a weather station [3].



Figure 1: The cavity tuning machine.

ARCHITECTURE

The software architecture of the CTM system is based on the concept of plug-ins, a solution built on the ability to dynamically load and execute specified components. The framework consists of a shell module and a set of plug-ins (see Fig. 2). The shell implements a queued state machine and provides the overall system control logic, data saving, control of plug-ins, and user interface integration. Each plug-in implements a separate measurement (e.g., eccentricity, field flatness) or functionality (e.g., positioning, model, assessment) and constitutes a complete module with its own user interface, logic and DAQ. A plug-in's front panel is integrated into the overall user interface. Plug-ins communicate via message queues.

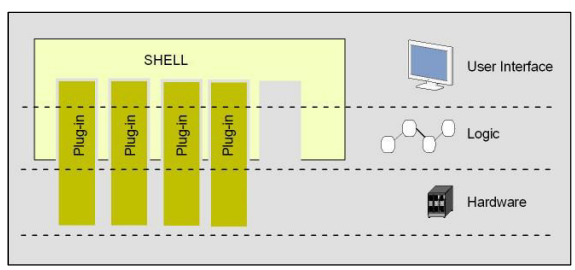


Figure 2: Plug-in architecture.

The system can operate in two modes: *manual* where the operator can use the controls available from the plug-in's front panel and *automatic* where the plug-in's front panel is disabled and the system controls the execution of plug-ins according to the logic specified in the script.

*Work supported by the U.S. Department of Energy under contract no. DE-AC02-07CH11359
#nogiec@fnal.gov

Copyright © 2013 CC-BY-3.0 and by the respective authors

A NEW FACILITY FOR TESTING SUPERCONDUCTING SOLENOID MAGNETS WITH LARGE FRINGE FIELDS AT FERMILAB

D. Orris, R. Carcagno, A.M. Makulski, J. Nogiec, R. Pilipenko, R. Rabehl, C. Sylvester, M. Tartaglia, Fermilab, Batavia, IL, USA

Abstract

Testing superconducting solenoid magnets with no iron flux return can be problematic for a magnet test facility due to the large magnetic fringe fields generated. These large external fields can interfere with the operation of equipment while precautions must be taken for personnel supporting the test. The magnetic forces between the solenoid under test and the external infrastructure must also be taken under consideration. A new test facility has been designed and built at Fermilab specifically for testing superconducting magnets with large external fringe fields. This paper discusses the test stand design, capabilities, and details of the instrumentation and controls with data from the first solenoid tested in this facility: the Muon Ionization Cooling Experiment (MICE) coupling coil.

INTRODUCTION

There has recently been a need to test solenoid magnets at Fermilab that have no iron flux return so the fringe magnetic fields could be relatively large. The Muon Ionization Cooling Experiment (MICE) Coupling Coil (CC) solenoid is the first such solenoid intended to be tested.

Since the existing dewars at Fermilab's Magnet Test Facility (MTF) are not large enough to test a MICE CC solenoid a new cryostat would be required. In addition, the large fringe field that would be produced by the solenoid would interfere with operations at MTF. At full operating current (210A) the 600 Gauss line would be at a radius of 3m and the 5 Gauss line would be at a radius of 15m. The 5 Gauss level is the limit for personnel with pacemakers and the 600 Gauss level impacts both personnel safety as well as the operation of equipment.

Several options were researched and the final decision was to build the solenoid test facility (SolTF) at the Fermilab Central Helium Liquefier (CHL) [1]. This location was selected because it had adequate space for the large test cryostat and the large fringe magnetic fields would not impact personnel and equipment operations: Personnel access could be managed to meet safety requirements. In addition, there was a sufficient source of liquid helium available to operate the new test facility.

SOLENOID TEST FACILITY

The new solenoid test facility (SolTF) would have to meet the cryogenic cooling, mechanical support, powering, quench protection, and data acquisition requirements for testing the MICE coupling coil at Fermilab. Table 1 lists some of the MICE CC specifications that SolTF must accommodate.

Table 1: MICE Coupling Coil Specifications for Testing

Parameter	Specification
Coil Design	96 Layers, 166 Turns in Series
Superconductor Strand	Cu/NbTi (MRI) 1.0 mm x 1.65 mm
Magnet Outer Structure Diameter	1860 mm
Magnet Weight	2.2 Tons
Cryogenic Cooling	Conduction Cooled
Helium Flow Rate	10 g/s
Cool Down Delta-T Limit	50 K Across the Magnet
Magnet Inductance	596 H
Maximum Current (4.5 K)	220 A
Stored Energy @220A	14.4 MJ
Peak Field (on axis)	2.6 T
Peak Field (on coil)	7.5 T
5G, 100 G, & 600 G Lines	15 m, 5m, 3m

Solenoid Test Cryostat

The cryostat used for the solenoid test facility was transferred to Fermilab from the National High Magnetic Field Laboratory (NHMFL) at Florida State University. The stainless steel vacuum vessel is 3.34m outer diameter, 3.32m inner diameter, and 2.7m high. The MICE CC coil would be tested in this cryostat using liquid helium conduction cooling.

The MICE CC solenoid is supported by a dished head assembly and four stainless steel rods each connected to a support bracket. The four support brackets are attached to the magnet with a G-10 block sandwiched between them to minimize heat conduction to the coil. G-10 rods between the support brackets and the cryostat wall prevent the magnet form moving horizontally. Although the cryostat was located as far as practical from the building's support columns and other fixed ferromagnetic material, tilt switches and displacement sensors were installed to monitor the magnet's vertical motion, if any, due to forces generated between the magnet and external magnetic material. Figure 1 is shows a 3-D model of the cryostat with the MICE CC solenoid.

Operated by Fermi Research Alliance, LLC under Contract No. De-AC02-07CH11359 with the United States Department of Energy.

Copyright © 2013 CC-BY-3.0 and by the respective authors

ISBN 978-3-95450-138-0

STATUS OF PXIE 200 OHM MEBT KICKER DEVELOPMENT*

Gregory Warren Saewert#, Mohamed H. Awida, Brian Chase, Howard Pfeffer, Dan Wolff,
Fermilab, Batavia, IL 60510, USA
Daniil Frolov, Kuban State University, Krasnodar, Russia

Abstract

The proposed Project X machine at Fermilab must deliver a widely varying bunch pattern to provide beam to several experiments quasi-simultaneously. H- Beam is delivered to the 2.1 MeV Medium Energy Beam Transport (MEBT) section at 162.5 MHz continuous wave (CW) by a radio frequency quadrupole magnet (RFQ). Unnecessary beam bunches will be selectively chopped out in the MEBT by two identical choppers on a bunch-by-bunch basis and stopped by an absorber. The Project X Injector Experiment (PXIE) will be the test bed to demonstrate a chopper's ability to form an arbitrary bunch pattern. Presently two kicker system versions are under development. One proposed version is a 50 Ω structure driven by a ±250 V linear amplifier. The second proposed version is a 200 Ω helical, microstrip line structure driven by a 500 V bipolar switch. This paper describes the development status of the 200 Ω version and includes the design concept, comparison of 3D modelling work with prototype measurements, 200 Ω hardware description and progress with the driver.

SYSTEM REQUIREMENTS

The challenge for this application is the bandwidth requirement to chop beam continuously. Beam will be delivered to a number of experiments "at the same time", so kicking patterns would vary depending upon the needs of the experiments. Thus, the frequency at which bunches change from being kicked in and out will vary from 1 to 35 MHz average and 81.25 MHz peak for about 20 alternating bunches. This 200 Ω chopper offers a design solution by taking advantage of reduced power requirement and includes the development of a suitable driver.

Beam beta in the MEBT is .067 at 2.1 MeV, so the kicker can be a traveling wave structure (the "kicker") to slow down the propagating voltage pulse to match the beam velocity. The chopper consists of two 50 cm long traveling wave kickers parallel to each other on opposite sides of the beam. Applied voltage to the parallel kickers will always be of opposite polarity.

The MEBT's lattice allows for a chopper either to apply a voltage to only kick beam out to the absorber (the unipolar scheme), or to kick beam both in and out with opposite polarity voltages (the bipolar scheme). The unipolar scheme requires applying 0 V and 500 V and the bipolar scheme ±250 V. Voltage tolerance is ±25 V.

* Operated by Fermi Research Alliance, LLC, under Contract No. DE-AC02-07CH11359 with the United States Department of Energy
# saewert@fnal.gov

SYSTEM DESIGN

Component power dissipation is a big issue, and current flowing in the kicker does nothing to kick beam. These facts made it appealing to design a higher impedance system than 50 Ω. Power delivered to the load is a factor of four lower at 200 Ω, and the kicker structure's RF I^2R losses in the vacuum are lower by a factor of 16 (all other physical characteristics being the same). The downside is that all system components need to be developed. Figure 1 is the block diagram of intended system.

Helical Kicker

Meander line kickers have been implemented. However, limited power handling and evident pulse distortion suggested considering alternatives. Helical structures have also been built [1]. Constructing a cylindrically helical, 175 Ω microstrip line demonstrated promising results. Subsequent ~200 Ω versions with good mechanical uniformity resulted in good enough performance to proceed with the 200 Ω idea.

The helical wire is #13 flat magnet wire (.105" x .041") held above a copper ground tube by four ceramic spacers. This wire size was chosen to be stiff to hold its shape yet easy enough to wind tightly on a mandrel by hand. Electrodes, each 2-cm wide and .61 cm long, are attached to each turn of wire at the point closest to the beam. Beam aperture between the two facing helices is 16 mm. Figure 2a shows a photograph of a kicker prototype.

The single helix electrical characteristics and performance are affected when the two helices are positioned alongside each other, as in Fig. 2a, and driven with opposite polarities. The electrical effects are that impedance is lowered and propagation velocity reduced at the 3-5% level. Also, the helix microstrip line alone exhibits 900 MHz bandwidth but drops to about 600 MHz due to the second helix's proximity. Therefore, electrical measurements of a single helix are only valid when a zero voltage plane is installed to electrically mirror the missing helix. A metal surface positioned at beam-centre needs to extend the length of the helix, be parallel to the electrodes and grounded to the copper ground tube at both ends.

Magnetic coupling of the helical microstrip line geometry affects its characteristic impedance. The geometry for this 200 Ω helix would be 140 Ω line if laid out flat.

Estimated RF I^2R losses in the wire are about 6 W. However, the design requirements call for handling 40 W of inadvertent beam striking each helix. The ceramic spacers supporting the helix will conduct the heat to the copper ground tube. This nominal 1" diameter copper

Copyright © 2013 CC-BY-3.0 and by the respective authors

ISBN 978-3-95450-138-0

STORAGE RING AND INTERACTION REGION MAGNETS FOR A $\mu^+\mu^-$ HIGGS FACTORY*

A.V. Zlobin#, Y.I. Alexahin, V.V. Kapin, V.V. Kashikhin, N.V. Mokhov, S.I. Striganov, I.S. Tropin, FNAL, Batavia, IL 60510, USA

Abstract

A low-energy Muon Collider (MC) offers unique opportunities to study the recently found Higgs boson. However, due to a relatively large beam emittance with moderate cooling in this machine, large-aperture high-field superconducting (SC) magnets are required. The magnets need also an adequate margin to operate at a large radiation load from the muon decay showers. General specifications of the SC dipoles and quadrupoles for the 125 GeV c.o.m. Higgs Factory with an average luminosity of ~$2\cdot10^{31}$ $cm^{-2}s^{-1}$ are formulated. Magnet conceptual designs and parameters are reported. The impact of the magnet fringe fields on the beam dynamics as well as the IR and lattice magnet protection from radiation are also reported and discussed.

INTRODUCTION

The major advantage of a μ+μ- collider-based Higgs Factory (HF) [1] is the possibility of direct precise measurement of the Higgs boson mass and width. According to the general concept of such a machine [2], muons - in order to keep their longitudinal emittance and energy spread low - undergo only partial cooling leaving their transverse emittance relatively high (see Table 1). Therefore quite small values (a few cm) of the β-function at the Interaction Point (IP) are required resulting in a large beam size in the Final Focus (FF) quadrupoles.

Together with the necessity of magnets and detector protection from the muon decay showers, this leads to very large magnet apertures imposing challenging engineering constraints for magnet design and creating beam dynamics issues with magnet field quality and fringe fields.

Table 1: Higgs Factory Parameters

Parameter	Unit	Value
Circumference	m	300
Beam energy	GeV	62.5
Transverse emittance, $\varepsilon_{\perp N}$	(π)mm·rad	0.3
Longitudinal emittance, $\varepsilon_{\parallel N}$	(π)mm·rad	1.0
Beam energy spread	%	0.003
β^*	cm	2.5
Repetition rate	Hz	30
Muons/bunch	-	2×10^{12}
Average luminosity	$cm^{-2}s^{-1}$	2.5×10^{31}

Table 1 gives basic parameters of the HF Storage Ring (SR) preliminary design presented in [3]. The conceptual design and analysis of the Interaction Region (IR) large-aperture magnets has shown that the IR magnets with apertures ~500 mm and operation fields ~12 T are feasible using the Nb_3Sn technology.

This paper continues the design studies of the HF IR and SR magnets. The impact of the magnet field quality and fringe fields on the beam dynamics, the IR and lattice magnet protection from radiation are also discussed.

STORAGE RING LATTICE

The HF lattice layout and the beam sizes are shown in Fig. 1 for parameters given in Table 1. The IR includes FF quadruplet (with first quadrupole Q1 at 3.5 m from IP) and dipoles generating dispersion for subsequent 3-sextupole chromaticity correction [4]. The latter is necessary despite small energy spread to compensate the path length increase due to betatron oscillations. The matching section allows for β^* variation in wide range.

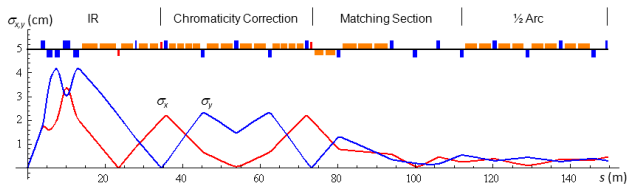


Figure 1: Layout and beam sizes in HF half-ring. Quadrupole magnets are shown in blue, dipoles in orange and sextupole correctors in red color.

MAGNET REQUIREMENTS

Table 2 shows the IR magnet parameters discussed in [3]. The orbit sagitta in IR dipoles is quite large – 8.1 cm. However, it does not affect the IR dipole bore diameter since it is determined by a large vertical beam size.

Table 2: IR Magnet Specifications

Parameter	Q1	Q2	Q3	Q4	B1
$10\sigma_{max}$ (mm)	234	411	339	415	405
G_{nom} (T/m)	74	-36	44	-25	0
B_{nom} (T)	0	2	0	2	8
L_{mag} (m)	1.00	1.40	2.05	1.70	4.10
Coil aperture (mm)	267	444	372	448	438
Quantity	1	2	1	1	2

Tables 3-4 present the maximum values of main parameters for the dipoles (B) and quadrupoles (Q) used in the chromaticity section (CS), the matching section (MS) and the arc (ARC). The most challenging magnets are the CS dipoles (B_{CS}), some MS dipoles (B_{MS}I) and the arc dipoles (B_{ARC}) which need high nominal operation field up to 10 T. This field level requires using the Nb_3Sn technology.

* Work supported by Fermi Research Alliance, LLC, under contract No. DE-AC02-07CH11359 with the U.S. Department of Energy and by the U.S. Department of Energy Muon Accelerator Program.
# zlobin@fnal.gov

Copyright © 2013 CC-BY-3.0 and by the respective authors

ISBN 978-3-95450-138-0

HELICAL MUON BEAM COOLING CHANNEL ENGINEERING DESIGN *

G. Flanagan#, R. P. Johnson, S. Kahn, F. Marhauser, M. Neubauer
Muons, Inc., Batavia, 60510 IL, USA
M. L. Lopes, N. Andreev, R. Bossert, J. Tomkins, S. Krave, K. Yonehara
Fermilab, Batavia, 60510 IL, USA

Abstract

The Helical Cooling Channel (HCC), a novel technique for six-dimensional (6D) ionization cooling of muon beams, has shown considerable promise based on analytic and simulation studies. However, the implementation of this revolutionary method of muon cooling requires new techniques for the integration of hydrogen-pressurized, high-power RF cavities into the low-temperature superconducting magnets of the HCC. We present the progress toward a conceptual design for the integration of 805 MHz RF cavities into a 10 T Nb_3Sn based HCC test section. The concept we present includes a decoupling of the RF and magnetic channels and the pressure and thermal barriers needed within the cryostat to maintain operation of the magnet at 4.2 K while operating the RF and energy absorber at a higher temperature.

INTRODUCTION

A HCC consisting of a pressurized gas absorber imbedded in a magnetic channel that provides solenoid, helical dipole and helical quadrupole fields has shown considerable promise in providing six-dimensional cooling for muon beams. The energy lost by muons traversing the gas absorber needs to be replaced by inserting RF cavities into the lattice. Replacing the substantial muon energy losses using RF cavities with reasonable accelerating fields will require a significant fraction of the channel length be devoted to RF. However, to provide the maximum phase space cooling and minimal muon losses, the helical channel should have a short period and length. Demonstrating the technology of such a cooling channel would represent enormous progress toward the next energy frontier machine. We propose to design and build the 10 T, 805 MHz segment of a HCC. This corresponds to the second section of the HCC design discussed in [1].

KEY TECHNOLOGICAL BARRIERS

The key technological barriers include cooling of the helical solenoid coils made of the low temperature superconductor (LTS) in the presence of RF cavities embedded in the channel and operation of RF cavities in the presence of a magnetic field. Recent results [2,3] show pressurizing the RF cavities may solve the latter challenge. The first challenge, we believe, can be addressed by reducing the size of each RF cavity utilizing a low loss dielectric insert to ease physical constraints for a given frequency. This allows enough room between the cavities and the coils for the magnet coils, the magnet cryostat, the hydrogen pressure vessel, and the RF coaxial feeds to the individual cavities. Calculations show that the heat loads will be tolerable and RF breakdown of the inserts will be suppressed by the pressurized hydrogen gas. The work done on this problem is one of the key accomplishments of the project and has led to a solution to the engineering problem of feeding the RF power through the magnet cryostat.

The following sections describe more fully the dielectric cavity design concepts and the design concept for an integrated 10 T, 805 MHz HCC.

DIELECTRIC LOADED CAVITIES

We have reported progress on the design and testing of dielectric loaded cavities for a HCC in detail elsewhere [3,4]. Here we give a summary and then devote more time to the alternative technology of re-entrant cavities (see next section). The key idea behind using dielectric loaded cavities is the reduction of cavity radius and the associated easing of engineering demands that comes along with it. One can decouple the RF and magnetic channels.

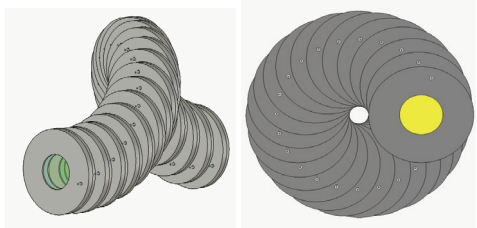


Figure 1: (Left) Illustration of RF cavities aligned to fit inside a HS magnet and cryostat. (Right) The end view shows the dielectric-filled region of the cavity (gray), where the yellow area corresponds to the region that the beam passes through. The small holes indicate the locations of the power feeds. Beryllium grids separate the cavities to make them RF pillboxes while not impeding oxygen-doped hydrogen flow. These are some of the building blocks of the integrated channel (see Figures 4 and 5).

RE-ENTRANT RF CAVITY ALTERNATIVE

As an alternative to using dielectric inserts for reducing the size of the RF cavities in order to fit them into a magnetic channel, we also consider a re-entrant RF structures. It is known that the cavity frequency can be lowered if one employs a half/quarter wave type upper torso. This increases the magnetic field at the perimeter.

*Work supported under U.S. DOE Grant Application Number DE-SC0006266
#flanagan@muonsinc.com

Copyright © 2013 CC-BY-3.0 and by the respective authors

DISPOSITION OF WEAPONS-GRADE PLUTONIUM WITH GEM*STAR

R.P. Johnson*, G. Flanagan, F. Marhauser, Muons, Inc., Batavia, IL, USA
C. D. Bowman, R. B. Vogelaar, ADNA Corp., Los Alamos, NM, USA

Abstract

An accelerator system like the SNS at ORNL can generate spallation neutrons to convert fertile elements like U238 in spent nuclear fuel (SNF) or Th232 into fissile isotopes to provide high temperature heat using technology developed at the ORNL Molten Salt Reactor Experiment. In the Green Energy Multiplier * Subcritical Technology Alternative Reactor (GEM*STAR) [1], the accelerator allows subcritical operation (no Chernobyls), the molten salt fuel allows volatiles to be continuously removed (no Fukushimas), and the SNF does not need to be enriched or reprocessed (to minimize weapons proliferation concerns). The molten salt fuel and the relaxed availability requirements of process heat applications imply that the required accelerator technology is available now. The accelerator can also be used to control the burning of fissile isotopes developed for weapons. A new opportunity is being considered by Russian and American scientists to use GEM*STAR to reduce the world inventory of weapons-grade plutonium leaving only remnants that are permanently unusable for nuclear weapons. This application could expedite the exploitation of this new accelerator-driven technology.

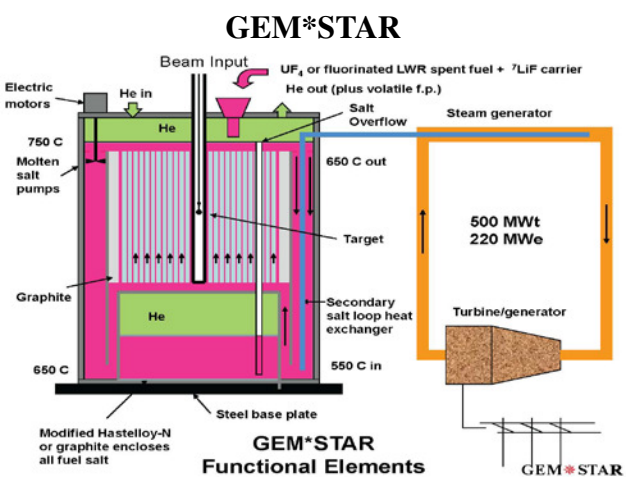


Figure 1: Conceptual arrangement of a GEM*STAR reactor unit configured to produce electricity. To produce diesel fuel, the secondary salt loop heats CH2 and H2O to produce CO and H2 for the Fischer-Tropsch process.

GEM*STAR is a graphite-moderated, thermal-spectrum, molten salt fueled reactor that is operated using an external accelerator to direct protons onto an internal spallation target. GEM*STAR can be operated with many fuels, without redesign, for process heat and/or for electricity generation. Figure 1 shows its basic components, where the active volume is 93% graphite (gray) and 7% molten salt made up of an appropriate eutectic mixture of lithium, uranium, plutonium, and/or thorium fluorides with a melting point above 500 C. Safety features of the design include the 500 MWt power output design limit, corresponding to not needing 1) a critical mass of fissile material for operation or 2) "defense in depth" measures for loss-of-coolant accidents since the heat generated by decays of fission products after the accelerator is turned off can be dissipated by passive external air cooling.

A helium flow over the hot core removes volatile radioactive isotopes and carries them to a relatively small underground tank where they are separated out cryogenically or with a centrifuge and then safely stored while they decay. This reduces the inventory of volatile isotopes in the reactor by a factor of a million compared to reactors used at Fukushima.

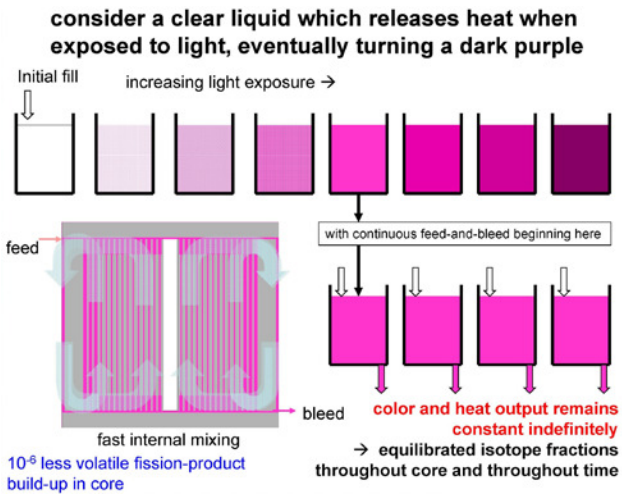


Figure 2: Concept of operating with equal fill and removal rates to maintain a constant reactor performance.

An essential feature of the design is the concept of feeding the reactor with a steady flow of fuel such that the concentration of fission products within the reactor stays constant for most of the 40-year reactor lifetime. As the fuel is fed into the reactor at a rate that maintains the 500 MWt output, an equal amount leaves the core through the salt overflow shown in figure 1 into a storage area under the core. Figure 2 shows an equivalent diagram of how the concentration of fission products reaches an equilibrium that can be maintained by this concept of adding molten salt fuel and removing it at the same rate.

Although the first approach to equilibrium takes some time (~5 years), a subsequent reactor can use the molten salt accumulated under the first reactor to start in an equilibrated state. Note that the heat from decaying reaction products will keep the overflow liquid from

* rol@muonsinc.com

ISBN 978-3-95450-138-0

Copyright © 2013 CC-BY-3.0 and by the respective authors

A DIPOLE MAGNET FOR THE FRIB HIGH RADIATION ENVIRONMENT NUCLEAR FRAGMENT SEPARATOR*

S.A. Kahn#, A. Dudas, G. Flanagan, J. Nipper, Muons, Inc., Batavia, IL 60510, USA
M.D. Anerella, R.C. Gupta, J. Schmalzle, BNL, Upton, NY 11973, USA

Abstract

Magnets in the fragment separator region of the Facility for Rare Isotope Beams (FRIB) would be subjected to extremely high radiation and heat loads. Critical elements of FRIB are the dipole magnets which are used to select the desired isotopes. Since conventional NbTi and Nb_3Sn superconductors must operate at 4.5 K, the removal of the large heat load generated in these magnets would be difficult. High temperature superconductors (HTS) have been shown to be radiation resistant and can operate in the 40 K temperature range where heat removal is an order of magnitude more efficient than at 4.5 K. The coils of this magnet must accommodate the large curvature from the 30° bend that the magnet will subtend. This paper will describe the magnetic and conceptual design for these magnets.

INTRODUCTION

The FRIB facility at MSU will provide isotope beams for physics research with intensities not available elsewhere [1]. The facility will enable scientists to study the properties of nucleonic matter providing insight into the nuclear processes in stars as well as tests fundamental symmetries in nuclear physics. Large quantities of various isotopes are produced when a high power 400 kW linac beam hits the target. FRIB will have the ability to accommodate various primary beams from protons to uranium with energies up to 200 MeV/u. The beams will be incident on a carbon target to produce a variety of secondary nuclides with various ionic charge states. The fragment separator which follows the target consists of a series of three quadrupole magnets to provide focusing and two dipole bend magnets to select the desired nuclei. The beam enters the first dipole magnet with a spread of rigidities. The undesired nuclides are removed with a beam dump between the two dipole magnets.

As the production rate for a specific rare isotope can be very small, the magnets in the fragment separator will have large apertures and strong magnetic fields to maximize the collection of these rare isotopes. The radiation level in the fragment separator magnets is quite high and these magnets need to be radiation resistant. The radiation dose seen by the first quadrupole after the target is estimated to be 2.5×1015 neutrons/cm2 per year (10 MGy/year) [2] which corresponds to 10 kW/m of deposited power. The deposited power will drop by an order of magnitude before reaching the first bending dipole. The high radiation environment influences the magnet design and the choice of materials used. Although NiTi and Nb3Sn are robust conductor materials in radiation, they must operate at 4.5 K which is not practical, since the anticipated heat load would be difficult and expensive to remove at that temperature. HTS conductors are reasonably resistant against radiation and have a significant current density at 40 K where the heat capacity of the refrigerants is much larger and the Carnot efficiency is greater making heat removal easier.

Brookhaven National Laboratory has been involved in an R&D program to develop the quadrupole magnets for pre-fragment separator at FRIB [3,4,5,6] using HTS conductor. The design of the fragment separator dipole magnets will rely on the technology that was learned.

MAGNETIC DESIGN

The design parameters of the fragment separator dipole magnet are shown in Table I. There are two such magnets in the fragment separator which is used to select the desired nuclide. Each of these magnets bends the beam by 30º with a nominal field of 2 T. The magnet should have field uniformity better than 0.7% over the useful beam aperture for operating field between 0.5 and 2.0 T. We have chosen a superferric design for this magnet where HTS coils are used to magnetize the iron which provides the desired field. The coils surround the iron poles and are enclosed in their individual cryostat. The coil and cryostat package are recessed behind the iron pole to protect them from a direct exposure to the radiation from the beam. However, the main source of radiation is from neutrons that penetrate into the coils. Most of the radiation and associated heat will be deposited into the iron yoke which is at room temperature. It is estimated that ~1 kW will be deposited into coil cryostats. Figure 1 shows a sketch of the sector bend magnet where only one half of the upper half of the iron is shown. The upper and lower coils must each carry 256 kA-turns to produce the design 2 T field in the beam aperture.

Table I: Fragment Separator Dipole Magnet Design Parameters.

Parameter	Value
Bending Radius	4 m
Bend Angle	30º
Magnetic Length along Beam Path	2.094 m
Nominal Central Field	2.0 T
Operating Field Range	0 to 2.2 T
Field Uniformity in Good Field Region	<0.7 %
Good Field Width in Bend Plane	0.3 m
Good Field Height in Non-Bend Plane	0.2 m
Total Current Required in Each Coil	256 kA-turns
Operating Temperature	40 K

*Work supported by US DOE grants DE-SC-0006273 and DE-AC02-98CH10886
#kahn@muonsinc.com

Copyright © 2013 CC-BY-3.0 and by the respective authors

RADIATION TOLERANT MULTIPOLE CORRECTOR COILS FOR FRIB QUADRUPOLES*

S.A. Kahn#, Muons, Inc., Batavia, IL 60510, U.S.A.
R.C. Gupta, BNL, Upton, NY 11973, U.S.A.

Abstract

Multipole correction insert coils with significant field strength are required inside the large aperture superconducting quadrupole magnets in the fragment separator section of the Facility for Rare Isotope Beams (FRIB). Corrector coils made with copper can not create the required field and conventional low temperature superconductors are not practical in the fragment separator magnets which will operate at 40-50 K. The corrector coils for this application should be made of HTS as are the main quadrupole coils in this magnet. There is a significant advantage to using HTS in these coils as it can withstand the high radiation and heat load that will be present. This paper will describe the innovative design suitable for coils with the complex end geometry of cylindrical coils. We will look at the forces in the corrector coils from the main quadrupole fields and anticipate possible coil distortions.

INTRODUCTION

The FRIB facility will provide isotope beams for physics research with intensities not available elsewhere. Large quantities of various isotopes will be produced when a high power (400 kW) linac beam from protons to uranium hits the target. The magnets in the fragment separator region, which selects the rare nuclides from the multitude of secondary fragments, would be subject to extremely high radiation and high heat loads [1,2]. Figure 1 shows a sketch of the first part of the FRIB fragment separator. The first quadrupole magnet after the target will see a flux of 2.5×10^{15} neutrons/cm^2 corresponding to 10 MGy/year. Similar high heat loads are faced by other quadrupole and corrector magnets in the fragment separator region. The baseline fragment separator design for the first several quadrupoles is based on HTS magnet operating at 38-50 K as the removal of a heat load of this magnitude would be difficult and expensive for NbTi or Nb_3Sn superconductors since they are operated at 4.2 K. HTS on the other hand have a significant critical current density at 40 K where the Carnot efficiency is greater and the heat capacity of the refrigerants is significantly higher making heat removal easier.

Corrector magnet inserts, which will be placed between the beam tube and quadrupole coils would face the same challenging situation as the other magnets in the fragment separator region. As corrector magnet inserts made with copper coils do not generate enough field strength and because conventional superconductors would not be practical in this environment, HTS wound coils will be necessary for these corrector inserts.

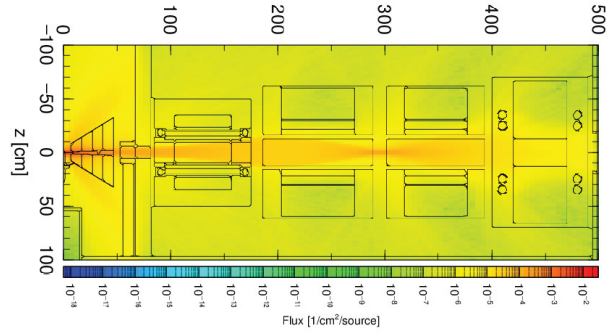


Figure 1: Proton flux seen in the first three quadrupoles of the fragment selector at FRIB. The figure is from ref [2].

CORRECTOR COIL DESCRIPTION

Seven quadrupole magnets in the fragment separator require multipole corrector inserts. Table 1 shows the beam line elements that follow the target. Table 2 shows the quadrupole, sextupole and octopole strengths for the quadrupole magnets that require multipole corrections [3]. The component strengths are evaluated at the reference radius shown in the table.

Table 1: Beam-line Elements in the Fragment Separator

Magnet	Half-gap (mm)	Field or Gradient	Length (m)	Element Position
Quad 1	100	-8,47 T/m	0.55	1.175
Quad 2	120	14.27 T/m	0.65	2.280
Quad 3	160	-11.67T/m	0.65	3.280
Octopole	130	163 T/m^3	0.50	4.570
Quad 4	140	6.53 T/m	0.55	5.350
Dipole 1	100 H, 150 V	2 T	1.75	6.900
Sextupole	100 H, 120 V	-42 T/m^2	0.40	9.320
Dipole 2	100 H, 200 V	-2 T	1.75	10.64
Quad 5	200	10 T/m	0.55	12.24
Quad 6	150	-4.95 T/m	1.357	13.54
Quad 7	160	4.2 T/m	1.357	15.51

The physical length of these inserts range from 0.6 to 0.7 m, with the effective length of the magnet being ~20% shorter. The inner radius of the octopole insert is between 75 and 110 mm adjusted to the various quadrupole apertures and the sextupole insert inner radius will be 5 mm larger than the corresponding octopole insert. The largest quadrupole pole tip field is 2.5 T, so the field at the insert coils is about 2 T. The design will assume that the sextupole and octopole fields at the insert coil radius are 0.25 T. The multipole coils should be shaped on a

*Work supported by DOE STTR grant DE-SC0006273.
#kahn@muonsinc.com

Copyright © 2013 CC-BY-3.0 and by the respective authors

ISBN 978-3-95450-138-0

ELLIPTICAL MUON HELICAL COOLING CHANNEL COILS*

S.A. Kahn#, G. Flanagan, Muons, Inc., Batavia, IL, 60510, USA
M.L. Lopes, K. Yonehara, FNAL, Batavia, IL 60510, USA

Abstract

A helical cooling channel (HCC) consisting of a pressurized gas absorber imbedded in a magnetic channel that provides solenoid, helical dipole and helical quadrupole fields has shown considerable promise in providing six-dimensional phase space reduction for muon beams. The most effective approach to implementing the desired magnetic field is a helical solenoid (HS) channel composed of short solenoid coils arranged in a helical pattern. The HS channel along with an external solenoid allows the B_z and B_ϕ components along the reference orbit to be set to any desired values. To set dB_ϕ/dr to the desired value for optimum focusing requires an additional variable to tune. We shall show that using elliptical shaped coils in the HS channel allows the flexibility to achieve the desired dB_ϕ/dr on the reference orbit without significant change to B_z and B_ϕ.

INTRODUCTION

A muon beam cooling technique, using a continuous gaseous hydrogen absorber inside a helical solenoid channel has shown promise to reduce muon phase space. This goal of this technique is to create bright muon beams with small emittance for use in particle accelerators and storage rings. Of particular interest is the development of a muon collider, which requires the reduction of the beam phase space by at least a factor of 10^6. Simulations have shown that the HCC can provide a significant phase space reduction [1]. The HCC is composed of a magnetic channel filled with pressurized H_2 gas absorber to reduce the particle energy. The lost energy is replaced in the longitudinal direction by RF. The desired field in the magnetic channel is comprised of helical dipole, helical quadrupole and solenoid components [2]:

Helical Dipole:

$$b_\phi = 2b_d I_1(k\rho)\cos(\phi - kz)/k\rho$$
$$b_\rho = 2b_d I_1'(k\rho)\sin(\phi - kz)$$
$$b_z = -k\rho b_\phi$$

Helical Quadrupole:

$$b_\phi = \frac{2b_q}{k^2\rho} I_2(2k\rho)\cos 2(\phi - kz - \phi_2)$$
$$b_\rho = \frac{2}{k} b_q I_2'(2k\rho)\sin 2(\phi - kz - \phi_2)$$
$$b_z = -k\rho b_\phi$$

where b_d and b_q are the dipole and quadrupole strengths, respectively, at $\rho = 0$. Implementing this channel with helical harmonic coils is difficult since $I_n(nk\rho)$ grows exponentially at large radius and the channel has large apertures. The HCC magnetic channel will be implemented with short solenoid coils arranged along the helical reference orbit. Figure 1 is a sketch of the helical solenoid (HS) channel [3]. This approach minimizes the magnetic field at the coils. To be effective the B_ϕ, B_z and dB_ϕ/dr of the HS at the reference orbit must match values from the theoretical formulae. B_ϕ and B_z can be set by HS coil current and adjusting an external solenoid field $B_{solenoid}$ (shown in Fig. 1). dB_ϕ/dr is important to control the beam focusing in the channel. To set this variable to an arbitrary value desired to optimize the channel requires an additional degree of freedom. In this paper we explore deforming the circular solenoids into elliptical rings to control the field gradient.

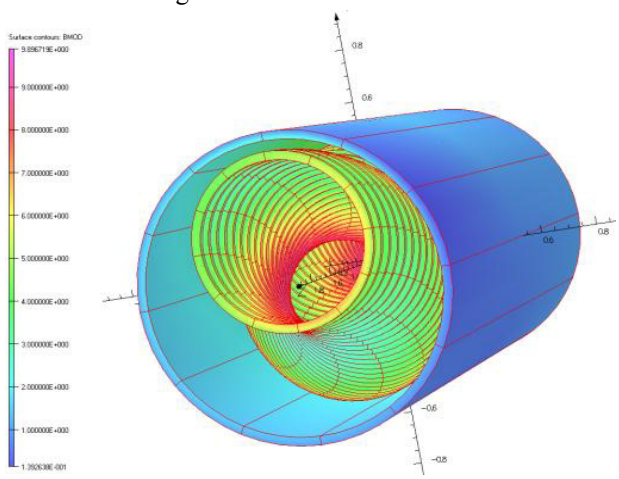


Figure 1: 3D layout of coils for the HCC channel. Note that the HS coils are placed in an external solenoid field.

Table 1: Field Properties of the Sections of the HCC Cooling Channel.

Section	λ	B_ϕ	dB_ϕ/dr	B_z	f
Units	m	T	T/m	T	MHz
1,2	1.0	1.29	-0.50	-4.25	325
3	0.9	1.43	-0.62	-4.73	325
4	0.8	1.61	-0.79	-5.32	325
5	0.5	2.58	-2.01	-8.51	650
6	0.4	3.22	-3.14	-10.63	650
7	0.3	4.30	-5.58	-14.18	650
8	0.3	4.30	-5.58	-14.18	1300

HCC CHANNEL DESIGN

The HCC channel that is proposed is divided into eight sections with each section providing a smaller final equilibrium emittance which requires progressively larger fields. The design field for each section is shown in

*Work supported by U.S. DOE STTR/SBIR grant DE-SC00006266
#kahn@muonsinc.com

Copyright © 2013 CC-BY-3.0 and by the respective authors

SIMULATION WORKSTATION

Thomas J. Roberts#, Muons, Inc., Batavia, IL 60510 USA

Abstract

The Simulation Workstation is a software toolkit that provides a universal Graphical User Interface to most particle simulation codes. This includes: constructing and displaying the simulated system graphically, running multiple simulation codes from a single system description, displaying particle tracks or histories with the objects of the system, flexibly generating plots and histograms, and comparing the results from multiple simulations. The workstation itself knows very little about particle simulations -- that knowledge is contained in the simulation codes themselves. As a consequence, the workstation can handle essentially any problem that any of the supported simulation codes can simulate. These include: beam optics calculations, ion source design, muon cooling channels, spacecraft radiation levels, nuclear reactors, complex shielding calculations, and accelerator driven subcritical reactors. The workstation offers interfaces to most CAD/CAE programs, enabling workflows that include multi-physics analysis by other programs. The Simulation Workstation will be portable among all major operating systems, will be freely available as open-source software, and will initially support these simulation codes: G4beamline [1], MCNP6 [2], and MAD-X [3]; additional codes can be added by users.

INTRODUCTION

When teaching beam dynamics and accelerator physics to students, user-friendly graphical tools are a big advantage, as they permit the construction and exploration of models with very little overhead. And for today's technology-driven students of the "Nintendo generation", graphical interfaces meet their expectations far better than text-based tools. Moreover, there are dozens of modeling codes available, so having a common user interface that can be used with multiple simulation codes will be a major advantage. Existing tools fall short of what is needed.

While the workstation has been designed with students in mind, accelerator physicists will also find it useful in dealing with the plethora of modeling tools and their different languages and data formats. The internal representation of the system is specifically designed to be useable as a text-based description of the system, and to make it easy for users to interface it to essentially any accelerator-modeling tool, regardless of its description language. In particular, this will make it straightforward to use fast but less realistic codes to design and optimize a system, and then use slower but more realistic codes to evaluate its performance. Graphical interfaces are emphasized, making it easy to construct the system graphically, display the system and its beam, and use on-screen controls to vary parameters and observe their effects immediately. Such exploration is essential to give students insight into how systems behave, and can be valuable to the experienced accelerator physicist, for tasks such as evaluating different techniques for tuning a system before it is built.

The user interface is centered around objects, which can be individual accelerator components, or arbitrarily complex collections of components with specified spatial relationships. Objects are stored in Libraries, which can easily be shared with other users. The use of URL-based component libraries will encourage collaboration among geographically diverse teams.

The Simulation Workstation provides the user with a single user interface to construct, design, optimize, analyze, and explore systems involving charged particle beams and other radiation. It is specifically designed to be interoperable with just about any existing simulation or beam optics code. This is possible for one simple reason: they necessarily have a common domain, with common concepts, common objects, and common operations. By abstracting these common elements into a new specification language, called *LinguaFranca*, a single GUI program can indeed interface to many simulation codes with relatively little effort. LinguaFranca has been specifically designed to make it easy to *instantiate* its description for other codes to read. Instantiation is not machine translation, which is known to be a difficult problem, but rather is performed by a sophisticated text-processing system that has been told by human developers how each LinguaFranca primitive is represented in the language of each simulation code.

The architecture of the Simulation Workstation is to be an overall control program that orchestrates the assembly of the various pieces required to prepare, perform, and analyze a simulation. Thus the user works with a single user interface to perform all related tasks. While it relies on interfaces to the simulation codes, the adaptation is always in the workstation, and no simulation code needs to be modified in order to work with it (some codes will benefit from modifications, especially on Windows).

The Simulation Workstation will be portable among the major operating systems (Windows, Linux, Mac OS X), and will be released as open-source software. This is the same overall commercialization model as for our highly successful program G4beamline [1]. The key to G4beamline's popularity is its excellent user interface; this project was inspired by that interface, and by what we perceived as ways to improve it. But rather than just improve this one code, we have chosen to design and develop a system that is customizable to improve the user experience for all related simulation codes.

tjrob@muonsinc.com

ISBN 978-3-95450-138-0

Copyright © 2013 CC-BY-3.0 and by the respective authors

STATUS OF SPALLATION NEUTRON SOURCE CRYOGENIC TEST FACILITY (CTF)*

M. Howell#, A. Coleman, B. DeGraff, S-H. Kim, T. Neustadt, J. Proulx, J. Saunders, W. Strong, D. Vandygriff, ORNL, Oak Ridge, TN 377831, USA
T. Xu, FRIB, East Lansing, MI 48824, USA

Abstract

The Spallation Neutron Source (SNS) is building Superconducting Radio Frequency (SRF) processing and testing facilities to support the reliability and sustainability goals of the enterprise. In addition, these facilities position the SNS superconducting linac (SCL) for improvement programs and future upgrades. Some of the testing facilities require cryogenic helium at both 4 K and 2 K. Currently, the Central Helium Liquefier (CHL) supplies 4 K helium to the linear accelerator and excess capacity is utilized to supply the test cave. As more facilities become available and testing is more frequent, it is essential to separate testing in the SRF facility from the operation of the accelerator. This paper describes the cryogenic system and the commissioning of that system at SNS to facilitate SRF testing needs. The initial phase of the project was to supply 4 K helium to a Vertical Test Area (VTA) and the test cave which is capable of housing either the Horizontal Test Apparatus (HTA) or a cryomodule. The scope of the initial phase of this project has been expanded. The system will be outfitted with warm pumping capability to produce 2 K helium in the testing systems. In addition, a liquid helium fill station will be incorporated to fill portable Dewars.

INTRODUCTION

The Spallation Neutron Source contains a superconducting linear accelerator which consists of eleven medium beta and twelve high beta cryomodules. The availability and reliability of the cryomodules has been high. However, the superconducting section of the linear accelerator has not met the energy specification of 1 GeV [1]. To increase the energy of the beam and meet future upgrade requirements, the performance of multiple cryomodules must be improved. To improve these cavities, there are two options. These cavities can be replaced which will involve removing, disassembling, and rebuilding cryomodules. This approach is cost prohibitive. A second option is to implement additional processing or conditioning of the superconducting cavities. SNS is currently installing and developing superconducting radiofrequency processing and test facilities to develop methodology in increasing beam energy and facilitating necessary repairs. The CTF refrigeration system will provide helium at both 4 K and 2 K to the SRF test facilities.

Multiple repairs of cryomodules have been performed at SNS by in house staff. These include tuner repairs, removal of HOM antennas, and repair of helium circuit, beam line vacuum and insulating vacuum leaks. In one case, a mild plasma processing was applied to a cryomodule to improve its performance [2]. After repair, the cryomodules have been qualified in the test cave using the CHL to supply helium. This couples the testing and qualification process to the actual operation of the linear accelerator. The implementation of the CTF decouples these two differing objectives.

DESIGN OVERVIEW

The original scope of the CTF refrigeration system was to provide 4 K helium to the test cave and the VTA [3]. This scope has been expanded to include adding 2 K capability through the use of a warm pumping system. Because the availability of liquid helium has been scarce, a liquid helium fill station to supply portable Dewars to the neutron instrument and sample environment areas has also been added to the scope. By having this subsystem, the liquid supply chain issues can be mitigated with the helium gas storage that is normally available in the CHL. A block flow diagram of the CTF system is included below in Fig. 1.

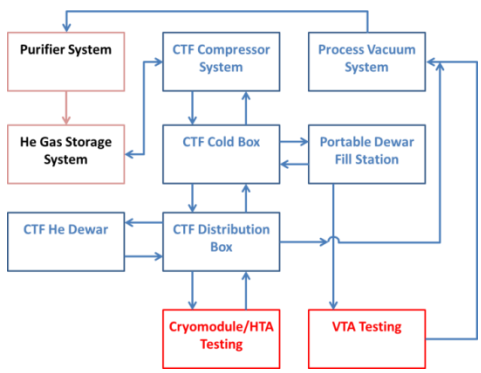


Figure 1: CTF Block Flow Diagram.

As system design has progressed and operational experience has increased, the cryogenic loads in the various testing modes have been further defined. Table 1 summarizes the estimated cryogenic loads of the various test modes. These loads are based on actual test results observed during operation of cryomodules in the test cave.

Table 1: Cryogenic Load Design Criteria

Test System	Nominal T_{bath}(K)	Primary Load (W)	Shield Load @4K (W)	Coupler Flow (g/s)
Cryomodule Test	4	400	200	< 0.5
	2	80	200	< 0.5
HTA Test (single cavity)	4	100	120	< 0.5
	2	20	120	< 0.5
VTA Test (CW)	4	600	None	NA
	2	150	None	NA

Copyright © 2013 CC-BY-3.0 and by the respective authors

RECENT IMPROVEMENTS IN PARTICLE SIMULATION SUPPORT IN ANALYST-MP*

J. F. DeFord, B. Held, A. Nichols, AWR Corporation, Mequon, WI 53092, USA

Abstract

Recent work on the Analyst product has simplified model development, improved result visualization, and added particle simulation functionality. The Analyst user interface has been updated with a new control layout, and support for automatic session recording, variables/expressions for all inputs, and units. For the study of multipacting and dark current phenomena a new volumetric particle source has been deployed, and changes to the way secondary generations are managed has simplified the identification of multipacting resonances.

INTRODUCTION

Analyst is a finite element-based tool used for design and optimization of three-dimensional structures in microwave engineering. In development of new particle accelerators, Analyst is used on a variety of components including RF modules, feed systems, deflectors, etc. When applied to the multipacting problem, driven RF or eigenmode calculations are performed to obtain field distributions, and these are then used in a separate particle simulation to search for particle resonances.

Recent work has improved the particle tracking algorithms and emission models [1]. The current version of the code employs a statistical secondary emission model that produces from an impact a set of zero or more electrons whose count and properties are obtained from samples of random variables that collectively enforce observed secondary emission behaviour [2]. The Analyst user interface has also been updated in response to user experience in the old system. Development on the particle simulation engine has focused on changes that make it easier to identify and interpret multipacting behaviour. These changes are discussed in the following sections.

VOLUMETRIC PARTICLE SOURCING

Previous versions of Analyst used a simple primary emission model for multipacting simulation. This model emitted one or more particles from each element face that lay on the model boundary. Particles were emitted at regular intervals during the first RF period, and subsequent particle motion and deterministic secondary generation were used to identify resonances. This technique is very efficient, but it does not necessarily require fewer emissions than a volumetric launch if one is to avoid missing resonances.

In addition to supporting primary emission from surfaces, Analyst now also allows initiation of particles in the volume by emitting a specified number from each mesh element (triangle or tetrahedron) during the first RF cycle. The position, direction vector, and emission time of each particle are all randomly chosen. The initial velocity of each particle is obtained by sampling a random variable, with the number of particles emitted per element controlled by a user input, and is typically of order 10^2.

As expected, the efficiency with which resonances are identified is a function of the choice of initial velocity distribution. Robust multipacting resonances involve low energy electrons because it is primarily low energy impacts (< 5 keV) that yield multiple secondary particles. Higher energy impacts can result in single reflected or re-diffused secondary particles, but do not contribute to gain in multipacting resonances. Consequently, initiating particles with high energy is usually of little utility in identifying resonances. In the low energy regime we studied the effects of using different velocity distribution functions, including a delta function (specified value), uniform over a range of values, and Boltzmann with a peak matching the secondary emission yield peak of surface material. We concluded that these functions were largely equivalent in initiating resonances in test structures, and the simplest approach of giving all of the particles the same initial energy (in the 100s of eV) is perfectly adequate. This value is an input parameter in the software, which defaults to the peak energy of the true secondary yield curve. Note that this choice does not imply that only particles with comparable energy exist in the simulation to initiate resonances. High-field regions will accelerate particles to high energies, and subsequent interaction with cavity walls will typically scatter some of these particles into low-field areas. However, with this approach the preponderance of particles in low field regions will be in an energy range to yield true secondaries on impact with common metals, increasing the odds that a resonance will be discovered if one is supported by the geometry/field-structure.

Volumetric sourcing produces an initial cloud of particles that rapidly dissipates, primarily due to collisions with cavity walls that produce no secondary particles. What remains after a few RF cycles is predominantly secondary particles that are in a resonance (Figure 1).

MULTIPROCESSING

Particle tracking is done by secondary generation, with each generation completed before the next one is started. Between generations secondary particles are redistributed across available processors to balance the computational load. Dependence of particle populations on processor count is undesirable, even when it does not lead to

*Work supported by DOE SBIR grant SC0002604.

ISBN 978-3-95450-138-0

Copyright © 2013 CC-BY-3.0 and by the respective authors

PARAMETER OPTIMIZATION FOR MULTI-DIMENSIONAL LASER COOLING OF AN ION BEAM IN THE STORAGE RING S-LSR*

Z. He#, FRIB, Michigan State University, USA; Tsinghua University, China
J. Wei, FRIB, Michigan State University, USA
K. Osaki, H. Okamoto, Hiroshima University, Japan
A. Noda, M. Nakao, National Institute of Radiological Science, Japan
H. Souda, Gunma University Heavy Ion Medical Centre, Japan
Y. Yuri, TARRI, Japan Atomic Energy Agency, Japan
K. Jimbo, IAE, Kyoto University, Japan

Abstract

S-LSR is a compact ion cooler ring built in ICR, Kyoto University, aiming at creating ultra-low temperature ion beam by laser cooling. In order to approach lowest possible temperature at S-LSR in an experiment, parameters of laser cooling should be carefully chosen by simulation. This paper mainly concerns optimization of laser cooling parameters and prediction of possible low limit of beam temperature at S-LSR. Firstly, the adiabatic capture process of ion beam is introduced and studied. Then, different laser profile parameters are compared and an optimized value is chosen. After that, optimized solenoid field strength for 3-D coupling is proposed. At last, by choosing the parameters proposed, the lowest beam temperature achievable for S-LSR is predicted to be 10 K in transverse direction and 0.05 K in longitudinal direction.

INTRODUCTION

Cold beam, or low emittance beam, usually means less beam loss and smaller necessary beam aperture. Considerable effort towards ultra-cold beam was devoted in 1990's by two European teams (the TSR group at Max Planck Institute [1, 2] and the ASTRID group at Aarhus University [3, 4]). Both teams applied the laser cooling technique [5, 6] to various heavy ions and succeeded in reducing the longitudinal beam. However, the possible lowest emittance is limited by the linear coherent resonance crossing unavoidable in both TSR and ASTRID rings [4, 7, 8]. S-LSR [9], a compact ion cooler ring built in ICR, Kyoto University, has a potential to overcome the difficulties encountered by the European teams. For instance, we can reduce the betatron phase advance per single lattice period near or even below 90 degrees and avoid strong beam heating due to the linear resonance crossing. It is also possible to employ the resonant coupling method (RCM) [10, 11] and enables us to produce an ultimate ion beam that has a temperature near the absolute zero in all three dimensions [12, 13]. This paper mainly concerns optimization of laser cooling parameter and prediction of low limit of beam temperature at S-LSR.

* This work was supported by the U.S. National Science Foundation under Grant No. PHY-11-02511, Advanced Compact Accelerator Development project of MEXT, and Global COE program.
#hez@frib.msu.edu

BUNCHED-BEAM LASER COOLING

S-LSR is a compaction cooler ring with an electron cooling system and a laser cooling system. It has six-fold symmetric lattice and each lattice consists of a bending magnetic two quadruples and one 1.86 m long drift line, two of which are occupied by an electron cooler and a laser-beam interaction section as Fig. 1. A 40 keV Mg^+ beam is injected continuously into the ring and captured and bunched by a RF cavity. The laser is set co-propagating with the Mg^+ beam and is slightly tuned below the transmission frequency of the beam. With the synchrotron motion of bunched-beam, particles automatically falls into the cooling region of the laser, thus making bunched-beam cooling possible by single laser. [14]

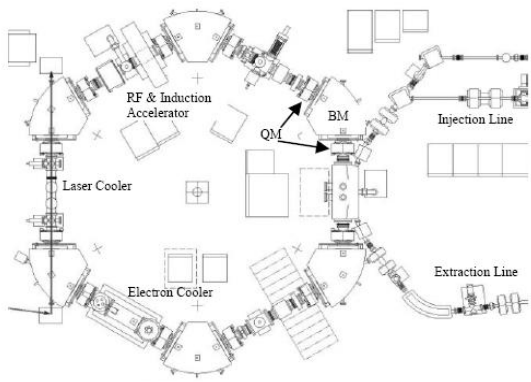


Figure 1: Layout of the ion storage ring [9].

In order to realize multi-dimensional laser cooling, the idea of RCM has been induced [10, 11]. In S-LSR, we adjust the working point around (ν_x, ν_y, ν_z) = (2.075, 1.120, 0.075) for 2-D cooling and working point around (2.075, 1.075, 0.075) for 3-D cooling. Longitudinal direction and horizontal direction are coupled by dispersion; horizontal direction and vertical direction are coupled by solenoid field.

Simulations are specially designed for this single laser bunched-beam cooling experiment at S-LSR. The parameters are all chosen according to the data or past experiment result of S-LSR. A molecular dynamic simulation code, CRYSTAL, developed for the laser-cooling and crystalline-beam study, was used [12].

Copyright © 2013 CC-BY-3.0 and by the respective authors

APS FAST ORBIT FEEDBACK SYSTEM UPGRADE*

R. Lipa, N. Arnold, H. Bui, G. Decker, T. Fors, R. Laird, F. Lenkszus,
A. Scaminaci, N. Sereno, S. Shoaf, ANL, Argonne, IL 60439, USA

Abstract

A real-time feedback double-sector controller (RTFB DSC) for the APS Upgrade has been under design for the past year. Using the Xilinx Zynq-7000 All Programmable System on a Chip FPGA residing on the ZC706 board as the base platform, the upgrade path interfaces to the existing accelerator system and modernizes the beam position monitoring and feedback systems. The modernized system increases the RTFB system sample rate from 1.5 kHz to 22.6 kHz. We report the plan for sector-by-sector upgrades that will occur during system shutdowns and allow the upgraded sectors to operate with the existing sectors. The mapping of the RTFB DSC architecture is shown utilizing the targeted FPGA features. These features include the dual ARM Cortex™ A9 processors, multi-port DDR3 memory controllers, gigabit transceivers, and the programming logic interconnect for implementing advanced orbit feedback controller algorithms using floating-point DSP operations. The RTFB DSC FPGA architecture is revealed as well as subsequent progress on the chassis implementation.

INTRODUCTION

The RTFB DSC of the APS storage ring upgrade increases the processing power using modernized electronics to provide the functions, calculations, and interfaces of the present-day system and to improve the beam stability by increasing the sample rate to target a closed-loop bandwidth of at least 200 Hz. The network interface elements and functions on the RTFB DSC incorporate the EPICS software environment to control the process variables to configure and monitor the RTFB system. The RTFB DSC gigabit transceiver cores receive and transmit the global BPM error matrix over the real-time data highway (DH). The digital signal processing cores calculate the corrector drive vector using a response matrix multiplication and global BPM error vectors to obtain the local portion of the corrector drive vectors. The correction is then applied to the steering corrector power supplies located in that double sector. The RTFB DSC interfaces to a disparate and evolving set of equipment. The RTFB DSC advantageously uses the programmable FPGA features to attach to the various rates and protocols used by different equipment. The modern FPGA's integrated features, such as high-performance embedded processors, integrated DDR3 cores, numerous DSP and BRAM cores, gigabit Ethernet controllers, and gigabit transceiver blocks, along with the programmable fabric, allow decreasing the sample period and reducing the delay in correcting the electron orbit.

*Work supported by U.S. Department of Energy, Office of Science, under Contract No. DE-AC02-06CH11357

RTFB DSC SYSTEM ARCHITECTURE

The real-time feedback double-sector controller functions in the middle of the following existing [1] and proposed storage ring elements: monopulse rf beam position monitors (BPMs), Bergoz (i.e., narrowband) BPMs, existing x-ray BPMs, steering corrector power supplies, the Experimental Physics and Industrial Control System (EPICS), the timing and event systems, the low-level rf systems, and a machine (i.e., storage ring) protection system. The modernized RTFB DSC FPGA also provides the capability to interface to commercial BPMs (e.g., Libera Brilliance+ [2]) and to commercial x-ray data acquisition systems (e.g., Libera Photon [3]). Figure 1 is a block diagram of the system showing the RTFB DSC and the other storage ring elements and the interconnections. The upgrade design shows the mapping of the RTFB DSC architecture to a realizable modern implementation.

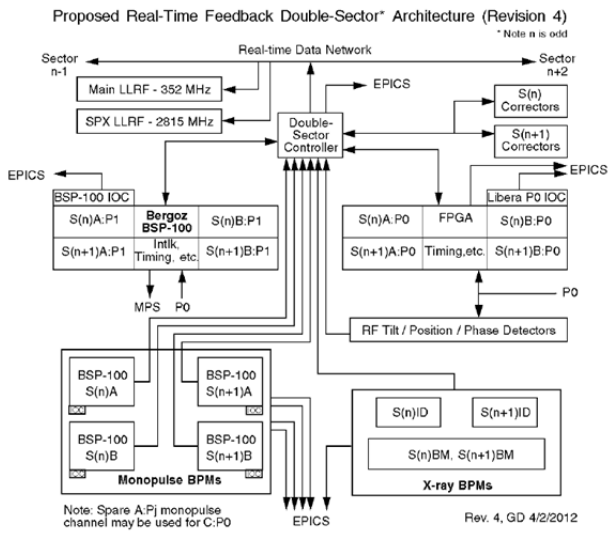


Figure 1: Real-time feedback double-sector controller architecture.

RTFB DSC IMPLEMENATION

The architecture maps into three functional chassis: 1) the APS2VME crate, which interfaces to the exiting reflective memory and EPICS networks; 2) the RTFB DSC chassis, which uses the ZC706 board [4] with its FPGA Mezzanine Connectors (FMC) for interfaces; and 3) the CMPSI-II chassis, which uses a KC705 board [5] and its FMC connectors interfaces as shown in Figure 2.

Copyright © 2013 CC-BY-3.0 and by the respective authors

ISBN 978-3-95450-138-0

LINEAR ANALYSIS FOR SEVERAL 6-D IONIZATION COOLING LATTICES*

J. Scott Berg, Robert B. Palmer, Diktys Stratakis, BNL, Upton, NY, 11973, USA†

Abstract

In muon accelerators, ionization cooling is the only viable option for reducing the muon beam emittance to values necessary for a muon collider. An ionization cooling lattice requires a large momentum acceptance, small beta functions, an extremely large dynamic aperture, and a modest amount of dispersion to have good performance. The latter values are a function of beam momentum. One step in understanding the lattice performance is to determine these quantities for a lattice cell being studied. This is modestly more complex than usual since the lattice is generally highly coupled. We first review the general method for computing these quantities for a general lattice. Then we look at several lattices of interest, compute these quantities, and relate their values and momentum dependencies to the performance of the lattices.

ANALYSIS

To try to understand the behavior of cooling lattices, one can used standard techniques for analyzing accelerator lattices. These systems are highly coupled, and they are non-symplectic due to the presence of cooling. The symplecticity is further complicated by the use of kinetic momenta in most tracking codes. Use of canonical momenta would be challenging due to the strong transverse vector potentials that arise from the use of solenoids, but would arise in any case due to the use of short cells and large beam sizes. Symplecticity can be further compromised by use of a non-symplectic integrator with step sizes larger than needed for machine precision and magnetic field approximations that are not divergence-free.

Fixed Energy

At fixed energies, we find the closed orbit through a single cooling cell, then look at the linear map about that closed orbit. We then find the eigenvalues and eigenvectors of the linear map to get the tunes and the beta functions. More specifically, if M is the linear map about the closed orbit, then we find a matrix A such that $MA = AR$, where R is in the form

$$\begin{bmatrix} \lambda_1\cos\mu_1 & \lambda_1\sin\mu_1 & 0 & 0 \\ -\lambda_1\sin\mu_1 & \lambda_1\cos\mu_1 & 0 & 0 \\ 0 & 0 & \lambda_1\cos\mu_2 & \lambda_1\sin\mu_2 \\ 0 & 0 & -\lambda_1\sin\mu_2 & \lambda_1\cos\mu_2 \end{bmatrix} \quad (1)$$

Since M is not necessarily symplectic, we allow $\lambda_k \neq 1$.

We find the lattice parameters as a function of energy. We will not study energies for which the lattice does not have stable orbits in the sense that R is of the form (1).

The matrix A is not uniquely defined. There are three different degrees of freedom. First, one can exchange the first two columns of A with the last two columns, which corresponds to swapping the eigenvalues. Second, one can change the sign of one of the first two columns of A, which corresponds to changing the sign of μ_1 (similarly for the last two columns and the sign of μ_2). Finally, one can multiply A on the right by a matrix of the form (1) (but with different parameters than R). We will define A sufficiently to accomplish three goals: to resolve the sign ambiguity in μ_k in R; to be able to compute the beta functions; and to ensure that the two sets of eigenvalues and the beta functions are continuous functions of the energy (so that the 1 and 2 indices don't swap arbitrarily).

For a given energy, we scale both $\boldsymbol{a}_{2k-1}$ and $\boldsymbol{a}_{2k}$ ($\boldsymbol{a}_j$, $1 \leqslant j \leqslant 4$, is the jth column of A) by the same value, and possibly change the sign of $\boldsymbol{a}_{2k}$, so that $\boldsymbol{a}_{2k-1}^T J \boldsymbol{a}_{2k} = 1$, where

$$J = \begin{bmatrix} 0 & 1 & 0 & 0 \\ -1 & 0 & 0 & 0 \\ 0 & 0 & 0 & 1 \\ 0 & 0 & -1 & 0 \end{bmatrix} \quad (2)$$

and the order of coordinates is (x, p_x, y, p_y). If we change the sign of $\boldsymbol{a}_{2k}$, we also change the sign of μ_k. There is still an arbitrary rotation on the right side of A; we will insure that subsequent results are independent of that rotation.

Say we compute A_1 and A_2 for nearby energies. We would expect these matrices to be nearly the same, except for an arbitrary rotation on the right side of each one. If the columns of these matrices are $\boldsymbol{a}_{1;j}$ and $\boldsymbol{a}_{2;j}$, we compute the matrix S_{kl} with elements $s_{kl;ij} = \boldsymbol{a}_{2;2k-2+i}^T J \boldsymbol{a}_{1;2l-2+j}$. If $\det S_{11} > \det S_{12}$, then the columns of A_1 and A_2 refer to corresponding eigenvectors. If not, then the eigenvectors are in a different order in A_1 and A_2, and for one of the matrices the first pair of columns should be swapped with the second pair, and the eigenvalues should be swapped as well.

Each eigenvector pair describes a corresponding set of Courant-Snyder lattice functions. They relate the beam size and angular divergence to the area traced out by an ellipse. Since with coupling, oscillation is not in a fixed plane, the corresponding quantities must be independent of direction. They must also be independent of the arbitrary rotation on the right side of A. By analogy to the usual quantities, we can then define

$$\beta_k = a_{1,2k}^2 + a_{1,2k+1}^2 + a_{3,2k}^2 + a_{3,2k+1}^2 \quad (3)$$

* This manuscript has been authored by employees of Brookhaven Science Associates, LLC under Contract No. DE-AC02-98CH10886 with the U.S. Department of Energy. The United States Government retains a non-exclusive, paid-up, irrevocable, world-wide license to publish or reproduce the published form of this manuscript, or allow others to do so, for United States Government purposes.

† jsberg@bnl.gov

Copyright © 2013 CC-BY-3.0 and by the respective authors

A PLANAR SNAKE MUON IONIZATION COOLING LATTICE *

Robert B. Palmer, J. Scott Berg, Diktys Stratakis, BNL, Upton, Long Island, New York, USA

Abstract

Muon Colliders require cooling in six dimensions (x, x',y, y', t, E). Several ionization 6D cooling lattices, using vacuum acceleration, are reviewed: RFOFO lattices, both curved [1] and rectilinear [2] cool one sign to low emittances; A Helical FOFO snake [3] cools both signs, but not to low emittances. A Planar Snake [4] lattice is proposed that cools both muon signs, and appears suitable for low emittances. The parameters and performance for an example suitable for the early stages of cooling is given.

INTRODUCTION

The Muon Accelerator Program (MAP) [5] is studying Muon Colliders with center of mass energies from 125 GeV to several TeV. All require 6 dimensional (x, x',y, y', E, t) cooling to transverse emittances of $\approx$ 0.31 mm, and longitudinal emittances $\approx$ 1.5 mm.

In transverse ionization cooling, in a low Z absorber (hydrogen or Lithium Hydride), both transverse and longitudinal momentum are lost. Radio-frequency (rf) cavities (only vacuum rf is considered in this paper) then restore the longitudinal momentum, leaving the reductions of the transverse components. Multiple scattering leads to a minimum (equilibrium) emittance that is proportional to the betatron $\beta_\perp$ divided by the relativistic β of the muon momentum.

For cooling in the longitudinal dimension, emittance exchange is required. Two methods are illustrated in Fig. 1a and b. In a), a wedge absorber is placed in a region with dispersion, so higher momentum muons have more energy loss than those lower. In b) a plane slab absorber is placed where there is angular dispersion. Emittance exchange can also be achieved in a Helical Cooling Channel [6] where absorbing material is everywhere while higher momenta have longer paths.

Periodic lattices allow lower transverse betatron lengths $\beta_\perp$, but introduce integer and half integer resonances defining the operating momentum range. Figure 2a, b, and c show three cases:

a) Simple lattices of equi-spaced solenoids operate above the single π resonance.

b) Bi-periodic lattices [7], with pairs of coils spaced by longer drifts operate between the 2π and π resonances and have an attractively level $\beta_\perp$ between these resonances.

c) Lattices with more complex coils sequences, such as the Helical FOFO Snake and Planar snake, which both operate between the 3π and 2π resonances.

* Work supported by US Department of Energy under contract DE-AC02-98CH10886

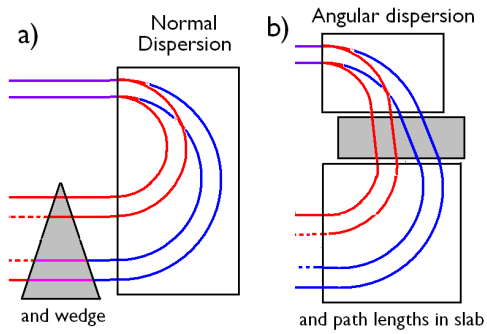


Figure 1: Emittance Exchange: a) using dispersion & wedge absorbers; b) using angular dispersion & slab absorbers.

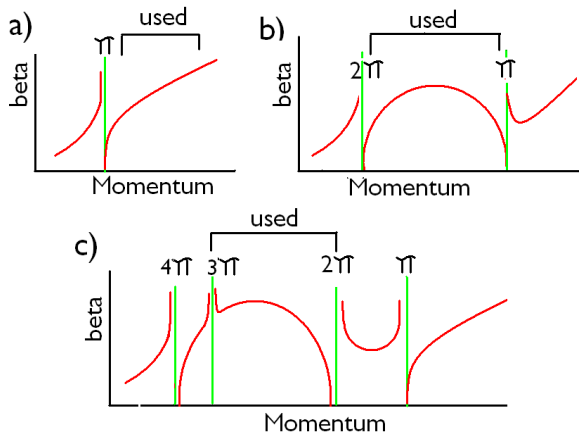


Figure 2: Lattice types: a) Simply periodic alternating solenoids; b) Bi-periodic alternating solenoids; c) Higher tune lattices (Helical Snake & Planar Snake).

GEOMETRIES

Figure 3 shows three lattice geometries. They could be curved, but we consider only straight geometries here.

RFOFO & RFOFO Rectilinear Lattices

Using alternating solenoids, Balbekov [2] has shown that the required dispersions can be generated by small tilts of the coils in either a simply periodic (FOFO) or bi-periodic (RFOFO) lattice. The tilts are small and alternate to generate periodic dipole fields (Fig. 3a). The performance of these lattices is essentially the same as with curved lattices [8], but with simpler engineering. Recent simulations [9, 10], have shown cooling from emittances close to those simulated from the initial phase rotation (15 mm transverse, 45 mm longitudinal) to that required in the baseline design (0.31 mm transverse and 1.5 mm longitudinal) with acceptable particle loss (of order 50%).

Copyright © 2013 CC-BY-3.0 and by the respective authors

ISBN 978-3-95450-138-0

SRF AND RF SYSTEMS FOR CeC PoP EXPERIMENT*

S. Belomestnykh#,1,2, I. Ben-Zvi1,2, C. H. Boulware3, J. C. Brutus1, T. L. Grimm3,Y. Huang1, D. Kayran1, X. Liang2, V. Litvinenko1,2, P. McIntosh4, A. Moss4, P. Orfin1, I. Pinayev1, T. Rao1, M. Ruiz Osés2, B. Sheehy1, J. Skaritka1, K. Smith1, R. Than1, J. Tuozzolo1, E. Wang1, A. Wheelhouse4, Q. Wu1, T. Xin2, Wencan Xu1, A. Zaltsman1
1) Brookhaven National Laboratory, Upton, NY 11973-5000, U.S.A.
2) Stony Brook University, Stony Brook, NY 11794, U.S.A.
3) Niowave, Inc., Lansing, MI 48906, U.S.A.
4) STFC/DL/ASTeC, Daresbury, Warrington, Cheshire, UK,WA4 4AD

Abstract

Efforts to experimentally prove the concept of coherent electron cooling are underway at BNL. A short 22 MeV linac will provide high charge, low repetition rate beam to cool a single ion bunch stored in RHIC. The linac will consist of a 112 MHz SRF gun, two 500 MHz normal conducting bunching cavities and a 704 MHz five-cell accelerating SRF cavity. The paper describes the SRF and RF systems, the linac layout, and discusses the project status, first test results and schedule.

INTRODUCTION

Coherent electron Cooling (CeC) is a technique promising significant luminosity improvement in high-energy hadron-hadron and electron-hadron colliders [1]. A Proof-of-Principle (PoP) experiment is under preparation at BNL to demonstrate its feasibility [2, 3]. This experiment aims to cool only one ion bunch stored in RHIC, requiring a high-bunch-charge (up to 5 nC), but low-repetition-rate electron beam. The bunch repetition frequency (78 kHz) is equal to the revolution frequency of ion bunches in RHIC. A short 22 MeV superconducting linac is being built to provide such beam [4]. The linac includes two superconducting RF (SRF) systems and one normal conducting RF system. The two SRF systems are a 112 MHz Quarter Wave Resonator (QWR) SRF photoemission electron gun [5] and a 704 MHz SRF booster cavity cryomodule. The normal conducting RF system comprises two copper bunching cavities [6] to provide velocity modulation for shortening the electron bunches between the two SRF cryomodules. The linac layout is shown in Figure 1. In this paper we describe the SRF and RF systems, report on the project status and test results, and discuss testing and commissioning plans.

112 MHz QWR SRF GUN

A superconducting 112 MHz quarter-wave resonator was developed by collaborative efforts of BNL and Niowave, Inc. [7, 8]. The gun operates at 4.5 K with liquid helium provided from a quiet helium source via the cryomodule cryogenic tower. We expect to achieve the

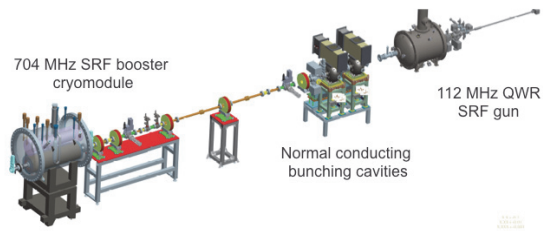


Figure 1: Layout of the CeC PoP linac.

cavity quality factor of 1.8×10^9. The QWR's center conductor geometry naturally accommodates a half-wavelength choke joint and allows mechanical decoupling of the cathode assembly from the niobium cavity [9]. A low-RF-loss photocathode stalk operates at room temperature. It is hollow, allowing inserting a small photocathode pack via a load lock system. We plan to use multi-alkali (CsK_2Sb or NaK_2Sb) photocathodes illuminated with a green (532 nm) light from a laser to generate the electron beam.

The 112 MHz gun is equipped with a dual-purpose fundamental RF power coupler / fine frequency tuning assembly [9]. The fine frequency tuning with a range of about 3 kHz will be used for remote frequency adjustment. It will complement a larger range (>78 kHz) tuner, which will be used only for an initial frequency set up. The mechanical design of the fundamental power coupler (FPC) is described elsewhere [10]. A focusing solenoid is placed on top of the FPC close to the cryomodule's beam exit flange.

After the first cryomodule cold test at Niowave in December of 2010 [7], the gun has undergone modifications. A new cryostat was designed and fabricated to be compatible with BNL's safety requirements and to have appropriate interfaces for installation in RHIC tunnel. The modified gun was cold tested again at Niowave in December of 2012 and February of 2013. During the tests we encountered multipacting zones at very low fields, which were processed only after we modified the RF input coupler to increase its coupling. Eventually, the gun reached an accelerating voltage of 0.92 MV, limited by an insufficient radiation shielding of the experimental set up. Figure 2 shows the gun cavity performance during the cold test.

*Work is supported by Brookhaven Science Associates, LLC under contract No. DE-AC02-98CH10886 with the US DOE.
#sbelomestnykh@bnl.gov

Copyright © 2013 CC-BY-3.0 and by the respective authors

NOVEL MECHANICAL DESIGN FOR RHIC TRANSVERSE STOCHASTIC COOLING KICKER

C.J. Liaw, J.M. Brennan, S. Bellavia, J. Tuozzolo, K. Mernick, M. Myers
Brookhaven National Laboratory, Upton, NY 11973, U.S.A.

Abstract

Based on the beam emittance measurement from the pickup, the RHIC Stochastic Cooling kicker uses sixteen narrowband high Q cavities (from 5 to 8 GHz) to kick (or to cool) the bunched beam on each of the two transverse planes in the two rings. The cavities are integrated to two pairs of cavity plates and installed in two UHV chambers. The new kicker features scissor like driving mechanism, frictionless flexure joints, water cooled cavity plates, small frequency shift (less than 0.05%) during the operation and maintenance free. Novel mechanical designs, including cavity plate, vacuum, cooling, driving mechanism, and support structure design, are presented. Structural and thermal analyses, using ANSYS, were performed to confirm chamber structural stability and to calculate the cavity plate deformation due to thermal and mechanical load. Good agreement between the calculated cavity plate deflection and the expected plate deformation from the cavity frequency shift measurements has been achieved. Three assemblies utilizing this design (1 for the vertical and 2 for the horizontal plane) were completed for the FY2012 run. Successful performance has been reported.

INTRODUCTION

RHIC has successfully employed the stochastic cooling technique to counteract the emittance growth in the high frequency bunched beam due to Intra Beam Scattering (IBS) in the past several runs [1]. Two essential components, a pickup (to measure the beam emittance in the transverse directions) and a kicker (to cool the beam transversely), are required for the transverse stochastic cooling. The new pickup design has been reported elsewhere [2]. This paper will focus on the mechanical design of the new transverse stochastic cooling kicker.

To minimize the input power, high Q resonant cavities were chosen as the new kicker in RHIC [3]. During the early stage kicker development, RHIC received a few stochastic cooling tanks from Fermilab as a gift, which were originally developed for the FNAL Tevatron. To take advantage of these tanks, the FNAL original vacuum chambers and the driving mechanisms [4] were used to accommodate those cavities and to drive them from the cooling position (with a smaller aperture) to the standby position (with a larger aperture for the injected beam). There are several disadvantages with these designs: (1) The cavity plate guide shafts could get stuck in vacuum, (2) The beryllium copper RF spring fingers could lose their contact with the beam pipe, (3) The actuator could deliver an excessive force to bend the shaft, (4) The vacuum space is too small for the application, and (5) The cavity frequencies are not repeatable.

The newly developed transverse stochastic cooling kicker has addressed all the mechanical problems described above. Novel mechanical designs for the system are described below. Structural and thermal analysis results are also presented.

DESIGN REQUIREMENTS

The mechanical design requirements for the new transverse stochastic cooling kicker are: (1) To provide 16 high Q cavities, spanning the bandwidth of 5 to 8 GHz in 200 MHz intervals, for each kicker, (2) To split the cavities on the median plane and integrate them into two pairs of cavity plates, (3)To maintain repeatable cavity resonant frequencies, with a frequency shift of no more than 0.05% of their frequencies, (4) To provide a reliable actuator for the cavity plates, (5) To keep the cavity aperture at 20 mm, during the operation, and at no less than 124 mm, when not in use, (6) To provide a sufficient space in the vacuum chamber for an easy access and the installation of the cavity plates, (7) To provide adequate structural stability of the vacuum chambers and the support stands, and (8) To provide a bakable (up to 200°C) and maintenance free vacuum design.

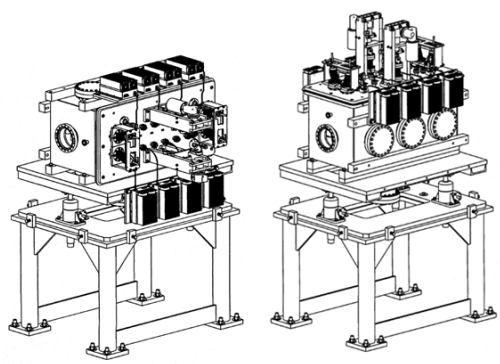


Fig. 1: One Half of a Horizontal and a Vertical Transverse Stochastic Cooling Kicker Assembly.

*Work supported by Brookhaven Science Associates, LLC under Contract No. DE-AC02-98CH10886 with the U.S. Department of Energy

Copyright © 2013 CC-BY-3.0 and by the respective authors

ISBN 978-3-95450-138-0

ROBUST MECHANICAL DESIGN FOR RHIC TRANSVERSE STOCHASTIC COOLING PICKUP

C.J. Liaw, J.M. Brennan, J. Tuozzolo, K. Mernick, V. De Monte, M. Myers
Brookhaven National Laboratory, Upton, NY 11973, USA

Abstract

The RHIC transverse Stochastic Cooling Pickup uses a pair of high resolution 4-8 GHz frequency band planar loop arrays to measure the Schottky signals from the bunched beams in the two transverse planes of the two rings. Precision alignment between the two 381 mm long array boards was achieved by surveying two specially designed alignment fixtures outside the vacuum chamber and using a pair of high resolution, motor controlled, and force balanced actuators. Robust mechanical design was achieved by excluding wearable mechanical joints and fragile electronics inside the vacuum chamber. Both mechanical designs and structural analysis results, for the vacuum chamber and for the array board supports, are presented. Two horizontal and two vertical plane pickups have been fabricated and installed in RHIC for the FY2012 run. Successful performance has been reported.

INTRODUCTION

The injected ion beams inside the two RHIC rings have a typical bunch rate of 10 MHz with 5 ns in length. The number of particles per bunch varies from 2 x 10^8 (for uranium) [1] to 1.5 x 10^9 (for gold) [2]. Due to intra-beam scattering (IBS), beam emittance would grow and reduce the intensity and the lifetime of the beam. RHIC has been successfully applying the stochastic cooling technique to correct this problem in the past 10 years. Based on the experience, a new transverse stochastic cooling system, which includes a broad band pickup and a kicker, has been developed recently. This paper will focus on the mechanical design of the new pickup.

McGinnis (1991) [3] developed a 4-8 GHz bandwidth bunched beam Stochastic Cooling Arrays for the Fermilab Tevatron. Due to the strong coherent frequency components presented in the high frequency bunched beam, the common mode Schottky signals from the two planar loop couplers must be subtracted before taking the measurement, which requires a high precision and repeatable mechanical alignment between the two arrays [3]. Hurh (1993) [4] designed a bunched beam Stochastic Cooling Tank for the FNAL Tevatron, which integrated the loop arrays into a vacuum chamber. The arrays were driven by two stepper motors through two guided plungers, which could provide different apertures for the changing beam size. Hurh's original design, however, has a few disadvantages, which include (1) The Teflon coated array board guiding shafts and the piezoelectric crystal inchworm motor could get stuck in vacuum, (2) The two pieces design BeCu image current transition assembly could buckle and reduce the aperture unexpectedly, and (3) The BeCu spring fingers on the image current transition assembly could lose their elastic strength and the contact forces on the beam pipe after the vacuum bake out.

Wei (2004) [5] applied the coasting beam theory and demonstrated that a 3-D stochastic cooling system with a 4-8 GHz bandwidth could effectively counteract IBS in RHIC. The 4-8 GHz Bunched Beam Stochastic Cooling Arrays, which were developed by McGinnis, were therefore adopted and retrofitted to become the sensor in the new pickup design. The newly developed transverse stochastic cooling pickup has addressed all the mechanical problems described above. Both mechanical designs and the supporting structural analysis results are presented below.

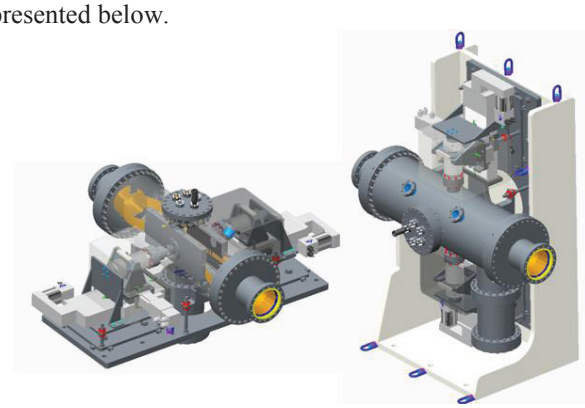


Figure 1: Horizontal and vertical stochastic cooling pickup.

MECHANICAL DESIGN OF THE TRANSVERSE STOCHASTIC PICKUP

The transverse stochastic cooling pickup could be installed either horizontally or vertically (see Fig. 1) to measure the Schottky signals from the RHIC bunched beam in the corresponding planes. The pickup integrates a pair of printed planar loop arrays, produced by Fermilab [3], with two aluminum backing boards being retrofitted into the newly designed UHV chamber. Two pickup leads and a proximity sensor (which is a pair of gold plated SST spring fingers, made by Lairtech) are provided on the two 381 mm x 152 mm x 17.5 mm array boards. Each array board is cantilever supported by a motor controlled precision linear stage, which is mounted on a four axes (X-Y-Z-theta) adjustable table. The linear stages provide a fine tuning on the relative alignment between two array boards in the X and the Z (or beam) direction. The alignment accuracy between the two array boards is required to be maintained within 50 microns

*Work supported by Brookhaven Science Associates, LLC under Contract No. DE-AC02-98CH10886 with the U.S. Department of Energy.

Copyright © 2013 CC-BY-3.0 and by the respective authors

HIGH INTENSITY RHIC LIMITATIONS DUE TO SIGNAL HEATING OF THE CRYOGENIC BPM CABLES *

P. Thieberger, C. Pai, K. Mernick, T. Miller, M. Minty, K. Hamdi, A. Ghosh and J. D'Ambra
Collider Accelerator Department, Brookhaven National Laboratory, Upton NY 11973, USA

Abstract

The signal cables from the beam position monitors (BPMs) in the cryogenic sections of the Relativistic Heavy Ion Collider (RHIC) need to satisfy somewhat conflicting requirements. On the one hand, the cryogenic load due to heat conduction along the cable needs to be small, which led to the use of stainless steel jacketed cables with Tefzel insulation. On the other hand, radio frequency losses need to be reasonably small to reduce heating due to dissipated signal power. As the beam intensity in RHIC increased over the years, and the bunches are becoming shorter, a point is being rapidly approached where these cables will soon become a performance limiting factor. Here we describe an extensive study of this problem including cable loss measurements as a function of temperature and frequency, characterization of the copper center conductor, and simulations using Particle Studio (PS) and ANSYS.

INTRODUCTION

The signal heating limitations of the RHIC cryogenic BPM cables were recognized and analyzed in 1995 [1, 2]. In particular, the Tefzel insulator has an operational temperature limit of 150 °C. Continuing RHIC upgrades to higher luminosities will hopefully lead next year [3] to the new goal of 111 bunches of 3E11 protons each with an RMS bunch length of 20 cm (henceforth the "upgraded beam"). The cable limit is expected to be approached, and more detailed estimates have now been performed to ensure safe and reliable operation.

CABLE LOSS MEASUREMENTS

Cable losses as a function of frequency were measured with a signal analyzer at eleven temperatures ranging from 4 K to the maximum operating temperature of the cable which is 423 K (150 °C). To perform these measurements at the various temperatures two different cryostats, an ice bath and an oven were used. A spare RHIC 125 cm long BPM cable was formed into a 10 cm diameter spiral and connected to two lead-in cables of the same type.

To take into account the temperature dependent losses in these lead-in cables, a short (8 cm long) "dummy" connection was used as shown in the Fig.1 inset, and the results shown in figure 1 were obtained by subtracting at each temperature the losses measured with the dummy from the ones measured with the sample under identical conditions. The frequency range up to 500 MHz contains over 95% of the signal power for 20 cm rms bunches.

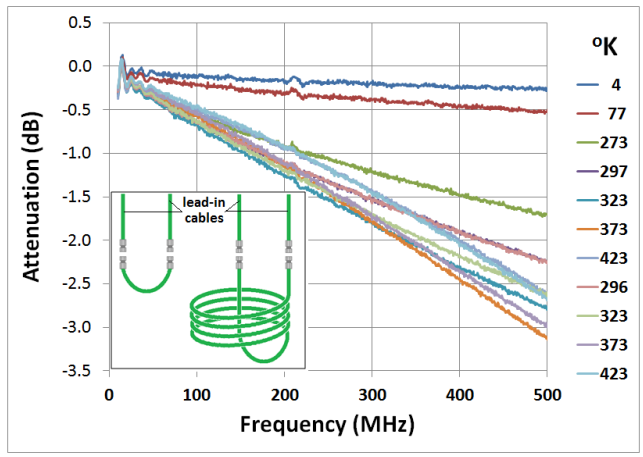


Figure 1: Cable attenuation as function of frequency measured at 11 temperatures ranging from 4 K to 423 K; the operating temperature limit for the cable.

From these curves, the losses per unit length are later calculated considering an effective cable length of 125 – 8 = 117 cm where 8 cm is the length of the "dummy" connection. The Fig. 1 data show that above ~180 MHz, some of the lower temperature losses are larger than losses at higher temperatures. This surprising behavior, which was confirmed by repeating the measurements with different signal analyzers, is probably due to peculiarities in the dielectric losses in the Tefzel insulator.

THERMAL CONDUCTIVITY

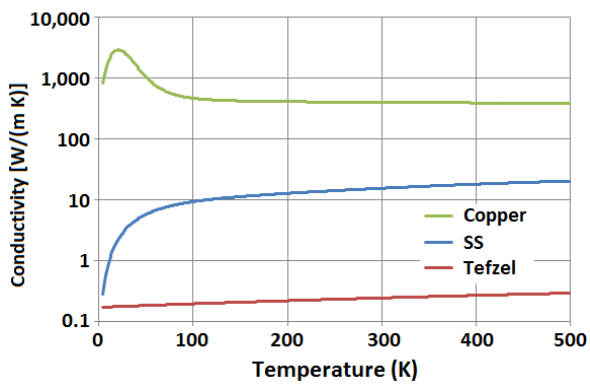


Figure 2: Thermal conductivities used for the simulations.

* Work supported by Brookhaven Science Associates, LLC under Contract No. DE-AC02-98CH10886 with the U.S. Department of Energy.

Copyright © 2013 CC-BY-3.0 and by the respective authors

ISBN 978-3-95450-138-0

UPGRADING THE RHIC BEAM DUMP FOR HIGHER INTENSITY*

C. Montag, S. Nayak, L. Ahrens, W. Fischer, H. Hahn, C.J. Liaw,
J. Mi, T. Roser, P. Thieberger, J. Tuozzolo, K. Yip, W. Zhang
BNL, Upton, NY 11973, USA

Abstract

Mechanical analysis of the RHIC beam dump window has shown that present heavy ion beam intensities are close to the tolerable limit, and will likely exceed that limit in future runs. Two approaches to upgrade the abort system for those projected higher intensities have been studied, namely replacing the existing window, and adding a vertical kicker that distributes the individual bunches more evenly across the window, thus reducing the heat load. We present the results of these studies and the present status of the upgrade project.

INTRODUCTION

The RHIC beam is aborted by a set of five kickers that deflect it horizontally into the dump. The dumped beam first passes through a 50 cm long C-C carbon block that dilutes its emittance before it exits the RHIC vacuum enclosure through a pair of 17-7 PH steel windows. Outside the beam vacuum, the aborted beam is diluted further by a second carbon block before it is absorbed by a massive steel block.

The RHIC beam dump system was originally designed for a 100 GeV/nucleon gold bunch intensity of $1 \cdot 10^9$ Au ions/bunch in 56 bunches. During the 13 years of RHIC operation, the actual beam intensity has been increased by more than a factor 2, to $1.3 \cdot 10^9$ Au bunches in 111 bunches. In addition, stochastic cooling [1] now results in much smaller emittances than originally envisioned during the RHIC design phase [2]. These developments led to a re-evaluation of the integrity of the vacuum window.

NUCLEAR INTERACTION AND MULTIPLE SCATTERING IN THE C-C CARBON BLOCK

Due to stochastic cooling the Au beam emittance in RHIC depends strongly on the bunch intensity. A simple scaling law can be derived from the fact that cooling rate and intrabeam scattering (IBS) growth rate counterbalance each other in the equilibrium.

With the cooling rate scaling with the bunch intensity as

$$\tau_{\mathrm{cool}}^{-1} \propto \frac{1}{N} \tag{1}$$

and the IBS emittance growth rate scaling as

$$\tau_{\mathrm{IBS}}^{-1} \propto \frac{N}{\epsilon_\perp^2 \epsilon_{\mathrm{L}}}, \tag{2}$$

Table 1: Double-Gaussian Fit Parameters for the Energy Deposition for Two Different Beam Emittances

emittance $[\pi\mathrm{mm\,mrad}]$	4	8
bunch intensity 10^9	0.7	1.6
A_1 $[\mathrm{MeV/cm^3}]$	$43.0 \cdot 10^{13}$	$66.8 \cdot 10^{13}$
σ_1 [mm]	0.51	0.62
A_2 $[\mathrm{MeV/cm^3}]$	$0.77 \cdot 10^{13}$	$1.74 \cdot 10^{13}$
σ_2 [mm]	5.25	5.26

where $\epsilon_\perp$ and ϵ_{L} are the transverse and longitudinal emittances, respectively, the transverse emittance is therefore proportional to the bunch intensity [3]

$$\epsilon_\perp \propto N \tag{3}$$

for a constant longitudinal emittance ϵ_{L}. This scaling rule agrees well with simulation results that show a transverse equilibrium normalized 95 percent emittance of $4\pi\mathrm{mm\,mrad}$ for $0.7 \cdot 10^9$ Au ions/bunch, and $8\pi\mathrm{mm\,mrad}$ for $1.6 \cdot 10^9$ Au ions/bunch [3].

The interaction of a single incoming bunch with the C-C carbon block and the resulting energy deposition is simulated using the code MCNPX [4]. Nuclear interaction and multiple scattering in the C-C carbon block widens the distribution and reduces the peak intensity of the round Gaussian beam, while at the same time producing significant non-Gaussian tails. The resulting distribution is described by a double-Gaussian fit as

$$\rho(r) = A_1 \exp\left(-\frac{r^2}{2\sigma_1^2}\right) + A_2 \exp\left(-\frac{r^2}{2\sigma_2^2}\right), \tag{4}$$

where r is the radial particle coordinate, and A_1, A_2 and σ_1, σ_2 are the normalized amplitudes and RMS widths of the double-Gaussian distribution. Table 1 lists the double-Gaussian fit parameters for two different emittances. Together with the abort kicker pulse shape, the spatial energy distribution on the abort kicker window for the entire 111 bunches can then be calculated.

MECHANICAL AND THERMAL STRESS IN THE WINDOW

The RHIC beam dump system aborts the beam by applying a horizontal kick. The pulse shape of these abort kickers is designed such that after an initial fast rise that kicks the first bunch across the septum, the remaining bunches are spread out in a straight line by an oscillatory behavior of the kick, as shown in Figure 1.

* Work supported by Brookhaven Science Associates, LLC under Contract No. DE-AC02-98CH10886 with the U.S. Department of Energy.

Copyright © 2013 CC-BY-3.0 and by the respective authors

OPTIMIZATION OF THE CAPTURE SECTION OF A STAGED NEUTRINO FACTORY*

H.K. Sayed,† H.G. Kirk, Brookhaven National Laboratory, Upton, NY 11973, USA
K.T. McDonald, Princeton University, Princeton, NJ 08544, USA

Abstract

A proposed staged Neutrino Factory, producing lower muon intensity of 10^{20} muons per year and 10-14 GeV muon beam energy, initially requires target station for 1 MW proton beam power with a proton beam energy of 3 GeV, which could be upgraded to the full power of 4 MW at 8-GeV beam energy. The optimization of the initial Target Station and the following Decay Channel and Buncher/Phase Rotator are discussed.

INTRODUCTION

In the baseline Neutrino Factory / Muon Collider design [1], sketched in Fig. 1, the muon beam is produced from pion decay by bombarding a liquid-mercury-jet target with a 4-MW pulsed proton beam, which delivers an intense muon beam of 10^{14} muons/sec from the incident beam of 10^{15} proton/s. In the proposed staged Neutrino Factory [2] with a 1-MW proton beam of 3-GeV energy, the Target Station uses a solid graphite target and produces a muon intensity of 10^{20} per year The target is embedded in a 15 (or 20) T solenoid magnet for the pion collection, shown in Fig. 2, which is followed by a lower field Decay Channel. The baseline design of the Target Station/Decay Channel will be retained during later stages of the Neutrino Factory to save the cost at the time of upgrade to the full 4-MW scenario.

The target and proton beam sizes and their tilt angles in the initial 3-GeV configuration are given in Table 1, which configuration produces 0.42 muons/protons at the end of the Target System.

Table 1: Proton Beam and Graphite Target Parameters for the Staged Neutrino Factory

Carbon rod target	Proton beam
Length 0.72 [m]	$\sigma_t = 2$ [nsec]
Diameter 0.692 [cm]	$\sigma_{x,y} = 0.0865$ [cm]
Angle to solenoid axis 42 mrad	42 mrad

The adiabatic variation in solenoid field strength along the beam near the target performs an emittance exchange affects the performance of the downstream Buncher, Phase Rotator, and Cooling Channel [3]. An optimization was performed using the MARS15 (2012) [4] and ICOOL [5] codes in which the rate of change of the field along the pion beam near the target was varied to maximize the number of muons that falls within the acceptance of the downstream accelerator chain (muons within 201.25 MHz RF bunches with momentum in the range 100300 MeV/c, transverse amplitude squared less than 0.03 m and longitudinal amplitude squared less than 0.15 m [3]).

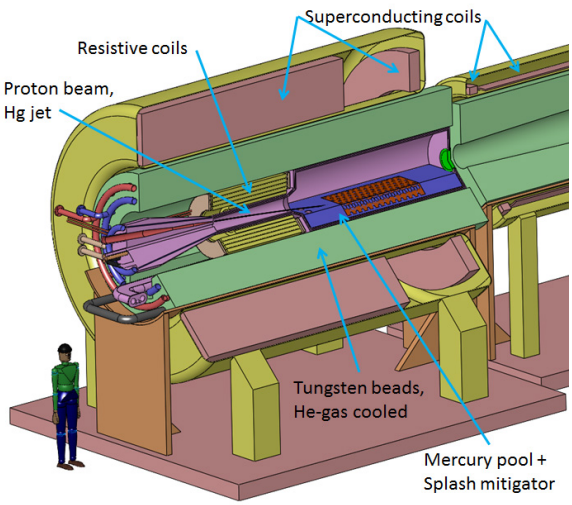


Figure 2: Neutrino Factory/Muon Collider target system.

The Target System utilizes a magnetic-field profile that peaks at $B_i = 15$ T at the target and tapers down to $B_f = 2.5$ T over a distance of $L_{\rm taper}$. In this study we optimized the length of this tapering solenoid $L_{\rm taper}$. The effect of solenoid-field profile on the captured-particle count and their phase-space distribution was studied by simulating the particles captured at the target and transported through the rest of the Front End. Various axial-field profiles were considered, based on an inverse-cubic form [6], from which the off-axis fields were calculated using Maxwellian series expansions. A sample of the axial-field profiles studied is shown in Fig. 3.

PION PRODUCTION AND CAPTURE AT THE TARGET

The MARS15 code [4] was used to simulate the particle production off the graphite target, using an incident 3-GeV proton beam with delta-function time distribution.

* Work supported by the US DOE Contract No. DE-AC02-98CHI10886.
† hsayed@bnl.gov

ISBN 978-3-95450-138-0

Copyright © 2013 CC-BY-3.0 and by the respective authors

A HIGH-PERFORMANCE RECTILINEAR FOFO CHANNEL FOR MUON COOLING*

D. Stratakis#, J. S. Berg, R. B. Palmer, Brookhaven National Laboratory, Upton NY, USA
V. I. Balbekov, Fermi National Accelerator Laboratory, Batavia IL, USA

Abstract

An ionization cooling channel is a tightly spaced lattice containing absorbers for reducing the momentum of the muon beam, rf cavities for restoring the longitudinal momentum and solenoids for focusing the beam. Such a lattice is an essential step for a Muon Collider. Here, we explore a new scheme for designing ionization cooling channels for muon related applications. In this scheme, emittance reduction is achieved within a rectilinear channel with wedge absorbers for cooling and tilted solenoids for emittance exchange. Such configuration addresses several of the engineering challenges of a conventional helical channel. We numerically examine the performance of our proposed channel and compare it against conventional designs. We also review the conductor current densities requirements for all of the simulated scenarios.

INTRODUCTION

A key technical challenge in the development of a Muon Collider is that the phase space of the beam that comes from pion decay greatly exceeds the acceptance of downstream accelerators system. Therefore, a cooling channel is required. Given the short life time of a muon particle, ionization cooling is the only practical method that can be realized.

Over the past decade several progresses have been made in the design and simulation of 6D RFOFO cooling rings [1] based on emittance exchange. This is generally accomplished by using a wedge shaped absorber in a region with dispersion. Particles with higher energies will pass through more material than particles with lower energy as a result of dispersion, eventually leading to reduction of longitudinal emittance. Such rings have been shown to provide an impressive to two order magnitude reduction of the normalized 6D phase-space volume with a transmission well above 50%. In order to avoid the complexity arising from the required injection and extraction systems, those rings involved without loss in performance to a RFOFO helical channel [2], commonly known as the Guggenheim. A chief advantage of the Guggenheim is that avoids any issues related to absorber overheating.

Although a helical lattice can be advantageous in paper, still many questions remain. For instance, the beam can be intercepted by the fringe fields from the nearby solenoids. In addition, engineering constraints may arise at the last stages as the radius of curvature becomes less than 1.5 m. To further relax the aforementioned constraints we design and simulate here a rectilinear FOFO snake channel which has been proposed recently by one of the authors [3] and show that it can offer the same performance as the Guggenheim. In particular, we show that by applying a novel tapering scheme in which numerous parameters of the structure change from stage to stage based on the emittance reduction rate and transmission, we can achieve a good cooling efficiency that remains flat through the channel. This is because the beam emittance is always above the equilibrium emittance.

DESIGN PARAMETERS

The main issue with a channel of a fixed radius, cell length, and frequency is its gradual loss of cooling efficiency. Therefore, to keep the cooling process going we examine a tapered channel in which various parameters change in order to avoid reaching equilibrium. In this scheme, parameters such as cell length and radius of curvature progressively change from stage to stage based on the emittance reduction rate and transmission. Recent studies have shown [4] that such a concept improves performance substantially. In addition, with this approach the same emittance can be obtained in much shorter scale.

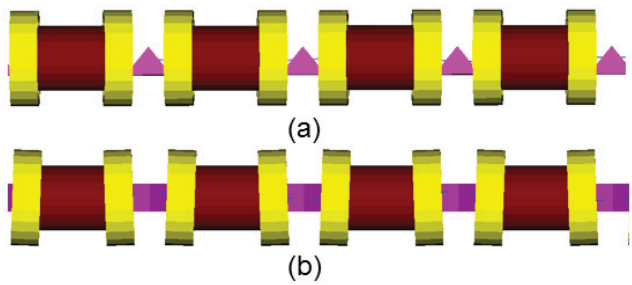


Figure 1: Conceptual design of our proposed rectilinear cooling channel: (a) Top view; (b) Side view. Note that the coils (yellow) are slightly tilted to generate dispersion.

At the first stage of the tapered channel the focusing will be relatively weak to avoid excessive angular divergence that can arise from the large transverse emittance of the initial muon beam. However, the weak focusing implies that the beta function and thus the equilibrium emittance are also relatively large, so the transverse cooling weakens as the limit is approached. To avoid this, this stage is terminated and we couple into the next stage that has a lower beta. This is achieved by simultaneously scaling down the cell dimensions and raising the strength of the on-axis solenoidal field. As a result this will produce a piecewise multi-stage shaped channel where each stage will consist of a series of

*Work supported by DE-AC02-98CH10886
#diktys@bnl.gov

Copyright © 2013 CC-BY-3.0 and by the respective authors

SPACE-CHARGE LIMITATIONS ON THE FINAL STAGES OF A MUON COLLIDER COOLING CHANNEL*

D. P. Grote#, Lawrence Livermore National Laboratory, Livermore, CA, USA
D. Stratakis, R. B. Palmer, J. S. Berg, Brookhaven National Laboratory, Upton, NY, USA

Abstract

Muon Colliders use ionization cooling to reduce the emittance of the muon beam prior to acceleration. At the last stages of the cooling channel, the bunch has 4×10^{12} muons, an average momentum of 200 MeV/c, and an rms bunch of 2 cm. With this beam intensity and relatively low momentum, we expect space charge effects to have a significant impact on beam dynamics. Here, with the aid of the particle-in-cell code Warp, a 3D model is developed to examine space-charge for muon cooling lattices and some recent results are presented. The model includes 6D cooling with wedge shaped absorbers. We show that space-charge under certain conditions can cause a notable particle loss. Furthermore, we discuss some potential space-charge compensation mechanisms.

INTRODUCTION

A complete scheme for cooling a muon beam sufficiently for use in a muon collider has been previously described [1]. This scheme uses separate 6D ionization cooling channels for the two signs of the particle charge. In each, a channel first reduces the emittance of a train of muon bunches until they can be injected into a bunch-merging system. The single muon bunches, one of each sign, are then sent through a second tapered 6D cooling channel where the transverse emittance is reduced as much as possible and the longitudinal emittance is cooled to a value below that needed for the collider. The beam can then be recombined and sent through a final cooling channel using high-field solenoids that cools the transverse emittance to the required values for the collider. The baseline cooling requirement for cooling is shown in Fig. 1.

Theoretical estimates predict that at the last stages of the post-bunch-merge 6D cooling channel the rms bunch length is just 2 cm and contains $4\text{x}10^{12}$ muons. Thus, the peak current becomes ~4 kA at a ~200 MeV/c momentum. Due to this large current, space-charge forces can be present and thus, there is cause for concern that the existing 6D cooling lattice design may not work so well. Recent studies [2] with the Warp PIC code [3] confirmed this fact since it was shown that longitudinal space-charge can oppose cooling while simultaneously it causes severe particle losses. To reduce the space charge effects, the overall lattice was redesigned with a higher longitudinal emittance target, increased from 1.5 to 2.0. We note that those previous studies were assuming a matrix for longitudinal cooling and thus, the effect of a real absorber wedge was not taken into account. This paper will present results from recent studies on simulating full 3D space-charge effects on muon cooling lattices with more realistic wedge shaped absorbers.

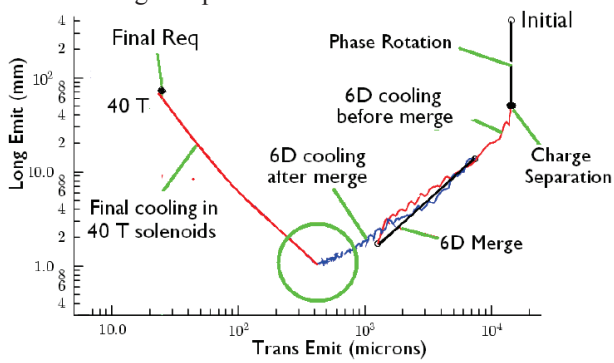


Figure 1: Baseline cooling requirement for the Muon Collider.

LATTICE DESIGN

In order to cool towards the micron scale emittances required for a Muon Collider a 16-stage tapering channel has been proposed. A detailed description of this lattice can be found elsewhere [4]. In this scheme, we apply the concept of tapering [5] where parameters such as cell length, focusing and radius of curvature progressively change from stage to stage based on the emittance reduction rate and transmission.

A segment of one stage of our proposed cooling system is shown in Fig. 2(a). Each stage consists of straight section with a number of identical cells like the one shown in Fig. 2(b) and Fig. 2(c). The coils (yellow) are

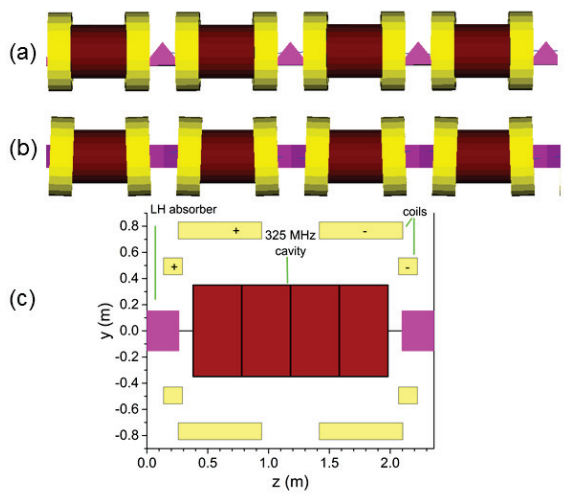


Figure 2: Cooling scheme for the Muon Collider. Fig. (c) depicts one lattice cell. The tilts of the magnets are not shown.

*Work supported by DE-AC02-98CH10886.
#dpgrote@lbl.gov

Copyright © 2013 CC-BY-3.0 and by the respective authors

ISBN 978-3-95450-138-0

RF CAVITY PHASE CALIBRATION USING ELECTROMAGNETIC PICKUPS*

B. Durickovic†, D. Constan-Wahl, J. Crisp, G. Kiupel, S. Krause, D. Leitner,
S. Nash, R. Rencsok, J.A. Rodriguez, R. Webber, W. Wittmer,
NSCL/FRIB, East Lansing, MI 48824, USA

Abstract

A method is presented using electromagnetic pickup probes for RF cavity phase calibration. (We used capacitive style pickup probes.) Pickup probes provide fast readings, and measurements of the phase difference between a pair of pickup probes provides enough information about the phase-energy curve to yield a fit for the zero-crossing phase. We present an overview of the algorithm and measurement results of an implementation on the ReA3 reaccelerator.

INTRODUCTION

The Facility for Rare Isotope Beams (FRIB) is a heavy ion fragmentation facility to produce rare isotopes far from stability for low energy nuclear science. The facility will utilize a high-intensity, superconducting heavy-ion driver linac to provide stable ion beams from protons to uranium at energies greater than $200\ \mathrm{MeV/u}$ and at a beam power of up to $400\ \mathrm{kW}$ [1]. The baseline design for the linac comprises over 300 accelerating superconducting cavities. A precondition for tuning the linac is calibrating the radio frequency (RF) phase of each of these cavities, which requires a phase scan combined with energy measurements. With such a large number of cavities as it is planned for FRIB, a need arises for an automated approach to calibrating cavity phase.

RF cavity phase calibration is the process of calibrating the cavity phase relative to the phase of the accelerated beam. For this purpose, the zero-crossing phase points (the phase points at which the cavity does not provide any acceleration) are determined. There are two such points in a full 360-degree phase range ($180°$ apart from each other), and we use the one on the bunching side of the phase slope as the reference. The value of the zero-crossing depends on the beam energy, thus the cavities need to be calibrated for every new energy tune. Therefore, cavity phase calibration is a necessary recurring task in operations.

We approached the concrete problem of calibrating the cavity phases on the ReA3 accelerator at Michigan State University [2], which is currently being commissioned. Prior to the installation of Beam Position Monitors (BPMs) in the ReA3 accelerator, the only method available for cavity phase calibration was energy measurements from silicon foil detectors. As these measurements are inherently slow, calibrating the six accelerating cavities currently installed in ReA3 could take up to several hours. Since capacitive style electromagnetic pickup probes provide fast readings, we explored the application of pickup probes for inferring the beam energy and thereby calibrating cavity phase. The capacitive style pickup probes we used were the two BPMs installed on the ReA3 beam line. The details of the BPMs in the ReA3 accelerator are presented in Rodriguez et al. [3]. The phase readouts were averaged over the four buttons for each BPM, so that for this purpose, the BPMs were effectively used only as electromagnetic pickup probes.

PRINCIPLE

The readouts from two pickup probes separated by a certain distance provide the phase difference of bunches at the two locations. It is important to keep in mind, though, that this is not the absolute phase difference, but its value modulo $360°$. In other words, the pickup probes do not provide information about the total number of bunches between the two locations, but only the fraction of the RF period that represents the "incomplete last bunch." The number of "complete bunches" between the two locations needs to be evaluated by other means. As will be shown, however, knowing this information exactly is not essential for the applicability of the method we are presenting.

The phase difference $\Delta\varphi$ between the pickup probes can be translated into the time of flight via

$$t(\Delta\varphi; n) = T_{RF}\left(n + \frac{\Delta\varphi}{360°}\right), \qquad (1)$$

where n is the truncated number of bunches between the pickup probes, T_{RF} is the RF period, and t is the time of flight. The integer n decreases with beam energy, and within energies attainable in the ReA3 accelerator (without deceleration), and with the BPMs separated by $2.08\ \mathrm{m}$, it ranges from 14 (for the beam energy after the RFQ of $600\ \mathrm{keV/u}$) to 8 (for the maximum beam energy after the linac of $1.9\ \mathrm{MeV/u}$). Translating the time of flight (1) into energy (non-relativistically), we obtain the dependence of energy per nucleon E/m on the phase difference $\Delta\varphi$:

$$\frac{E}{m}(\Delta\varphi; n) = \frac{1}{2}\left(\frac{Lf_{RF}}{n + \frac{\Delta\varphi}{360°}}\right)^2, \qquad (2)$$

where L is the distance between the pickup probes, and $f_{RF} = 1/T_{RF}$ is the RF frequency. Equation (2) can be in-

* Work supported by Michigan State University FRIB funds and by the U.S. Department of Energy Office of Science under Cooperative Agreement DE-SC0000661

† durickovic@frib.msu.edu

Copyright © 2013 CC-BY-3.0 and by the respective authors

MICE SPECTROMETER SOLENOID MAGNETIC FIELD MEASUREMENTS

M. Leonova# *on behalf of the MICE collaboration*
Fermilab, Batavia, IL 60510, USA

Abstract

The Muon Ionization Cooling Experiment (MICE) is designed to demonstrate ionization cooling in a muon beam. Its goal is to measure a 10% change in transverse emittance of a muon beam going through a prototype Neutrino Factory cooling channel section with an absolute measurement accuracy of 0.1%. To measure emittances, MICE uses two solenoidal spectrometers, with Solenoid magnets designed to have 4 T fields, uniform at 3 per mil level in the tracking volumes. Magnetic field measurements of the Spectrometer Solenoid magnet SS2, and analysis of coil parameters for input into magnet models will be discussed.

INTRODUCTION

The MICE experiment [1] located at Rutherford Appleton Laboratory consists of a dedicated beam line, which generates muons in a range of input momenta between 140 and 240 MeV/c and emittances between 2 and 10 π mm, and a cooling cell sandwiched between particle identification detectors (PID) and Spectrometer Solenoids (SS) equipped with scintillating fiber trackers, see Fig. 1. The cooling cell is designed to reduce the transverse emittance of a passing muon beam by about 10% using the ionization cooling principle.

Each spectrometer consists of a 4 T superconducting solenoid, and a tracker [2] composed of five planar scintillating-fibre stations, whose pacing has been chosen to optimize the performance of the reconstruction (track-finding efficiency and parameter resolution). Together, the spectrometers are required to determine the expected relative change of approximately 10% between the "before" and "after" beam transverse emittances with a precision of ±1% (i.e. 0.1% absolute measurement of the emittance). Therefore, the fields in the tracking volume should be known with high accuracy.

The MICE SSs were built at Wang NMR (Livermore, CA, USA). A schematic representation of the magnet (not drawn to scale) is shown in Fig. 2. The cryostat consists of a liquid helium vessel, an 80 K thermal shield, cold mass supports and a stainless steel vacuum vessel with 40-cm diameter bore. Each solenoid consists of five superconducting Nb-Ti coils wound on a single aluminum mandrel. Two Matching coils (M1, M2) match the muon beam in the SSs to the beam in the cooling cell. Two End coils (E1, E2) positioned around a Center coil (C) are designed to generate a uniform 4 T field over a 110-cm-long and 30-cm-diameter volume. The coil parameters

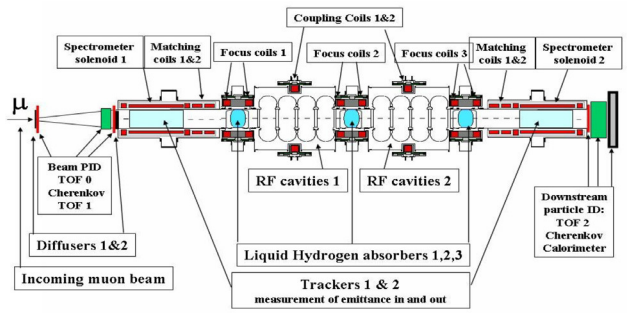


Figure 1: Layout of the MICE cooling cell. It is a prototype of a cooling channel section for use in a Neutrino Factory or a Muon Collider.

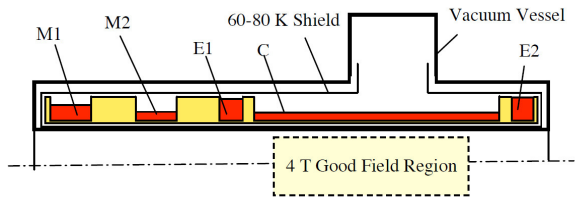


Figure 2: Top half of a schematic cross-section of one of the MICE SS.

	Match 1	Match 2	End 1	Center	End 2
Inner Coil Radius (mm)	258	258	258	258	258
Coil Thickness (mm)	46.165	30.925	60.905	22.125	67.783
Coil Length (mm)	201.268	199.492	110.642	1314.30	110.642
Current Center Axial Position* (mm)	124.00	564.00	964.00	1714.00	2464.00
Current Center Radial Position* (mm)	281.083	273.463	288.453	269.063	291.891
Coil Average J (A mm-2)	137.67	147.77	124.28	147.66	127.09
Number of Layers per Coil	42	28	56	20	62
Number of Turns per Layer	115	114	64	768	64
Total Number of Turns	4830	3192	3584	15360	3968
Design Current (A)**	264.83	285.60	233.68	275.52	240.21
Coil Self Inductance (H)^	12.0	5.0	9.0	40.0	11.3
Coil Stored Energy (MJ)**	0.42	0.20	0.26	1.55	0.32
Peak Field in Coil (T)**	5.30	4.32	5.68	4.24	5.86
Temperature Margin at 4.2 K (K)**	~1.6	~1.8	~1.5	~2.0	~1.5

* Based on Z = 0 is at the match coil end of the magnet cold mass (The center of MICE in these coordinates is at Z = -3487 mm) R = is the axis of the magnet (the MICE axis).
** This is at the maximum design current, which is based on the worst-case currents for the five coils.
^ The inductance of the two end coils and the center coil in series is about 74 H.

Figure 3: As built parameters of the second MICE SS.

given in Fig. 3 [3] are "as built", which are different from the original design and design by vendor. Each coil layer was thicker than anticipated with fewer turns per layer, thus, the currents in the coils were adjusted accordingly.

A model of the solenoids (together with other magnets, equipment and structures in the MICE experimental hall) will be used to simulate the fields for each momentum/emittance case for use in MICE data analysis. Thus, the magnetic field mapping is important to verify the coil geometry for the model and effects of magnetic material (detector shielding) on the field.

mleonova@fnal.gov
Work supported by US DOE under contract DE-AC02-07CH11359.

ISBN 978-3-95450-138-0

Copyright © 2013 CC-BY-3.0 and by the respective authors

STATUS OF THE MUON IONIZATION COOLING EXPERIMENT (MICE)*

Y. Torun, Illinois Institute of Technology, Chicago, IL 60616, USA†
M. Zisman, LBNL, Berkeley, CA 94720, USA
for the MICE Collaboration

Abstract

A muon collider and a muon-based neutrino factory are attractive options for particle physics. Their realization requires demonstration of muon ionization cooling, the only technique to rapidly reduce the emittance of the short lived tertiary muon beam. MICE, performed by a team from the U.S., Europe, and Asia at Rutherford Appleton Laboratory, will provide this demonstration. The experiment comprises one cell of a representative cooling channel, bracketed upstream and downstream by muon detection stations, each with a spectrometer solenoid (SS). Characterization of the RAL/ISIS muon beam line is complete. Fabrication of the two SS is nearly complete, with one having passed its acceptance tests, and the second nearly ready for testing. The first focus coil is presently being tested, with a second unit ready shortly. The cold mass for the coupling coil prototype is under test and its cryostat is in fabrication. Other required hardware, including RF cavities and liquid-H absorbers, is also being built. Their status and plans for carrying out the experiment are described.

CONCEPT AND STAGING

Ionization cooling of muons involves reducing the total momentum through energy loss while replenishing the component along the reference orbit with acceleration. MICE is a demonstration of muon cooling using a full cooling cell surrounded by tracking and particle identification detectors to measure each muon before and after it traverses the cell [1]. This way, a virtual beam can be constructed in software and its emittance measured with unprecedented precision. The goal is to measure a reduction of order 10% in normalized transverse emittance with a relative precision of 1% under different configurations of input beam and magnetic channel optics. Figure 1 shows the staging of the experiment. Step I, aimed at characterizing the beam using the particle identification detectors, is now complete. In addition, preliminary momentum reconstruction and emittance measurements were performed at this stage using the time-of-flight (TOF) detectors [2]. Reconstructed trace space distributions agree well with simulations for different combinations of momentum (140, 200 and 240 MeV/c) and normalized transverse emittance (3π, 6π and 10π mm). The first measurement of cooling with absorbers will take place in Step IV [3]. This will be followed by the final stage (Step VI) with the full cooling channel cell in place including RF acceleration [4].

* This work was supported by the Office of Science, U.S. Department of Energy under DOE contract number DE-AC02-05CH11231

† torun@iit.edu

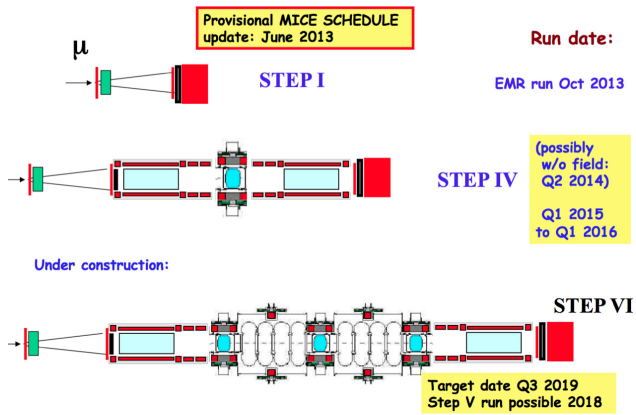


Figure 1: MICE staging and schedule.

BEAMLINE

A target system [5] utilizing a linear electromagnetic drive moves a Ti cylinder vertically toward the edge of the shrinking proton beam envelope just before extraction. In addition, a vertical closed orbit bump has been developed to steer the ISIS beam to meet the target at the correct phase and reduce losses in the machine induced by the MICE target [6]. Figure 2 shows the beamline elements and instrumentation. The pion beam from the target is captured by a quadrupole triplet (Q1-3) and momentum selected in a dipole (D1) before being directed into a decay solenoid (DS). A variable thickness proton absorber at the exit of the DS is used to remove protons from the beam. Momentum selection on the muons from pion decay is performed by

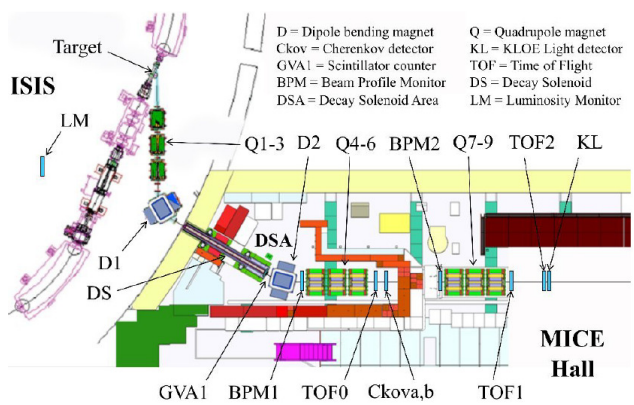


Figure 2: MICE beamline and instrumentation.

Copyright © 2013 CC-BY-3.0 and by the respective authors

A CHARGE SEPARATION STUDY TO ENABLE THE DESIGN OF A COMPLETE MUON COOLING CHANNEL*

C. Yoshikawa#, C. Ankenbrandt, R. P. Johnson, Muons, Inc., Batavia, IL 60510, U.S.A.
Y. Derbenev, V. Morozov, JLAB, Newport News, VA 23606, U.S.A.
D. Neuffer, K. Yonehara, Fermilab, Batavia, IL 60510, U.S.A.

Abstract

The most promising designs for 6D muon cooling channels operate on a specific sign of electric charge. In particular, the Helical Cooling Channel (HCC) and Rectilinear RFOFO designs are the leading candidates to become the baseline 6D cooling channel in the Muon Accelerator Program (MAP). Time constraints prevented the design of a realistic charge separator, so a simplified study was performed to emulate the effects of charge separation on muons exiting the front end of a muon collider. The output of the study provides particle distributions that the competing designs will use as input into their cooling channels. We report here on the study of the charge separator that created the simulated particles.

INTRODUCTION

One of the most challenging components for a muon collider is the 6D cooling channel that must cool muons by six orders of magnitude in phase space before they decay (τ=2.2μs). The two most promising candidates are the Helical Cooling Channel [1,2] and Rectilinear RFOFO [3] designs. The Muon Accelerator Program (MAP) is a national effort headed at Fermilab that is charged with accessing the feasibility of building a muon collider and/or a neutrino factory based on a muon storage ring. A down-select competition between these contenders had been announced over the summer of 2013 with the expectation for each design to have results of simulations of all components in their channel by end of calendar 2013. Both concepts operate on a single sign of electric charge of the muon, but a charge separator had not been designed. The tight time constraint forbade the design of a realistic charge separator, so a study was performed to emulate the effects of a simplified charge separator on muons exiting the front end of a muon collider. The output of the study provides particle distributions that the competing designs will use as input into their cooling channels.

INITIAL STUDY

This study benefits from an earlier effort [4] that used bent solenoids to separate the opposite charges in the beam. Upon scrutiny of that study, we realized that it was possible to design a configuration that would separate the charges without the need to accelerate the muons above the momentum of 250 MeV/c expected from the front end of the system. A cartoon of the coil configurations that illustrate the basic layout of the charge separator is shown in Figure 1. There are two bent solenoids; the first "forward bend" (shown in white in Figure 1(a)) separates the charged beams vertically, while the second "reverse bend" (shown in red and blue in Figure 1) directs each beam back into the mid-plane. Each bend has three sectors: two "Norem matching" sectors [5] of half a Larmor oscillation length ($\lambda_L/2$) each and a mid-sector that has half the bending radius (and thus twice the vertical displacement angle) to adjust the vertical displacement at the end of the first bend. One of the beams will need to drift in a straight solenoid for a full λ_L in order to create separation between the two reverse bend sets of coils. For consistency with the earlier study, we chose the μ+ beam to traverse the longer path. Since there is no RF in the separator, the beam in the longer path is subject to larger longitudinal emittance growth, and that drives the performance of the charge separator. We will thus design to optimize the μ^+ beam and subsequently analyse the μ^- beam in the shorter channel.

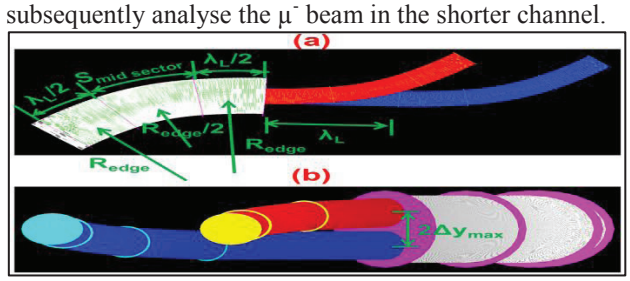


Figure 1: Cartoon of coil configuration illustrating the concept of a charge separator from a top view (a) and at the downstream end looking upstream (b).

A SIMPLIFIED CHARGE SEPARATOR

Designing a realistic charge separator will involve:

1. Dealing with fringe fields at the end of the forward bend and start of the two smaller solenoids.
2. Dealing with fringe fields between the two downstream solenoids.
3. Possibly tilting the coils in the downstream segments if the path difference introduced by the vertical displacement of the coils has a negative impact on performance.

The above complications and the time constraints motivated the need for a simulation setup that can extract the effects of a properly designed charge separator without having to design a realistic charge separator. Such a setup is illustrated in Figure 2 where the simple charge separator is introduced by way of two separate channels, one for each sign. Each channel incorporates large radii coils throughout both bends as well as in the

*Work supported in part by DOE STTR grant DE-SC0007634
#cary.yoshikawa@muonsinc.com

Copyright © 2013 CC-BY-3.0 and by the respective authors

ISBN 978-3-95450-138-0

MAGNETIC BUNCH COMPRESSION FOR A COMPACT INVERSE COMPTON SOURCE

B.R.P. Gamage[1*] and T. Satogata[1,2]
[1]Center for Accelerator Science, Old Dominion University, Norfolk VA, 23529, USA
[2]Thomas Jefferson National Accelerator Facility, Newport News VA, 23606, USA

Abstract

A compact electron accelerator suitable for inverse Compton source applications is in design at the Center for Accelerator Science (CAS) at Old Dominion University (ODU). Here we discuss two options for transverse magnetic bunch compression and final focus, each involving a 4-dipole s-chicane with M_{56} tunable over a range of 1.5-2.0m with independent tuning of the final focus to an interaction point β*=5mm. One design has no net bending, while the other has net bending of 90 degrees and is suitable for compact corner placement.

INTRODUCTION

There is significant interest in X-ray sources beyond those available at large third-generation, lab-based synchrotron light sources. Medical phase imaging, and industrial applications have been developed that have motivated development of compact light sources based on inverse Compton scattering (ICS) [1] that provide single beamline operation at a cost of about $10-15M. A compact ICS source is in design at the ODU CAS with an X-ray energy of up to 12 keV, flux of approximately 1.6×10^{14} photon/sec, and average brilliance of 1.5×10^{15} photon/$(\mathrm{s} \cdot \mathrm{mm}^2 \cdot \mathrm{mrad}^2 \cdot 0.1\%\mathrm{BW})$ [2].

This project consists of an optimized 500 MHz superconducting electron gun, 4K 500 MHz superconducting spoke cavity linac [3], and a bunch compressor to provide a short, high-brightness electron bunch to collide with an incoming laser beam to produce inverse Compton scattered photons. The electron beam requirements are shown in Table 1. The bunch length requirement of a few ps and energy spread requirement of 3×10^{-4} indicate the need for small longitudinal emittance (<7 eV-m) and well-corrected bunch compression. A practical system will also have tunable M_{56} to optimize the scattered photon beam.

Table 1: Electron Beam Parameters at Collision

Parameter	Value	Units
Energy	25	MeV
Bunch charge	10	pC
Repetition rate	100	MHz
Average current	1	mA
Normalized emittance	0.1	mm·mrad
$\alpha^*_{x,y}$, $\beta^*_{x,y}$	0, 5	-, mm
FWHM bunch length	3.0 (0.9)	psec (mm)
RMS energy spread	7.5	keV

DESIGN PHILOSOPHY

Traditionally dispersion-free chicanes are used for magnetic bunch compression, with $M_{56} < 0$ and $T_{566} > 0$[4]. However, these chicanes are not very compact and cancel dispersion only to odd orders. M_{56} tunability is also directly connected to the chicane transverse dimension, and so is limited.

For a compact design with tunable M_{56}, we have been investigating 4-dipole s-chicanes that alternate the bending directions of the center dipoles. A chicane of this type was investigated for the final bunch compressor of TTF-FEL [5]. S-shaped compressors are dispersion free to all orders, have greater M_{56} tunability, and can be wrapped in on themselves with large central bend angles to be made compact. As described in [5], M_{56} is tunable by adjusting the central dipole angle.

Initial designs considered combining quadrupoles in the compressor with quadrupoles outside the compressor to tune the final focus. However, the aggressiveness of the design final focusing to $\beta^* = 5$mm is best handled with a separate independent low-beta focus section. This sacrifices some small measure of compactness of the design, but greatly improves the orthogonality of tuning knobs for achromaticity, M_{56}, final focusing, and upstream matching. The linac design for this ICS suggests that a reasonable range for M_{56} tuning is 1.5-2.0m.

A typical s-shaped chicane compressor ensures achromaticity by having a net horizontal phase advance of 2π, with a pair of symmetrically-placed horizontal focusing quadrupoles to tune achromaticity and a vertical focusing quadrupole at the center symmetry point to control vertical betas. Here the compact design pushes us towards stronger focusing, and we investigate two designs: one with net 3π phase advance and a net 90° bend for corner use, and one with net 4π phase advance for larger dispersion and M_{56} lever arm. M_{56} is tunable for both designs by adjusting the center symmetric bend angles and rematching achromaticity and final focus.

DESIGNS AND RESULTS

We use elegant from the APS for lattice design, optimization, and particle tracking, including simulation of short quadrupole end effects as described in the next section. Each lattice has three quadrupoles in two symmetric families between the center dipoles. For a given central

* Author email: bgama002@odu.edu

Copyright © 2013 CC-BY-3.0 and by the respective authors

IMPROVEMENT OF DIGITAL FILTER FOR THE FNAL BOOSTER TRANSVERSE DAMPERS

T. Zolkin*, The University of Chicago, Department of Physics, Chicago, IL 60637–1434, USA
N. Eddy†, V. Lebedev‡, FNAL, Batavia, IL 60510–5011, USA

Abstract

Fermilab Booster has two transverse dampers which independently suppress beam instabilities in the horizontal and vertical planes. A suppression of the common mode signal is achieved by digital notch filter which is based on subtracting beam positions for two consecutive turns. Such system operates well if the orbit position changes sufficiently slow. Unfortunately it is not the case for FNAL Booster where the entire accelerating cycle consists of about 20000 turns, and successful transition crossing requires the orbit drifts up to about 10 μm/turn, resulting in excessive power, power amplifier saturation and loss of stability. To suppress this effect we suggest an improvement of the digital filter which can take into account fast orbit changes by using bunch positions of a few previous turns. To take into account the orbit change up to N-th order polynomial in time the system requires $(N+3)$ turns of "prehistory". In the case of sufficiently small gain the damping rate and the optimal digital filter coefficients are obtained analytically. Numerical simulations verify analytical theory for the small gain and predict a system performance with gain increase.

INTRODUCTION

Consider a paraxial transverse motion of the particle with equilibrium energy in a circular accelerator. For further calculations we will be neglecting a coupling between transverse planes and consider only one of them for simplicity. Neglecting nonlinear effects, in an approximation of linear optics, the dynamics of a particle can be described by the "time" evolution of the betatron state-vector, $\tilde{\zeta}(s) = [q(s), p(s)]^{\mathrm{T}}$, where the variable s is the path length along the closed orbit and plays the role of time, q is the particle deviation in considered transverse direction with respect to the closed orbit, and $p = d\,q(s)/ds$ is canonically conjugated momentum.

The canonical transformation to the so-called normalized coordinates $(p, q) \to (\mathcal{P}, \eta)$:

$$\begin{aligned} \eta(s) &= q(s)/\sqrt{\beta(s)}, \\ \mathcal{P}(s) &= p(s)\sqrt{\beta(s)} + q(s)\,\frac{\alpha(s)}{\sqrt{\beta(s)}}, \end{aligned}$$

where $\beta(s)$ is a beta-function and $\alpha(s) = -\frac{1}{2}\,d\beta(s)/ds$, is performed in order to reduce the motion (from an initial position s_1 to a final one s_2) to the pure rotation of new normalized vector $\zeta(s) = [\eta(s), \mathcal{P}(s)]^{\mathrm{T}}$:

$$\begin{bmatrix} \eta(s_2) \\ \mathcal{P}(s_2) \end{bmatrix} = \begin{bmatrix} \cos\mu_{12} & \sin\mu_{12} \\ -\sin\mu_{12} & \cos\mu_{12} \end{bmatrix} \begin{bmatrix} \eta(s_1) \\ \mathcal{P}(s_1) \end{bmatrix},$$

where $\mu_{12} = \psi(s_2) - \psi(s_1)$ and $\psi(s)$ is a betatron phase advance

$$\psi(s) = \int_0^s \frac{d\bar{s}}{\beta(\bar{s})}.$$

Damper System

A general transverse damper is an active feedback system consisting of pickup station which measures the beam position, and a kicker which is located downstream and damps the betatron oscillations of the beam as a whole by applying an appropriate kick (see Fig. 1).

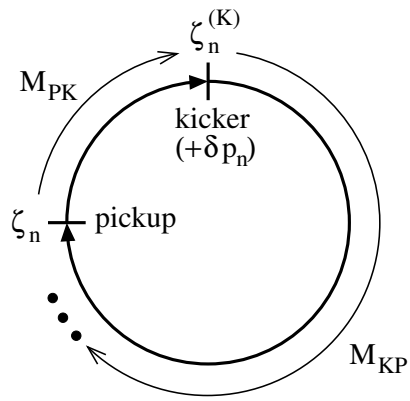


Figure 1: Schematic plot of the one turn transformation of the betatron state-vector in a lattice with damper.

For further considerations we will denote as ζ_n and $\zeta_n^{(\mathrm{K})}$ the normalized betatron-state vector on the n-th turn at the locations of the pickup and the kicker respectively, as $M_{\mathrm{PK}}(\mu_1)$ and $M_{\mathrm{KP}}(\mu_2)$ the transport matrices between pickup and kicker and between kicker and pickup, where $\mu_{1,2}$ are phase advances corresponding to those matrices, and as δp_n the change of particle momentum applied at the n-th turn by kicker. The above determines the betatron tune $\mu_0 = \mu_1 + \mu_2$.

Thereby, a one-turn map that recursively defines a new state-vector at the pickup location can be written as, [1]:

$$\zeta_{n+1} = M_{\mathrm{KP}}\,\zeta_n^{(\mathrm{K})} = M_{\mathrm{KP}}\left(M_{\mathrm{PK}}\,\zeta_n + \begin{bmatrix} 0 \\ \delta p_n \end{bmatrix}\right). \quad (1)$$

* zolkin@uchicago.edu
† eddy@fnal.gov
‡ val@fnal.gov

ISBN 978-3-95450-138-0

Copyright © 2013 CC-BY-3.0 and by the respective authors

FAST FPGA BASED LOW-TRIGGER-JITTER WAVEFORM GENERATOR METHOD FOR BARRIER-BUCKET ELECTRONICS AT FAIR*

E. Bayer†, P. Zipf, University of Kassel, Kassel, Germany
H. Klingbeil, A. Klaus, GSI Helmholtz Centre, Darmstadt, Germany

Abstract

A new method for low trigger-jitter waveform generation is presented. The targeted application is the time-delayed, trigger synchronous waveform generation. The method can be implemented on a single FPGA, which drives an ADC. The phase-jitter between a trigger signal fed to the FPGA and the generated single sine waveform is σ= 40 ps and 275 ps peak-to-peak. The response time of the wave form generator is 50 ns. The amplitude and the offset of each sine wave can also be manipulated in real time. The waveform generator was designed for the use in the Barrier-Bucket system of the SIS100 synchrotron at the new Facility for Antiproton and Ion Research (FAIR) in Darmstadt, Germany.

INTRODUCTION

The GSI Helmholtz Centre for Heavy Ion Research in Darmstadt, Germany is an accelerator facility for High Energy Physics (HEP) research. In collaboration with 16 countries and physicists from all over the world, the Facility for Antiproton and Ion Research (FAIR) will be built as a major extension of the existing facility and will be one of the largest accelerator facilities in the world.

The presented waveform generator method is designed for the use in the pre-compression stage of the new SIS100 synchrotron. The existing SIS18 will be used as booster and will inject bunches of particles into 8 of 10 SIS100 buckets. After the particles have been accelerated to the final speed in the SIS100, they have to be compressed to a single bunch that takes 1/3 of the circumference. The preferred method to perform this task is called Barrier-Bucket. In this method, the amplitude of the bucket forming sine waves, which hold the bunches, is decreased adiabatically. After a certain time the bunches merge into a single long particle bunch in between the remaining sine waves. Now, to compress the beam without the loss of particles, one wave has to be moved towards the other adiabatically, means in steps less than 1 ns. Both sine waves have to be generated synchronously to the revolution trigger, coming from the Central Control System, which controls also the amplitude and the voltage offset of the sine waves. The BB-method is illustrated in Fig. 1. The constraints for the waveform generation system, listed in Table 1, are given by the physics of the accelerator and the desired bunch quality.

The task is therefore to gain control over the phase of the generated single sine waves in the sub nano-second region with a low response time. For this purpose a new waveform generation method was developed and implemented.

* Work supported by EU, EURONS contract No. 506065.
† e.bayer@gsi.de

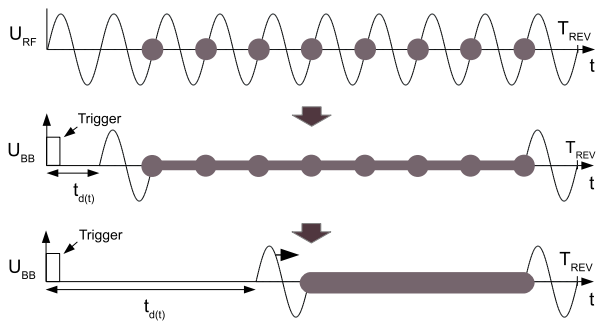


Figure 1: The procedure for beam pre-compression with the Barrier Bucket method (simplified).

Table 1: Specifications for the Barrier-Bucket Low-Level RF-System

Parameter	Value
Barrier Frequency f_b	1.5 $\pm$ 0.2 MHz
Revolution Period T_{REV} (= Trigger Period)	9.1 to 3.7 μs
Moving Time T_{MOV}	10 to 200 ms
Moving Step Resolution $\Delta t_{d(t)}$	$\leq$ 1ns
BB signal rise/fall time t_R and t_F	$\leq$ 10ns

We will introduce the new method in the next section. In the section "Design" the design structure and operation are explained. Subsequently, the measured performance of the system will be presented, followed by a conclusion.

WAVE GENERATION METHOD

In existing asynchronous triggered DDS methods, the incoming trigger signal is sampled with the internal system-clock frequency f_{sys}. As soon as a 0/1 transition is detected, a Digital-Analog-Converter (DAC) is driven by the system-clock and fed with the grid points of the desired waveform. The standard deviation of the resulting trigger-waveform jitter equals then $1/(f_{sys} \cdot \sqrt{12})$. To overcome this limitation, additional effort is necessary on both sides - on the input processing as well as on the signal synthesis part. The given task can therefore be divided into two subtasks. First, the relation of the incoming trigger-signal phase to the system-clock signal phase $\Delta\Phi$ has to be determined with a higher precision than simply by sampling the trigger signal and second, the generation of the phase accurate sine wave using this information. This procedure is illustrated in Fig. 2. In the following sections, the methods for a high precision phase measurement and for phase accurate signal generation are introduced.

Copyright © 2013 CC-BY-3.0 and by the respective authors

STUDY OF MICROPHONICS COMPENSATION FOR SRF CAVITY*

Z. Zheng[#,1,2], S. Zhao[1], Z. Liu[1], D. Morris[1], J. Wei[1], Y. Zhang[1]
[1]Facility for Rare Isotope Beams, Michigan State University, East Lansing, Michigan, USA
[2]Tsinghua University, Beijing, China

Abstract

Microphonics and Lorentz Force detune the resonance frequency of a SRF cavity, leading to perturbations of the amplitude and phase of its accelerating field. Although this disturbance could be compensated by a piezo-electric tuner or with additional RF power, these two methods have conflicts, which is observed as unstable RF fields in a recent experiment. These conflicts could be explained by a model. Further experiments on ReA3 [1] cryomodule validates a conflict suggested by the model. Overall optimization of control algorithm is still needed to effectively combine the two methods.

INTRODUCTION

Microphonics and Lorentz Force Detuning are major disturbances to the accelerating field of an SRF cavity. Usually, people can invest more RF power into the cavity to compensate these effects. However, RF power is expensive, especially for high gradient SRF cavities. An economical substitute is piezo-electric tuner, which sense and compensate the vibration with a fast feedback system. But the compensation is relatively rough, compared with the RF power method. It seems natural to combine the rough and cheap tuner with fine RF power to get an effective and affordable compensation. As we expect a stable accelerating field by simultaneously applying both tuners, we did observe strong interference between them. Section 1 describes these observations.

To understand the conflict in the combo control, we have developed a model in MATLAB. The model reveals a conflict that is resulted from a time delay of piezo tuner control response. When high frequency modulation is induced by RF power modulation, such a time delay corresponds to a large phase difference, which could amplify the unwanted oscillations rather than suppress them.

We added a low pass filter to verify our speculation. The phase fluctuation has been suppressed from ±7° to ±4°, but not completely eliminated. Although the combo control uses two compensation methods simultaneously, their control algorithms are in fact separate. Apparently we need an overall optimization for the combo control algorithm that includes piezo's time delay into consideration.

In this paper, we also compared performance of ADRC algorithm on the piezo tuner with the common PI algorithm. Although ADRC appears to be more efficient than PI in simulation [2], their experimental performance are comparable. Section 2 describes our observation.

CONFLICTS IN THE COMBO CONTROL

To compensate microphonics, a piezo tuner was installed on the quarter-wave resonator (QWR) in ReA3. However, it was only used to suppress helium pressure fluctuations (<1 Hz), not microphonics (>1 Hz). A major source of the microphonics is the vibration of the QWR, with a resonate frequency ~38 Hz. To test the

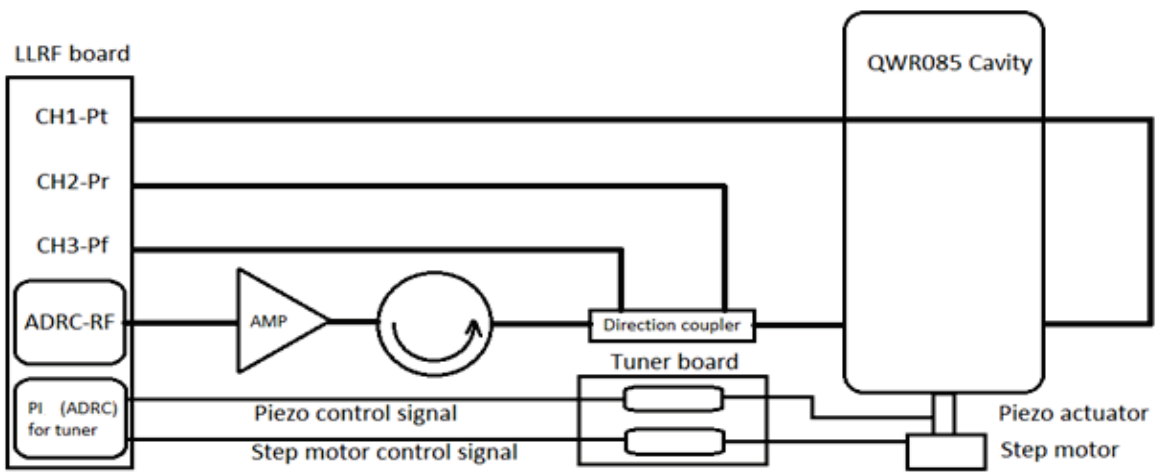


Figure 1: Test setup for a ReA3 cavity. CH1, CH2 and CH3 are three channels on the LLRF board receiving transmit (Pt), reflect (Pr) and forward power (Pf). RF power is controlled with ADRC. Piezo tuner is controlled by PI and later by ADRC.

*Work supported by the U.S. Department of Energy Office of Science under Cooperative Agreement DE-SC0000661.
#zhengw@frib.msu.edu

Copyright © 2013 CC-BY-3.0 and by the respective authors

ISBN 978-3-95450-138-0

NEXT GENERATION CW REFERENCE CLOCK TRANSFER SYSTEM WITH FEMTOSECOND STABILITY

P. Orel, S. Zorzut, P. Lemut, R. Hrovatin, Instrumentation Technologies, Solkan, Slovenia
S.G. Hunziker, V. Schlott, Paul Scherrer Institute, Villigen, Switzerland

Abstract

Present and future fourth generation light sources, such as the Swiss FEL, are placing strict requirements on current CW reference clock transfer systems. Both the added jitter and the long-term stability criteria need to be in the range of a few femtoseconds. In order to meet these requirements, the existing Libera Sync CW transfer system has been redesigned. All of the aspects of the system design have been revised and improved, from new measuring methods and better evaluation of components to careful pre-design testing and simulation. New fiber link topology, new approaches in thermal stabilization, improved power supply distribution and interconnection of carefully selected electrical and state-of-the-art optical components has led to a significant reduction in added jitter and excellent long-term stability of the system. Measurements repeatedly show the jitter performance to be below 6 fs_{rms}, integrated over the frequency range of 10 Hz to 10 MHz. Preliminary measurements of the long-term stability place the system in the range of a few tens of femtoseconds peak-to-peak of drift per day.

INTRODUCTION

Free Electron Lasers (FEL) require high performance synchronization throughout the entire machine; otherwise, its performance may be degraded or even fail. Typically, this high performance synchronization system is composed of two key subsystems. One is the source where a Reference Master Oscillator (RMO) is used. Its frequency range spans from a few 100 MHz to a few GHz. It has high close-in spectral purity and extremely stable frequency. The other extremely important element is the reference clock transfer system. Its goal is to deliver the reference signal to the users in either the optical or electrical domains while preserving initial reference clock signal purity and stability.

Typical requirements in terms of added jitter and long-term phase stability are below 10 fs for jitter and below 40 fs for phase stability per day [1]. For distances greater that 100m, the use of optical fibers as a transmission media is recommended since they exhibit low insertion loss, are insusceptible to EM interference and are reasonably inexpensive. Within the optical domain, two approaches are available.

The first is a pulsed-based system that uses the Michelson interferometer to detect optical path changes. The benefit of this approach is excellent long-term stability.

The other approach is based on a continuous wave (CW) modulation of an optical carrier in which phase detection and stabilization are done in the radio frequency (RF) domain. It offers the advantage of a system restart without re-tuning, high reliability and lower cost [2].

The Libera Sync 3 transfer system presented in this article is based on the CW modulation scheme.

THEORY OF OPERATION

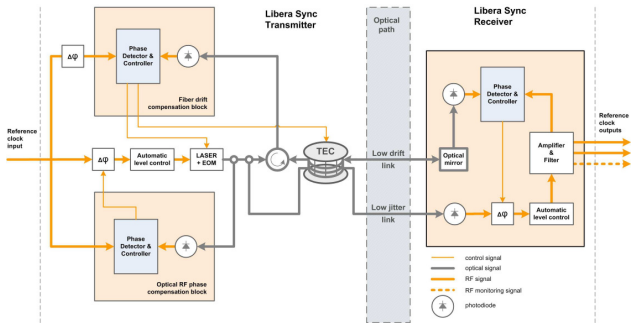


Figure 1: Block diagram of the system.

The figure above is a block diagram of the system that shows the basic principle of operation. The system is composed of a transmitter and a receiver units connected by two optical fiber links. The transmitter input signal is the CW RF reference clock signal coming from the RMO. This signal modulates the 1550 nm optical carrier through an electro-optical modulator. The optical signal is then split and fed into two separate paths. One of the signals along with the on-board control circuitry is used for link phase drift compensation and is partly reflected back at the receiver side. The other path is used for transfer of the low-added jitter signal. In the receiver, both incident optical signals are demodulated back into the RF domain.

In the transmitter unit, the fiber drift compensation is done by comparing the demodulated reflected signal phase with the phase of the input reference signal. The optical path compensation is provided using two principles. The slow changes are compensated by cooling or heating a fiber spool. The temperature of the fibers on the spool is changed in the opposite direction from the temperature change on the optical path between the transmitter and the receiver. Faster changes are compensated by changing the laser source temperature and thus the optical carrier wavelength. In this manner, the optical path is artificially extended or shrunk by taking advantage of the chromatic dispersion in the interconnection fiber.

To overcome optical limitations, two fibers are used, the first one for the transfer of a low-noise signal and the second one for the transfer of a low-drift reference signal.

Copyright © 2013 CC-BY-3.0 and by the respective authors

ISBN 978-3-95450-138-0

ENERGY DEPOSITION IN THE SECTOR 37 SCRAPER OF THE ADVANCED PHOTON SOURCE STORAGE RING*

J. C. Dooling†, M. Borland, Y. C. Chae, and R. Lindberg, ANL, Argonne, IL 60439, USA

Abstract

The horizontal scraper in the sector 37 straight section of the Advanced Photon Source storage ring serves as a diagnostic to probe both the edge of the beam as well as the physical aperture when the store is lost. Initially, the scraper was meant only to be a diagnostic; high-density, short-radiation-length material used in the device was intended to stop halo, not the full beam. Damage to this device was recently discovered, and as a result, we began an effort to model and improve the scraper. Modeling with `elegant` provides loss distributions for several scenarios such as muting one or both rf systems in combination with firing injection kickers. The loss distributions are used as input to a MARS model of the scraper. Beam dumps from 100 mA dissipate a total of 2600 J. Most of this energy is not deposited locally; however, depending on the geometry and physical make-up, sufficient power density exists to damage the device on beam-facing surfaces. Testing is currently planned to examine the suitability of different beam-facing materials. Because of non-local energy deposition, we are evaluating the secondary role for this scraper as a spoiler rather than a beam dump.

INITIAL DAMAGE AND TESTING

During the Spring 2011 APS shutdown, damage to the sector 37 (S37) scraper was observed, and the device was removed from the storage ring (SR). A photograph of the damaged region is presented in Figure 1; the view is looking downstream. The thickness of the W is 2.54 cm. The

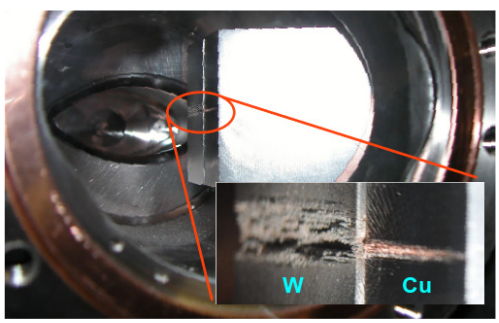


Figure 1: S37 scraper after removal from the SR in April 2011. View is looking downstream.

S37 scraper shown in Fig. 1 had been in use for seven years. The scraper was rebuilt using the same geometery and materials with the intention of employing the device only for diagnostics and collimation while a new design was considered. The rebuilt scaper was reinstalled in the SR in January 2012. Because of installation issues, the device was not used until the final day of the Spring 2012 run when beam dump studies were carried out. After shutdown the device was removed from the SR. During the study, beam was purposely dumped on the scraper using both 24-bunch and hybrid fill patterns. An image of the tungsten region damaged by 24-bunch beam dumps is presented in Figure 2.

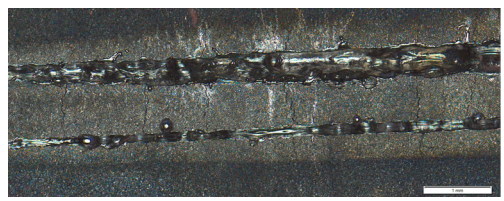
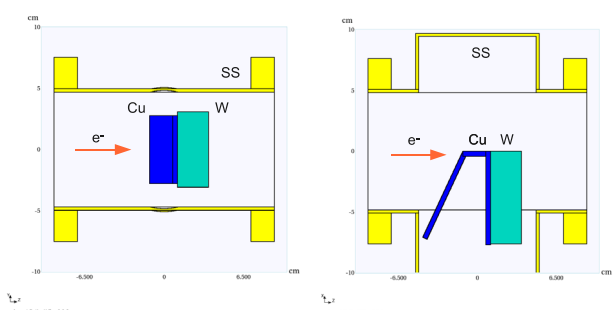


Figure 2: Tungsten region of the rebuilt S37 scraper after removal from the SR in May 2012. Beam motion: left to right.

SIMULATIONS

The particle-matter interaction program MARS [1] is used to estimate energy deposition within the scraper employing loss distributions generated with `elegant` [2]. The scraper components included in the MARS model that directly interact with the beam are shown in Figure 3; the beam travels from left to right. The tapered upstream portion is water-cooled copper. The downstream part is composed of scintered tungsten and is not directly water cooled.



(a) y-z view, x=-1.1 cm (b) x-z view, y=0 cm

Figure 3: Sector 37 baseline scraper geometry modeled in MARS; a) an elevation view at the edge of the scraper (x=-1.1 cm) and b) a plan view at beam elevation (y=0).

The loss distribution is generated by `elegant` for a hy-

* Work supported by the U.S. Department of Energy, Office of Science, under contract number DE-AC02-06CH11357.

† jcdooling@anl.gov

ISBN 978-3-95450-138-0

Copyright © 2013 CC-BY-3.0 and by the respective authors

ANDROID APPLICATION FOR ACCELERATOR PHYSICS AND ENGINEERING CALCULATIONS

M. Borland *

Abstract

Smartphones and tablets are increasingly capable computational devices, with fast processors and high-resolution displays. They are also nearly ubiquitous, suggesting that they can support the need of physicists and engineers to perform quick calculations in situations where using a full-blown simulation is not necessary or expedient. In this paper, we report on the design, features, and capabilities of an Android application inspired by these ideas. The application is called "TAPAs," which stands for Toolkit for Accelerator Physics on Androids. As the name—meant invoke the popular snacks of Spanish cuisine— suggests, the application provides a varied selection of calculations for electron storage rings, electron linear accelerators, electron guns, free-electron lasers, undulator design, synchrotron radiation, and engineering. The calculations are organized into separate sub-applications, which share input values to allow performing related calculations without re-entering data. The application is free of advertising and is available free of charge on the Google Play store.

INTRODUCTION

Physicists and engineers have long needed the ability to perform quick "back of the envelope" calculations. This need arises during discussions, meetings, and conferences, when running a simulation code is not possible or would take too long. It also arises in day-to-day work as one explores ideas at one's desk. The ability to perform a quick, reasonably accurate calculation can sometimes make all the difference between being productive and pursing a dead-end idea.

Such calculations may be performed mentally, with a pad and pencil, or with a hand-held calculator. Depending on one's ability to remember the appropriate equations, one might use a published handbook, memorized equations, or a "cheat sheet." In the not-to-distant past, it was not uncommon to have a programmable calculator that facilitated common calculations. At present, one is more likely to have a smartphone or tablet close by than a programmable calculator. Hence, it makes sense to develop smartphone or tablet "apps" to address the need for quick calculations.

Inspired by these ideas, we developed an Android application that performs a number of useful calculations of the sort that commonly come up in day-to-day work. The Android platform was chosen for its open-source nature and the low cost of entry for devices and development. Unlike other smartphone platforms, the Android Software Development Kit (SDK) is free and available for essentially all platforms, which allowed using Linux for development.

We used the Eclipse Integrated Development Environment (IDE), which is advantageous in that it helps one quickly learn both the Java language and the specific methods provided by Android. The web contains many resources, such as Android tutorials and user forums (e.g., StackExchange).

The application is called TAPAs, which stands for "Toolkit for Accelerator Physics for Androids" and also is meant to bring to mind the popular snacks of Spanish cuisine. The application is free of advertising and is available free of charge on the Google Play store.

SOFTWARE DESIGN

Those who are uninterested in software design may wish to skip this section, as it has little to do with how the application is used or what it can do. This section also assumes some familiarity with Android development.

The root activity of the application, MainActivity, is an extension of the ListActivity class, which presents a set of choices as a simple vertical list. In addition, MainActivity provides pop-up dialog using AlertDialog that acquaints users with recent changes. The SharedPreferences facility is used to remember the major and minor version of the last invocation, so that the pop-up dialog appears only on the first invocation of a new version. Finally, MainActivity loads a set of name/value pairs into a hash table, which provides default values for entries in the various calculations. As calculations are used, the values in the table are updated so that other applications have access to the new data. The hash table is part of a class that is implemented as a "static singleton," which means that there is only one instance of the class and it is shared by all methods that attempt to instantiate the class.

Below the main list are a series of sublists that are also instances of ListActivity. The activities in each sublist are implemented using an ActivityWithMenu class derived from the Activity class. As the name suggests, this new class provides an activity class with a predefined menu. This menu is used to control some basic settings of the application. The settings are saved between invocations and shared among activities using the SharedPreferences class. The widgets for each activity are embedded in a vertically-scrolled list, which helps in accommodating various screen sizes.

Individual calculation activities typically consist of a list of numerical entry and output widgets, in some cases accompanied by graphics. The numerical entry widgets use the EditNumber class, which extends EditText. This class provides two entry methods, one being a simple numerical

* michael.d.borland@gmail.com

Copyright © 2013 CC-BY-3.0 and by the respective authors

ISBN 978-3-95450-138-0

CRYOMODULE PERFORMANCE OF THE MAIN LINAC PROTOTYPE CAVITY FOR CORNELL'S ENERGY RECOVERY LINAC*

N. Valles†, R. Eichhorn, F. Furuta, M. Gi, D. Gonnella, D. Hall, Y. He, V. Ho, G. Hoffstaetter, M. Liepe, T. O'Connell, S. Posen, P. Quigley, J. Sears and V. Veshcherevich
Cornell University, CLASSE, Ithaca, NY 14853, USA

Abstract

Energy Recovery Linacs (ERLs) require strong damping of higher-order modes in main linac cavities to avoid beam loss from beam break-up effects. In addition, the cavities need to have very high intrinsic quality factors to minimize the size of cryogenic plants in CW cavity operation. We present world record results for a fully equipped multicell cavity in a cryomodule, reaching intrinsic quality factors at operating accelerating field of Q_0(E =16.2 MV/m, 1.8 K) $> 6.0 \times 10^{10}$ and Q_0(E =16.2 MV/m, 1.6 K) $= 1.0 \times 10^{11}$, corresponding to a residual surface resistance of 1.1 nΩ, which is more than three times better than the Q_0 design specification.

INTRODUCTION

Cornell University is developing a 5 GeV energy recovery linac (ERL). The SRF main linac of this ERL is designed to support high current beams, each at 100 mA with 77 pC bunch charge (one beam is accelerated and the returning beam is decelerated in the main linac), with small emittance.[1] These demanding beam requirements set tight constraints for electromagnetic and higher-order mode properties of the 1.3 GHz main-linac cavities.[2, 3] In addition to these RF properties of the cavity, the feasibility of operating a 5 GeV SRF linac in continuous wave mode requires the main-linac cavities to have 1.8 K quality factors of at least 2×10^{10} at E_{acc}=16.2 MV/m.[1]

Eventually, six 7-cell cavities along with other instrumentation will be commissioned within a prototype main linac cryomodule (MLC).[4] The precursor to the MLC is the horizontal test cryomodule (HTC) which can contain a single 7-cell cavity, two higher-order mode (HOM) absorbers and other experimental instrumentation.

The first prototype cavity has been fabricated,[5] and is being qualified in the HTC through several stages of hardware implementation. By performing measurements at various stages of implementation, the effects on the quality factor and higher-order mode spectrum can be characterized systematically, leading to tight control of the performance of the structure. In total, there are three verification stages, which have been discussed elsewhere.[6] The instrumentation effecting fundamental mode performance is summarized in Table 1.

Table 1: Key Elements Affecting the 7-cell's HOM Spectrum Incorporated in Each Iteration of the Horizontal Test Cryomodule Experiments. The fundamental mode couples to the on-axis input coupler with $Q_{ext} = 9 \times 10^{10}$ and the high-power coupler with $Q_{ext} = 5 \times 10^{7}$.

Stage	RF input method	HOM absorbers
HTC-1	On-axis coupler	none
HTC-2	High-power input coupler	none
HTC-3	High-power input coupler	2 SiC absorbers

Meeting gradient and quality factor specifications in each of these tests demonstrates the feasibility of the all the main systems needed for the MLC.

This paper details the final results of the three HTC experimental runs, focusing on the fundamental mode properties. Investigations of the higher-order mode spectrum are presented elsewhere.[7] We present quality factor measurements for all three tests and demonstrate that the cavity fabricated at Cornell exceeds design specifications.

METHODS

Cavity Preparation and Cryomodule Assembly

The construction[8] and preparation of the prototype main-linac 7-cell cavity, ERL 7.1, for HTC-1 has been described elsewhere.[5] An overview is presented here.

Following fabrication, ERL 7.1 received a 10 μm BCP, a 16 hour high-pressure rinse (HPR), was then cleanly assembled and baked at 120°C for 48 hours. The cavity was vertically tested, and found to exceed quality factor and gradient specifications. The cavity's Q vs E curve only showed mild medium field Q slope and reached 26 MV/m, limited by available RF power.

Following the successful vertical test, while maintaining a clean RF surface, the cavity was outfitted with a helium jacket, and installed in a horizontal test cryomodule for HTC-1. An axial RF coupler, (fundamental mode $Q_{ext} = 9 \times 10^{10}$) similar to the one used in the vertical test, was installed on the end of the cavity.

At the next stage of the tests, HTC-2, a high-power side mounted RF input coupler was added to the HTC-1 assembly. This antenna couples to the fundamental mode with $Q_{ext} = 4.5 \times 10^{7}$, so is strongly over coupled.

The final stage of the HTC tests, HTC-3, added beamline higher-order mode absorbers at each end of the cavity.

* Work supported by NSF Grants NSF DMR-0807731 and NSF PHY-1002467
† nrv5@cornell.edu

ISBN 978-3-95450-138-0

Copyright © 2013 CC-BY-3.0 and by the respective authors

FERMILAB MUCOOL TEST AREA CAVITY CONDITIONING CONTROL USING LABVIEW

D.W. Peterson, Fermi National Accelerator Laboratory*, Batavia, IL 60510, USA
Y. Torun, Illinois Institute of Technology, Chicago, IL 60616, USA

Abstract

Automated RF cavity conditioning controls have been implemented in the Fermilab MuCool Test Area using National Instruments LabVIEW. Display of RF parameters, cavity gradient and diagnostic signals are provided for real-time monitoring. Oscilloscope traces and operating parameters are logged automatically. Gradient ramping and cavity breakdown detection allow unattended operation. Key parameters are made available to the Fermilab ACNET system for viewing by users.

SYSTEM OVERVIEW

The MuCool Test Area (MTA) consists of a beamline stub and experimental hall off of the 400 MeV H- section of the Fermilab LINAC [1]. The hall contains power supplies and cryogenics for a 5T superconducting solenoid as well as RF feeds for high power 201 MHz and 805 MHz. Cavity conditioning is currently performed at 805 MHz at up to 13 MW of RF power [2][3][4].

The computer test system consists of a Dell GX620 computer running National Instruments (NI) LabVIEW 2012[5]. Waveforms are acquired with the NI PCI-5105 60 MS/s, 12-Bit, 8-Channel Digitizer/Oscilloscope card. A GPIB bus communicates with the HP E4400B RF Signal Generator, LeCroy 625Zi oscilloscope, and Tektronix DPO7104 oscilloscope.

Triggering of acquisitions is by the RF gate TTL signal from a master timing distribution module. Additional signals into the PCI digitizer card are a diode detected sample of the cavity RF probe signal, a sample of the waveguide reflected power, and an optional signal from a cavity photo detector.

SOFTWARE DESIGN

The MuCool Cavity Test software has evolved over more than six years of activity [6][7]. LabVIEW has been used throughout the process. This latest version has implemented some important new features:

- A simplified user interface with multiple floating front panel windows.
- Cavity waveform analysis during each pulse, including cavity breakdown detection.
- A new cavity tuning algorithm.
- Gradient ramping and breakdown recovery.
- Verbose log files.
- Cavity waveforms are periodically saved to disk and can be viewed later.
- Breakdown events are recorded along with data from preceding and following pulses.
- A few key parameters are available on the ACNET control system.

User Interface

LabVIEW routines are called virtual instruments (VIs). Each VI has a front panel for user interaction and a block diagram that defines the program execution. In the cavity conditioning system the main front panel provides a general view of the cavity signals and pulse status. It also provides a launch point for the cavity conditioning control VIs, such as tuner control and cavity waveform analysis. Figure 1 shows the general flow of the program. Figure 2 shows the layering of various VI front panels. During any given user interaction, the panel of interest can be brought to the foreground or minimized as needed. Additional VIs are available for the user to set the data logging interval and to enter comments into the log file.

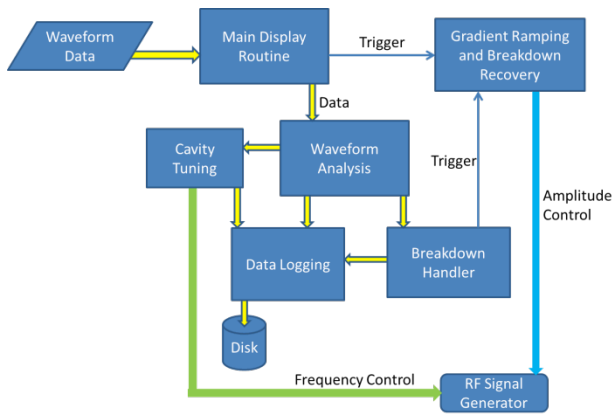


Figure 1: Simplified block diagram of the cavity conditioning program.

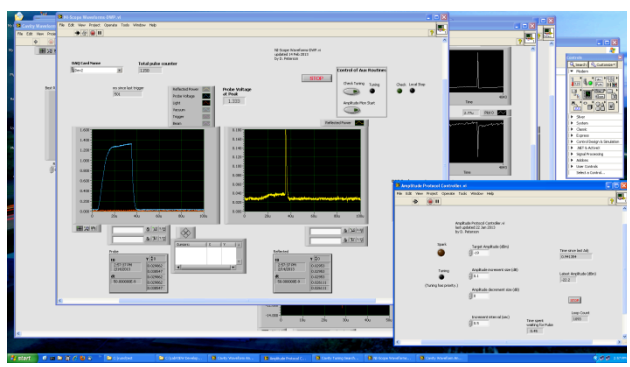


Figure 2: Screen capture of the overall user interface showing the layering of multiple VI front panels.

* Operated by Fermi Research Alliance, LLC, under Contract No. DE-AC02-07CH11359 with the United States Department of Energy

Copyright © 2013 CC-BY-3.0 and by the respective authors

SSR1 CRYOMODULE DESIGN FOR PXIE*

T. Nicol#, S. Cheban, M. Chen, M. Merio, Y. Orlov, D. Passarelli, T. Peterson, V. Poloubotko, O. Pronitchev, L. Ristori, I. Terechkine, Fermilab, Batavia, IL 60510, U.S.A,
P. Bhattacharyya, Variable Energy Cyclotron Centre, Kolkata, India

Abstract

Project X is a proposed proton accelerator complex intended to support Fermilab's role in intensity frontier research over the next several decades. It will replace the existing 40-year-old injector complex and add powerful new capabilities to support a large number of experiments in the energy range from 1 to 120 GeV.

Fermilab is planning a program of research and development aimed at testing of critical components. This program, known as the Project X Injector Experiment (PXIE), is being undertaken as a major element of the ongoing Project X R&D program.

PXIE contains two superconducting cavity cryomodules, one utilizing half-wave resonators (HWR), and the other, single spoke resonators (SSR). The first SSR cryomodule, known as SSR1 contains eight cavities and four solenoids in the following order: C–S–C–C–S–C–C–S–C–C–S–C, as well as active steering elements.

This paper describes the design of the SSR1 cryomodule and includes discussions of the system interfaces, vacuum vessel, magnetic and thermal shields, insulating and support systems, cavities, tuners, input couplers, focusing elements, and current leads.

INTRODUCTION

The SSR1 cryomodule will operate with continuous wave (CW) RF power and support peak currents of 5 mA chopped with varying patterns to yield an average beam current of 1 mA. The RF power per cavity at 1 mA average current and 2.2 MV accelerating voltage (β=0.22) should not exceed 4 KW with an overhead reserved for microphonics control.

The current beam optics design for Project X requires that the SSR1 cryomodule contains eight cavities and four solenoids in the following order: C–S–C–C–S–C–C–S–C–C–S–C. Horizontal and vertical dipole correctors are located inside each solenoid. A four-electrode beam position monitor (BPM) is located at each solenoid.

The intent is that this cryomodule has all external connections to the cryogenic, RF, and instrumentation systems made at removable junctions at the cryomodule itself. The only connection to the beamline is the beam pipe itself which will be terminated by "particle free" valves at both ends. Minimizing mean time between failure and repair and in-situ repair of some internal systems are important design considerations in the cryomodule design.

Figure 1 shows the linac layout including the location of the SSR1 cryomodule.

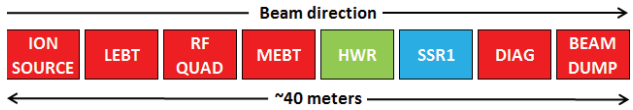


Figure 1: PXIE layout.

CRYOMODULE DESIGN

Eventually, Project X will require several different cryomodule designs for cavities operating at 162.5, 325, 650, and 1300 MHz. The SSR1 for PXIE is the first of these being developed at Fermilab. Details of individual cryomodule components are described below.

Cryogenic Systems and Vacuum Interfaces

There are two ways that cryogenic and vacuum systems are distributed to individual modules in superconducting magnets or cavity strings. Coarse segmentation refers to systems in which the cryogenic circuits and insulating vacuum inside individual cryostats are more or less continuous for long lengths, at least over the length of several cryomodules. Fine segmentation, refers to systems in which the insulating vacuum and the cryogenic circuits are confined to an individual cryomodule, the only connection between modules being the at beam tube. Fine segmentation is the configuration choice for Project X and PXIE cryomodules. Each individual vacuum vessel will be closed at both ends and the cryogenic circuits will be fed through bayonet connections at each cryomodule. Each cryomodule will have its own connection to the insulating vacuum pumping system. Also, each cryomodule will have its own 2 K heat exchanger and pressure relief line exiting near the middle of the module. This configuration provides flexibility in terms of cryomodule replacement and cooldown and warm-up times at the expense of requiring more individual cryogenic connections, cold-to-warm transitions at each end of each cryomodule, and extra space at each interconnect to close the beam tube.

Vacuum Vessel

The vacuum vessel serves to house all the cryomodule components in their as-installed positions, to provide a secure anchor to the tunnel floor, to insulate all cryogenic components in order to minimize heat load to 80 K, 4.5 K, and 2 K, as well as maintain the insulating vacuum. It is 1.219 m (48 inches) in diameter.

Magnetic Shield

Just inside the vacuum vessel, nearly in contact with the inner wall, is a magnetic shield to shield the cavities from the earth's field. Preliminary tests show that a 1.5 mm-thick mu-metal shield at room temperature reduces

* Supported by FRA under DOE Contract DE-AC02-07CH11359
# tnicol@fnal.gov

Copyright © 2013 CC-BY-3.0 and by the respective authors

ISBN 978-3-95450-138-0

ENERGY DEPOSITION IN MAGNETS AND SHIELDING OF THE TARGET SYSTEM OF A STAGED NEUTRINO FACTORY*

P. Snopok,† Illinois Institute of Technology, Chicago, Illinois 60616, USA
N. Souchlas, Particle Beam Lasers, Northridge, CA 91324, USA
H.G. Kirk, Brookhaven National Laboratory, Upton, NY 11973, USA
K.T. McDonald, Princeton University, Princeton, NJ 08544, USA
C.T. Rogers, Rutherford Appleton Laboratory, Chilton, Didcot, Oxon, UK
X. Ding, UCLA, Los Angeles, CA 90095, USA

Abstract

In the Neutrino Factory and Muon Collider muons are produced by firing high energy protons onto a target to produce pions. The pions decay to muons which are then accelerated. This method of pion production results in significant background from protons and electrons, which may result in heat deposition on superconducting materials and activation of the machine preventing manual handling. In this paper we discuss the design of a secondary particle handling system. The system comprises a solenoidal chicane that filters high momentum particles, followed by a proton absorber that reduces the energy of all particles, resulting in the rejection of low energy protons that pass through the solenoid chicane. We detail the design and optimization of the system and energy deposition and shielding analysis in MARS15(2012).

INTRODUCTION

The baseline target concept for a Muon Collider or a Neutrino Factory [1] is a free jet of mercury impacted by a 4-MW, 8-GeV proton beam at 50 Hz within a 20-T magnetic field [2]. The magnetic field is produced by a coaxial array of cryogenically cooled superconducting (SC) coils and water-cooled resistive magnets. The superconducting coils are protected from secondary radiation from the target by internal shielding of He-gas-cooled tungsten beads.

The design proton beam energy and power will be approached in stages [2], beginning with a 1-MW, 3-GeV proton beam. A solid carbon target can be used in the initial stage, and replaced with a mercury target module at a later stage when higher beam power is utilized.

The 20-T field on the target is reduced to 1.5 T in a tapering field profile over $\approx$ 5 m, beyond which is an $\approx$ 60-m-long, 1.5-T solenoidal Decay Channel where secondary pions decay to form the muon beam. Roughly 10% of the proton beam power is transported into the Decay Channel [3, 4], mainly via soft protons from breakup of target nuclei, and energetic protons scattered from the beam. These protons would be transported by the Decay Channel into subsequent components of the Muon Collider/Neutrino Factory Front End [5], the Buncher, Phase Rotator, and Ionization Cooling sections. To minimize radiation damage to these components, and to keep their activation low enough that hands-on maintenance is feasible, the secondary protons should be removed from the Decay Channel. This is to be accomplished via a bent-solenoid chicane [6], sketched in Fig.1, in which most proton of energy above 500 MeV are deflected out of the Decay Channel, and by a 10-cm-thick Be absorber which removes most protons of lower energy.

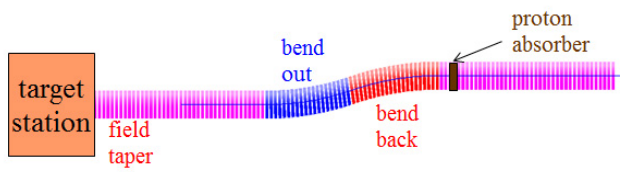


Figure 1: Sketch of the pion-production and Decay Channel, including a chicane to suppress energetic protons and an absorber for soft protons.

ENERGY DEPOSITION STUDIES

The higher-energy particles (mostly protons) which leave the beam in the chicane would pass through the coils of the bent solenoids unless the latter have adequate internal shielding. As for the superconducting coils of the target-system upstream of the chicane, we desire that the maximum energy deposition in the coils be less that 0.1 mW/g to permit an operational lifetime greater than 10 years of 10^7 s. This criterion is taken from studies [7] conducted for the ITER project.

To evaluate the amount of shielding required for the magnets of the Decay Channel chicane, we used a MARS15(2012) [8] simulation with field maps generated by G4beamline [9]. A preliminary version of these studies was reported in [10].

Given the complicated geometry of the chicane, adding tungsten shielding was not straightforward using only MARS extended geometry. However, a recently developed ROOT-based geometry framework [11] for MARS has made the task manageable with a wide variety of basic volumes provided by the ROOT TGeo module. The

*Work supported by the US DOE Contract No. DE-AC02-98CHI10886.
† psnopok@iit.edu

Copyright © 2013 CC-BY-3.0 and by the respective authors

OPTIMIZATION OF PARTICLE PRODUCTION FOR A STAGED NEUTRINO FACTORY*

X. Ding†, UCLA, Los Angeles, CA 90095, USA
H.G Kirk, Brookhaven National Laboratory, Upton, NY 11973, USA
K.T. McDonald, Princeton University, Princeton, NJ 08544, USA
J.J. Back, University of Warwick, Coventry CV4 7AL, UK

Abstract

A first stage of a Neutrino Factory based on muon beams might use a pulsed 3-GeV proton beam with 1-MW average power. We report on optimization of particle production by a carbon target inside a solenoid magnet for this scenario.

INTRODUCTION

The ultimate option for the final stage of a Neutrino Factory (NF) in the Muon Accelerator Program [1] is to use a 8-GeV (or more) proton beam of 4-MW average power interacting with a free-flowing mercury jet to create copious amounts of pions that are captured in a high-field solenoid magnet system. Two capture systems, referred to as IDS120h and IDS120j, as sketched in Fig. 1 have been used for the present study. Figure 2 shows that the axial magnetic field for both the IDS120h tapers adiabatically from 20 T and the IDS120j tapers from 15 T around the target to 1.5 T at the end of the target system. The inner radius of superconducting coils (SC) in the region surrounding the mercury jet target region is 120 cm to permit sufficient internal tungsten shielding for a 10-year operational lifetime of the SC coils against radiation damage [2].

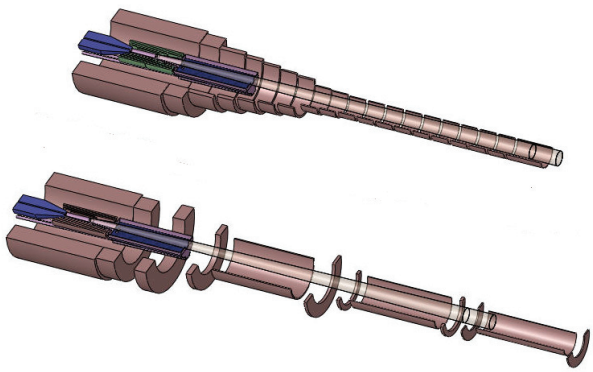


Figure 1: Lower half of the IDS120h (top) and IDS120j (bottom) target system.

A key feature in the staging scenarios [1] for a Neutrino Factory is initial operation of the proton driver at 3-GeV beam energy and 1-MW average beam power. As was noted in previous study, a radiation-cooled graphite target is a viable option for a 1-MW proton beam [3].

The particle production at the target depends on the target geometry as shown in Fig. 3, which illustrates the length and radius of the target, the radius of the proton beam, the orientation of the proton beam relative to the magnetic field, and the angle of the beam and target relative to each other (both of which lie in a vertical plane).

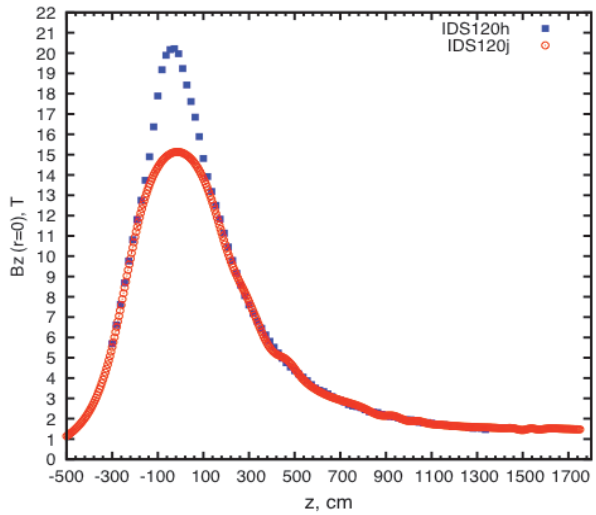


Figure 2: Longitudinal magnetic field along the solenoid axis of SC coils in the IDS120h (dashed line) and IDS120j (solid line) front-end channel.

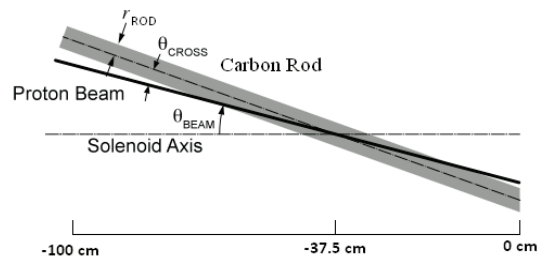


Figure 3: The carbon-target geometry. The proton beam and carbon target cross at z = -37.5 cm. The proton beam is launched at z = -100 cm.

In this paper, we report on the optimization of particle production (pion and muon yields) by a carbon target inside a solenoid magnet of IDS120h or IDS120j configuration. The pions and muons of interest for a Neutrino Factory are those with kinetic energies between 40 and 180 MeV, and we report rates of these at the transverse planes z = 0 m (downstream end of the beam/target interaction region) and z = 50 m.

We used four modes of the MARS15(2012) code [4] (denoted MARS15 below), as well as the FLUKA code [5]. The MARS15 modes used in this study were

*Work supported in part by US DOE Contract NO. DE-AC02-98CH110886.
†xding@bnl.gov

ISBN 978-3-95450-138-0

Copyright © 2013 CC-BY-3.0 and by the respective authors

A BUNCH LENGTH MONITOR FOR JLAB 12 GeV UPGRADE*

M. M. Ali, A. Freyberger, G. Krafft, J. Gubeli
Jefferson Lab, Newport News,VA 23606, USA

Abstract

A continuous non-invasive bunch length monitor for the 12 GeV upgrade of Jefferson Lab will be used to determine the bunch length of the beam. The measurement will be done at the fourth dipole of the injector chicane at 123 MeV using the coherent synchrotron light emitted from the dipole. The estimated bunch length is 333 fs. A vacuum chamber will be fabricated and a Radiabeam real time interferometer will be used. In this paper, background, the estimated calculations and the construction of the chamber will be discussed

INTRODUCTION

In recent days, many accelerators use short electron bunches. Measuring bunch length is important for operating and characterizing the accelerator. Bunch length measurement can be classified as invasive techniques such as zero-phasing [1] and deflecting cavity [2] or non-invasive techniques such as electro-optical sampling [3] and interferometers [4],[5]. In Jefferson Laboratory (JLab), we are going to measure the bunch length for the 12 Gev upgrade using the radiabeam Real time interferometer (RTI) [6]. The RTI is a solid state, compact and non-destructive. The experiment will be based on the Synchorotron light which will be emitted from the last bending magnet of the injector chicane. When the bunch length of the electron beam is shorter than the radiation wavelength, the electrons radiate in phase and the radiation power becomes proportional to the square of number of electrons per bunch (N^2) [7].

$$P_{total}(\lambda) = P(\lambda)[N + N(N-1)f(\lambda)] \quad (1)$$

where $P(\lambda)$ is the power radiated by single electron and $f(\lambda)$ is the form factor given by

$$f(\lambda) = |\int S(z) exp(\frac{-2\pi i z}{\lambda}) dz|^2 \quad (2)$$

where S(z) is the normalized longitudinal distribution function, z is the longitudinal position of the electrons and λ is the radiation wavelength. The form factor equals zero when the radiation is incoherent & equals one when the radiation is coherent.

COMPRESSION CALCULATION

In accelerator beam optics, the equation for an ellipse is normalized so ϵ the area of ellipse divided by π is on the right hand side. The general equation is given by

$$\gamma(\Delta\phi)^2 + 2\alpha(\Delta\phi)(\Delta E) + \beta(\Delta E)^2 = \epsilon \quad (3)$$

By compression, we desire to convert a horizontal upright ellipse to a tilted ellipse. The transformation array is given by

$$\begin{bmatrix} \Delta\phi' \\ \Delta E' \end{bmatrix} = \begin{bmatrix} M_{11} & M_{12} \\ M_{12} & M_{22} \end{bmatrix} \begin{bmatrix} \Delta\phi \\ \Delta E \end{bmatrix} \quad (4)$$

Equation(4) can be written as

$$\begin{bmatrix} \Delta\phi \\ \Delta E \end{bmatrix} = \begin{bmatrix} (M^{-1})_{11} & (M^{-1})_{12} \\ (M^{-1})_{12} & (M^{-1})_{22} \end{bmatrix} \begin{bmatrix} \Delta\phi' \\ \Delta E' \end{bmatrix} \quad (5)$$

Substituting by the values of it from eq.(5) into equation(3) and adding the terms of $(\Delta\phi')^2$, $(\Delta E')^2$ and $\Delta\phi'\Delta E'$, then the tilted ellipse twiss parameters will be

$$\gamma_1 = (M_{11}^{-1})^2\gamma_0 + 2(M_{11}^{-1})(M_{21}^{-1})\alpha_0 + (M_{21}^{-1})^2\beta_0 \quad (6)$$

$$\begin{aligned}\alpha_1 = {} & (M_{11}^{-1})(M_{12}^{-1})\gamma_0 \\ & + \left[(M_{11}^{-1})(M_{22}^{-1}) + (M_{12}^{-1})(M_{21}^{-1})\right]\alpha_0 \\ & + (M_{21}^{-1})(M_{22}^{-1})\beta_0 \end{aligned} \quad (7)$$

$$\beta_1 = (M_{12}^{-1})^2\gamma_0 + 2(M_{12}^{-1})(M_{22}^{-1})\alpha_0 + (M_{22}^{-1})^2\beta_0 \quad (8)$$

Assume that the longitudinal phase space distribution is a horizontal upright ellipse before compression with $\sigma_{\phi 0}$ and σ_{E0} as initial values for the bunch length and energy respectively. After the compression it will be $\sigma_{\phi,opt}$ and $\sigma_{E,opt}$ as shown in figure(1). let *M* be the magnification factor, so the bunch length will be compressed by a factor $\frac{1}{M}$ and to achieve the maximum minimum energy spread after compression, *M* must equal $\frac{\sigma_{\phi 0}}{\sigma_{\phi,opt}}$.

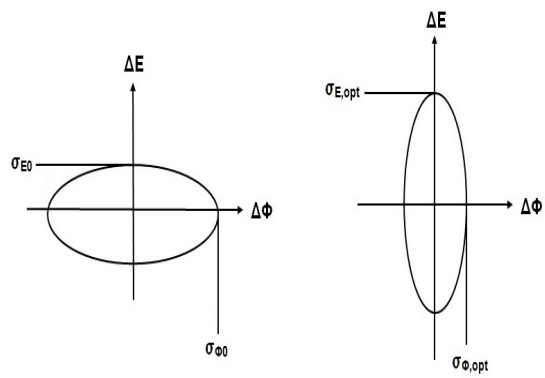


Figure 1: Phase space before & after compression.

* Work supported by the U.S. Department of energy under U.S. DOE Contract No. DE-AC05-06OR23177

Copyright © 2013 CC-BY-3.0 and by the respective authors

A HIGH-INTENSITY NEUTRON PRODUCTION SOURCE BASED ON ROTARY VALVING*

B. Rusnak, P. Fitsos, J. M. Hall, R. Souza, P. Peaslee, LLNL, Livermore, CA 94550

Abstract

As part of the effort to develop a fast neutron imaging capability at LLNL, a novel windowless deuterium gas target was developed for use with high-intensity pulse deuteron beams to generate neutrons via the $D(d,n)^3He$ reaction. The system was designed to create high-velocity, cross-flowing gas to minimize rarefaction due to beam heating in the target gas. The system also employs a unique gas beam stop to minimize knock-on neutrons from implanted deuterons over time. A prototype system employing rotary valving to generate and modulate gas flow, and a rotating aperture to minimize gas back streaming into the beamline vacuum system, was designed and built. Design details and supporting analyses of the gas dynamics of the system are presented.

INTRODUCTION

Investigating low-density features and materials that are heavily shielded within high-density materials is a challenge for x-ray techniques due to the attenuation of the x rays in the high-Z outer materials. Using the high penetrability of fast neutrons to create radiographic images is an alternative technique demonstrated to be very effective at creating cubic-millimeter-scale resolution images in heavily shielded low-Z test objects [1]. Technology development in the pursuit of creating a fast neutron imaging capability as a complimentary non-destructive evaluation (NDE) diagnostic to x rays has been on going at LLNL for the last decade [2].

Neutron Source Requirements

To achieve high penetrability in a variety of potential high Z materials, a 10-MeV neutron energy was chosen. In addition, this energy would not create short-lived activation products in air due to the $^{16}O(n,p)^{16}N$ reaction, which has a threshold above 10 MeV. The rapid decay of ^{16}N produces a background of high-energy gammas that are not only a radiological hazard but can degrade image resolution. To minimize image degradation due to an excess of scattered lower energy neutrons, the source neutrons also needed to be quasi-monoenergetic. For this application, having the energy width be approximately 10% was acceptable. To achieve nominal cubic-millimeter resolution, the source spot size needed to be at most 1.5 mm in diameter. These requirements placed significant constraints on the system and have strongly influenced the technology development path.

*This work performed under the auspices of the U. S. Department of Energy by Lawrence Livermore National Laboratory under contract DE-AC52-07NA27344.

Production Target Resolution Requirements

Production of quasi-monoenergetic high-energy neutrons can be readily achieved by impinging a deuteron ion beam onto a fixed length of high-pressure deuterium gas via the $D(d,n)^3He$ reaction. The maximum final neutron energy is determined by the incoming beam kinetic energy plus the Q value of the fusion reaction of 3.3 MeV, and the energy width of the neutron beam is directly related to the ion beam energy loss as the beam subtends the length gas cell. For this application, the deuterium gas cell is nominally 1.5 mm in diameter and 40 mm long. A deuteron beam of 7 MeV will be used to create ~10 MeV neutrons with a nominal 1 MeV energy width with 90% of the beam being in a forward directed.

Production Target Intensity Requirements

The neutron source intensity desired is 10^{11} n/sec/st at zero degrees. This was set by the goal of realizing a full 256-image computed tomographic (CT) reconstruction of a heavily shielded object in a nominal work shift. To achieve this intensity, 300 uA of average beam current will need to interact with nominally 3-bar deuterium gas at ambient temperature in the gas cell volume.

The small source spot size required for high-resolution imaging will create very high deposited power densities on any materials the beam interacts with, including any solid-material window typically used for making deuterium-gas neutron targets. This is due to the high energy loss of ion beams in solids at these low energies. Operating such a windowed source lends itself to DC accelerators as these provide the lowest possible average power for a given spot size in the window compared to pulsed beam structures. A great deal of experimentation over the years has shown that most windowed gas cells with millimeter-scale focal spots only achieve ~20–30 uA of average current before failure [3]. Given the factor of 10 higher beam currents needed to make the intensity requirements, an alternate approach to windowed gas cells was needed.

Another significant challenge due to the small spot size was stopping and disposing of the unreacted beam after the gas cell. For any solid high-Z stop, since the beam loses only 10% of its energy and does not appreciably enlarge when interacting with the deuterium gas, the beam stop needs to absorb 90% of the beam power over a stopping range of tens of microns. While grazing incident and rotating stop ideas were considered to prevent melting, there was concern that the density variations produced for the neutron beam would result in unwanted shadows on the radiographs, that the solid material would be damaged over time due to the pulsed nature of the

Copyright © 2013 CC-BY-3.0 and by the respective authors

ISBN 978-3-95450-138-0

ION-IRRADIATION RESPONSE OF GAFCHROMIC FILMS AND THEIR APPLICATION TO THE MEASUREMENT OF THE TRANSVERSE BEAM INTENSITY DISTRIBUTION

Yosuke Yuri, Tomohisa Ishizaka, Takahiro Yuyama, Ikuo Ishibori, and Susumu Okumura,
Takasaki Advanced Radiation Research Institute, Japan Atomic Energy Agency,
1233 Watanuki-machi, Takasaki, Gunma, Japan

Abstract

The response of radiochromic films, Gafchromic HD-810 and EBT2, was investigated using MeV/u-class proton and heavy-ion beams to apply the films to a measurement technique of the transverse beam intensity distribution at an azimuthally-varying-field cyclotron of Japan Atomic Energy Agency. The optical density of the irradiated films increased linearly with the particle fluence of the beam in a low-fluence region. The linear-response range of the fluence strongly depended on ion species as well as on the film type. By analyzing the film response to absorbed dose, it was found that the sensitivity of the film decreased for a beam with higher linear energy transfer. Based on the linear response of the Gafchromic film, we measured the relative intensity distribution of a large-area ion beam focused with multipole magnets. It was demonstrated that the present technique was useful for evaluation of the size and uniformity of the ion beam.

INTRODUCTION

Precise, handy evaluation of the transverse intensity distribution of a large-area ion beam with various ion species is required for materials and biological researches at the accelerator facility TIARA of Japan Atomic Energy Agency (JAEA). Radiochromic films, Gafchromic HD-810 and EBT2 (Ashland Inc.) [1], were, therefore, adopted as a possible measurement technique of the transverse beam intensity distribution. Various properties of the film, such as high spatial resolution (below 1 mm), large size (over 100 cm^2), thinness (for the penetration of a low-energy ion beam), and easy handling, are advantageous to the present purpose.

A beam irradiation experiment was carried out systematically in order to determine the applicability of Gafchromic films to various ion beams at the azimuthally-varying-field (AVF) cyclotron in TIARA [2]. Their response characteristics were investigated in a wide fluence range. Furthermore, the optical-density response of the films was analyzed in terms of linear energy transfer (LET) and dose [3]. Based on the linear-response characteristics of the films, we measured the relative intensity distribution of a large-area beam focused with multipole magnets [4] and evaluated the size and uniformity of the beam.

FLUENCE RESPONSE

HD-810 and EBT2 films were irradiated uniformly with 10-MeV ^{1}H, 13-MeV/u ^{40}Ar, and 3.5-MeV/u ^{129}Xe beams from the AVF cyclotron. The irradiated films were read at a resolution of 127 dpi with a general-purpose flat-bed scanner, LiDE50 (Canon Inc.), to digitize them into TIFF-formatted images with 16-bit RGB color intensity values. The film scanning was performed in more than one day after irradiation to prevent short-term color variation after irradiation. The optical density d_X in each color channel X (red, green, or blue) was determined from the equation: $d_X = \log_{10}((2^{16}\text{-}1)/I_X)$, where I_X is the 16-bit intensity value.

The response of HD-810 films irradiated with the ion beams is shown as a function of the fluence in Fig. 1. The increment of the optical density depends on the color channels for each ion species. The optical density obtained from the red channel is the largest at a given fluence in the linear-response region, while that from the blue channel is the least sensitive. This reflects that the film absorption sensitivity is higher in the longer wavelength region. Thus, the intensity distribution of the beam can be measured in a wide fluence range with a moderate signal-to-noise ratio by choosing an appropriate color channel of the scanned image. The range of the response curves shifted drastically toward a lower-fluence region for heavier-ion beams, as clearly seen in Fig. 1.

For EBT2, the optical density only of the green channel exhibited the linear response in a low-fluence range. The linear-response range is one order of magnitude lower than that of HD-810.

DOSE RESPONSE

The strong dependence of the film response on ion species, as shown in Fig. 1, is probably due to the difference of the LET in the active layer of the film. To see this, the particle fluence F is transformed into the dose D using the following relation: $D = c\,(LET/\rho)\,F$, where ρ is the density of the active layer of the film and c is a constant. The LETs of the beams at each layer of the films can be determined using SRIM code [5]. For example, the average LETs in the active layer (ρ = 1.08 g/cm^3) of HD-810 are 5.0×10^0, 1.2×10^3, and 1.1×10^4 keV/μm for the H, Ar, and Xe ion beams in the present case, respectively.

The response curves of the three ion species are replotted as a function of the average dose in the active layer of HD-810 in Fig. 2. For the proton beam, the linear response in Fig. 2(a) is similar to those observed in previous studies in spite of the differences in proton energy and scanners [6-8]. Although the linear-response dose range has been partially overlapped with the manufacturer's specifications (10~400 Gy) of the film in

Copyright © 2013 CC-BY-3.0 and by the respective authors

ISBN 978-3-95450-138-0

SIMULATION OF X-BAND LINAC NEUTRON SOURCE

K. Tagi#, K. Dobashi, T. Fujiwara, and M. Uesaka, University of Tokyo, Tokyo, Japan
M. Yamamoto, Accuthera Inc., Kawasaki, Japan

Abstract

In Tokyo University, there is a plan of development of electron linac neutron source because the research reactor "Yayoi" was decommissioned and a new neutron source is required. This linac will be introduced in the core of the reactor, so measurement of nuclear fuel materials can be expected. The application of this research is to measure more accurate nuclear data of some atomic fuel materials. It is necessary for analysing debris in Fukushima 1st nuclear power plant.

30 MeV X-band linac is used and neutrons are generated by interactions between bremsstrahlung x-rays and materials. In this research, the thermal electron gun, the buncher and the target for the linac are optimized for generating as many neutrons as possible. Uranium can be used as target materials, so high neutron flux was gained from the calculation.

INTRODUCTION

Nuclear data, neutron cross section, is important because it can be applied to development of new reactor and analysis of debris in Fukushima 1st nuclear power plant. However, this data, especially the data of nuclear fuel materials, such as U, Pu, and Am, is not so correct. Figure 1 shows experimental data of total cross section of Pu-239 [1]. You can understand the accuracy of the peak at 1 eV is low. In addition, measurement of this data hasn't been done recently.

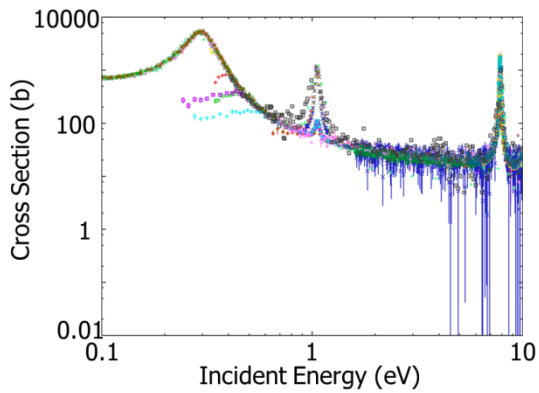


Figure 1: Experimental data of total cross section of Pu-239 [1].

Energy resolution is very important for the measurement of debris. The relation between time and energy is given by the equations

$$T[\mu s] = \frac{72.3L[\mathrm{m}]}{\sqrt{E[\mathrm{eV}]}}, \frac{\Delta E}{E} = -\frac{\Delta T}{T}. \quad (1)$$

For measuring data in 1% energy resolution, 1 μs is necessary when length of beam line is 5 m and beam energy is 10 eV, and 100 ns is necessary when length of beam line is 40 m and beam energy is 100 keV. So short pulse width is necessary for high energy resolution measurement. Pulse width of electron linac is much shorter than that of proton accelerator, so electron linac is suitable for our research.

PURPOSE

The purpose of my research is the development of electron linac driven neutron source for nuclear data measurement. Linac will be installed into the core of the "Yayoi" reactor which is now under decommissioning because in Yayoi, handling nuclear fuel materials are permitted. The reason why X-band linac is used for our neutron source is it enables us to set the accelerator in the core. But the klystron will be set out of the core.

COMPTON SCATTERING X-RAY SOURCE

For preliminary test of neutron source installation, 30 MeV X-band Linac has been tested. The Linac was originally designed for Compton scattering monochromatic X-ray source [2], shown in Figure 2. It is consisted of 3 MeV RF gun, alpha magnet, 30 MeV accelerator tube, and laser.

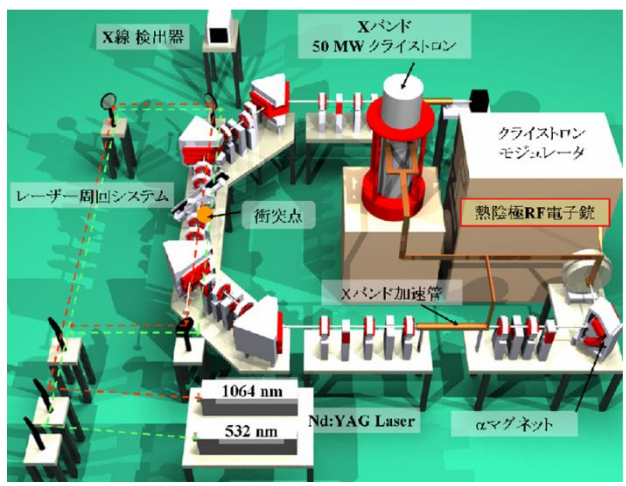


Figure 2: Compton scattering x-ray source.

In December 2012, the experiment of the RF electron gun was done. Figure 3 shows the current of it. The RF gun has is emittance, low current, and stability problem, so it is not suitable for neutron source.

Some part of this system, the RF source, the accelerator tube and the cooling system, will be used in the new neutron source. However, as I explained, RF gun is not suita-

Copyright © 2013 CC-BY-3.0 and by the respective authors

ISBN 978-3-95450-138-0

DIRECT DIAGNOSTIC TECHNIQUE FOR A HIGH INTENSITY LASER BASED ON LASER COMPTON SCATTERING*

R. Sato†, Y. Yoshida, K. Nonomura, K. Sakaue, A. Endo, M. Washio
Waseda University, Tokyo, Japan

Abstract

In laser produced plasma (LPP) EUV source, high intensity pulse CO_2 laser is essential for plasma generation. To achieve high conversion efficiency and stable EUV power, we would like to measure laser profile in collision point and make feedback system. There is no way to directly measure a high intensity laser profile at the focus point. Therefore, we have been developing laser profiler based on laser Compton scattering. Laser profile can be measured by scanning focused electron beam while measuring Compton scattering signal. We use compact electron accelerator based on Cs-Te photocathode RF gun at Waseda university. Electron beam is focused by solenoid lens. We simulated beam size using GPT, obtained beam size of 10 μm rms. We measured beam size by Gafchromic film HD-810. We have succeeded in observing minimum beam size of about 20 μm rms. In this conference, we will report result of simulation, beam size measurements, and the present progress.

INTORODUCTION

Extreme ultraviolet lithography (EUVL) is the next generation lithography for integrated circuit fabrication at 22nm half pitch mode [1]. In EUVL, several 100W EUV light is based on Sn plasma produced by CO_2 laser. CO_2 laser is required more than 100 kHz repetition rate, 200 mJ, 100 μm spot size and 10 ns pulse duration. To achieve high conversion efficiency and stable EUV power, we would like to measure laser profile in collision point and make feedback system. However, there is no way to directly measure such high power laser profile.

We have been developing laser profiler based on laser Compton scattering (LCS). Laser profile can be measured by scanning focused electron beam while measuring Compton scattering signal. If both laser and electron beam have a gaussian distribution, the observed profile of Compton signal as a function of electron position is a gaussian distribution. Observed rms width can be written down as;

$$\sigma = \sqrt{\sigma_{\mathrm{laser}}^2 + \sigma_{\mathrm{electron}}^2} \qquad (1)$$

where σ_{laser} is the laser beam size, $\sigma_{\mathrm{electron}}$ is the electron beam size. If the electron beam size is much smaller than that of laser, the observed profile would be equivalent to the laser profile. To scan electron beam from various direction and reconstruct image used CT technique, we can obtain 2D laser profile.

Focused electron beam is a key issue of this method. The more electron beam is focused, the higher resolution laser profile we can obtain. To achieve small beam spot, we use low emittance electron accelerator and special design solenoid lens. In this paper, we discuss GPT simulation and results of beam size measurement by Gafchromic film.

ACCELERATOR SYSTEMS

A photocathode rf gun is one of the most high quality electron source. Because of high gradient electric field on the cathode, it can generate small emittance beam. At Waseda university, we have been performed the high quality electron beam generation and applied research experiments, such as laser Compton soft-Xray generation [2] and pulse radiolysis [3].

The cavity structure is based on the design of the BNL Type IV, which have 1.6 cell structure. The rf frequency is 2856 MHz. The cavity is able to produce low emittance beam with 5 MeV beam energy. We use Cs-Te photocathode which have a high quantum efficiency and achieve 1 nC / bunch. The seed laser is Nd:YLF mode lock oscillator with 119 MHz frequency. We use LN intensity modulator to pick pulse train, it chooses the number of pulses from 1 pulse to 100 pulses. The pulse trains are amplified by Yb fiber amplifier and LD pumped amplifier 4 pass system. After two amplifications, IR pulses are converted to UV pulses by two nonlinear doubling crystals.

The experiment set up is shown in Fig. 1. There are beam diagnostic instruments. A current transfer measure beam charge and pulse train stability. Alumina fluorescent plate (Demarquest Co.) beam profile monitor is located behind solenoid magnets. 45 degree bending magnet is used for energy measurement. Our accelerator system is characterized it's small structure, the total length is less than 3 m.

For this experiment, we designed new solenoid lens. The

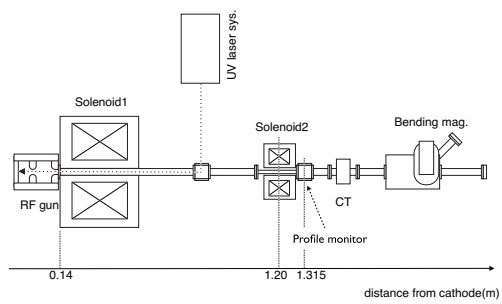


Figure 1: Schematic design of Waseda beam line.

* Work supported by NEDO(New Energy and Industrial Technology Development Organization).
† wase-nishicab61@akane.waseda.jp

Copyright © 2013 CC-BY-3.0 and by the respective authors

CONCEPTUAL PHYSICS DESIGN FOR THE CHINA-ADS LINAC

J.Y. Tang*, P. Cheng, H.P. Geng, Z. Guo, Z.H. Li, C. Meng, H.F. Ouyang, S.L. Pei, B. Sun, J.L. Sun, F. Yan, C. Zhang, Z. Yang, IHEP, CAS, Beijing 100049, China
Y. He, Y. Yang, IMP, CAS, Lanzhou 730000, China

Abstract

The China-ADS project was launched in 2011 to pursue the R&D on key technologies towards a final demonstration facility on ADS with the capability of more than 1000 MW thermal power. The driver linac is defined to be 1.5 GeV in energy, 10 mA in current and in CW operation mode. It employs the superconducting structures except the RFQs. To meet the extremely high reliability and availability, the linac is designed with much installed margin and fault tolerance, including hot-spare injectors and local compensation method for key element failures. The accelerator complex consists of two parallel 10-MeV injectors, a joint medium-energy beam transport line, a main linac and a high-energy beam transport line. The conceptual physics design including beam dynamics studies with multiparticle simulations is presented here.

INTRODUCTION

The C-ADS (or China-ADS) project is a strategic plan to solve the nuclear waste problem and the resource problem for nuclear power plants in China. With its long-term planning, the project will be conducted in three or four major phases with the final goal to build a demo transmutation facility by 2032.

The C-ADS accelerator complex is a large CW proton linac consisting of several sections and uses superconducting (SC) acceleration structures except the RFQs, which is under developing in collaboration at IHEP and IMP. The main design specifications for the proton beam at the ultimate stage are shown in Table 1.

Table 1: Specifications for the C-ADS Linac

Particle	Proton	Unit
Energy	1.5	GeV
Current	10	mA
Beam power	15	MW
RF frequency	(162.5)/325/650	MHz
Duty factor	100	%
Beam Loss	<1	W/m
Beam trips/year[1]	<25000 <2500 <25	1s<t<10s 10s<t<5m t>5m

DESIGN CONSIDERATIONS

The C-ADS linac is designed to have very high beam power and very high reliability, which surpasses those of the existing proton linacs by far. However, several proposed CW proton/deuteron linac projects such as Project-X [1-2], EFIT or MYRRHA [3], IFMIF [4] and EURISOL [5], etc. are good models for the physics design and technical design of the accelerator. In addition, some pulsed high power proton linacs and some CW heavy ion linacs using SC cavities also serve as good reference examples. Although most of the design philosophy for the linac has been addressed by previous literatures, we still list the main principles here: 1) the whole linac consists of SC cavities except the RFQ which is room-temperature; 2) installed redundancy for all the parts of the accelerator will be applied; 3) as low as possible beam losses along the linac, with an upper limit of 1 W/m in warm sections and even lower in cold sections; 4) the acceleration efficiency and the number of cavity types will be balanced; 5) different transverse focusing structures are used to follow the acceleration structures and beam properties in different acceleration sections; 6) tune depression will be controlled to stay in the emittance dominated regime preferably; 7) the growths in both the rms emittance and halo emittance should be controlled strictly, and the ratio of acceptance and rms emittance should be kept large to avoid severe beam beams; 8) the phase advance per period is controlled below 90° to avoid parametric resonances.

DIFFERENT ACCELERATION SECTIONS

The linac consists of two injectors, a special medium-energy beam transfer line (MEBT2), and the main linac, as shown in Figure 1. Two identical injectors will be operated in the mode of one as the hot-spare of the other to provide quick switch in case of failure of the one in delivering beam to the main linac, which is considered crucial to achieve very high reliability of the whole accelerator. MEBT2 is to transport and match the beam from either of the two injectors to the main linac. However, in the early developing phase two different approaches of injector will be developed in parallel by two different teams. At a later phase, a decision based on the R&D development will be made about which injector scheme will be used in the future phase. The main linac section that consists of different acceleration sections will be developed in phases.

*tangjy@ihep.ac.cn

Copyright © 2013 CC-BY-3.0 and by the respective authors

ISBN 978-3-95450-138-0

THZ BAND HORN ANTENNAS DESIGN

T.V. Bondarenko, S.M. Polozov, A.Yu. Smirnov,
National Research Nuclear University MEPhI, Moscow, Russia

Abstract

The report is concerned with the development of the irradiating antennas for THz radiation source. The THz radiation is irradiated by relativistic high brightness electron bunch traveling through the Cherenkov decelerating capillary channel [1]. Irradiation systems are built as horn antennas type with circular and rectangular cross-sections. Irradiating antennas are constructed directly to the open end of the capillary channel and are used for the THz radiation directivity enhancement after passing through the capillary output. The investigation of the horns directivities were performed using the far-field analysis of the emerging radiation. The antennas were also investigated to perform low values of the reflected power.

INTRODUCTION

High-power THz radiation source based on photoinjector and decelerating capillary channel is now one of the most discussable compact facilities providing monochromatic THz radiation of power high enough to be used for cargo introscopy [2].

Facility is based on two main parts: accelerating structure and decelerating radiating channel. Capillary is placed right after the accelerating structures and is made of copper with either dielectric coated inner surface or corrugated surface.

For effective irradiation of THz radiation from the capillary structure the high values of capillary RF matching with the open space and high directivity values are out to be fulfilled. Capillary that irradiates in the free space with its open end doesn't provide enough directivity that can be seen from the angular pattern shown in the Fig. 1. To enhance the directivity of the radiation the open end of the capillary must be attached to the irradiating antenna. As the capillary has a circular cross-section the optimal geometry of the horn is based on the horn antenna that is directly fitted to the metal parts of the capillary and is fabricated with it as a whole entity.

Main parameters of the antenna are the directivity, angle between the longitudinal axis and main lobe, main lobe angular width and horn power reflection coefficient. Angular width of the main lobe is the parameter defining the distance between two directions of the lobe with 3dB power decay between them. Important parameter is also bandwidth of the horn that is defined as frequency difference between horn working frequency (resonant frequency of the capillary) and the frequency of horn -20dB power reflection level.

There are several different types of horn designs. This article is concerned with the modelling of the horns with circular and rectangular cross sections. All antennas are discussed for the metal Cherenkov irradiating capillary with 300 μm aperture and 31 μm polytetrafluoroethylene coating on the metal surface. Resonant frequency of this type of capillary is 0.96 THz. Work band on the level of -3 dB of the maximal power transmission is 3.2%.

CIRCULAR HORN ANTENNA

Circular antenna is the most conventional type of antenna for such devices (Fig. 2). The model of the horn was built and calculated using the CST Microwave Studio [3]. To define the maximum effective horn parameters the electrodynamics characteristics were studied while varying the horn geometrical parameters. The opening angle was varied while the horn length was kept L=1 mm (fig. 3). After that with the angle equal 14.5 degrees (that corresponds to maximal directivity of the horn) length of the horn was varied (Fig. 3). The investigations were held in the frequency band of 0.7-1.1 THz.

The graphs in the Fig. 3 show that the increase of the horn opening angle decreases its directivity and bandwidth. Main lobe width is increased at the same time. Variation of the horn length leads to the enhancement of the directivity at the 4.8 mm length and then results in its reduction with higher values of the parameter. Inverse relationships are specific for main lobe direction and angular width.

Minimum of the reflection coefficient is defined at the 1 THz region for all discussed geometries. Opening angle enhancement leads to growth of the reflection on the resonant frequency value and bandwidth of the horn decreases. The frequency dependent values of the power reflection coefficients for varying geometrical sizes are depicted in the Fig. 4.

For more clearance the visualization of the horn directivity the directional diagrams are depicted in the Fig. 5. The diagrams are shown for the maximal directivity case of the horn antenna (length of the horn is 4.8 mm and 14.5 degrees opening angle). For maximal values of the mail lobe angular width the same graphs are shown in the Fig. 6. Antenna has corresponding parameters: 4.8 mm length and 57 degrees opening angle.

Characters of all dependences confirm the convention model of horn antennas modeling for lower frequency ranges.

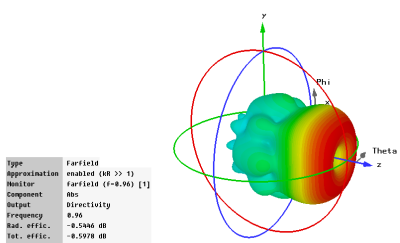


Figure 1: Directivity diagram of the open capillary end.

Copyright © 2013 CC-BY-3.0 and by the respective authors

ANALYSIS OF PROPAGATED EFFECTS IN PROTON DEPTH-DOSE DISTRIBUTION CURVES DUE TO INITIAL BEAM ENERGY SPREAD

S. Zalel*, J.F. Piech, UROP students, Imperial College London
M. Aslaninejad, P. A. Posocco#, Imperial College London

Abstract

Proton therapy treatment planning uses depth-dose distribution curves of single initial beam energies to create Spread spread Out Bragg Peaks (SOBP). These are used to target specific regions in the body. However, the initial energy spread of the beams leads to an uncertainty in beam energy, affecting the dose distribution. In this paper, previous work (M. Aslaninejad et al., 2011: 189–196) on the depth-dose distribution of proton beams using inelastic-collision cross sections of liquid water is extended into use with chromatic beams. The effect of the initial energy spread on depth-dose distribution curves, the distal dose and the SOBP are discussed. Limits on beam energy spread are suggested.

INTRODUCTION

Proton therapy is advantageous over conventional radiation therapy as particles lose most of their energy at a particular location, depending on their initial energy. This effect is usually represented by means of depth-dose distribution curves. These are characterised by the Bragg Peak (BP) where the relative dose reaches a sharp maximum. As the range and shape of the BP depends on initial beam energy, the energy spread of protons within a beam distorts the theoretical BP and potentially compromises the effectiveness of the treatment. In this paper we extend previous work to account for the energy spread within a therapeutic proton beam.

Depth-dose distribution curves are a useful tool indicating which region will be most affected by incoming radiation. In the code developed in [1] depth-dose distribution curves in water are created by modelling proton beams using a combination of semi-empirical models and the Bethe-Bloch theory. At energies below 1 MeV the cross section is defined by a combination of semi-empirical models, such as the model of ionization processes by Rudd et al.. The stopping cross section gives information on the energy transferred per unit length as a function of particle energy. The total stopping cross section is the sum of the stopping cross sections of all interactions contributing to energy. Nuclear processes are disregarded.

The Bethe-Bloch formula is a good approximation for calculating energy lost per distance travelled for fast charged particles (i.e. with energies higher than 1MeV). Equation 1 shows the Bethe-Bloch formula according to Groom and Klein [2]:

$$\frac{1}{\rho}\frac{dE}{dx} = Kz^2\frac{Z}{A}\frac{1}{\beta^2}\left[\frac{1}{2}\ln\frac{2m_e c^2\beta^2\gamma^2 T_{max}}{I^2} - \beta^2 - \frac{\delta(\beta\gamma)}{2}\right], \quad (1)$$

where z it the charge of the incident particle, Z and A are the atomic number and the atomic mass of the absorber, respectively. I is the mean excitation energy, $\delta(\beta\gamma)$ is the density effect correction to ionisation energy loss and β and c are the usual relativistic factors. T_{max} is the maximum kinetic energy which can be imparted to a free electron in a single collision.

Other considerations that were taken into account in the code are:

- Straggling model: range travelled by individual protons is governed by a Gaussian distribution.
- Fragmentation: effectively reduced fluence attributed to proton decay.

These lead to the broad-beam depth-dose curve characterised by increased peak width and reduced peak height. Multiple scattering was also considered; this changes the shape of the depth-distribution by changing the ratio of peak to entrance dose.

EXTENSION TO CHROMATIC BEAMS

In the discussion above proton beams of single defined energies are used. However, real beams are characterised by an energy spread. This is due to individual characteristics of the accelerator, beam transport, and collimation system [3]. The width of the initial energy spectrum is expressed as a percentage error in the initial beam energy and is estimated in the order of magnitude of ±1% [4]. In this paper a superposition of Gaussian probability weighted monochromatic beams was used to simulate chromatic depth-dose distribution curves and values of up to 2% sigma have been used for several initial beam energies. This analytical method is a good approximation for the peak itself, however the shape of the tail is affected largely by other factors and may vary further from the model used [3].

The Effect of Energy Spread on the Bragg Peak

The depth dose distributions curves created for single proton Bragg peaks as function of the initial beam energy spread were used to study the effect of the chromatic beam on the treatment. The depth dose distributions of the proton beams were modelled along a 1-D axis being the path of the proton. Effects of 3-D scattering were not included.

Depth-dose distribution curves of varying initial energy spreads were produced for 70, 100, 150, 200 and 250 MeV to cover the entire range of energies used for treatment, with energy spreads of 0.1%, 0.2%, 0.5%, 1% and 2% sigma.

Figure 1 shows the effects of increasing energy spread on the BP for a 200 MeV proton beam. Due to the

*Supported by the Anglo Israel Association
#p.posocco@imperial.ac.uk

Copyright © 2013 CC-BY-3.0 and by the respective authors

ISBN 978-3-95450-138-0

A NOVEL SOLUTION FOR FFAG PROTON GANTRIES

J. Pasternak*, Imperial College London / RAL, STFC
P.R.N. Holland, G.W. Walton, UROP students, Imperial College London
M. Aslaninejad, Imperial College London
P. A. Posocco, Imperial College London / The Cockroft Institute / Gunnar Nilssons Cancerstiftelse

Abstract

In the recent years FFAG gantries have been studied for medical applications, but none has so far been realised. The FFAG solution would reduce the complexity of beam line set-up, its weight and therefore the cost of the rotating support, in particular for heavy ions. The Imperial College London is using the experience gained in the Pamela Project and in the design and commissioning of EMMA to work on a solution of a non-scaling FFAG gantry, which could potentially fulfil the full requirements for the spot scanning - parallel beam treatment technique, and provides an easy interface to the upstream accelerator. The preliminary results will be presented in this paper.

INTRODUCTION

The research on Fixed Field Alternating Gradient (FFAG) accelerators was restarted after long period of silence in recent years, which triggered the successful construction and operation of several scaling machines in Japan and the world's first linear Non-Scaling one - EMMA [1] in the UK. Following these vigorous progress it was proposed to apply the FFAG principle for next generation hadron therapy machines [2] aiming to reduce the cost of treatment by utilising the very strong focusing and high repetition rate offered by FFAGs to make the machine dimensions more compact and the treatment time shorter.

In modern hadron therapy applications it is preferred to use the gantry as the final beam transport system, which allows to precisely vary the beam angle at the patient in the large range simultaneously allowing to carefully control the beam spot size and position in the spot scanning. Although the existing gantry solutions (non-FFAG type) have been constructed and are in operation, they consist of room temperature iron magnet system with a very large weight and overall dimensions, which is a significant fraction of the total cost of the facility.

FFAG solutions for proton and carbon gantries have been proposed [2, 3], which allow to greatly reduce the size and weight of the gantry by using superconducting magnets. Stable particle orbits exist in such gantry for the broad momentum range eliminating a need for magnets' ramp or requiring to ramp only between small number of operational regimes, which offers an opportunity to reduce the treatment time. Thus FFAG gantries will contribute in decreasing the cost of modern hadron therapy facilities. It may be fed by any conventional medical accelerator including cyclotron or by a future medical FFAG.

* j.pasternak@imperial.ac.uk

FFAG gantries studied so far were based either on linear non-scaling magnets, scaling ones or such that break only partially the scaling law. This paper describes a novel gantry type using nonlinear non-scaling FFAG magnets, which explicitly violates the scaling law maintaining the zero-chromatic condition.

NONLINEAR NON-SCALING FFAG GANTRY DESIGN

Requirements and Assumptions

As the starting point of the study the classical shape of the gantry is assumed, in which the beam is firstly deflected outwards from the common incoming beam/patient axis, which also serves as gantry axis of rotation. Secondly the beam is deflected in opposite direction cancelling the initial negative angle and finally bending by the final 90° pointing at the patient. If this configuration is rotated using the incoming beam as the axis of rotation, it allows for the full flexibility in the choice of the treatment angle in a very broad angular range.

As the goal a gantry for proton therapy was chosen as it allows an easy comparison with other existing gantries and can be further extrapolated to a carbon case. It was also decided that the operation energy range of 100-200 MeV is potentially interesting especially for applications in paediatrics and is also quite ambitious at the start.

To simplify the orbit matching in the presence of rotation for different energies, zero dispersion condition is preferred at the input of the gantry. To avoid any correlations between the beam position and energy, zero dispersion at the patient is also required. The identity matrix is needed as the total betatron transfer map through the gantry, which will allow to set the particular condition required for treatment downstream the gantry in the non-rotating part and transparently reproduce it at the patient position simplifying the gantry operation.

Linear Optics Design

In order to minimize the orbit excursion in an FFAG many short cells are required with a very strong focusing. As the compromise between the orbit excursion, the maximum value of the magnetic field and space constraints in the magnet design, the design of the first bend consists of 8 identical FDF triplet cells, with the total deflection angle of -72°. As the preliminary studies showed that zero dispersion is preferred also at the end of the negative bend section as it minimises the orbit distortion downstream, the phase advance of $\pi/2$ rad per

Copyright © 2013 CC-BY-3.0 and by the respective authors

ISBN 978-3-95450-138-0

A READY-TO-USE APPLICATION OF LASER-PLASMA ACCELERATORS USING GABOR LENSES

R.M. Nichols*, UROP student, Imperial College London
M. Aslaninejad, N.P. Dover#, Z. Najmudin, J.K. Pozimski, Imperial College London
P. A. Posocco, Imperial College London / The Cockcroft Institute / Gunnar Nilssons Cancerstiftelse

Abstract

A realistic particle distribution for a proton beam generated by laser-plasma interaction is required in order to simulate its transport through a Gabor lens system intended for use in radiobiology experiments. A stack of radiochromic films were exposed to a laser-driven proton beam of 25 MeV at the Vulcan Petawatt Experiment at Rutherford Lab and subsequently analysed to find the energy deposited per film and therefore the energy spectrum of the beam. Combined with the information on the radial profile of the dose in the films, it was possible to generate an idealised particle distribution. This distribution was sampled and used as a realistic proton source in a simulation through the Gabor lens system published at IPAC'13, scaled down to 4 MeV to fit the radiobiology experiment requirements.

INTRODUCTION

An intense beam of ions is generated when a solid target, several microns thick, is irradiated by a high intensity laser pulse [eg. 1, 2]. In such a scheme, the laser ionises the surface of the target and accelerates electrons to high energies. These electrons travel through the target and upon exiting the target result in the generation of huge quasi-static electric fields, due to charge separation. This field accelerates the ions at the target surface, which are often protons, carbon and oxygen ions from the typical hydrocarbon layer on the target surface [3, 4].

Ion beams accelerated in this way have attracted interest in recent years due to their potential for use in radiotherapy and a number of other applications [5]. There has been considerable investment in recent years into hadron therapy, which can provide more targeted therapy for deep-seated tumours than conventional x-ray or electron radiotherapy. Current systems for proton therapy are extremely costly and laser-accelerated beams could offer in the long-term simple and compact treatment devices and therefore significantly reduce treatment costs. Meanwhile, while still requiring further development before being suitable for treatment, they are sufficient to allow biologists to study the effect particles produce in cells, and are already far more convenient than electrostatic accelerators commonly used for this purpose. Experimental radiobiology with particles is an area that has been only partially explored and with a strong impact on the modalities of particles delivery to patients and treatment outcomes.

We believe that laser-plasma accelerators of the current generation combined with a novel optical system based on Gabor lenses [6] is an ideal candidate for this application. If proven effective, Gabor lenses can be scaled to higher energies and thus easily applied to future laser-driven particle sources in a clinical environment.

THE PARTICLE DISTRIBUTION

The Vulcan Petawatt laser was focused to a focal spot of 4 μm (FWHM) at 45 angle of incidence onto a 100 μm thick Al target. The resultant accelerated proton beam was diagnosed using a film stack positioned 7.4 cm from the target. The stack itself is 0.66 cm thick and consisted of Al shielding followed by layers of RadioChromic Films, which darken when exposed to dose, alternated with spacers of either Fe or Al.

The set of RCFs (data taken in 2012) were scanned and the intensity value for each pixel was converted to dose by calibrating with pixel intensity values of images of RCFs exposed to known doses of radiation.

Calibration of the Films

Calibration images were obtained by scanning RCFs that had been exposed in three separate experiments when films were exposed to known doses of radiation using the Scanditronix MC 40 cyclotron at the University of Birmingham. In the area selected, the median pixel value is found for each of the colour channels of the image. A median is used rather than a mean as it will not be affected by outliers (caused by, for example, dust on the film). These values are then compared to the dose known to have irradiated the calibration films.

The results of the calibration are shown in Figure 1, in which the pixel intensity values are plotted as function of their known doses. The red channel is more sensitive than the green or blue channels and so it reaches its saturation point at a much lower dose. Therefore the red channel was used for the lower doses and the blue channel for the higher doses. The calibration switch point between the two channels was chosen at 200 Gy.

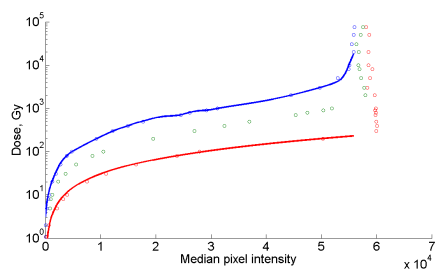


Figure 1: Calibration of how the red, green and blue channels of images of RCF respond to irradiation.

* Supported by the UK Engineering and Physics Research Council
# nicholas.dover08@imperial.ac.uk

ISBN 978-3-95450-138-0

Copyright © 2013 CC-BY-3.0 and by the respective authors

CHARACTERISATION OF NITROGEN CLUSTERS AND GAS JET TARGETS UNDER VARIED NOZZLE GEOMETRIES

C. Hughes, N.P. Dover*, Z. Najmudin, P.A. Posocco, Imperial College London

Abstract

Gas jets are widely used for targets in laser-plasma driven article acceleration experiments. Optimising the mechanism requires tailored gas jet density profiles. Therefore, high density gas profiles have been investigated and characterised using different types of nozzles: sonic, supersonic, slit and supersonic slit. Gas jet profile optimisation was examined using nozzles of different diameters while varying gas pressure between 0 and 100 bar and valve opening duration. Gas jets produced by the nozzles were characterised using an optical probe laser. The gas jet density profile was measured through interferometry which was captured using a CCD camera. A second camera was used to record the Rayleigh scattering from the laser to confirm the presence clustering in nitrogen at high pressures.

INTRODUCTION

Recent research into laser-plasma ion acceleration has demonstrated beams with various characteristics from a number of different target types. The use of solid targets presented two widely investigated mechanisms: target normal sheath acceleration (TNSA) and radiation pressure acceleration (RPA) [1]. For applications that require high energies and monoenergetic beams, RPA is seen as the more desirable mechanism for acceleration due to the characteristics of the accelerated beams, though has been difficult to achieve in experiments [2][3]. Solid targets can add complications to the ion source as they require very high laser contrast to avoid their destruction, create debris, result in multispecies beams, and may cause difficulty for high repetition rate systems for applications.

Gas jet targets have been seen to offer a solution to these issues. Gas jet targets have been widely used for laser wakefield electron acceleration [4], and some more recent studies for ion acceleration. For example, recent experiments have demonstrated monoenergetic proton beams from the interaction of a CO2 laser with gas jets [5], generated from the laser radiation pressure acting on a low density, but opaque, plasma. Interest in gas targets has led to the development and subsequent optimisation. The acceleration mechanism can be optimised via tailored gas jet density profiles through altering nozzle geometry (Figure 1).

Under high pressure and specific conditions a range of gases have been found to form small grouping of atoms which are loosely bound to each other through their Van der Waals forces. These are known as gas clusters. The formation of clustering in supersonic gas jets is a concept that has been observed for many years, along with their dependency on pressure and nozzle size [6]. Clustering gases are of interest in targetry mainly in relation to high intensity laser-plasma interaction as they provide very high absorption of laser energy [7]. It has also been shown that high pressure gas clustering can be utilised as targets in ion acceleration [8]. More recently, an experiment has been reported investigating a selection of nozzle geometries: sonic, supersonic, slit and supersonic slit (Figure 2).

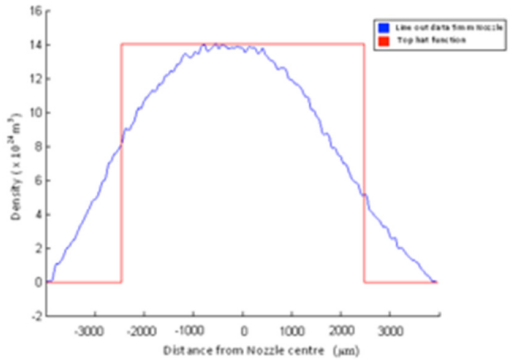


Figure 1: Ideal gas jet would possess a density profile that follows the shape of a top hat function. Actual jets do not produce such a steep density gradient.

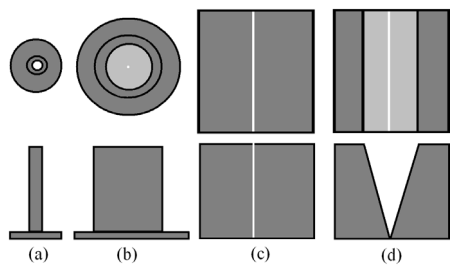


Figure 2: Examples of nozzle geometries for (a) sonic nozzle (b) conical nozzle (c) slit nozzle (d) supersonic slit nozzle.

EXPERIMENTAL SET-UP

Nozzles

A selection of nozzles was used to produce gas jets bearing different characteristics due to their geometries. Additionally, the effect of placing an insulator before the nozzles was investigated (Figure 3). These included a 10 mm diameter conical supersonic nozzle with an entrance aperture of 2 mm, a 2 mm diameter conical sonic nozzle and a slit nozzle. The slit nozzle was shaped with pliers from a 2 mm sonic nozzle to approximate the properties for this geometry. The slit dimensions were verified the CCD camera. This set up was found to be able to observe clusters in argon gas through a probing laser and the resulting Rayleigh scattering [9].

* nicholas.dover08@imperial.ac.uk

Copyright © 2013 CC-BY-3.0 and by the respective authors

CONSTRUCTION AND TESTING OF THE DUAL SLOT RESONANCE LINAC*

N. Barov, D. Newsham, R.H. Miller, FAR-TECH, Inc., San Diego, CA 92121

Abstract

The dual slot resonance (DSR) linac is a novel method of providing enhanced coupling to a coupled cavity linac system, resulting in very strong coupling. For the 11-cell, 2856 MHz structure described here, the acceleration mode bandwidth is about 650 MHz, which is an order of magnitude greater than many traditional side-coupled and axis-coupled linacs. The strong coupling promotes phase and amplitude stabilization, and offers decreased sensitivity to fabrication errors. We describe the construction, tuning, and RF conditioning of the prototype structure.

INTRODUCTION

The basic concept of the DSR linac was reported in [1], and that article contains a more in-depth explanation of this linac type. FAR-TECH was granted a patent for this technology [2]. The geometry of a pair of linac cells is shown in Figure 1, which shows a half-geometry of the vacuum region inside the linac structure. A group of two resonant slots connect two adjacent linac cells through an intervening swept triangular volume which we refer to as a "void". The void region serves to provide RF coupling between the two slots. Each group of two slots has two collective resonant modes: a mode at around 1 GHz, and the working mode at the target operating frequency of 2.856 GHz. The mode split between these collective modes is so large that the pair of slots can effectively be considered a single oscillator at 2.856 GHz. The two slots serve the same purpose as a coupling cell in a side coupled linac. The advantages of the DSR linac include: a very large coupling with about 22% bandwidth, a compact geometry, no additional radial space required for the coupling cells, and shunt impedance competitive with a side-coupled linac. Simulations with HFSS [3] and with Omega3P [4] predict a shunt impedance ZT^2 of 85 $\mathrm{M\Omega/m}$. This is competitive with other linac designs featuring large coupling such as the PWT design [5], and is slightly less efficient than an equivalent side-coupled linac, which might have about 8-10% higher ZT^2 with the same basic cavity and nose cone shape. The linac is designed for the UCLA Pegasus laboratory to aid in ultra-short electron bunch experiments [6] by boosting the beam energy by a design 10 MeV. The linac can also be operated in bunching phase, which will further shorten the bunch length and enable better resolution for experiments such as electron diffraction studies. It is hoped that the DSR linac design will also find uses in industrial and medical applications.

* Work supported by DOE Office of High Energy Physics, DOE-SBIR #DE-FG02-08ER85034

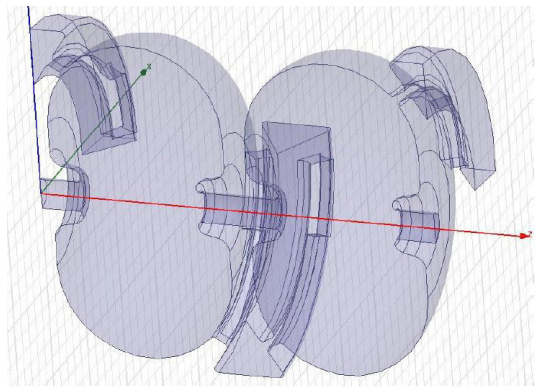


Figure 1: HFSS geometry used to model two cells of the DSR linac.

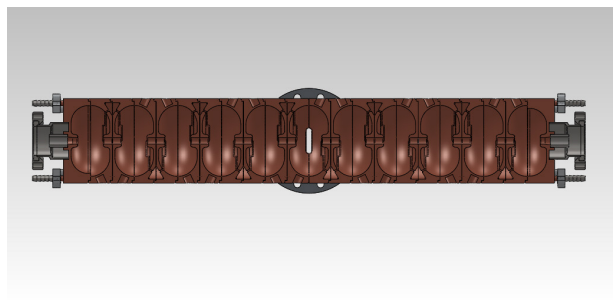


Figure 2: A cross section view of the 11-cell DSR linac.

DESIGN AND CONSTRUCTION

Design

An 11-cell DSR linac was designed with HFSS and Omega3P, as shown in Figure 2. End cells were transversely displaced in order to limit dipole kicks, and the central coupling cell shape was designed to minimize the mode pull due to the RF coupler. The linac is cooled with four cooling tubes running the length of the structure. The RF connection is via a WR284 waveguide and Skarpaas flange, and vacuum connections to the beamline are made with 2.75 inch ConFlat flanges. The beam clear aperture diameter is 8 mm. The band surrounding the accelerating mode extends from 2.513 to 3.153 GHz, making the frequency spacing from the accelerating mode to the closest nearby modes 45 MHz in our 11-cell structure. In a linac with $\pi/2$ phase advance per cell, the dispersion curve should be closed by tuning the even and odd oscillators to the proper frequency. The tolerance for the amount of closure depends on the overall bandwidth, and we have estimated that a residual stop band of as much as 3 MHz will not harm the electrical properties of the structure. Time

Copyright © 2013 CC-BY-3.0 and by the respective authors

ISBN 978-3-95450-138-0

DESIGN OF A COMPACT X-BAND LINAC STRUCTURE FOR KAERI-RTX-ISU MEDICAL CYBERKNIFE PROJECT

C. Eckman[1*], P. Buaphad[1], Y. Kim[1,2], T. Downer[1], A. Andrews[1], B. N. Lee[3], B. C. Lee[3], S. Y. Ryoo[4]
[1]Department of Physics, Idaho State University, Pocatello, ID 83209, USA
[2]Thomas Jefferson National Accelerator Facility, Newport News, VA 23606, USA
[3]Korea Atomic Energy Research Institute, Daejeon 305-353, Korea
[4]Radiation Technology eXcellence, Daejeon 305-353, Korea

Abstract

Recently, the Advanced Accelerator and Ultrafast beam Lab (AAUL) at Idaho State University (ISU), has been developing an X-band linac for the medical CyberKnife project by collaborating with Korean Atomic Energy Research Institute (KAERI) and Radiation Technology eXcellence (RTX) [1–3]. The medical CyberKnife is essentially an X-band linac, which is attached to a robotic arm for precise cancer treatment. The X-band linac has considerable advantages in cancer treatment over C-band or other RF linacs, partly due to its compact size and light weight. These qualities make the X-band linac easier to attach to a robotic arm, thus making it more maneuverable. Other advantages include a higher accelerating gradient and a higher shunt impedance. Since high mobility is necessary for precise cancer treatment, the compact X-band RF linac was selected for the CyberKnife project. This paper describes detailed design processes of the X-band linac structure, which was done with 2D SUPERFISH and 3D CST MICROWAVE STUDIO (CST MWS) electromagnetic simulation programs.

INTRODUCTION

Recently, ISU AAUL, KAERI, and RTX have been developing an X-band Standing Wave (SW) RF linac for the CyberKnife robotic radiosurgery system. CyberKnife is a non-invasive cancer treatment technique, which can be used for a multitude of cancers or tumors in the human body [4]. By adjusting a robotic arm housing the X-band linac precisely, CyberKnife can target with pinpoint accuracy. The X-band linac is used to deliver high doses of radiation directly to the cancer or tumorous areas. This process is a major improvement over older and harsher cancer treatment techniques and has the potential to save thousands of lives. The expected parameters of the X-band linac for the CyberKnife project is summarized in Table 1. The X-band linac consists of a π-mode SW linac structure with 15 cells and a coupler as shown in Fig. 1. By using the π-mode, a higher shunt impedance and a higher gradient can be obtained [5]. For the RF power source of the linac, an X-band coaxial pulsed magnetron manufactured by L-3 Communications was selected [6]. Therefore, the linac was optimized to make an RF resonance at 9.3 GHz.

* cryptoscientia@gmail.com

Table 1: Parameters of an Optimized X-band Linac

Parameter	Value	Unit
length of the linac	0.25	m
initial beam energy from gun	20	keV
maximum beam energy at linac exit	6	MeV
RF frequency	9.3	GHz
maximum RF input power	2.36	MW
shunt impedance	78	MΩ/m
maximum energy gain per cell	400	keV
unloaded quality factor	8306	·
external quality factor	7099	·

By knowing the RF resonant frequency, the cell lengths and cell radii of the linac structure can be calculated in advance. The cell length l of the π-mode SW linac structure is given by

$$l = \beta \frac{\lambda_{RF}}{2}, \quad (1)$$

where β is the relativistic velocity of electrons, and λ_{RF} is the RF wavelength of the linac structure [1]. In our linac design, the bunching cells in the linac structure correspond to the cells where β is smaller than 0.95. All these initial conditions were used in 2D SUPERFISH simulation to find a basic geometry of the linac structure. A MATLAB program was developed to work in conjunction with the 2D SUPERFISH program to design basic geometries of each bunching cell and nominal accelerating cell. These individual cells are then combined in series to form a full linac structure with good electric field symmetry. Therefore, we can save our working time to find full geometry of the X-band linac structure with good electric field symmetry by using the homemade MATLAB and SUPERFISH combined program. Then, 3D CST MWS was used to optimize the linac structure and coupler by starting with the full geometry generated by the MATLAB and SUPERFISH combined program. Once the design is completed with CST MWS, it will serve as a blueprint for an actual working model.

2D SUPERFISH SIMULATION

SUPERFISH is a 2D electromagnetic field solver created and distributed by the Los Alamos National Laboratory to evaluate cylindrically symmetric RF accelerator cavities [7]. The cells in the X-band SW RF linac structure

Copyright © 2013 CC-BY-3.0 and by the respective authors

ISBN 978-3-95450-138-0

COMPACT SCHEME FOR LASER-FREE THZ-SUB-THZ SOURCE*

A. V. Smirnov#, RadiaBeam Technologies Inc., Santa Monica, CA 90404, USA

Abstract

Undulator-free schemes based on resonant Cherenkov radiation in a small insertion device driven by a few MeV RF electron injector and alpha-magnet are considered. S- and C-band RF guns are compared to X-band multi-cell microlinac. Preference is given to planar radiator and wide quasi-flat sub-ps bunches that can be obtained with alpha magnet. It is shown that up to a milli-joule of sub-THz energy can be produced within a macropulse.

INTRODUCTION

Relatively insignificant number of facilities such as synchrotron radiation sources and free electron lasers (FELs) around the world are dedicated specifically to the THz range to deliver substantial power to users. Obviously, more facilities are needed to cover the rapidly growing demand in dedicated sources for THz science and technology [1]. However, conventional radiation facilities based on FELs, electron storage rings, and/or energy recovery linacs (ERLs) are too large, expensive, and not readily available for a broader community of researchers, investigators, scientists and commercial applicants to operate it on a flexibly customized, on-demand, independent base. For narrow bandwidth radiation generation, resonant Cherenkov resonant radiation is an attractive alternative to undulator radiation due to relative frequency independency from the beam energy (for relativistic beams) and due to the much higher equivalent shunt impedance. Coherence is provided by the Cherenkov synchronism between the microbunches and fundamental (or one of the lowest) eigenmode(s) along the interaction space hundreds of wavelengths long.

THE CONCEPT

This source concept illustrated in Fig. 1 can be utilized for container inspection, screening, safe imaging, cancer diagnostics, surface defectoscopy, and many other applications. Substantial average power can be provided by using thermionic, plasma [2], field [3] or secondary emission [4] that can be perfectly combined with RF cavity.

The THz radiation is generated by beam pre-bunching and chirping in the RF gun, followed by microbunching in a magnetic compressor and resonant Cherenkov radiation of an essentially flat beam in a robust, planar, structure with mm-sub-mm gap. The proof-of-principle has been successfully demonstrated recently on a 5 MeV beam driven by an L-band thermionic injector [5].

We calculate the energy radiated by a single microbunch using the modal energy loss found analytically with the eigenmode excitation theory applied in time domain [6] for matched outcoupling without trapped modes as follows:

$$W_{lb} \approx \frac{\omega}{4}\frac{rL}{Q}\frac{(q|\Phi|)^2}{|1-\beta_{gr}/\beta|}\left(\frac{1-\exp(-\alpha L)}{\alpha L}\right)^2, \qquad (1)$$

where $\omega = 2\pi f = h(\omega)v$ is the circular frequency of the resonant Cherenkov radiation, $h(\omega)$ is the wavenumber defined by the structure dispersion, q is the bunch charge, $r = E_z^2/dP/dz$ is the shunt impedance, $\beta = v/c$, Q is the Q-factor, $Q|\beta-\beta_{gr}|>>1$, $\alpha = \pi f/Qv_{gr}$ is the attenuation, and $\Phi = \exp\left(-(\omega\sigma_t)^2/2\right)$ is the formfactor for a Gaussian bunch having rms duration σ_t. Note Eq. (1) applied to, e.g., the 270 GHz setup [7], gives 9 μJ energy which is the same as measured [7].

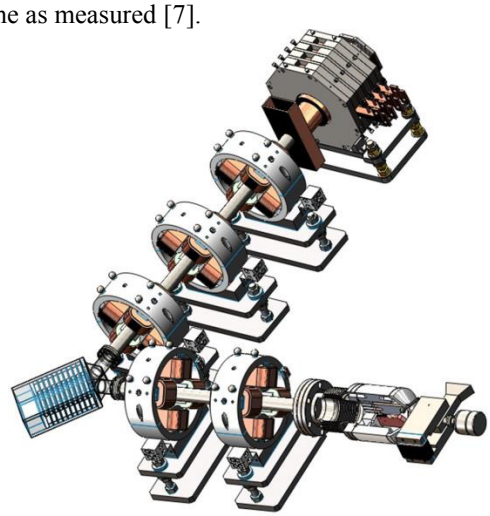


Figure 1: Schematics of the THz source beamline composed by quadrupoles, PM α-magnet, Cherenkov radiator, dipole magnet, and THz beam output.

Below we consider only briefly key features of beam dynamics, slow-wave structure, and general beamline design.

PLANAR CHERENKOV RADIATOR

Electromagnetic and mechanical engineering of a planar radiator [5,8,9] is used here as a prototype for a 0.67 THz radiator design shown in Fig. 2. The structure parameters are the following: r/Q=8 kΩ/m at 3 mm width of the grating, 0.6 mm interaction gap and 42 μm grove height; Q=1410, and 1" structure length.

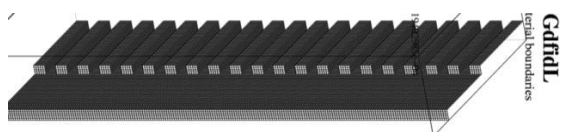


Figure 2: 20-period, bottom-half fragment of the planar radiator structure in GdfidL model (antenna horn is not shown).

*Work supported by US DoE Contract DE- SC-FOA-0000760
#asmirnov@radiabeam.com.

Copyright © 2013 CC-BY-3.0 and by the respective authors

ISBN 978-3-95450-138-0

ADAPTATION OF THE ISIS INDUCTION-CELL DRIVER TO A LOW-IMPEDANCE *X*-PINCH DRIVER

R.V. Shapovalov, W. Beezhold, V.I. Dimitrov (deceased), and R.B. Spielman
Idaho Accelerator Center, Pocatello, ID 83201, USA

Abstract

In this paper we summarize the work done to design a system to non-destructively convert the Idaho State Induction System (ISIS) induction cell driver (ICD) to a low impedance pulse power driver for *x*-pinch applications. The simulation results show that such a driver can supply about 300-kA peak current with about 70-ns rise time (10-90%). However, simulations also show that the negative reflective wave is formed, which can cause the destruction of the ISIS ICD's pulse forming line (PFL). Particular attention was taken to simulate the effect of misfire of one of the PFLs. To reduce the amplitude of this destructive wave, high power damping resistors should be placed after the output of each PFL. This would result in the maximum current achievable by this driver to be limited to about 200-kA peak value.

OVERVIEW

ISIS is a high-intensity, pulsed-power electron accelerator able to supply about 80 GW of power in a 35-nanosecond pulse [1]. It was donated to the Idaho State University by Titan Pulse Sciences, Inc. in 2002, and its primary purpose has been to serve as a radiation source for radiation effect testing in biological and semiconductor systems [2]. The power supply of ISIS [3] is composed from a Marx generator and five separate PFLs. Forty oil-filled, 77-ns-long cables connect the power supply to each acceleration unit (AU) of ISIS. The power supply of the ISIS is shown in Fig. 1. Each PFL produces a perfect 84-ns long, flat-topped 300-kV pulse which is directly used to accelerate electrons inside each AU.

In order to convert the ISIS power supply to a low-impedance *x*-pinch driver, an impedance transformer was designed [4]. The impedance transformer is the most important part of the *x*-pinch driver and serves to combine five, 300-kV outputs of the ISIS' induction cell driver (5 Ω each) into one, low-impedance (<1 Ω), 40-80 kV output to be fed to the *x*-pinch chamber. Analysis of the ISIS induction-cell driver showed that the most suitable spot for tapping its output pulse is at the end of the water-filled PFLs before the oil-filled connectors to the high-voltage cables [4].

We present the electrical circuit simulation results of proposed ISIS' based *x*-pinch driver. LTspice [5] simulations show that after directly connecting the output of each PFL to the impedance transformer and feeding the output pulse to *x*-pinch load, such a *x*-pinch driver can supply about 300-kA peak current with about 150-ns rise time (Fig. 3a). However, simulations also show, that the negative reflective wave is formed, which can cause the destruction of the ISIS PFL. Particular attention was taken to simulate the effect of misfire of one of the PFLs (Fig. 3b). To reduce the amplitude of this destructive wave, a high-power damping resistor should be placed after the output of each PFL. This would result in the maximum current achievable by this driver to be limited to about 200-kA peak value (Fig. 4a).

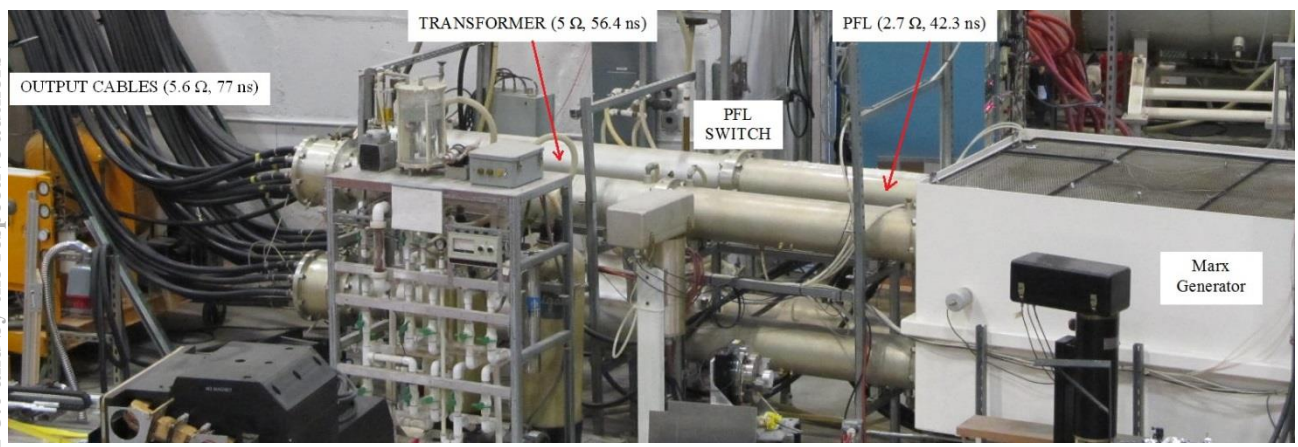


Figure 1: ISIS power supply.

Copyright © 2013 CC-BY-3.0 and by the respective authors

ISBN 978-3-95450-138-0

TRANSVERSE BEAM TRANSFER FUNCTIONS VIA THE VLASOV EQUATION*

M. Blaskiewicz†, V.H. Ranjbar
BNL Upton NY 11973 USA

Abstract

A semi-numerical method of integrating the Vlasov equation to obtain beam transfer functions directly as a function of frequency is presented. The results are compared with beam transfer functions calculated via particle tracking and excellent agreement is shown. The technique works well with both transverse wakes and detuning wakes from space charge.

INTRODUCTION AND THEORY

The stability and response properties of particle beams are encapsulated in beam transfer functions (BTFs) [1, 2, 3]. BTFs are relatively easy to measure making their accurate calculation of great practical interest. In this paper we will present two independent ways to calculate bunched beam transverse beam transfer functions, and show their agreement for some challenging parameters. To begin let θ denote azimthh, which increases by 2π each turn. Let t be clock time and let τ denote particle arrival time with respect to the synchronous particle so that $\theta = \omega_0(t-\tau)$, with ω_0 the synchronous angular revolution frequency. We use θ as the time-like variable and, to make a precise cross check possible, take linear rf so that

$$\frac{d\tau}{d\theta} = Q_s\epsilon \qquad \frac{d\epsilon}{d\theta} = -Q_s\tau, \tag{1}$$

where Q_s is the synchrotron tune and ϵ is the energy variable. with We consider a single transverse variable x and uniform focusing. Collective forces are taken in the continuum approximation with $dx/d\theta = p$ and

$$\begin{aligned}\frac{dp}{d\theta} &= -Q_\beta^2(\epsilon)x + F_e(\theta,\tau)\\ &+ 2Q_\beta\Delta Q_{sc}(\tau)[x-\bar{x}(\theta,\tau)]\\ &- \frac{q}{2\pi P_0\omega_0}\int_0^{2\tau_b} W_\perp(\tau_1)D(\theta,\tau-\tau_1)d\tau_1,\end{aligned} \tag{2}$$

where $Q_\beta(\epsilon) = Q_0 + Q_s\epsilon\omega_0\xi/\eta$ is the betatron tune, with chromaticity ξ and frequency slip factor η, $F_e(\theta,\tau)$ is the external driving force, $\Delta Q_{sc}(\tau)$ is the space charge tune shift as a function of longitudinal position in the bunch, and $\bar{x}(\theta,\tau)$ is the average beam offset. The wall induced forces are due the the transverse wake potential $W_\perp(\tau)$ and driven by the instantaneous dipole moment $D(\theta,\tau) = \bar{x}(\theta,\tau)I(\tau)$ with $I(\tau)$ the bunch current, q the particle charge, and P_0 the synchronous momentum. The force is limited to a single bunch of full length $2\tau_b$ but can be extended to uniformly filled rings.

To solve (1) and (2) using the Vlasov equation first introduce amplitude angle variables defined by $\tau = a\sin\psi$ $\epsilon = a\cos\psi$. Since all particle have constant a,

$$\frac{\partial F}{\partial\theta} + p\frac{\partial F}{\partial x} + \frac{dp}{d\theta}\frac{\partial F}{\partial p} + Q_s\frac{\partial F}{\partial\psi} = 0, \tag{3}$$

where $dp/d\theta$ is given by Eq (2). We normalise F so that $F dx dp a da d\psi$ is the number of particles in the phase space volume. To continue we define 3 transverse moments [4],

$$\{X(\psi,a,\theta),P,\Psi\} = \int dxdpF(x,p,a,\psi,\theta)\{x,p,1\}. \tag{4}$$

This gives

$$\frac{\partial X}{\partial\theta} + Q_s\frac{\partial X}{\partial\psi} = P(\psi,a,\theta), \tag{5}$$

$$\begin{aligned}\frac{\partial P}{\partial\theta} + Q_s\frac{\partial P}{\partial\psi} &= -Q_\beta^2(\epsilon)X + F_e(\theta,\tau)\Psi\\ &+2Q_\beta\kappa\left[X\int d\epsilon\Psi - \Psi\int d\epsilon X\right]\\ &-\frac{q\Psi}{2\pi P_0\omega_0}\int_0^\infty d\tau_1 W_\perp(\tau_1)q\int d\epsilon X(\epsilon,\tau-\tau_1)\end{aligned} \tag{6}$$

where $\Delta Q_{sc}(\tau) = \kappa\int d\epsilon\Psi$, $\bar{x}(\tau)\int d\epsilon\Psi = \int d\epsilon X$ and, for example,

$$\int d\epsilon X \equiv \int a_1 da_1 d\psi_1\delta(a\sin\psi - a_1\sin\psi_1)X(\psi_1,a_1,\theta),$$

and the occurences of τ and ϵ in (6) are understood to be shorthand for the amplitude angle representations. Next we substitute (5) in (6) and drop second partial derivatives with respect to ψ. We take $F_e(\theta,\tau) = F_0(\tau)\exp(-iQ\theta)$, and we take $X = X_1\exp(-iQ\theta - i\xi\omega_0\tau/\eta)$, with $Q = Q_0 + \Delta Q$. This yields

$$\left\{\Delta Q + iQ_s\frac{\partial}{\partial\psi} + \Delta Q_{sc}(a\sin\psi)\right\}X_1(\psi,a) = \tilde{F}(\tau)\Psi(a), \tag{7}$$

where

$$\begin{aligned}\tilde{F}(\tau) &= \frac{-e^{i\xi\omega_0\tau/\eta}F_0(\tau)}{2Q_0} + \kappa\int d\epsilon X_1\\ &+q^2\int_0^\infty d\tau_1\frac{W_\perp(\tau_1)e^{i\xi\omega_0\tau_1/\eta}}{4\pi Q_0P_0\omega_0}\int d\epsilon X_1(\epsilon,\tau-\tau_1).\end{aligned} \tag{8}$$

* Work performed under the auspices of the United States Department of Energy
† blaskiewicz@bnl.gov

ISBN 978-3-95450-138-0

Copyright © 2013 CC-BY-3.0 and by the respective authors

CONTROL OF INTRABUNCH DYNAMICS AT CERN SPS RING USING 3.2 GS/s DIGITAL FEEDBACK CHANNEL*

C. Rivetta†, J. D. Fox, J. M. Cesaratto, J. Dusatko, M. Pivi, K. Pollock, O.Turgut
SLAC National Accelerator Laboratory, Stanford, CA USA
H. Bartosik, W. Hofle, G. Kotzian, K. Li, CERN, Geneva, Switzerland

Abstract

The feedback control of intra-bunch instabilities driven by electron-cloud or strong head-tail interaction requires bandwidth sufficient to sense the vertical position and apply correction fields to multiple sections of a nanosecond-scale bunch. These requirements impose challenges and limits in the design of the feedback channel.

We present experimental measurements taken from the CERN SPS machine development studies with an intra-bunch feedback channel prototype. The performance of a 3.2 GS/s digital processing system is evaluated, quantifying the effect of noise and limits of the feedback channel in the bunch stability as well as transient and steady state motion of the bunch. The controllers implemented are general purpose 16 tap FIR filters and the impact on the bunch stability of controller parameters are analyzed and quantified. These studies, based on the limited feedback prototype, are crucial to validate reduced models of the system and macro-particle simulation codes, including the feedback channel. These models will allow us to predict the beam dynamics and controller limits when future wideband hardware is installed in the final prototype to stabilize multiple bunches.

INTRODUCTION

Intrabunch instabilities induced by electron-cloud (ECI) and strong head-tail interactions (TMCI) limiting factors to reach the maximum beam currents in the SPS and LHC rings [1]. Feedback techniques can stabilize bunch instabilities induced by electron cloud and strong head-tail interactions. The application of feedback control to stabilize the bunch is challenging because it requires large bandwidth to sense the transverse position and apply correcting fields to multiple sections of a nanosecond-scale bunch. These requirements impose technology challenges and limits in the design. The goal is to design a feedback control channel and to develop the hardware of a control system prototype to prove principles and evaluate the limitations of this technique by stabilizing a few bunches in the CERN SPS machine. This paper presents results from measurements conducted at SPS and validation studies of models of the feedback system using those measurements.

* Work supported by the U.S. Department of Energy under contract DE-AC02-76SF00515 and the US LHC Accelerator Research Program (LARP).

† rivetta@slac.stanford.edu

FEEDBACK SYSTEM

A single bunch wideband digital feedback system has been developed to explore new technology and control techniques. The implementation of this system is based on a reconfigurable FPGA and ADC/DAC operating at 3.2 GS/s. The system is synchronized with the SPS RF clock and is able to perform diagnostic functions, set feedback parameters and record the bunch motion at selected intervals [2]. The present studies were conducted using an existing stripline device as a kicker with 160 MHz bandwidth. Future tests will be conducted using new wideband kickers, which are currently under development [3]. The four-electrode kicker is driven by 4- 90W amplifiers of 1GHz bandwidth. The pickup signal is equalized to compensate the frequency response of the device and the cables. The controller is implemented using a bank of simple FIR filters, processing each individual ADC samples across the bunch. The prototype is capable of setting 16-tap filters, and during the test 5-taps and 7-taps were used. Additionally, the filter parameters can be changed during the run, allowing to vary the controllers in the feedback system to process the bunch motion signals.

Feedback Model

The block diagram of the feedback system including noise sources and external signal perturbations is depicted in Fig. 1. The main blocks in this figure are modeled in both macro-particle simulation codes and tools where the bunch dynamics is represented by reduced order models to assess the stability margins of the system and study the bunch performance under the influence of noise and external perturbations. These models have to be validated

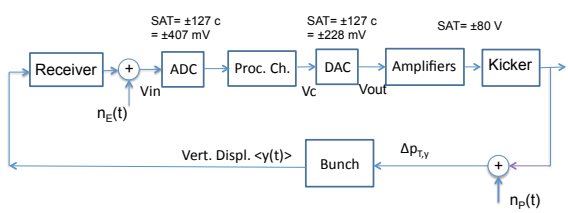


Figure 1: Block diagram feedback system.

with measurements in the SPS to be able to predict future operation conditions and evaluate the impact of limitations and non-linearities in the feedback hardware on the bunch stability and performance. The frequency response of the receiver and the RF power stage have been measured and appropriated models are included in the simulation tools [4].

Copyright © 2013 CC-BY-3.0 and by the respective authors

ISBN 978-3-95450-138-0

SIMULATION STUDY ON TRANSVERSE LASER COOLING AND ORDERING OF HEAVY-ION BEAMS IN A STORAGE RING

Yosuke Yuri, Takasaki Advanced Radiation Research Institute, Japan Atomic Energy Agency,
1233 Watanuki-machi, Takasaki, Gunma, Japan

Abstract

The formation of three-dimensionally ultralow-temperature ion beams by means of laser cooling in a storage ring is studied with the molecular dynamics approach in which stochastic interaction between laser photons and ions is incorporated. The transverse motion of a coasting beam is cooled indirectly through horizontally-displaced lasers and resonant coupling at several different operating points. The indirect transverse cooling rate depends on the displacement and detuning of the lasers as well as on momentum dispersion. In the ultralow-temperature equilibrium state, a 3D ordered (but not crystalline) structure can be formed depending on laser-cooling conditions. The characteristics of the Coulomb-ordered beam are discussed in contrast to a 3D crystalline beam.

INTRODUCTION

Three-dimensional (3D) beam cooling is essential in order to generate an ultralow-emittance beam in a storage ring. It is expected that, at ultralow emittance, the beam is Coulomb-ordered where the relative particle configuration is arranged in order and, in the zero-emittance limit, Coulomb-crystallized where the betatron and synchrotron oscillations are fully suppressed [1]. A longitudinal, one-dimensional (1D) ordering phenomenon was already observed experimentally in ultralow-current (about 10^3 ions in the ring) ion beams using electron cooling [2-4]. It has been found, by theoretical studies, that ions in the ordered beam do not pass through each other longitudinally [5-7]. As to crystalline beams, however, even a 1D string crystal has not been realized up to now in spite of a laser-cooling experimental effort at a cooler storage ring S-LSR in Kyoto University [8]. It is actually very difficult to observe phase transition of a very low-intensity (about 10 ions per bunch) bunched beam clearly although the feasibility of 1D and 2D crystalline beams was predicted with a molecular dynamics (MD) simulation [9, 10].

We have recently demonstrated the feasibility of the three-dimensionally ordered state of an ion beam with 3D laser cooling for the first time [11]. In these proceedings, more detail MD simulation results are given on transverse laser cooling and the ordered state of heavy-ion beams. The stress is put on various characteristics of the Coulomb-ordered beam.

SIMULATION PARAMETERS

A dedicated MD simulation code CRYSTAL, in which stochastic interaction between laser photons and ions is incorporated, is employed for the present study [9]. An actual beam and lattice parameters of S-LSR (see Fig. 1) has been considered. The superperiodicity of the ring is six. The ring can fulfill the following requirements to reach an ultralow-temperature state of an ion beam [1, 12]: First, the storage ring must be operated below transition energy. Second, the bare betatron tune $\nu_{x,y}$ must be less than 0.35 per lattice period to avoid linear resonances at ultralow temperature. More desirably, it must be below 0.25 to avoid linear resonance crossing in the cooling process [13].

A coasting beam of 40-keV $^{24}Mg^{+}$ ions is assumed. The space-charge force is calculated efficiently by imposing a periodic boundary condition in the longitudinal direction. The initial transverse rms emittance and longitudinal rms momentum spread of the beam have been chosen from the recent experimental observation [8].

One co-propagating and one counter-propagating Gaussian cooling lasers with the waist radius of 5 mm are applied along one of the straight sections in the ring. The direct longitudinal laser-cooling force is extended to the horizontal direction through momentum dispersion by horizontally displacing the two Gaussian laser beams [14, 15, 10]. Moreover, the vertical direction is coupled with the horizontal one through a weakly-excited solenoid magnet by applying a resonant coupling scheme [16]. Three different operating points ($\nu_x = \nu_y = (\nu_0 =)$ 1.44, 1.60, and 1.90), which fulfil the above tune requirement, are chosen for comparison. To reduce the longitudinal momentum spread, the frequencies of the lasers are

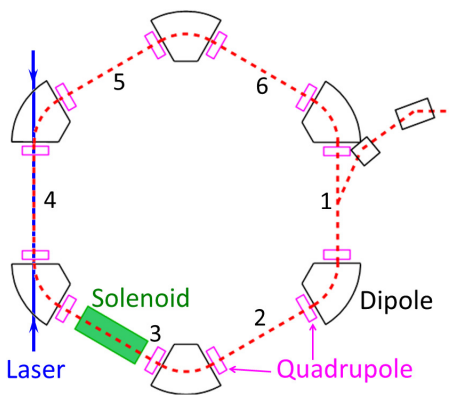


Figure 1: Schematic drawing of S-LSR. The circumference of the ring is 22.56 m. Six bending dipole and 12 quadrupole magnets have been excited so that the six-fold lattice superperiodicity can be realized. Numbers (1 to 6) in the figure express the number of straight sections for convenience. Two cooling lasers are injected along the fourth straight section. A solenoid magnet, installed in the middle of the third straight section, is excited for horizontal-vertical coupling.

Copyright © 2013 CC-BY-3.0 and by the respective authors

ELECTRON CLOUD MEASUREMENTS USING A SHIELDED PICKUP IN A QUADRUPOLE AT CESRTA*

J.P. Sikora†, M.G. Billing, J.V. Conway, J.A. Crittenden
J.A. Lanzoni, Y. Li, CLASSE, Ithaca, New York 14853 USA

Abstract

We have recently constructed a shielded pickup in a quadrupole magnet for time-resolved detection of electron cloud. Cloud electrons pass into the detector through an array of small holes in the wall of the beam-pipe that shield the collecting electrode from the direct beam signal. There are two collectors, each aligned on a pole face: one near the longitudinal center of the quadrupole, the other in the fringe field. The signals from the collectors are recorded with a digital oscilloscope. We present a summary of the design, construction and commissioning of this device, as well as initial beam measurements. This work was performed at the Cornell Electron Storage Ring which has been reconfigured as a test accelerator (CESRTA) with positron or electron beam energies ranging from 2 GeV to 5 GeV.

INTRODUCTION

Investigation of electron cloud (EC) growth and decay is an important part of the CESRTA program. Shielded pickups (SPU) in two field free regions have been in use since 2009 and significant progress has been made in connecting simulations with data from these detectors [1]. Parameters used in simulation of the electron cloud are tuned to match the data, including modeling of the detectors . The introduction of dipole or quadrupole fields makes this connection more difficult, mostly in accurate modeling of the detectors rather than modeling of the electron cloud. There was an interest in constructing a simple device that would give time-resolved information about the EC density in a quadrupole field since there is some evidence and modeling that electron cloud could be trapped there [2, 3, 4].

The quadrupole shielded pickup (QSPU) is based on the successful design of the SPU. An important part of that design is the array of holes that connect the vacuum space to the detector. The 1:3 diameter to depth ratio of the holes provides significant attenuation of the direct beam signal [5]. This is important, since a typical direct beam signal will be tens of volts, while the largest (unamplified) electron cloud signals that we have seen are tens of millivolts. Even with this attenuation, some direct beam signal is visible in the detector output.

*This work is supported by the US National Science Foundation PHY-0734867, PHY-1002467 and the US Department of Energy DE-FC02-08ER41538, DE-SC0006505.

† jps13@cornell.edu

QSPU DETECTOR

The QSPU has two collectors, both aligned with a pole face as shown in Fig. 1: one in the longitudinal center of the quadrupole , the other is located in the fringe field. This paper contains data only from the centered detector.

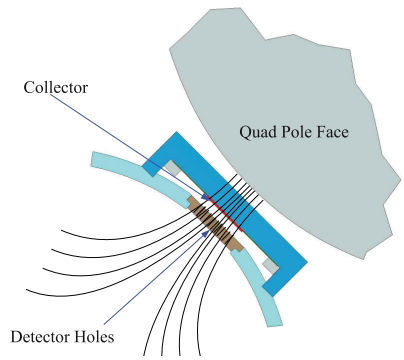


Figure 1: The QSPU detector is centered on one of the quadrupole pole faces. The rectangular collector is 10 x 100 mm copper on kapton centered longitudinally along the pole face behind an array of holes in the beam-pipe wall.

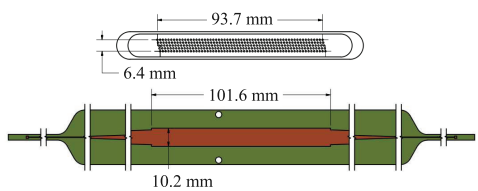


Figure 2: The 5 x 60 array of 0.79 mm diameter holes allow cloud electrons in the beam-pipe to enter the detector. The wall thickness is 2.4 mm. Electrons are collected on the copper flex circuit and the signal routed to feed-throughs at either end of the quadrupole chamber (not shown).

In the QSPU, the collector is an approximately 10 x 100 mm copper rectangle on a 0.13 mm thick kapton flex circuit with a ground plane shown in Fig. 2. Tapered striplines on the flex circuit couple the signal to SMA vacuum feed-throughs approximately 1 m apart at either end of the quadrupole chamber. For comparison, the collector in the field free SPU, is a 1.7 cm diameter button of the type used for beam position monitors.

Copyright © 2013 CC-BY-3.0 and by the respective authors

ISBN 978-3-95450-138-0

EXPERIMENTAL STUDY OF HALO FORMATION IN SPACE CHARGE DOMINATED BEAM*

H. D. Zhang#, B. L. Beaudoin, R. A. Kishek,
University of Maryland, College Park, MD 20742, USA

Abstract

Beam halos are a group of particles with low density that are far away from the well-defined central beam core and have large transverse velocities. Beam losses from halos can require a larger aperture and impose restrictions on the beam current. Several theoretical techniques have been applied to analyze and understand halo formation, including the particle-core model, the free energy model as well as particle in cell (PIC) simulations. However, few experiments on beam halos have been carried out. Here, we describe an experimental study at the University of Maryland to understand and characterize space-charge induced halo formation. The experiments are conducted on the University of Maryland Electron Beam (UMER) and the results are compared with PIC simulations using WARP.

INTRODUCTION

Halo is generally understood as a population of particles that do, or will reach large transverse radii relative to a more intense, centralized beam core. It is associated with emittance growth, degradation of beam quality and particle loss [1]. Several analytic models such as the particle-core model [2] and the free energy model [3] are derived either to depict the process of halo formation or to describe the associated emittance growth. Many theoretical and simulation studies developed these ideas and discussed various mechanisms for halo formation. However, fewer experimental studies have been performed as it is hard to obtain a halo free beam, a crucial component to identify different mechanisms or sources for halo formation. The LEDA experiment [4] is an example for demonstrating agreement with the particle-core model. But its propagation length is limited and it is no longer operational. In this paper, we discuss a method to get a halo-free beam though envelope match and skewness correction. Based on the matched beam, we perform a mismatch experiment as well as a skewness test to verify the sources of halo formation in UMER. Then, we generate a pure breathing mode mismatch, and compare experiments with simulations to confirm this mode.

EXPERIMENT SETUP

UMER

UMER [5], is small compact electron ring with a low energy (10 keV) but relatively high beam current (0.6-100 mA). It is designed to study the physics of electron beams from the emittance dominated regime to space charge dominated regime. The results can be scaled to higher energy beams with higher mass. Fig. 1 shows a schematic of the UMER layout, and Table 1 lists its key parameters and Table 2 lists the beam parameters we will use in this discussion.

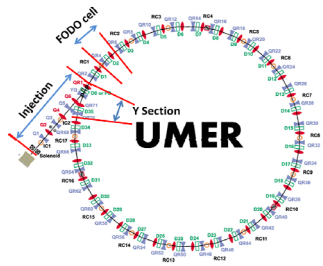


Figure 1: Diagram of UMER.

Table 1: UMER Design Parameters [5]

Parameter	Value
$\beta = v / c$	0.2
Pulse Length	20-120 ns
Beam Energy	10 keV
Current	0.6-100 mA
Ring Circumference	11.52 m
Lap Time	197 ns
Pulse Repetition Rate	10-60 Hz
FODO Period	0.32 m
Zero-current Phase Advance	0.760

Table 2: Beams in UMER [5]

Aperture#	r_0 (mm)	I (mA)	ε (μm)	χ
1	0.875	6	16.8	0.605
2	1.5	21	30.0	0.901

Image System

An imaging system was designed and dedicated for this work utilizing Ethernet cameras, in order to take and process images quickly. A system illustration is shown in Fig. 2. The cameras are connected to a control PC through a gigabyte Ethernet switch. The camera control PC can also control the magnets though the main control PC by sending an appropriate command. The whole system is integrated by a Matlab GUI code. It includes a camera control panel, Magnet control panel, image display and calculation panel, and the Auto picture scan panel. It allows one to change camera settings and take beam images, in order to calculate transverse beam parameters; such as centroid, size and rotation angle. This system can also be used for injection scan (empirical method discussed later) and phase space tomography.

*Work supported by the US Dept. of Energy, office of Science,
#haozhang@umd.edu

Copyright © 2013 CC-BY-3.0 and by the respective authors

SNS PERFORMANCE AND THE NEXT GENERATION OF HIGH POWER ACCELERATORS*

J. Galambos#, on behalf of the SNS team, ORNL, Oak Ridge, TN 37830, USA

Abstract

The SNS accelerator at ORNL has been operating near the MW level for several years now. This presentation discusses the successes and challenges, new insight gained and lessons learned with regard to the operation of a modern high power accelerator. In particular, issues with the RFQ, the target and the superconducting RF linac are discussed. Also future high power proton accelerator plans and development needs are discussed.

RECENT SNS OPERATIONAL EXPERIENCE

The Spallation Neutron Source (SNS) accelerator reached the 1 MW operational power level in 2009. Over the past two years beam power has been run between 0.85 MW and 1 MW, as indicated in Fig. 1, with reduced power operation driven by considerations beyond accelerator components. For example the past year of operation, beam power was reduced to preserve target lifetime due to a target spare shortage. However, for the past few weeks, the operational power level has been increased up to 1.2 MW.

Extended running periods without power increase in 2010 – 2011 coincided with increased accelerator availability, as shown in Figure 2. After steady rises in operational hours and beam availability through 2011, the past 2 years show decreases in both these figures. These are due to target failures at the end of FY 2012, and the start of 2013 that severely reduced operational hours and negatively impacted the beam availability. The target issue is discussed in more detail below. Discounting the target failures, the accelerator availability for the years 2011-2013 was 92%, 94% and 89% (YTD) respectively.

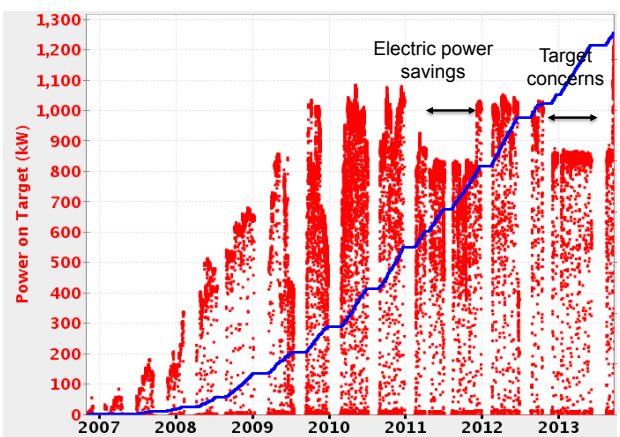


Figure 1: Power history of the SNS accelerator.

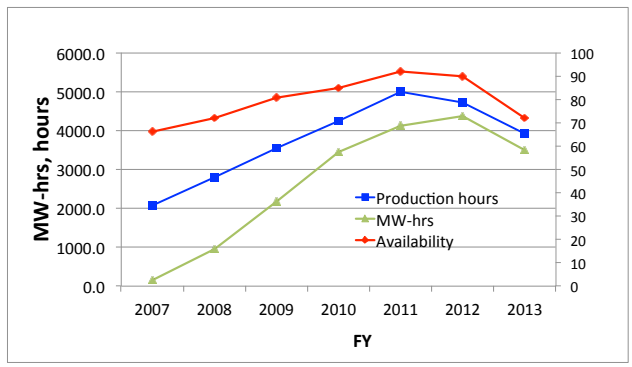


Figure 2: Operation hours and availability since initial operations in 2007.

RFQ Issues

The SNS RFQ experienced 2 detuning incidents in 2003 and 2009, which required retuning of the RFQ in order to operate. From the period mid-2011 through mid-2012 a reduction of beam current measured downstream of the RFQ was observed for all ion sources [1] (see Figure 3). This prompted a measurement of the field profile in the RFQ, and yet another perturbation was observed (see Figure 4). Interestingly, this field disturbance did not prevent operation of the RFQ, only a reduction in beam transmission. The first extended outage that allowed for retuning the field was summer of 2013. However, while there are suspected causes of the first two detuning incidents, this latest incident remains unexplained.

The field profile changes discussed above are likely specific issues related to the manufacturing of this RFQ. However, another perhaps more generic RFQ issue has been observed. This is the issue of discharge heating in the RFQ (in addition to the normal RF induced copper hearting [2]. The discharge related heating can be significant (~ 10% of total heat load) and is not constant, but rather dependent on the gas load history into the RFQ. Also it can change suddenly, complicating the cooling system and resonance control, which is designed for slower heat load changes. To accommodate this complication the low level RF control has been modified to provide fast modulation of the RFQ pulse length to help control the resonance error. However the additional pulse length margin used for this function is becoming limited as we reach the design pulse length of the machine (1 ms), and a new mitigation technique is being sought.

*This work was supported by SNS through UT-Battelle, LLC, under contract DE-AC05-00OR22725 for the U.S. DOE
jdg@ornl.gov

Copyright © 2013 CC-BY-3.0 and by the respective authors

ISBN 978-3-95450-138-0

THE EUROPEAN SPALLATION SOURCE

Mats Lindroos*, Mohammad Eshraqi and David McGinnis, ESS AB, Lund, Sweden

Abstract

The European Spallation Neutron Source project includes a 5 MW superconducting linac, and aims for initial operation at 1.5 MW in 2019 with 5 MW capacity installed for 2023. Design considerations including the work done to find the minimum cost for preserved beam power will be discussed. This will include discussions on lessons learnt from SNS regarding e.g. superconducting RF performance and RF power sources. The design and construction plans and status will be described.

NEUTRON USAGE AND HISTORICAL BACKGROUND

The neutron beams are being used extensively in science and industry to investigate the properties of matter. The beams of neutrons are used to monitor the structure of the matter in atomic levels using scattering methods. These methods give a high precision information about matter and the high penetration property of neutron makes it the only probe for these measurements.

Most existing neutron sources in Europe are based on nuclear reactors. This approach has been taken to its limits set by both technical issues such as cooling but also by licensing which is non-trivial for any facility using fissile material. Compared to existing spallation sources ESS will be 30 times brighter and it will be the first spallation source with a time averaged flux of neutrons as high as the best research reactors. Europe has today over 5000 researchers who use neutrons and this community is asking for a new intense source of neutrons.

The need for the European Spallation Source (ESS) [1] was articulated 20 years ago but a decision to build it in Lund in Sweden was only taken in May 2009. A series of meetings organized in 1991 and 1992 by Forchungszentrum Jülich (FZ-J) and Rutherford Appleton Laboratory (RAL) explored the basis for an advanced accelerator driven pulsed spallation source, which later formed the basis for the specification for ESS [2]. The decision to site it in Lund was the final stage of a process initiated by the European Commission and steered by the European Strategy Forum on Research Infrastructures (ESFRI). ESFRI was created in 2002 and is a strategic instrument of EC to develop the scientific integration of Europe and to strengthen its international outreach [3].

* mats.lindroos@esss.se

THE ESS FACILITY

The spallation cross section for protons on heavy nuclei increases as a function of proton energy up to several tens of GeV [4]. Nonetheless it is generally agreed that a kinetic proton energy between 1-3 GeV is optimal for practical target and moderator designs, and in order to keep the shielding requirements reasonable.

The ESS accelerator design has gone through several evolutions. In 2002 a fully normal conducting design was proposed [5] in parallel to a pre-dominantly superconducting design derived from the CONCERT project [6]. In 2003 a new design was presented [2] with two front-ends consisting of ion-source, Radio Frequency Quadrupole (RFQ) and a Drift-Tube Linac (DTL) up to 20 MeV. The beams of the two front-ends were merged at 20 MeV and further accelerated in normal conducting structures up to 400 MeV and superconducting structures up to 1334 MeV. The facility had both a long pulse target station and a storage and accumulation ring for a short pulse target. To enable low loss injection into the accumulator ring H^- ions were proposed to be accelerated at a total beam power of 10 MW. In 2009, the competing ESS-Bilbao [7] team and the ESS-Scandinavia [8, 9] team both proposed a simplified 5 MW design with protons accelerated to 2.5 GeV by a mostly superconducting linac with only one front-end to avoid the complex merging stage and higher beam energy to lower the required beam current. The requirement for a short pulse target station was also dropped to reduce cost. This makes it possible to accelerate H^+ ions, which should reduce losses due to intra-beam stripping of H^- ions and simplifies the ion source design.

The last design iteration was undertaken after cost objectives were set in autumn 2012. The main changes were: i) the implementation of energy staging to ease installation and commissioning, ii) the removal of cryomodules with RF systems and compensate by using operational experience from SNS and run the linac more aggressively, iii) the removal of additional cryomodules with RF systems and compensate by increasing the peak field in the cavities from 40 MV/m to 45 MV/m and iv) introducing new Multi Beam (MB) IOT technology for the high beta linac RF system in the baseline. For the staged commissioning the plan is to start with 1.5 MW in 2019 and complete remaining installation of linac to 2.0 GeV to provide 5 MW of beam by 2022. The staging doesn't only leave more time for installation but it also creates more time for the development of MB-IOTs.

As a result of this series of optimization and iterations the ESS linac beam current is proposed to be 62.5 mA and the final energy is fixed to 2.0 GeV to provide 125 MW of

Copyright © 2013 CC-BY-3.0 and by the respective authors

ISBN 978-3-95450-138-0

PROGRESS TOWARDS THE FACILITY FOR RARE ISOTOPE BEAMS*

J. Wei[#1], D. Arenius[2], N. Bultman[1], F. Casagrande[1], C. Compton[1], K. Davidson[1], J. DeKamp[1], B. Drewyor[1], K. Elliott[1], A. Facco[1,4], V. Ganni[2], P. Gibson[1], T. Glasmacher[1], K. Holland[1], M. Johnson[1], S. Jones[1], R.E. Laxdal[5], D. Leitner[1], M. Leitner[1], G. Machicoane[1], F. Marti[1], D. Morris[1], J. Nolen[1,3], J. Ozelis[1], S. Peng[1], J. Popielarski[1], L. Popielarski[1], E. Pozdeyev[1], T. Russo[1], K. Saito[1], J. Savino[1], R. Webber[1], M. Williams[1], T. Xu[1], Y. Yamazaki[1], A. Zeller[1], Y. Zhang[1], Q. Zhao[1]
[1] Facility for Rare Isotope Beams, Michigan State University, East Lansing, MI 48824 USA
[2] Thomas Jefferson National Laboratory, Newport News, VA 23606, USA
[3] Physics Division, Argonne National Laboratory, Argonne, IL 60439, USA
[4] INFN - Laboratori Nazionali di Legnaro, Legnaro (Padova), Italy
[5] TRIUMF, Vancouver, Canada

Abstract

The Facility for Rare Isotope Beams (FRIB) is based on a continuous-wave superconducting heavy ion linac to accelerate all the stable isotopes to above 200 MeV/u with a beam power of up to 400 kW. At an average beam power approximately two-to-three orders-of-magnitude higher than those of operating heavy-ion facilities, FRIB stands at the power frontier of the accelerator family - the first time for heavy-ion accelerators. To realize this innovative performance, superconducting RF cavities are used starting at the very low energy of 500 keV/u, and beams with multiple charge states are accelerated simultaneously. Many technological challenges specific for this linac have been tackled by the FRIB team and collaborators. Furthermore, the distinct differences from the other types of linacs at the power front must be clearly understood to make the FRIB successful. This report summarizes the technical progress made in the past years to meet these challenges.

INTRODUCTION

During the past decade, facilities like the Spallation Neutron Source (SNS), the Japan Proton Accelerator Research Complex (J-PARC) and the PSI accelerator advanced the frontier of proton beam power by an order of magnitude to 1 MW level (Fig. 1) [1]. On the other hand, facilities for heavy ions has been at the 1 kW level of average beam power. FRIB currently designed and ready for civil construction at the Michigan State University will advance the frontier of heavy-ion beam power by two-to-three orders-of-magnitude to 400 kW.

On August 1, 2013, the Department of Energy's Office of Science approved Critical Decision-2 (CD-2), Approve Performance Baseline, and Critical Decision-3a (CD-3a), Approve Start of Civil Construction and Long Lead Procurements, for the FRIB construction project. The Total Project Cost for FRIB is $730M, of which $635.5M will be provided by DOE and $94.5M will be provided by Michigan State University. The project will be completed by 2022. "When completed, FRIB will provide access to completely uncharted territory at the limits of nuclear stability, revolutionizing our understanding of the structure of nuclei as well as the origin of the elements and related astrophysical processes."

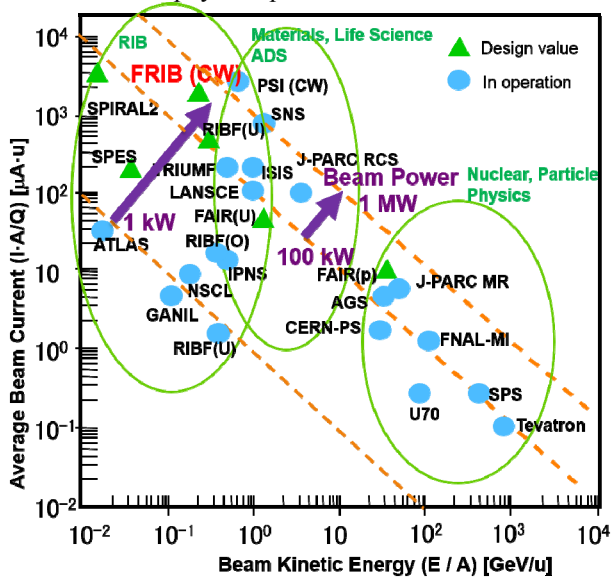


Figure 1: Average beam power as a function of the kinetic beam energy for various operating and proposed proton and heavy-ion accelerator projects.

The FRIB driver accelerator is designed to accelerate all stable ions to energies > 200 MeV/u with beam power on the target up to 400 kW (Table 1) [2]. As shown in Fig. 2, the driver accelerator consists of Electron Cyclotron Resonance (ECR) ion sources; a low energy beam transport containing a pre-buncher and electrostatic deflectors for machine protection; a Radiofrequency Quadrupole (RFQ) linac; linac segment 1 (with Quarter-wave Resonators (QWR) of β_0=0.041 and 0.085) accelerating the beam up to 20 MeV/u where the beam is stripped to higher charge states; linac segments 2 and 3 (with Half-wave Resonators (HWR) of β_0=0.29 and 0.53) accelerating the beam > 200 MeV/u; folding segments to confine the footprint and facilitate beam collimation; and a beam delivery system to transport to the target a tightly

*Work supported by the U.S. Department of Energy Office of Science under Cooperative Agreement DE-SC0000661
#wei@frib.msu.edu

Copyright © 2013 CC-BY-3.0 and by the respective authors

ISBN 978-3-95450-138-0

STATUS OF THE RARE ISOTOPE REACCELERATOR FACILITY REA*

D. Leitner[1,2], D. Alt[2], T. M.Baumann[2], C. Benatti[2], K. Cooper[2], B. Durickovich[1], K. Kittimanapun[2], S. Krause[2], A. Lapierre[2], L. Ling-Ying[2], F. Montes[2], D. Morrissey[2], S. Nash[2], R. Rencsok[2], A. J. Rodriguez[1], C. Sumithrarachchi[2], S. Schwarz[2], M. Steiner[2], M. Syphers[2], S. Williams[2], W. Wittmer[1], X. Wu[1]

[1]Facility for Rare Isotope Beams, Michigan State University, East Lansing, MI 48824 USA
[2]NSCL, Michigan State University, East Lansing, MI 48824, USA

Abstract

The Facility for Rare Isotope Beams (FRIB) is currently in the preliminary design phase at Michigan State University (MSU) [1]. FRIB consists of a driver linac for the acceleration of heavy ion beams, followed by a fragmentation target station and a ReAccelerating facility (ReA). While FRIB is expected to start commissioning in 2018, the first stage of ReA called ReA3 is already under commissioning [2, 3]. ReA was connected to the Coupled Cyclotron Facility at MSU in 2012 and has delivered its first radioactive ion beam to the experimental hall in 2013. An overview of the facility will be discussed. In addition, this paper focuses on the technical progress and first commissioning results with radioactive ion beams.

INTRODUCTION

Nuclear science research requires reaccelerated radioactive isotope ion beams in a range of kinetic energies from thermal energies to near 20 MeV/nucleon. Isotope Separation On-line (ISOL) and Projectile Fragmentation (PF) are the two most common methods used to produce high quality radioactive ions beams (RIBs) for the various nuclear science experiments. In the ISOL technique the RIBs are produced in a thick target from which they have to diffuse out before they can be ionized and used as radioactive beams. While this technique offers unmatched yields for a number of isotopes, chemically reactive isotope are more difficult and slow to extract.

Projectile fragmentation on the other hand can be used for a broad range of interesting nuclei, since the reaction products recoil out of the target in forward direction, which makes the production method chemically indifferent. In order to separate the desired isotope from the bulk of the other reaction products, in-flight fragmentation facilities are often combined with a high acceptance fragment separator [4]. This combination offers a versatile method to develop a wide range of isotopes in a short time. As an example, in the 10 years of operation of Coupled Cyclotron Facility at Michigan State University more than 1000 rare isotope beams have been produced and more than 870 have been delivered to users for experiments [5]. The energy however of those radioactive beams are close to the primary driver beam energy (80-150MeV/nucleon) which can be too high for some nuclear physics experiments.

The physics reach can be further enriched if such a facility is combined with a gas stopper and a re-accelerator. Then in addition to the fast RIBs of 50 to a few 100MeV/u, high quality beams can be provided from the lowest energies of a few 10s of keV/nucleon (for trapping and spectroscopy experiments) to an energy range between a few 100 keV/nucleon and 20

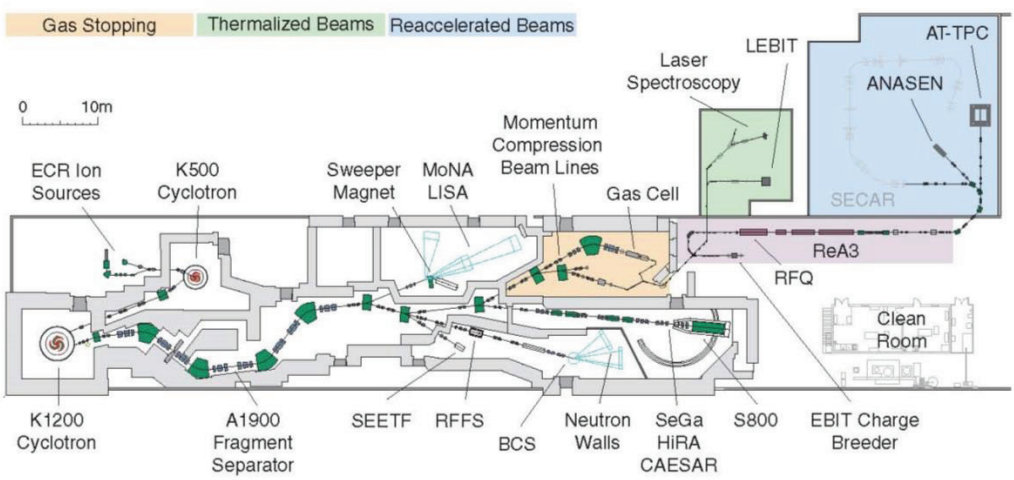


Figure 1: Facility layout of the National Superconducting Cyclotron Laboratory with the Coupled Cyclotron Facility and the newly commissioned gas stopping area and reaccelerated radioactive ion beam capabilities[5].

Copyright © 2013 CC-BY-3.0 and by the respective authors

SUPERCONDUCTING GANTRY AND OTHER DEVELOPMENTS AT HIMAC

Y. Iwata*, K. Noda, T. Shirai, T. Murakami, T. Fujita, T. Furukawa, K. Mizushima, Y. Hara, S. Suzuki, S. Sato, and K. Shouda, NIRS, 4-9-1 Anagawa, Inage, Chiba 263-8555, Japan
T. Fujimoto, and H. Arai, AEC, 3-8-5 Konakadai, Inage, Chiba 263-0043, Japan
T. Ogitsu, KEK, 1-1 Oho, Tsukuba, Ibaraki 305-0801, Japan
T. Obana, NIFS, 322-6 Oroshi-cho, Toki-city 509-5292, Japan
N. Amemiya, Kyoto Univ., Kyoto-Daigaku-Katsura, Nishikyo, Kyoto 615-8510, Japan
T. Orikasa, S. Takayama, Y. Nagamoto, and T. Yazawa, Toshiba Corp., 1-1-1 Shibaura, Minatoku, Tokyo 105-8001, Japan

Abstract

New developments at HIMAC include a superconducting carbon gantry, a new therapy area with three new treatment rooms, and substantial enhancements to the synchrotron extraction system to enable energy-variation through multiple flattops within a synchrotron cycle to match characteristics of the gantry and three-dimensional raster scanning. The carbon gantry consists of ten combined-function superconducting magnets, allowing a very compact geometry – the length and the radius of the gantry are approximately 13 and 5.5 m, respectively, comparable to the dimensions of existing proton gantries. Further, these superconducting magnets are designed for fast slewing of the magnetic field to follow the multiple flattop operation of the synchrotron. In this paper, the recent developments of HIMAC are presented.

INTRODUCTION

Heavy-ion cancer-therapy using the Heavy-Ion Medical Accelerator in Chiba (HIMAC) has been carried out since June 1994. The successful cancer treatments have led us to construct a new treatment facility [1]. The new treatment facility equips with three treatment rooms; two of them have both horizontal and vertical fixed-irradiation-ports, and the other is a rotating gantry port as schematically shown in Fig. 1. For all the ports, the three-dimensional raster-scanning irradiation method with pencil beam will be employed [2].

In raster-scanning irradiation, a target is directly irradiated with high-energy carbon-ions, after being accelerated by a synchrotron ring. Since the position of the focused beam on a target is controlled by the fast horizontal and vertical scanning-magnets, the lateral dose distribution is determined by these scanning magnets. On the other hand, the depth dose-distribution is determined by beam energy. To control the depth dose-distribution, it is preferable to change the beam energy directly by the accelerators, instead of using energy degraders, since energy degraders may broaden the spot size of the beam on a target, and concurrently produce secondary fragments, which could adversely affect the depth dose-distribution.

To quickly change the energy of the beam, as provided by the synchrotron ring, we developed a multiple-energy operation with extended flattops [3]. The proposed operation enables us to provide carbon ions having various energies in a single synchrotron cycle; namely, the beam energy would be successively changed within a single synchrotron pulse. With this operation, the beam range could be controlled without using any energy degraders.

To further obtain precise dose distributions, we developed an isocentric superconducting rotating-gantry for carbon therapy [4]. This rotating gantry is designed to transport carbon ions having 430 MeV/u to an isocenter with irradiation angles of over ±180 degrees, and is further capable of performing the fast raster-scanning irradiation. The combined-function superconducting magnets will be employed for the rotating gantry. Use of the superconducting magnets with optimized beam optics allow a compact gantry design with a large scan size at the isocenter; the length and the radius of the gantry will be approximately 13 and 5.5 m, respectively, which are comparable to those for the existing proton gantries. This rotating gantry is currently under construction, and will be installed in the room G of the new treatment facility.

We report the recent developments of the multiple flattop operation as well as the superconducting rotating-gantry.

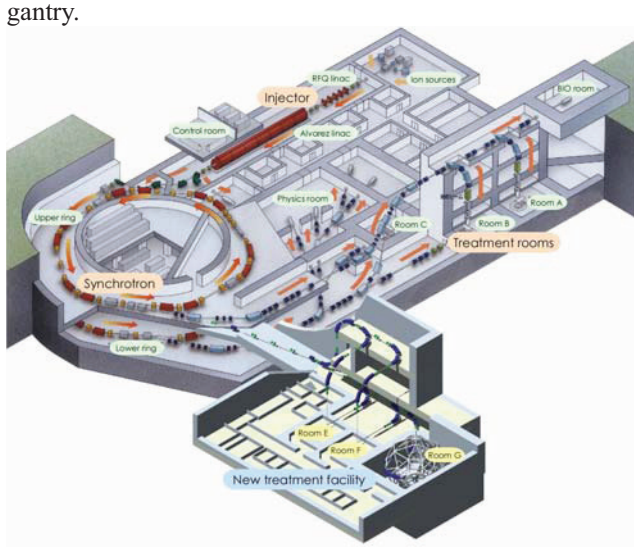


Figure 1: Layout of the HIMAC complex.

*corresponding author. E-mail: y_iwata@nirs.go.jp (Y. Iwata)

ISBN 978-3-95450-138-0

Copyright © 2013 CC-BY-3.0 and by the respective authors

ADVANCES IN SUPERCONDUCTING UNDULATORS *

Y. Ivanyushenkov#, Advanced Photon Source, ANL, Argonne, IL 60439, USA

Abstract

Superconducting technology could be employed for building undulators with enhanced parameters for synchrotron light sources and free-electron lasers. Expected and measured performance of superconducting undulators will be presented. Although superconducting technology is already working in superconducting wigglers, the development of superconducting undulators was slowed down by a variety of challenges that will be discussed. Possible solutions with examples will be presented. Finally, an overview of recent developments in superconducting undulators is presented in this paper.

INTRODUCTION

Insertion devices (IDs) are essential parts of modern and future light sources. The trends for IDs of future light sources are reviewed in [1]. Until now most IDs have been built using permanent magnets as a source of magnetic flux. At the same time, there is a growing interest in electromagnetic devices that use superconducting windings. As a matter of fact, superconducting wigglers are a well-established technology; such IDs are being used in many synchrotron light sources [1]. In comparison, the development of superconducting undulators is lagging behind the progress being made with superconducting wigglers.

This paper follows the review of developments in superconducting insertion devices given in [2] and concentrates on superconducting undulators (SCUs). The motivation of developing SCUs is first discussed, followed by a list of challenges. Examples of recent developments towards finding the solutions are then given. Finally, an overview of activities in superconducting undulators is presented.

SCU MOTIVATION

Interest in SCUs is stimulated by the fact that the SCUs can reach, for the same vacuum gap and period length, higher field events with respect to cryogenic permanent magnet undulators (CPMUs)—the state-of-the-art of permanent-magnet-based undulators. The undulator peak field for both technologies is compared in Table 1 [3]. In this table, NbTi-APC refers to a NbTi-superconductor with artificial pinning centers (APC).

A similar comparison is given in [4]. A careful analysis of CPMU and SCU technologies concludes that above the period length of 10 mm SCUs produce the highest fields. For the smaller period lengths, CPMUs can compete with NbTi SCUs, whereas Nb_3Sn or NbTi-APC devices are still superior.

*Work supported by by U.S. Department of Energy, Office of Science, under Contract No. DE-AC02-06CH11357.

#yury@aps.anl.gov

Table 1: CPMU and SCU Comparison [3]

	CPMU PrFeB	SCU NbTi	SCU NbTi-APC
Undulator period, mm	15	15	15
Magnetic gap, mm	5.2	6	6
Undulator peak field B, T	1.0	1.18	1.46
Undulator parameter K	1.40	1.65	2.05

SCU CHALLANGES

Development of SCUs is progressing relatively slowly due to several challenges. The first one concerns the requirement of high quality field from an undulator magnet. The second one is operating the SCU magnet coils at high current densities and providing adequate cooling in the presence of beam heating.

The first and second field integrals should be kept at a minimum to avoid electron beam position deviation by the undulator magnetic field. To achieve the highest performance of an undulator at higher harmonics, the phase error should also be kept at a level of a few degrees RMS. Those requirements are not easily achievable for multipole magnetic structures.

Cooling complex multi-coil superconducting magnetic structures of SCUs in the presence of heating by an electron beam is another challenging task. The possible solutions are discussed below.

SCU MAGNET

Magnet Design

A planar SCU generates a periodic magnetic field in a plane. For this, a set of linear currents is required as a minimum [5]. For practical reasons, a set of small racetrack coils (with dimensions of few a cm in height by a few cm in length) is used forming a multi-coil structure supported by a magnet former. The coils are usually vertically oriented due to a relatively short (15-30 mm) period length in the undulators. One undulator period contains two coils with the currents going in opposite directions. A magnet former, or a core, can be made of magnetic or non-magnetic material. A complete SCU magnetic structure is then made of two such magnets separated by a magnetic gap where a beam vacuum chamber can be located [6].

Such a magnetic design is adopted in the SCUs for the National Synchrotron Radiation Research Center (NSRRC), Taiwan [7], Advanced Photon Source (APS), USA [8], Diamond Light Source (DLS), UK [9], and Shanghai Synchrotron Radiation Facility (SSRF), China [10]. In the SCU for ANKA there is no beam vacuum

Copyright © 2013 CC-BY-3.0 and by the respective authors

DEVELOPMENT AND OPERATION OF THE SNS FAST CHOPPER SYSTEMS*

R. Saethre, D. Anderson, C. Deibele, V. Peplov, M. Stockli
ORNL, Oak Ridge, TN 37831, USA

Abstract

The Spallation Neutron Source (SNS) at Oak Ridge National Laboratory requires fast chopper systems to create a series of mini-pulses of H^- ions in the Linear Accelerator (LINAC) for injection into the accumulation ring. The fast chopper systems are in the front end of the accelerator with one chopper in the Low Energy Beam Transport (LEBT), immediately upstream of the Radio Frequency Quadrupole (RFQ), and another chopper in the Medium Energy Beam Transport (MEBT), downstream of the RFQ, where the beam energy is approximately 2.5 MeV. Clean bunching requires fast rise and fall time and low jitter to minimize the amount of charge in the ring extraction gap. The chopper systems operate at a burst frequency of 1 MHz and a burst width of greater than 1 ms and burst frequency of 60 Hz. The choppers have had historical reliability issues, especially in the LEBT system. This paper describes the development of reliable LEBT and MEBT choppers and the operational performance since SNS commissioning in 2006.

INTRODUCTION

A layout of the Spallation Neutron Source (SNS) at Oak Ridge National Laboratory is shown in Figure 1. The SNS consists of a Linear Accelerator (LINAC) which injects H^- beam pulses into a proton accumulation ring where they are extracted and transported to a liquid mercury target to generate neutrons for studying neutron sciences. The ion source in the front end system [1] produces an H^- beam that is chopped into mini-pulses for injection into the LINAC. The beam is accelerated through the LINAC and transported through the high energy beam transport (HEBT) section where it is injected into the accumulation ring. More than 1000 turns can be accumulated before the beam is extracted from the ring for transport to the mercury target. Four bipolar high voltage pulse generators in the Low Energy Beam Transport (LEBT) [2-4] section and two unipolar high voltage pulse generators in the Medium Energy Beam Transport (MEBT) [5-8] section create the beam mini-pulses.

The pulse generators and the structures they drive have had many reliability issues which have required extensive research and development to rectify. This paper summarizes the LEBT and MEBT chopper systems function, failure history, and development of reliable modules. It is focused on the reliability of the LEBT high voltage pulse generators used to apply pulses to the lens segments. Detailed descriptions of the LEBT and MEBT structure improvements can be found in the references.

*Work performed at Oak Ridge National Laboratory, which is managed by UT-Battelle, LLC, under contract DE-AC05-00OR22725 for the U.S. Department of Energy.

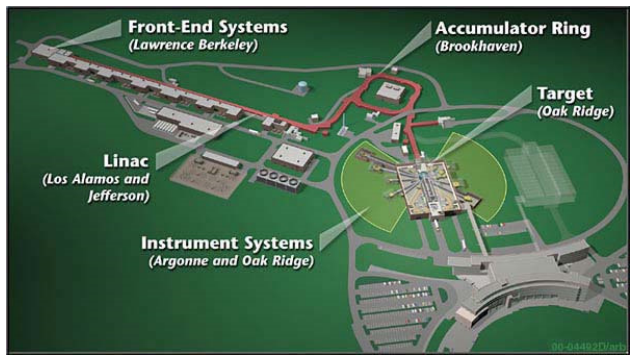


Figure 1: Layout of the Spallation Neutron Source in Oak Ridge, TN.

CHOPPER TIMING REQUIREMENTS FOR BEAM EXTRACTION

The choppers operate by generating fast rise/fall time high voltage pulses interspersed with periods of no high voltage, effectively deflecting the beam from the beamline to a target to generate gaps in the beam. The extraction kicker rise time sets the minimum gap required for the high voltage pulse generators used for chopping in the LEBT and MEBT. The beam gap in the accumulation ring must be clean and wide enough for the extraction kickers to fully turn on. If the head and tail of the beam in the ring are not sharp or the gap is not free of protons, the extraction kickers will partially deflect the beam during kicker turn on, causing activation of the extraction septum magnet.

The extraction kicker system consists of fourteen pulse forming networks (PFNs) located in the Ring Service Building, driving fourteen kicker magnets in the Ring Tunnel. Due to the design of the PFN, the rise time is fixed at approximately 200 ns. Figure 2 is a graph of the rise time of the extraction kicker magnet current.

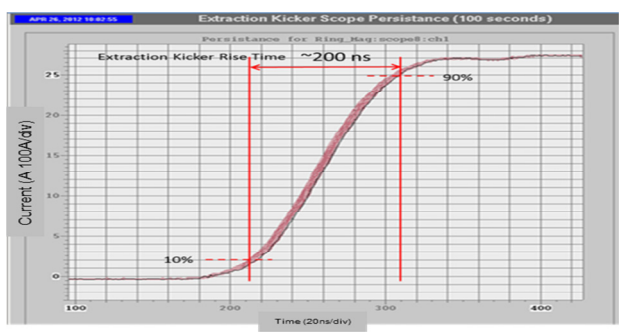


Figure 2: Extraction kicker rise time.

Copyright © 2013 CC-BY-3.0 and by the respective authors

ISBN 978-3-95450-138-0